

UC Davis

Research reports

Title

Investigation of the Effect of Pavement Deflection on Vehicle Fuel Consumption: Field Testing and Empirical Analysis

Permalink

<https://escholarship.org/uc/item/8zc70841>

Authors

Butt, Ali Azhar
Harvey, John
Fitch, Dillon
et al.

Publication Date

2022

DOI

10.7922/G2X34VRF

Investigation of the Effect of Pavement Deflection on Vehicle Fuel Consumption: Field Testing and Empirical Analysis

Authors:

Ali Azhar Butt, John T. Harvey, Dillon Fitch, Sampat Kedarisetty, Jeremy D. Lea, Jon Lea, and Darren Reger

Partnered Pavement Research Center (PPRC) Project Number 4.53 (DRISI Task 2691):
Investigation of the Effect of Pavement Deflection on Vehicle Fuel Consumption:
Field Testing and Empirical Analysis

PREPARED FOR:

California Department of Transportation
Division of Research, Innovation, and System Information
Office of Materials and Infrastructure

PREPARED BY:

University of California
Pavement Research Center
UC Davis, UC Berkeley




TECHNICAL REPORT DOCUMENTATION PAGE

1. REPORT NUMBER UCPRC-RR-2021-03	2. GOVERNMENT ASSOCIATION NUMBER	3. RECIPIENT'S CATALOG NUMBER
4. TITLE AND SUBTITLE Investigation of the Effect of Pavement Deflection on Vehicle Fuel Consumption: Field Data Collection, Data Processing, and Empirical Analysis		5. REPORT PUBLICATION DATE January 2022
7. AUTHOR(S) Ali Azhar Butt (ORCID 0000-0002-4270-8993), John T. Harvey (ORCID 0000-0002-8924-6212), Dillon Fitch (ORCID 0000-0003-3760-322X), Sampat Kedarisetty (ORCID 0000-0002-5584-5380), Jeremy D. Lea (ORCID 0000-0003-3445-8661), Jon Lea (ORCID 0000-0003-0999-469X), and Darren Reger		6. PERFORMING ORGANIZATION CODE
9. PERFORMING ORGANIZATION NAME AND ADDRESS University of California Pavement Research Center Department of Civil and Environmental Engineering, UC Davis 1 Shields Avenue Davis, CA 95616		8. PERFORMING ORGANIZATION REPORT NO. UCPRC-RR-2021-03 UCD-ITS-RR-21-94
12. SPONSORING AGENCY AND ADDRESS California Department of Transportation Division of Research, Innovation, and System Information P.O. Box 942873 Sacramento, CA 94273-0001		10. WORK UNIT NUMBER
15. SUPPLEMENTAL NOTES doi:10.7922/G2X34VRF		11. CONTRACT OR GRANT NUMBER 65A0542
16. ABSTRACT The results presented in this report are part of Phase II of a two-phase study. Based on the results from mechanistic models of additional fuel consumption in vehicles due to the structural response of the pavement structure, Phase I of this study concluded that pavement has a small but important enough effect on vehicle fuel consumption to warrant field investigation. The goal of the Phase II study was to measure vehicle fuel consumption in the field on different pavement types in winter and summer and at different speeds, and to use the data collected to develop empirical models for this fuel-consumption effect. The field investigation presented in this report included 21 California pavement sections with different pavement types: flexible, semi-rigid, jointed plain concrete, continuously reinforced concrete, and composite structures. The vehicles selected and instrumented for the fuel economy measurements included a five-axle semi-trailer tractor, a diesel truck, a sports utility vehicle (SUV), a gasoline-fueled car, and a diesel-fueled car. Vehicles were run on cruise control and data were recorded at 45 and 55 mph on state roads and at 35 and 45 mph on local roads. The data from the field investigation were analyzed and used to develop an empirical modeling framework considering road geometry, wind, temperature, and pavement structural and surface (roughness and texture) effects on vehicle fuel consumption. Based on the final framework, a final empirical model was developed for each section. The report presents results of a factorial analysis of the effects of each variable using the final model for each vehicle type on each pavement type and in different California climate regions. The within-section variability is almost always greater than the variability between sections for a given pavement type and efficiency condition (tailwind, speed, and climate region) and the within-section variability is also usually larger than the variability between pavement types. Only the data for the heavy heavy-duty truck (HHDT) showed any meaningful difference in results between sections, but that variability is not tied to pavement type and is only present under certain conditions of speed, tailwind, and air temperature (tied to climate region). These results indicate that missing variables (or errors in the existing variables) need to be reduced in further experiments to observe measurable effects of pavements on fuel consumption in real-world driving. While air temperature interacted with cruise control speed for the HHDT, there was a lack of clear evidence that asphalt roads cause more fuel consumption for the HHDT even under the conditions where the most possible effect of pavement type was found. This suggests that pavement type is not the correct explanation for that variation. Instead, the variation in the effect of air temperature by cruise control speed for the HHDT likely has to do with differences in engine efficiency under different conditions.		13. TYPE OF REPORT AND PERIOD COVERED Research Report November 2014 to December 2020
17. KEY WORDS pavement deflection, deflection energy, excess fuel consumption, fuel economy, field testing, mechanistic-empirical analysis, energy models, forward modeling	14. SPONSORING AGENCY CODE	
19. SECURITY CLASSIFICATION (of this report) Unclassified	18. DISTRIBUTION STATEMENT No restrictions. This document is available to the public through the National Technical Information Service, Springfield, VA 22161	21. PRICE None
20. NUMBER OF PAGES 709	21. PRICE None	

Reproduction of completed page authorized

UCPRC ADDITIONAL INFORMATION

1. DRAFT STAGE Final	2. VERSION NUMBER 1				
3. PARTNERED PAVEMENT RESEARCH CENTER STRATEGIC PLAN ELEMENT NUMBER 4.53	4. DRISI TASK NUMBER 2691				
5. CALTRANS TECHNICAL LEAD AND REVIEWER(S) D. Maskey	6. FHWA NUMBER CA222691A				
7. PROPOSALS FOR IMPLEMENTATION					
8. RELATED DOCUMENTS Harvey, J., Lea, J.D., Kim, C., Coleri, E., Zaabar, I., Louhghalam, A., Chatti, K., Buscheck, J., and Butt, A.A. 2016. <i>Simulation of Cumulative Annual Impact of Pavement Structural Response on Vehicle Fuel Economy for California Test Sections</i> (Research Report: UCPRC-RR-2015-05). Davis and Berkeley, CA: University of California Pavement Research Center. https://escholarship.org/uc/item/3p8312vs .					
9. LABORATORY ACCREDITATION The UCPRC laboratory is accredited by AASHTO re:source for the tests listed in this report					
10. SIGNATURES					
A. A. Butt FIRST AUTHOR	J. T. Harvey TECHNICAL REVIEW	D. Spinner EDITOR	J. T. Harvey PRINCIPAL INVESTIGATOR	D. Maskey CALTRANS TECH. LEAD	T. J. Holland CALTRANS CONTRACT MANAGER

Reproduction of completed page authorized

TABLE OF CONTENTS

LIST OF FIGURES	v
LIST OF TABLES	xx
PROJECT OBJECTIVES	xxii
EXECUTIVE SUMMARY	xxiii
LIST OF ABBREVIATIONS	xxxiv
1 INTRODUCTION	1
1.1 Overall Study and Phase I Summary	5
1.2 Project Goal and Objective	8
1.3 Report Organization	9
2 FIELD INVESTIGATION, EXPERIMENT DESIGN, AND DATA COLLECTION	11
2.1 Field Test Sections Experiment Design	11
2.1.1 Field Test Section Characterization	16
2.1.2 Laboratory Testing	23
2.2 Fuel Economy Testing and Data Collection	26
2.2.1 Vehicles	26
2.2.2 Fuel Use Measurement Equipment	28
2.2.3 Climate Data Collection Equipment During Field Testing	28
2.2.4 Fuel Economy Testing Protocol	29
2.2.5 Fuel Economy Data Collection	30
3 DATA MANAGEMENT PROCESS	33
3.1 Summary of Data Collected	33
3.1.1 Weather Station Data	33
3.1.2 Profile Data	34
3.1.3 Gradient Data	34
3.1.4 Fuel Consumption Data (OBD Data)	35
3.2 Data Cleaning	36
3.2.1 Raw Data Verification and Completeness	38
3.2.2 First Order Data Cleaning	40
3.2.3 Selection of Subsection Length for Analysis	42
3.2.4 Data Compilation	49
3.2.5 Second Order Data Cleaning	50
3.3 Data Verification	52
4 EMPIRICAL DATA ANALYSIS AND MODELING	61
4.1 Empirical Modeling of Vehicle Fuel Consumption	61
4.1.1 Examination of Autocorrelation	63
4.1.2 Model Structure	65
4.2 Model Results	67
4.2.1 Model Predictions	68
4.2.2 Control Characteristics	70
4.2.3 Primary Pavement Effects	83
5 CONCLUSIONS	99
REFERENCES	101
Appendix A: Test Sections Location, Average Roughness, and Macrotexture	105
Appendix B: Pavement Structure Information from Ground Penetrating Radar and Site Investigation	131
Appendix C: Laser Texture Scanner Results	159
Appendix D: Temperature Profiles	161
Appendix E: Test Section Profile Graphs	167

Appendix F: Pavement Gradient Data From Different Sources	189
Appendix G: Dynamic Shear Modulus Versus Frequency Sweep Master Curves	
for Asphalt Surface Pavement Sections	217
Appendix H: Information About Vehicles	231
Appendix I: Tire Hardness.....	233
Appendix J: Tire Pressure Monitoring Study	237
Appendix K: Fuel Quality Study	243
Appendix L: Air Density Calculations	247
Appendix M: Determining the Relationship Between RPM and Vehicle Speed	251
Appendix N: Determining Pavement Temperatures	255
Appendix O: Number of Test Replicates and Graphs of Fuel Rate Data for Different Vehicles	287
Appendix P: Graphs of Fuel Rate, Roughness, Gradient, Headwind, and Speed per Vehicle Type	
per Section per Season	297
Appendix Q: Quantitative Summaries of Vehicle Empirical Models.....	671

LIST OF FIGURES

Figure 1.1: Summary of Phase II tasks.	9
Figure 2.1: FWD deflection bowl in wheelpath at transverse joint on jointed plain concrete section PH01 under 60 kN load for summer and winter test cycles.	18
Figure 2.2: FWD deflection bowl in wheelpath at mid-slab on jointed plain concrete section PH03 under 52 kN load for summer and winter test cycles.	18
Figure 2.3: FWD test in wheelpath on flexible section PH10 under 35 kN load for summer and winter test cycles.	19
Figure 2.4: FWD test in wheelpath on semi-rigid section PH16 under 63 kN load for summer and winter test cycles.	19
Figure 2.5: FWD test in wheelpath on composite section PH19 under 34 kN for summer and winter test cycles.	20
Figure 2.6: FWD test in wheelpath on continuously reinforced concrete section PH20 under 56 kN load for summer and winter test cycles.	20
Figure 2.7: Procedure to slice different layers from each lift from a core sample.	23
Figure 2.8: Vehicles used in the study.	27
Figure 3.1: Data handling and cleaning process.	37
Figure 3.2: Fuel consumption of F-450 on PH03-Yol505-JPC section at 55 mph in two different gears.	39
Figure 3.3: Average elevation and subsection length plot for subsection length of 480 ft.	43
Figure 3.4: Average elevation and subsection length plot for subsection length of 300 ft.	44
Figure 3.5: Average elevation and subsection length plot for subsection length of 240 ft.	45
Figure 3.6: Average elevation and subsection length plot for subsection length of 180 ft.	46
Figure 3.7: Average elevation and subsection length plot for subsection length of 90 ft.	47
Figure 3.8 (a) and (b): Example plots of RVE analysis based on IRI.	49
Figure 3.9: Example plot of car fuel consumption and vehicle speed data used to identify bad data.	51
Figure 3.10: Example of tagging runs for car speed data on Section PH07.	52
Figure 3.11: Fuel rate, vehicle speed, effective headwind, air density, gradient, and IRI for each subsection and multiple runs: summer nighttime testing using car at 45 mph on section PH02.	54
Figure 3.12: Fuel rate, vehicle speed, effective headwind, air density, gradient, and IRI for each subsection and multiple runs: summer daytime testing using HHDT at 55 mph on section PH09.	56
Figure 3.13: Fuel rate, vehicle speed, effective headwind, air density, gradient, and IRI for each subsection and multiple runs: winter daytime testing using HHDT at 55 mph on section PH09.	57
Figure 3.14: Fuel rate, vehicle speed, effective headwind, air density, gradient, and IRI for each subsection and multiple runs: winter daytime testing using SUV at 45 mph on section PH21.	58
Figure 3.15: Fuel rate, vehicle speed, effective headwind, air density, gradient and IRI for each subsection and multiple runs: winter daytime testing using SUV at 55 mph on section PH21.	59
Figure 4.1: Directed acyclic graph representing the conceptual model of vehicle fuel consumption.	61
Figure 4.2: Simplified directed acyclic graph representing the conceptual model used for linear regression.	63
Figure 4.3: Time series fuel consumption predictions for first experimental run on PH01 for all the vehicles. ...	69
Figure 4.4: Time series fuel consumption predictions for first experimental run on PH02 for all the vehicles. ...	70
Figure 4.5: Conditional effect of cruise control speed on the fuel consumption of the car (left) and F-450 (right).	71
Figure 4.6: Conditional effect of cruise control speed on the fuel consumption of the SUV (left) and HHDT (right).	72
Figure 4.7: Conditional effect of elevation gradient on the fuel consumption of the car (top left), SUV (top right), F-450 (bottom left), and HHDT (bottom right).	73
Figure 4.8: Conditional effect of air temperature on the fuel consumption of the car (top left), SUV (top right), F-450 (bottom left), and HHDT (bottom right).	75

Figure 4.9: Conditional effect of air temperature by cruise control speed on the fuel consumption of the car (top left), SUV (top right), F-450 (bottom left), and HHDT (bottom right).....	76
Figure 4.10: Conditional effect of effective tailwind on the fuel consumption of the car (top left), SUV (top right), F-450 (bottom left), and HHDT (bottom right).....	78
Figure 4.11: Conditional effect of roughness and texture on the fuel consumption of the car.	79
Figure 4.12: Conditional effect of roughness and texture on the car’s fuel consumption by cruise control speed.	80
Figure 4.13: Conditional effect of roughness and texture on the fuel consumption of the SUV.....	80
Figure 4.14: Conditional effect of roughness and texture on the SUV’s fuel consumption by cruise control speed.	81
Figure 4.15: Conditional effect of roughness and texture on the fuel consumption of the F-450.....	81
Figure 4.16: Conditional effect of roughness and texture on the F-450’s fuel consumption by cruise control speed.	82
Figure 4.17: Conditional effect of roughness and texture on the fuel consumption of the HHDT.	82
Figure 4.18: Conditional effect of roughness and texture on the HHDT’s fuel consumption by cruise control speed.	83
Figure 4.19: Car scenario for the Central Coast Region.	85
Figure 4.20: Car scenario for the Desert Region.....	86
Figure 4.21: Car scenario for the High Mountain Region.....	87
Figure 4.22: Car scenario for the Inland Valley Region.	88
Figure 4.23: SUV scenario for the Central Coast Region.	89
Figure 4.24: SUV scenario for the Desert Region.....	90
Figure 4.25: SUV scenario for the High Mountain Region.	91
Figure 4.26: SUV scenario for the Inland Valley Region.	92
Figure 4.27: F-450 scenario for the Central Coast Region.....	93
Figure 4.28: F-450 scenario for the Desert Region.	94
Figure 4.29: F-450 scenario for the High Mountain Region.....	95
Figure 4.30: F-450 scenario for the Inland Valley Region.....	96
Figure 4.31: HHDT scenario for the Central Coast Region.	97
Figure 4.32: HHDT scenario for the Desert Region.	97
Figure 4.33: HHDT scenario for the High Mountain Region.	98
Figure 4.34: HHDT scenario for the Inland Valley Region.	98
Figure A.1: Pavement test sections located in California, shown on Google Maps.	105
Figure A.2: PH01 is a northbound concrete pavement section and PH02 is a southbound concrete pavement section on Highway 113 in Yolo County on Google Maps.	106
Figure A.3: PH01 location on Google Earth.	106
Figure A.4: PH02 location on Google Earth.	107
Figure A.5: On-site location photograph of PH02.	107
Figure A.6: PH03 is a northbound concrete and PH04 is a southbound composite pavement section on Highway 505 in Yolo County on Google Earth.	108
Figure A.7: PH03 location on Google Earth.	108
Figure A.8: PH03 on-site location photograph during falling weight deflectometer (FWD) closures.	109
Figure A.9: PH04 location on Google Earth.	109
Figure A.10: PH04 on-site location photograph.	110
Figure A.11: PH07 is a northbound asphalt pavement section on CR98 on Google Maps.	110
Figure A.12: PH07 location on Google Earth.	111
Figure A.13: PH07 on-site location photograph from Google Maps.	111
Figure A.14: PH08 is an eastbound asphalt pavement section on CR29 on Google Maps.....	112
Figure A.15: PH08 location on Google Earth.	112
Figure A.16: PH08 on-site location photograph from Google Maps.	113

Figure A.17: PH09 is a northbound asphalt pavement section and PH10 is a southbound asphalt pavement section on Highway 113 in Sutter County on Google Maps.....	113
Figure A.18: PH09 location on Google Earth.....	114
Figure A.19: PH10 location on Google Earth.....	114
Figure A.20: On-site location photograph of PH09 (right lane) and PH10 (left lane) from Google Maps.....	115
Figure A.21: PH11 is a northbound and PH12 is a southbound pavement section on Highway 113 in Sutter County on Google Maps.....	115
Figure A.22: PH11 location on Google Earth.....	116
Figure A.23: PH12 location on Google Earth.....	116
Figure A.24: On-site location photograph of PH11 (right lane) and PH12 (left lane) from Google Maps.....	117
Figure A.25: PH13 is a northbound and PH14 is a southbound pavement section on Highway 113 in Sutter County on Google Maps.....	117
Figure A.26: PH13 location on Google Earth.....	118
Figure A.27: PH14 location on Google Earth.....	118
Figure A.28: On-site location photograph of PH13 (right lane) and PH14 (left lane) from Google Maps.....	118
Figure A.29: PH15 is an eastbound pavement section on CR32B (Chiles Road) on Google Maps.....	119
Figure A.30: PH15 location on Google Earth.....	119
Figure A.31: On-site location photograph of PH15 (right lane) from Google Maps.....	120
Figure A.32: PH16 is an eastbound semi-rigid pavement section and PH17 is a westbound semi-rigid pavement section on Highway 132 in Stanislaus County on Google Maps.....	120
Figure A.33: PH16 location on Google Earth.....	121
Figure A.34: PH17 location on Google Earth.....	121
Figure A.35: On-site location photograph of PH16 (right lane) and PH17 (left lane) from Google Maps.....	121
Figure A.36: PH19 is a northbound pavement section, and PH18 and PH20 are southbound pavement sections on I-5 in Kern County on Google Maps.....	122
Figure A.37: PH18 location on Google Earth.....	122
Figure A.38: PH19 location on Google Earth.....	123
Figure A.39: PH20 location on Google Earth.....	123
Figure A.40: PH19 On-site location photograph during coring pavement sample under Caltrans closure.....	124
Figure A.41: On-site location photograph of PH20 (right lane) during Caltrans closure.....	124
Figure A.42: PH21 is a northbound concrete pavement section and PH22 is a southbound concrete pavement section on Highway 99 in Sutter County on Google Maps.....	125
Figure A.43: PH21 location on Google Earth.....	126
Figure A.44: PH22 location on Google Earth.....	126
Figure A.45: PH21 On-site location photograph from Google Maps.....	127
Figure A.46: PH23 is a westbound concrete pavement section on CR32A in Yolo County on Google Maps.....	127
Figure A.47: PH23 location on Google Earth.....	128
Figure A.48: PH23 (right lane) on-site location photograph from Google Maps.....	128
Figure A.49: Roughness and macrotexture scale for the test sections factorial.....	129
Figure B.1: GPR data for section PH01.....	131
Figure B.2: GPR data for section PH02.....	132
Figure B.3: GPR data for section PH03.....	132
Figure B.4: GPR data for section PH04.....	133
Figure B.5: Pavement core and subgrade soil sample locations for PH04 from Google Maps.....	134
Figure B.6: Pavement core sample for PH04.....	134
Figure B.7: Pavement core and subgrade soil sample locations for PH08 from Google Maps.....	135
Figure B.8: Pavement core sample for PH08.....	136
Figure B.9: GPR data for sections PH09, PH11, and PH13.....	137
Figure B.10: Pavement core and subgrade soil sample locations for PH09 from Google Maps.....	137
Figure B.11: Pavement core sample for PH09.....	138
Figure B.12: Pavement core and subgrade soil sample locations for PH10 from Google Maps.....	139

Figure B.13: Pavement core sample for PH10.....	139
Figure B.14: Pavement core and subgrade soil sample locations for PH11 from Google Maps.....	141
Figure B.0.15: Pavement core sample for PH11.....	141
Figure B.16: Pavement core and subgrade soil sample locations for PH12 from Google Maps.....	142
Figure B.17: Pavement core sample for PH12.....	143
Figure B.18: Pavement core and subgrade soil sample locations for PH13 from Google Maps.....	144
Figure B.19: Pavement core sample for PH13.....	144
Figure B.20: Pavement core and subgrade soil sample locations for PH14 from Google Maps.....	145
Figure B.21: Pavement core sample for PH14.....	146
Figure B.22: Pavement core and subgrade soil sample locations for PH15 from Google Maps.....	147
Figure B.23: Pavement core sample for PH15.....	147
Figure B.24: GPR data for section PH16.....	148
Figure B.25: Pavement core and subgrade soil sample locations for PH16 from Google Maps.....	149
Figure B.26: Pavement core sample for PH16.....	149
Figure B.27: Pavement core and subgrade soil sample locations for PH17 from Google Maps.....	150
Figure B.28: Pavement core sample for PH17.....	151
Figure B.29: GPR data for section PH18.....	152
Figure B.30: Pavement core and subgrade soil sample locations for PH18 from Google Maps.....	152
Figure B.31: Pavement core sample for PH18.....	153
Figure B.32: GPR data for section PH19.....	154
Figure B.33: Pavement core and subgrade soil sample locations for PH19 from Google Maps.....	155
Figure B.34: Pavement core sample for PH19.....	155
Figure B.35: GPR data for section PH21.....	156
Figure B.36: GPR data for section PH22.....	157
Figure B.37: Pavement core sample location for PH23 from Google Maps.....	158
Figure B.38: Pavement core sample for PH23.....	158
Figure D.1: Temperature profile of section PH04.....	161
Figure D.2: Temperature profile of section PH08.....	161
Figure D.3: Temperature profile of section PH09.....	162
Figure D.4: Temperature profile of section PH10.....	162
Figure D.5: Temperature profile of sections PH11 and PH12.....	163
Figure D.6: Temperature profile of sections PH13 and PH14.....	163
Figure D.7: Temperature profile of section PH15.....	164
Figure D.8: Temperature profile of sections PH16 and PH17.....	164
Figure D.9: Temperature profile of section PH18.....	165
Figure E.1: Roughness, mean profile depth, and grade data plots for section PH01.....	167
Figure E.2: Roughness, mean profile depth, and grade data plots for section PH02.....	168
Figure E.3: Roughness, mean profile depth, and grade data plots for section PH03.....	169
Figure E.4: Roughness, mean profile depth, and grade data plots for section PH04.....	170
Figure E.5: Roughness, mean profile depth, and grade data plots for section PH07.....	171
Figure E.6: Roughness, mean profile depth, and grade data plots for section PH08.....	172
Figure E.7: Roughness, mean profile depth, and grade data plots for section PH09.....	173
Figure E.8: Roughness, mean profile depth, and grade data plots for section PH10.....	174
Figure E.9: Roughness, mean profile depth, and grade data plots for section PH11.....	175
Figure E.10: Roughness, mean profile depth, and grade data plots for section PH12.....	176
Figure E.11: Roughness, mean profile depth, and grade data plots for section PH13.....	177
Figure E.12: Roughness, mean profile depth, and grade data plots for section PH14.....	178
Figure E.13: Roughness, mean profile depth, and grade data plots for section PH15.....	179
Figure E.14: Roughness, mean profile depth, and grade data plots for section PH16.....	180
Figure E.15: Roughness, mean profile depth, and grade data plots for section PH17.....	181
Figure E.16: Roughness, mean profile depth, and grade data plots for section PH18.....	182

Figure E.17: Roughness, mean profile depth, and grade data plots for section PH19.	183
Figure E.18: Roughness, mean profile depth, and grade data plots for section PH20.	184
Figure E.19: Roughness, mean profile depth, and grade data plots for section PH21.	185
Figure E.20: Roughness, mean profile depth, and grade data plots for section PH22.	186
Figure E.21: Roughness, mean profile depth, and grade data plots for section PH23.	187
Figure F.1: Section PH01 grade plots for 165 ft. (50 m) subsections from three data sources.	191
Figure F.2: Section PH01 elevation plots for 90 ft. (27 m) subsections from four data sources.	191
Figure F.3: Section PH02 grade plots for 165 ft. (50 m) subsections from three data sources.	192
Figure F.4: Section PH02 elevation plots for 90 ft. (27 m) subsections from four data sources.	193
Figure F.5: Section PH03 grade plots for 165 ft. (50 m) subsections from three data sources.	194
Figure F.6: Section PH03 elevation plots for 90 ft. (27 m) subsections from four data sources.	194
Figure F.7: Section PH04 grade plots for 165 ft. (50 m) subsections from three data sources.	195
Figure F.8: Section PH04 elevation plots for 90 ft. (27 m) subsections from four data sources.	195
Figure F.9: Section PH07 elevation plots for 30 ft. (9 m) subsections.	196
Figure F.10: Section PH08 elevation plots for 30 ft. (9 m) subsections.	197
Figure F.11: Section PH09 grade plots for 165 ft. (50 m) subsections from three data sources.	198
Figure F.12: Section PH09 elevation plots for 90 ft. (27 m) subsections from four data sources.	199
Figure F.13: Section PH10 grade plots for 165 ft. (50 m) subsections from three data sources.	200
Figure F.14: Section PH10 elevation plots for 90 ft. (27 m) subsections from four data sources.	200
Figure F.15: Section PH11 grade plots for 165 ft. (50 m) subsections from three data sources.	201
Figure F.16: Section PH11 elevation plots for 90 ft. (27 m) subsections from four data sources.	201
Figure F.17: Section PH12 grade plots for 165 ft. (50 m) subsections from three data sources.	202
Figure F.18: Section PH12 elevation plots for 90 ft. (27 m) subsections from four data sources.	202
Figure F.19: Section PH13 grade plots for 165 ft. (50 m) subsections from three data sources.	203
Figure F.20: Section PH13 elevation plots for 90 ft. (27 m) subsections from four data sources.	204
Figure F.21: Section PH14 grade plots for 165 ft. (50 m) subsections from three data sources.	205
Figure F.22: Section PH14 elevation plots for 90 ft. (27 m) subsections from four data sources.	205
Figure F.23: Section PH15 elevation plots for 30 ft. (9 m) subsections.	206
Figure F.24: Section PH16 grade plots for 165 ft. (50 m) subsections from three data sources.	206
Figure F.25: Section PH16 elevation plots for 90 ft. (27 m) subsections from four data sources.	207
Figure F.26: Section PH17 grade plots for 165 ft. (50 m) subsections from three data sources.	208
Figure F.27: Section PH17 elevation plots for 90 ft. (27 m) subsections from four data sources.	208
Figure F.28: Section PH18 grade plots for 165 ft. (50 m) subsections from three data sources.	209
Figure F.29: Section PH18 elevation plots for 90 ft. (27 m) subsections from four data sources.	209
Figure F.30: Section PH19 grade plots for 165 ft. (50 m) subsections from three data sources.	210
Figure F.31: Section PH19 elevation plots for 90 ft. (27 m) subsections from four data sources.	211
Figure F.32: Section PH20 elevation plots for 90 ft. (27 m) subsections from four data sources.	212
Figure F.33: Section PH21 grade plots for 165 ft. (50 m) subsections from three data sources.	213
Figure F.34: Section PH21 elevation plots for 90 ft. (27 m) subsections from four data sources.	214
Figure F.35: Section PH22 grade plots for 165 ft. (50 m) subsections from three data sources.	215
Figure F.36: Section PH22 elevation plots for 90 ft. (27 m) subsections from four data sources.	215
Figure F.37: Section PH23 elevation plots for 30 ft. (9 m) subsections.	216
Figure G.1: Frequency sweep master curves for the reference temperature of 77°F (25°C) for PH04 layer 1. .	217
Figure G.2: Frequency sweep master curves for the reference temperature of 77°F (25°C) for PH04 layer 2. .	217
Figure G.3: Frequency sweep master curves for the reference temperature of 77°F (25°C) for PH08 layer 1. .	218
Figure G.4: Frequency sweep master curves for the reference temperature of 77°F (25°C) for PH09 layer 1. .	218
Figure G.5: Frequency sweep master curves for the reference temperature of 77°F (25°C) for PH09 layer 2. .	219
Figure G.6: Frequency sweep master curves for the reference temperature of 77°F (25°C) for PH09 layer 3. .	219
Figure G.7: Frequency sweep master curves for the reference temperature of 77°F (25°C) for PH10 layer 1. .	220
Figure G.8: Frequency sweep master curves for the reference temperature of 77°F (25°C) for PH10 layer 2. .	220
Figure G.9: Frequency sweep master curves for the reference temperature of 77°F (25°C) for PH10 layer 3. .	221

Figure G.10: Frequency sweep master curves for the reference temperature of 77°F (25°C) for PH11 layer 1.....	221
Figure G.11: Frequency sweep master curves for the reference temperature of 77°F (25°C) for PH11 layer 2.....	222
Figure G.12: Frequency sweep master curves for the reference temperature of 77°F (25°C) for PH12 layer 1.....	222
Figure G.13: Frequency sweep master curves for the reference temperature of 77°F (25°C) for PH12 layer 2.....	223
Figure G.14: Frequency sweep master curves for the reference temperature of 77°F (25°C) for PH12 layer 3.....	223
Figure G.15: Frequency sweep master curves for the reference temperature of 77°F (25°C) for PH12 layer 4.....	224
Figure G.16: Frequency sweep master curves for the reference temperature of 77°F (25°C) for PH13 layer 1.....	224
Figure G.17: Frequency sweep master curves for the reference temperature of 77°F (25°C) for PH14 layer 1.....	225
Figure G.18: Frequency sweep master curves for the reference temperature of 77°F (25°C) for PH15 layer 1.....	225
Figure G.19: Frequency sweep master curves for the reference temperature of 77°F (25°C) for PH15 layer 2.....	226
Figure G.20: Frequency sweep master curves for the reference temperature of 77°F (25°C) for PH16 layer 1.....	226
Figure G.21: Frequency sweep master curves for the reference temperature of 77°F (25°C) for PH16 layer 2.....	227
Figure G.22: Frequency sweep master curves for the reference temperature of 77°F (25°C) for PH16 layer 3.....	227
Figure G.23: Frequency sweep master curves for the reference temperature of 77°F (25°C) for PH17 layer 1.....	228
Figure G.24: Frequency sweep master curves for the reference temperature of 77°F (25°C) for PH18 layer 1.....	228
Figure G.25: Frequency sweep master curves for the reference temperature of 77°F (25°C) for PH18 layer 2.....	229
Figure G.26: Frequency sweep master curves for the reference temperature of 77°F (25°C) for PH19 layer 1.....	229
Figure I.1: Car tires hardness readings.....	233
Figure I.2: SUV tire hardness data.....	234
Figure I.3: F-450 tire hardness data.....	235
Figure I.4: HHDT tire hardness data.....	236
Figure J.1: Outside air temperature versus tire temperature during nighttime testing with F-450.....	238
Figure J.2: Outside air temperature versus tire temperature during daytime testing with F-450.....	238
Figure J.3: Vehicle fuel consumption versus tire pressure during nighttime testing with F-450.....	239
Figure J.4: Vehicle fuel consumption versus tire pressure during daytime testing with F-450.....	239
Figure J.5: Tire pressure versus the normalized time during nighttime testing with SUV.....	240
Figure J.6: Tire pressure versus the normalized time during daytime testing with SUV.....	240
Figure K.1: Calorific values in MJ/kg of gas and diesel samples collected in summer and winter testing cycles in 2016.....	244
Figure M.1: Average fuel consumption of F-450 truck at constant speed of 45 mph.....	251
Figure M.2: Slow and fast acceleration of the F-450 truck.....	252
Figure M.3: Relationship between RPM and car speeds in different gears.....	253
Figure M.4: Relationship between RPM and SUV speeds in different gears.....	253
Figure M.5: Relationship between RPM and F-450 speeds in different gears.....	254
Figure M.6: Relationship between RPM and HHDT speeds in different gears.....	254
Figure N.1: Typical structure modeled in Abaqus.....	255
Figure N.2: Solar data locations in Northern California in the Sacramento region.....	257
Figure N.3: Solar data location in Southern California in the Bakersfield region.....	258
Figure N.4: Prediction and calibration of pavement temperatures for CR29.....	259
Figure N.5: Air, pavement surface, and one-third depth temperatures on 01/27/2016 testing day.....	261
Figure N.6: Air, pavement surface, and one-third depth temperatures on 08/10/2016 testing day.....	261
Figure N.7: Air, pavement surface, and one-third depth temperatures on 08/02/2016 testing day.....	262
Figure N.8: Air, pavement surface, and one-third depth temperatures on 02/12/2016 testing day.....	262
Figure N.9: Air, pavement surface, and one-third depth temperatures on 07/14/2016 testing day.....	263
Figure N.10: Air, pavement surface, and one-third depth temperatures on 02/12/2016 testing day.....	263
Figure N.11: Air, pavement surface, and one-third depth temperatures on 07/14/2016 testing day.....	264
Figure N.12: Air, pavement surface, and one-third depth temperatures on 02/08/2016 testing day.....	264
Figure N.13: Air, pavement surface, and one-third depth temperatures on 08/04/2016 testing day.....	265
Figure N.14: Air, pavement surface, and one-third depth temperatures on 02/08/2016 testing day.....	265
Figure N.15: Air, pavement surface, and one-third depth temperatures on 08/04/2016 testing day.....	266
Figure N.16: Air, pavement surface, and one-third depth temperatures on 02/08/2016 testing day.....	266

Figure N.17: Air, pavement surface, and one-third depth temperatures on 08/04/2016 testing day.....	267
Figure N.18: Air, pavement surface, and one-third depth temperatures on 02/16/2016 testing day.....	267
Figure N.19: Air, pavement surface, and one-third depth temperatures on 07/27/2016 testing day.....	268
Figure N.20: Air, pavement surface, and one-third depth temperatures on 02/16/2016 testing day.....	268
Figure N.21: Air, pavement surface, and one-third depth temperatures on 07/27/2016 testing day.....	269
Figure N.22: Air, pavement surface, and one-third depth temperatures on 01/27/2016 testing day.....	269
Figure N.23: Air, pavement surface, and one-third depth temperatures on 08/10/2016 testing day.....	270
Figure N.24: Air, pavement surface, and one-third depth temperatures on 08/02/2016 testing day.....	270
Figure N.25: Air, pavement surface, and one-third depth temperatures on 02/05/2016 testing day.....	271
Figure N.26: Air, pavement surface, and one-third depth temperatures on 07/25/2016 testing day.....	271
Figure N.27: Air, pavement surface, and one-third depth temperatures on 02/05/2016 testing day.....	272
Figure N.28: Air, pavement surface, and one-third depth temperatures on 07/25/2016 testing day.....	272
Figure N.29: Air, pavement surface, and one-third depth temperatures on 02/05/2016 testing day.....	273
Figure N.30: Air, pavement surface, and one-third depth temperatures on 07/25/2016 testing day.....	273
Figure N.31: Air, pavement surface, and one-third depth temperatures on 02/05/2016 testing day.....	274
Figure N.32: Air, pavement surface, and one-third depth temperatures on 07/25/2016 testing day.....	274
Figure N.33: Air, pavement surface, and one-third depth temperatures on 02/05/2016 testing day.....	275
Figure N.34: Air, pavement surface, and one-third depth temperatures on 07/25/2016 testing day.....	275
Figure N.35: Air, pavement surface, and one-third depth temperatures on 02/05/2016 testing day.....	276
Figure N.36: Air, pavement surface, and one-third depth temperatures on 07/25/2016 testing day.....	276
Figure N.37: Air, pavement surface, and one-third depth temperatures on 01/26/2016 testing day.....	277
Figure N.38: Air, pavement surface, and one-third depth temperatures on 08/08/2016 testing day.....	277
Figure N.39: Air, pavement surface, and one-third depth temperatures on 07/26/2016 testing day.....	278
Figure N.40: Air, pavement surface, and one-third depth temperatures on 01/26/2016 testing day.....	278
Figure N.41: Air, pavement surface, and one-third depth temperatures on 08/08/2016 testing day.....	279
Figure N.42: Air, pavement surface, and one-third depth temperatures on 07/26/2016 testing day.....	279
Figure N.43: Air, pavement surface, and one-third depth temperatures on 02/02/2016 testing day.....	280
Figure N.44: Air, pavement surface, and one-third depth temperatures on 08/09/2016 testing day.....	280
Figure N.45: Air, pavement surface, and one-third depth temperatures on 07/15/2016 testing day.....	281
Figure N.46: Air, pavement surface, and one-third depth temperatures on 02/02/2016 testing day.....	281
Figure N.47: Air, pavement surface, and one-third depth temperatures on 08/09/2016 testing day.....	282
Figure N.48: Air, pavement surface, and one-third depth temperatures on 07/15/2016 testing day.....	282
Figure N.49: Air, pavement surface, and one-third depth temperatures on 02/11/2016 testing day.....	283
Figure N.50: Air, pavement surface, and one-third depth temperatures on 07/20/2016 testing day.....	283
Figure N.51: Air, pavement surface, and one-third depth temperatures on 07/22/2016 testing day.....	284
Figure N.52: Air, pavement surface, and one-third depth temperatures on 02/11/2016 testing day.....	284
Figure N.53: Air, pavement surface, and one-third depth temperatures on 07/20/2016 testing day.....	285
Figure N.54: Air, pavement surface, and one-third depth temperatures on 07/22/2016 testing day.....	285
Figure O.1: Fuel rate versus RPM for car for all speeds and sections.	292
Figure O.2: Fuel rate versus RPM for SUV for all speeds and sections.	293
Figure O.3: Fuel rate versus RPM for F-450 for all speeds and sections.....	294
Figure O.4: Fuel rate versus RPM for HHDT for all speeds and sections.	295
Figure O.5 Fuel consumption versus engine RPM for all four vehicles on all 23 sections.	296
Figure P.1: Car data on Section PH01.....	297
Figure P.2: Car data on Section PH01.....	298
Figure P.3: Car data on Section PH01.....	299
Figure P.4: Car data on Section PH01.....	300
Figure P.5: Car data on Section PH01.....	301
Figure P.6: Car data on Section PH01.....	302
Figure P.7: Car data on Section PH02.....	303
Figure P.8: Car data on Section PH02.....	304

Figure P.9: Car data on Section PH02.....	305
Figure P.10: Car data on Section PH02.....	306
Figure P.11: Car data on Section PH02.....	307
Figure P.12: Car data on Section PH02.....	308
Figure P.13: Car data on Section PH03.....	309
Figure P.14: Car data on Section PH03.....	310
Figure P.15: Car data on Section PH03.....	311
Figure P.16: Car data on Section PH03.....	312
Figure P.17: Car data on Section PH03.....	313
Figure P.18: Car data on Section PH04.....	314
Figure P.19: Car data on Section PH04.....	315
Figure P.20: Car data on Section PH04.....	316
Figure P.21: Car data on Section PH04.....	317
Figure P.22: Car data on Section PH04.....	318
Figure P.23: Car data on Section PH07.....	319
Figure P.24: Car data on Section PH07.....	320
Figure P.25: Car data on Section PH07.....	321
Figure P.26: Car data on Section PH07.....	322
Figure P.27: Car data on Section PH07.....	323
Figure P.28: Car data on Section PH07.....	324
Figure P.29: Car data on Section PH08.....	325
Figure P.30: Car data on Section PH08.....	326
Figure P.31: Car data on Section PH08.....	327
Figure P.32: Car data on Section PH08.....	328
Figure P.33: Car data on Section PH08.....	329
Figure P.34: Car data on Section PH08.....	330
Figure P.35: Car data on Section PH09.....	331
Figure P.36: Car data on Section PH09.....	332
Figure P.37: Car data on Section PH09.....	333
Figure P.38: Car data on Section PH09.....	334
Figure P.39: Car data on Section PH10.....	335
Figure P.40: Car data on Section PH10.....	336
Figure P.41: Car data on Section PH10.....	337
Figure P.42: Car data on Section PH10.....	338
Figure P.43: Car data on Section PH11.....	339
Figure P.44: Car data on Section PH11.....	340
Figure P.45: Car data on Section PH11.....	341
Figure P.46: Car data on Section PH11.....	342
Figure P.47: Car data on Section PH12.....	343
Figure P.48: Car data on Section PH12.....	344
Figure P.49: Car data on Section PH12.....	345
Figure P.50: Car data on Section PH12.....	346
Figure P.51: Car data on Section PH13.....	347
Figure P.52: Car data on Section PH13.....	348
Figure P.53: Car data on Section PH13.....	349
Figure P.54: Car data on Section PH13.....	350
Figure P.55: Car data on Section PH14.....	351
Figure P.56: Car data on Section PH14.....	352
Figure P.57: Car data on Section PH14.....	353
Figure P.58: Car data on Section PH14.....	354
Figure P.59: Car data on Section PH15.....	355

Figure P.60: Car data on Section PH15.....	356
Figure P.61: Car data on Section PH15.....	357
Figure P.62: Car data on Section PH15.....	358
Figure P.63: Car data on Section PH15.....	359
Figure P.64: Car data on Section PH15.....	360
Figure P.65: Car data on Section PH15.....	361
Figure P.66: Car data on Section PH16.....	362
Figure P.67: Car data on Section PH16.....	363
Figure P.68: Car data on Section PH16.....	364
Figure P.69: Car data on Section PH16.....	365
Figure P.70: Car data on Section PH17.....	366
Figure P.71: Car data on Section PH17.....	367
Figure P.72: Car data on Section PH17.....	368
Figure P.73: Car data on Section PH17.....	369
Figure P.74: Car data on Section PH18.....	370
Figure P.75: Car data on Section PH18.....	371
Figure P.76: Car data on Section PH19.....	372
Figure P.77: Car data on Section PH19.....	373
Figure P.78: Car data on Section PH20.....	374
Figure P.79: Car data on Section PH20.....	375
Figure P.80: Car data on Section PH21.....	376
Figure P.81: Car data on Section PH21.....	377
Figure P.82: Car data on Section PH21.....	378
Figure P.83: Car data on Section PH21.....	379
Figure P.84: Car data on Section PH22.....	380
Figure P.85: Car data on Section PH22.....	381
Figure P.86: Car data on Section PH22.....	382
Figure P.87: Car data on Section PH22.....	383
Figure P.88: Car data on Section PH23.....	384
Figure P.89: Car data on Section PH23.....	385
Figure P.90: Car data on Section PH23.....	386
Figure P.91: Car data on Section PH23.....	387
Figure P.92: Car data on Section PH23.....	388
Figure P.93: Car data on Section PH23.....	389
Figure P.94: SUV data on Section PH01.....	390
Figure P.95: SUV data on Section PH01.....	391
Figure P.96: SUV data on Section PH01.....	392
Figure P.97: SUV data on Section PH01.....	393
Figure P.98: SUV data on Section PH01.....	394
Figure P.99: SUV data on Section PH01.....	395
Figure P.100: SUV data on Section PH02.....	396
Figure P.101: SUV data on Section PH02.....	397
Figure P.102: SUV data on Section PH02.....	398
Figure P.103: SUV data on Section PH02.....	399
Figure P.104: SUV data on Section PH02.....	400
Figure P.105: SUV data on Section PH02.....	401
Figure P.106: SUV data on Section PH03.....	402
Figure P.107: SUV data on Section PH03.....	403
Figure P.108: SUV data on Section PH03.....	404
Figure P.109: SUV data on Section PH03.....	405
Figure P.110: SUV data on Section PH03.....	406

Figure P.111: SUV data on Section PH03.	407
Figure P.112: SUV data on Section PH04.	408
Figure P.113: SUV data on Section PH04.	409
Figure P.114: SUV data on Section PH04.	410
Figure P.115: SUV data on Section PH04.	411
Figure P.116: SUV data on Section PH04.	412
Figure P.117: SUV data on Section PH04.	413
Figure P.118: SUV data on Section PH07.	414
Figure P.119: SUV data on Section PH07.	415
Figure P.120: SUV data on Section PH07.	416
Figure P.121: SUV data on Section PH07.	417
Figure P.122: SUV data on Section PH07.	418
Figure P.123: SUV data on Section PH07.	419
Figure P.124: SUV data on Section PH08.	420
Figure P.125: SUV data on Section PH08.	421
Figure P.126: SUV data on Section PH08.	422
Figure P.127: SUV data on Section PH08.	423
Figure P.128: SUV data on Section PH08.	424
Figure P.129: SUV data on Section PH09.	425
Figure P.130: SUV data on Section PH09.	426
Figure P.131: SUV data on Section PH09.	427
Figure P.132: SUV data on Section PH10.	428
Figure P.133: SUV data on Section PH10.	429
Figure P.134: SUV data on Section PH10.	430
Figure P.135: SUV data on Section PH10.	431
Figure P.136: SUV data on Section PH11.	432
Figure P.137: SUV data on Section PH11.	433
Figure P.138: SUV data on Section PH11.	434
Figure P.139: SUV data on Section PH11.	435
Figure P.140: SUV data on Section PH12.	436
Figure P.141: SUV data on Section PH12.	437
Figure P.142: SUV data on Section PH12.	438
Figure P.143: SUV data on Section PH12.	439
Figure P.144: SUV data on Section PH13.	440
Figure P.145: SUV data on Section PH13.	441
Figure P.146: SUV data on Section PH13.	442
Figure P.147: SUV data on Section PH13.	443
Figure P.148: SUV data on Section PH14.	444
Figure P.149: SUV data on Section PH14.	445
Figure P.150: SUV data on Section PH14.	446
Figure P.151: SUV data on Section PH14.	447
Figure P.152: SUV data on Section PH15.	448
Figure P.153: SUV data on Section PH15.	449
Figure P.154: SUV data on Section PH15.	450
Figure P.155: SUV data on Section PH15.	451
Figure P.156: SUV data on Section PH15.	452
Figure P.157: SUV data on Section PH15.	453
Figure P.158: SUV data on Section PH16.	454
Figure P.159: SUV data on Section PH16.	455
Figure P.160: SUV data on Section PH16.	456
Figure P.161: SUV data on Section PH16.	457

Figure P.162: SUV data on Section PH17.	458
Figure P.163: SUV data on Section PH17.	459
Figure P.164: SUV data on Section PH17.	460
Figure P.165: SUV data on Section PH17.	461
Figure P.166: SUV data on Section PH18.	462
Figure P.167: SUV data on Section PH18.	463
Figure P.168: SUV data on Section PH19.	464
Figure P.169: SUV data on Section PH19.	465
Figure P.170: SUV data on Section PH20.	466
Figure P.171: SUV data on Section PH20.	467
Figure P.172: SUV data on Section PH21.	468
Figure P.173: SUV data on Section PH21.	469
Figure P.174: SUV data on Section PH21.	470
Figure P.175: SUV data on Section PH21.	471
Figure P.176: SUV data on Section PH22.	472
Figure P.177: SUV data on Section PH22.	473
Figure P.178: SUV data on Section PH22.	474
Figure P.179: SUV data on Section PH22.	475
Figure P.180: SUV data on Section PH23.	476
Figure P.181: SUV data on Section PH23.	477
Figure P.182: SUV data on Section PH23.	478
Figure P.183: SUV data on Section PH23.	479
Figure P.184: SUV data on Section PH23.	480
Figure P.185: SUV data on Section PH23.	481
Figure P.186: F-450 data on Section PH01.	482
Figure P.187: F-450 data on Section PH01.	483
Figure P.188: F-450 data on Section PH01.	484
Figure P.189: F-450 data on Section PH01.	485
Figure P.190: F-450 data on Section PH01.	486
Figure P.191: F-450 data on Section PH01.	487
Figure P.192: F-450 data on Section PH02.	488
Figure P.193: F-450 data on Section PH02.	489
Figure P.194: F-450 data on Section PH02.	490
Figure P.195: F-450 data on Section PH02.	491
Figure P.196: F-450 data on Section PH02.	492
Figure P.197: F-450 data on Section PH02.	493
Figure P.198: F-450 data on Section PH03.	494
Figure P.199: F-450 data on Section PH03.	495
Figure P.200: F-450 data on Section PH03.	496
Figure P.201: F-450 data on Section PH03.	497
Figure P.202: F-450 data on Section PH03.	498
Figure P.203: F-450 data on Section PH03.	499
Figure P.204: F-450 data on Section PH04.	500
Figure P.205: F-450 data on Section PH04.	501
Figure P.206: F-450 data on Section PH04.	502
Figure P.207: F-450 data on Section PH04.	503
Figure P.208: F-450 data on Section PH04.	504
Figure P.209: F-450 data on Section PH04.	505
Figure P.210: F-450 data on Section PH07.	506
Figure P.211: F-450 data on Section PH07.	507
Figure P.212: F-450 data on Section PH07.	508

Figure P.213: F-450 data on Section PH07.....	509
Figure P.214: F-450 data on Section PH07.....	510
Figure P.215: F-450 data on Section PH07.....	511
Figure P.216: F-450 data on Section PH08.....	512
Figure P.217: F-450 data on Section PH08.....	513
Figure P.218: F-450 data on Section PH08.....	514
Figure P.219: F-450 data on Section PH08.....	515
Figure P.220: F-450 data on Section PH08.....	516
Figure P.221: F-450 data on Section PH08.....	517
Figure P.222: F-450 data on Section PH09.....	518
Figure P.223: F-450 data on Section PH09.....	519
Figure P.224: F-450 data on Section PH09.....	520
Figure P.225: F-450 data on Section PH09.....	521
Figure P.226: F-450 data on Section PH10.....	522
Figure P.227: F-450 data on Section PH10.....	523
Figure P.228: F-450 data on Section PH10.....	524
Figure P.229: F-450 data on Section PH10.....	525
Figure P.230: F-450 data on Section PH11.....	526
Figure P.231: F-450 data on Section PH11.....	527
Figure P.232: F-450 data on Section PH11.....	528
Figure P.233: F-450 data on Section PH11.....	529
Figure P.234: F-450 data on Section PH12.....	530
Figure P.235: F-450 data on Section PH12.....	531
Figure P.236: F-450 data on Section PH12.....	532
Figure P.237: F-450 data on Section PH12.....	533
Figure P.238: F-450 data on Section PH13.....	534
Figure P.239: F-450 data on Section PH13.....	535
Figure P.240: F-450 data on Section PH13.....	536
Figure P.241: F-450 data on Section PH13.....	537
Figure P.242: F-450 data on Section PH14.....	538
Figure P.243: F-450 data on Section PH14.....	539
Figure P.244: F-450 data on Section PH14.....	540
Figure P.245: F-450 data on Section PH14.....	541
Figure P.246: F-450 data on Section PH15.....	542
Figure P.247: F-450 data on Section PH15.....	543
Figure P.248: F-450 data on Section PH15.....	544
Figure P.249: F-450 data on Section PH15.....	545
Figure P.250: F-450 data on Section PH15.....	546
Figure P.251: F-450 data on Section PH15.....	547
Figure P.252: F-450 data on Section PH16.....	548
Figure P.253: F-450 data on Section PH16.....	549
Figure P.254: F-450 data on Section PH16.....	550
Figure P.255: F-450 data on Section PH16.....	551
Figure P.256: F-450 data on Section PH17.....	552
Figure P.257: F-450 data on Section PH17.....	553
Figure P.258: F-450 data on Section PH17.....	554
Figure P.259: F-450 data on Section PH17.....	555
Figure P.260: F-450 data on Section PH18.....	556
Figure P.261: F-450 data on Section PH18.....	557
Figure P.262: F-450 data on Section PH19.....	558
Figure P.263: F-450 data on Section PH19.....	559

Figure P.264: F-450 data on Section PH20.....	560
Figure P.265: F-450 data on Section PH20.....	561
Figure P.266: F-450 data on Section PH21.....	562
Figure P.267: F-450 data on Section PH21.....	563
Figure P.268: F-450 data on Section PH21.....	564
Figure P.269: F-450 data on Section PH21.....	565
Figure P.270: F-450 data on Section PH22.....	566
Figure P.271: F-450 data on Section PH22.....	567
Figure P.272: F-450 data on Section PH22.....	568
Figure P.273: F-450 data on Section PH22.....	569
Figure P.274: F-450 data on Section PH23.....	570
Figure P.275: F-450 data on Section PH23.....	571
Figure P.276: F-450 data on Section PH23.....	572
Figure P.277: F-450 data on Section PH23.....	573
Figure P.278: F-450 data on Section PH23.....	574
Figure P.279: F-450 data on Section PH23.....	575
Figure P.280: HHDT data on Section PH01.....	576
Figure P.281: HHDT data on Section PH01.....	577
Figure P.282: HHDT data on Section PH01.....	578
Figure P.283: HHDT data on Section PH01.....	579
Figure P.284: HHDT data on Section PH01.....	580
Figure P.285: HHDT data on Section PH01.....	581
Figure P.286: HHDT data on Section PH02.....	582
Figure P.287: HHDT data on Section PH02.....	583
Figure P.288: HHDT data on Section PH02.....	584
Figure P.289: HHDT data on Section PH02.....	585
Figure P.290: HHDT data on Section PH02.....	586
Figure P.291: HHDT data on Section PH02.....	587
Figure P.292: HHDT data on Section PH03.....	588
Figure P.293: HHDT data on Section PH03.....	589
Figure P.294: HHDT data on Section PH03.....	590
Figure P.295: HHDT data on Section PH03.....	591
Figure P.296: HHDT data on Section PH03.....	592
Figure P.297: HHDT data on Section PH03.....	593
Figure P.298: HHDT data on Section PH04.....	594
Figure P.299: HHDT data on Section PH04.....	595
Figure P.300: HHDT data on Section PH04.....	596
Figure P.301: HHDT data on Section PH04.....	597
Figure P.302: HHDT data on Section PH04.....	598
Figure P.303: HHDT data on Section PH04.....	599
Figure P.304: HHDT data on Section PH07.....	600
Figure P.305: HHDT data on Section PH07.....	601
Figure P.306: HHDT data on Section PH07.....	602
Figure P.307: HHDT data on Section PH07.....	603
Figure P.308: HHDT data on Section PH07.....	604
Figure P.309: HHDT data on Section PH07.....	605
Figure P.310: HHDT data on Section PH08.....	606
Figure P.311: HHDT data on Section PH08.....	607
Figure P.312: HHDT data on Section PH08.....	608
Figure P.313: HHDT data on Section PH08.....	609
Figure P.314: HHDT data on Section PH08.....	610

Figure P.315: HHDT data on Section PH08.	611
Figure P.316: HHDT data on Section PH09.	612
Figure P.317: HHDT data on Section PH09.	613
Figure P.318: HHDT data on Section PH09.	614
Figure P.319: HHDT data on Section PH09.	615
Figure P.320: HHDT data on Section PH10.	616
Figure P.321: HHDT data on Section PH10.	617
Figure P.322: HHDT data on Section PH10.	618
Figure P.323: HHDT data on Section PH10.	619
Figure P.324: HHDT data on Section PH11.	620
Figure P.325: HHDT data on Section PH11.	621
Figure P.326: HHDT data on Section PH11.	622
Figure P.327: HHDT data on Section PH11.	623
Figure P.328: HHDT data on Section PH12.	624
Figure P.329: HHDT data on Section PH12.	625
Figure P.330: HHDT data on Section PH12.	626
Figure P.331: HHDT data on Section PH12.	627
Figure P.332: HHDT data on Section PH13.	628
Figure P.333: HHDT data on Section PH13.	629
Figure P.334: HHDT data on Section PH13.	630
Figure P.335: HHDT data on Section PH13.	631
Figure P.336: HHDT data on Section PH14.	632
Figure P.337: HHDT data on Section PH14.	633
Figure P.338: HHDT data on Section PH14.	634
Figure P.339: HHDT data on Section PH14.	635
Figure P.340: HHDT data on Section PH15.	636
Figure P.341: HHDT data on Section PH15.	637
Figure P.342: HHDT data on Section PH15.	638
Figure P.343: HHDT data on Section PH15.	639
Figure P.344: HHDT data on Section PH15.	640
Figure P.345: HHDT data on Section PH15.	641
Figure P.346: HHDT data on Section PH16.	642
Figure P.347: HHDT data on Section PH16.	643
Figure P.348: HHDT data on Section PH16.	644
Figure P.349: HHDT data on Section PH16.	645
Figure P.350: HHDT data on Section PH17.	646
Figure P.351: HHDT data on Section PH17.	647
Figure P.352: HHDT data on Section PH17.	648
Figure P.353: HHDT data on Section PH17.	649
Figure P.354: HHDT data on Section PH18.	650
Figure P.355: HHDT data on Section PH18.	651
Figure P.356: HHDT data on Section PH19.	652
Figure P.357: HHDT data on Section PH19.	653
Figure P.358: HHDT data on Section PH20.	654
Figure P.359: HHDT data on Section PH20.	655
Figure P.360: HHDT data on Section PH21.	656
Figure P.361: HHDT data on Section PH21.	657
Figure P.362: HHDT data on Section PH21.	658
Figure P.363: HHDT data on Section PH21.	659
Figure P.364: HHDT data on Section PH22.	660
Figure P.365: HHDT data on Section PH22.	661

Figure P.366: HHDT data on Section PH22.	662
Figure P.367: HHDT data on Section PH22.	663
Figure P.368: HHDT data on Section PH23.	664
Figure P.369: HHDT data on Section PH23.	665
Figure P.370: HHDT data on Section PH23.	666
Figure P.371: HHDT data on Section PH23.	667
Figure P.372: HHDT data on Section PH23.	668
Figure P.373: HHDT data on Section PH23.	669

LIST OF TABLES

Table 1.1: Descriptive Statistics for EFC Results for Site-Specific Traffic and Climate of Asphalt-Surfaced Test Sections	7
Table 2.1: Phase II Sections and Location Details	13
Table 2.2: Data Collected on All Field Sections	14
Table 2.3: Lift Type and Thickness (in ft.) of Core Samples Collected from Different Pavements	24
Table 2.4: Subgradient Soil Classification Results	26
Table 3.1: Section Directions in Global Coordinate System	34
Table 4.1: Cross Validation Prediction of HHDT Model With and Without Autoregressive Errors	64
Table 4.2: Scenario Regions and Associated Temperatures	84
Table 4.3: Scenarios for Each Vehicle	84
Table B.1: Layer Thicknesses Recorded from the Core Sample for PH04	135
Table B.2: Layer Thicknesses Recorded from the Core Sample for PH09	138
Table B.3: Layer Thicknesses Recorded from the Core Sample for PH10	140
Table B.4: Layer Thicknesses Recorded from the Core Sample for PH11	142
Table B.5: Layer Thicknesses Recorded from the Core Sample for PH12	143
Table B.6: Layer Thicknesses Recorded from the Core Sample for PH15	147
Table B.7: Layer Thicknesses Recorded from the Core Sample for PH16	150
Table B.8: Layer Thicknesses Recorded from the Core Sample for PH17	151
Table B.9: Layer Thicknesses Recorded from the Core Sample for PH18	153
Table B.10: Layer Thicknesses Recorded from the Core Sample for PH19	156
Table C.1: Laser Texture Scanning (LTS) Locations, Test Dates, and Results for All Pavements Considered in This Study	159
Table F.1: Recent Construction Dates and Information for the Sections	189
Table H.1: Vehicle and Fuel Types, Number of Axles and Wheels	231
Table H.2: Vehicle Loads and Tire Inflated Pressures	231
Table H.3: Axle Loads, Tire Contact Area, and Tire Loads	232
Table H.4: Axle and Tire Spacings in Centimeters	232
Table J.1: Average Time Taken to Reach Maximum Operating Pressure for the Vehicles Tested with TPMS	241
Table J.2: Average Time Taken to Reach the Section Locations	241
Table K.1: Percentage Ethanol Content per Gasoline Fuel Sample Collected During Winter and Summer Economy Fuel Testing	245
Table K.2: Density, Relative Density and American Petroleum Institute (API) Gravity of Gasoline and Diesel Fuel Samples	245
Table L.1: Total Air Pressure at Different Elevations	249
Table N.1: Parameter Values for Layer Properties Used in Temperature Prediction	256
Table N.2: Calibration Factor and Standard Error for Temperature Prediction Model	260
Table O.1 Number of Test Replicates per Vehicle per Section	287
Table O.2: Number of Observations per Gear per Vehicle	291
Table Q.1: Quantitative Summaries of Vehicle Empirical Models	671

DISCLAIMER

This document is disseminated in the interest of information exchange. The contents of this report reflect the views of the authors who are responsible for the facts and accuracy of the data presented herein. The contents do not necessarily reflect the official views or policies of the State of California or the Federal Highway Administration. This publication does not constitute a standard, specification or regulation. This report does not constitute an endorsement by the California Department of Transportation of any product described herein.

For individuals with sensory disabilities, this document is available in alternate formats. For information, call (916) 654-8899, TTY 711, or write to California Department of Transportation, Division of Research, Innovation and System Information, MS-83, P.O. Box 942873, Sacramento, CA 94273-0001.

ACKNOWLEDGMENTS

The University of California Pavement Research Center (UCPRC) acknowledges the following individuals and organizations who contributed to the project:

- Deepak Maskey, Joseph Holland, and Nick Burmas from California Department of Transportation
- Adam Chavez and Johnny Kalush of Chavez Trucking for arranging heavy heavy-duty truck participation
- Julian Brotschi, Jonny Hoang, Mayra Velasquez, and the UCPRC laboratory staff for helping with data collection, archiving, and several other major project tasks
- Irwin Guada and Angel Mateos of the UCPRC for helping with road-closure arrangements and shear testing of core samples
- Mark Hannum of the UCPRC for profile testing on all the test sections
- Mike Nicholas and the Institute of Transportation Studies University of California, Davis, for lending their onboard diagnostic devices
- Prof. Bryan Jenkins and graduate student Li Wang from the Department of Biological and Agricultural Engineering at University of California, Davis, for their help with bomb calorimeter testing
- David Spinner and Camille Fink of the UCPRC for the editing and publication of this report

We also want to thank the following people for their support of, continuous help with, and involvement in this project:

- Michigan State University: Prof. Karim Chatti, Prof. Imen Zaabar and Danilo Balzarini
- Oregon State University: Prof. Erdem Coleri and Mostafa Estaji
- University of Massachusetts Dartmouth: Prof. Arghavan Louhghalam

PROJECT OBJECTIVES

This study, Partnered Pavement Research Center Strategic Plan Element (PPRC SPE) 4.53, is a continuation of PPRC SPE 4.49 (Verification of Pavement Structure and Deflection Effects on Vehicle Fuel Economy and GHG Emissions). The Phase I research program SPE 4.49 involved reviewing different models for energy and additional vehicle fuel consumed by the structural response of pavements, collecting data for characterization of dynamic properties of pavement on a set of California test sections, predicting deflection and vehicle fuel use, and reviewing the results. The goal of the Phase II program, completed in SPE 4.53, was to measure fuel consumption on the same and/or new sets of pavements and to finalize the development of calibrated and validated models for vehicle energy consumption due to pavement deflection for use in pavement management and design. Both empirical modeling and mechanistic-empirical modeling were included in the scope of this project.

The goal of Phase II (SPE 4.53) was achieved by completing the following tasks:

1. Update the modeling results, including completion of the concrete modeling approaches by Oregon State University (OSU) and Michigan State University (MSU), complete the modeling of the Phase I field test sections, and model all the Phase II section factorials.
2. Update the factorial of test sections and characterizing the test sections through field measurements.
3. Measure and analyzing fuel economy on the Phase II test sections.
4. Develop empirical models of the effects of pavement on fuel economy.
5. Perform mechanistic-empirical analysis using the HDM-4 model of the effects of pavement on fuel economy.
6. Validate and calibrate the dissipated energy models from MSU, OSU, and MIT.
7. Compare the measurement and modeling results.
8. Perform forward modeling and simulations of the effects of pavement structural response on vehicle fuel economy for typical pavement structures, traffic, and climate conditions in California using the empirical and mechanistic models.
9. Prepare reports that document the study and its results.

This report documents the work of Tasks 2 through 4. Other tasks are documented in separate reports.

EXECUTIVE SUMMARY

Pavement characteristics can influence the fuel efficiency of vehicles and, therefore, related greenhouse gases and air pollution emissions through what is called pavement-vehicle interaction. Pavement-vehicle interaction mechanisms that increase vehicle fuel use are roughness, macrotexture, and structural response. Structural response is the energy consumed by the viscoelastic deflection of the pavement due to the application of a vehicle load. Asphalt-bound materials and subgrade soils are the typical pavement layers that consume this additional energy because they have a viscoelastic rather than elastic response when they deflect under a vehicle load. Compared to structural response, roughness and texture are well understood pavement characteristics.

The 2015 Federal Highway Administration (FHWA) report *Towards Sustainable Pavement Systems* summarized the state of field experimental measurement and model validation for the effects of pavement structural response on vehicle fuel use. There has not been any major field study since its publication, other than the study presented in this report. A summary from the FHWA report shows that several field experiments have been conducted. However, none of these experiments were comprehensive with respect to pavement and vehicle types, and they did not characterize the pavement structural responses under different temperature conditions and loading durations that control the viscoelastic response. A comprehensive field evaluation of the influence of structural response on vehicle fuel economy had not been completed prior to the study presented in this UCPRC report.

The purpose of this project is to develop, calibrate, and validate models for vehicle energy consumption due to pavement structural response for use in network-level pavement management systems and project-level design. The project is divided into two phases. In Phase I, three different pavement structural response energy dissipation models were used to estimate excess fuel consumption (EFC) for a range of California pavements and then calibrated with field data. EFC is defined as the additional fuel required to propel a vehicle on a pavement that is less than ideal for fuel consumption compared with the amount required on a pavement with no structural response, very low roughness, and sufficient macrotexture to provide good skid resistance.

The Phase I factorial of pavement field sections on the California state highway network included 20 asphalt- and concrete-surfaced pavements with different structure types that were characterized by their viscoelastic properties for the layers expected to dissipate energy through viscoelasticity. The layers characterized for viscoelastic properties were the asphalt layers for the asphalt-surfaced pavements and the subgrades for the concrete-surfaced pavements. Phase I of the study was completed in 2015, and it included development of an approach for simulation of the annual EFC from structural response for a factorial of the vehicles, traffic flows, speed distributions, and climate regions typical of California. The simulation approach was applied to a factorial of typical California

situations using the energy consumption models from Oregon State University (OSU), Michigan State University (MSU), and the Massachusetts Institute of Technology (MIT). The conclusion of the simulations was that excess fuel consumption due to structural response has a small but important effect on the overall EFC of vehicles and that it is highly dependent on the pavement structure. Results from all the models indicated that the effects of structural response are especially important for the overall EFC of heavy vehicles, such as trucks and buses.

Based on the results in the Phase I report, which indicated that structural response was large enough to be included in consideration of the effects of pavement on excess fuel consumption, a Phase II work plan was prepared.

The goal of the Phase II program was to measure fuel consumption on the same and/or new sets of pavements and to finalize the development of calibrated and validated models for vehicle energy consumption due to pavement deflection for use in pavement management and design. Both empirical modeling and mechanistic-empirical (ME) modeling were included in the scope of this project. The mechanistic-empirical modeling of the Phase II test sections is reported separately.

The goal of Phase II was achieved by updating the OSU, MSU, and MIT mechanistic modeling results and ME modeling using the HDM-4 model, measuring and analyzing fuel economy on the Phase II test sections, and comparing the modeling and empirical results. The final tasks of Phase II are simulating typical pavement structures, traffic, and climate conditions in California using the empirical and/or mechanistic models and preparing reports.

To meet the goal of Phase II, an experiment was designed to include the different types of pavements and vehicles, different traffic speeds, and different pavement temperatures that exist in California. The pavement type factorial included California's most common pavement types. The road sections for the fuel economy testing were selected based on the following criteria:

- The *slope/gradient of the pavement* is a major contributor to vehicle fuel consumption. An uphill slope increases fuel consumption and a downhill slope decreases it. To minimize the effects of EFC due to pavement surface gradient, sections with a slope of less than 0.5% were sought.
- The fuel consumption of vehicles moving on *horizontal curves* is affected by curvature forces. Therefore, straight test sections were selected.
- The *length of the road section* had to be long enough for vehicles to reach a steady speed so they could collect enough vehicle fuel consumption data.

- *Safety* requires that pavement section characterization using destructive and nondestructive procedures be performed in closures with moving traffic and that test vehicles can operate safely at relatively low speeds. Therefore, only sections that allowed these conditions to be met were included in the factorial.
- Because the fuel use testing needed to be performed at different times of the year to capture different temperature conditions, it was important to only include test sections for which *no pavement maintenance was scheduled*; otherwise, the study goal would be negated. Information was gathered from Caltrans and counties for candidate sections to ensure that no major pavement maintenance was scheduled between the winter and summer of 2016.
- *Road roughness* has an important effect on vehicle fuel consumption. Except for a few high roughness sections to be used for comparison, most of the sections selected had low roughness to minimize the effects of roughness on fuel use and to help isolate the structural response effect.

Once these revised criteria were determined for Phase II, the Phase I sections were reviewed to determine which ones met them and which did not. The Phase I sections that did not meet the revised criteria were replaced by new sections that did meet the criteria. The resulting 21 test sections across Northern and Central California were selected based on this road section selection protocol. Most of the sections are on the state highway network, with the rest consisting of county roads. The selected pavement structures included:

- Sections with a portland cement concrete (PCC) surface
 - Six jointed plain concrete pavements (JPCPs) (without dowels)
 - One continuously reinforced concrete (CRC) pavement
- Sections with a hot mix asphalt (HMA) surface
 - Eight flexible pavements (asphalt layers on unbound bases) with and without rubberized surfaces and open-graded surfaces and a range of thicknesses and stiffnesses
 - Three semi-rigid pavements (asphalt layers over cement-treated base)
 - Three composite pavements (asphalt overlays on cracked and sealed JPCPs without dowels)

The pavement sections structures were characterized according to their structure (material types, thicknesses, and stiffnesses), surface roughness, and texture. Information on the selected sections was gathered from Caltrans automated pavement condition surveys (APCS) and ground-penetrating radar (GPR) databases. Field tests—consisting of deflection testing with the falling weight deflectometer at several temperatures, International Roughness Index (IRI), laser texture scanning, and subsurface temperature measurements (asphalt sections only)—were performed on each section. Pavement section cores were also collected and used for thickness verification and testing of the asphalt materials for dynamic shear modulus using a frequency and temperature

sweep approach in the laboratory. Subgrade samples were laboratory tested for their soil classification. GPR data were not available for the county road sections.

The following five vehicles were selected for the fuel economy testing:

- A five-axle semi-trailer truck, called a heavy heavy-duty truck (HHDT), 2013 Peterbilt 388, with two single-axle trailers
- A single-rear-axle dual-tire diesel truck, 2011 Ford 450 (F-450)
- A sport utility vehicle (SUV), 2014 Ford Explorer
- A gasoline-powered car, 2015 Chevrolet Impala
- A diesel-powered car, 2015 Chevrolet Cruze

Newer vehicle models were selected for the test. To avoid variability in driving behavior, one driver was assigned to each vehicle for the entire test, except for the SUV, which had different drivers during the summer and winter test cycles. Since the weights of the SUV drivers varied, sandbags were placed in the vehicle when the lighter driver was behind the wheel to maintain the total weight.

The HHDT was loaded with crushed aggregate, and this load was maintained during the summer and winter testing so that the load on the axles remained the same. The F-450 truck was loaded with bricks, which were secured on a wooden pallet and wrapped with plastic sheets so their moisture content did not change. Its axle loads were checked at a weigh station, and its pallet was positioned to make sure that the axle loads during each test cycle were consistent.

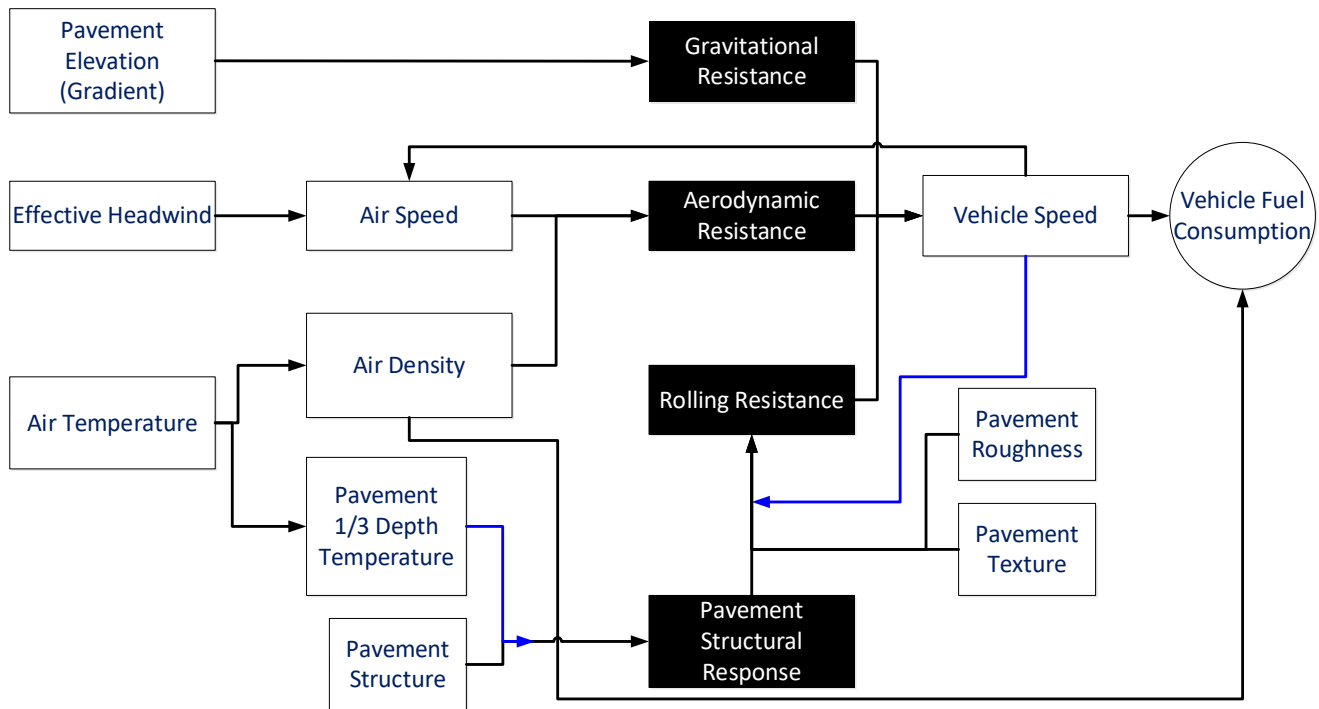
Onboard diagnostic (OBD) devices were used to measure fuel consumption data of the vehicles for this study. Solar-powered wireless weather stations with a connected data logger were used to collect data on wind speed, wind direction, air and pavement temperatures, and dew point during the fuel economy testing. During the nighttime testing, the weather stations used a battery that had been charged in the daytime by solar energy. A testing protocol was written and followed for the fuel economy testing. The planned data collection schedule called for testing in the cold (January to March) and hot (July to August) seasons of 2016 (trials were also conducted before the actual plan was followed.) Vehicles were serviced and their axle loads were measured before the start of each testing cycle. Before the first testing season, a tire pressure and temperature study was completed to determine the time needed for the vehicle tires to reach stable temperatures and tire pressures, as tire pressure changes affect vehicle fuel consumption.

The maximum number of replicate passes that could be made on each section depended on the testing time period available, which was often determined by changes in wind speed and temperatures as well as the length of the section (i.e., it took less time to drive on shorter sections, and therefore more replicates were recorded). Although a minimum of 6 good replicates were recommended, the target was 8 to 12 good replicate runs at each speed on each section in each season.

Data collected and stored in relational databases included the weather station data, profile data, gradient data, and fuel consumption (OBD) data. After organizing and sorting the raw data files, the study team filtered and processed the data that were relevant to the study. The raw data were checked for completeness after each testing day. Although most of the datasets were found to be complete for the analysis, a few had failures. This required going back into the field to generate new explanatory data that could be correlated to the data collected during the fuel economy testing. Vehicle speed, gear, and fuel consumption relationships per vehicle, corrupted or unrecorded climate data, and incomplete pavement surface temperature data were some datasets that were affected and are discussed in detail in the report.

Datasets from all of the instruments were aligned using time stamps and location identification fields. The data from each test section were divided into subsections with the goal of finding the shortest subsection length that had the lowest variance of roughness and gradient within it and that still had sufficient data points to provide a reliable mean. After considering subsection lengths from 30 to 480 ft. (9 to 146 m), it was determined that 90 ft. (27 m) was the longest subsection length that could be used. Additional data quality checks were performed after subsectioning.

The initial step in modeling was to develop a broad conceptual model of the primary variables believed to influence fuel consumed of a vehicle driven on cruise control. The following figure presents a directed acyclic graph of the key variables and causal links. The goal of this framework was to examine if the effects of pavement on fuel efficiency could be observed in the field based on experimental design and to explore the relative magnitude of those effects. Detailed theories of pavement structural responses that are covered in other modeling frameworks were not considered in this approach.



Note: Black arrows indicate a causal effect direction, white boxes indicate measured predictor variables, black boxes indicate unmeasured constructs, white circle represents the outcome, and blue arrows indicate moderating effects (interactions).

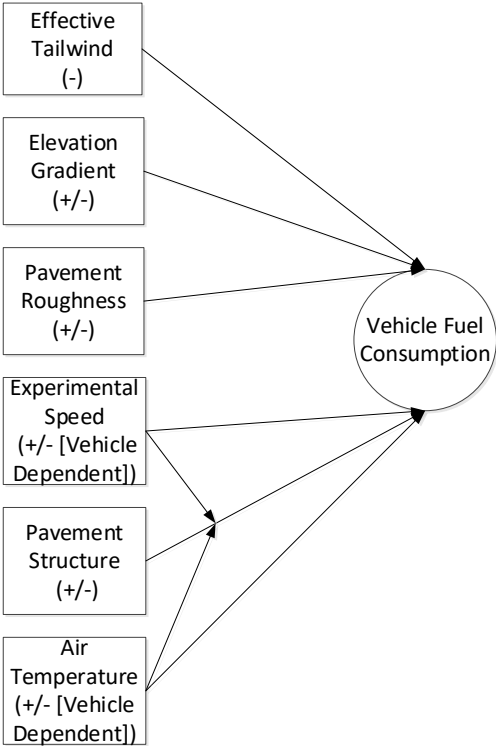
Directed acyclic graph representing the conceptual model of vehicle fuel consumption.

Translating the conceptual model shown in the figure to statistical models proved challenging. As the conceptual model indicates, clear feedback loops in the model cannot be handled in most statistical modeling frameworks, such as linear regression. While some more complex modeling frameworks (e.g., structural equation models) allow such feedbacks, the other complexities of the data (e.g., serial autocorrelation, large number of records, and multilevel structure) forced the need for a parsimonious statistical framework.

Fuel consumed is modeled through linear regression because it is a continuous variable. While fuel consumed cannot be negative, the model is not constrained to positive reals because in some cases zero fuel was recorded in a subsection; this could be due to cruise control adjustment by the vehicle when traveling downhill. Because all the complexities presented in the figure could not be included in a linear regression, the conceptual model was simplified to model fuel consumption using linear regression by removing the feedbacks; the most important simplification made was the removal of the vehicle's real-time speed. Real-time speed is managed/adjusted by the vehicle controller once cruise control is set, and it acts as a mediating variable for all the upstream effects on fuel consumption (e.g., gradient, pavement structure, and others as shown in the figure). By removing real-time speed, the conceptual model can be revised with direct causal links from the explanatory variables to the response variable (fuel consumed).

Several other casual links in the model were also simplified, such as not including separate variables for air and pavement temperatures in the statistical models because of extreme collinearity between those two explanatory variables. This collinearity is due to pavement temperature mediating the effect of air temperature on the structural response. Instead, the model used only air temperature, which was interpreted as having an effect on fuel consumption through two pathways. The first is air density changes that alter aerodynamic resistance, and slight changes to combustion efficiency, if any. The second pathway arises from pavement temperature changes that result in varying losses in vehicle energy attributable to changes in rolling resistance from changes in the pavement’s structural response.

Vehicle speed was kept as a categorical variable (e.g., the speed that cruise control was set at in the experimental run) so that the potential interactions of temperature, speed, and pavement type could be compared. Finally, pavement macrotexture (mean profile depth [MPD]) was also removed from the models after testing revealed that it had little to no effect on fuel consumption. The resulting final simplified model is presented in the following figure.



Note: White boxes indicate measured predictor variables, and white circle represents the outcome. Arrows leading to other arrows indicate moderating effects (interactions).

Simplified directed acyclic graph representing the conceptual model used for linear regression.

The data in this experiment has strong temporal (serial) autocorrelation. Using autocorrelation function plots of linear model residuals, models that were created without accounting for temporal order of the data revealed considerable autocorrelation for nearly every experimental run (99% of the runs). This autocorrelation arises from the fact that the vehicle controller is constantly adjusting fuel consumption as the vehicle experiences forces from aerodynamic resistance, gravity, and rolling resistance. Strong autocorrelation has the potential to bias the estimation of the parameters relating the predictor variables to fuel consumption and has the potential to greatly reduce the predictive ability of the model if not properly removed or modeled.

Several methods were used to examine the autocorrelation and account for it in the models. Analysis of the results with the different methods suggests that the models without the autocorrelation term are likely producing slightly biased estimates for gradient and pavement roughness. More importantly, however, it shows that the model without the autocorrelation term is not adequately representing the uncertainty and variability of all of the estimates of pavement type.

To analyze the full data, the study employed multilevel linear regression models. They were used to analyze each experimental run for the autocorrelation parameters, and by pavement structure to analyze for the main effects. The models were framed by experimental runs and by pavement structure because the experimental design created grouped data (i.e., data repeatedly collected on each pavement structure one run at a time in different conditions). More specifically, the models have varying intercepts (mean effects) for each pavement type (section) and varying slopes by those pavement types for experimental speeds and air temperatures and for their interactions. The models' errors are assumed to be autocorrelated with a lag of one subsection, within each experimental run.

Because of the numerous complexities in the linear regression, a flexible and robust Bayesian modeling framework was used. The models were estimated using the R package BRMS (Bayesian Regression Models using “Stan”) as an interface for the Stan statistical environment. By using this estimation procedure, the full uncertainty in the primary effects of concern (e.g., pavement structures) on the fuel economy is considered. A separate model for each of the four vehicles was estimated because of the differences in fuel type (diesel versus gasoline) and, thus, energy density; this implies that the fuels consumed by the cars and trucks are not comparable. The data for the two vehicles with the same fuel type were not pooled because in that case interactions would have been needed for all the variables by vehicle leading to three-way interactions with varying slopes, and these interactions were computationally too costly.

Given the large amount of data and separate models for each vehicle, the model runtimes were already burdensome for testing (ranging from 2 to 9 days). Furthermore, the intent was to have a separate model for each vehicle class

type so that when these vehicle fuel consumption empirical models are used in the models, such as a life cycle assessment use stage model, better fuel consumption predictions could be made based on vehicle class types. No advantage was seen for having one model with four distinct vehicle types in it because vehicle type is not a continuum (there are distinct types) and because the vehicles used in the experiment are reasonably representative of the typical classifications of vehicles in the fleet.

In a sample of experimental runs on each road, the 95% prediction interval nearly always includes the observed fuel consumed. In general, the predictions for each vehicle type are consistently accurate across vehicles and roads. The models rely heavily on the autoregressive error term to accurately predict fuel consumption, which is further confirmed by the cross validation presented in the methods section.

Characteristics such as air temperature, effective tailwind, cruise control speed, and elevation gradient have measurable effects on the vehicle's fuel consumption. However, because the effect of pavement on vehicle fuel consumption is the focus of this study, these variables are considered control variables. Of the five control characteristics, cruise control speed has the strongest effect on fuel consumption, but its effect varies by vehicle. Elevation gradient has the next strongest effect of the control characteristics considered on the vehicle's fuel consumption. Elevation gradient has a positive relationship with fuel consumption for all the vehicle types. A 1% increase in elevation gradient has a predicted 5% to 10% increase in fuel consumption across all the vehicles. The effect of gradient is stronger on the car and SUV than on the F-450 and HHDT.

The effect of air temperature on fuel consumption varies across the vehicles. In theory, air temperature has two competing effects on fuel consumption. Because air temperature influences air density, it also influences fuel combustion and aerodynamic drag. In this experiment, air temperature increases resulted in less fuel consumption, indicating that the increased temperatures caused combustion to be more efficient, and less drag. However, a competing effect also resulted because higher air temperatures also influence the structural response of some pavements (e.g., those surfaced with viscoelastic asphalt materials). The model predictions aligned with the theory of air temperature being negatively associated with fuel consumption for all the vehicles, though the effects for the HHDT were negligible compared to those for other vehicles. In general, an increase in 20°F (11°C) has a predicted 0% to 6% reduction in fuel consumption across all the vehicles.

An examination of the interaction between air temperature and cruise control speed showed varied effects on fuel use. The only clear interaction between air temperature and cruise control speed was seen in the HHDT: air temperature had a positive effect on fuel consumption when cruising at 35 mph (56 km/hr), no effect when cruising at 45 mph (72 km/hr), and a strong negative effect when cruising at 55 mph (88 km/hr). For the HHDT,

these interactions may be due to differences in combustion efficiency and drag at the different cruising speeds, but at slow speeds they may also be partially due to the effects of pavement (i.e., warmer air causing asphalt-surfaced pavements to soften and absorb more energy from the heavy HHDT). However, a further analysis that focused on the specific pavements suspected of causing this effect (presented in Section 4.2.3) indicates this may not be the case.

Effective tailwind has a consistently positive effect on fuel consumption across all the vehicles, but the magnitude of the effect is negligible from the model results. This is likely because the experiment was designed to limit the effect of wind by testing only when the wind speed was less than 5 mph (8 km/hr), and most of the tests involving wind conditions resulted in effective tailwinds between -2 and 2 mph (-3.2 and 3.2 km/hr).

In general, the models show that pavement roughness and texture had little effect on fuel consumption across all the vehicles. This is partially because the experiment was designed to limit the effect of these pavement variables. But even on the few subsections that were rough (> 168 in./mi. [2.68 m/km] IRI) or had high-texture (> 1.20 mm MPD), the fuel consumption predicted was similar to that of the smooth and low-texture subsections.

To examine the effects of pavement type on fuel consumption, a factorial sensitivity analysis was completed with the final model with three scenarios for three primary variables (tailwind, temperature, and vehicle speed) to provide a clearer understanding about how pavement types influence fuel consumption. The three scenarios for each variable were selected to produce an inefficient condition, a median condition, and an efficient condition. The temperatures for the three scenarios (inefficient condition, median condition, and efficient condition) vary for each of the four different California regions considered. Permutations of factor levels across three variables were not run; rather the scenarios considered the inefficient condition, median condition, and efficient condition for all three variables at the same time. The scenarios include no elevation gradient, low roughness, and low texture. This resulted in a total of 16 simulations (four regions by four cars) for each of the three scenarios.

The results of the scenario analysis suggest that the effects of pavement type on fuel consumption are too small to be estimated. Further, the variation in fuel consumption on each unique road given in the three scenarios is much larger than the variation in fuel consumption between roads for a given scenario. This indicates that the “control” variables have a much larger effect on fuel consumption than pavements.

The primary conclusion drawn from the results of the study is that the magnitude of a pavement structure type’s influence on fuel consumption from the measurement campaign of this study is too small for meaningful conclusions about the effect of pavement type for broad classes of pavements (e.g., concrete and asphalt) to be

drawn, based on the size of the dataset used in this project and the effort required to control the variables in the experimental design. The within-section variability is almost always greater than the variability between sections for a given pavement type and efficiency condition (tailwind, speed, and climate region), and the within-section variability is also usually larger than the variability between pavement types. Only the data for the heavy heavy-duty truck (HHDT) showed any meaningful difference in results between sections, but that variability is not tied to pavement type and is only present in conditions that are extremely inefficient for fuel consumption. These results indicate that missing variables (or errors in this study's existing variables) need to be reduced in any future experiments to observe the measurable effects of pavements on fuel consumption in real-world driving.

While air temperature interacting with cruise control speed had an effect on fuel consumption for the HHDT, there is a lack of clear evidence from this study that asphalt roads cause more fuel consumption for the HHDT in inefficient conditions. This suggests that pavement type is not the correct explanation for that variation. Instead, the variation in effect of air temperature by cruise control speed for the HHDT likely has to do with differences in engine efficiency under different conditions.

The modeling results, documented in other reports that are part of this study, show very small changes in additional fuel consumption from structural response under most conditions, which is commensurate with the difficulty in measuring these changes in the field. Modeling shows that the most significant effects occur under conditions (hot pavement and slow-moving heavy vehicles) that are very difficult to measure for long enough sections on the state highway and local road networks to produce safe vehicle operations. It is therefore recommended that the inability of this study to find a consistent measurable effect of structural response on fuel use not be used as a reason to exclude structural response from consideration in life cycle assessment.

LIST OF ABBREVIATIONS

AB	Aggregate base
ACF	Autocorrelation function
APCS	Automated pavement condition surveys
CAN	Control area network
CRCP	Continuously reinforced concrete pavement
EFC	Excess fuel consumption
FHWA	Federal Highway Administration
FWD	Falling weight deflectometer
GHG	Greenhouse gas
GLONASS	Global Navigation Satellite System
GPR	Ground-penetrating radar
GPS	Global positioning system
HHDT	Heavy heavy-duty truck
HMA	Hot mix asphalt
IRI	International Roughness Index
JPCP	Jointed plain concrete pavement
LCA	Life cycle assessment
LTS	Laser texture scanning
MAE	Mean absolute error
MPD	Mean profile depth
MTD	Mean texture depth
OBD	Onboard diagnostic (device)
PCC	Portland cement concrete
PMS	Pavement management system
PPRC	Partnered Pavement Research Center
PVI	Pavement-vehicle interaction
REV	Representative elementary volume
RMSE	Root mean square error
RPM	Revolutions per minute
SR	Semi-rigid
SUV	Sport utility vehicle
UV	Ultraviolet

SI* (MODERN METRIC) CONVERSION FACTORS

APPROXIMATE CONVERSIONS TO SI UNITS				
Symbol	When You Know	Multiply By	To Find	Symbol
LENGTH				
in.	inches	25.40	millimeters	mm
ft.	feet	0.3048	meters	m
yd.	yards	0.9144	meters	m
mi.	miles	1.609	kilometers	km
AREA				
in ²	square inches	645.2	square millimeters	mm ²
ft ²	square feet	0.09290	square meters	m ²
yd ²	square yards	0.8361	square meters	m ²
ac.	acres	0.4047	hectares	ha
mi ²	square miles	2.590	square kilometers	km ²
VOLUME				
fl. oz.	fluid ounces	29.57	milliliters	mL
gal.	gallons	3.785	liters	L
ft ³	cubic feet	0.02832	cubic meters	m ³
yd ³	cubic yards	0.7646	cubic meters	m ³
MASS				
oz.	ounces	28.35	grams	g
lb.	pounds	0.4536	kilograms	kg
T	short tons (2000 pounds)	0.9072	metric tons	t
TEMPERATURE (exact degrees)				
°F	Fahrenheit	(F-32)/1.8	Celsius	°C
FORCE and PRESSURE or STRESS				
lbf	pound-force	4.448	newtons	N
lbf/in ²	pound-force per square inch	6.895	kilopascals	kPa
APPROXIMATE CONVERSIONS FROM SI UNITS				
Symbol	When You Know	Multiply By	To Find	Symbol
LENGTH				
mm	millimeters	0.03937	inches	in.
m	meters	3.281	feet	ft.
m	meters	1.094	yards	yd.
km	kilometers	0.6214	miles	mi.
AREA				
mm ²	square millimeters	0.001550	square inches	in ²
m ²	square meters	10.76	square feet	ft ²
m ²	square meters	1.196	square yards	yd ²
ha	hectares	2.471	acres	ac.
km ²	square kilometers	0.3861	square miles	mi ²
VOLUME				
mL	milliliters	0.03381	fluid ounces	fl. oz.
L	liters	0.2642	gallons	gal.
m ³	cubic meters	35.31	cubic feet	ft ³
m ³	cubic meters	1.308	cubic yards	yd ³
MASS				
g	grams	0.03527	ounces	oz.
kg	kilograms	2.205	pounds	lb.
t	metric tons	1.102	short tons (2000 pounds)	T
TEMPERATURE (exact degrees)				
°C	Celsius	1.8C + 32	Fahrenheit	°F
FORCE and PRESSURE or STRESS				
N	newtons	0.2248	pound-force	lbf
kPa	kilopascals	0.1450	pound-force per square inch	lbf/in ²

*SI is the abbreviation for the International System of Units. Appropriate rounding should be made to comply with Section 4 of ASTM E380. (Revised April 2021)

1 INTRODUCTION

The pavements that cars and trucks use influence the fuel mileage of these vehicles. While the impact of pavements on a single vehicle’s fuel mileage is small relative to the impacts attributable to a number of other factors—such as the effects of air resistance at highway speeds, underinflated tires, vertical gradients, and inefficient driving behaviors—their effect is of interest because it impacts every vehicle on the road, which can make its cumulative result large. Generally, the effect of non-ideal in-service pavement is less than an approximate 3% increase in fuel use compared to an “ideal” pavement.

Pavement characteristics such as roughness, texture, and structural response can influence the fuel efficiency of vehicles and, therefore, related greenhouse gases (GHG) and air pollution emissions through what is called pavement-vehicle interaction (PVI). Harvey et al. detailed the abovementioned pavement characteristics (1). Briefly, *roughness* can be defined as the irregularities on the surface with wavelengths of 1.6 to 164 ft. (0.5 to 50 m). It affects the responses of the tire sidewalls and shock absorbers and is typically influenced most by paving practice and the presence of distresses (cracking, rutting, faulting) on the surface. *Texture* is the finish of a pavement surface with wavelengths of 0.02 to 2 in. (0.5 to 50 mm). It primarily interacts with the footprint of the tire and is typically influenced most by aggregate size and gradation for asphalt surfaces and the surface finish type (tining, grinding, grooving) on concrete surfaces. *Structural response* is the energy consumed by the viscoelastic deflection of the pavement due to the application of a vehicle load. Asphalt-bound materials and subgrade soils are the typical pavement layers that consume this additional energy because they are viscoelastic rather than elastic. This can be modeled either as the viscoelastic energy dissipation in the pavement as a vehicle wheel passes or as the equal energy dissipation of the delayed response of the pavement to the vehicle load causing the vehicle to move “uphill” on the deflection bowl (2–12). In this report, the terms *structural response* and *deflection* are used interchangeably.

Compared to structural response, roughness and texture are well understood pavement characteristics. Models for their effects on fuel use have been calibrated with field experiments through the NCHRP 1-45 project (13).

The 2015 Federal Highway Administration (FHWA) report *Towards Sustainable Pavement Systems* (14) summarized the state of field experimental measurement and model validation for the effects of pavement structural response on vehicle fuel use. There has not been any major field study since its publication, other than the study presented in this report. The following is a summary of the work done up to 2014 and included in the FHWA report:

A number of field studies have been performed to measure the effects of pavement type on vehicle fuel economy, including those by Zaniewski et al. (15), Taylor and Patten (16), Ardekani and Sumitsawan (17), Bienvenu and Jiao (18), and Hultqvist (19). For automobile traffic, the study by Zaniewski et al. (15) showed no measurable difference in fuel economy between asphalt and concrete pavement. The study by Taylor and Patten (16) had limited results for an automobile driven over 11 test sections that included concrete, asphalt, and composite (asphalt surface over concrete) paved roads in Ontario and Quebec; two seasons (winter and summer) and two travel speeds (37 and 62 mph [60 and 100 km/hr]) were included. All of the pavement sections had International Roughness Index (IRI) values less than 126 inches/mile (2 m/km) and the IRI was considered directly in the results, but the study did not control for or measure pavement surface texture. Of the statistically significant results, the study showed a small increase in fuel use for asphalt pavement compared to concrete pavement for one season, and a small increase in fuel use for concrete pavement compared to composite for one season (the opposite was observed for the other season). The pavements considered by Ardekani and Sumitsawan (17) consisted of four rough to extremely rough urban streets (IRI values of 170 to 325 inches/mile [2.7 to 5.2 m/km]) tested using a Chevy Astro van with a relatively small number of replicate runs and no consideration of texture or roughness. The study by Hultqvist (19) in Sweden showed about a 1% difference in fuel economy for cars when tested on one asphalt and one concrete pavement on the same route in the Swedish summer. However, the authors concluded that these results were primarily due to the higher macrotexture from studded tire use on the asphalt pavement based on modeling results. The pavement structures were not characterized for their stiffnesses.

Noting possible problems with measurements in two earlier phases of work, Taylor and Patten (16) performed a Phase III study on the Canadian pavements listed above using a heavy articulated truck outfitted with different weights and running at two travel speeds (37 and 62 mph [60 and 100 km/hr]) to establish if loading was a contributing factor to truck fuel consumption differences among the three different pavement types (concrete, asphalt, and composite). Testing was performed under different seasonal conditions in eastern Canada. The study found statistically significant fuel use savings for trucks traveling on concrete pavements for most of the five seasons and day/night conditions across the range of vehicle loadings, with greater differences noted at 37 mph (60 km/hr) (1.3% to 3.9%) than at 62 mph (100 km/hr) (0.8% to 1.8%). The study also found statistically significant fuel saving results for most of the seasonal and day/night conditions for concrete pavements compared to composite pavements, again with larger differences at 37 mph (60 km/hr) (1.9% to 6.0%) than at 62 mph (100 km/hr) (0.8% to 3.1%). Interestingly, statistically significant results under the hottest conditions on summer days found the opposite result, with the trucks consuming less fuel on composite pavements than on concrete pavements,

with larger differences at 37 mph (60 km/hr) (2.4% to 3.0%) than at 62 mph (100 km/hr) (about 1.4%). The models developed in the Phase III study also noted that “The insensitivity of the fuel consumption differences to temperature, load and speed is somewhat counterintuitive to the engineering physical models”; however, no explanation for this lack of sensitivity was identified in the study. Thicknesses of the pavement structures were noted, but no structural evaluation or characterization of the pavements (other than being classified as asphalt, concrete, or composite) was included in the analyses of the fuel consumption results. Texture was not measured or considered.

Coast-down measurements were also performed as part of the Taylor and Patten (16) study on the asphalt and concrete sections to measure rolling resistance. Coast-down tests consist of measuring how far a vehicle (the loaded truck in this case) will roll without braking and after shutting off the engine and putting the transmission in neutral. The results showed no significant differences between the asphalt and concrete structures included in the fuel economy studies.

The truck results from the study by Hultqvist (19) showed up to a 5% to 7% difference in fuel efficiency for heavy vehicles operating on hot days on one concrete and one asphalt pavement. The differences were attributed to a combination of structural responsiveness and macrotexture, with macrotexture levels higher on the asphalt pavement while the IRI was slightly higher on the concrete pavement. The effects of texture and structural responsiveness were not separated for the truck measurements, and the authors expressed concern about the presence of relatively strong winds during testing. As noted previously, the pavement structures were not characterized for their stiffnesses. The Swedish study is unique in that the sections were used to check a mechanistic model of pavement energy consumption from vehicles called VETO (20) which showed results similar to the measurements for the test sections. Many of the models in VETO are similar to those in HDM-4.

A field study by Bienvenu and Jiao (18) along 28 miles of Interstate 95 in Florida indicated that passenger vehicles on a concrete pavement use 3.2% less fuel compared to asphalt pavement. The study also showed that, along the same corridor, loaded tractor trailers traveling on the concrete pavement experienced 4.5% better fuel economy than on the asphalt pavement. The asphalt pavement consisted of 9.25 in. (235 mm) of asphalt (including an open-graded friction course) on 5 in. (125 mm) aggregate base and 12 in. (300 mm) of treated subgrade. The concrete pavement consisted of a 13 in. (330 mm) JPCP [jointed plain concrete pavement] resting on a 1 in. (25 mm) asphalt-treated permeable base and 4 in. (100 mm) asphalt base. The pavement structures were not characterized for their structural responsiveness nor were the surface textures measured or considered.

The previously cited study by Chatti and Zaabar (13) had as a secondary objective the evaluation of fuel economy for vehicles traveling on asphalt and concrete pavements. It included 11 pavement sections in Michigan divided between asphalt and concrete, five types of vehicles operating at different speeds, daytime winter and summer measurements (for most vehicles), and ranges of roughness and texture levels. As with the other studies cited, there was very little characterization of the pavement structure besides being noted as being either asphalt or concrete. The results of the study indicated that “pavement type [does] not affect the fuel consumption of any vehicle class except for heavy trucks.” More detailed analysis of the same data indicated that articulated (heavy) trucks and light trucks had statistically significant higher fuel consumption, with about a 4% difference for the heavy trucks when operated on asphalt pavements included in the study at 35 mph (56 km/hr) in the daytime in the summer, but there [sic] no statistically significant difference at speeds of 45 or 55 mph (72 or 88 km/hr) or when the trucks operated during the winter. As noted, there was no characterization of the pavement structures in terms of the structural responsiveness to vehicle operating conditions and temperature that would permit generalized application to other structures and other temperature and loading conditions.

From the review of the various studies noted here, it can be said with reasonable certainty that the influence of structural responsiveness on fuel economy and associated environmental impacts has not been comprehensively validated with an experiment that has accounted for the broad range of environmental conditions or the various types of pavement structures used in the nation’s highway network (e.g., composite pavements, semi-rigid pavements, rubberized and polymer modified mixtures, doweled and nondoweled JPCP, and CRCP). The field studies conducted to date to measure the effects of dissipated energy on vehicle fuel efficiency suffer from a serious lack of characterization of the pavement structures in terms of their structural responsiveness to loading as a function of the stiffness and thickness of the pavement layers or the viscoelastic nature of the materials under different conditions of temperature and traffic speed. Without consideration of those variables, it is difficult to use the results for model validation. And, without validated models, it is difficult to calculate the net results of all of the variables affecting this mechanism. The structural responsiveness to vehicle loading of pavements depends on subgrade, sub-base, and base support conditions, and, particularly for asphalt pavements, the temperature and time of loading. Further, these responses change as the pavement materials age and deteriorate. Therefore, consideration of pavement structural responsiveness effects must be analyzed separately for each project considering the intersection of structural responsiveness, traffic levels, traffic speeds and pavement temperatures, and the moisture conditions in the underlying unbound layers, which vary widely with daily and seasonal climatic fluctuations.

While it is known that water, snow, and ice on the pavement will also impact rolling resistance, the fuel economy studies cited above were all carried out under dry pavement conditions (21). Modeling results from Sweden (22) indicate that water depths [on the surface of the pavement] of 0.039, 0.078, and 0.156 in. (1, 2, and 4 mm) can increase vehicle fuel use by 30%, 90%, and nearly 80%, respectively, compared to dry pavement (21). These results indicate that pavement designs and materials that can remove water from the pavement surface quickly may contribute to substantial reductions in fuel use and environmental impact, particularly in areas with high rainfall; they will also contribute positively to overall safety. In general, open-graded friction courses and directional texturing are used on asphalt and concrete surfaces, respectively, to reduce water depths under tires. Some of these textures also tend to increase macrotexture and might slightly reduce fuel consumption. It should be noted that these modeling results are also not yet validated.

This summary shows that a number of field experiments have been conducted and that one study was used to calibrate a mechanistic model for pavement energy dissipation under moving vehicles. However, none of these experiments were comprehensive with respect to pavement and vehicle types, and the pavement structural responses under different temperature conditions and loading durations that control the viscoelastic response were not characterized. A comprehensive field evaluation of the influence of structural response on vehicle fuel economy had not been completed prior to the study presented in this report. This means that models for structural response effects of vehicle fuel use have not been calibrated for a range of different pavement types and traffic and climatic conditions.

1.1 Overall Study and Phase I Summary

This work is part of Caltrans/UCPRC (University of California Pavement Research Center) participation in the MIRIAM (Models for rolling resistance In Road Infrastructure Asset Management systems) initiative, an ongoing series of studies conducted by a consortium of European national highway research laboratories, Caltrans, the UCPRC, and, more recently, the FHWA. The purpose of the project discussed in this report is to develop, calibrate, and validate models for vehicle energy consumption due to pavement structural response for use in network-level pavement management systems (PMS) and project-level design.

The project is divided into two phases. In Phase I (Partnered Pavement Research Center Strategic Plan Element [PPRC SPE] 4.49), three different pavement structural response energy dissipation models were used to estimate excess fuel consumption (EFC) for a range of California pavements and then calibrated with field data. EFC is defined as the additional fuel required to propel a vehicle on a pavement that is less than ideal condition for fuel

consumption compared with the amount required on an ideal pavement. An ideal pavement is defined as having the following characteristics:

- No fuel consumption caused by structural response
- Very low roughness, defined as an IRI value of 0.6 m/km (38 in./mi.)
- Sufficient macrotexture to provide good skid resistance, defined as a mean profile depth (MPD) of 0.5 mm

The factorial of pavement field sections on the California state highway network included 20 asphalt- and concrete-surfaced pavements with different structure types that were characterized by their viscoelastic properties for the layers expected to dissipate energy through viscoelasticity. The layers characterized for viscoelastic properties were the asphalt layers for the asphalt-surfaced pavements and the subgrades for the concrete-surfaced pavements.

Phase I of the study was completed in 2015 and its outcome was documented in two reports: (1) a report documenting field characterization of the Phase I test sections and mechanistic modeling of energy consumption due to structural response that has not been published (23) and (2) a published report on the simulations of the effects of pavement on vehicle fuel use and GHG emissions (1).

The results of the modeling in Phase I of the study were used to develop an approach for simulation of the annual EFC from structural response for a factorial of the vehicles, traffic flows, speed distributions, and climate regions typical of California. The modeling study included a preliminary sensitivity analysis of the EFC from structural response (EFC_s) to the variables in the factorial.

The Phase I study concluded that EFC_s has a small but important effect on the overall EFC of vehicles and that the effect is highly dependent on the pavement structure. Phase I compared the EFC of roughness, macrotexture, and structural response (1,23) across the Phase I test sections, which were generally selected for their lack of excessive roughness (the large majority have IRI less than approximately 81 in./mi. [1.3 m/km]). The average results across the sections for each vehicle type and model approach showed that the ratio of average EFC_s between heavy vehicles (trucks) and light vehicles (60% cars and 40% sport utility vehicles [SUVs]) is 15:1, 6.1:1, and 6.6:1 for the three structural responses considered in the study. (These responses are referred to by the university teams that developed the models as the MIT model, the MSU model, and the OSU model.) Results from all the models indicated that the effects of structural response are especially important for the overall EFC of heavy vehicles, such as trucks and buses. The results of the simulations also showed that the EFC on the asphalt-surfaced pavements were approximately 1.4 times greater in California's hotter Desert and Inland Valley climate regions than those in the cooler Central and South Coast climate regions.

Table 1.1 shows that the effects of EFC_S were smaller than the combined effects on EFC from roughness (EFC_{IRI}) and macrotexture (EFC_{MPD}): EFC_S was between 14% and 19% of the combined effects of roughness and macrotexture from the MIT model, between 29% and 33% from the MSU model, and between 15% and 21% from the OSU model. These results indicate that while structural response has a small effect, it should not be ignored.

Table 1.1. Descriptive Statistics for EFC Results for Site-Specific Traffic and Climate of Asphalt-Surfaced Test Sections

Statistic	EFC_S^1 (mL/km/vehicle, [% of EFC_{IRI} + EFC_{MPD}])			EFC_{IRI} and EFC_{MPD}^2 (mL/km/vehicle)
	MIT	MSU	OSU/Lyon	
Minimum	0.02 (14%)	0.04 (29%)	0.03 (21%)	0.14
Average	0.12 (14%)	0.28 (33%)	0.18 (21%)	0.85
Maximum	0.61 (19%)	0.92 (29%)	0.48 (15%)	3.2

Notes: EFC_S = excess fuel consumption from structural response; EFC_{IRI} = excess fuel consumption from roughness in terms of International Roughness Index (IRI); EFC_{MPD} = excess fuel consumption from macrotexture in terms of mean profile depth (MPD); sections were selected for mostly low IRI and macrotexture

¹ Relative to no structural response

² Relative to IRI = 38 in./mi. (0.6 m/km) and MPD = 0.5 mm

Each structural response model produced a different result, though all were of a similar magnitude. It was concluded that without field validation, there was no way to determine which modeling approach was the most appropriate. Moreover, given the small sample of each pavement type in the factorial analyzed, a difference was found in how the three models ranked the pavement types in terms of EFC from best (lowest EFC) to worst (highest EFC): on average, the MIT model ranked the composite, flexible, and semi-rigid pavements as 1, 2, and 3, respectively, while the OSU and MSU models ranked them as 3, 2, and 1. It must be noted that the MIT model used the approach of modeling energy dissipation as the delayed response of the pavement to the vehicle load causing the vehicle to move “uphill” on the deflection bowl, while both the MSU and OSU models used different implementations of the approach to model viscoelastic energy dissipation in the pavement structure. The Phase I study recommended the following (23):

Use the model results to simulate the annual vehicle excess fuel consumption caused by pavement structural response on each of the asphalt-surfaced test sections for typical traffic and climate in California and to compare those results with the excess fuel consumption caused by roughness and surface macrotexture, and then prepare a report summarizing the results. Based on those results regarding the importance of fuel consumption attributed to structural response, include in the report a recommendation regarding the need for Phase II experimental work.

Based on the results in the Phase I report, which indicated that structural response was large enough to be included in consideration of the effects of pavement on excess fuel consumption, a Phase II work plan was prepared with the nine tasks shown in Section 1.2. That work plan was approved, and the work was completed.

1.2 Project Goal and Objective

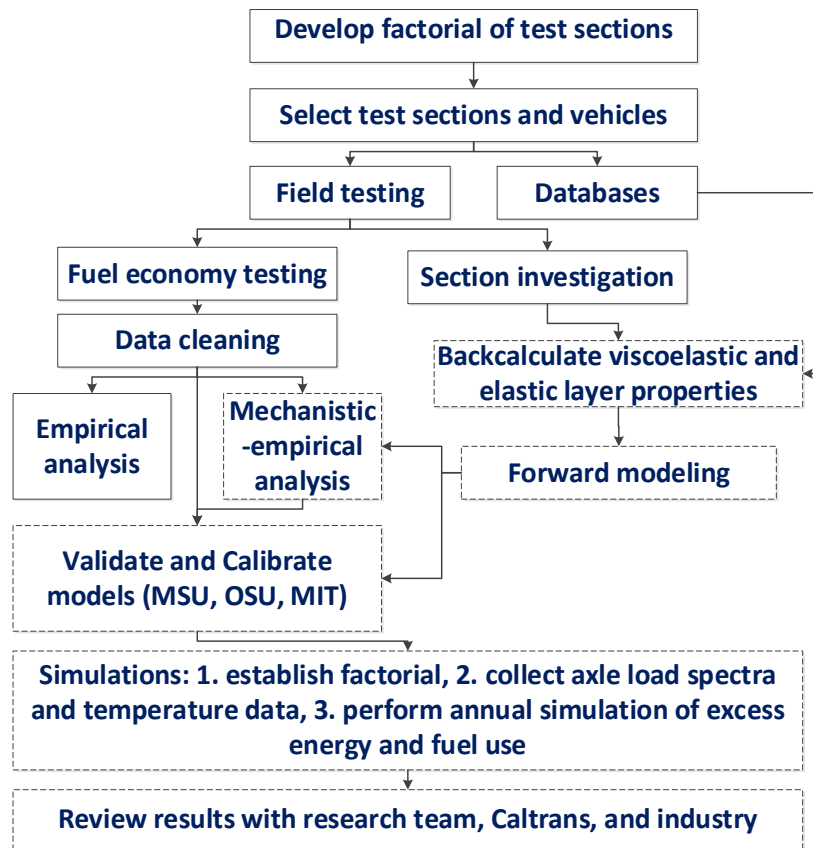
This study, Partnered Pavement Research Center Strategic Plan Element (PPRC SPE) 4.53, is a continuation of PPRC SPE 4.49 (Verification of Pavement Structure and Deflection Effects on Vehicle Fuel Economy and GHG Emissions). The Phase I research program SPE 4.49 involved reviewing the different models for energy and additional vehicle fuel consumed by the structural response of pavements, collecting data for characterization of dynamic properties of pavement on a set of California test sections, predicting deflection and vehicle fuel use, and reviewing the results. The goal of the Phase II program, completed in SPE 4.53, was to measure fuel consumption on the same and/or new sets of pavements and to finalize the development of calibrated and validated models for vehicle energy consumption due to pavement deflection for use in pavement management and design. Both empirical modeling and mechanistic-empirical modeling were included in the scope of this project.

The goal of Phase II (SPE 4.53) was achieved by completing the following tasks:

1. Update the modeling results, including completion of the concrete modeling approaches by Oregon State University (OSU) and Michigan State University (MSU), complete the modeling of the Phase I field test sections, and model all the Phase II section factorials.
2. Update the factorial of test sections and characterizing the test sections through field measurements.
3. Measure and analyze fuel economy on the Phase II test sections.
4. Develop empirical models of the effects of pavement on fuel economy.
5. Perform mechanistic-empirical analysis using the HDM-4 model of the effects of pavement on fuel economy.
6. Validate and calibrate the dissipated energy models from MSU, OSU, and MIT.
7. Compare the measurement and modeling results.
8. Perform forward modeling and simulations of the effects of pavement structural response on vehicle fuel economy for typical pavement structures, traffic, and climate conditions in California using the empirical and mechanistic models.
9. Prepare reports that document the study and its results.

This report documents the work of Tasks 2 through 4. Other tasks are documented in separate reports.

Figure 1.1 summarizes all the tasks in Phase II of the study.



Note: Tasks shown in bold type with solid borders are documented in this report.

Figure 1.1: Summary of Phase II tasks.

The models developed, validated, and calibrated in this project can be used as vehicle fuel consumption models in the pavement life cycle use stage as well as in the Caltrans PMS to predict fuel consumption, GHGs, and other environmental effects contributed by different pavement surfaces and under different climate conditions on the California highway network.

1.3 Report Organization

In Chapter 2 of this report, the field investigation, experiment design, and data collection methods are described. This includes the field and laboratory methods used to characterize the field test sections, descriptions of the vehicles and vehicle instrumentation, the temperature and wind speed measurement methods, and the protocol used to measure fuel use on each section. Chapter 3 documents the processes used to analyze data and separate valid data from instrument errors and other measurement errors. The chapter also presents the methods used to correctly synchronize all of the data types in time and space. Chapter 4 discusses the empirical data analysis and modeling on the final data set. This includes examination of significant autocorrelation issues between several important variables and, after resolution of those issues, the final model structure. The chapter presents analysis

of the ability of the model to match measured results and the results of application of the model to a parametric sensitivity study. Chapter 5 shows the conclusions drawn from the field investigation and empirical modeling.

2 FIELD INVESTIGATION, EXPERIMENT DESIGN, AND DATA COLLECTION

To meet the goal of Phase II, an experiment was designed to include the different types of pavements and vehicles, different traffic speeds, and different pavement temperatures that exist in California. This chapter describes the experiment design and the data collection methods.

2.1 Field Test Sections Experiment Design

The pavement type factorial included California's most common pavement types. The road sections for the fuel economy testing were selected based on the following criteria:

- The *slope/gradient of the pavement* is a major contributor to vehicle fuel consumption. An uphill slope increases fuel consumption and a downhill slope decreases it. To minimize the effects of excess fuel consumption (EFC) due to pavement surface gradient, sections with a slope of less than 0.5% were sought.
- The fuel consumption of vehicles moving on *horizontal curves* is affected by curvature forces. Therefore, it is ideal to have test sections that are straight to eliminate the effect of curvature forces.
- The *length of the road section* had to be long enough for vehicles to reach a steady speed, so they could collect enough vehicle fuel consumption data.
- *Safety* requires that pavement section characterization using destructive and nondestructive procedures be performed in closures with moving traffic and that test vehicles can operate safely at relatively low speeds. Therefore, only sections that allowed these conditions to be met were included in the factorial.
- Because the fuel use testing needed to be performed at different times of the year to capture different temperature conditions, it was important to only include test sections for which *no pavement maintenance was scheduled*; otherwise, the study goal would be negated. Information was gathered from Caltrans and counties for candidate sections to ensure that no major pavement maintenance was scheduled between the winter and summer of 2016.
- *Road roughness* has an important effect on vehicle fuel consumption. With the exception of a few high roughness sections to be used for comparison, most of the sections selected had low roughness to minimize the effects of roughness on fuel use and to help isolate the structural response effect.

Once these revised criteria were determined for Phase II, the Phase I sections were reviewed to determine which ones met them and which did not. The Phase I sections that did not meet the revised criteria were replaced by new sections that did meet the criteria. The resulting 21 test sections across Northern and Central California shown in Table 2.1 were selected based on this road section selection protocol. Appendix A includes photographs of each test section and a map with the locations of all sections.

The selected pavement structures included:

- Sections with a portland cement concrete (PCC) surface
 - Six jointed plain concrete pavements (JPCPs) (without dowels)
 - One continuously reinforced concrete (CRC) pavement
- Sections with a hot mix asphalt (HMA) surface
 - Eight flexible pavements (asphalt layers on unbound bases) with and without rubberized surfaces and open-graded surfaces and a range of thicknesses and stiffnesses
 - Three semi-rigid pavements (asphalt layers over cement-treated base)
 - Three composite pavements (asphalt overlays on cracked and sealed JPCPs, typically without dowels)

The pavement sections structures were characterized according to their structure (material types, thicknesses, and stiffnesses), surface roughness, and texture. (For more details on section roughness and MPD, see Appendix A.) Information on the selected sections was gathered from Caltrans automated pavement condition surveys (APCS) and ground-penetrating radar (GPR) databases. Field tests—consisting of deflection testing with the falling weight deflectometer (FWD) at several temperatures, International Roughness Index (IRI), laser texture scanning (LTS), and subsurface temperature measurements (asphalt sections only)—were performed on each section. Pavement section cores were also collected and used for thickness verification and testing of the asphalt materials for dynamic shear modulus using a frequency and temperature sweep approach in the laboratory. Subgrade samples were laboratory tested for their soil classification. The data collected are summarized in Table 2.1 and Table 2.2. The GPR data showing the underlying structure (from the 2010–2011 Caltrans survey of the state network) are shown in Appendix B for the sections for which data were available. GPR data were not available for the county road sections.

Table 2.1: Phase II Sections and Location Details

Section Codes	Pavement Type	District	County	Route	Outer-most Lane #	Direction	Post-Mile (Start)	Post-Mile (End)	Section Length (mi.)	Start (Lat, Long)	End (Lat, Long)
Six Jointed Plain Concrete Pavement Sections (all without dowels)											
PH01	Concrete	3	YOL	113	2	N	4.5	6	1.5	38.59452, -121.76698	38.61508, -121.76659
PH02	Concrete	3	YOL	113	2	S	6	4.5	1.5	38.61506, -121.76698	38.59452, -121.76742
PH03	Concrete	3	YOL	505	2	N	0.7	6.3	5.6	38.537451, -121.95283	38.616341, -121.95322
PH21	Concrete	3	SUT	99	2	N	31.6	33.6	2	39.155849, -121.635194	39.185780, -121.63475
PH22	Concrete	3	SUT	99	2	S	33.7	31.55	2.2	39.187073, -121.635127	39.154779, -121.63553
PH23 ^a	Concrete	—	YOL	CR32A	1	W	County Road (CR)		1.3	38.564668, -121.642591	38.559458, -121.66622
Eight Flexible Pavement Sections											
PH07 ^a	HMA	—	YOL	CR98	1	N	County Road (CR)		1.8	38.592331, -121.803074	38.617869, -121.80292
PH08 ^a	HMA	—	YOL	CR29	1	E	County Road (CR)		2	38.590626, -121.854847	38.590576, -121.81807
PH09	HMA	3	SUT	113	1	N	5.35	10	5.6	38.875246, -121.705889	38.953002, -121.67680
PH10	HMA	3	SUT	113	1	S	10	5.35	5	38.949366, -121.678005	38.879900, -121.70416
PH11	HMA	3	SUT	113	1	N	12	14	2	38.971943, -121.672018	39.000470, -121.67197
PH12	HMA	3	SUT	113	1	S	14	12	2	39.000470, -121.67203	38.971943, -121.67207
PH13	HMA	3	SUT	113	1	E	15	16	1.2	39.003163, -121.660342	39.003278, -121.63827
PH14	HMA	3	SUT	113	1	W	16	15	1.1	39.003307, -121.639388	39.003205, -121.66038
Three Semi-Rigid Pavement Sections											
PH15 ^a	HMA	—	YOL	CR32B	1	E	County Road (CR)		0.8	38.554729, -121.684886	38.557708, -121.67154
PH16	HMA	10	STA	132	1	E	20.4	22.8	2.4	37.638301, -120.89714	37.638695, -120.85348
PH17	HMA	10	STA	132	1	W	22.8	20.4	2.4	37.638743, -120.853468	37.638346, -120.89714

Three Composite Pavement Sections											
PH04	HMA	3	YOL	505	2	S	6.3	0.7	5.5	38.614511, -121.953558	38.536294, -121.95317
PH18	HMA	6	KER	5	2	S	56.3	54.2	2.1	35.4388929, -119.452387	35.418706, -119.42466
PH19	HMA	6	KER	5	2	N	52.9	56.3	3.4	35.405332, -119.405833	35.438312, -119.45099
One Continuously Reinforced Concrete Pavement Section											
PH20	Concrete	6	KER	5	2	S	54.2	52.5	1.6	35.418603, -119.424555	35.402670, -119.402785

^a Indicates county road.

Table 2.2: Data Collected on All Field Sections

Section Codes	FWD Test Date	Surface Temperature Range	FWD Dates	Surface Temperature Range	Average IRI (in./mi.)	Average MTD (micron)	Average MPD (micron)	Layer Thicknesses from Cores	Section Labels
	Low Temperature (°F)		High Temperature (°F)			Concrete	Asphalt		
Six Jointed Plain Concrete Pavement Sections									
PH01	17-Nov-15	64-68	21-Jun-16	86-104	60	379	—	No Cores Taken	PH01-YOL113N-JPC
PH02	17-Nov-15	51-61	20-Jun-16	95-110	68	589	—	No Cores Taken	PH02-YOL113S-JPC
PH03	18-Nov-15	62-65	14-Jun-16	68-104	60	505	—	No Cores Taken	PH03-YOL505N-JPC
PH21	17-Mar-16	53-74	15-Sep-16	62-95	55	503	—	No Cores Taken	PH21-YOL99N-JPC
PH22	17-Mar-16	80-94	16-Sep-16	75-108	55	425	—	No Cores Taken	PH22-YOL99S-JPC
PH23	16-Mar-16	59-86	3-Jun-16	95-119	142	825	—	PCC 7.5"	PH23-YOL-CR32AW-JPC
Eight Flexible Pavement Sections									
PH07 ¹	18-Mar-16	65-85	29-Jun-16	98-124	73	—	648	HMA 6" AB 13.5" ASB 11"	PH07-YOL-CR98N-HMA
PH08	18-Mar-16	64-104	30-Jun-16	104-131	213	—	861	HMA 4"	PH08-YOL-CR29E-HMA
PH09	3-Nov-15	68-74	24 and 25-Aug-16	91-104	55	—	1,220	RHMA-O 1" HMA 2.4" HMA 3"	PH09-SUT113N-RHMA-O
PH10	10-Nov-15	69-81	24 and 25-Aug-16	98-119	63	—	1,010	RHMA-O 1" HMA 3" HMA 3" HMA 2.4"	PH10-SUT113S-RHMA-O
PH11	4-Nov-15	64-72	13-Sep-16	75-81	100	—	749	HMA 1.5" HMA 2.64"	PH11-SUT113N-HMA

Section Codes	FWD Test Date	Surface Temperature Range	FWD Dates	Surface Temperature Range	Average IRI (in./mi.)	Average MTD (micron)	Average MPD (micron)	Layer Thicknesses from Cores	Section Labels
PH12	4-Nov-15	64-81	13-Sep-16	89-104	106	—	830	HMA 1" RHMA-G 1" HMA 1.8" HMA 2.75" HMA 2.87"	PH12-SUT113S-HMA
PH13	5-Nov-15	51-79	14-Sep-16	100-112	120	—	540	HMA 2.17"	PH13-SUT113N-HMA
PH14	5-Nov-15	59-79	14-Sep-16	107-115	125	—	710	HMA 3.74"	PH14-SUT113S-HMA
Three Semi-Rigid Pavement Sections									
PH15 ¹	7-Apr-16	69-92	18-Aug-16	75-126	97	—	520	HMA 2" HMA 3.5"	PH15-YOL-CR32BE-HMA
PH16	12-Nov-15	42-68	23-Aug-16	82-104	66	—	945	RHMA-G 1.7" HMA 2" HMA 1.5" HMA 2.2"	PH16-STAI32E-RHMA-G
PH17	12-Nov-15	62-75	23-Aug-16	104-122	69	—	834	RHMA-G 2" HMA 2.4"	PH17-STAI32W-RHMA-G
Three Composite Pavement Sections									
PH04	19-Nov-15	46-64	15-Jun-16	75-101	57	—	1,090	RHMA-G 1.2" HMA-O 1.2" HMA 2"	PH04-YOL505S-RHMA-G
PH18	22-Mar-16	77-88	7-Jun-16	95-115	60	—	2,360	HMA-O 1" HMA 2.75" HMA 1.2"	PH18-KER5S-HMA-O
PH19	23-Mar-16	51-72	8-Jun-16	85-122	40	—	1,200	RHMA-G 1.2" HMA 1.2"	PH19-KER5N-RHMA-G
One Continuously Reinforced Concrete Pavement Section									
PH20 ²	22-Mar-16	53-74	7-Jun-16	111-124	100	747	—	CRCP 13.2" HMA (Type A) 3" Class 2 AS 8.4"	PH20-KER5S-CRCP

¹ Pavement layer information and layer thicknesses were obtained from Yolo County.

² Pavement layer information and layer thicknesses were obtained from Caltrans.

Notes:

- PCC: Portland cement concrete
- AB: Aggregate base
- ASB/AS: Aggregate sub-base
- HMA: Hot mix asphalt
- RHMA-G: Rubberized hot mix asphalt, gap graded
- RHMA-O: Rubberized hot mix asphalt, open graded
- HMA-O: Open-graded hot mix asphalt
- CRCP: Continuously reinforced concrete pavement
- IRI: International Roughness Index
- MTD: Mean texture depth
- MPD: Mean profile depth

2.1.1 *Field Test Section Characterization*

Road closures were required for field investigation of the pavement sections. Caltrans closures on state highways and contracted closures on county roads were set up for each section in the winter and summer cycles. Field tests included FWD testing, LTS testing, and temperature profiling. Pavement cores and subgradient samples were collected during the closures. FWD testing was carried out during both winter and summer cycles, and all other tests and sample collections were completed in the summer. The surface profile was measured during the winter season using an inertial profiler. The following subsections present short summaries of the field tests.

2.1.1.1 Coring and Subgrade Soil Sampling

During the FWD testing closures in the summer of 2016, two to four 6 in. (150 mm) diameter cores were collected from each asphalt-surfaced section by coring through the asphalt and bound layers. No coring was done on the CRCP section. Of the five JPCP sections, only one was cored, as it was built in the 1940s and cross-section layer thickness data were unavailable for it. Only the top 8 in. (200 mm) from the surface of the pavements were cored and collected as samples. If the core broke in the hole, only the upper broken lift core sample was collected. Coring locations within the sections were as follows:

- For fixed closures, the cores were collected from the start and end of the closures within the section.
- For moving closures, the cores were collected from the start and end of the section.

Coring was only carried out between the wheelpaths, and the holes were filled with either standard cold asphalt patching materials or county-recommended patching materials. The cores were labeled following the standard UCPRC procedure. The core information, including the location (GPS), thickness, lift type, section number, and other information were then logged in the core data sheets as presented in Appendix A.

Subgrade soil samples were collected from the side of the road rather than from under the pavement after removing 3 to 5 in. (75 to 125 mm) of the soil layer to ensure that no debris or organic material on the surface was included in the sample. On sections built on embankment, the soil sample was taken from the shoulder.

2.1.1.2 Falling Weight Deflectometer (FWD) Tests

Nondestructive pavement surface deflection measurements were used to backcalculate the stiffness of each pavement structural layer and the subgrade resilient modulus. The FWD tests were conducted in both the winter and summer seasons using a Dynatest® Heavy Weight Deflectometer to capture the effects of pavement temperatures on the viscoelastic properties of the asphalt materials, seasonal moisture effects in the unbound layers, and joint interlock at the JPCP transverse joints.

Three drop heights were used to apply average loads of approximately 5,000, 8,000, and 12,000 lb. (approximately 25, 35, and 55 kN). Two repetitions for each weight drop height were applied at each station in each section. Impact load deflections were measured by sensors (geophones) that were mounted radially from the center of the load plate with offsets of 0 in. (0 mm), 7.99 in. (200 mm), 11.8 in. (300 mm), 17.7 in. (450 mm), 23.6 in. (600 mm), 35.4 in. (900 mm), 47.2 in. (1.2 m), and 59 in. (1.5 m). Complete time histories of the load pulse and deflections were collected to allow backcalculation of the viscoelastic properties of the asphalt concrete in the flexible, semi-rigid, and composite pavements, and the subgrade in the jointed plain concrete and continuously reinforced concrete pavements.

The number of stations tested for deflection varied depending on the traffic closure durations permitted on each section by Caltrans or the county, and on the length of the section and, therefore, the travel distance between stations. Deflection stations were evenly spaced along the length of the sections. For all pavement types, deflection readings were measured in the right wheelpath in the outer (truck) lane. For JPCP, the deflections were measured in the outer wheelpath on the intact slabs at the mid-slab as well as close at the transverse joint, with the FWD placed so that the sensors at 7.9 in. (200 mm) and 11.8 in. (300 mm) from the load were on each side of the joint.

Examples of sensor readings on different types of pavement under different loads are presented in Figure 2.1 to Figure 2.6. The figures show typical deflection bowl shapes.

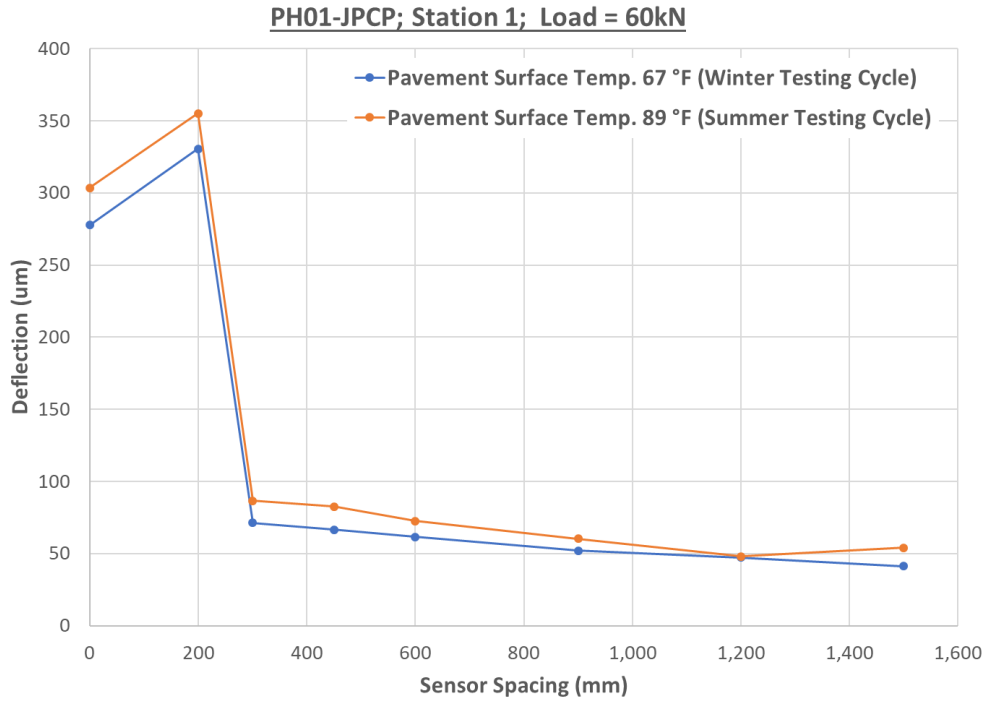


Figure 2.1: FWD deflection bowl in wheelpath at transverse joint on jointed plain concrete section PH01 under 60 kN load for summer and winter test cycles.

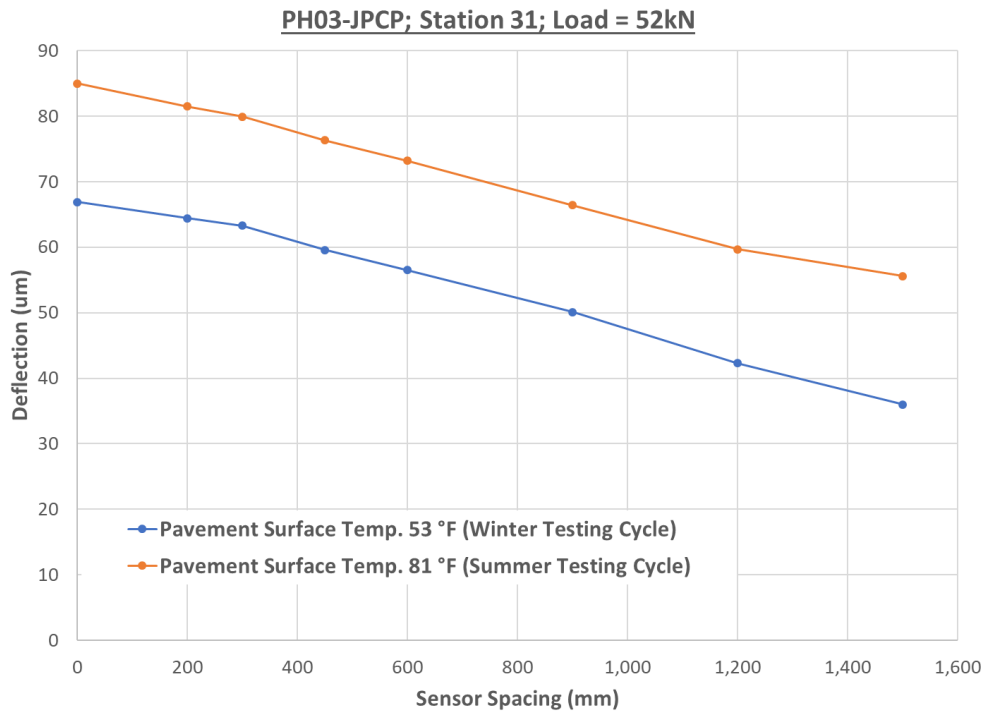


Figure 2.2: FWD deflection bowl in wheelpath at mid-slab on jointed plain concrete section PH03 under 52 kN load for summer and winter test cycles.

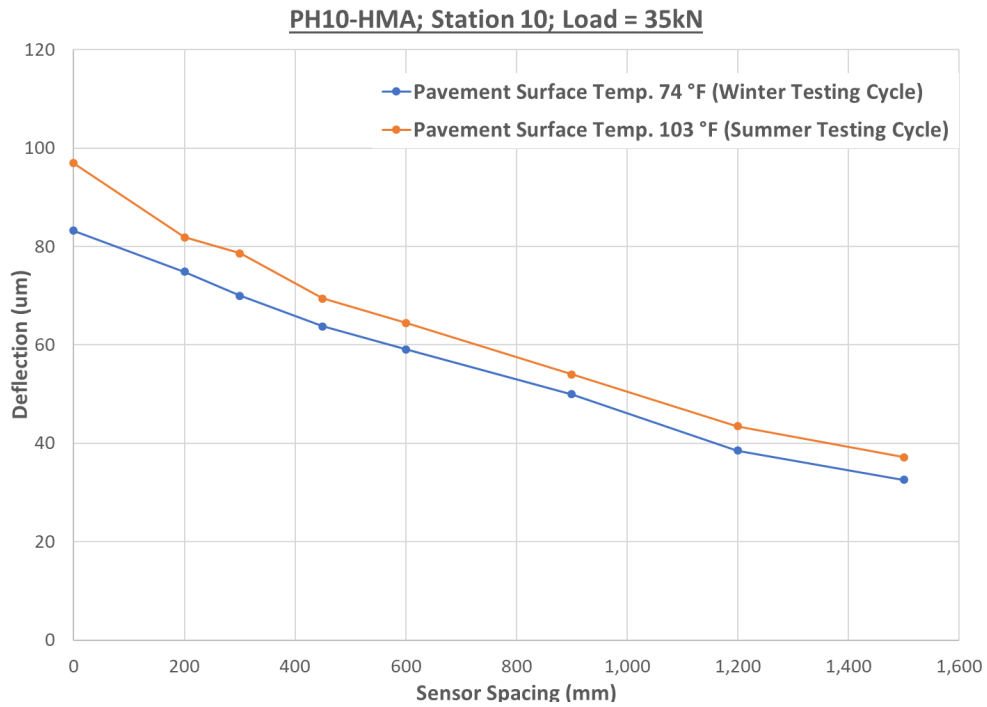


Figure 2.3: FWD test in wheelpath on flexible section PH10 under 35 kN load for summer and winter test cycles.

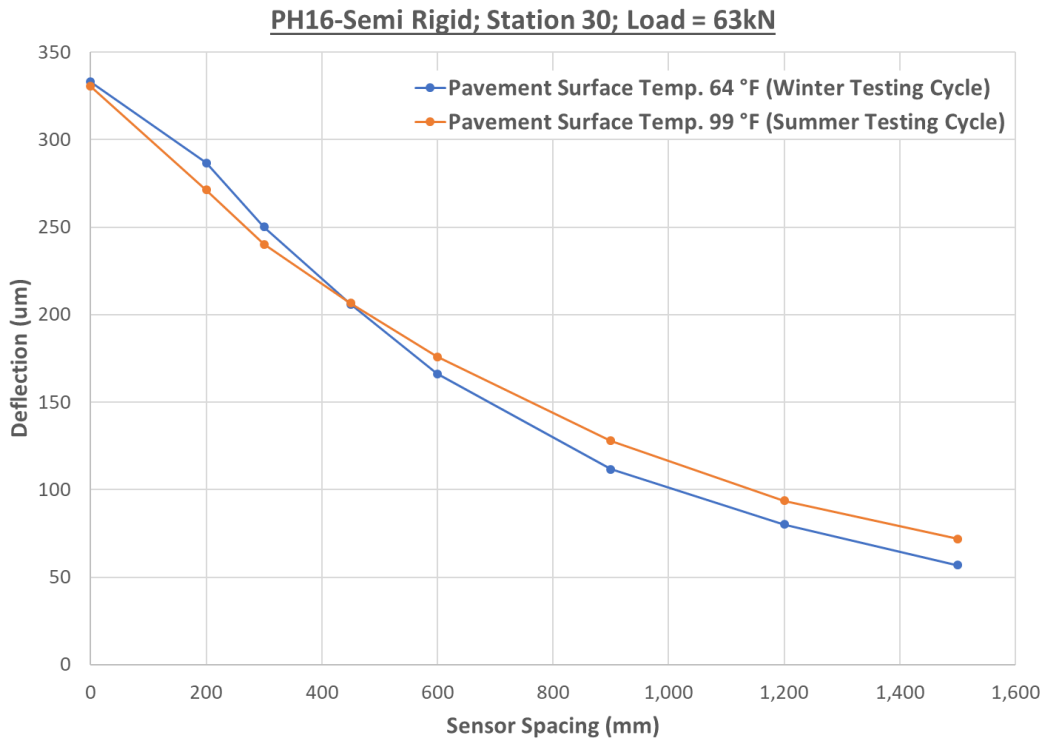


Figure 2.4: FWD test in wheelpath on semi-rigid section PH16 under 63 kN load for summer and winter test cycles.

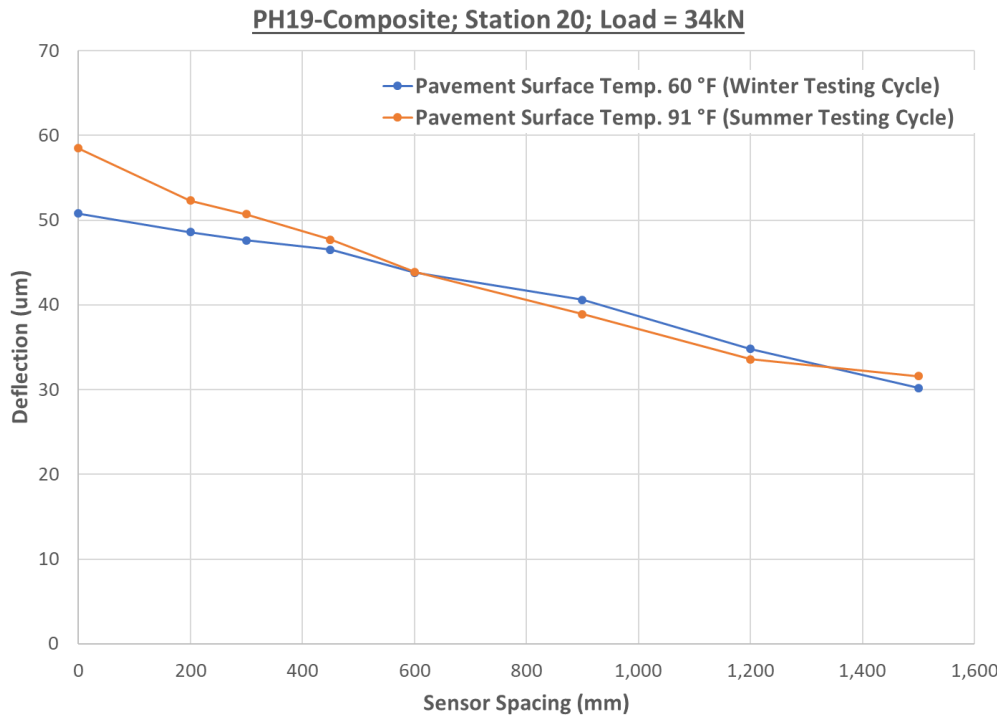


Figure 2.5: FWD test in wheelpath on composite section PH19 under 34 kN for summer and winter test cycles.

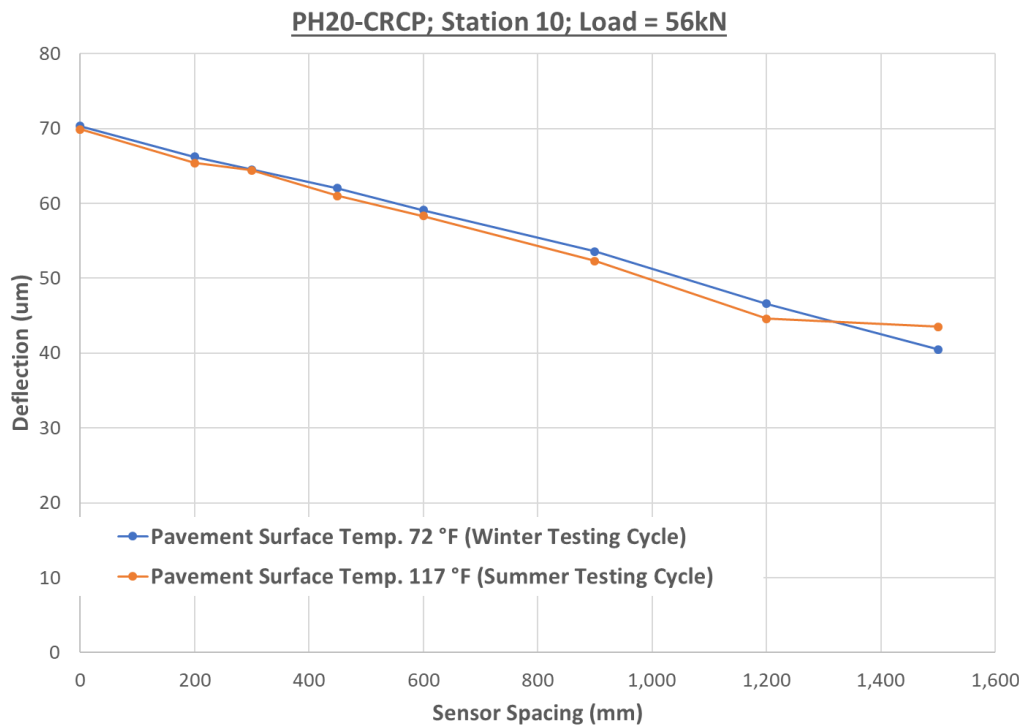


Figure 2.6: FWD test in wheelpath on continuously reinforced concrete section PH20 under 56 kN load for summer and winter test cycles.

2.1.1.3 Laser Texture Scanner Tests

A laser texture scanner (LTS) is a stationary device that scans a pavement surface to measure its macrotexture. The scanner measures the macrotexture of a square of pavement surface approximately 4 in. by 4 in. (102 mm by 102 mm). LTS testing was conducted during the summer traffic closures, and measurements of the mean profile depth (MPD) on the surface of asphalt pavements and of the mean texture depth (MTD) on the surface of concrete pavement sections were recorded. Macrotexture measurements took 15 minutes at each of the two to three separate locations tested along the section. The measurements of MPD for asphalt surfaces and MTD for concrete surfaces for all the test sections are presented in Appendix C.

2.1.1.4 Temperature Profiling

Pavement surface and subsurface temperature data are required for backcalculation of the asphalt pavement stiffnesses; therefore, temperature profiling was also conducted during the summer cycle traffic closures. A hole was drilled in the pavement and the debris was sucked out of the hole using an air vacuum. The hole was then filled with motor oil, and an 8 in. (200 mm) long fabricated thermocouple was inserted in the hole. The first 15 minutes of readings were discarded. Temperature readings were then recorded at every 2 in. (50 mm) depth at 15-minute intervals. It was not possible on some asphalt-surfaced pavements and on the concrete pavement types (JPCP and CRCP) to set up and maintain an in-depth pavement temperature monitoring station to collect temperature profile data because it was unsafe or because local government authorities would not grant permission to drill or core. Instead, for these cases, temperature gradients were estimated using the BELLS3 temperature equation.¹ The measured temperature profiles for all the asphalt-surfaced test sections are presented in Appendix D.

2.1.1.5 Inertial Profiler Tests

The road profile was measured using the UCPRC profiler vehicle, which is equipped with a Dynatest[®] Mk-III road surface profiler. This device has laser instruments that measured the pavement profile in the left and right wheelpaths. The profiler used a RoLine[®] laser on the right wheelpath to measure the pavement profile on concrete pavements. The profiler vehicle was also equipped with a high-resolution dot laser with sampling capability of up to 64 kHz. This laser was used to collect profile data from which a continuous longitudinally measured texture was calculated in the right wheelpath.² The linear measurement of macrotexture using the profiler was applicable only for asphalt-surfaced pavements and could not be used for surfaces with directional texture, such as tined, diamond-ground, or grooved concrete pavements. The profile data were used to calculate the IRI of all the

¹ <https://www.fhwa.dot.gov/publications/research/infrastructure/pavements/ltp/98085/tempred.cfm>.

² Texture is measured as mean profile depth (MPD) for asphalt surfaces and mean texture depth (MTD) for concrete surfaces.

pavement types. Data from the RoLine[®] sensor in the right wheelpath were used for the IRI of concrete-surfaced pavements, while data from the normal-speed dot laser in the left wheelpath and the high-speed dot laser in the right wheelpath were used for the asphalt-surfaced pavements. The averaged IRI and MPD or MTD values for each section are shown in Table 2.2. The IRI profile (in./mi.), MPD (micron), and pavement vertical gradient (%) of all the sections are presented in Appendix E.

2.1.1.6 Vertical Gradient Estimation

A pavement's vertical slope (gradient) affects vehicle fuel consumption significantly, increasing fuel use when the vehicle goes uphill and decreasing when it goes downhill. Even very small gradients over short sections of pavement can cause fuel use changes that are of a similar order of magnitude to fuel use changes caused by pavement structural response. Therefore, accurate and precise section gradients were necessary for the analysis. This study used several data sources selected after comparison to see which ones best reflected realistic gradient readings. Three major sources were used to determine gradients for each state highway network section:

1. Measurements from FWD testing: A Trimble[™] global positioning system (GPS) was attached to the FWD in this study to record the elevation of each FWD test station on the section.
2. Measurements from Google Maps[™]: Elevation values were found for each 165 ft. (50 m) subsection length, and the gradient was determined between elevation values.
3. Measurements from Caltrans databases: Caltrans collects APCS data on state highways using a highly precise gyroscope and accelerometers linked to a GPS (IMUs).³ This enables the collection of inertially corrected position measurements with post-processed GPS data. This unit has a 2 in. (5 cm) height measurement accuracy in most cases. The sections' locations and elevation data were extracted from Caltrans databases and compared; the data collected includes 2010/2011 GPR, 2011 APCS, 2012 APCS, and 2015 APCS.

For the county road sections (PH07, PH08, PH15, and PH23), in addition to methods (1) and (2) stated above, a third method was used where a Garmin Edge[®] 520 GPS (with Global Navigation Satellite System [GLONASS] enabled) was placed in a vehicle. Gradient data were then collected while driving on the sections slow enough (10 to 20 mph [16 to 32 km/hr]) to capture maximum data points. Enabling GLONASS (Russian 31 satellite system) and GPS (US satellite system) settings in Garmin allowed the GPS unit to connect to more than 50 satellites, which permitted measurements even at higher speeds.

The vertical gradient graphs for all the sections are presented in Appendix F.

³ www.applanix.com/downloads/products/specs/POS-LV-Datasheet.pdf

2.1.2 Laboratory Testing

In the laboratory, field sample cores were checked visually and the materials and thicknesses in the layers of their cross sections were measured. Frequency sweep shear tests were also performed to determine the HMA shear stiffness master curves. Finally, subgrade classifications for the subgrade samples collected from each pavement section location were completed. In this way, the pavement structure in each test section was defined and their backcalculated layer stiffnesses were determined.

After the field sample cores were examined visually to see the different layers (lifts), they were marked and cut into separate lifts, as shown in Figure 2.7. A frequency sweep shear test was then performed on each trimmed lift sample. The lift types and thicknesses (in ft.) of core samples are shown in Table 2.3.

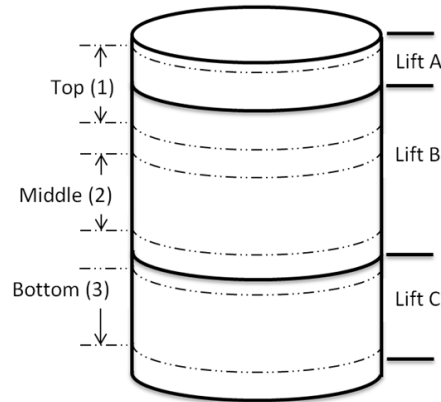


Figure 2.7: Procedure to slice different layers from each lift from a core sample.

Table 2.3: Lift Type and Thickness (in ft.) of Core Samples Collected from Different Pavements

Core ID	Thick Lift 1	Type Lift 1	Thick Lift 2	Type Lift 2	Thick Lift 3	Type Lift 3	Thick Lift 4	Type Lift 4	Thick Lift 5	Type Lift 5
PH04-C1	0.1	RHMA-G	0.1	HMA-O	0.17	HMA				
PH04-C2	0.1	RHMA-G	0.1	HMA-O	0.17	HMA				
PH08-C1	0.33	HMA								
PH08-C2	0.2	HMA								
PH09-C1	0.08	RHMA-O	0.2	HMA	0.25	HMA				
PH09-C2	0.08	RHMA-O	0.2	HMA						
PH09-C3	0.08	RHMA-O	0.2	HMA	0.25	HMA	0.3	HMA		
PH10-C1	0.08	RHMA-O	0.25	HMA	0.25	HMA	0.2	HMA		
PH10-C2	0.08	RHMA-O	0.2	HMA	0.25	HMA	0.2	HMA		
PH10-C3	0.1	RHMA-O	0.2	HMA	0.25	HMA				
PH11-C1	0.18	HMA								
PH11-C2	0.125	HMA	0.22	HMA						
PH11-C3	0.4	HMA								
PH12-C1	0.08	HMA	0.08	RHMA-G	0.15	HMA	0.23	HMA	0.24	HMA
PH12-C2	0.17	HMA	0.12	HMA	0.1	HMA	0.2	HMA		
PH12-C3	0.17	HMA	0.1	HMA						
PH13-C1	0.18	HMA								
PH13-C2	0.12	HMA								
PH14-C1	0.31	HMA								
PH14-C2	0.15	HMA								
PH15-C1	0.17	HMA	0.3	HMA						
PH15-C2	0.17	HMA	0.25	HMA						
PH15-C3	0.18	HMA	0.25	HMA						
PH15-C4	0.15	HMA	0.2	HMA						
PH16-C1	0.15	RHMA-G	0.33	HMA						
PH16-C2	0.14	RHMA-G	0.17	HMA	0.125	HMA	0.18	HMA		
PH17-C1	0.17	RHMA-G	0.2	HMA						
PH18-C1	0.08	HMA-O	0.2	HMA						

Core ID	Thick Lift 1	Type Lift 1	Thick Lift 2	Type Lift 2	Thick Lift 3	Type Lift 3	Thick Lift 4	Type Lift 4	Thick Lift 5	Type Lift 5
PH18-C2	0.08	HMA-O	0.23	HMA	0.1	HMA				
PH19-C2	0.1	RHMA-G	0.1	HMA						
PH19-C3	0.09	RHMA-G	0.15	HMA						

Notes:

- RHMA-G: Rubberized hot mix asphalt, gap graded
- RHMA-O: Rubberized hot mix asphalt, open graded
- HMA: Hot mix asphalt
- HMA-O: Open-graded hot mix asphalt

Laboratory frequency sweep shear tests (AASHTO T 320) were performed on each core lift (trimmed core) from the field section core samples. The frequency sweep included three temperatures (50°F [10°C], 77°F [25°C], and 104°F [40°C]) at 10 loading frequencies of 0.01 Hz, 0.02 Hz, 0.05 Hz, 0.1 Hz, 0.2 Hz, 0.5 Hz, 1 Hz, 2 Hz, 5 Hz, and 10 Hz. The frequency sweep master curves were developed for a reference temperature of 77°F (25°C) and are presented in Appendix G. Although the test results were not used for viscoelastic model development, they were used for comparison with the shape of the master curves from FWD backcalculations for reasonableness.

Subgrade soils were subjected to wet and dry sieve analyses and Atterberg limits tests to determine their Unified Soil Classification System (USCS) classifications. The results are presented in Table 2.4.

Table 2.4: Subgradient Soil Classification Results

Section	Liquid Limit	Plastic Limit	Plasticity Index	General Type	USCS (ASTM D 2487)	General Type
PH01	31.5	14.8	17	Coarse-grained	SC	Clayey Sand
PH02	47.2	18.8	28	Coarse-grained	SC	Clayey Sand
PH03 (sample 1)	42.1	13.0	29	Coarse-grained	SC	Clayey Sand
PH03 (sample 2)	45.1	20.0	25	Fine-grained	CL	Lean Clay
PH04 (sample 1)	34.2	15.6	19	Fine-grained	CL	Lean Clay
PH04 (sample 2)	40.9	14.9	26	Fine-grained	CL	Lean Clay
PH07	31.3	14.9	16	Fine-grained	CL	Lean Clay
PH08	46.4	13.5	33	Fine-grained	CL	Lean Clay
PH09	49.3	17.8	31	Fine-grained	CL	Lean Clay
PH10	29.7	18.0	12	Fine-grained	CL	Lean Clay
PH11 and PH12	26.3	12.9	13	Coarse-grained	SC	Clayey Sand
PH13 and PH14	26.8	14.3	13	Coarse-grained	SC	Clayey Sand
PH15	62.5	20.9	42	Fine-grained	CH	Sandy Fat Clay
PH16 and PH17	22.4	12.4	10	Coarse-grained	SC	Clayey Sand
PH18	—	Non-plastic	0	Coarse-grained	SM	Silty Sand
PH19 (sample 1)	—	Non-plastic	0	Coarse-grained	SM	Silty Sand
PH19 (sample 2)	—	Non-plastic	0	Coarse-grained	SM	Silty Sand
PH20	—	Non-plastic	0	Coarse-grained	SM	Silty Sand
PH21	—	Non-plastic	0	Coarse-grained	SM	Silty Sand
PH23	32.2	15.7	17	Fine-grained	CL	Lean Clay with sand

2.2 Fuel Economy Testing and Data Collection

2.2.1 Vehicles

A range of lightweight to heavyweight vehicles were identified in the data collection plan. The vehicle factorial included gasoline- and diesel-fueled vehicles as well as hybrid and electric vehicles. However, hybrid and electric

vehicles were not included in the study due to time constraints and the onboard diagnostic (OBD) device's limited ability to collect fuel economy data for these vehicle types. Further, vehicle selection was limited by vehicle availability and OBD data collection capability. Based on the factorial, the five vehicles shown in Figure 2.8 were selected for the fuel economy testing:

- A five-axle semi-trailer truck, called a heavy heavy-duty truck (HHDT), 2013 Peterbilt 388, with two single-axle trailers
- A single-rear-axle dual-tire diesel truck, 2011 Ford 450 (F-450)
- A sport utility vehicle (SUV), 2014 Ford Explorer
- A gasoline-powered car, 2015 Chevrolet Impala
- A diesel-powered car, 2015 Chevrolet Cruze

Newer vehicle models were selected for the test, as technology is advancing and newer engines are built to be more fuel efficient than older ones. To avoid variability in driving behavior, one driver was assigned to each vehicle for the entire test, with the exception of the SUV, which had different drivers during the summer and winter test cycles. Since the weights of the SUV drivers varied, sandbags were placed in the vehicle when the lighter driver was behind the wheel to maintain the total weight.

The HHDT was loaded with crushed aggregate, and this load was maintained during the summer and winter testing so that the load on the axles remained the same. The F-450 truck was loaded with bricks, which were secured on a wooden pallet and wrapped with plastic sheets so their moisture content did not change. Its axle loads were checked at a weigh station, and its pallet was positioned to make sure that the axle loads during each test cycle were consistent. Vehicle weights, axle loads, axle spacing, and other information were recorded for all the vehicles and are presented in Appendix H.



Note: Left to right: diesel-powered car, HHDT, F-450 truck, SUV, gasoline-powered car)

Figure 2.8: Vehicles used in the study.

New tires were mounted on the vehicles for the fuel economy data collection. The vehicles were driven on trial sections for two days, so the tires were broken in and had initial aging. The drivers also used those two days to familiarize themselves with the testing protocol. To prevent further aging of the tires between the summer and winter testing, the tires were removed from the vehicles and stored in a cold container. An Intercomp® durometer was used to measure the hardness and aging of the tires, and each tire was marked at three separate locations so the measurements could be taken at the same spot every time. Per the durometer manufacturer's instructions, the device was calibrated by pressing the probe onto a flat solid surface (wood) and setting the knob to zero. No significant change was seen in tire hardness during the test cycles. Plots showing the hardness of the tires, measured in Ha, for each vehicle during the winter and summer test cycles are presented in Appendix I.

2.2.2 Fuel Use Measurement Equipment

Onboard diagnostic (OBD) devices from HEM Data™ were used to measure fuel consumption of the vehicles used in this study. These devices were equipped with data-logging capability and a slot for a memory drive to record the data being output from the vehicle electronics. The OBD device was connected (usually under the dashboard) to the vehicle's OBD connector to access data from the engine control unit, which is also referred to as the vehicle's engine management system. Certain data could be collected from a vehicle via its OBD device as preprogrammed by each vehicle manufacturer. Additional types of data could be recorded by the OBD device but required that it be reprogrammed. Data received by the OBD is usually sampled in series and collection of additional parameters requires more time, resulting in longer times between parameter recording cycles. Because of the short time that it took to traverse subsections with the constant vertical gradient within each test section, it was important to have several vehicle instrument scans recorded for each test section. Therefore, the OBD devices for each vehicle were programmed to record only the data that were required for the study purposes.

The possibilities of recording flow in the fuel pipeline or connecting a device directly to the vehicle's control area network (CAN) in order to record fuel consumption data were discussed and were included as an option in the study's test plan. However, as the vehicles were to be driven on state and county roads, these alterations of the engine controls and components were not pursued for safety reasons. Only OBD devices were used to collect fuel consumption data from each vehicle.

2.2.3 Climate Data Collection Equipment During Field Testing

Solar-powered Davis Instruments Vantage Pro2™ wireless weather stations with a connected data logger were used to collect data on wind speed, wind direction, air and pavement temperatures, and dew point during the fuel

economy testing. During the nighttime testing, the weather stations used a battery that had been charged during the daytime by solar energy.

2.2.4 Fuel Economy Testing Protocol

A testing protocol was written and followed for the fuel economy testing. The planned data collection schedule called for testing in the cold (January to March) and hot (July to August) seasons of 2016. Trials were also conducted before the actual plan was executed. Vehicles were serviced and their axle loads were measured before the start of each testing cycle. Testing times were mainly between 9 a.m. and 4 p.m. during the day and 11 p.m. and 6 a.m. Both test crew safety and public safety was always the first priority, so the test times were selected to match periods of lower traffic flow. Before each day's testing, the vehicles were driven for at least 20 mi. to warm up their engines. Before the first testing season, a tire pressure and temperature study was completed to determine the time needed for the vehicle tires to reach stable temperatures and tire pressures, as tire pressure changes affect vehicle fuel consumption. Details of this study are found in Appendix J.

The vehicles were run on the sections in a convoy, with a space of at least three sedan car lengths (approximately 45 ft. [14 m]) kept between the vehicles to minimize drafting and other tailgate effects. Also, to help minimize the effects of air disturbance, the order of the vehicles in the convoy was based on size, with the smallest vehicle, the gasoline car, in the lead, followed by the SUV, the F-450, and the HHDT. The diesel car was included as the last vehicle in the convoy (behind the HHDT) to serve as a pilot car to warn drivers that slow-moving vehicles were operating ahead of it.⁴ Although the data from the diesel car were collected, they were not used in the final analysis due to the car's frequent braking and acceleration and the tailgate effect from the HHDT.

Amber lights were mounted on all the vehicles, and magnetic safety signs (indicating a slow-moving vehicle) were installed on the rear and the driver side of all the vehicles. Testing was only performed in the right lane. The testing protocol required drivers to stay in the same path on each replicate pass on the test section and to minimize vehicle wander. The same protocol was followed for all the testing cycles to maintain consistency during the summer and winter as well as the daytime and nighttime testing cycles. The testing protocols included the following:

- No testing was to be performed when the pavement was wet or damp or when winds were above 5 mph (8 km/hr).
- Tire pressures were to be checked each day before testing.

⁴ Average speed on California freeways is 75 to 80 mph (121 to 129 km/hr), which is much greater than the test vehicles speeds of 35 to 55 mph (56 to 88 km/hr).

- The air conditioning, fan, and heater were to be turned off during the testing, as these vehicle accessories draw power, and therefore consume more fuel. Drivers were to wear warmer clothes when it was cold. In summer, drivers could use the fans powered by a small car-mountable battery, and it was recommended that they cool themselves by taking frequent, short breaks after every two to four runs (depending on section length).
- Most of the vehicles' windows were to be closed at all times during the tests because lowering them would affect fuel consumption, especially for the smaller vehicles. Only the HHDT could have its driver's side window open during winter and summer testing cycles, to accommodate its driver's special needs.
- Vehicle headlights were kept on during both nighttime and daytime testing because of the need to keep accessory loads constant.
- The radio was always turned on during the testing to help the drivers stay awake. When the driver required quiet time, the volume was turned down.
- The testing was always to be done with vehicles using automated vehicle speed control (cruise control). This protocol was included because during trial testing it was found that driving behavior and speed could not be controlled sufficiently without cruise control. Speed control was found to have a time lag as it reacted to vehicle speed changes due to even small changes in vertical gradient and/or wind speed or direction. However, this lag was considered in the analysis of the fuel use data.
- Vehicles were to be fueled to 100% before testing and refueled during the testing if the fuel tank became less than 90% full. This was done because the amount of fuel in the fuel tank affects the vehicle's total weight, hence affecting fuel consumption.
- As fuel quality may affect fuel consumption, vehicles were to be fueled at stations providing the same brand. Since most of the test sections were close to the city of Davis, fueling was done at the UC Davis fleet services fuel station. Except for a few instances when the test sections were too far from the HHDT's fuel source, it too was mainly fueled at one source. It should be noted that fuel use may have been affected by California's requirement that an oxygenated (lower-energy density) fuel formula be used in winter to minimize air pollution. When vehicles refueled, samples were collected and sealed in glass bottles. Bomb calorimeter tests were performed on these samples later to determine if any variability in fuel energy content had affected the vehicles' fuel consumption. Details of these tests and their results are available in Appendix K.

2.2.5 Fuel Economy Data Collection

At least 20 minutes prior to testing, weather stations were set up on the test sites at pre-identified locations that were determined to be safe and free of obstructions. The weather stations recorded wind speed, wind direction,

and pavement and air temperatures during the testing. A team member was assigned to monitor the weather station; the location of the weather station was also where drivers could park their vehicles to rest. Walkie-talkies were provided to all team members for communication purposes. The weather station monitor kept track of the number of test run replicates on a sheet, directed the team, and recorded if there was a problem with any of the vehicles on the run that required a repeat run. Vehicle speeds were set using cruise control to collect fuel consumption data at 45 and 55 mph (72 and 88 km/hr) on all state highway sections and at 35 and 45 mph (56 and 72 km/hr) on all county roads.

The maximum number of replicate passes that could be made on each section depended on the testing time period available, which was often determined by changes in wind speed and temperatures as well as the length of the section (i.e., it took less time to drive on shorter sections, and therefore more replicates were recorded). Although a minimum of 6 good replicates were recommended, the target was 8 to 12 good replicate runs at each speed on each section in a given season.

The OBD device installed in each vehicle was programmed to record the parameters identified as necessary to calculate the vehicle's fuel consumption. The OBD devices recorded data every 0.02 second for all vehicles except the HHDT, where data was recorded every 0.004 second. Weather station data were recorded every minute.

3 DATA MANAGEMENT PROCESS

This chapter describes the processes used to store data, the equations for calculating parameters, and the processes for performing quality checks and identifying the subsection lengths used to produce the final data set for empirical modeling and for comparison with mechanistic models.

3.1 Summary of Data Collected

Microsoft® *Access*® and *PostgreSQL* were used to develop the study's database.

3.1.1 Weather Station Data

Weather station data for each testing day per section were extracted using *WeatherLink* 6.0.3 software. The data included date, time, air density, hourly air temperature, maximum and minimum air temperatures, humidity, dew point, hourly and maximum wind speeds, wind direction, barometric pressure, heat index, heating and cooling degree days, rain rate, rainfall, solar radiation, solar energy, temperature-humidity-wind index, temperature-humidity-sun-wind index, ultraviolet (UV) index, UV dose, pavement surface temperature, and wind run. The data were extracted from the software as comma-separated value (.csv) files.

Air density is a calculated value, and no sensor in a weather station can determine it. However, the air density values calculated by the weather station unit in this study were not used because the section elevation information at each location was incorrectly inputted into the weather station software each test day. As a result, air density was calculated after the testing was completed. The parameters required to calculate air density are the section's elevation (where the weather station was installed), atmospheric pressure, and the dew point measured at the weather station. Details of the air density calculation are reported in Appendix L.

Sensors in the weather station measured the wind direction and wind speed each minute. The wind direction was measured in 22.5-degree intervals from the north. The component of the wind speed in the direction of the section (the headwind) was calculated.⁵ As all the sections selected for testing were straight, determining the angles of the section lengths from the north was straightforward and are presented in Table 3.1.

⁵ If the wind direction was against the traffic flow, it is referred as *headwind*, and if the wind direction was in the direction of travel of the vehicle, it is referred to as *tailwind*.

Table 3.1: Section Directions in Global Coordinate System

Section ID (PH)	Section Angle from North (degrees)	General Direction ^a
1	0.96	N
2	180.96	S
3	359.79	N
4	179.79	S
7	0.27	N
8	90.11	E
9	16.37	N
10	196.37	S
11	359.89	N
12	179.89	S
13	90.40	E
14	270.40	W
15	76.50	E
16	89.20	E
17	269.20	W
18	131.97	S
19	312.03	N
20	131.97	S
21	0.65	N
22	180.65	S
23	254.27	W

^a North = N, South = S, East = E, West = W

3.1.2 Profile Data

The profile data collected were GPS location; right, center, and left wheelpath sensor data; International Roughness Index (IRI) calculated at 3.28 ft. (1 m) intervals; macrotexture; and elevation. The data were extracted as response (.rsp) files. Data from the .rsp files were then extracted using MATLAB[®], and plots were prepared in the R programming language. The plots are presented in Appendix D.

3.1.3 Gradient Data

After reviewing the gradient data for each section from the different sources (measurements from FWD testing, Google Maps[™], and Caltrans databases) described in Section 2.1.1.6 and presented in Appendix F, Caltrans 2015 automated pavement condition survey (APCS) data were chosen to use for the state highway sections and collected Garmin GPS elevation data for the county road sections.

At times, the Trimble[™] GPS used for FWD testing had difficulty connecting to high numbers of satellites. Therefore, the elevation data it collected sometimes showed irregular spikes, and it was difficult to gauge its

accuracy compared to data from other sources. One possible reason for this difficulty could be that the FWD did not stop at the measurement location long enough, as this type of testing usually takes less than a minute at each point on the section. Elevation data collected from Google Maps was also found to be problematic, as it had too much noise.

The data selected for use for the state highway sections came from the 2015 Caltrans APCS. These data were the most recent (fuel economy testing was conducted in 2016) and most accurate (few sections were identified to have undergone maintenance between 2011 and 2015, as can be seen in Table F.1 in Appendix F) of the four Caltrans sources compared (2010/2011 GPR, 2011 APCS, 2012 APCS).

Due to the reasons noted above, the Trimble™ GPS and Google Maps elevation data were not used for the county road sections. Instead, elevations measured by the Garmin Edge®520 GPS were selected.

3.1.4 Fuel Consumption Data (OBD Data)

As explained in Section 2.2.2, every vehicle manufacturer allows certain data to be accessible through an OBD. Therefore, the OBD was programmed to extract the parameters necessary to compute fuel consumption for each vehicle. The data parameters chosen for this experiment are as follows:

Car and SUV

The data that the OBD devices recorded in their memory drives included time, vehicle speed, air flow rate, fuel level input, latitude, longitude, elevation, velocity, and various satellite information. The data were collected every 0.02 second by the OBDs from the vehicles' control area network (CAN). Mass air flow (*maf*) data in grams per second were used to determine the amount of fuel that was used in gallons per second for each collected data point by using Equation (3.1):

$$IFC = \frac{maf}{fps * lfps * gfps} \quad (3.1)$$

Where:

IFC = instantaneous fuel consumption in gallons per hour

fps = 14.7, the number of grams of air per gram of gasoline

lfps = 454, the number of grams of fuel per pound of fuel

gfps = 6.701, the number of pounds of fuel per gallon of fuel

Medium truck (F-450)

The OBD recorded time, vehicle speed, engine fuel rate, fuel level input, latitude, longitude, elevation, velocity, and various satellite information every 0.02 second. Engine fuel rate measured in liters per hour was converted to gallons per second to calculate the fuel consumption at each collected data point.

Five-axle semi-trailer truck (HHDT)

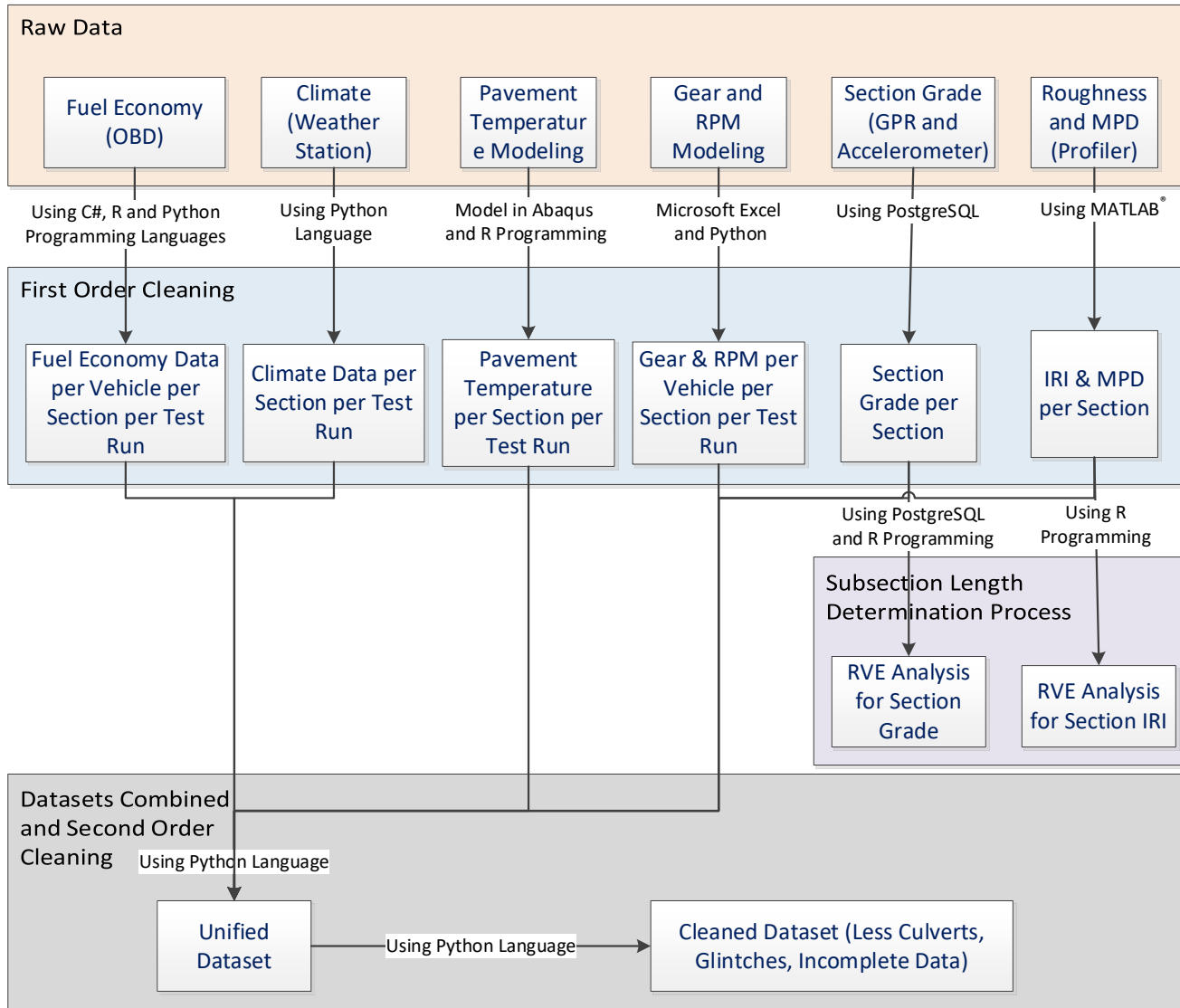
The OBD recorded time, wheel-based vehicle speed, engine fuel rate, engine instantaneous fuel economy, engine inlet air mass flow rate, latitude, longitude, elevation, velocity, and various satellite information every 0.004 second. Engine fuel rate measured in liters per hour was converted to gallons per second to calculate the fuel consumption at each collected data point.

3.2 Data Cleaning

After organizing and sorting the raw data files, the study team filtered and processed the data that were relevant to the study. The software used for data processing and storing were Microsoft® *Access*®, *PostgreSQL*, *Abaqus*, *MATLAB*®, and Microsoft® *Excel*®; the programming languages included Python, R, and C#. The steps taken to prepare the data for analysis and modeling (mechanistic-empirical and empirical) are shown in Figure 3.1 and listed as follows:

1. Raw data verification and completeness check
2. First order data cleaning
3. Data aggregation
4. Data compilation
5. Second order data cleaning

Each of these steps is described in more detail in the following sections of this chapter.



Note: RVE = representative volume element.

Figure 3.1: Data handling and cleaning process.

3.2.1 *Raw Data Verification and Completeness*

The raw data were checked for completeness after each testing day; that is, it was confirmed that the device collected data. The data were plotted using Microsoft® *Excel*® and Python to see the trends and shapes of the graphs to ensure that the data made sense and were complete. Although most of the datasets were found to be complete for the analysis, a few had failures. This required going back into the field to generate new explanatory data that could be correlated to the data collected during the fuel economy testing. Vehicle speed, gear and fuel consumption relationships per vehicle, corrupted or unrecorded climate data, and incomplete pavement surface temperature data were some datasets that were affected, and they are discussed in detail in the following subsections.

3.2.1.1 Same Speed, Different Gear

The fuel economy data showed that the F-450 truck was not recording repeatable fuel consumption on replicate runs at the same speed on the same section. The data showed two different fuel consumption ranges that were wide apart, as can be seen in Figure 3.2. It was assumed that the OBD had some technical issues and that replacing it might solve the data recording issues. Additional fuel economy data were collected using a new OBD, but the issue persisted.

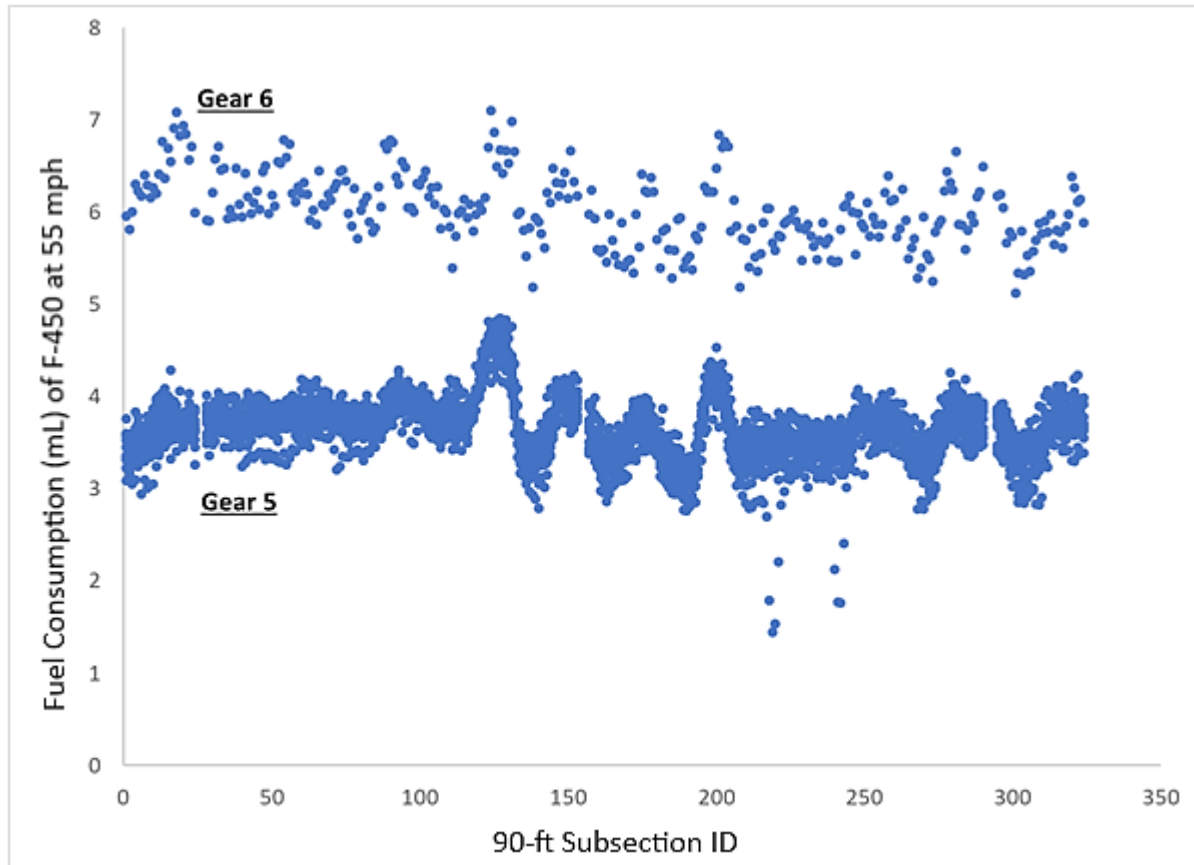


Figure 3.2: Fuel consumption of F-450 on PH03-Yol505-JPC section at 55 mph in two different gears.

It was then hypothesized that the variation in the fuel consumption results might be due to a difference in the vehicle’s revolutions per minute (RPM), which changes with different gears. It was thought that the F-450 truck, while moving to reach the control speed on the test section, was either accelerating or decelerating before cruise control was turned on at the test speed. As some of the automatic transmission’s control speeds were at the gear-change point, the truck may have achieved cruise speed in either a lower or higher gear. To test this hypothesis, the OBD device was configured to record the vehicle speed, fuel consumption, and RPM of the F-450 truck. The loaded vehicle was then driven on a remote county road, and several scenarios were investigated:

1. Driving with cruise control at 45 mph (72 km/hr) in different gears (operating the gears manually)
2. Slowly accelerating to higher speeds
3. Accelerating as fast as possible to the control speeds

The results were then compared to the fuel economy data collected for this project and the hypothesis was proven to be correct. The data from the other vehicles and sections were rechecked. Very few runs for other vehicles were found to have the same problem, and those runs were removed from the dataset. However, it was important to

determine the gear and RPM for each vehicle at each vehicle speed, as it is not speed that determines fuel consumption but rather a combination of speed, gear, and RPM. Therefore, all the vehicles were reviewed, and a detailed investigation was performed. An empirical relationship was established between speed and RPM for each gear for each vehicle. These relationships were used to calculate the RPM for each vehicle speed in the fuel economy data collected. The details of this separate study along with the empirical relationships found for each speed per vehicle are presented in Appendix M.

3.2.1.2 Climate Data

There were a few times when the weather station did not record any data even though it was operational during the testing time; it is unclear why this happened. In these situations, climate information was collected from the nearest weather station to the testing site.

3.2.1.3 Pavement Temperature Measurement Data

Other significant issues identified in the weather station data occurred with the pavement temperature data collection. For reasons that have not been determined, the temperature probe at the weather stations on occasion did not record the pavement temperatures that were being collected during the fuel economy testing. Additionally, traffic safety concerns prevented installation of the temperature probe on several state highway sections. Therefore, to determine pavement surface and subsurface temperatures in these situations, a temperature model developed by Li (24) was used to predict the temperature regime in the test section pavement structure.

The process of determining pavement surface temperatures and temperatures at one-third depth of the pavement using Li's model is discussed in detail in Appendix N.

3.2.2 *First Order Data Cleaning*

The data that met the requirements of the experiment were extracted from the raw data files. That is, data were continuously collected over the course of the day, but only data collected following the protocols (see Section 2.2.4) were qualified for the analysis.

3.2.2.1 Fuel Economy Data

Fuel economy data was extracted from the .csv files. The start and end GPS coordinates of each section (identified in Table 2.1 and discussed in Section 2.1) were used as points in what is referred to as the rectangle method to

extract the data from the raw files. C# programming was used to define a rectangle within which the data of interest lie for each section.

Test speed was the next data reviewed. Of the five test vehicles, the HHDT took the longest time to reach the test speed on a section. Therefore, section limits were adjusted (after data extraction from raw files) based on the GPS coordinates at which the HHDT reached the test speed. To keep the section lengths similar and comparable between the vehicles, HHDT test speed determined the start and end point of a section. The data were extracted using the R programming language for the three test speeds: 55±1 mph and 45±1 mph for state highway sections, and 45±1 mph and 35±1 mph for county road sections.

For the data to be properly aligned to all other datasets, it was necessary for the location and time data in the OBD datasets to be accurate. The HEM Data™ OBD comes with two separate units mounted on the same chip: (1) a GPS data logger that records location, speed, and time every second and (2) a unit that records vehicle data (every 0.02 second for car, SUV, and F-450 and 0.004 sec for HHDT, as mentioned in Section 3.1.4). As these units recorded data at different time intervals, a linear interpolation of the GPS data (location, speed, and time) was done to match the time interval of the vehicles' data readings using Equation (3.2):

$$x(j, t) = x(t) \left(1 + \frac{j}{n}\right) \quad (3.2)$$

Where j is the interpolation step out of n steps between pre-existing time steps $t-1$ and t for a variable x .

3.2.2.2 Data with Important Location Information

Determining location information—section and subsection gradient, roughness, and macrotexture data—was important so that the OBD data could be aligned with this dataset. The data that matched the start and end GPS coordinates finalized in Section 3.2.2.1 were extracted using *PostgreSQL* (for gradient) and *MATLAB*® (for IRI and mean profile depth [MPD]/mean texture depth [MTD]).

3.2.2.3 Data with Important Time Information

Time information from the weather station data was important so that the OBD data could be aligned with this dataset. The weather stations were turned on at least 30 minutes before the fuel economy testing and were turned off after the testing and data collection were completed for the testing day. A Python program was used to convert the date-time data to separate date and time data.

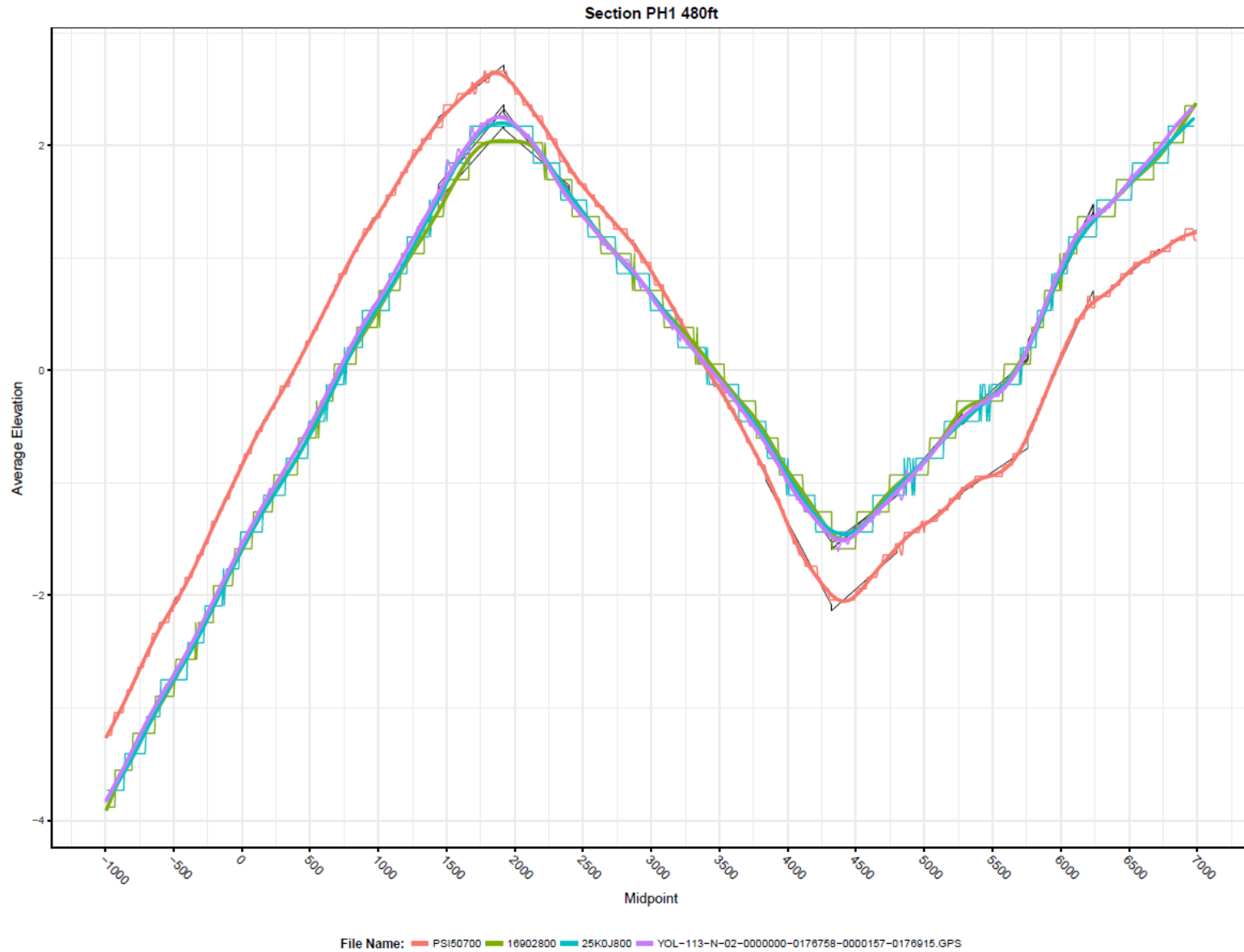
3.2.3 *Selection of Subsection Length for Analysis*

Each instrument records data at different intervals as was discussed earlier. The time or distance interval between two consecutive data points for all the datasets recorded was different for each data type. In addition, use of average values over an entire section or large subsections would result in loss of important information, as there was important variation within each section. The use of average values over small subsections would also result in higher variance of the mean because of the few data points used to establish the average. Gradient and roughness are not randomly distributed. They have spatial variation that is correlated with the distance between any two points (semi-variance), and gradient tends to have inherent dominant wavelengths because of natural features and how roads are constructed. Also, gradient and IRI are not point measurements. Gradient is, by definition, the slope between any two points. IRI is the result of a viscoelastic mechanical simulation of vehicle suspension operating along a profile that has time dependence and, therefore, length dependence.

The goal was to find the shortest subsection length that had the lowest variance of roughness and gradient within it and that still had sufficient data points to provide a reliable mean. Eight subsection lengths were considered: 30, 60, 90, 120, 180, 240, 300, and 480 ft. (9, 18, 27, 36.5, 55, 73, 91, and 146 m).

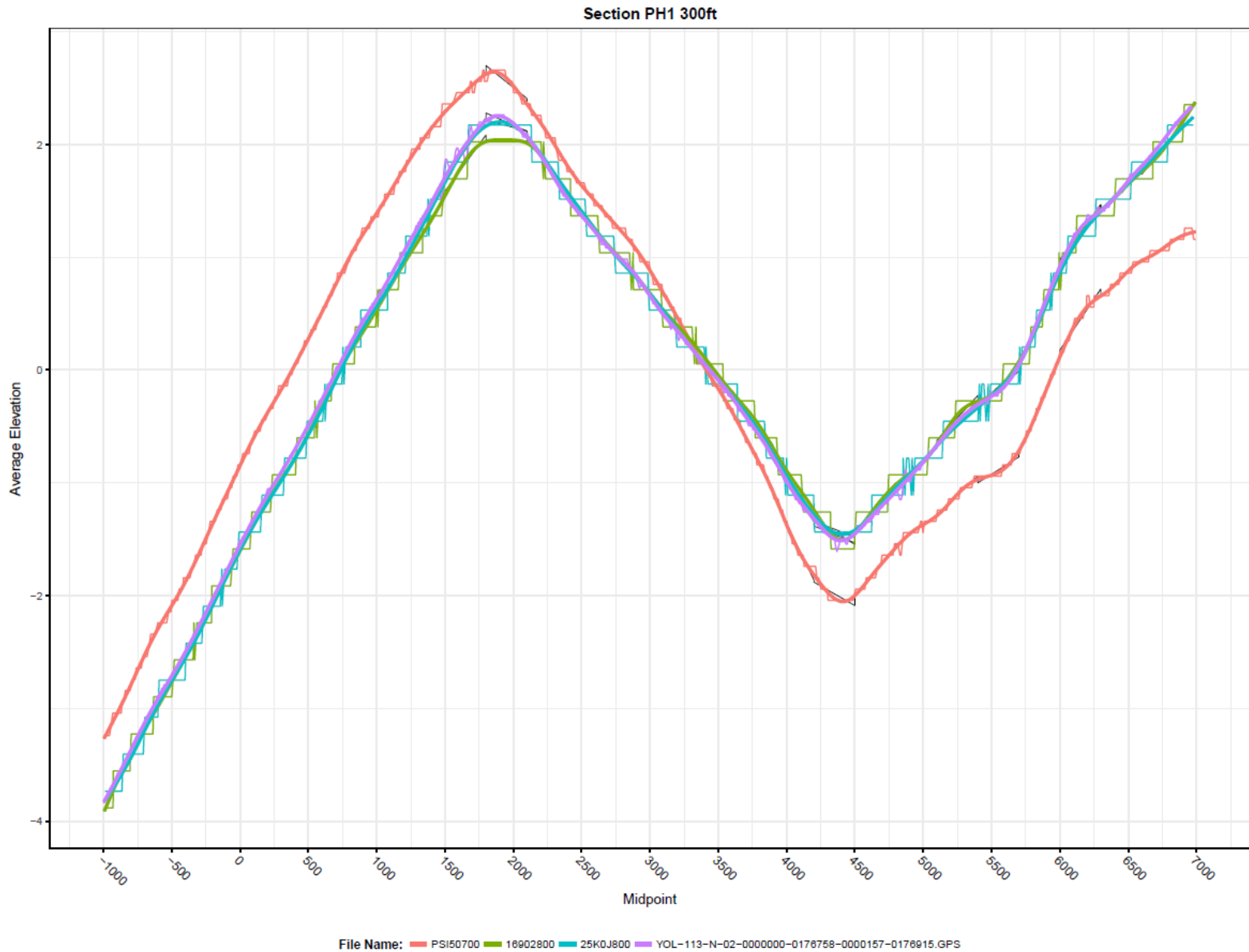
3.2.3.1 Subsection Analysis Using Gradient Data

Average elevation/slope were used for the subsection analysis in which the entire section was divided into equal subsection lengths (30, 60, 90, 120, 180, 240, 300, and 480 ft.). The slope of each subsection was then calculated, and the linear model was fitted on slope data plots of the section. Example plots for section PH01 are presented from Figure 3.3 to Figure 3.7 for five subsection lengths (480, 300, 240, 180, 90 ft.). The linear model fit, seen as a black line plot on each figure, is the smoothing trend line showing the best fit; locations where it peaks, mainly where the subsection length is small, represent poor fit.



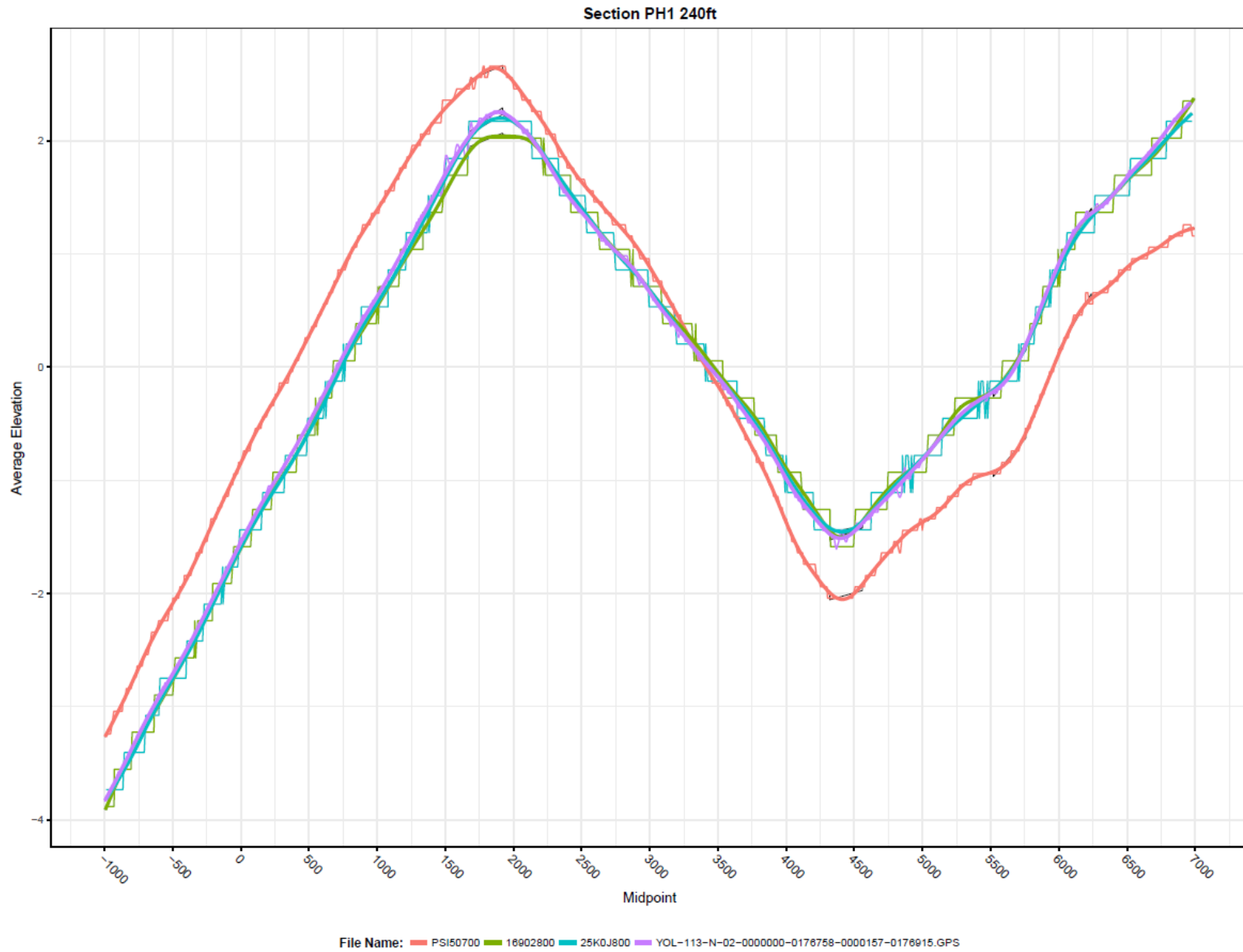
Note: PSI50700 [2015 APCS data] is selected for the analysis and the black line plot represents the linear model fit of elevation per subsection length.

Figure 3.3: Average elevation and subsection length plot for subsection length of 480 ft.



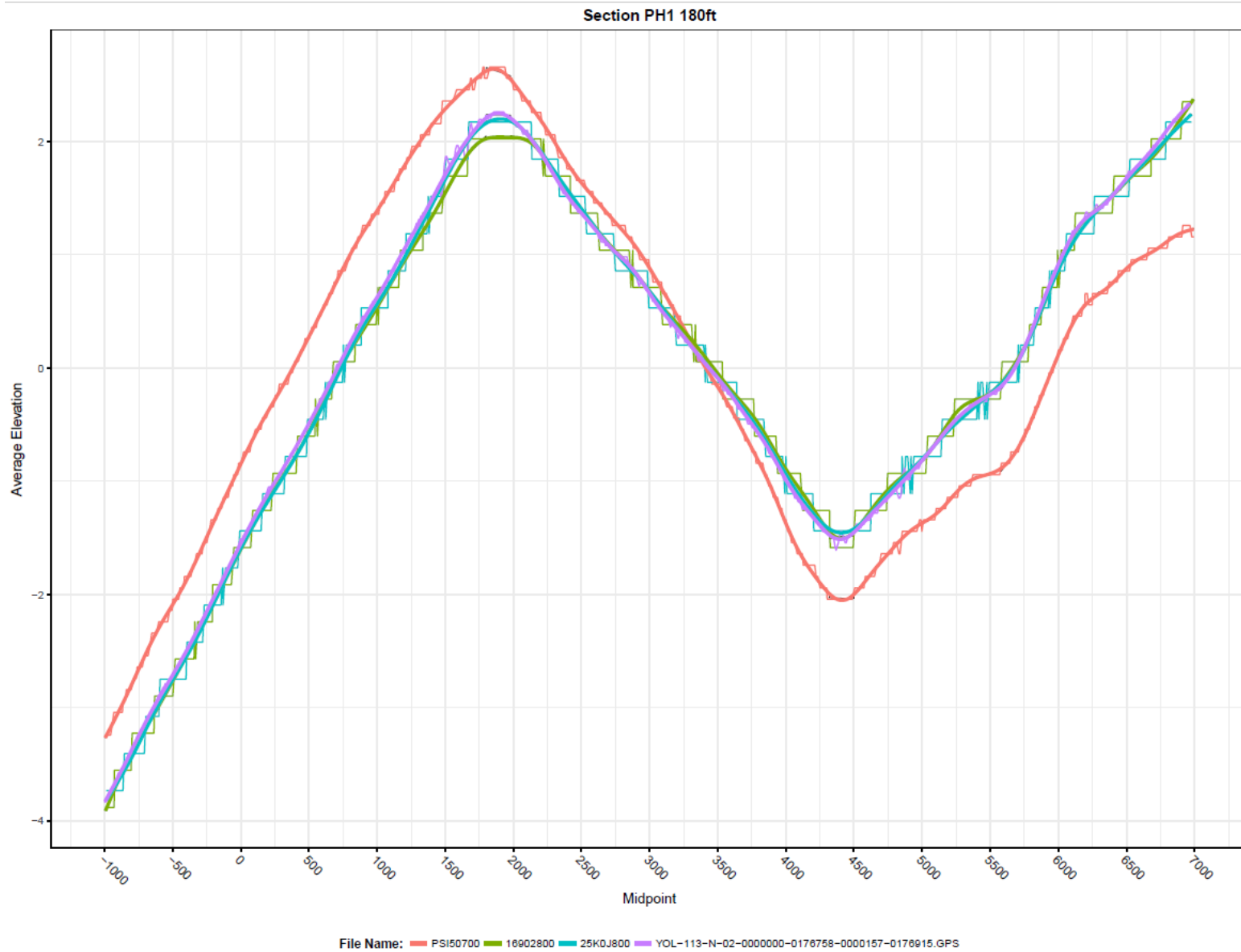
Note: PSI50700 [2015 APCS data] is selected for the analysis and the black line plot represents the linear model fit of elevation per subsection length.

Figure 3.4: Average elevation and subsection length plot for subsection length of 300 ft.



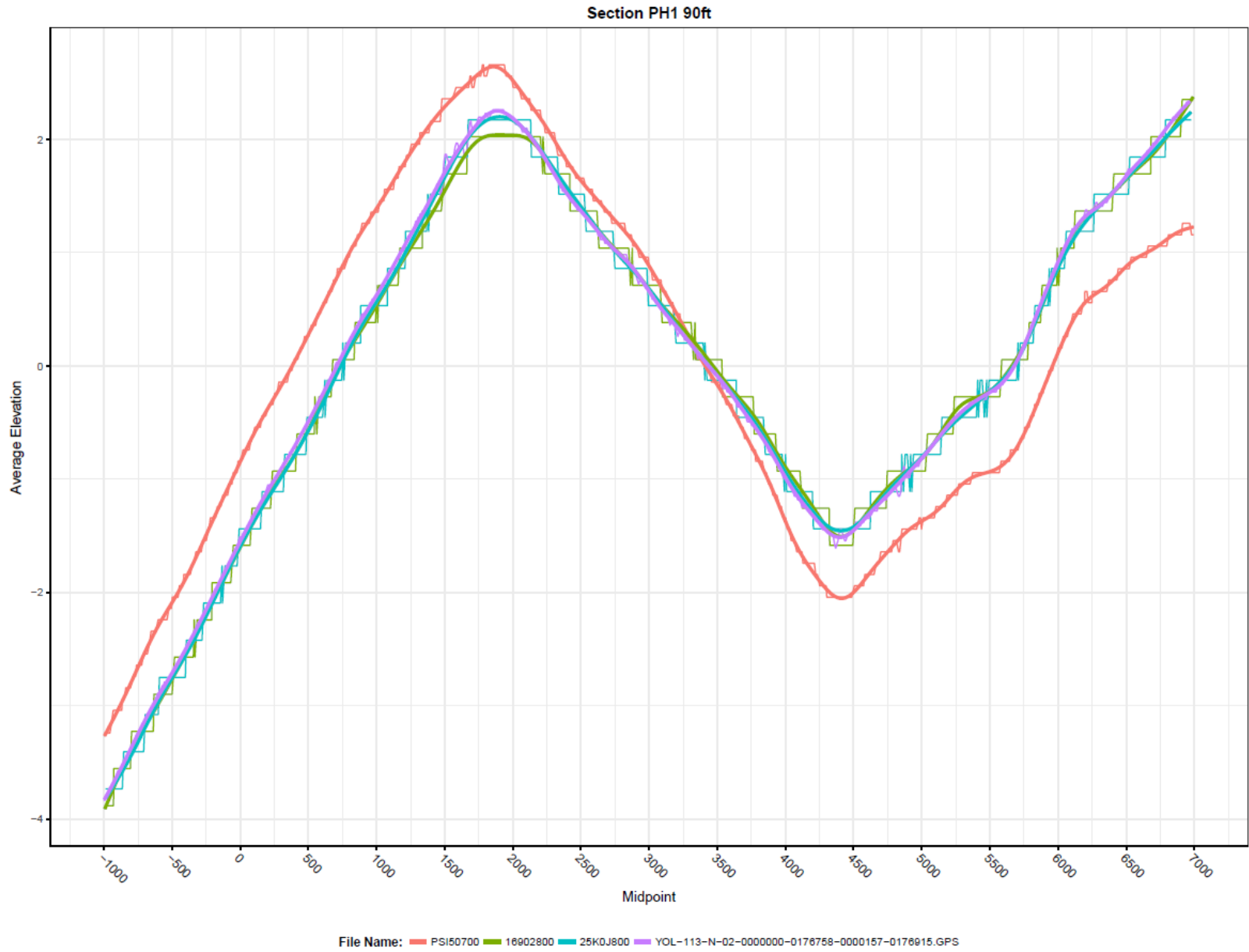
Note: PSI50700 (2015 APCS data) is selected for the analysis and the black line plot represents the linear model fit of elevation per subsection length.

Figure 3.5: Average elevation and subsection length plot for subsection length of 240 ft.



Note: PSI50700 (2015 APCS data) is selected for the analysis and the black line plot represents the linear model fit of elevation per subsection length.

Figure 3.6: Average elevation and subsection length plot for subsection length of 180 ft.



Note: PSI50700 (2015 APCS data) is selected for the analysis and the black line plot represents the linear model fit of elevation per subsection length.

Figure 3.7: Average elevation and subsection length plot for subsection length of 90 ft

Each plot was studied, and the following observations were made:

- Figure 3.3 (PH01 480 ft. [146 m]; the section was divided into subsection lengths of 480 ft.). At several locations (1500 to 2000, 4250 to 4500, 5500 to 5750, 6250), the linear model fit did not capture the slopes of the subsections correctly.
- Figure 3.4 (PH01 300 ft. [91 m]; the section was divided into subsection lengths of 300 ft.). At the locations around 1750 and 4500, the subsection slopes are positive. However, the linear model fits to present negative slopes for those subsections.
- Figure 3.5 (PH01 240 ft. [73 m]; the section was divided into subsection lengths of 240 ft.). At the locations between 4250 and 4500, the subsection slopes are negative. However, the linear model fits to present positive slopes for those subsections.
- Figure 3.6 (PH01 180 ft. [55 m]; the section was divided into subsection lengths of 180 ft.). The subsection lengths are small enough to best fit the average elevation data of the section. However, there are locations, such as between 1750 and 2000 and 4250 and 500, where the linear model lines are still visible.
- Figure 3.7 (PH01 90 ft. [27 m]; the section was divided into subsection lengths of 90 ft.). The linear model line hides under the average elevation data (orange line; 2015 APCS data). That is, it is at this subsection length that the linear model perfectly fits on the average elevation data of the subsections.

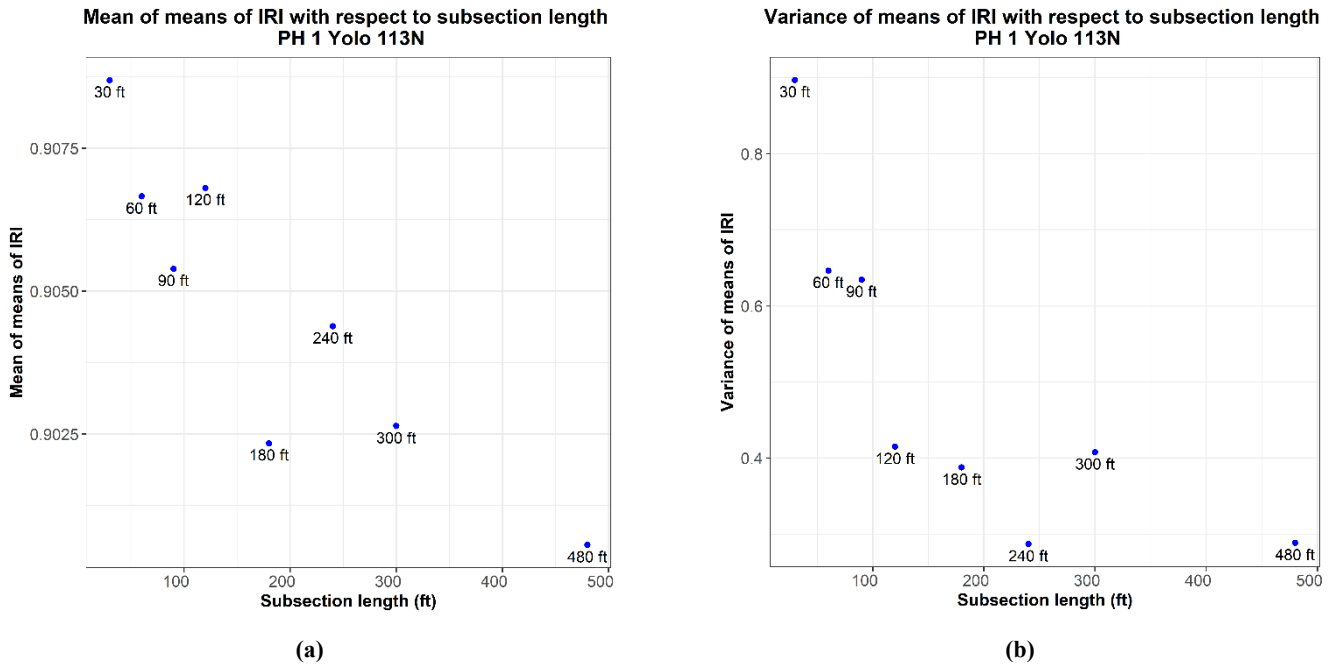
The same process was followed to look at other section plots. The next step was to study the variance of the mean of IRI for the sections at different subsection lengths.

3.2.3.2 Subsection Analysis Using Roughness (IRI) Data

Inertial profile data were recorded every 3.28 ft. (1 m) by the profiler. Analysis based on IRI was focused on the right wheelpath as being representative of the pavement roughness condition, because only the right wheelpath had a laser compatible with concrete pavement. The analysis method used is called the representative volume element (RVE) method. This was done in three steps:

1. The entire section was divided into equal subsection lengths of 30, 60, 90, 120, 180, 240, 300, and 480 ft. (9, 18, 27, 36.5, 55, 73, 91, and 146 m). The mean of IRI for each subsection was calculated.
2. The mean of the means of IRI for each subsection (calculated in the previous step) were then determined. This resulted in mean (for a section) of means (subsections) of IRI data for different subsection lengths (30, 60, 90, 120, 180, 240, 300, and 480 ft.).
3. The variance of the means of IRI were then calculated.

The mean and variance of the means of IRI were plotted for each section for all the subsection lengths considered. Figure 3.8 (a) and (b) shows example plots for PH01. It can be seen in Figure 3.8 (b) that the variance of the means of IRI reduces with an increase of the subsection lengths. Similar trends were seen for all the other sections.



Note: The data labels in the figures represent the mean and variance of the means of IRI values for the complete section based on subsection lengths.

Figure 3.8 (a) and (b): Example plots of RVE analysis based on IRI.

Based on the subsection analysis using gradient (slope), it was determined that 90 ft. (27 m) was the largest subsection length that could be used. The difference of variance of means of IRI between 90 ft. and larger subsection lengths was not that large. Therefore, the sections were divided into 90 ft. subsection lengths.

3.2.4 Data Compilation

Section 3.2.3 discussed how all the datasets for a section (less climate data, for which time was an important parameter) were adjusted to have the same starting and ending location for the shortest run length that had consistent speeds for all vehicles. The fuel consumption data for all the replicates per vehicle per section (as discussed in Section 3.2.2.1) were averaged for 90 ft. (27 m) subsection lengths. The section investigation data (as discussed in Section 3.2.2.2) were also averaged for 90 ft. subsection lengths. The date and time of the fuel consumption data for all the replicates per vehicle per section averaged for 90 ft. subsection lengths were aligned with the date and time of the weather station data.

3.2.5 *Second Order Data Cleaning*

Once all the runs per section per testing season per vehicle were sorted, the next step was to further clean the data to remove any outliers missed in the first order data cleaning. The subsections data from before, over, and after the culverts that were present in a few sections were treated as anomalies and removed from the datasets. Then an outlier analysis was performed on the replicate fuel consumption readings of a vehicle for each 90 ft. (27 m) subsection. The interquartile range rule (IQR) was used to determine the outliers. Two flag columns were created in the dataset, one with 1.5 IQR and the other with 2.5 IQR.

Plots of the datasets after the second order cleaning exercise still showed outliers. An example of car fuel consumption and vehicle speed data on section PH01 during summer nighttime testing is shown in Figure 3.9. The top plot in the figure shows fuel consumption versus distance, and the bottom plot shows vehicle speed versus distance. The two plots in the figure shows similar trends, but runs 3 and 15 show different trends at the beginning of the section. In the case of run 3, the vehicle accelerates while it reaches the cruise control speed. This causes the fuel consumption to increase to approximately 6.5 mL per subsection and then rapidly drop, before stabilizing close to the section average of 1.7 mL per subsection. This increase and decrease of fuel consumption are clearly related to vehicle speed adjustment, either by cruise control or the drivers' efforts to reach the test speed. Similar trends were visible for other vehicles on other sections, which indicates a few runs where the vehicles were unable to reach the testing speed on certain test sections or where drivers applied their brakes before completing the data collection on the entire section.

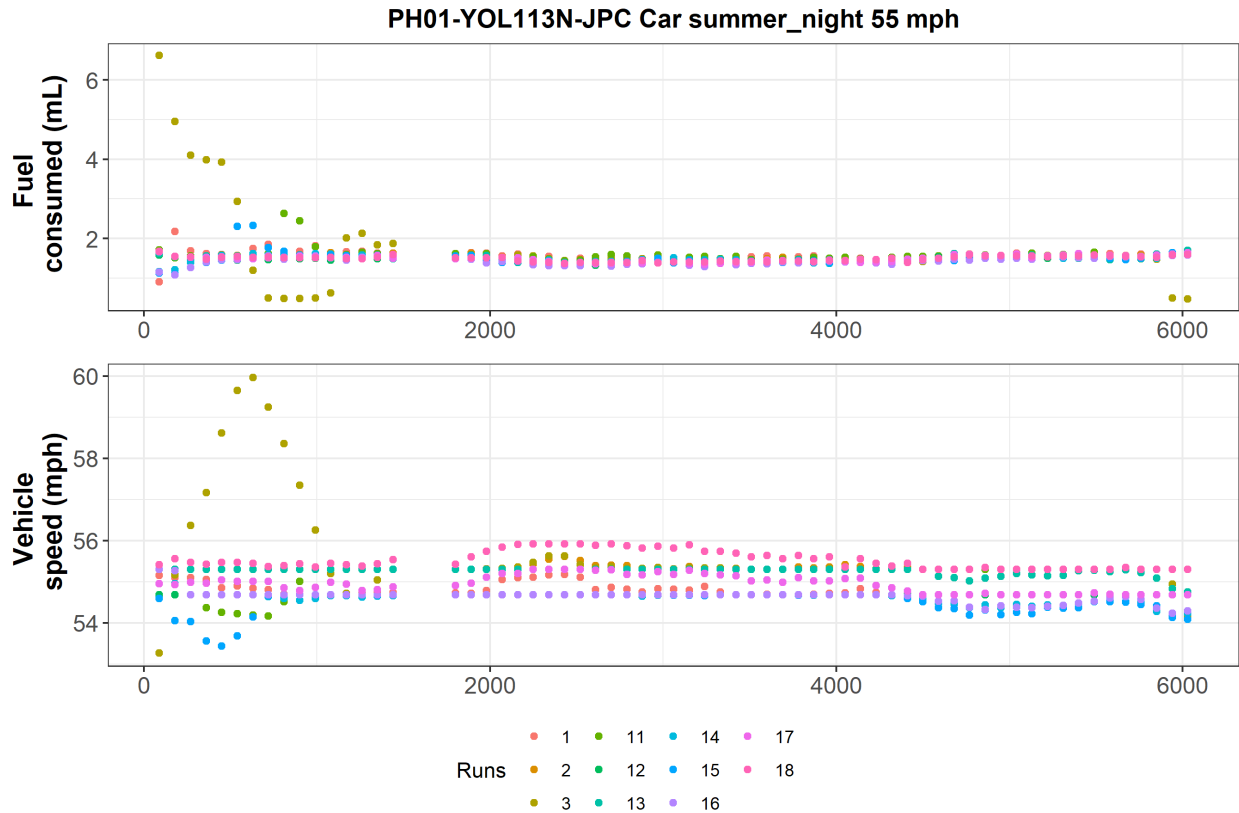


Figure 3.9: Example plot of car fuel consumption and vehicle speed data used to identify bad data.

A separate identification process was used to find the exact subsection numbers that showed bad speeds. This procedure included plotting all the runs (vehicle speed versus subsection ID) of a vehicle per section per testing day (fuel consumption data collection day) and then flagging each subsection and runs using four different flags: “bad,” “bad begin,” “bad end,” and “good” (see Figure 3.10):

- The “bad” categorization is used when the entire run has inconsistent observations and the data show that the vehicle was not at the testing speed.
- “Bad begin” refers to the runs where at the beginning of the run the vehicle either accelerated or decelerated.
- “Bad end” refers to the runs where at the end of the run the vehicle either accelerated or decelerated.
- “Good” refers to the runs free of aberrations.

All but the good runs were removed from the dataset. It is important to note that arriving at an unbiased dataset was the goal of the data cleaning exercise. In this experiment, the length of the sections and the number of replicates were the two most important parameters. Dropping too many runs reduced the number of replicates, while truncating too many subsections from the start and end of the section reduced the section length. Thus, if

the speed at the beginning or end of the run was within a 1 mph (1.6 km/hr) range of the average speed of that run, the data were marked as good. If one or two runs out of seven had a bad start or a bad end, the entire run was deleted; however, if a few runs showed similar behavior, no data were truncated.

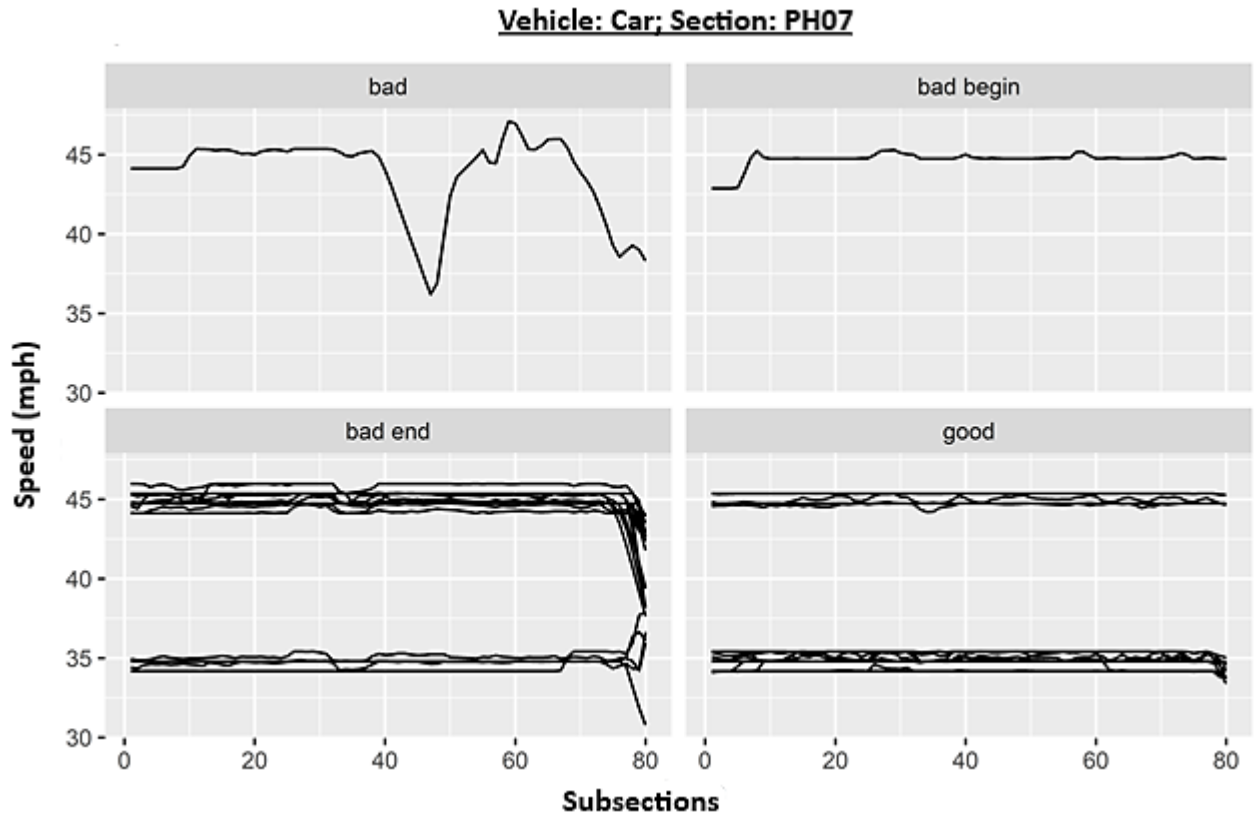


Figure 3.10: Example of tagging runs for car speed data on Section PH07.

After data cleaning, the final total number of runs and replicates for each vehicle per speed per section per season were tabulated and are shown in Appendix O.

3.3 Data Verification

The data were next visually checked by plotting cleaned OBD data (fuel rate and vehicle speed), climate data (headwind/tailwind [mph] and air density [lb./ft³]), and pavement section data (gradient [%] and IRI [in./mi.]) on the same figure. The trends were studied to verify they were correct, and the different data types were checked to be correctly synced. Figures for each vehicle on each section per speed and testing season are presented in Appendix P. A few example figures are presented and interpreted in the following discussion.

Figure 3.11 is an example plot of data for the car running at 45 mph (72 km/hr) on section PH02 (JPC pavement) during nighttime summer testing. The figure is divided into three sections represented by colored boxes containing

two figures each. The top blue box presents OBD data, the middle red box the climate data, and the bottom green box the pavement section data. The blue box in the figure embeds two plots of fuel rate (mL/s) and vehicle speed (mph) versus the subsections. The red box contains two plots of effective headwind (mph) and air density (lb/ft³) versus subsections. The green box contains two plots of gradient (%) and IRI (in./mi.) versus the subsections. Each dot in the figure is the average data value on a 90 ft. (27 m) subsection.

Each colored dot in the figure represents a single run-on section PH02 by the car at 45 mph (72 km/hr) during the nighttime summer testing. Each plot shows the data for section gradient and IRI, which do not change during the runs. Therefore, they were only collected once, before the fuel economy testing. The data missing between subsections 35 and 40 were removed in the cleaning process (see Section 3.2.5) because they were collected on a culvert⁶ on section PH02.

A common observation for all the figures is that the vehicle fuel consumption or fuel rate trends follow the section gradient profile (i.e., an increase in gradient results in an increase in fuel rate, and a decrease in gradient causes the vehicle to consume less fuel). If the trend is not observed to be the same for certain subsections during a run, then other factors—such as aerodynamics (headwind and/or air density) and pavement roughness—may have affected fuel consumption. As cruise control was used in the experiment, the vehicle’s computer continuously evaluated the resistance to flow and tried to keep the vehicle running at a predetermined constant speed during the testing.

⁶ Culverts and bridges are not part of this study.

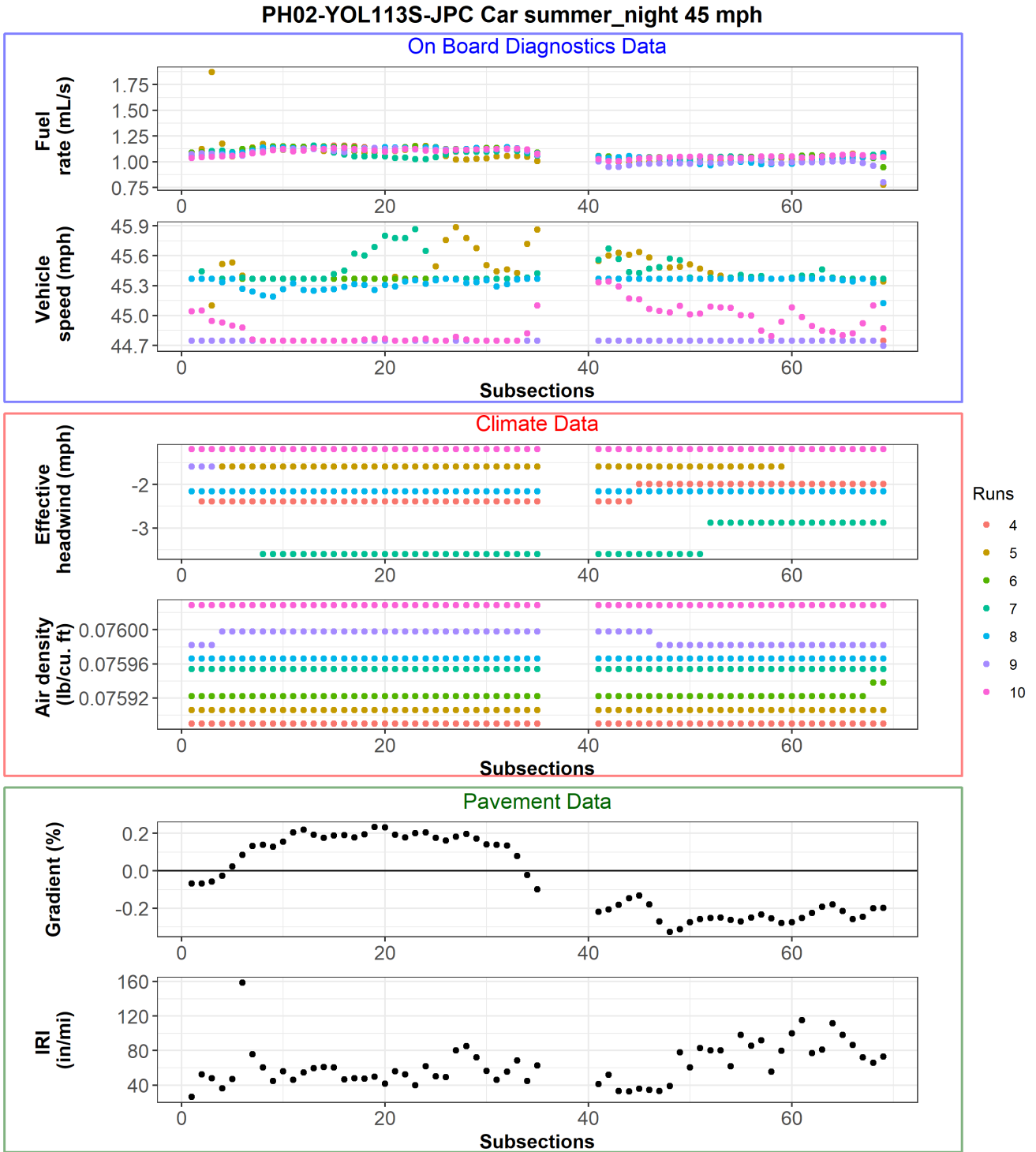


Figure 3.11: Fuel rate, vehicle speed, effective headwind, air density, gradient, and IRI for each subsection and multiple runs: summer nighttime testing using car at 45 mph on section PH02.

Figure 3.12 and Figure 3.13 are examples of the HHDT running at 55 mph (88 km/hr) on section PH09 (asphalt pavement) on a summer day and a winter day, respectively. (Note: To show the distinctive trends and plot profiles,

the Y-axis scale in both figures has not been fixed.) In both seasons, the fuel rate change is within 2 mL/s for the first 175 90 ft. subsections (15,750 ft. [4,800 m] from the start of the section). This is because the gradient did not change (within 0.1% range). But, as soon as a change in gradient is observed (subsections 175 to 190), the fuel rate changed as well. A similar trend can be seen in the vehicle speed plot. Although the change is very small (0.2 mph [0.3 km/hr]), it is clearly visible in the figures.

A general trend observed in almost all the cases (for all the vehicles on all the sections) is that the fuel rate (and fuel consumption) during winter is higher than during summer. The factors that may have caused this increase in fuel consumption during winter could be air density, the use of oxygenated (lower-energy density) fuel, and/or vehicle engine behavior (25).

The air density was always observed to be higher during the winter season than the summer season due to the low air temperatures. Considering the current example, the average air density for the winter testing day can be read as 0.076 lb./ft³ (1.22 kg/m³; see Figure 3.13) and for the summer testing day as 0.071 lb./ft³ (1.14 kg/m³; see Figure 3.12). The increased air density increases the vehicle's flow resistance, resulting in greater fuel consumption. A study by the US Environmental Protection Agency (US EPA), as temperatures dropped from 75 to 45°F (24 to 7°C), fuel consumption by vehicles in urban areas increased by 12% to 28% (25). Bomb calorimeter testing was performed on the fuel samples collected during the winter and summer testing cycles, and it was found that there was a slight reduction (around 1 MJ/kg) in the calorific value of gas in the oxygenated winter fuel blend. This may have resulted in increased fuel consumption during the winter testing cycle (see Appendix K for details).

With an increase in vehicle speed within a single gear, an increase in fuel rate is obvious, as can be seen in all the cases in this study. Figure 3.14 and Figure 3.15 present examples of the SUV running on section PH21 (JPCP) during a winter testing day at 45 mph and 55 mph (72 km/hr and 88 km/hr), respectively. During the 45 mph testing, the average recorded fuel rate of the SUV was 1.3 mL/s, while at 55 mph (on the same section during the same testing day) it was around 1.75 mL/s.

Plots of fuel consumption per vehicle on all the sections versus vehicle engine RPM for each vehicle are presented in Appendix O.

PH09-SUT113N-RHMA-O HHDT summer_day 55 mph

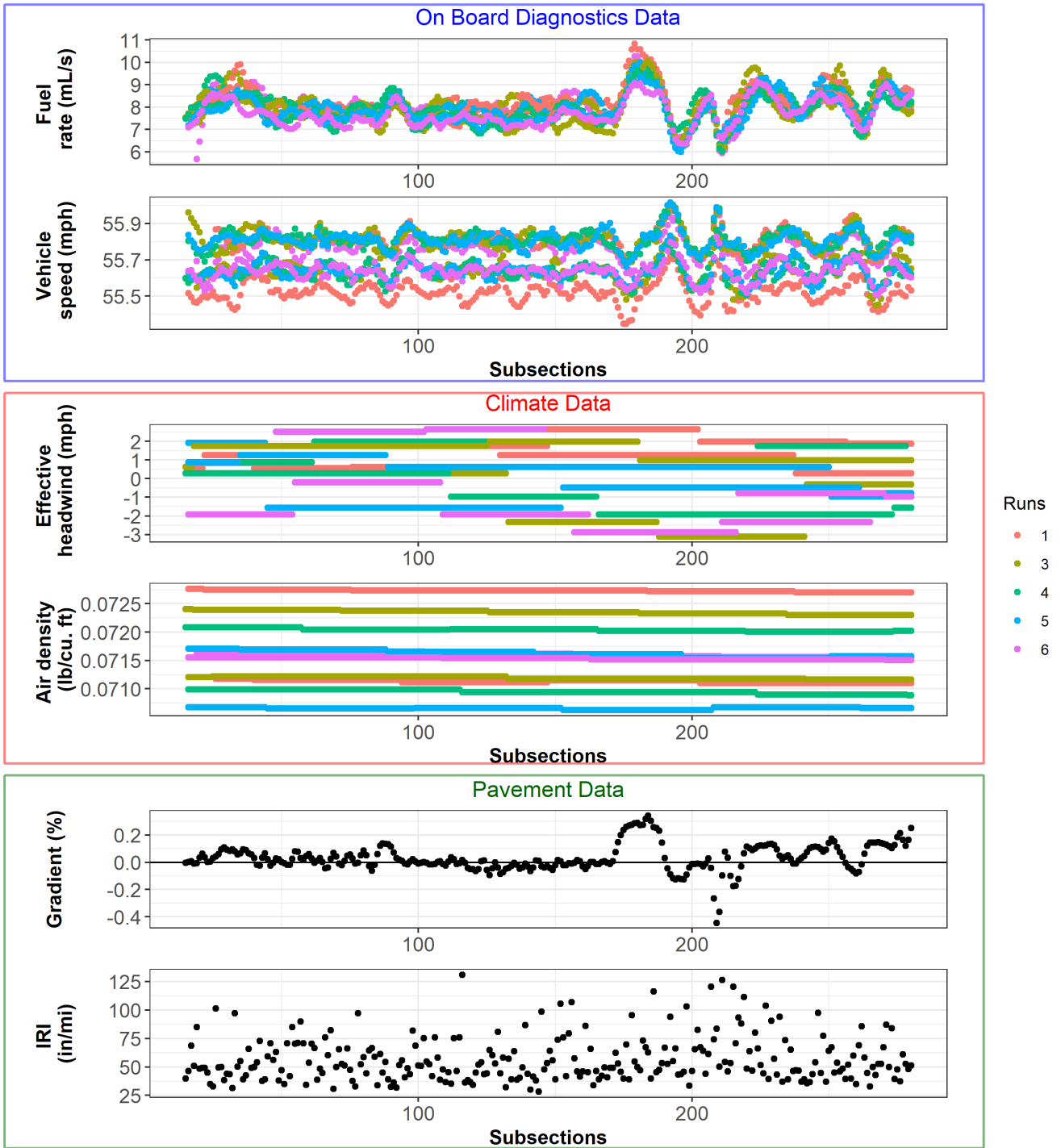


Figure 3.12: Fuel rate, vehicle speed, effective headwind, air density, gradient, and IRI for each subsection and multiple runs: summer daytime testing using HHDT at 55 mph on section PH09.

PH09-SUT113N-RHMA-O HHDT winter_day 55 mph

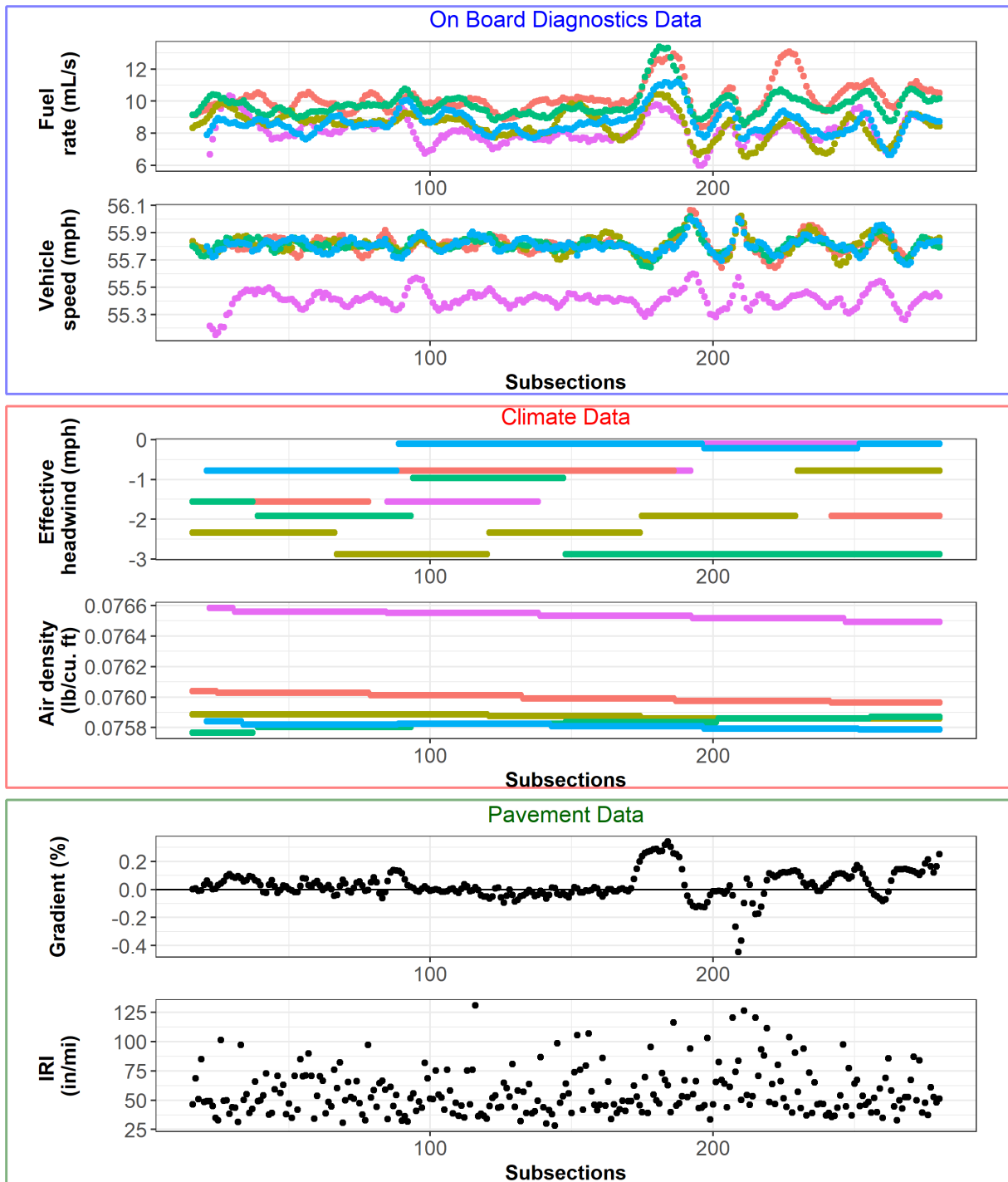


Figure 3.13: Fuel rate, vehicle speed, effective headwind, air density, gradient, and IRI for each subsection and multiple runs: winter daytime testing using HHDT at 55 mph on section PH09.

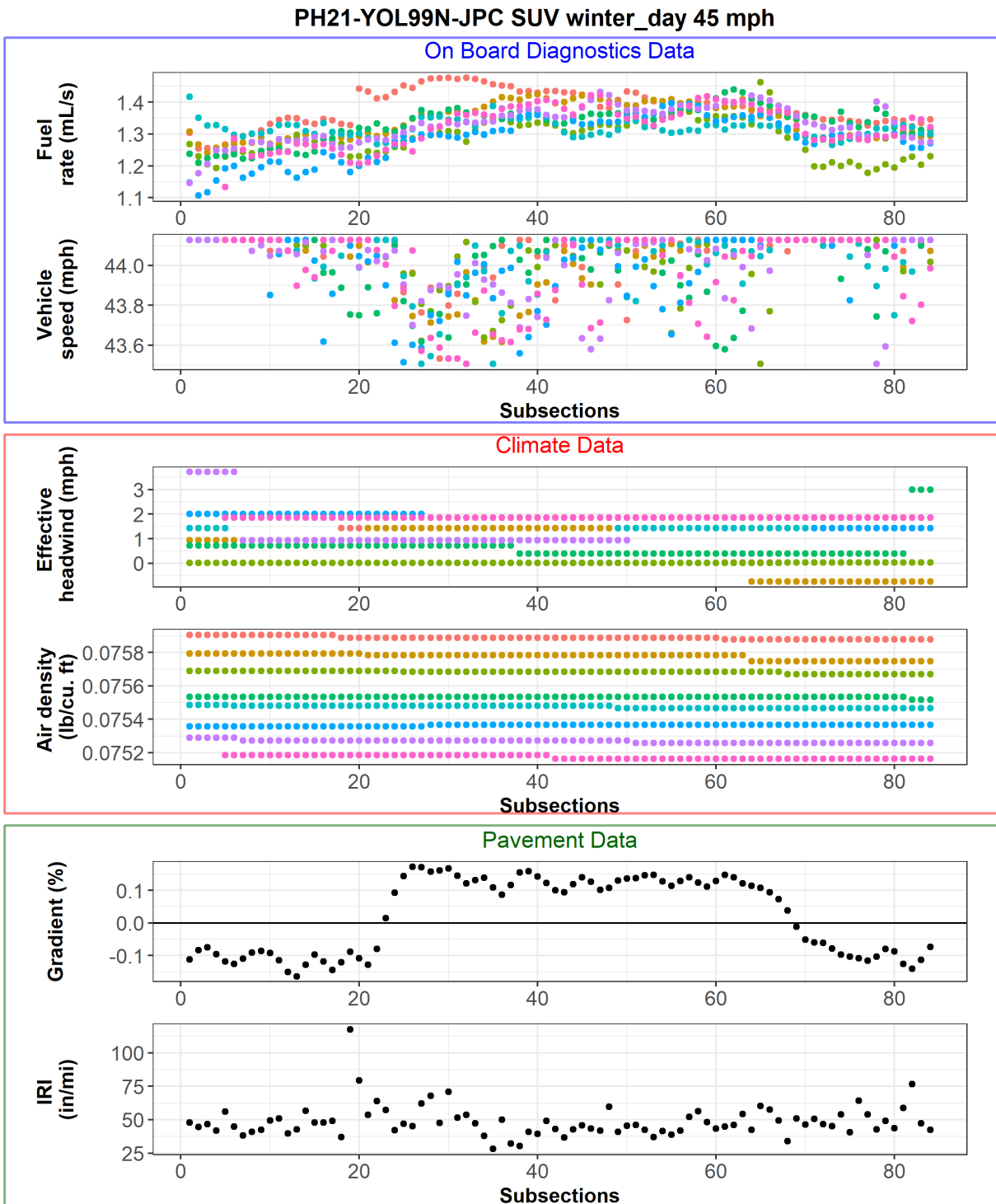


Figure 3.14: Fuel rate, vehicle speed, effective headwind, air density, gradient, and IRI for each subsection and multiple runs: winter daytime testing using SUV at 45 mph on section PH21.

PH21-YOL99N-JPC SUV winter_day 55 mph

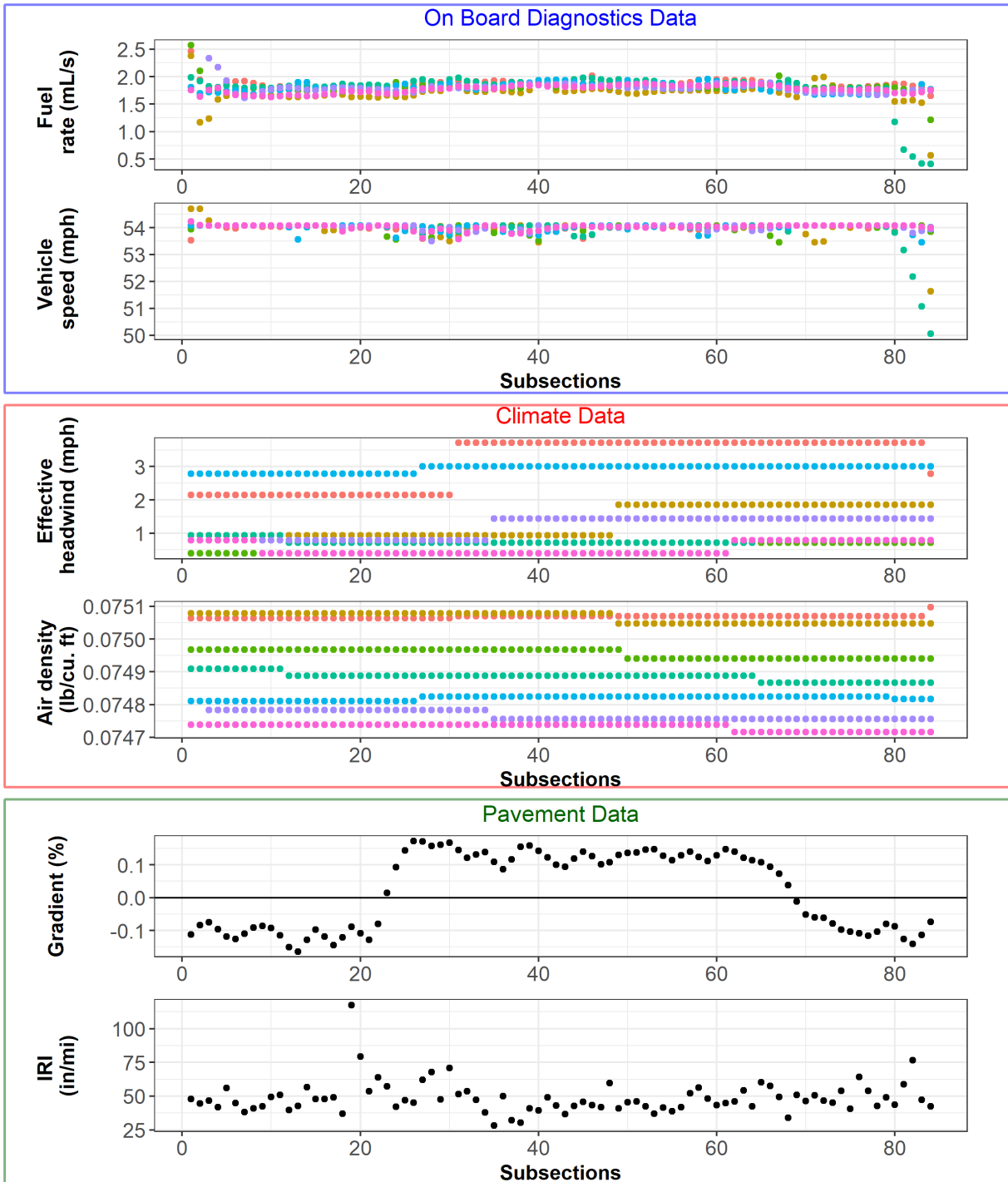


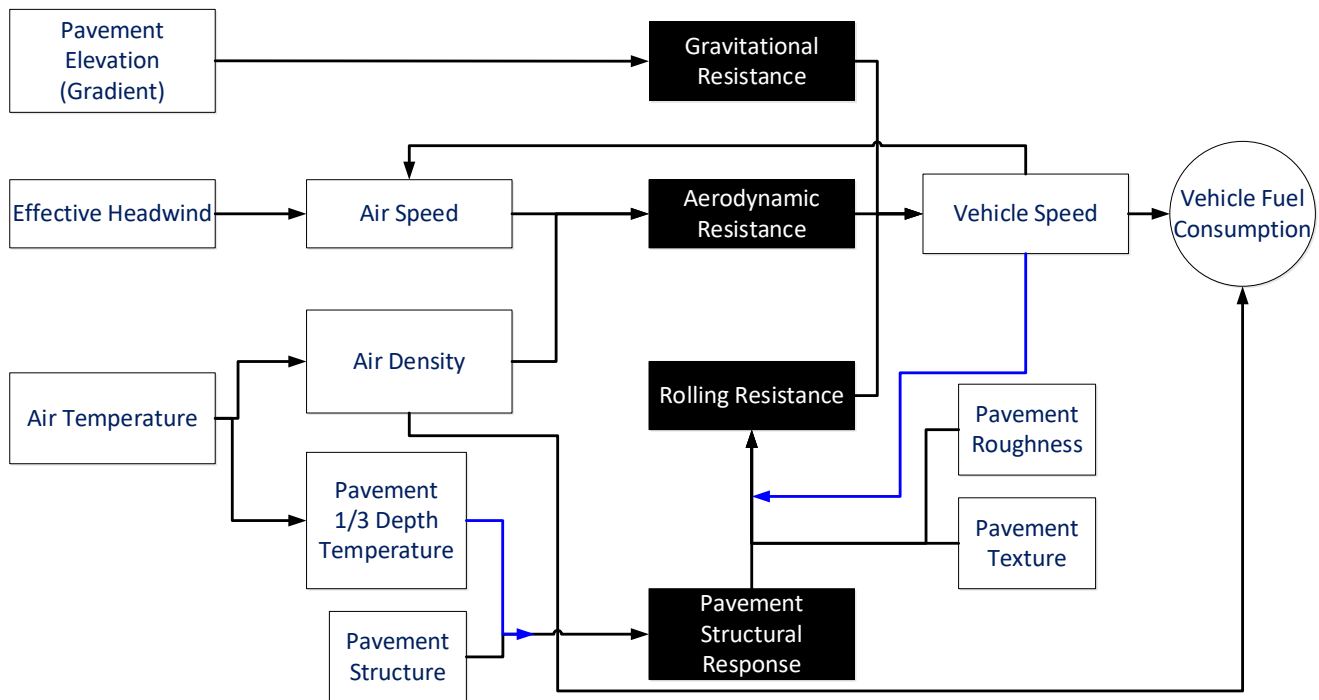
Figure 3.15: Fuel rate, vehicle speed, effective headwind, air density, gradient and IRI for each subsection and multiple runs: winter daytime testing using SUV at 55 mph on section PH21.

4 EMPIRICAL DATA ANALYSIS AND MODELING

This chapter documents the process of formulating and then creating an empirical model. The modeling process was made difficult by the experiment’s number of explanatory variables, feedback loops, and interactions.

4.1 Empirical Modeling of Vehicle Fuel Consumption

The initial step in modeling was to develop a broad conceptual model of the primary variables believed to influence the fuel consumed by a vehicle driven on cruise control. Figure 4.1 presents a directed acyclic graph of the key variables and causal links. The goals of this framework were to examine if the effects of pavement on fuel efficiency could be observed in the field on the basis of experimental design, and to explore the relative magnitude of those effects. Detailed theories of pavement structural responses that are covered in other modeling frameworks were not considered in this approach.



Note: Black arrows indicate a causal effect direction, white boxes indicate measured predictor variables, black boxes indicate unmeasured constructs, white circle represents the outcome, and blue arrows indicate moderating effects (interactions).

Figure 4.1: Directed acyclic graph representing the conceptual model of vehicle fuel consumption.

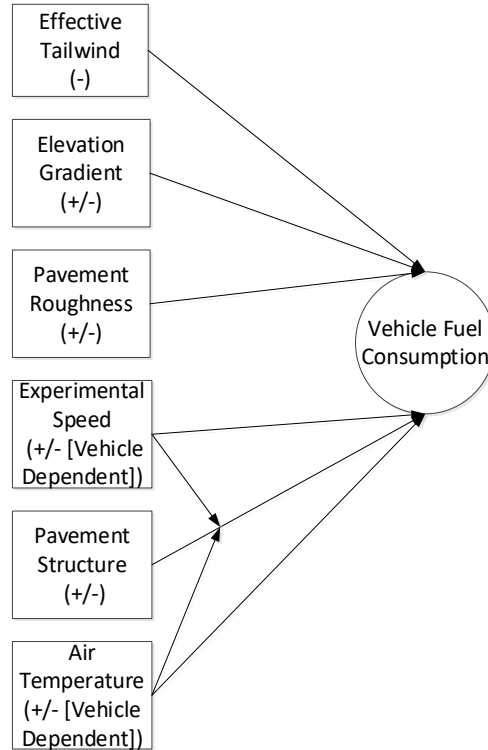
Translating the conceptual model shown in Figure 4.1 to statistical models proved challenging. As the conceptual model indicates, clear feedback loops in the model cannot be handled in most statistical modeling frameworks, such as linear regression. While some more complex modeling frameworks (e.g., structural equation models)

allow such feedbacks, the other complexities of the data (e.g., serial autocorrelation, large number of records, and multilevel structure) forced the need for a parsimonious statistical framework.

Fuel consumed is modeled through linear regression because it is a continuous variable. While fuel consumed cannot be negative, the model is not constrained to positive reals because in some cases zero fuel was recorded in a subsection; this could be due to cruise control adjustment by the vehicle when traveling downhill. As mentioned previously, all the complexities presented in Figure 4.1 could not be included in a linear regression. Thus, to model fuel consumption using linear regression, the conceptual model was simplified to remove the feedbacks; the most important simplification made was the removal of the vehicle's real-time speed. Real-time speed is managed/adjusted by the vehicle controller once cruise control is set, and it acts as a mediating variable for all the upstream effects on fuel consumption (e.g., gradient, pavement structure, and others, as shown in Figure 4.1). By removing real-time speed, the conceptual model can be revised with direct causal links from the explanatory variables to the response variable (fuel consumed).

Several other casual links in the model were also simplified, such as not including separate variables for air and pavement temperatures in the statistical models because of extreme collinearity between those two explanatory variables. This collinearity is due to pavement temperature mediating the effect of air temperature on the structural response, as shown in Figure 4.1. Instead, the model used only air temperature, which was interpreted as having an effect on fuel consumption through two pathways. The first is air density changes that alter aerodynamic resistance, and slight changes to combustion efficiency, if any. The second pathway arises from pavement temperature changes that result in varying losses in vehicle energy attributable to changes in rolling resistance from changes in the pavement's structural response.

Vehicle speed was kept as a categorical variable (e.g., the speed that cruise control was set at in the experimental run) so that the potential interactions of temperature, speed, and pavement type could be compared. Finally, pavement macrotexture (mean profile depth [MPD]) was also removed from the models after testing revealed that it had little to no effect on fuel consumption. The resulting final simplified model is presented in Figure 4.2.



Note: White boxes indicate measured predictor variables, and the white circle represents the outcome. Arrows leading to other arrows indicate moderating effects interactions).

Figure 4.2: Simplified directed acyclic graph representing the conceptual model used for linear regression.

4.1.1 Examination of Autocorrelation

The data in this experiment have strong temporal (serial) autocorrelation. Using autocorrelation function (ACF) plots of linear model residuals, models that were created without accounting for temporal order of the data revealed considerable autocorrelation for nearly every experimental run (99% of the runs). This autocorrelation arises from the fact that the vehicle controller is constantly adjusting fuel consumption as the vehicle experiences forces from aerodynamic resistance, gravity, and rolling resistance. Strong autocorrelation has the potential to bias the estimation of the parameters relating the predictor variables to fuel consumption, and it has the potential to greatly reduce the predictive ability of the model if not properly removed or modeled. The following methods were used to examine the autocorrelation and account for it in the models.

4.1.1.1 Comparison of Predictive Ability of Linear Regression Models Considering Autoregressive Error Structure Using Repeat Cross Validation

Using the heavy heavy-duty truck (HHDT) data, repeat cross validation was performed for a model with and without an autoregressive error structure. The HHDT data were chosen for this examination because it was

assumed that these data have the largest signal-to-noise ratio of all the vehicles with respect to effects from pavement parameters. Test and training data were created using the following procedure:

1. To select four experimental runs for each cross classification of the variables listed and call them the test data, use stratified random sampling (by temperature category [$> 75^{\circ}\text{F}$ and $\leq 75^{\circ}\text{F}$ (25°C)], pavement structure type, and experimental speed [35, 45, and 55 mph (56, 72, and 88 km/hr)]) without replacement.
2. Use the same stratified random sampling scheme as in step 1, but sample only from the remaining data (without replacing the test data), and call this the training data.
3. Repeat steps 1 and 2 ten times.
4. Run each of the two statistical models on each of the 10 training datasets resulting in 20 model fits (10 for each model).
5. For each model fit that is not rejected, calculate the root mean square error (RMSE) and the mean absolute error (MAE) by using the testing data for prediction.

The results of this examination is presented in Table 4.1, which shows that the model with the autoregressive error term, AR (1), consistently outperforms the model without that term.

Table 4.1: Cross Validation Prediction of HHDT Model With and Without Autoregressive Errors

Cross Validation Run	Model with AR (1)		Model without AR (1)	
	RMSE	MAE	RMSE	MAE
1	0.43	0.25	1.15	0.85
2	0.59	0.41	1.37	0.98
3	0.40	0.25	1.26	0.91
4	0.51	0.28	2.70	1.53
5	0.45	0.25	5.09	1.60
6	0.39	0.24	1.58	1.09
7	0.44	0.25	1.30	0.93
8	0.58	0.41	1.04	0.75
9	0.41	0.24	1.48	1.02
10	0.40	0.25	1.33	0.94
Average	0.46	0.28	1.83	1.06

4.1.1.2 Compare Regression Coefficients of the Linear Regression Model

Using the same two models, one with and one without the autoregressive error term, with the full dataset, the predicted conditional effects were plotted, and a visual comparison was made between the mean parameter values and between their uncertainties. Since the autoregressive term is estimated at 0.97 (95% confidence interval from 0.97 to 0.98), the AR (1) model suggests very strong one-lag correlation, meaning correlation between observations for any two 90 ft. (27 m) subsections adjacent in time and space, unaccounted for in the model without the AR (1) term. However, all regression parameters show similar conditional effects with the following

exceptions. The AR (1) model reports slightly less of an effect from gradient and more uncertainty in the effect. It also shows slightly less of an effect of pavement roughness and more uncertainty in the effect. Finally, the AR (1) model shows much larger standard deviations for the varying effects and more uncertainty. All of these differences suggest that the models without the AR (1) term are likely producing slightly biased estimates for gradient and pavement roughness. More importantly, however, it shows that the model without the AR (1) term is not adequately representing the uncertainty and variability of all of the estimates of pavement type.

For the following are reasons the AR (1) model form was chosen for further study/investigation:

1. It more closely represents the data-generating mechanism (e.g., a vehicle controller on conventional cruise control depends on forces in the past).
2. It shows more conservative estimates of effects and more conservative estimates of the variability within-pavement type.
3. It shows consistent improvement in prediction based on repeat cross validation.

4.1.2 Model Structure

To analyze the full data, the study employed multilevel linear regression models. They were used to analyze each experimental run for the autocorrelation parameters, and by pavement structure to analyze for the main effects. The models were framed by experimental runs and by pavement structure because the experimental design created grouped data (i.e., data repeatedly collected on each pavement structure one run at a time in different conditions). More specifically, the models have varying intercepts (mean effects) for each pavement type (section) and varying slopes by the interactions of those pavement types with experimental speeds and air temperatures. The models' errors are assumed to be autocorrelated with a lag of one subsection, often termed linear regression with AR (1) errors within each experimental run. This is nearly analogous to a grouped time series model with covariates. The grouped AR (1) error structure reduced autocorrelation for a large majority of experimental runs. Models with additional autoregressive terms were considered, but they resulted in increased model runtimes without decreasing the autocorrelation. Any residual autocorrelation from the chosen models should not bias the magnitude of the main effects but may slightly underestimate the uncertainty of the effects.

Because of the numerous complexities in the linear regression, a flexible and robust Bayesian modeling framework was used. The models were estimated using the R package BRMS (Bayesian Regression Models using “Stan”) as an interface for the Stan statistical environment. By using this estimation procedure, the full uncertainty in the primary effects of concern (e.g., pavement structures) on the fuel economy is considered. A separate model for each of the four vehicles was estimated because of the differences in fuel type (diesel versus gasoline) and,

therefore, energy density; this implies that the fuels consumed by the cars and trucks are not comparable because of different energy densities. The data for the two vehicles with the same fuel type were not pooled because in that case interactions would have been needed for all the variables by vehicle leading to three-way interactions with varying slopes, and these interactions were computationally too costly. Given the large amount of data and separate models for each vehicle, the model runtimes were already burdensome for testing (ranging from 2 to 9 days). Furthermore, it was intentional to have a separate model for each vehicle class type so that when these vehicle fuel consumption empirical models are used in the models, such as a life cycle assessment use stage model, better fuel consumption predictions could be made based on vehicle class types. No advantage was seen for having one model with four distinct vehicle types in it because vehicle type is not a continuum (there are distinct types) and because the vehicles used in the experiment are reasonably representative of the typical classifications of vehicles in the fleet.

The general model equation is as follows:

$$\begin{aligned}
 F_i &\sim \text{Normal}(\mu_i, \sigma) \\
 \mu_i &= A_i + \beta_{S45,i}S45_i + \beta_{S55,i}S55_i + \beta_{S35T,i}T_i + \beta_{S45T,i}S45_iT_i + \beta_{S55T,i}S55_iT_i \\
 &\quad + \beta_G G_i + \beta_{ET}ET_i + \beta_{S35LR}LR_i + \beta_{S35LT}LT_i + \varepsilon_{run}[i] \\
 A_i &= \alpha + \alpha_{segment}[i] \\
 \beta_{S45,i} &= \beta_{S45} + \beta_{S45,segment}[i] + \beta_{S45LR}LR_i + \beta_{S45LT}LT_i \\
 \beta_{S55,i} &= \beta_{S55} + \beta_{S55,segment}[i] + \beta_{S55LR}LR_i + \beta_{S55LT}LT_i \\
 \beta_{T,i} &= \beta_T + \beta_{T,segment}[i] \\
 \beta_{S45T,i} &= \beta_{S45T} + \beta_{S45T,segment}[i] \\
 \beta_{S55T,i} &= \beta_{S55T} + \beta_{S55T,segment}[i] \\
 \varepsilon_{run}[i] &= \rho \varepsilon_{run}[i-1] \\
 \begin{bmatrix} \alpha_{segment} \\ \beta_{S45,segment}[i] \\ \beta_{S55,segment}[i] \\ \beta_{T,segment}[i] \\ \beta_{S45T,segment}[i] \\ \beta_{S55T,segment}[i] \end{bmatrix} &\sim \text{Normal} \left(\begin{bmatrix} 0 \\ 0 \\ 0 \\ 0 \\ 0 \\ 0 \end{bmatrix}, \begin{bmatrix} \sigma_\alpha \\ \sigma_{\beta_{S45}} \\ \sigma_{\beta_{S55}} \\ \sigma_{\beta_T} \\ \sigma_{\beta_{S45T}} \\ \sigma_{\beta_{S55T}} \end{bmatrix} \right) \\
 \alpha &\sim \text{Normal}(0, 4) \\
 (\beta_{S45}, \dots, \beta_{LT}) &\sim \text{Normal}(0, 2) \\
 \sigma &\sim \text{Half Student-t}(3, 0, 4) \\
 (\sigma_\alpha, \dots, \sigma_{\beta_{S55T}}) &\sim \text{Half Student-t}(3, 0, 4) \\
 \rho &\sim \text{Normal}(0, 1), \text{ constrained by } -1 < \rho < 1
 \end{aligned}$$

Where F_i is the fuel consumed (mL) on a 90 ft. (27 m) subsection i , $S45_i$ is an indicator for when cruise control speed is at 45 mph (72 km/hr), $S55_i$ is an indicator for when cruise control speed is at 55 mph (88 km/hr), T_i is temperature ($^{\circ}\text{F}$), G_i is elevation gradient, ET_i is the effective tailwind (m/s), LR_i is an indicator for low pavement

roughness ($IRI < 168$ in./mi. [2.68 m/km]), and LT_i is an indicator for low pavement texture ($MPD < 1.2$ mm). μ_i is the linear model for mean fuel consumed (mL), and σ is the standard deviation of fuel consumed. μ_i consists of a series of terms. A_i is the intercept linear model with α as the grand mean and $\alpha_{segment[i]}$ as the segment mean indexed by subsection i when experimental speed is 35 mph (56 km/hr, base experimental speed). All the other variables are at their means (or at 0 for indicator variables). $\beta_{S45,i}$ is the linear model for experimental speed effects at 45 mph with β_{S45} as the mean effect of 45 mph speed. $\beta_{S45,segment[i]}$ is the vector of segment level effects of 45 mph speed. $\beta_{S55,i}$ is the linear model for experimental speed effects at 55 mph with β_{S55} as the mean effect of 55 mph speed, and $\beta_{S55,segment[i]}$ is the vector of segment level effects of 55 mph speed. $\beta_{T,i}$ is the linear model for air temperature effects with β_T as the grand mean effect of air temperature and $\beta_{T,segment[i]}$ as the vector of segment level effects of air temperature. $\beta_{S45T,i}$ is the linear model for the interaction of experimental speed of 45 mph and temperature effects with β_{S45T} as the mean interaction effect of 45 mph speed and air temperature. $\beta_{S45T,segment[i]}$ is the vector of segment level interaction effects of 45 mph speed and air temperature. $\beta_{S55T,i}$ is the linear model for the interaction of experimental speed of 55 mph and temperature effects with β_{S55T} as the mean interaction effect of 55 mph speed and air temperature. $\beta_{S55T,segment[i]}$ is the vector of segment level interaction effects of 55 mph speed and air temperature. $\varepsilon_{run[i]}$ is the linear model for the regression errors ρ representing the serial correlation with the prior subsection i within each experimental run. All other β parameters describe the conditional association between fuel consumed and the variables in their products.

All the effects that vary by test section are modeled in a multilevel fashion where they are assumed to be normally distributed with mean zero and independent standard deviations (i.e., this model assumes the varying effects have zero correlation). Other models including correlation structures were explored, but they all showed very little varying effect correlation and resulted in much longer model runtimes. All parameters are given “weakly informative” priors—including distributions for regression parameter and student distribution for standard deviations—to reduce the risk of overfitting. All such priors are common choices when estimating multilevel models in Stan (26).

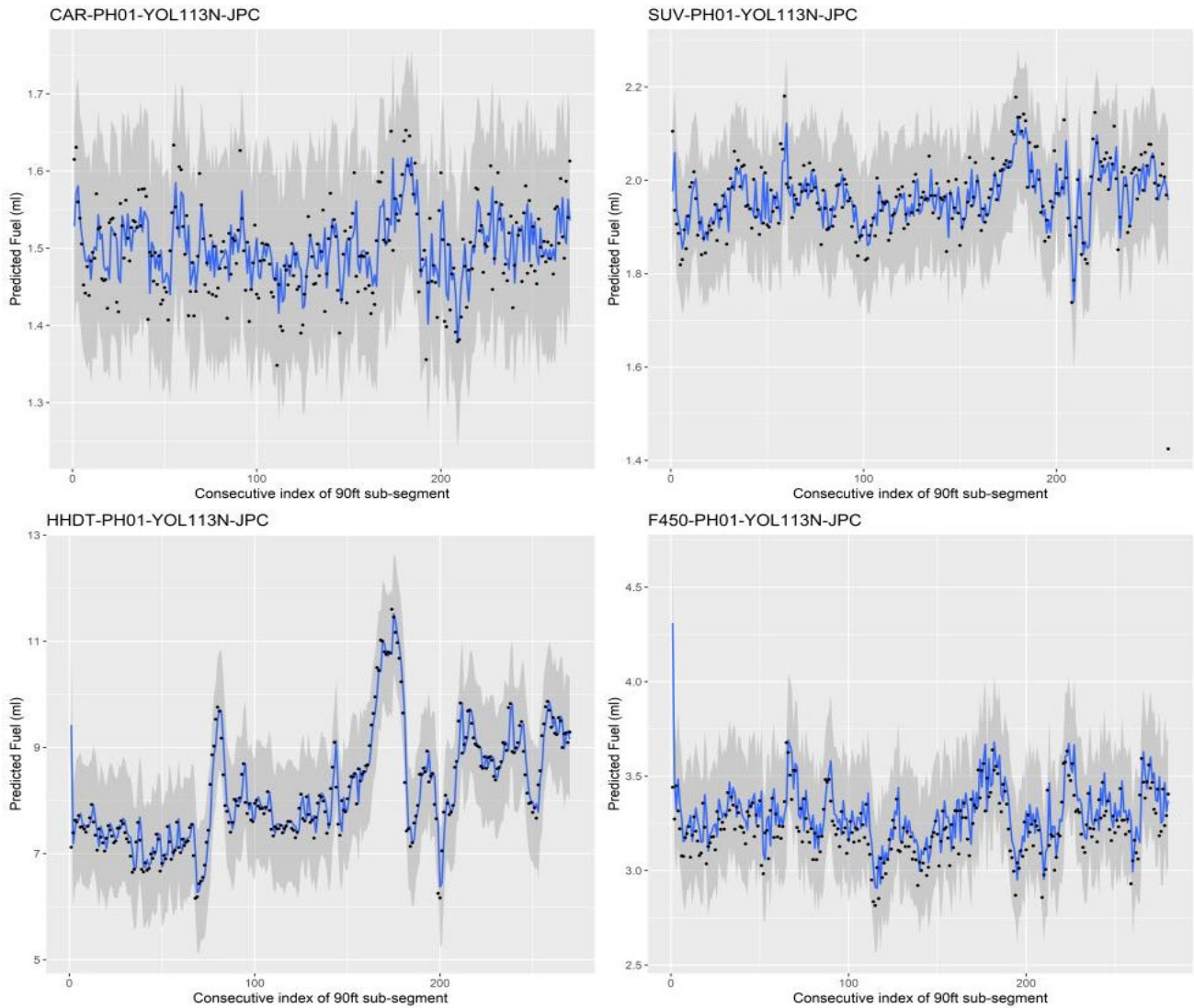
4.2 Model Results

In the following sections, visuals are produced from the models to infer model prediction and conditional effects of variables. Predictions are evaluated based on subsection level values including the autoregressive parameter and presented on the outcome scale of milliliters (mL) of fuel consumed. Conditional effects of each variable are evaluated based on holding all other variables at their mean (for continuous variables) and selecting the most common value for each category (e.g., 45 mph [72 km/hr] for vehicle speed) when calculating the predicted fuel

consumption. These plots are commonly called counterfactual predictions. Quantitative summaries of the empirical models are presented in Appendix Q.

4.2.1 Model Predictions

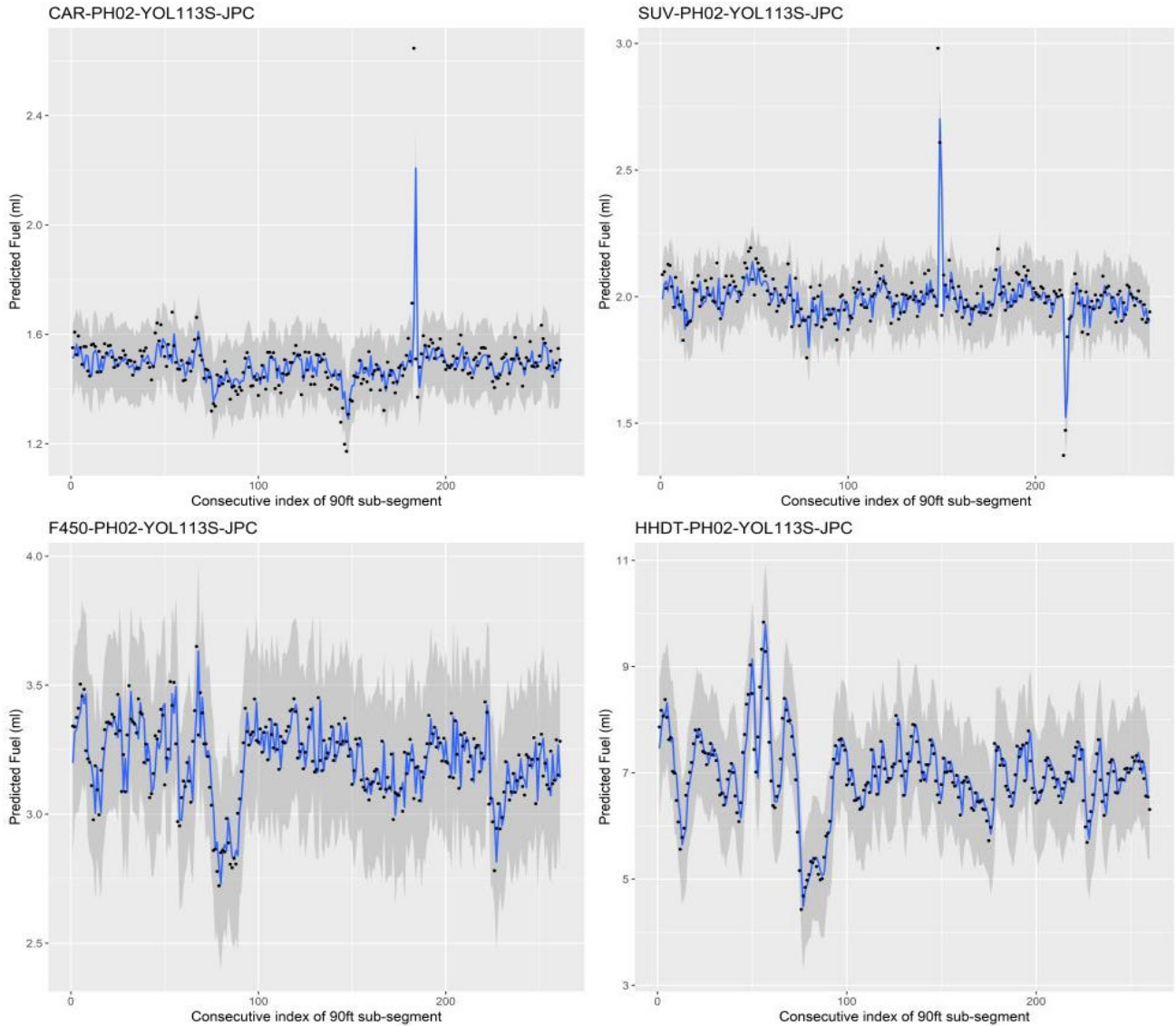
In a sample of experimental runs on each road (e.g., Figure 4.3 and Figure 4.4), the 95% prediction interval nearly always includes the observed fuel consumed. In general, the predictions for each vehicle type are consistently accurate across vehicles and roads. The few cases where the models fail are at the beginning of experimental runs, because there is no prior fuel consumption to condition on, and in cases where outliers exist (e.g., a few observations in Figure 4.3 are outside the 95% prediction interval). This indicates that the models rely heavily on the autoregressive error term to accurately predict fuel consumption, which is further confirmed by the cross validation presented in the methods section.



Notes:

- Y-axis scales are different because the fuel consumption per vehicle ranges are very different.
- Gray area indicates 95% prediction interval, blue line indicates model prediction, and black dots are observations.

Figure 4.3: Time series fuel consumption predictions for first experimental run on PH01 for all the vehicles.



Notes:

- Y-axis scales are different because the fuel consumption per vehicle ranges are very different.
- Gray area indicates 95% prediction interval, blue line indicates model prediction, and black dots are observations.

Figure 4.4: Time series fuel consumption predictions for first experimental run on PH02 for all the vehicles.

4.2.2 Control Characteristics

Characteristics such as air temperature, effective tailwind, cruise control speed, and elevation gradient have measurable effects on vehicle fuel consumption. However, because the effect of pavement on vehicle fuel consumption is the focus of this study, these variables are considered control variables.

4.2.2.1 Cruise Control Speed

Of the five control characteristics, cruise control speed has the strongest effect on fuel consumption, but its effect varies by vehicle, as shown in Figure 4.5 and Figure 4.6. For example, the 35 mph (56 km/hr) cruise control speed shows the highest fuel consumption for the car and F-450, while the 55 mph (88 km/hr) cruise control speed shows the highest fuel consumption for the SUV and HHDT. For all vehicles, the 45 mph (72 km/hr) cruise control speed shows the lowest fuel consumption. The effect of a 10 mph (16 km/hr) difference in cruise control speed accounts for an approximately 3% to 26% difference in fuel consumption across all the vehicles. The effect of vehicle speed on fuel use varies depending on how fast a vehicle is traveling, and the effects are inverse. Specifically, when traveling at lower speeds, which use less fuel-efficient lower gears, fuel use increases. But, when a vehicle travels faster and uses a more efficient high-speed gear, aerodynamic resistance increases, also increasing fuel use. A third effect is that on pavements with viscoelastic structural response, faster speeds result in higher stiffness for the viscoelastic materials and therefore less fuel consumption due to structural response. The speeds at which vehicles shift gears differs between vehicles, as was discussed in Chapter 3.

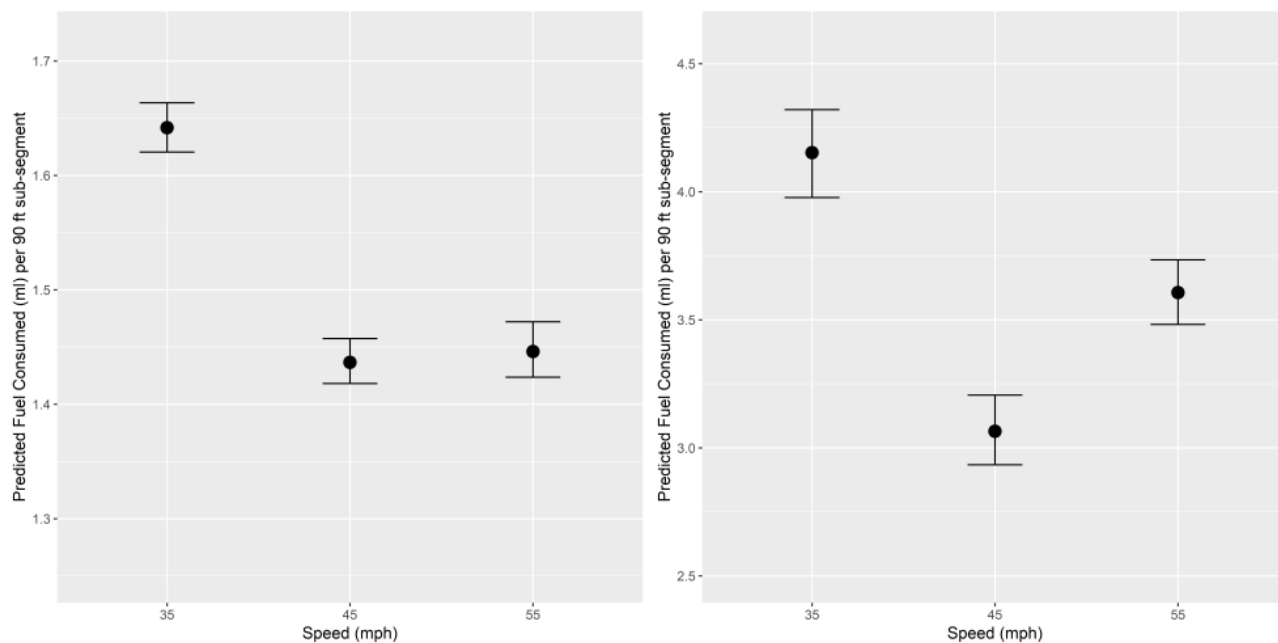


Figure 4.5: Conditional effect of cruise control speed on the fuel consumption of the car (left) and F-450 (right).

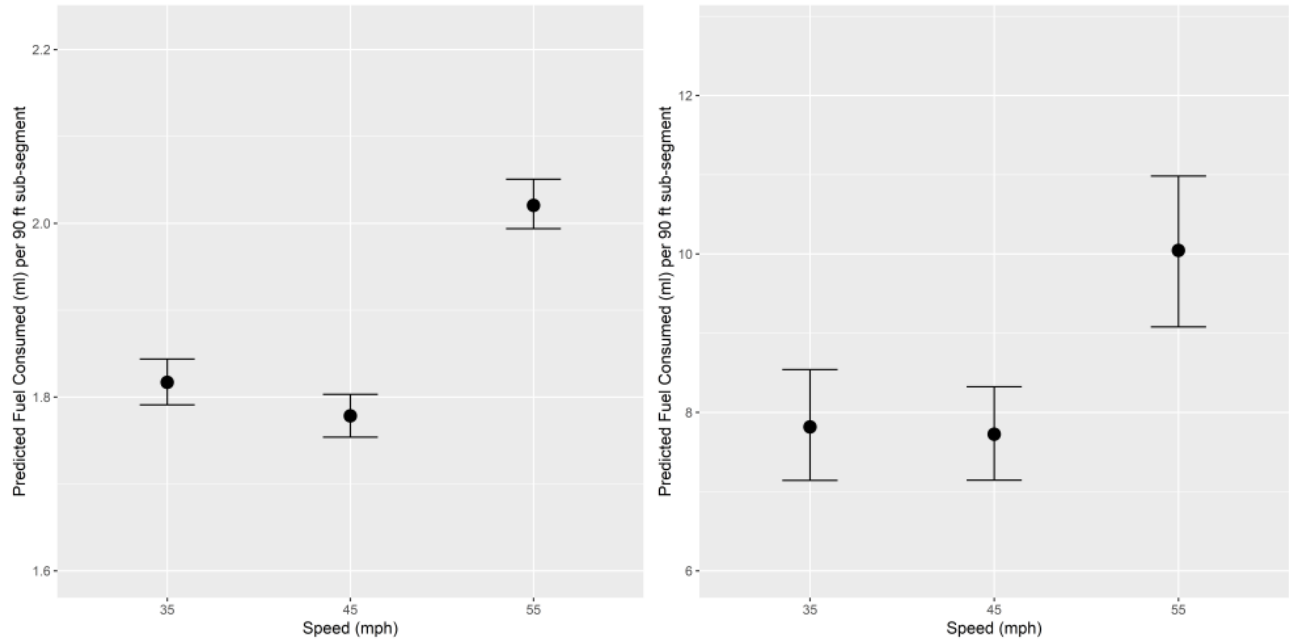


Figure 4.6: Conditional effect of cruise control speed on the fuel consumption of the SUV (left) and HHDT (right).

4.2.2.2 Elevation Gradient

Elevation gradient has the next strongest effect of the control characteristics considered related to vehicle fuel consumption. Elevation gradient has a positive relationship with fuel consumption for all the vehicle types, as can be seen in Figure 4.7. A 1% increase in elevation gradient has a predicted 5% to 10% increase in fuel consumption across all the vehicles. The effect of gradient is stronger on the car and SUV than on the F-450 and HHDT.

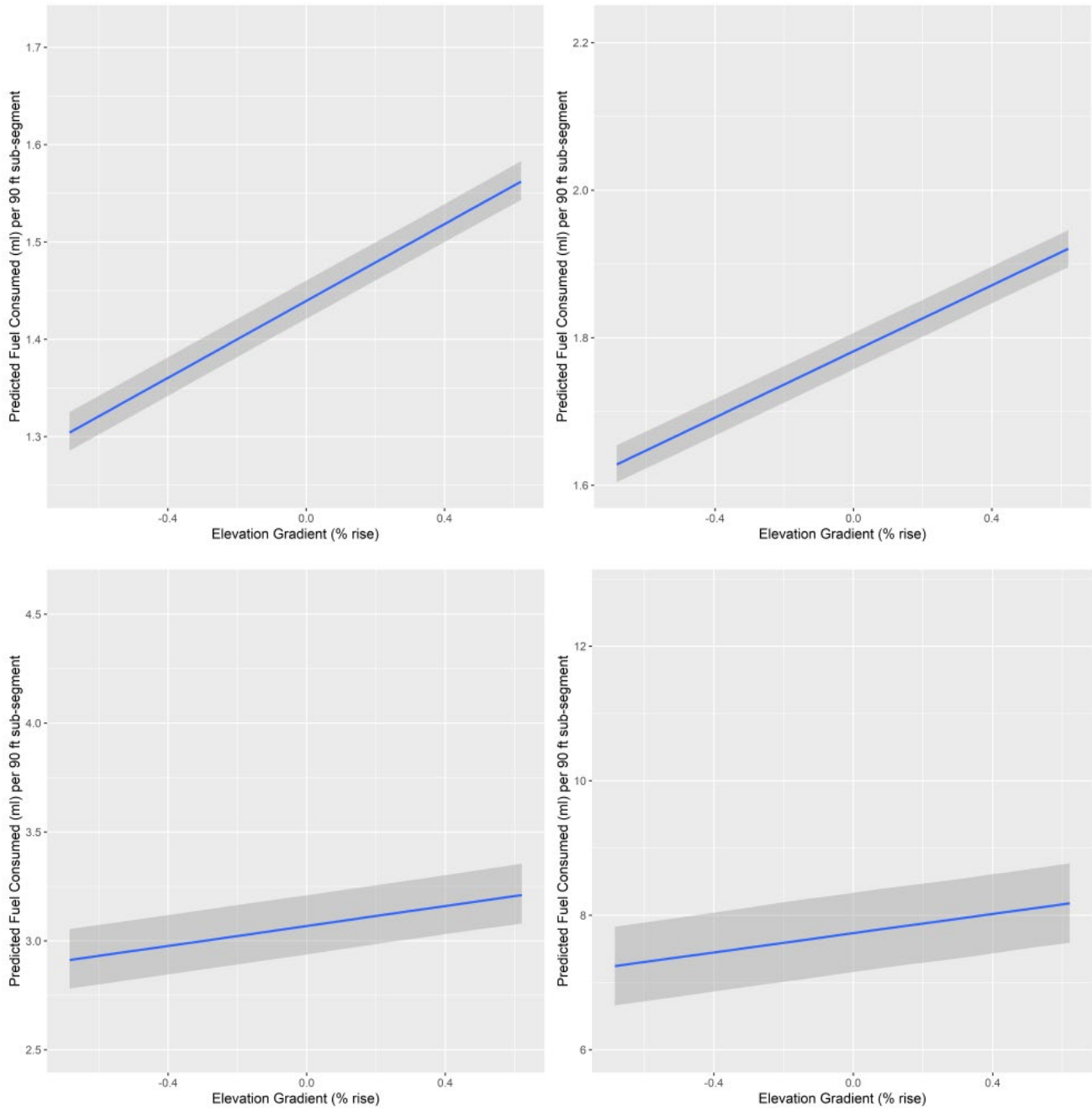


Figure 4.7: Conditional effect of elevation gradient on the fuel consumption of the car (top left), SUV (top right), F-450 (bottom left), and HHDT (bottom right).

4.2.2.3 Air Temperature

The effect of air temperature on fuel consumption varies across the vehicles. In theory, air temperature has two competing effects on fuel consumption. Because air temperature influences air density, it also influences fuel combustion and aerodynamic drag; in this experiment, air temperature increases resulted in less fuel consumption, indicating that the increased temperatures caused combustion to be more efficient, and less drag. However, a

competing effect also resulted because higher air temperatures also influence the structural response of some pavements (e.g., those surfaced with viscoelastic asphalt materials, an effect discussed later).

The model predictions aligned with the theory of air temperature being negatively associated with fuel consumption for all the vehicles, as shown in Figure 4.8, though the effects for the HHDT were negligible compared to those for other vehicles. In general, an increase in 20°F (11°C) has a predicted 0% to 6% reduction in fuel consumption across all the vehicles.

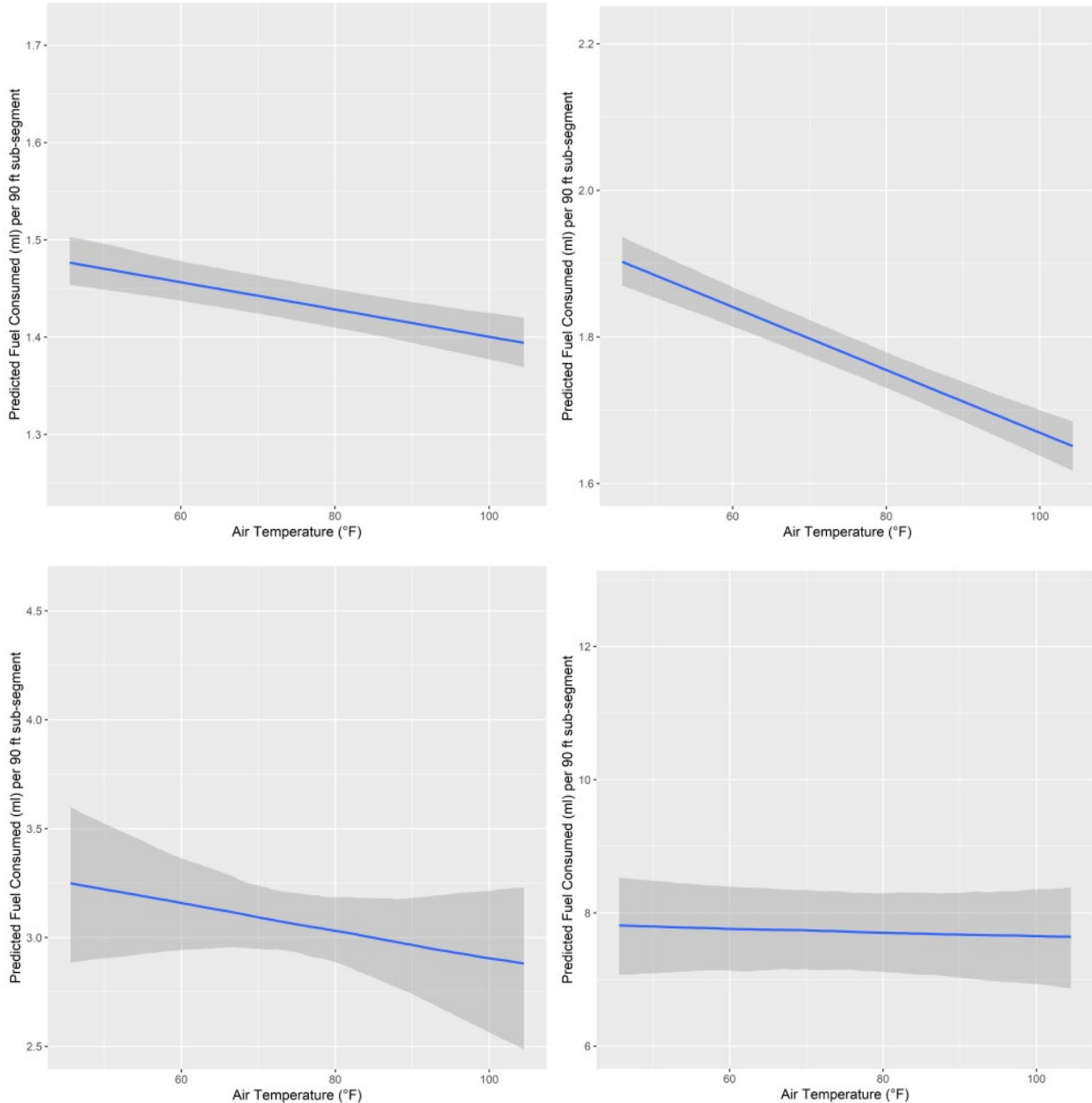


Figure 4.8: Conditional effect of air temperature on the fuel consumption of the car (top left), SUV (top right), F-450 (bottom left), and HHDT (bottom right).

4.2.2.4 Interaction Between Air Temperature and Cruise Control Speed

An examination of the interaction between air temperature and cruise control speed showed varied effects on fuel use. The effects of air temperature on fuel consumption by the car and SUV showed no signs of varying by cruise control speed. Although the F-450 showed a slight positive effect of air temperature on fuel consumption at the slowest cruise control speed of 35 mph (56 km/hr), this effect is highly uncertain. The only clear interaction between air temperature and cruise control speed was seen in the HHDT: air temperature had a positive effect on

fuel consumption when cruising at 35 mph (56 km/hr), no effect when cruising at 45 mph (72 km/hr), and a strong negative effect when cruising at 55 mph (88 km/hr). For the HHDT, these interactions may be due to differences in combustion efficiency and drag at the different cruising speeds, but at slow speeds they may also be partially due to the effects of pavement (i.e., warmer air causing asphalt-surfaced pavements to soften and absorb more energy from the heavy HHDT), as seen in Figure 4.9. However, a further analysis that focused on the specific pavements suspected of causing this effect (presented in Section 4.2.3) indicates this may not be the case.

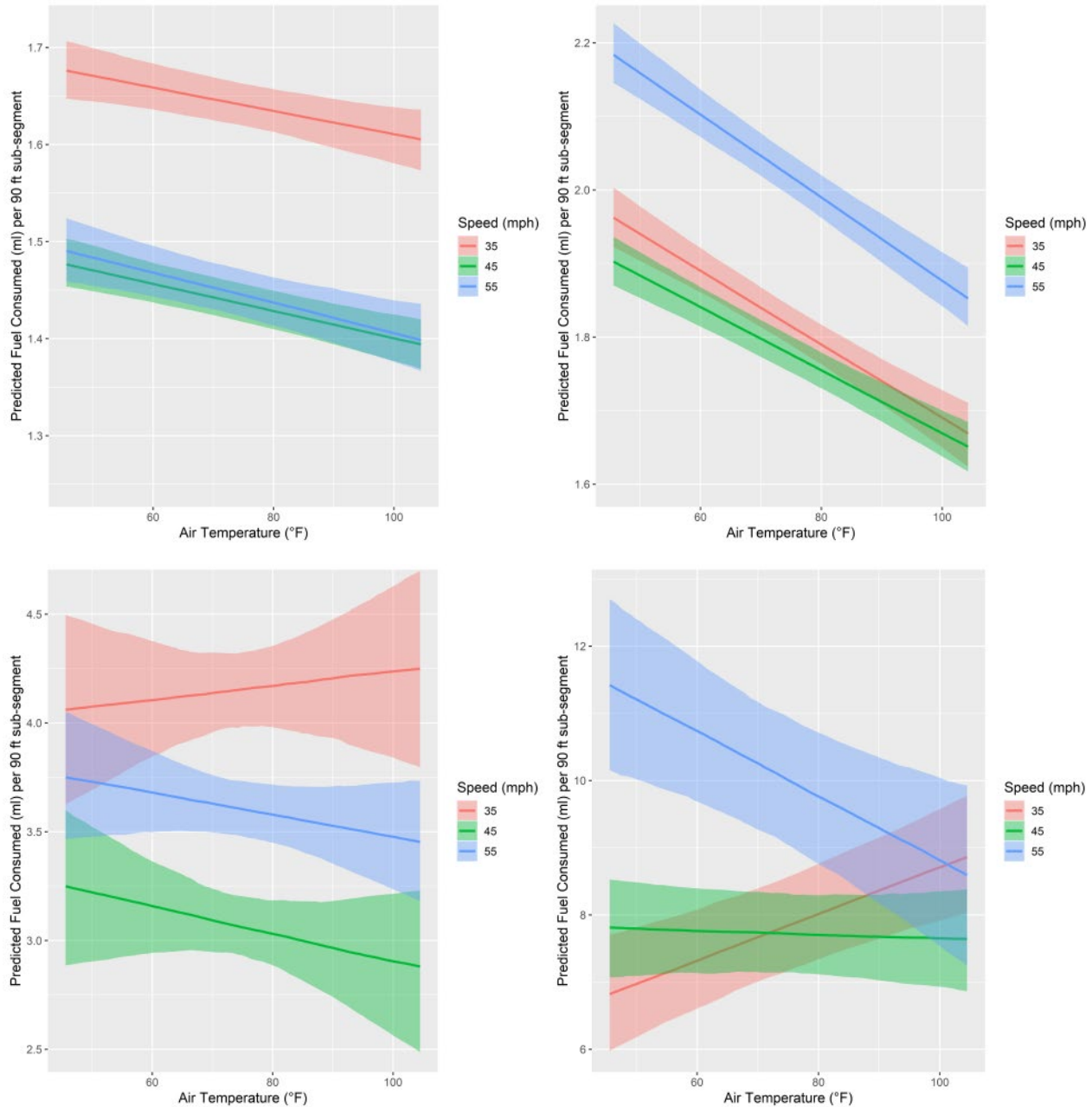


Figure 4.9: Conditional effect of air temperature by cruise control speed on the fuel consumption of the car (top left), SUV (top right), F-450 (bottom left), and HHDT (bottom right).

4.2.2.5 Effective Tailwind

Effective tailwind has a consistently positive effect on fuel consumption across all the vehicles, but the magnitude of the effect is negligible from the model results, as shown in Figure 4.10. This is surprising, especially considering the frontal area of the HHDT. However, because the experiment was designed to limit the effect of wind by testing only when the wind speed was less than 5 mph (8 km/hr), most of the tests involving wind conditions resulted in ineffective tailwinds between -2 and 2 mph (-3.2 and 3.2 km/hr).

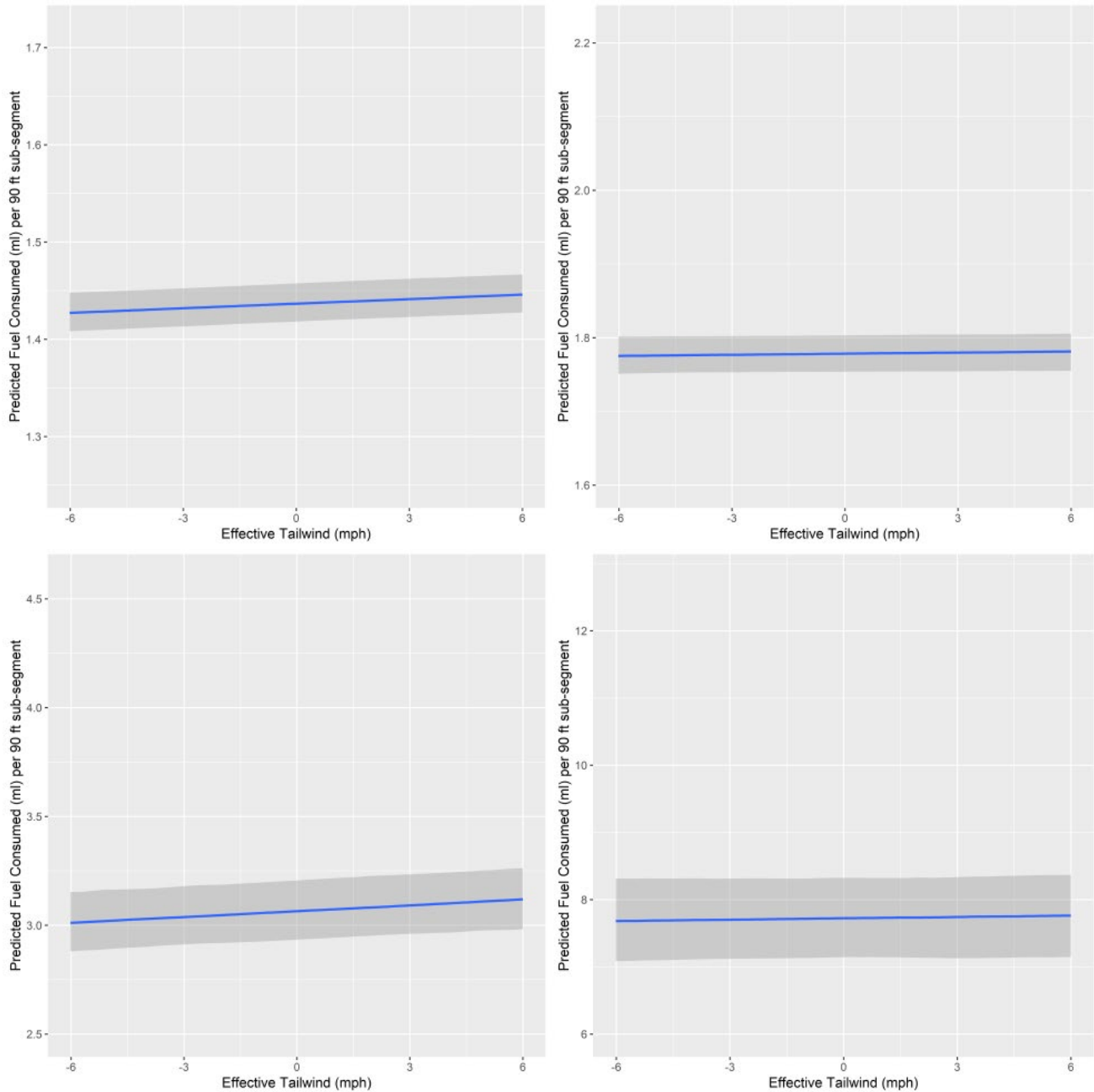


Figure 4.10: Conditional effect of effective tailwind on the fuel consumption of the car (top left), SUV (top right), F-450 (bottom left), and HHDT (bottom right).

4.2.2.6 Pavement Roughness and Texture

In general, the models show that pavement roughness and texture had little effect on fuel consumption across all the vehicles. This is partially because the experiment was designed to limit the effect of these pavement variables. But even on the few subsections that were rough (> 168 in./mi. [2.68 m/km] IRI) or had high-texture (> 1.20 mm MPD), the fuel consumption predicted was similar to that of the smooth and low-texture subsections.

The effect of roughness and texture on the car’s fuel consumption was confidently observed to be near zero (Figure 4.11). Even when varying the effect of roughness and texture by speed, little to no effect on fuel consumption was observed (Figure 4.12). The conditional effects with great uncertainty are the ones that have inadequate data for those combinations of values. For example, the car never ran at 35 mph (56 km/hr) on a section with MPD greater or equal to 1.20 mm, so the estimated effect of that combination is very uncertain (Figure 4.12).

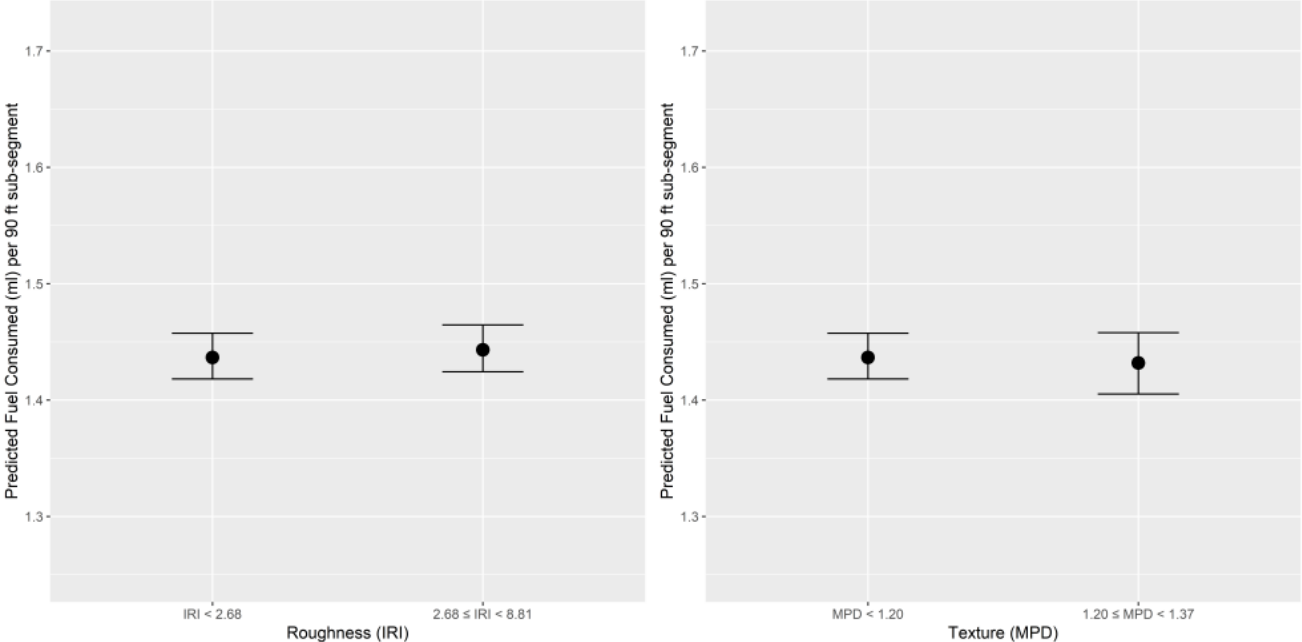


Figure 4.11: Conditional effect of roughness and texture on the fuel consumption of the car.

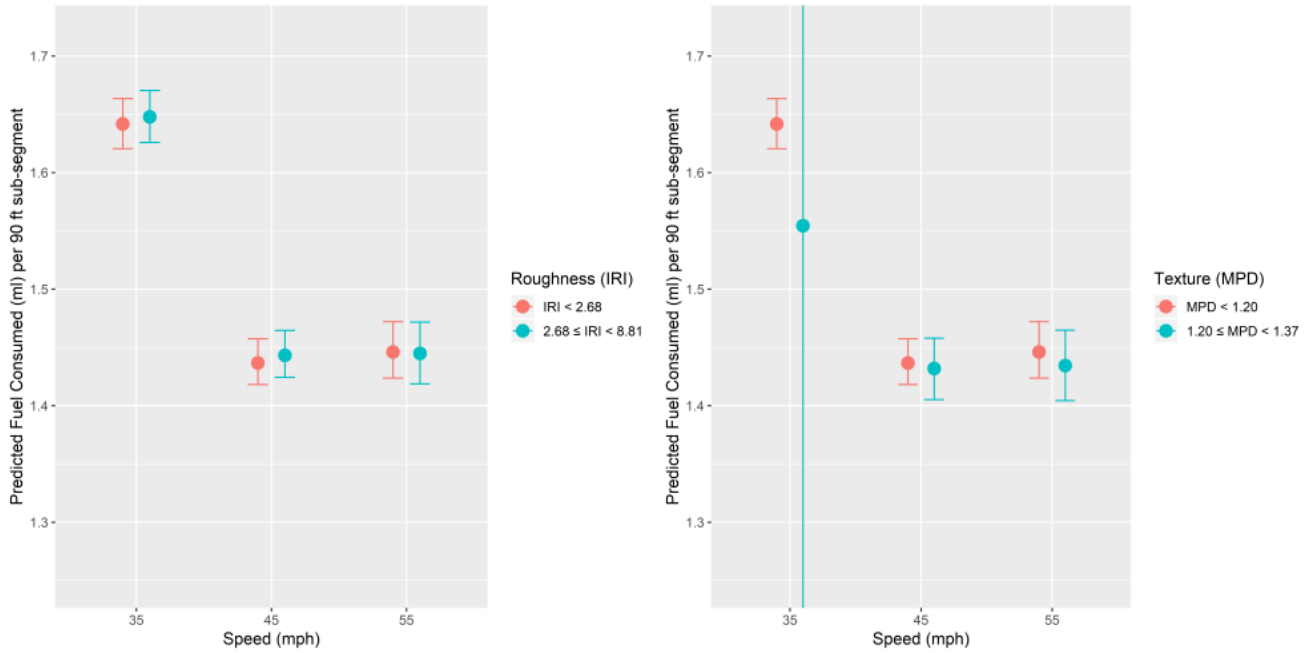


Figure 4.12: Conditional effect of roughness and texture on the car’s fuel consumption by cruise control speed.

The effect of roughness and texture on the SUV’s fuel consumption was also confidently near zero (Figure 4.13). Further, no effect on fuel consumption was observed even when varying the effect of roughness and texture by speed (Figure 4.14).

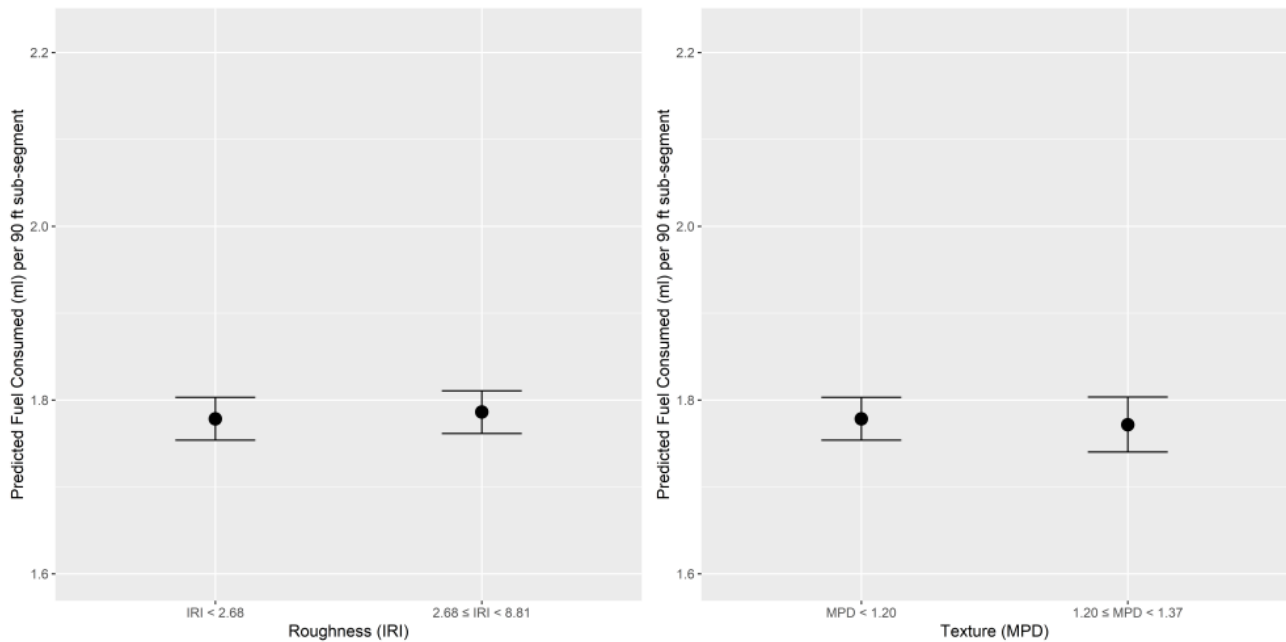


Figure 4.13: Conditional effect of roughness and texture on the fuel consumption of the SUV.

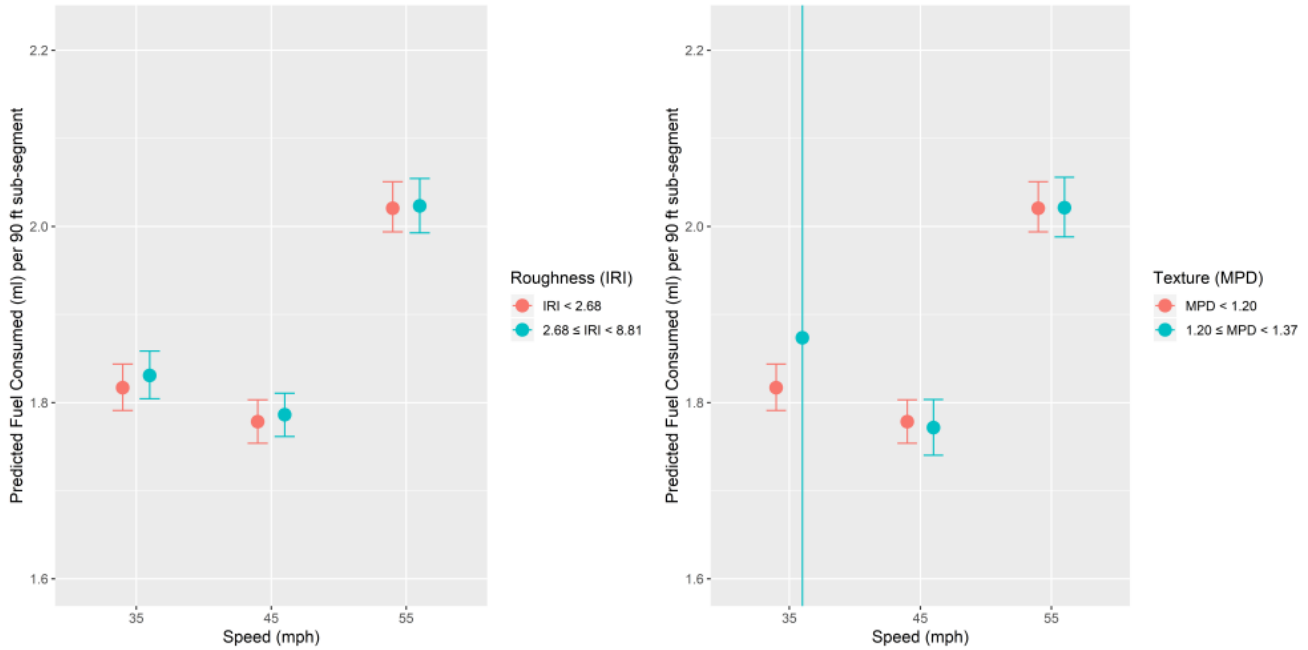


Figure 4.14: Conditional effect of roughness and texture on the SUV’s fuel consumption by cruise control speed.

The effect of roughness and texture on the fuel consumption of the F-450 was also confidently near zero (Figure 4.15). No effect on fuel consumption was observed even when varying the effect of roughness and texture by speed (Figure 4.16).

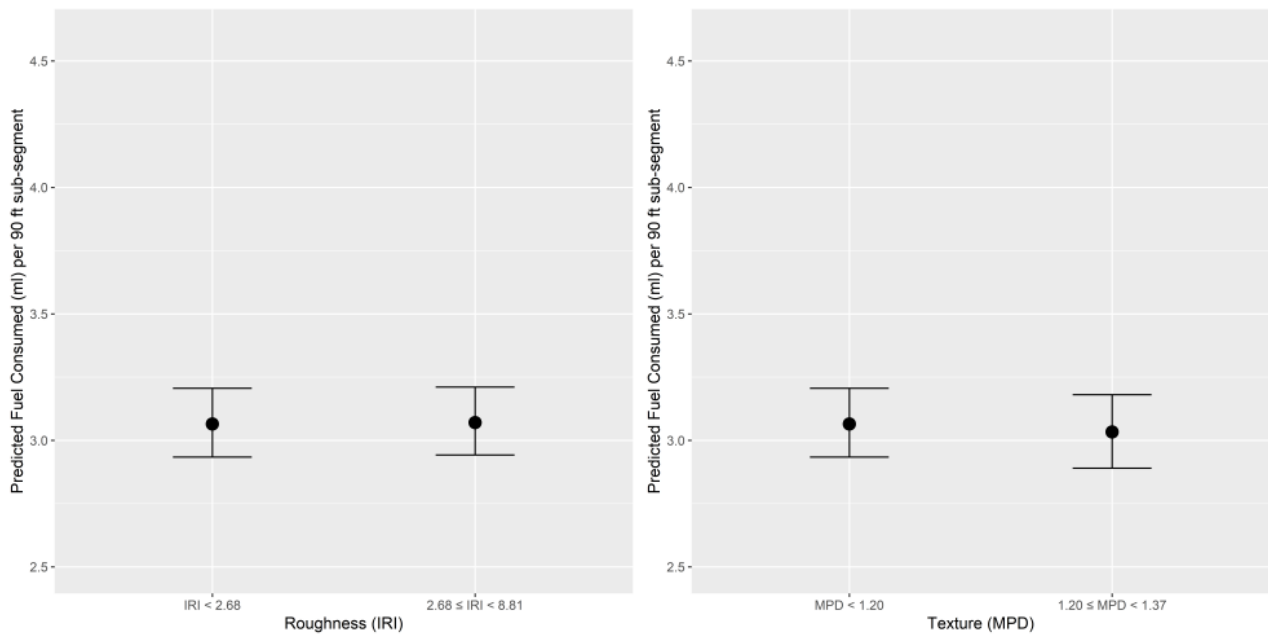


Figure 4.15: Conditional effect of roughness and texture on the fuel consumption of the F-450.

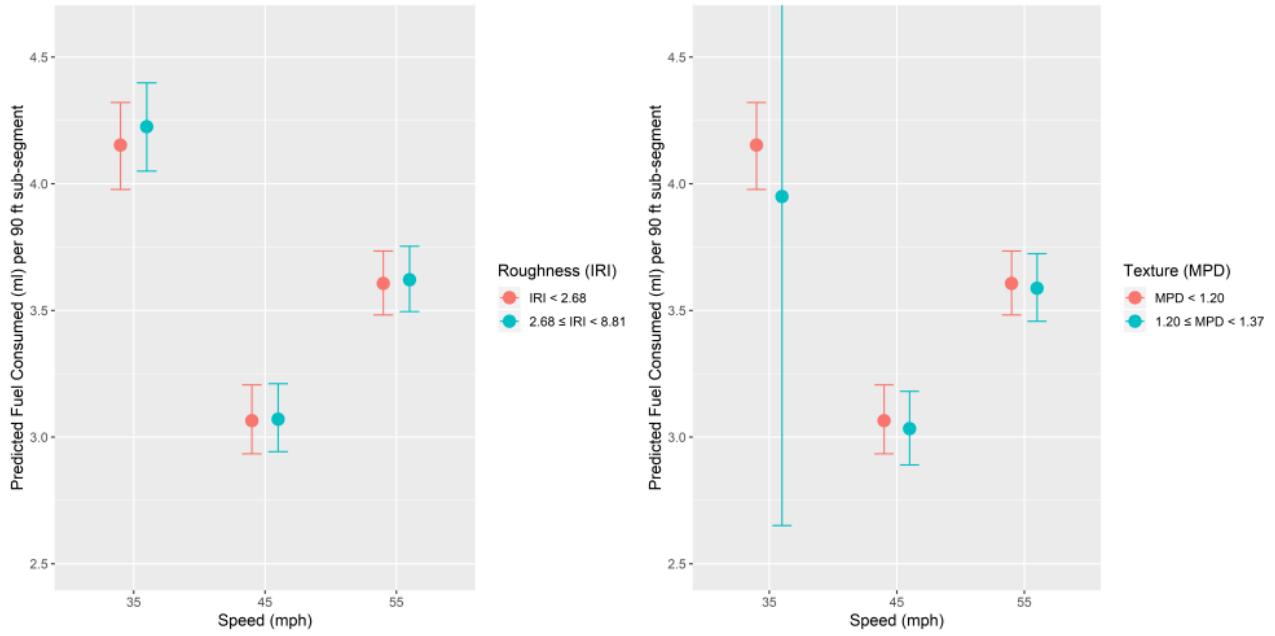


Figure 4.16: Conditional effect of roughness and texture on the F-450’s fuel consumption by cruise control speed.

The effect of roughness and texture on the fuel consumption of the HHDT was also confidently near zero (Figure 4.17). No change in the HHDT’s fuel consumption was observed even when varying the effect of roughness and texture by speed (Figure 4.18).

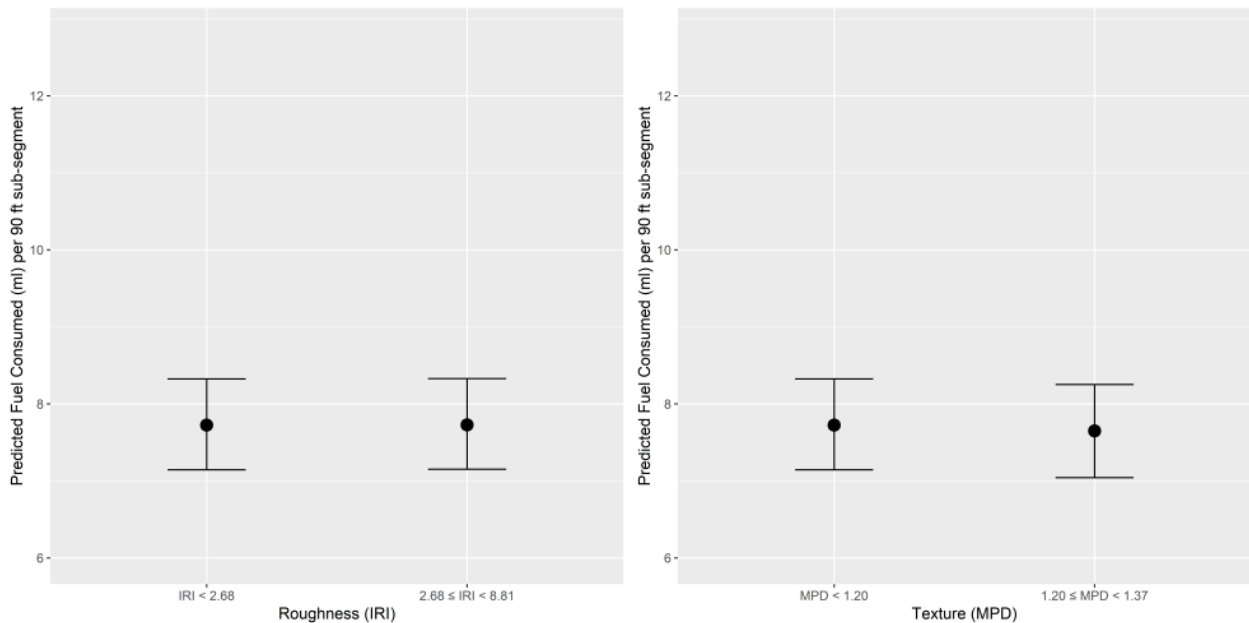


Figure 4.17: Conditional effect of roughness and texture on the fuel consumption of the HHDT.

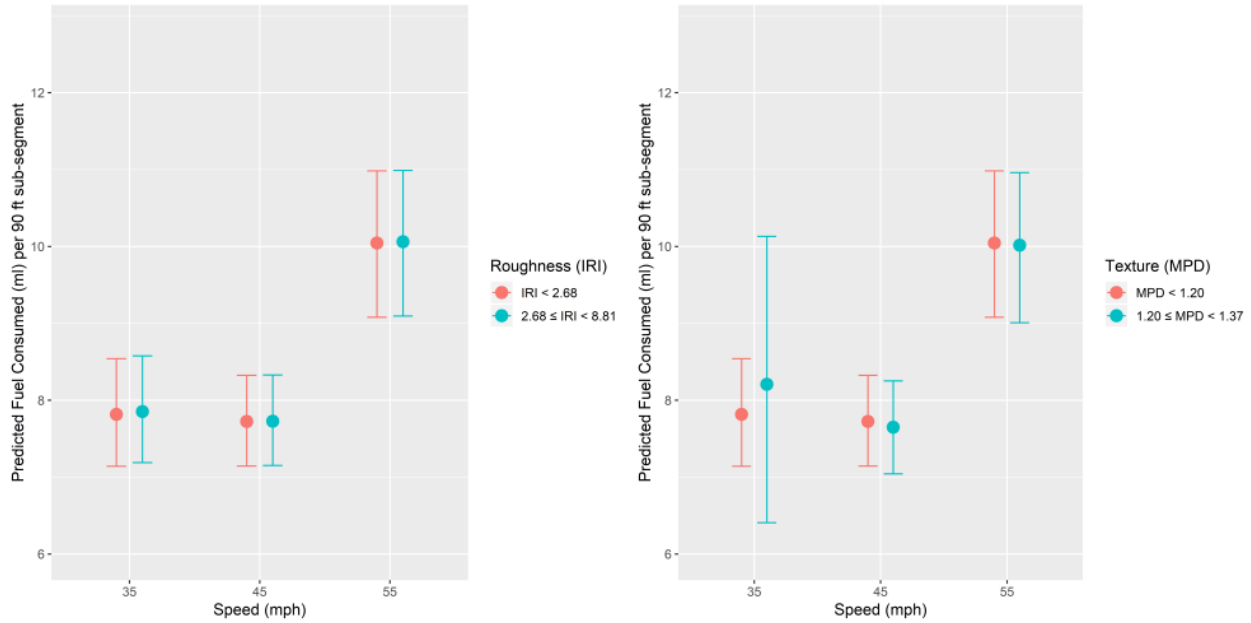


Figure 4.18: Conditional effect of roughness and texture on the HHDТ’s fuel consumption by cruise control speed.

4.2.3 Primary Pavement Effects

This experiment was designed to evaluate the effects of several pavement types—*asphalt, composite, concrete, continuously reinforced concrete (CRC), and semi-rigid (SR)*—on fuel consumption and to examine how those effects vary on different roads with those pavement types. A factorial sensitivity analysis was run with three scenarios for three primary variables (tailwind, temperature, and vehicle speed) to more clearly understand how pavement types influence fuel consumption. The three scenarios for each variable were selected to produce an inefficient condition, a median condition, and an efficient condition. The temperatures for the three scenarios (inefficient condition, median condition, and efficient condition) vary for each of the four different California regions considered (Central Coast [San Francisco], Inland Valley [Sacramento], High Mountain [South Lake Tahoe], and Desert [Daggett]), as shown in Table 4.2. The full set of scenarios, with three values for each of the three variables for the four vehicles is shown in Table 4.3. Permutations of factor levels across three variables were not run; rather, the scenarios considered the inefficient condition, median condition and efficient condition for all three variables at the same time. The scenarios include no elevation gradient, low roughness, and low texture. This resulted in a total of 16 simulations (four regions by four cars) for each of the three scenarios. The scenarios help provide inference about the specific pavements across a variety of environmental conditions, which should help inform policy about pavement guidance in different regions of California.

Table 4.2. Scenario Regions and Associated Temperatures

Four Caltrans Climate Regions	Air Temperatures	°C	°F
Central Coast (San Francisco, CA)	Daily minimum ¹	5	41
	Daily maximum ¹	23	74
	10-year annual average ²	14	58
Inland Valley (Sacramento, CA)	Daily minimum ¹	2	36
	Daily maximum ¹	35	95
	10-year annual average ²	17	62
High Mountain (Reno, NV/South Lake Tahoe, CA)	Daily minimum ¹	-9	16
	Daily maximum ¹	33	92
	10-year annual average ²	13	55
Desert (Daggett, CA)	Daily minimum ¹	0	32
	Daily maximum ¹	41	106
	10-year annual average ²	21	69

¹ The daily maximum and minimum air temperatures were determined within the 30-year averaged year (1961–1990): Harvey, J., Chong, A., and Roesler, J. 2000. *Climate Regions for Mechanistic-Empirical Pavement Design in California and Expected Effects on Performance*. CAL/APT Program, Pavement Research Center, Institute of Transportation Studies, University of California, Berkeley.

² 10-year annual average air temperature period (January 1, 2009–December 31, 2018) from National Centers for Environmental Information (www.ncdc.noaa.gov)

Table 4.3. Scenarios for Each Vehicle

Scenario	Vehicle	Effective Tailwind (mph)	Air Temperature	Cruise Control Speed (mph)
Efficient	Car	+5 mph	Regional daily maximum	45
	SUV	+5 mph	Regional daily maximum	45
	F-450	+5 mph	Regional daily maximum	45
	HHDT	+5 mph	Regional daily minimum	35
Median	Car	0 mph	Regional 10-year annual average	55
	SUV	0 mph	Regional 10-year annual average	35
	F-450	0 mph	Regional 10-year annual average	55
	HHDT	0 mph	Regional 10-year annual average	45
Inefficient	Car	-5 mph	Regional daily minimum	35
	SUV	-5 mph	Regional daily minimum	55
	F-450	-5 mph	Regional daily maximum	35
	HHDT	-5 mph	Regional daily minimum	55

The results of the scenario analysis suggest that the effects of pavement type on fuel consumption are too small to be estimated. Further, the variation in fuel consumption on each unique road given in the three scenarios is much larger than the variation in fuel consumption between roads for a given scenario. This indicates that the “control” variables have a much larger effect on fuel consumption than pavements. The specific scenario results are presented by vehicle in the following discussion.

The car scenarios show comparable fuel consumption across all the pavement types in all the efficiency condition scenarios. The three semi-rigid (SR) pavement sections show slightly less variation in fuel consumption than the other pavement types, and the one continuously reinforced concrete (CRC) section shows slightly less fuel consumption across all the scenarios. The median and efficient conditions show similar fuel consumption within the region, and the inefficient condition always shows greater fuel consumption. Figure 4.19 to Figure 4.22 show all the car scenarios for all the four regions and sections.

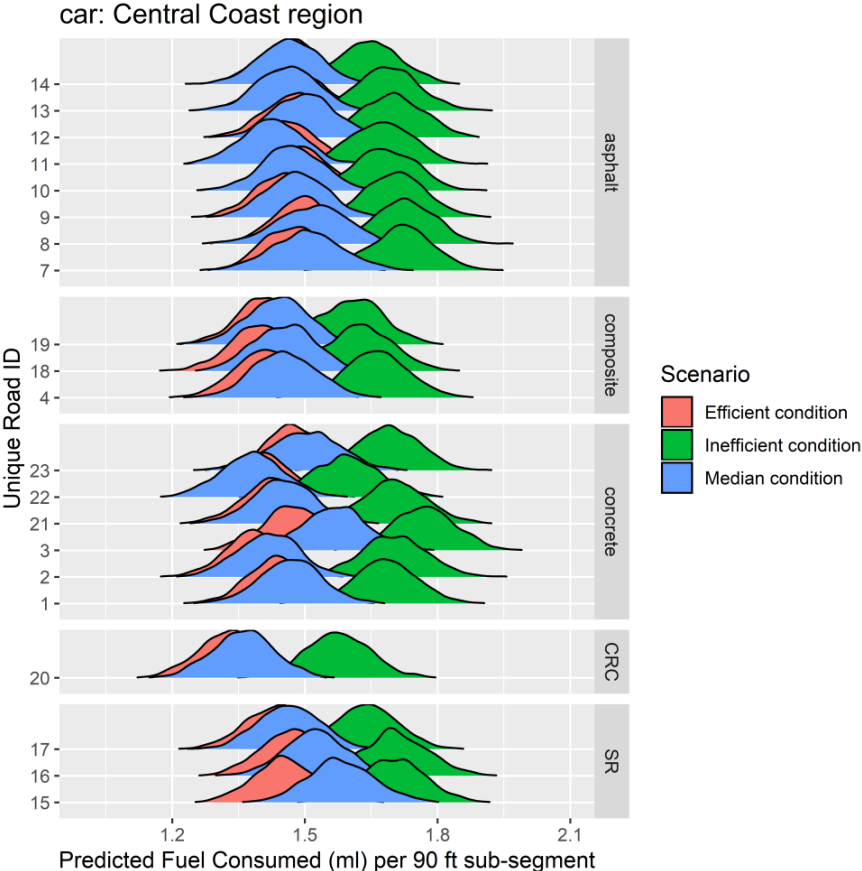


Figure 4.19: Car scenario for the Central Coast Region.

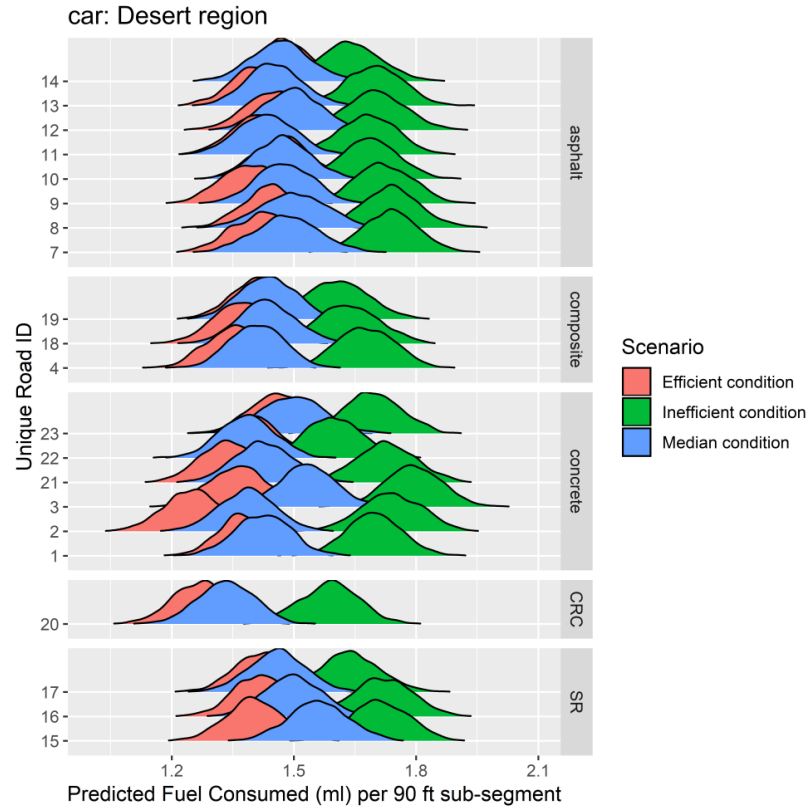


Figure 4.20: Car scenario for the Desert Region.

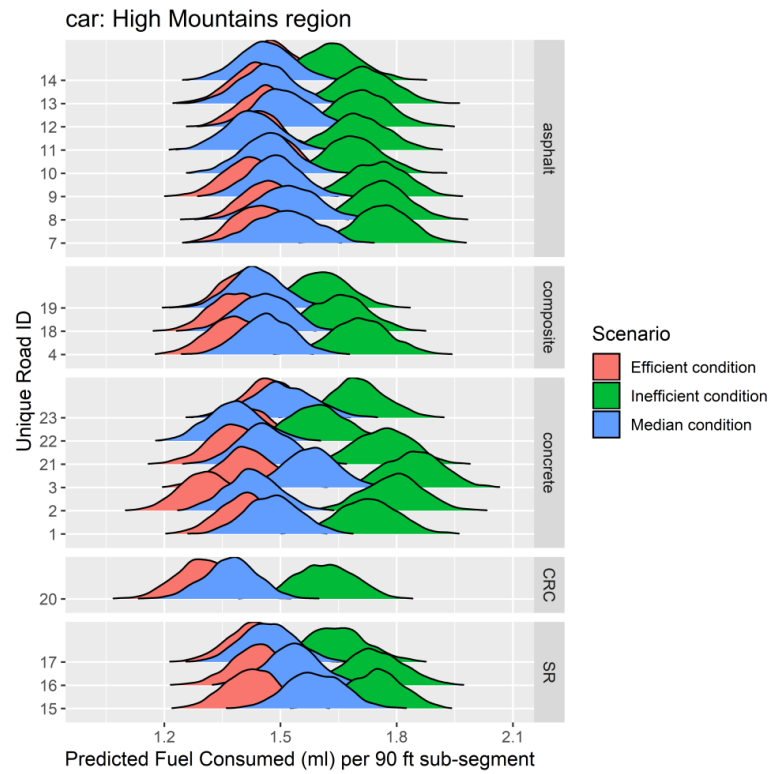


Figure 4.21: Car scenario for the High Mountain Region.

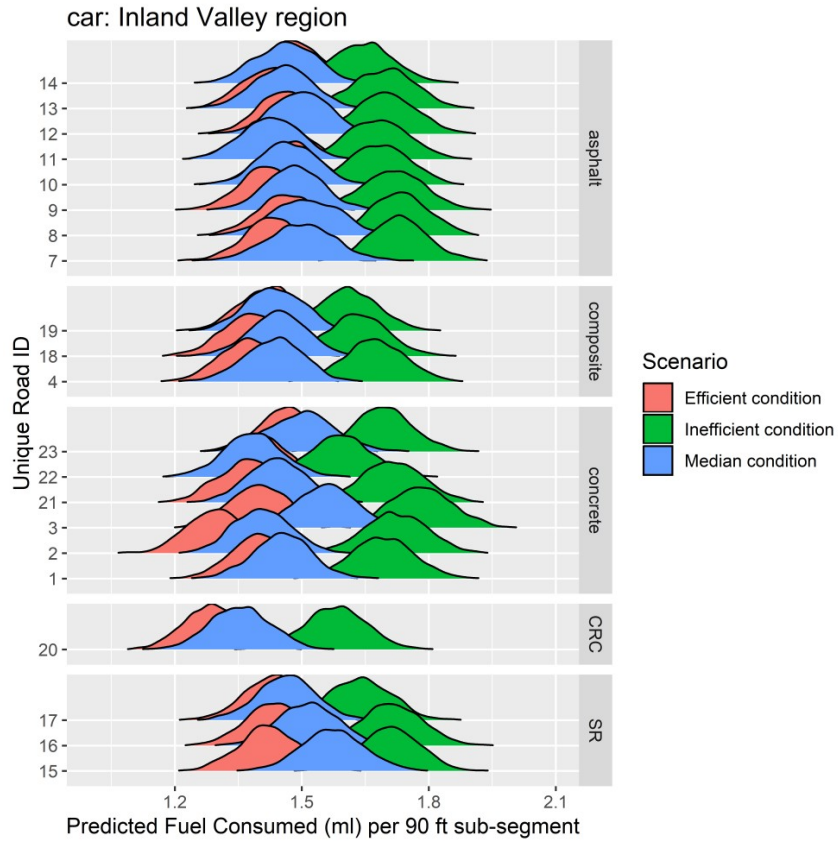


Figure 4.22: Car scenario for the Inland Valley Region.

The SUV scenarios show comparable fuel consumption across all the pavement types for all efficiency condition scenarios. Unlike the car, the SUV shows wider variation in fuel consumed within each road type, but the variation between roads is still small. The SUV scenarios show that the efficient and median conditions differ from each other more than those same conditions for the car, suggesting the fuel consumption of the SUV is more responsive to changes in the “control” variables. Figure 4.23 to Figure 4.26 show all the SUV scenarios for all four regions and sections.

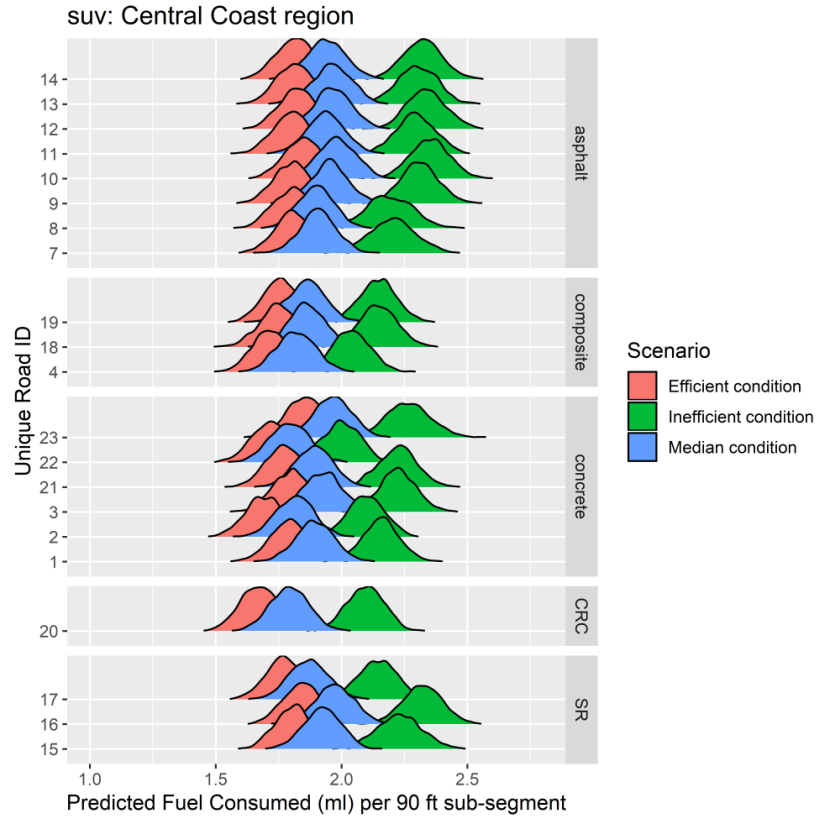


Figure 4.23: SUV scenario for the Central Coast Region.

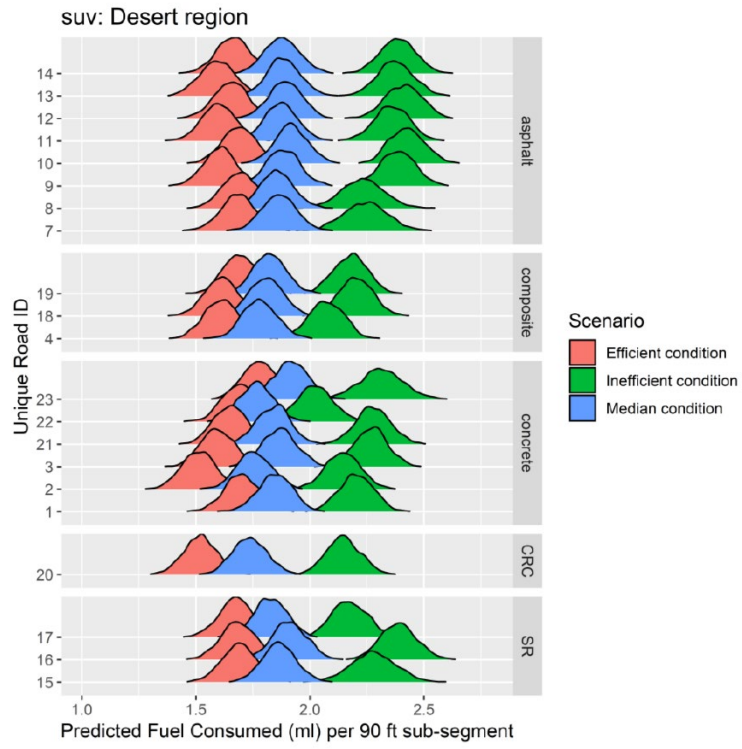


Figure 4.24: SUV scenario for the Desert Region.

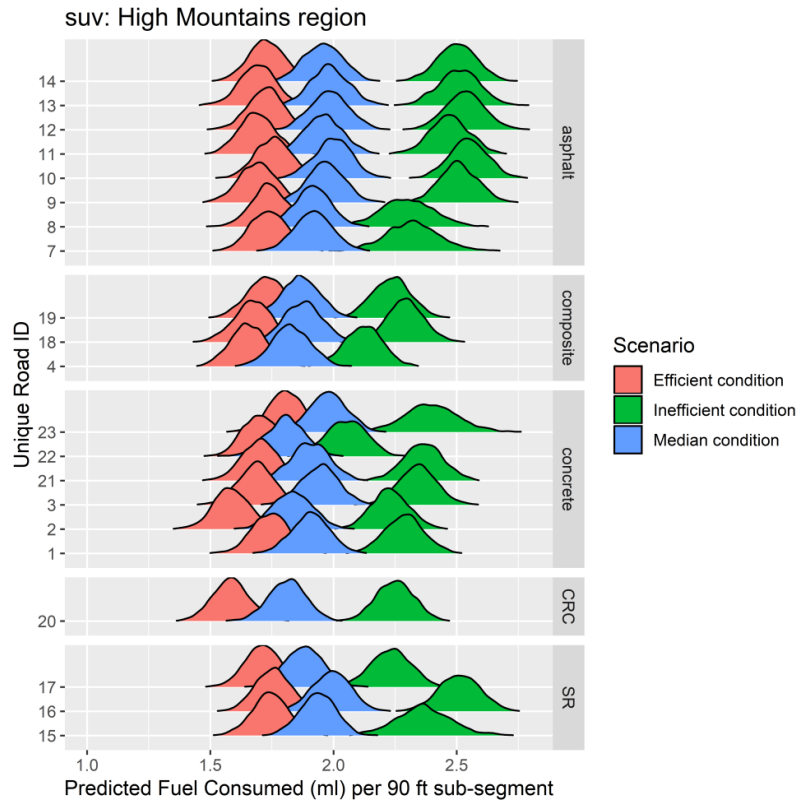


Figure 4.25: SUV scenario for the High Mountain Region.

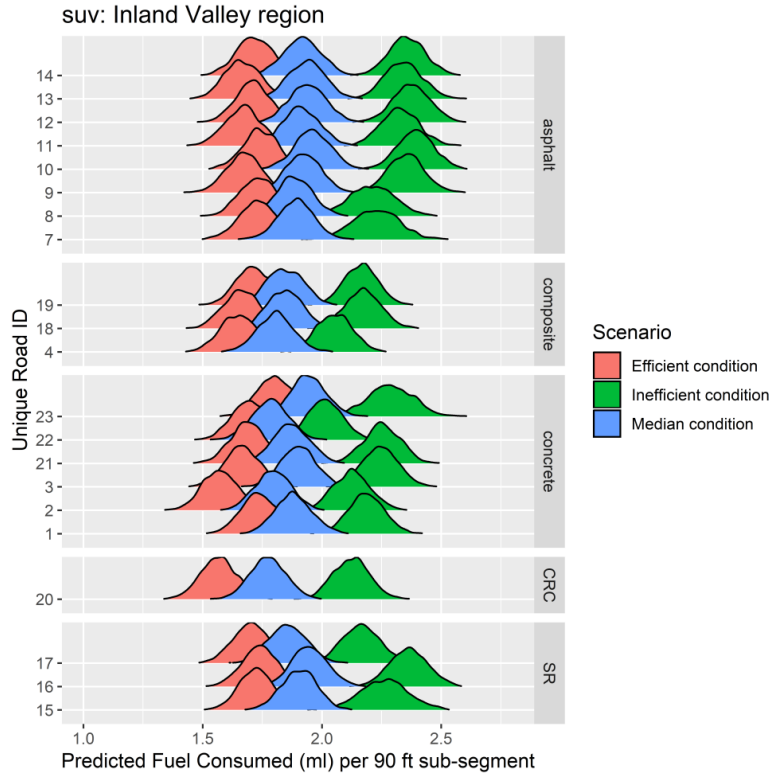


Figure 4.26: SUV scenario for the Inland Valley Region.

The F-450 scenarios show similar results to the car and SUV scenarios: greater within-pavement-type variation by scenario compared to between-pavement-type variations (Figure 4.27 to Figure 4.30). Most striking are the few outliers in the F-450 results. PH07 (an asphalt pavement) shows much greater fuel consumption in the inefficient condition compared to the other asphalt roads. Furthermore, this effect is exacerbated in the Desert and High Mountain region scenarios. Another outlier is PH23 (a concrete pavement type). In all scenarios, PH23 exhibits the opposite effect of the scenarios from all the other roads. That is, the inefficient condition shows the lowest fuel consumption across all regions for the F-450. Both PH07 and PH23 are county roads, while PH07 is a newly paved asphalt road and PH23 is very old (built in the 1940s) JPCP.

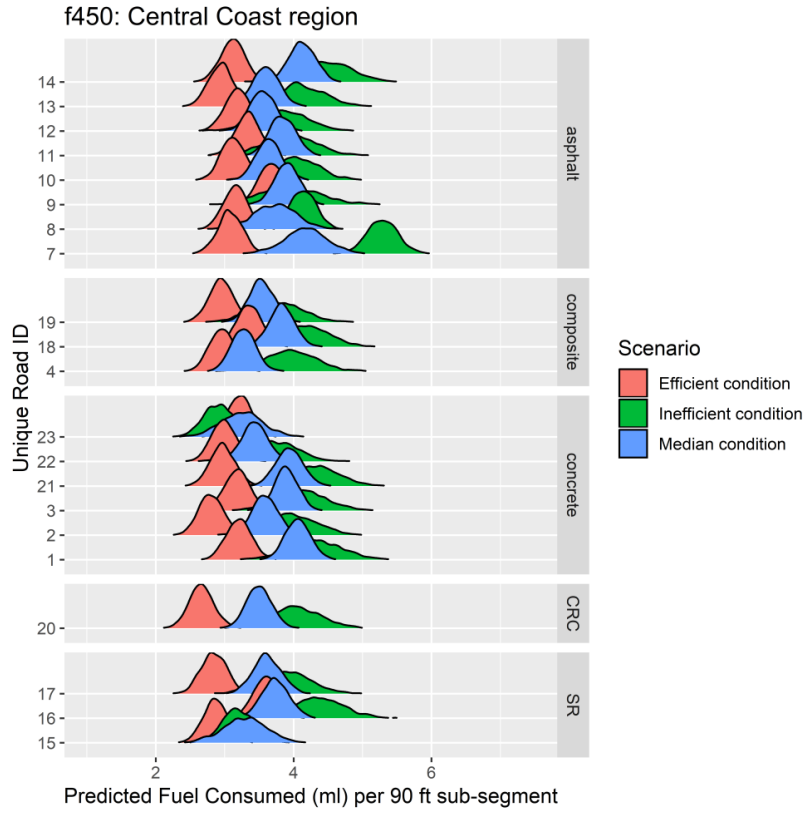


Figure 4.27: F-450 scenario for the Central Coast Region.

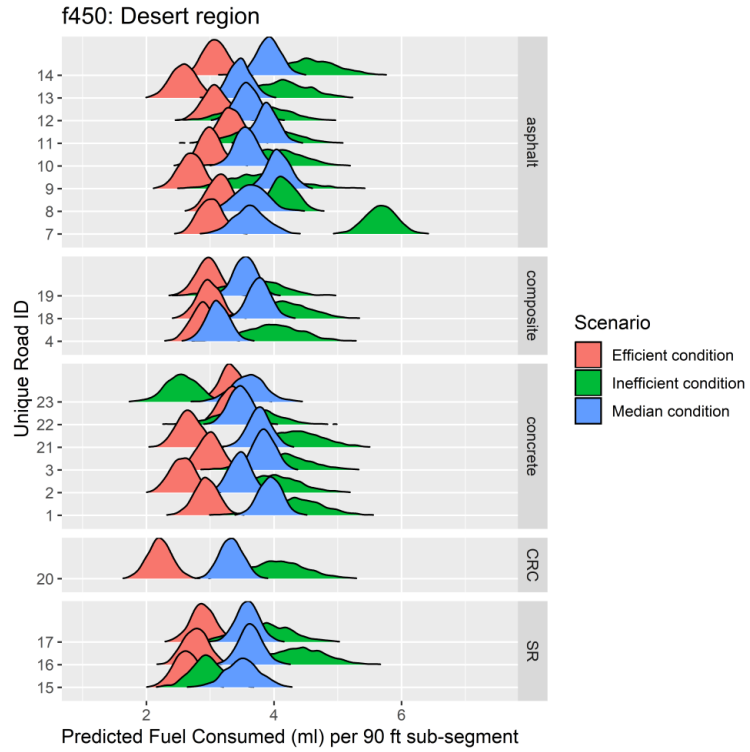


Figure 4.28: F-450 scenario for the Desert Region.

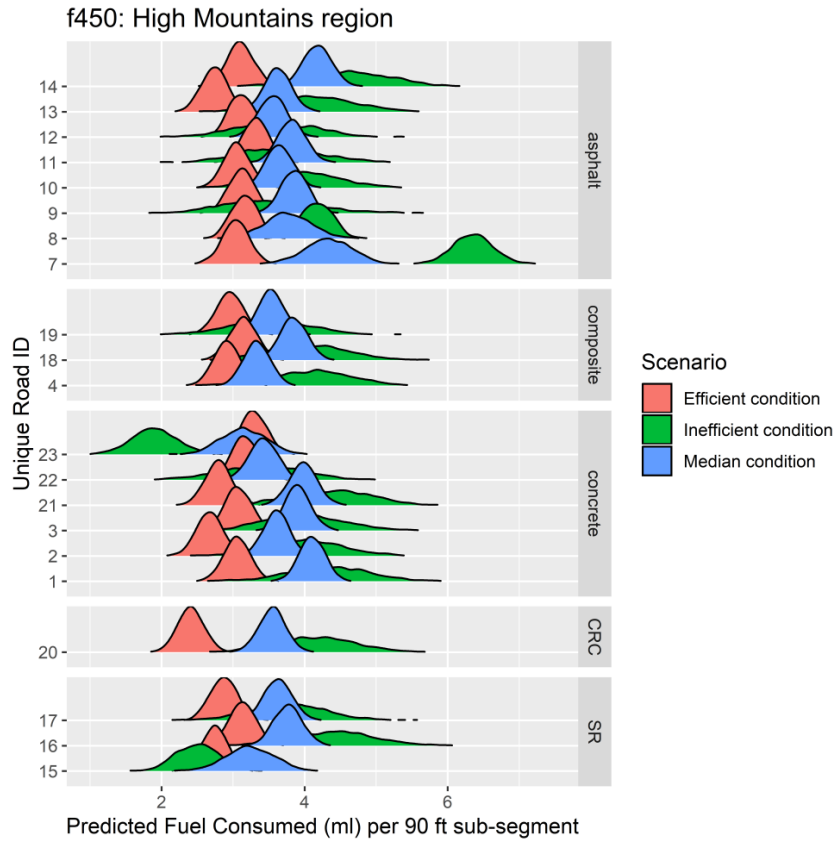


Figure 4.29: F-450 scenario for the High Mountain Region.

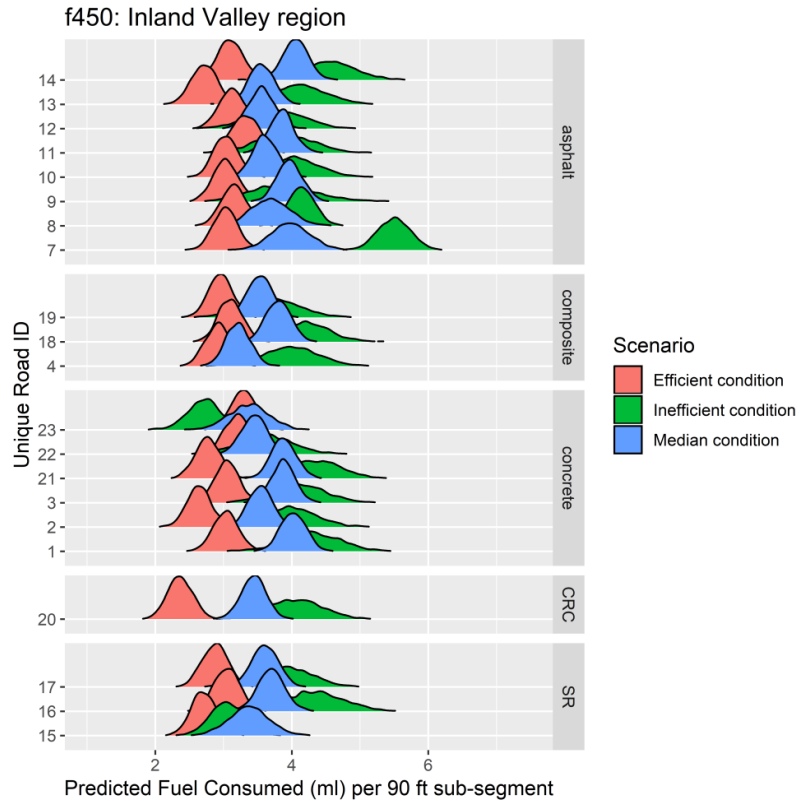


Figure 4.30: F-450 scenario for the Inland Valley Region.

In general, the HHDT scenarios show greater within-pavement-type variation by scenario compared to between-road variations. However, unlike the other vehicles, the HHDT results show large between-pavement-type variability in the inefficient condition. For example, within the Central Coast Region, the HHDT is predicted to consume only 3.5 mL of fuel per 90 ft. (27 m) subsection on PH11 (an asphalt pavement section), but around 18.5 mL of fuel per 90 ft. subsection on PH01 (a concrete pavement section). However, in the median and efficient conditions, the predicted fuel consumption for PH11 and PH01 are comparable (between 6 and 10 mL of fuel per 90 ft. subsection). While this is an extreme example, the green curves from Figure 4.31 to Figure 4.34 clearly show much larger variation, suggesting some differences that are unexplained by the “control” variables. Although the HHDT shows this extreme variation for the inefficient condition, the variation between pavement types is negligible, with the exception of PH01.

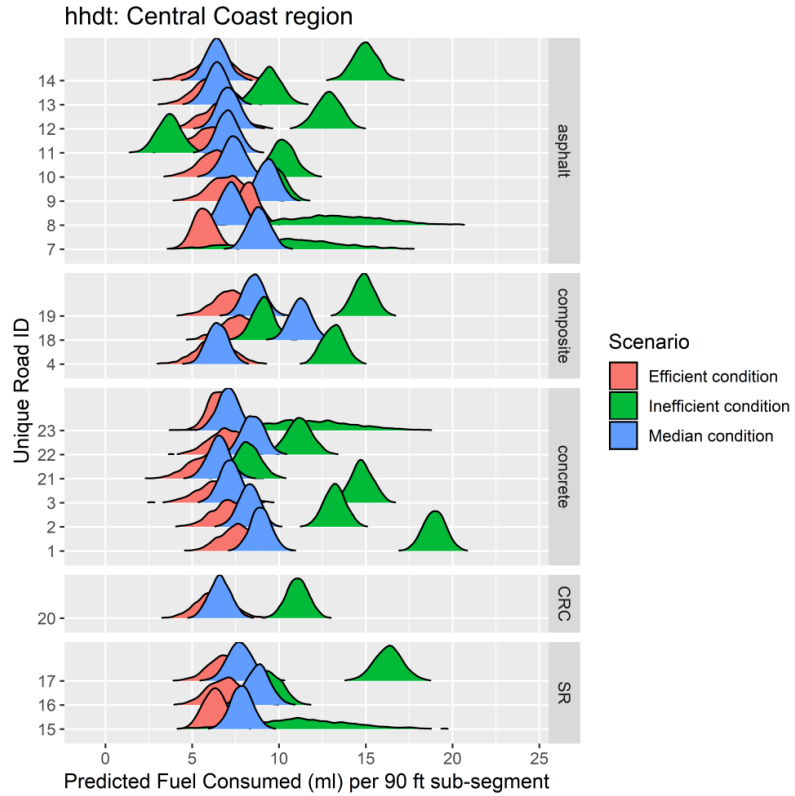


Figure 4.31: HHDT scenario for the Central Coast Region.

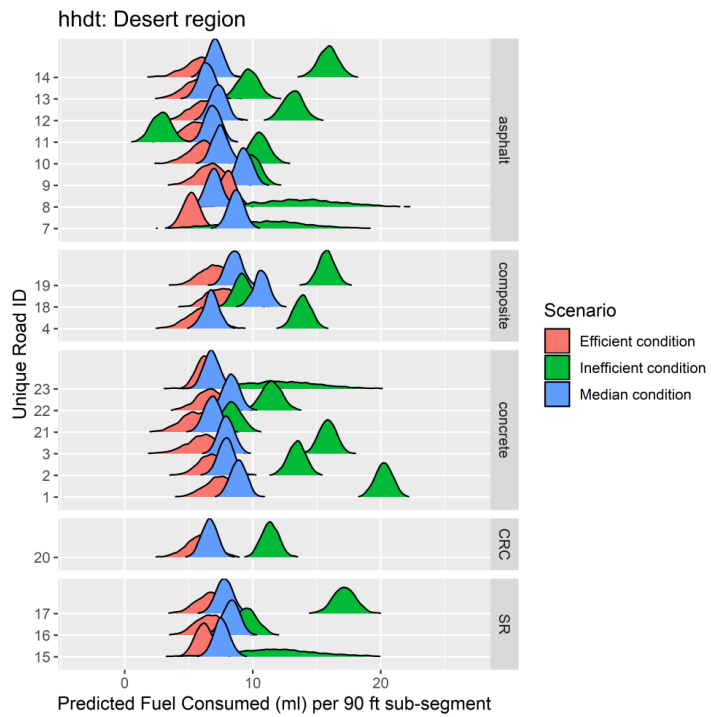


Figure 4.32: HHDT scenario for the Desert Region.

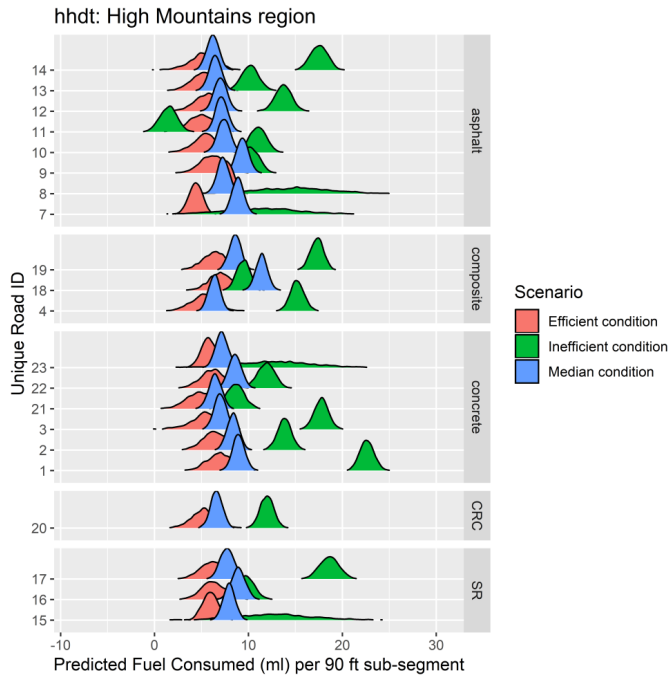


Figure 4.33: HHDT scenario for the High Mountain Region.

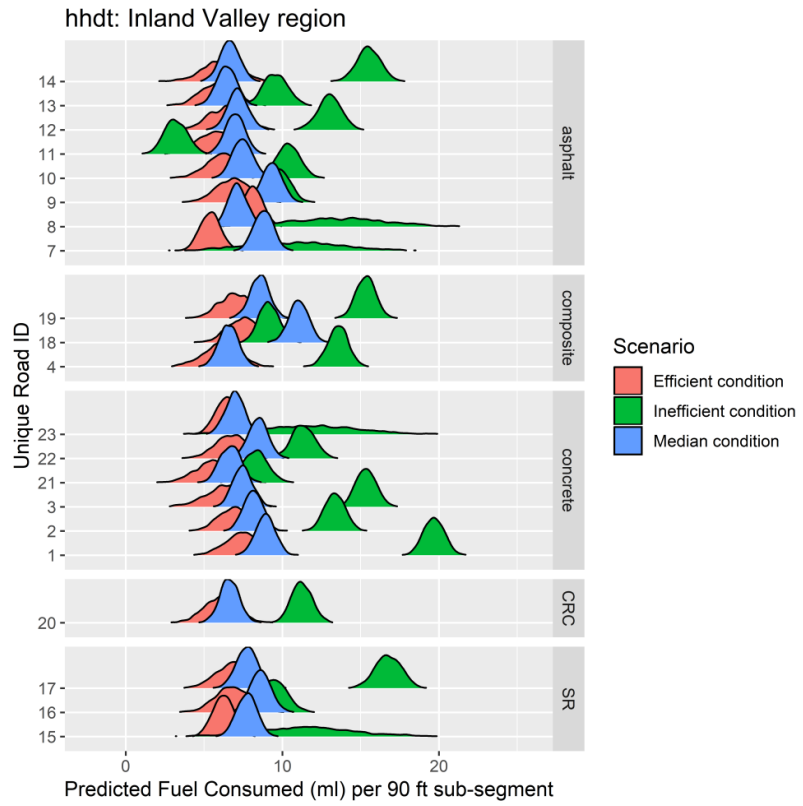


Figure 4.34: HHDT scenario for the Inland Valley Region.

5 CONCLUSIONS

The primary conclusion drawn from the results of the study is that the magnitude of a pavement structure type's influence on fuel consumption from the measurement campaign of this study is too small for meaningful conclusions about the effect of pavement type for broad classes of pavements (e.g., concrete and asphalt) to be drawn, based on the size of the dataset used in this project and the effort required to control the variables in the experimental design. The within-section variability is almost always greater than the variability between sections for a given pavement type and efficiency condition (tailwind, speed, and climate region), and the within-section variability is also usually larger than the variability between pavement types. Only the data for the heavy heavy-duty truck (HHDT) showed any meaningful difference in results between sections, but that variability is not tied to pavement type and is only present in conditions that are extremely inefficient for fuel consumption. These results indicate that missing variables (or errors in this study's existing variables) need to be reduced in any future experiments to observe the measurable effects of pavements on fuel consumption in real-world driving.

While air temperature interacting with cruise control speed had an effect on fuel consumption for the HHDT, there is a lack of clear evidence from this study that asphalt roads cause more fuel consumption for the HHDT in inefficient conditions. This suggests that pavement type is not the correct explanation for that variation. Instead, the variation in effect of air temperature interacting with cruise control speed for the HHDT likely has to do with differences in engine efficiency under different conditions.

The modeling results, documented in other reports that are part of this study, show very small changes in additional fuel consumption from structural response under most conditions, which is commensurate with the difficulty in measuring these changes in the field. Modeling shows that the most significant effects occur under conditions (hot pavement and slow-moving heavy vehicles) that are very difficult to measure for long enough sections on the state highway and local road networks to produce safe vehicle operations. It is therefore recommended that the inability of this study to find a consistent measurable effect of structural response on fuel use not be used as a reason to exclude structural response from consideration in life cycle assessment.

REFERENCES

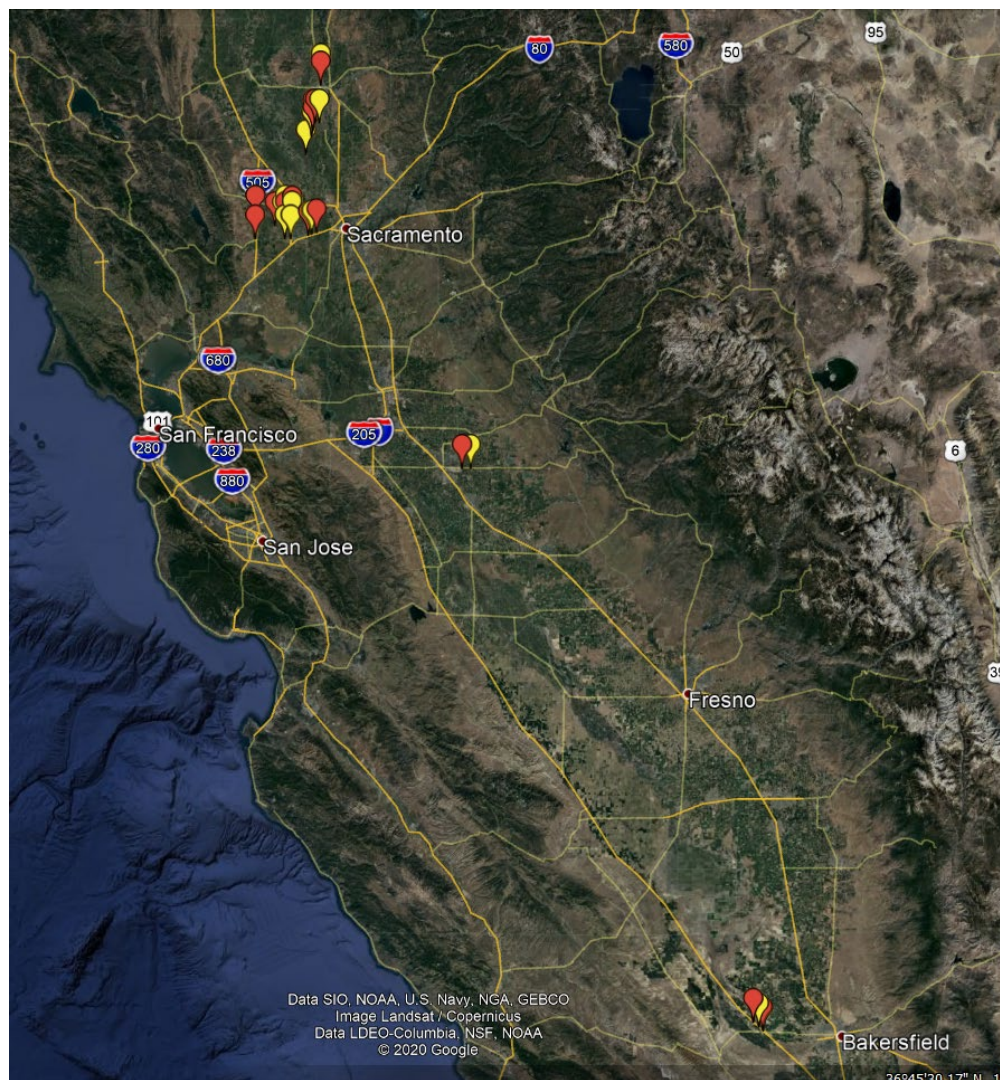
1. Harvey, J.T., Lea, J.D., Kim, C., Coleri, E., Zaabar, I., Louhghalam, A., Chatti, K., Buscheck, J., and Butt, A. 2016. *Simulation of Cumulative Annual Impact of Pavement Structural Response on Vehicle Fuel Economy for California Test Sections* (Research Report: UCPRC-RR-2015-05). Davis and Berkeley, CA: University of California Pavement Research Center. <https://escholarship.org/uc/item/3p8312vs>.
2. Flügge, W. 1975. *Viscoelasticity*. Berlin, Germany: Springer Verlag.
3. Kelly, J.M. 1962. “Moving Load Problems in the Theory of Viscoelasticity.” PhD diss.. Stanford University.
4. Huang, Y. H. 1967. “Stresses and Displacements in Viscoelastic Layered Systems under Circular Loaded Areas.” Presented at Second International Conference on Asphalt Pavements, Ann Arbor, MI.
5. Perloff, W.H. and Moavenzadeh, F. 1967. “Deflection of Viscoelastic Medium Due to a Moving Load.” Presented at Second International Conference on Asphalt Pavements, Ann Arbor, MI.
6. Hopman, P.C. 1993. *VEROAD: A Linear Viscoelastic Multilayer Program for the Calculation of Stresses, Strains and Displacements in Asphaltic Road Constructions. Part 1: A Viscoelastic Halfspace*. Delft, Netherlands: University of Technology.
7. Hajj, E.Y., Sebaaly, P.E., and Siddharthan, R.V. 2006. “Response of an Asphalt Pavement Mixture Under a Slow Moving Truck.” In *Asphalt Concrete: Simulation, Modeling, and Experimental Characterization*. Proceedings of R. Lytton Symposium on Mechanics of Flexible Pavements, Baton Rouge, LA, June 1–3, 2005.
8. Thom, N.H., Lu, T., and Parry, T. 2010. “Fuel Consumption Due to Pavement Deflection Under Load.” Presented at Second International Conference on Sustainable Construction Materials and Technologies, Ancona, Italy, June 28–30, 2010.
9. Akbarian, M., Moeini-Ardakani, S., Ulm, F.J., and Nazzal, M. 2012. “Mechanistic Approach to Pavement–Vehicle Interaction and Its Impact on Life-Cycle Assessment.” *Transportation Research Record* 2306, no. 1: 171–179.
10. Pouget, S., Sauzéat, C., Benedetto, H., and Olard, F. 2012. “Viscous Energy Dissipation in Asphalt Pavement Structures and Implication for Vehicle Fuel Consumption.” *Journal of Materials in Civil Engineering* 24, no. 5: 568–576.
11. Chupin, O., Piau, J.M., and Chabot, A. 2013. “Evaluation of the Structure-Induced Rolling Resistance (SRR) for Pavements Including Viscoelastic Material Layers.” *Materials and Structures* 46, no. 4: 683–696.
12. Loughalam, A., Akbarian, M., and Ulm, F.J. 2014. “Flügge’s Conjecture: Dissipation- Versus Deflection-Induced Pavement-Vehicle Interactions (PVI).” *Journal of Engineering Mechanics* 140, no. 8.
13. Chatti, K., and Zaabar, I. 2012. *Estimating the Effects of Pavement Condition on Vehicle Operating Costs* (NCHRP Report 720). Washington, DC: Transportation Research Board..

14. Van Dam, T. J., Harvey, J.T., Muench, S., Smith, K.D., Snyder, M.B., Al-Qadi, I.L., Ozer, H., Meijer, J., Ram, P.V., Roesler, J.R., and Kendall, A. 2015. *Towards Sustainable Pavement Systems: A Reference Document* (FHWA-HIF-15-002). Washington, DC: Federal Highway Administration. www.fhwa.dot.gov/pavement/sustainability/hif15002/hif15002.pdf.
15. Zaniewski, J.P., Butler, B.C., Cunningham, G., Elkins, G.E., Paggi, M.S., and Machemehl, R. 1982. *Vehicle Operating Costs, Fuel Consumption, and Pavement Type and Condition Factors* (FHWA/PL/82/001). Washington, DC: Federal Highway Administration. <https://rosap.nsl.bts.gov/view/dot/1012>.
16. Taylor, G.W., and Patten, J.D. 2006. *Effects of Pavement Structure on Vehicle Fuel Consumption—Phase III*. (CSTT-HVC-TR-068). Ottawa, Canada: Centre for Surface Transportation Technology.
17. Ardekani, S.A., and Sumitsawan, P. 2010. *Effect of Pavement Type on Fuel Consumption and Emissions in City Driving*. Alexandria, VA: Ready Mixed Concrete (RMC) Research & Education Foundation . <https://rmc-foundation.org/wp-content/uploads/2017/07/UTA-Fuel-Consumption-Emissions-Study-Final-3-10.pdf>.
18. Bienvenu, M., and Jiao, X. 2013. *Comparison of Fuel Consumption on Rigid Versus Flexible Pavements Along I-95 in Florida*. Miami, FL: Florida International University.
19. Hultqvist, B.A. 2013. *Measurement of Fuel Consumption on Asphalt and Concrete Pavements North of Uppsala: Measurements with Light and Heavy Goods Vehicle* (VTI Note 18–2013). Linköping, Sweden: Swedish National Road and Transport Research Institute (VTI). <http://vti.diva-portal.org/smash/get/diva2:669314/FULLTEXT01.pdf>.
20. Hammarström, U., and Karlsson, B. 1987. *VETO: A Computer Program for Calculating Transportation Costs as a Function of Road Standards*. Linköping, Sweden: Swedish National Road and Transport Research Institute (VTI).
21. Karlsson, R., Carlson, A., and Dolk, E. 2012. *Energy Use Generated by Traffic and Pavement Maintenance: Decision Support for Optimization of Low Rolling Resistance Maintenance Treatments* (VTI Note 36A–2012). Linköping, Sweden: Swedish National Road and Transport Research Institute (VTI). <http://vti.diva-portal.org/smash/get/diva2:669289/FULLTEXT01.pdf>.
22. Hammarström, U., Eriksson, J., Karlsson, R., and Yahya, M.R. 2012. *Rolling Resistance Model, Fuel Consumption Model and the Traffic Energy Saving Potential from Changed Road Surface Conditions* (VTI Report 748A). Linköping, Sweden: Swedish National Road and Transport Research Institute (VTI). <http://vti.diva-portal.org/smash/get/diva2:670621/FULLTEXT01.pdf>.
23. Coleri, E., Harvey, J., Zaabar, I., Louhghalam, A., and Chatti, K. 2016. “Model Development, Field Section Characterization, and Model Comparison for Excess Vehicle Fuel Use Attributed to Pavement Structural Response.” *Transportation Research Record* 2589, no.: 40–50.

24. Li, H. 2012. *Evaluation of Cool Pavement Strategies for Heat Island Mitigation: Improving Outdoor Thermal Environment in Hot Climates through Cool Pavement Design Strategies* (Research Report: UCD-ITS-RR-12-33). Davis, CA: Institute of Transportation Studies. escholarship.org/content/qt6mr4k9t1/qt6mr4k9t1_noSplash_9ab61b14762e84b7d61994b7aa5e0d1b.pdf?t=pyhuvvm.
25. Natural Resources Canada. 2014. *AutoSmart—Learn the Facts: Cold Weather Effects on Fuel Efficiency*. [Ottawa, Canada: Natural Resources Canada. www.nrcan.gc.ca/sites/www.nrcan.gc.ca/files/oe/pdf/transportation/fuel-efficient-technologies/autosmart_factsheet_3_e.pdf](http://www.nrcan.gc.ca/sites/www.nrcan.gc.ca/files/oe/pdf/transportation/fuel-efficient-technologies/autosmart_factsheet_3_e.pdf).
26. Stan Development Team. n.d. “Stan User’s Guide: Version 2.24.” https://mc-stan.org/docs/2_24/stan-users-guide/index.html#overview.

APPENDIX A: TEST SECTIONS LOCATION, AVERAGE ROUGHNESS, AND MACROTEXTURE

The test sections are located mainly around Sacramento and Bakersfield as shown in Figure A.1.



Note: Yellow marks represent the start point of sections and red marks represent the end points of sections.

Figure A.1: Pavement test sections located in California, shown on Google Maps.

The following discussion briefly describes the location of each test section and shows it on Google Maps. All the test sections lie in the outer lane/truck lane of a multilane highway or county road.

1. PH01 and PH02

PH01 is a northbound concrete pavement section and PH02 is a southbound concrete pavement section located on Highway 113 between Road 29 and Road 27 in Yolo County. The sections fall under Caltrans District 3 between postmile (PM) 4.5 and PM6. The location of the PH01 and PH02 sections is shown in Figure A.2 to Figure A.5.

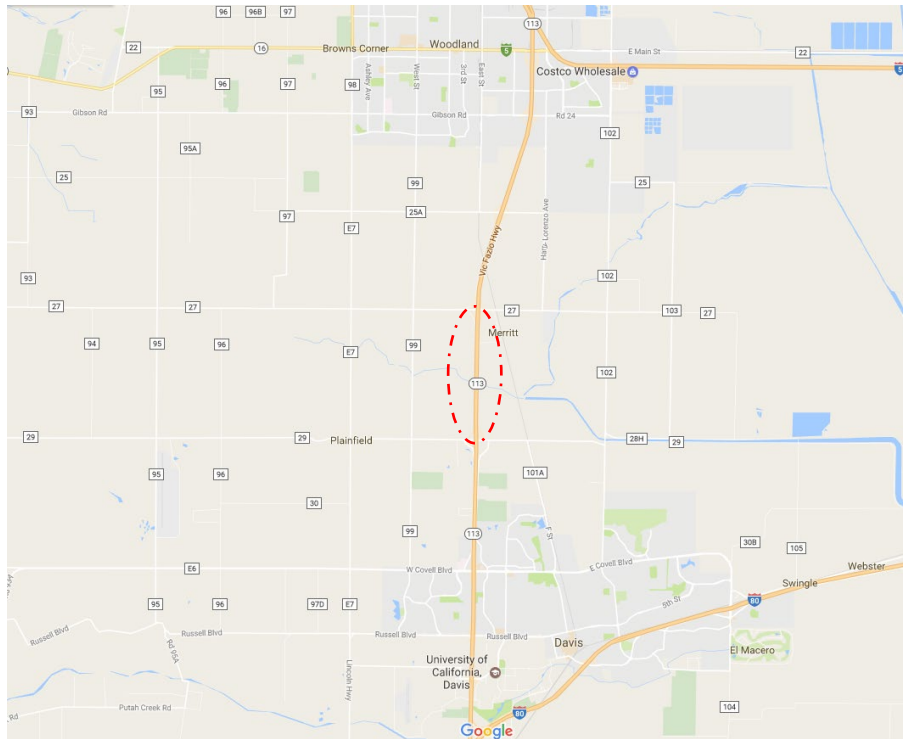


Figure A.2: PH01 is a northbound concrete pavement section and PH02 is a southbound concrete pavement section on Highway 113 in Yolo County on Google Maps.



Figure A.3: PH01 location on Google Earth.



Figure A.4: PH02 location on Google Earth.

An on-site photo of southbound section PH02 on Highway 113 is shown in Figure A.5. (PH01 is not shown, as it is the same pavement type as PH02.)



Figure A.5: On-site location photograph of PH02.

2. PH03 and PH04

PH03 is a northbound concrete pavement section and PH04 is a southbound composite pavement section located on Highway 505 between Road 27 and Road 32 in Yolo County. The sections fall under Caltrans District 3 between PM0.5 and PM6. The location of the PH03 and PH04 sections is shown in Figure A.6 to Figure A.10.

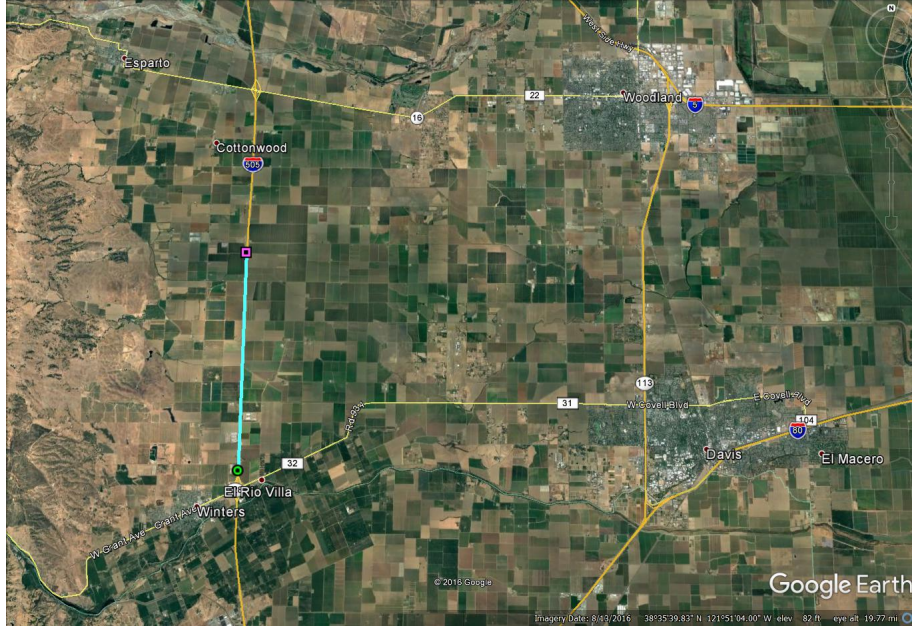


Figure A.6: PH03 is a northbound concrete and PH04 is a southbound composite pavement section on Highway 505 in Yolo County on Google Earth.



Figure A.7: PH03 location on Google Earth.



Figure A.8: PH03 on-site location photograph during falling weight deflectometer (FWD) closures.

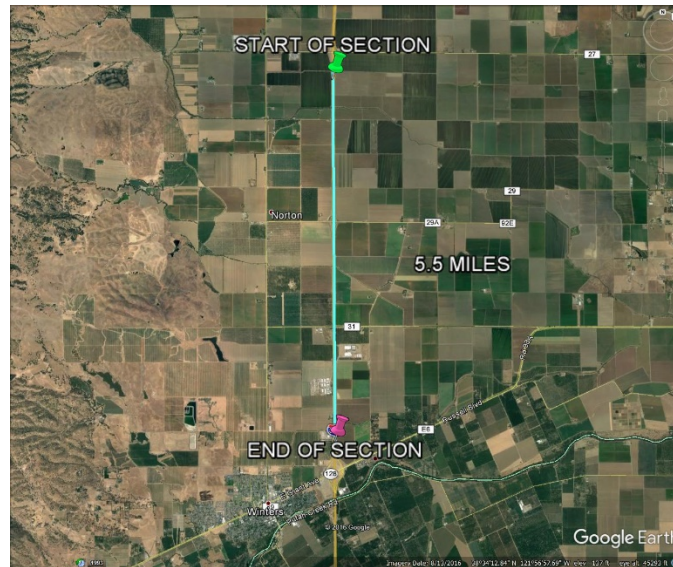


Figure A.9: PH04 location on Google Earth.



Figure A.10: PH04 on-site location photograph.

3. PH07

PH07 is a northbound asphalt pavement section located on county road 98 (CR98) between Road 27 and Road 29 in Yolo County and runs parallel to Highway 113. The location of the PH07 section is shown in Figure A.11 to Figure A.13.

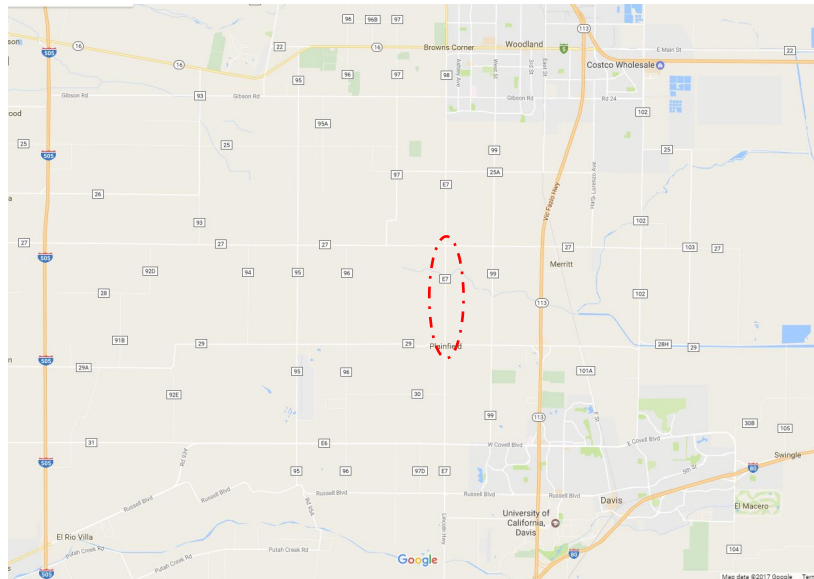


Figure A.11: PH07 is a northbound asphalt pavement section on CR98 on Google Maps.

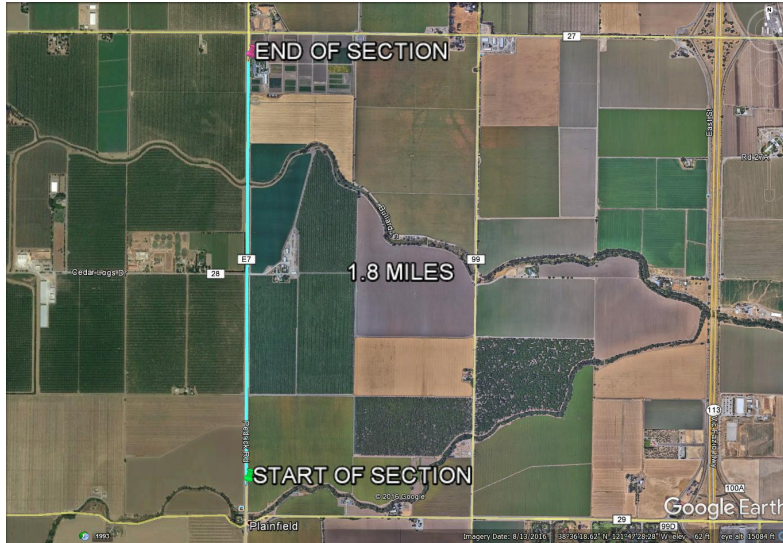


Figure A.12: PH07 location on Google Earth.



Figure A.13: PH07 on-site location photograph from Google Maps.

4. PH08

PH08 is an eastbound asphalt pavement section located on CR29 between Road 95 and Road 98 in Yolo County. The location of the PH08 section shown in Figure A.14 to Figure A.16.

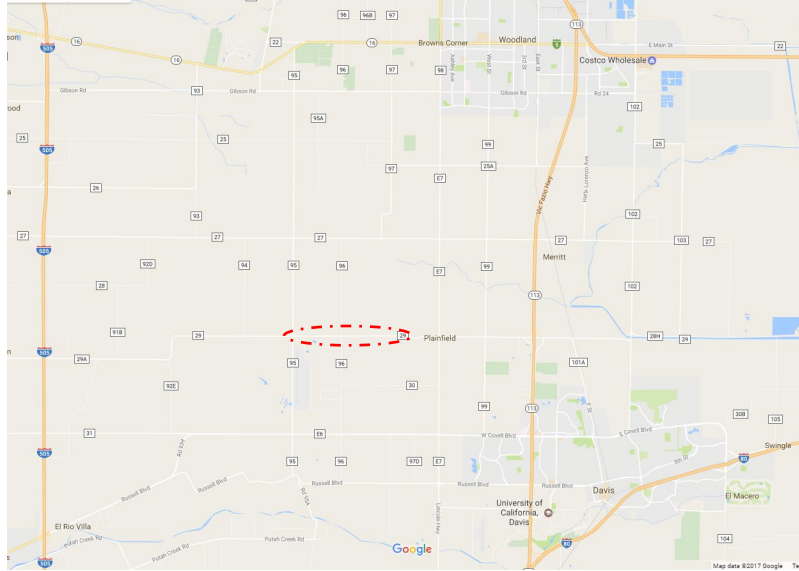


Figure A.14: PH08 is an eastbound asphalt pavement section on CR29 on Google Maps.



Figure A.15: PH08 location on Google Earth.



Figure A.16: PH08 on-site location photograph from Google Maps.

5. PH09 and PH10

PH09 is a northbound asphalt pavement section and PH10 is a southbound asphalt pavement section located on Highway 113 in Sutter County. The sections fall under Caltrans District 3 between PM5.35 and PM10. The location of the PH09 and PH10 sections is shown in Figure A.17 to Figure A.20.

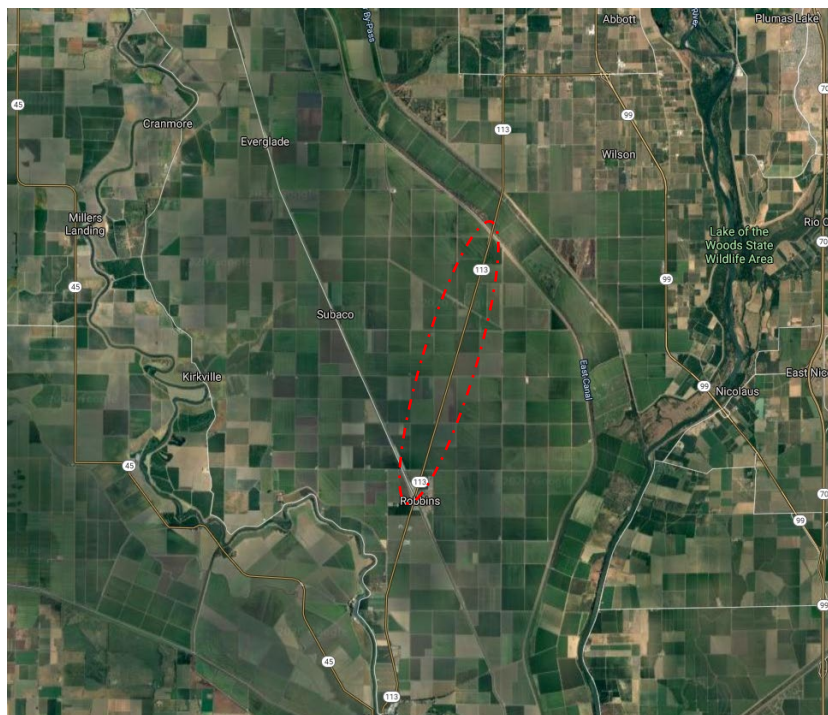


Figure A.17: PH09 is a northbound asphalt pavement section and PH10 is a southbound asphalt pavement section on Highway 113 in Sutter County on Google Maps.



Figure A.18: PH09 location on Google Earth.

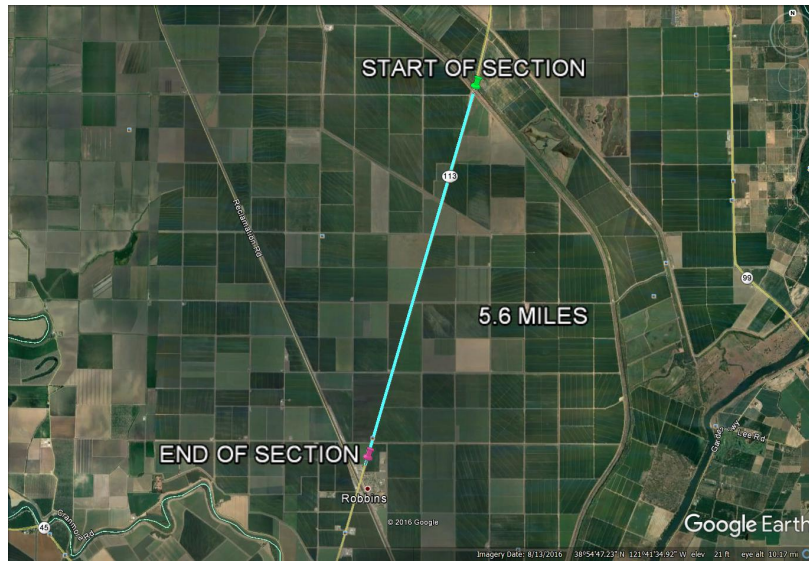


Figure A.19: PH10 location on Google Earth.



Figure A.20: On-site location photograph of PH09 (right lane) and PH10 (left lane) from Google Maps.

6. PH11 and PH12

PH11 is a northbound and PH12 is a southbound asphalt pavement sections located on Highway 113 in Sutter County. The sections fall under Caltrans District 3 between PM12 and PM14. The location of the PH11 and PH12 sections is shown in Figure A.21 to Figure A.24.



Figure A.21: PH11 is a northbound and PH12 is a southbound pavement section on Highway 113 in Sutter County on Google Maps.



Figure A.22: PH11 location on Google Earth.

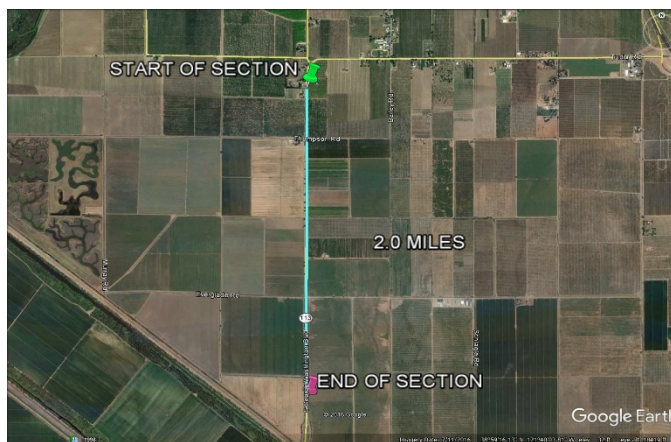


Figure A.23: PH12 location on Google Earth.



Figure A.24: On-site location photograph of PH11 (right lane) and PH12 (left lane) from Google Maps.

7. PH13 and PH14

PH13 is a northbound and PH14 is a southbound asphalt pavement sections located on Highway 113 in Sutter County. The sections fall under Caltrans District 3 between PM15 and PM16. The location of the PH11 and PH12 sections is shown in Figure A.25 to Figure A.28.



Figure A.25: PH13 is a northbound and PH14 is a southbound pavement section on Highway 113 in Sutter County on Google Maps.

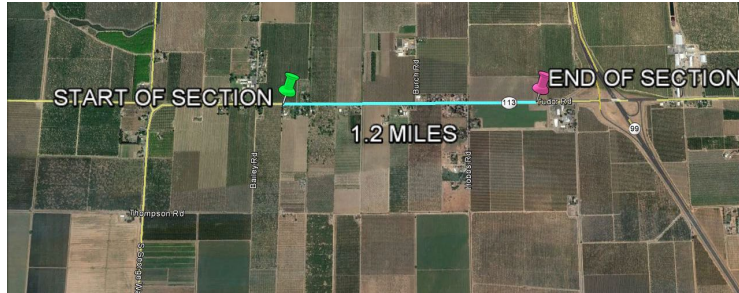


Figure A.26: PH13 location on Google Earth.

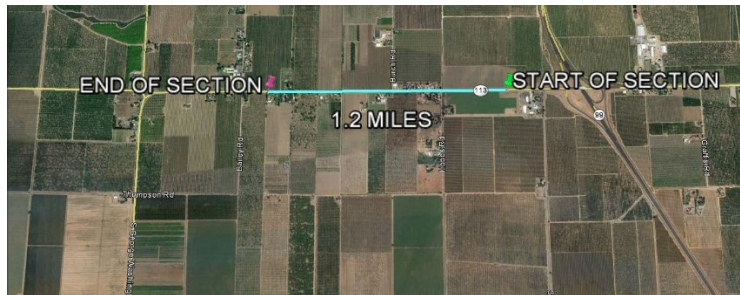


Figure A.27: PH14 location on Google Earth.



Figure A.28: On-site location photograph of PH13 (right lane) and PH14 (left lane) from Google Maps.

8. PH15

PH15 is an eastbound semi-rigid pavement section located on CR32B (Chiles Road) in Yolo County. The section runs parallel to I-80 northbound in Davis. The location of the PH15 section is shown in Figure A.29 to Figure A.31.

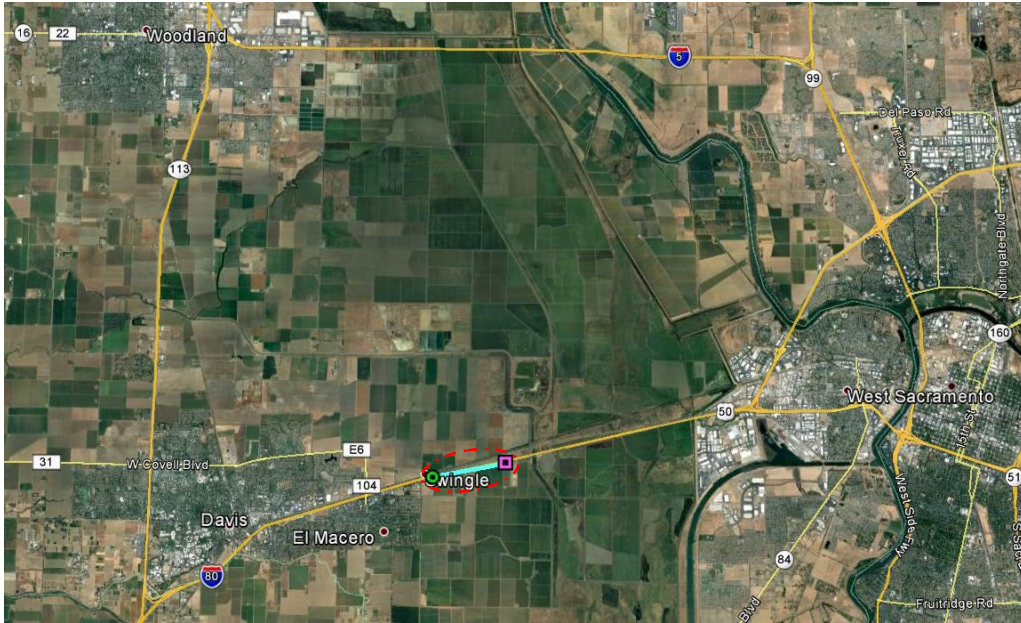


Figure A.29: PH15 is an eastbound pavement section on CR32B (Chiles Road) on Google Maps.

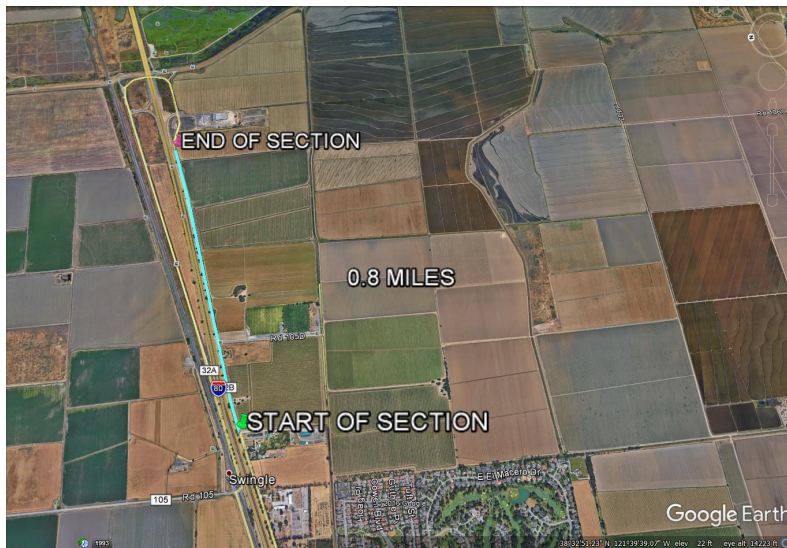


Figure A.30: PH15 location on Google Earth.



Figure A.31: On-site location photograph of PH15 (right lane) from Google Maps.

9. PH16 and PH17

PH16 is an eastbound semi-rigid pavement section and PH17 is a westbound semi-rigid pavement section located on Highway 132 in Stanislaus County. The sections fall under Caltrans District 10 between PM20.4 and PM22.8. The location of the PH16 and PH17 sections are shown in Figure A.32 to Figure A.35.

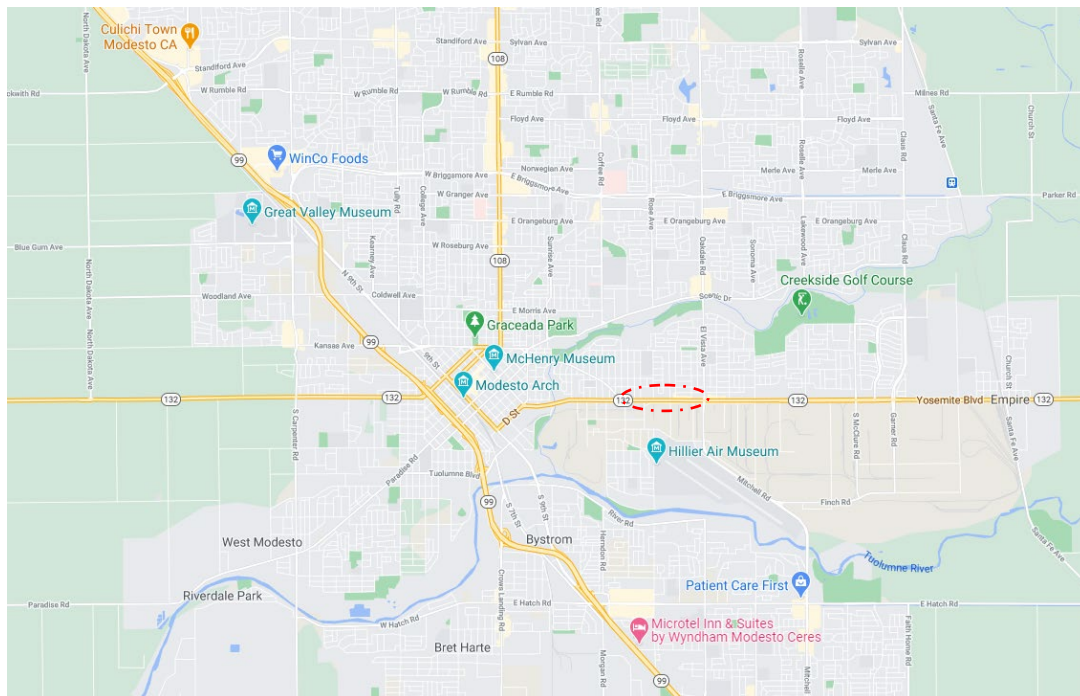


Figure A.32: PH16 is an eastbound semi-rigid pavement section and PH17 is a westbound semi-rigid pavement section on Highway 132 in Stanislaus County on Google Maps.

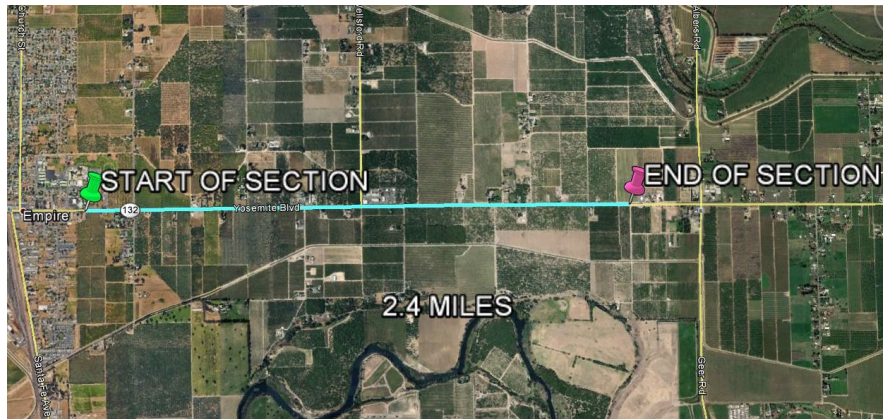


Figure A.33: PH16 location on Google Earth.

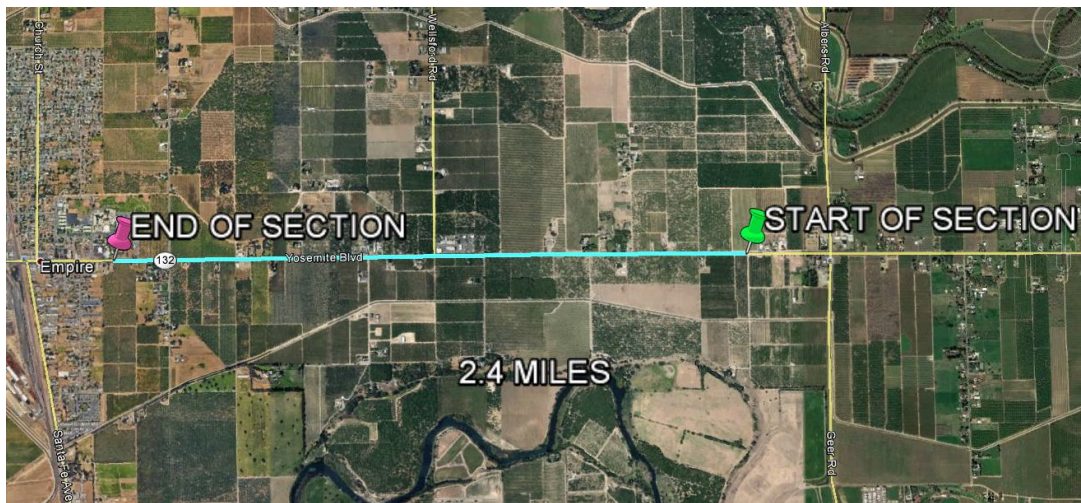


Figure A.34: PH17 location on Google Earth.



Figure A.35: On-site location photograph of PH16 (right lane) and PH17 (left lane) from Google Maps.

10. PH18, PH19 and PH20

PH18 is a southbound composite pavement section and PH19 is a northbound composite pavement section, while PH20 is a southbound continuously reinforced concrete pavement section located on Interstate Highway 5 (I-5) in Kern County. The sections fall under Caltrans District 10 between PM52.5 and PM56.3 located in Buttonwillow. The location of the PH18, PH19, and PH20 sections are shown in Figure A.36 to Figure A.41.

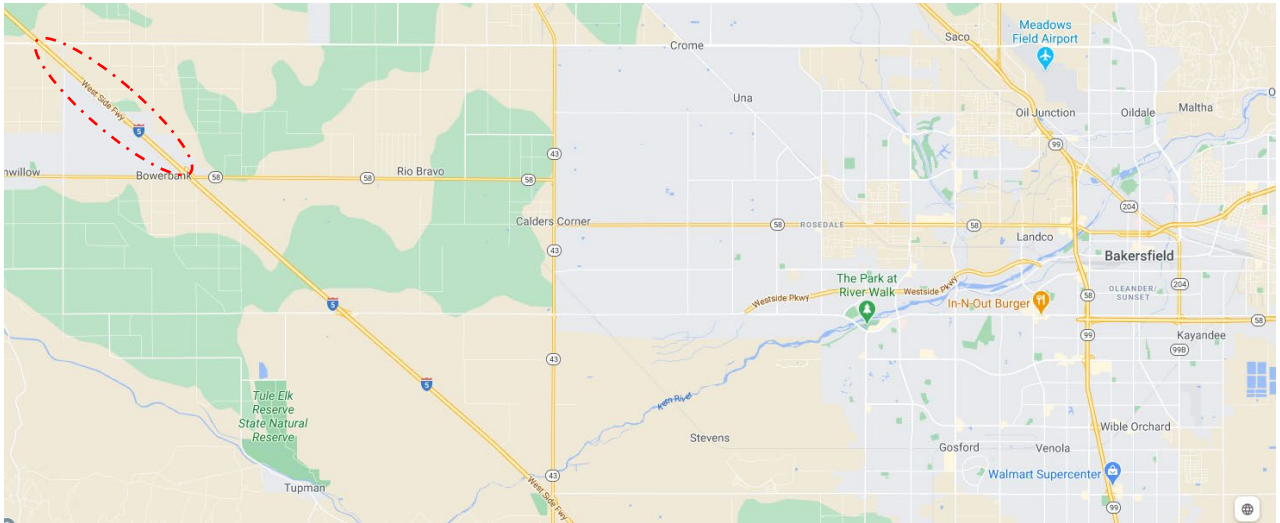


Figure A.36: PH19 is a northbound pavement section, and PH18 and PH20 are southbound pavement sections on I-5 in Kern County on Google Maps.



Figure A.37: PH18 location on Google Earth.



Figure A.38: PH19 location on Google Earth.



Figure A.39: PH20 location on Google Earth.



Note: PH18 is not shown as both PH18 and PH19 are the same pavement type.

Figure A.40: PH19 On-site location photograph during coring pavement sample under Caltrans closure.



Figure A.41: On-site location photograph of PH20 (right lane) during Caltrans closure.

11. PH21 and PH22

PH21 is a northbound concrete pavement section and PH22 is a southbound concrete pavement section located on Highway 99 in Sutter County. The sections fall under Caltrans District 3 between PM31.5 and PM33.7. The location of the PH21 and PH22 sections are shown in Figure A.42 to Figure A.45.

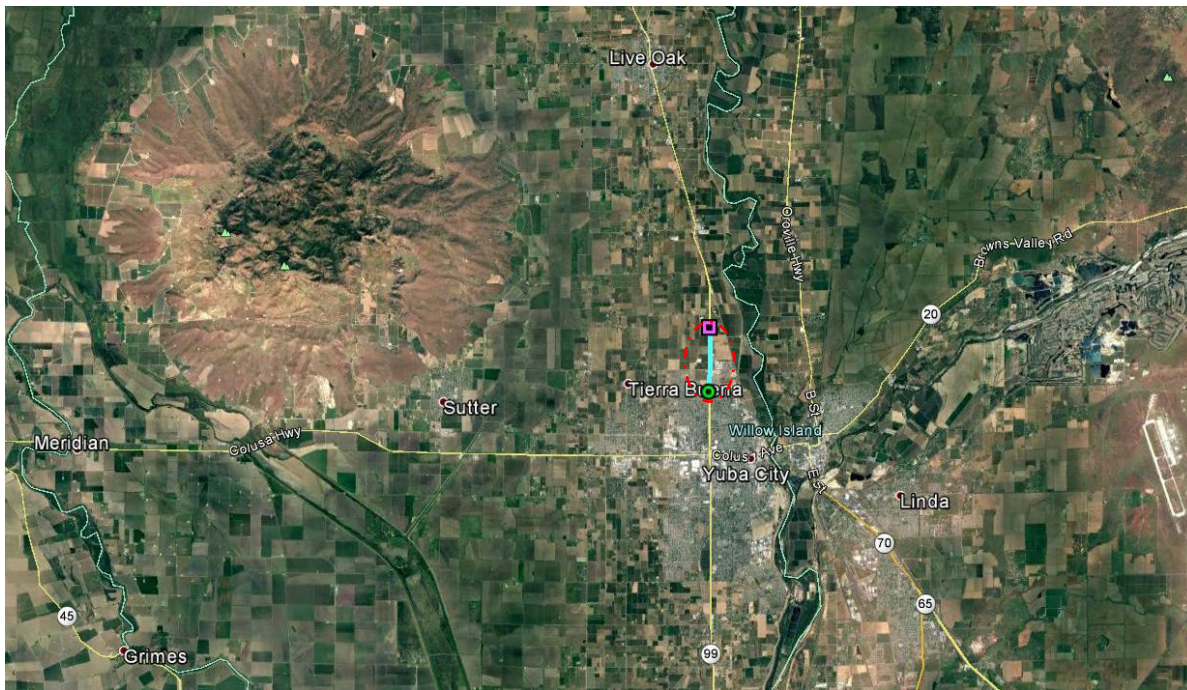


Figure A.42: PH21 is a northbound concrete pavement section and PH22 is a southbound concrete pavement section on Highway 99 in Sutter County on Google Maps.

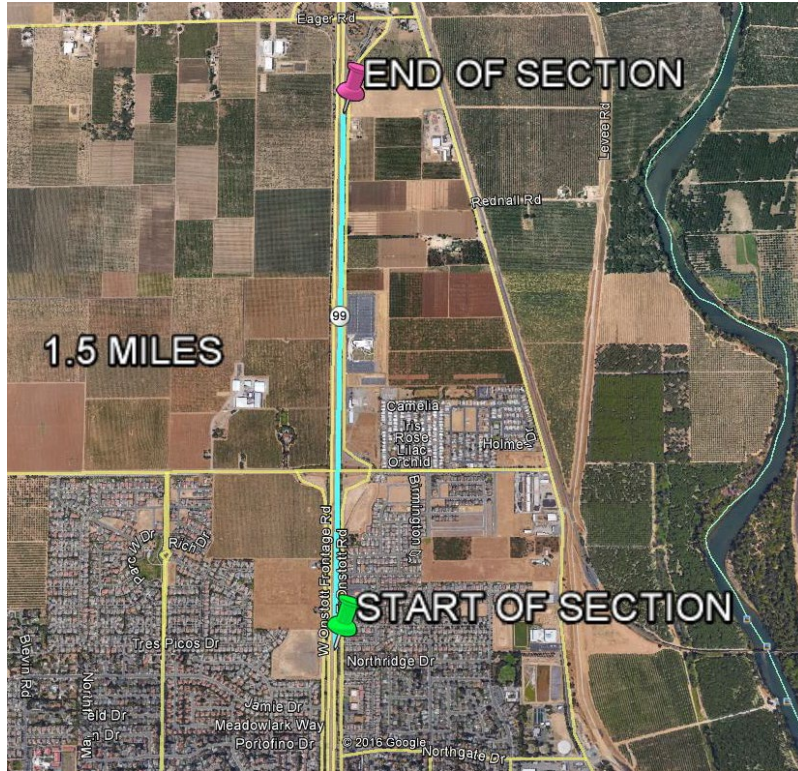


Figure A.43: PH21 location on Google Earth.



Figure A.44: PH22 location on Google Earth.



Note: PH22 is not shown as PH21 and PH22 are both the same pavement type.

Figure A.45: PH21 On-site location photograph from Google Maps.

12. **PH23**

PH23 is a westbound concrete pavement section located on CR32A in Yolo County. The section runs parallel to I-80 southbound in Davis. The location of the PH23 section is shown in Figure A.46 to Figure A.48.

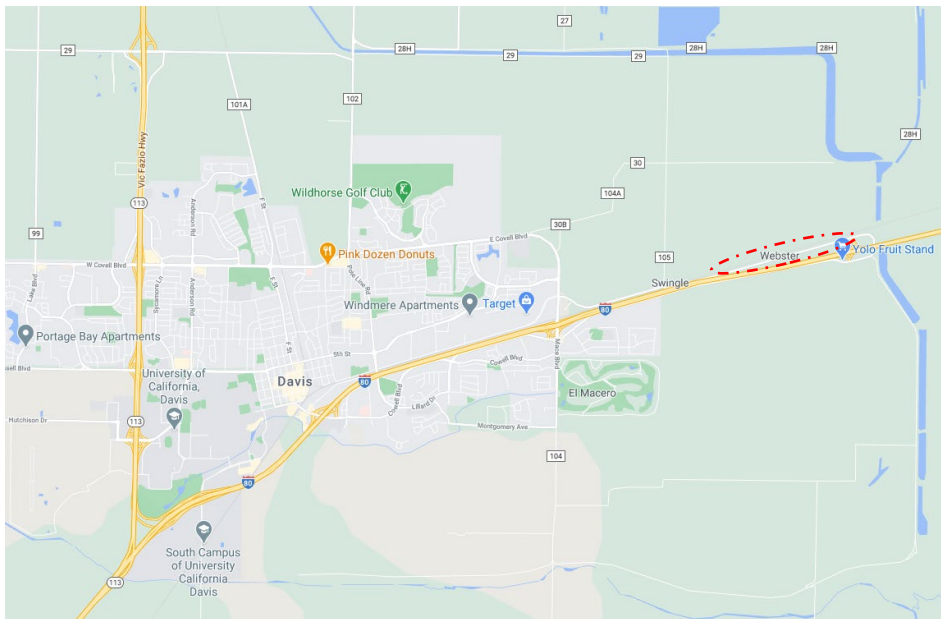


Figure A.46: PH23 is a westbound concrete pavement section on CR32A in Yolo County on Google Maps.

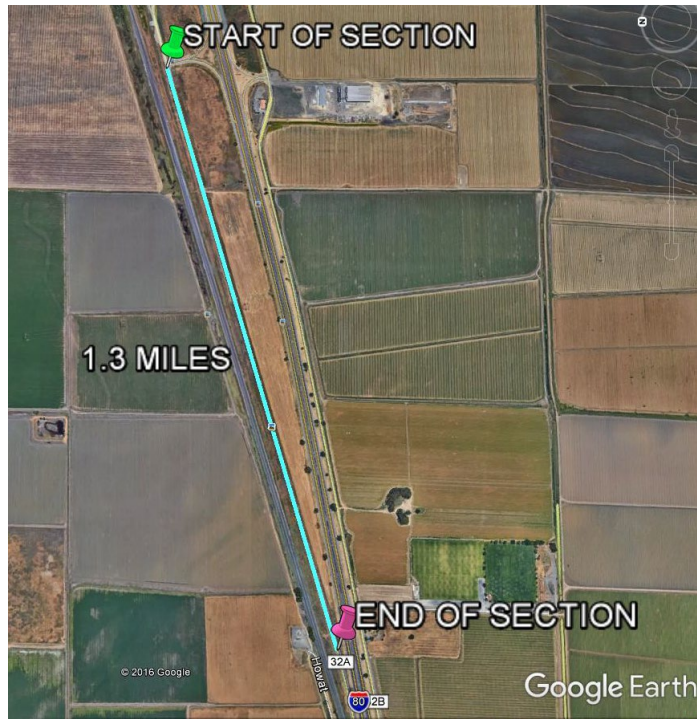


Figure A.47: PH23 location on Google Earth.



Figure A.48: PH23 (right lane) on-site location photograph from Google Maps.

Roughness and Macrotexture of Sections

Most of the sections selected for the study had low roughness and microtexture of less than 1 mm, with an exception for a few with high roughness as shown in Figure A.49.

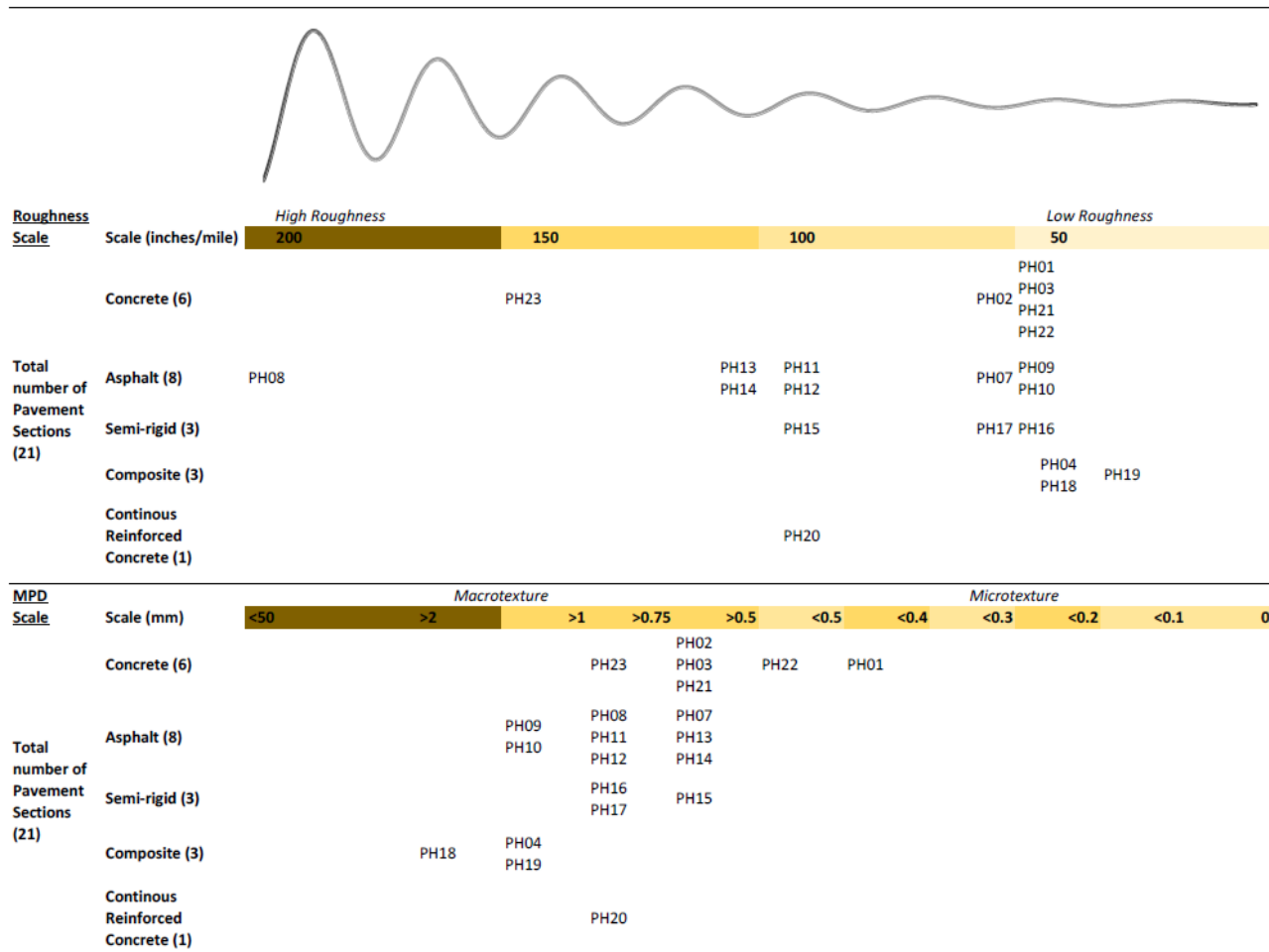


Figure A.49: Roughness and macrotecture scale for the test sections factorial.

APPENDIX B: PAVEMENT STRUCTURE INFORMATION FROM GROUND PENETRATING RADAR AND SITE INVESTIGATION

1. PH01, PH02, and PH03

Figure B.1 to Figure B.3 present pavement structure information using the data from ground penetrating radar (GPR). No cores were taken from concrete pavement sections.

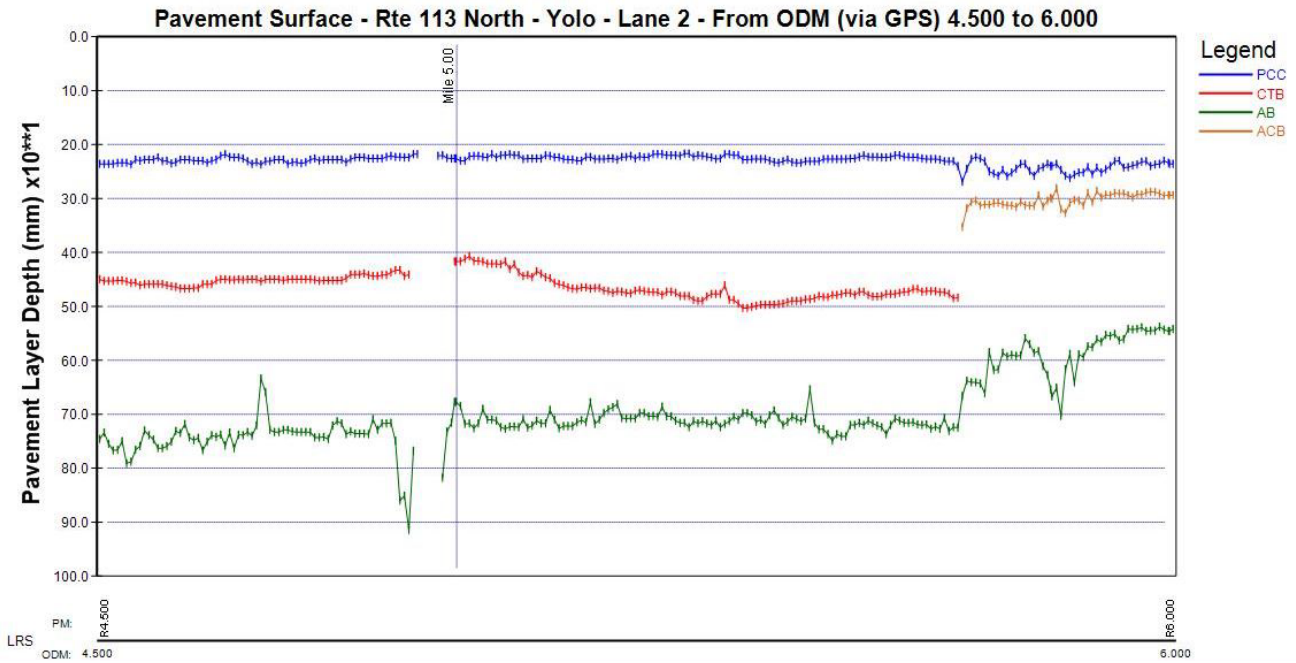


Figure B.1: GPR data for section PH01.

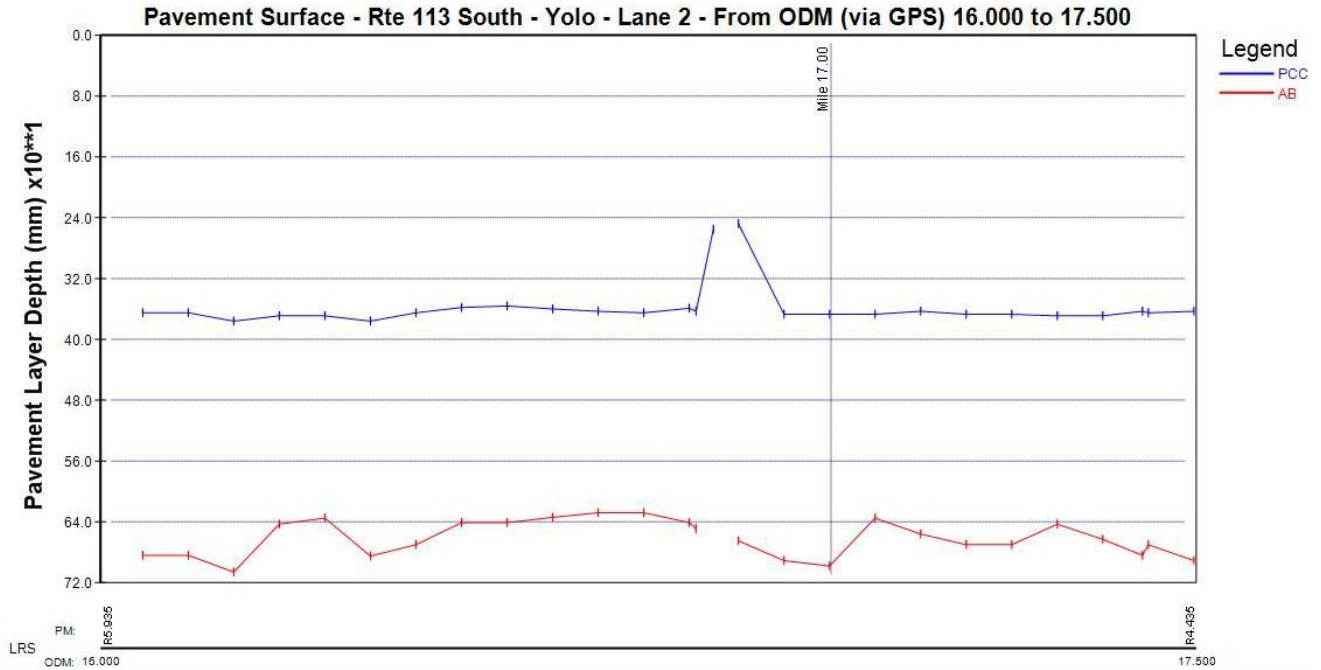


Figure B.2: GPR data for section PH02.

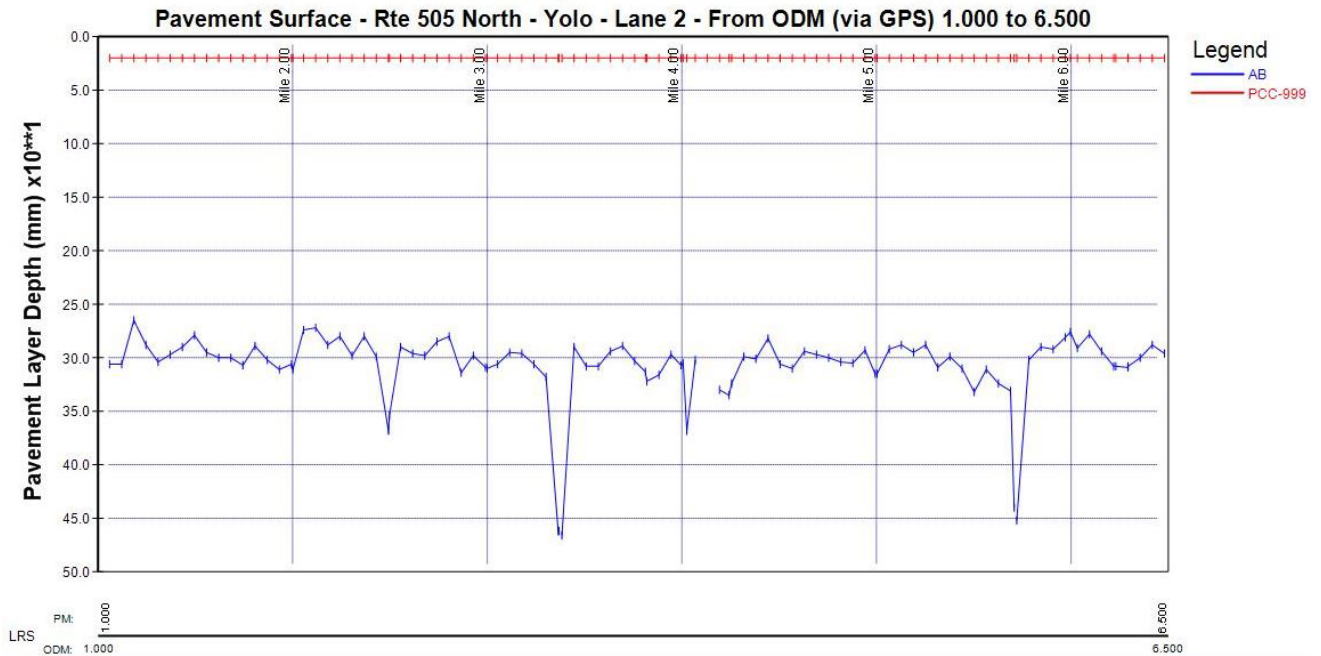


Figure B.3: GPR data for section PH03.

2. PH04

Figure B.4 presents pavement structure from the GPR data. A core was taken from the center of the outer lane during the FWD testing closures, as shown in in Figure B.5. The cored sample is shown in Figure B.6.

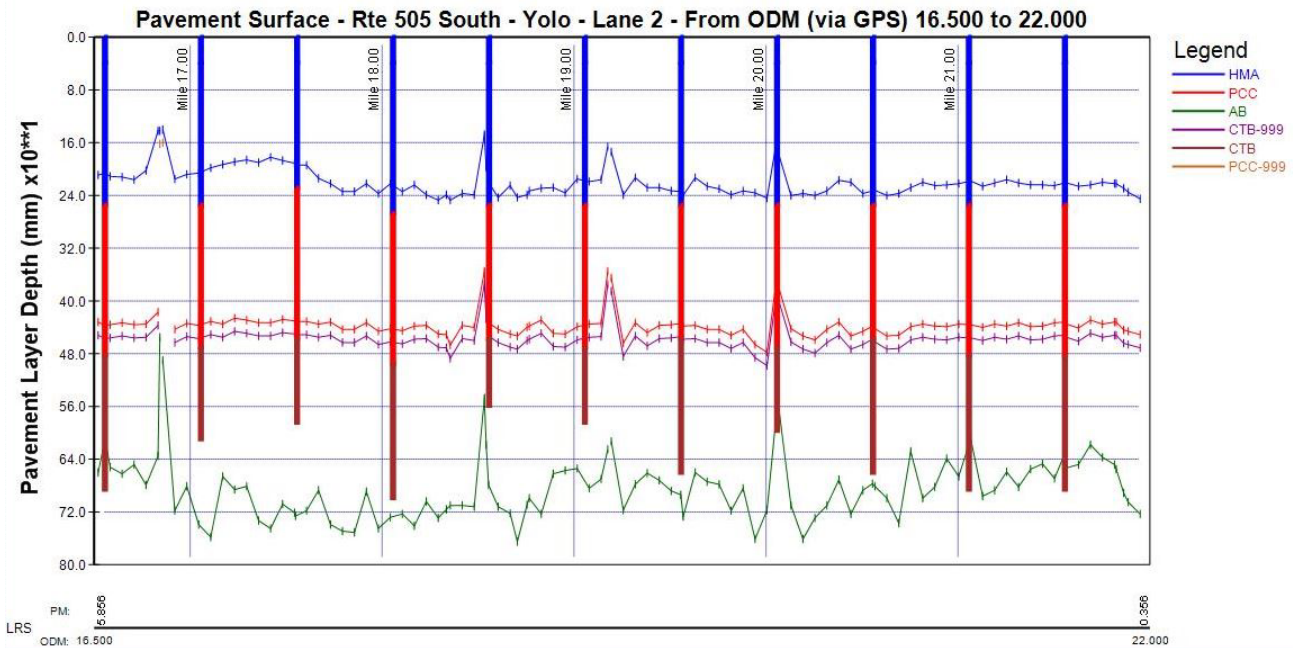


Figure B.4: GPR data for section PH04.

Date cored: 06/15/2016

District: 03

County: Yolo

Route: 505

Direction: Southbound

Lane number: 2/2

GPS coordinates of core location: (38.61434669, -121.95359999)

Postmile: 6.3

Cored ID: YOL505SB-PH04-C1

Shoulder soil classification: CL

Location description: After SB off-ramp RD 27 towards Winters



Figure B.5: Pavement core and subgrade soil sample locations for PH04 from Google Maps.

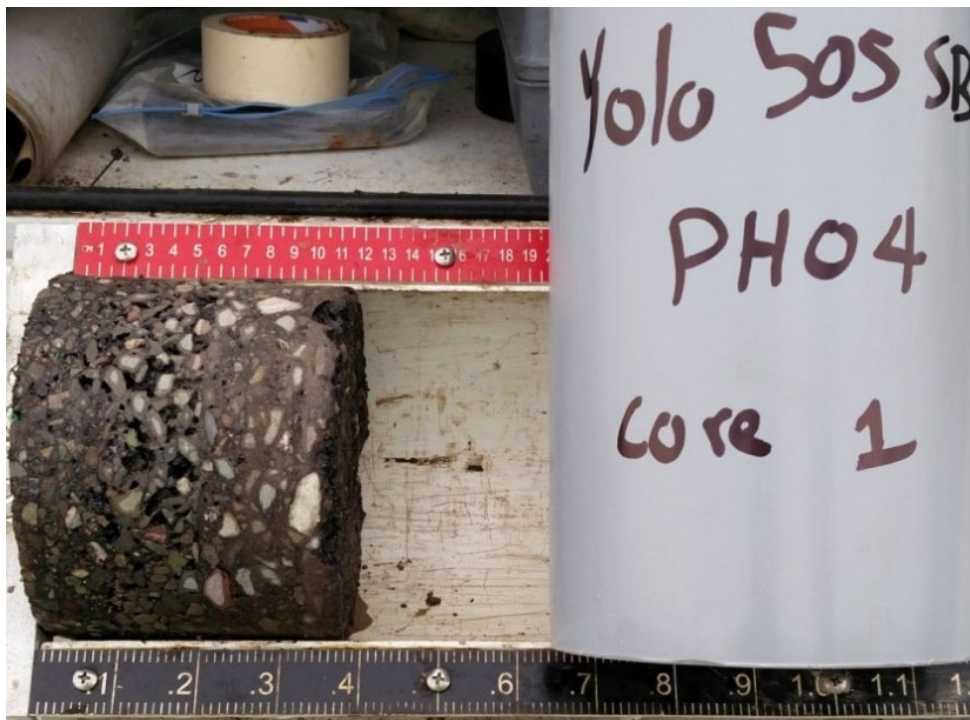


Figure B.6: Pavement core sample for PH04.

Information from the core sample is presented in Table B.1.

Table B.1: Layer Thicknesses Recorded from the Core Sample for PH04

Type	Thickness (in.)(mm)
RHMA-G	1.2 in. (30.5 mm)
HMA-O	1.2 in. (30.5 mm)
HMA	2.0 in. (51.8 mm)

Notes:

- RHMA-G = rubberized hot mix asphalt, gap-graded
- HMA-O = hot mix asphalt, open-graded
- HMA = hot mix asphalt

3. PH07 and PH08

Caltrans collects GPR data only on state highways, so no GPR data exists for PH07 and PH08. No cores were allowed to be taken on the newly built CR98 pavement section (PH07) in Yolo County. Figure B.7 shows the locations where the core and soil samples were collected. An HMA layer lift thickness of only 4 in. was recorded from the core, as shown in Figure B.8.

Cored: 06/30/2016

District: 03

County: Yolo

Route: 29

Direction: Eastbound

Lane number: 1/1

GPS coordinates of core location: (3859059664, -121.85390332)

Postmile: N/A

Cored ID: YOL29EB-PH08-C1

Shoulder soil classification: CL

Location description: After Aviation Avenue, near Yolo County Airport entrance



Figure B.7: Pavement core and subgrade soil sample locations for PH08 from Google Maps.



Figure B.8: Pavement core sample for PH08.

4. PH09

Figure B.9 presents pavement structure from the GPR data for PH09. A core was taken from the center of the lane during the FWD testing closures, as can be seen in Figure B.10. The cored sample can be seen in Figure B.11. Information from the core sample is presented in Table B.2.

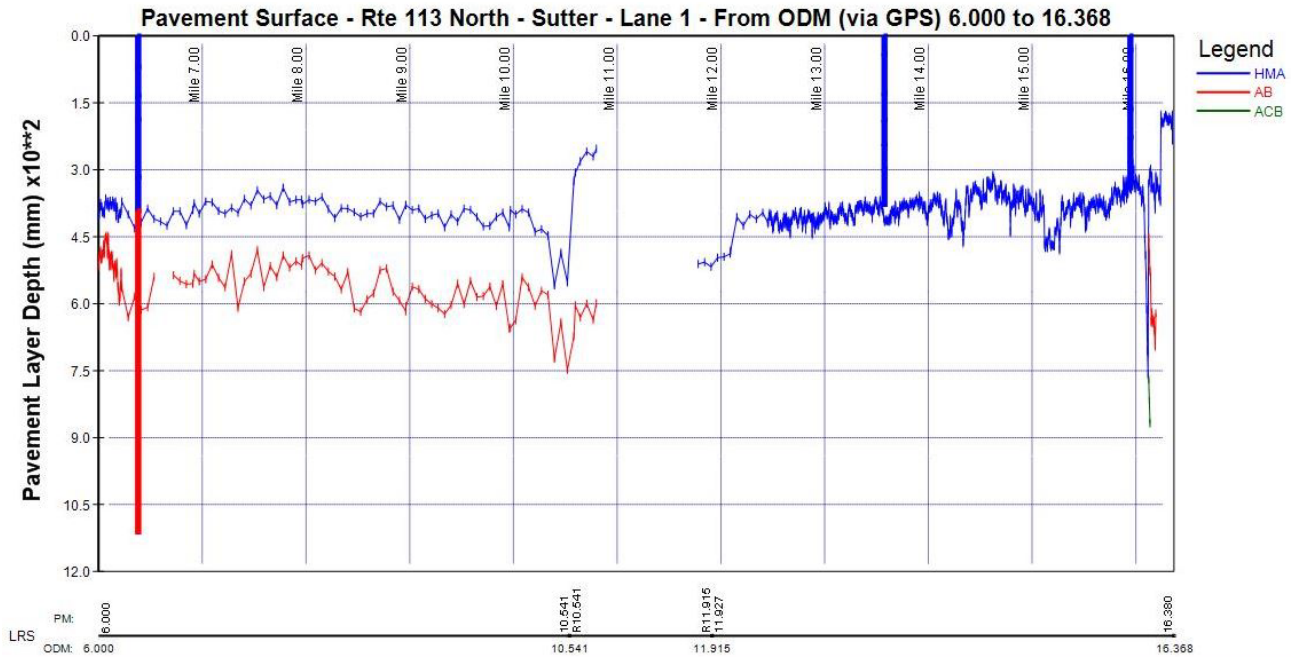


Figure B.9: GPR data for sections PH09, PH11, and PH13.

Cored: 08/25/2016

District: 03

County: Sutter

Route: 113

Direction: Northbound

Lane number: 1/1

GPS coordinates of core location: (38.92763334, -121.68608665)

Postmile: 9.0

Cored ID: SUT113NB-PH-09-C3

Shoulder soil classification: CL

Location description: At PM9.0, perpendicular to blue callbox



Figure B.10: Pavement core and subgrade soil sample locations for PH09 from Google Maps.



Figure B.11: Pavement core sample for PH09.

Table B.2: Layer Thicknesses Recorded from the Core Sample for PH09

Type	Thickness (in.)(mm)
RHMA-O	1.0 in. (24.4 mm)
HMA	2.6 in. (66 mm)
HMA	3.0 in. (76.2 mm)
HMA	3.6 in. (91.4 mm)

Notes:

- RHMA-O = rubberized hot mix asphalt, open-graded
- HMA = hot mix asphalt

5. PH10

No GPR data is available for PH10, as PH09 and PH10 are, respectively, single lane northbound and southbound state highways of similar structure without a median structure. A core was taken from the center of the lane during the FWD testing closures, as shown in Figure B.12. The cored sample is shown in Figure B.13. Information from the core sample is presented in Table B.3.

Date cored: 08/25/2016

District: 03

County: Sutter

Route: 113

Direction: Southbound

Lane number: 1/1

GPS coordinates of core location: (38.87705497, -121.70522333)

Postmile: 5.4

Cored ID: SUT113SB-PH10-C1

Shoulder soil classification: CL

Location description: Approximately 1,000 ft. north of Robbins, perpendicular to 65 mph sign



Figure B.12: Pavement core and subgrade soil sample locations for PH10 from Google Maps.



Figure B.13: Pavement core sample for PH10.

Table B.3: Layer Thicknesses Recorded from the Core Sample for PH10

Type	Thickness (in.)(mm)
RHMA-O	1.0 in. (24.4 mm)
HMA	3.0 in. (76.2 mm)
HMA	3.0 in. (76.2 mm)
HMA	2.4 in. (61 mm)

Notes:

- RHMA-O = rubberized hot mix asphalt, open-graded
- HMA = hot mix asphalt

6. PH11

Figure B.9 presents pavement structure from the GPR data for PH11. A core was taken from the center of the lane during the FWD testing closures, as shown in Figure B.14. The cored sample is shown in Figure B.15. Information from the core sample is presented in Table B.4.

Date cored: 09/13/2016

District: 03

County: Sutter

Route: 113

Direction: Northbound

Lane number: 1/1

GPS coordinates of core location: (38.97130667, -121.67199331)

Postmile: 12

Cored ID: SUT113NB-PH11-C1

Shoulder soil classification: CL

Location description: North of Sutter Causeway Bridge, past levee access roads



Figure B.14: Pavement core and subgrade soil sample locations for PH11 from Google Maps.

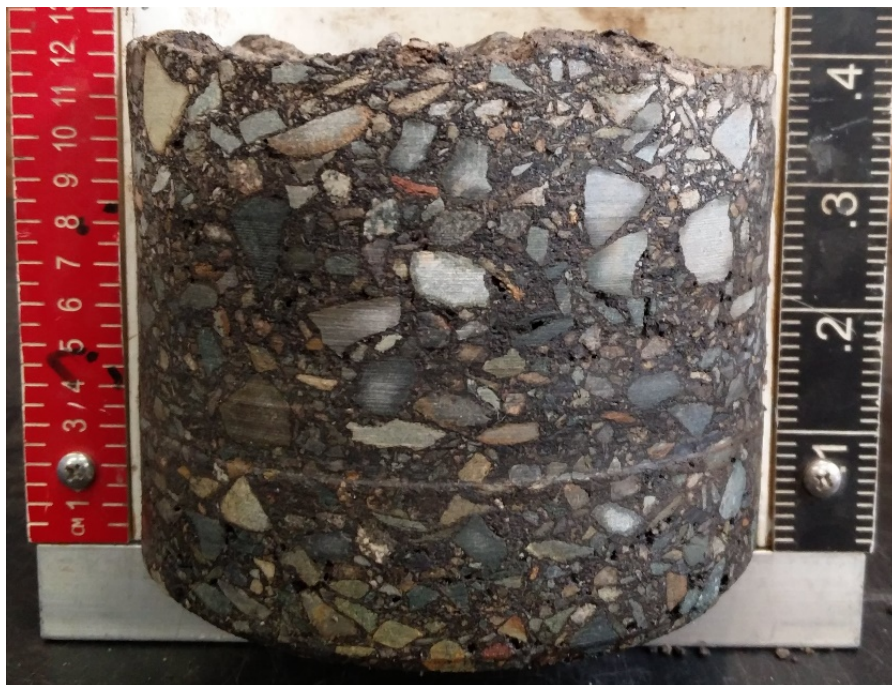


Figure B.0.15: Pavement core sample for PH11.

Table B.4: Layer Thicknesses Recorded from the Core Sample for PH11

Type	Thickness (in.)(mm)
HMA	1.5 in. (38 mm)
HMA	2.6 in. (67 mm)

Notes:
 - HMA = hot mix asphalt

7. PH12

No GPR data is available for PH12, as PH11 and PH12 are, respectively, single lane northbound and southbound state highways of similar structure without a median structure. A core was taken from the center of the lane during the FWD testing closures, as shown in Figure B.16. The cored sample is shown in Figure B.17. Information from the core sample is presented in Table B.5.

Date Cored: 09/13/2016 **District:** 03 **County:** Sutter
Route: 113 **Direction:** Southbound **Lane number:** 1/1
GPS coordinates of core location: (38.99873167, -121.67204335) **Postmile:** 14
Cored ID: SUT113SB-PH12-C1 **Shoulder soil classification:** SC
Location description: After Tudor Road South, George Washington Blvd turn, near old fruit stand building



Figure B.16: Pavement core and subgrade soil sample locations for PH12 from Google Maps.

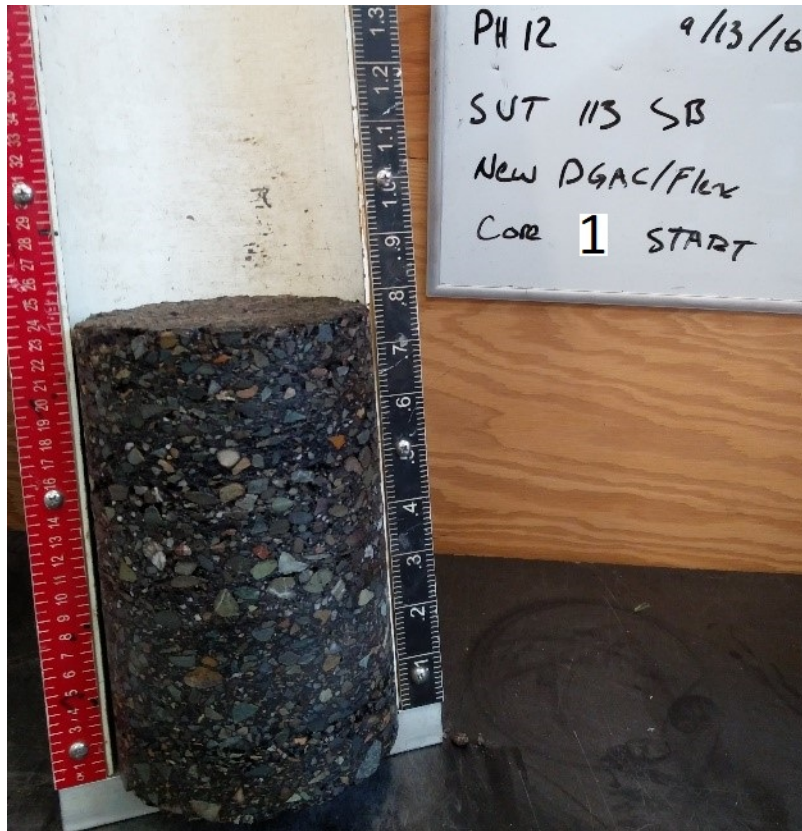


Figure B.17: Pavement core sample for PH12.

Table B.5: Layer Thicknesses Recorded from the Core Sample for PH12

Type	Thickness (in.)(mm)
HMA	1.0 in. (24.4 mm)
RHMA-G	1.0 in. (24.4 mm)
HMA	1.8 in. (45.7 mm)
HMA	2.8 in. (70 mm)
HMA	2.9 in. (73 mm)

Notes:

- RHMA-G = rubberized hot mix asphalt, gap-graded
- HMA = hot mix asphalt

8. PH13

Figure B.9 presents pavement structure from the GPR data for PH13. A core was taken from the center of the lane during the FWD testing closures, as shown in Figure B.18. The cored sample is shown in Figure B.19. An HMA layer lift thickness of only 2.2 in. was able to be cored from the pavement.

Date cored: 09/14/2016

District: 03

County: Sutter

Route: 113

Direction: Eastbound

Lane number: 1/1

GPS coordinates of core location: (39.00322499, -121.66152833)

Postmile: 15

Cored ID: SUT113EB-PH13-C1

Shoulder soil classification: SC

Location description: North of Sutter Causeway Bridge, past levee access roads



Figure B.18: Pavement core and subgrade soil sample locations for PH13 from Google Maps.



Figure B.19: Pavement core sample for PH13.

9. PH14

No GPR data is available for PH14, as PH13 and PH14 are, respectively, single lane northbound and southbound state highways of similar structure without a median structure. A core was taken from the center of the lane during the FWD testing closures, as shown in Figure B.20. The cored sample is shown in Figure B.21. An HMA layer lift thickness of only 3.7 in. was able to be cored from the pavement.

Date cored: 09/14/2016

District: 03

County: Sutter

Route: 113

Direction: Westbound

Lane number: 1/1

GPS coordinates of Core location: (39.00333166, -121.63879000)

Postmile: 16

Cored ID: SUT113WB-PH14-C1

Shoulder soil classification: SC

Location description: After off-ramp 113, near pavement overlay, perpendicular to telephone pole



Figure B.20: Pavement core and subgrade soil sample locations for PH14 from Google Maps.



Figure B.21: Pavement core sample for PH14.

10. PH15

Caltrans collects GPR data only on state highways, so no GPR data exists for PH15. Figure B.22 shows the locations where the core and soil samples were collected. An HMA layer lift thickness of only 4 in. was recorded from the core, as shown in Figure B.23. Information from the core sample is presented in Table B.6.

Date Cored: 08/18/2016

District: 03

County: Yolo

Route: CR32B

Direction: Eastbound

Lane number: 1/1

GPS coordinates of Core location: (38.55698668, -121.67480665)

Postmile: N/A

Cored ID: Yolo32b-PH15-C1

Shoulder Soil Classification: CH

Location Description: 300 ft. past Calfire Equipment Station entrance



Figure B.22: Pavement core and subgrade soil sample locations for PH15 from Google Maps.



Figure B.23: Pavement core sample for PH15.

Table B.6: Layer Thicknesses Recorded from the Core Sample for PH15

Type	Thickness (in.)(mm)
HMA	2.0 in. (52 mm)
HMA	3.6 in. (91.5 mm)

Notes:

- HMA = hot mix asphalt

11. PH16

Figure B.24 presents pavement structure from the GPR data for PH16. A core was taken from the center of the lane during the FWD testing closures, as shown in Figure B.25. The cored sample is shown in Figure B.26. Information from the core sample is presented in Table B.7.

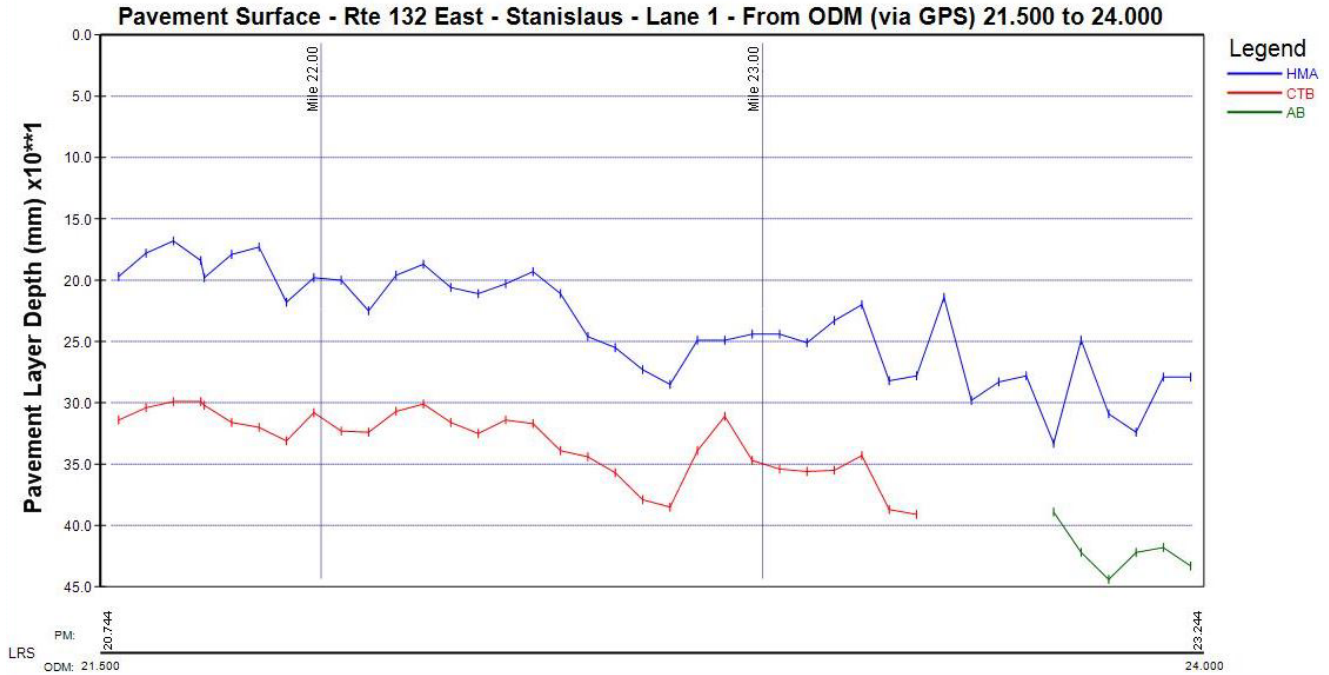


Figure B.24: GPR data for section PH16.

Date cored: 08/23/2016

District: 10

County: Stanislaus

Route: 132

Direction: Eastbound

Lane number: 1/1

GPS coordinates of core location: (37.63867168, -120.85489330)

Postmile: 22.8

Cored ID: STA132EB-PH16-C2

Shoulder soil classification: SC

Location description: 600 ft. from Triangle Ranch Road, at change in double yellow line near telephone pole



Figure B.25: Pavement core and subgrade soil sample locations for PH16 from Google Maps.

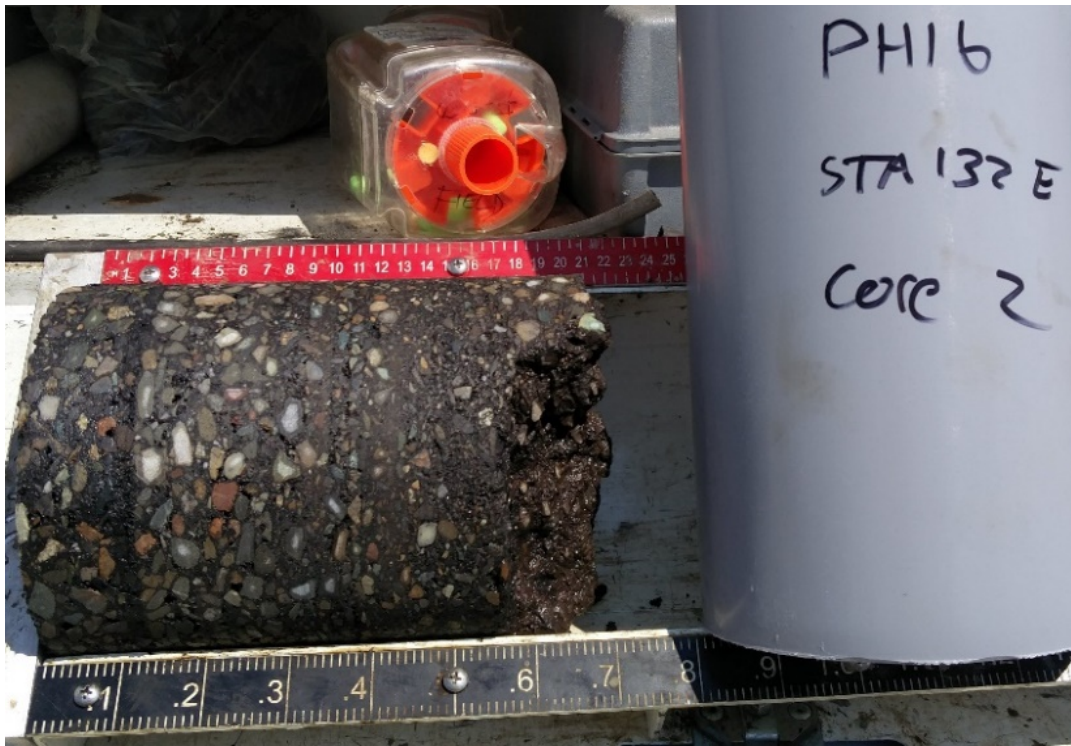


Figure B.26: Pavement core sample for PH16.

Table B.7: Layer Thicknesses Recorded from the Core Sample for PH16

Type	Thickness (in.)(mm)
RHMA-G	1.7 in. (42.7 mm)
HMA	2.0 in. (51.8 mm)
HMA	1.5 in. (38 mm)
HMA	2.2 in. (55 mm)

Notes:

- RHMA-G = rubberized hot mix asphalt, gap-graded
- HMA = hot mix asphalt

12. PH17

No GPR data is available for PH17, as PH16 and PH17 are, respectively, single lane northbound and southbound state highways of similar structure without a median structure. A core was taken from the center of the lane during the FWD testing closures, as shown in Figure B.27. The cored sample is shown in Figure B.28. Information from the core sample is presented in Table B.8.

Date cored: 08/23/2016

District: 10

County: Stanislaus

Route: 132

Direction: Westbound

Lane number: 1/1

GPS coordinates of core location: (37.63867168, -121.85489330)

Postmile: 22.8

Cored ID: STA132W-PH17-C1

Shoulder soil classification: SC

Location description: 600 ft. from Triangle Ranch Road, at change in double yellow line near telephone pole



Figure B.27: Pavement core and subgrade soil sample locations for PH17 from Google Maps.



Figure B.28: Pavement core sample for PH17.

Table B.8: Layer Thicknesses Recorded from the Core Sample for PH17

Type	Thickness (in.)(mm)
RHMA	2.0 in. (51 mm)
HMA	2.4 in. (61 mm)

Notes:

- RHMA = rubberized hot mix asphalt
- HMA = hot mix asphalt

13. PH18

Figure B.29 presents pavement structure from the GPR data for PH18. A core was taken from the center of the lane during the FWD testing closures, as shown in Figure B.30. The cored sample is shown in Figure B.31. Information from the core sample is presented in Table B.9.

Date cored: 06/07/2016

District: 06

County: Kern

Route: 5

Direction: Southbound

Lane number: 2/2

GPS coordinates of core location: (35.42255665, -119.42997334)

Postmile: 56.2

Cored ID: KER5PH18-C2

Shoulder soil classification: SM

Location description: 1,000 ft. before Buttonwillow rest stop

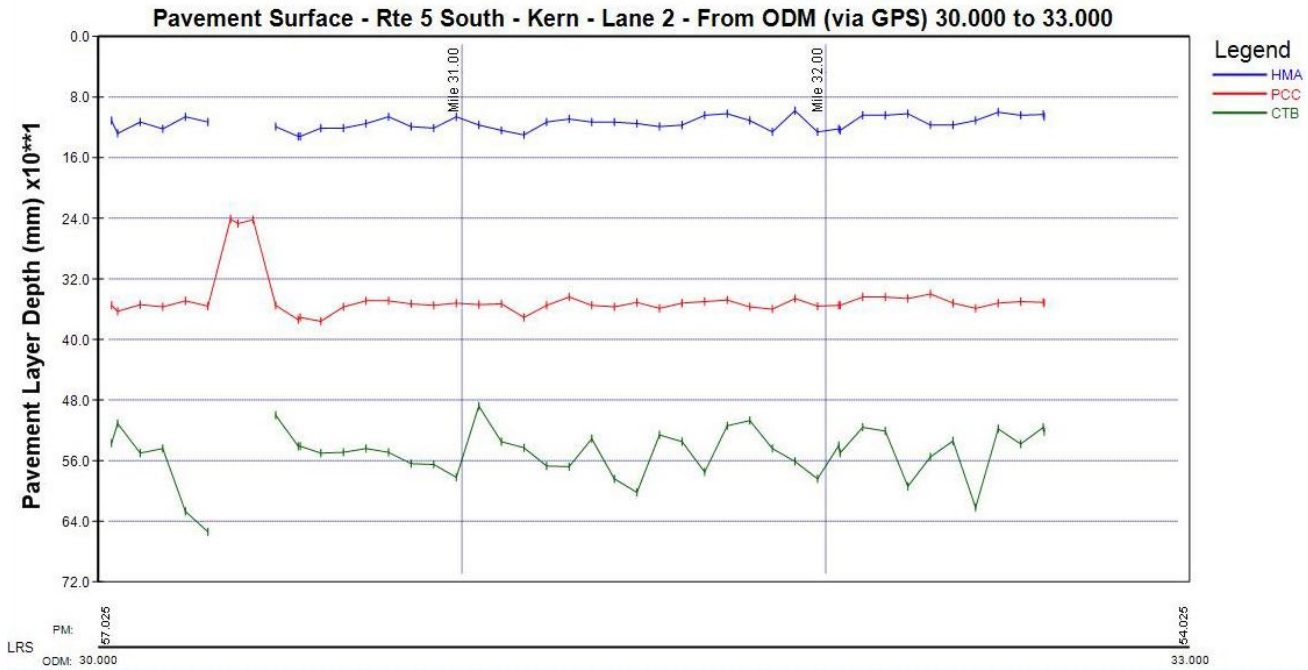


Figure B.29: GPR data for section PH18.



Figure B.30: Pavement core and subgrade soil sample locations for PH18 from Google Maps.



Figure B.31: Pavement core sample for PH18.

Table B.9: Layer Thicknesses Recorded from the Core Sample for PH18

Type	Thickness (in.)(mm)
HMA-O	0.9 in. (24 mm)
HMA	2.8 in. (70 mm)
HMA	1.1 in. (30 mm)

Notes:

- HMA-O = hot mix asphalt, open-graded
- HMA = hot mix asphalt

14. PH19

Figure B.32 presents pavement structure from the GPR data for PH19. A core was taken from the center of the lane during the FWD testing closures, as shown in Figure B.33. The cored sample is shown in Figure B.34. Information from the core sample is presented in Table B.10.

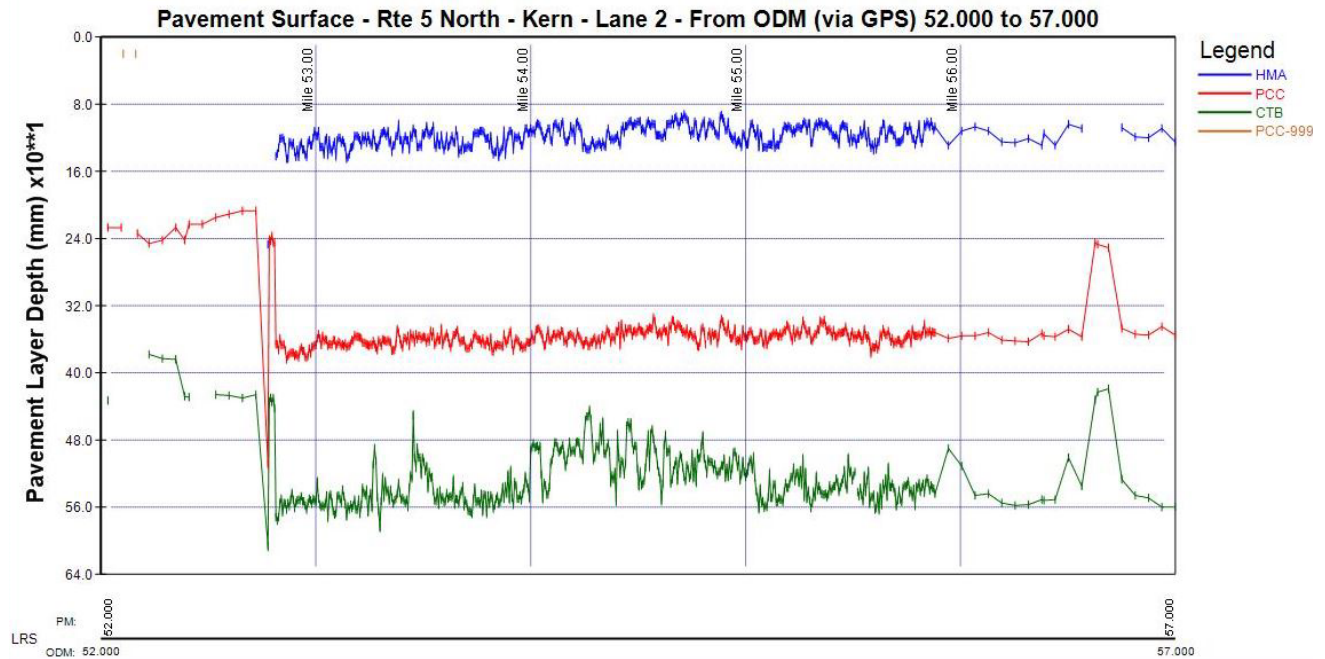


Figure B.32: GPR data for section PH19.

Date cored: 06/08/2016

District: 06

County: Kern

Route: 5

Direction: Northbound

Lane number: 2/2

GPS coordinates of core location: (35.42047665, -119.42654666)

Postmile: 54.28

Cored ID: KER5NB-PH19-C3

Shoulder soil classification: SM

Location description: 100 feet from I5 sign/light pole and PM 54.26, after off-ramp Buttonwillow rest stop



Figure B.33: Pavement core and subgrade soil sample locations for PH19 from Google Maps.

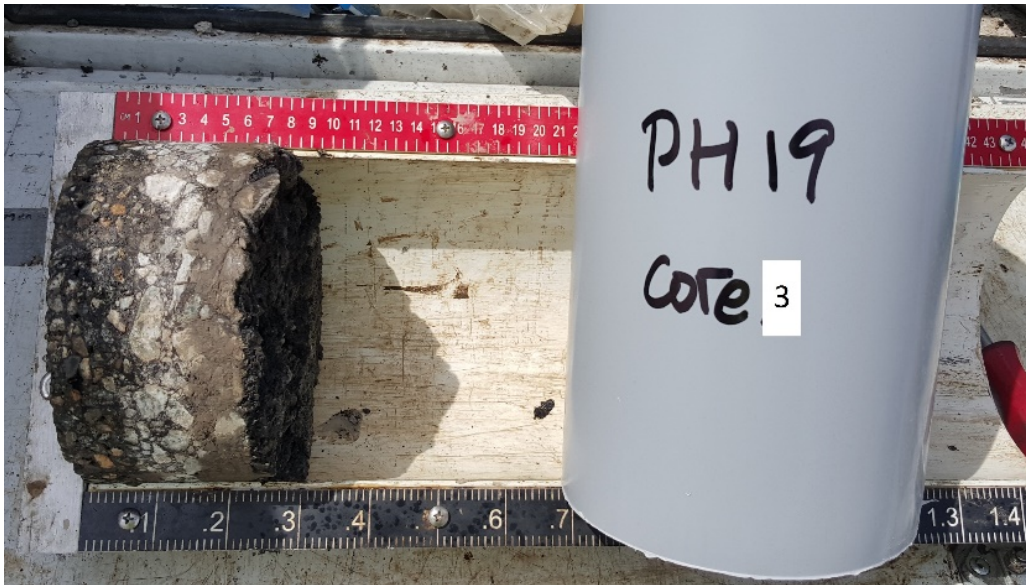


Figure B.34: Pavement core sample for PH19.

Table B.10: Layer Thicknesses Recorded from the Core Sample for PH19

Type	Thickness (in.)(mm)
RHMA-G	1.1 in. (27.4 mm)
HMA	1.8 in. (45.7 mm)

Notes:

- RHMA-G = rubberized hot mix asphalt, gap-graded
- HMA = hot mix asphalt

15. PH20, PH21, and PH22

Figure B.35 and Figure B.36 present pavement structure information for PH21 and PH22, respectively, using the data from GPR. No GPR information is available for PH20 pavement section, as a rehabilitation project converting the JPC pavement section to CRC pavement was taking place during the GPR testing/data collection. No cores were taken from concrete pavement sections.

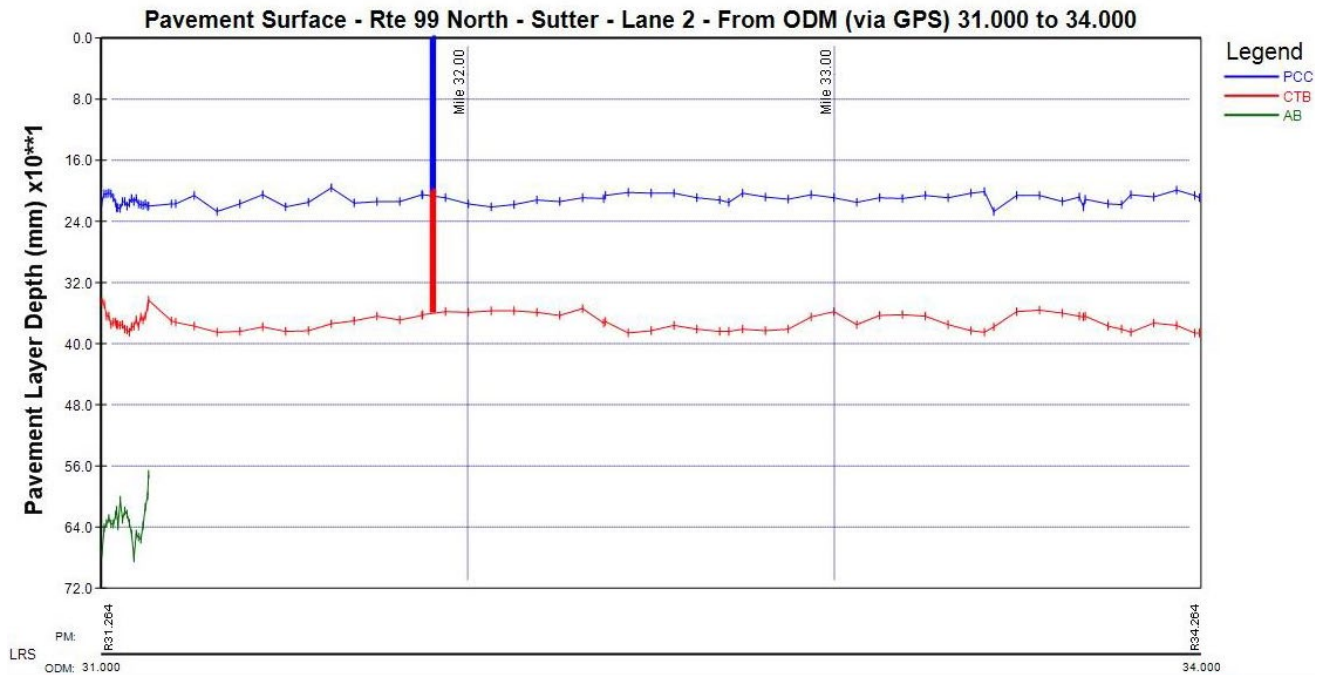


Figure B.35: GPR data for section PH21.

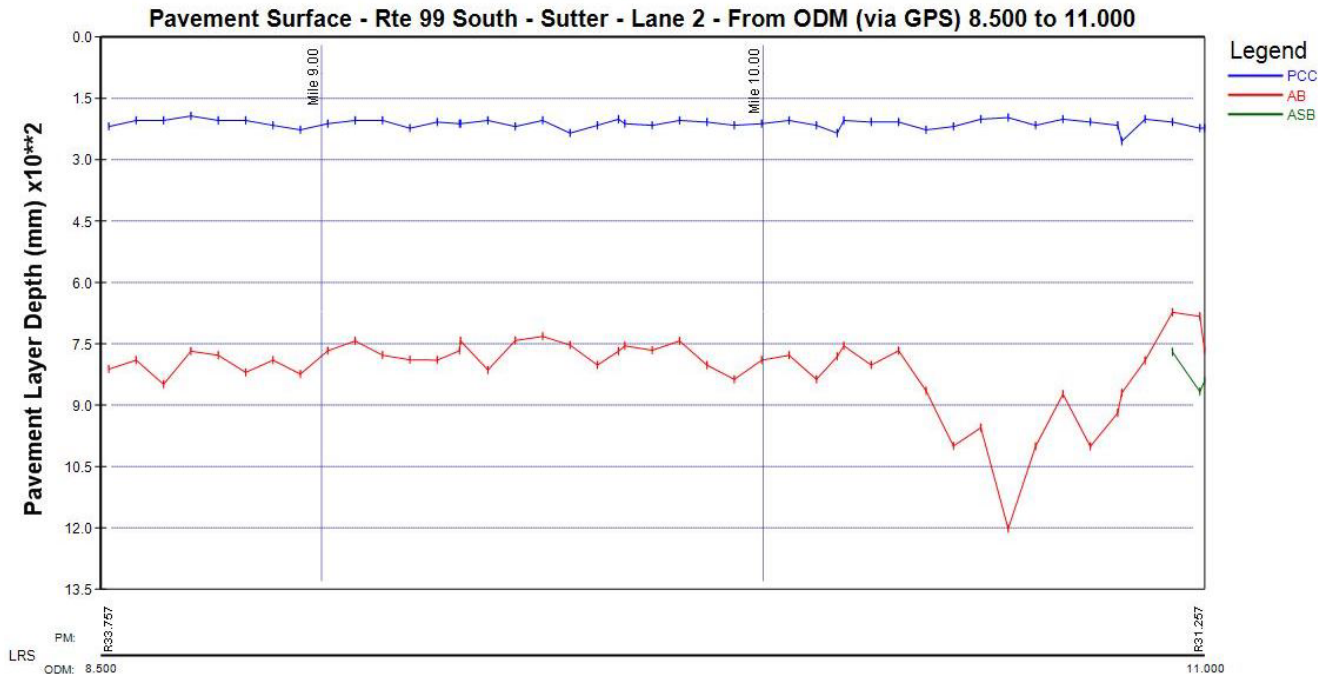


Figure B.36: GPR data for section PH22.

16. PH23

Caltrans collects GPR data only on state highways, so no GPR data exists for PH23. Of all the concrete sections, only PH23 had a core sample collected from it, as there was no information on the layer thickness of the pavement structure. Figure B.37 shows the locations where the core samples were collected. Only 7.4 in. of JPC layer lift thickness was recorded from the core as shown in Figure B.38.

Date cored: 06/03/2016

District: 03

County: Yolo

Route: 32A

Direction: Westbound

Lane number: 1/1

GPS coordinates of core location: (38.56851, -121.646427)

Postmile: N/A

Cored ID: YOL32A-PH23-C1

Shoulder soil classification: CL

Location description: West of I80 highway off-ramp, approximately 50 ft. west of electrical utility



Figure B.37: Pavement core sample location for PH23 from Google Maps.



Figure B.38: Pavement core sample for PH23.

APPENDIX C: LASER TEXTURE SCANNER RESULTS

Table C.1: Laser Texture Scanning (LTS) Locations, Test Dates, and Results for All Pavements Considered in This Study

Section ID	Pavement Type	Test date	LTS 1				LTS 2				LTS 3				LTS 4				AVG LTS							
			LTS 1 GPS	MPD 1	ETD 1	MPD 1	ETD 1	LTS 2 GPS	A MPD 2	A ETD 2	B MPD 2	B ETD 2	LTS 3 GPS	A MPD 3	A ETD 3	B MPD 3	B ETD 3	LTS 4 GPS		A MPD 4	A ETD 4	B MPD 4	B ETD 4			
PH01	JPC	6/21/2016	38.596176, -121.766880		0.367343		0.391058		-		-		-		-		-		-		-		-		0.37920	
PH02	JPC	6/20/2016	38.612850, -121.767035		0.6211066		0.5563211		-		-		-		-		-		-		-		-		0.58871	
PH03	JPC	6/14/2016	38.53883, -121.95282		0.4576731		0.4975704		38.61544, -121.95532		0.4894414		0.5746612		-		-		-		-		-		0.50484	
PH20	CRC	6/7/2016	35.411558, -119.420514		0.5737554		0.5231633		35.403016, -119.403340		0.9448361		0.9448361		-		-		-		-		-		0.74665	
PH21	JPC	9/15/2016	39.16376, -121.63509		0.5035594		0.588064		39.1843731, -121.63478		0.42446		0.496127		-		-		-		-		-		0.50305	
PH22	JPC	9/15/2016	39.163775, -121.635421		0.4052403		0.44537		-		-		-		-		-		-		-		-		0.42531	
PH23	JPC	6/3/2016	38.564076, -121.645453		0.7595035		0.7455865		38.560295, -121.662514		0.8978378		0.8976591		-		-		-		-		-		0.82515	
PH04	Composite	6/15/2016	38.61489, -121.95353	1.10124	1.142987		0.8662548		38.53731, -121.95317		1.097867		1.025311		-		-		-		-		-		1.09185	
PH07	HMA	6/29/2016	38.592835, -121.803061	0.726769	0.8662548		0.5975585		38.614853, -121.802919		0.5078563		0.4921486		-		-		-		-		-		0.64826	
PH08	HMA	6/30/2016	38.590641, -121.853951	0.9019302	0.5975585		0.9019302		38.590556, -121.825643		1.053813		0.895884		-		-		-		-		-		0.86072	
PH09	HMA	8/24 - 8/25	38.87678, -121.70529	1.319572	1.337232		0.9755558		38.89975, -121.69657		1.113893		1.097238		38.92745, -121.68605	1.286476	1.186046		-		-		-		1.22341	
PH10	HMA	8/24 - 8/25	38.92745, -121.68605	0.9755558	1.188191		0.9755558		38.90491, -121.69470		0.9907044		1.088943		38.87678, -121.70529	0.9437953	0.8748791		-		-		-		1.01034	
PH11	HMA	9/13/2016	38.971306, -121.671983	0.7297232	0.8616624		0.8616624		38.9858117, -121.672020		0.7059637		0.729213		38.984670, -121.672040	0.7035032			-		-		-		0.74601	
PH12	HMA	9/13/2016	38.998734, -121.672040	1.30954	0.820017		0.820017		38.985613, -121.672140		0.6507626		0.637669		38.971284, -121.672070	0.8250122	0.7324264		-		-		-		0.82924	
PH13	HMA	9/14/2016	39.003163, -121.661485	0.5301512	0.5365774		0.5365774		39.003203, -121.645667		0.5781323		0.5146221		-		-		-		-		-		0.53987	
PH14	HMA	9/14/2016	39.003237, -121.645668	0.487247	0.540767		0.540767		39.003198, -121.661478		0.856476		0.956813		-		-		-		-		-		0.71033	
PH15	Semi-rigid	8/18/2016	38.55700, -121.674461	0.5860646	0.5467719		0.5467719		38.55812, -121.66947		0.6097265		0.55878		38.55908, -121.66258	0.4481002	0.388928		-		-		38.56012, -121.65505	0.4887713	0.5357846	0.52037
PH16	Semi-rigid	8/23/2016	37.63835, -120.89255	0.9315349	1.031947		1.031947		37.63869, -120.85463		0.9479166		0.8694123		-		-		-		-		-		0.94520	
PH17	Semi-rigid	8/23/2016	37.63873, -120.85420	0.8791695	0.7881717		0.7881717		-		-		-		-		-		-		-		-		0.83367	
PH18	Composite	6/7/2016	35.43859, -119.452008	2.238109	2.367751		2.367751		35.435130, -119.446586		2.716897		2.127587		-		-		-		-		-		2.36259	
PH19	Composite	6/8/2016	35.40546, -119.405898	1.202935	1.422091		1.422091		35.420610, -119.426726		1.446272		1.290444		35.435130, -119.446586	0.8920054	0.9650432		-		-		-		1.20313	

APPENDIX D: TEMPERATURE PROFILES

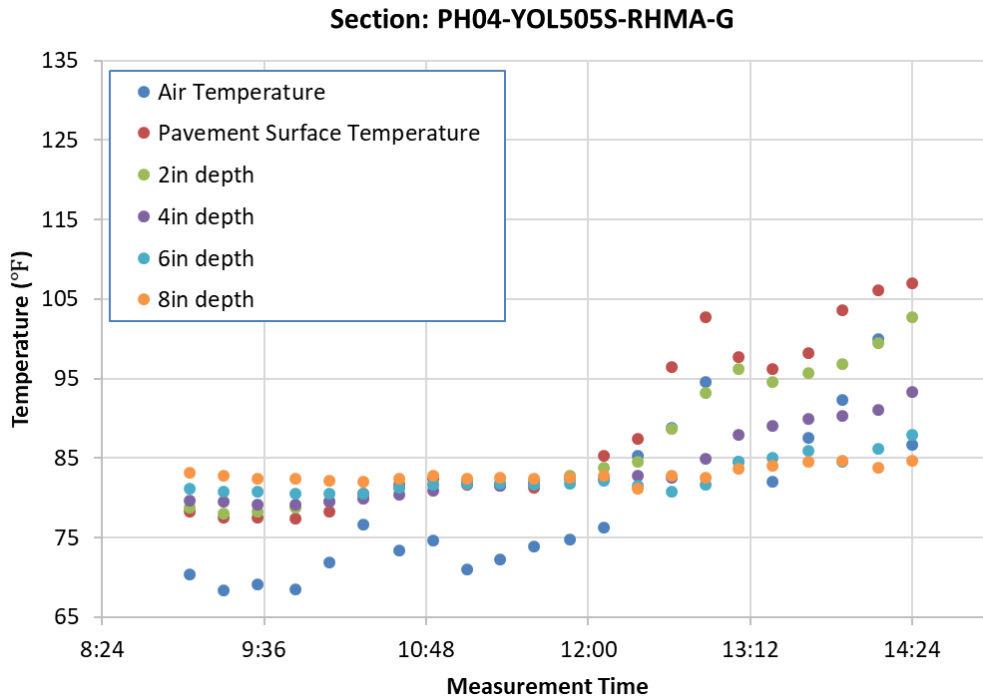


Figure D.1: Temperature profile of section PH04.

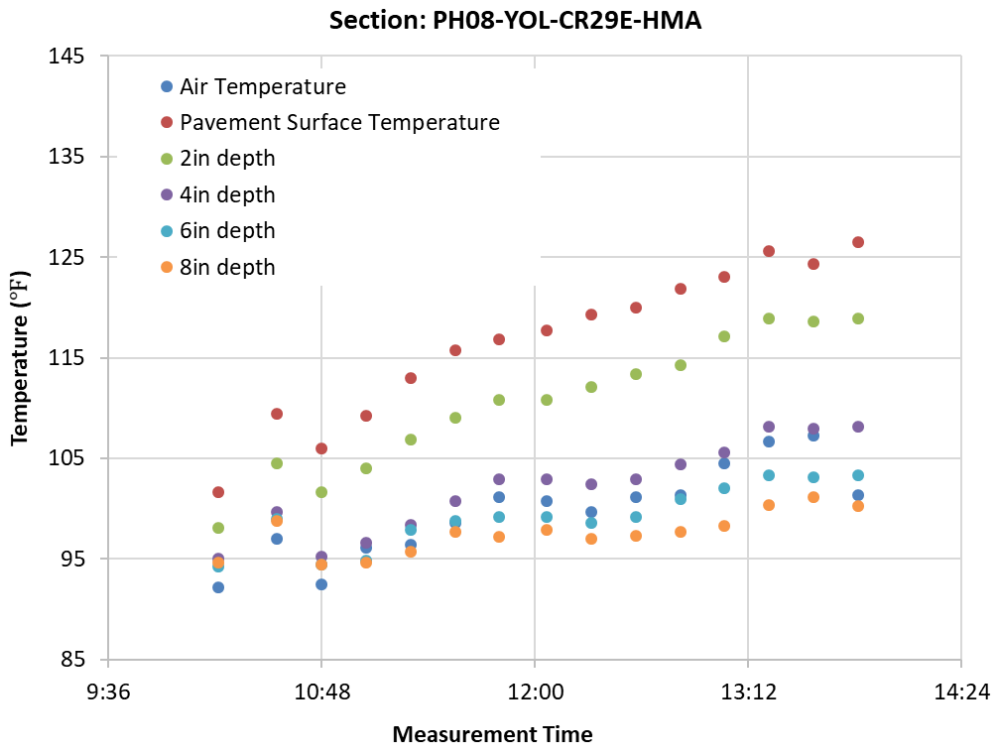


Figure D.2: Temperature profile of section PH08.

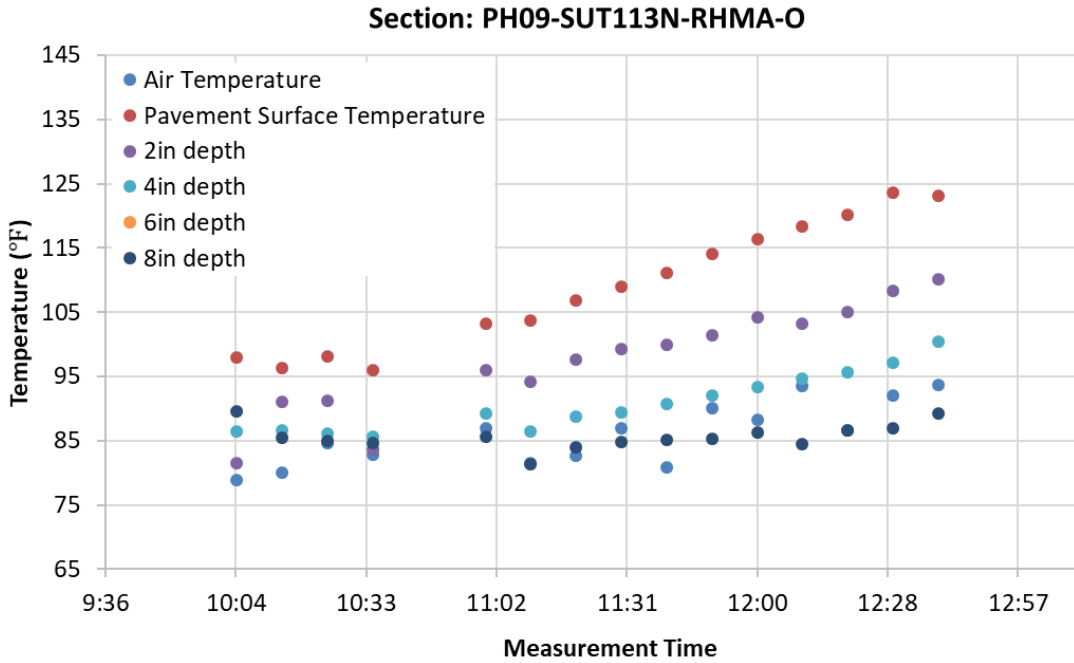


Figure D.3: Temperature profile of section PH09.

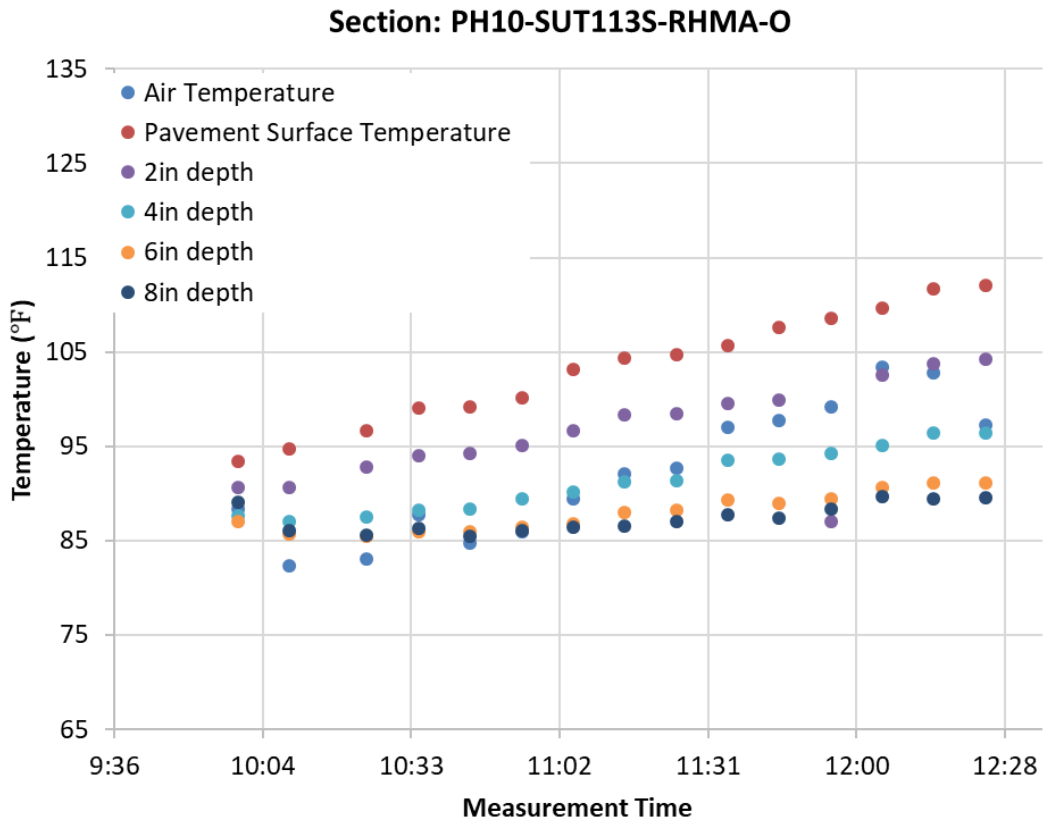


Figure D.4: Temperature profile of section PH10.

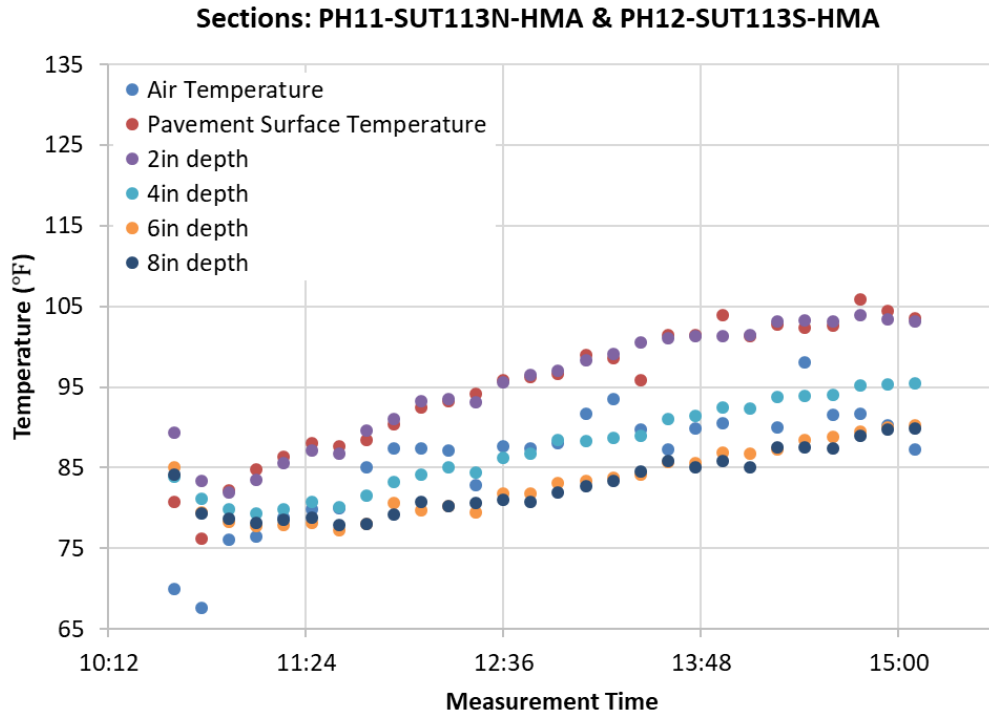


Figure D.5: Temperature profile of sections PH11 and PH12.

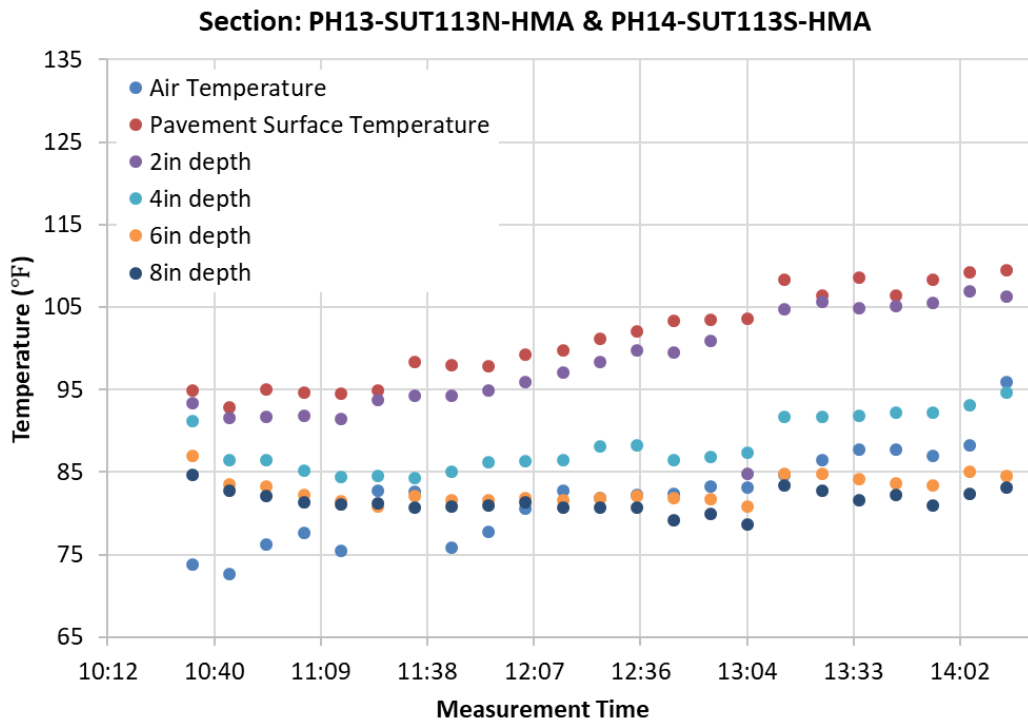


Figure D.6: Temperature profile of sections PH13 and PH14.

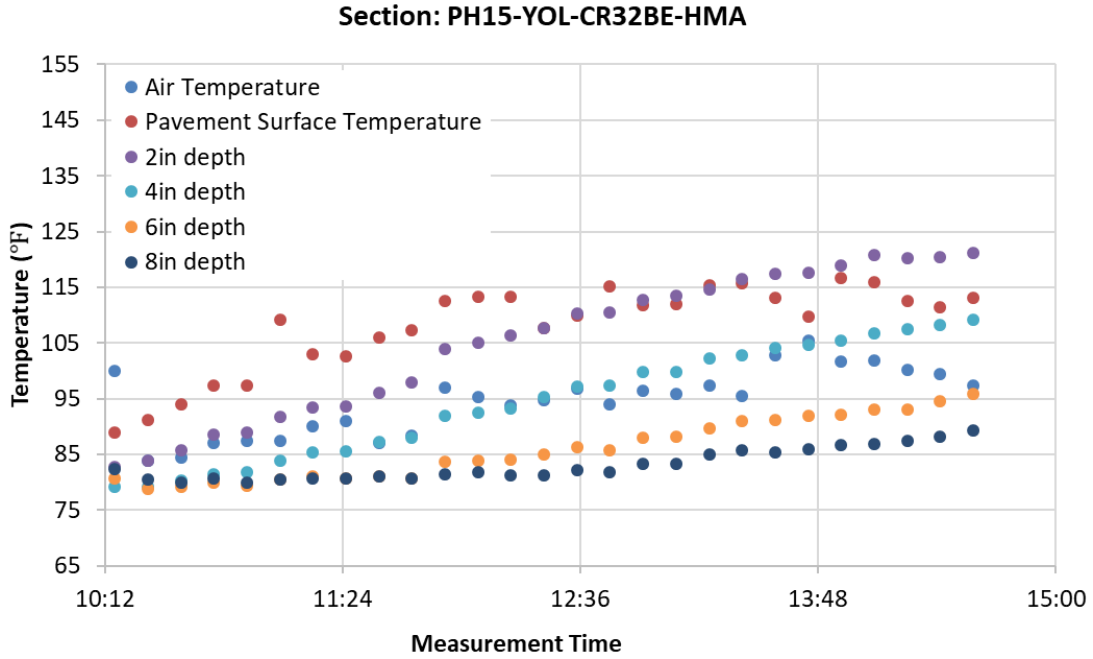


Figure D.7: Temperature profile of section PH15.

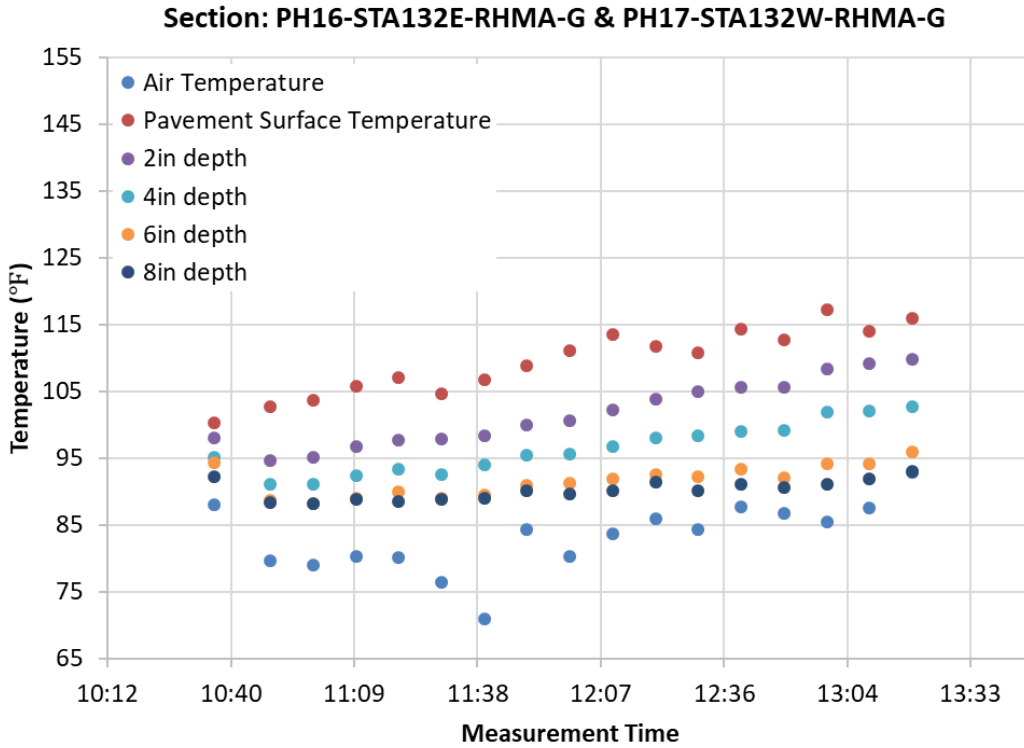


Figure D.8: Temperature profile of sections PH16 and PH17.

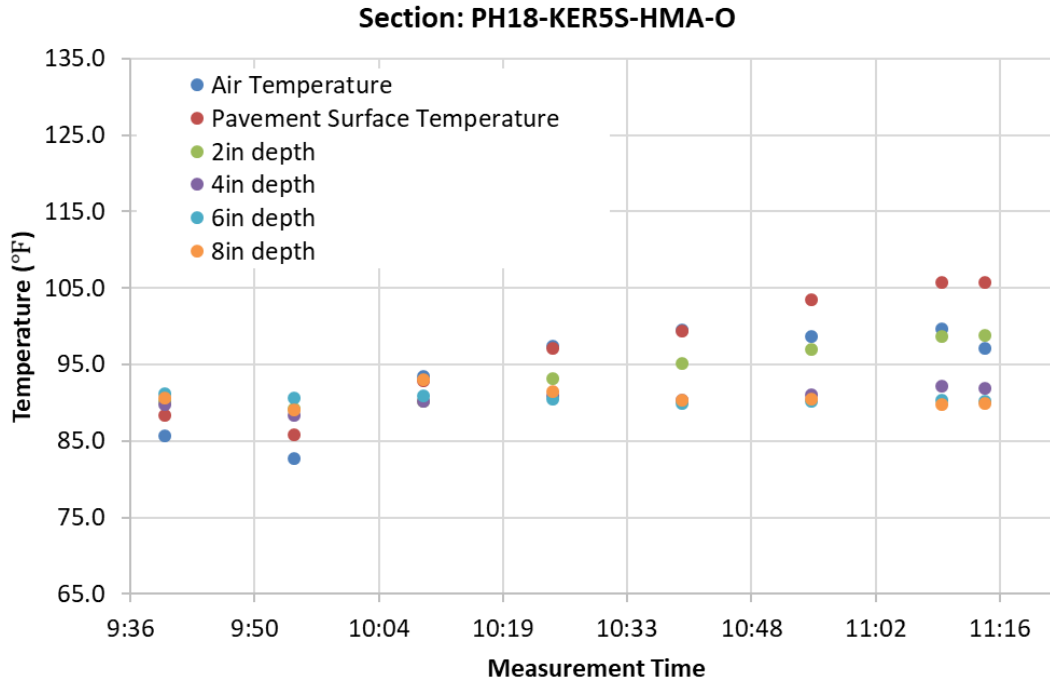


Figure D.9: Temperature profile of section PH18.

APPENDIX E: TEST SECTION PROFILE GRAPHS

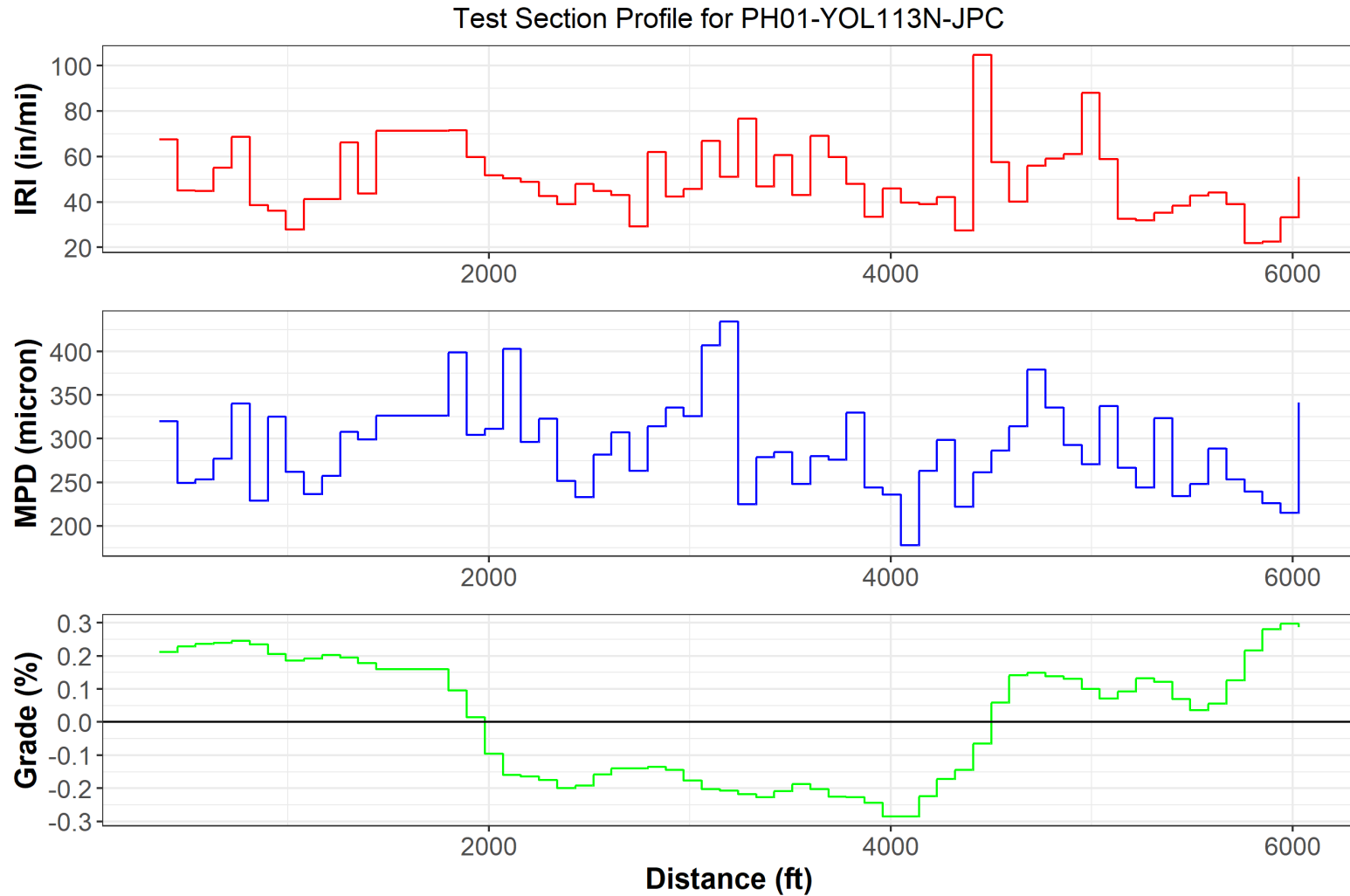


Figure E.1: Roughness, mean profile depth, and grade data plots for section PH01.

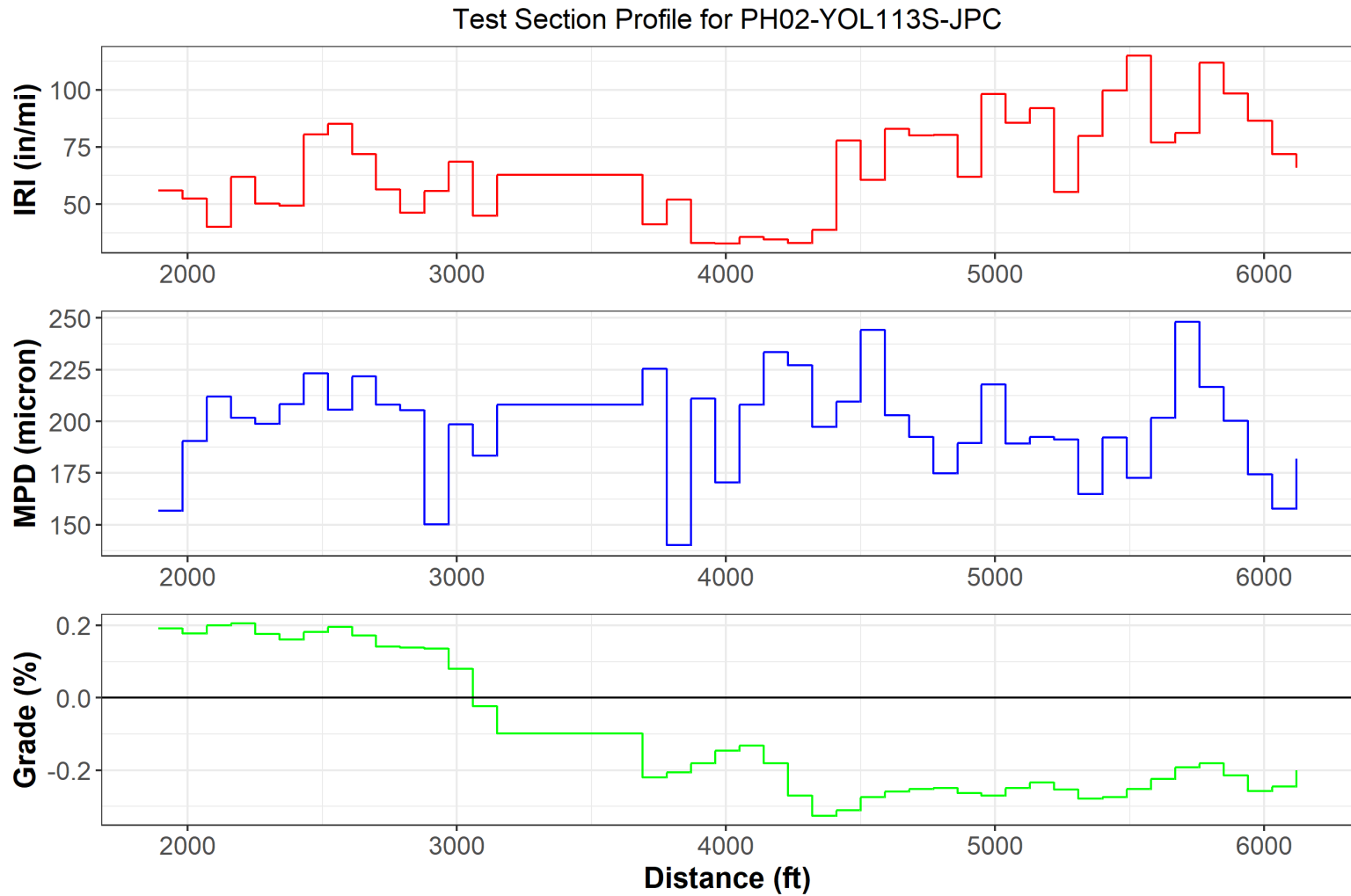


Figure E.2: Roughness, mean profile depth, and grade data plots for section PH02.

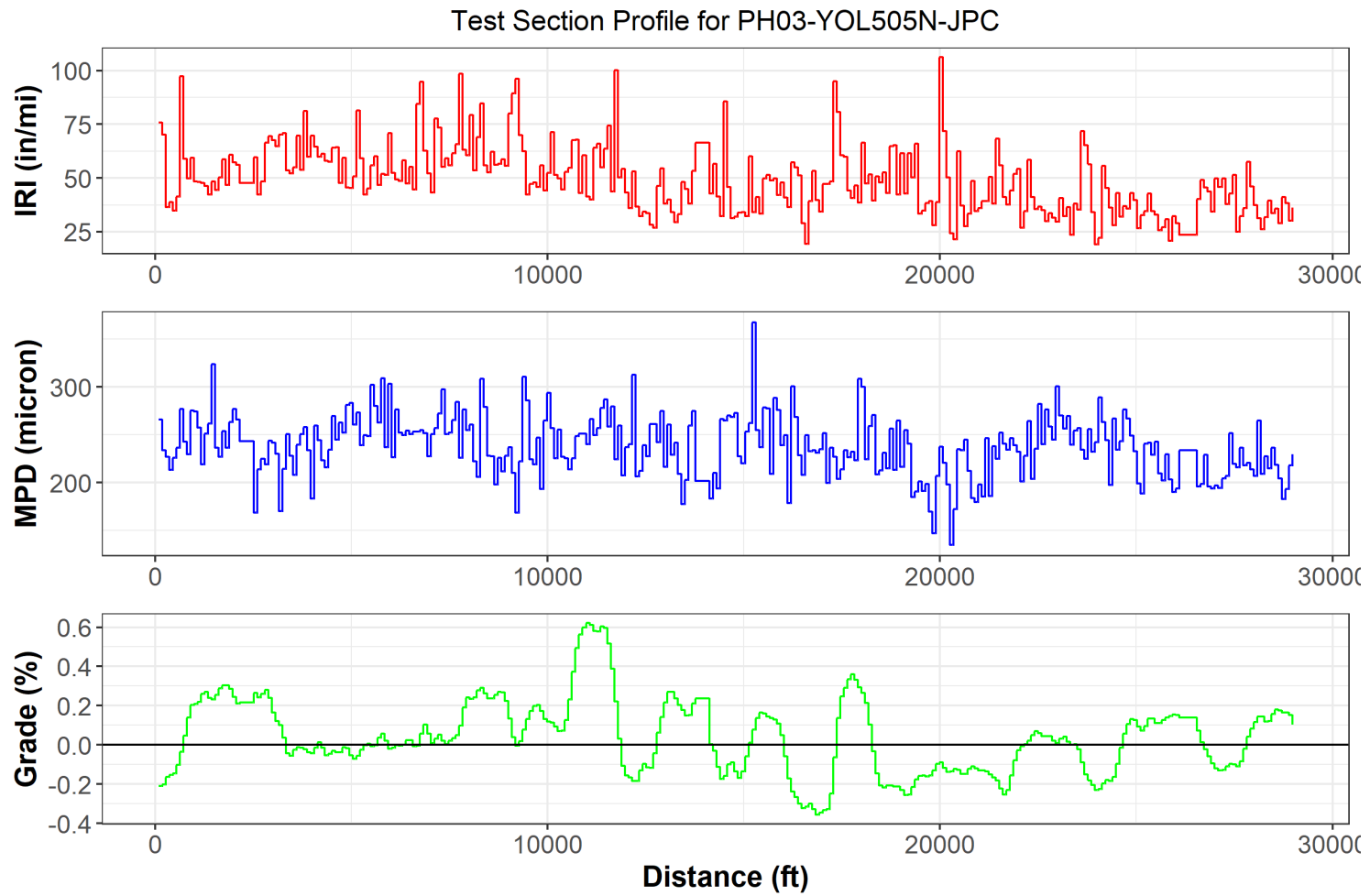


Figure E.3: Roughness, mean profile depth, and grade data plots for section PH03.

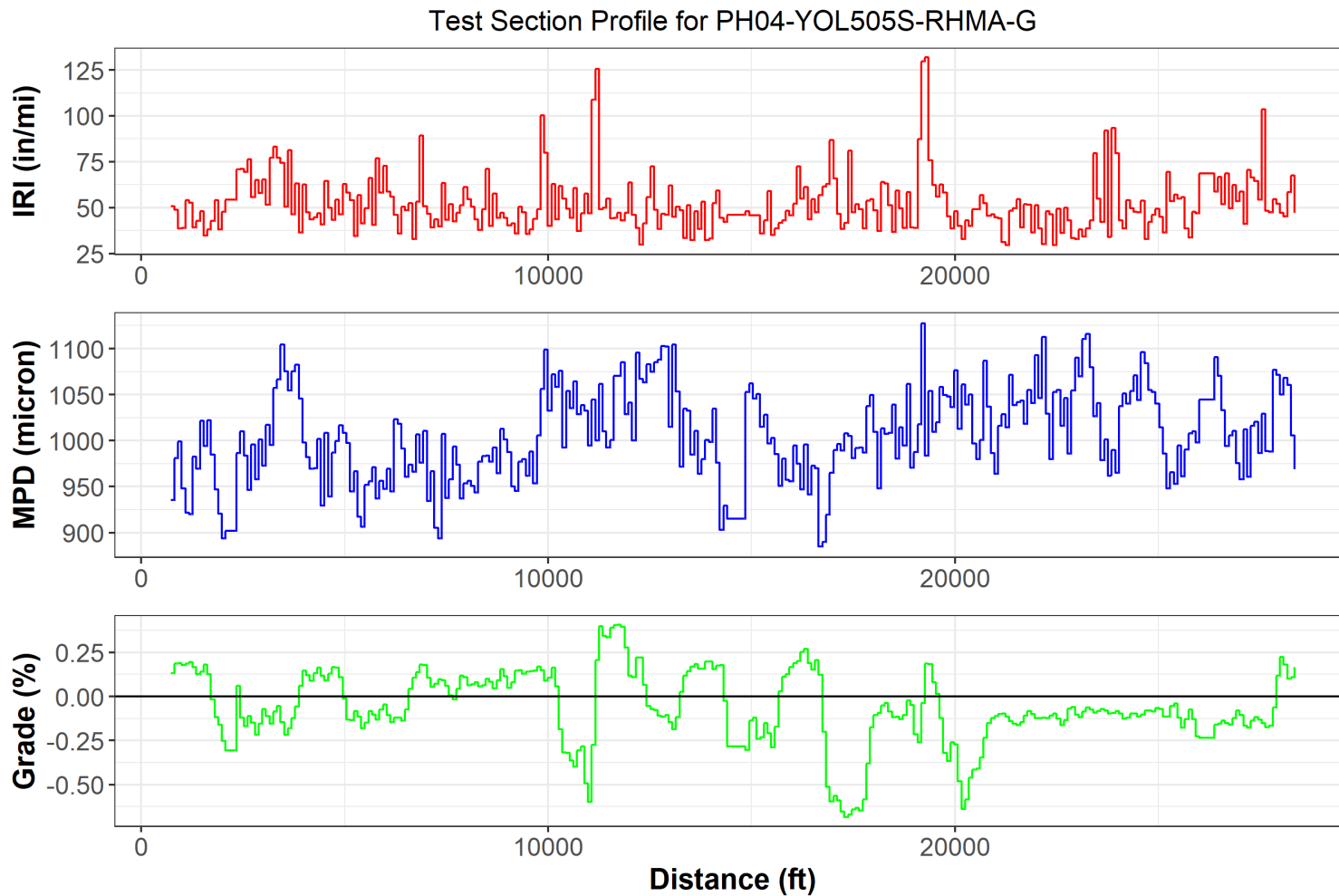


Figure E.4: Roughness, mean profile depth, and grade data plots for section PH04.

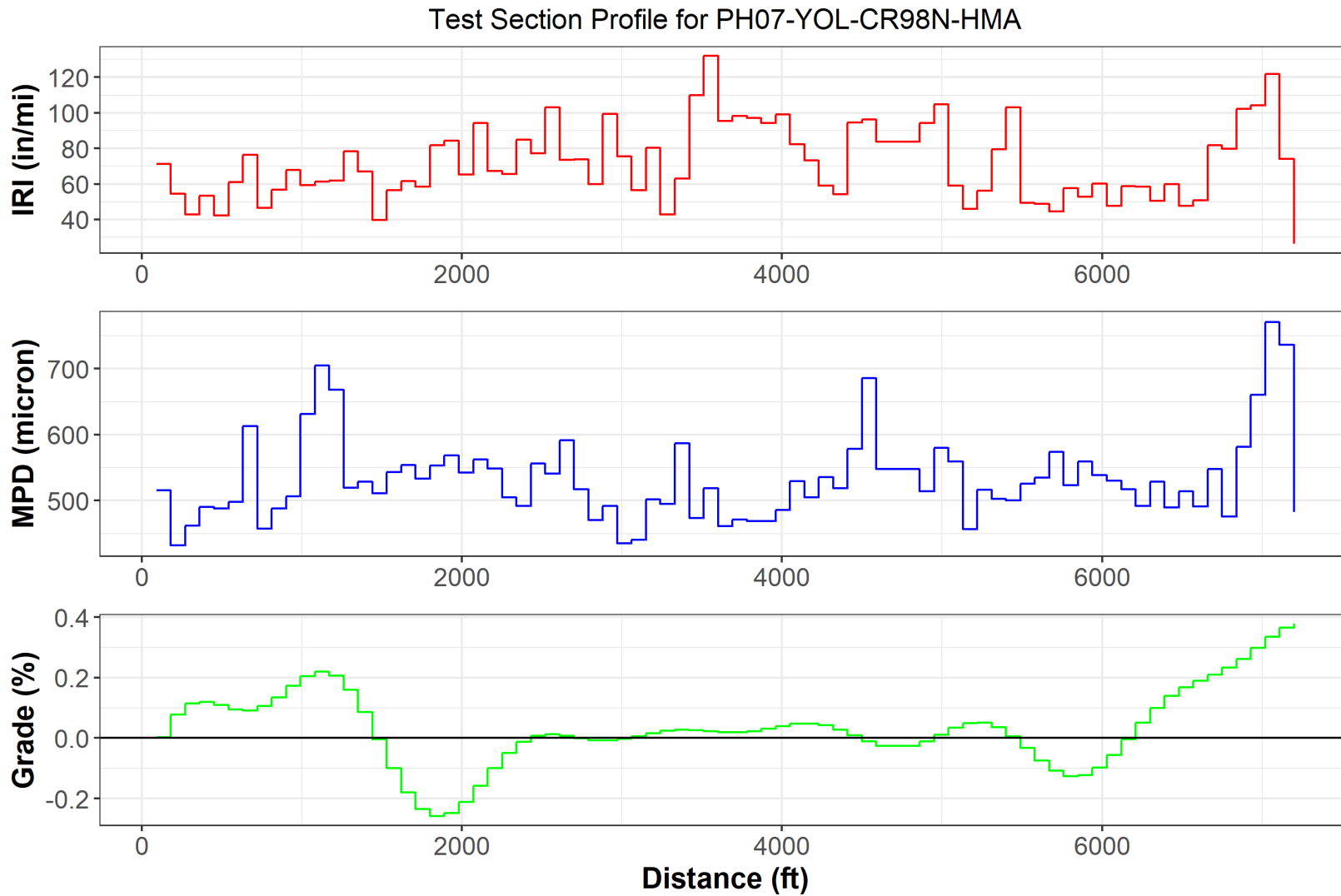


Figure E.5: Roughness, mean profile depth, and grade data plots for section PH07.

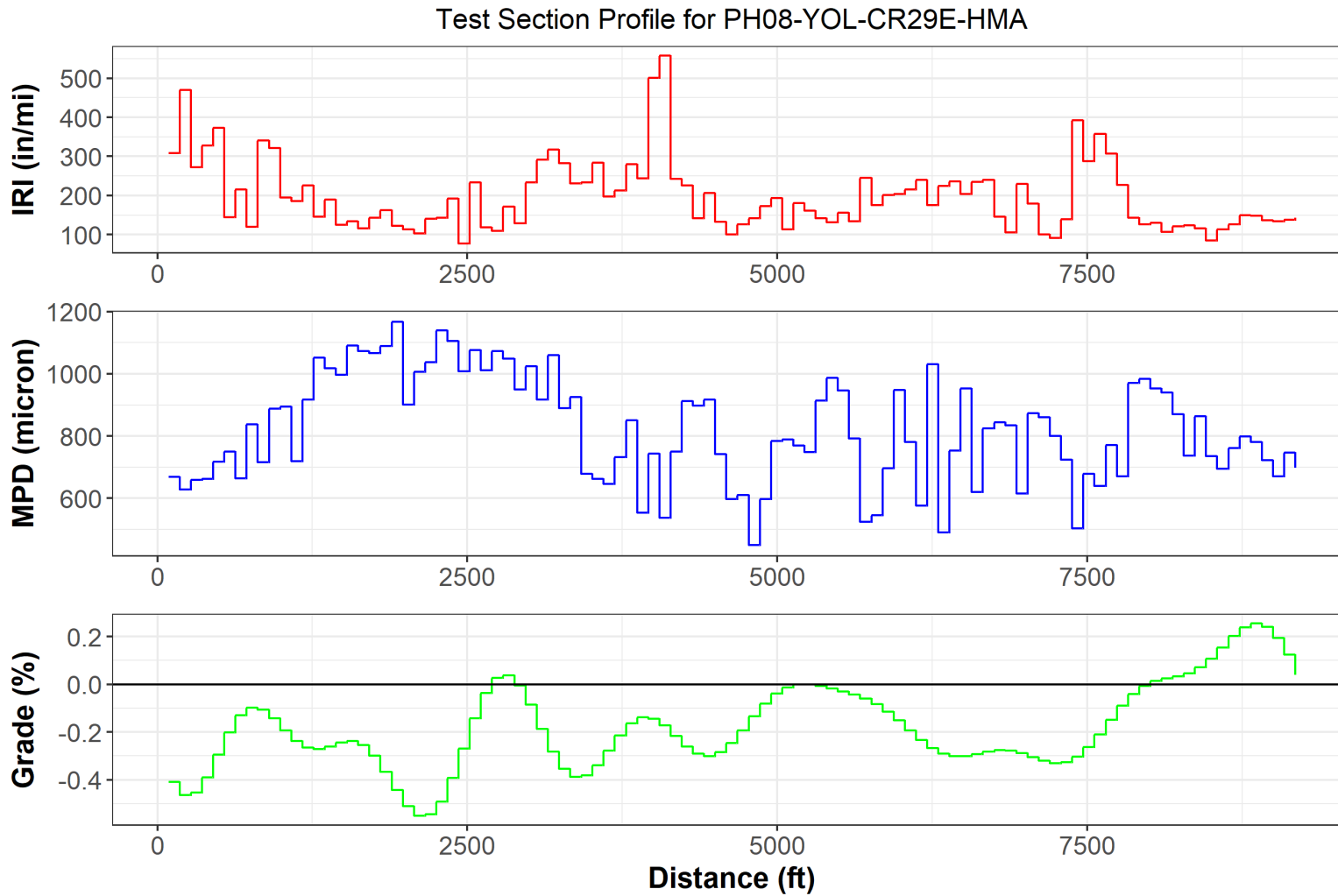


Figure E.6: Roughness, mean profile depth, and grade data plots for section PH08.

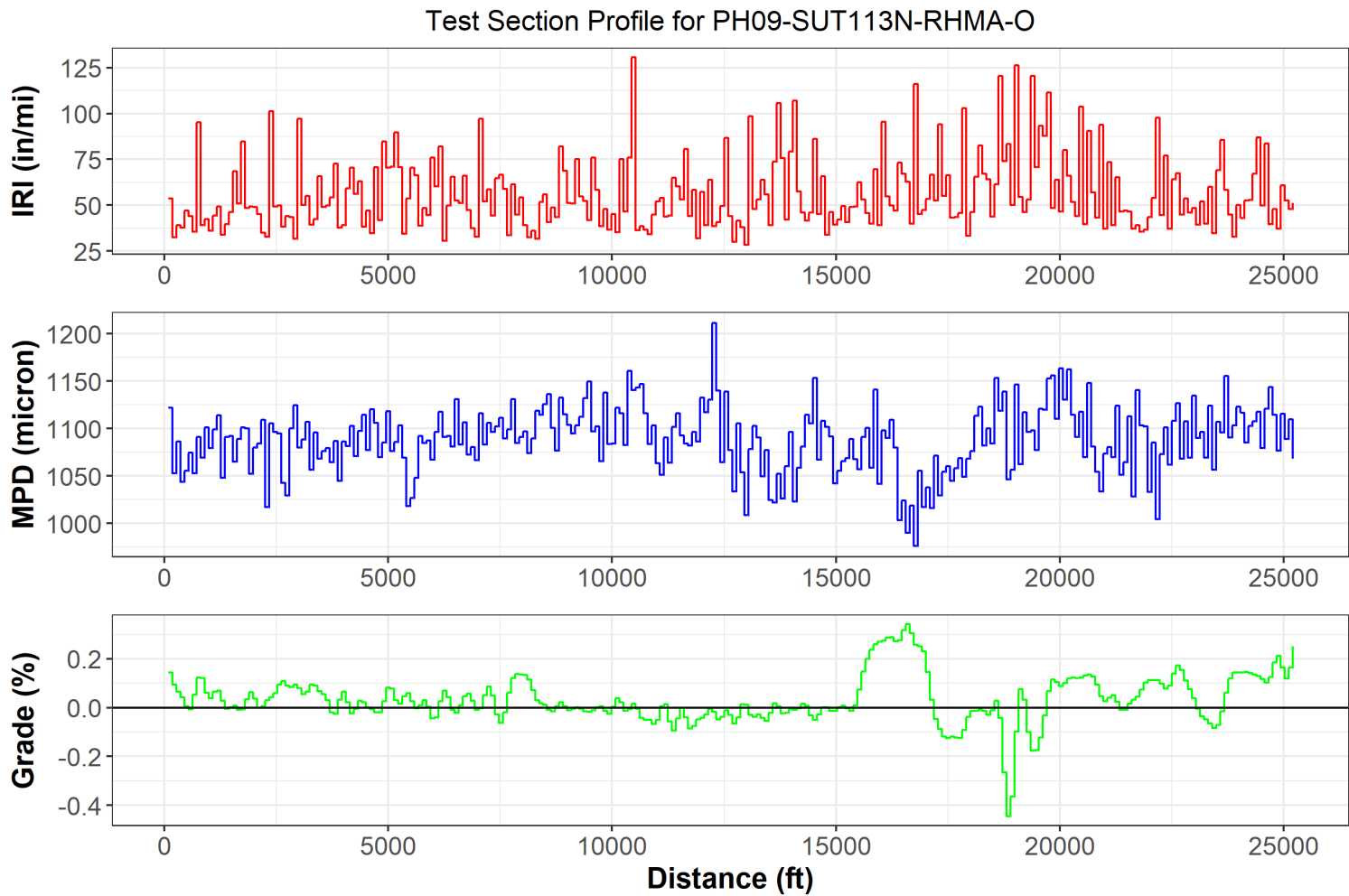


Figure E.7: Roughness, mean profile depth, and grade data plots for section PH09.

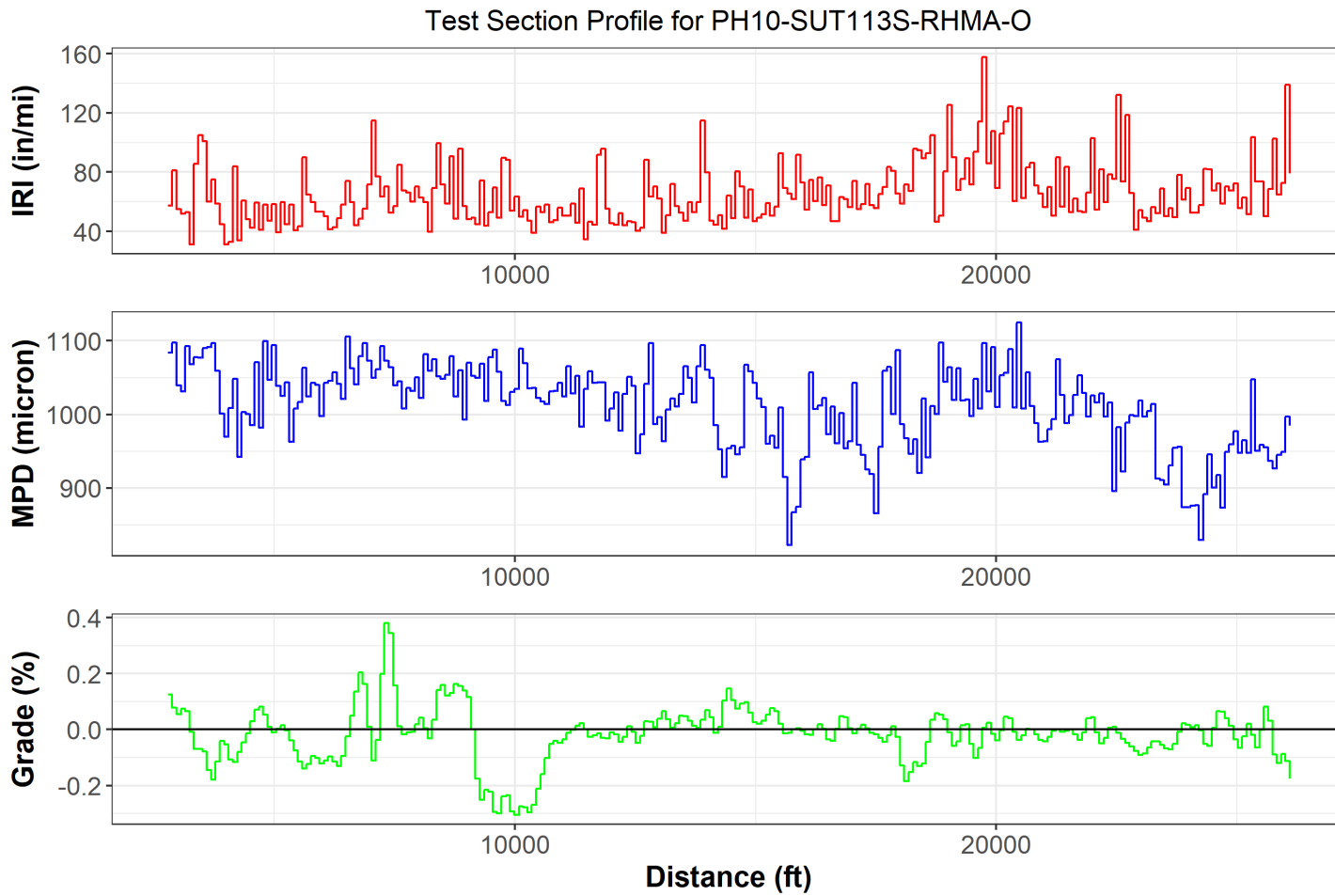


Figure E.8: Roughness, mean profile depth, and grade data plots for section PH10.

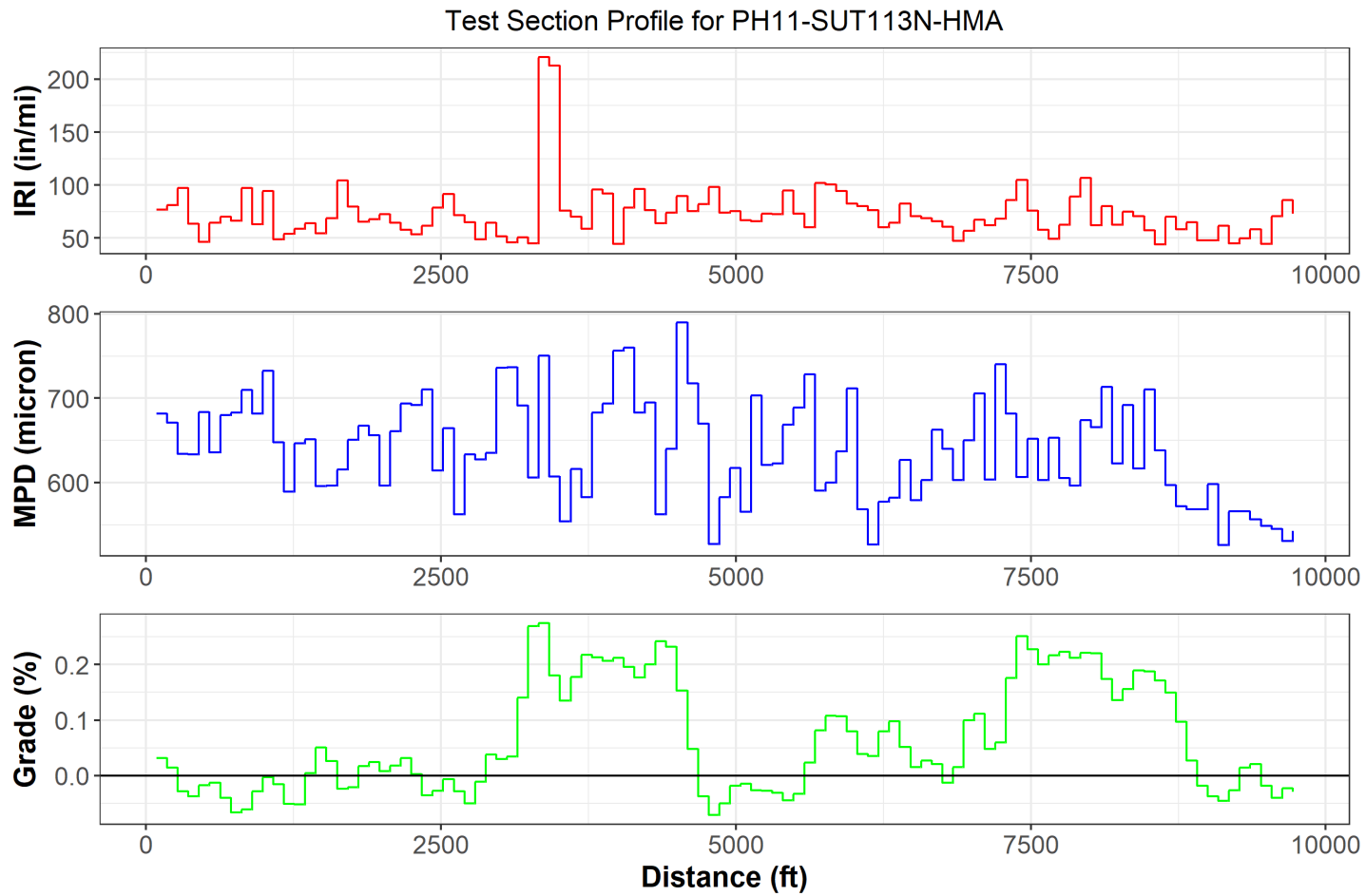


Figure E.9: Roughness, mean profile depth, and grade data plots for section PH11.

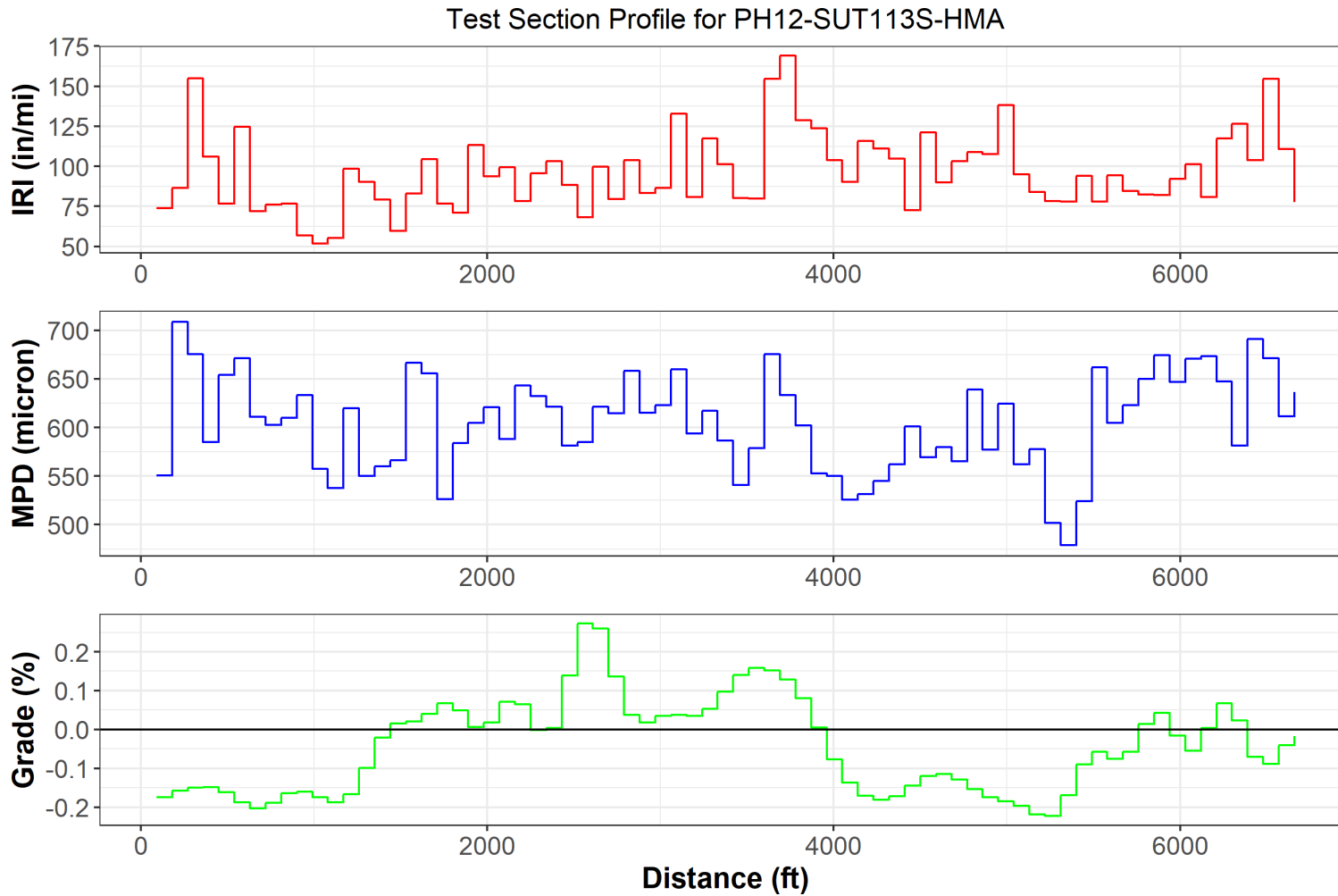


Figure E.10: Roughness, mean profile depth, and grade data plots for section PH12.

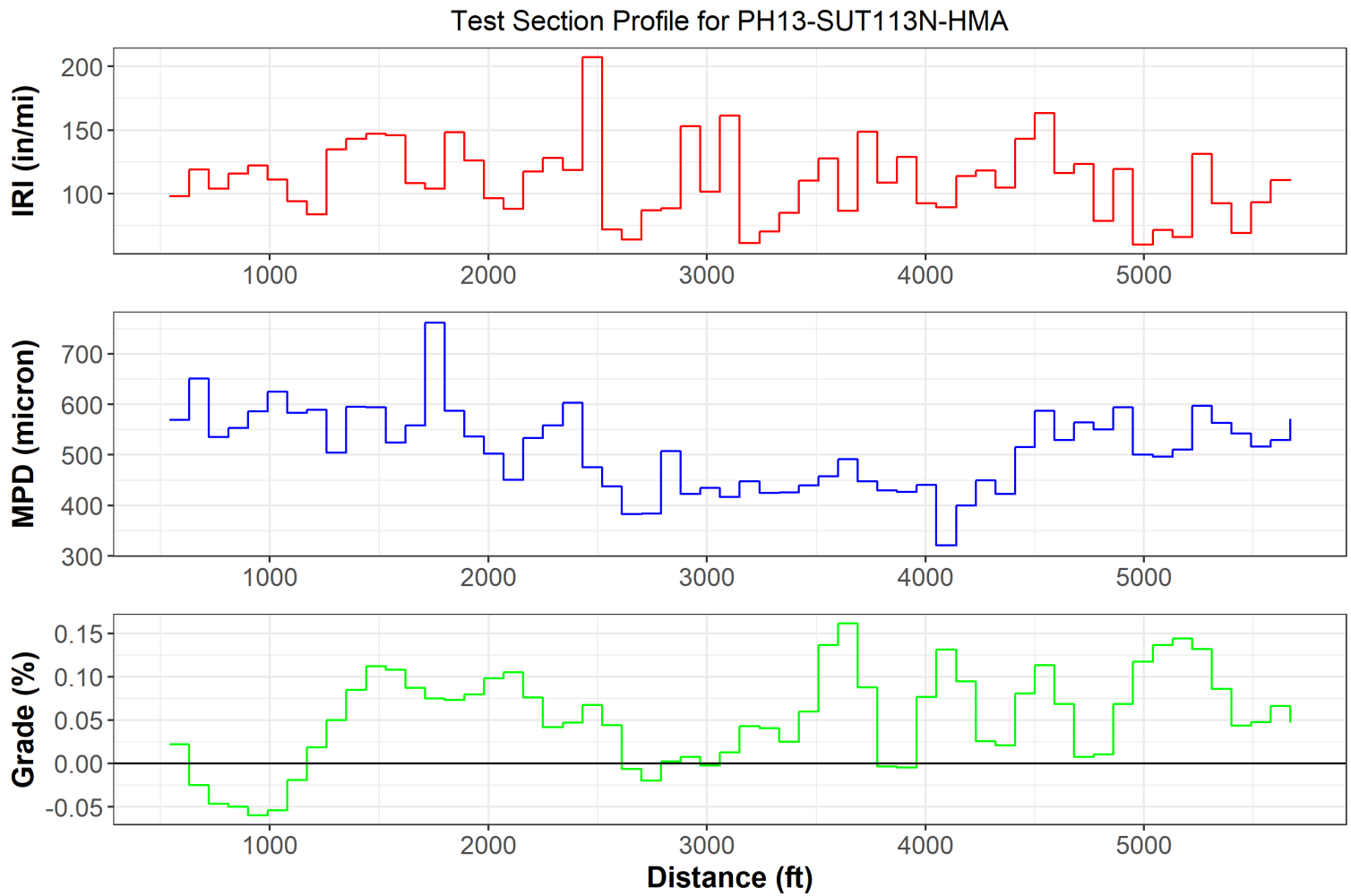


Figure E.11: Roughness, mean profile depth, and grade data plots for section PH13.

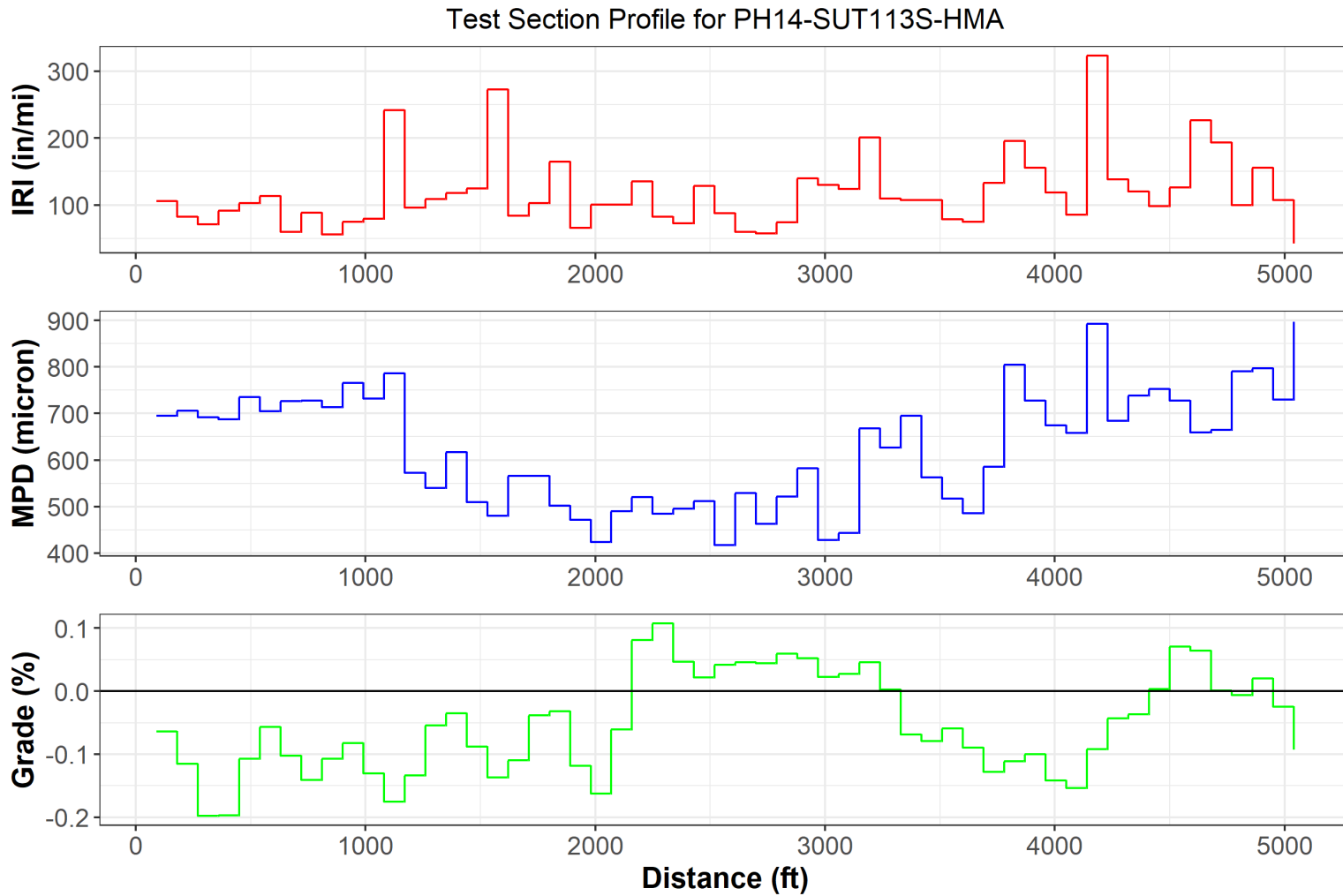


Figure E.12: Roughness, mean profile depth, and grade data plots for section PH14.

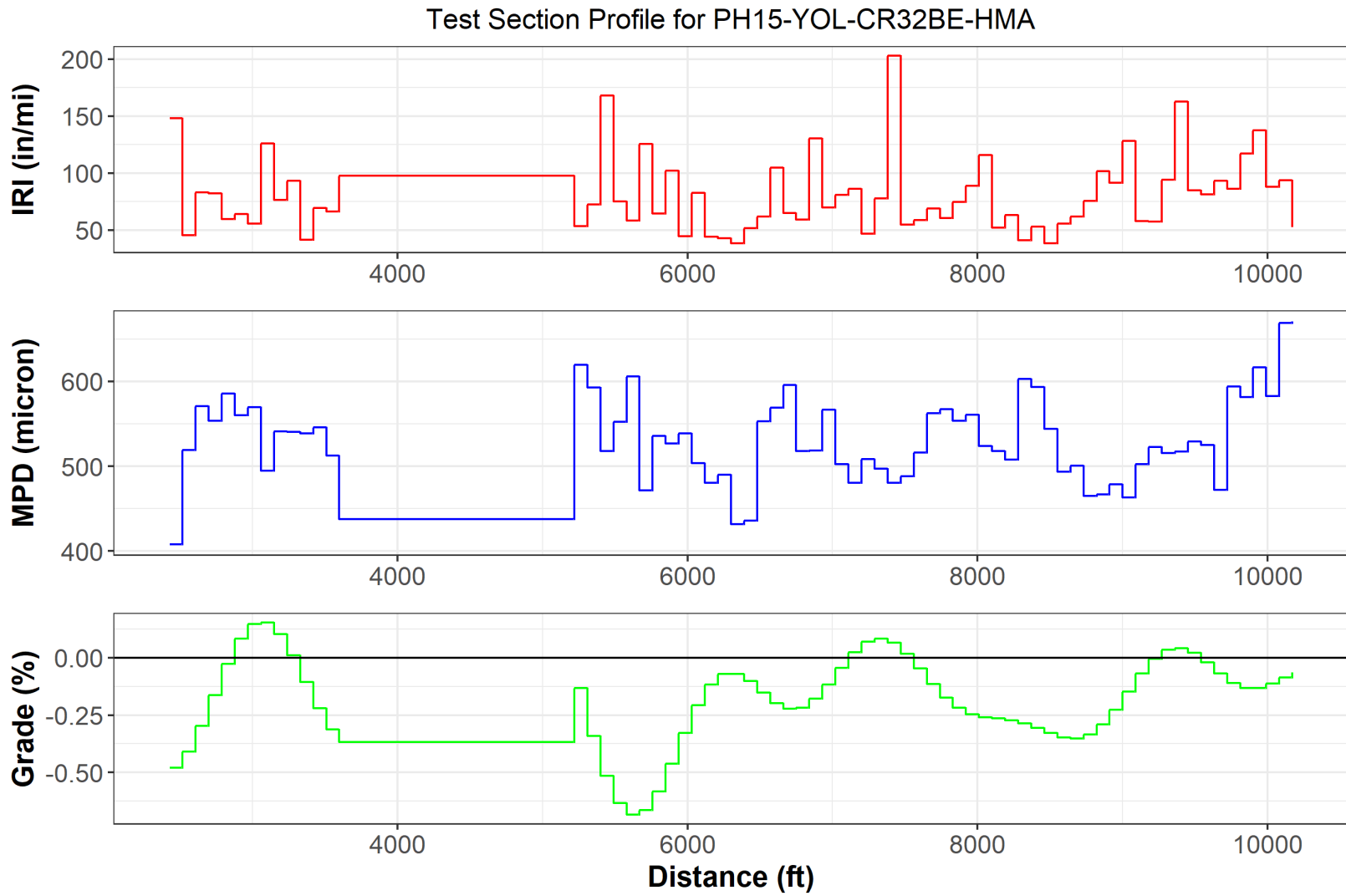


Figure E.13: Roughness, mean profile depth, and grade data plots for section PH15.

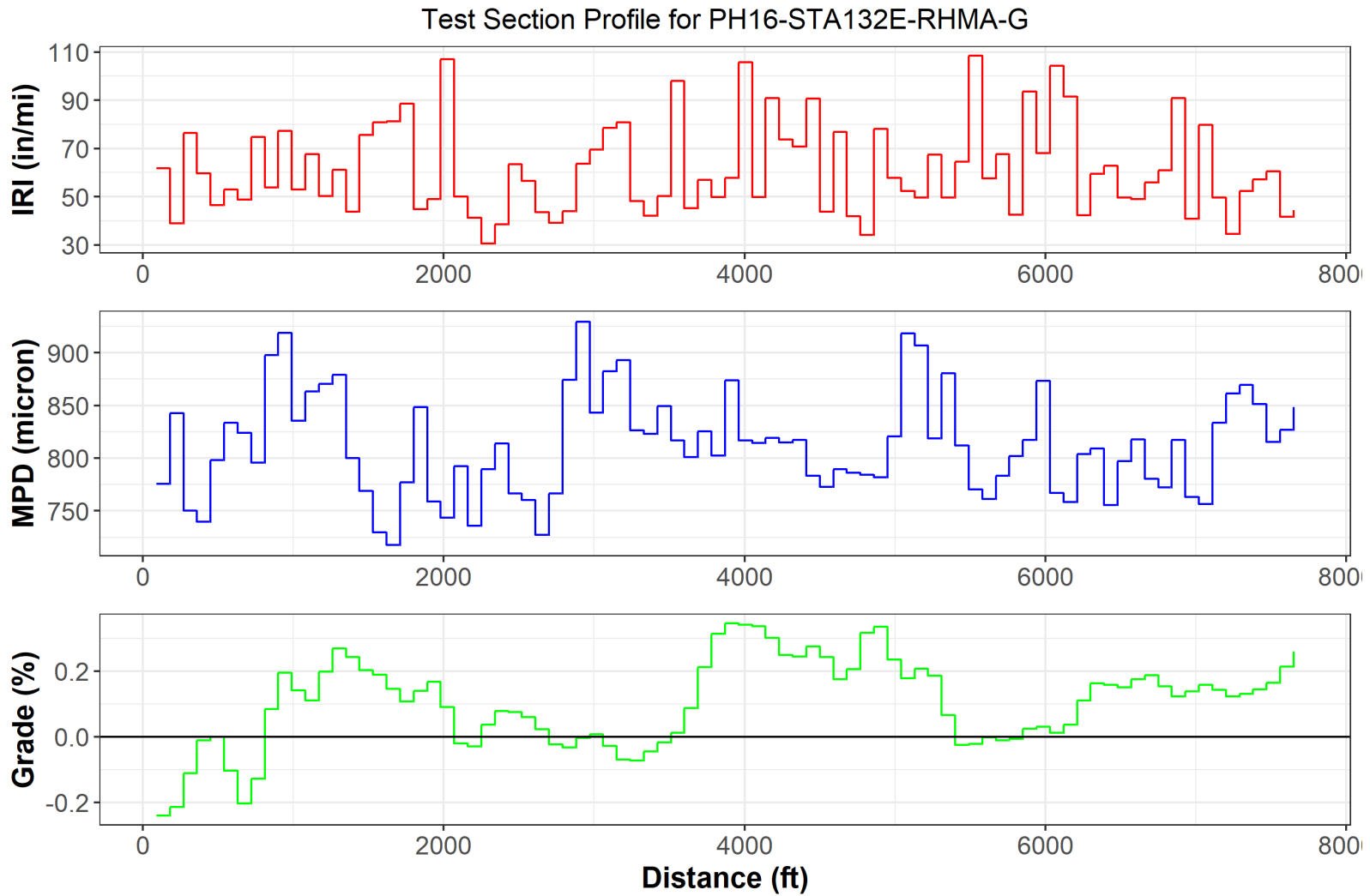


Figure E.14: Roughness, mean profile depth, and grade data plots for section PH16.

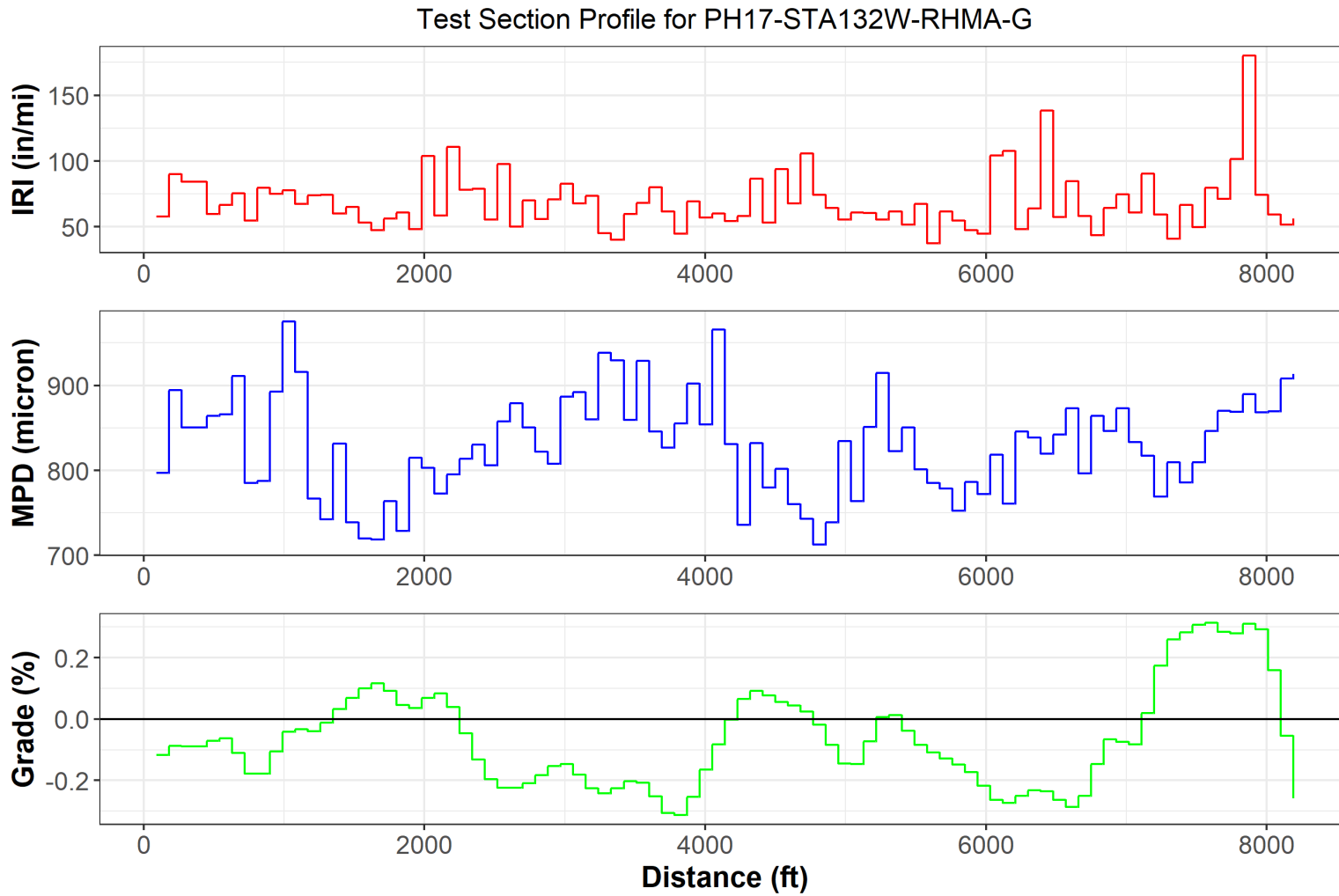


Figure E.15: Roughness, mean profile depth, and grade data plots for section PH17.

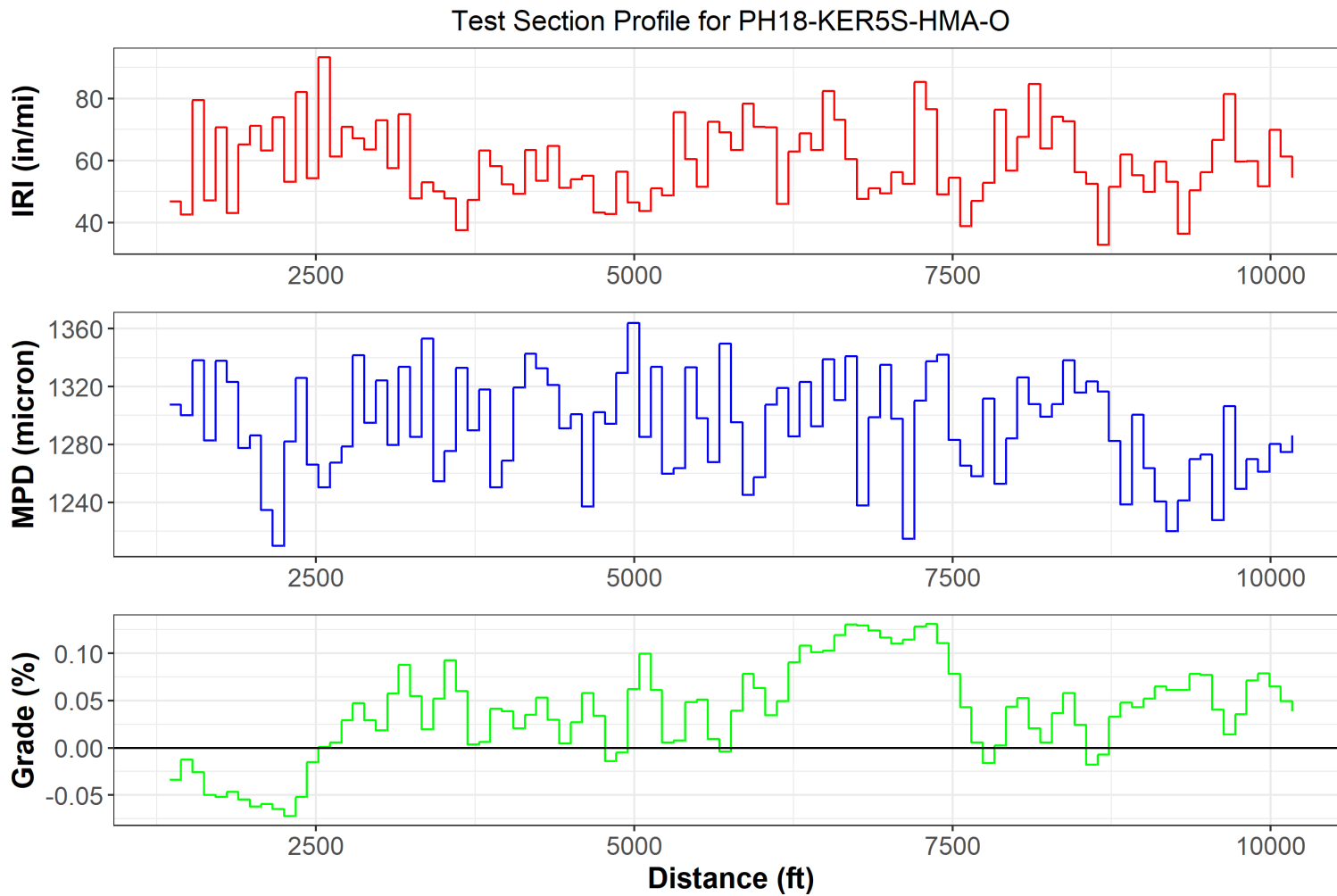


Figure E.16: Roughness, mean profile depth, and grade data plots for section PH18.

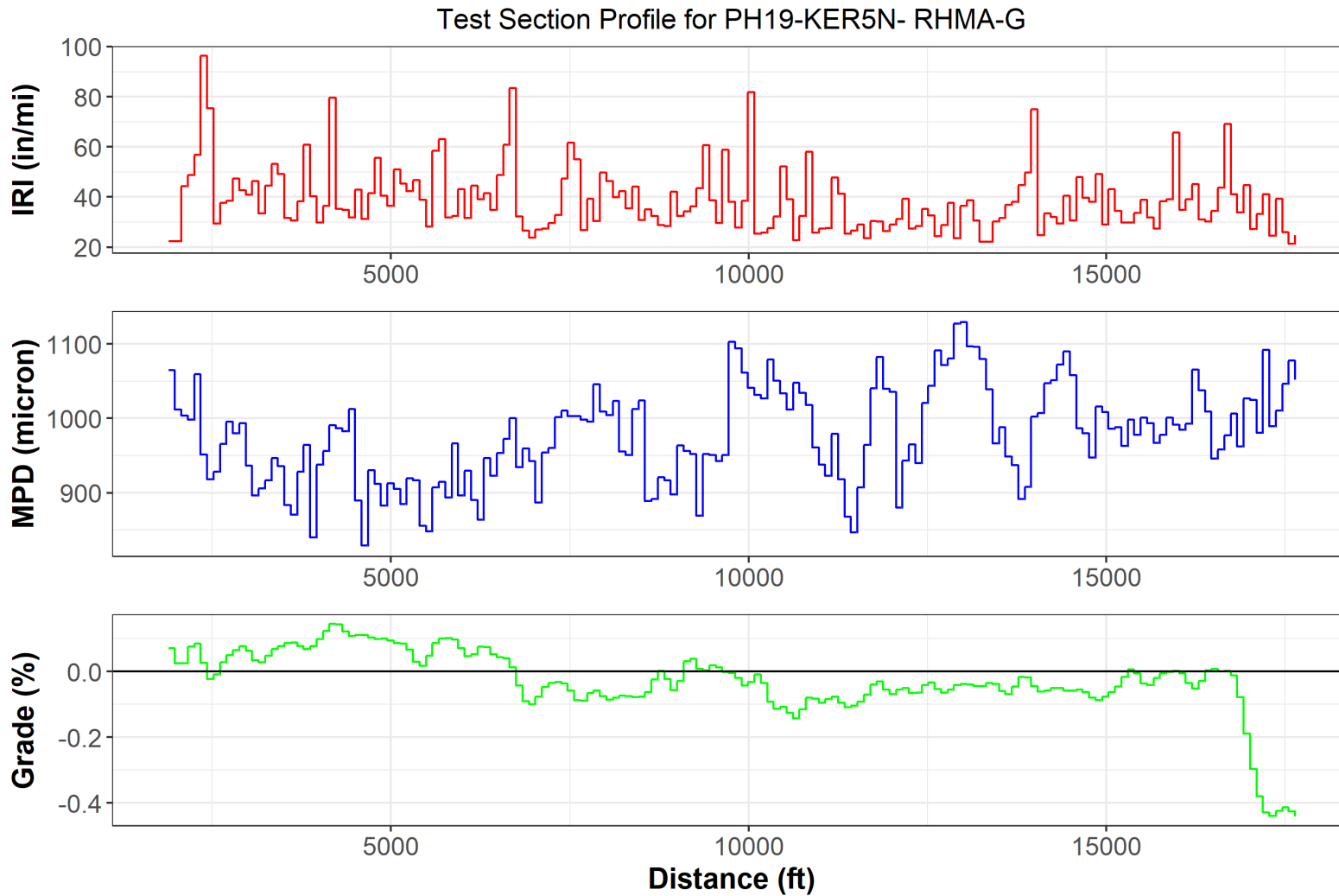


Figure E.17: Roughness, mean profile depth, and grade data plots for section PH19.

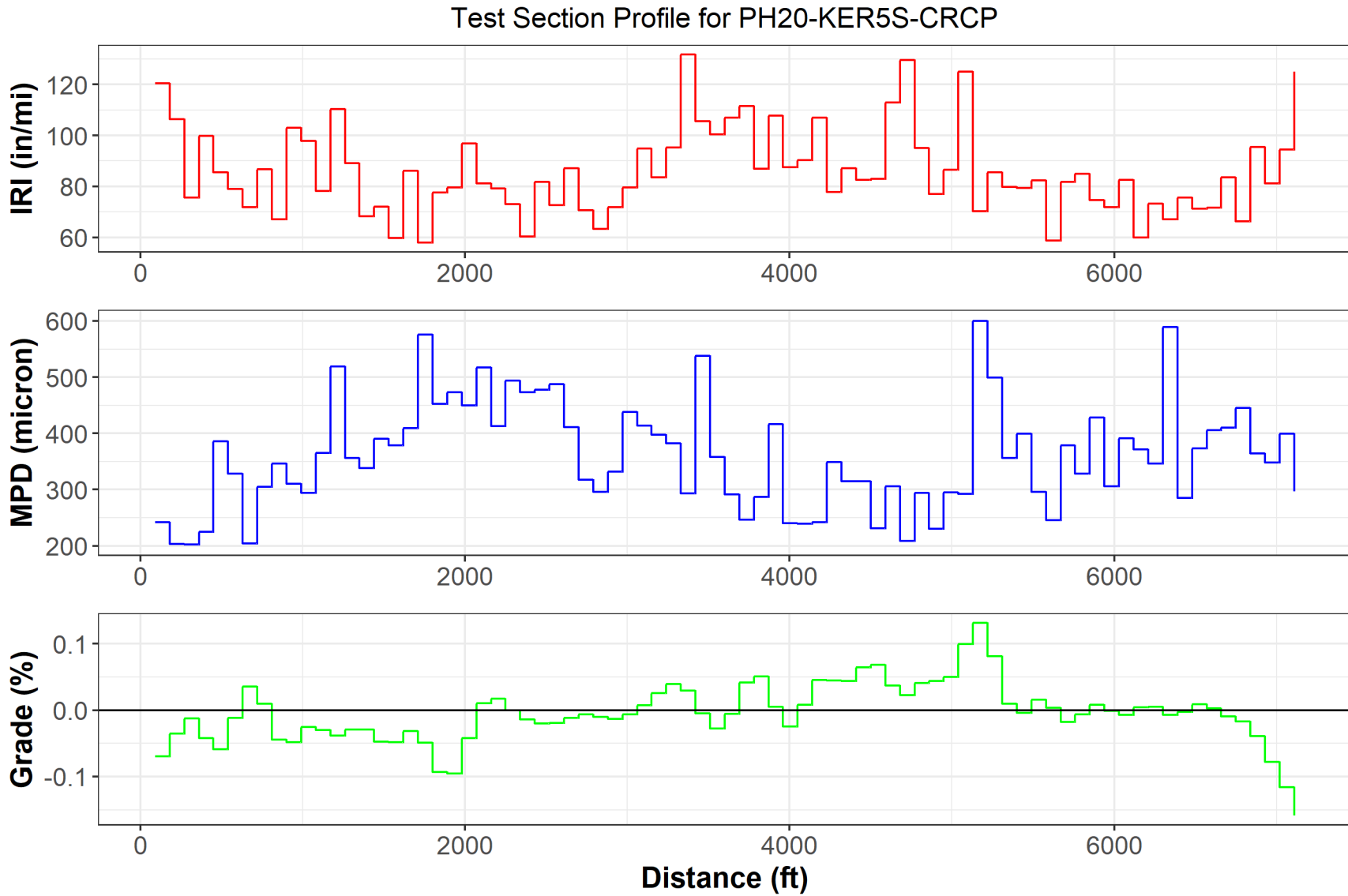


Figure E.18: Roughness, mean profile depth, and grade data plots for section PH20.

Test Section Profile for PH21-YOL99N-JPC

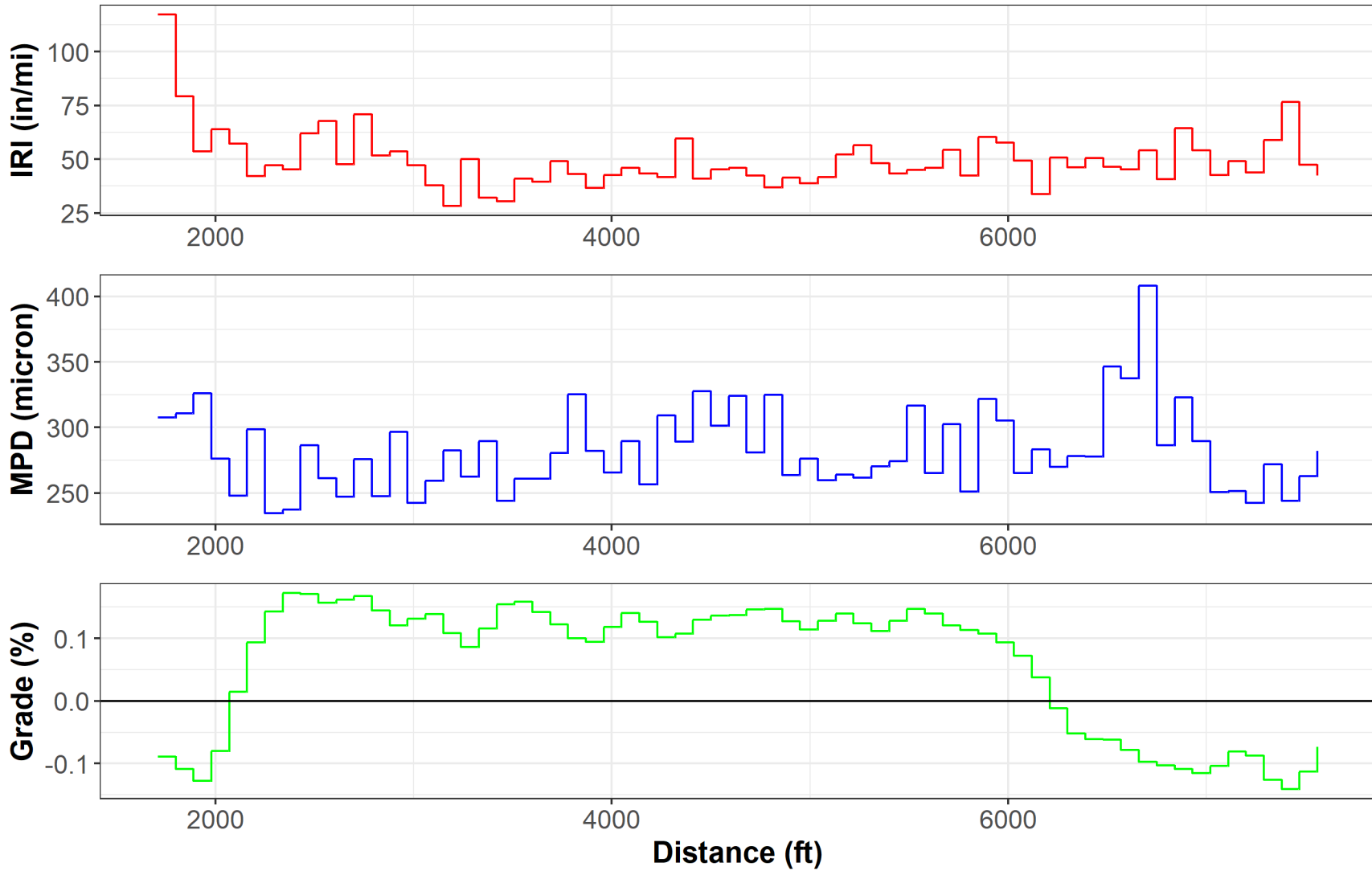


Figure E.19: Roughness, mean profile depth, and grade data plots for section PH21.

Test Section Profile for PH22-YOL99S-JPC

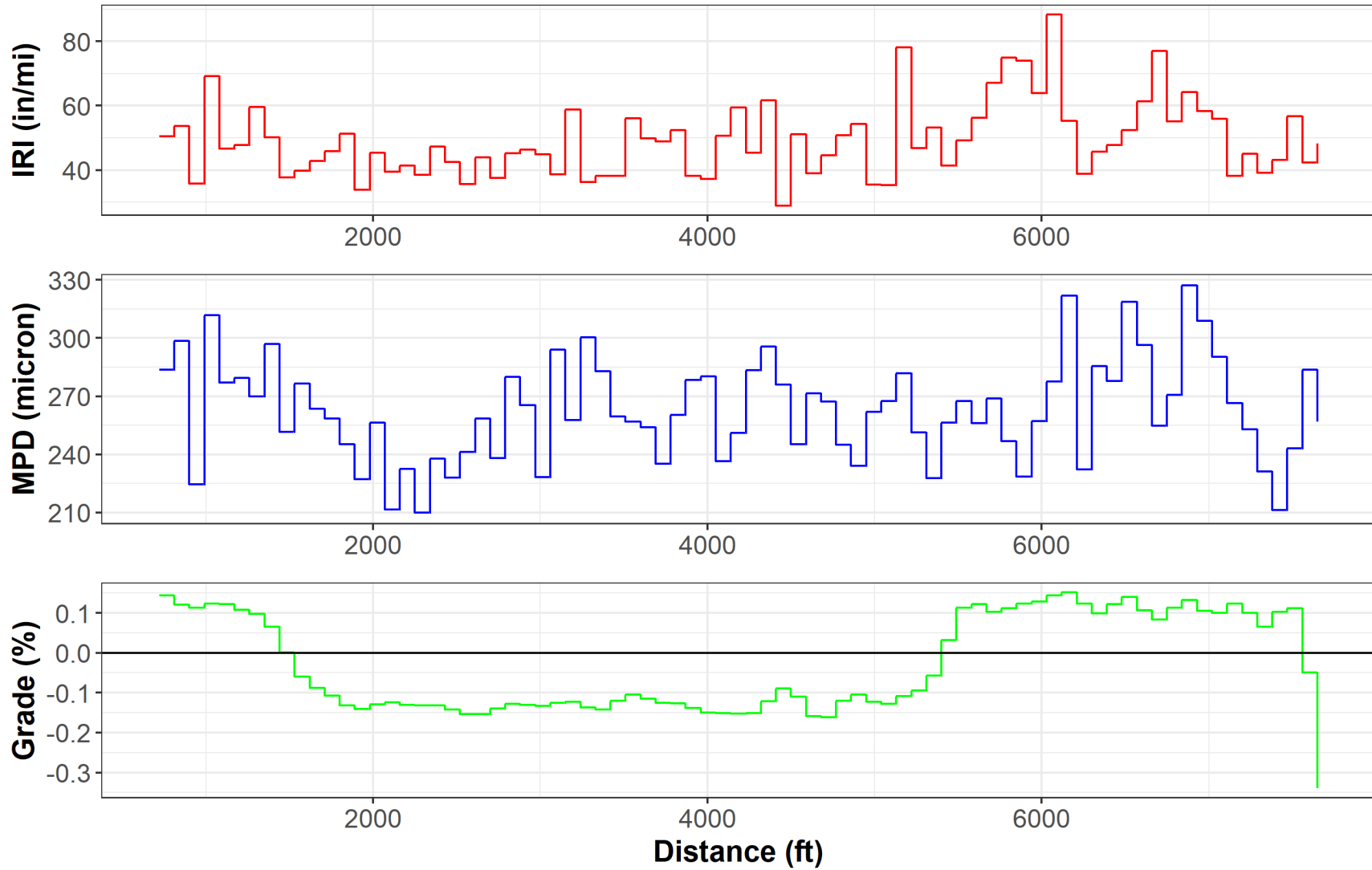


Figure E.20: Roughness, mean profile depth, and grade data plots for section PH22.

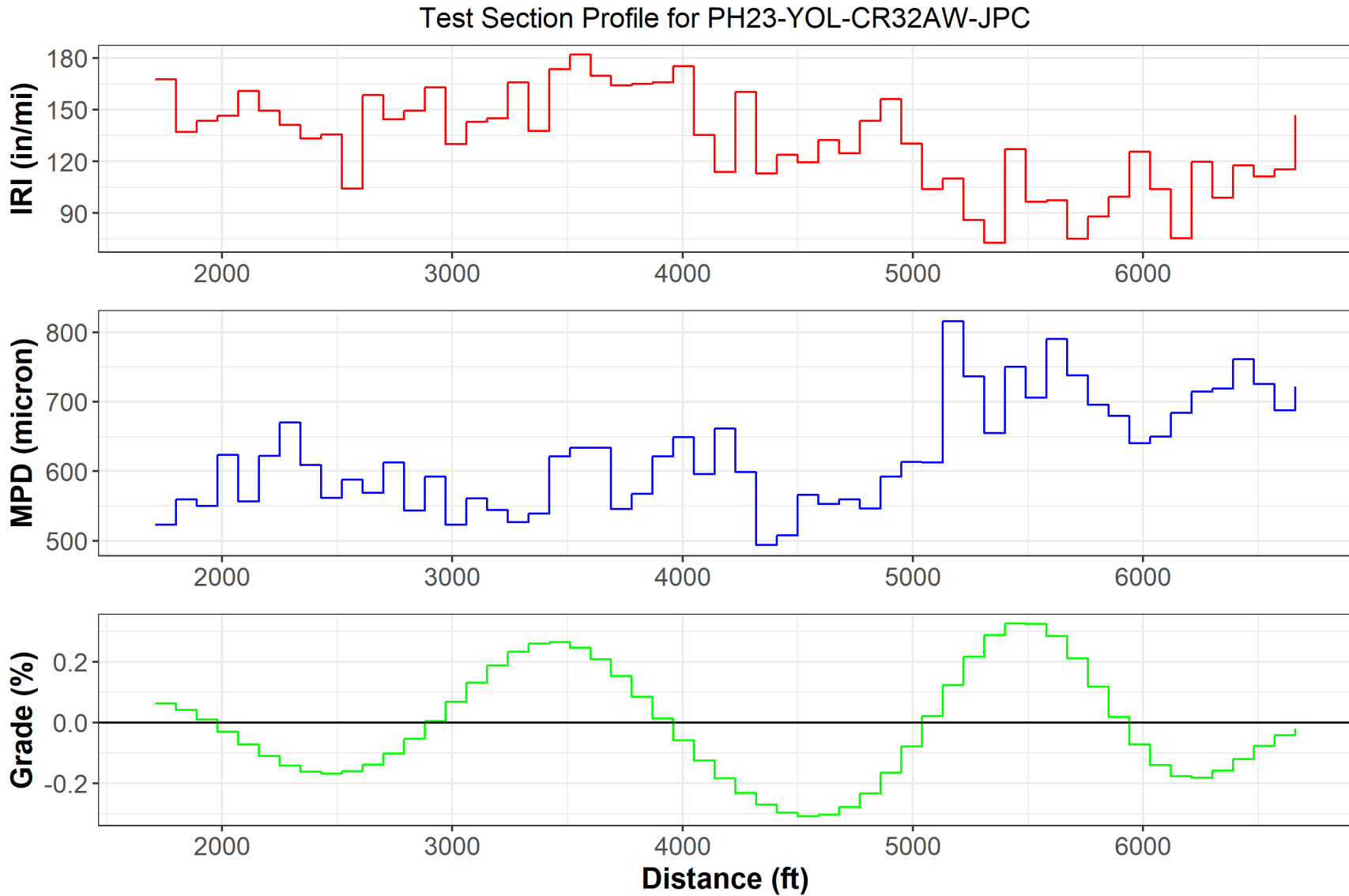


Figure E.21: Roughness, mean profile depth, and grade data plots for section PH23.

APPENDIX F: PAVEMENT GRADIENT DATA FROM DIFFERENT SOURCES

This study used several data sources to compare section gradients. The fuel consumption profile looks similar to that of the section gradient profile, as fuel consumption is highly affected by the pavement surface gradient (i.e., more fuel is used to drive uphill and less fuel is used to drive downhill). In this appendix, mainly two different types of graphs are presented:

1. Google Maps gradient (GMAPS), ground penetration radar vehicle data from Caltrans (GPR Van), and Trimble™ GPS (HP Gps) section grade (% per 165 ft. [50 m] subsection length) versus section length plots are presented in a graph for each state highway section.
2. GPR data 2011 (filename: *.GPS) and APCS 2011, 2012, and 2015 (database filenames: 25K0J800, 16902800, and PSI50700, respectively) average elevation (every 90 ft.) data per section versus section length are plotted for each state highway section.

State highway sections were used to determine the subsection length to average the section gradient data. Therefore, only the best data source available is presented for the county road sections (elevation was measured for PH07, PH08, PH15, and PH23 while driving slowly [10–20 mph] on the sections using a Garmin Edge® 520 GPS unit).

Using the APCS data, it was determined that there was some maintenance performed for some of the sections, as shown in Table F.1. The elevation of those sections changed, as reflected in the second group of graphs for each of the following sections.

Table F.1: Recent Construction Dates and Information for the Sections

Sections	Pavement Types	Construction Date from APCS¹	Construction Activity Notes from APCS¹
PH01	Concrete	12-Apr-2013	Grind and next generation grind of PCC ² , random slab replacement
PH02	Concrete	12-Apr-2013	Grind and next generation grind of PCC ² , random slab replacement
PH03	Concrete	12-Aug-2011	Grind PCC ² and slab replacement
PH21	Concrete	19-May-2011	Grind PCC ² for smoothness
PH22	Concrete	20-May-2011	No data available
PH09	Asphalt	31-Aug-2012	Cold plane 0.1ft. and 0.45 ft. HMA ³ overlay and 0.1 ft. RHMA-O ⁴ cap, 0.25 ft. dig outs

Sections	Pavement Types	Construction Date from APCS ¹	Construction Activity Notes from APCS ¹
PH10	Asphalt	31-Aug-2012	Cold plane 0.1 ft. and 0.45 ft. HMA ³ overlay and 0.1 ft. RHMA-O ⁴ cap, 0.25 ft. dig outs
PH11	Asphalt	28-May-2009	0.25 ft. dig outs and 0.10 ft. AC ⁵ overlay
PH12	Asphalt	28-May-2009	0.25 ft. dig outs and 0.10 ft. AC ⁵ overlay
PH13	Asphalt	No data available	No data available
PH14	Asphalt	No data available	No data available
PH16	Semi-Rigid	26-Jul-2006	Asphalt rubber chipseal
PH17	Semi-Rigid	26-Jul-2006	Asphalt rubber chipseal
PH04	Composite	26-Jun-2013	0.1 ft. RHMA-O ⁴ overlay and ramps, fog seal shoulders, crack seal
PH18	Composite	29-Mar-2002	Crack, seal, and overlay (25 mm OGAC ⁶ , 75 mm AC ⁵ , pavement reinforcing fabric and 30 mm AC ⁵ leveling course) (15.8-42.8, 52.8-62.6 Northbound, 30.8-36.4, 44.8-62.6 Southbound) and PCC ² grind and slab replacement
PH19	Composite	19-Jul-2012	Cold plane 0.0-0.08 ft. and place 0.07 ft. BWC ⁷ gap grade overlay
PH20	Continuously Reinforced Concrete Pavement	11-Jan-2013	R&R ⁸ #2 lane with CRCP ⁹ 14 ft. wide with AC ⁵ shoulder, R&R ⁸ random slabs, and grind #1

Note: PH07, PH08, PH15, and PH23 are county road sections, and their previous construction records were not available.

¹ APCS: Accelerated Pavement Condition Survey

² PCC: Portland cement concrete

³ HMA: Hot mix asphalt

⁴ RHMA-O: Rubberized hot mix asphalt, open-graded

⁵ AC: Asphalt concrete

⁶ OGAC: Open-graded asphalt concrete

⁷ BWC: Bonded wearing course

⁸ R&R: Remove and replace

⁹ CRCP: Continuously reinforced concrete pavement

1. PH01

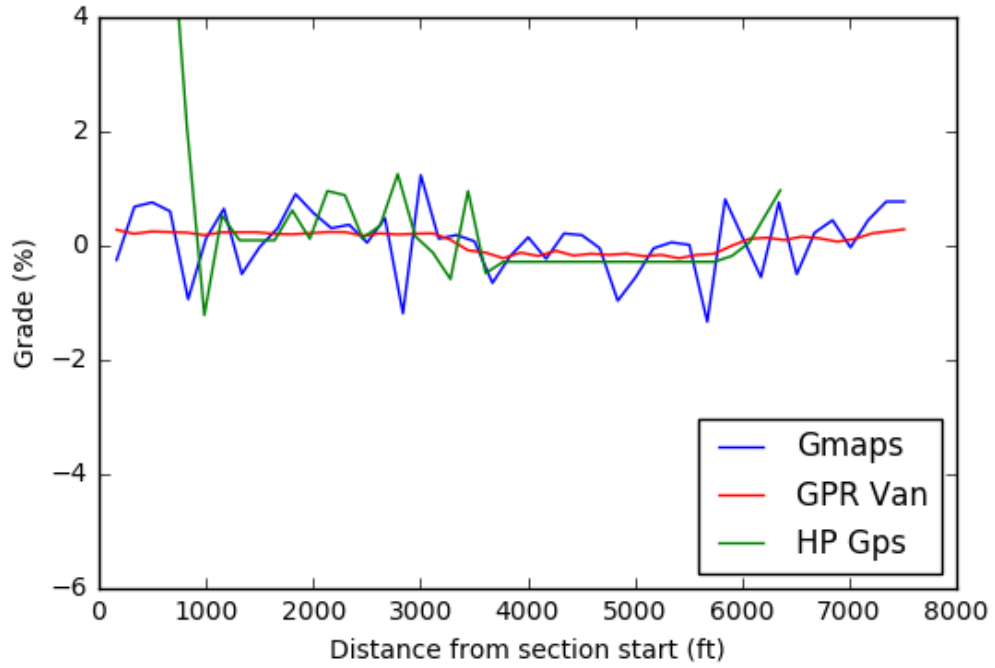


Figure F.1: Section PH01 grade plots for 165 ft. (50 m) subsections from three data sources.

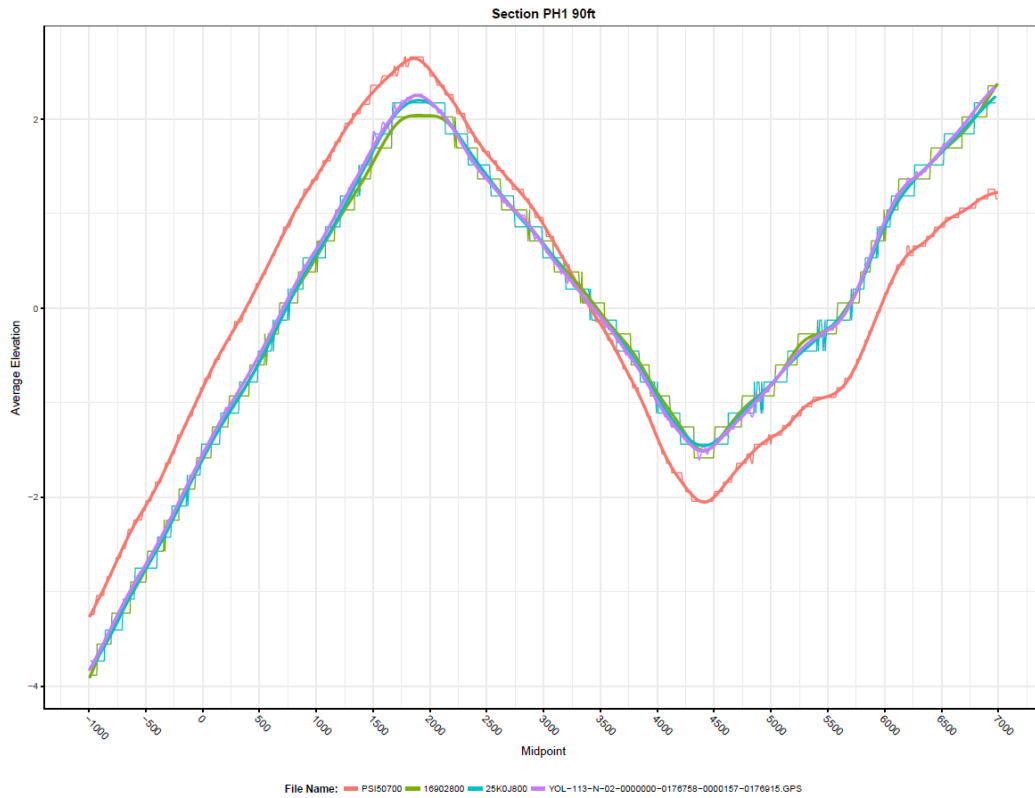


Figure F.2: Section PH01 elevation plots for 90 ft. (27 m) subsections from four data sources.

2. PH02

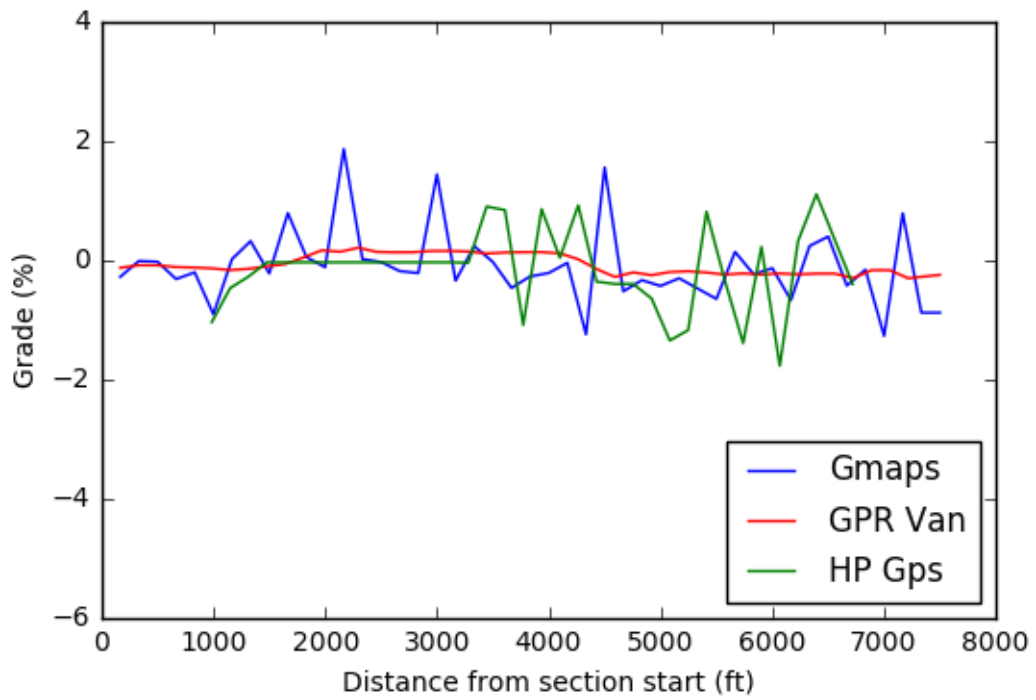


Figure F.3: Section PH02 grade plots for 165 ft. (50 m) subsections from three data sources.

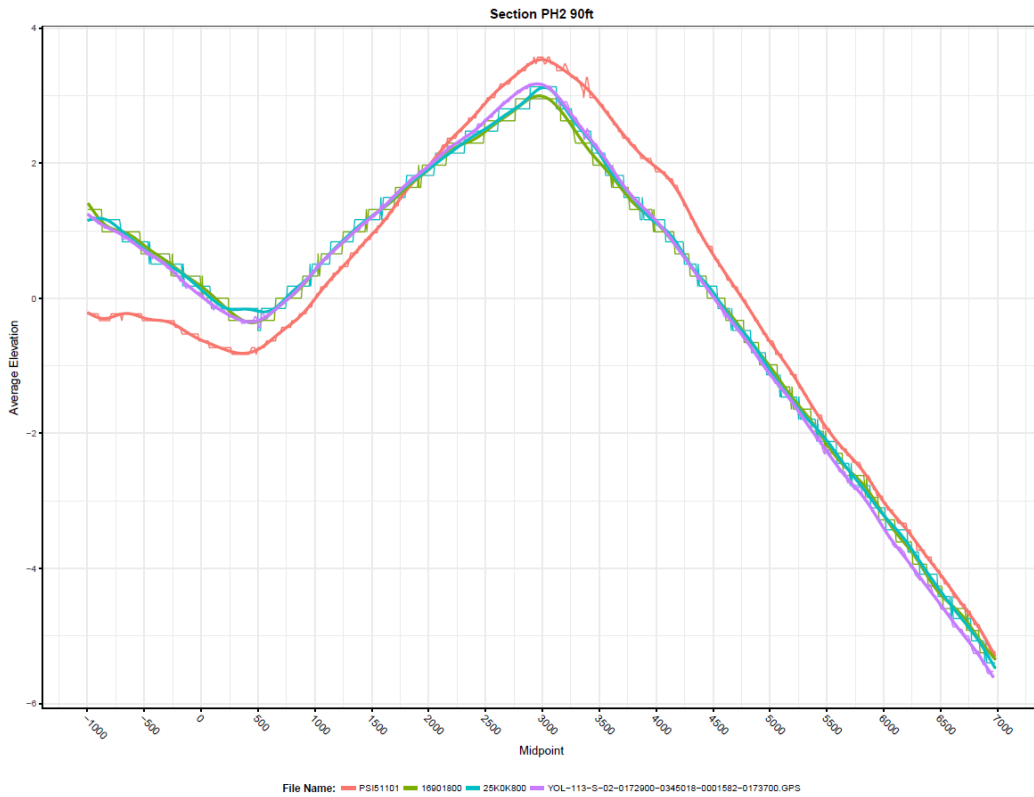


Figure F.4: Section PH02 elevation plots for 90 ft. (27 m) subsections from four data sources.

3. PH03

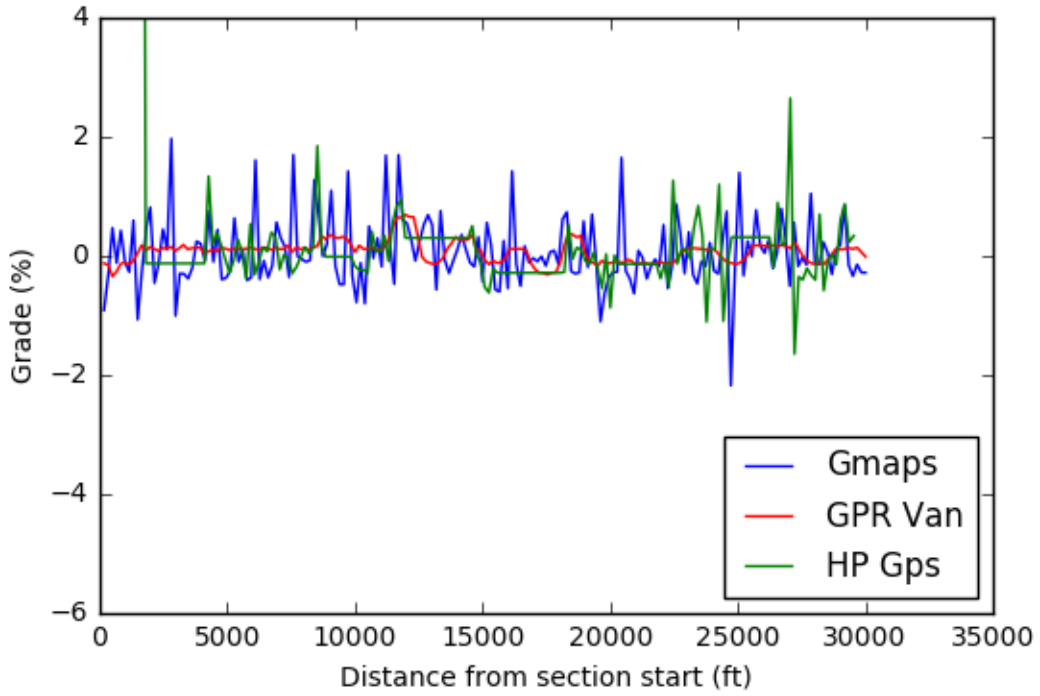


Figure F.5: Section PH03 grade plots for 165 ft. (50 m) subsections from three data sources.

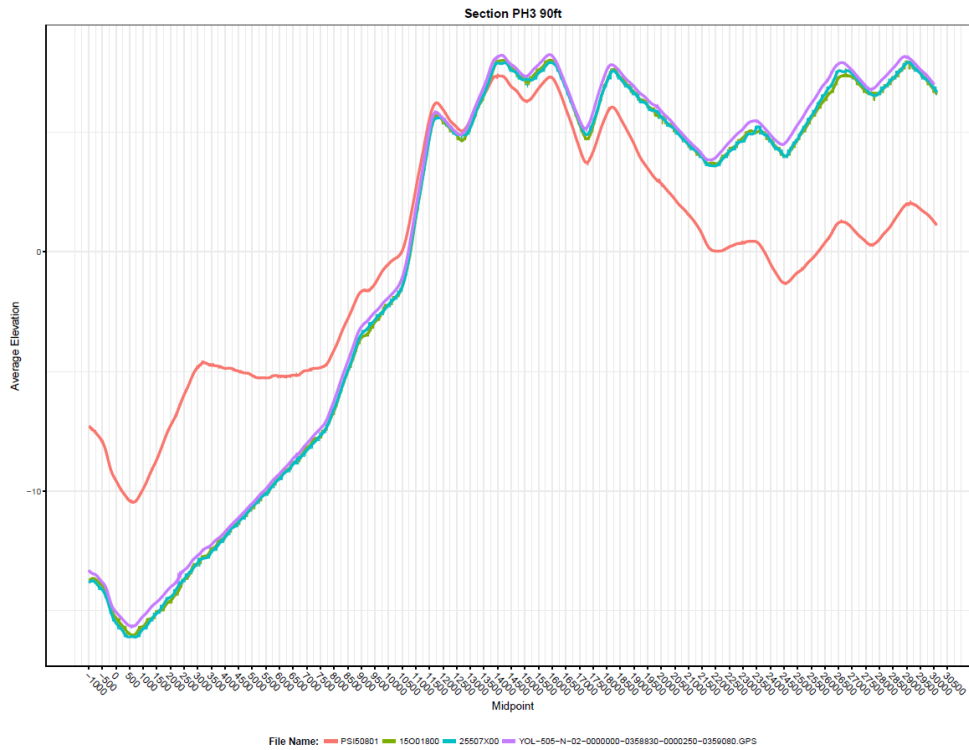


Figure F.6: Section PH03 elevation plots for 90 ft. (27 m) subsections from four data sources.

4. PH04

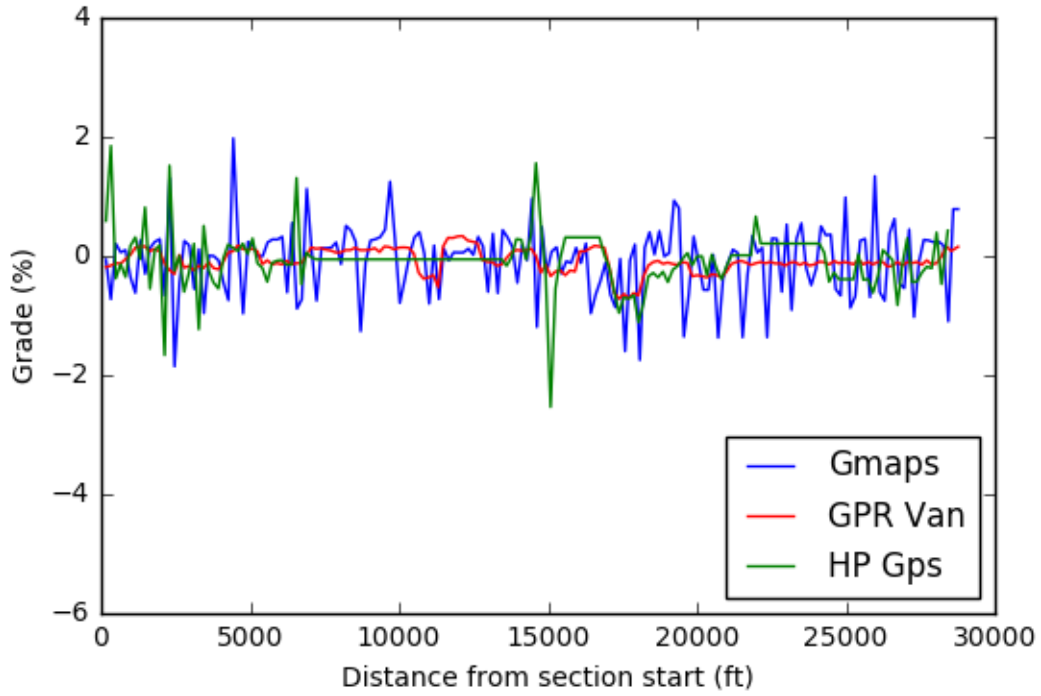


Figure F.7: Section PH04 grade plots for 165 ft. (50 m) subsections from three data sources.

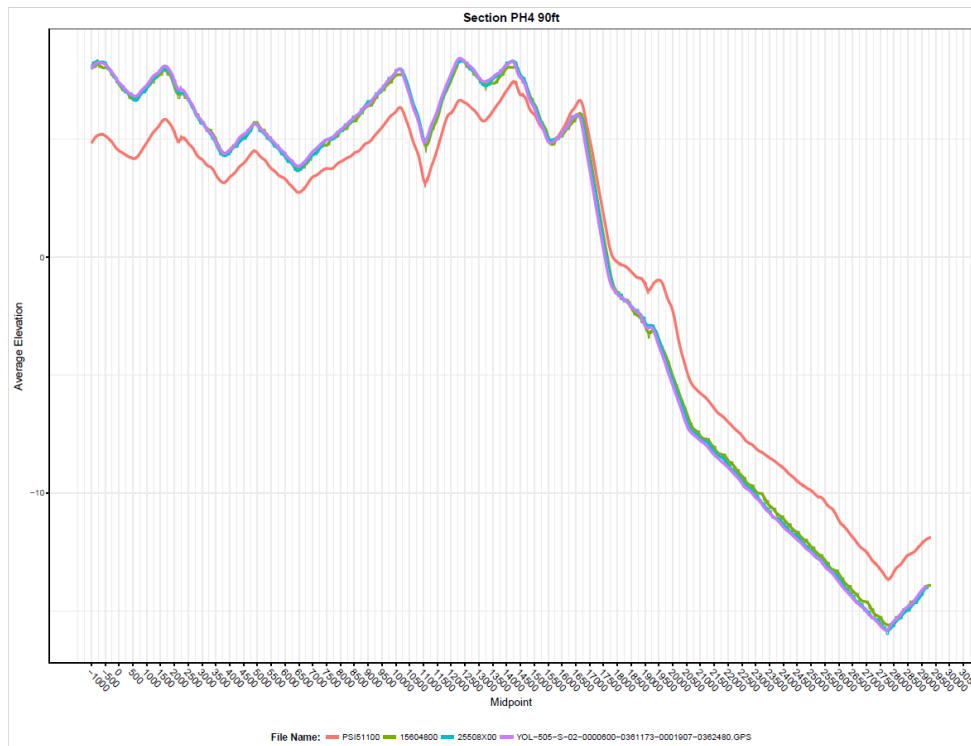


Figure F.8: Section PH04 elevation plots for 90 ft. (27 m) subsections from four data sources.

5. PH07

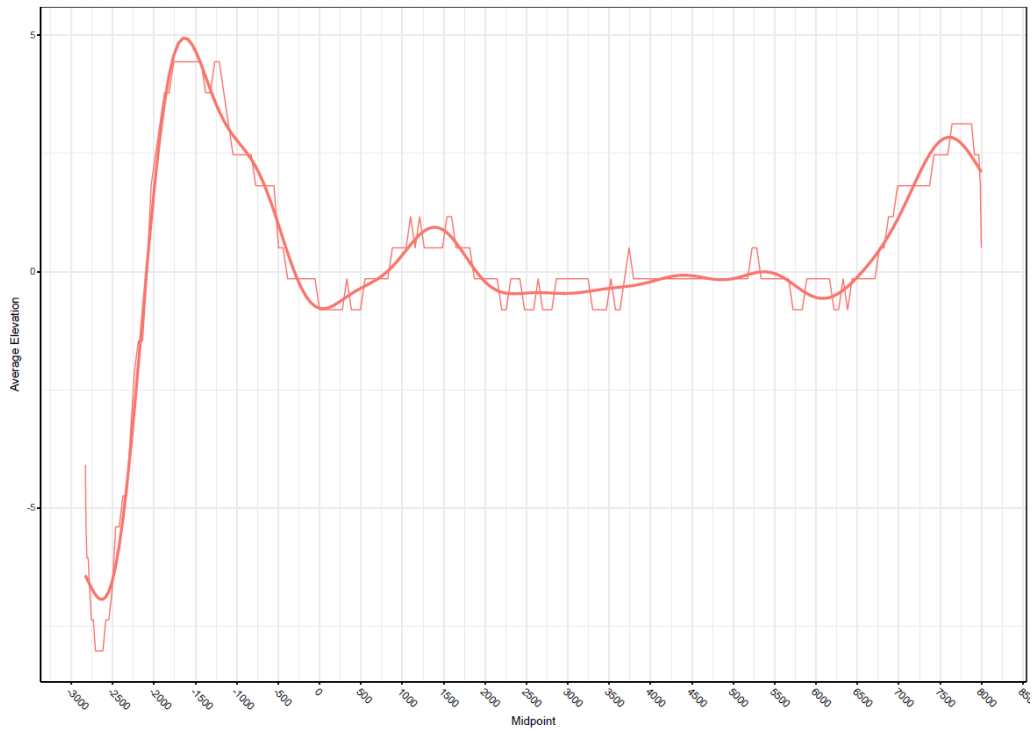


Figure F.9: Section PH07 elevation plots for 30 ft. (9 m) subsections.

6. PH08

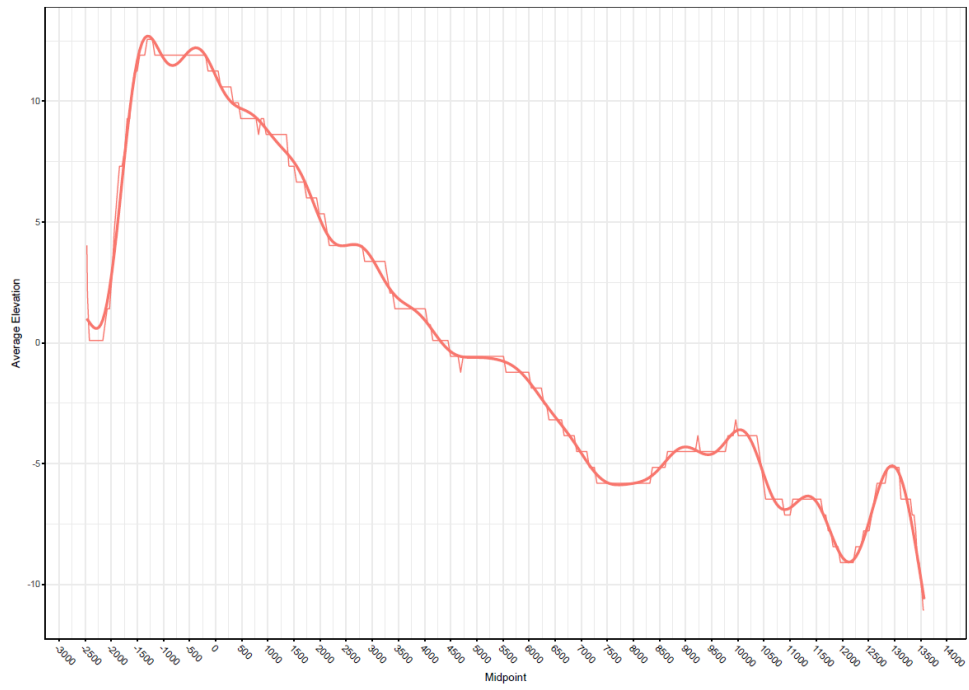


Figure F.10: Section PH08 elevation plots for 30 ft. (9 m) subsections.

7. PH09

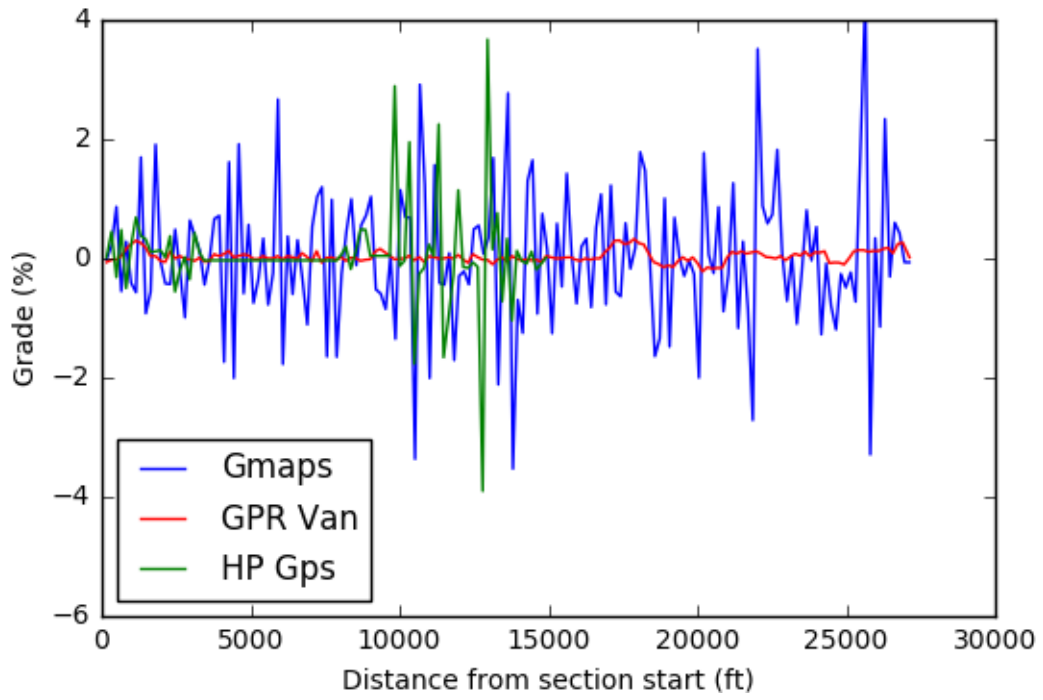


Figure F.11: Section PH09 grade plots for 165 ft. (50 m) subsections from three data sources.

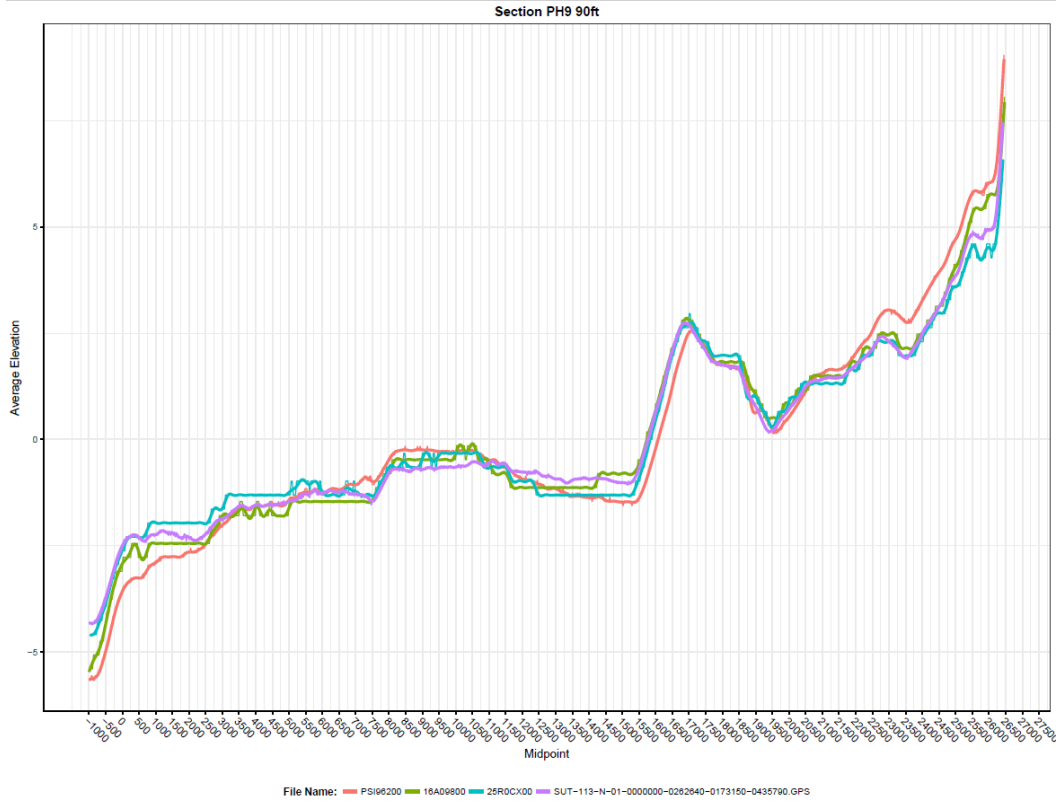


Figure F.12: Section PH09 elevation plots for 90 ft. (27 m) subsections from four data sources.

8. PH10

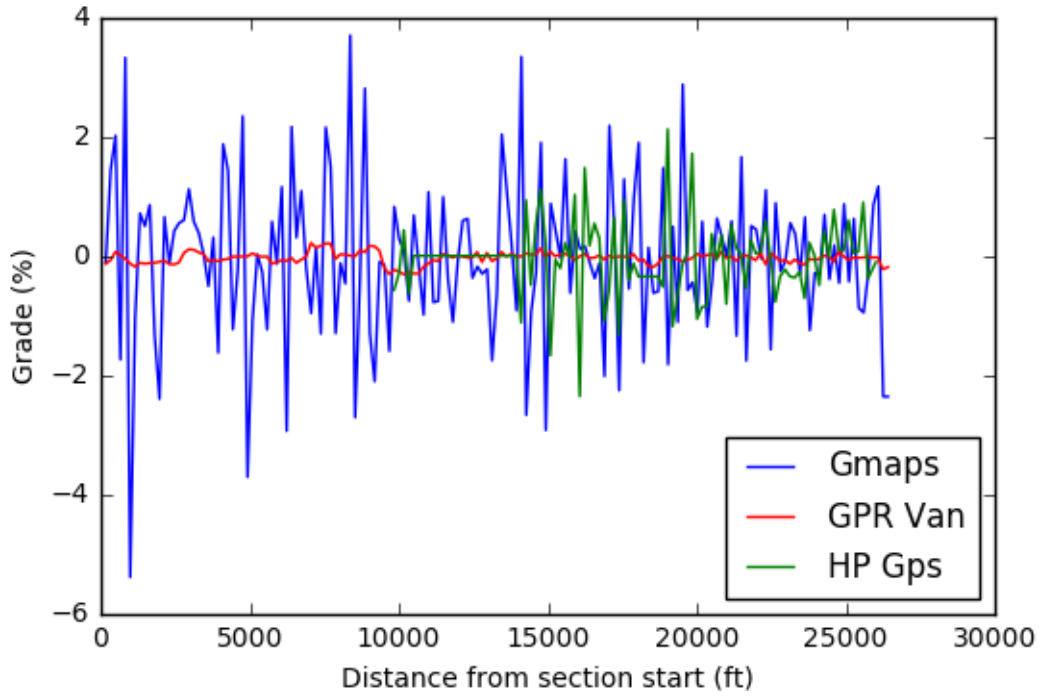


Figure F.13: Section PH10 grade plots for 165 ft. (50 m) subsections from three data sources.

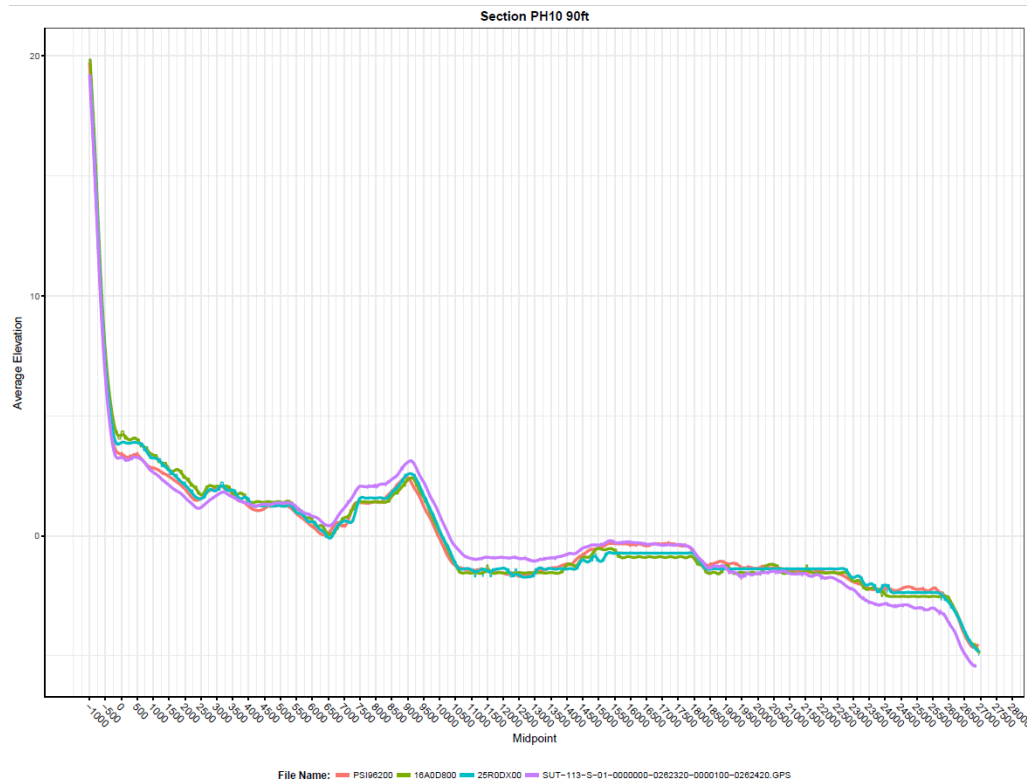


Figure F.14: Section PH10 elevation plots for 90 ft. (27 m) subsections from four data sources.

9. PH11

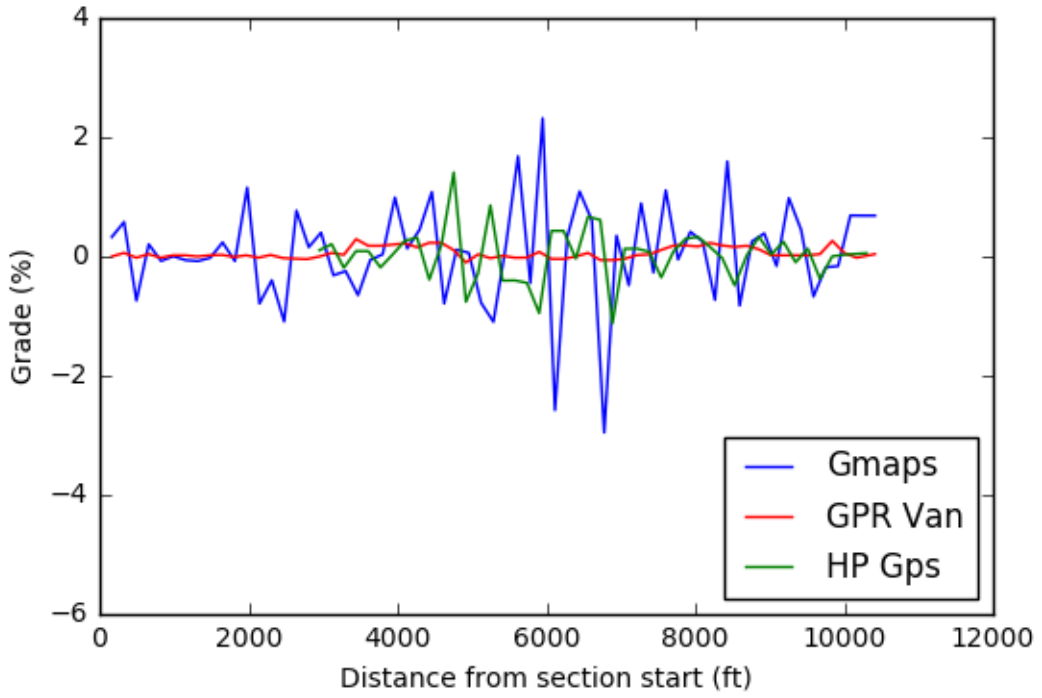


Figure F.15: Section PH11 grade plots for 165 ft. (50 m) subsections from three data sources.

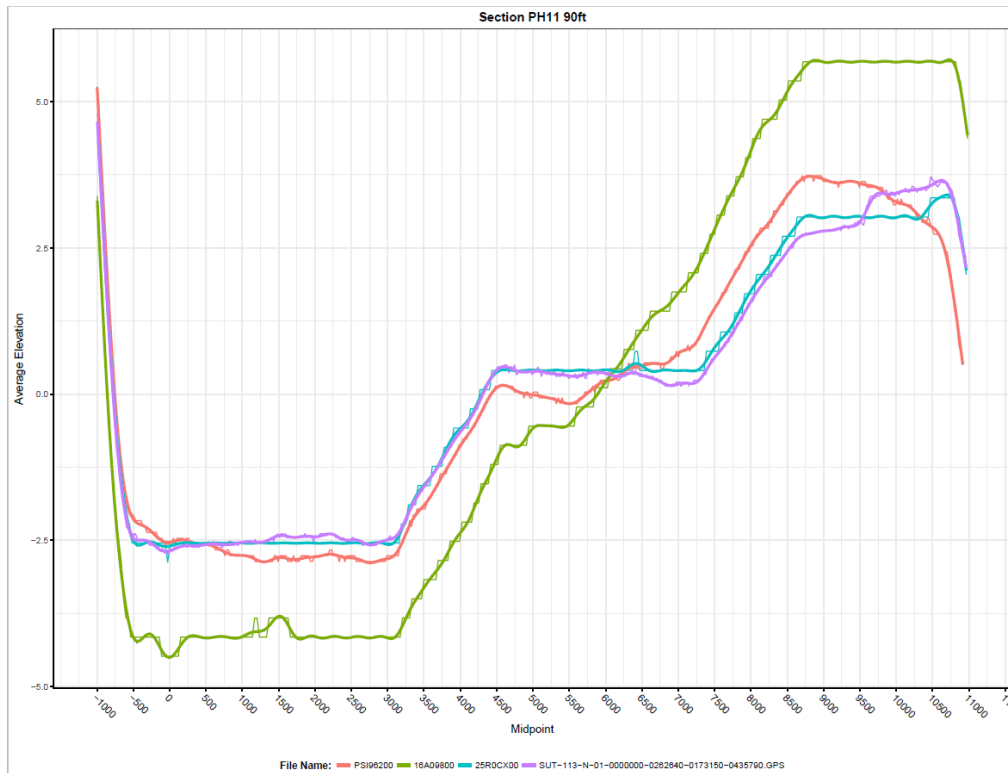


Figure F.16: Section PH11 elevation plots for 90 ft. (27 m) subsections from four data sources.

10. PH12

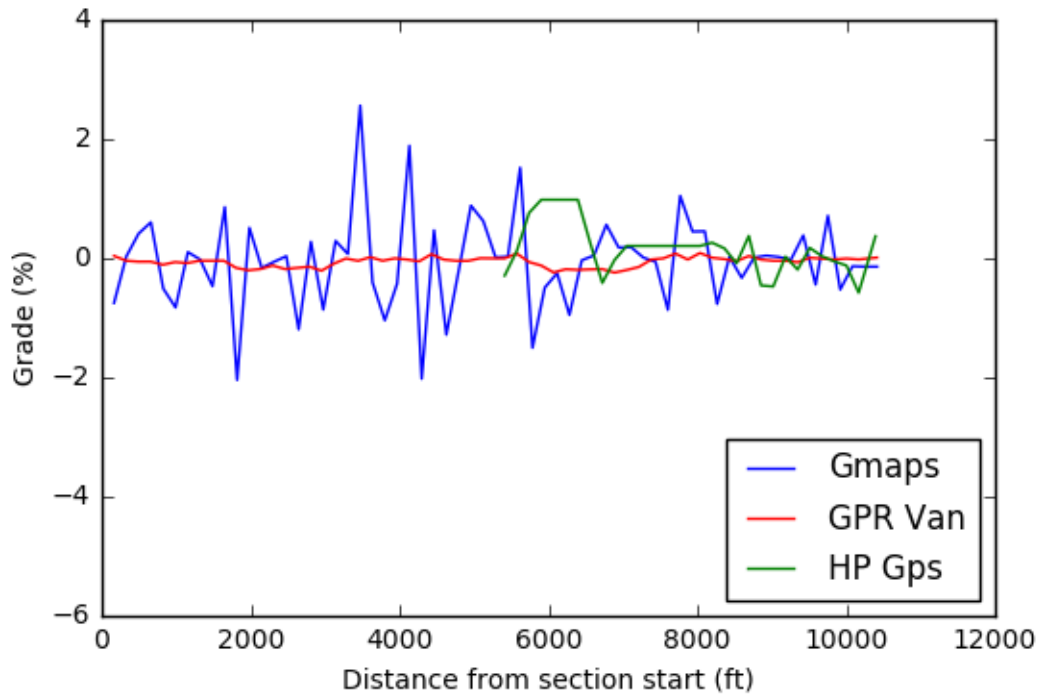


Figure F.17: Section PH12 grade plots for 165 ft. (50 m) subsections from three data sources.

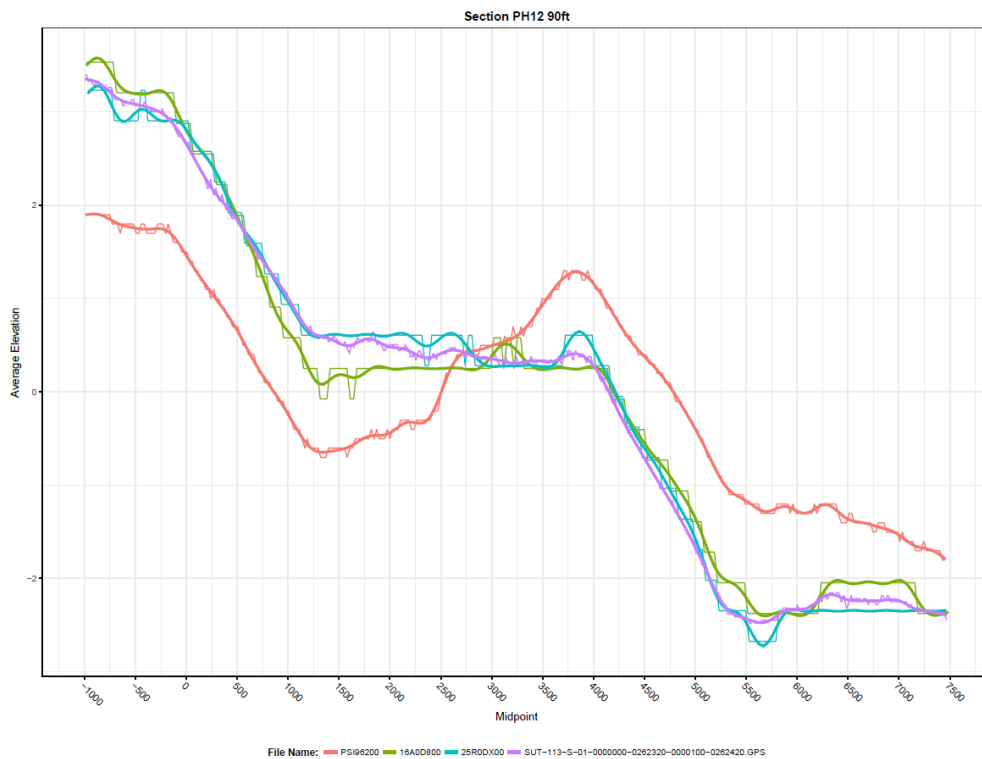


Figure F.18: Section PH12 elevation plots for 90 ft. (27 m) subsections from four data sources.

11. PH13

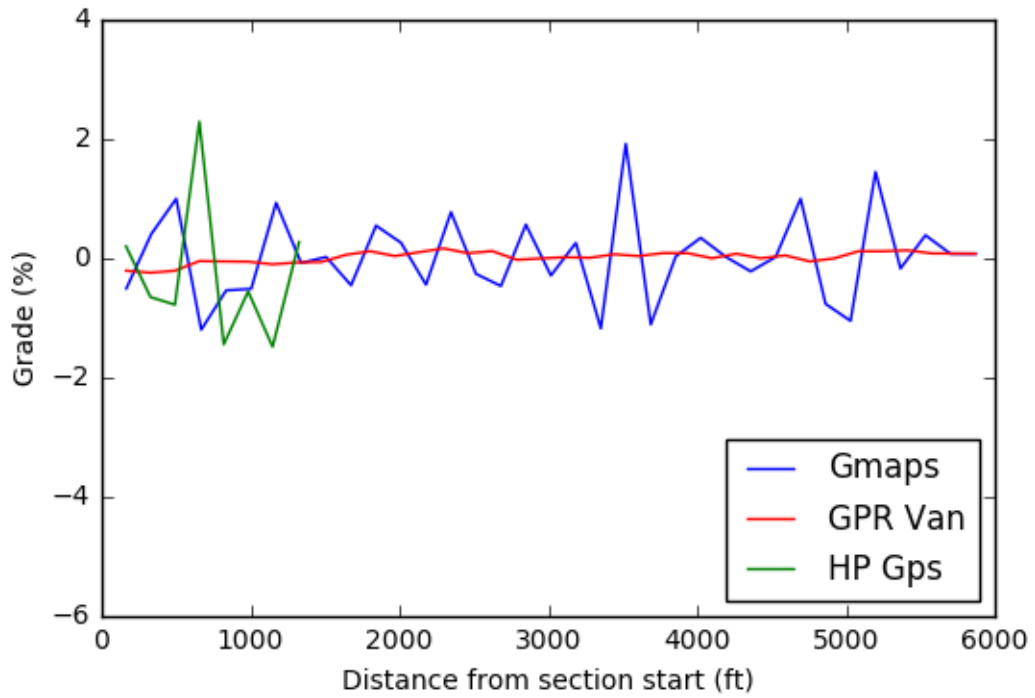


Figure F.19: Section PH13 grade plots for 165 ft. (50 m) subsections from three data sources.

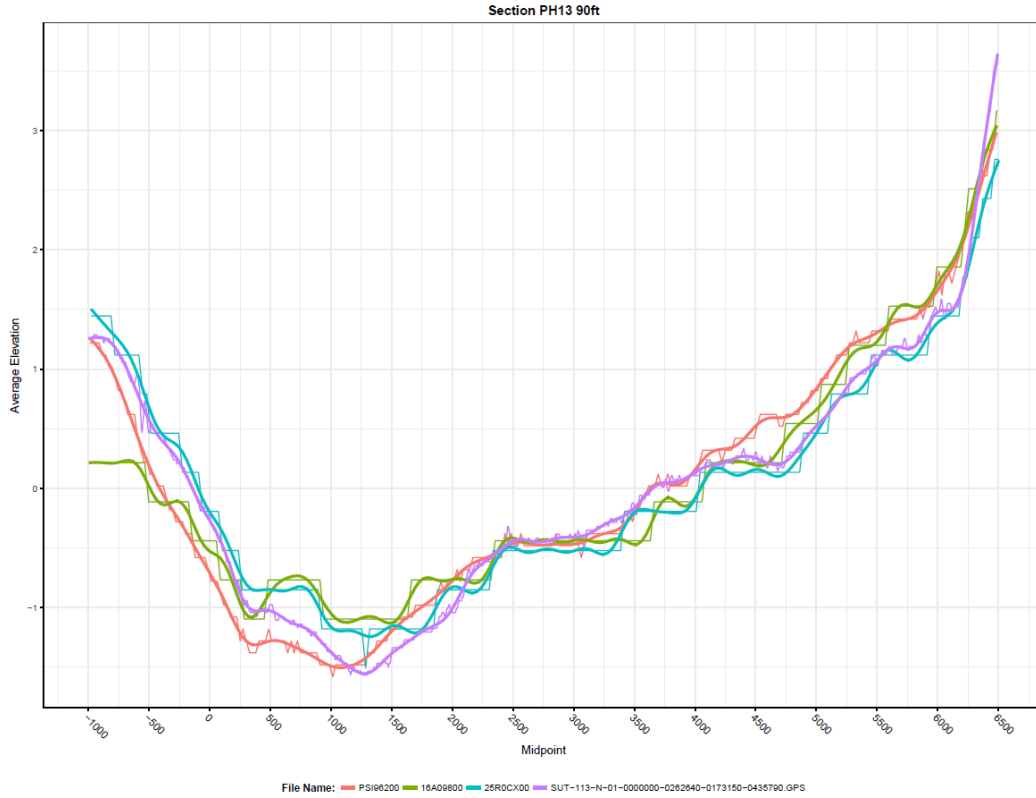


Figure F.20: Section PH13 elevation plots for 90 ft. (27 m) subsections from four data sources.

12. PH14

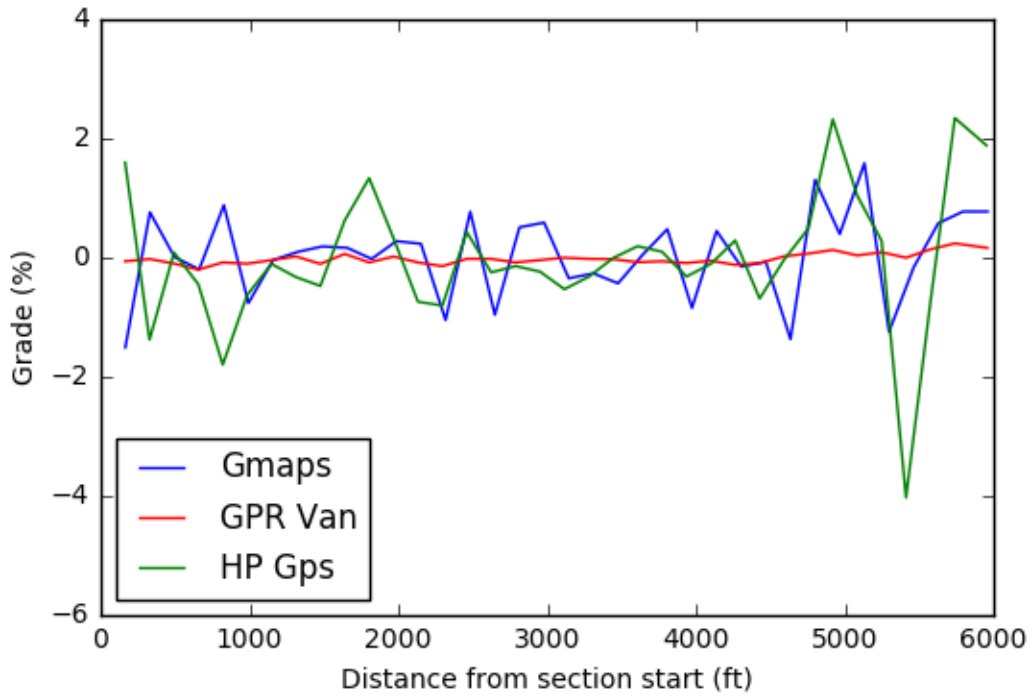


Figure F.21: Section PH14 grade plots for 165 ft. (50 m) subsections from three data sources.

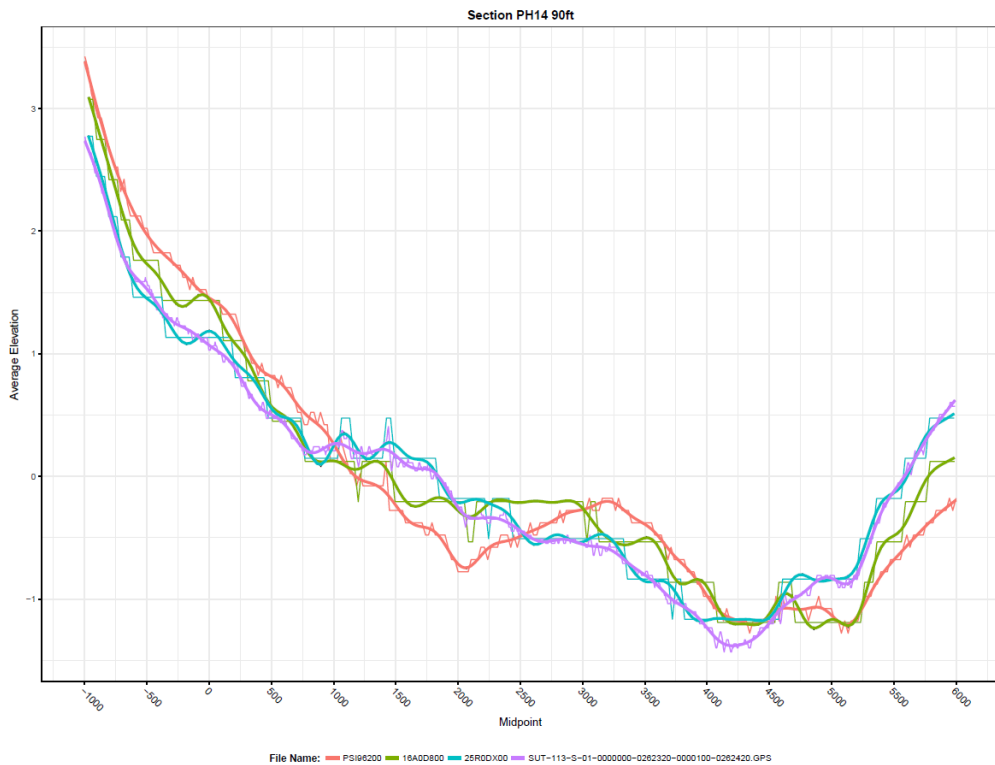


Figure F.22: Section PH14 elevation plots for 90 ft. (27 m) subsections from four data sources.

13. PH15

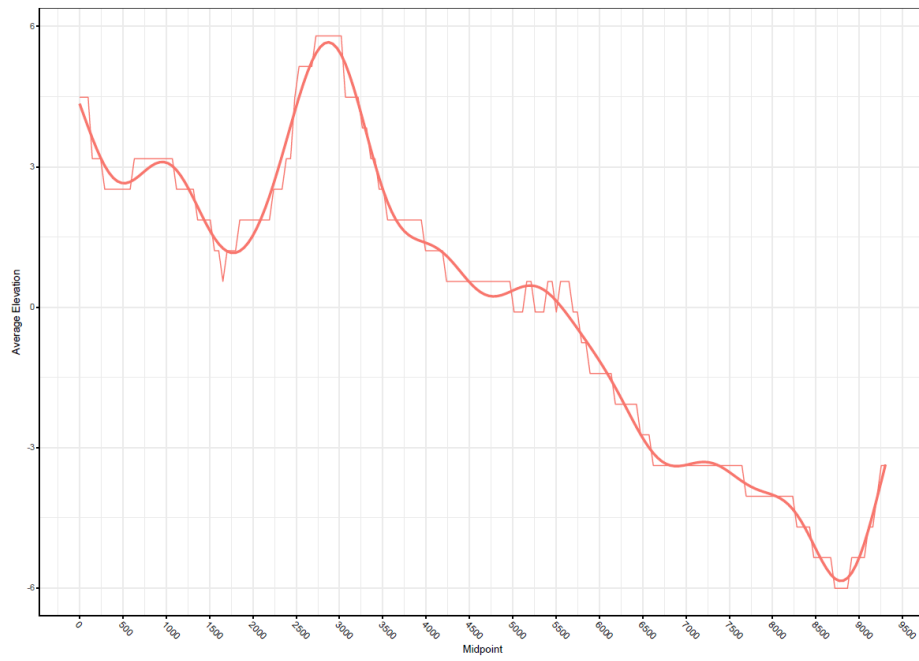


Figure F.23: Section PH15 elevation plots for 30 ft. (9 m) subsections.

14. PH16

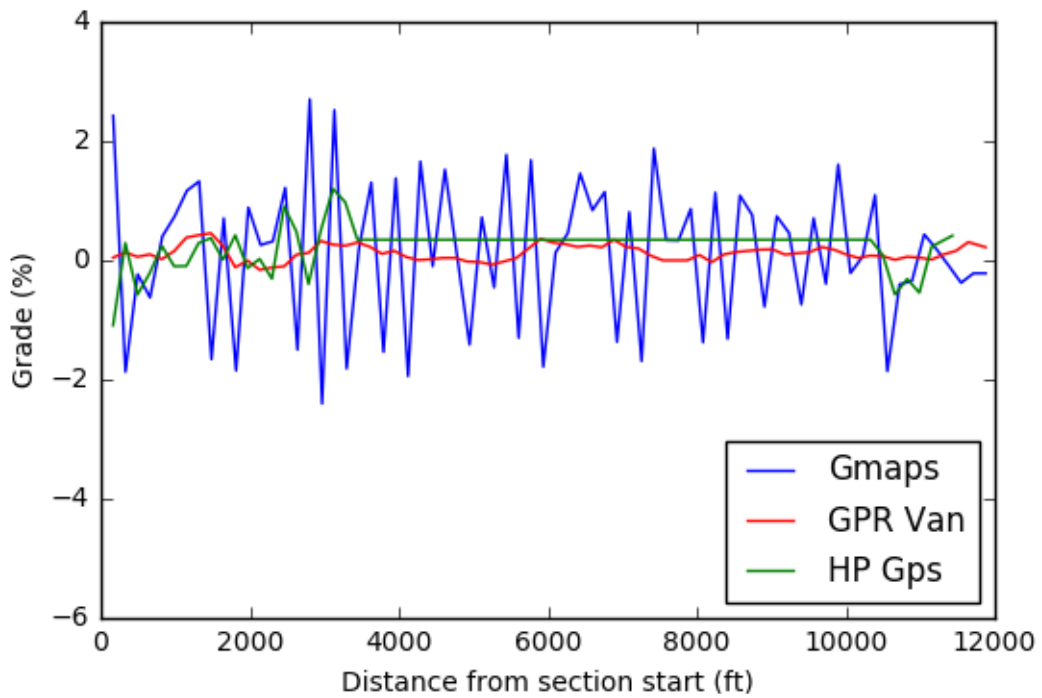


Figure F.24: Section PH16 grade plots for 165 ft. (50 m) subsections from three data sources.

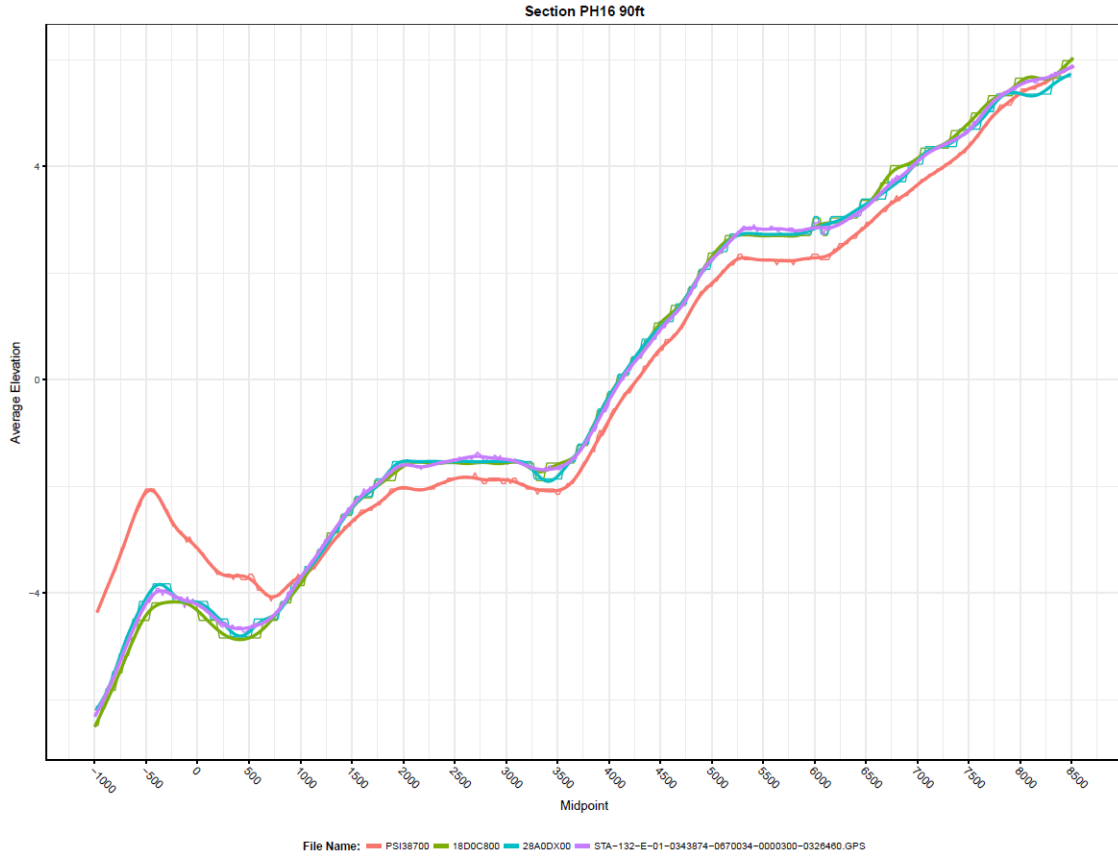


Figure F.25: Section PH16 elevation plots for 90 ft. (27 m) subsections from four data sources.

15. PH17

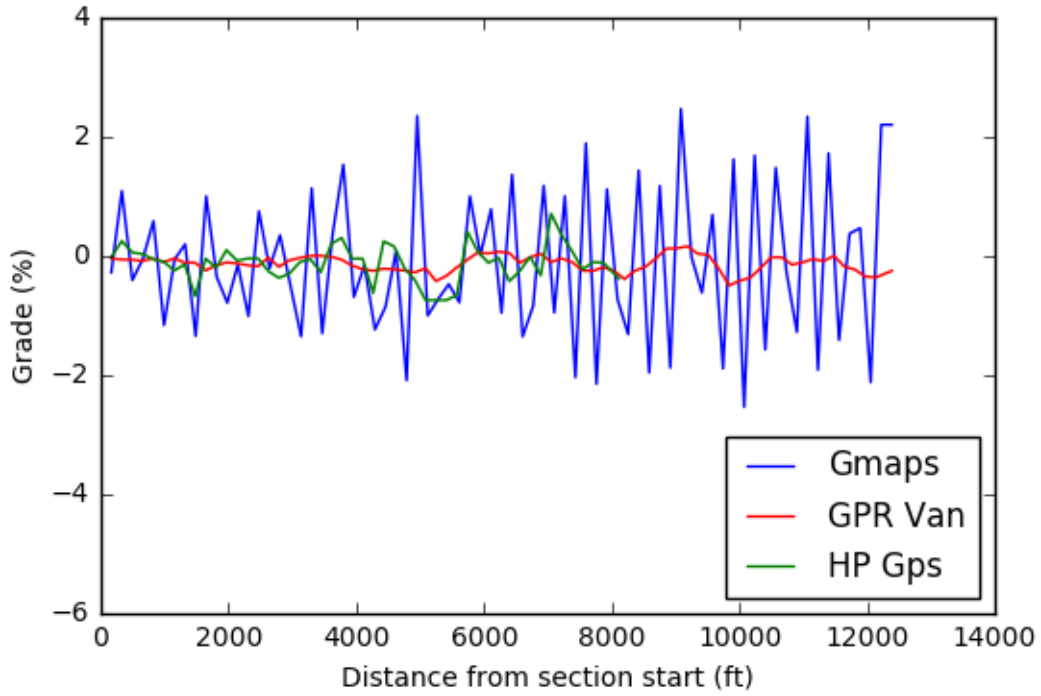


Figure F.26: Section PH17 grade plots for 165 ft. (50 m) subsections from three data sources.

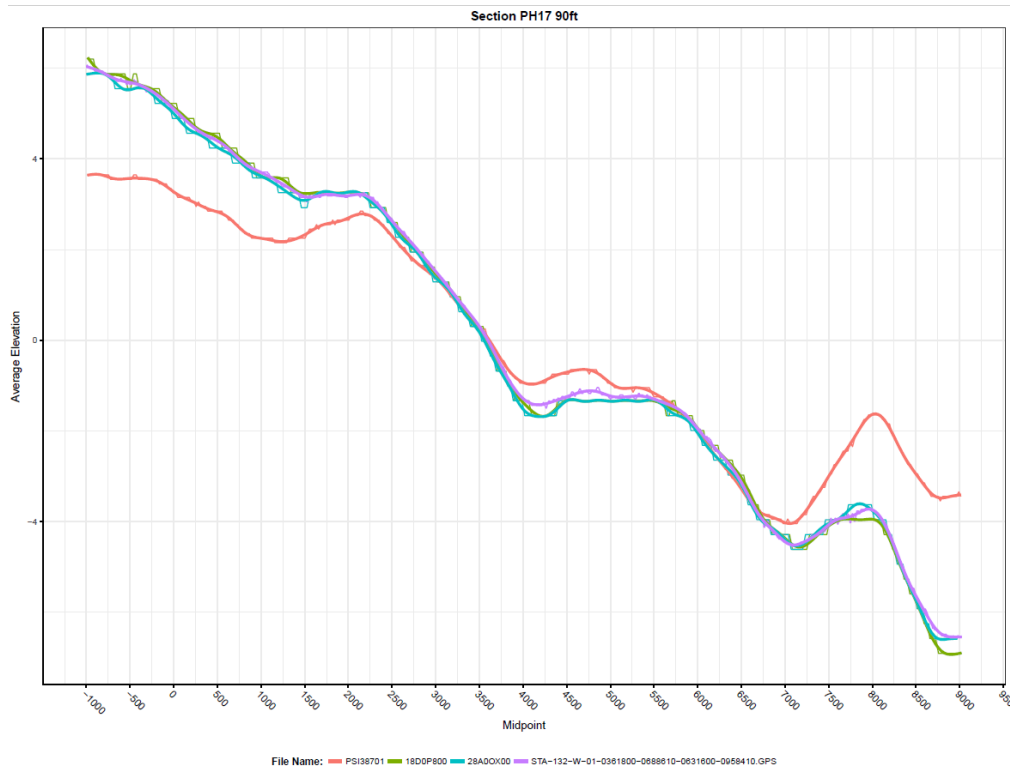


Figure F.27: Section PH17 elevation plots for 90 ft. (27 m) subsections from four data sources.

16. PH18

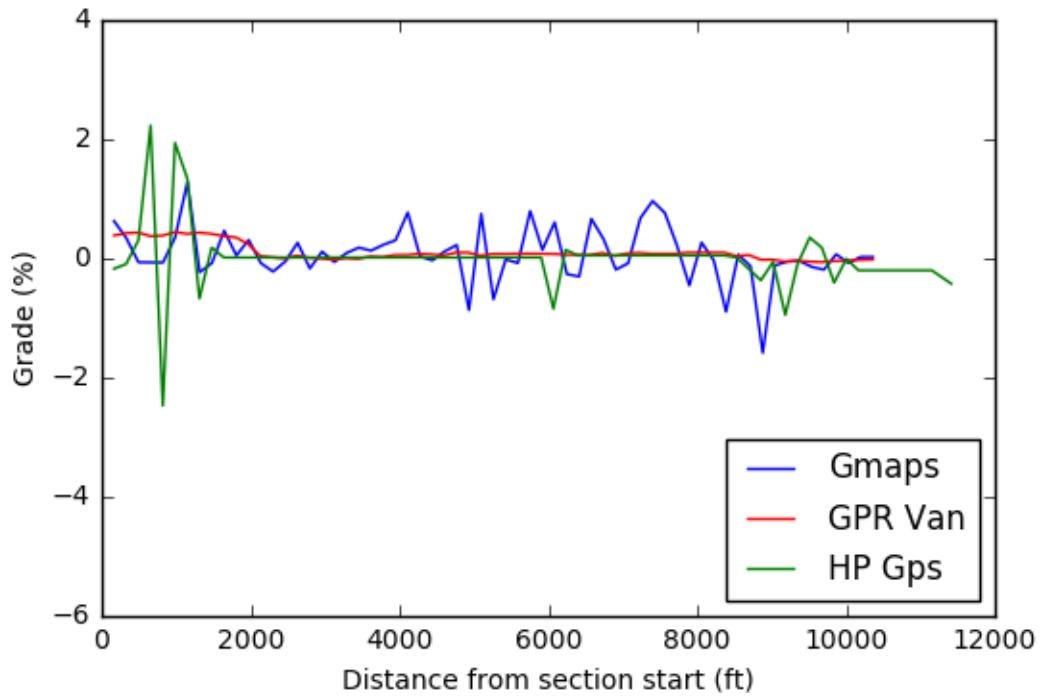


Figure F.28: Section PH18 grade plots for 165 ft. (50 m) subsections from three data sources.

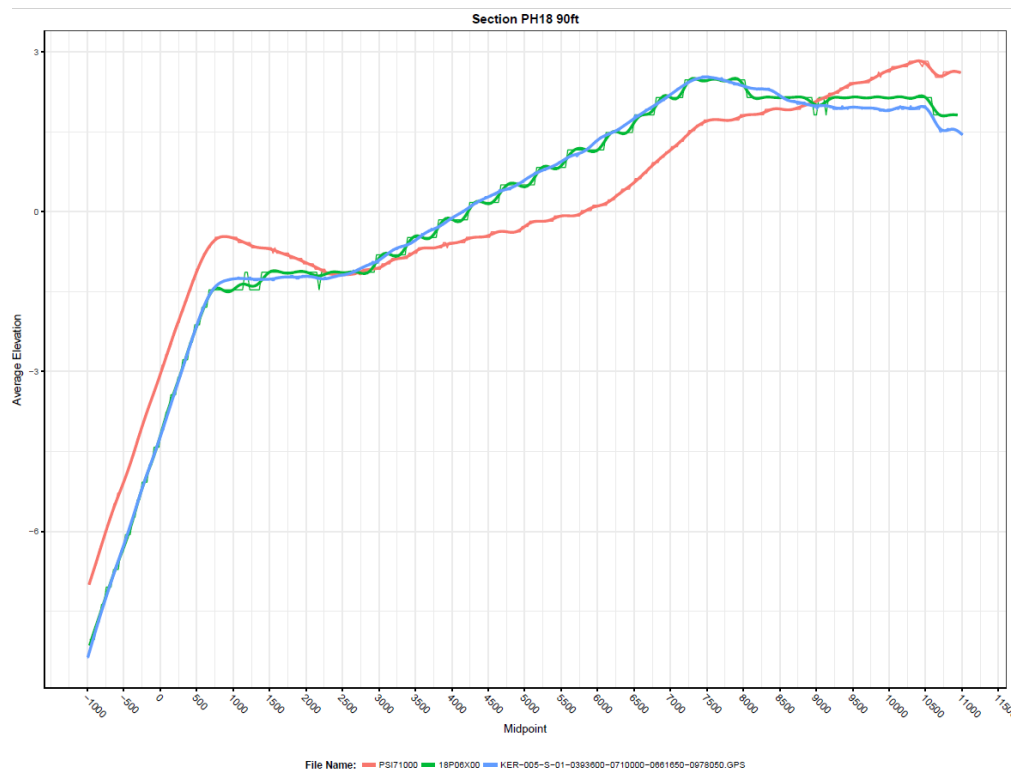


Figure F.29: Section PH18 elevation plots for 90 ft. (27 m) subsections from four data sources.

17. PH19

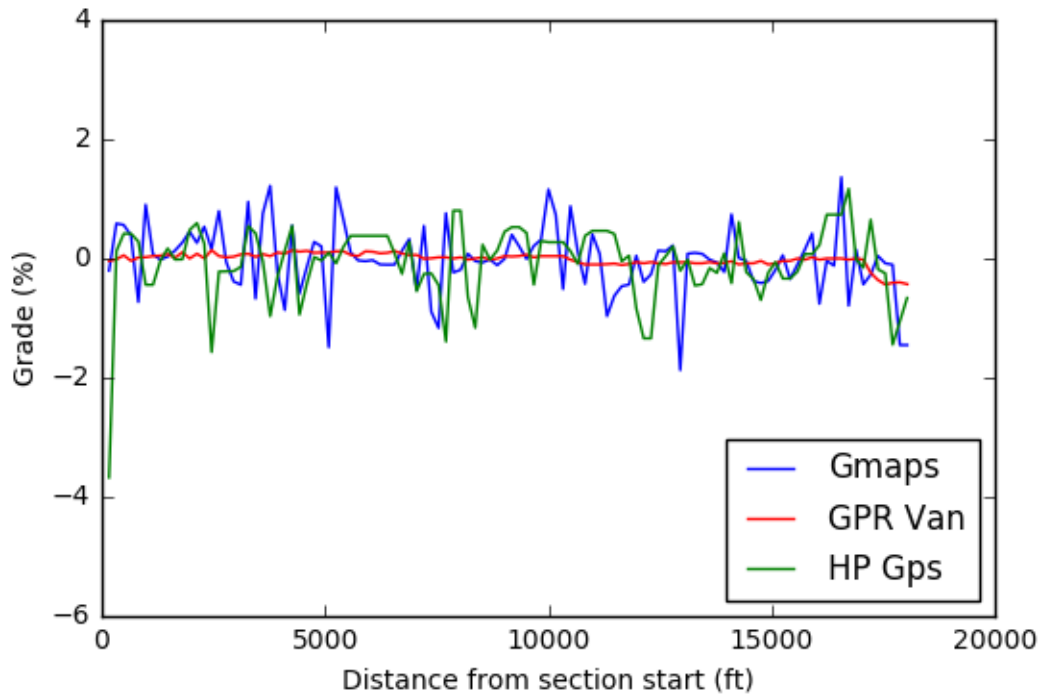


Figure F.30: Section PH19 grade plots for 165 ft. (50 m) subsections from three data sources.

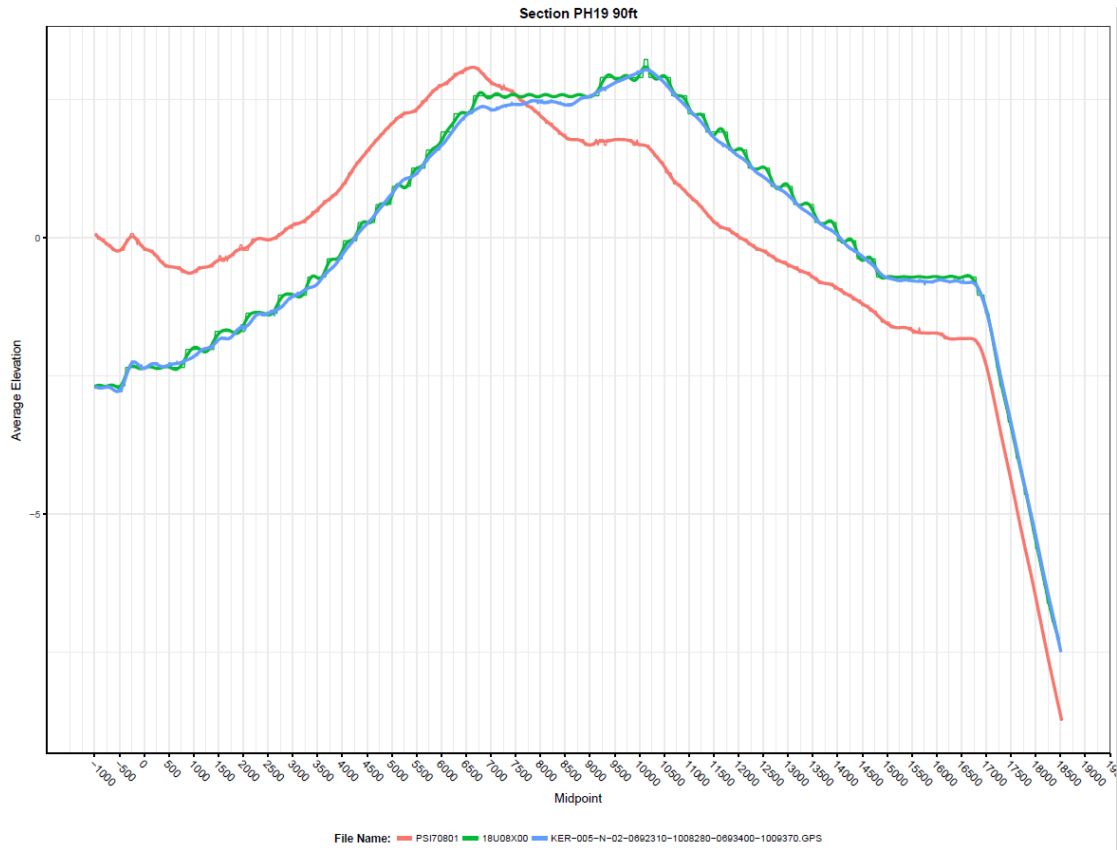


Figure F.31: Section PH19 elevation plots for 90 ft. (27 m) subsections from four data sources.

18. PH20

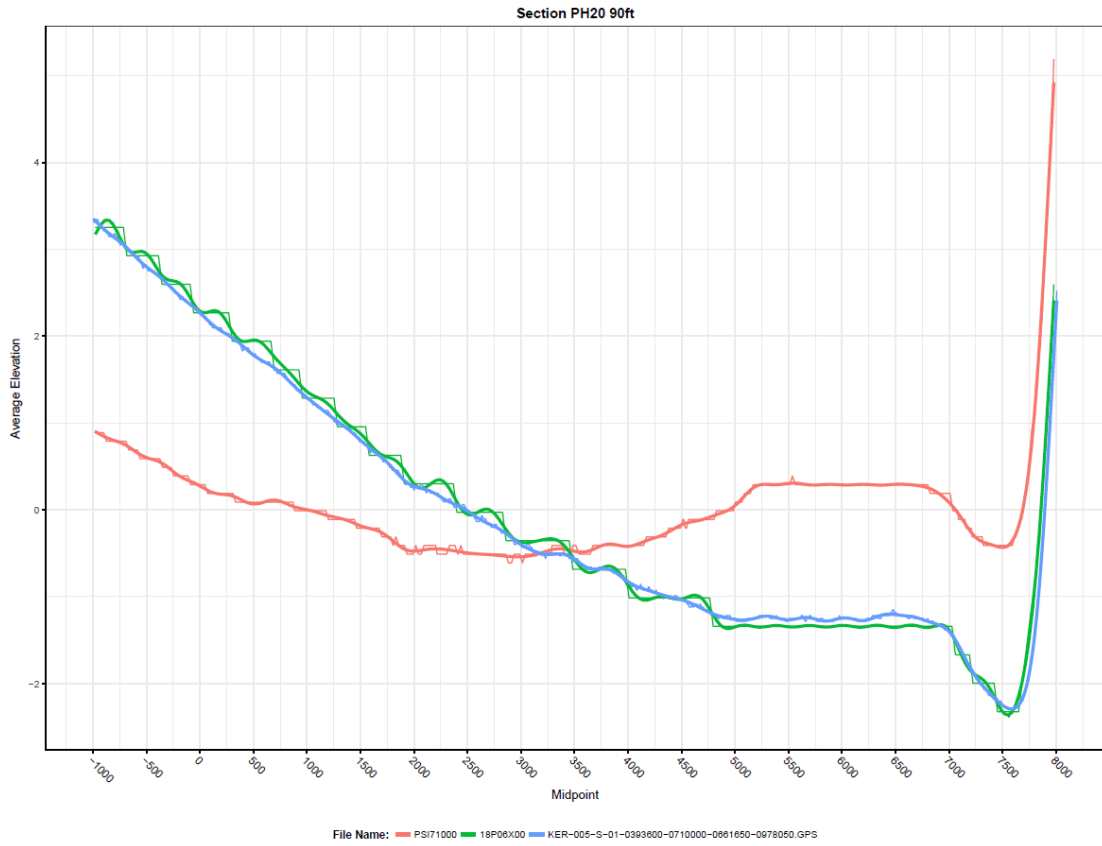


Figure F.32: Section PH20 elevation plots for 90 ft. (27 m) subsections from four data sources.

19. PH21

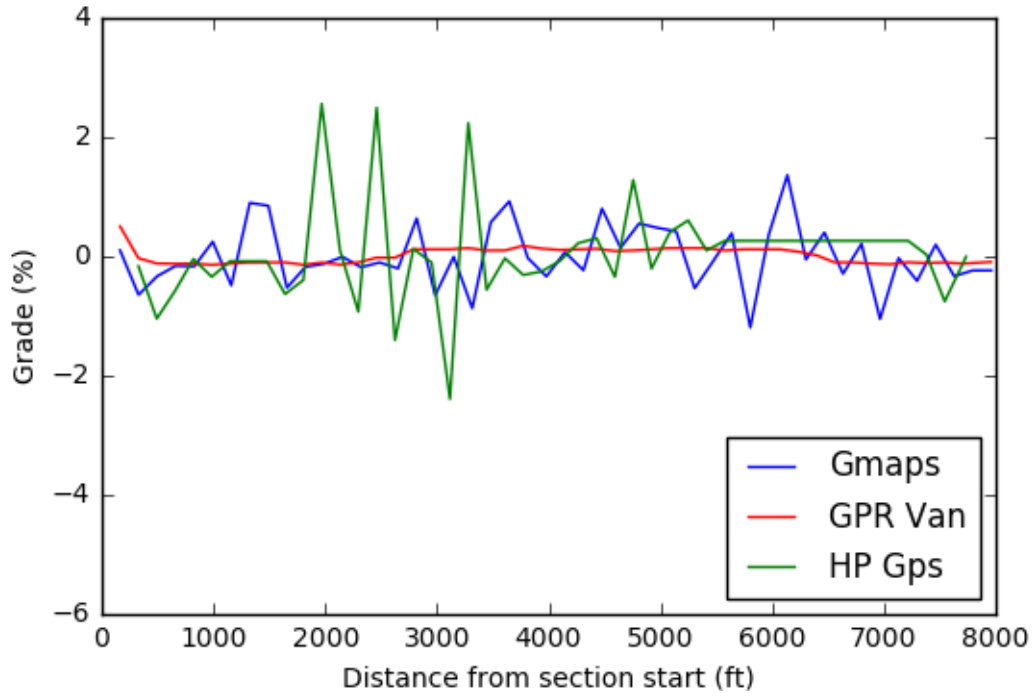


Figure F.33: Section PH21 grade plots for 165 ft. (50 m) subsections from three data sources.

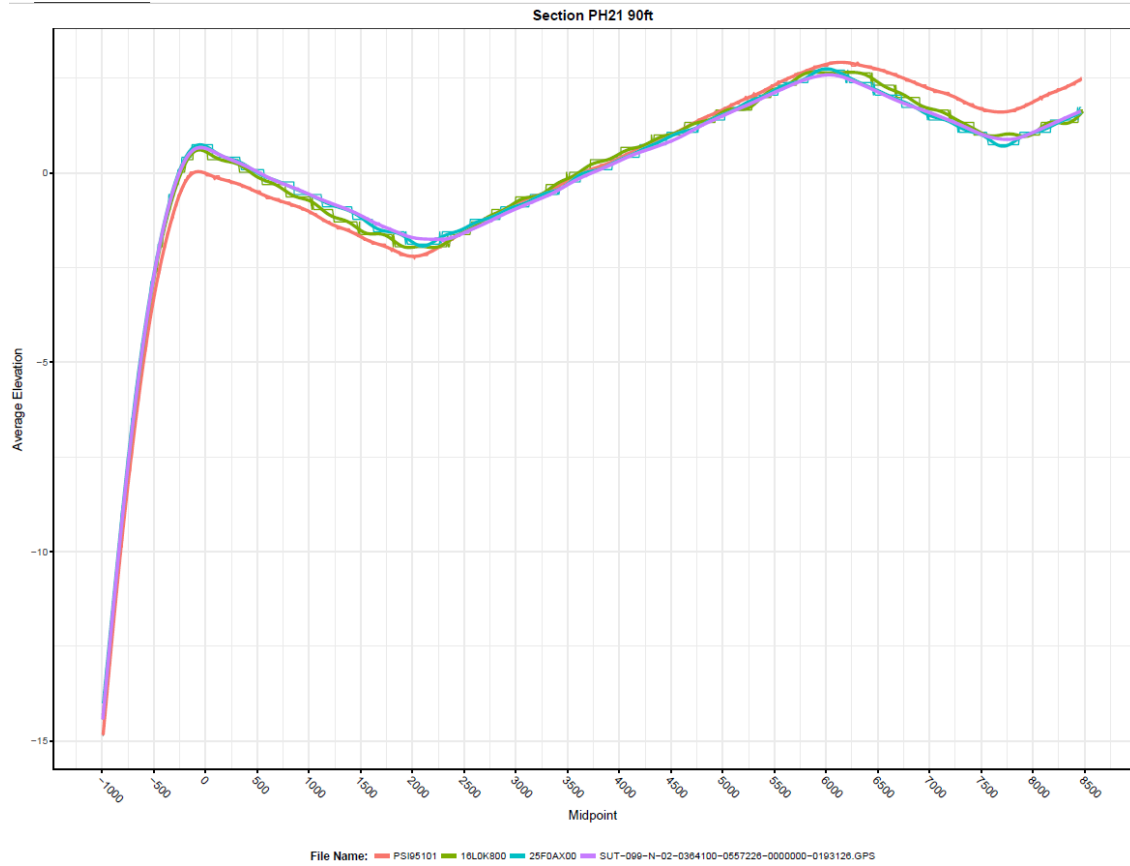


Figure F.34: Section PH21 elevation plots for 90 ft. (27 m) subsections from four data sources.

20. PH22

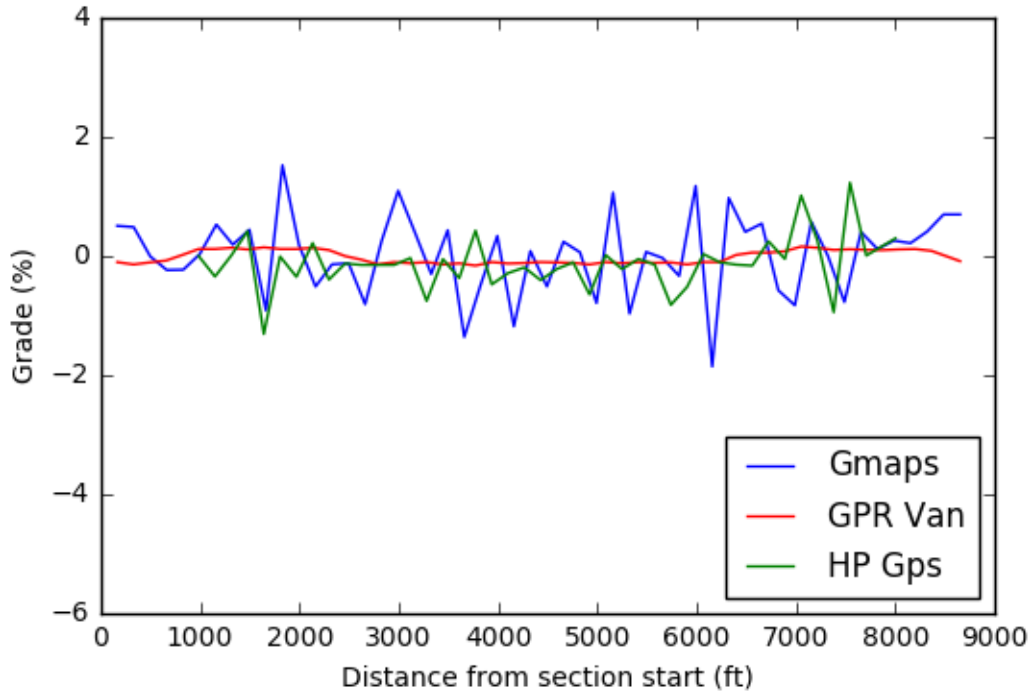


Figure F.35: Section PH22 grade plots for 165 ft. (50 m) subsections from three data sources.

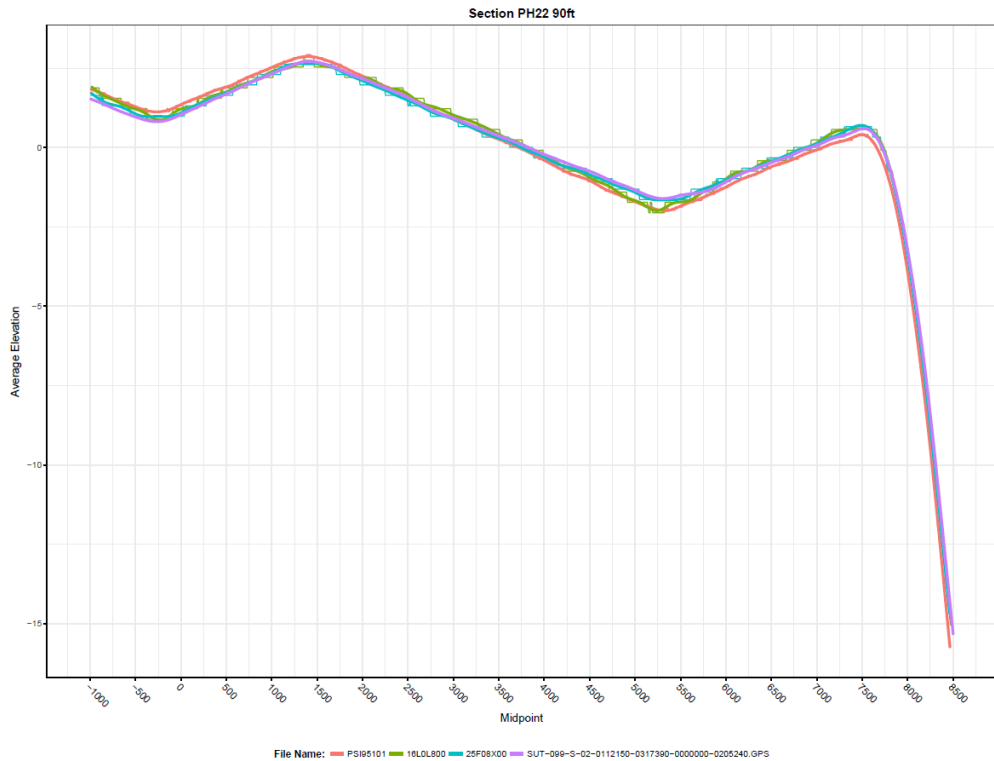


Figure F.36: Section PH22 elevation plots for 90 ft. (27 m) subsections from four data sources.

21. PH23

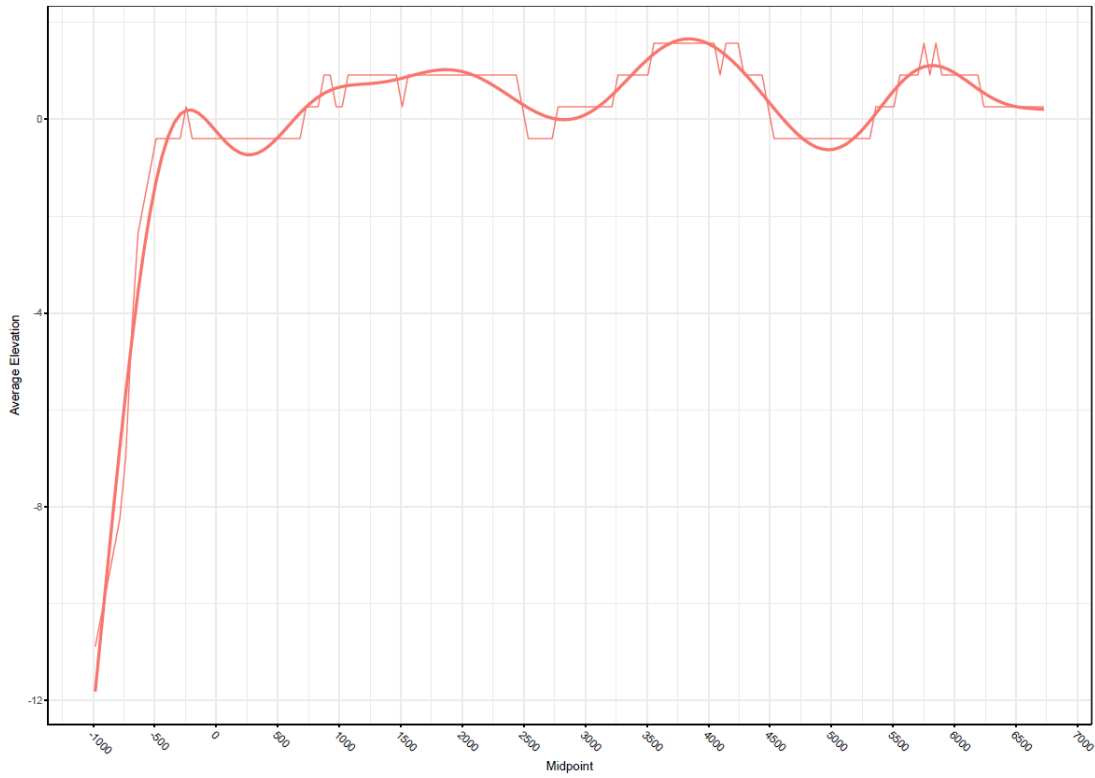


Figure F.37: Section PH23 elevation plots for 30 ft. (9 m) subsections.

APPENDIX G: DYNAMIC SHEAR MODULUS VERSUS FREQUENCY SWEEP MASTER CURVES FOR ASPHALT SURFACE PAVEMENT SECTIONS

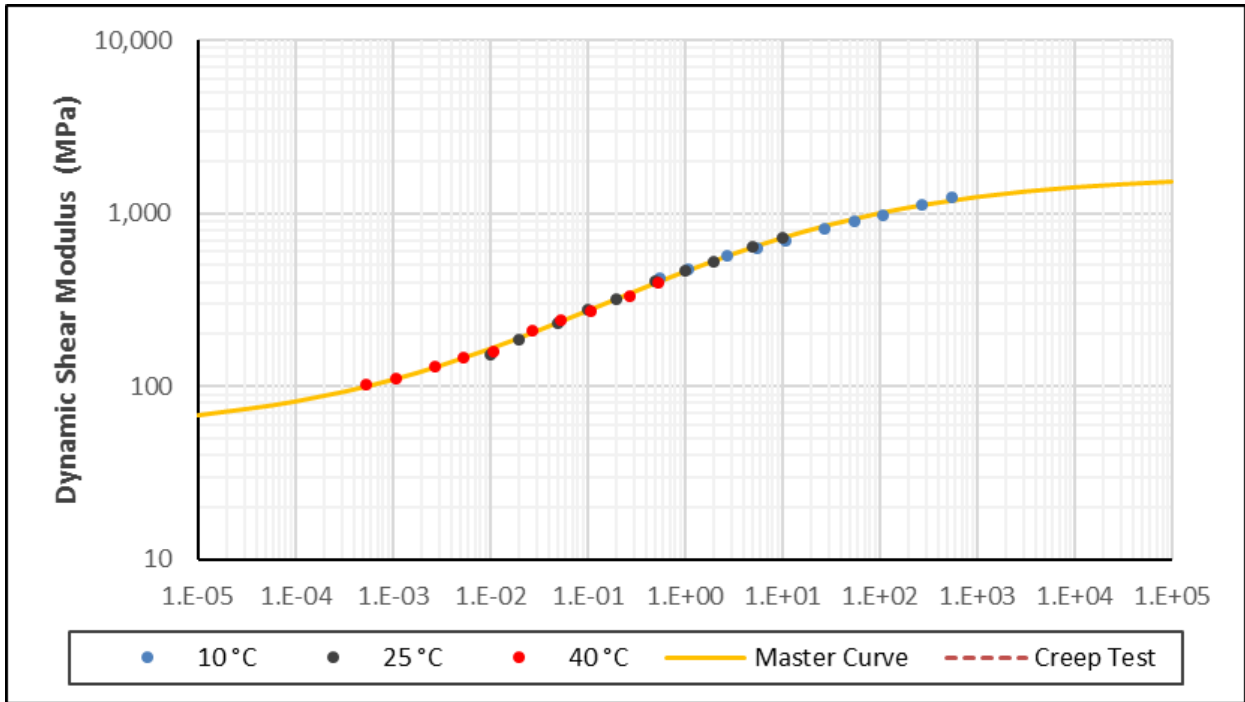


Figure G.1: Frequency sweep master curves for the reference temperature of 77°F (25°C) for PH04 layer 1.

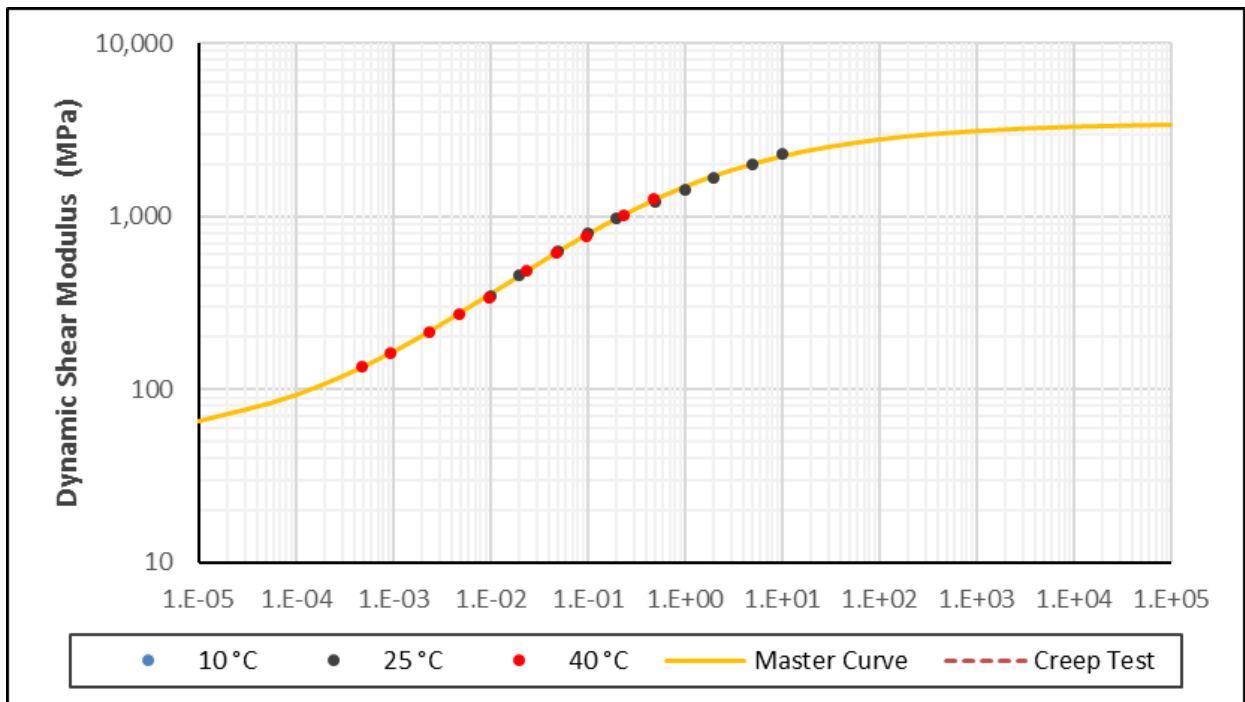


Figure G.2: Frequency sweep master curves for the reference temperature of 77°F (25°C) for PH04 layer 2.

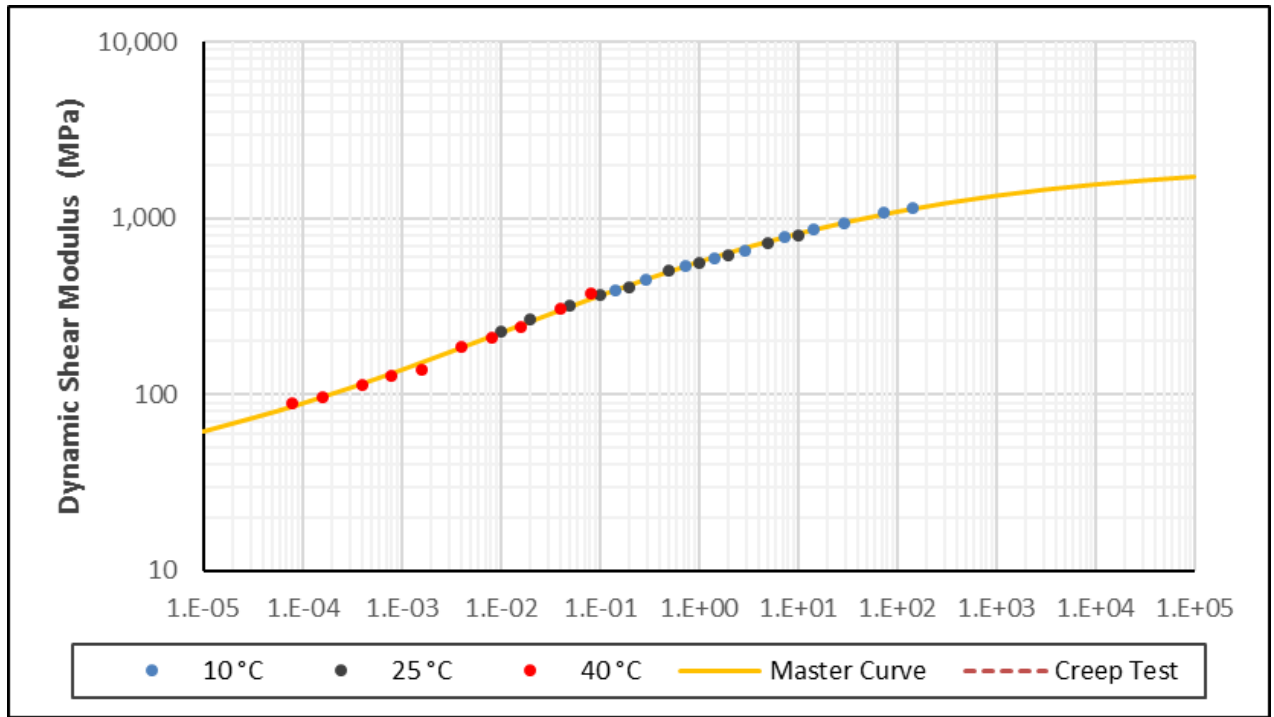


Figure G.3: Frequency sweep master curves for the reference temperature of 77°F (25°C) for PH08 layer 1.

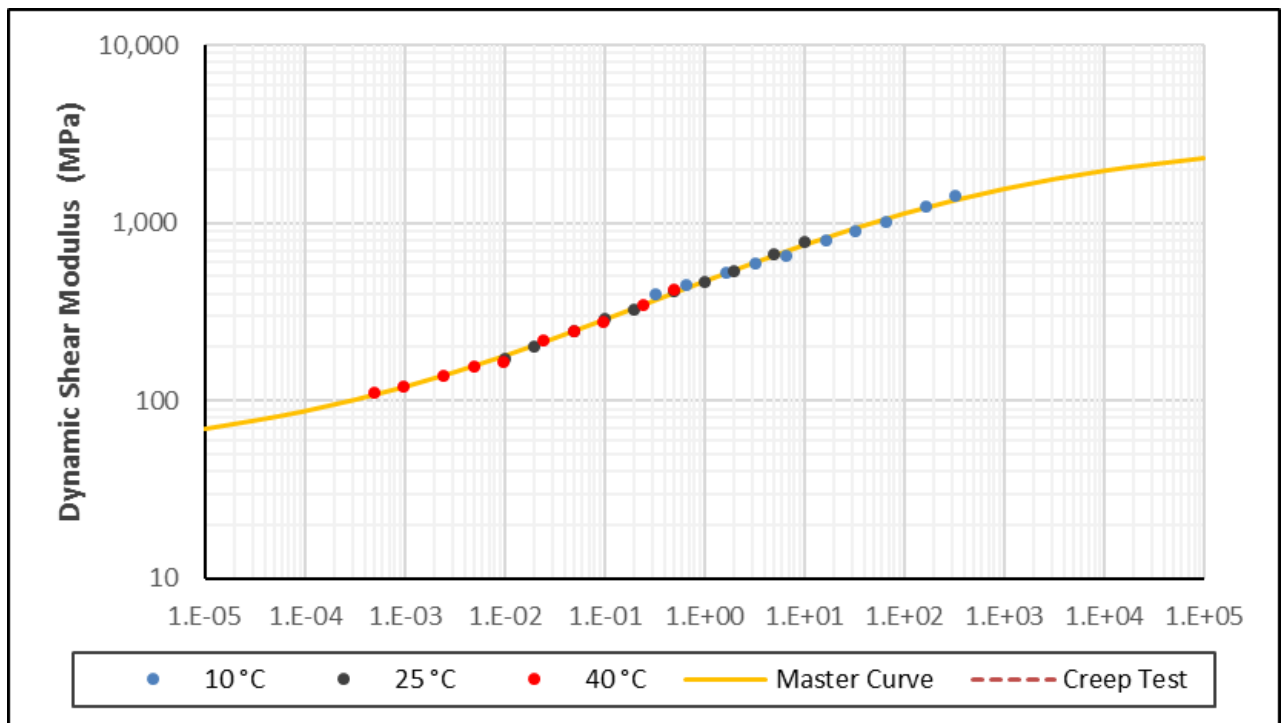


Figure G.4: Frequency sweep master curves for the reference temperature of 77°F (25°C) for PH09 layer 1.

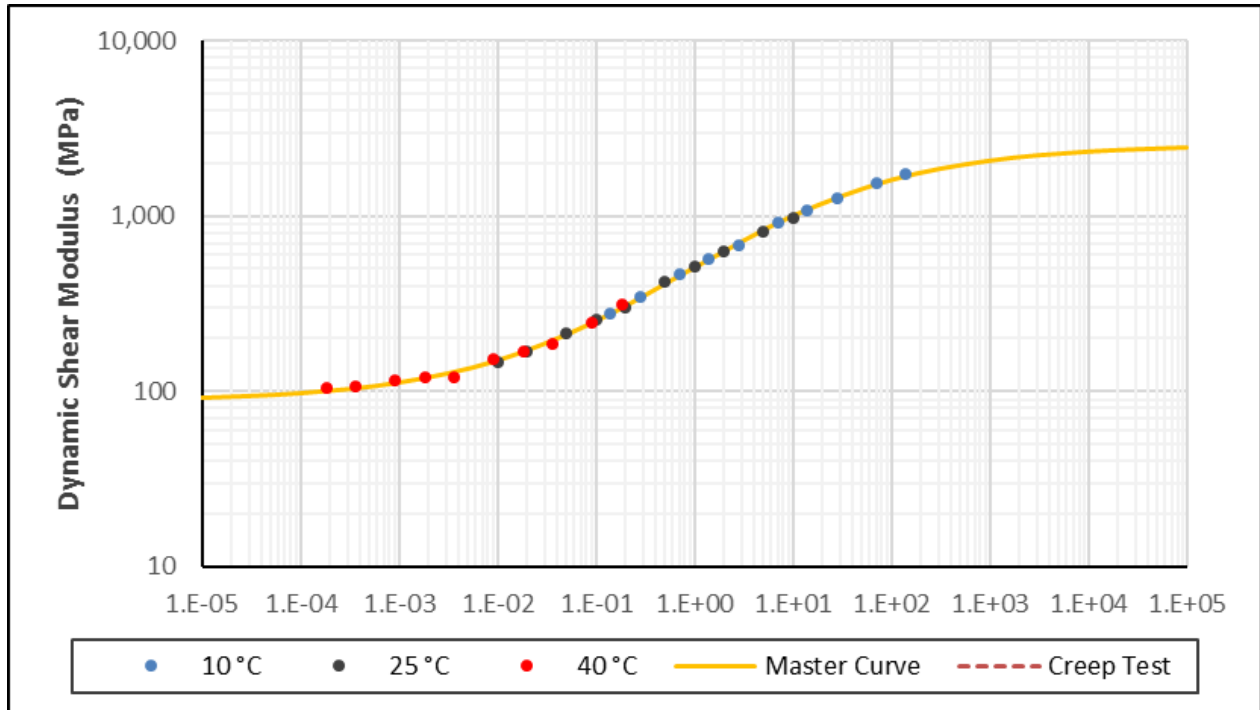


Figure G.5: Frequency sweep master curves for the reference temperature of 77°F (25°C) for PH09 layer 2.

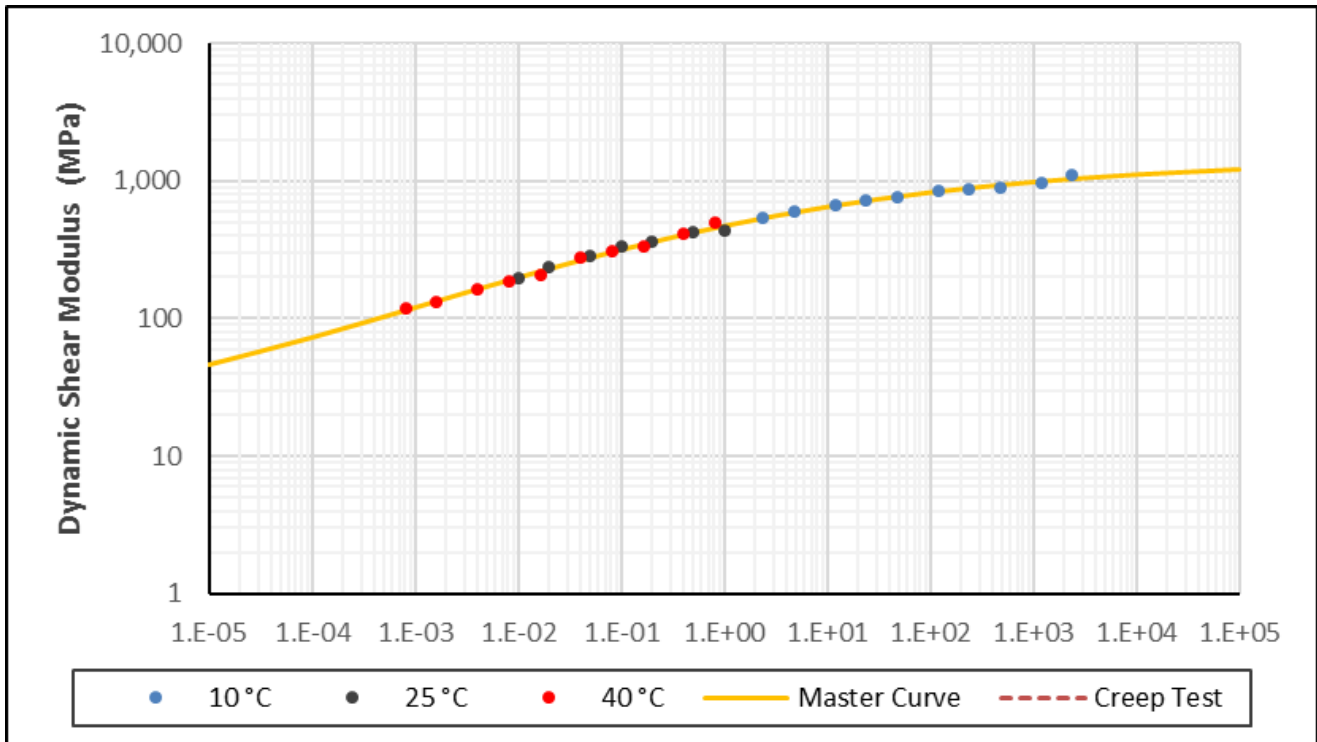


Figure G.6: Frequency sweep master curves for the reference temperature of 77°F (25°C) for PH09 layer 3.

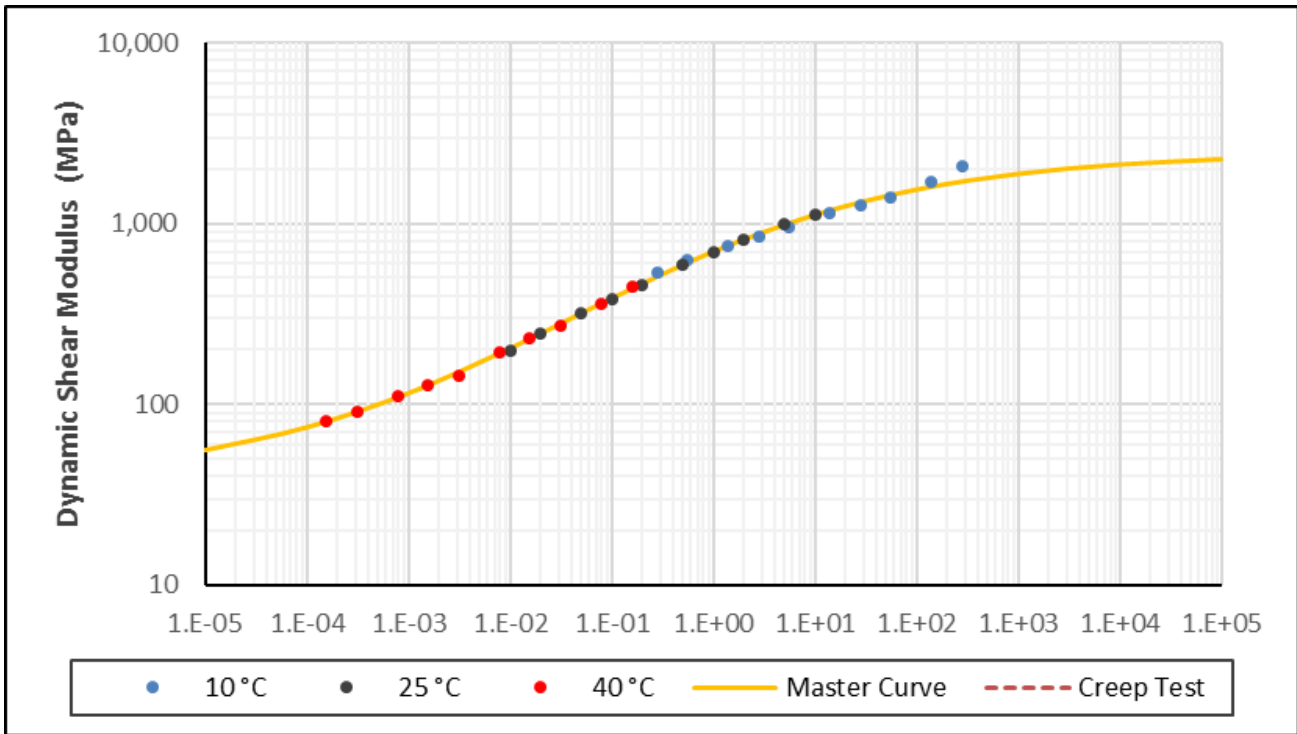


Figure G.7: Frequency sweep master curves for the reference temperature of 77°F (25°C) for PH10 layer 1.

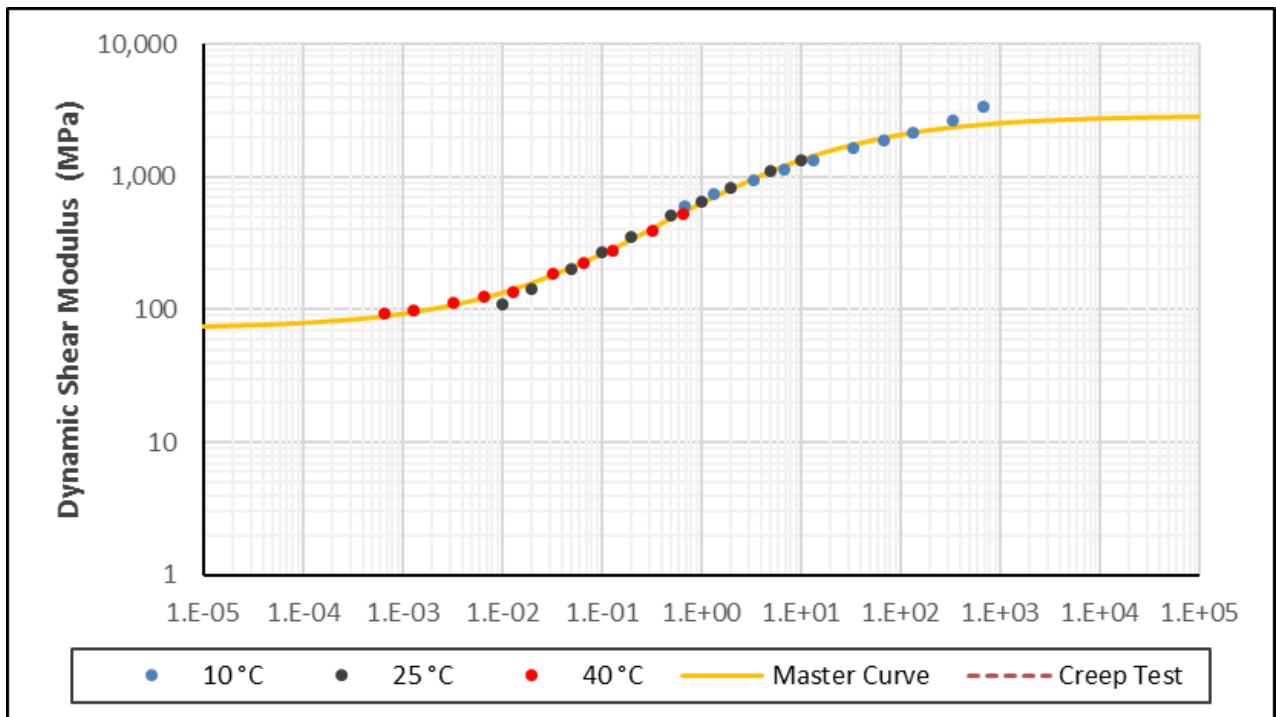


Figure G.8: Frequency sweep master curves for the reference temperature of 77°F (25°C) for PH10 layer 2.

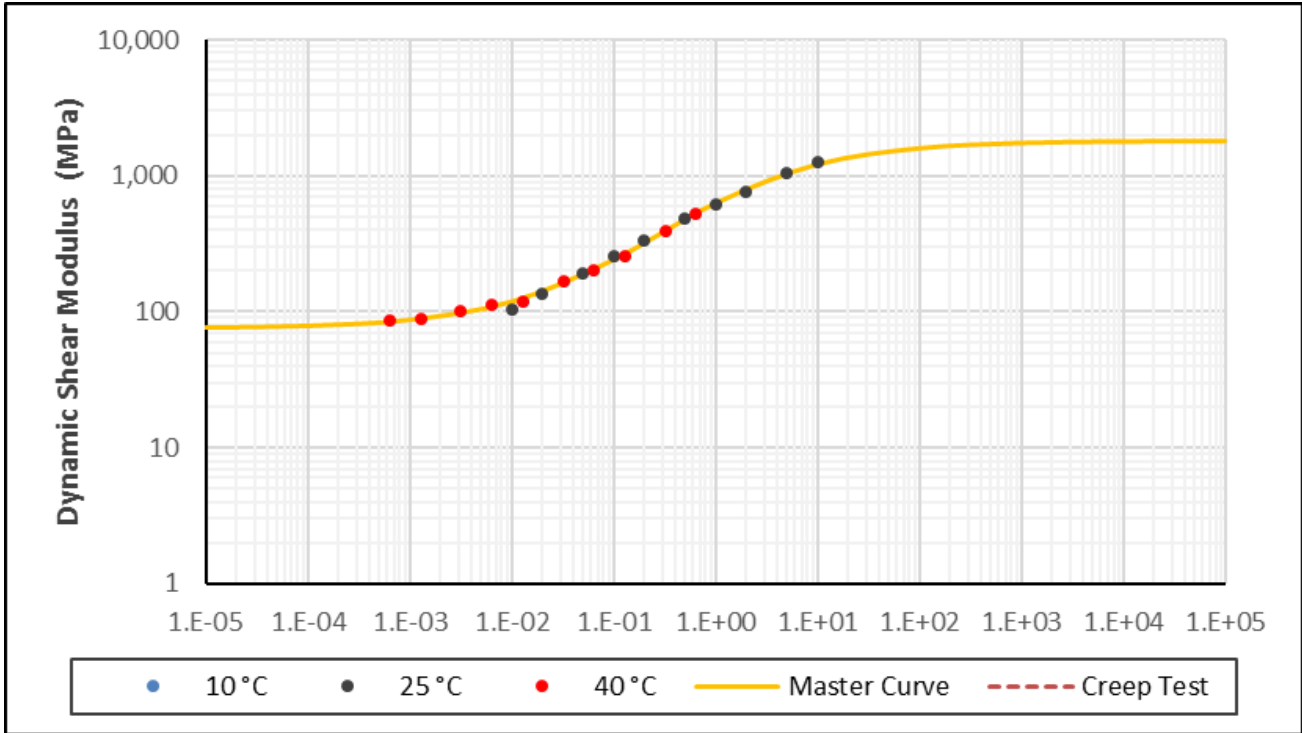


Figure G.9: Frequency sweep master curves for the reference temperature of 77°F (25°C) for PH10 layer 3.

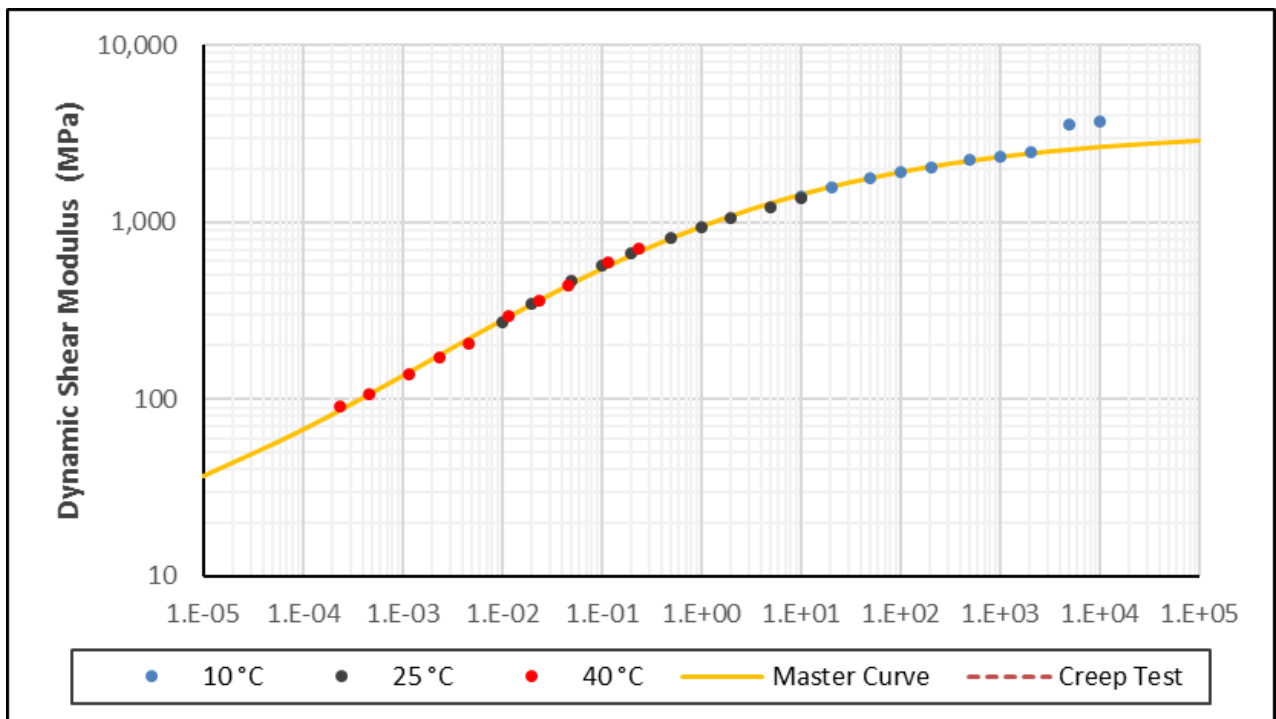


Figure G.10: Frequency sweep master curves for the reference temperature of 77°F (25°C) for PH11 layer 1.

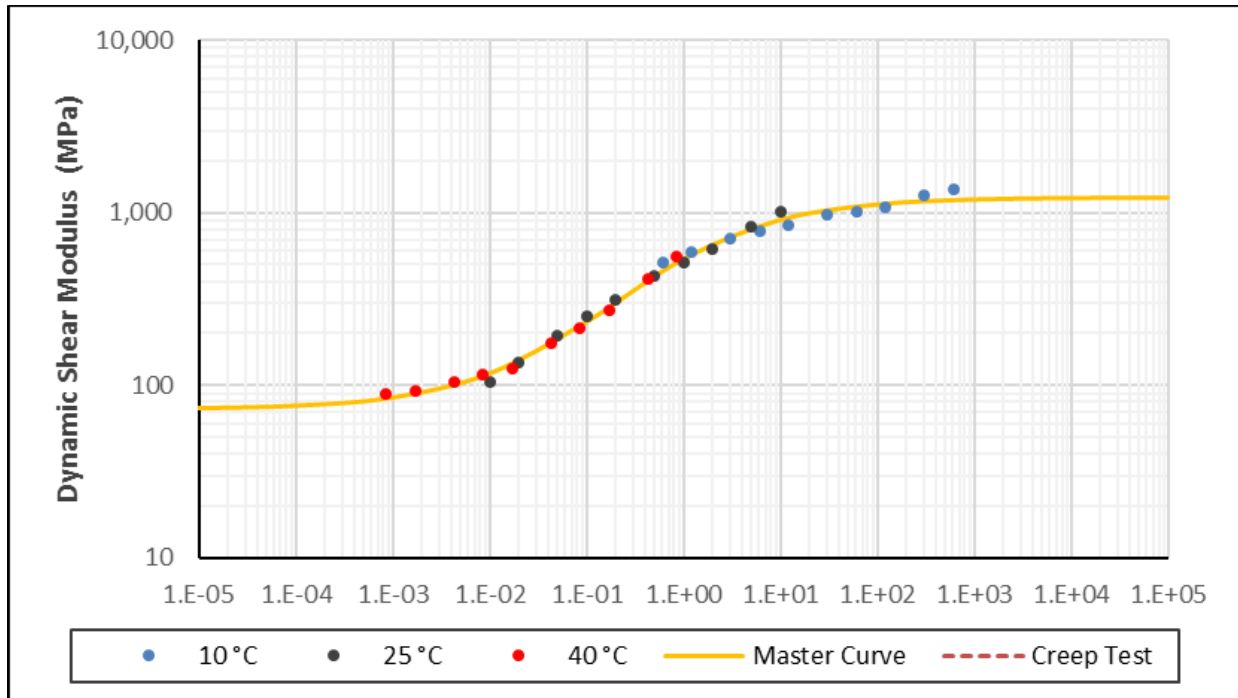


Figure G.11: Frequency sweep master curves for the reference temperature of 77°F (25°C) for PH11 layer 2.

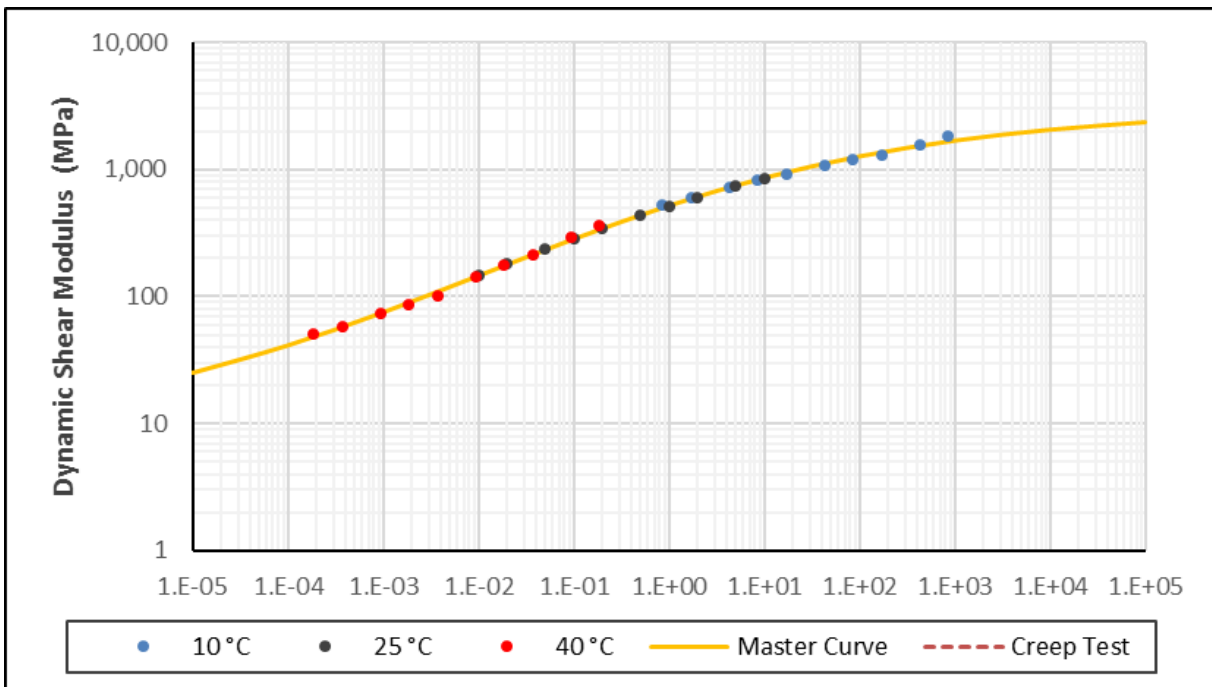


Figure G.12: Frequency sweep master curves for the reference temperature of 77°F (25°C) for PH12 layer 1.

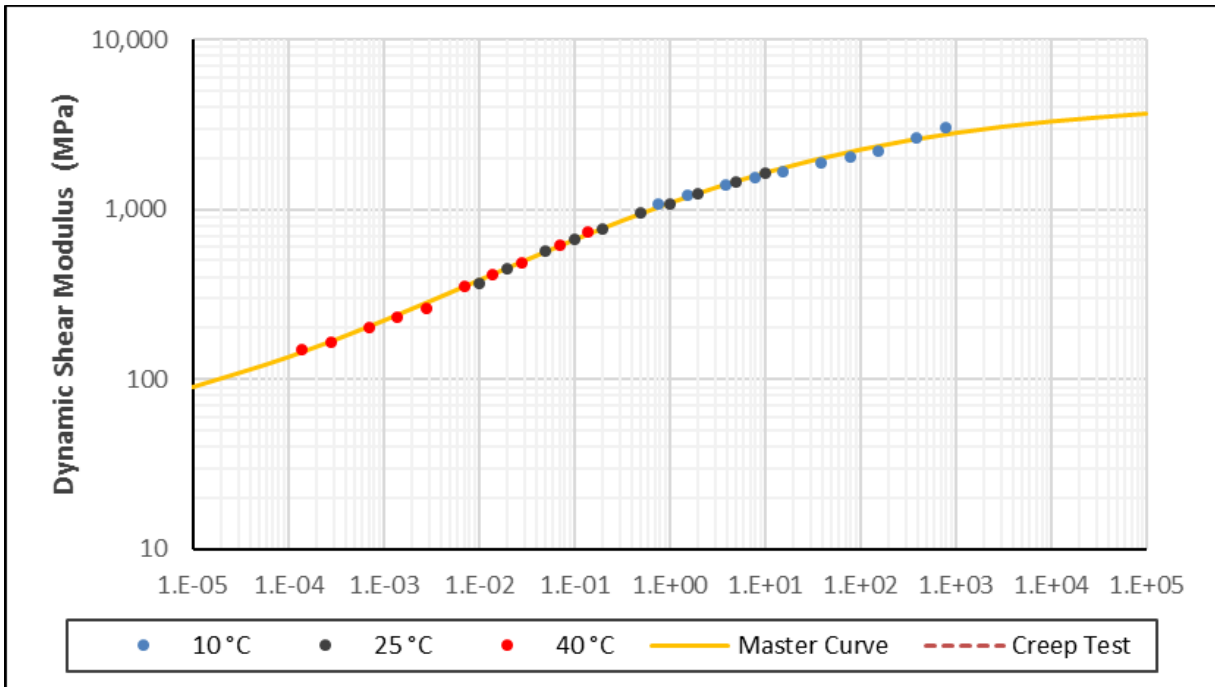


Figure G.13: Frequency sweep master curves for the reference temperature of 77°F (25°C) for PH12 layer 2.

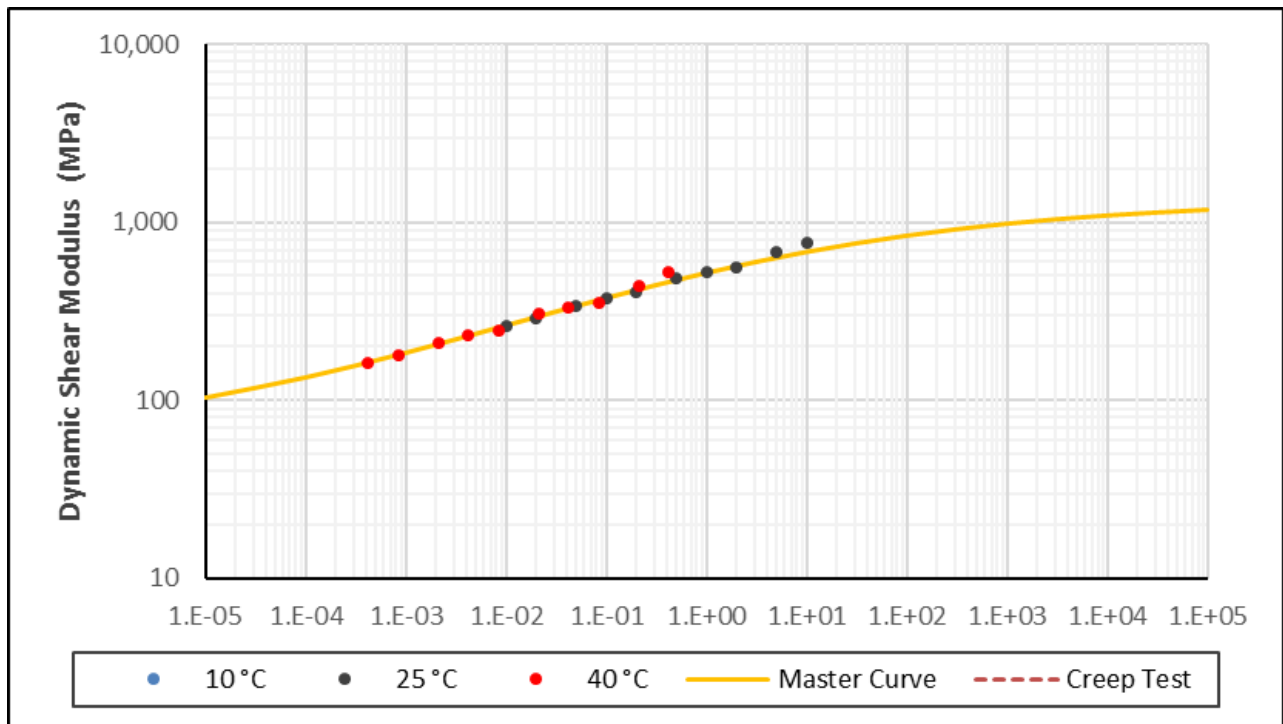


Figure G.14: Frequency sweep master curves for the reference temperature of 77°F (25°C) for PH12 layer 3.

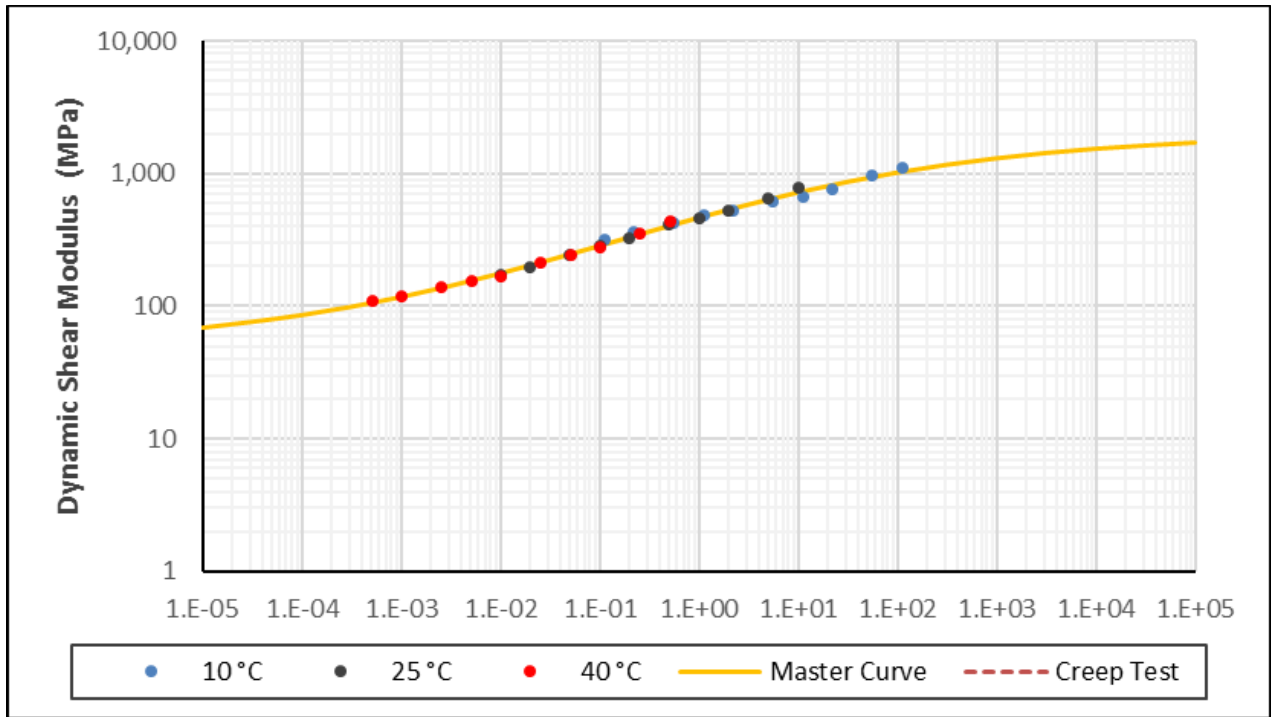


Figure G.15: Frequency sweep master curves for the reference temperature of 77°F (25°C) for PH12 layer 4.

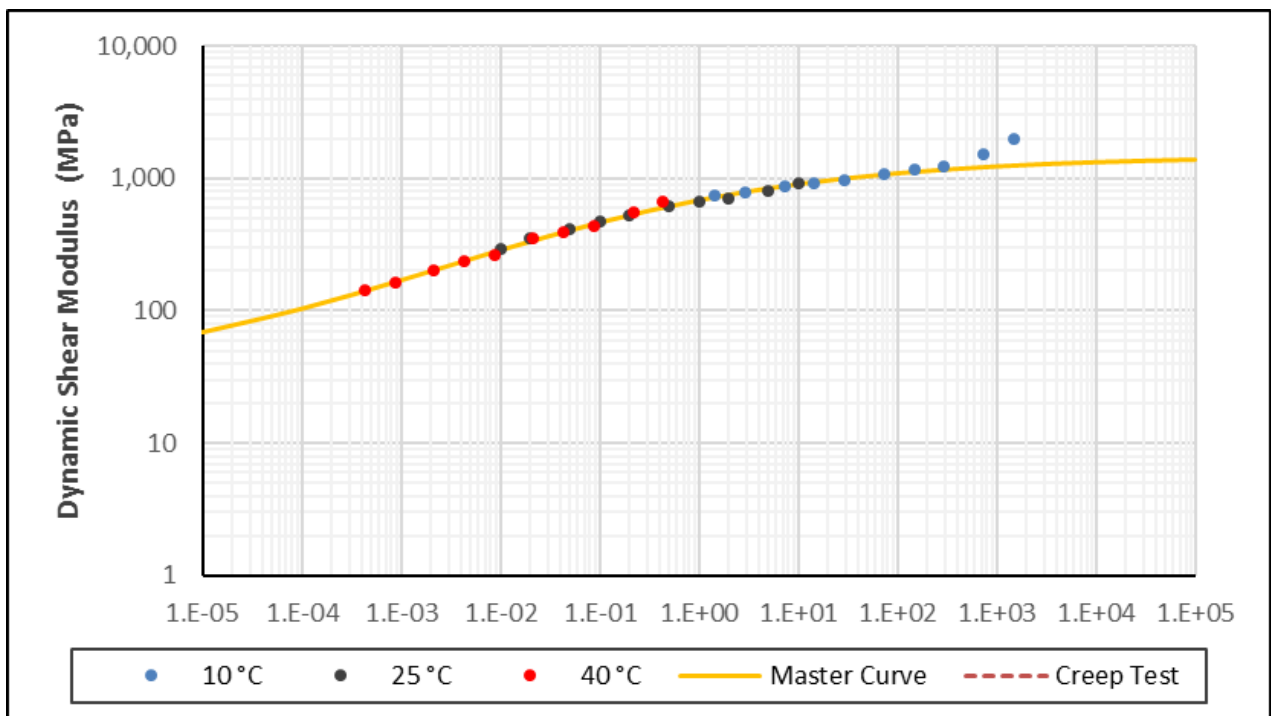


Figure G.16: Frequency sweep master curves for the reference temperature of 77°F (25°C) for PH13 layer 1.

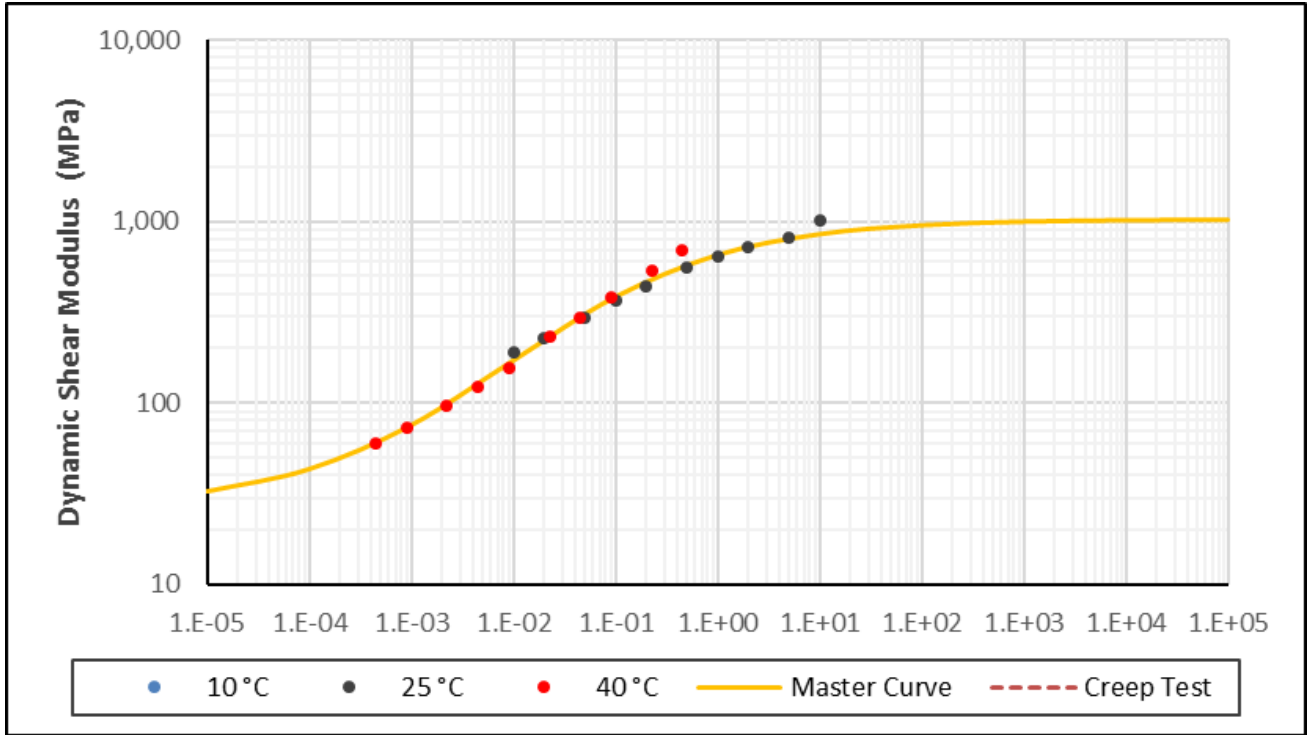


Figure G.17: Frequency sweep master curves for the reference temperature of 77°F (25°C) for PH14 layer 1.

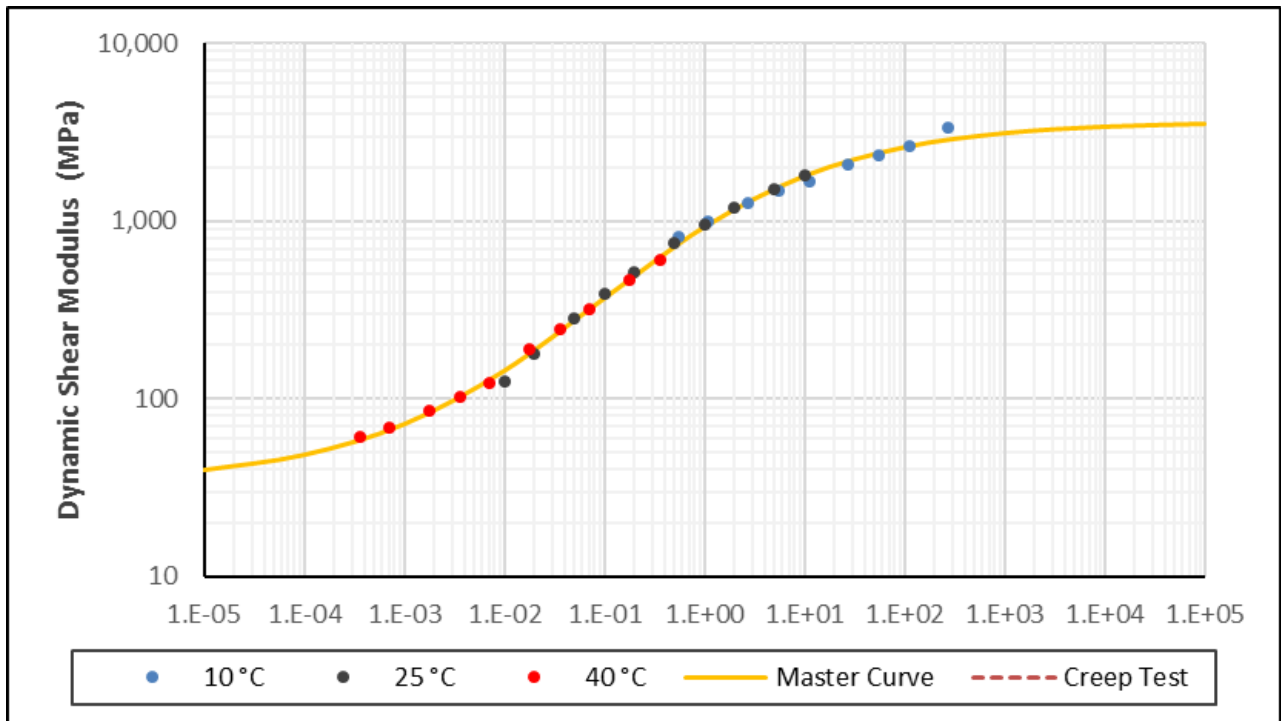


Figure G.18: Frequency sweep master curves for the reference temperature of 77°F (25°C) for PH15 layer 1.

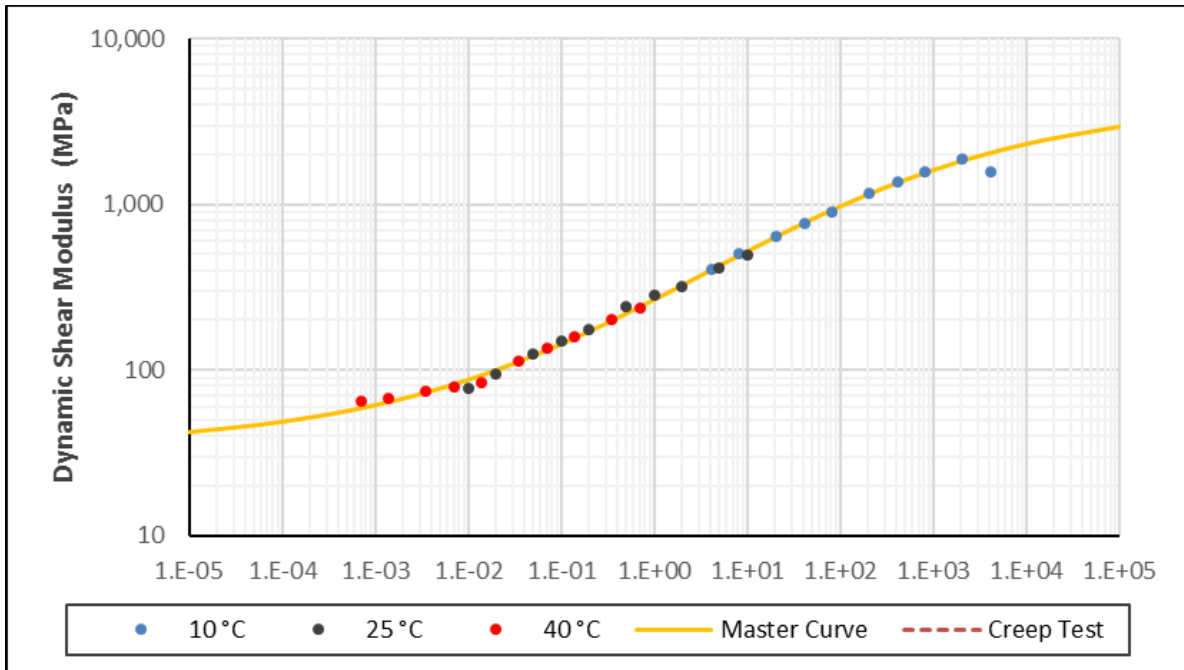


Figure G.19: Frequency sweep master curves for the reference temperature of 77°F (25°C) for PH15 layer 2.

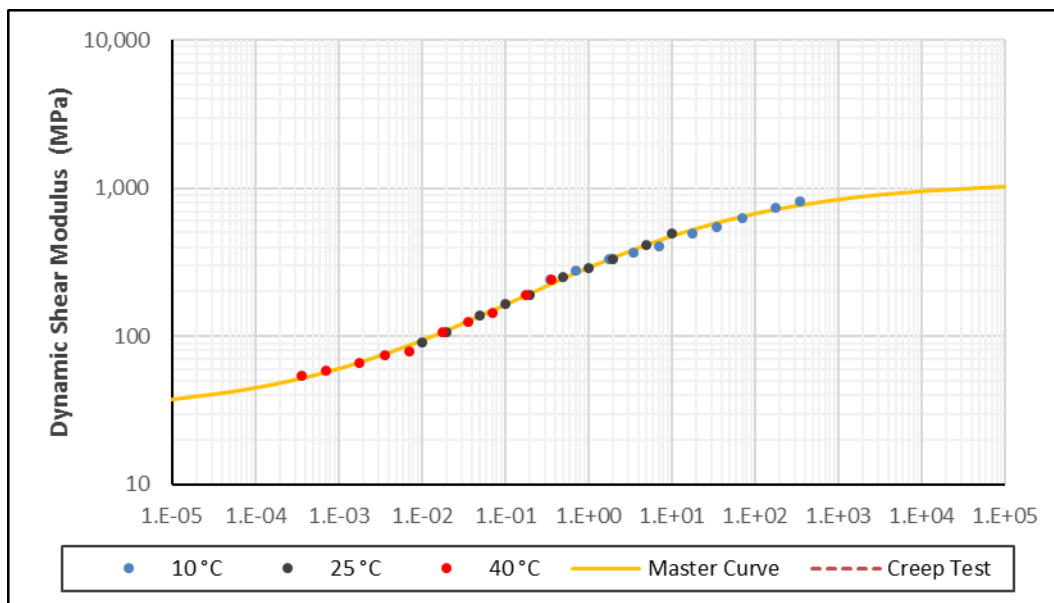


Figure G.20: Frequency sweep master curves for the reference temperature of 77°F (25°C) for PH16 layer 1.

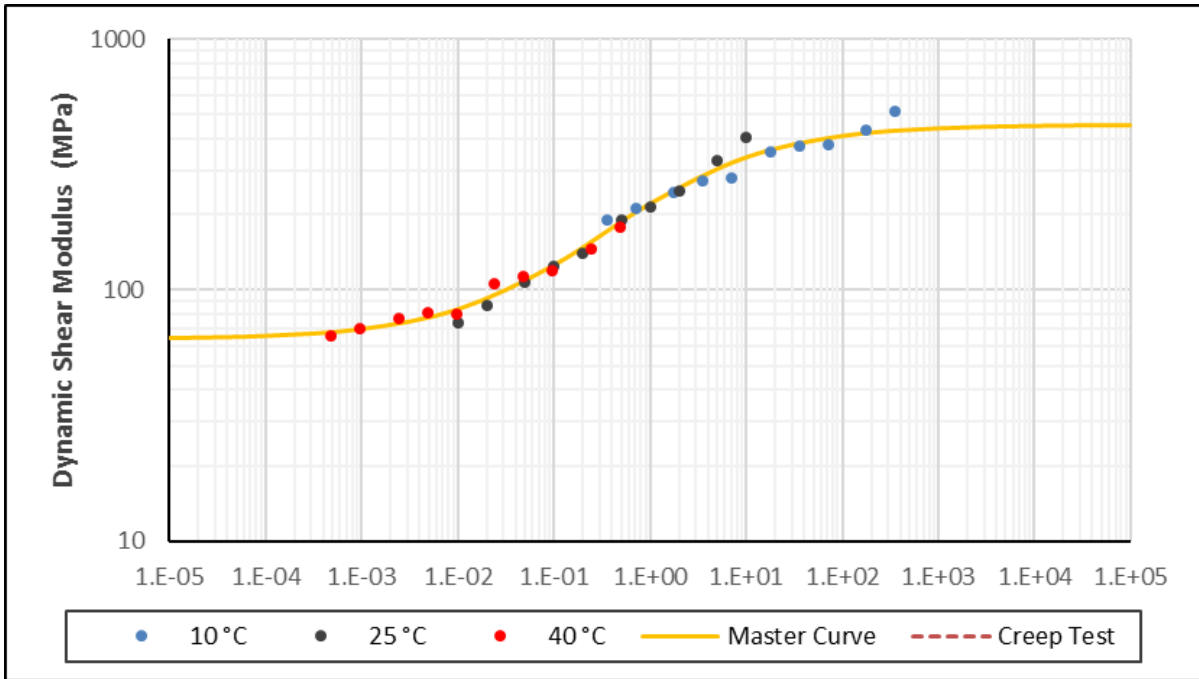


Figure G.21: Frequency sweep master curves for the reference temperature of 77°F (25°C) for PH16 layer 2.

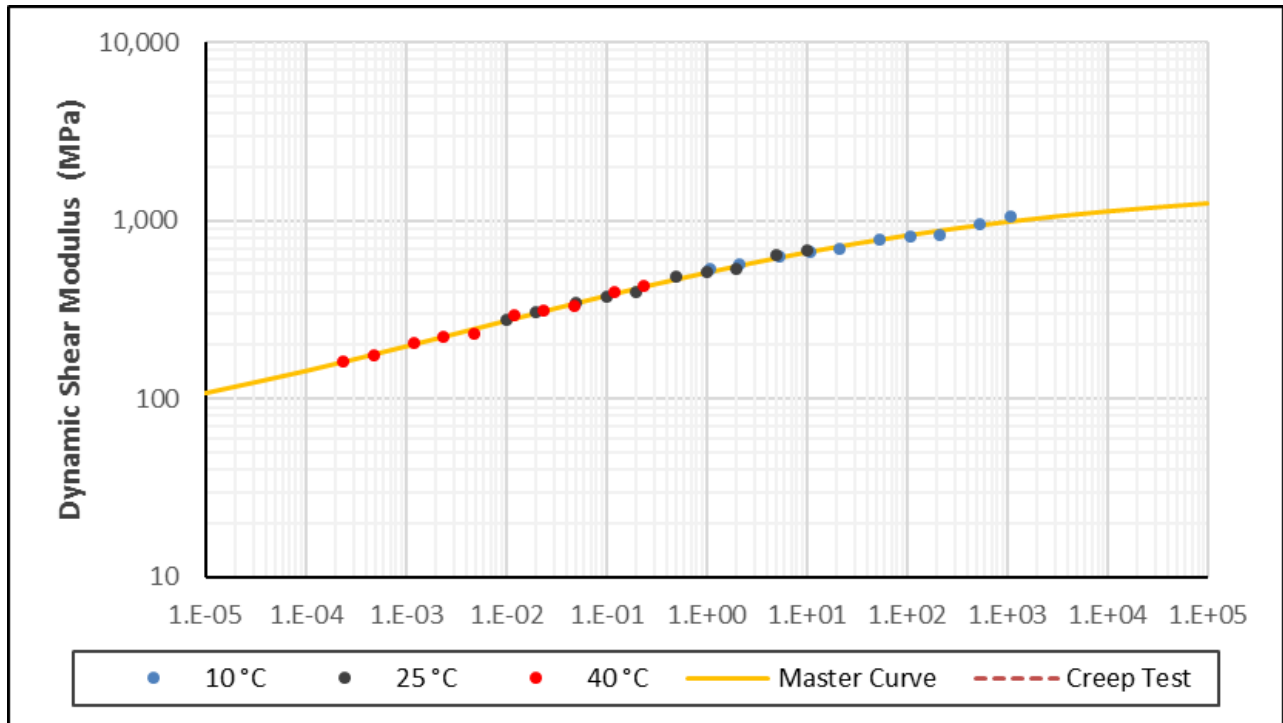


Figure G.22: Frequency sweep master curves for the reference temperature of 77°F (25°C) for PH16 layer 3.

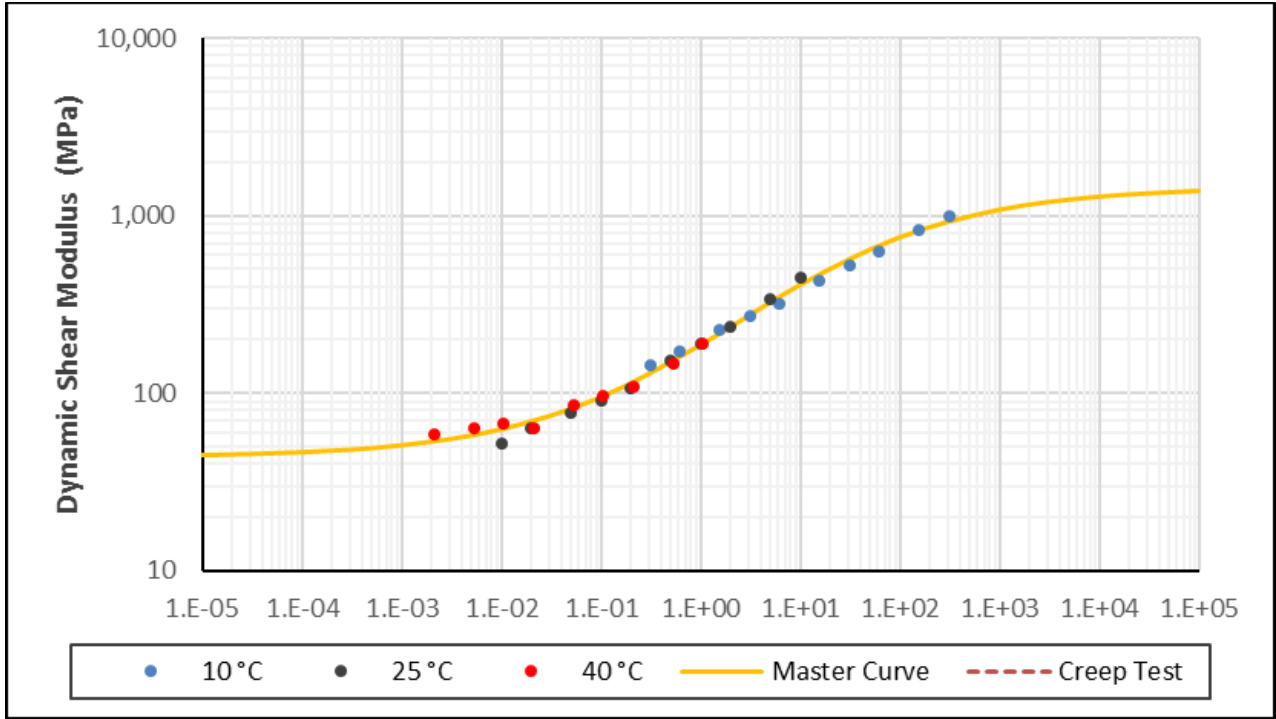


Figure G.23: Frequency sweep master curves for the reference temperature of 77°F (25°C) for PH17 layer 1.

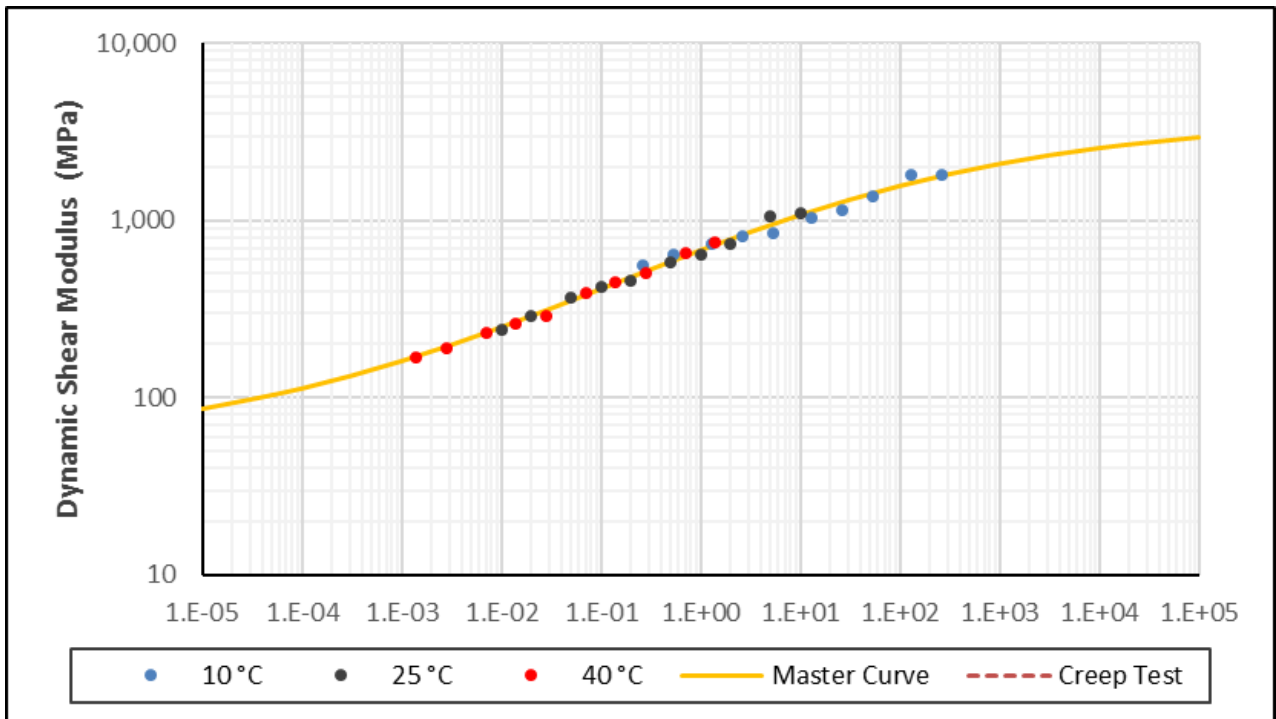


Figure G.24: Frequency sweep master curves for the reference temperature of 77°F (25°C) for PH18 layer 1.

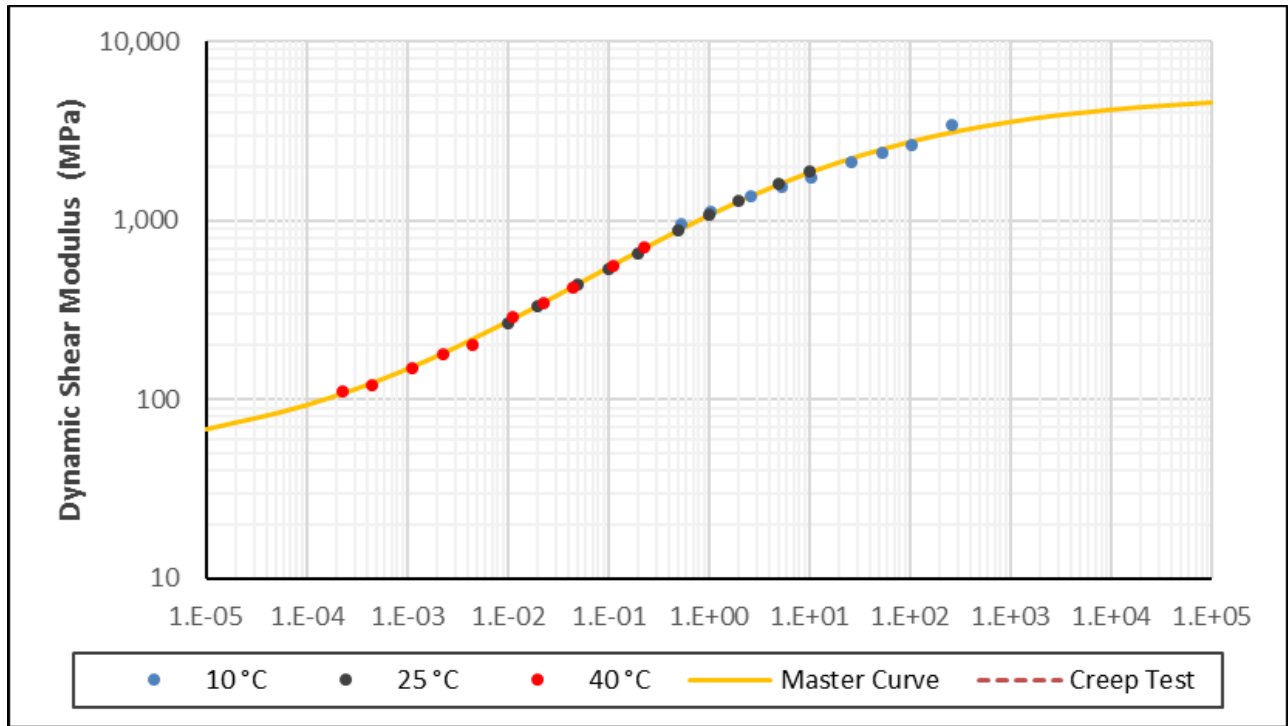


Figure G.25: Frequency sweep master curves for the reference temperature of 77°F (25°C) for PH18 layer 2.

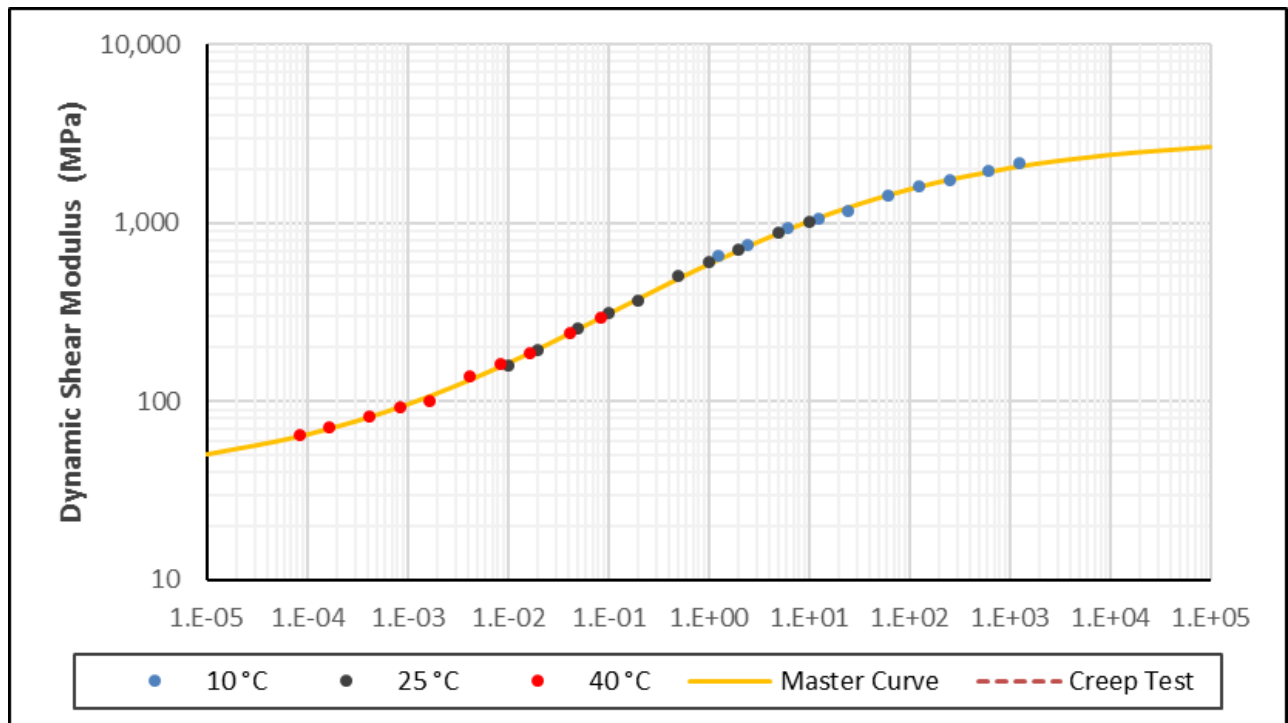


Figure G.26: Frequency sweep master curves for the reference temperature of 77°F (25°C) for PH19 layer 1.

APPENDIX F: INFORMATION ABOUT VEHICLES

Table H.1: Vehicle and Fuel Types, Number of Axles and Wheels

Vehicle Class	Fuel Type	Number of Wheels	Number of Axles	Number of Wheels				
				Front Axle	Rear Axle	Trailer 1 (Rear Axle)	Trailer 2 (Front Axle)	Trailer 2 (Rear Axle)
Car (2015 Chevy Impala)	Gas	4	2	2	2			
SUV (2014 Ford Explorer)	Gas	4	2	2	2			
Truck (2011 Ford 450 [F-450])	Diesel	6	2	2	4			
HHDT (2013 Peterbilt 388)	Diesel	18	5	2	4	4	4	4

Table H.2: Vehicle Loads and Tire Inflated Pressures

Vehicle	Axle Weight (lb.)		Driver Weight	Axle Weight (lb.)					Total Weight (lb.)	Total Load (kN)	Tire Pressure in PSI (kPa)		Time (mins) to Reach Operating Pressure
	Front	Rear		Adjusted Front	Adjusted Rear	Trailer1	Trailer2	Trailer2			Cold	Operating	
Car (gas)	2180	1540	220	2290	1650				3940	17.53	35 (242)	38 (262)	15–35
SUV	2520	2080	250	2645	2205				4850	21.57	35 (242)	38 (262)	22–44
F-450	5660	8980	220	5770	9090				14860	66.10	110 (758)	118 (814)	35-50
HHDT (Winter)	8960	18700	220	9070	18810	17387	17387	17387	80040	356.04	92 (632)	108 (742)	
HHDT (Summer)	9040	17820	220	9150	17930	17660	17660	17660	80060	356.12	92 (632)	108 (742)	
HHDT 2 ^a	9040	14820	220	9150	14930	14660	14660	14660	68060	302.75	92 (632)	108 (742)	
HHDT 3 ^b	9040	11820	220	9150	11930	11660	11660	11660	56060	249.37	92 (632)	108 (742)	

^a HHDT 2: 3,000 lb. are reduced from rear truck (summer) axle for forward modeling purposes.

^b HHDT 3: 6,000 lb. are reduced from rear truck (summer) axle for forward modeling purposes.

Table H.3: Axle Loads, Tire Contact Area, and Tire Loads

Vehicle Class	Front Axle		Rear Axle		Trailer 1 (Rear Axle)		Trailer 2 (Front Axle)		Trailer 2 (Rear Axle)	
	Load per Tire in lb. (kN)	Contact Area in ft ² (m ²)	Load per Tire in lb. (kN)	Contact Area in ft ² (m ²)	Load per Tire in lb. (kN)	Contact Area in ft ² (m ²)	Load per Tire in lb. (kN)	Contact Area in ft ² (m ²)	Load per Tire in lb. (kN)	Contact Area in ft ² (m ²)
Car (gas)	1144 (5.09)	0.209 (0.0194)	825 (3.67)	0.151 (0.014)						
SUV	1322 (5.88)	0.242 (0.0225)	1102 (4.9)	0.201 (0.0187)						
F-450	2884 (12.83)	0.170 (0.0158)	2273 (10.11)	0.133 (0.0124)						
HHDT(Winter)	4534 (20.17)	0.293 (0.0272)	4703 (20.92)	0.303 (0.0282)	4346 (19.33)	0.281 (0.0261)	4346 (19.33)	0.281 (0.0261)	4346 (19.33)	0.281 (0.0261)
HHDT (Summer)	4575 (20.35)	0.295 (0.0274)	4483 (19.94)	0.290 (0.0269)	4415 (19.64)	0.285 (0.0265)	4415 (19.64)	0.285 (0.0265)	4415 (19.64)	0.285 (0.0265)
HHDT 2 ^a	4575 (20.35)	0.295 (0.0274)	3732 (16.6)	0.241 (0.0224)	3664 (16.3)	0.237 (0.022)	3664 (16.3)	0.237 (0.022)	3664 (16.3)	0.237 (0.022)
HHDT 3 ^a	4575 (20.35)	0.295 (0.0274)	2983 (13.27)	0.193 (0.0179)	2916 (12.97)	0.188 (0.0175)	2916 (12.97)	0.188 (0.0175)	2916 (12.97)	0.188 (0.0175)

^a Due to reduced rear axle loads, load per tire for rear axles will be smaller. This is solely for forward modeling purposes.

Table H.4: Axle and Tire Spacings in Centimeters

Vehicle Class	UCPRC Measurements Axle Length in inches (cm)					Axle Spacing in inches (cm)				Space between Dual Tires in inches (cm)	
	Front Axle	Rear Axle	Trailer 1 (Rear Axle)	Trailer 2 (front Axle)	Trailer 2 (Rear Axle)	Front-Rear 1	Rear 1-Rear 2	Rear 2-Rear 3	Rear 3-Rear 4	Rear Axle	Trailer Axles
Car (gas)	62.2 (158)	62.2 (158)				108.3 (275)					
SUV	66.9 (170)	66.9 (170)				111.4 (283)					
F-450	74 (188)	71.7 (182)				200.8 (510)				3 (7.6)	
Truck	81.1 (206)	73.2 (186)	72 (183)	72 (183)	72 (183)	177.2 (450)	179.1 (455)	183.1 (465)	180 (457)	3.8 (9.7)	4.6 (11.6)

APPENDIX G: TIRE HARDNESS

The graphs of tire hardness for each tire per vehicle are shown in Figure I.1. “A1” in the legend stands for front axle and “A2” for drive axle. “D” stands for driver side and “P” for passenger side.

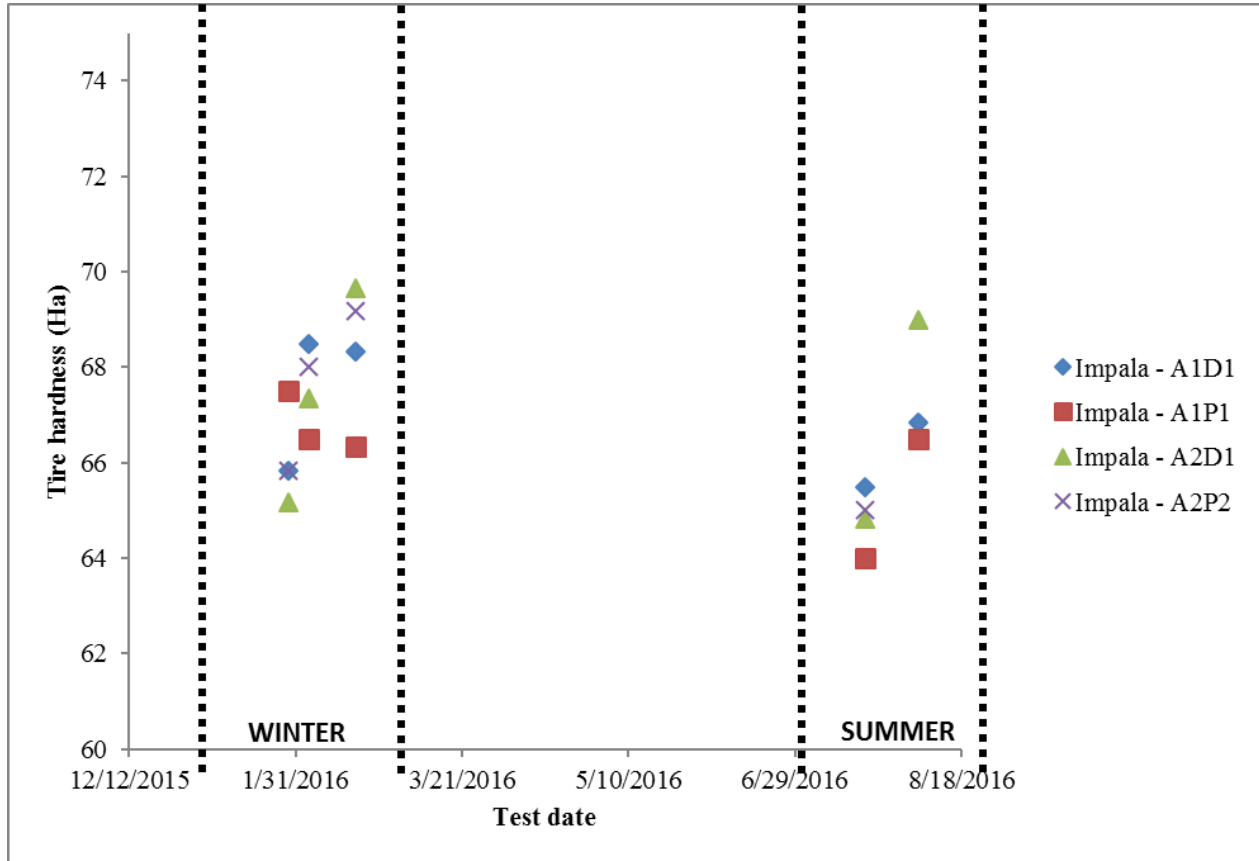


Figure I.1: Car tires hardness readings.

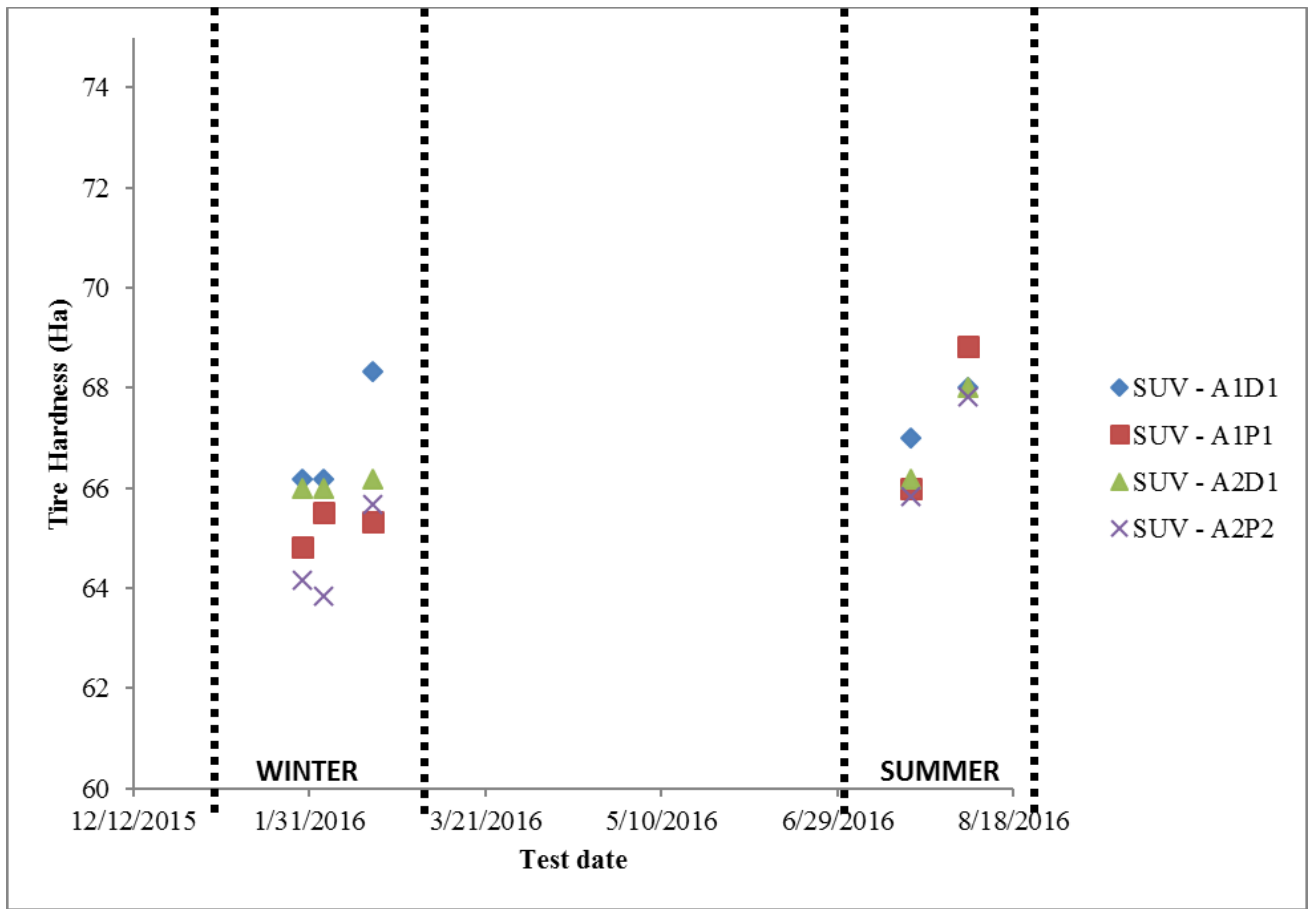


Figure I.2: SUV tire hardness data.

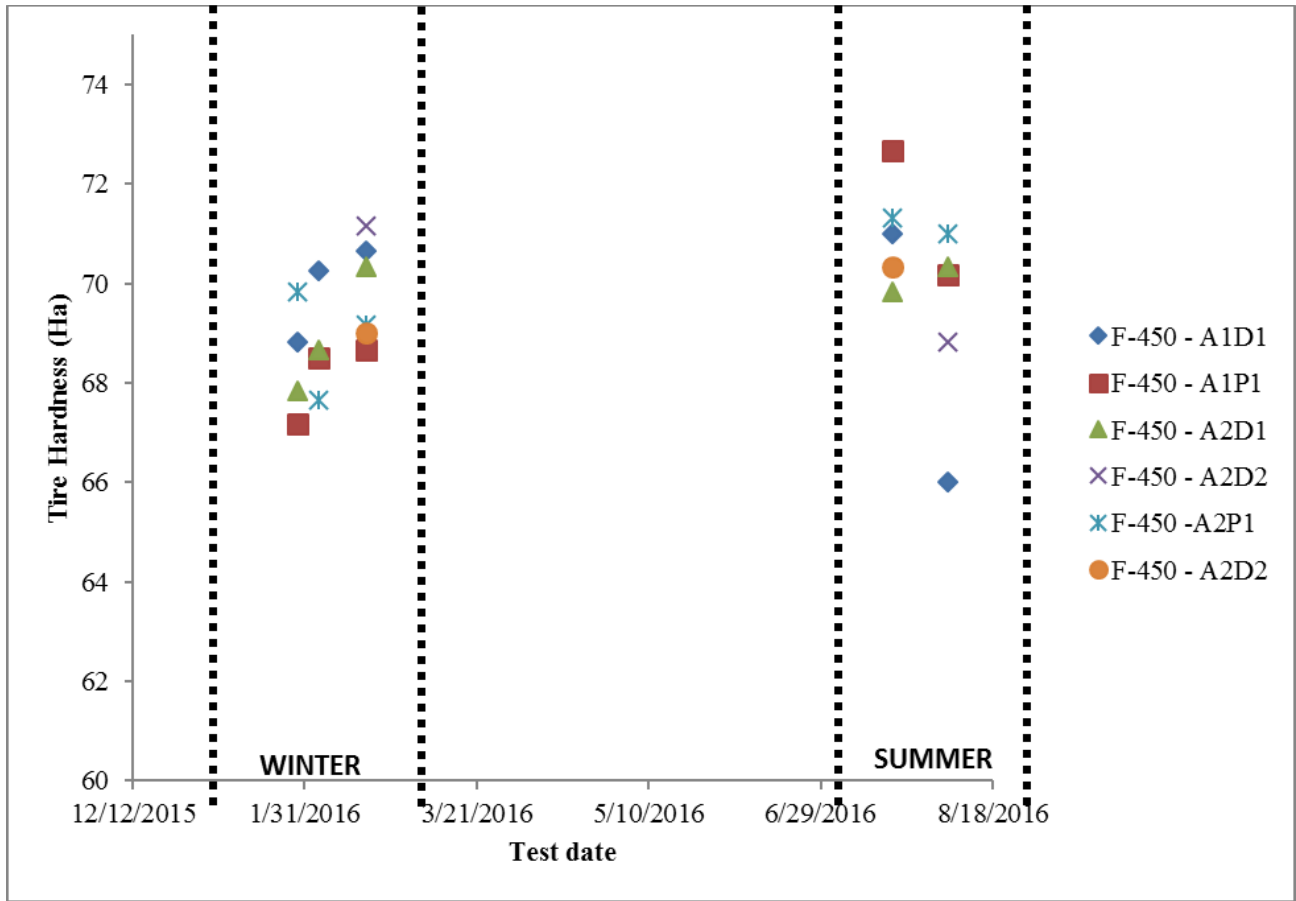


Figure I.3: F-450 tire hardness data.

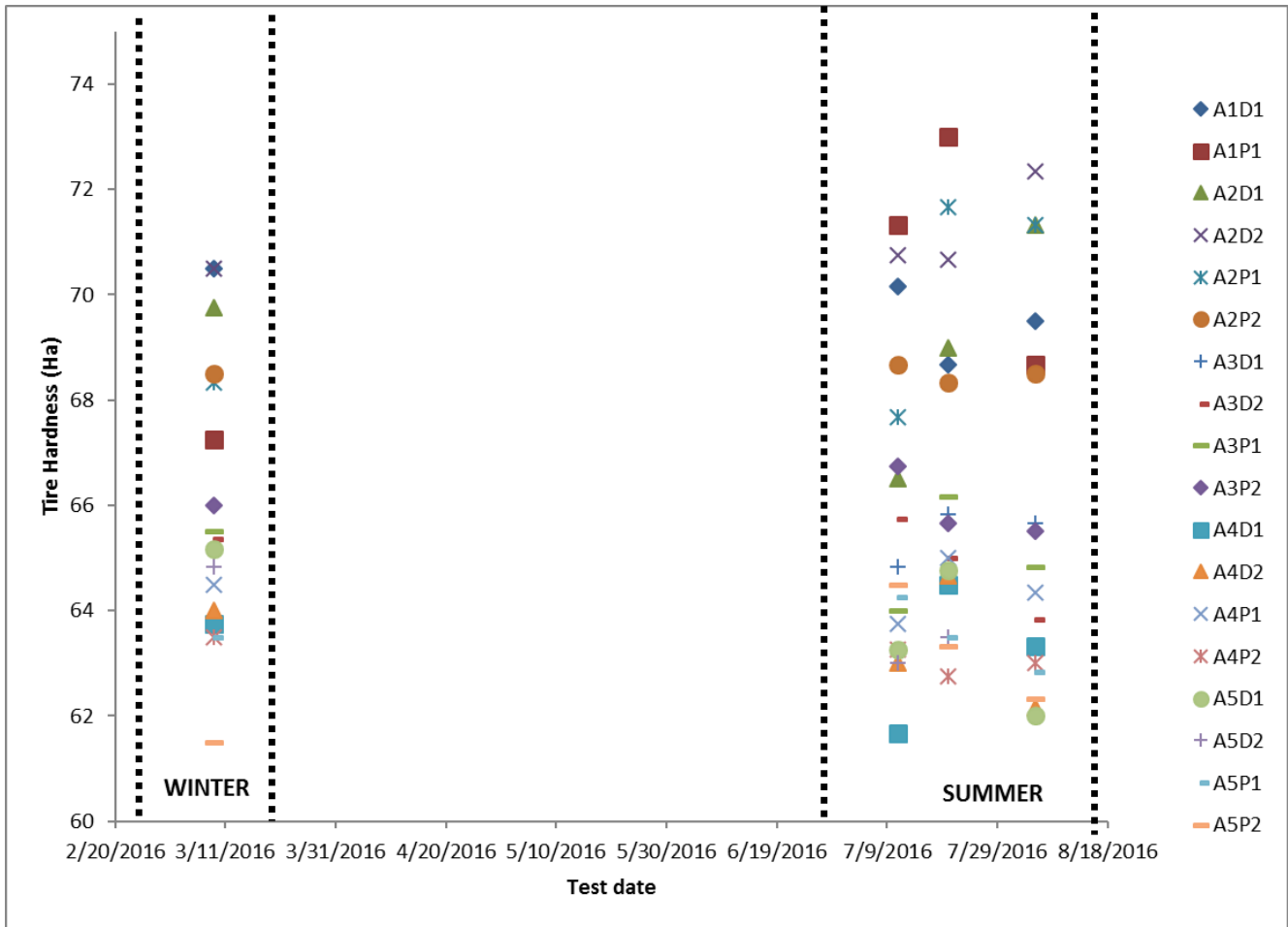


Figure I.4: HHDT tire hardness data.

APPENDIX H: TIRE PRESSURE MONITORING STUDY

Tire pressure is affected by a number of factors, including the rotation of the wheels (friction between the tires and the pavement), outside air temperature, inside and outside tire temperature, and sunlight. An increase in the temperature expands the tires, which increases the tire contact area with the pavement and may contribute to an increase in the vehicle's fuel consumption. To validate and calibrate the deflection energy fuel consumption models developed by MIT, MSU, and OSU, it was necessary to make sure that the fuel consumption data for each vehicle was being collected at the maximum operating pressure of the tires to minimize variability in the data. A tire pressure monitoring system (TPMS) was used for the study. The TPMS was mounted on the following vehicles: gasoline car, SUV, and Ford 450 (F-450). These vehicles were used for the fuel economy testing.

TPMS is an electronic system that can monitor tire pressures. A PressurePro® PULSE TPMS⁷ unit was used for this study. This unit could monitor up to 80 wheel positions and 5 vehicles and had the ability to measure tire pressures and temperatures every minute. It also had data logging capability and could record data in a connected memory drive. Wireless dynamic sensors were used that have 1 to 2% pressure measurement accuracy of up to 200 PSI and temperature resolution of 1.5 °C. Each sensor had a unique identification and was installed on the tire valve and synced to a PULSE monitoring unit that was powered by the vehicle. The tires that were used for the fuel economy testing were mounted to the vehicles, and the tests were conducted during cold (night) and warm (day) temperatures in the winter season. Tests were conducted for three tire pressures: standard (STD), 10% reduced pressure, and 20% reduced pressure for all vehicles. An onboard diagnostic (OBD) device was connected, and the tests were conducted during dry days and nights with wind speeds below 5 mph. TPMS data were first collected for the F-450 for two weeks and then for the car and SUV for another few weeks. Figure J.1 and Figure J.2 show how the outside air temperature affected the tire air temperature during the daytime (warm) and nighttime (cold) testing with the F-450 on section PH08. The rapid increase in tire temperature is due mainly to the rotation of the wheels. However, with an increase in air temperature, an increase in tire air temperature was observed, as presented in the following figures. A similar trend was observed for the other vehicles as well. Moreover, an increase in tire air pressure influenced fuel

⁷ <https://pressurepro.us/product-pulse.html>

consumption, as shown in Figure J.3 and Figure J.4 for the F-450. Similar trends were observed for all the other vehicles.

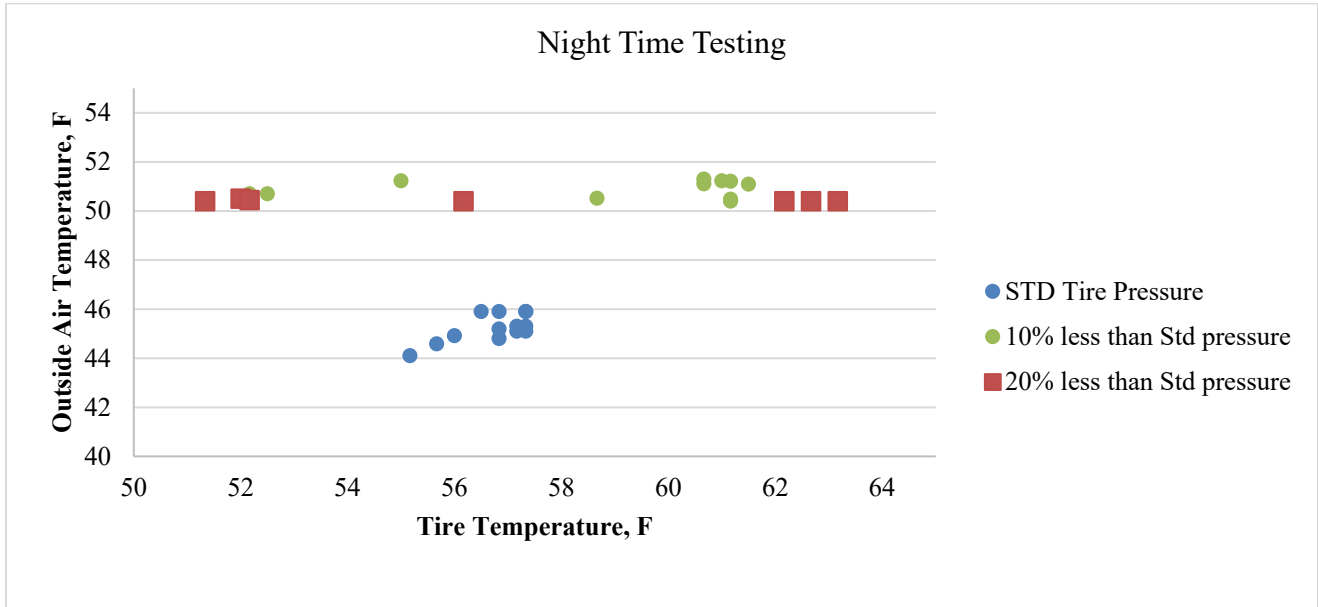


Figure J.1: Outside air temperature versus tire temperature during nighttime testing with F-450.

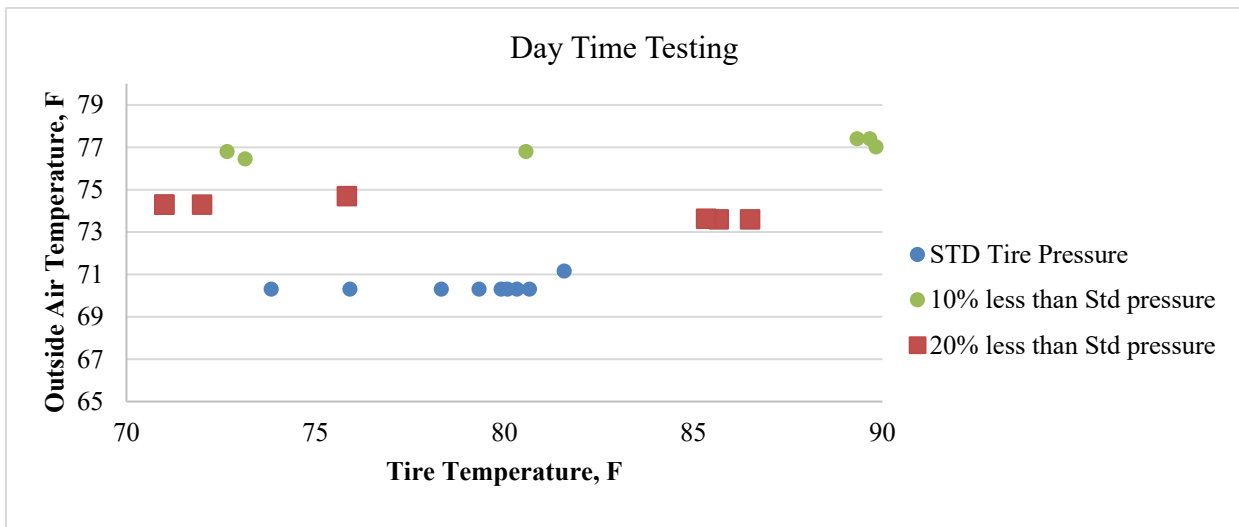


Figure J.2: Outside air temperature versus tire temperature during daytime testing with F-450.

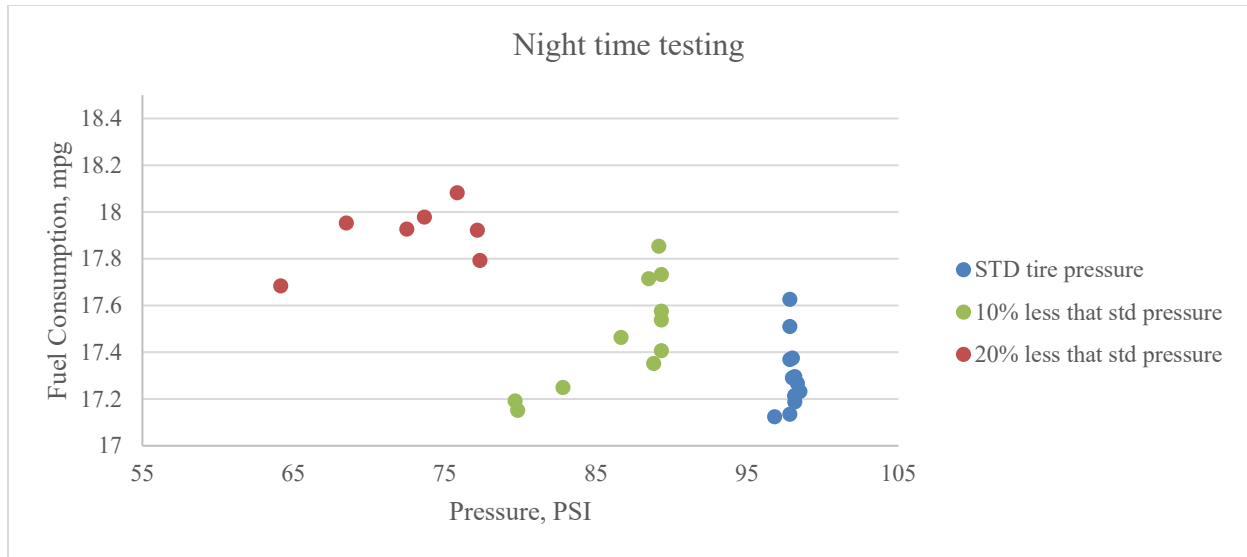


Figure J.3: Vehicle fuel consumption versus tire pressure during nighttime testing with F-450.

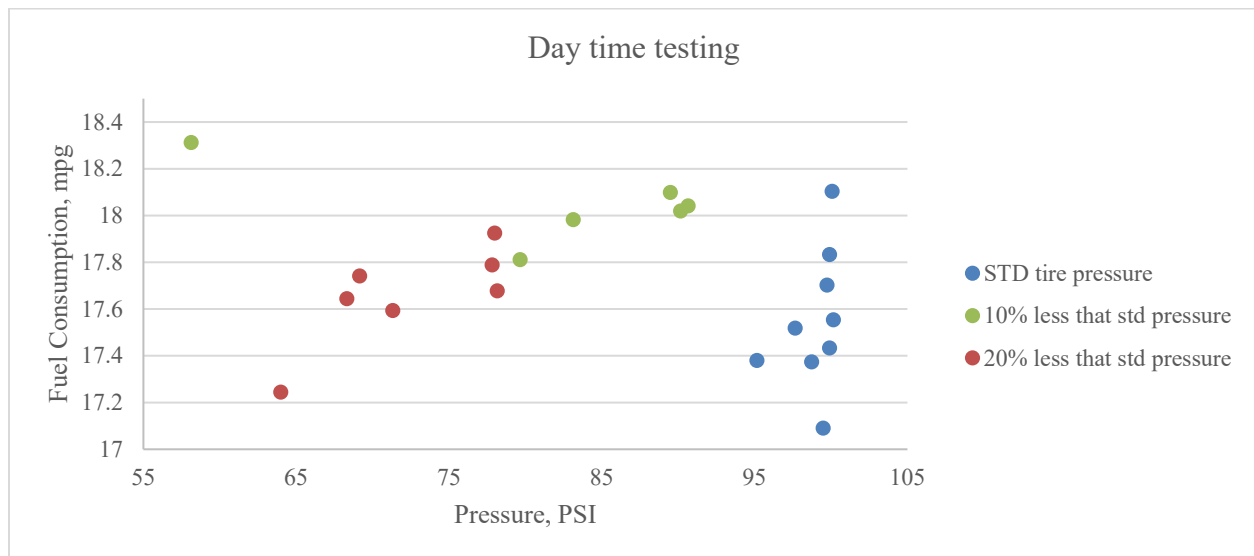


Figure J.4: Vehicle fuel consumption versus tire pressure during daytime testing with F-450.

In order to confirm that the vehicles were operating at maximum operating tire pressures, the change in tire pressures from the time the vehicles were connected to the tire pressure nozzle until they returned to the base stations were plotted. Figure J.5 shows an example of tire pressures for an SUV on section PH23. Similar trends were observed for all vehicles, and the results are reported in Table J.1. Table J.1 also shows the amount of time for each vehicle to reach the maximum operating tire pressure during cold and warm temperatures. Additionally, it shows the amount of time to reach the sections from the base station.

The base station for the truck was Chavez Trucking, which is seven miles from the University of California Pavement Research Center (UCPRC), and it took 15 minutes for the truck to reach the UCPRC, where it was dispatched to the sections.

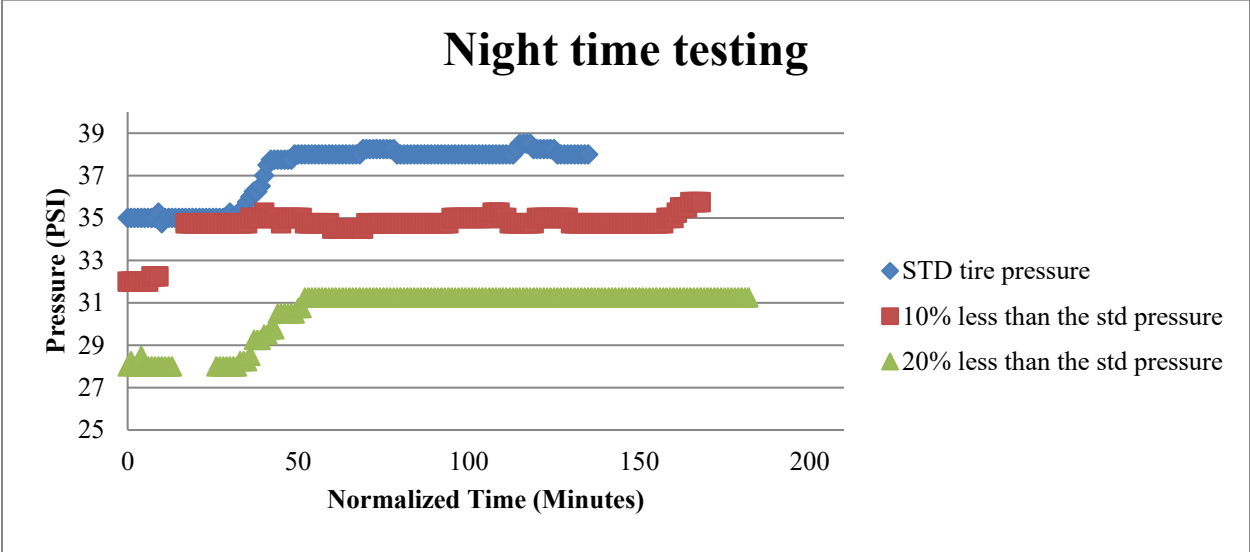


Figure J.5: Tire pressure versus the normalized time during nighttime testing with SUV.

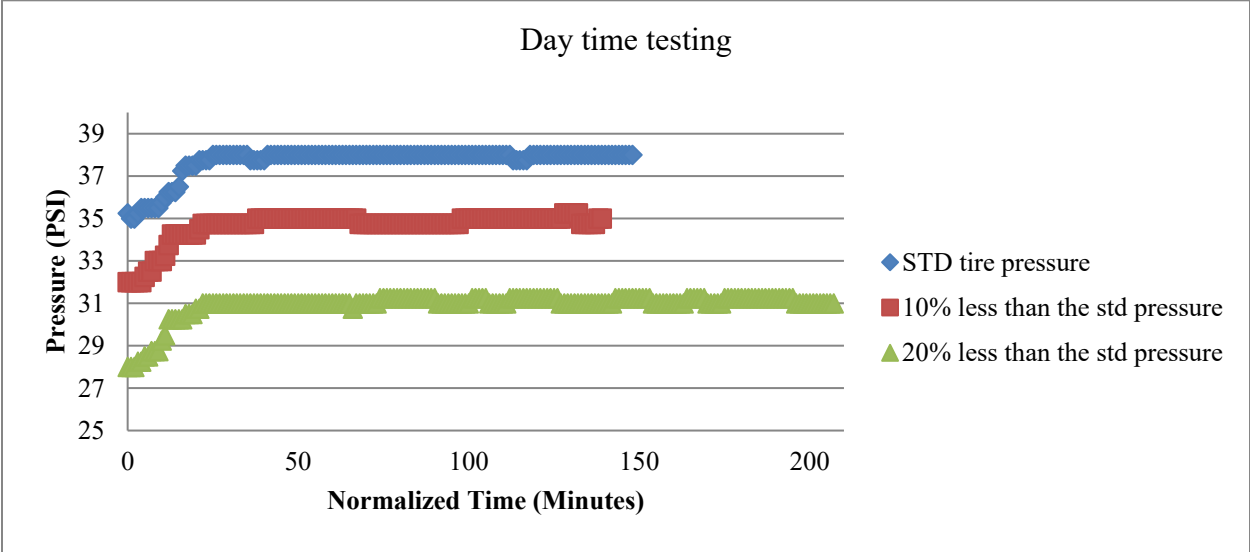


Figure J.6: Tire pressure versus the normalized time during daytime testing with SUV.

Table J.1: Average Time Taken to Reach Maximum Operating Pressure for the Vehicles Tested with TPMS

Vehicle	Air Temperature	Standard Pressure (PSI)	Maximum Operating Pressure (PSI)	Avg. Time to Maximum Operating Pressure (mins)
Car	Cold	35	37.5	35
	Warm	35	38	17
SUV	Cold	35	38	44
	Warm	35	38	22
F-450	Cold	89	98	35
	Warm	89	98	50

Table J.2: Average Time Taken to Reach the Section Locations

Section List	Base Station	Section Location	Distance from Base Station to Section Location (miles)	Time Taken to Reach the Section Location (mins)
PH01, PH02	UCPRC, Davis, CA	YOL113	8	10
PH03, PH04	UCPRC, Davis, CA	YOL505	15	20
PH07	UCPRC, Davis, CA	YOL98N	5	9
PH08	UCPRC, Davis, CA	YOL29E	12	17
PH09	UCPRC, Davis, CA	SUT113NE	30	35
PH10	UCPRC, Davis, CA	SUT113SW	52	61
PH11	UCPRC, Davis, CA	SUT113N	37	42
PH12	UCPRC, Davis, CA	SUT113S	48	56
PH13	UCPRC, Davis, CA	SUT113E	40	45
PH14	UCPRC, Davis, CA	SUT113W	47	55
PH15	UCPRC, Davis, CA	YOL32bE	9	14
PH16, PH17	UCPRC, Davis, CA	STA132	100	120
PH18, PH20	Motel 6, Buttonwillow, CA	KER5S	7	10
PH19	Motel 6, Buttonwillow, CA	KER5N	1	2
PH21, PH22	UCPRC, Davis, CA	SUT99	55	60
PH23	UCPRC, Davis, CA	YOL32aW	11	16

Note: The time taken to reach the section location does not include traffic congestion time, which in reality increases the tire pressure.

APPENDIX I: FUEL QUALITY STUDY

Fuels such as gasoline and diesel are energy resources built of chains of carbon and hydrogen that produce energy when combusted in the presence of oxygen. The quality of fuel affects a vehicle's efficiency, which affects its fuel consumption. During the fuel consumption data collection experiment in the winter and summer testing cycles, fuel samples (gas and diesel) were collected in sealed-cap glass bottles and were dated with a marker. Variability of fuel energy density was then determined using a bomb calorimeter test. A bomb calorimeter test measures the quantity of heat of combustible solids and liquids measured as the calorific value or heat of combustion of a sample. The calorific value is recorded as the number of heat units liberated by a unit mass of a sample burned with oxygen in a constant volume enclosure presented in Joules per gram of material, J/g.

The ASTM D5865 standard was followed to carry out calorific tests using a constant-volume adiabatic calorimetry (IKA C5003/C5001 calorimeter system). Prior to each fuel sample test in a bomb calorimeter, a benzoic acid tablet was combusted, and its value of 26.38 ± 0.25 kJ/g was confirmed to ensure the calorimeter was calibrated and performing according to standards. An enclosure was required in which the fuel could be contained. Bubble wrap was used for this, and the calorific value of bubble wrap was determined. Hence, the fuel calorific value was determined by subtracting the calorific value of bubble wrap from the calorific value obtained from the combustion of bubble wrap containing fuel. The results from the tests are presented in Figure K.1.

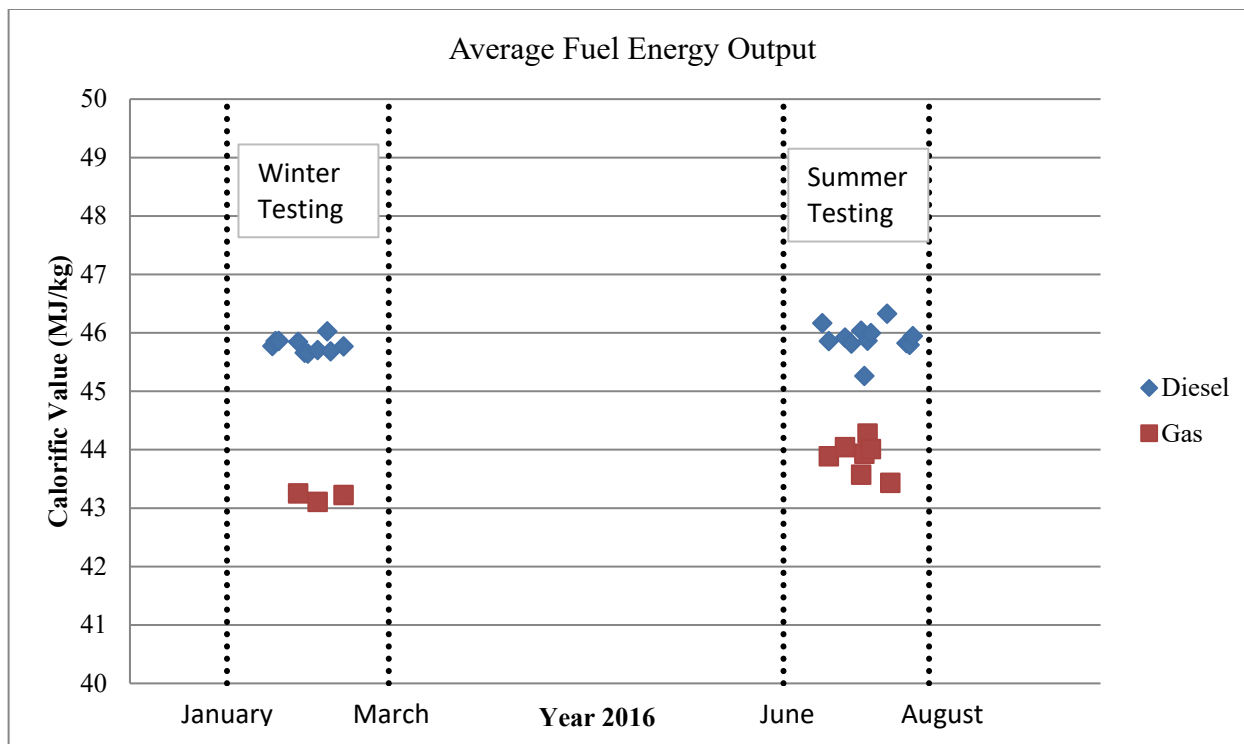


Figure K.1: Calorific values in MJ/kg of gas and diesel samples collected in summer and winter testing cycles in 2016.

No change in calorific value of diesel was observed in either of the testing cycles (summer and winter) from the bomb calorimeter testing. A slight reduction (< 1 MJ/kg) in calorific value of gas was seen in winter due to the difference in blends at different times of the year. In California, the fuel in the summer (summer blend) is different from that in the winter (winter blend), as the gasoline's density needs to be adjusted so that it can easily evaporate at a given temperature. This is determined by checking the Reid Vapor Pressure (RVP) of the fuel (lower RVP means low volatility). Winter gasoline blends contain higher additives (ethanol/butane) content, which increases fuel RVP (hence, more volatility) making fuel easier to evaporate in cold engines. According to the US Environmental Protection Agency (EPA), conventional summer-blend gasoline contains 1.7% more energy than winter-blend gasoline.⁸

An ethanol test was also conducted on the collected gasoline samples. The percent ethanol content determined in the gasoline fuel is reported in Table K.1. Density of fuel samples (gasoline and diesel) were also determined as reported in Table K.2.

⁸ <https://insights.ohio.aaa.com/what-to-know-about-gasoline-blends/>

Table K.1: Percentage Ethanol Content per Gasoline Fuel Sample Collected During Winter and Summer Economy Fuel Testing

Season	Date	Location	Ethanol Percentage in Fuel (%)
Winter	2/2/2016	Yolo505_1	Insufficient fuel quantity
Winter	2/2/2016	Yolo505_2	Insufficient fuel quantity
Winter	2/16/2016	STA132	Insufficient fuel quantity
Summer	7/15/2016	Yolo505_1	7.50
Summer	7/15/2016	Yolo505_2	7.50
Summer	7/20/2016	Yolo113N	9
Summer	7/25/2016	SUT113	8
Summer	7/26/2016	CR98	7.50
Summer	7/27/2016	STA132	6
Summer	7/25/2016	SUT113	9
Summer	8/3/2016	KERN5	6

Table K.2: Density, Relative Density and American Petroleum Institute (API) Gravity of Gasoline and Diesel Fuel Samples

Fuels	Gasoline	Diesel
Density (15°C/59°F) in g/mL	0.7336	0.7798
Relative Density (60/60°F)	0.7338	0.7801
API Gravity (60°F) in °API	61.3	49.9

APPENDIX J: AIR DENSITY CALCULATIONS

Aerodynamic forces can be defined as a combination of lift (deflecting a moving fluid) and drag (fluid resistance). Newton's second law of motion states that aerodynamic forces on a body are directly related to the change in momentum of the fluid with time (i.e., aerodynamic force is directly proportional to the density of the fluid).⁹ Aerodynamic force is one of the major factors that directly affects vehicles' fuel consumption. Every 2% reduction in aerodynamic drag can result in 1% fuel economy improvement.¹⁰ Therefore, accuracy of the air density and aerodynamic measurements is very important.

During the fuel economy field testing, weather stations were set up and a number of parameters were recorded. Air density calculations depend on the altitude at which a weather station is placed, and input is required for the air density calculations to be accurate. However, as the altitude input in the WeatherLink weather station was unchanged for all the field section locations, the air density data were considered inaccurate. Air density is a function of air temperature, relative humidity, absolute pressure, and saturated vapor pressure in the WeatherLink software. Due to the unavailable/unrecorded relative humidity and absolute pressure data from the weather station, the equation in the software could not be used. Thus, air density was calculated using other parameters, such as air temperature and dew point, recorded by the weather station during the fuel economy field testing. The total air pressure for each section elevation was determined. The procedure to calculate air density is described in the following discussion.

The following is the equation¹¹ used to determine air density at each weather station location during the fuel economy testing:

$$D = \left(\frac{P}{R_d \cdot T} \right) \cdot \left(1 - \frac{0.378 \cdot P_v}{P} \right)$$

Where:

D = Total air density (dry + moist), kg/m³

P_v = Water vapor pressure, Pa

P = Total air pressure (dry + moist), Pa

R_d = Gas constant for dry air, 287.05 J/(kg.K)

T = Air temperature, in Kelvin, K

⁹ <https://www.grc.nasa.gov/www/k-12/airplane/density.html>

¹⁰ <https://www.fleetequipmentmag.com/truck-trailer-aerodynamics-fuel-efficiency>

¹¹ Brutsaert 1982: <https://link.springer.com/book/10.1007%2F978-94-017-1497-6>

Air temperature was measured by the weather stations, while water vapor and total pressure were to be determined. Water vapor pressure was calculated based on the popular equation by Herman Wobus¹²:

$$E_s = \frac{eso}{P_E^8}$$

Where:

E_s = saturation water vapor pressure, mb

$eso = 6.1078$

$P_E = (c0+T.(c1+T.(c2+T.(c3+T.(c4+T.(c5+T.(c6+T.(c7+T.(c8+T.(c9))))))))))$

T = Air temperature, C

$c0 = 0.99999683$

$c1 = -0.90826951 \times 10^{-2}$

$c2 = 0.78736169 \times 10^{-4}$

$c3 = -0.61117958 \times 10^{-6}$

$c4 = 0.43884187 \times 10^{-8}$

$c5 = -0.29883885 \times 10^{-10}$

$c6 = 0.21874425 \times 10^{-12}$

$c7 = -0.17892321 \times 10^{-14}$

$c8 = 0.11112018 \times 10^{-16}$

$c9 = -0.30994571 \times 10^{-19}$

Water vapor pressure, P_v , is not calculated based on relative humidity, and air temperature, T , can be replaced by dew point, T_{dp} . By changing the air temperature value with dew point, saturated water vapor pressure equals water vapor pressure, $E_s = P_v$. In order to calculate total pressure, P , based on altitude of the test sections, the US standard atmosphere equation was used.¹³

$$P = P_b \cdot \left[\frac{T_b}{T_b + L_b \cdot (H - h)} \right]^{\frac{g \cdot M}{R \cdot L_b}}$$

¹² Schlatter and Baker, 1991: <http://icoads.noaa.gov/software/other/profs> and https://wahiduddin.net/calc/density_algorithms.htm

¹³ NASA: <https://ntrs.nasa.gov/archive/nasa/casi.ntrs.nasa.gov/19770009539.pdf>, US. Standard Atmosphere, 1976, U.S. Government Printing Office, Washington, D.C., 1976

Where:

P_b = Static pressure (atmospheric pressure above sea level), 101325 Pa

T_b = Standard temperature at which static pressure is measured, 288.15 K (15 C)

L_b = Standard temperature lapse rate, -0.0065 K/m

h = Height above sea level where static pressure is measured, 0 m

H = Height above sea level (elevation of the section above sea level), m

g = Gravitational acceleration, 9.80665 m/s²

R = Universal gas constant, 8.3144598 J/mol/K

M = Molar mass of Earth's air, 0.0289644 kg/mol

Total air pressure based on section location (where the weather station was placed) is shown in Table L.1.

Table L.1: Total Air Pressure at Different Elevations

Section	Weather Station GPS Location	Elevation, H (ft.)	Total Air Pressure, Pt (inhg)
PH01-YOL113N PH02 -YOL113S	38.59292°N -121.76641°E	45	29.87
PH03-YOL505N PH04-YOL505S	38.53230°N -121.95540°E	123	29.79
PH07-CR98N PH08-CR29E	38.59078°N -121.80294°E	61	29.86
PH09-SUT113N PH10-SUT113S	38.87082°N -121.70742°E	22	29.90
PH11-SUT113N1 PH12-SUT113S1 PH13-SUT113E PH14-SUT113W	38.97058°N -121.67188°E	32	29.89
PH15-CR32bE	38.56129°N -121.64483°E	19	29.90
PH16-STA132E PH17-STA132W	37.63862°N -120.89835°E	119	29.79
PH18-KER5S PH19-KER5N PH20-KER5S	35.40423°N -119.40263°E	289	29.61
PH21-SUT99N PH22-SUT99S	39.17040°N -121.63601°E	58	29.86
PH23-CR32aW	38.56532°N -121.63969°E	21	29.90

APPENDIX M: DETERMINING THE RELATIONSHIP BETWEEN RPM AND VEHICLE SPEED

Figure M.1 shows that the fuel consumption of the F-450 truck cruising at constant speed of 45 mph but in different gears (3, 4, 5 and 6); resultant fuel consumption was different in each gear even though the vehicle was running at a constant 45 mph speed. Thus, it is not inaccurate to say that the fuel consumption is dependent on not only the speed at which it is running but also the gear in which it is operating.

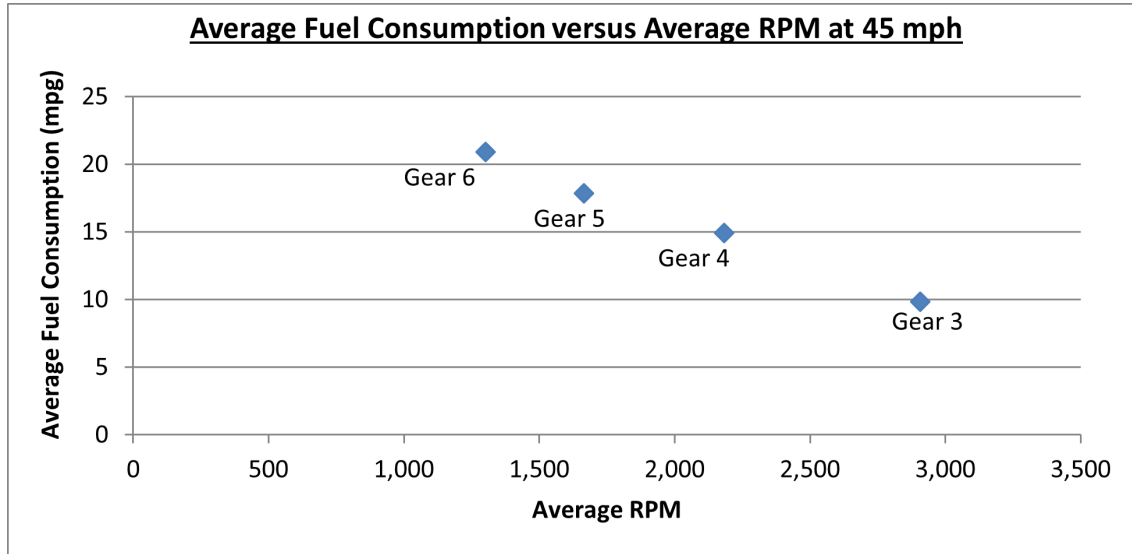


Figure M.1: Average fuel consumption of F-450 truck at constant speed of 45 mph.

Figure M.2 shows how slow and fast acceleration changes the RPM and F-450 speed curve. A gear shift between 40 and 50 mph for the F-450 can be seen in Figure M.2. Thus, it is possible that different fuel consumption values that were recorded for the F-450 during the fuel economy testing were for the same speed but different gears. The driver was either deaccelerating from a higher to a lower speed or was accelerating to a higher speed when the cruise control was turned on at 45 mph, resulting in cruising at a higher or a lower gear. This was an important observation. Therefore, it was necessary to investigate the gear in which the fuel economy data were collected for each speed for all the automatic transmission vehicles.

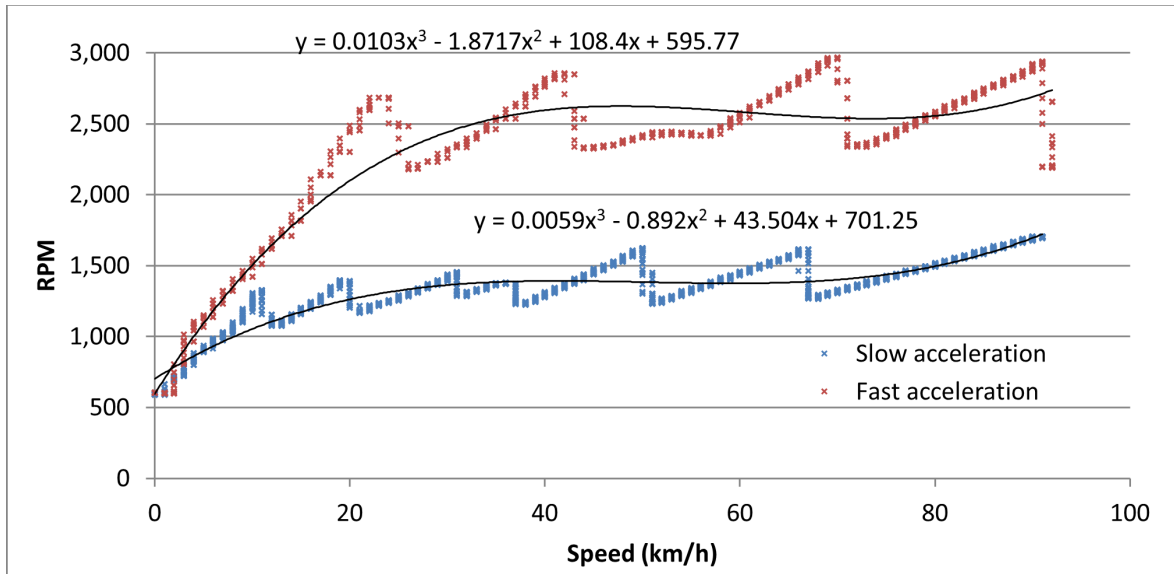


Figure M.2: Slow and fast acceleration of the F-450 truck.

The vehicles were run on different sections at different speeds in different gears by deactivating the automatic gear control and manually setting the shift for each vehicle. The RPM versus vehicle speed for each gear were then plotted, and empirical relationships were determined. It is important to mention here that RPM and speed have a linear relationship if the vehicle is operating in the same gear. The parabolic or cubic relationship of RPM and vehicle speeds (the example shown in Figure M.2) is suggested in other studies and in the Highway Development and Management Model (HDM-4), which was not used in this study. The linear relationships of RPM versus speed for each vehicle in each gear are presented in Figure M.3 to Figure M.6.

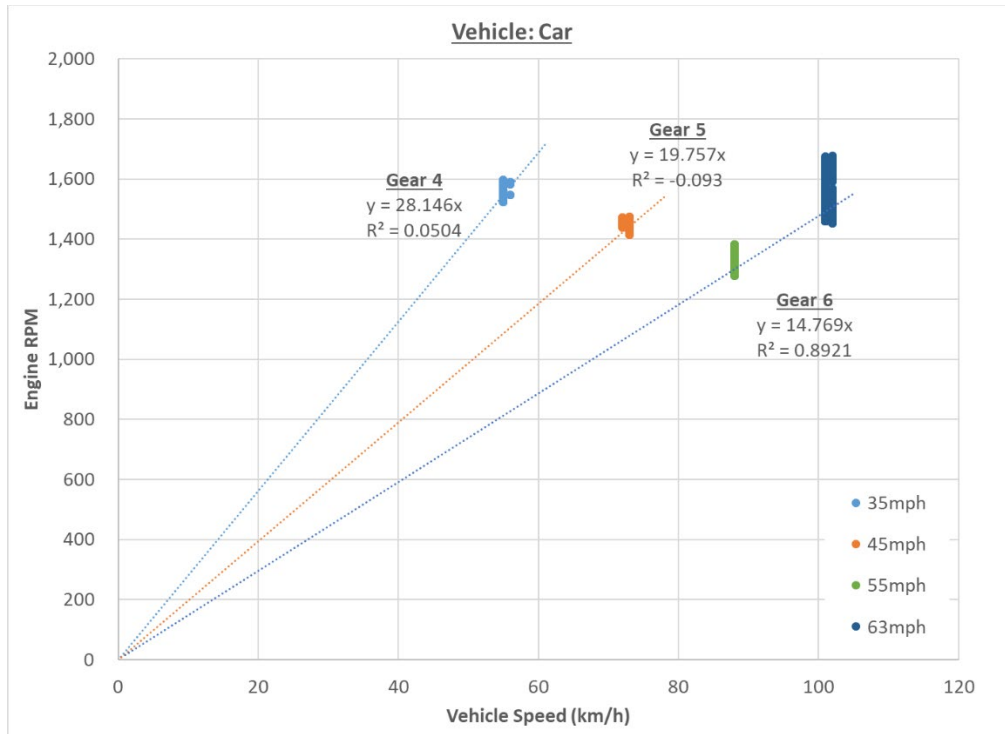


Figure M.3: Relationship between RPM and car speeds in different gears.

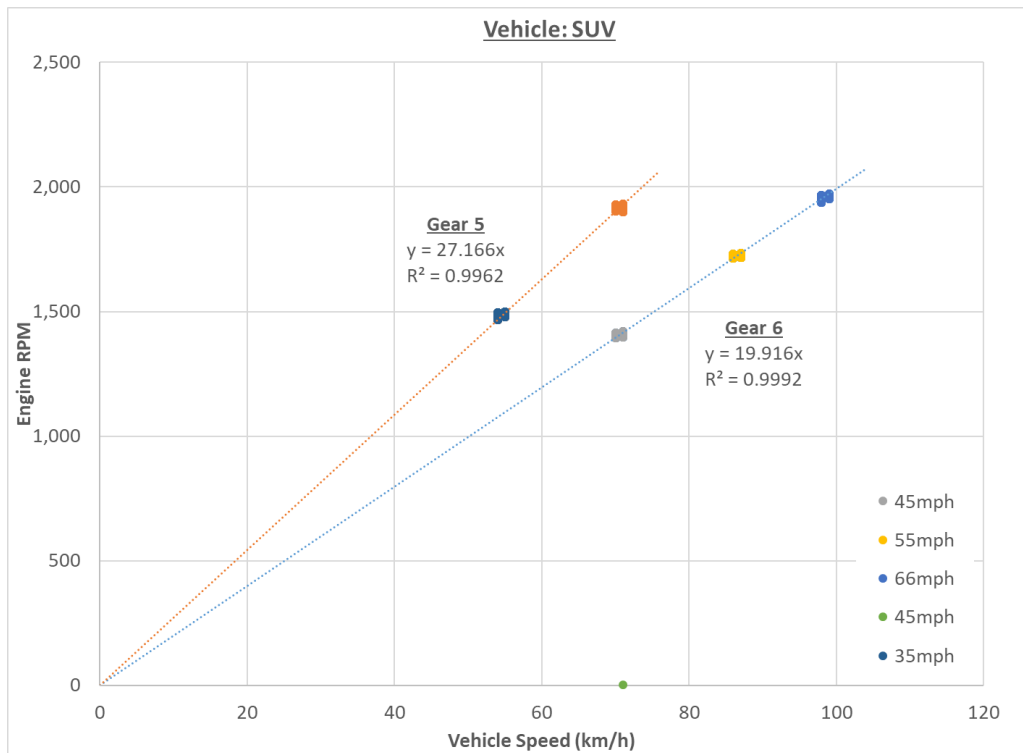


Figure M.4: Relationship between RPM and SUV speeds in different gears.

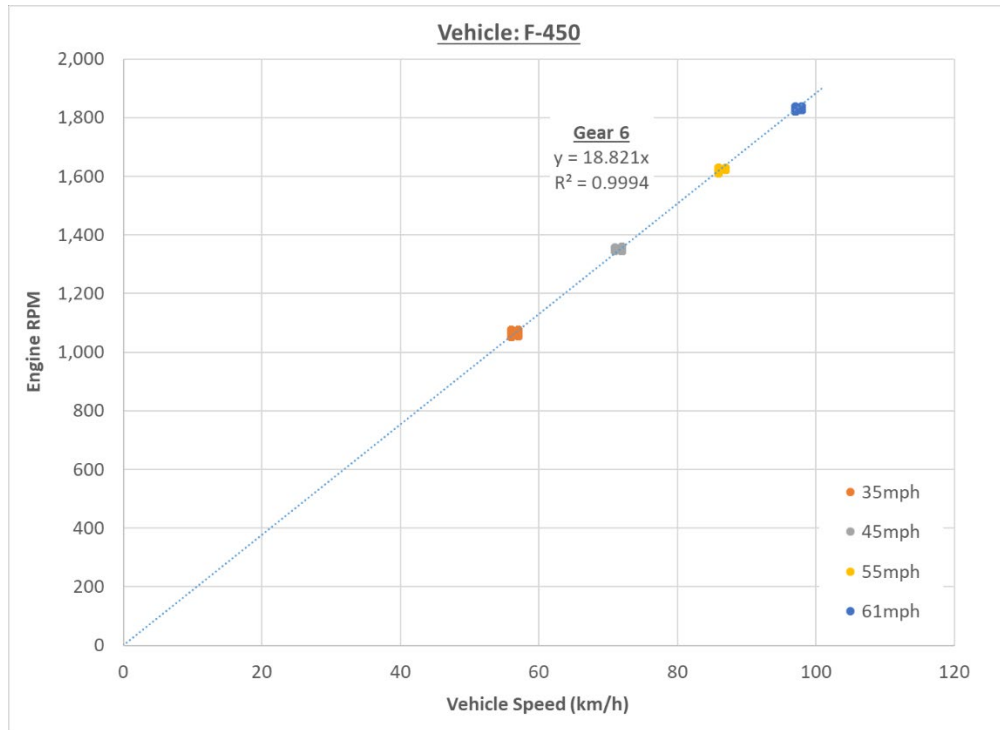


Figure M.5: Relationship between RPM and F-450 speeds in different gears.

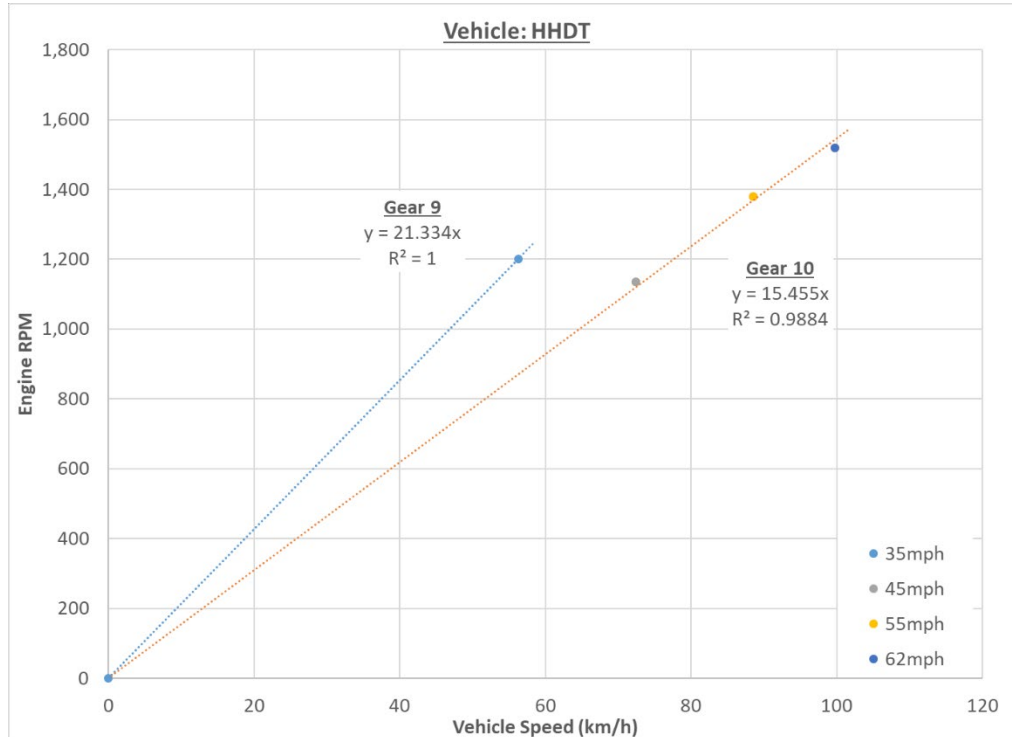


Figure M.6: Relationship between RPM and HHDT speeds in different gears.

APPENDIX N: DETERMINING PAVEMENT TEMPERATURES

A computer model developed by Li¹⁴ was used to simulate pavement behavior over time. The authors developed an Abaqus-based model that predicts heat transfer through a given structure and can be used to determine pavement surface and subsurface temperatures. Modeling was carried out using a finite element method, where the layers were split into smaller elements that are denser near the material edges and sparser as they move away from the layer boundaries. Figure N.1 shows a typical structure that was designed in the model. The environment above the pavement surface (denoted as “Air” in the figure) was also defined in the model. Simulations were then performed where the heat transfer from the air layer down to the subgrade was determined based on several known inputs and data.

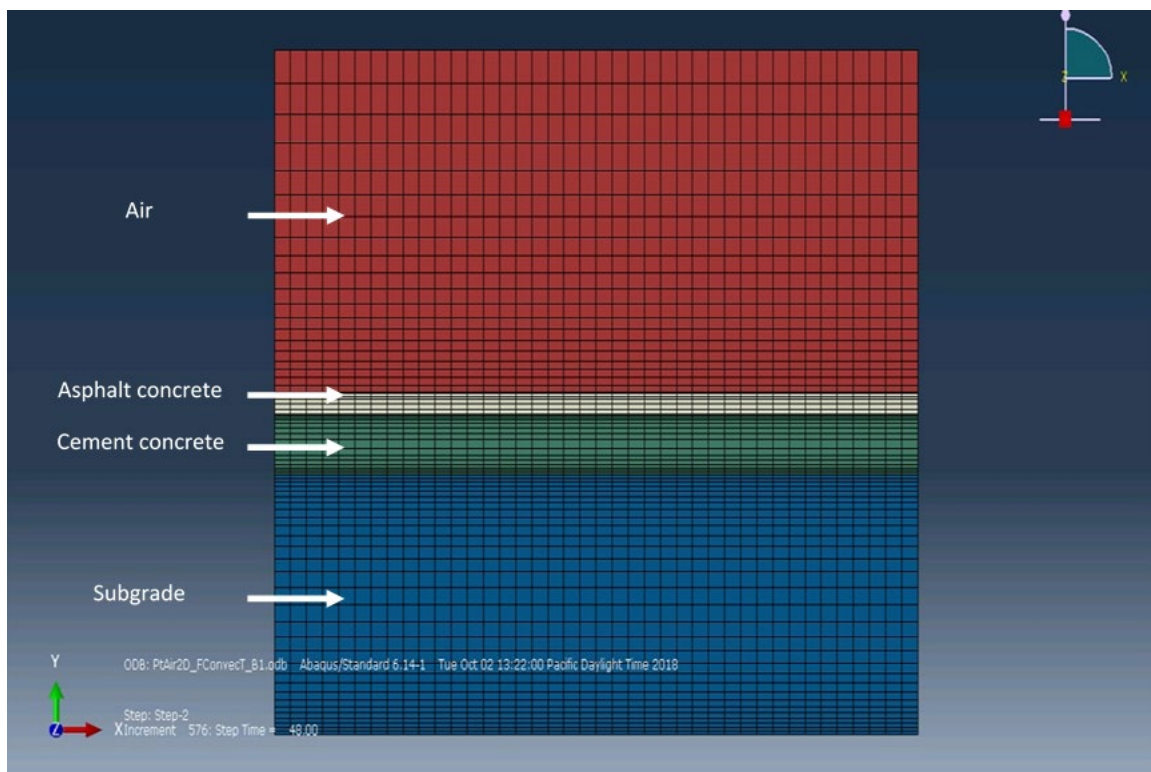


Figure N.1: Typical structure modeled in Abaqus.

Determining pavement surface and subsurface temperatures required a number of variables, which include:

1. Thermal conductivity of the layers [$W/(m \text{ } ^\circ C)$]
2. Density of the layers [kg/m^3]
3. Specific heat of the layers [$J/(kg \text{ } ^\circ C)$]

¹⁴https://escholarship.org/content/qt6mr4k9t1/qt6mr4k9t1_noSplash_9ab61b14762e84b7d61994b7aa5e0d1b.pdf?t=pyhuvvm

4. Emissivity of the layers
5. Ambient temperature during fuel economy testing period [°C]
6. Solar radiation during fuel economy testing period [W/m²]
7. Convection film coefficient [W/(m² °C)]
8. Wind speed (m/s)

Predicting the pavement temperatures for which no data were recorded involved three steps:

1. Collect pavement temperature data for all sections for two to three consecutive days and nights using two devices. The two instruments used were a temperature gun and a thermocouple. These were calibrated at the UCPRC before being used on the test sections.
2. Run the prediction model and calibrate the results for each section.
3. Use the solar radiation, air temperature, and wind speed data collected during the fuel economy testing in the prediction model to predict the pavement temperatures for that testing day per section. Then use the calibration factors determined in step 1 to get the final pavement temperature prediction.

Thermal conductivity and the density of the pavement layers were obtained from the literature surveys for different kinds of materials from Li. Albedos of the test sections were determined by visually comparing the known albedo surfaces with the test section surface photographs. Table N.1 shows the different values of the parameters used in this study for different layer types.

Table N.1: Parameter Values for Layer Properties Used in Temperature Prediction

Layers	Material	Albedo	Thermal Conductivity (W/(m. °C))	Heat Capacity (J/(kg. °C))	Density (kg/m ³)	Thermal Emissivity
Asphalt	RHMA-G	0.08	1.23	798	2200	0.8
Asphalt	HMA	0.08	1.73	852	2399	0.8
Concrete	Concrete-D	0.05	1.83	1001	2257	0.8
Base	CTB	N/A	1.4	920	1800	N/A
Subgrade	Soil	N/A	1.3	860	1700	N/A
Air	Air	N/A	0.00257	1006	1205	0.8

Notes:

- RHMA-G = hot mix asphalt, gap-graded
- HMA = hot mix asphalt (densely graded asphalt concrete)
- CTB = cement treated base

The most critical of these variables are the solar radiation on the pavement surface and the wind speed. The solar radiation data were obtained from the National Solar Radiation Database (NSRDB), which is hosted and maintained by the National Renewable Energy Laboratory (NREL). It provides solar radiation and cloud cover data for the entire United States as well as for other parts of South Asia and Mexico and Central America. NREL's

Physical Solar Model v3 is a mathematical model that uses data from different weather sources to predict the solar radiation in any given area or at a particular point. The wind speed data were the second critical component affecting pavement temperatures, and these data were obtained from historical databases of wind speeds from the Weather Underground online repository. This study used wind speed data from weather stations located near test sections; the data corresponded to the days when the pavement temperature data were collected. Figure N.2 and Figure N.3 show the test site locations for which the solar radiation and wind speed data were collected. The temporal resolution of the wind data varied from one minute to half an hour, and the model was correspondingly adjusted.

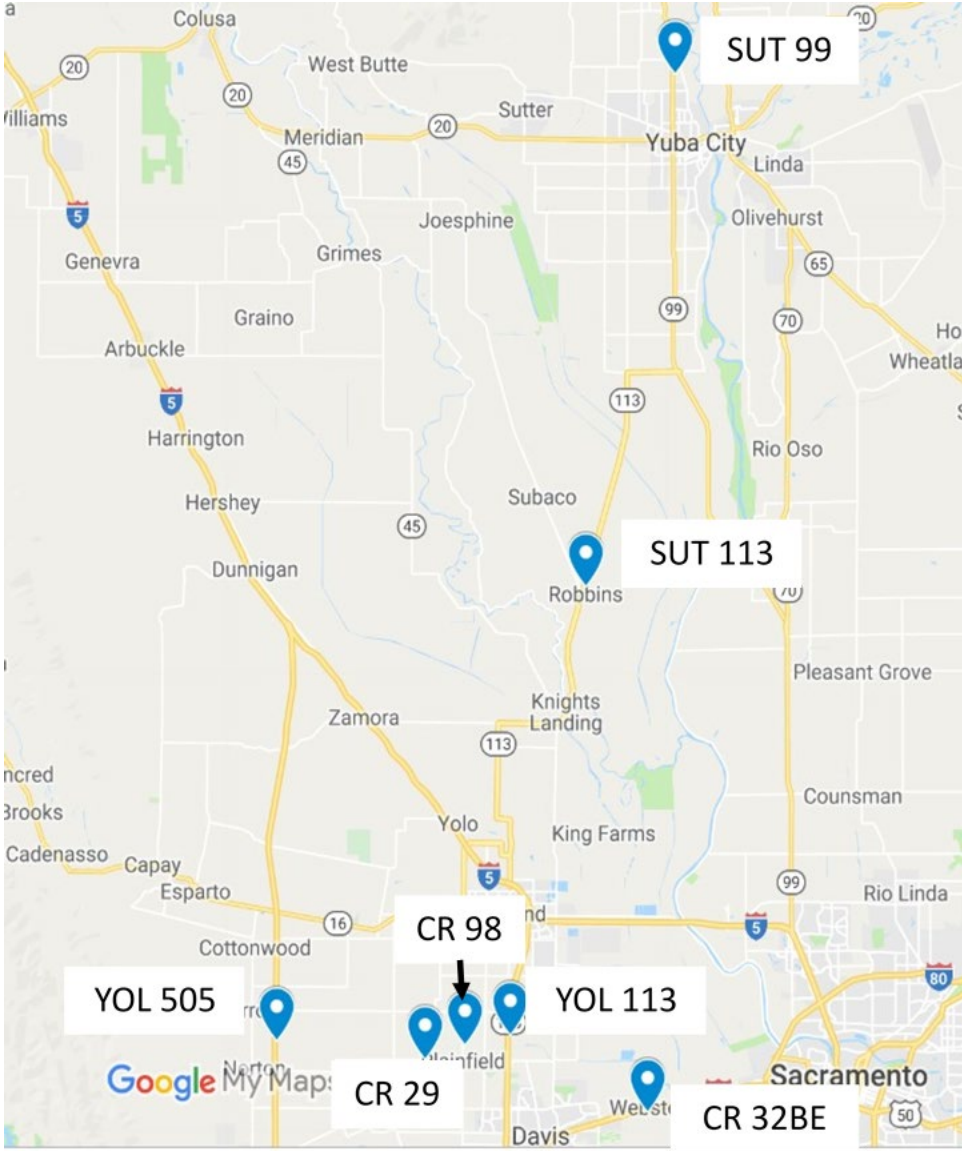


Figure N.2: Solar data locations in Northern California in the Sacramento region.

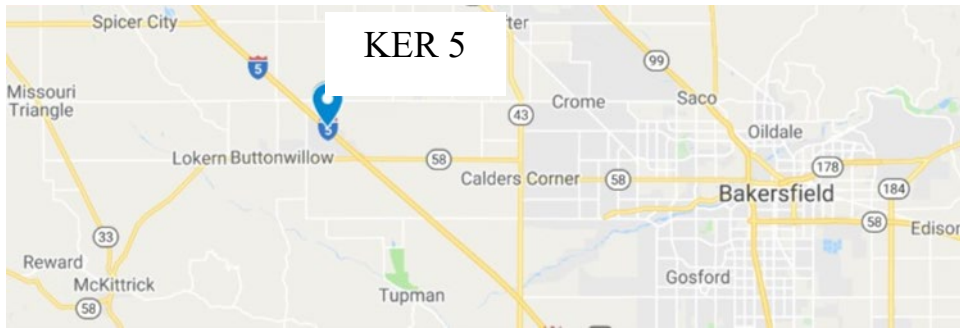
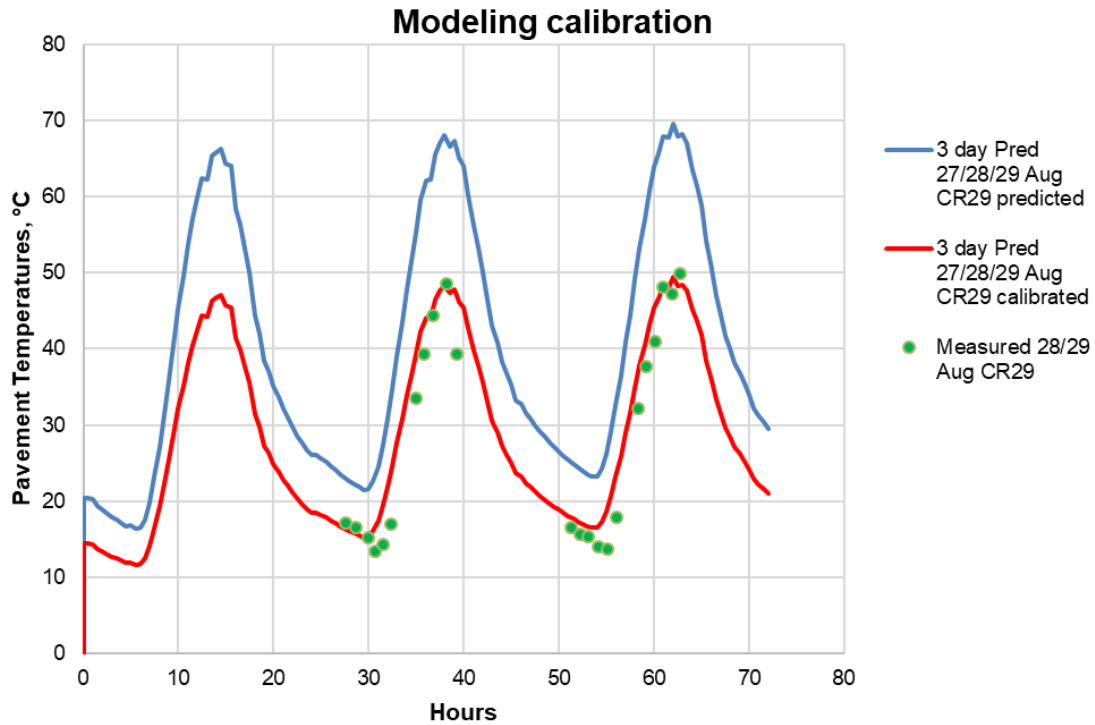


Figure N.3: Solar data location in Southern California in the Bakersfield region.

After the computer model predicted the surface pavement temperatures for each section, the next step was to calibrate the model with field collected data. Temperature gun and temperature measuring probe devices were used to measure two to three consecutive days on all test sections for which the pavement temperatures were to be predicted. Pavement surface temperature readings were recorded at 10- to 15-minute intervals during the hottest and coolest times of the day and night for two to three consecutive days. Simultaneously, the computer model was used to predict temperatures for the same days. The collected pavement temperature data were then plotted on the predicted pavement temperatures of the model. A random value was assigned to an adjustment parameter so that the predicted data aligned with the measured data. This parameter was defined as the calibration factor, which was unique for each section. An example plot of the CR29 prediction, measurement, and calibration is shown in Figure N.4.



Note: *Pred* is short for *prediction*.

Figure N.4: Prediction and calibration of pavement temperatures for CR29.

Using the solar radiation and wind speed data collected during the fuel economy testing, the prediction model was rerun for each section. The calibration factors (obtained for each section) were then multiplied by the pavement temperature predictions to obtain an accurate estimation of the pavement temperatures at the time of fuel economy testing for each run on each section. The calibration factors for all sections and the corresponding standard error between the predicted and measured temperatures are presented in Table N.2.

Table N.2: Calibration Factor and Standard Error for Temperature Prediction Model

PH	Calibration Factor	Standard Error
1	0.74	3.94
2	0.74	3.94
3	0.74	4.41
4	0.67	2.89
7	0.76	1.83
8	0.71	3.34
9	0.55	2.42
10	0.55	2.42
15	0.735	2.87
18	0.75	2.279
19	0.75	2.279
20	0.82	1.099
21	0.67	3.079
22	0.67	3.079

The final air temperatures, pavement temperatures, and temperatures at pavement one-third depth for each section during the fuel economy testing are presented from Figure N.5 to Figure N.54.

PH23-YOL-CR32AW-JPC winter day

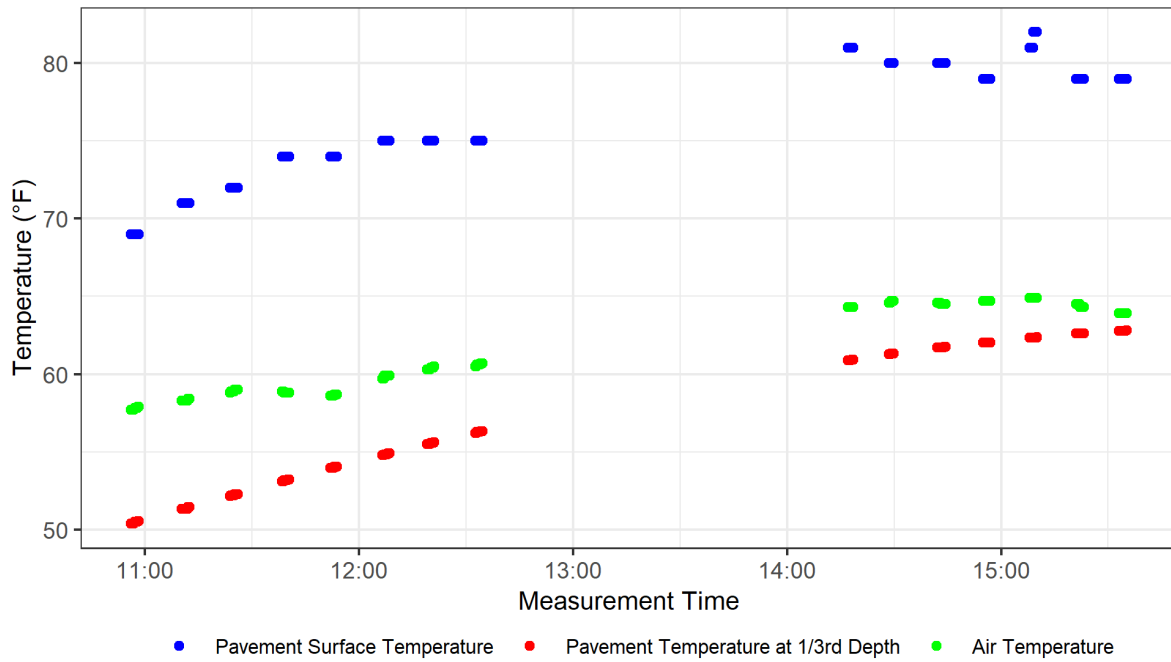


Figure N.5: Air, pavement surface, and one-third depth temperatures on 01/27/2016 testing day.

PH23-YOL-CR32AW-JPC summer night

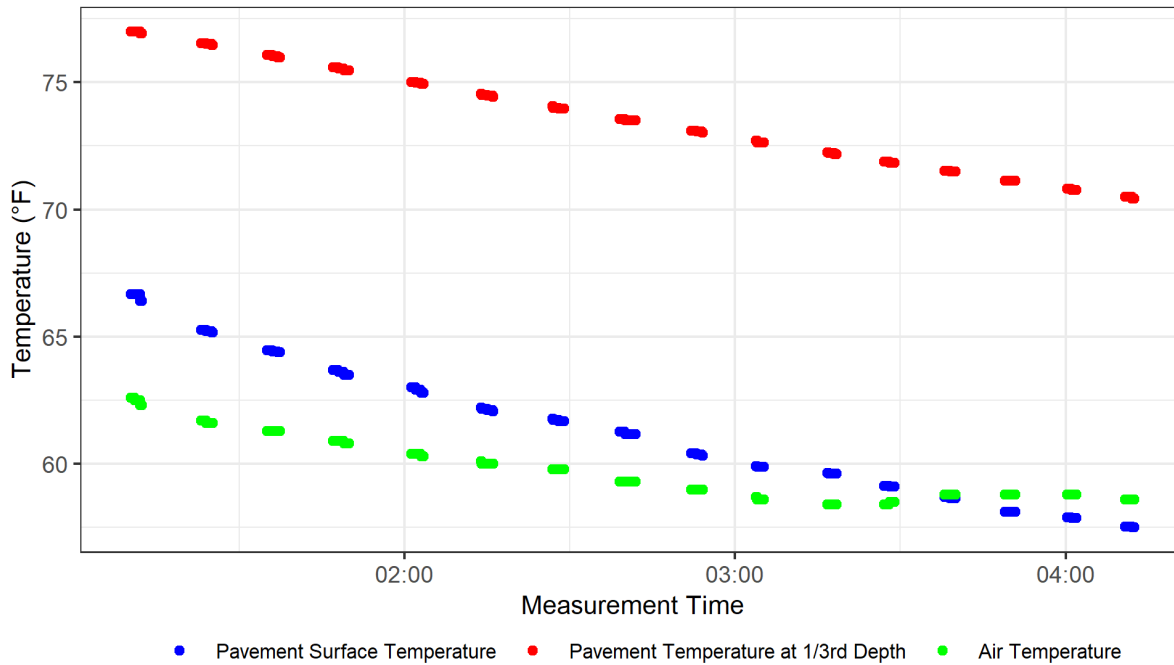


Figure N.6: Air, pavement surface, and one-third depth temperatures on 08/10/2016 testing day.

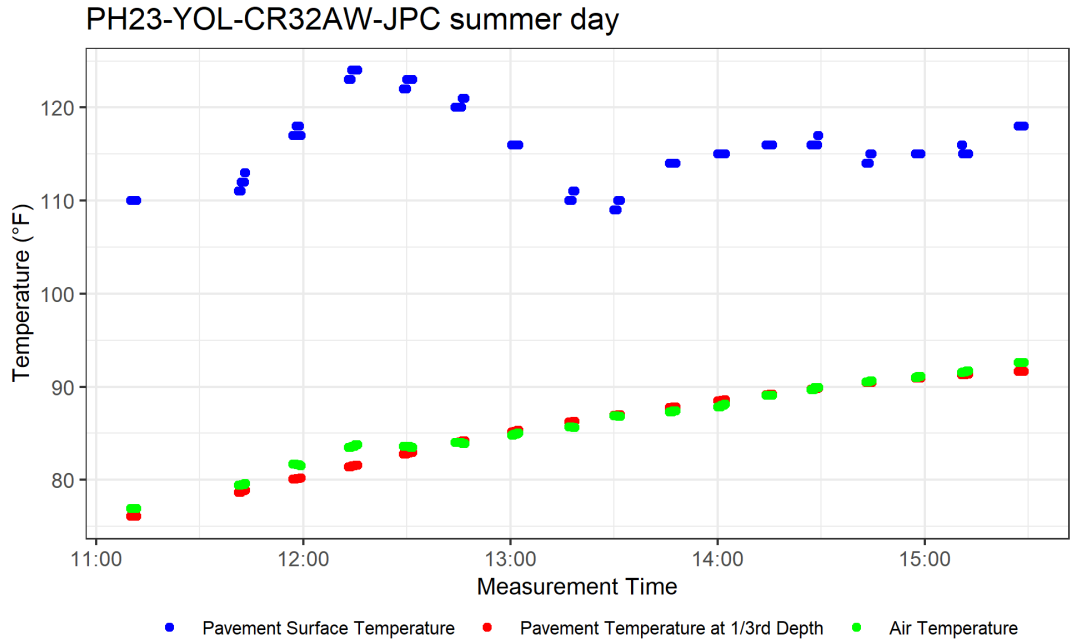


Figure N.7: Air, pavement surface, and one-third depth temperatures on 08/02/2016 testing day.

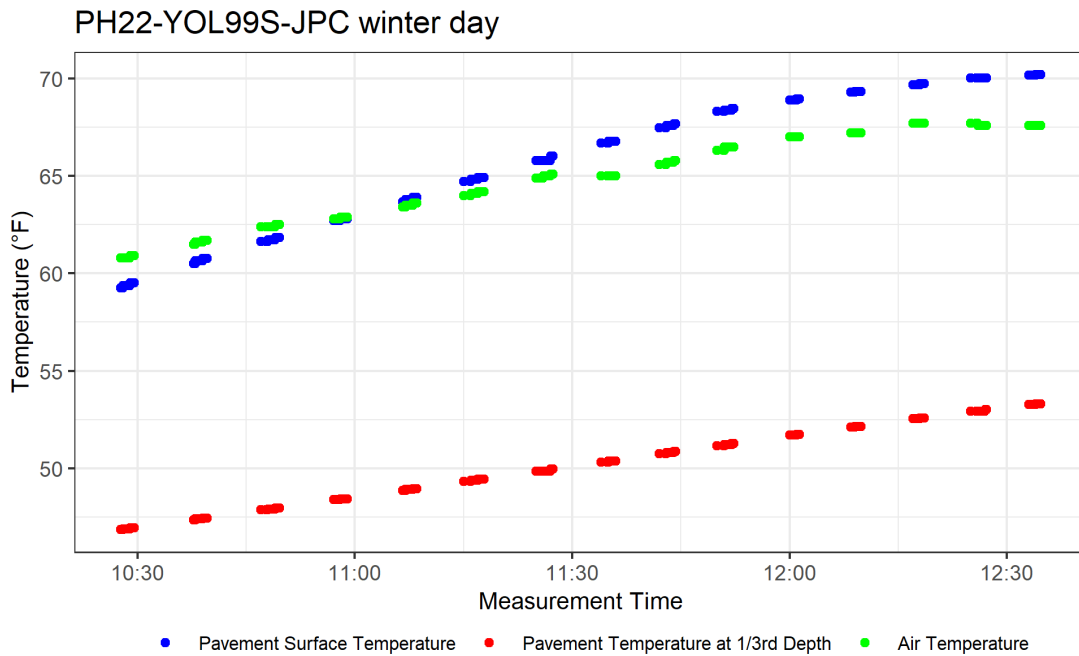


Figure N.8: Air, pavement surface, and one-third depth temperatures on 02/12/2016 testing day.

PH22-YOL99S-JPC summer day

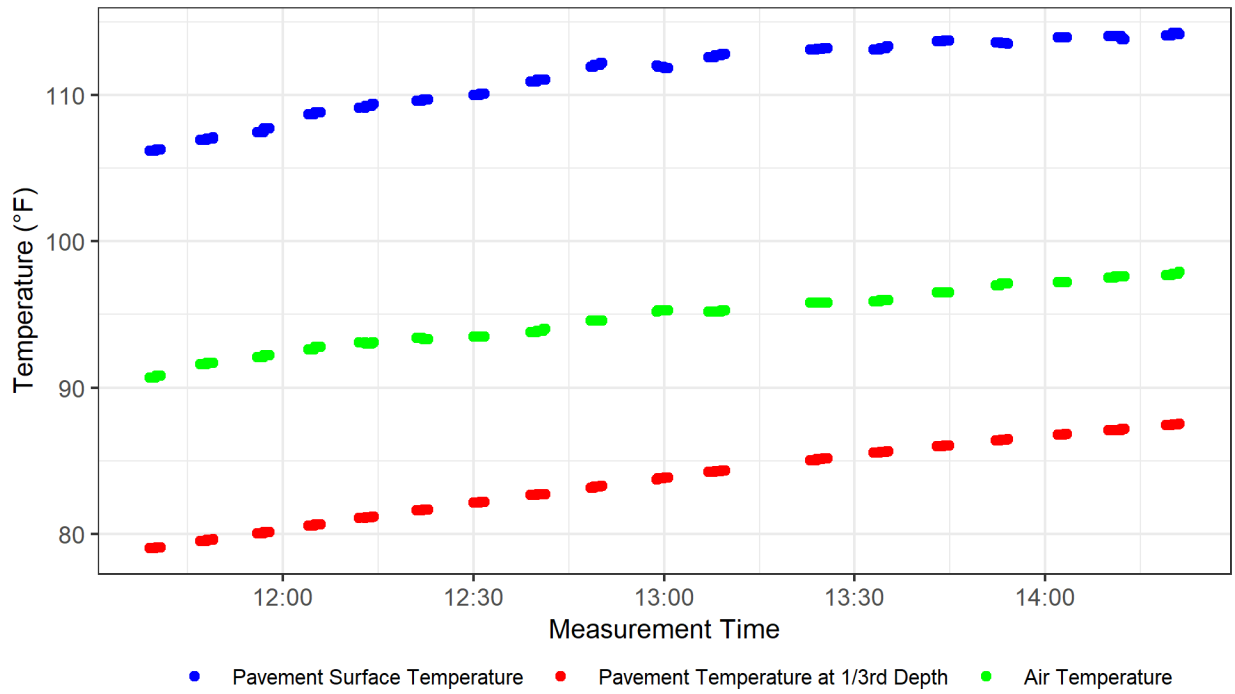


Figure N.9: Air, pavement surface, and one-third depth temperatures on 07/14/2016 testing day.

PH21-YOL99N-JPC winter day

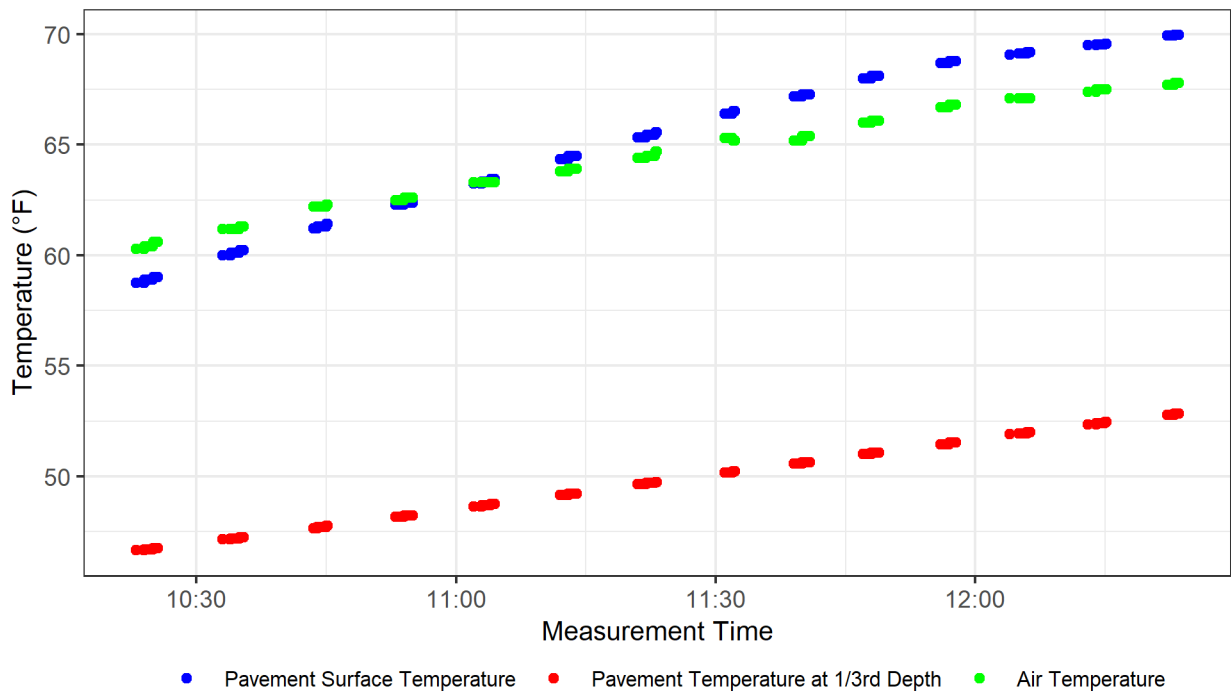


Figure N.10: Air, pavement surface, and one-third depth temperatures on 02/12/2016 testing day.

PH21-YOL99N-JPC summer day

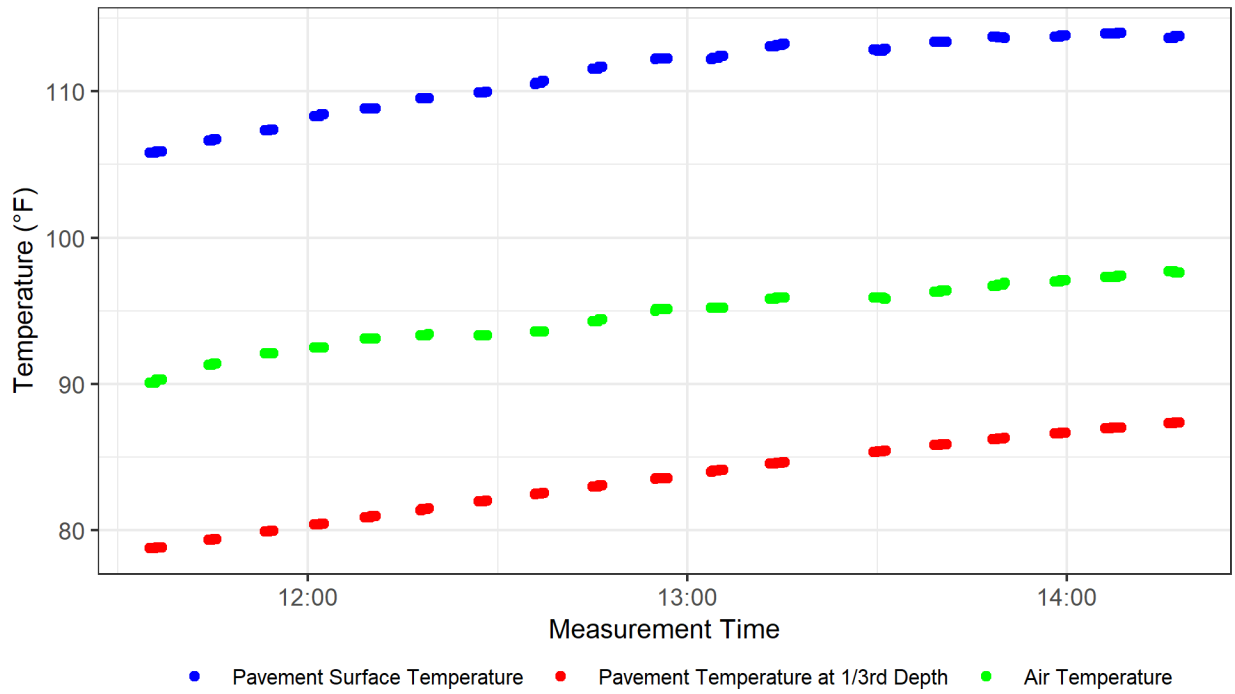


Figure N.11: Air, pavement surface, and one-third depth temperatures on 07/14/2016 testing day.

PH20-KER5S-CRCP winter night

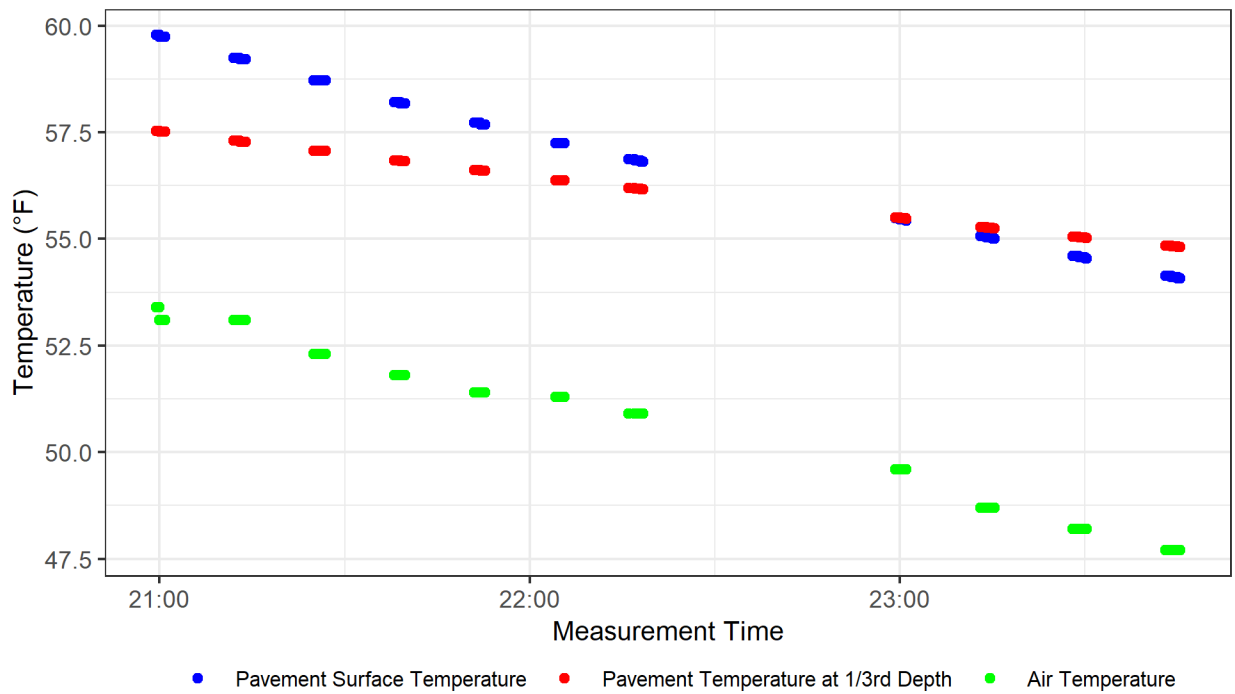


Figure N.12: Air, pavement surface, and one-third depth temperatures on 02/08/2016 testing day.

PH20-KER5S-CRCP summer day

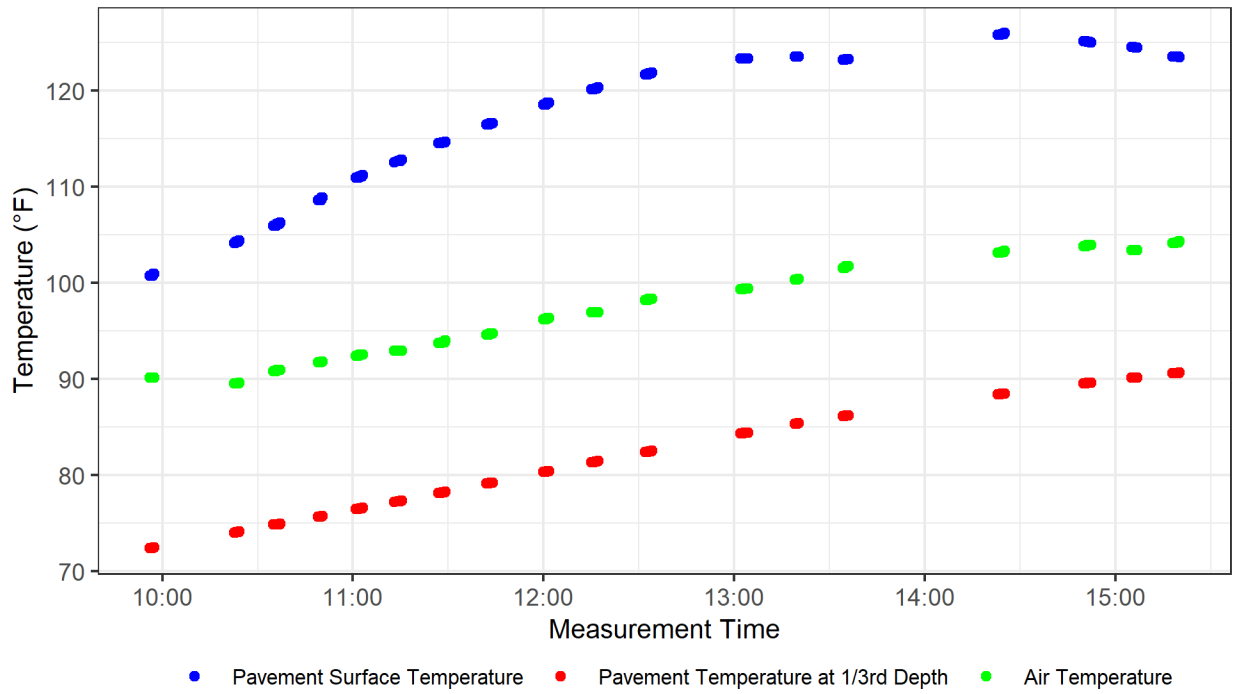


Figure N.13: Air, pavement surface, and one-third depth temperatures on 08/04/2016 testing day.

PH19-KER5N- RHMA-G winter night

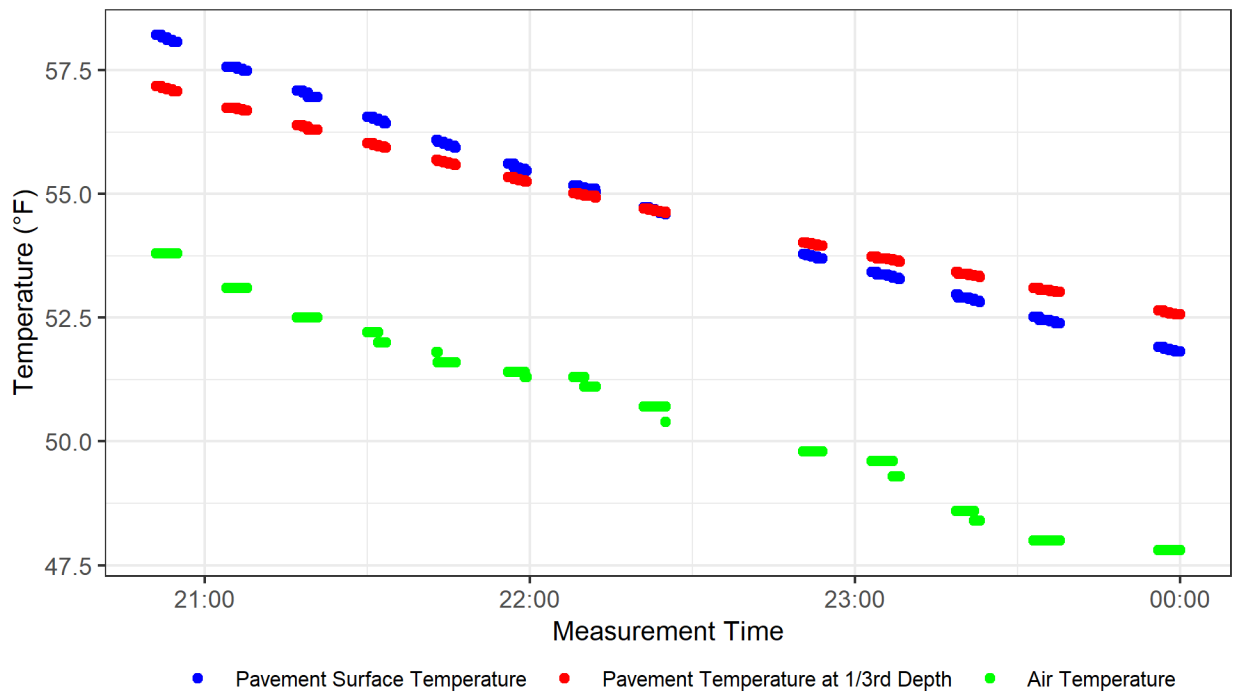


Figure N.14: Air, pavement surface, and one-third depth temperatures on 02/08/2016 testing day.

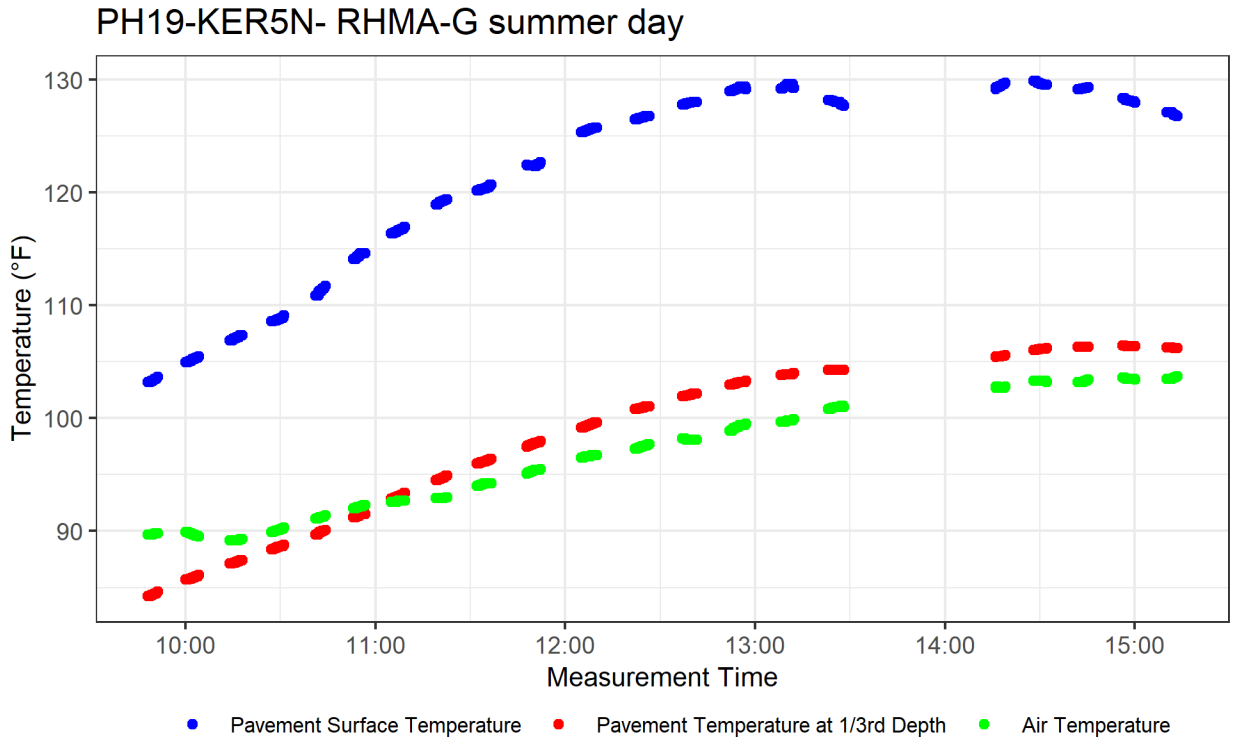


Figure N.15: Air, pavement surface, and one-third depth temperatures on 08/04/2016 testing day.

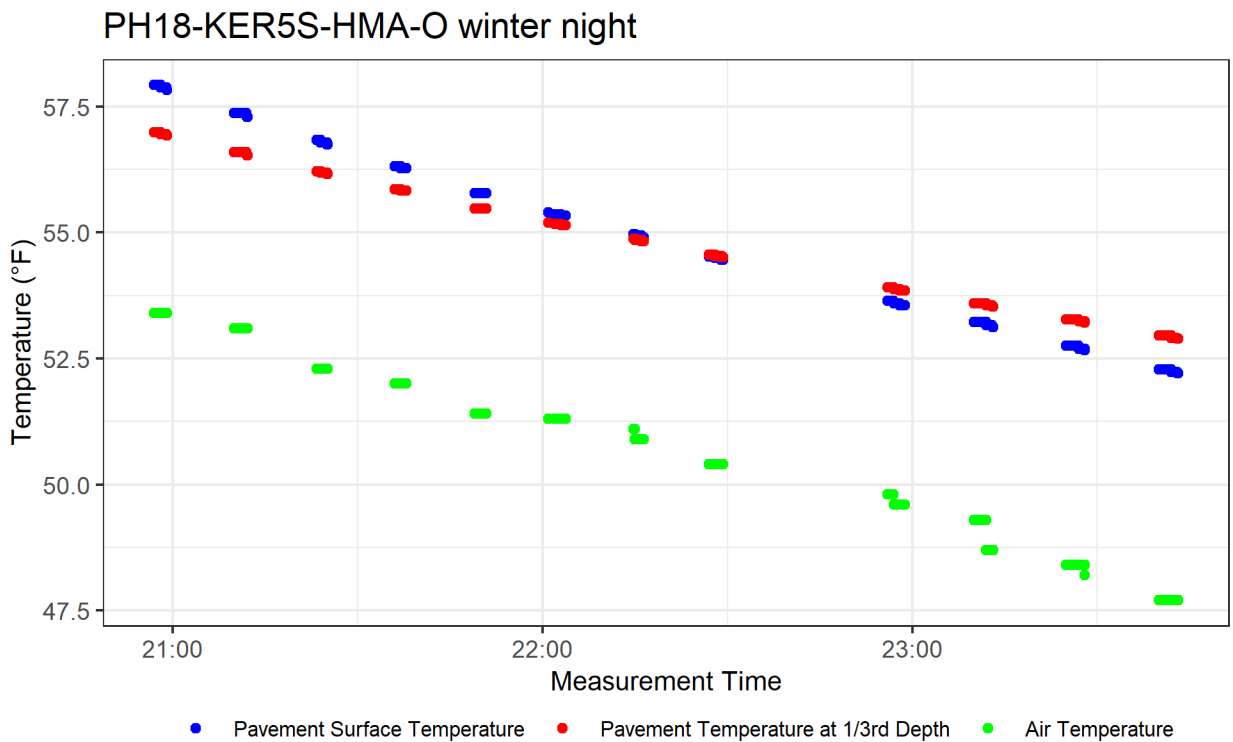


Figure N.16: Air, pavement surface, and one-third depth temperatures on 02/08/2016 testing day.

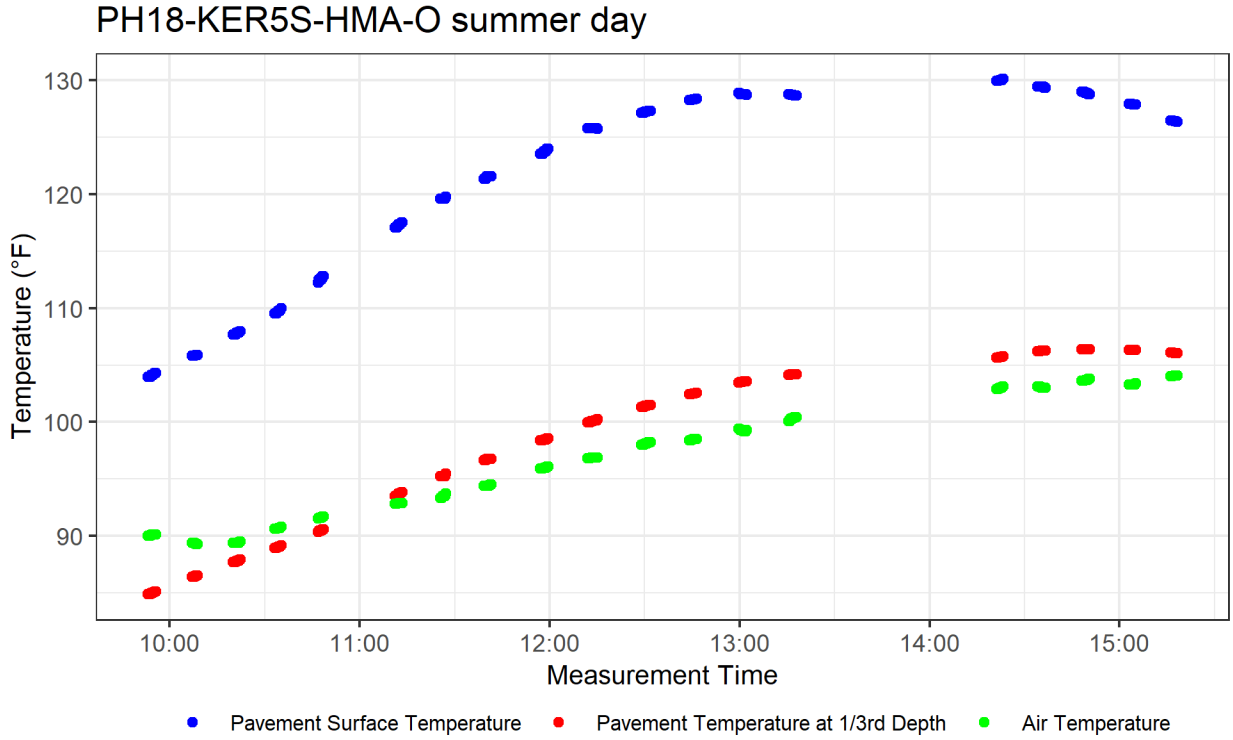


Figure N.17: Air, pavement surface, and one-third depth temperatures on 08/04/2016 testing day.

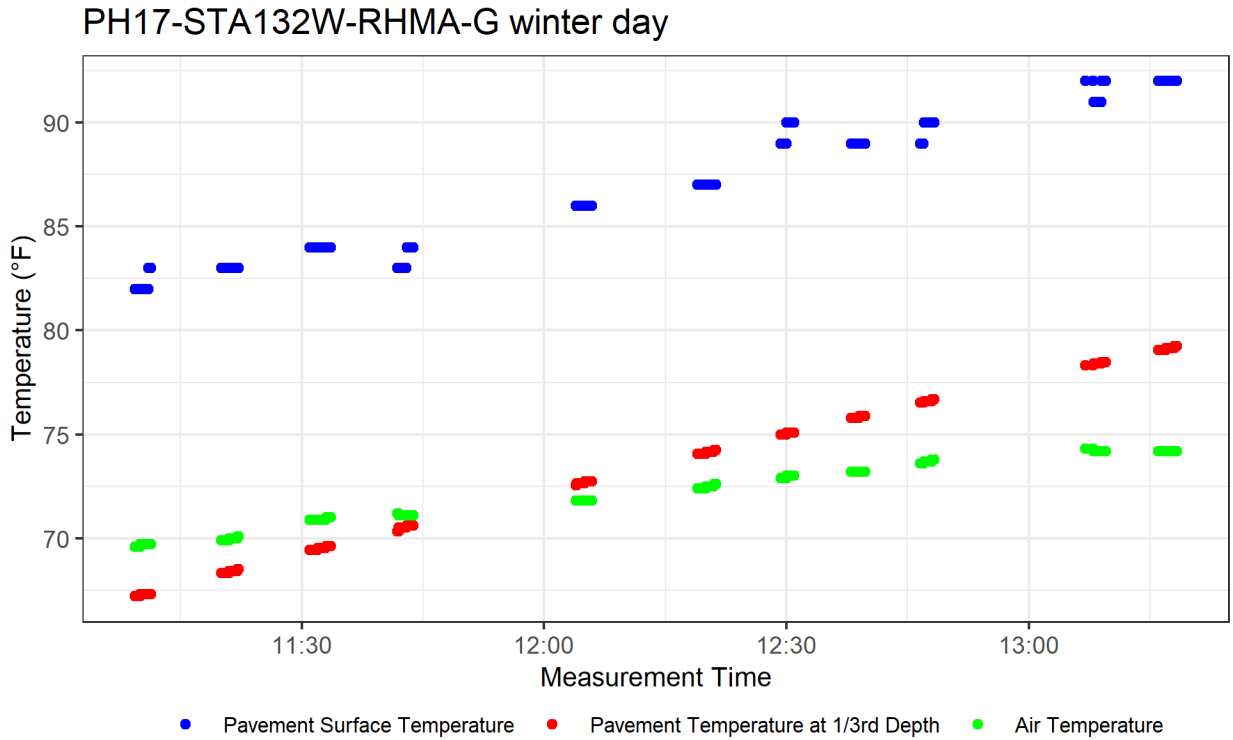


Figure N.18: Air, pavement surface, and one-third depth temperatures on 02/16/2016 testing day.

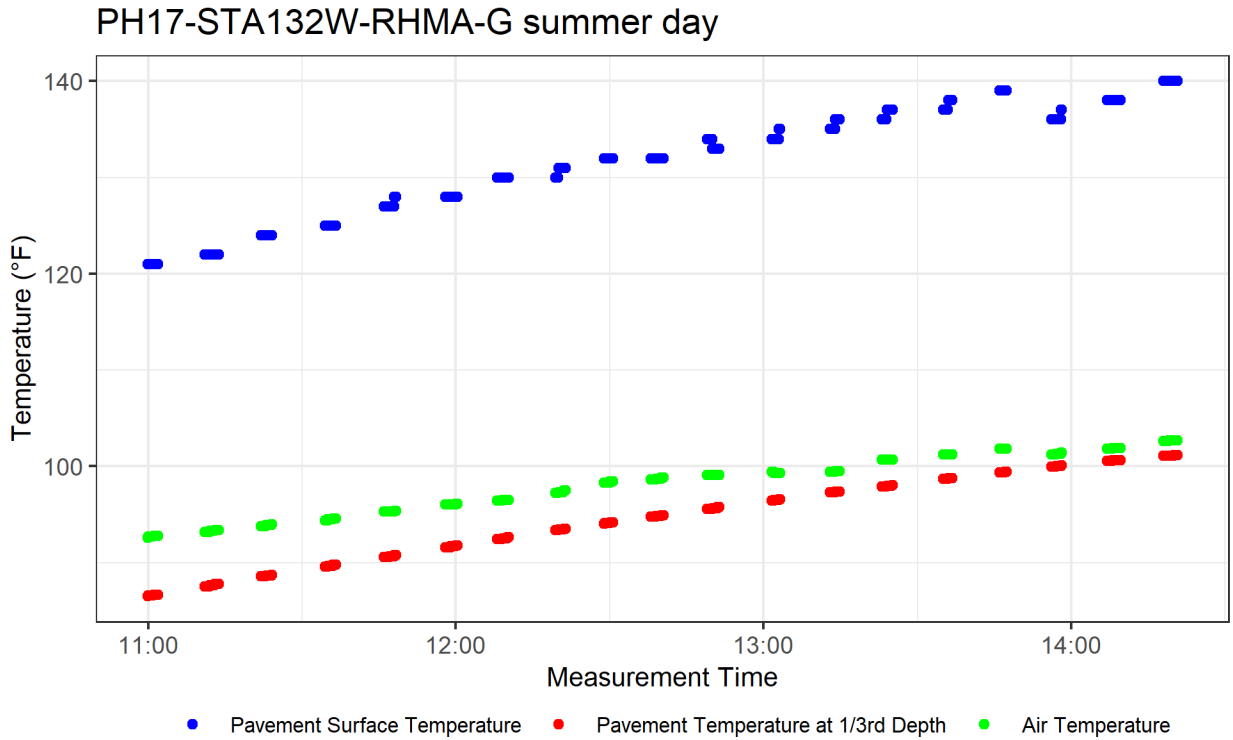


Figure N.19: Air, pavement surface, and one-third depth temperatures on 07/27/2016 testing day.

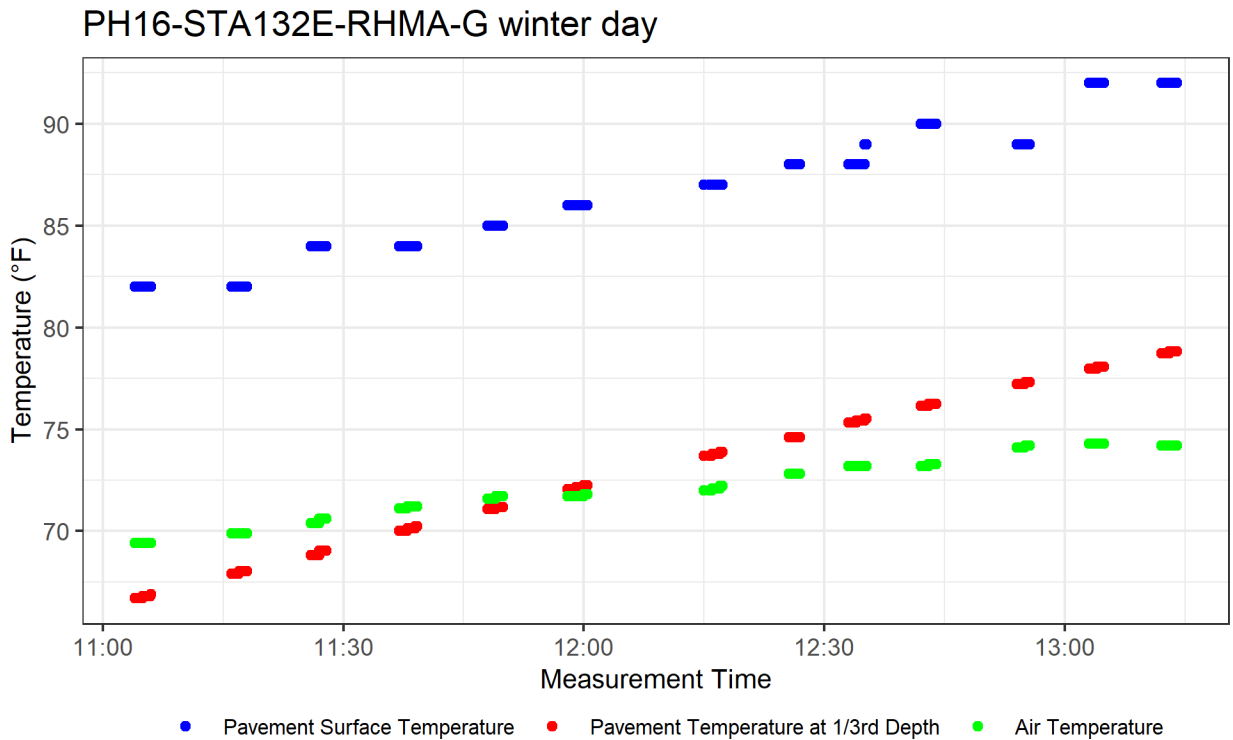


Figure N.20: Air, pavement surface, and one-third depth temperatures on 02/16/2016 testing day.

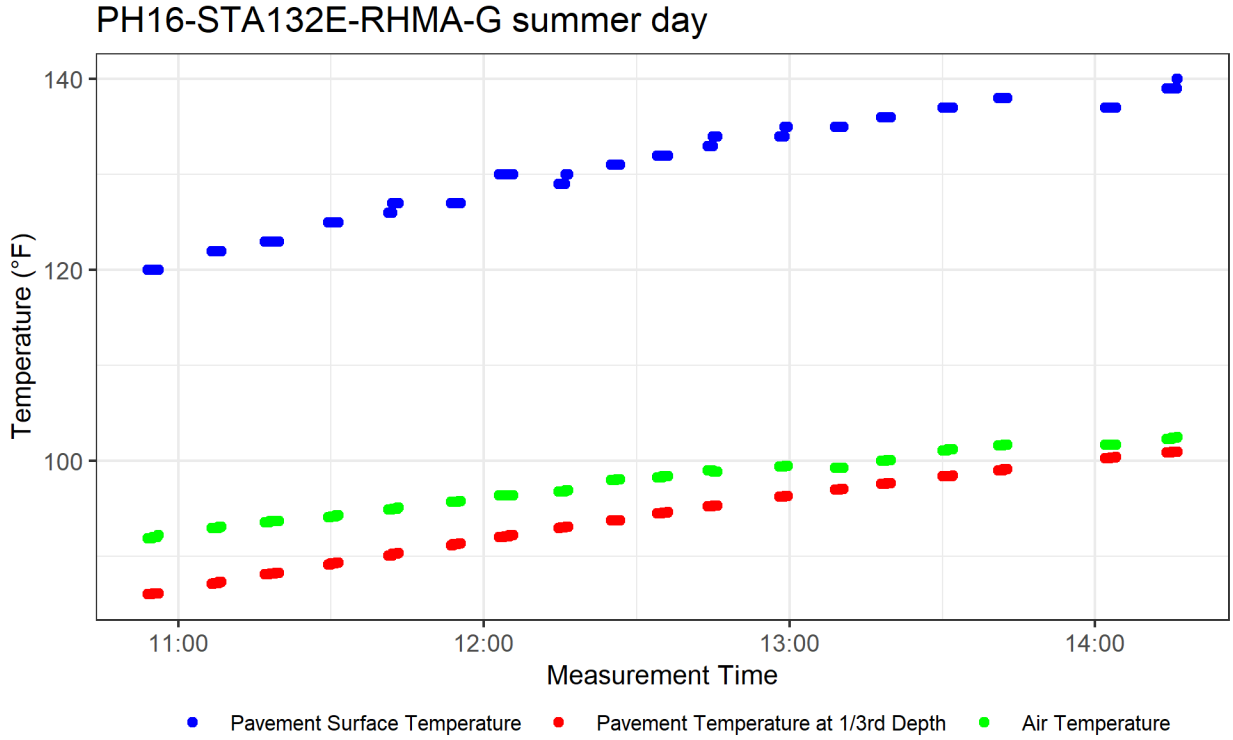


Figure N.21: Air, pavement surface, and one-third depth temperatures on 07/27/2016 testing day.

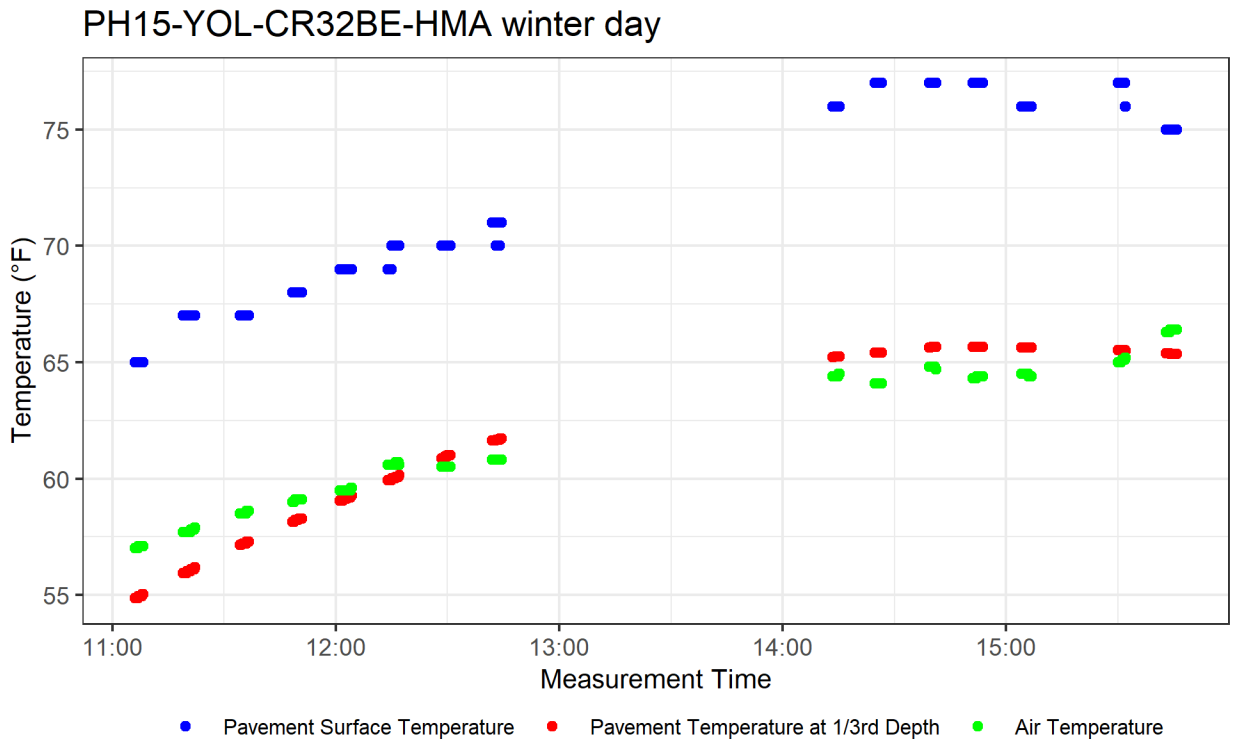


Figure N.22: Air, pavement surface, and one-third depth temperatures on 01/27/2016 testing day.

PH15-YOL-CR32BE-HMA summer night

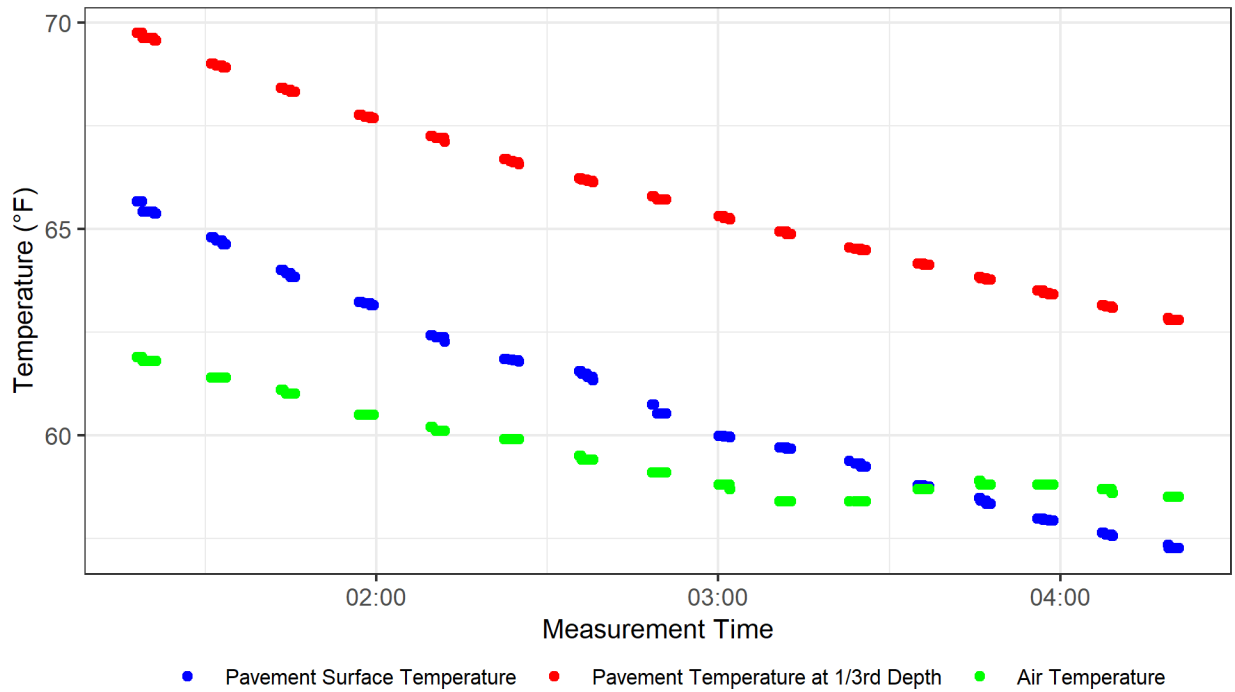


Figure N.23: Air, pavement surface, and one-third depth temperatures on 08/10/2016 testing day.

PH15-YOL-CR32BE-HMA summer day

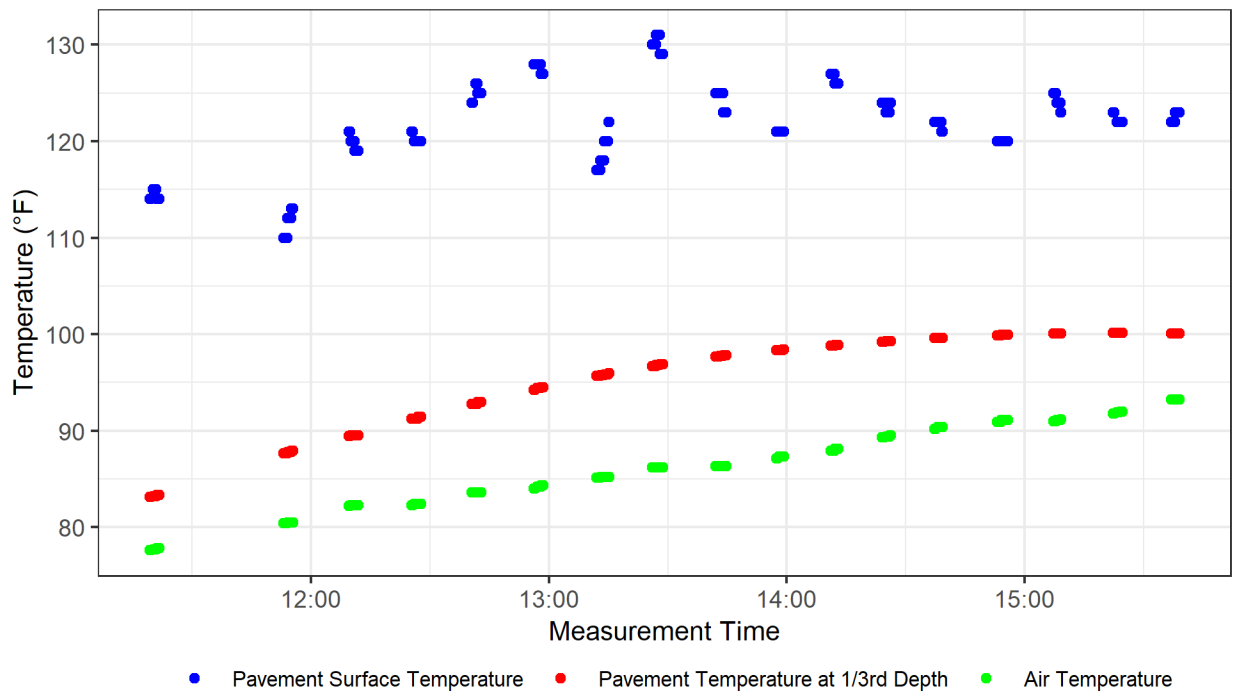


Figure N.24: Air, pavement surface, and one-third depth temperatures on 08/02/2016 testing day.

PH14-SUT113S-HMA winter day

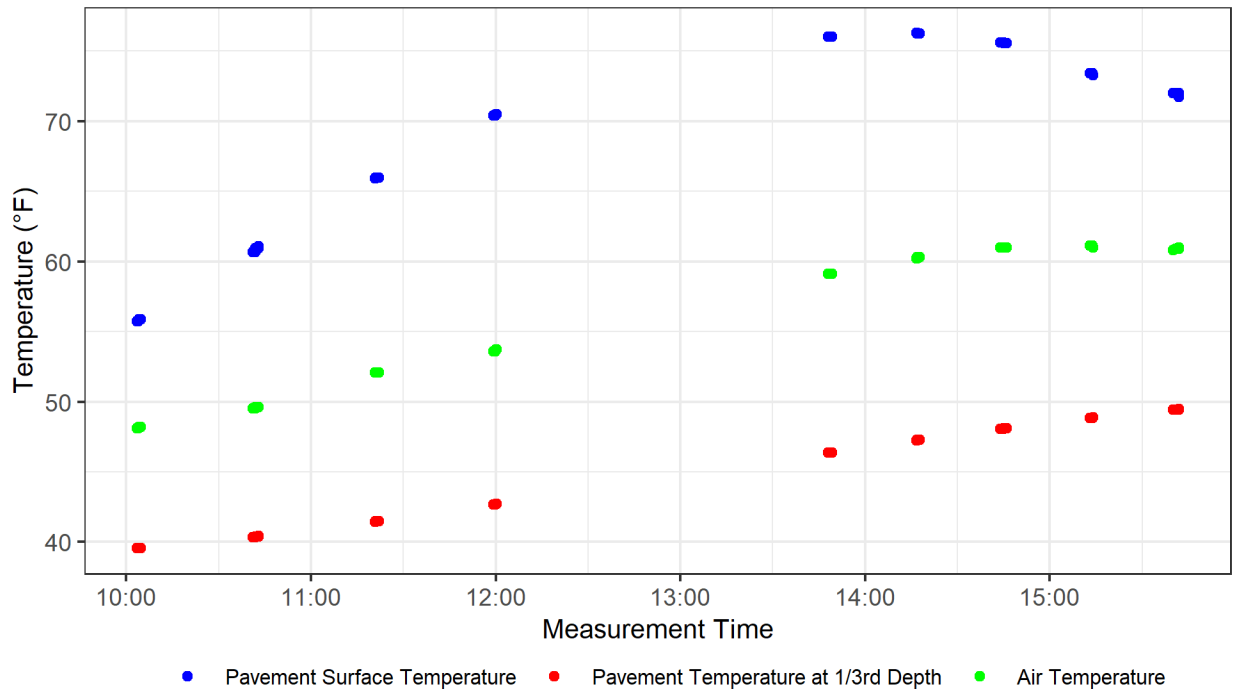


Figure N.25: Air, pavement surface, and one-third depth temperatures on 02/05/2016 testing day.

PH14-SUT113S-HMA summer day

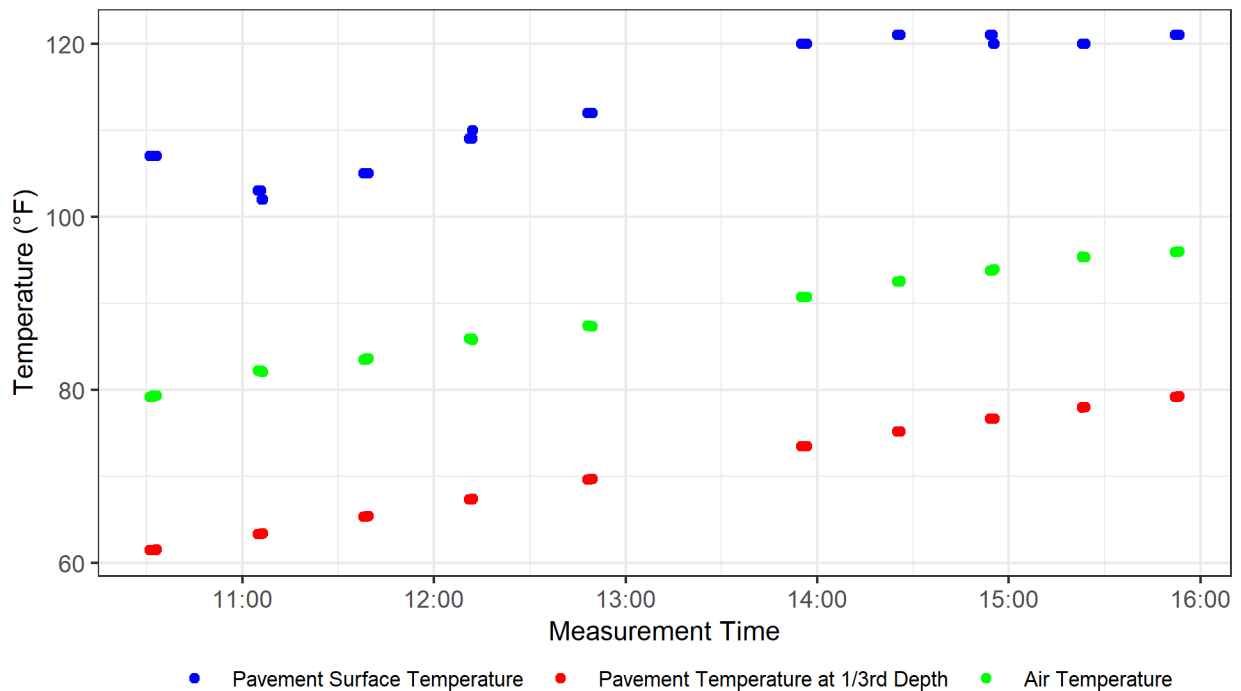


Figure N.26: Air, pavement surface, and one-third depth temperatures on 07/25/2016 testing day.

PH13-SUT113N-HMA winter day

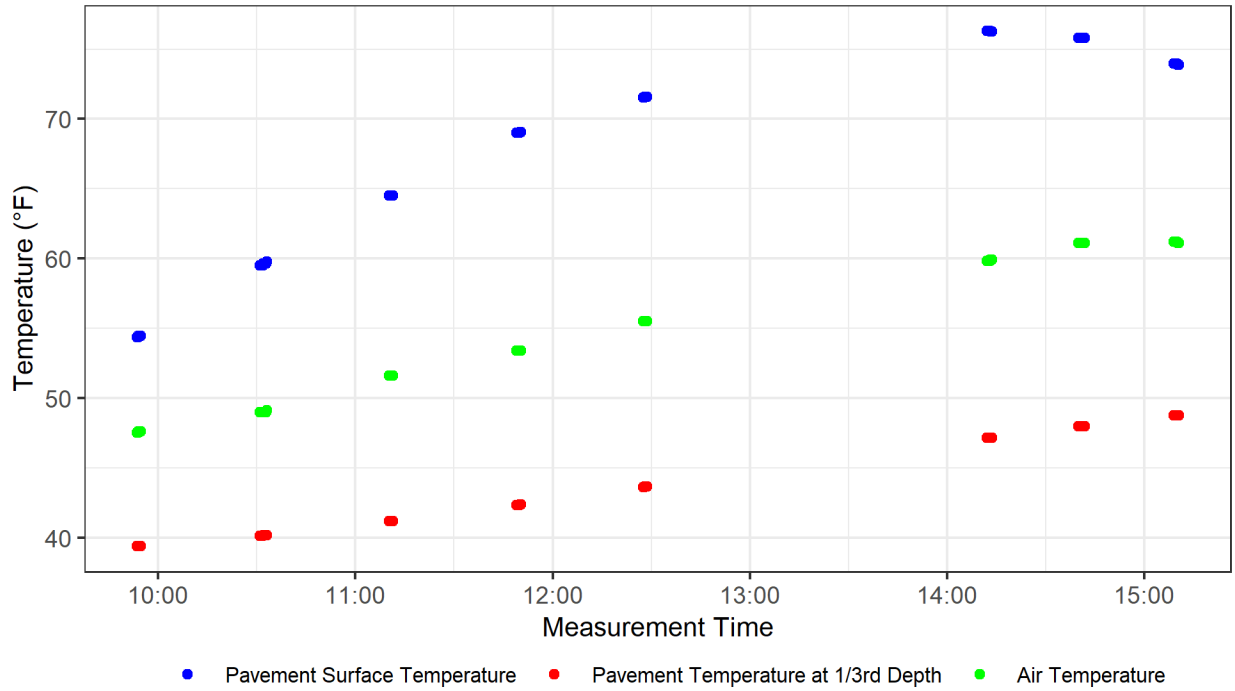


Figure N.27: Air, pavement surface, and one-third depth temperatures on 02/05/2016 testing day.

PH13-SUT113N-HMA summer day

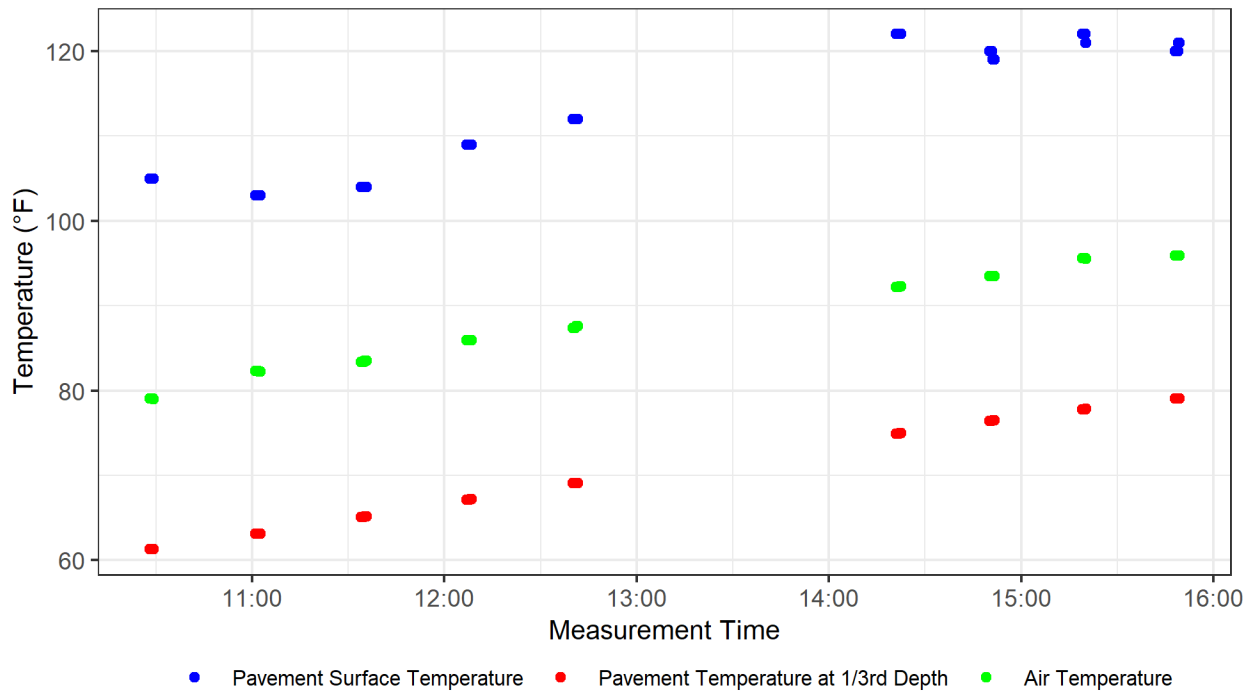


Figure N.28: Air, pavement surface, and one-third depth temperatures on 07/25/2016 testing day.

PH12-SUT113S-HMA winter day

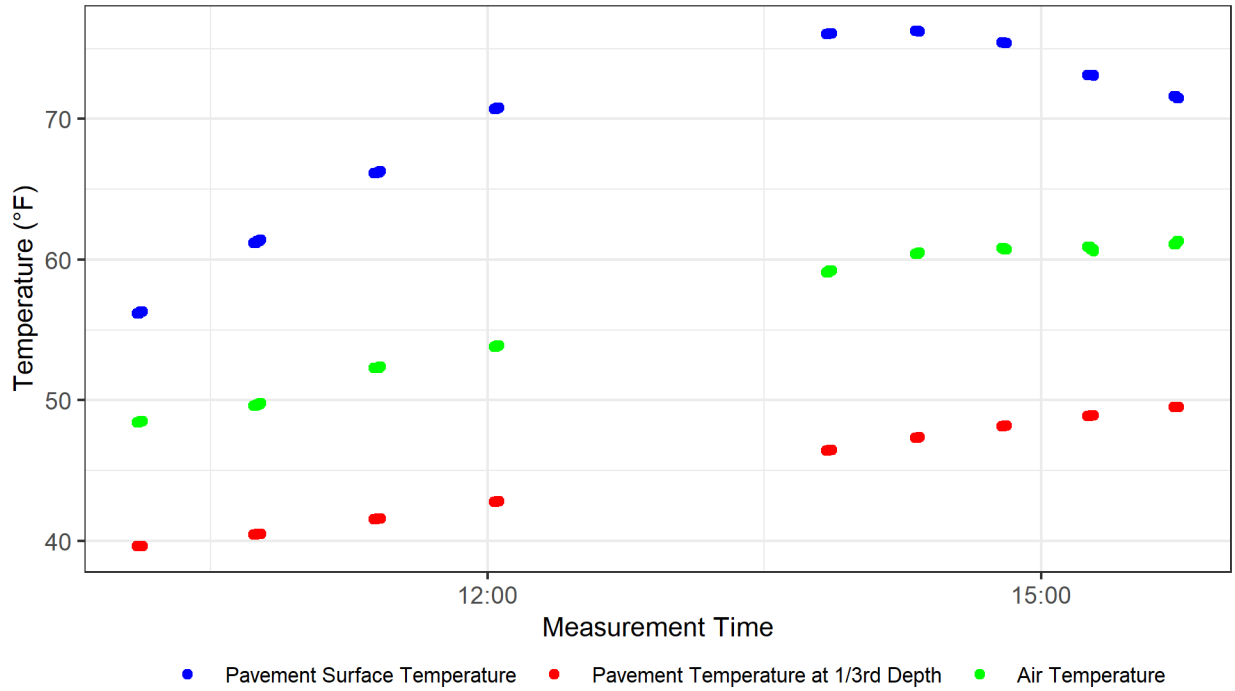


Figure N.29: Air, pavement surface, and one-third depth temperatures on 02/05/2016 testing day.

PH12-SUT113S-HMA summer day

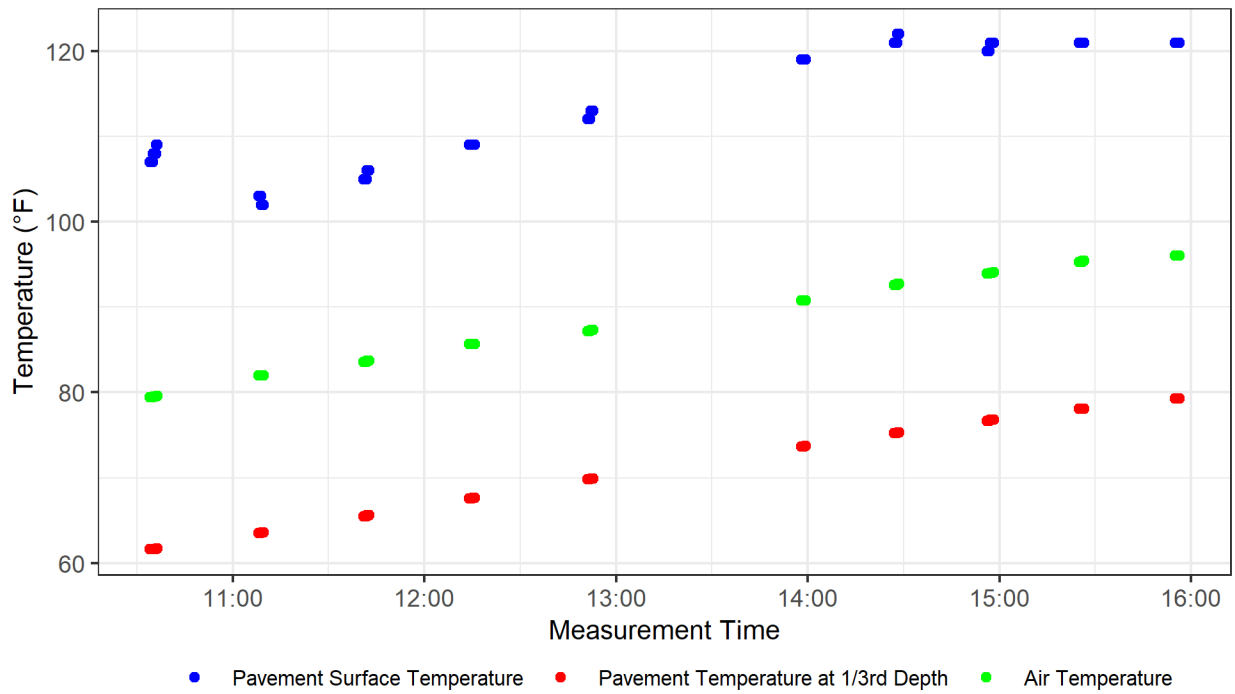


Figure N.30: Air, pavement surface, and one-third depth temperatures on 07/25/2016 testing day.

PH11-SUT113N-HMA winter day

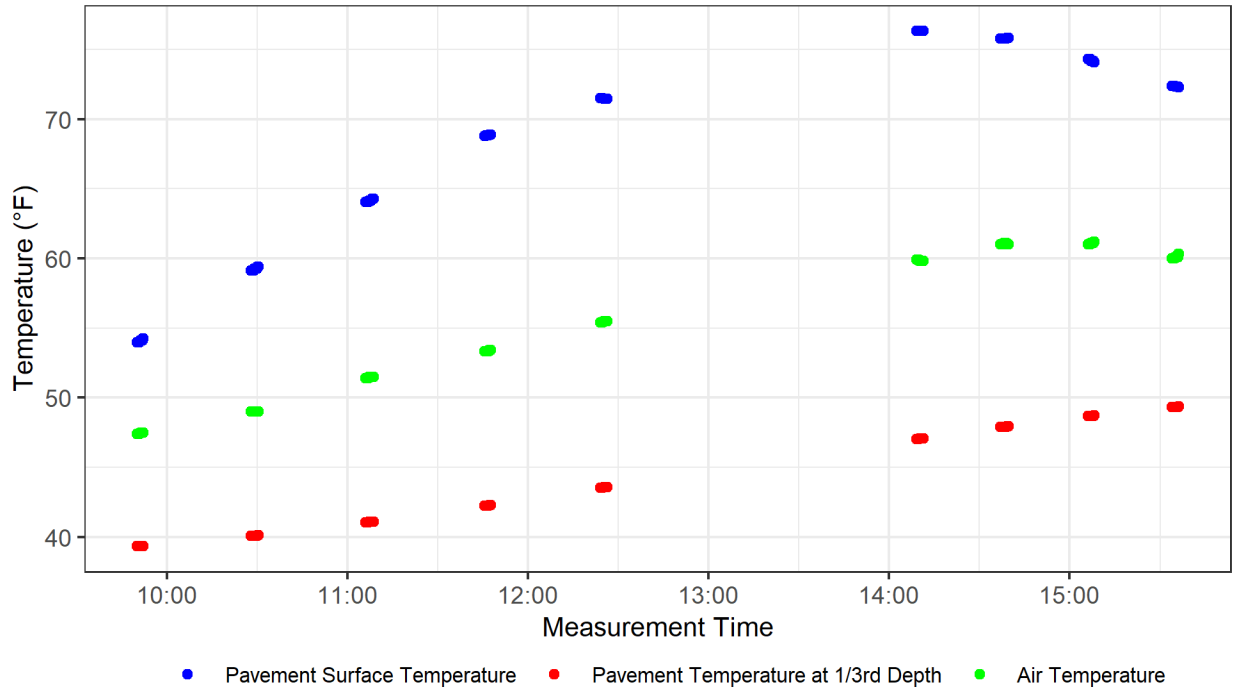


Figure N.31: Air, pavement surface, and one-third depth temperatures on 02/05/2016 testing day.

PH11-SUT113N-HMA summer day

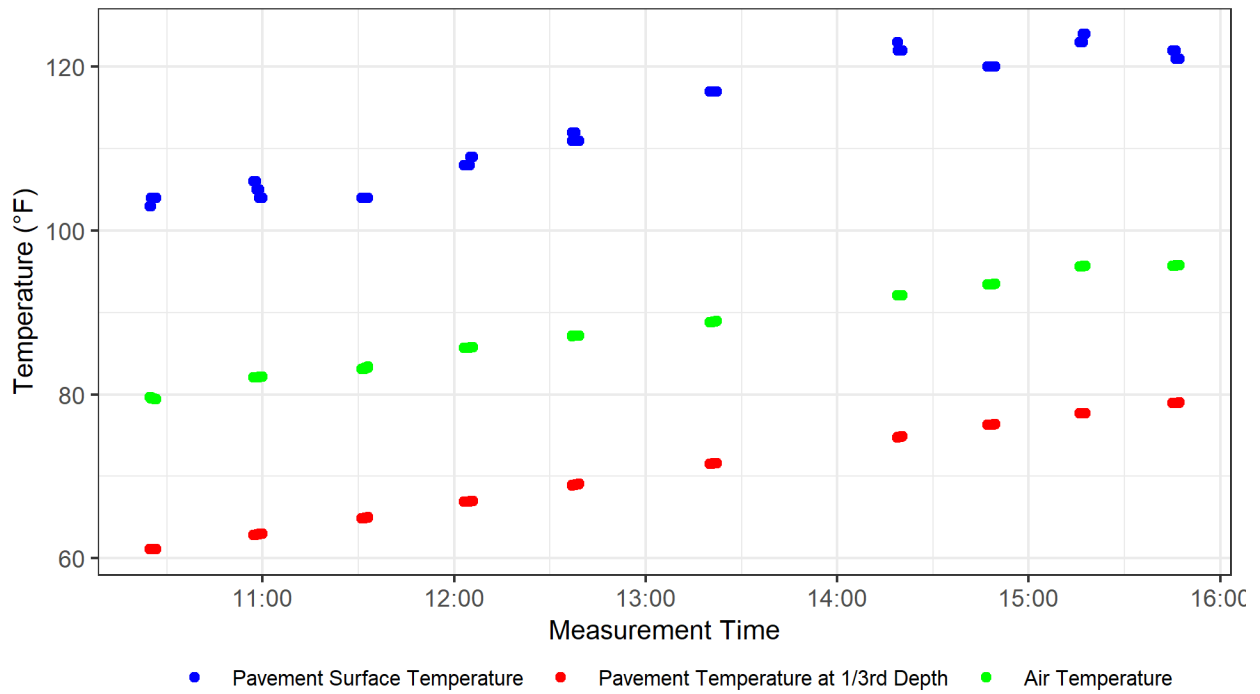


Figure N.32: Air, pavement surface, and one-third depth temperatures on 07/25/2016 testing day.

PH10-SUT113S-RHMA-O winter day

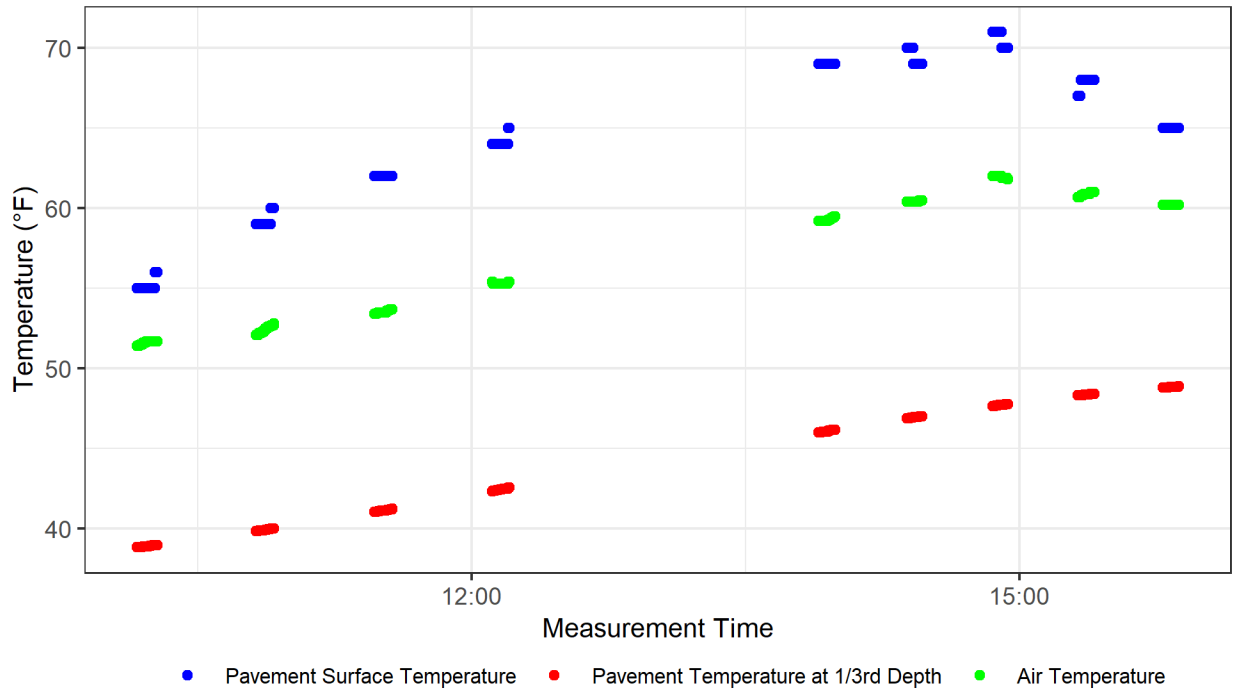


Figure N.33: Air, pavement surface, and one-third depth temperatures on 02/05/2016 testing day.

PH10-SUT113S-RHMA-O summer day

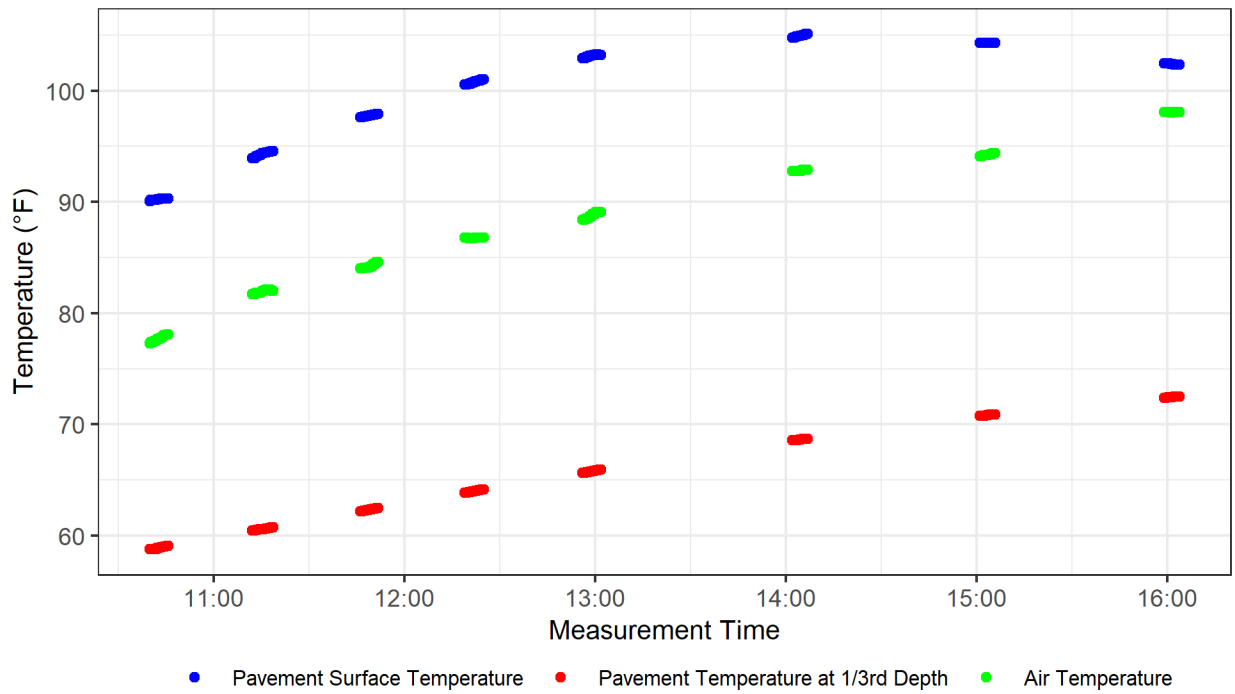


Figure N.34: Air, pavement surface, and one-third depth temperatures on 07/25/2016 testing day.

PH09-SUT113N-RHMA-O winter day

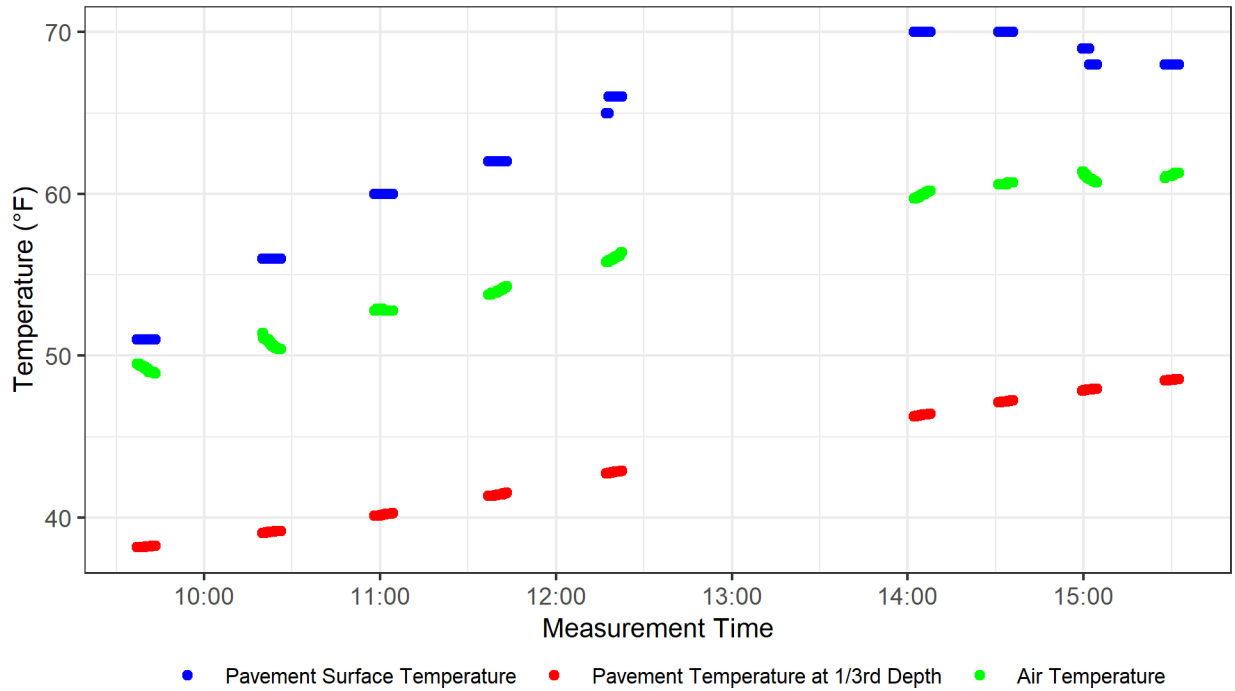


Figure N.35: Air, pavement surface, and one-third depth temperatures on 02/05/2016 testing day.

PH09-SUT113N-RHMA-O summer day

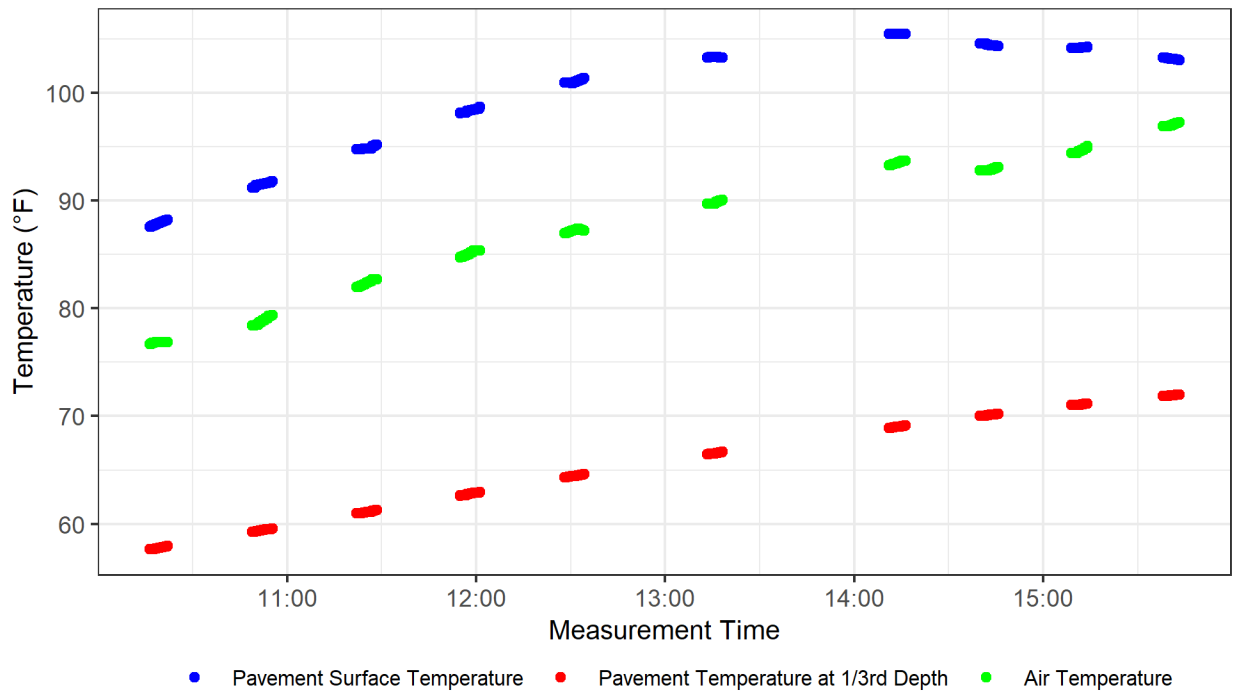


Figure N.36: Air, pavement surface, and one-third depth temperatures on 07/25/2016 testing day.

PH08-YOL-CR29E-HMA winter day

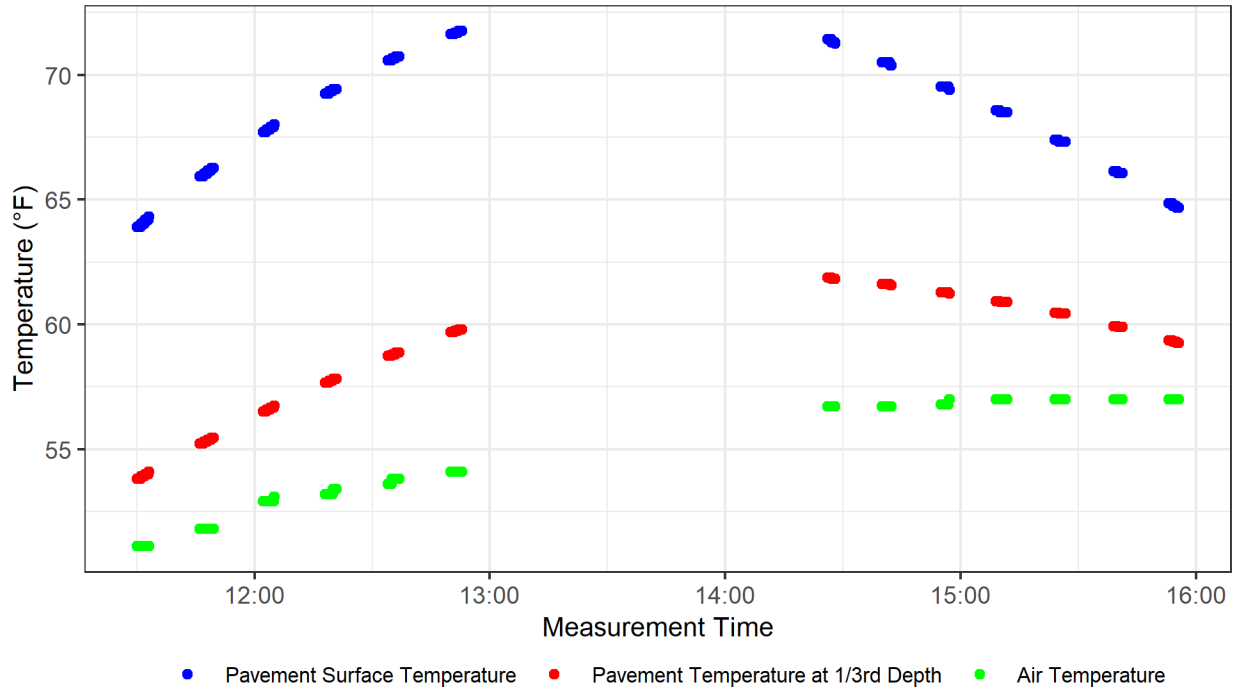


Figure N.37: Air, pavement surface, and one-third depth temperatures on 01/26/2016 testing day.

PH08-YOL-CR29E-HMA summer night

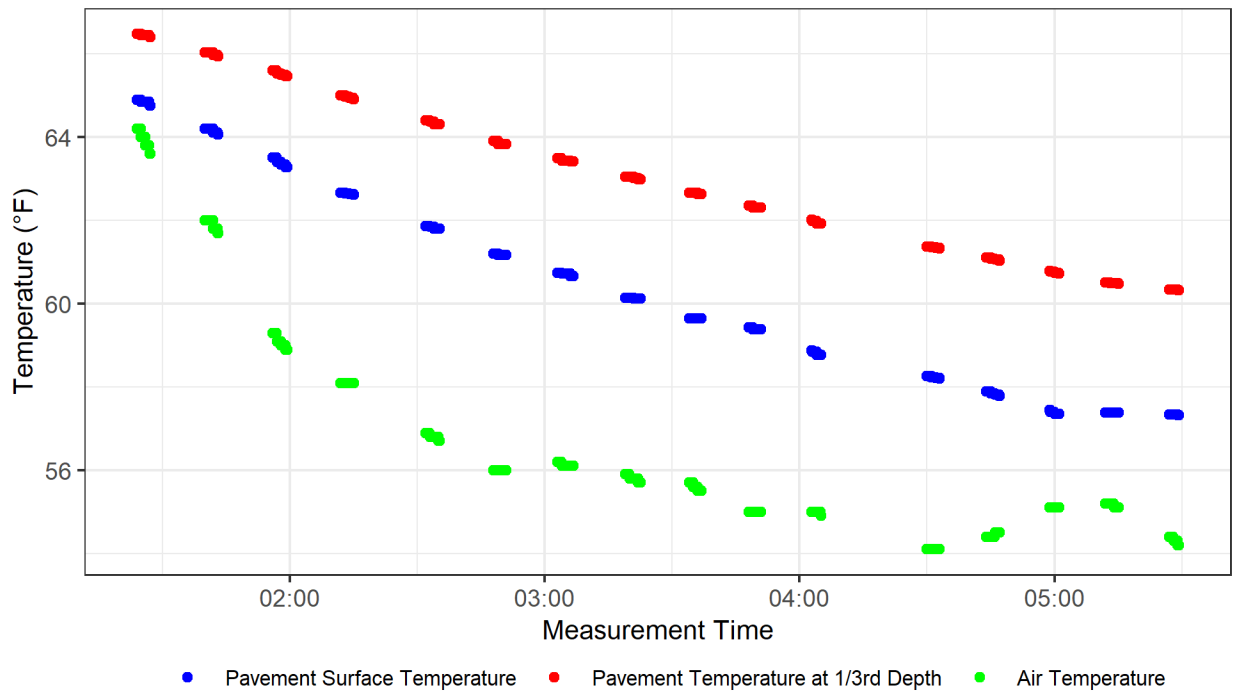


Figure N.38: Air, pavement surface, and one-third depth temperatures on 08/08/2016 testing day.

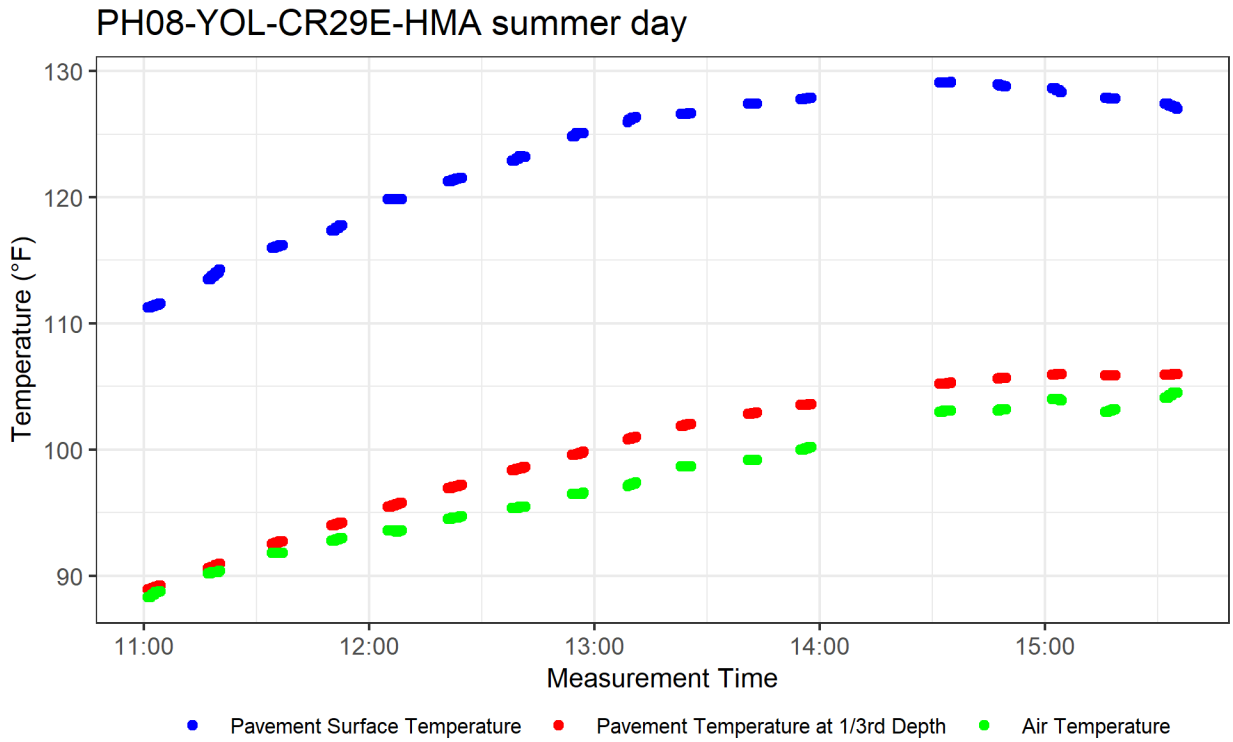


Figure N.39: Air, pavement surface, and one-third depth temperatures on 07/26/2016 testing day.

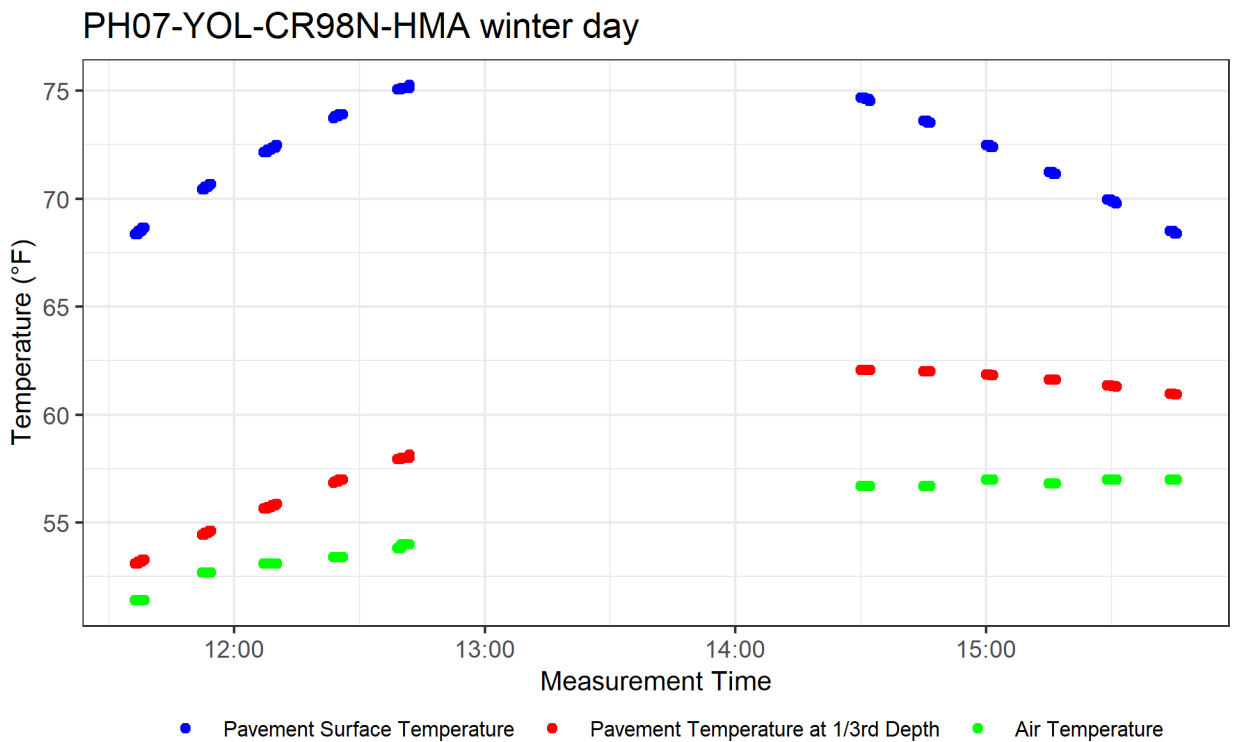


Figure N.40: Air, pavement surface, and one-third depth temperatures on 01/26/2016 testing day.

PH07-YOL-CR98N-HMA summer night

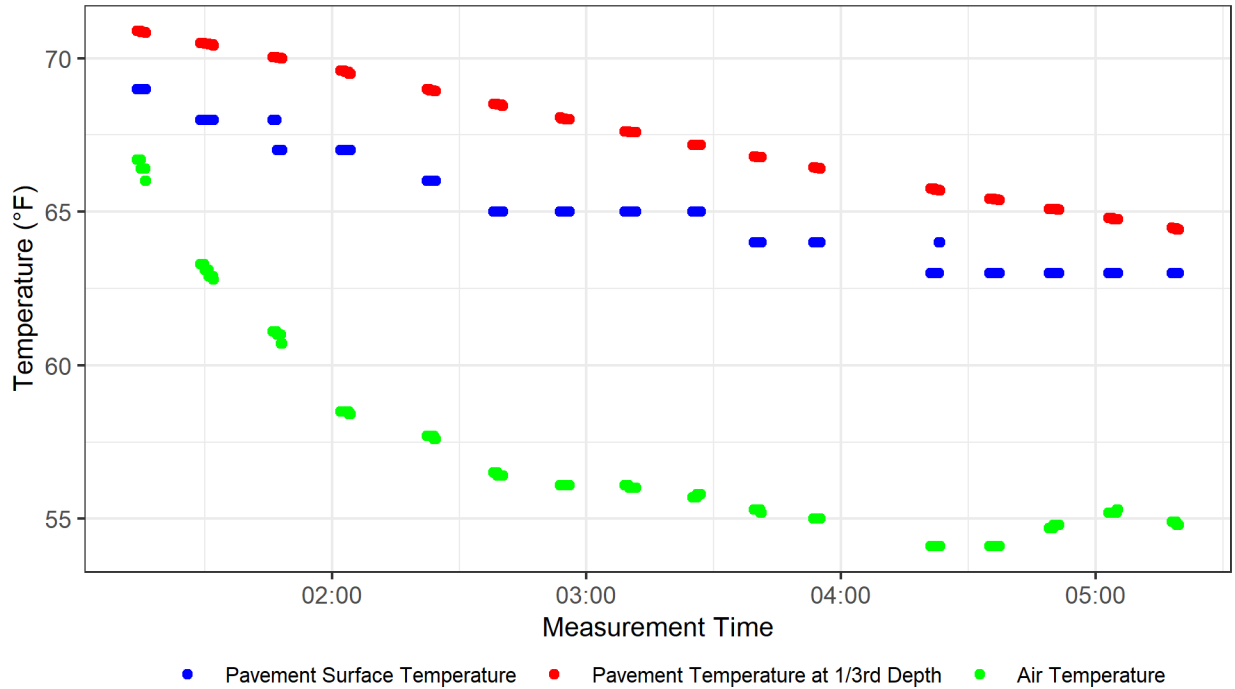


Figure N.41: Air, pavement surface, and one-third depth temperatures on 08/08/2016 testing day.

PH07-YOL-CR98N-HMA summer day

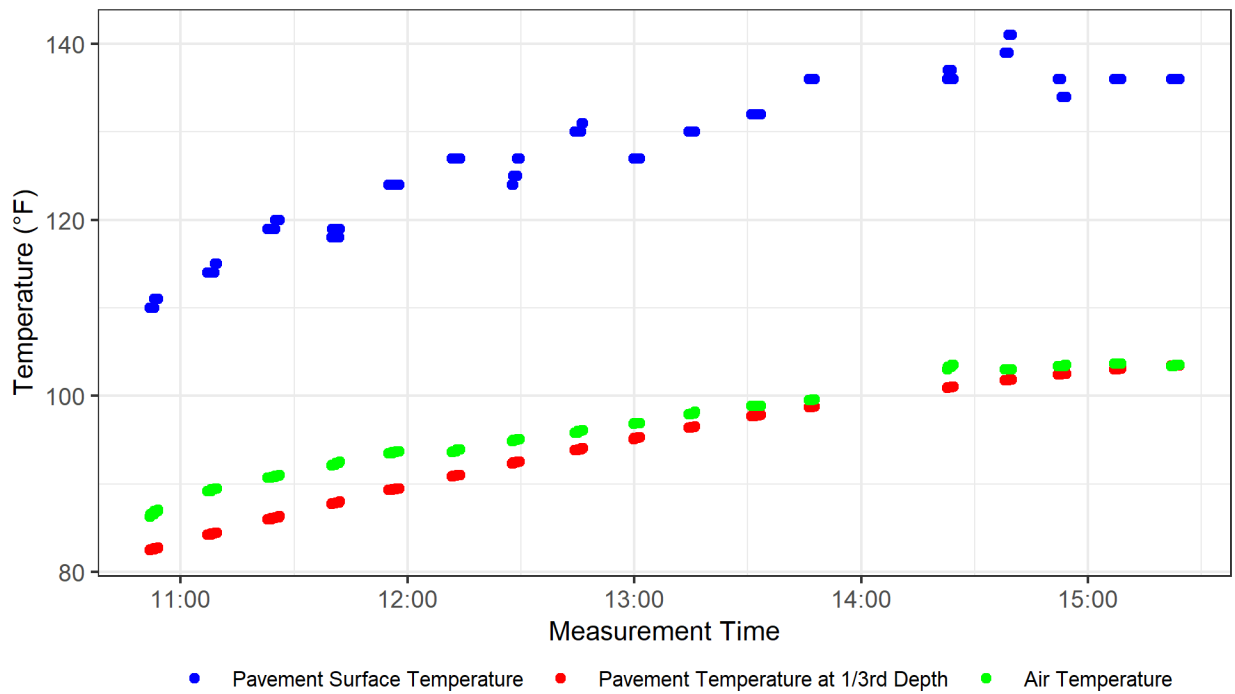


Figure N.42: Air, pavement surface, and one-third depth temperatures on 07/26/2016 testing day.

PH04-YOL505S-RHMA-G winter day

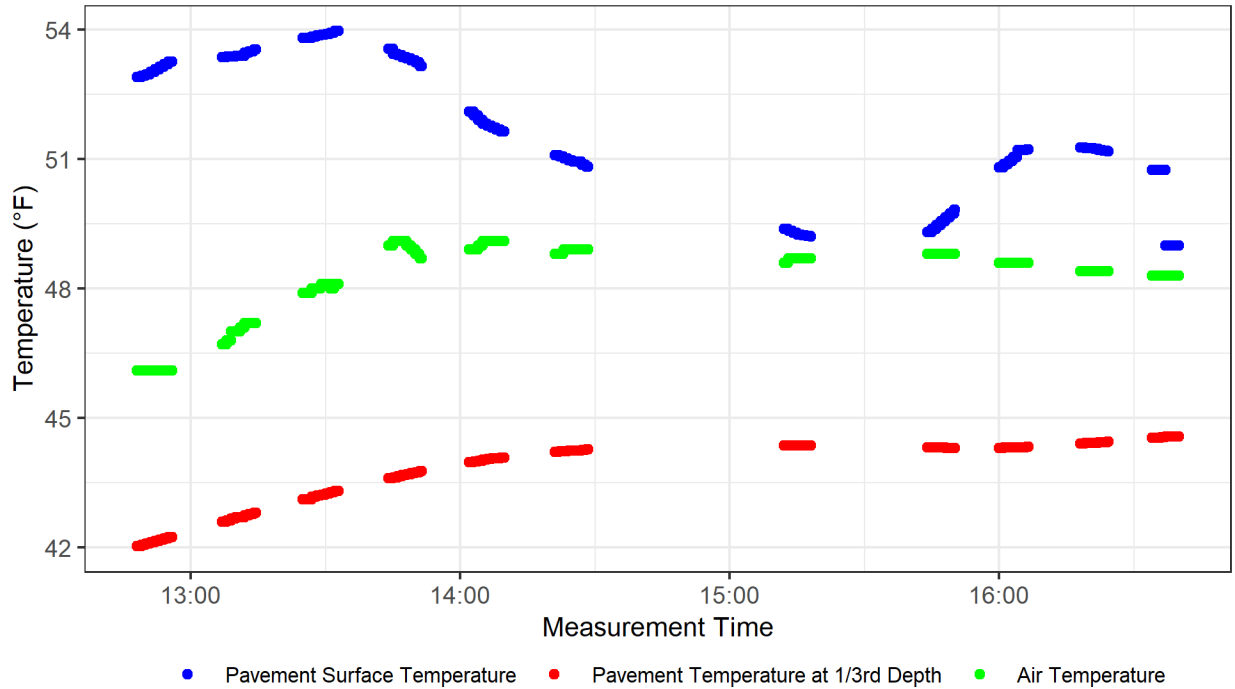


Figure N.43: Air, pavement surface, and one-third depth temperatures on 02/02/2016 testing day.

PH04-YOL505S-RHMA-G summer night

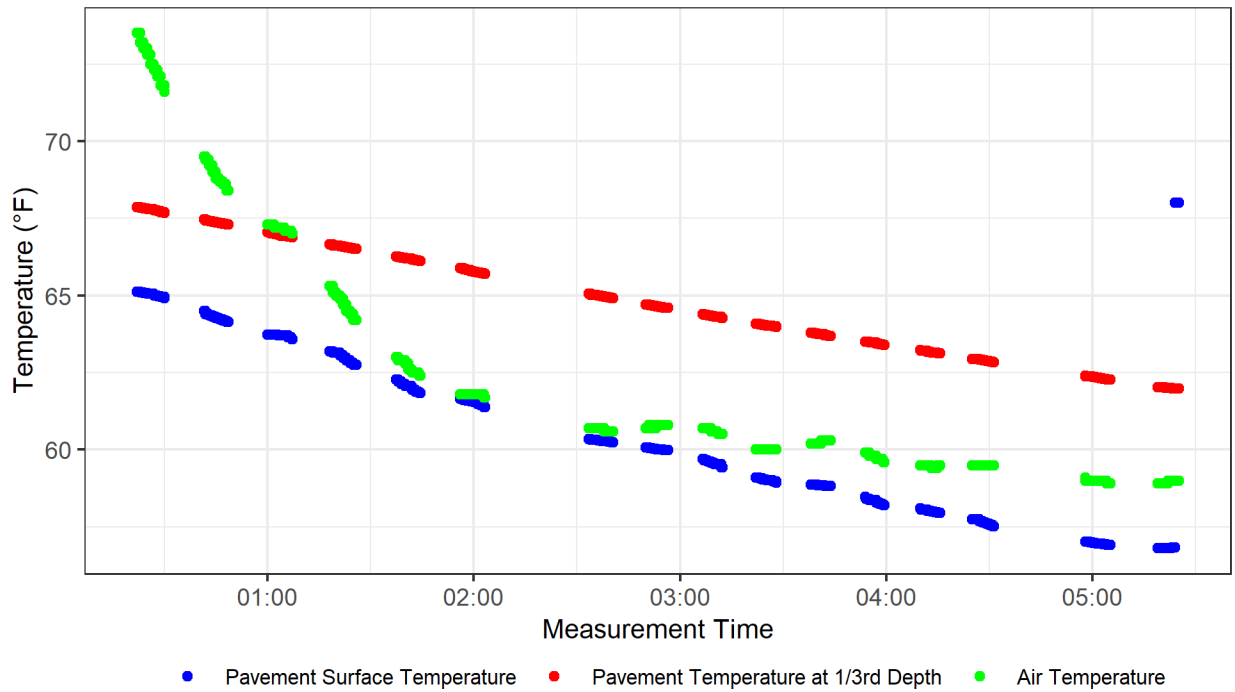


Figure N.44: Air, pavement surface, and one-third depth temperatures on 08/09/2016 testing day.

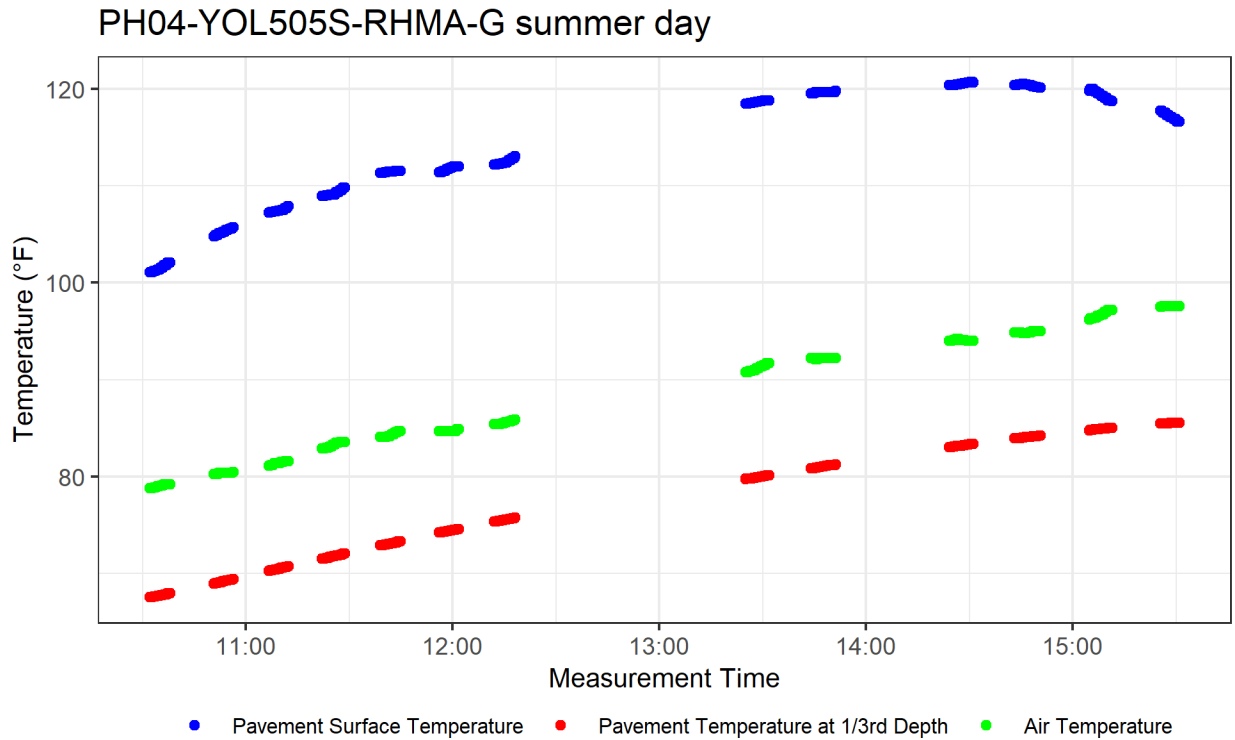


Figure N.45: Air, pavement surface, and one-third depth temperatures on 07/15/2016 testing day.

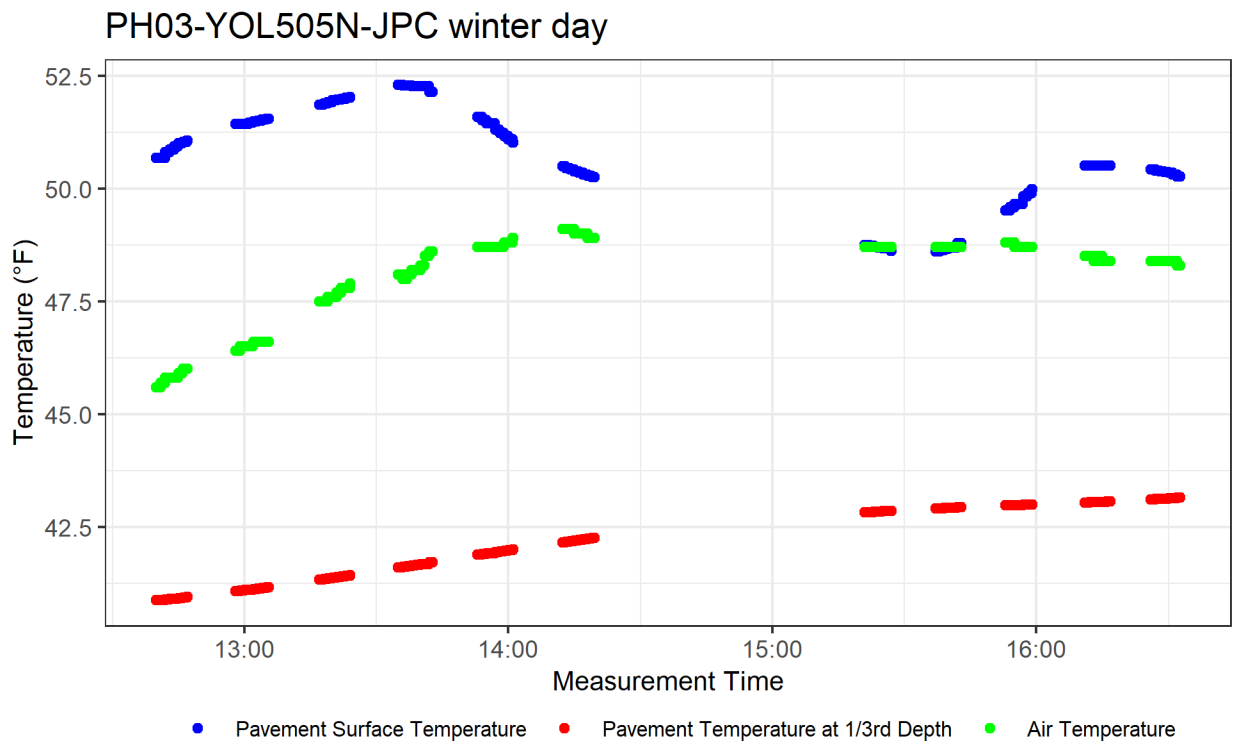


Figure N.46: Air, pavement surface, and one-third depth temperatures on 02/02/2016 testing day.

PH03-YOL505N-JPC summer night

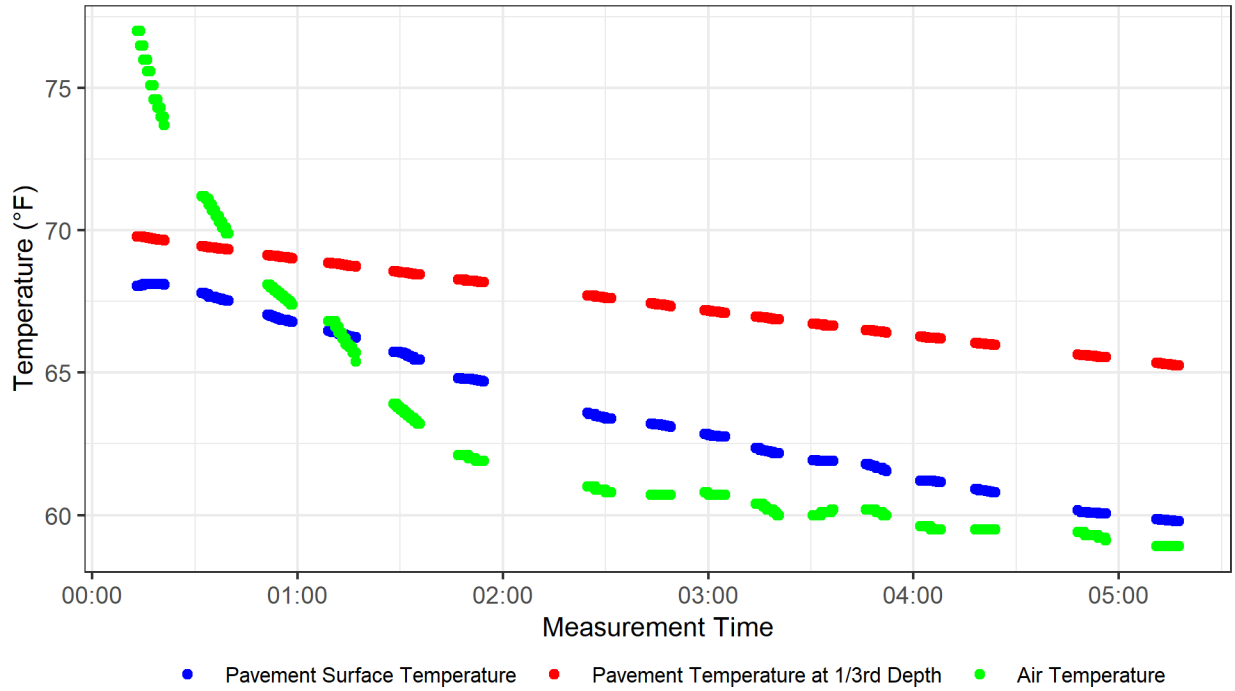


Figure N.47: Air, pavement surface, and one-third depth temperatures on 08/09/2016 testing day.

PH03-YOL505N-JPC summer day

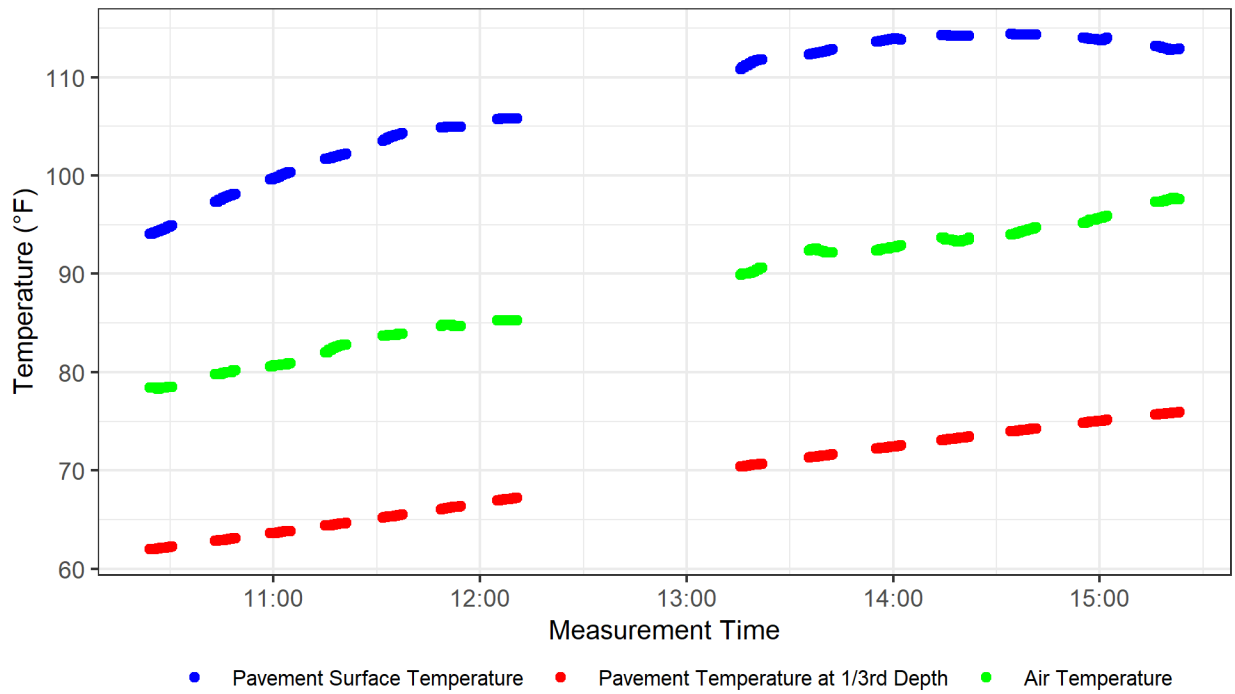


Figure N.48: Air, pavement surface, and one-third depth temperatures on 07/15/2016 testing day.

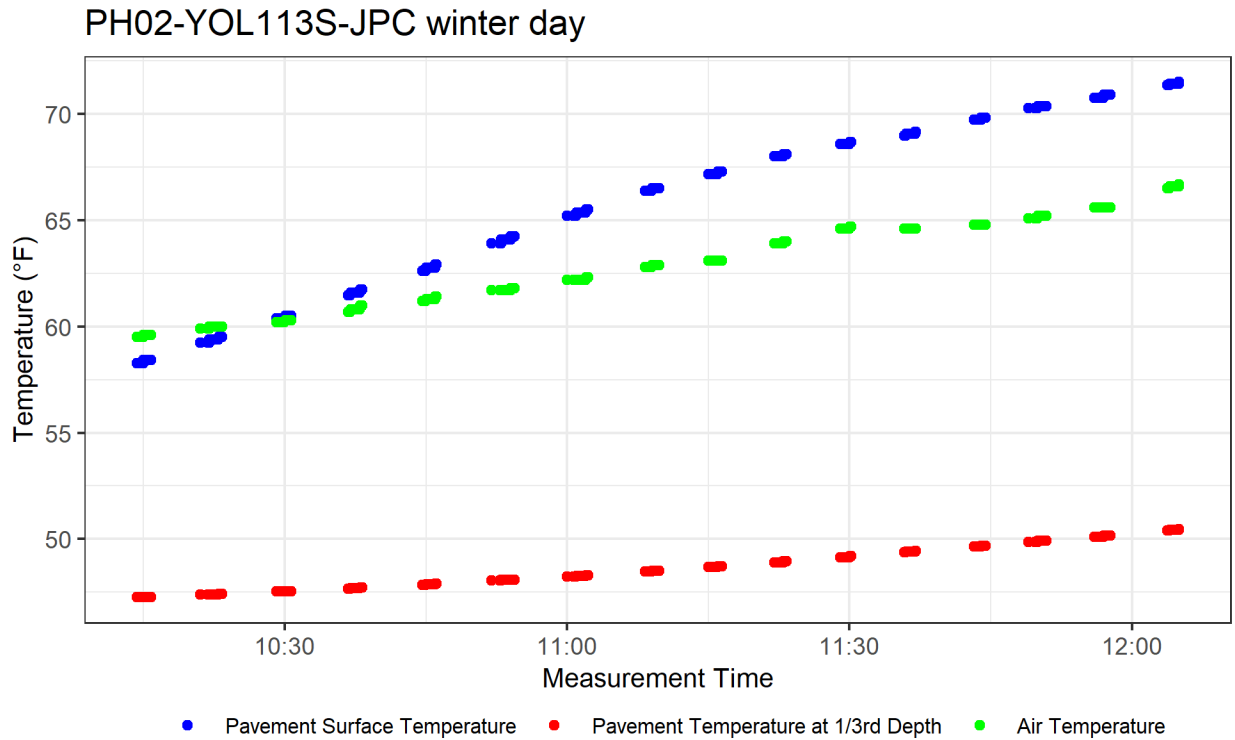


Figure N.49: Air, pavement surface, and one-third depth temperatures on 02/11/2016 testing day.

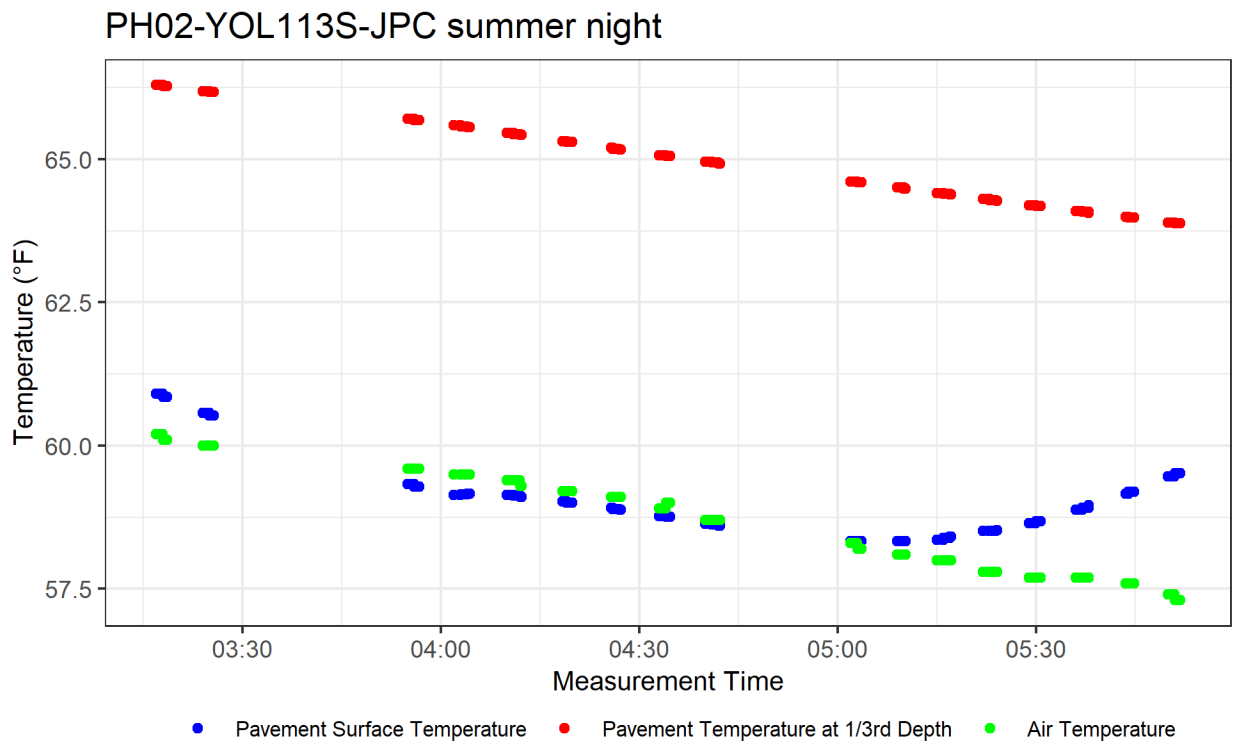


Figure N.50: Air, pavement surface, and one-third depth temperatures on 07/20/2016 testing day.

PH02-YOL113S-JPC summer day

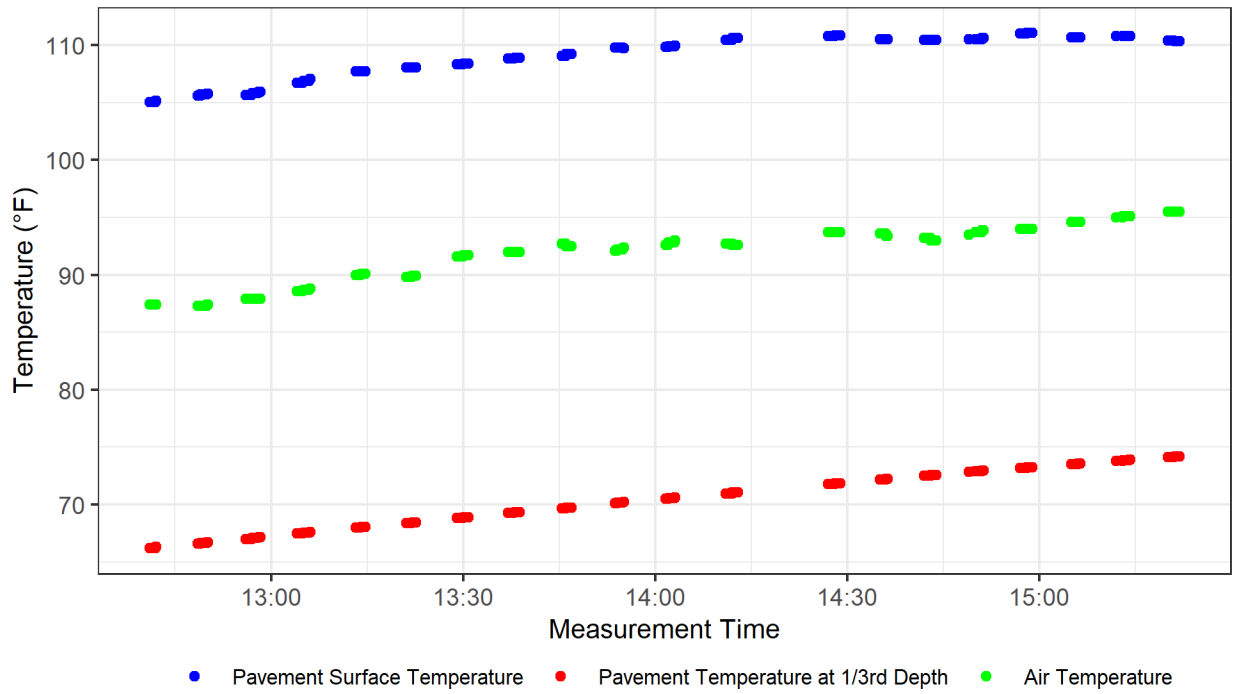


Figure N.51: Air, pavement surface, and one-third depth temperatures on 07/22/2016 testing day.

PH01-YOL113N-JPC winter day

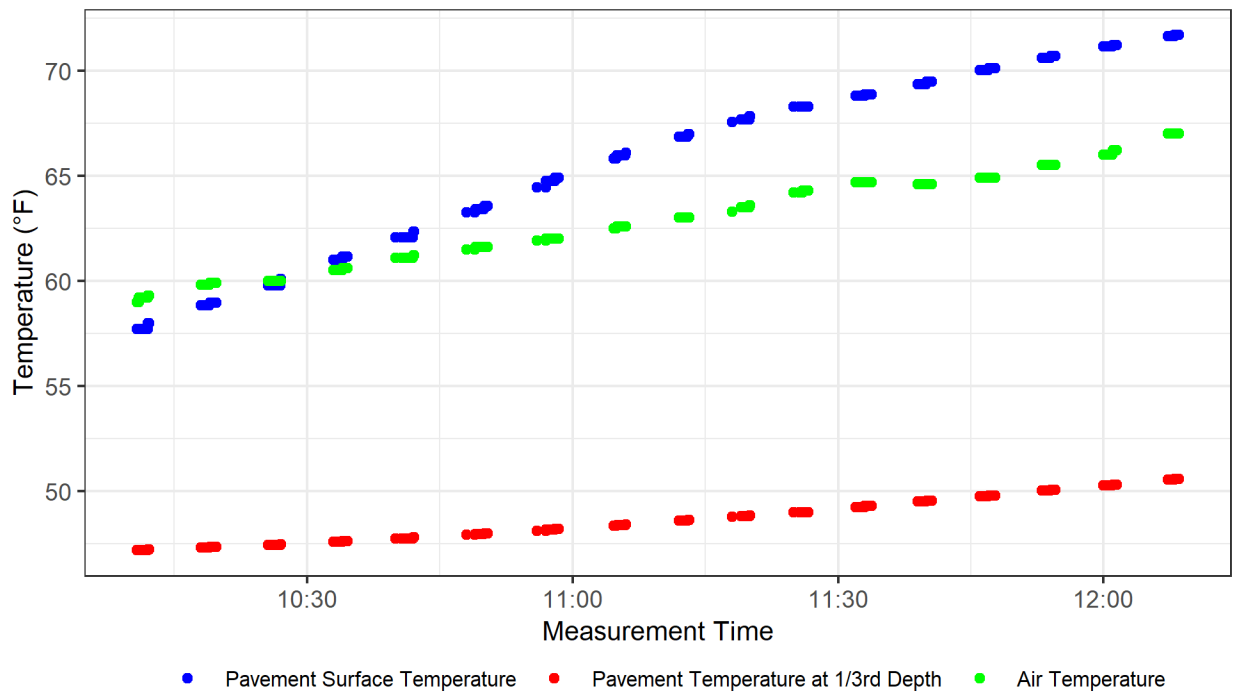


Figure N.52: Air, pavement surface, and one-third depth temperatures on 02/11/2016 testing day.

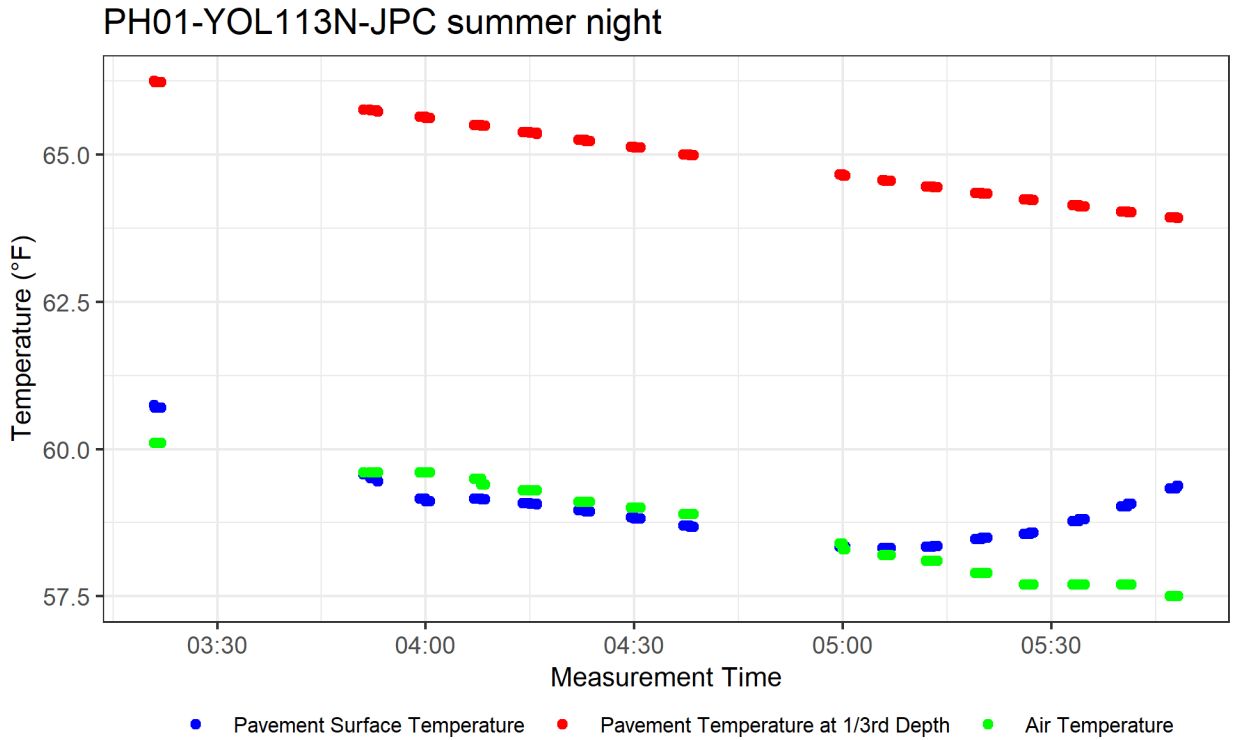


Figure N.53: Air, pavement surface, and one-third depth temperatures on 07/20/2016 testing day.

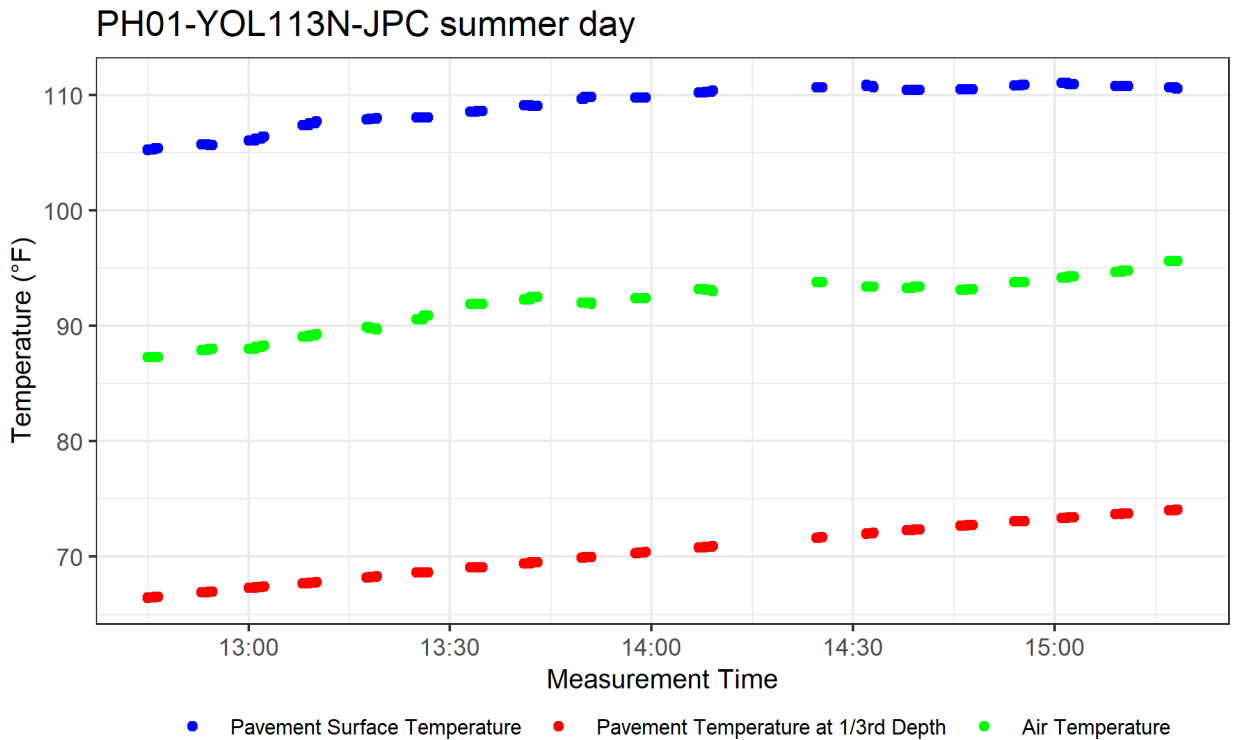


Figure N.54: Air, pavement surface, and one-third depth temperatures on 07/22/2016 testing day.

APPENDIX O: NUMBER OF TEST REPLICATES AND GRAPHS OF FUEL RATE DATA FOR DIFFERENT VEHICLES

The number of replicates that were performed by each vehicle on each section in each season at different speeds is presented in Table O.1.

Table O.1 Number of Test Replicates per Vehicle per Section

Vehicle	Sections	Season	Day/Night	Vehicle Speed (mph)		
				35	45	55
				Number of Test Replicates		
Car	PH01	Winter	Day		8	9
		Summer	Day		12	8
		Summer	Night		7	11
	PH02	Winter	Day		8	8
		Summer	Day		12	8
		Summer	Night		7	10
	PH03	Winter	Day		6	
		Summer	Day		7	6
		Summer	Night		8	8
	PH04	Winter	Day		6	
		Summer	Day		6	6
		Summer	Night		8	7
	PH07	Winter	Day	6	7	
		Summer	Day	8	6	
		Summer	Night	7	8	
	PH08	Winter	Day	6	7	
		Summer	Day	8	8	
		Summer	Night	8	8	
	PH09	Winter	Day		3	4
		Summer	Day		6	6
	PH10	Winter	Day		4	5
		Summer	Day		5	6
	PH11	Winter	Day		4	4
		Summer	Day		6	6
	PH12	Winter	Day		4	5
		Summer	Day		5	5
	PH13	Winter	Day		4	5
		Summer	Day		6	6
	PH14	Winter	Day		4	5
		Summer	Day		5	5
	PH15	Winter	Day	8	8	
		Summer	Day	8	9	
Summer		Night	5	8		
PH16	Winter	Day		4	7	
	Summer	Day		9	10	

	PH17	Winter	Day		6	8
		Summer	Day		9	12
	PH18	Winter	Night		7	9
		Summer	Day		9	8
	PH19	Winter	Night		7	8
		Summer	Day		8	8
	PH20	Winter	Night		8	7
		Summer	Day		8	8
	PH21	Winter	Day		8	7
		Summer	Day		9	8
	PH22	Winter	Day		7	7
		Summer	Day		9	8
PH23	Winter	Day	8	8		
	Summer	Day	8	8		
	Summer	Night	6	8		
F-450	PH01	Winter	Day		8	9
		Summer	Day		12	8
		Summer	Night		7	10
	PH02	Winter	Day		8	9
		Summer	Day		12	8
		Summer	Night		7	10
	PH03	Winter	Day		6	4
		Summer	Day		6	7
		Summer	Night		6	6
	PH04	Winter	Day		6	5
		Summer	Day		7	7
		Summer	Night		7	6
	PH07	Winter	Day	7	7	
		Summer	Day	9	7	
		Summer	Night	8	8	
	PH08	Winter	Day	7	7	
		Summer	Day	9	8	
		Summer	Night	8	8	
	PH09	Winter	Day		2	5
		Summer	Day		6	4
	PH10	Winter	Day		4	5
		Summer	Day		6	4
	PH11	Winter	Day		4	5
		Summer	Day		6	6
	PH12	Winter	Day		4	4
		Summer	Day		5	6
	PH13	Winter	Day		4	5
Summer		Day		6	6	
PH14	Winter	Day		4	5	
	Summer	Day		5	6	

	PH15	Winter	Day	8	8	
		Summer	Day	6	9	
		Summer	Night	8	7	
	PH16	Winter	Day		6	7
		Summer	Day		9	8
	PH17	Winter	Day		6	7
		Summer	Day		9	9
	PH18	Winter	Night		4	7
		Summer	Day		8	8
	PH19	Winter	Night		4	7
		Summer	Day		8	7
	PH20	Winter	Night		5	6
		Summer	Day		8	8
	PH21	Winter	Day		8	8
		Summer	Day		9	8
PH22	Winter	Day		8	7	
	Summer	Day		8	8	
PH23	Winter	Day	8	8		
	Summer	Day	5	9		
	Summer	Night	8	8		
HHDT	PH01	Winter	Day		8	9
		Summer	Day		11	8
		Summer	Night		7	9
	PH02	Winter	Day		8	8
		Summer	Day		12	8
		Summer	Night		7	10
	PH03	Winter	Day		6	5
		Summer	Day		7	7
		Summer	Night		8	8
	PH04	Winter	Day		6	5
		Summer	Day		6	7
		Summer	Night		8	8
	PH07	Winter	Day	5	6	
		Summer	Day	9	8	
		Summer	Night	8	8	
	PH08	Winter	Day	6	7	
		Summer	Day	9	8	
		Summer	Night	8	8	
PH09	Winter	Day		4	5	
	Summer	Day		6	5	
PH10	Winter	Day		4	5	
	Summer	Day		5	6	
PH11	Winter	Day		4	5	
	Summer	Day		6	6	
PH12	Winter	Day		4	5	
	Summer	Day		6	6	

	PH13	Winter	Day		4	4
		Summer	Day		6	6
	PH14	Winter	Day		4	5
		Summer	Day		6	6
	PH15	Winter	Day	8	7	
		Summer	Day	8	9	
		Summer	Night	8	8	
	PH16	Winter	Day		6	7
		Summer	Day		9	9
	PH17	Winter	Day		5	6
		Summer	Day		10	9
	PH18	Winter	Night		4	8
		Summer	Day		7	7
	PH19	Winter	Night		4	8
		Summer	Day		8	8
	PH20	Winter	Night		4	7
		Summer	Day		7	7
	PH21	Winter	Day		7	7
		Summer	Day		9	9
	PH22	Winter	Day		7	8
		Summer	Day		9	9
	PH23	Winter	Day	8	7	
		Summer	Day	8	9	
		Summer	Night	8	8	
SUV	PH01	Winter	Day		8	8
		Summer	Day		12	8
		Summer	Night		7	10
	PH02	Winter	Day		8	8
		Summer	Day		11	8
		Summer	Night		6	10
	PH03	Winter	Day		6	4
		Summer	Day		7	7
		Summer	Night		8	8
	PH04	Winter	Day		6	4
		Summer	Day		7	7
		Summer	Night		8	8
	PH07	Winter	Day	6	7	
		Summer	Day	8	7	
		Summer	Night	8	8	
	PH08	Winter	Day	7	8	
		Summer	Day	8	7	
		Summer	Night	8	7	
	PH09	Winter	Day		4	5
		Summer	Day		5	6
	PH10	Winter	Day		4	5
		Summer	Day		5	6

PH11	Winter	Day		4	4
	Summer	Day		6	6
PH12	Winter	Day		4	5
	Summer	Day		4	6
PH13	Winter	Day		4	4
	Summer	Day		6	6
PH14	Winter	Day		4	5
	Summer	Day		5	6
PH15	Winter	Day	8	8	
	Summer	Day	9	9	
	Summer	Night	8	8	
PH16	Winter	Day		6	6
	Summer	Day		9	9
PH17	Winter	Day		6	6
	Summer	Day		9	9
PH18	Winter	Night		4	6
	Summer	Day		8	8
PH19	Winter	Night		4	8
	Summer	Day		6	8
PH20	Winter	Night		5	5
	Summer	Day		8	8
PH21	Winter	Day		8	7
	Summer	Day		9	8
PH22	Winter	Day		7	7
	Summer	Day		9	8
PH23	Winter	Day	7	8	
	Summer	Day	9	9	
	Summer	Night	8	8	

The total number of observations per vehicle per gear are presented in Table O.2. First order cleaned fuel rate (mL/s) and RPM data for each vehicle for all sections are presented in Figure O.1 to Figure O.4. The combined data are presented in Figure O.5.

Table O.2: Number of Observations per Gear per Vehicle

Test Speeds	Car Gear	Number of Observations	SUV Gear	Number of Observations	F-450 Gear	Number of Observations ¹	HHDT Gear	Number of Observations
35	4	7,359	5	7,451	6	6,378	9	7,376
45	5	49,485	6	45,405	6	39,926	10	45,076
55	6	37,130	6	39,780	6	35,126	10	39,325
Total		93,974		92,636		81,430		91,777

¹ The number of observations for the F-450 were 89,969. However, 8,539 observations had to be removed from the dataset as the same test speeds were running in different gears (see Appendix M for details).

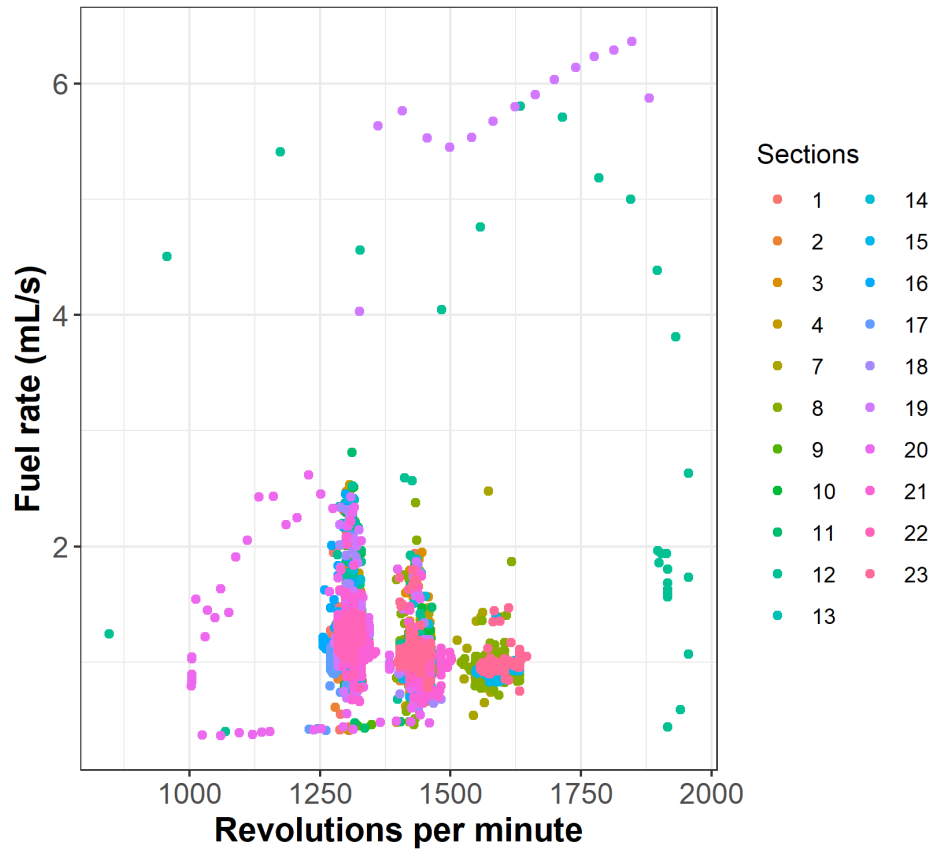


Figure O.1: Fuel rate versus RPM for car for all speeds and sections.

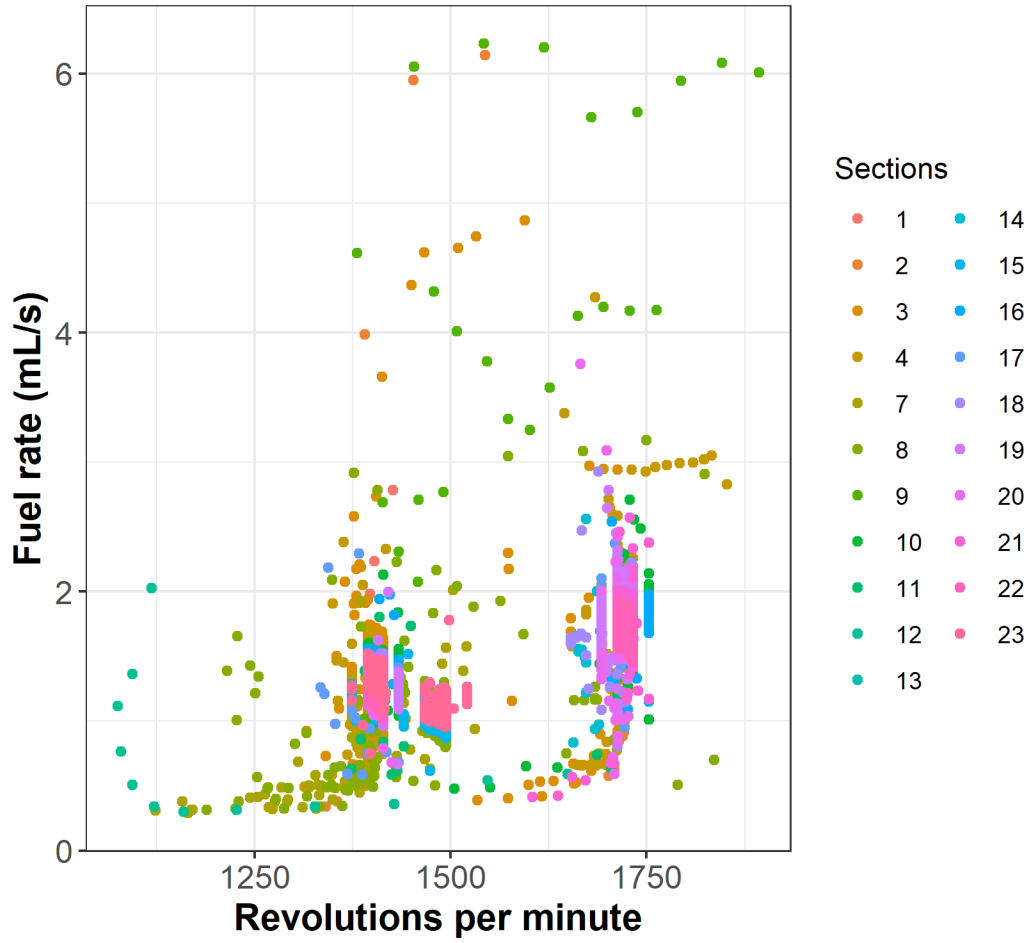


Figure O.2: Fuel rate versus RPM for SUV for all speeds and sections.

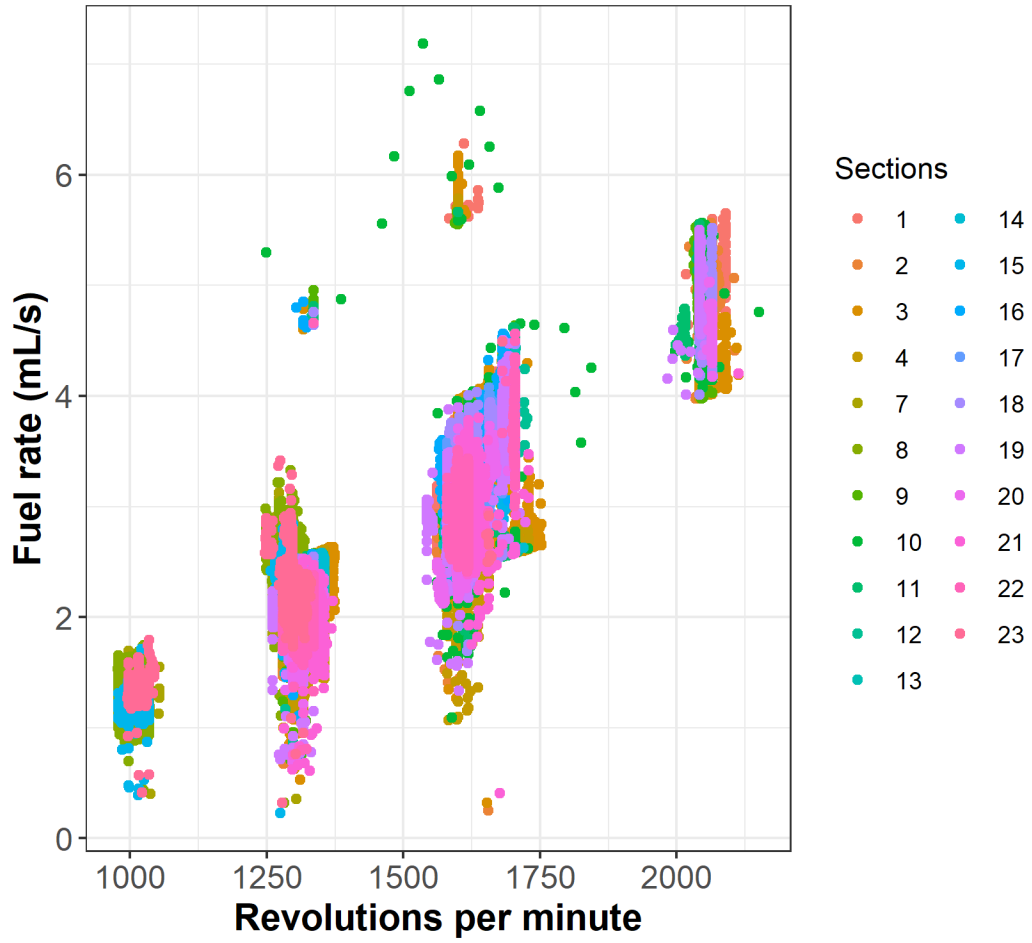


Figure O.3: Fuel rate versus RPM for F-450 for all speeds and sections.

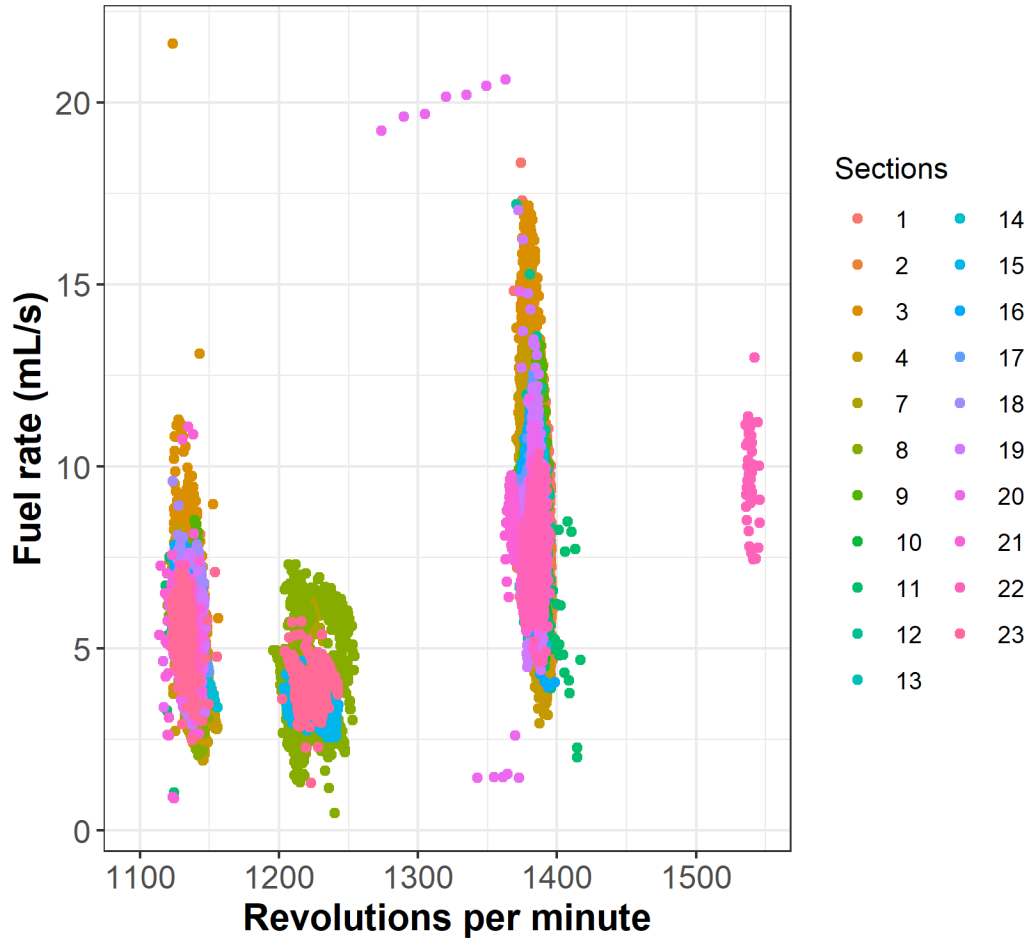


Figure O.4: Fuel rate versus RPM for HHDT for all speeds and sections.

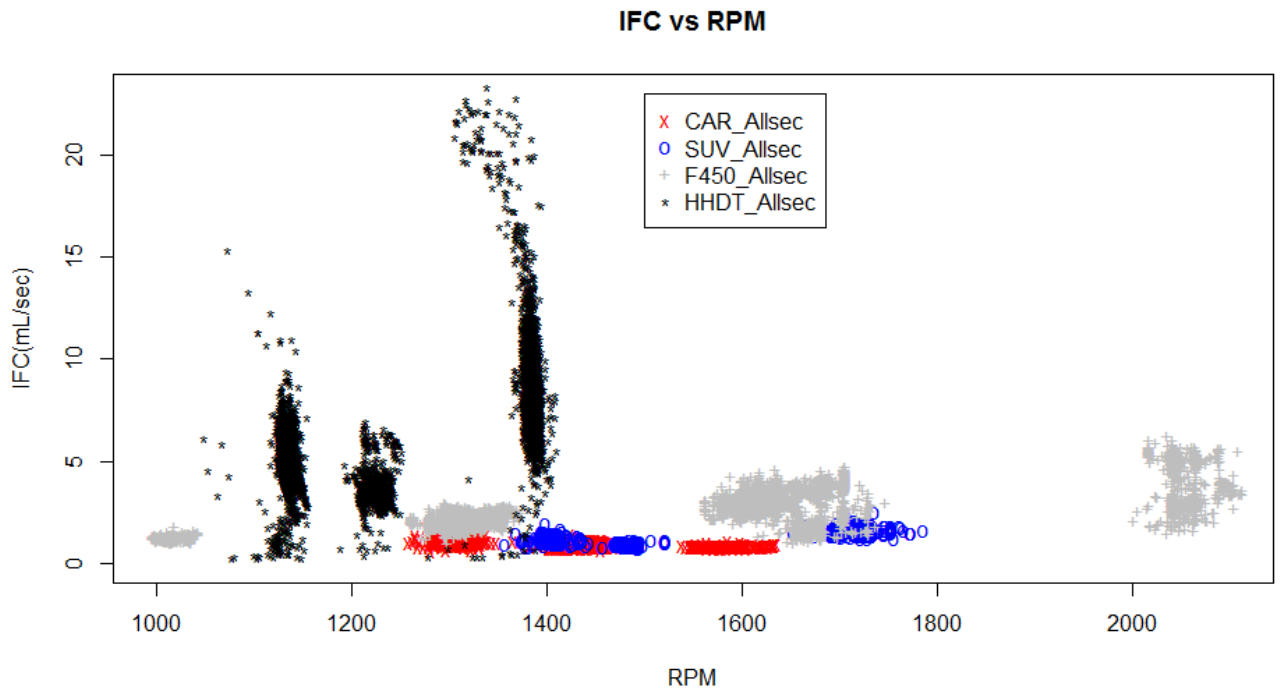


Figure O.5 Fuel consumption versus engine RPM for all four vehicles on all 23 sections.

APPENDIX P: GRAPHS OF FUEL RATE, ROUGHNESS, GRADIENT, HEADWIND, AND SPEED PER VEHICLE TYPE PER SECTION PER SEASON

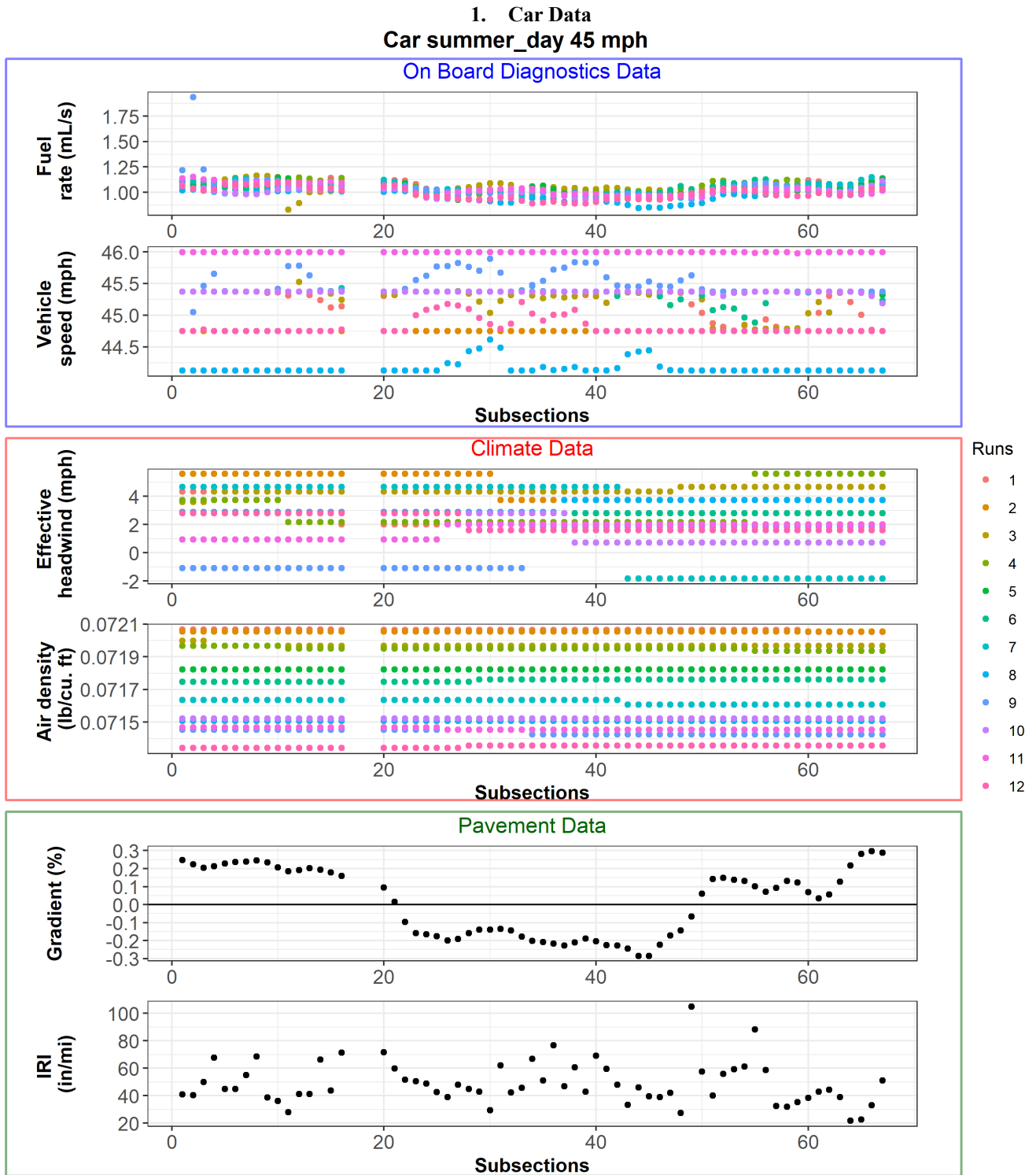


Figure P.1: Car data on Section PH01.

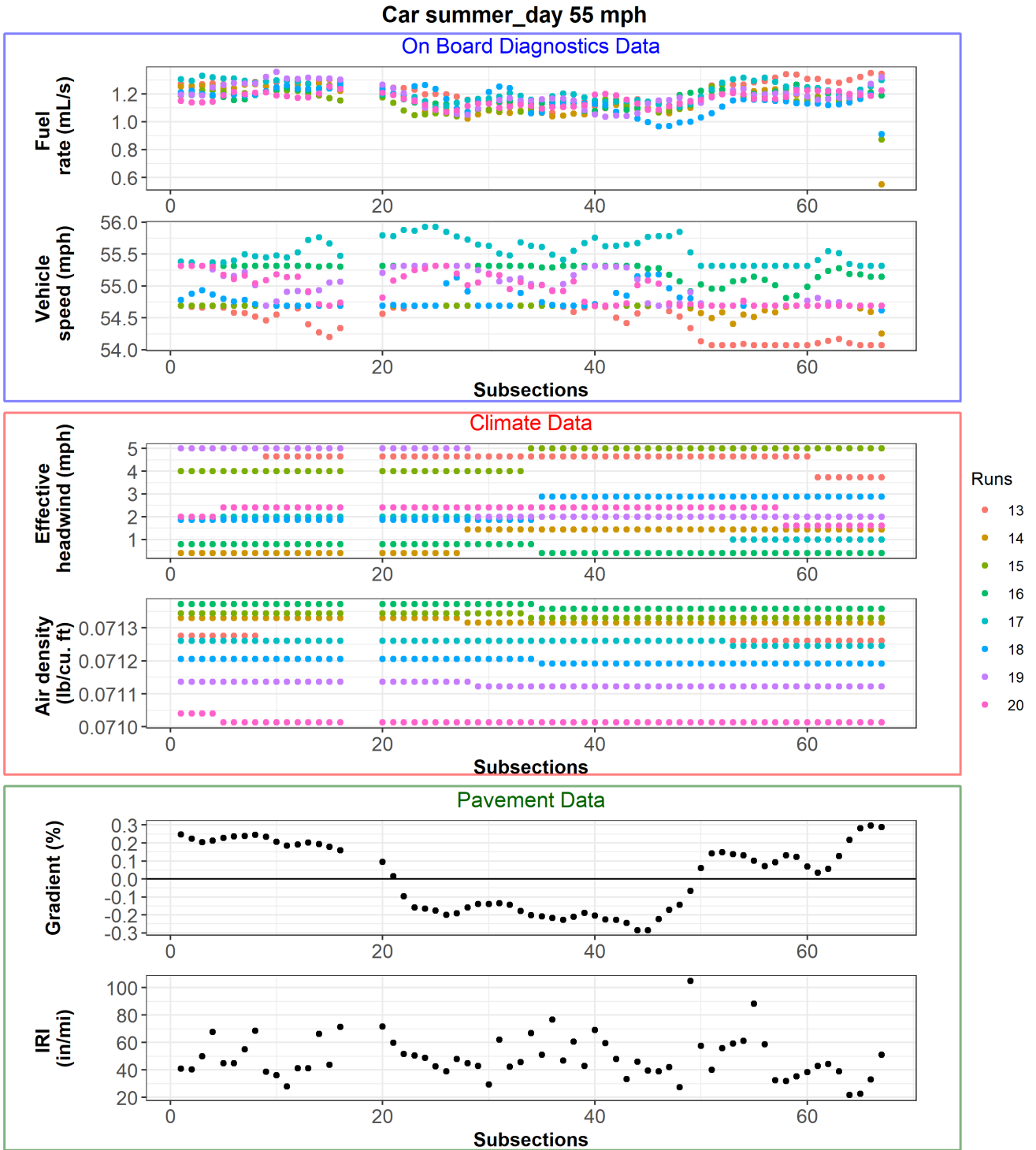


Figure P.2: Car data on Section PH01.

Car summer_night 45 mph

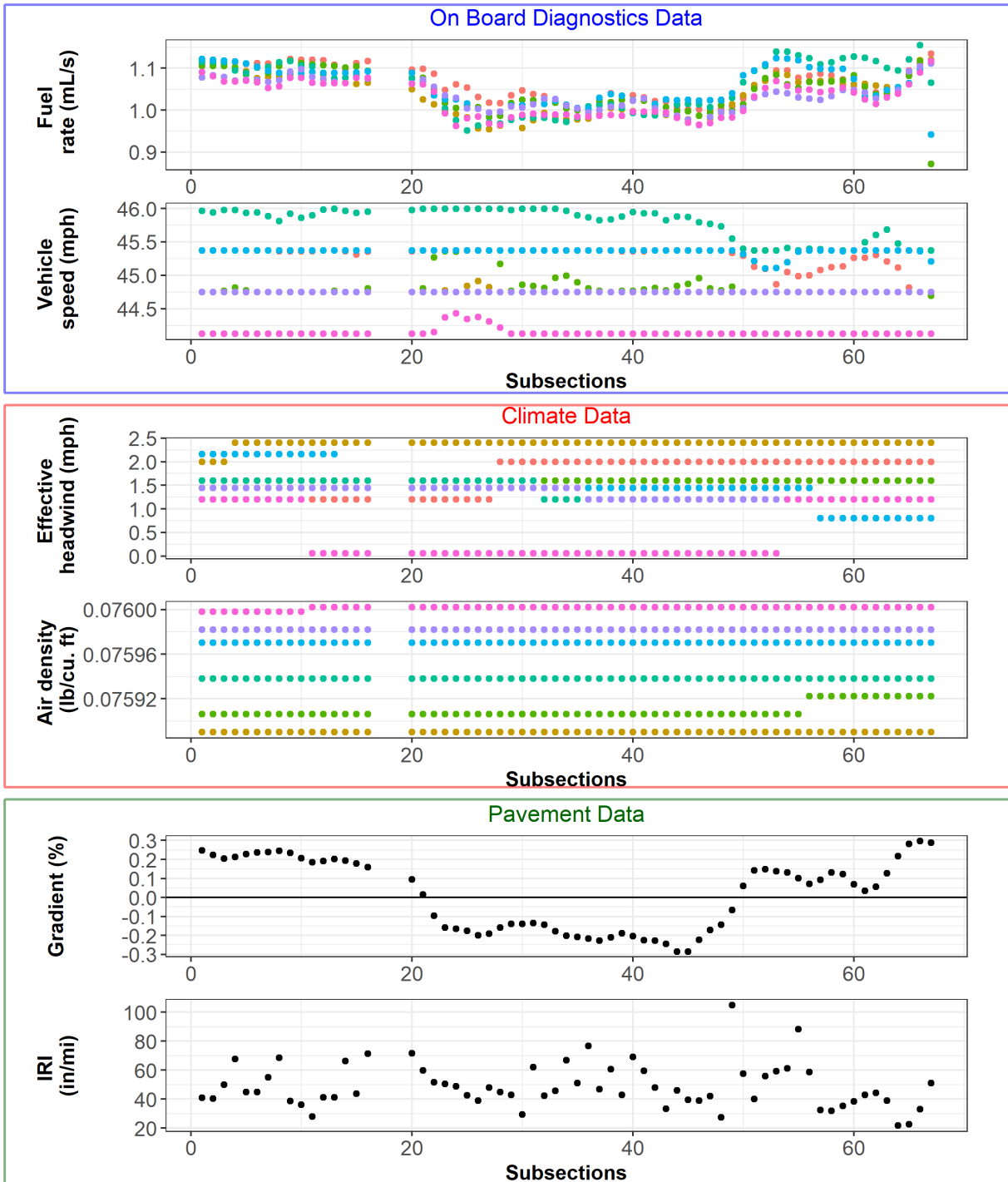


Figure P.3: Car data on Section PH01.

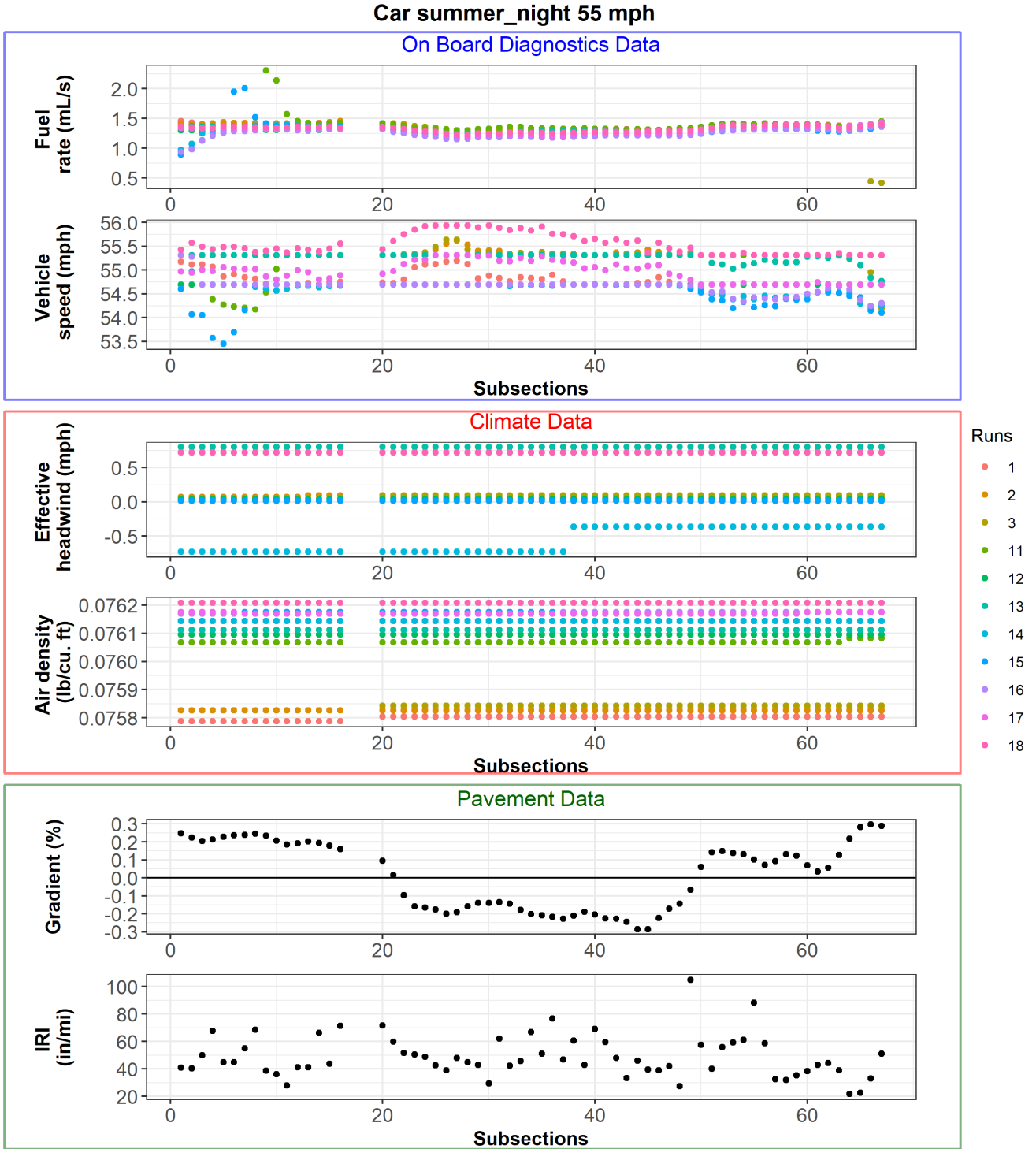


Figure P.4: Car data on Section PH01.

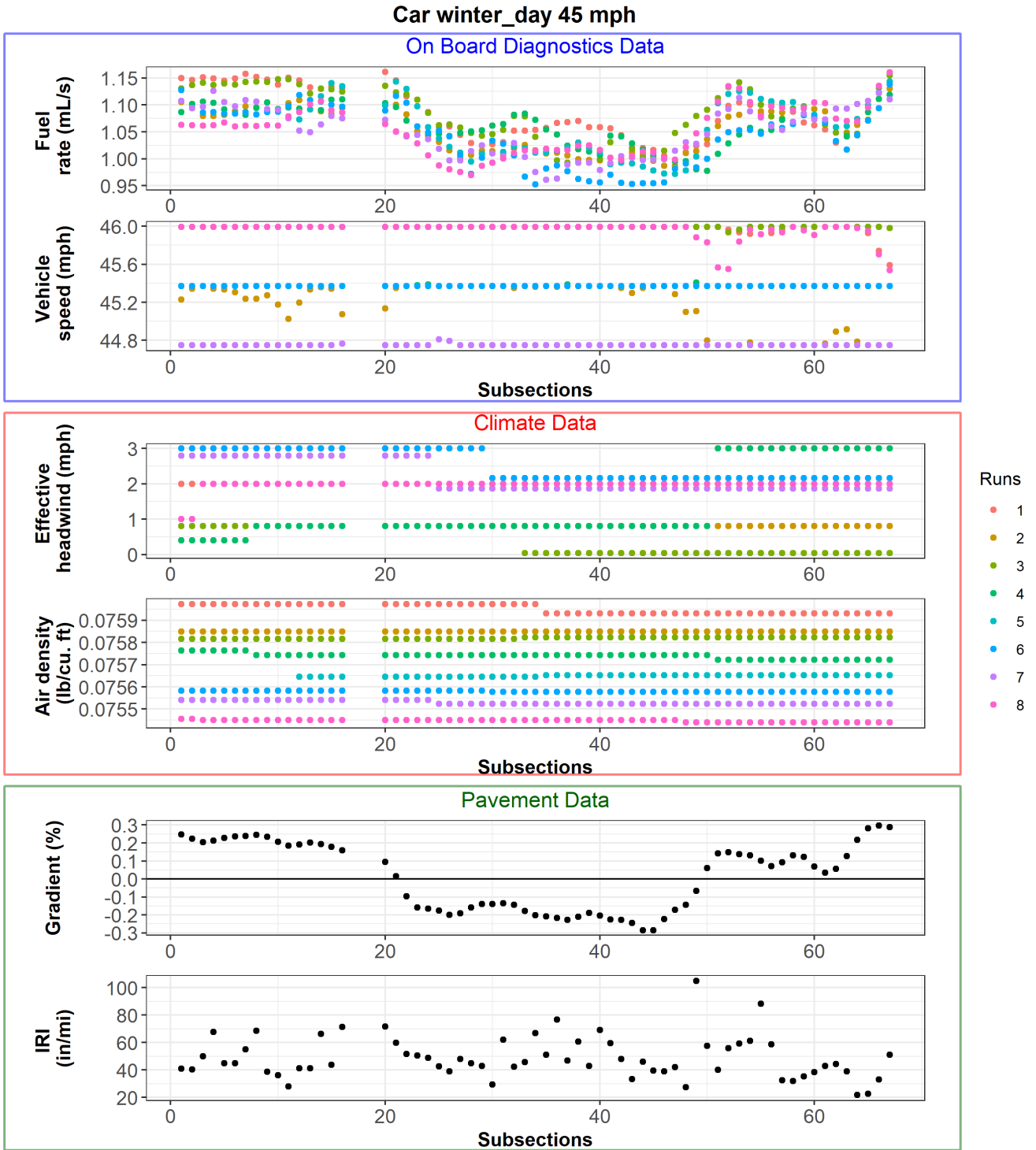


Figure P.5: Car data on Section PH01.

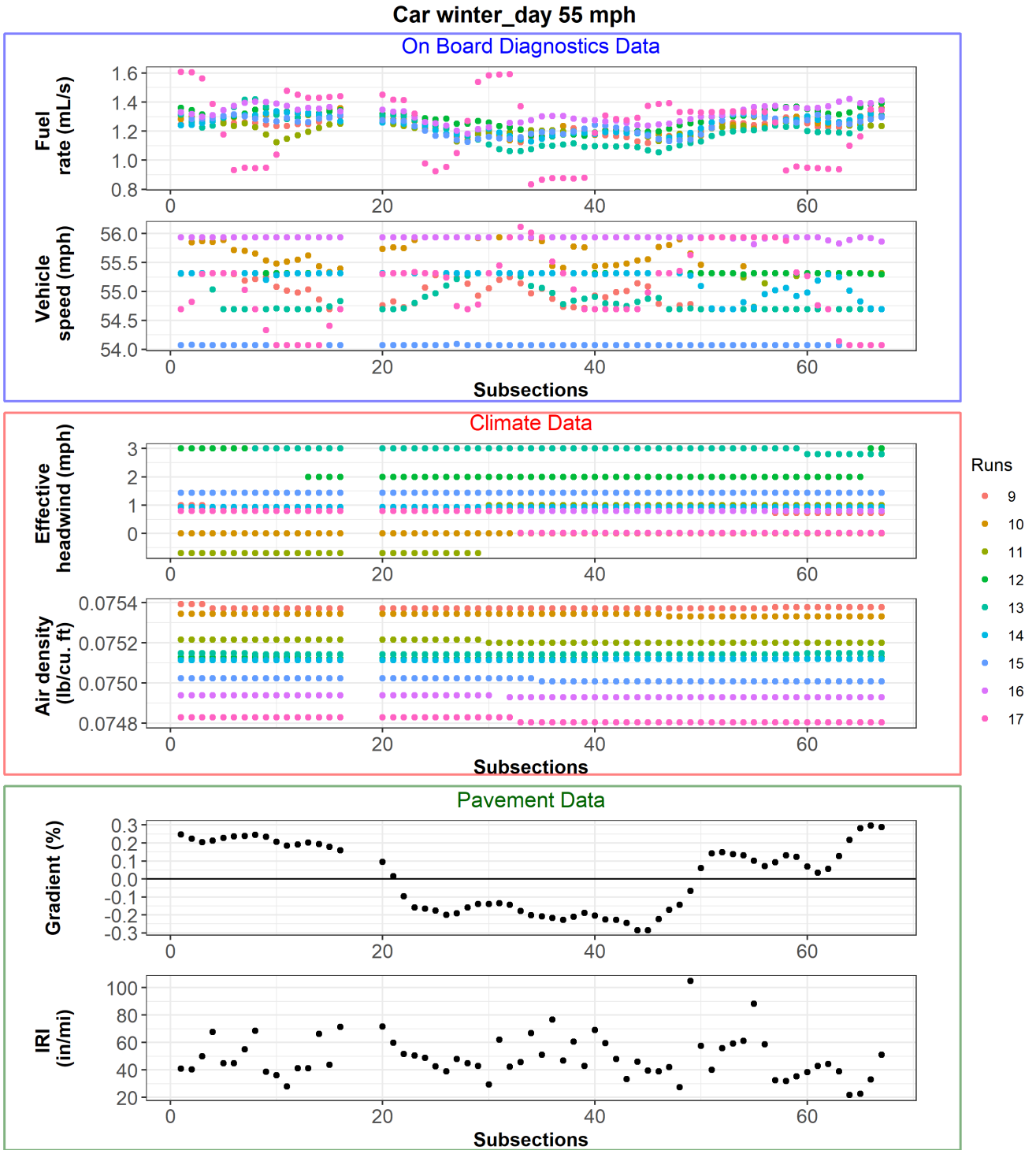


Figure P.6: Car data on Section PH01.

Car summer_day 45 mph

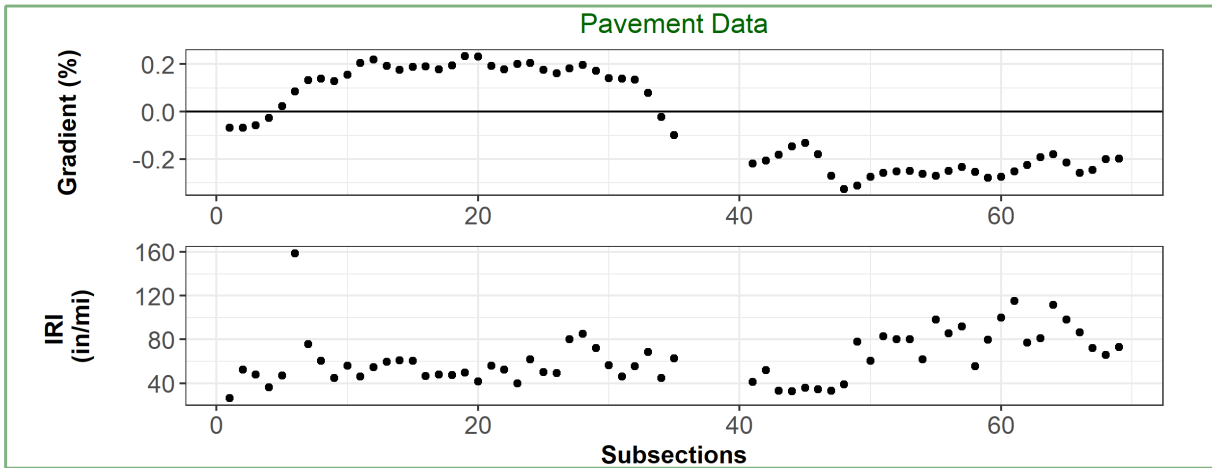
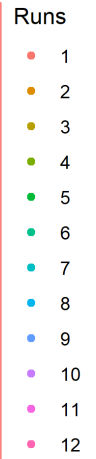
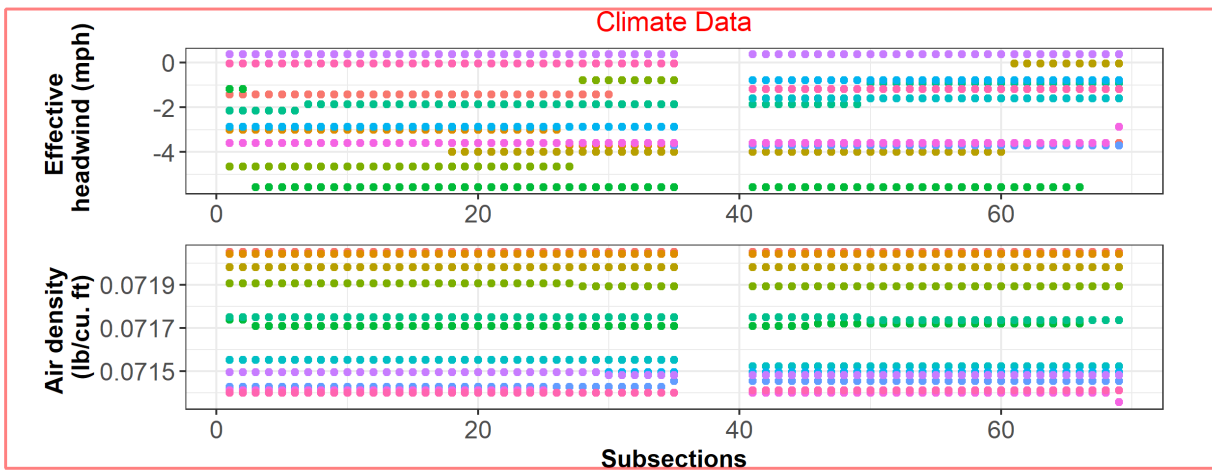
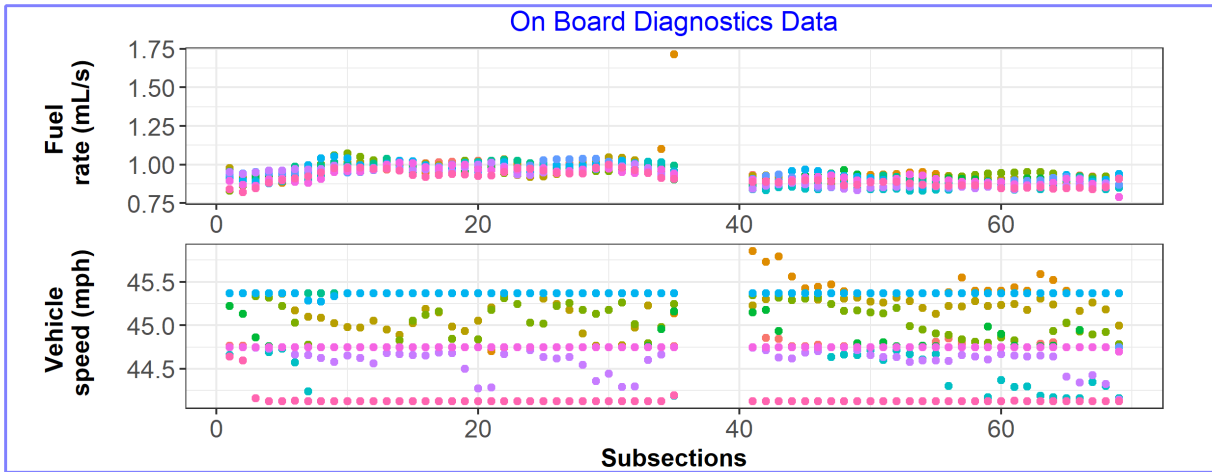


Figure P.7: Car data on Section PH02.

Car summer_day 55 mph

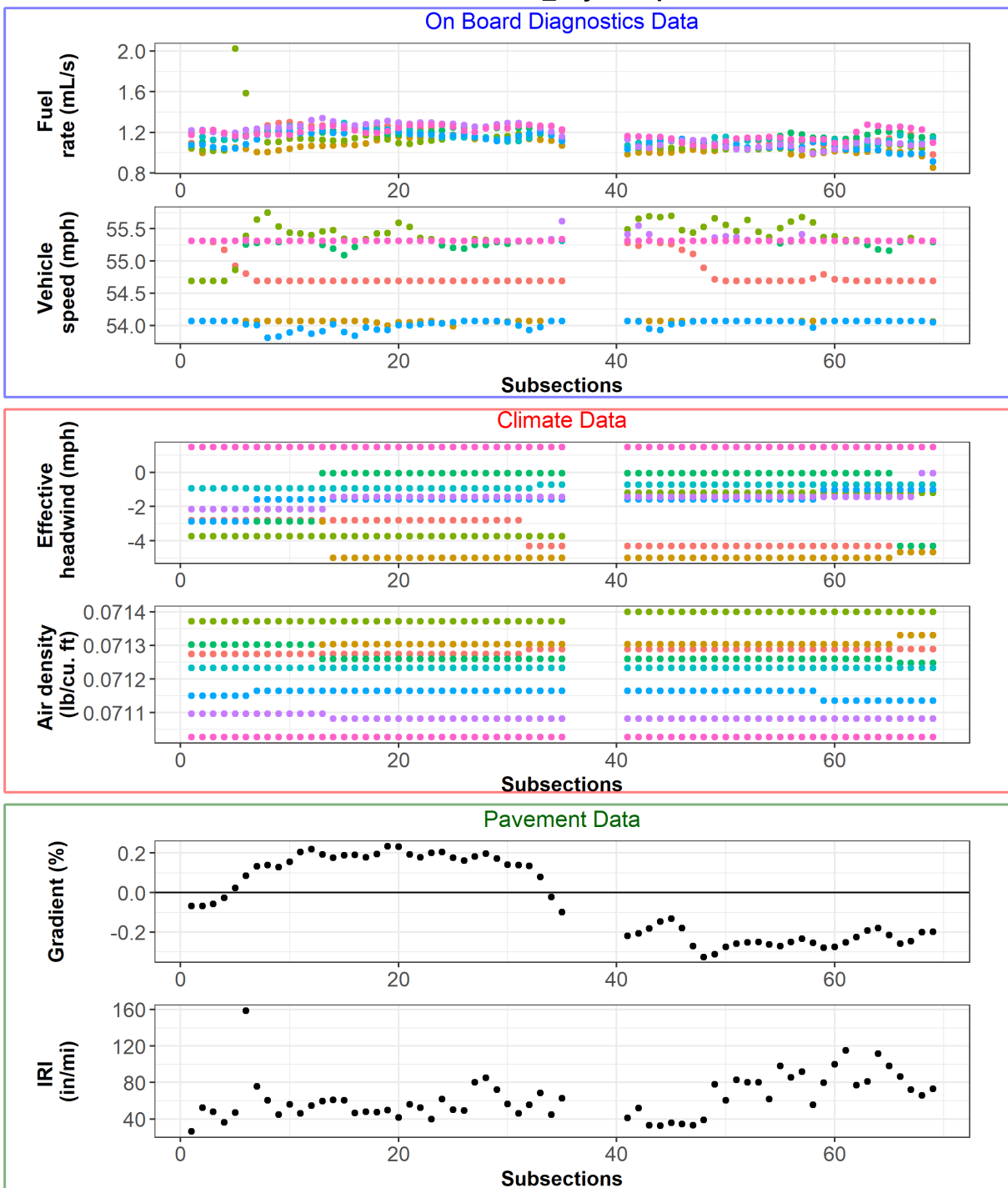
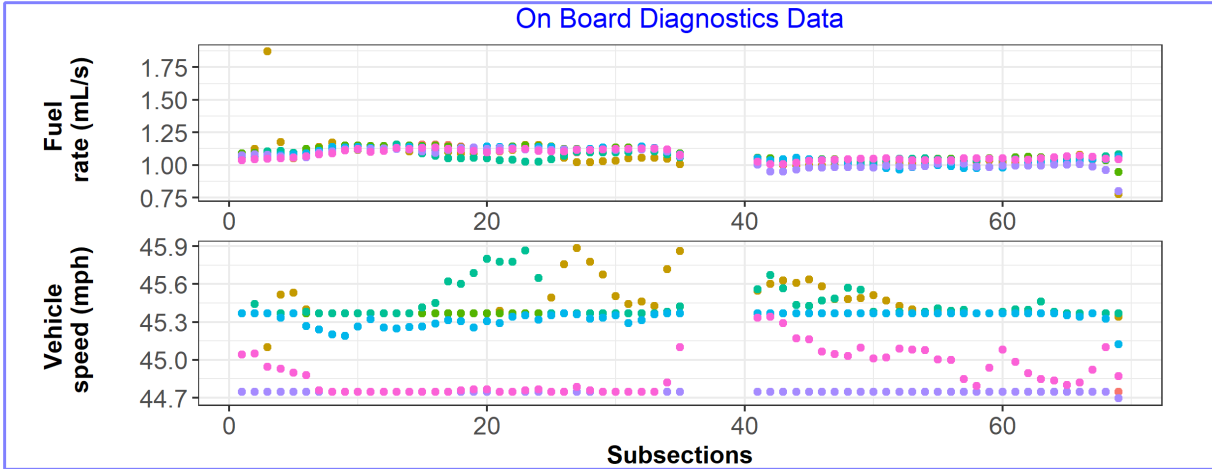


Figure P.8: Car data on Section PH02.

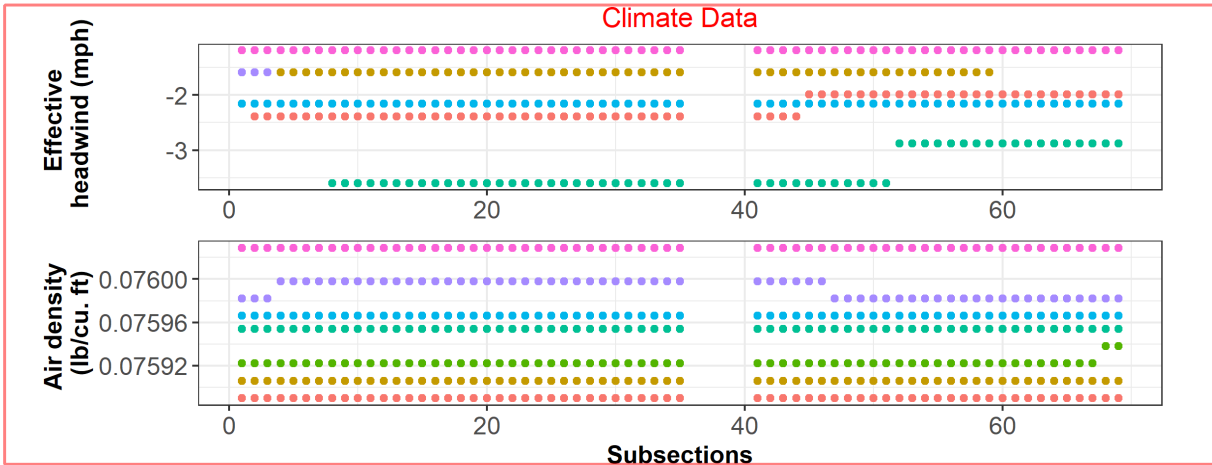
Car summer_night 45 mph

On Board Diagnostics Data



Subsections

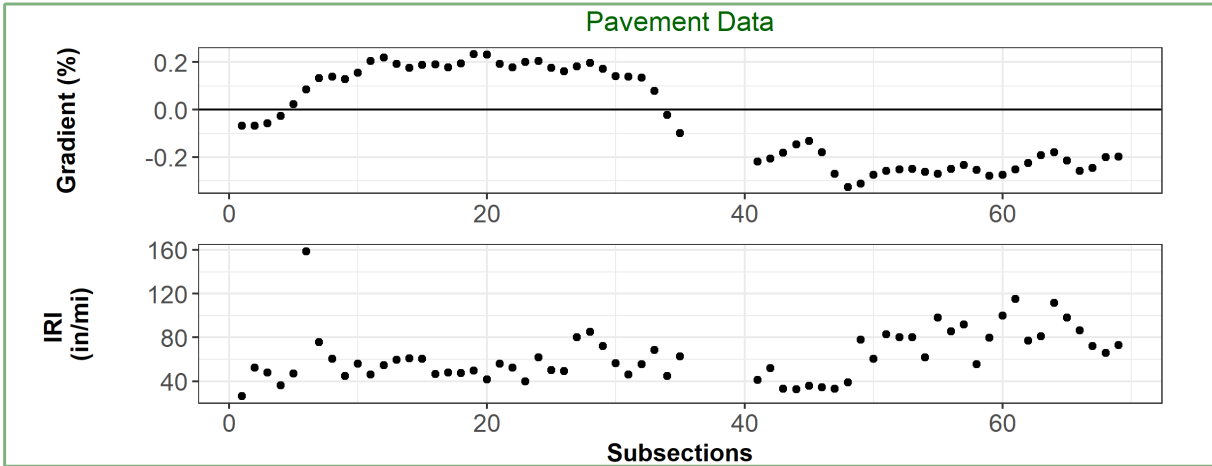
Climate Data



Subsections

- Runs
- 4
 - 5
 - 6
 - 7
 - 8
 - 9
 - 10

Pavement Data



Subsections

Figure P.9: Car data on Section PH02.

Car summer_night 55 mph

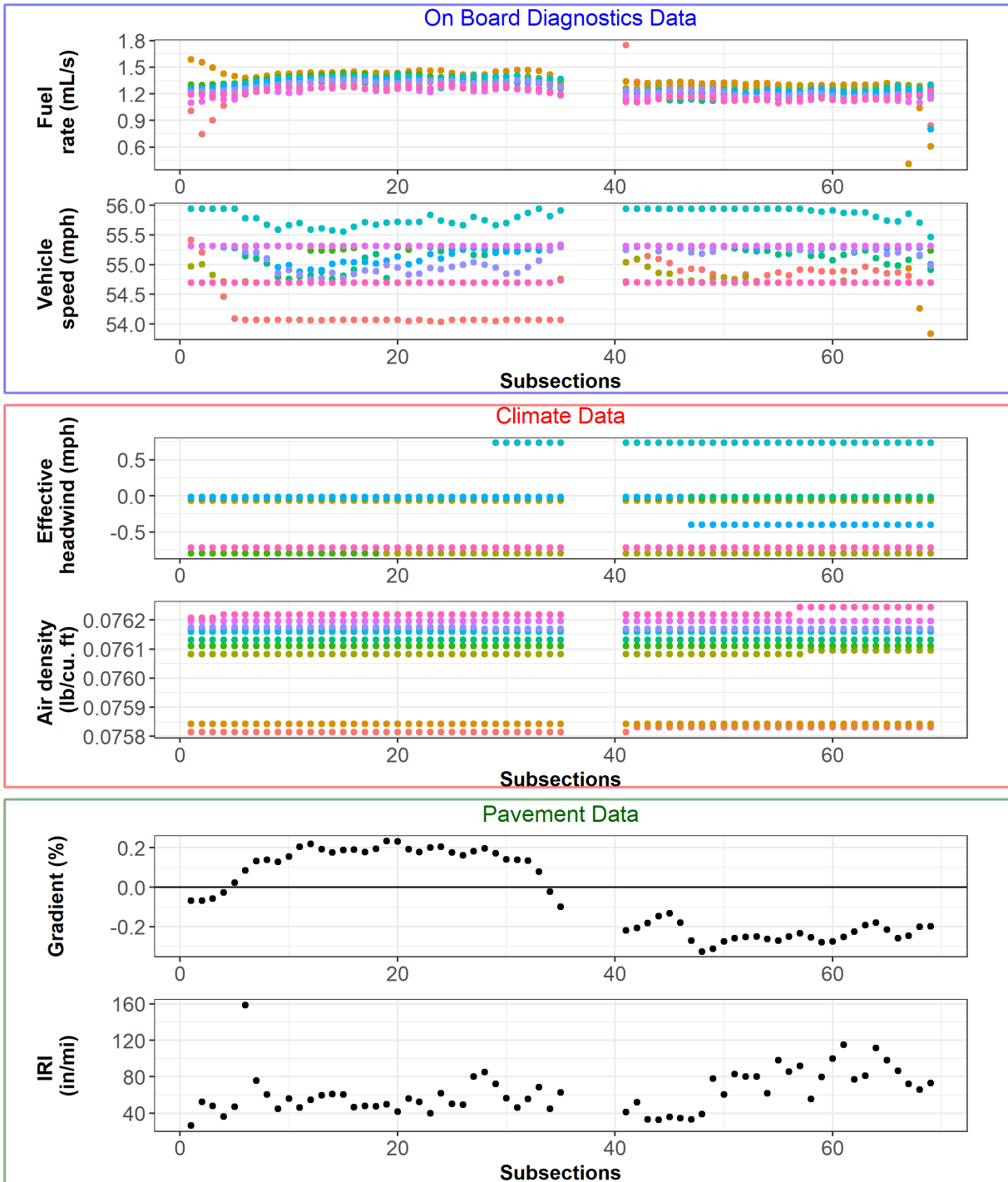


Figure P.10: Car data on Section PH02.

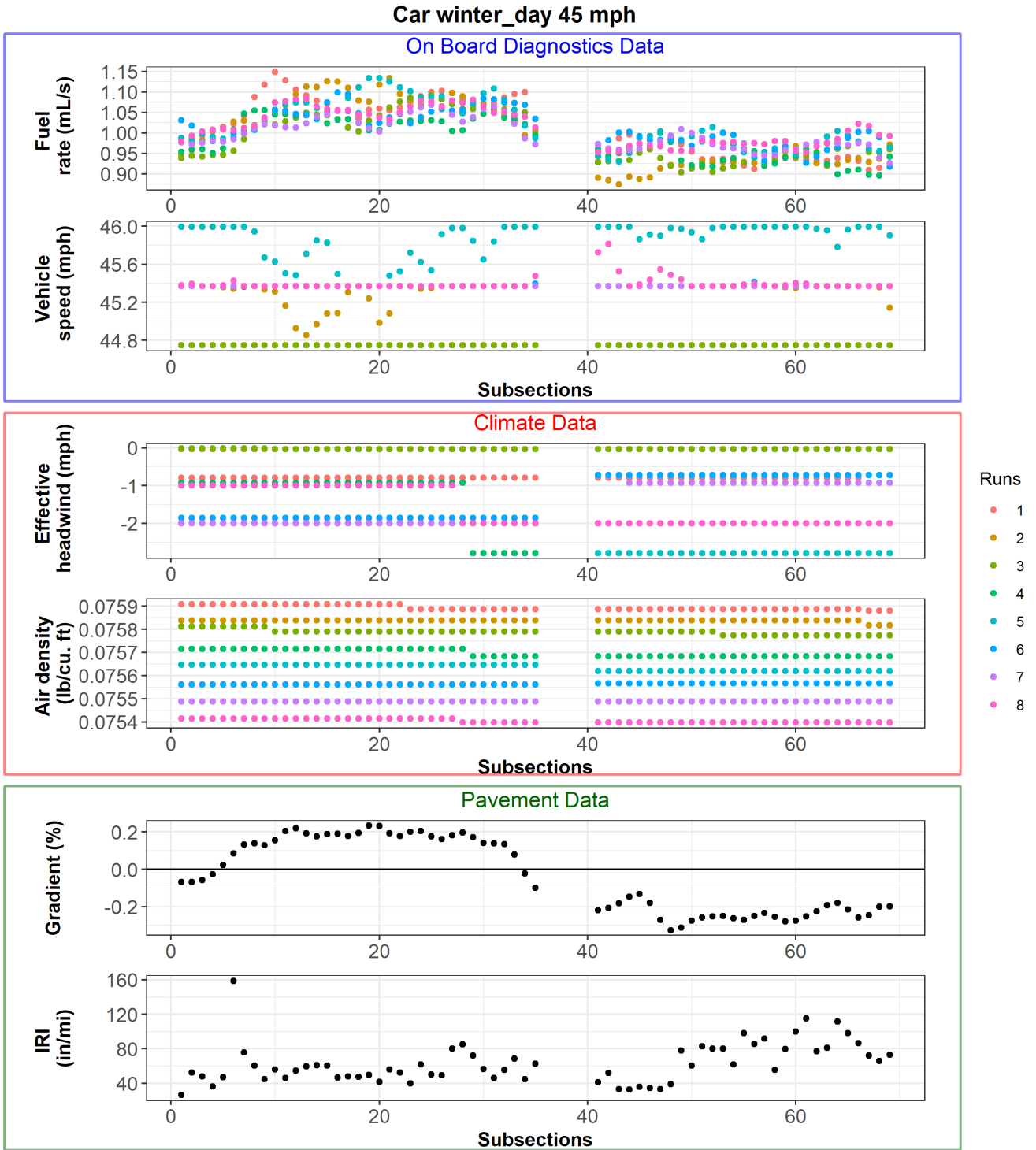


Figure P.11: Car data on Section PH02.

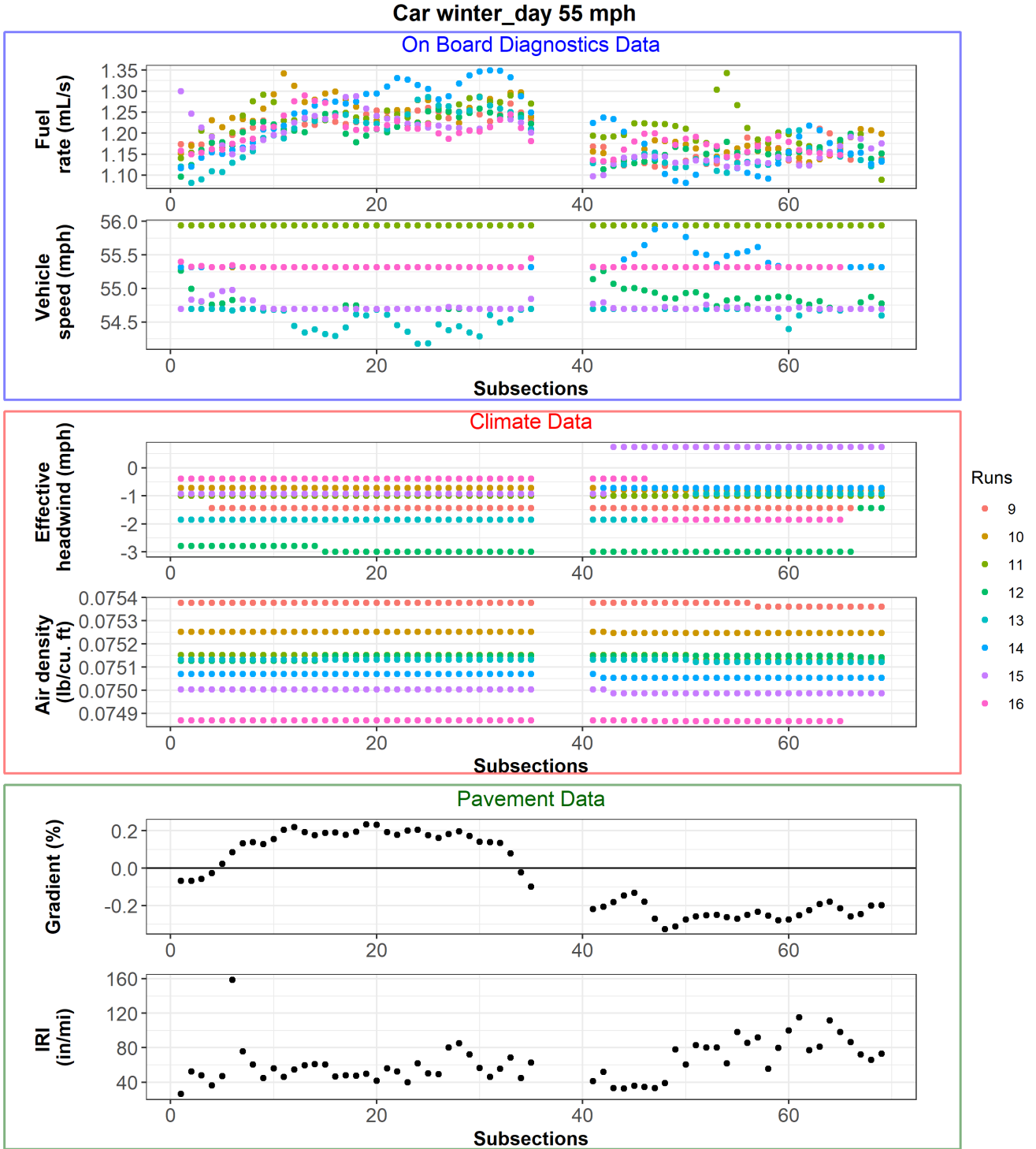


Figure P.12: Car data on Section PH02.

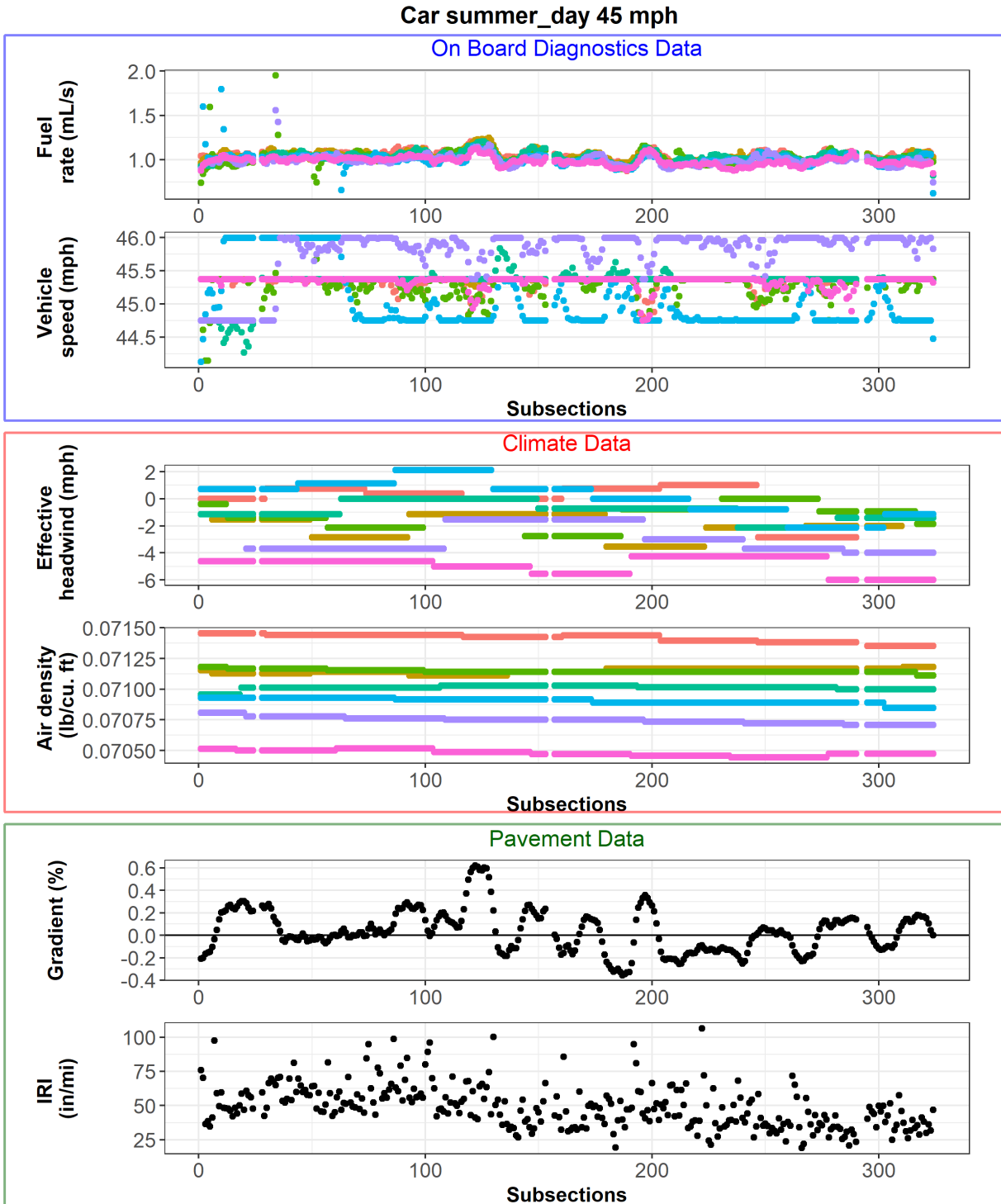


Figure P.13: Car data on Section PH03.

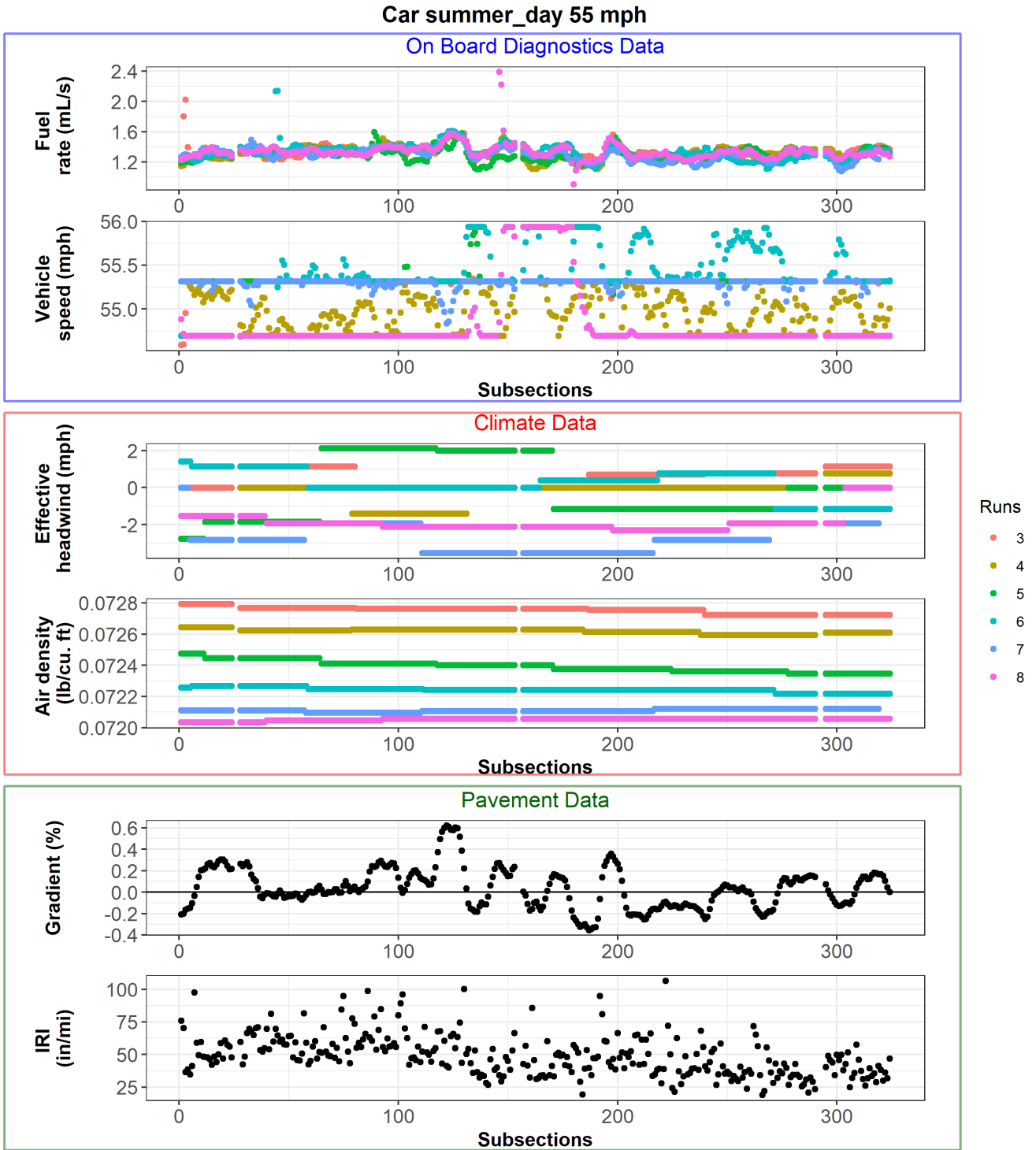


Figure P.14: Car data on Section PH03.

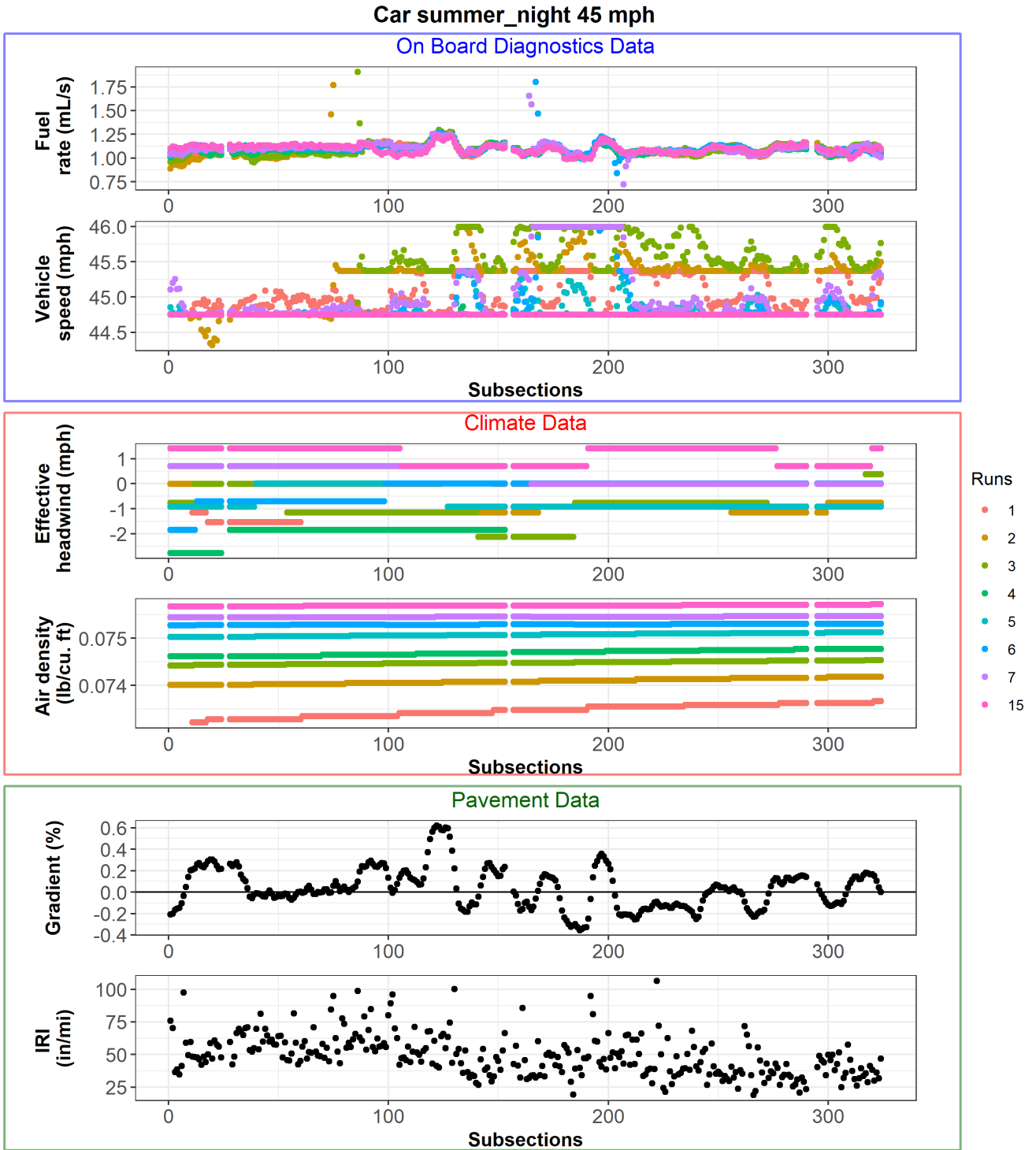


Figure P.15: Car data on Section PH03.

Car summer_night 55 mph

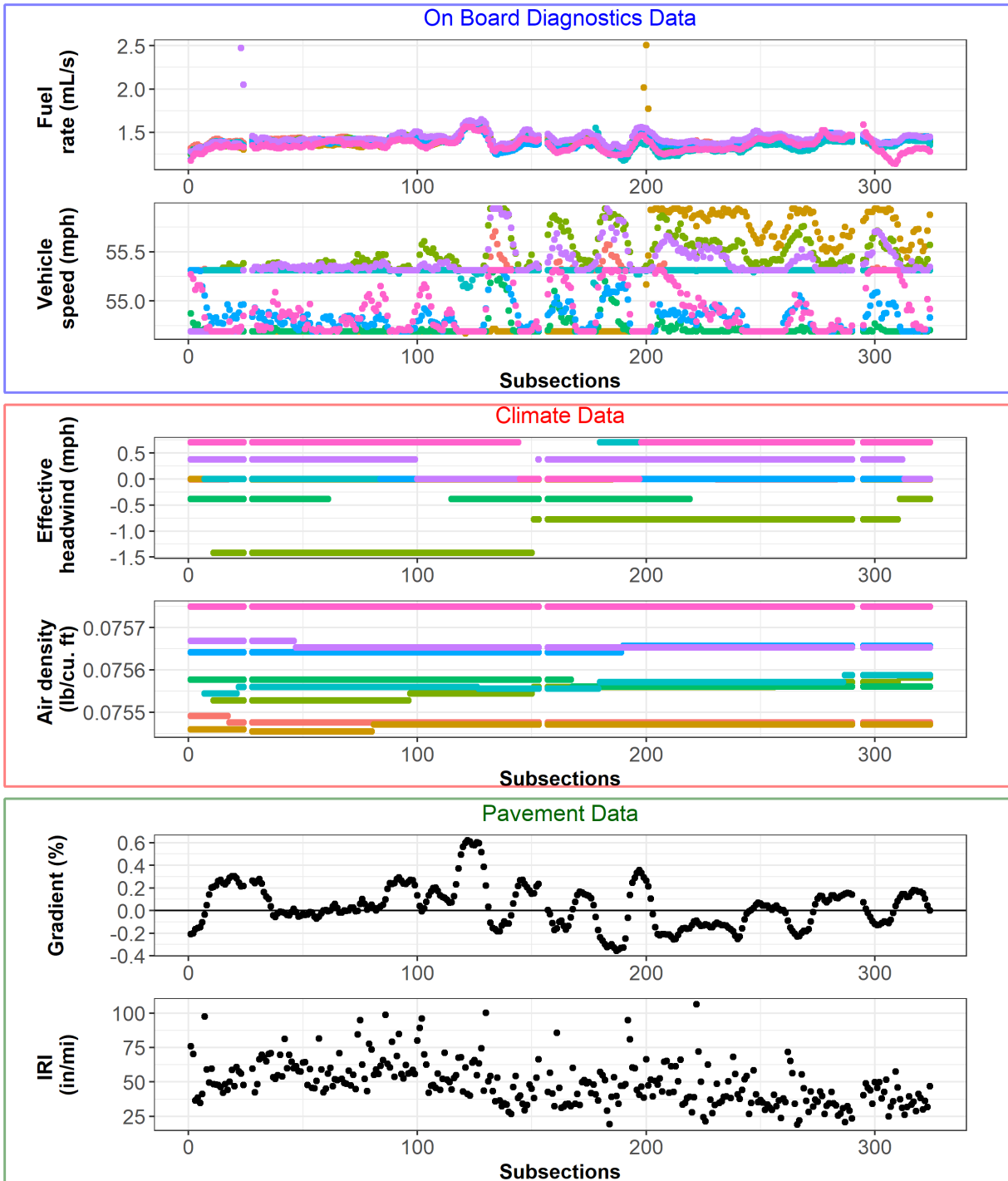


Figure P.16: Car data on Section PH03.

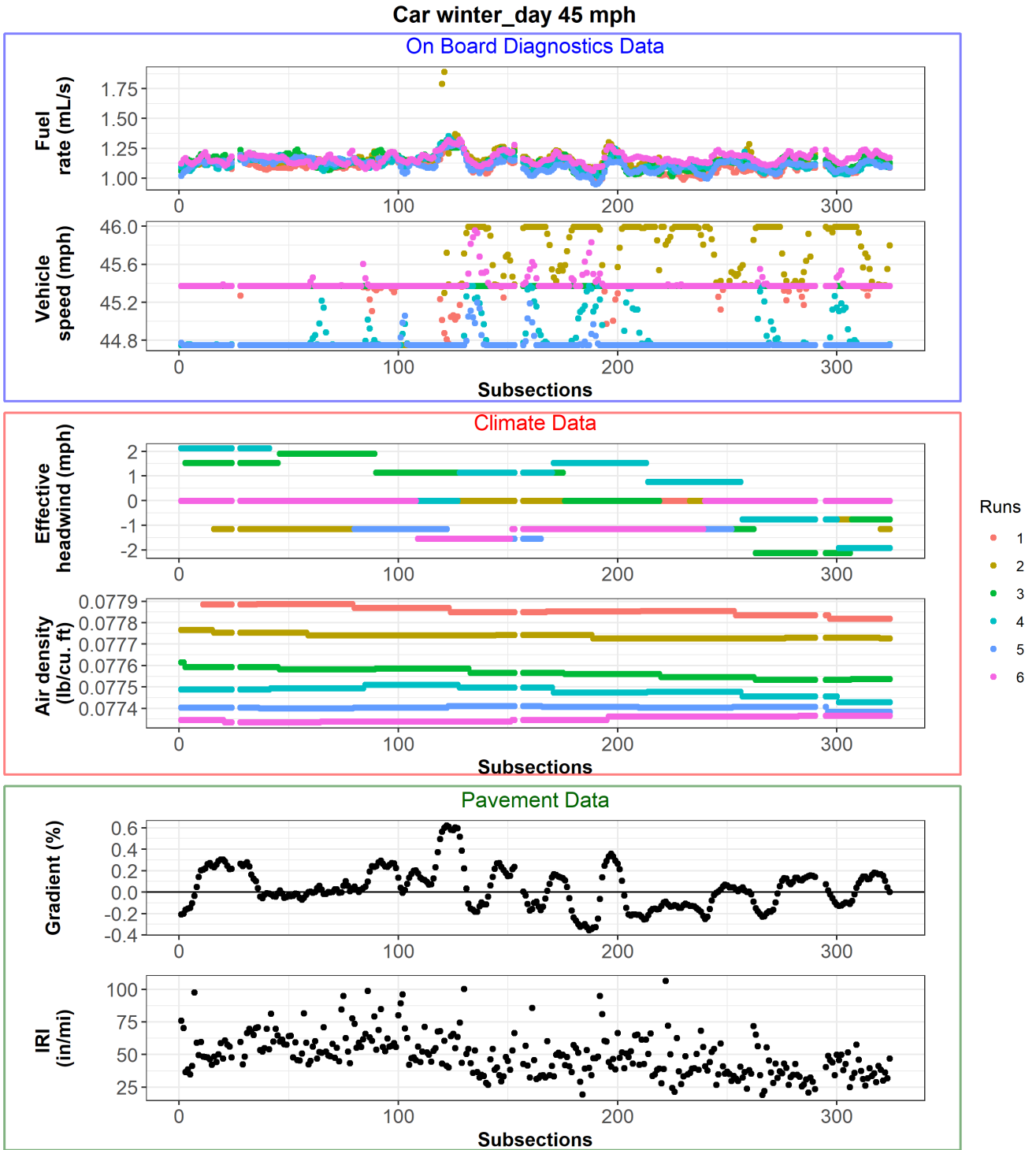


Figure P.17: Car data on Section PH03.

Car summer_day 45 mph

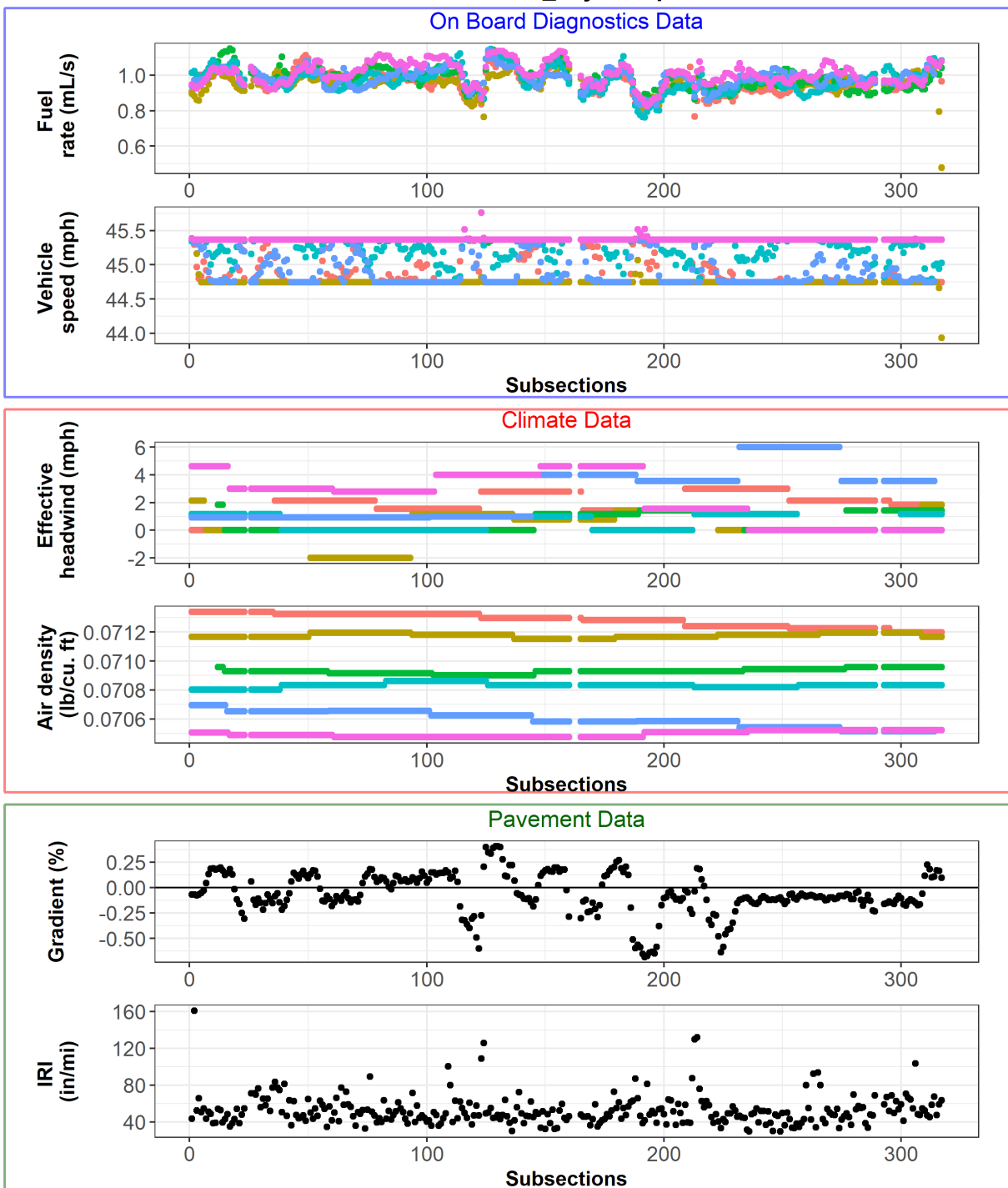


Figure P.18: Car data on Section PH04.

Car summer_day 55 mph

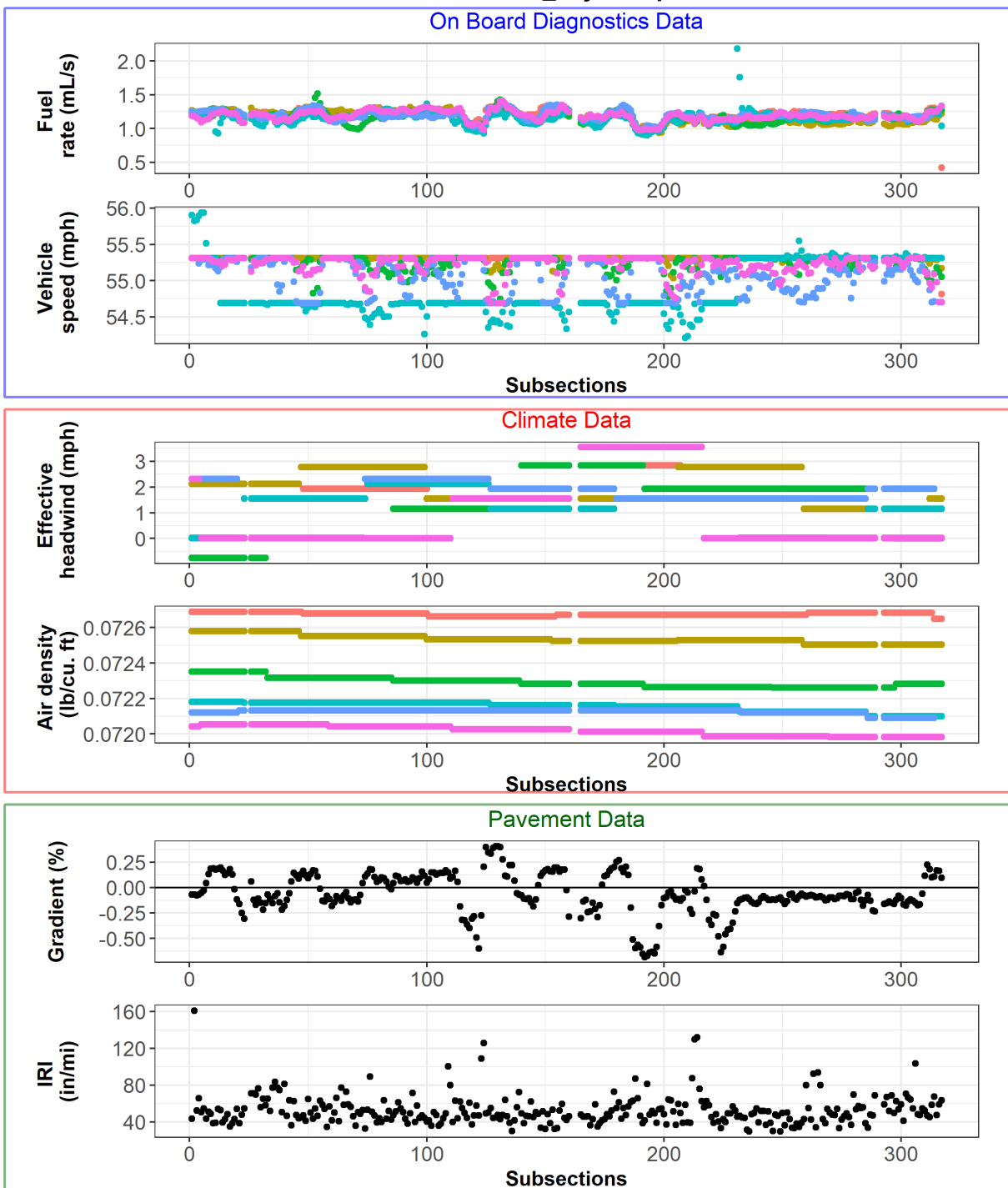


Figure P.19: Car data on Section PH04.

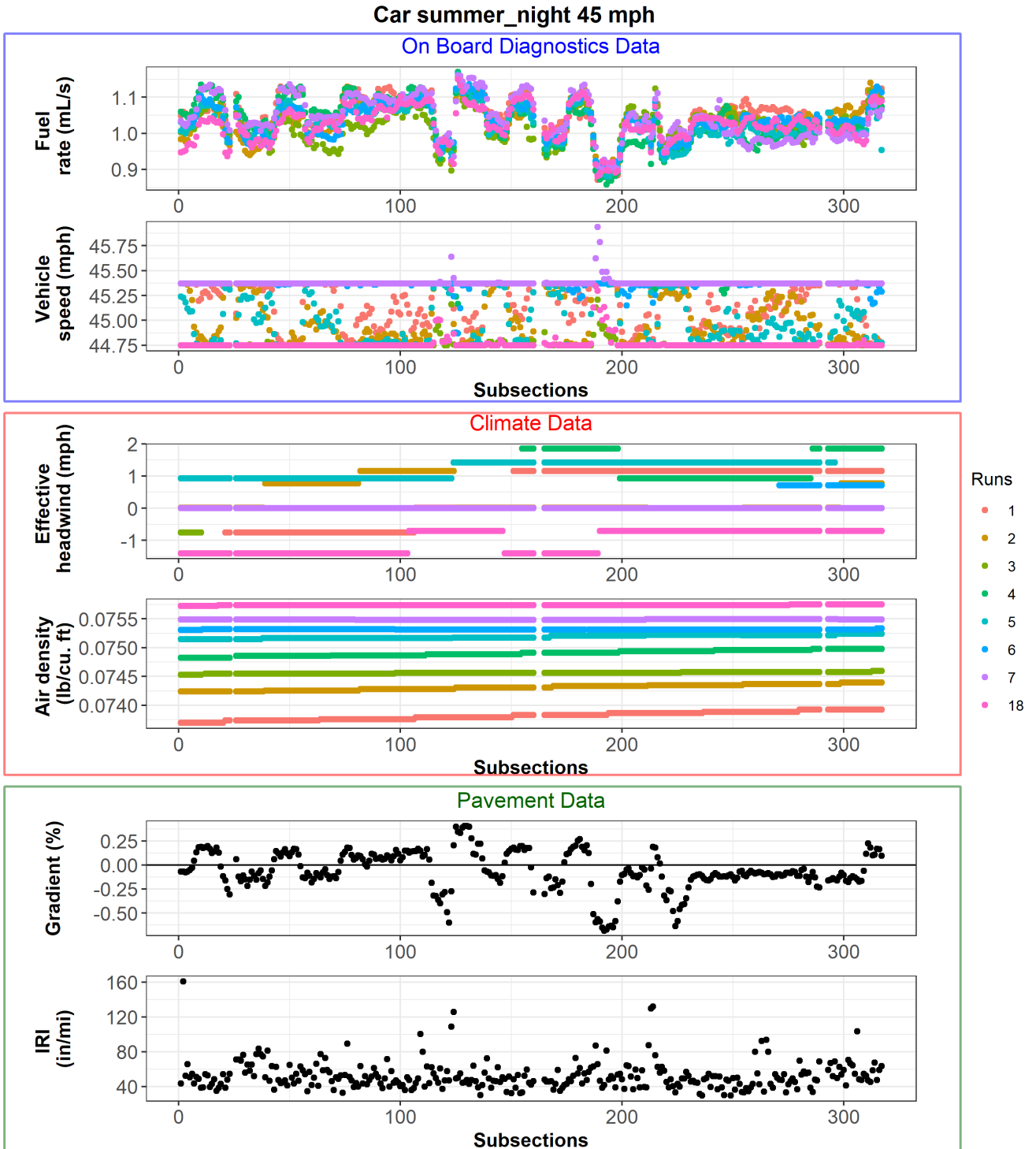


Figure P.20: Car data on Section PH04.

Car summer_night 55 mph

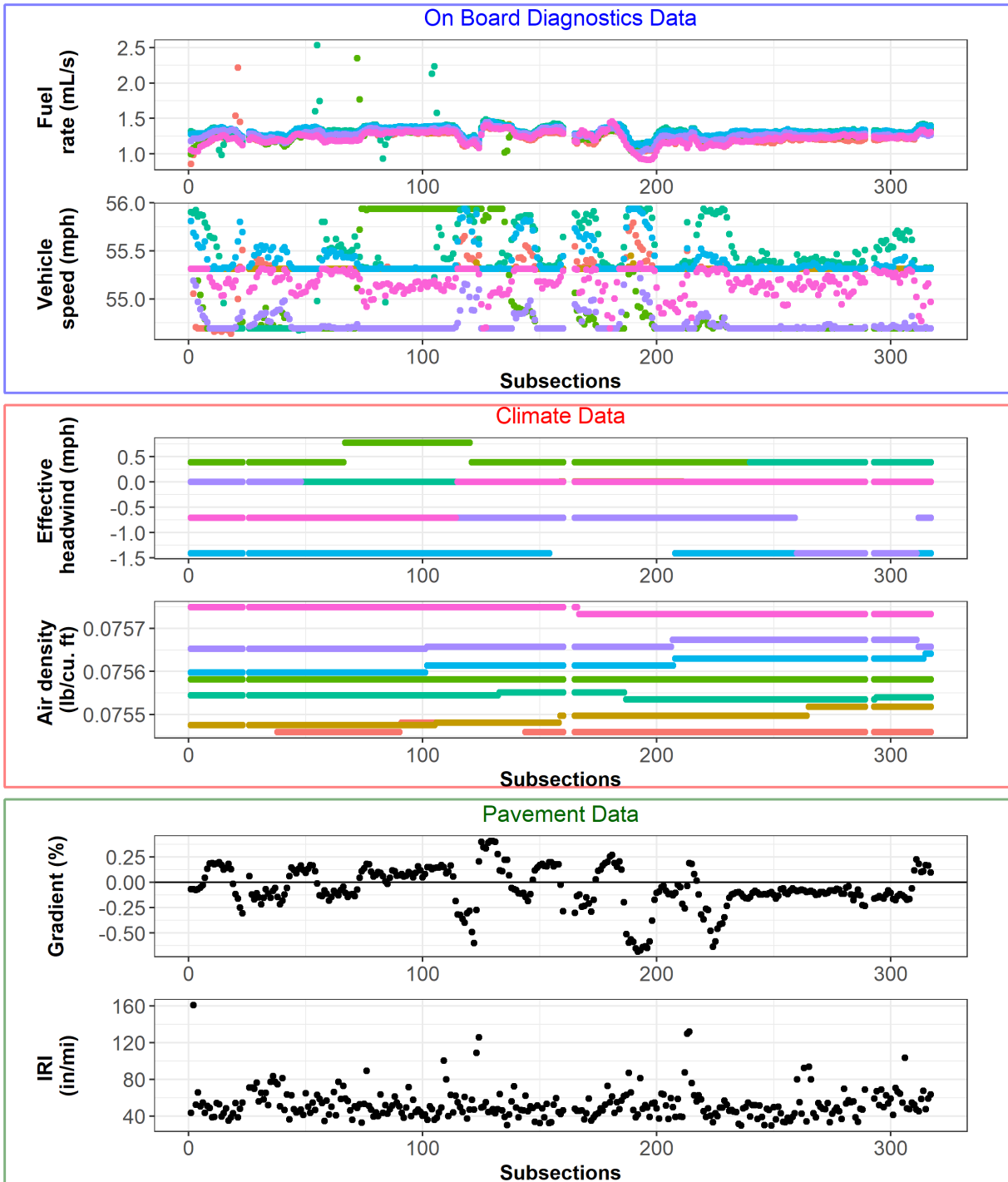


Figure P.21: Car data on Section PH04.

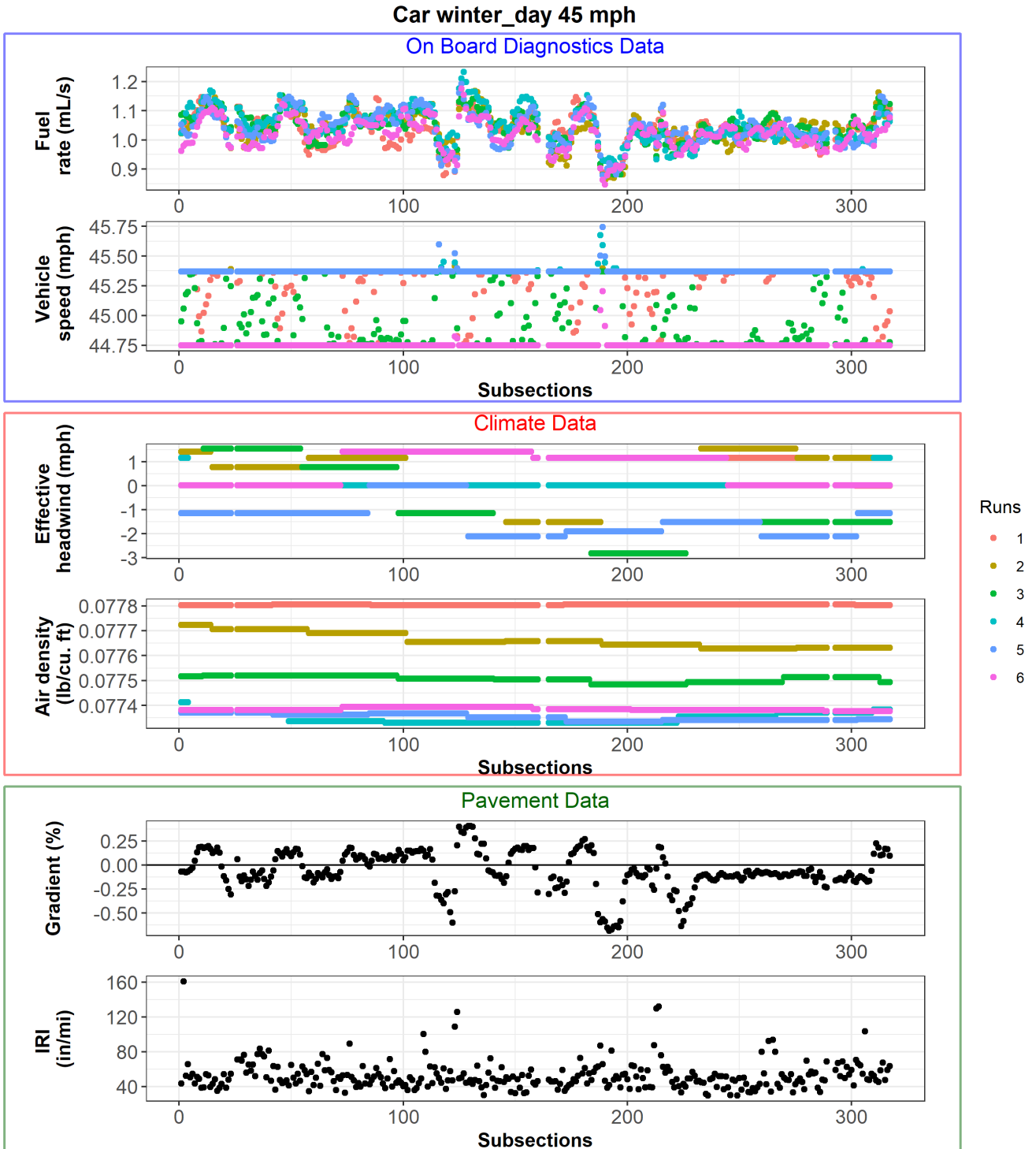


Figure P.22: Car data on Section PH04.

Car summer_day 35 mph

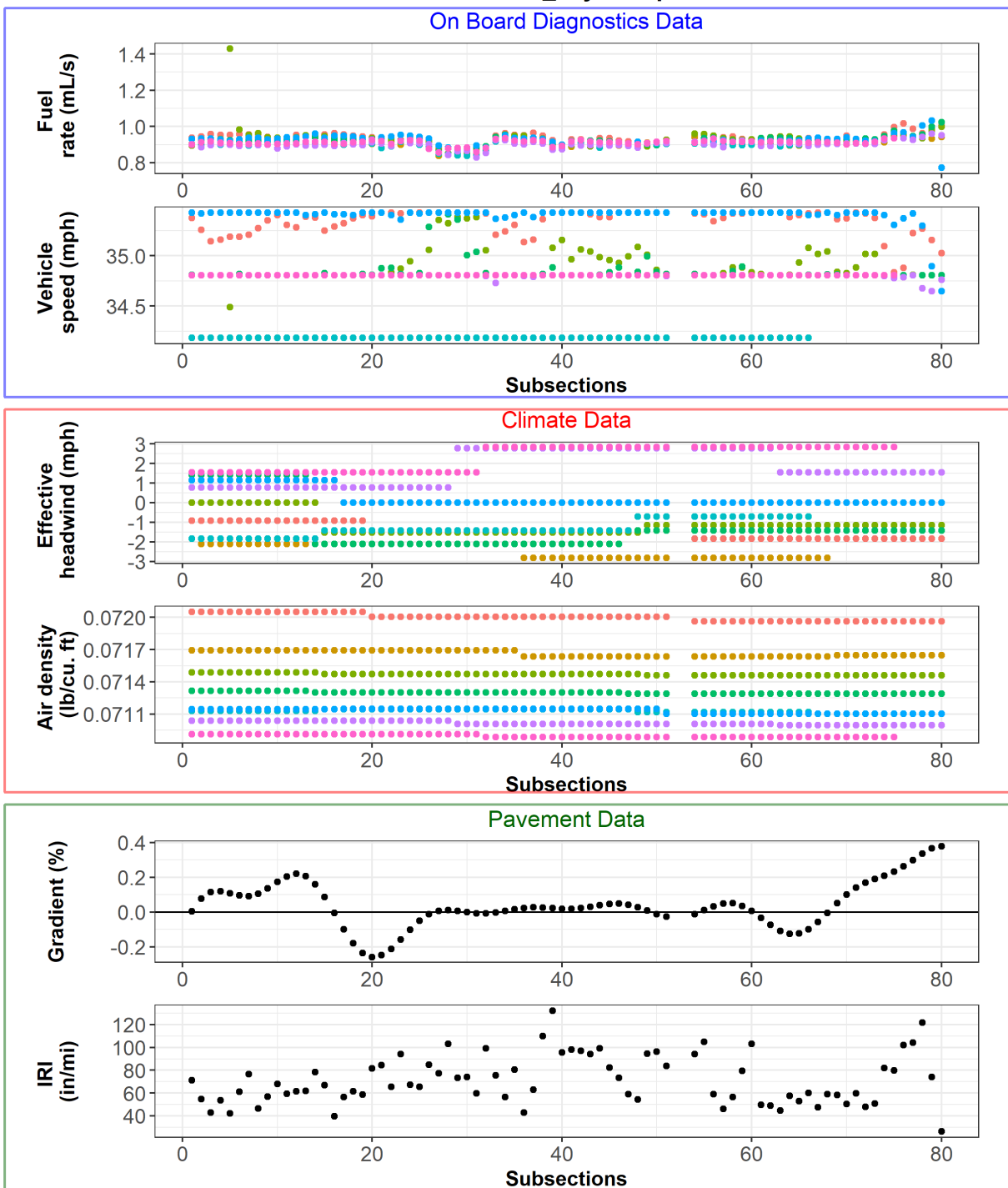


Figure P.23: Car data on Section PH07.

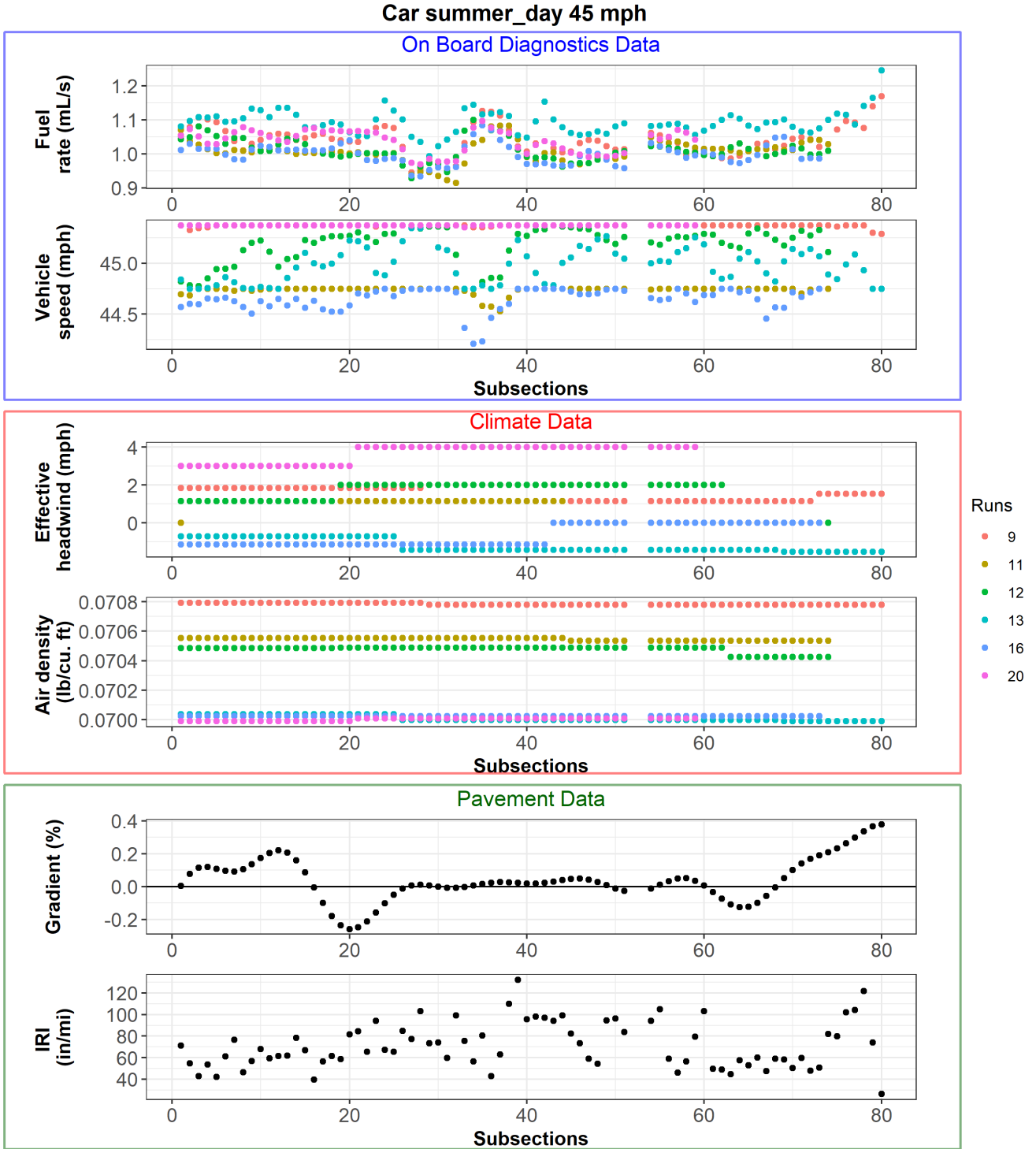


Figure P.24: Car data on Section PH07.

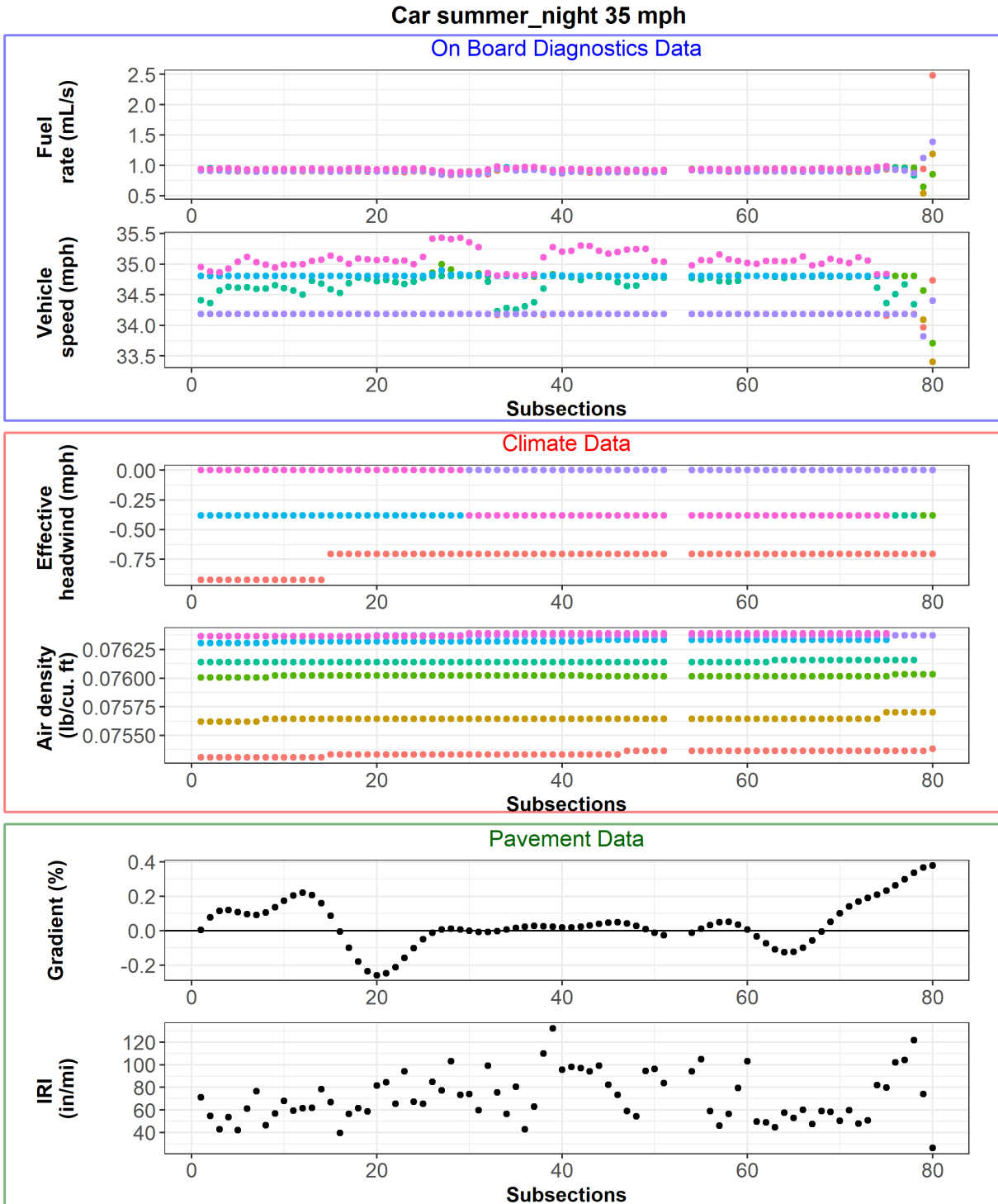


Figure P.25: Car data on Section PH07.

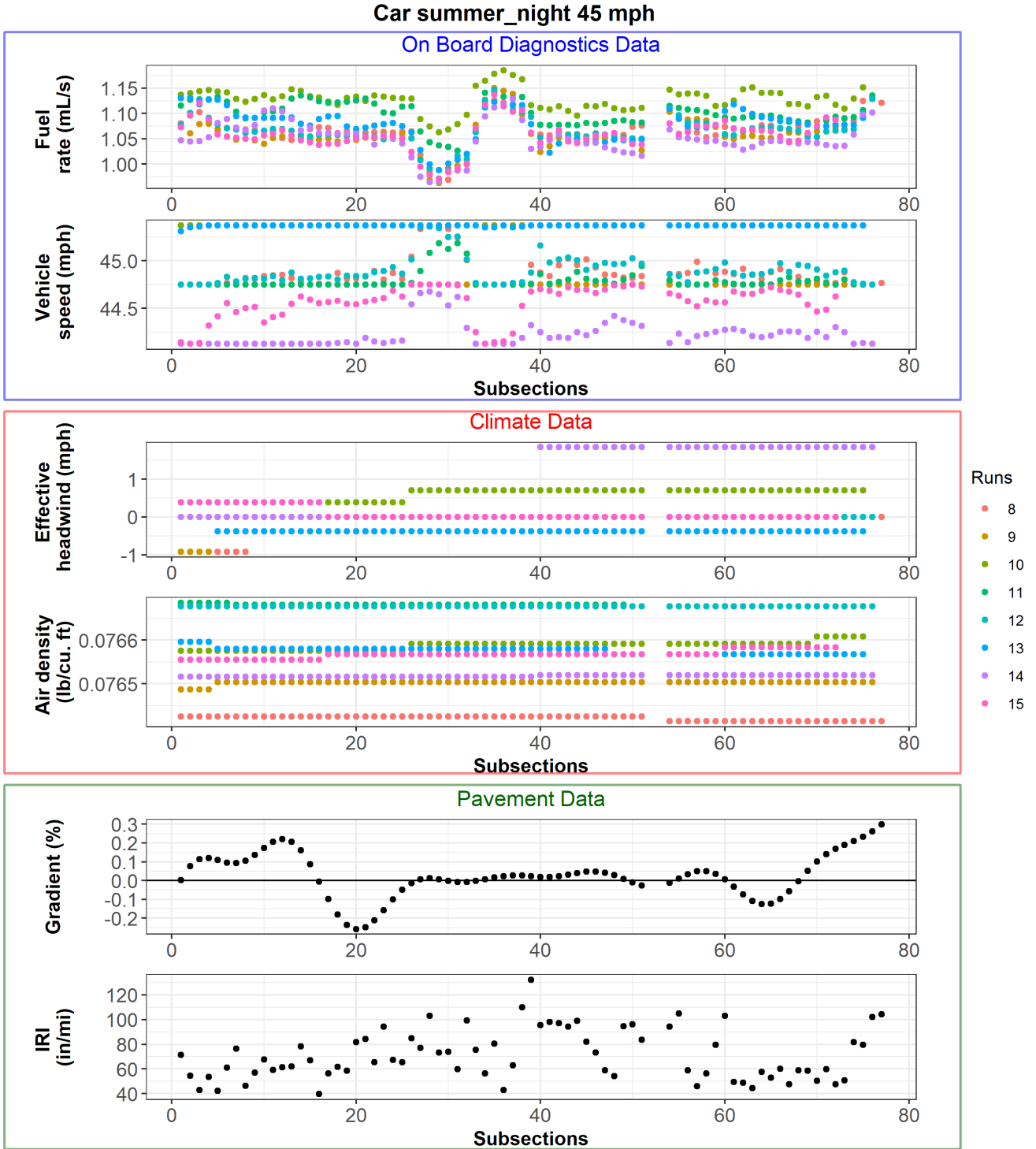
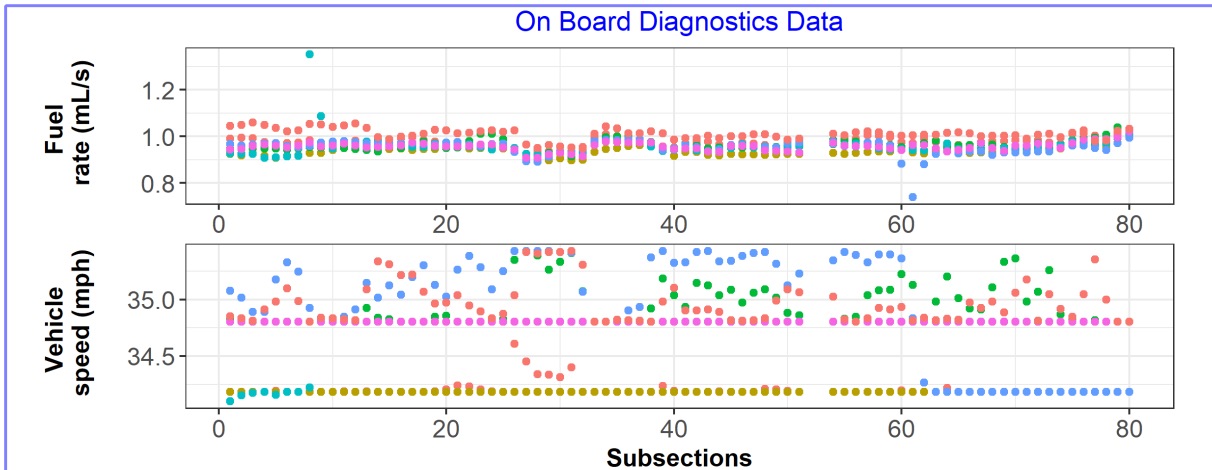


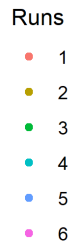
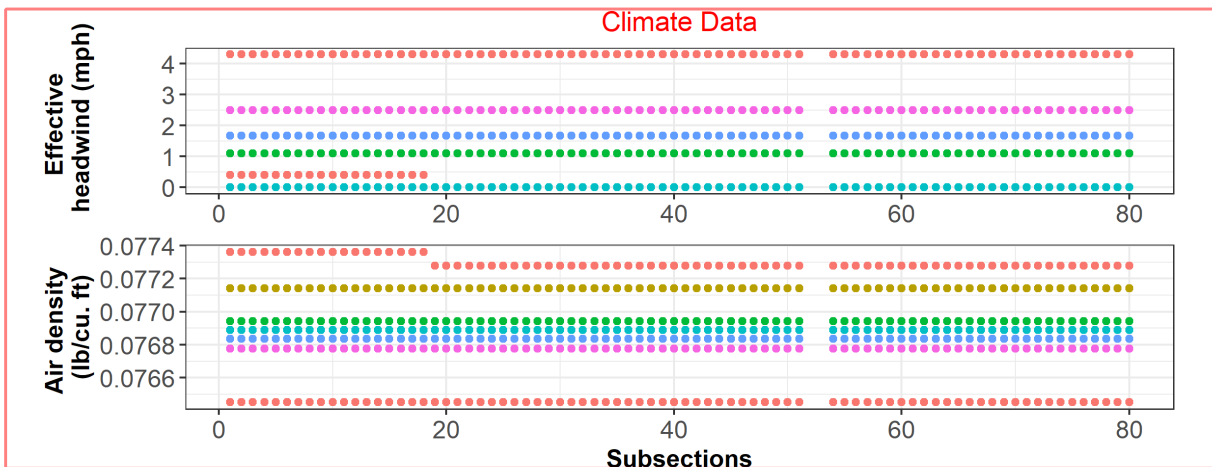
Figure P.26: Car data on Section PH07.

Car winter_day 35 mph

On Board Diagnostics Data



Climate Data



Pavement Data

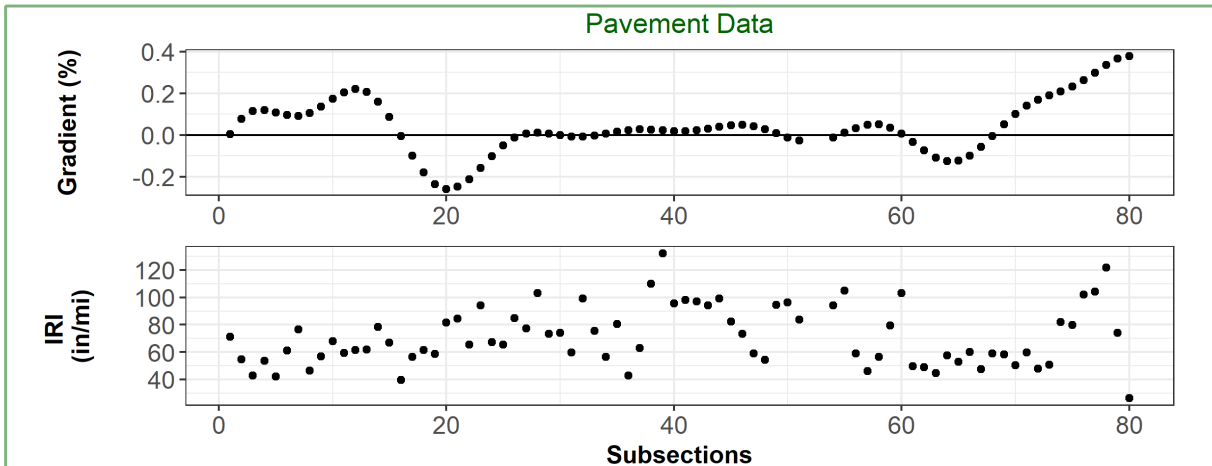
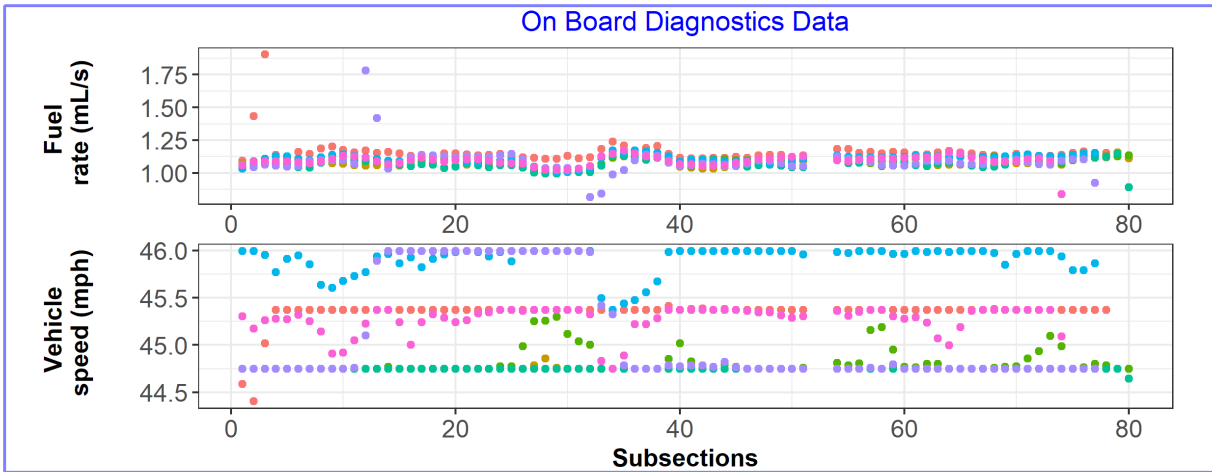


Figure P.27: Car data on Section PH07.

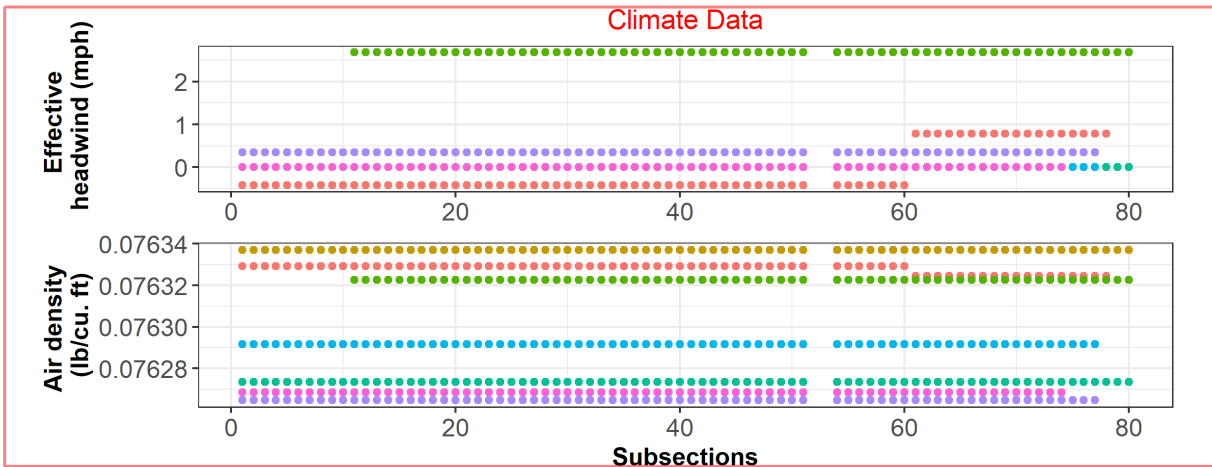
Car winter_day 45 mph

On Board Diagnostics Data



Subsections

Climate Data

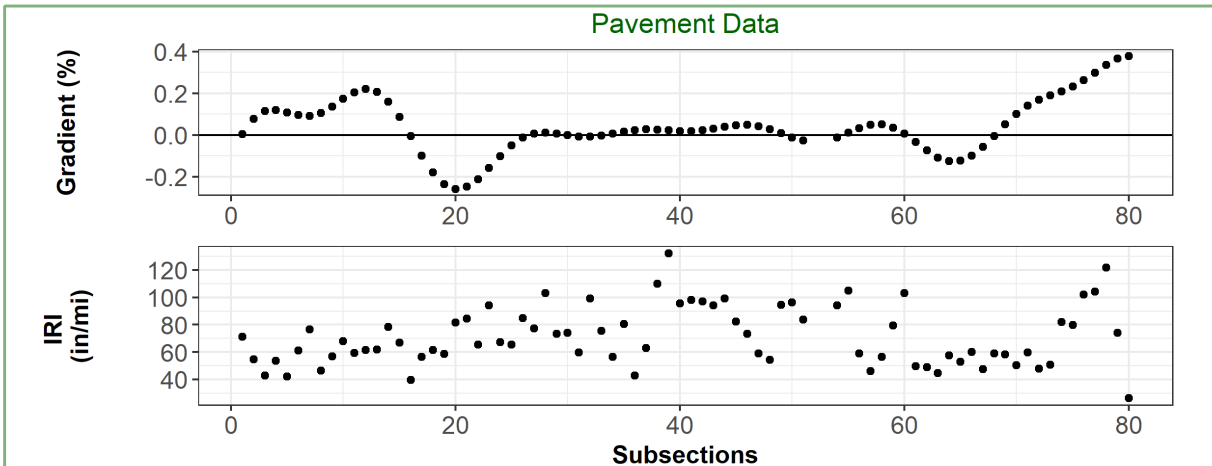


Subsections

Runs

- 2
- 3
- 4
- 5
- 6
- 7
- 8

Pavement Data

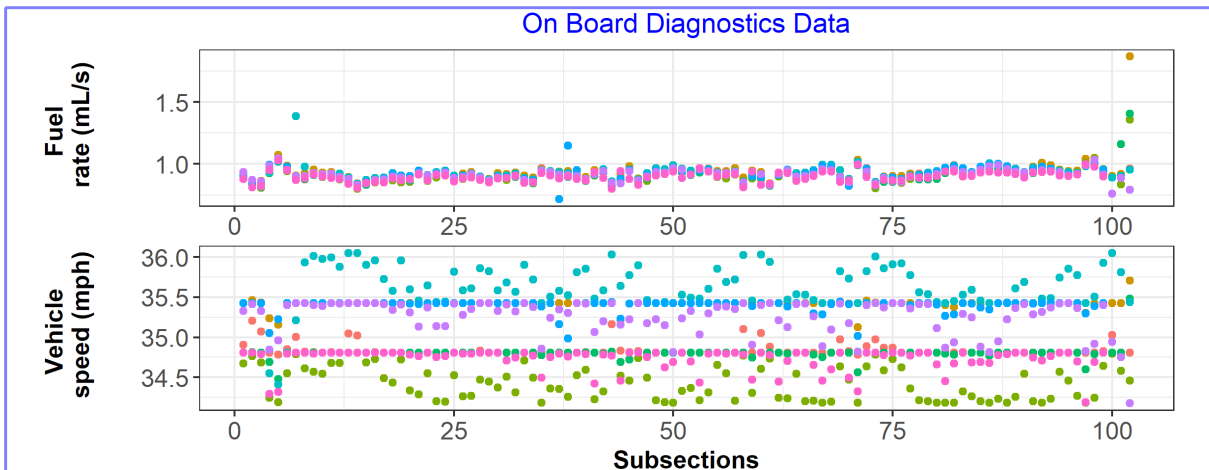


Subsections

Figure P.28: Car data on Section PH07.

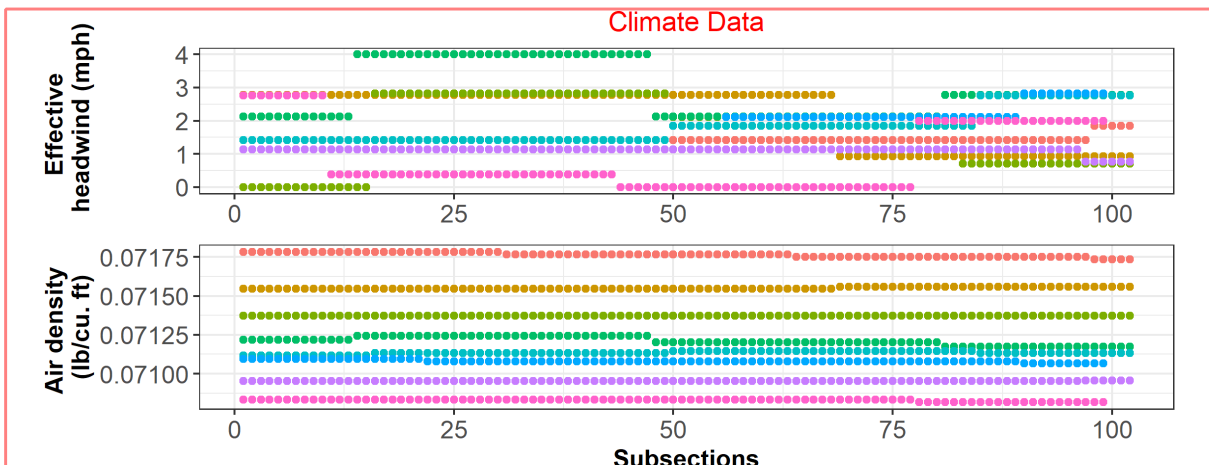
Car summer_day 35 mph

On Board Diagnostics Data



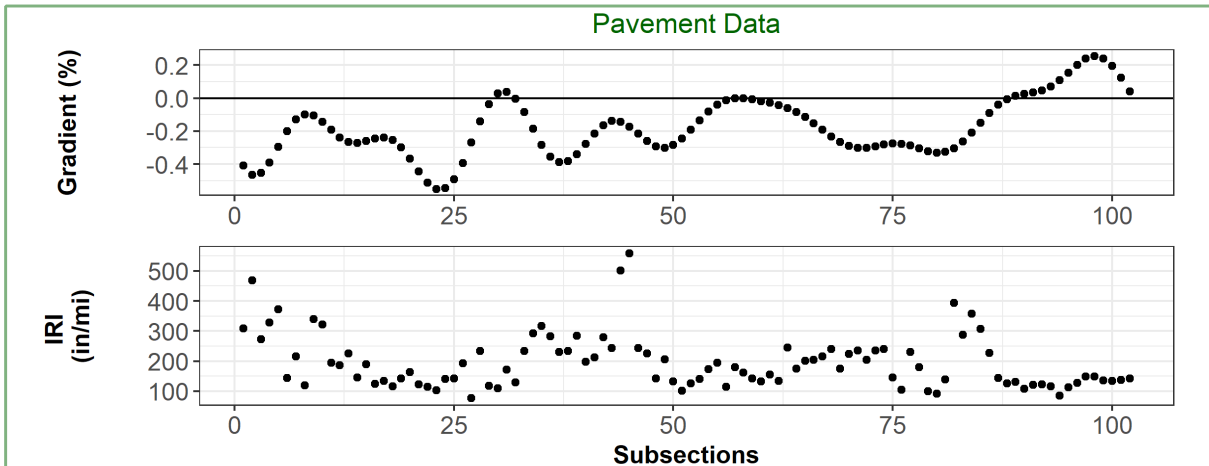
Subsections

Climate Data



Subsections

Pavement Data



Subsections

Runs

- 1
- 2
- 3
- 4
- 5
- 6
- 7
- 8

Figure P.29: Car data on Section PH08.

Car summer_day 45 mph

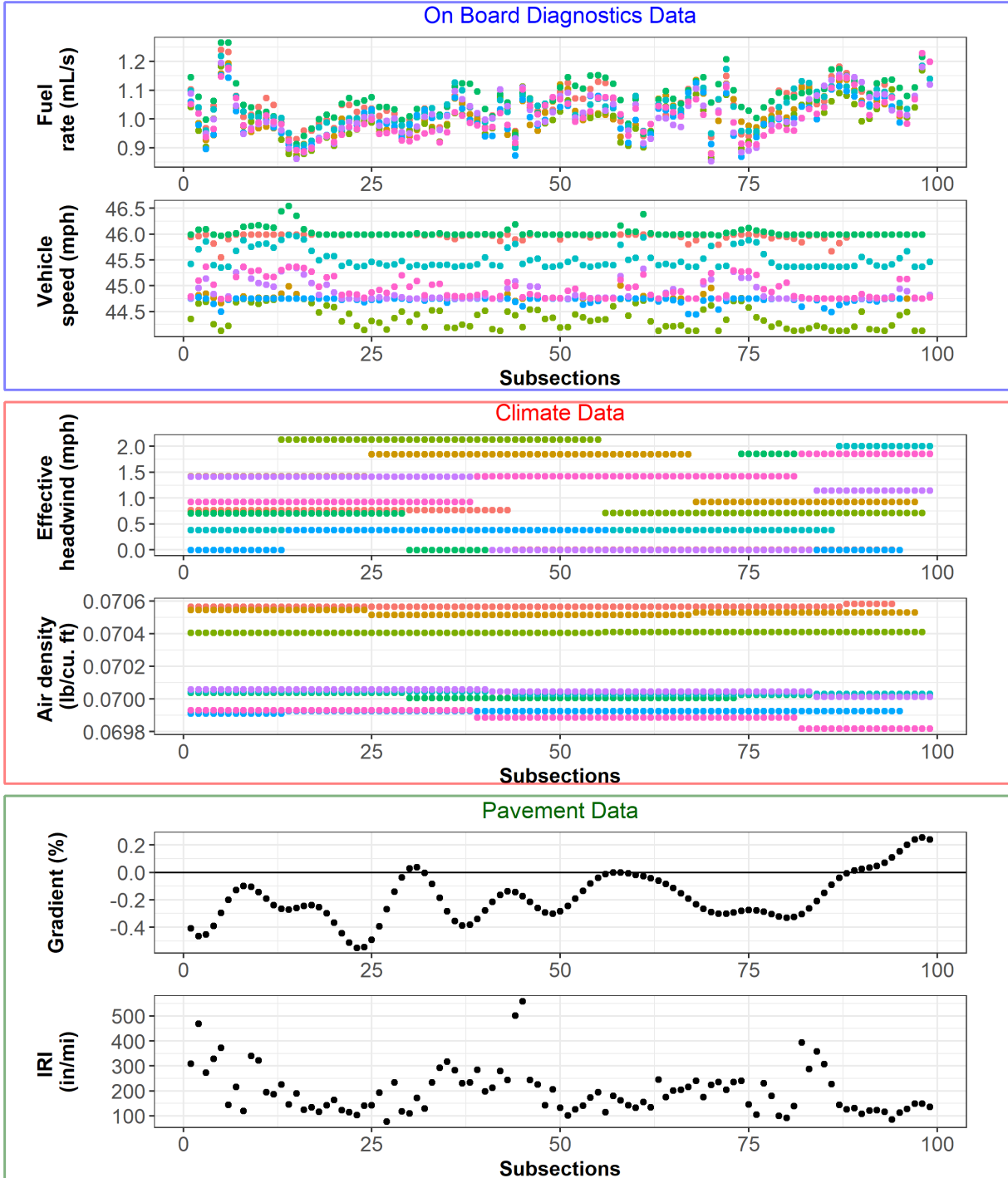


Figure P.30: Car data on Section PH08.

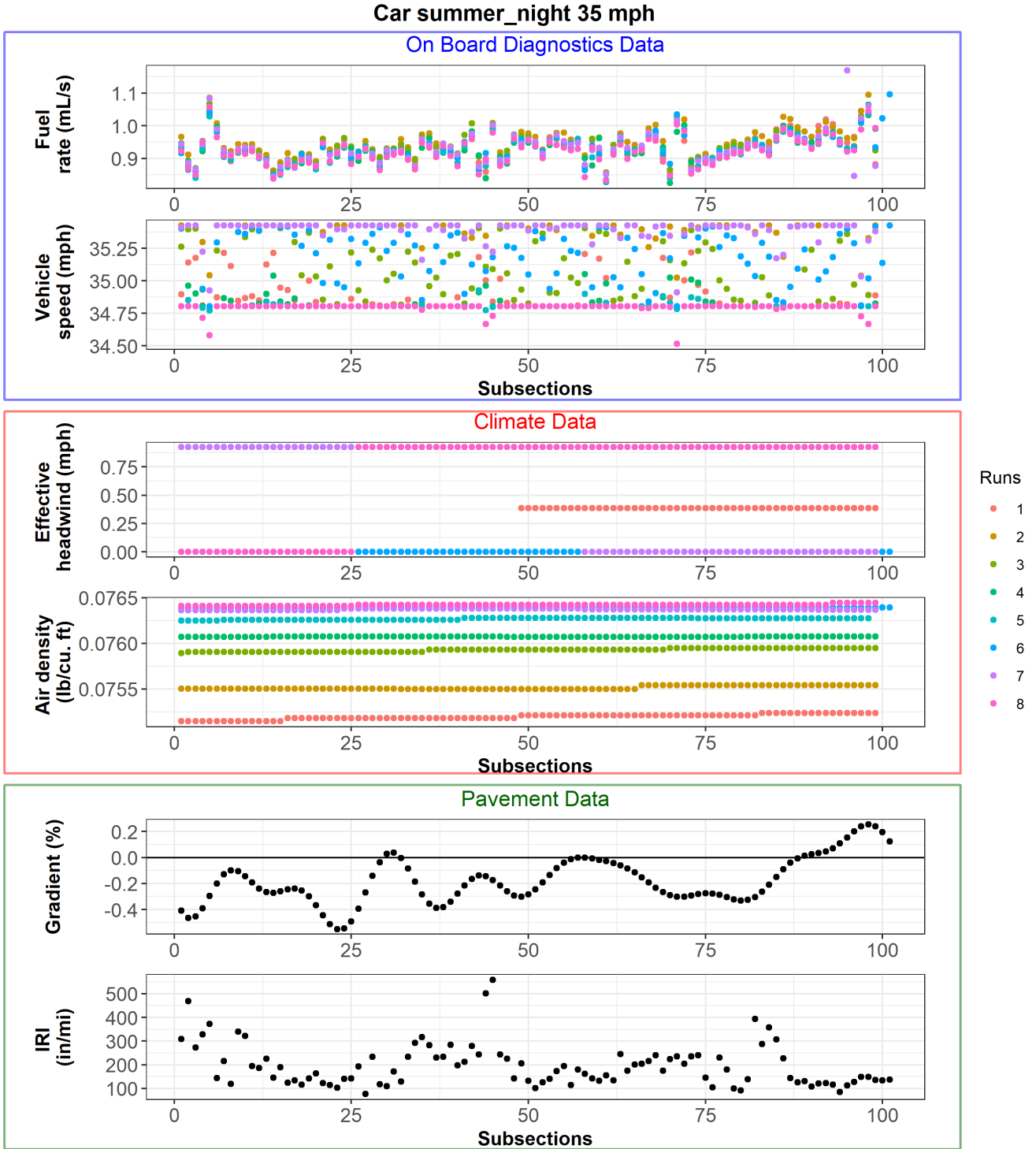
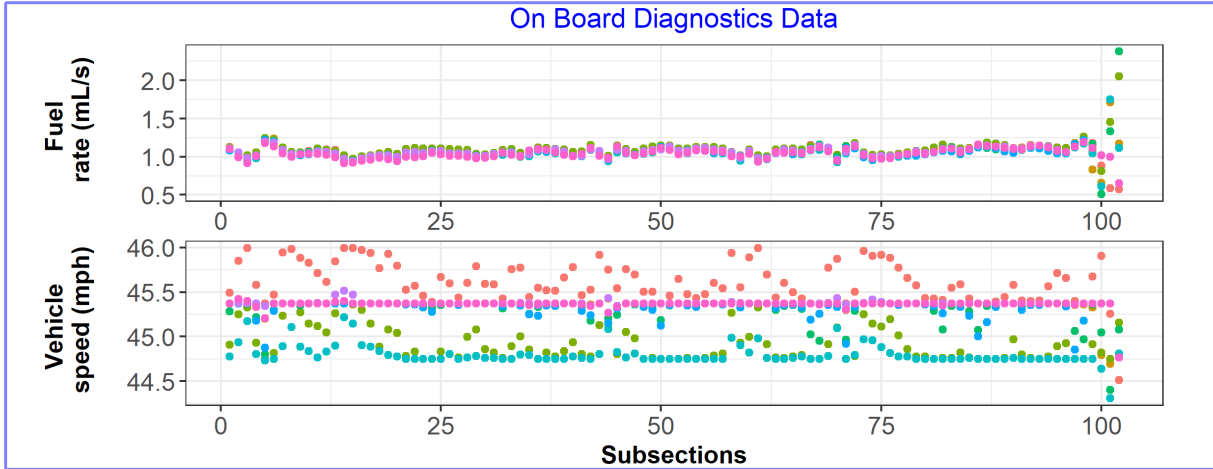
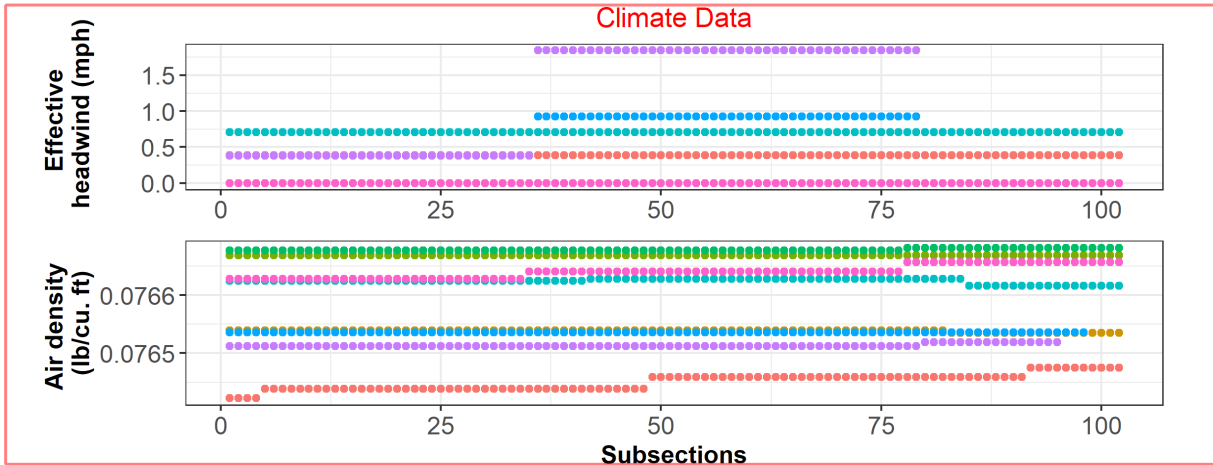


Figure P.31: Car data on Section PH08.

Car summer_night 45 mph
On Board Diagnostics Data



Climate Data



Pavement Data

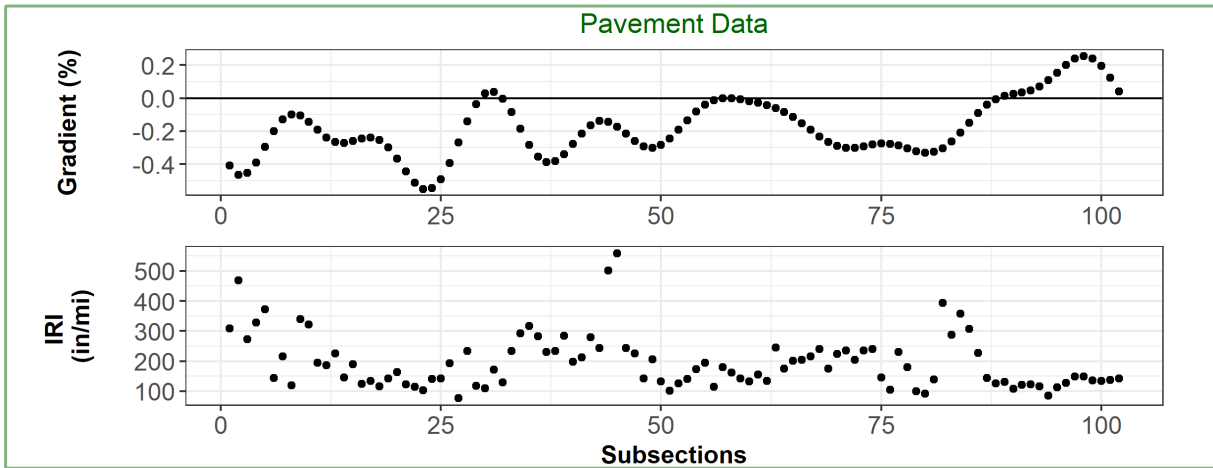


Figure P.32: Car data on Section PH08.

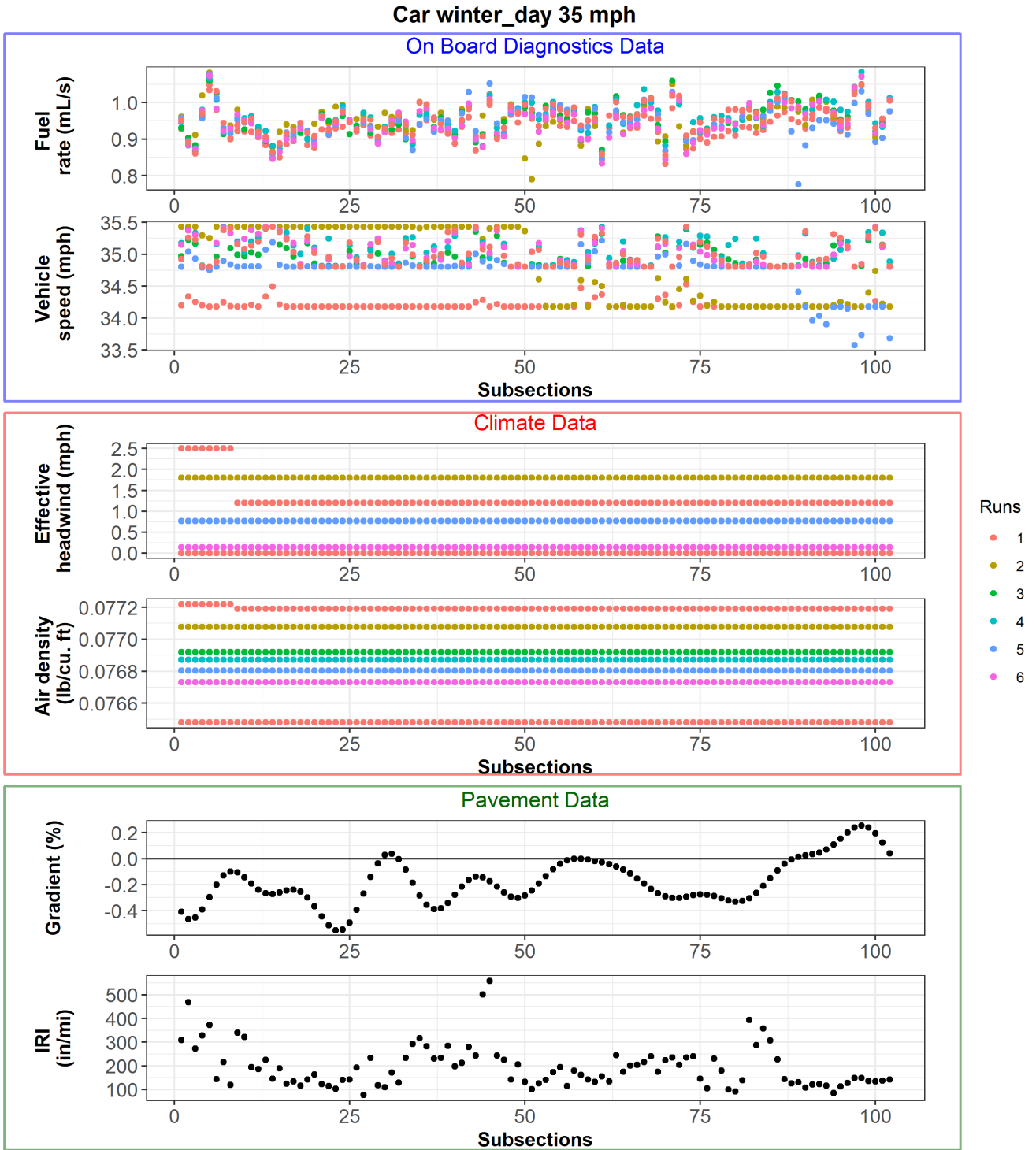


Figure P.33: Car data on Section PH08.

Car winter_day 45 mph

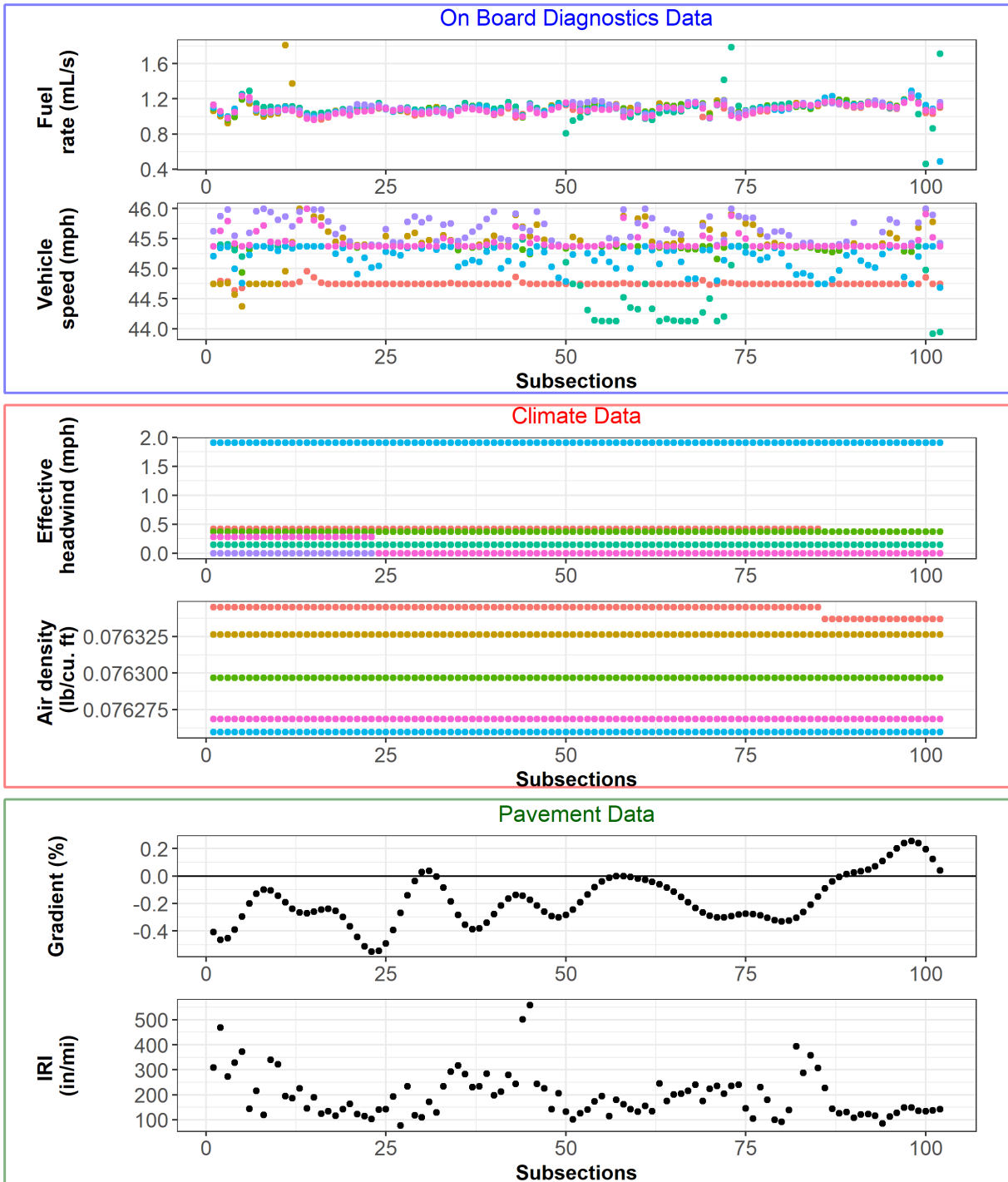


Figure P.34: Car data on Section PH08.

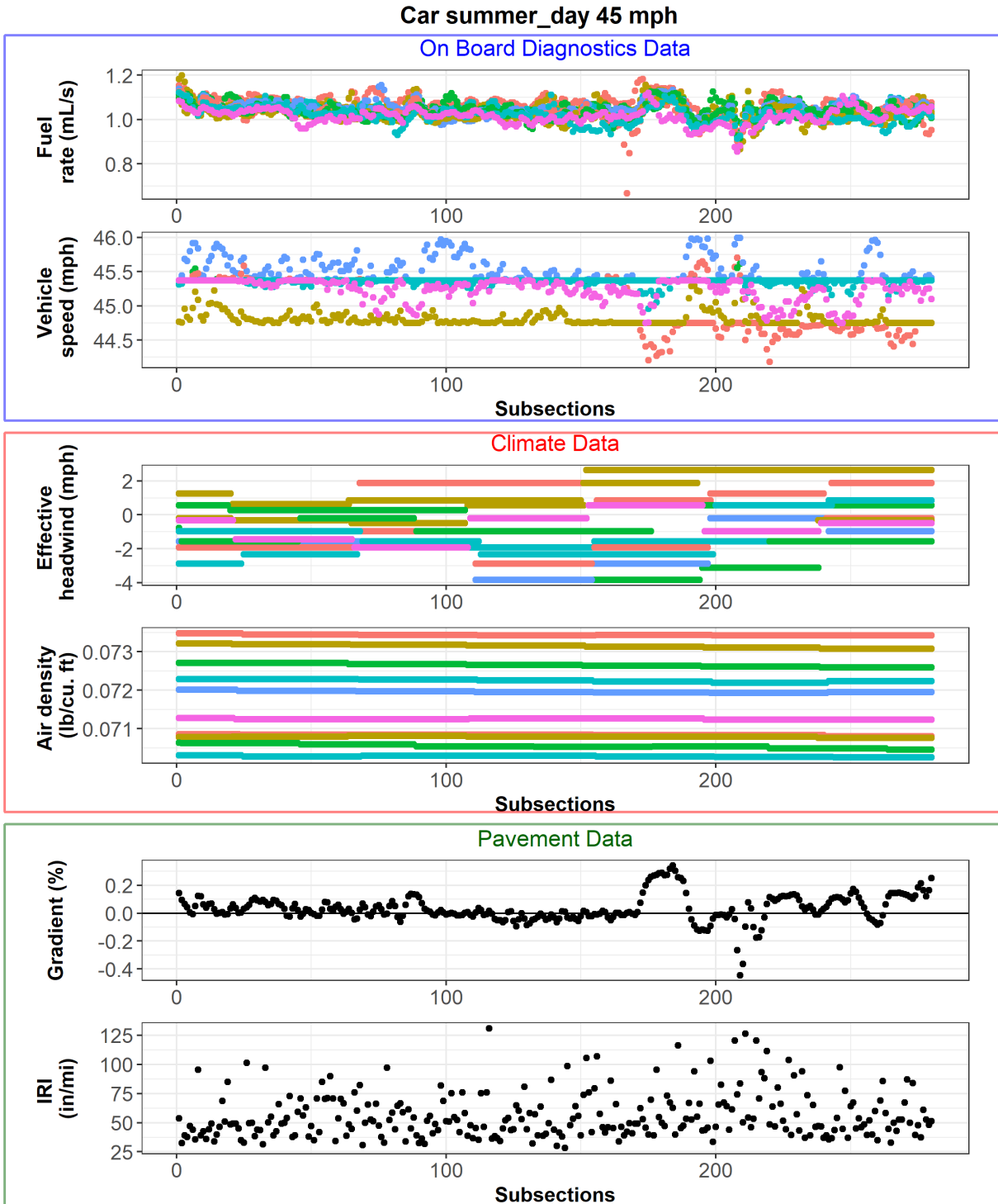


Figure P.35: Car data on Section PH09.

Car summer_day 55 mph

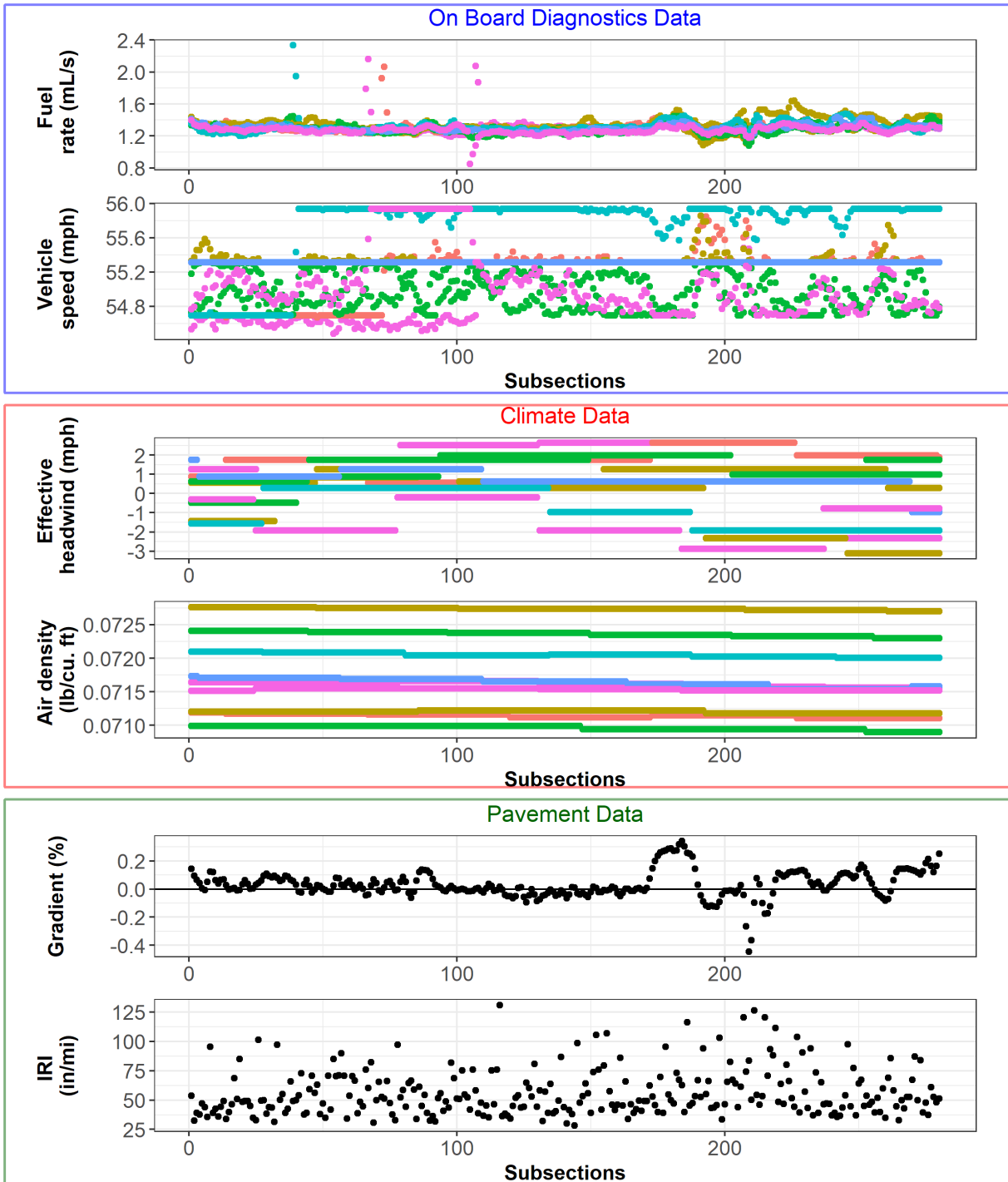


Figure P.36: Car data on Section PH09.

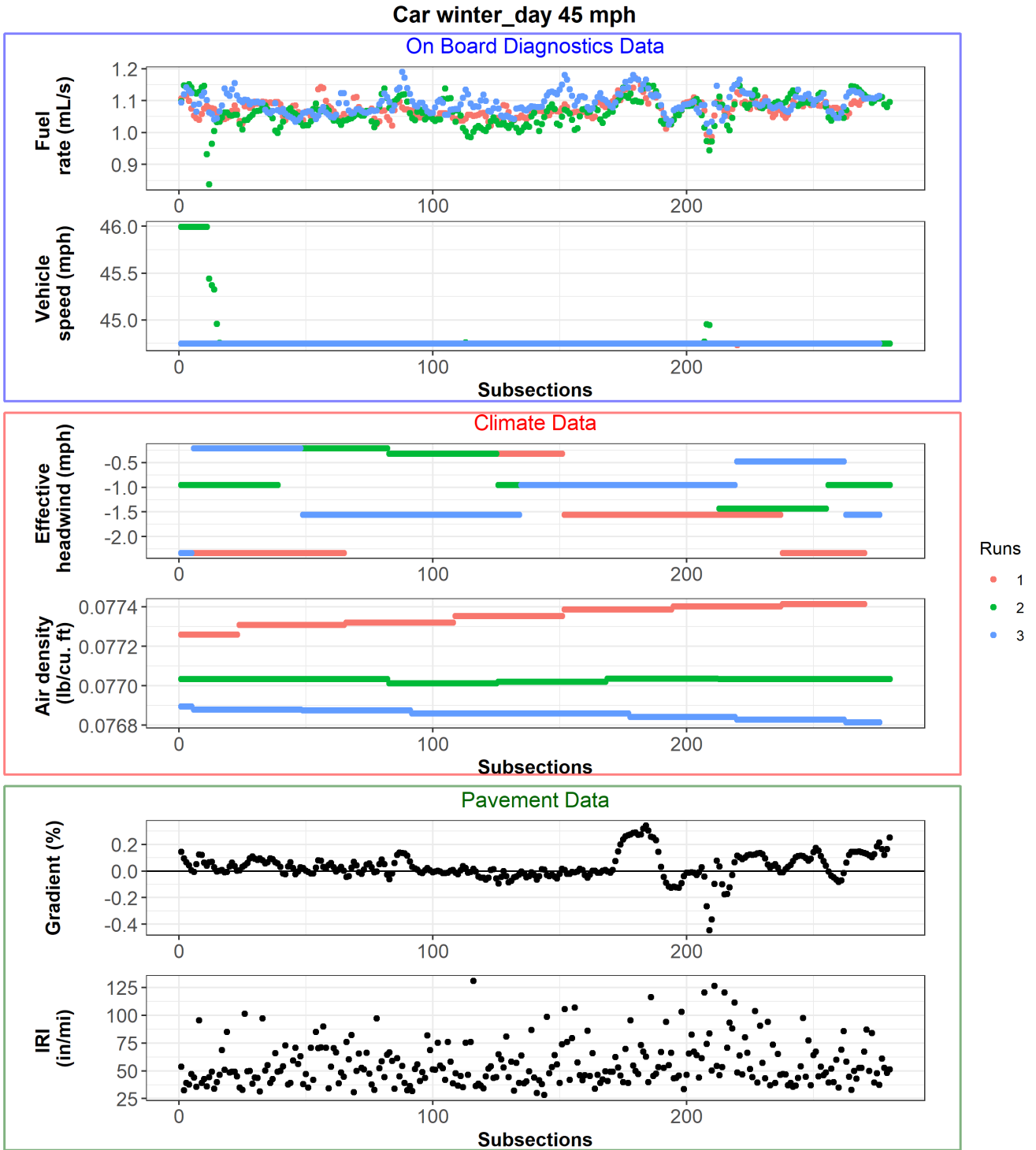


Figure P.37: Car data on Section PH09.

Car winter_day 55 mph

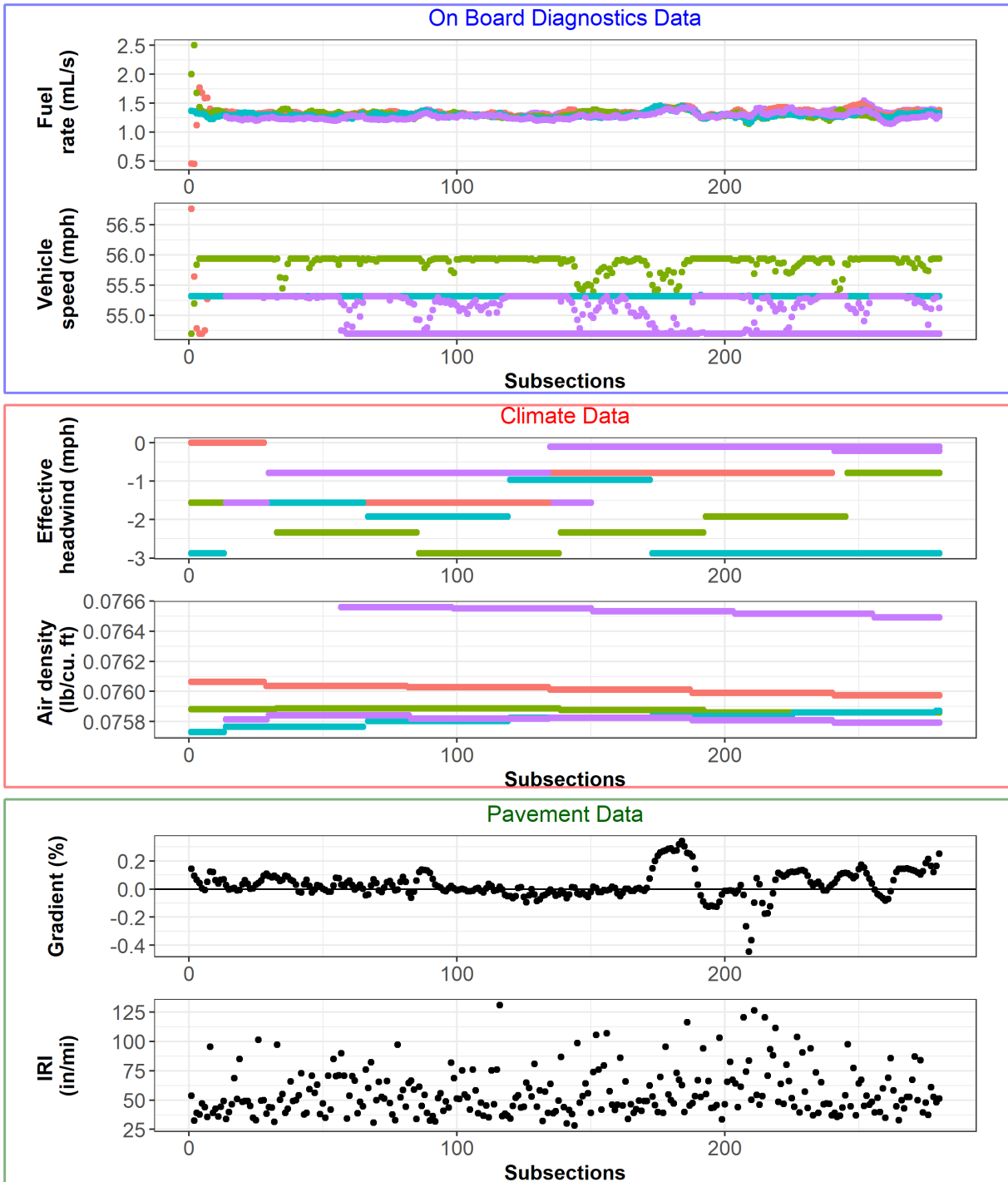


Figure P.38: Car data on Section PH09.

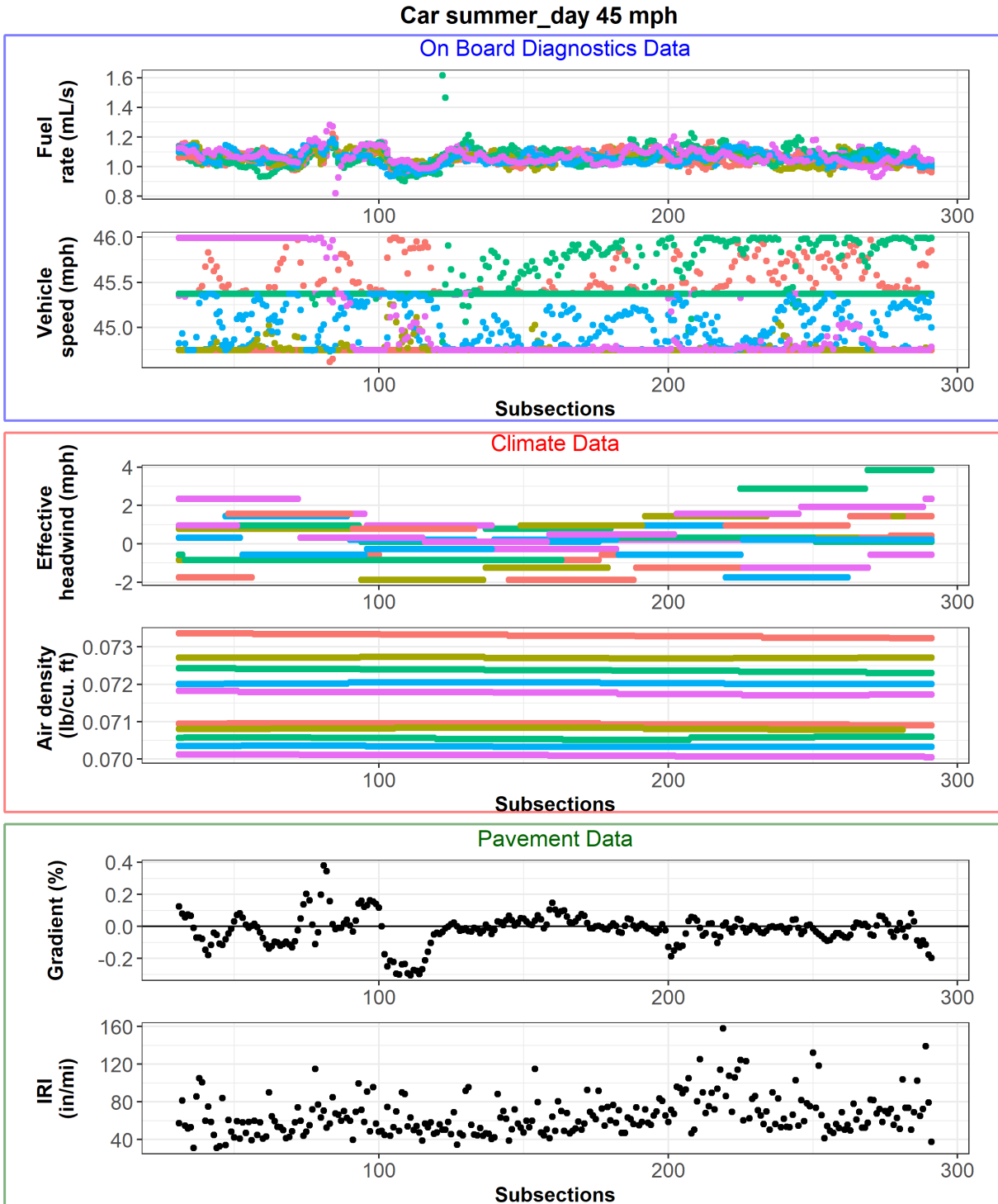


Figure P.39: Car data on Section PH10.

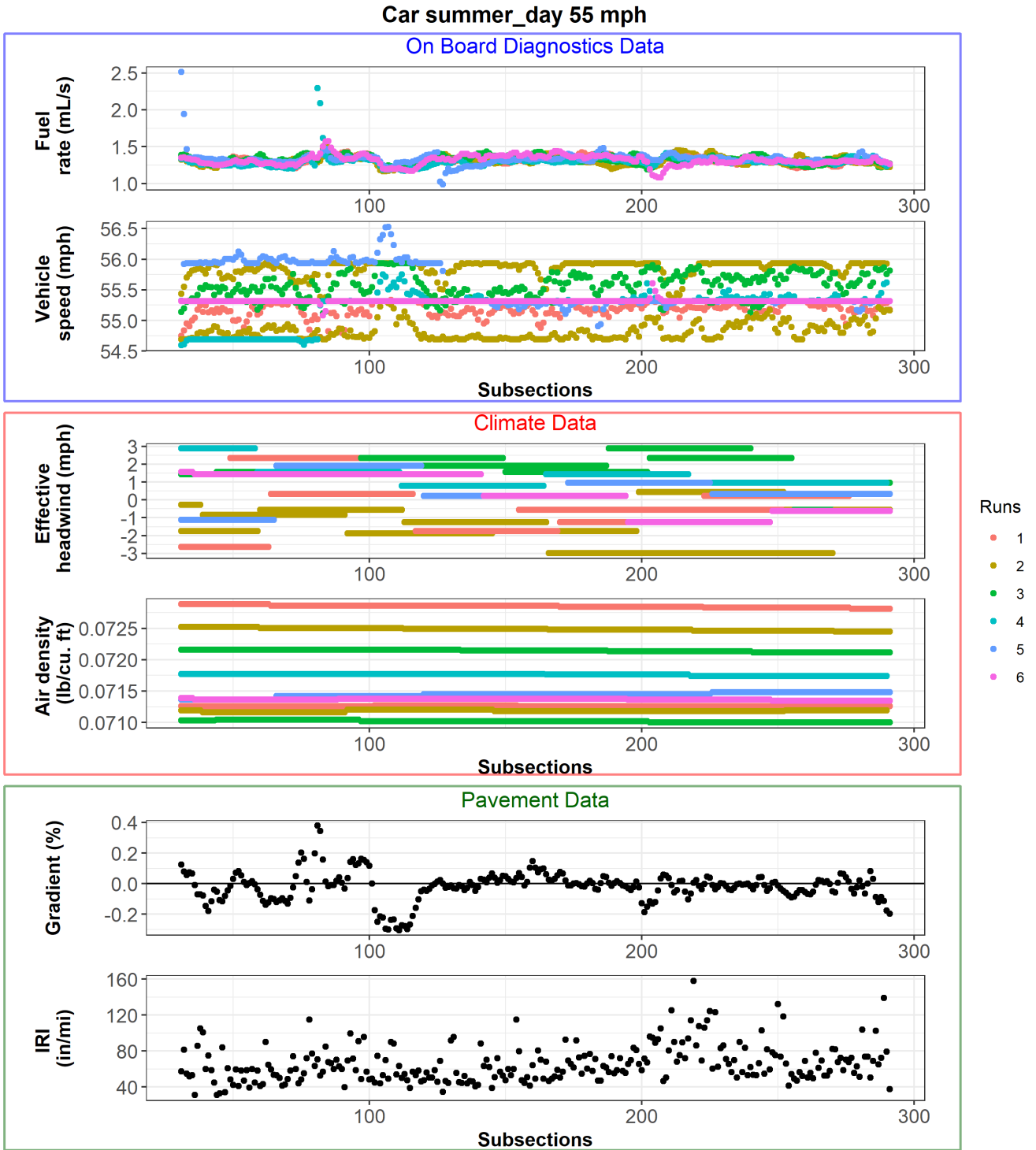


Figure P.40: Car data on Section PH10.

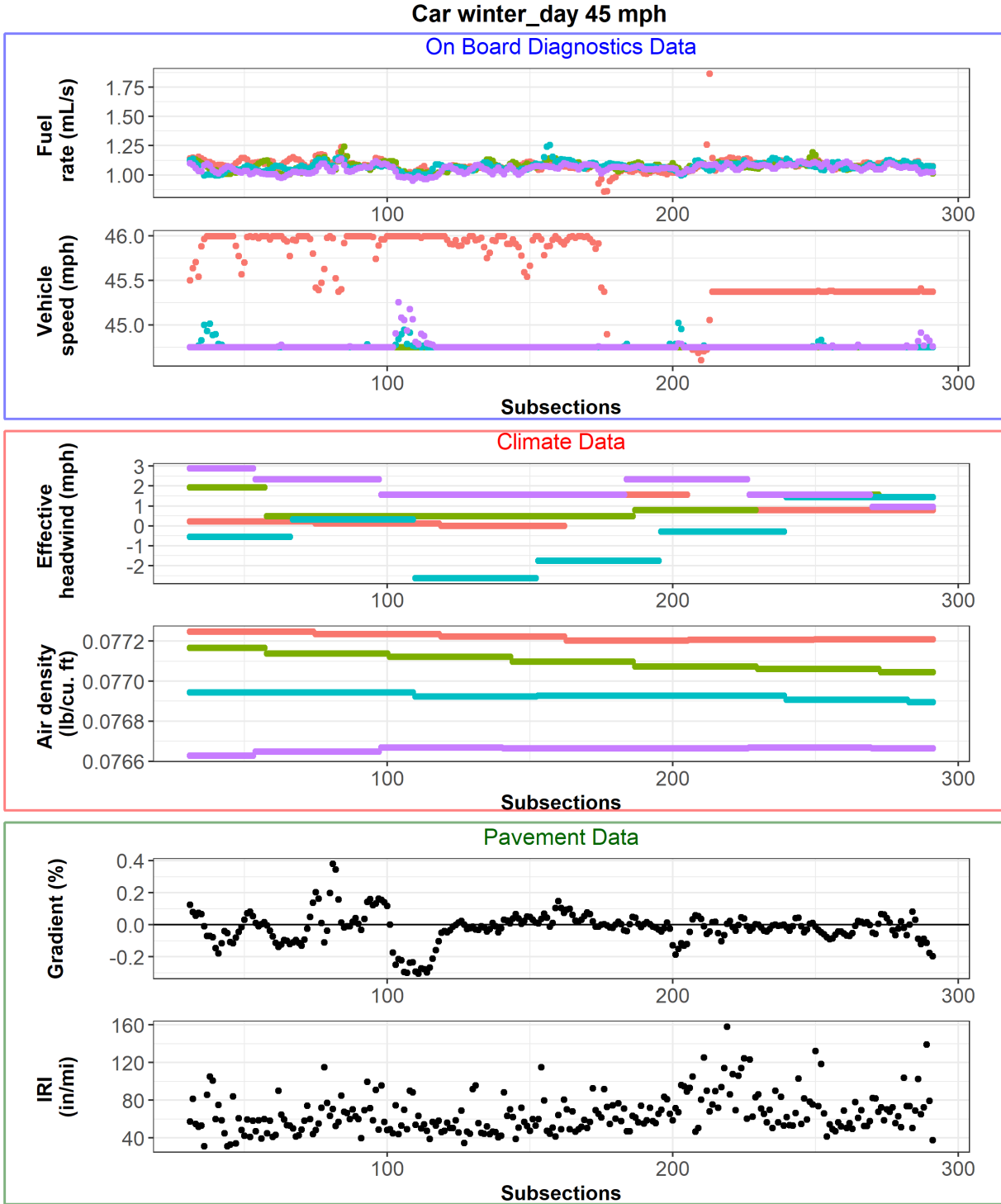


Figure P.41: Car data on Section PH10.

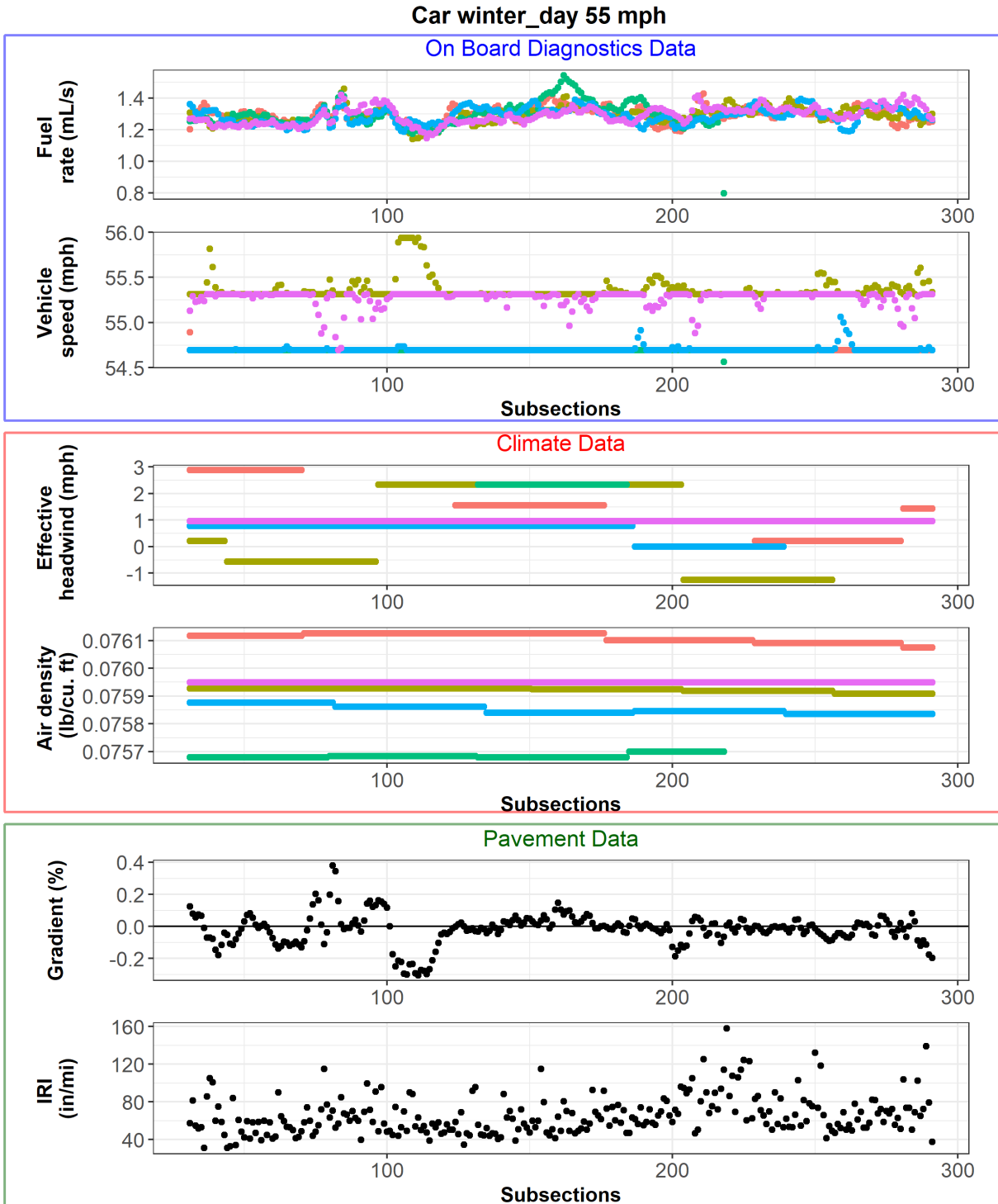
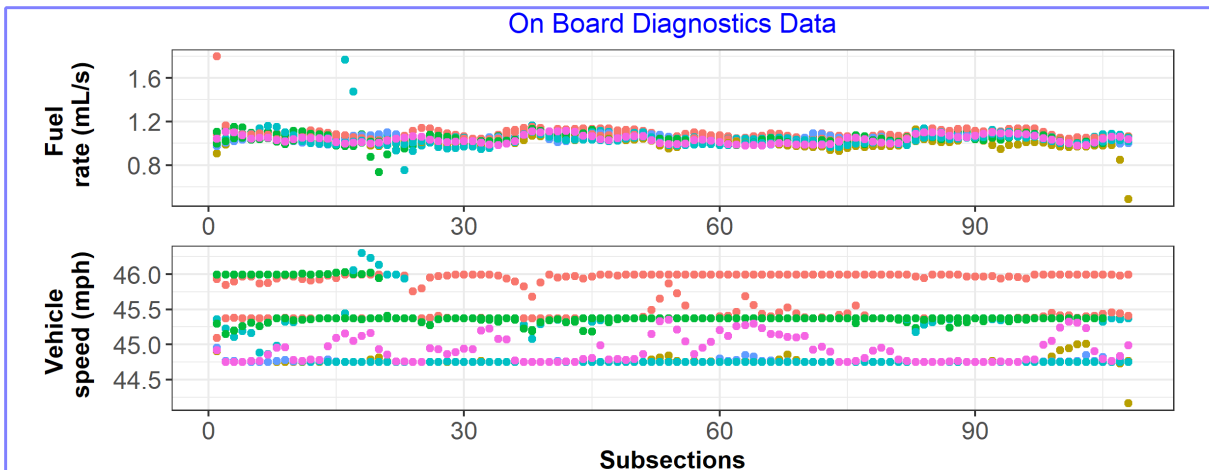


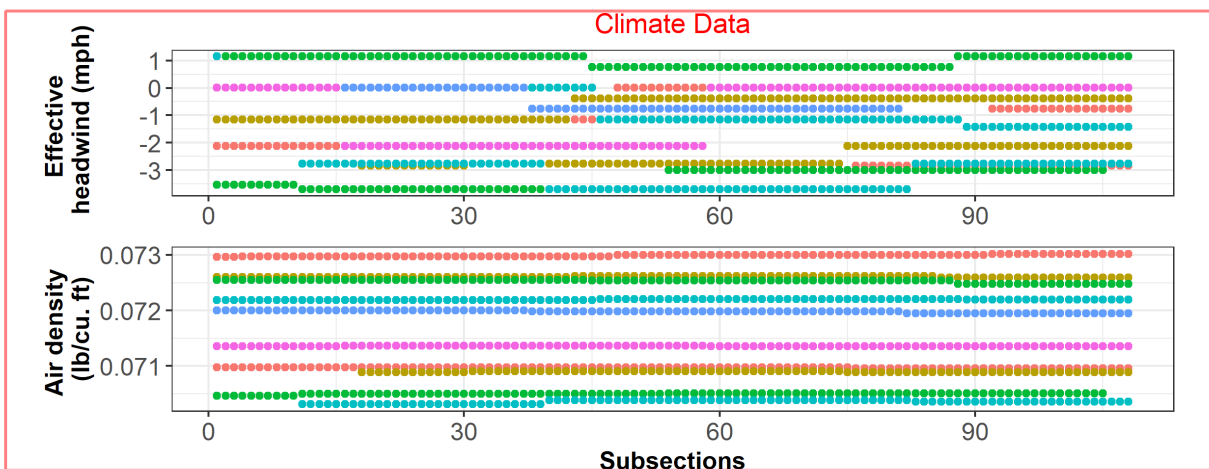
Figure P.42: Car data on Section PH10.

Car summer_day 45 mph

On Board Diagnostics Data



Climate Data



Runs

- 1
- 2
- 3
- 4
- 5
- 6

Pavement Data

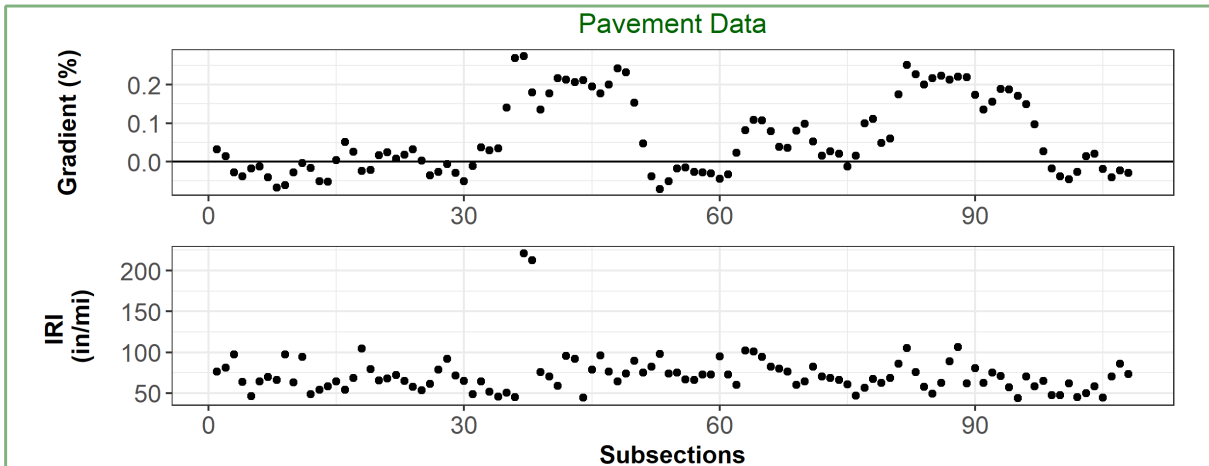


Figure P.43: Car data on Section PH11.

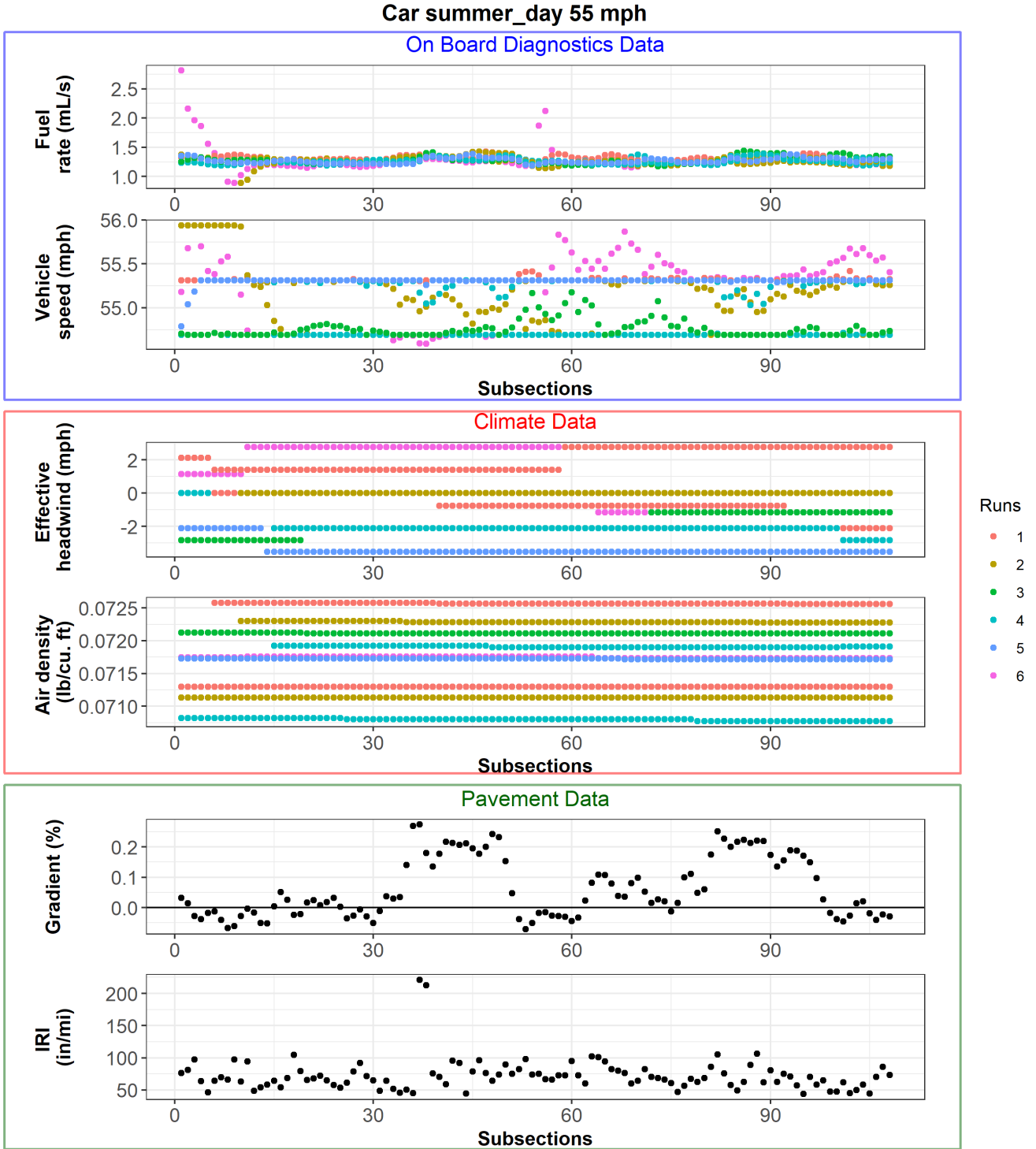


Figure P.44: Car data on Section PH11.

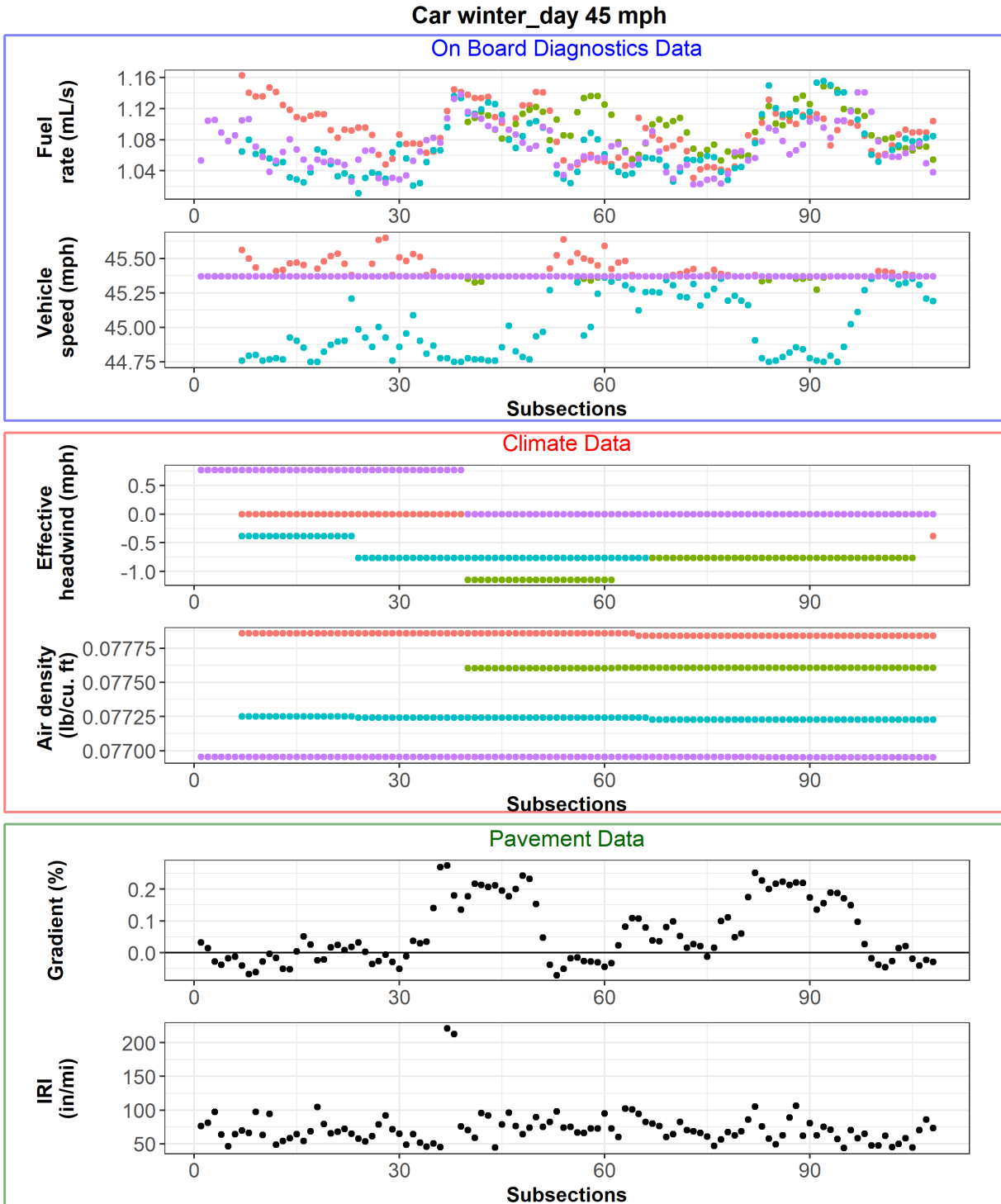


Figure P.45: Car data on Section PH11.

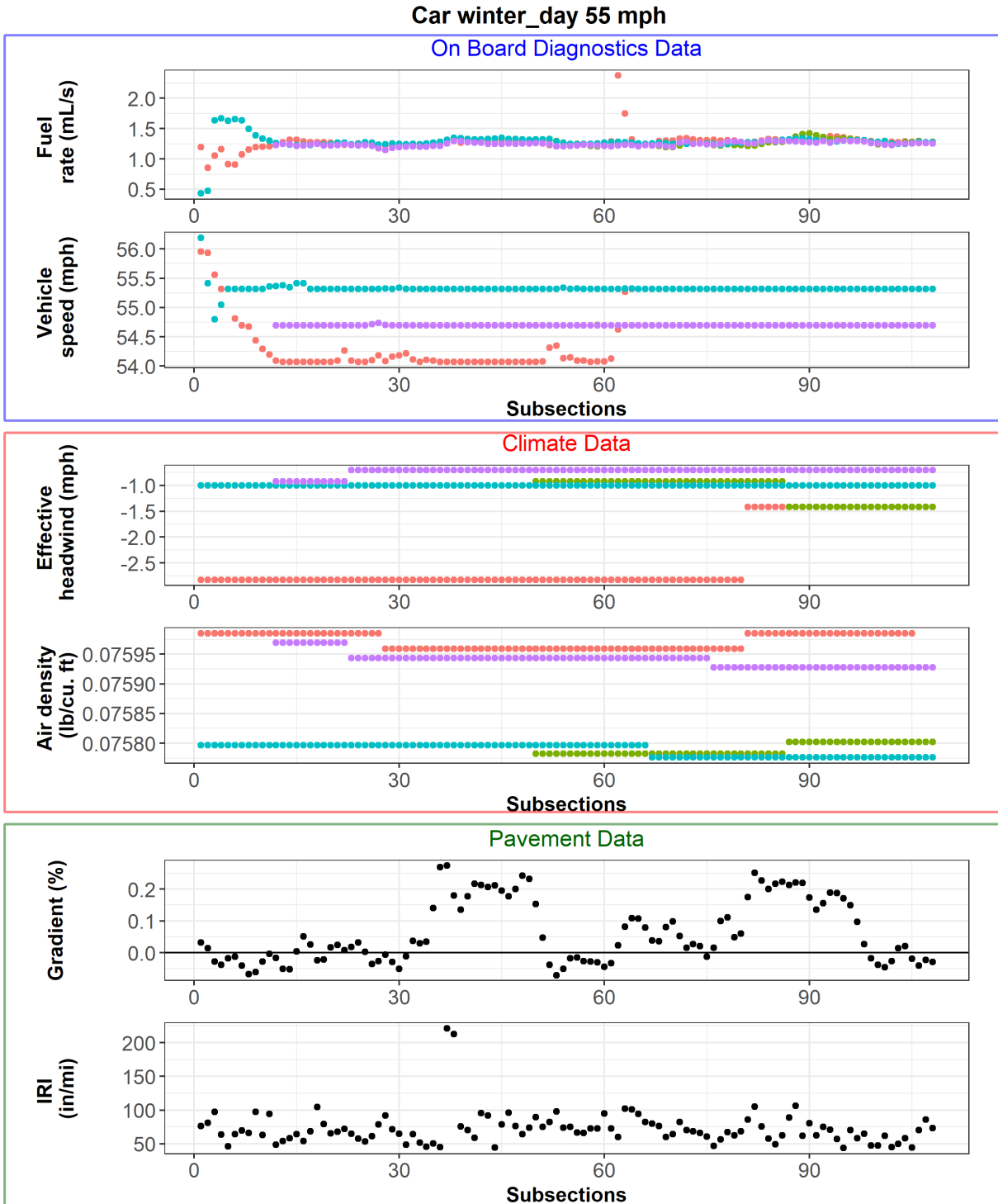


Figure P.46: Car data on Section PH11.

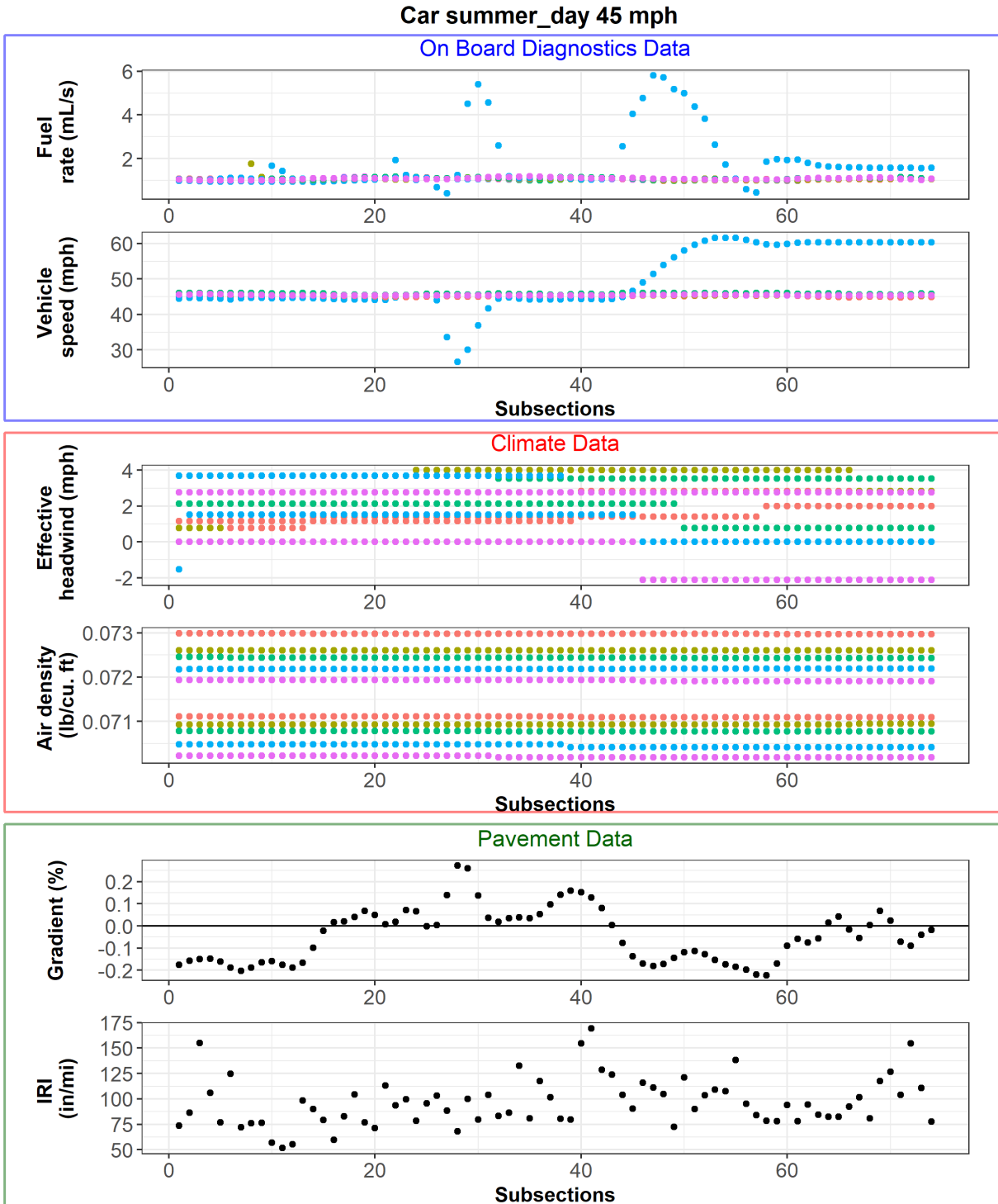


Figure P.47: Car data on Section PH12.

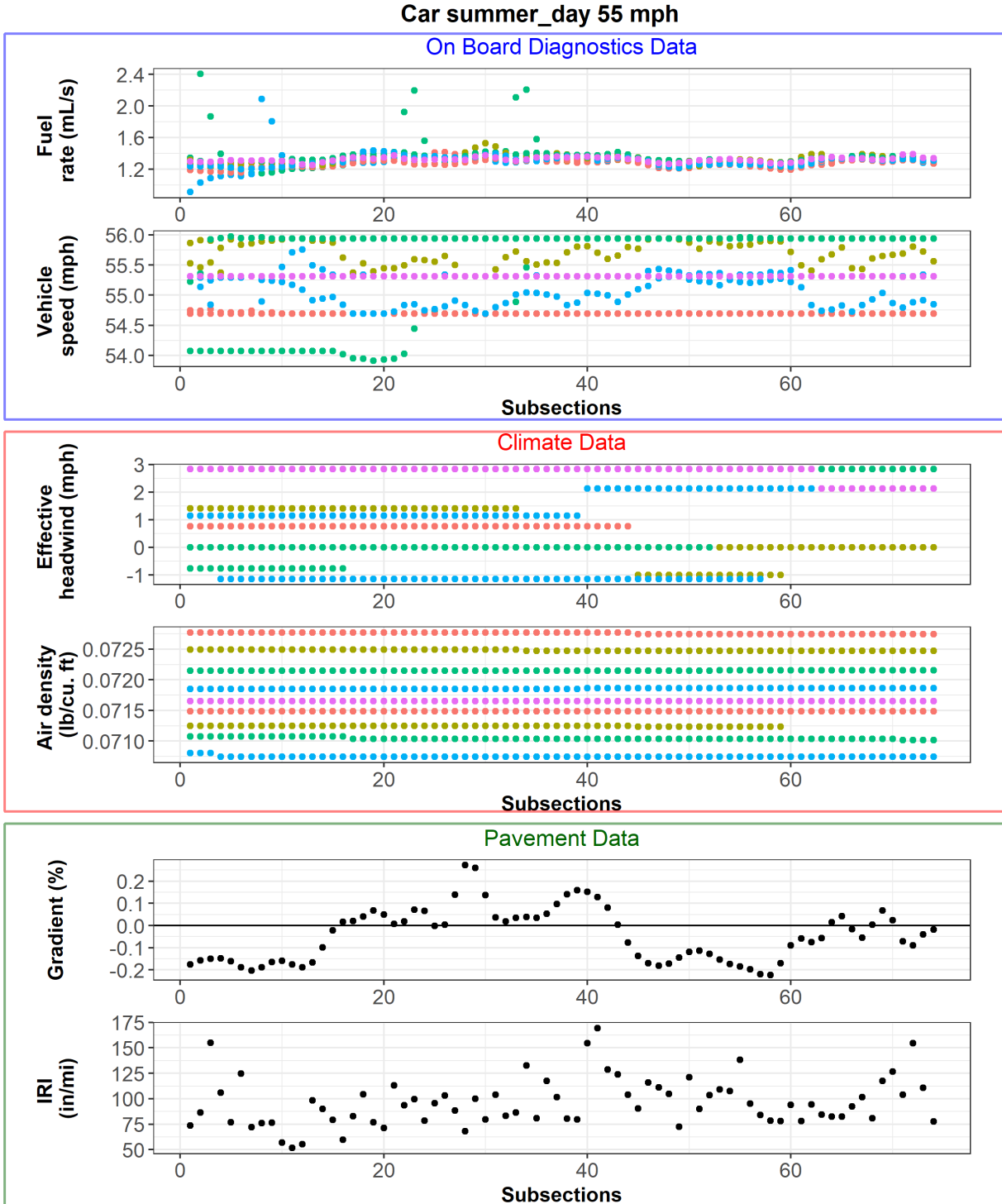


Figure P.48: Car data on Section PH12.

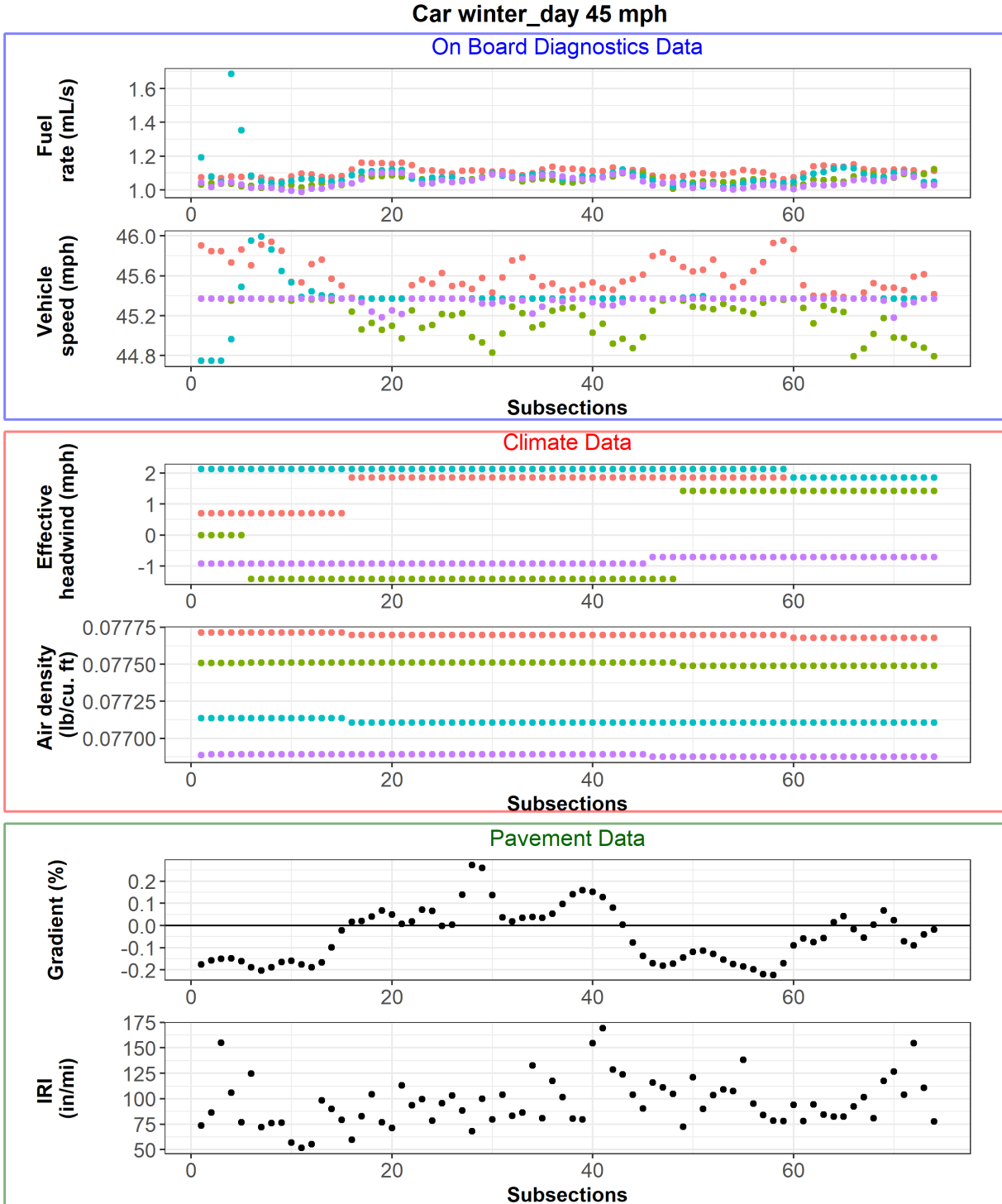


Figure P.49: Car data on Section PH12.

Car winter_day 55 mph

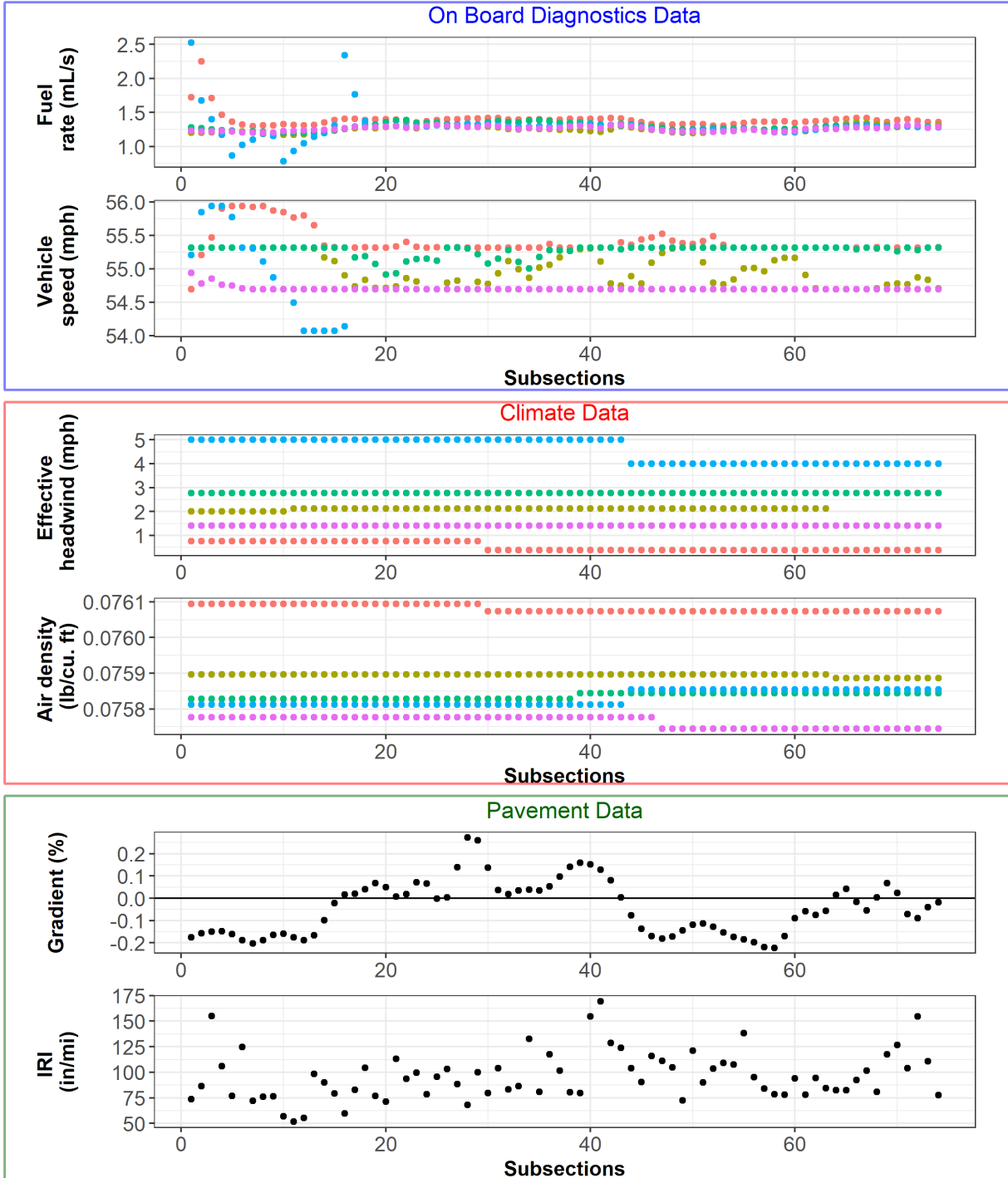


Figure P.50: Car data on Section PH12.

Car summer_day 45 mph

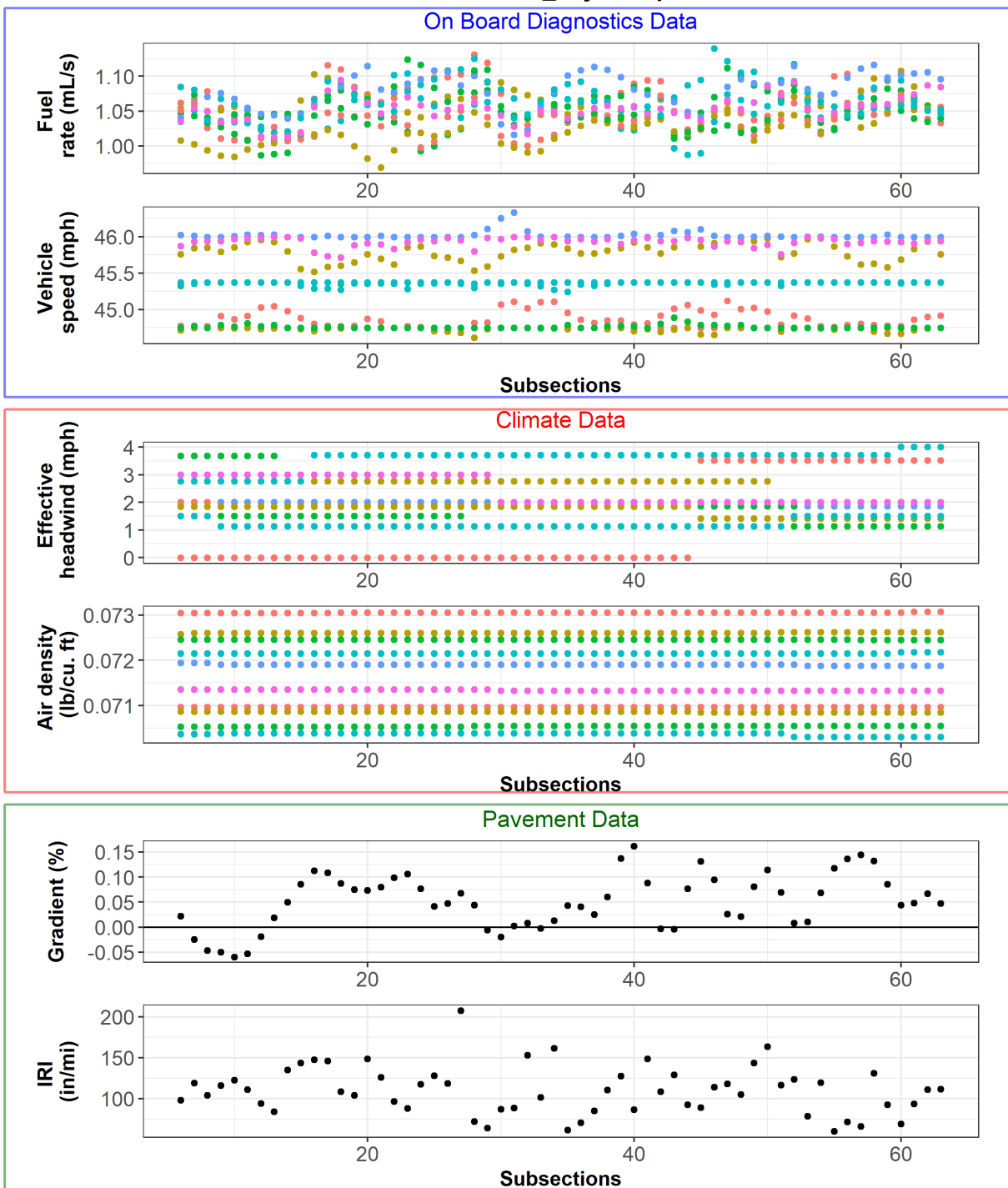
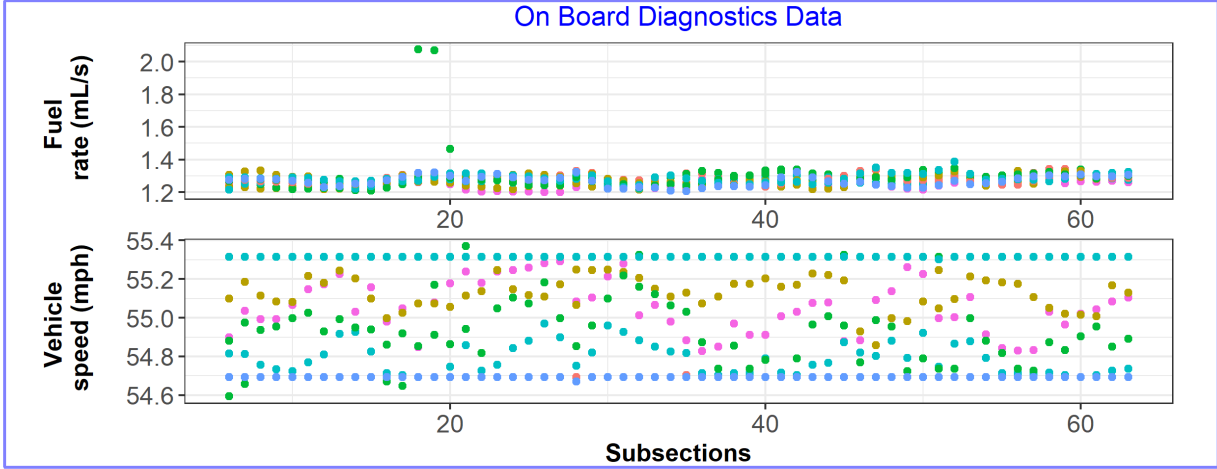


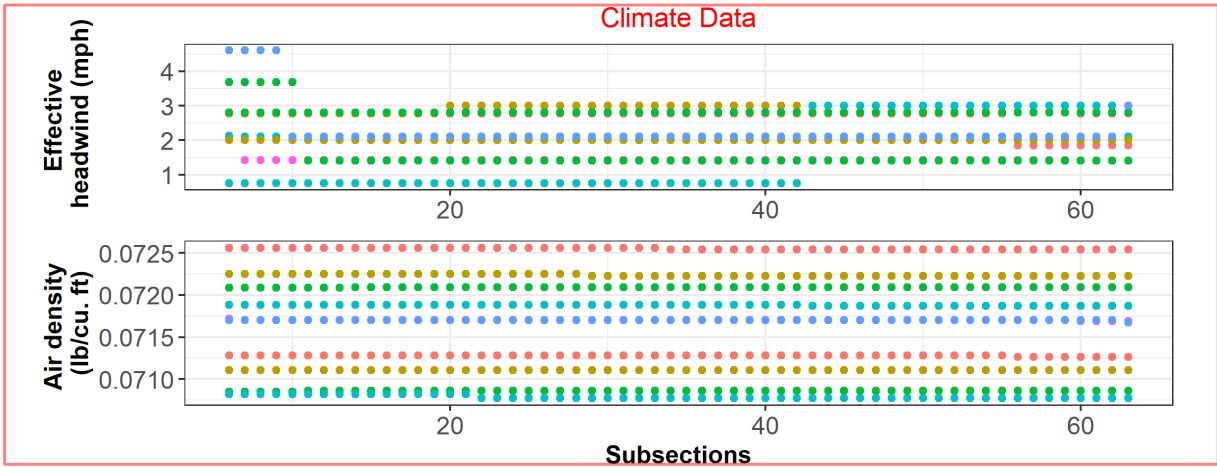
Figure P.51: Car data on Section PH13.

Car summer_day 55 mph

On Board Diagnostics Data



Climate Data



- Runs
- 1
 - 2
 - 3
 - 4
 - 5
 - 6

Pavement Data

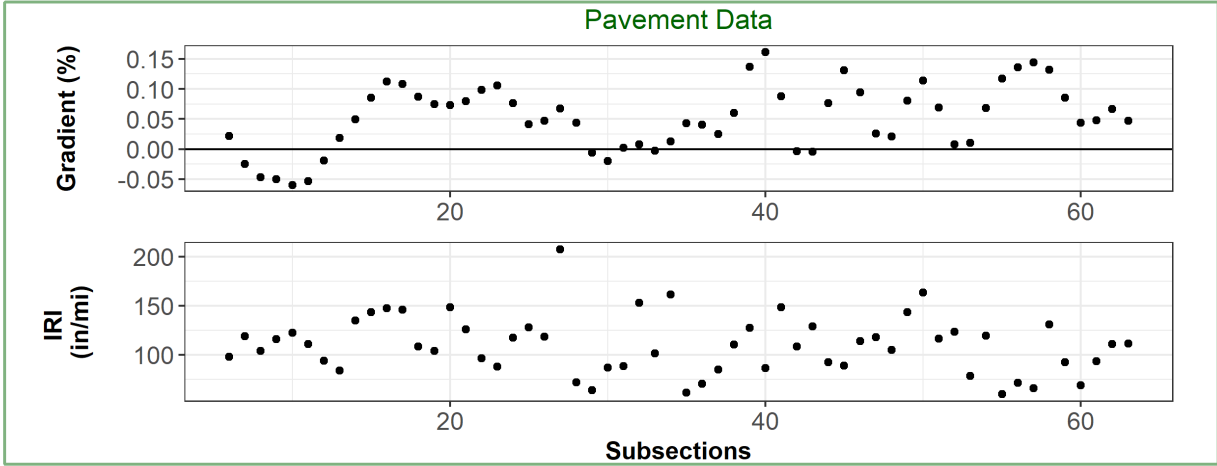


Figure P.52: Car data on Section PH13.

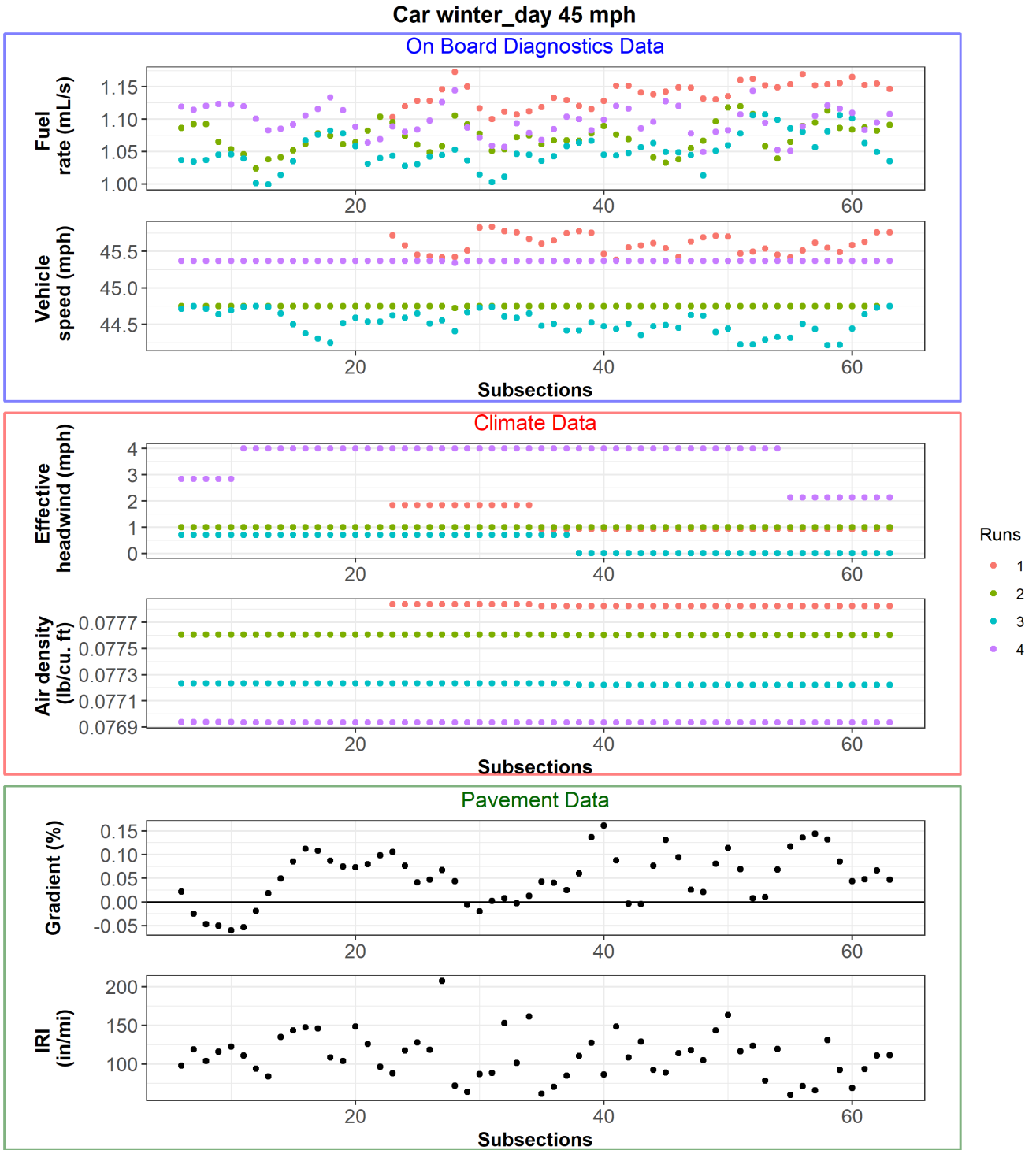


Figure P.53: Car data on Section PH13.

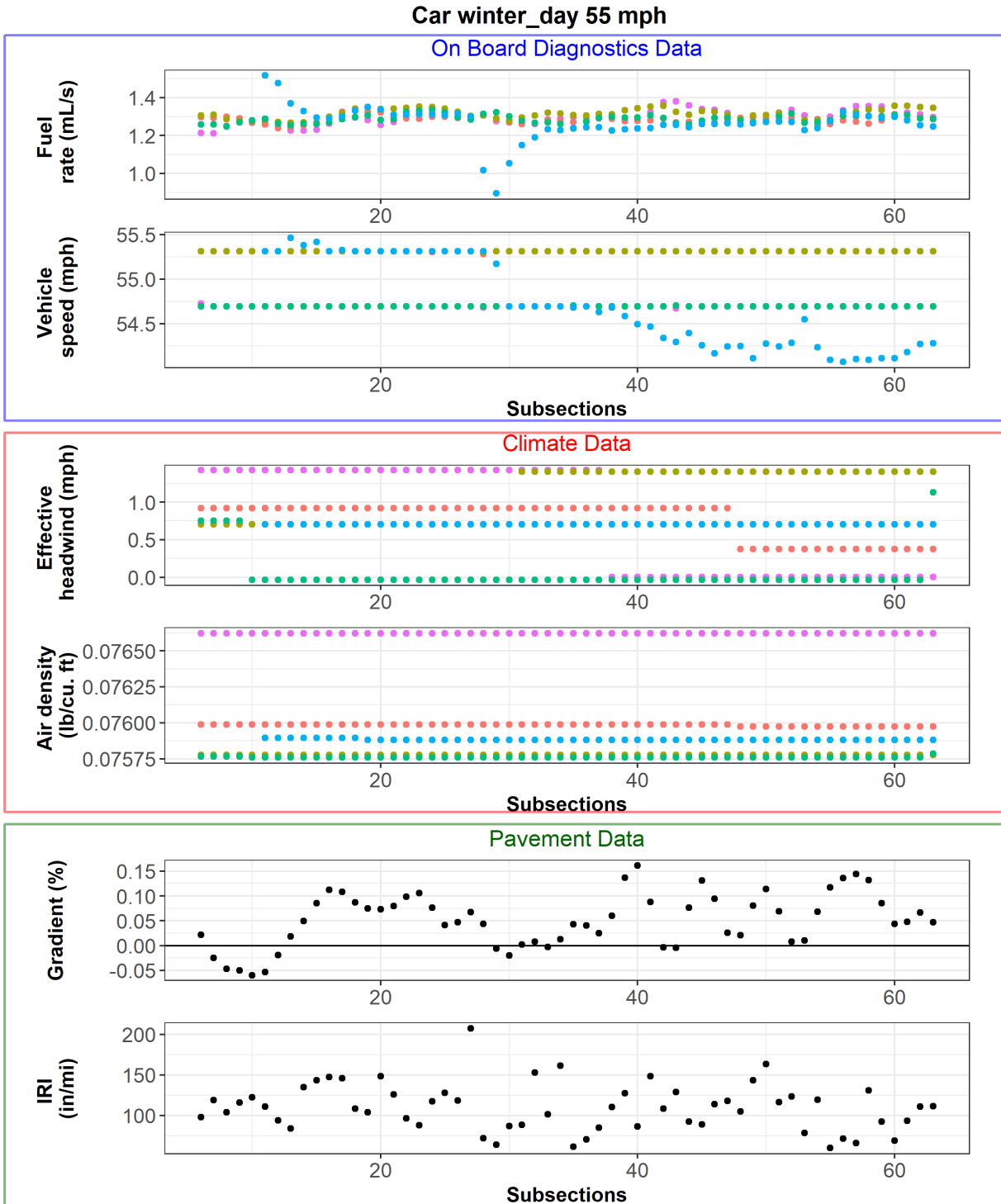


Figure P.54: Car data on Section PH13.

Car summer_day 45 mph

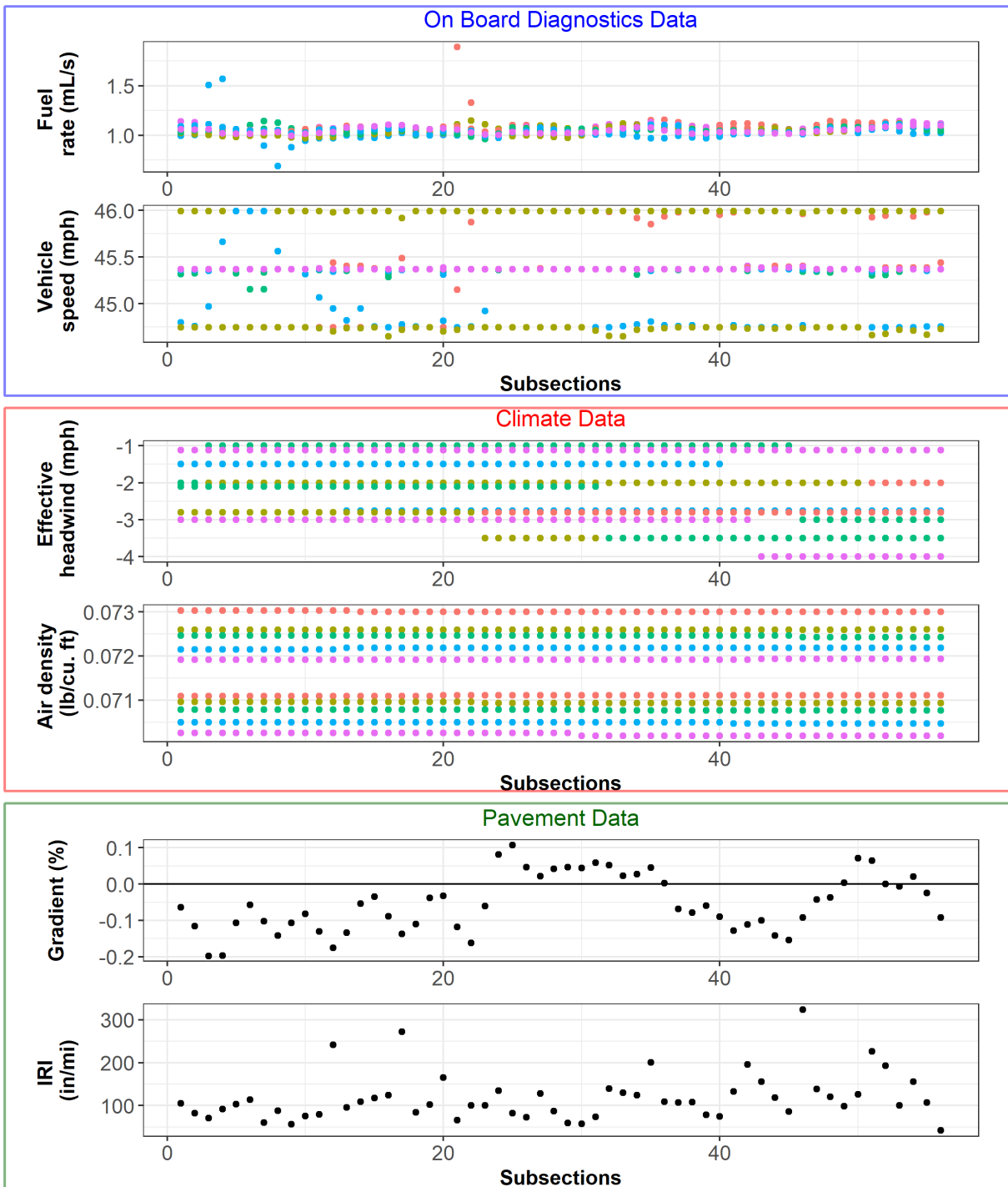


Figure P.55: Car data on Section PH14.

Car summer_day 55 mph

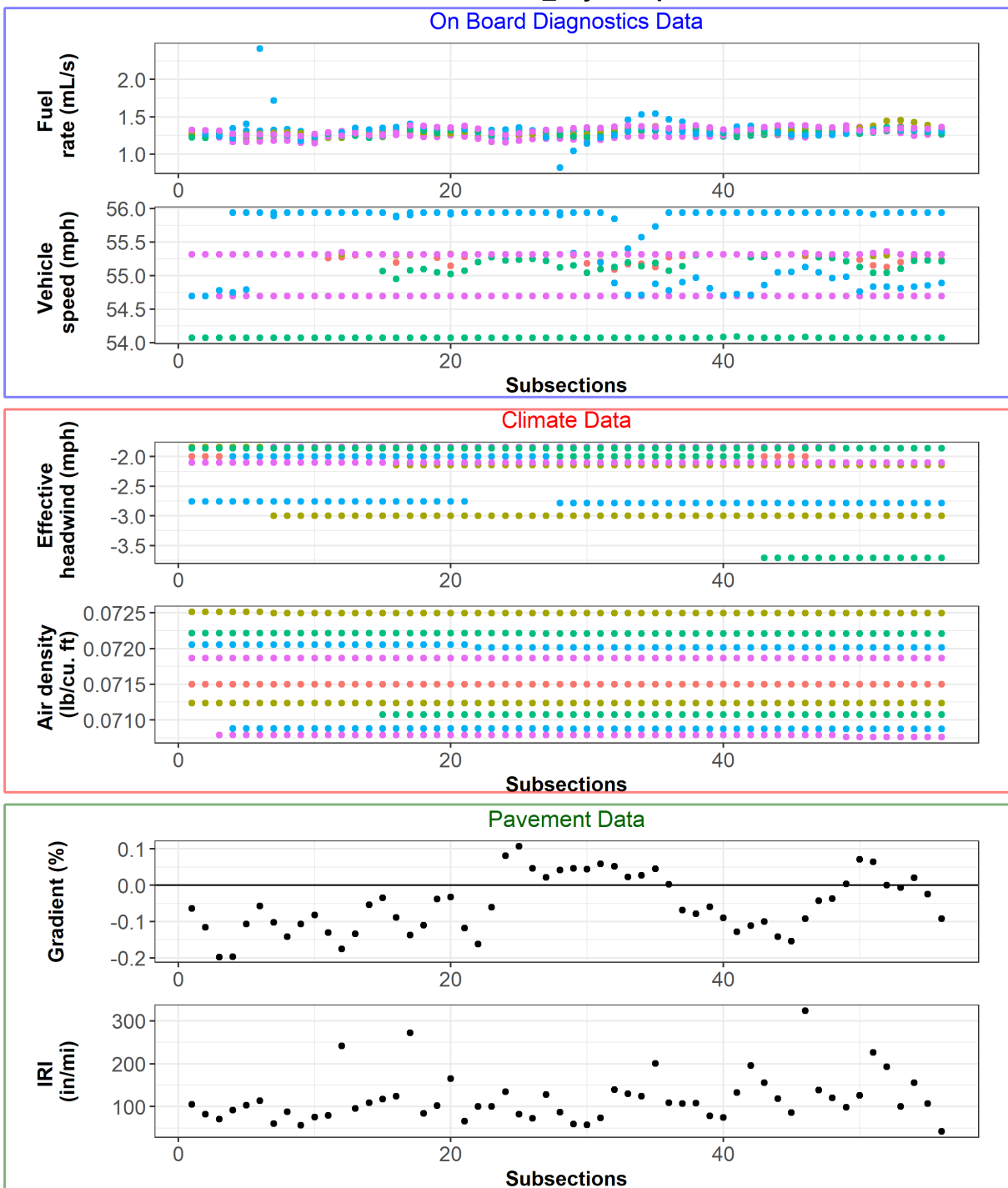


Figure P.56: Car data on Section PH14.

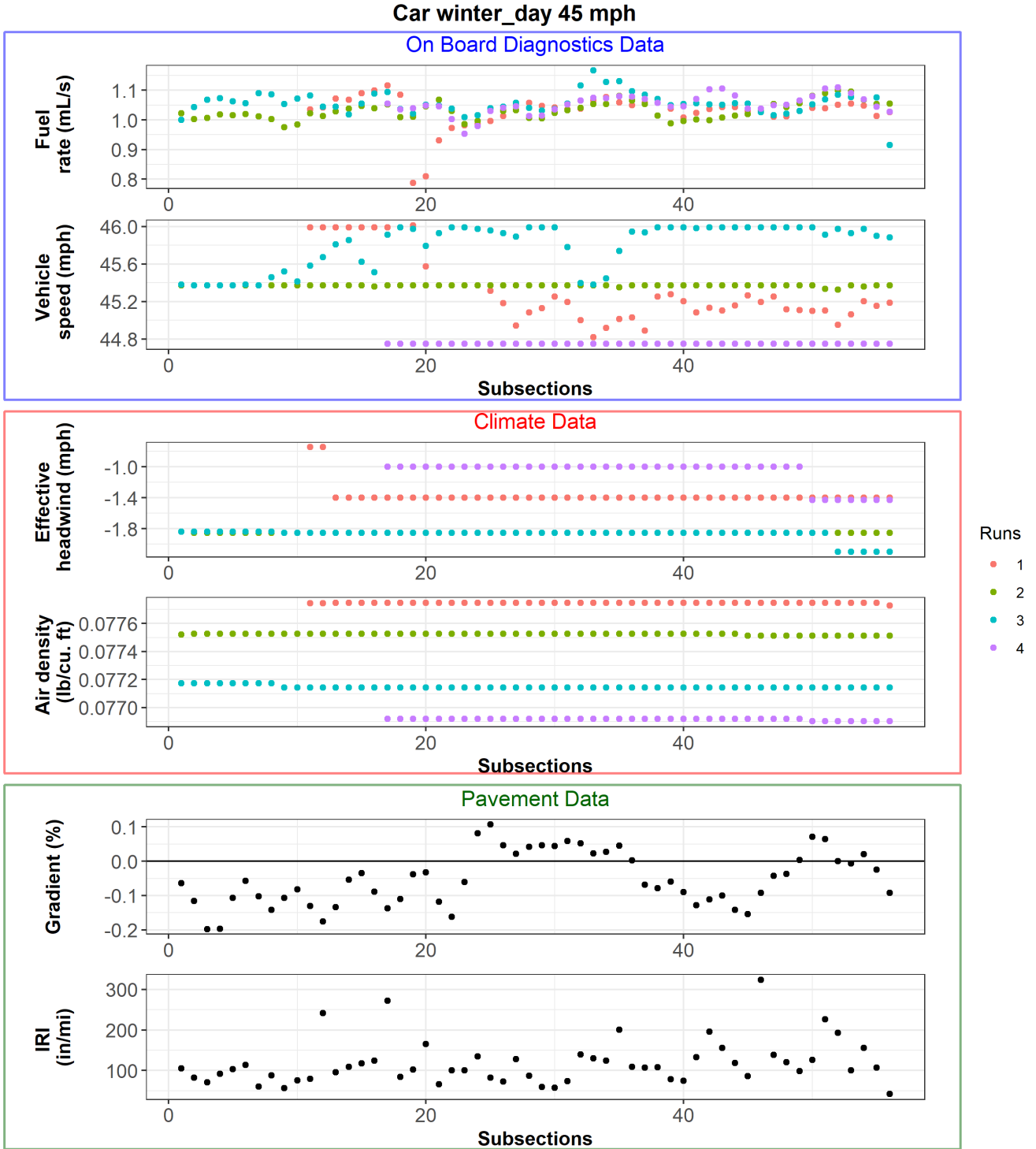


Figure P.57: Car data on Section PH14.

Car winter_day 55 mph

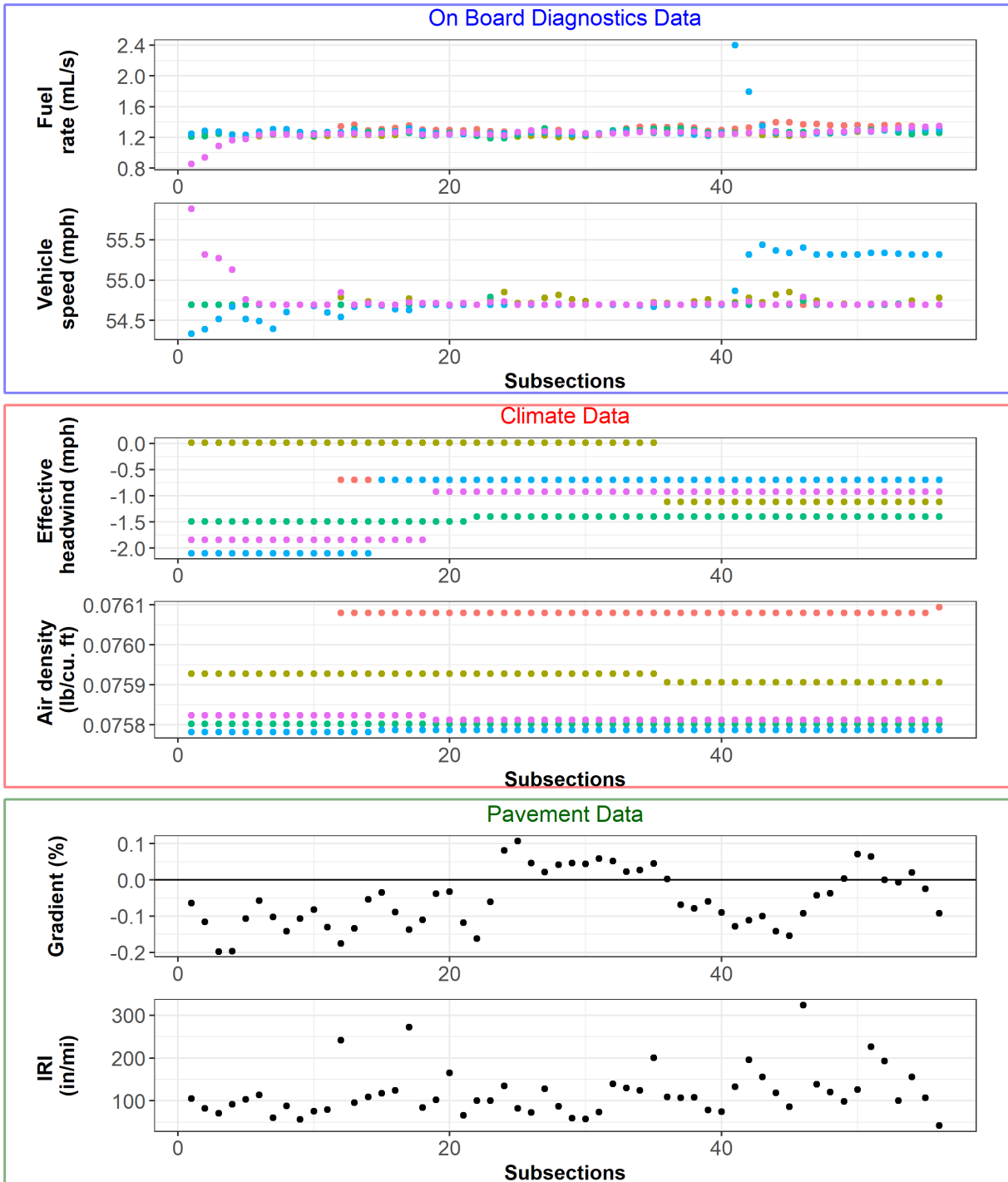


Figure P.58: Car data on Section PH14.

Car summer_day 35 mph

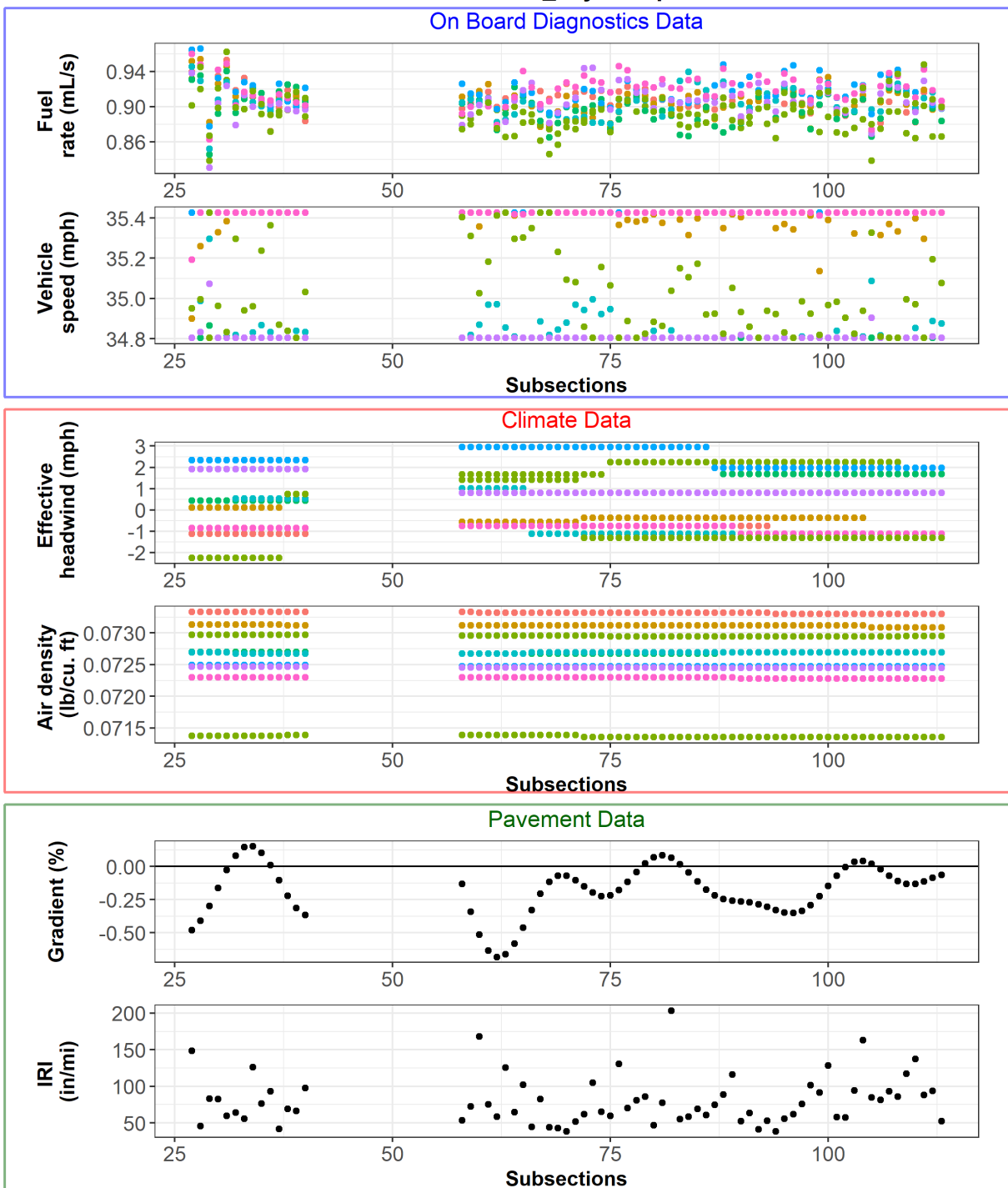


Figure P.59: Car data on Section PH15.

Car summer_day 45 mph

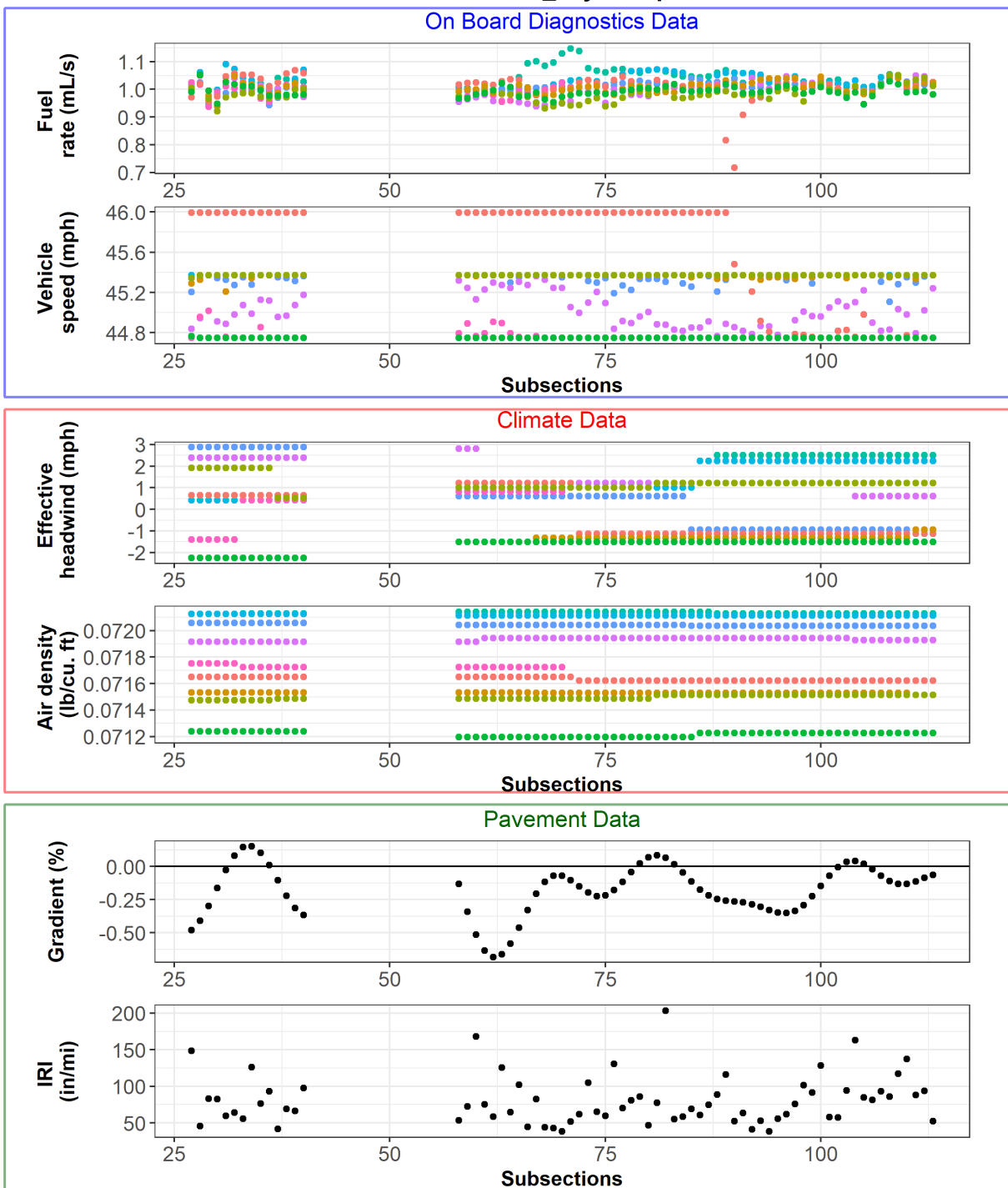


Figure P.60: Car data on Section PH15.

Car summer_day 55 mph

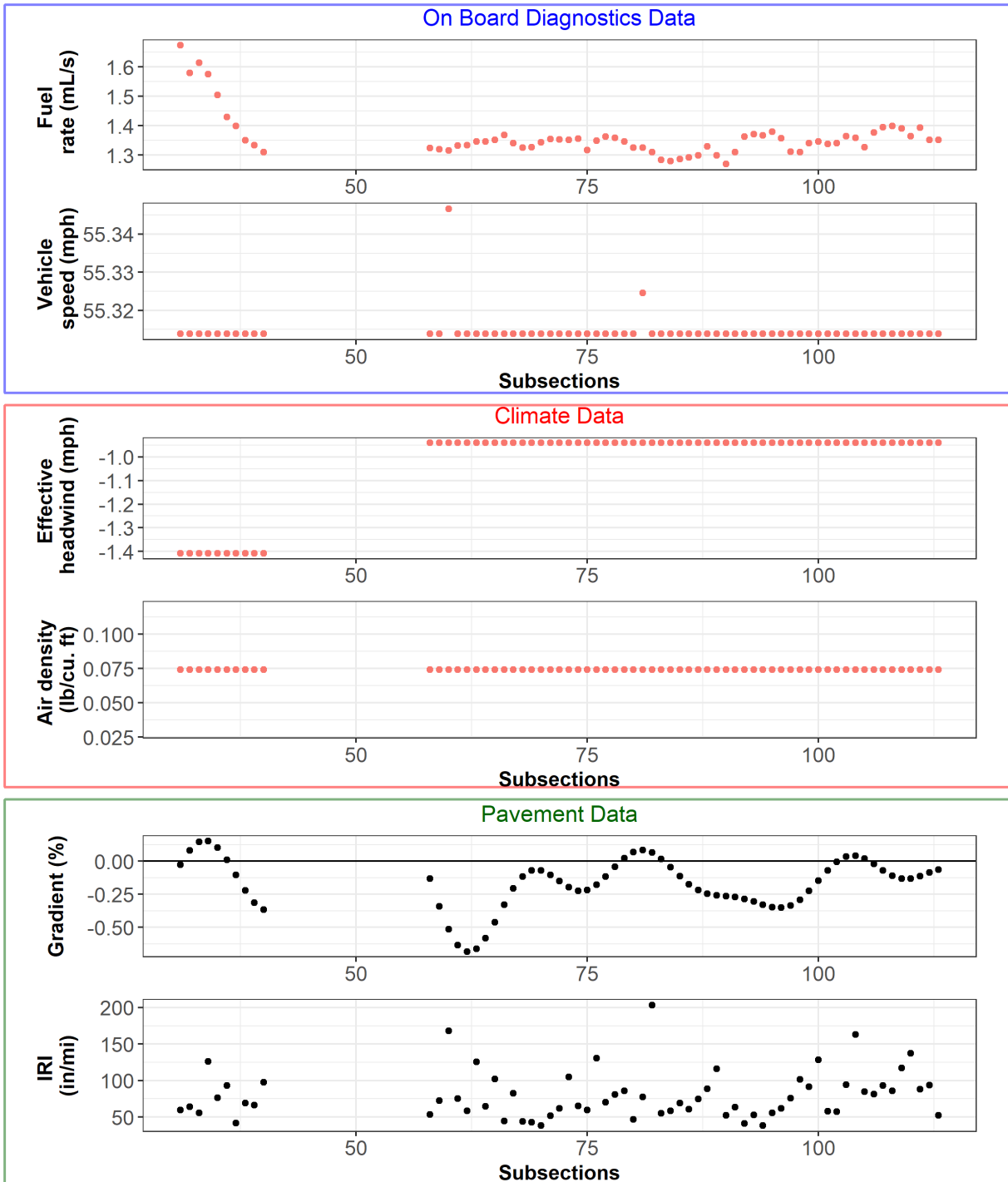


Figure P.61: Car data on Section PH15.

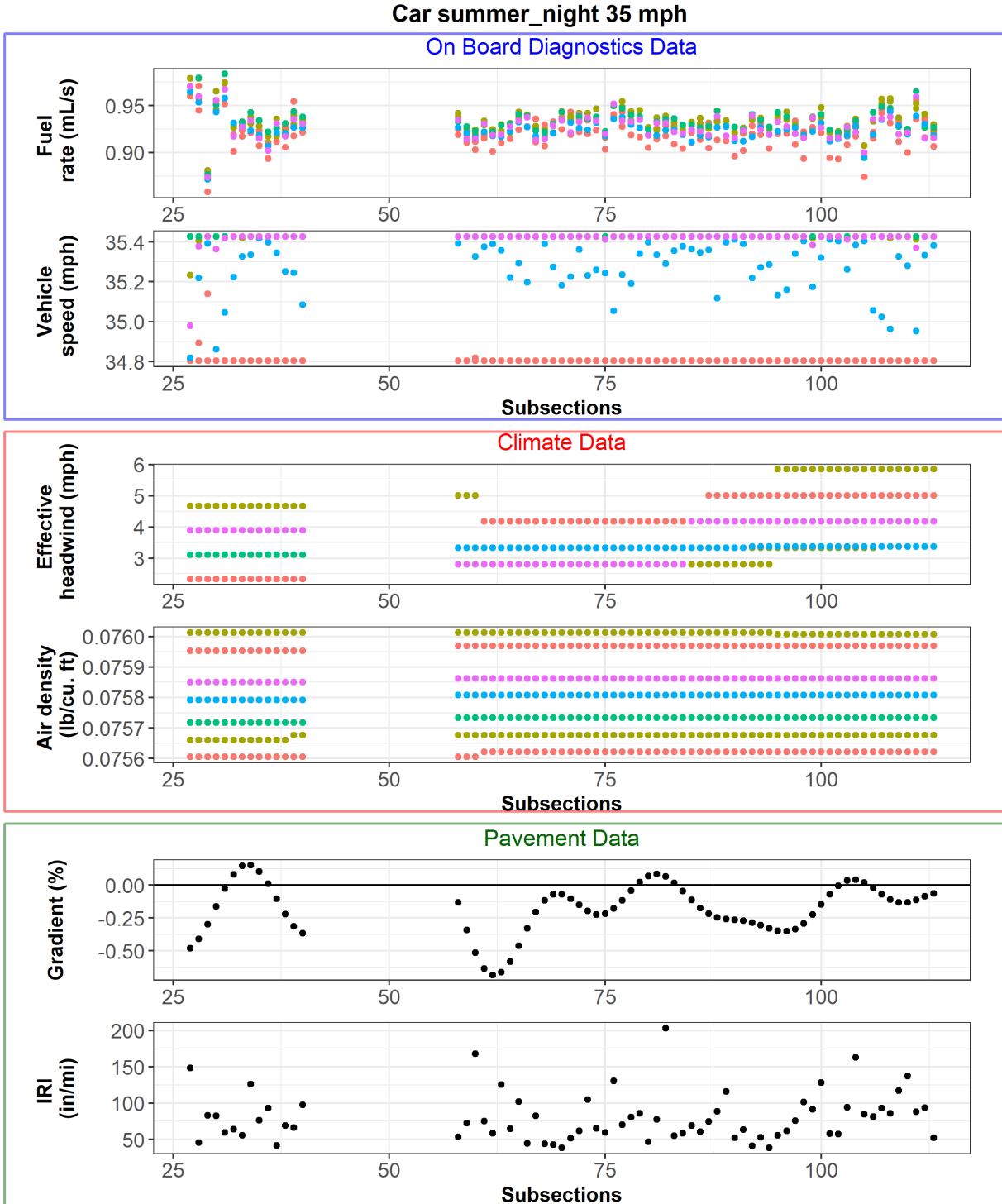


Figure P.62: Car data on Section PH15.

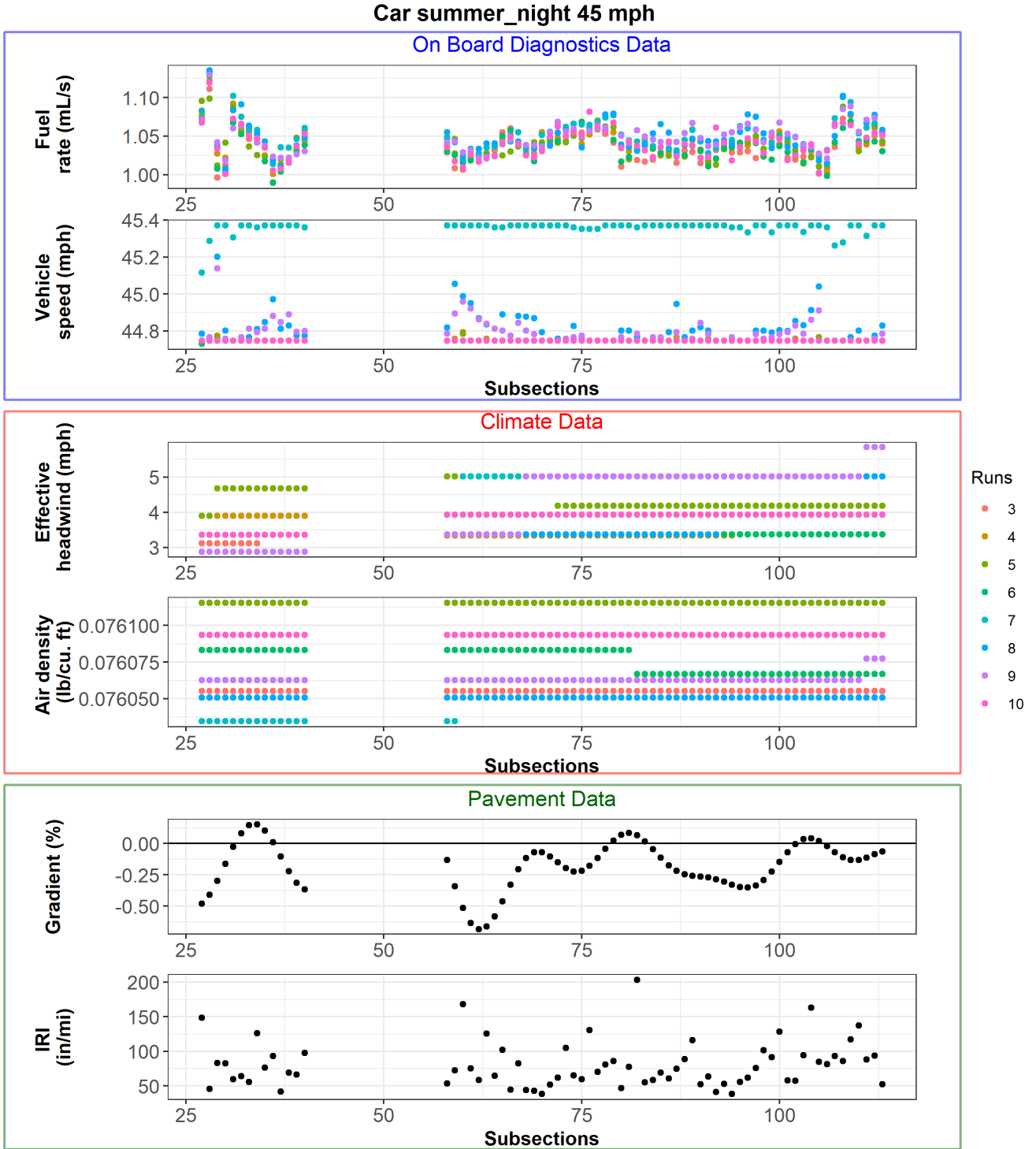


Figure P.63: Car data on Section PH15.

Car winter_day 35 mph

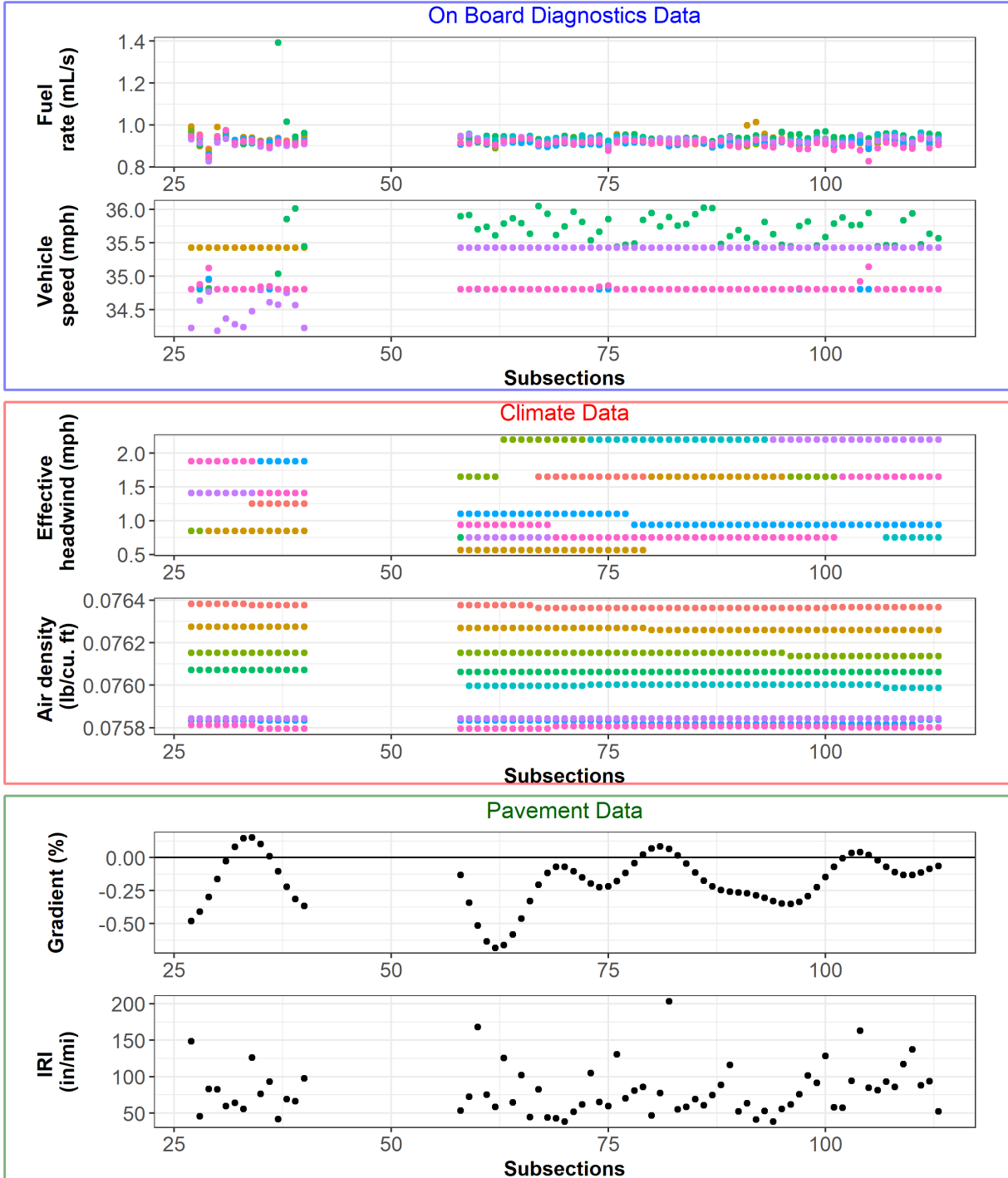


Figure P.64: Car data on Section PH15.

Car winter_day 45 mph

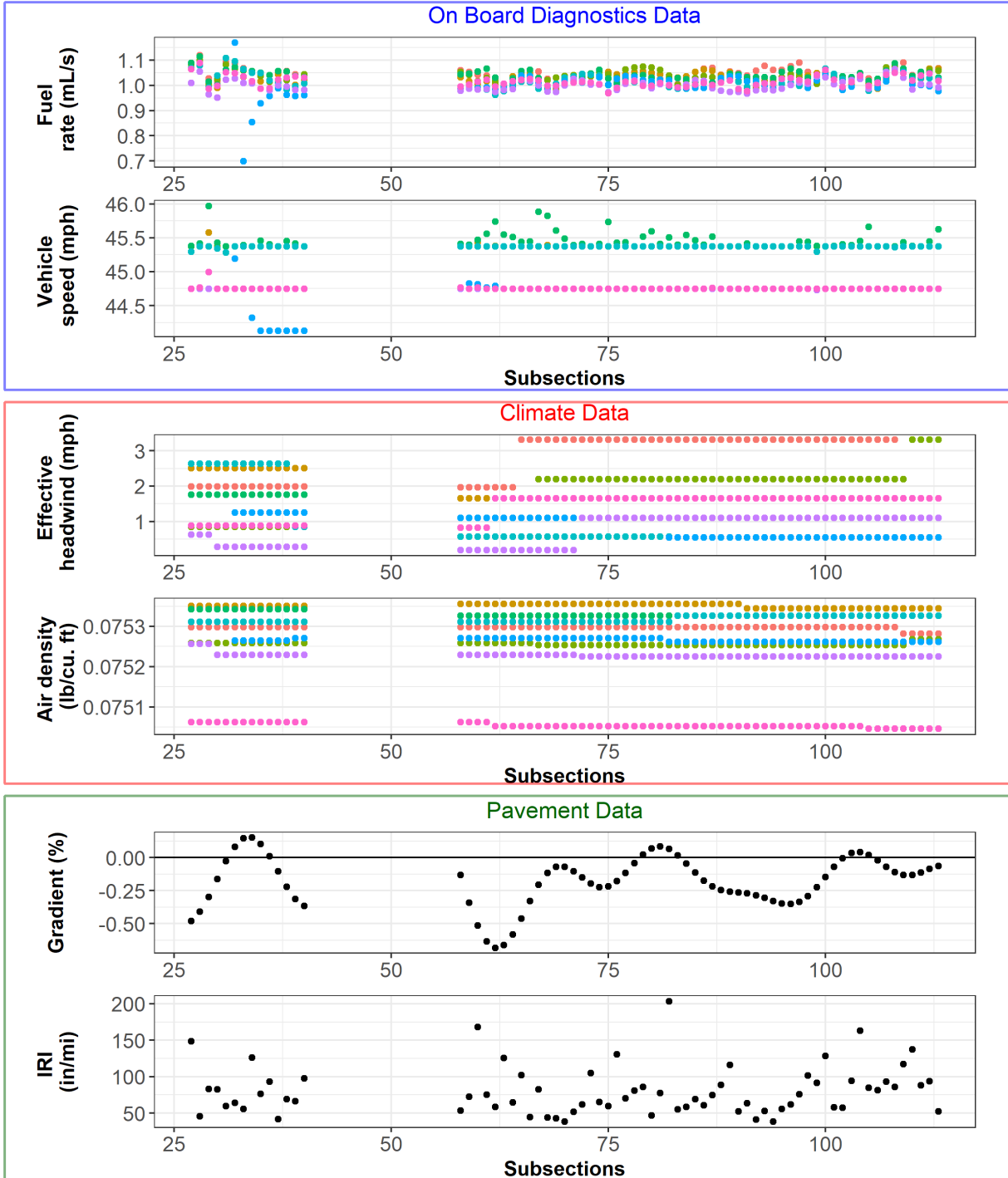


Figure P.65: Car data on Section PH15.

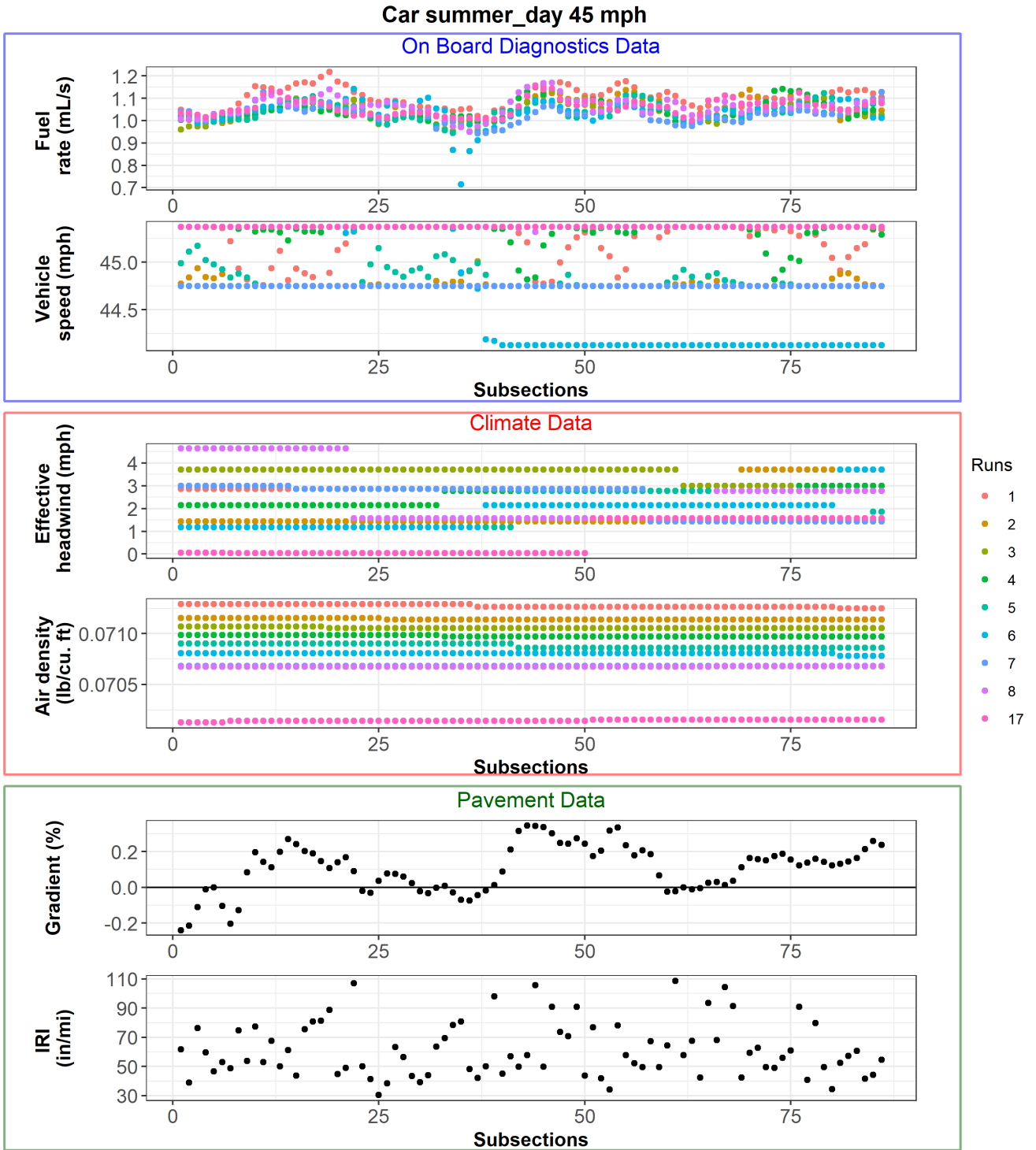


Figure P.66: Car data on Section PH16.

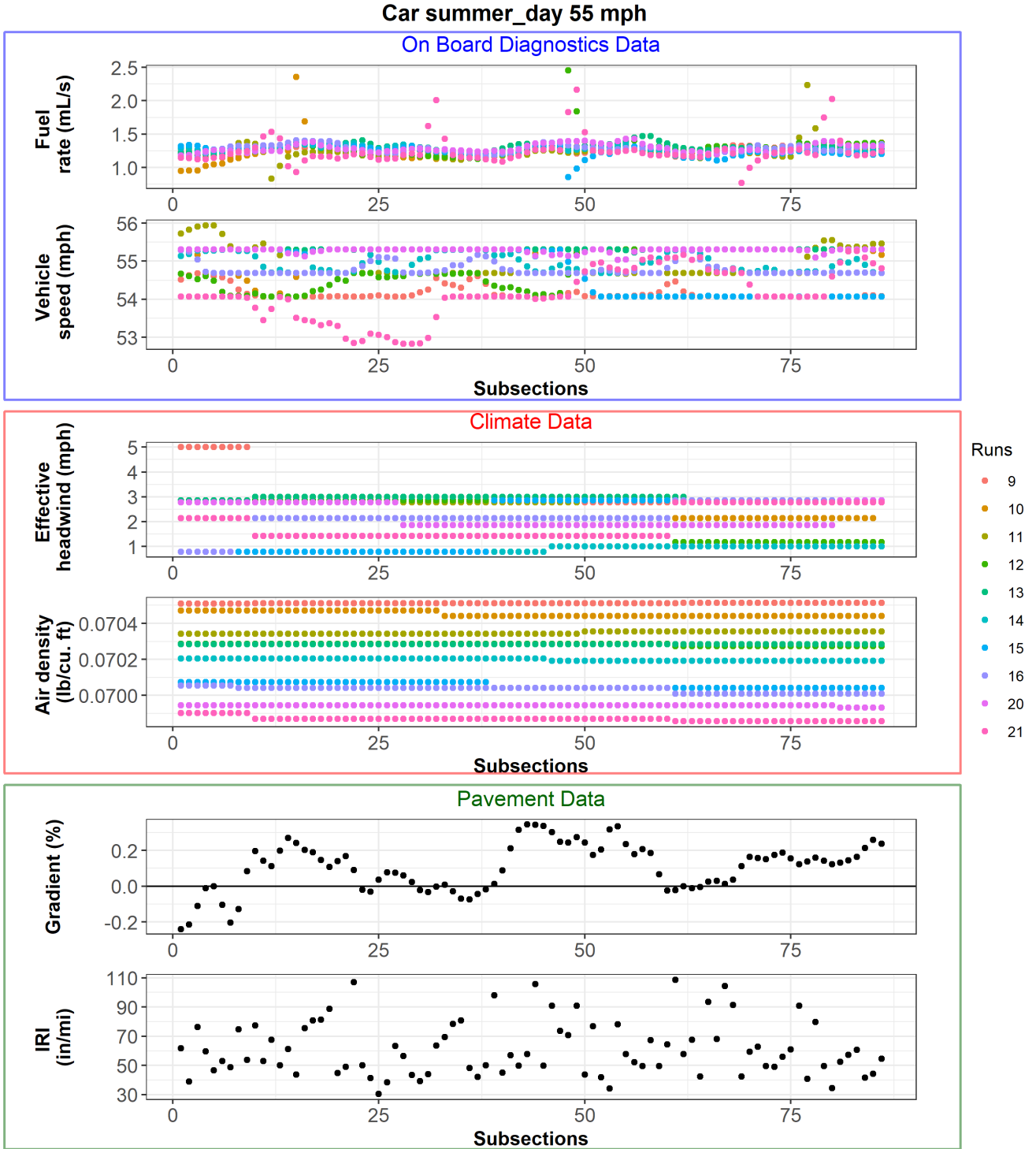


Figure P.67: Car data on Section PH16.

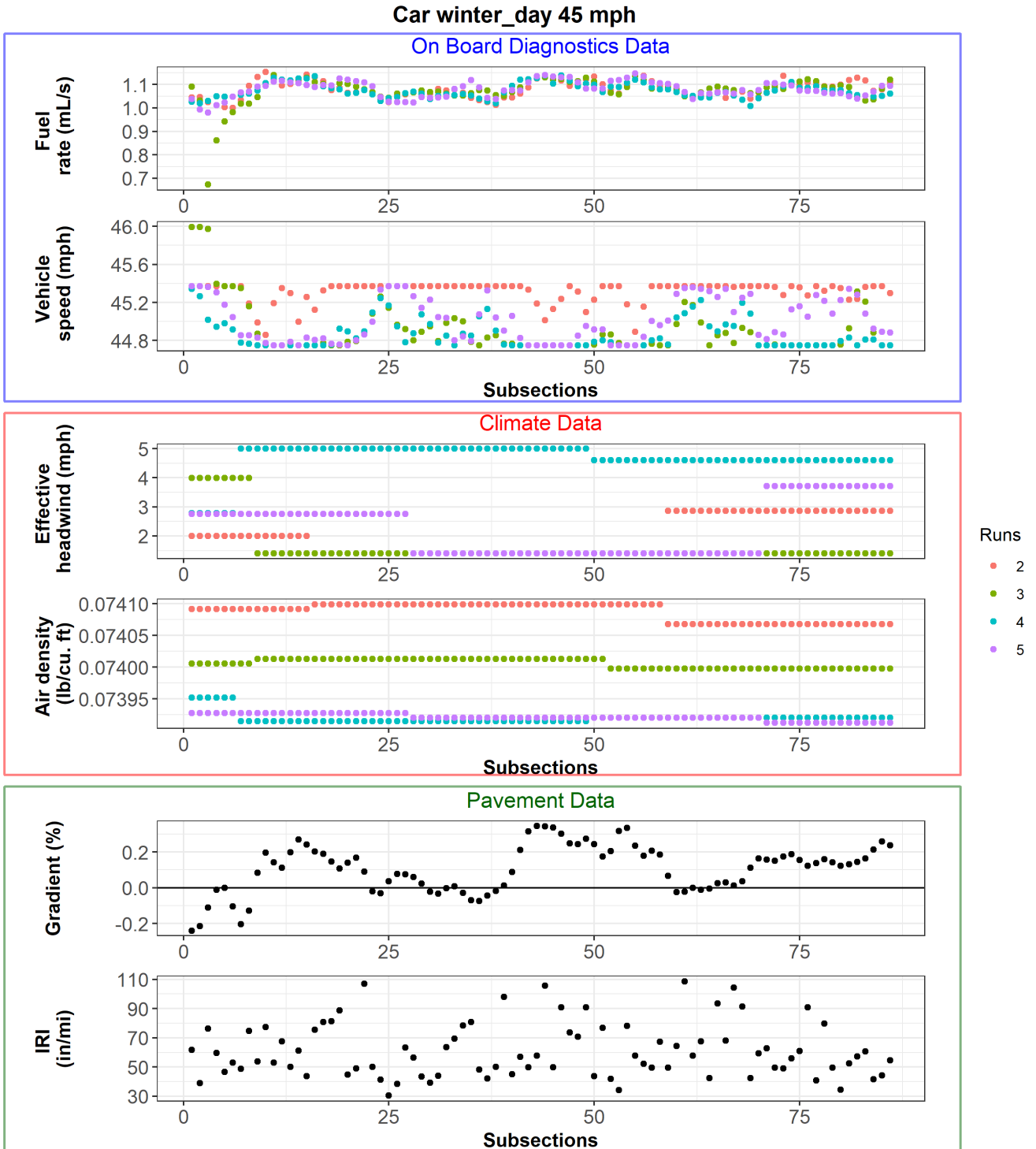
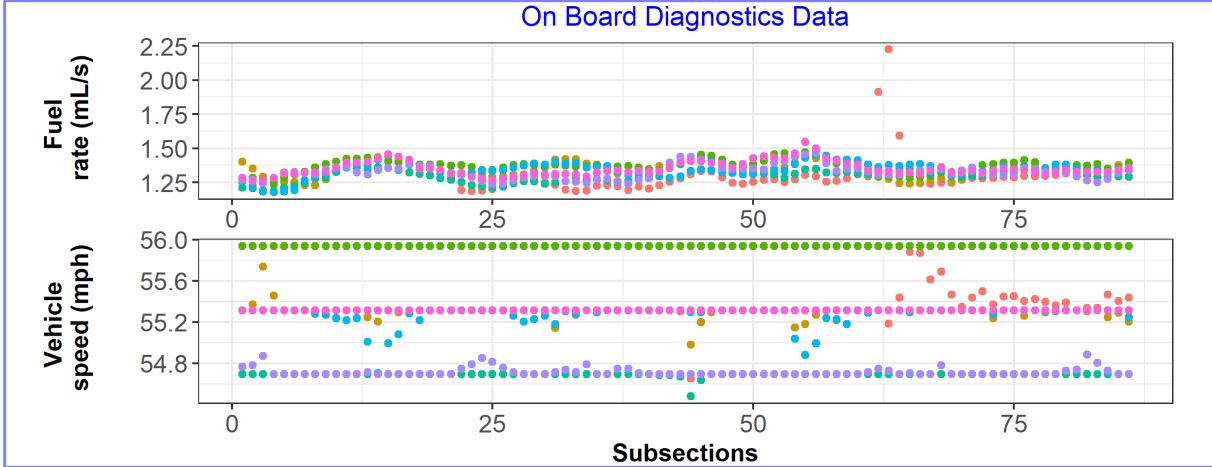


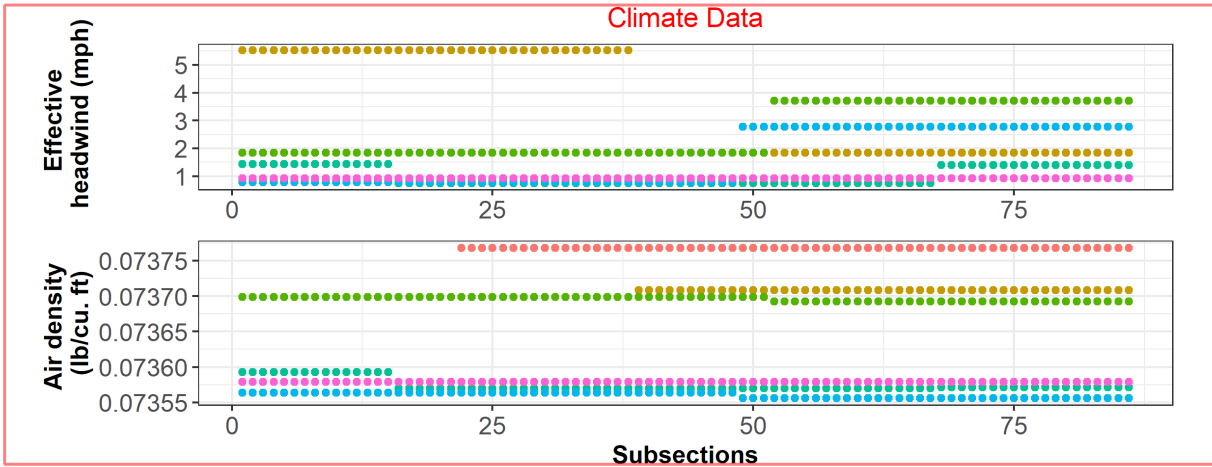
Figure P.68: Car data on Section PH16.

Car winter_day 55 mph

On Board Diagnostics Data



Climate Data



- Runs
- 2
 - 3
 - 4
 - 5
 - 6
 - 7
 - 8

Pavement Data

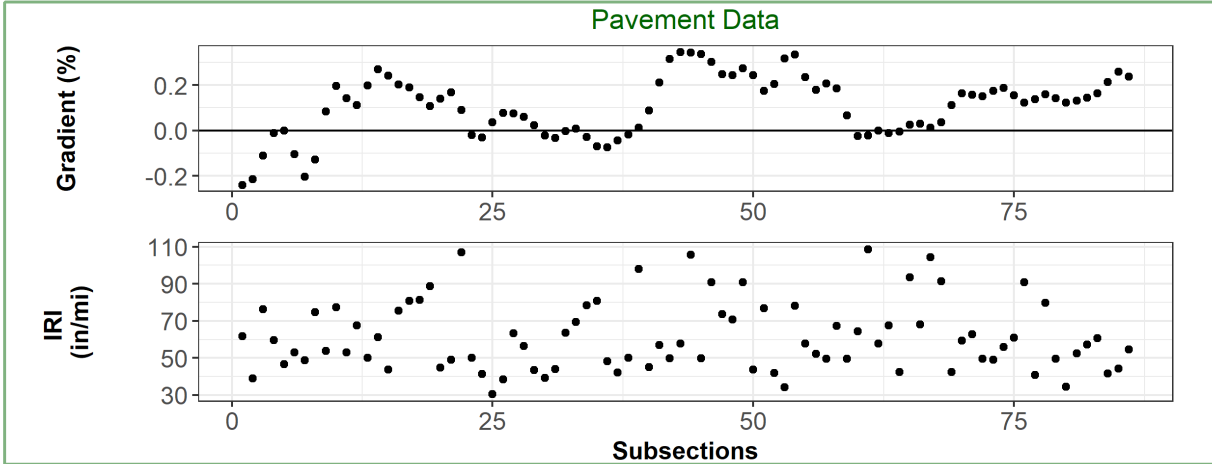


Figure P.69: Car data on Section PH16.

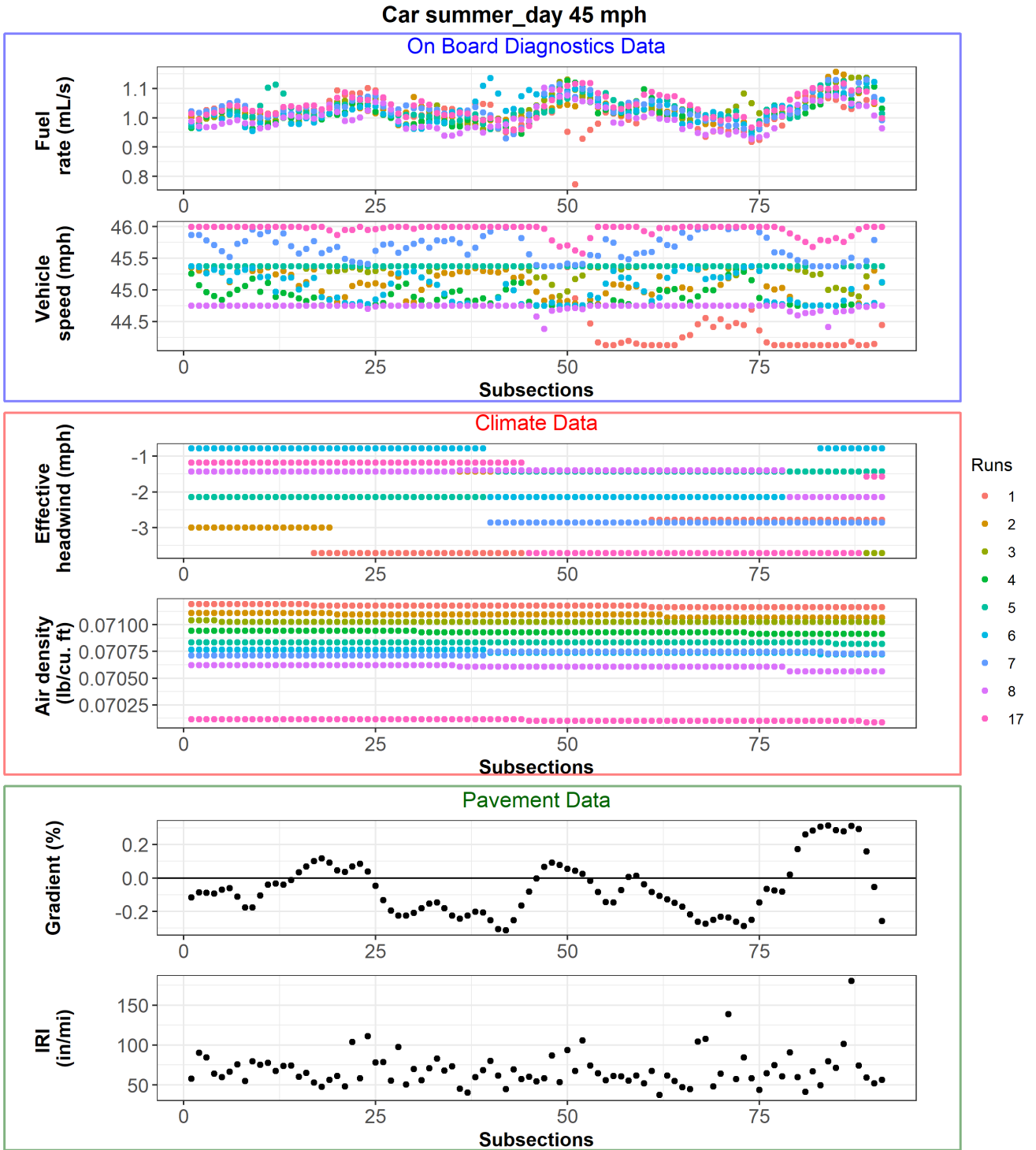


Figure P.70: Car data on Section PH17.

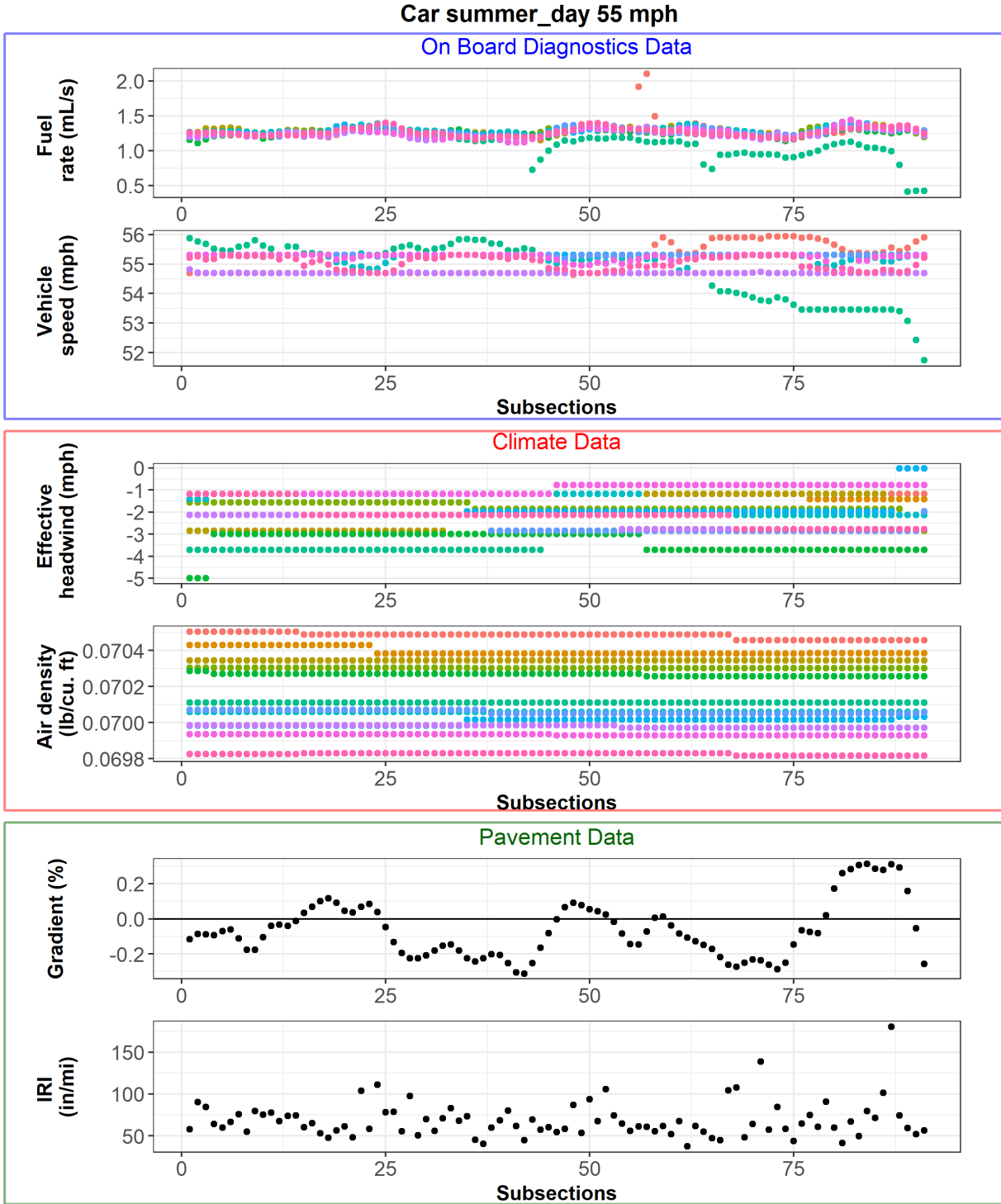


Figure P.71: Car data on Section PH17.

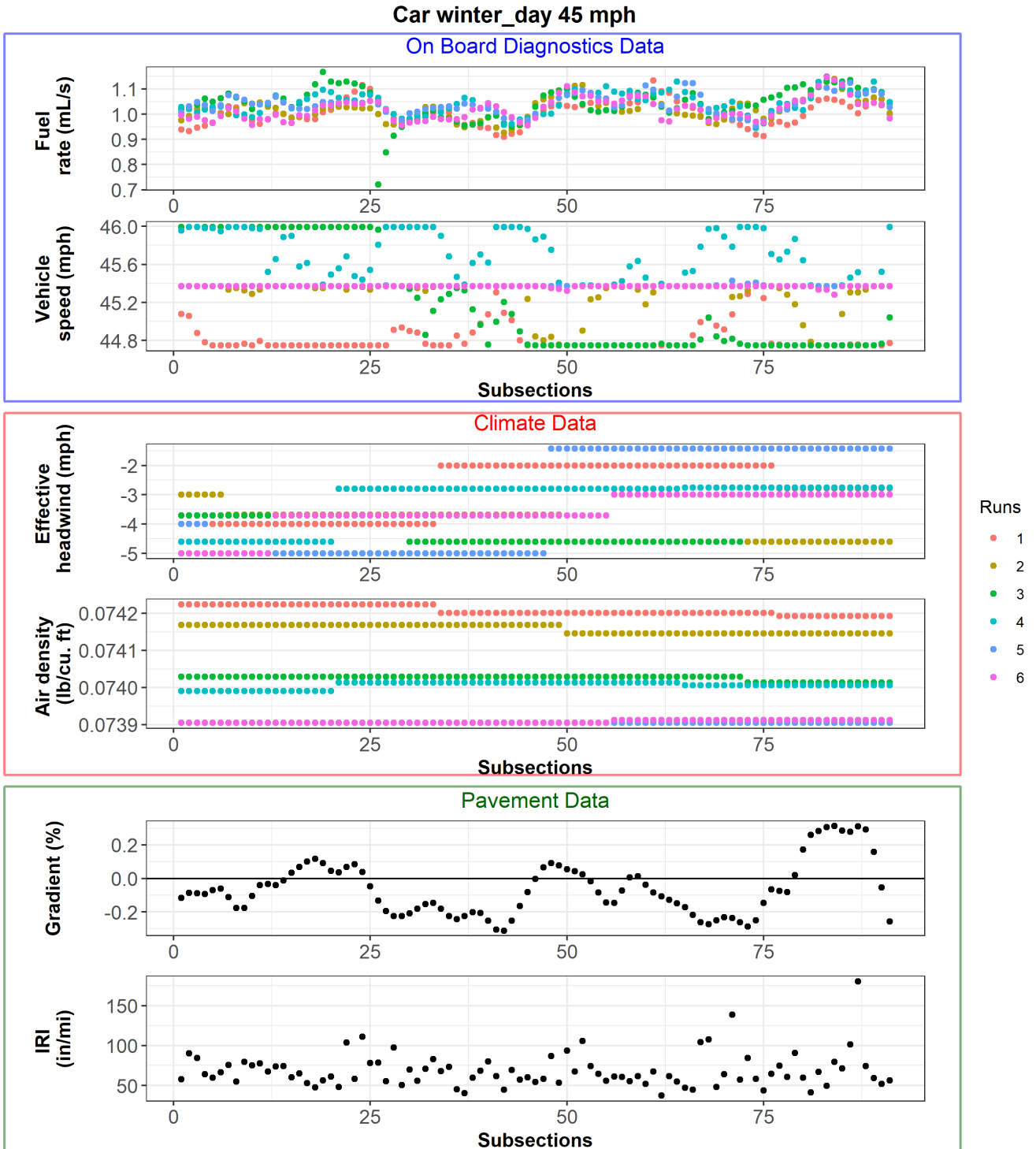


Figure P.72: Car data on Section PH17.

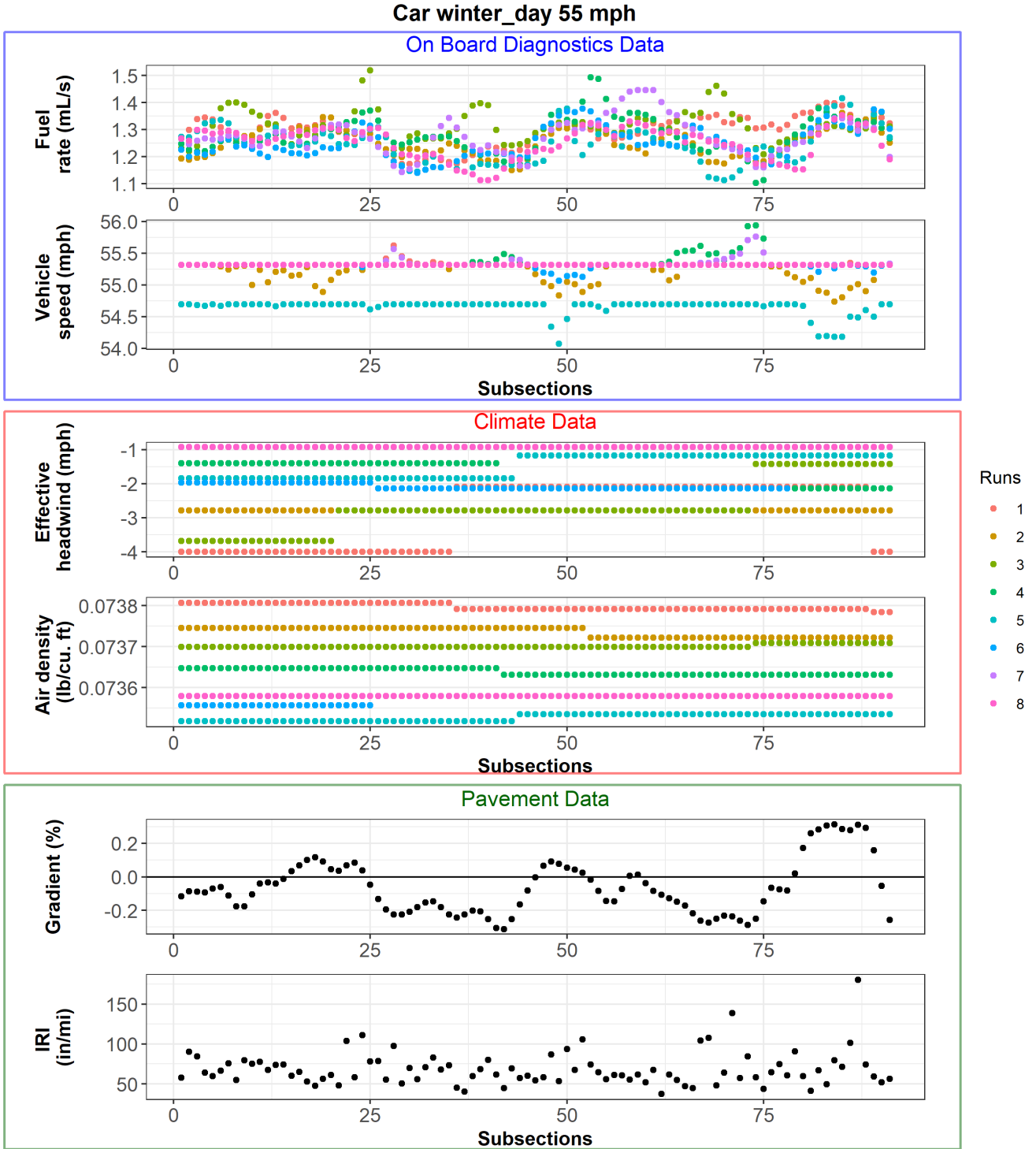


Figure P.73: Car data on Section PH17.

Car summer_day 45 mph

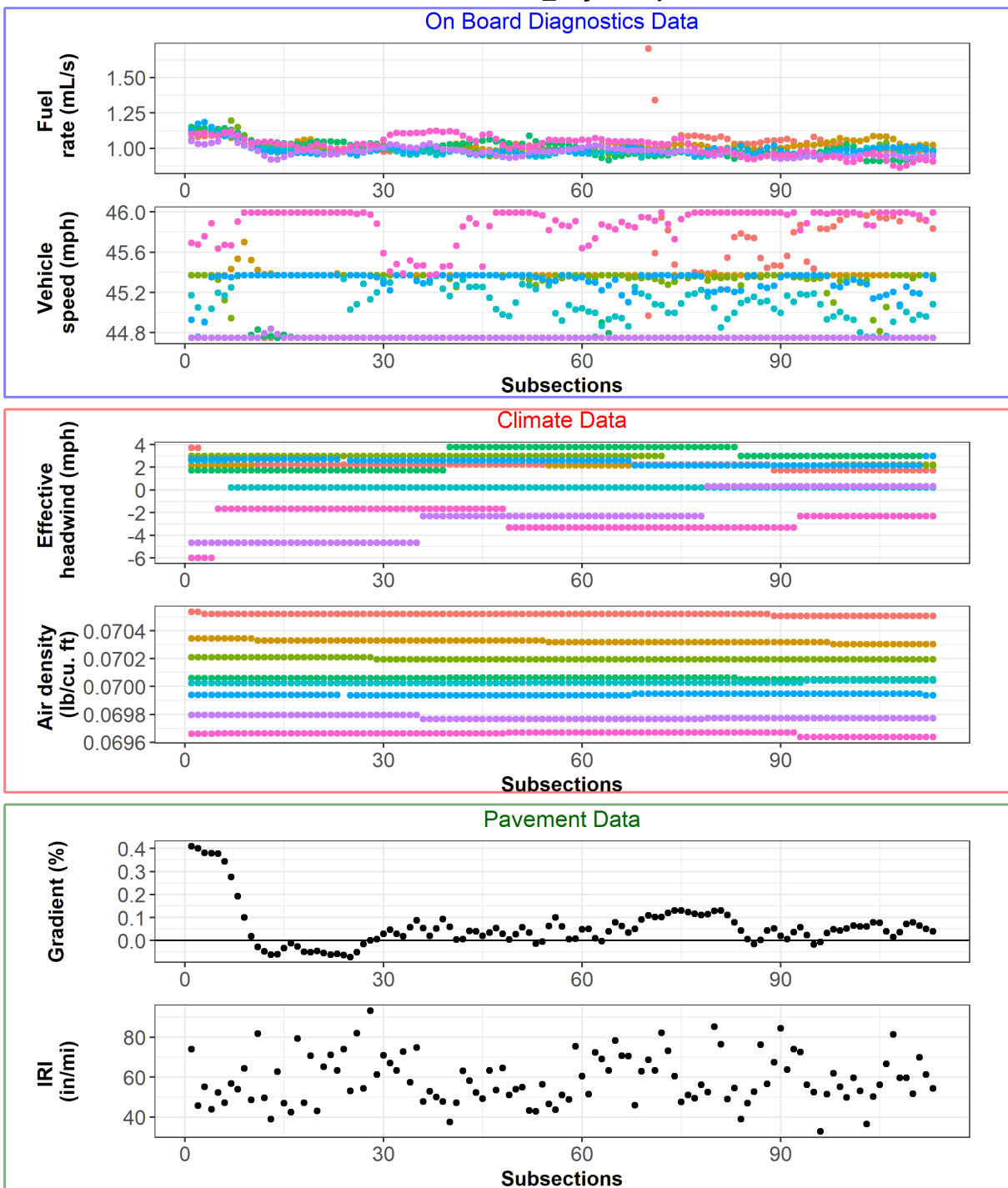


Figure P.74: Car data on Section PH18.

Car summer_day 55 mph

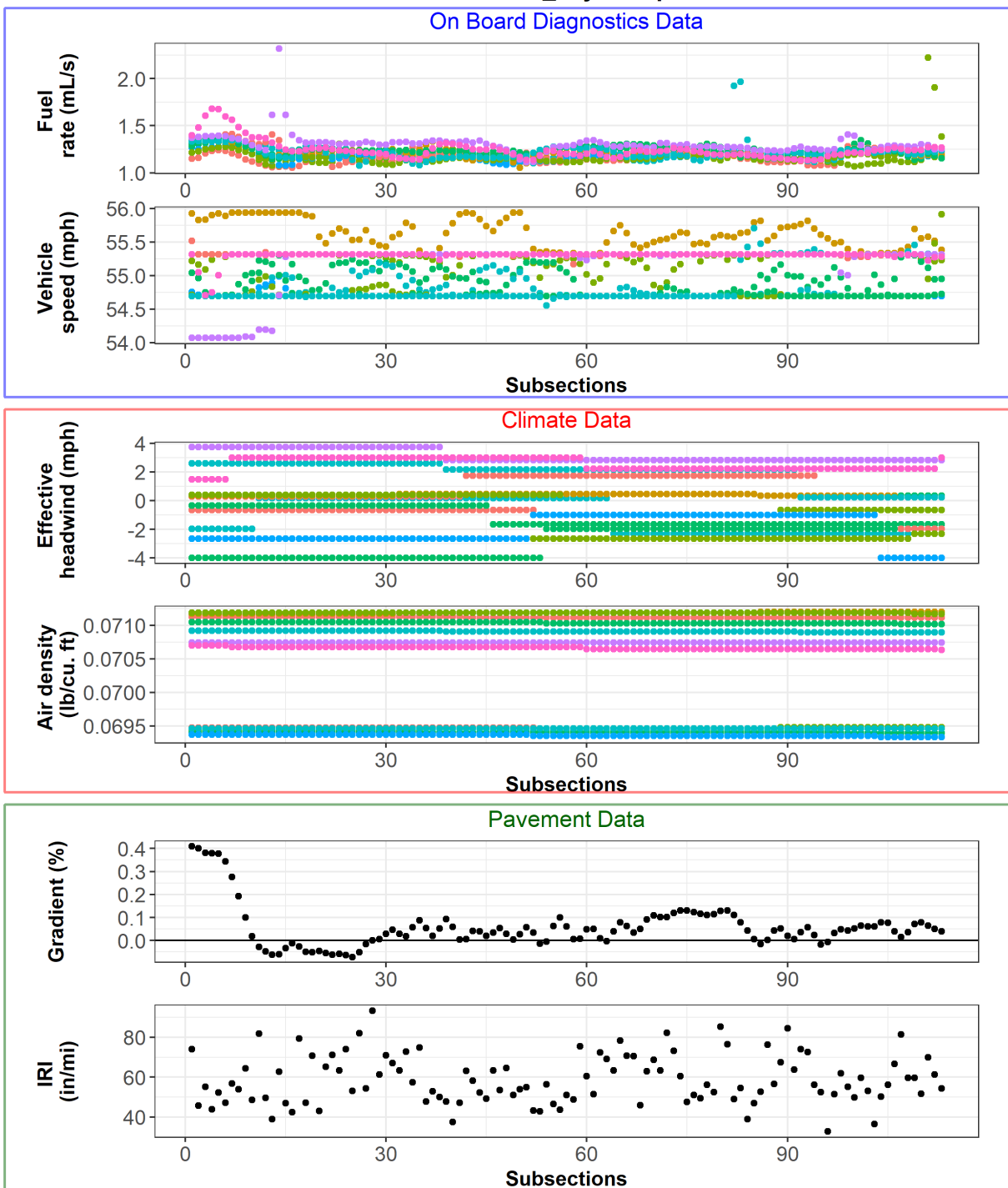


Figure P.75: Car data on Section PH18.

Car summer_day 45 mph

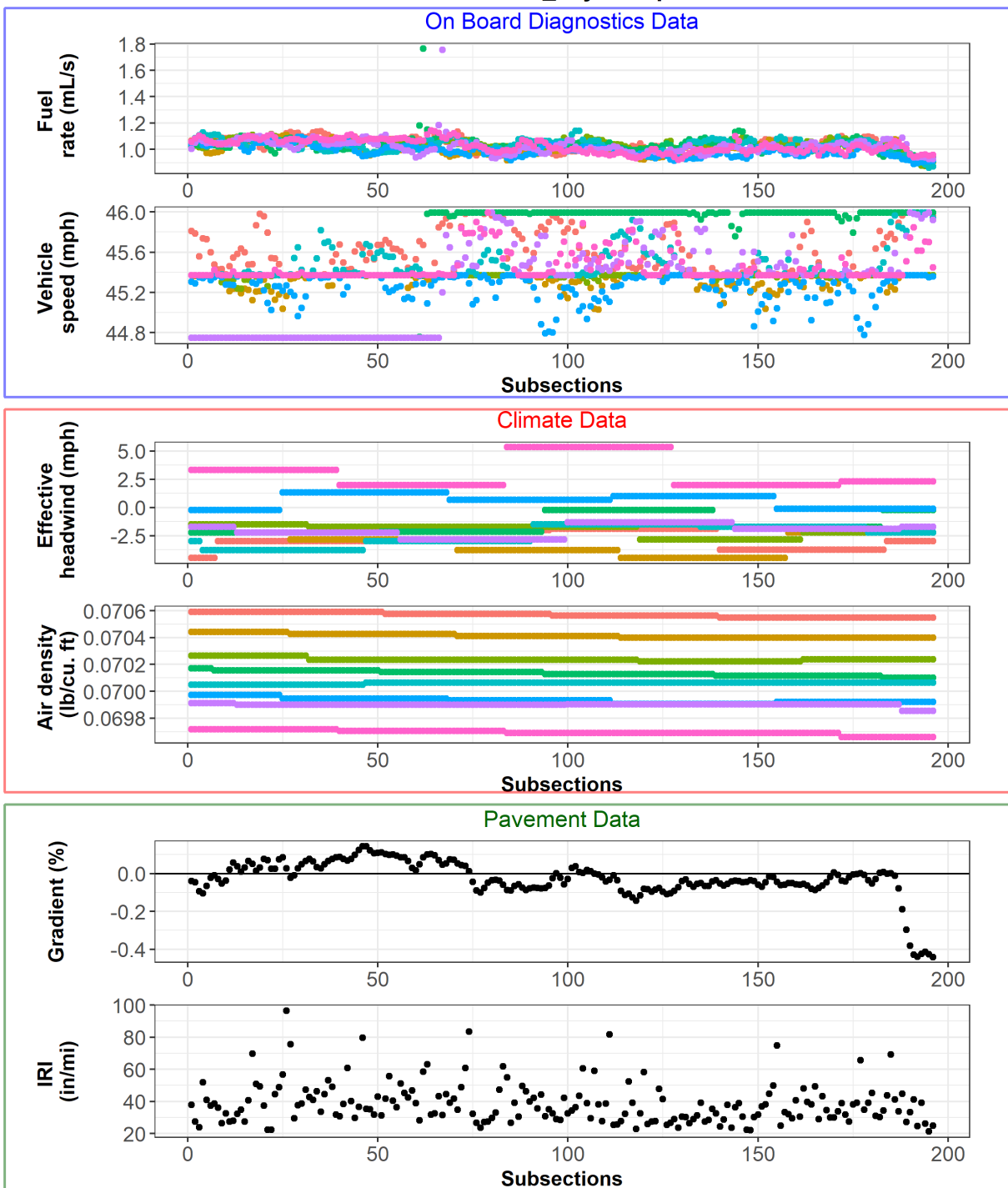


Figure P.76: Car data on Section PH19.

Car summer_day 55 mph

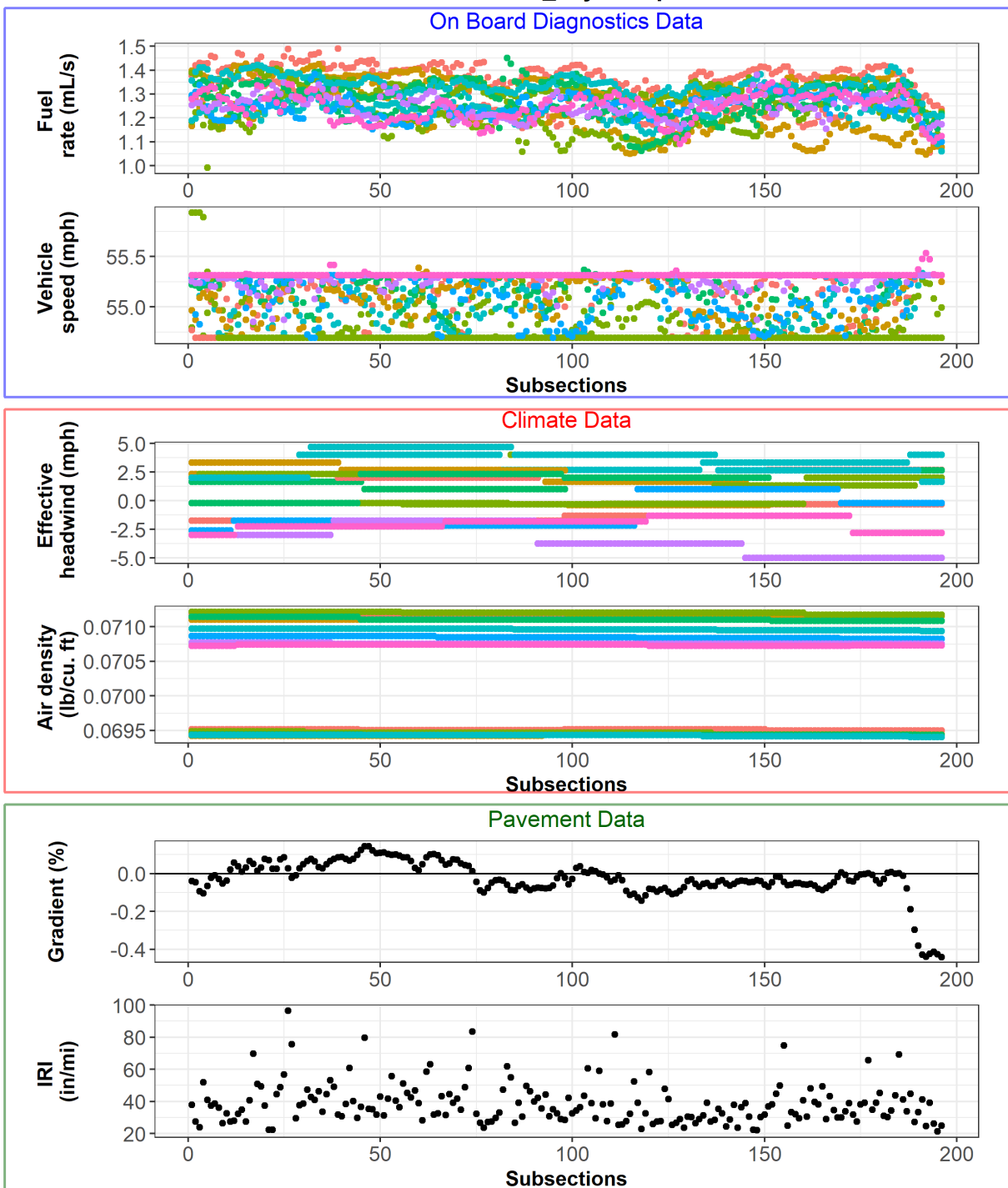


Figure P.77: Car data on Section PH19.

Car summer_day 45 mph

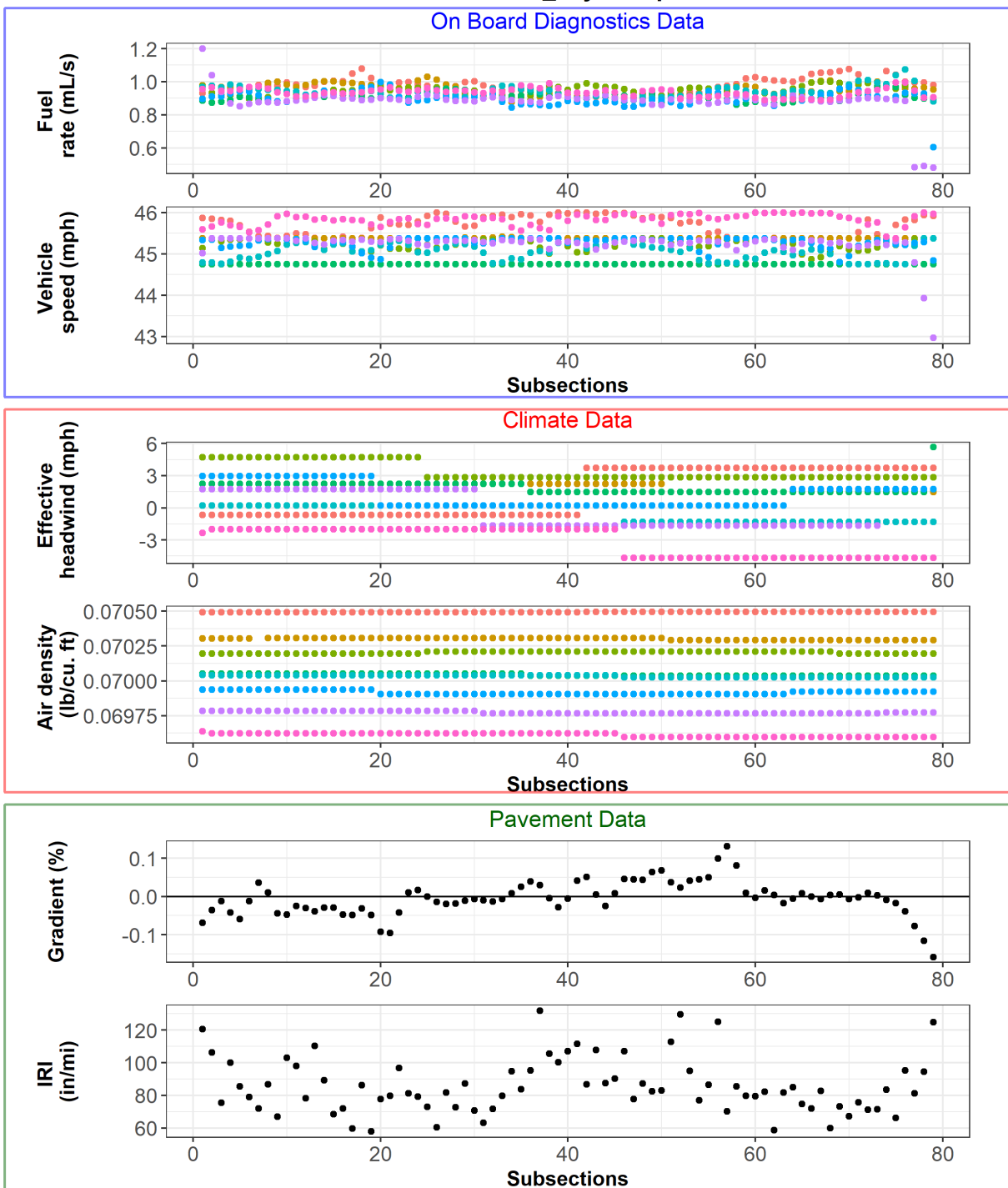


Figure P.78: Car data on Section PH20.

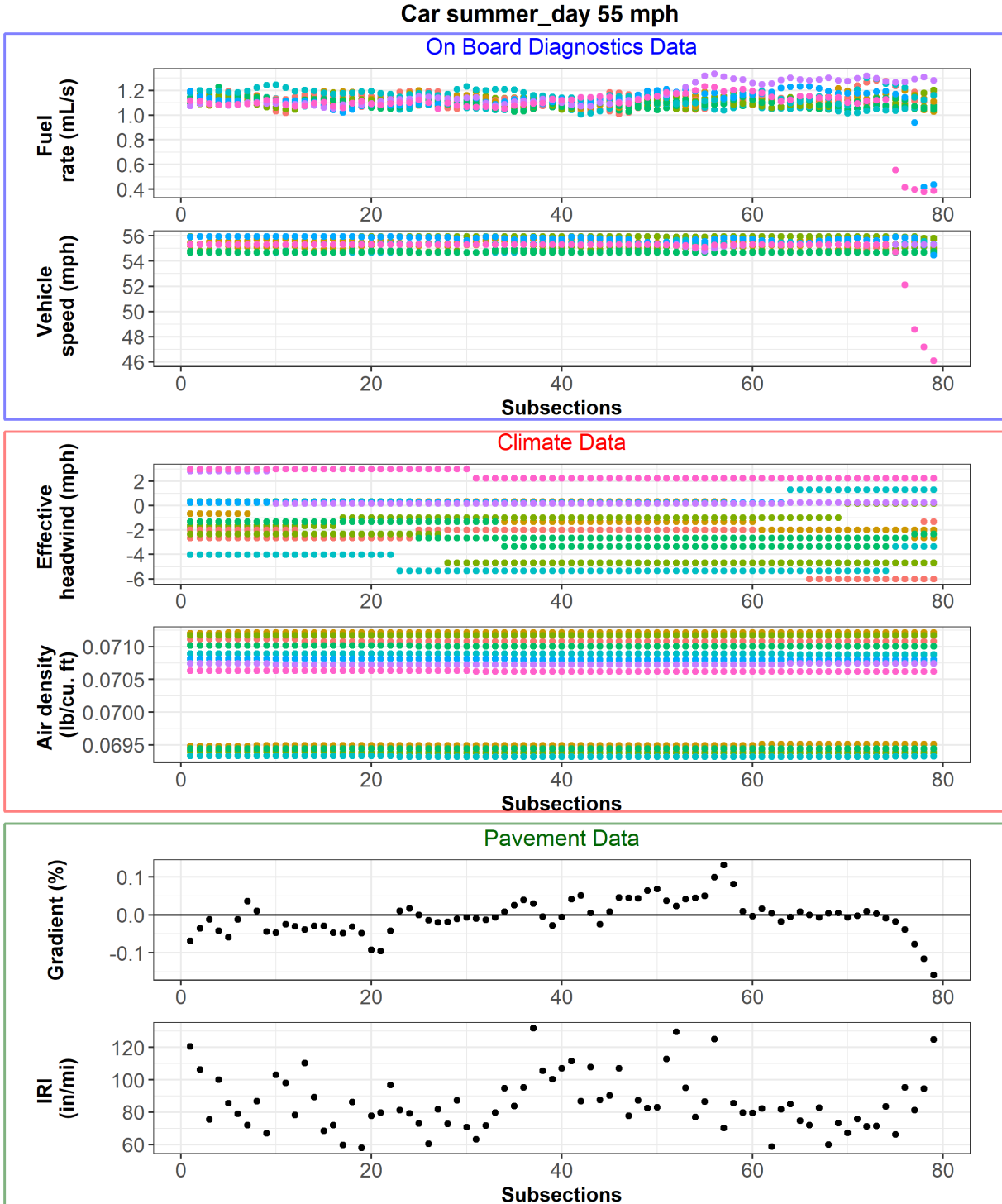


Figure P.79: Car data on Section PH20.

Car summer_day 45 mph

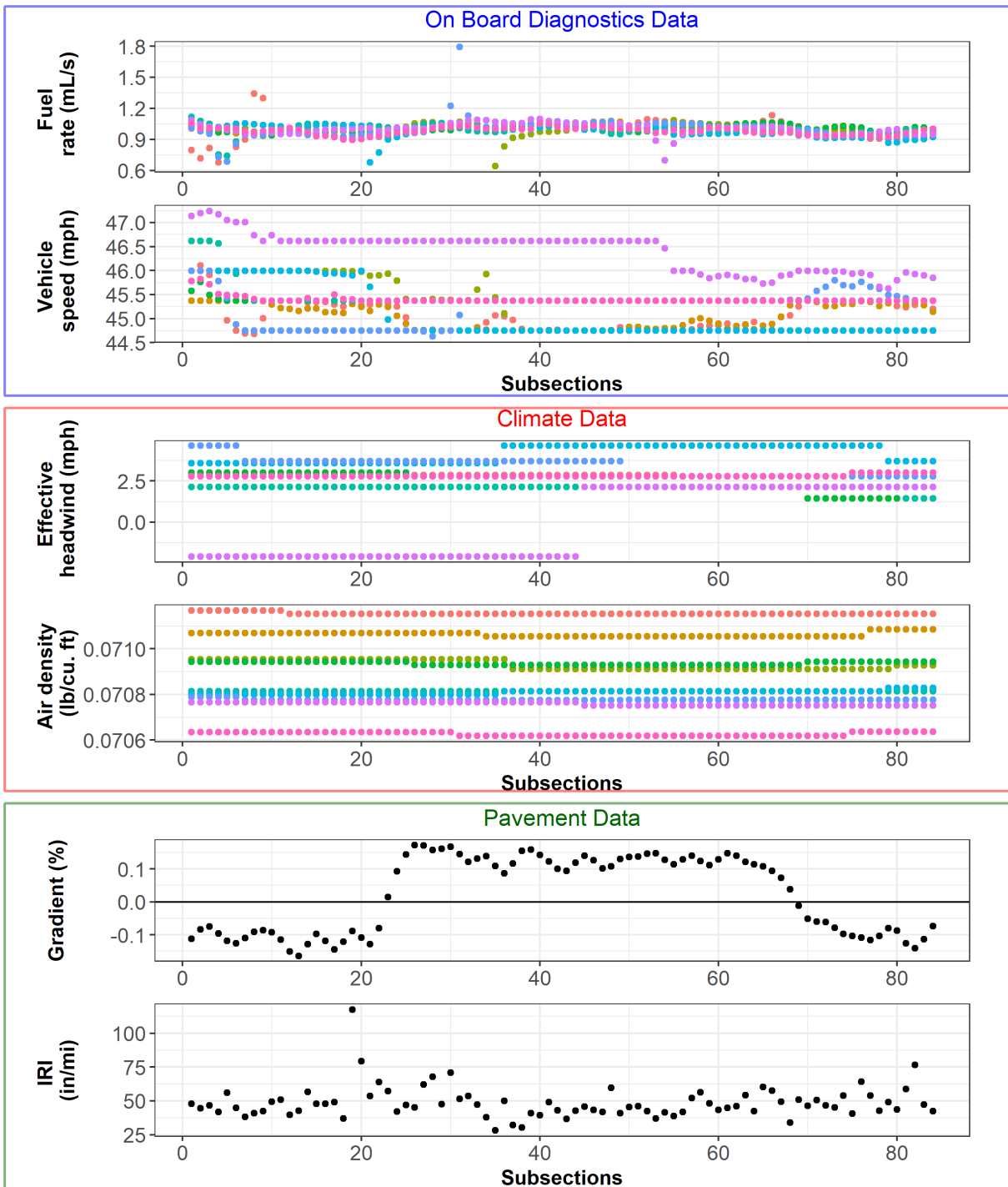


Figure P.80: Car data on Section PH21.

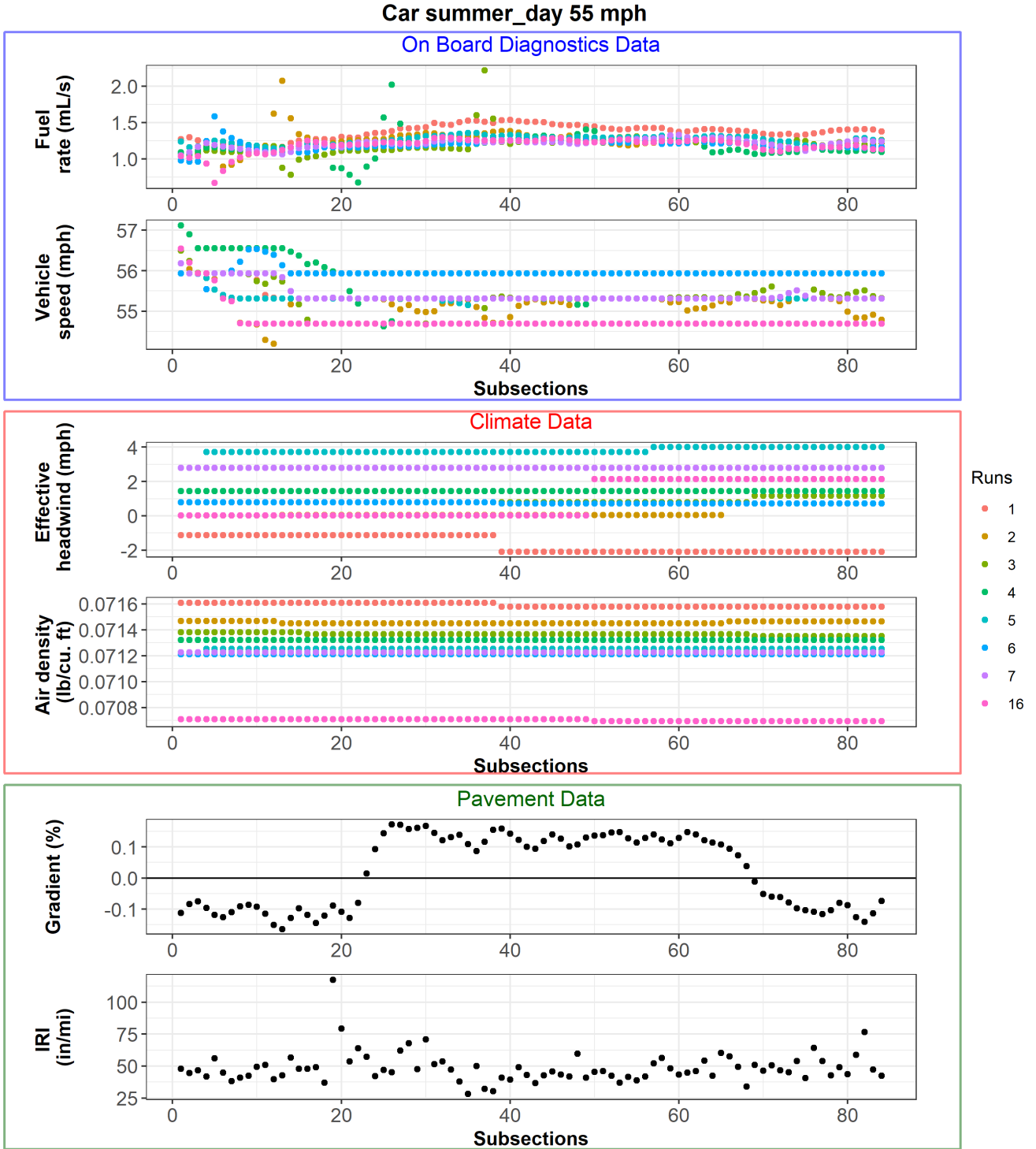


Figure P.81: Car data on Section PH21.

Car winter_day 45 mph

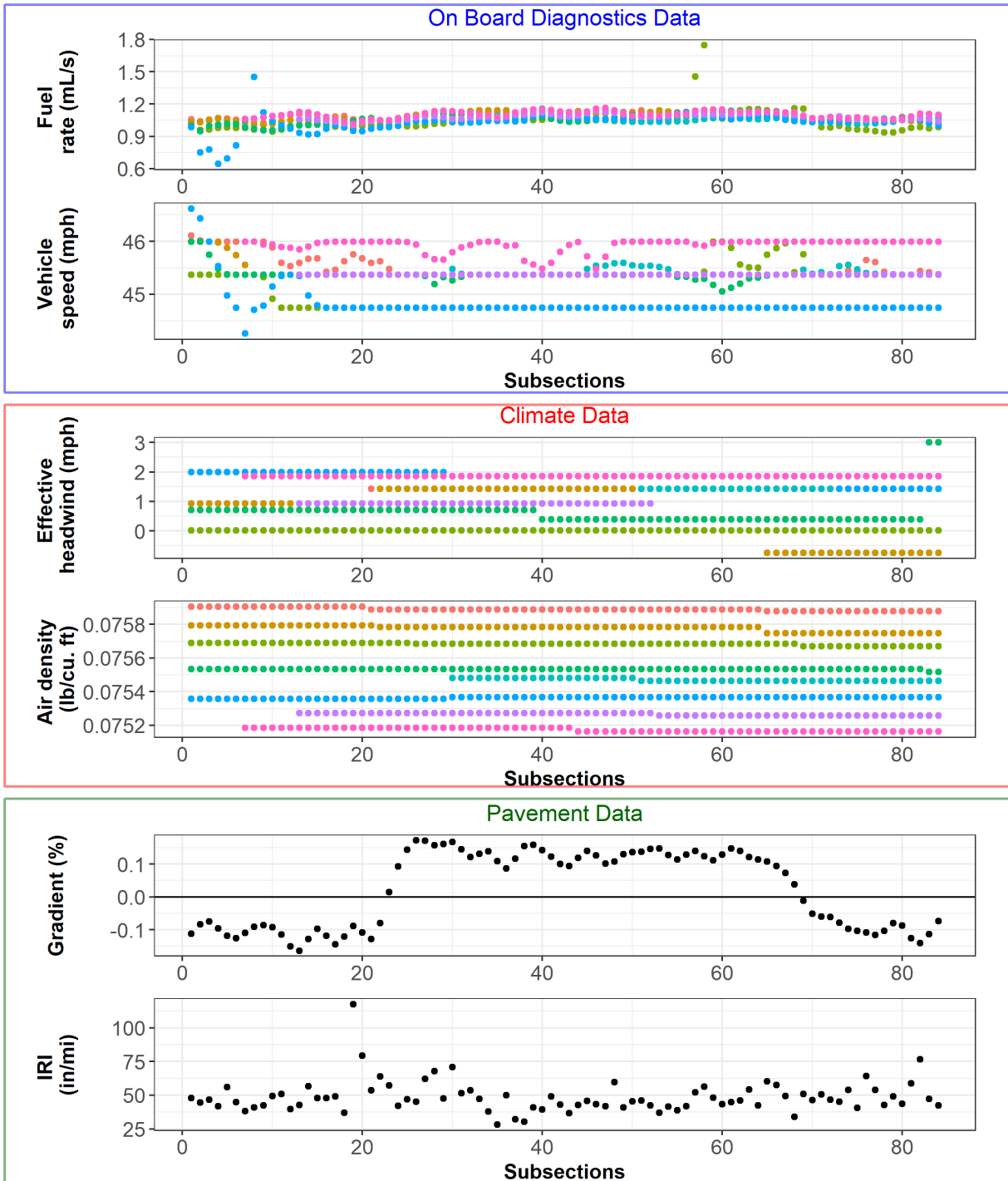
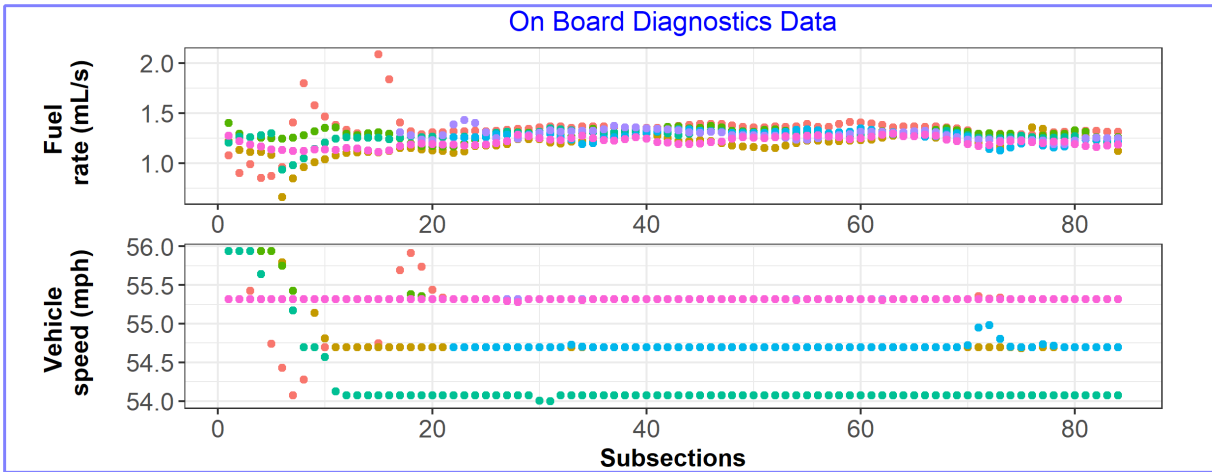


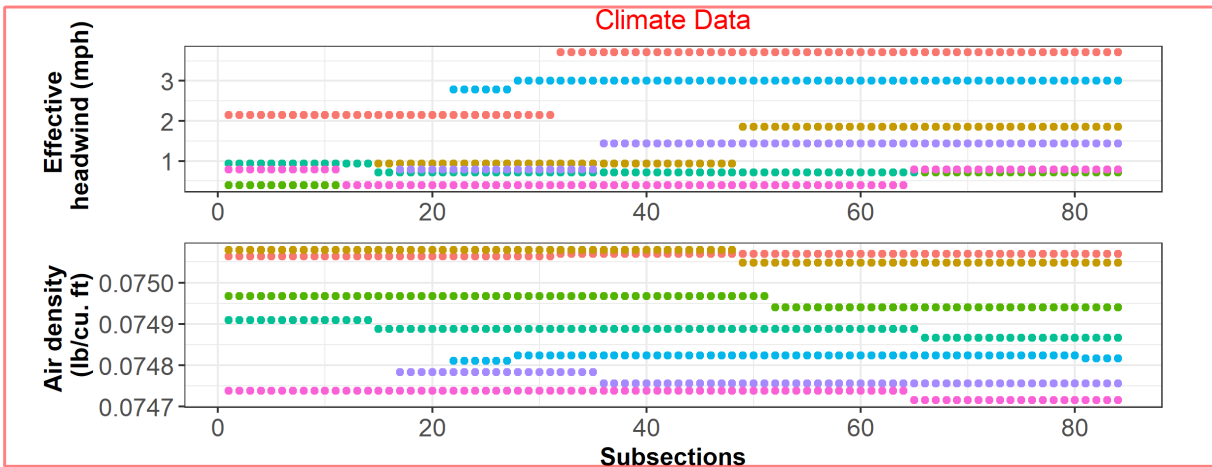
Figure P.82: Car data on Section PH21.

Car winter_day 55 mph

On Board Diagnostics Data



Climate Data



Pavement Data

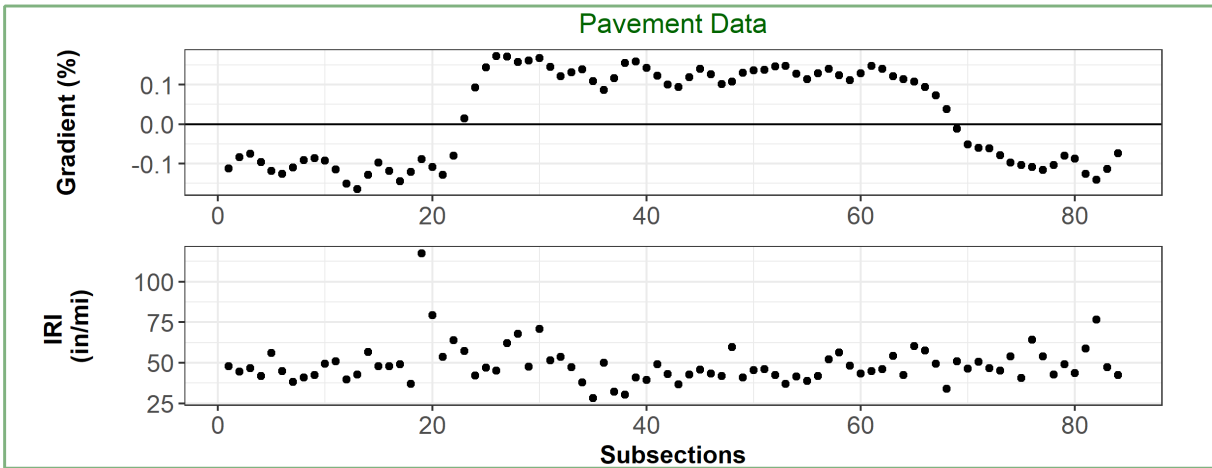


Figure P.83: Car data on Section PH21.

Car summer_day 45 mph

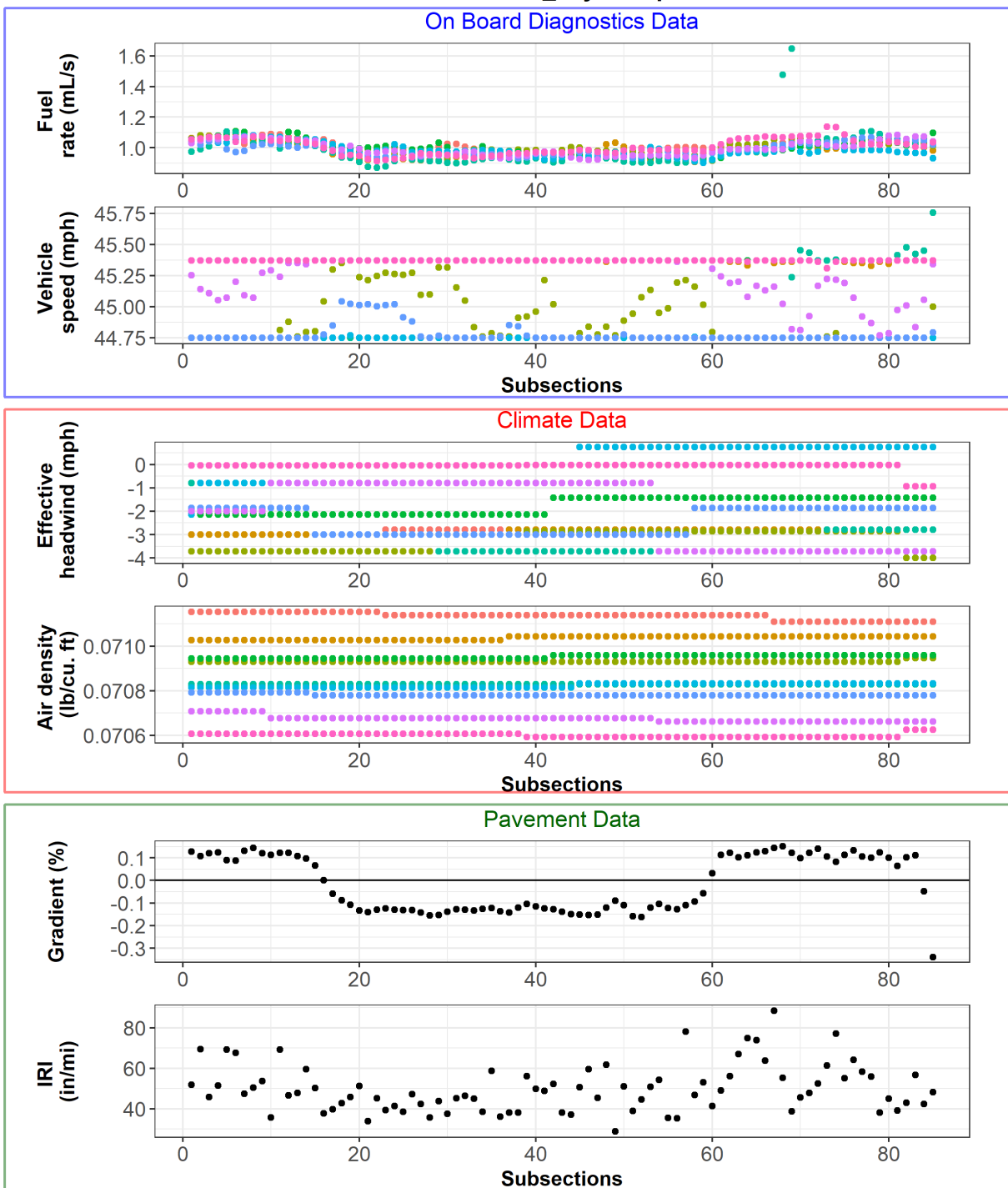


Figure P.84: Car data on Section PH22.

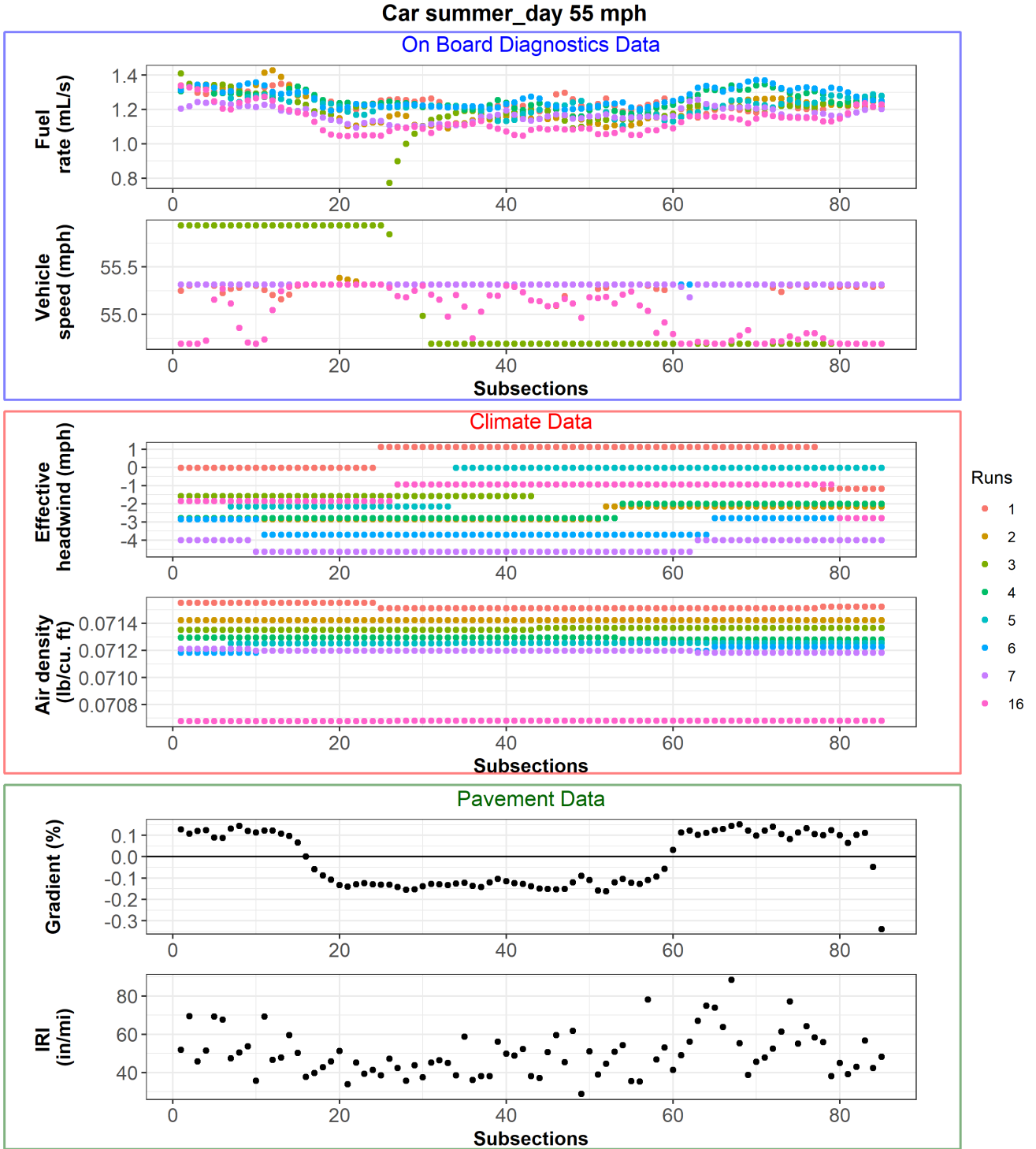


Figure P.85: Car data on Section PH22.

Car winter_day 45 mph

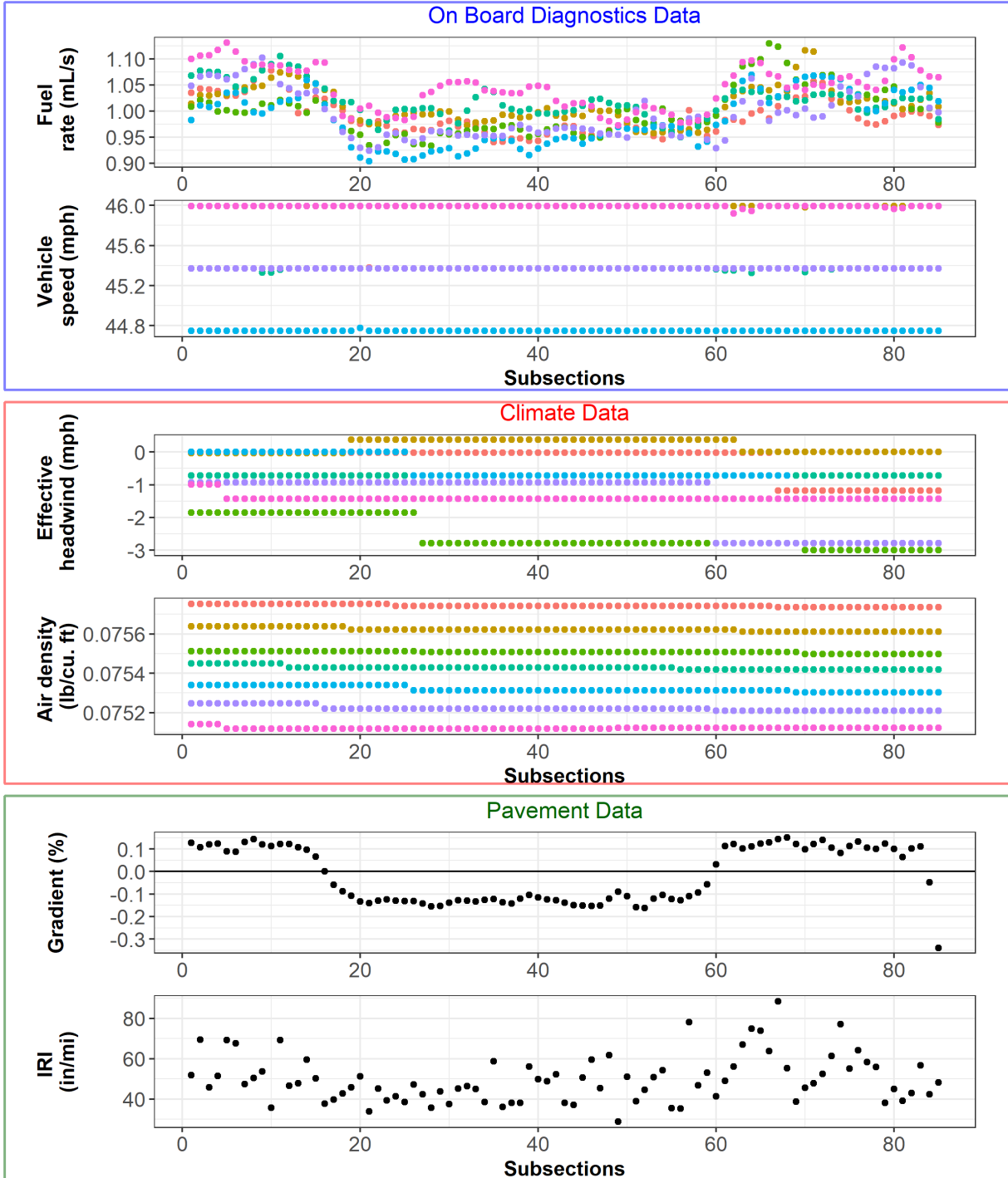


Figure P.86: Car data on Section PH22.

Car winter_day 55 mph

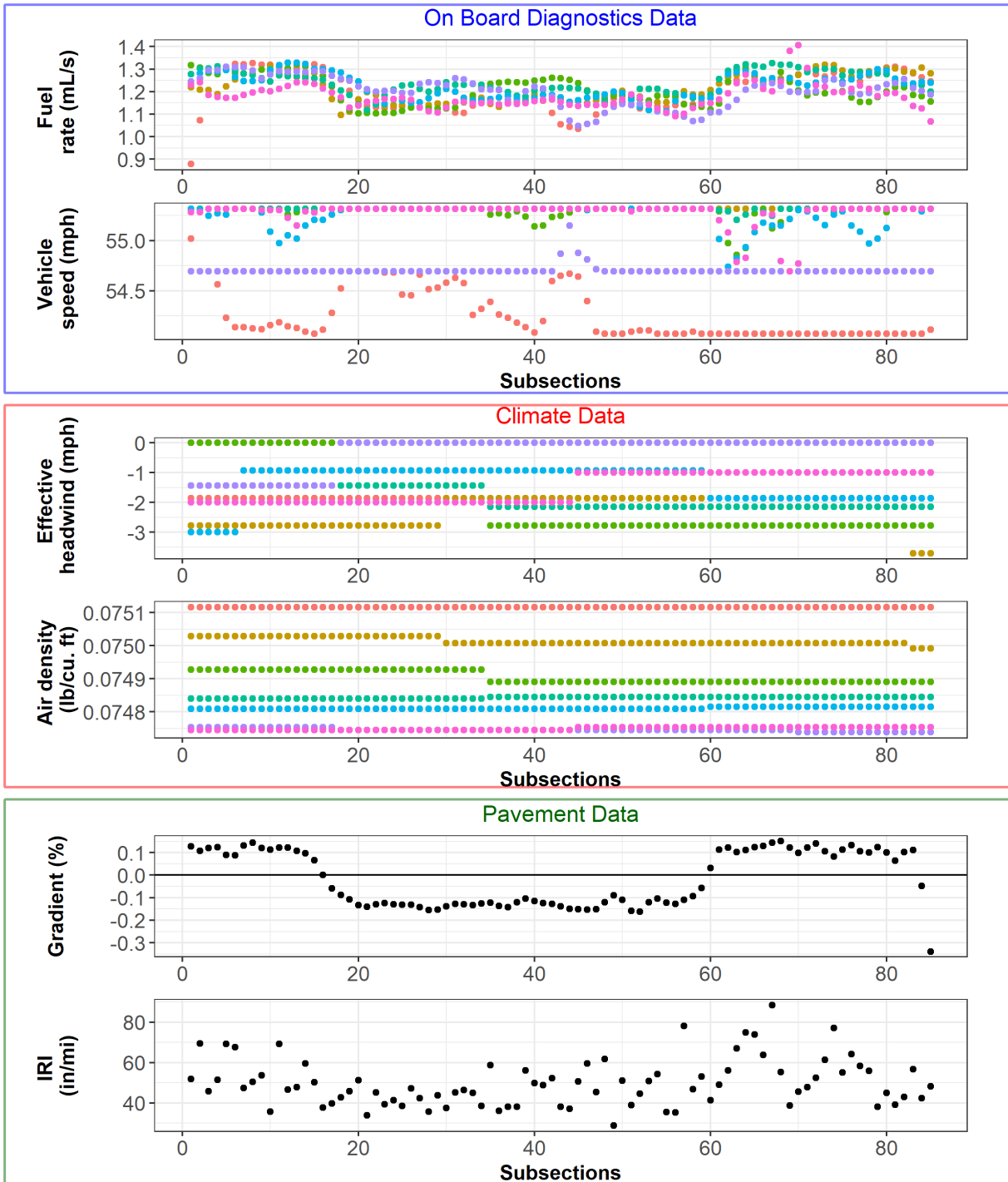


Figure P.87: Car data on Section PH22.

Car summer_day 35 mph

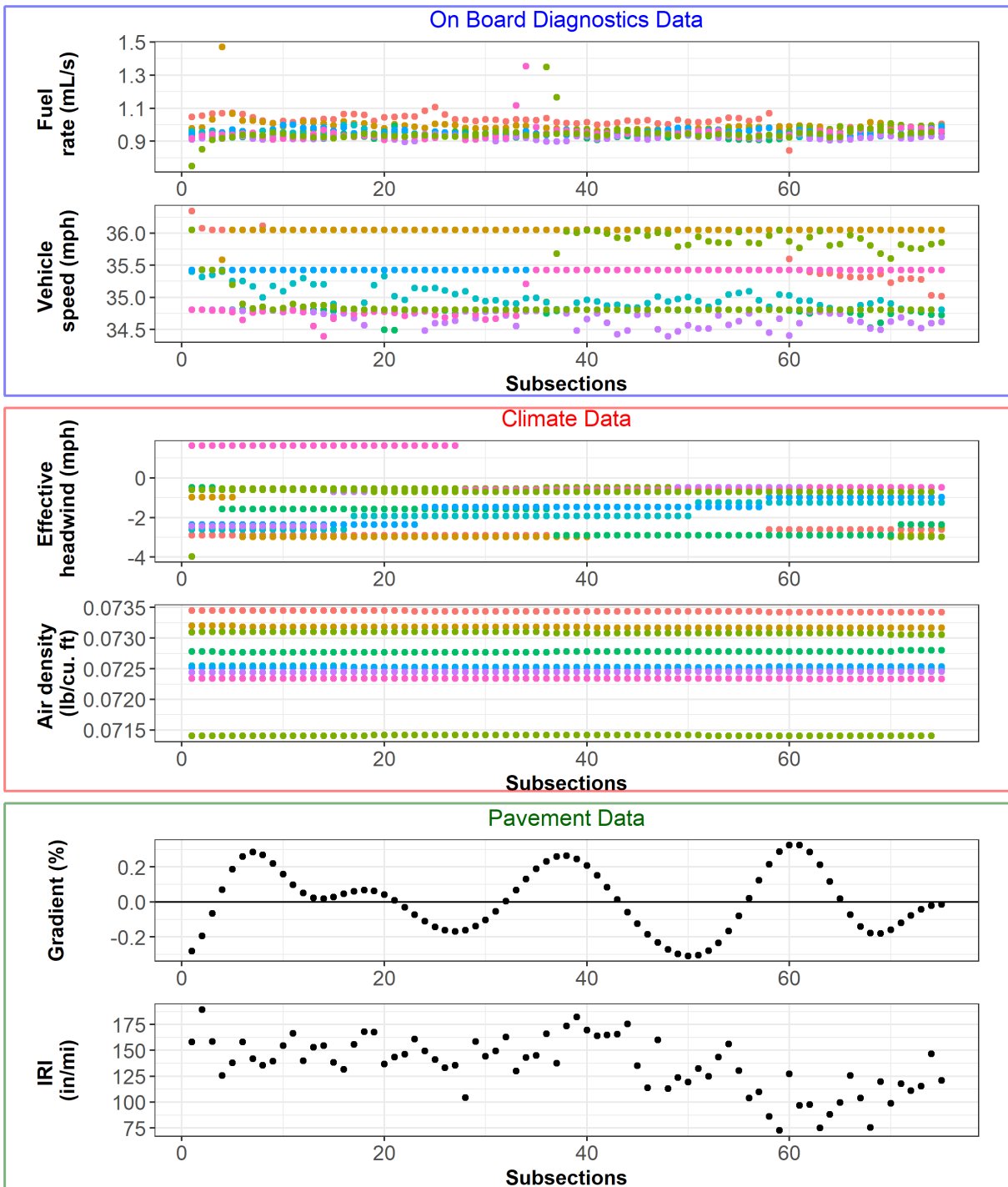


Figure P.88: Car data on Section PH23.

Car summer_day 45 mph

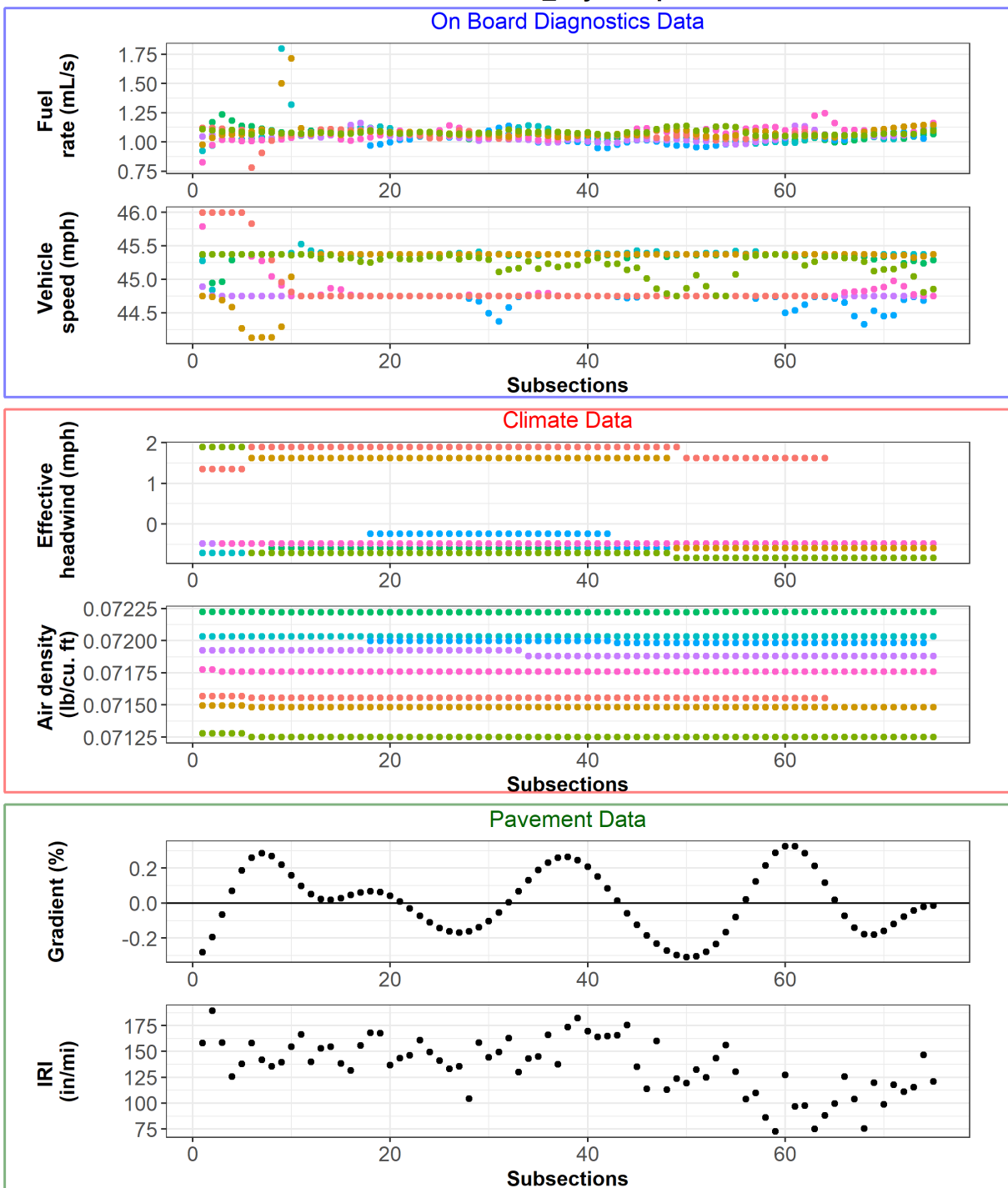


Figure P.89: Car data on Section PH23.

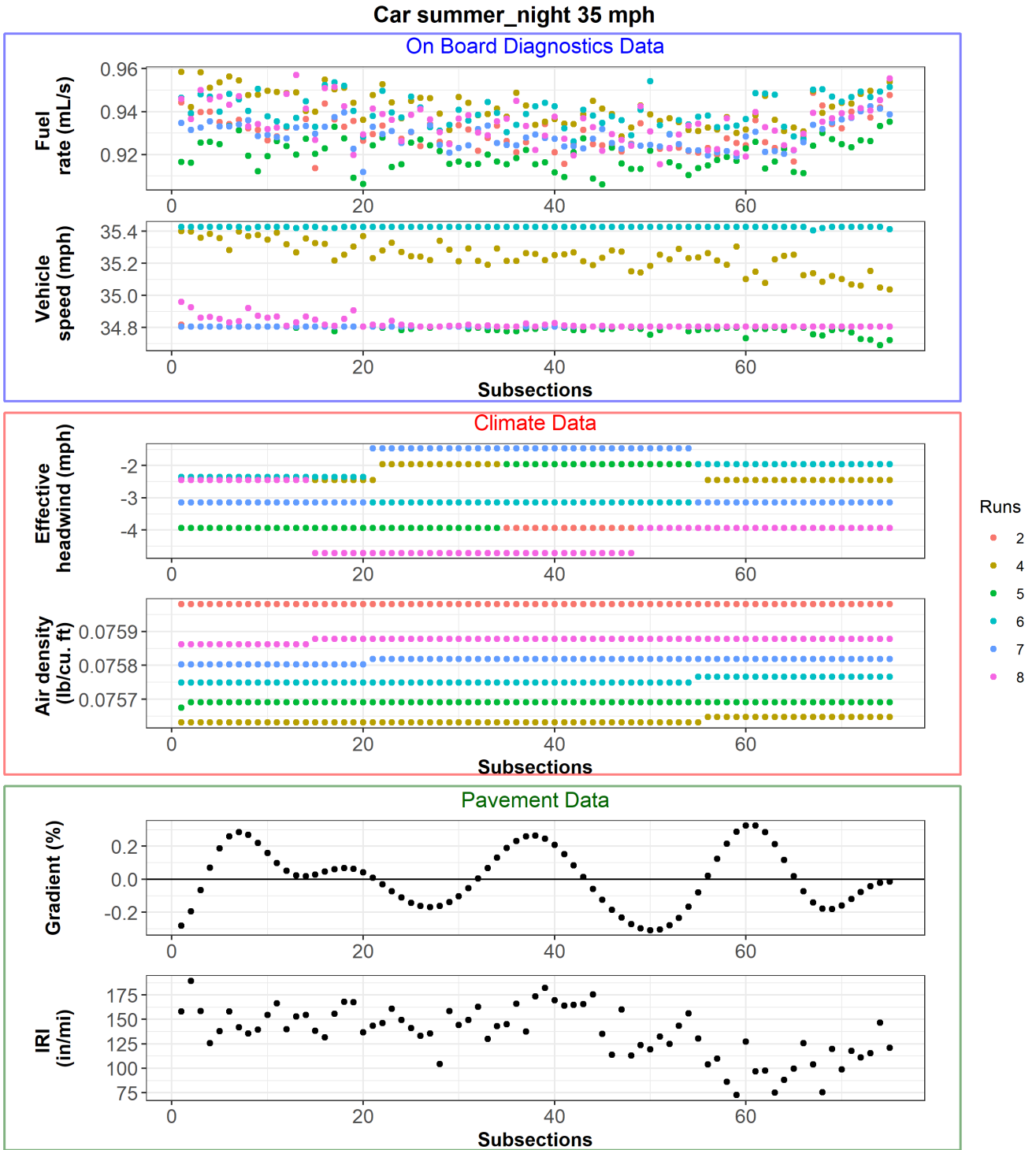


Figure P.90: Car data on Section PH23.

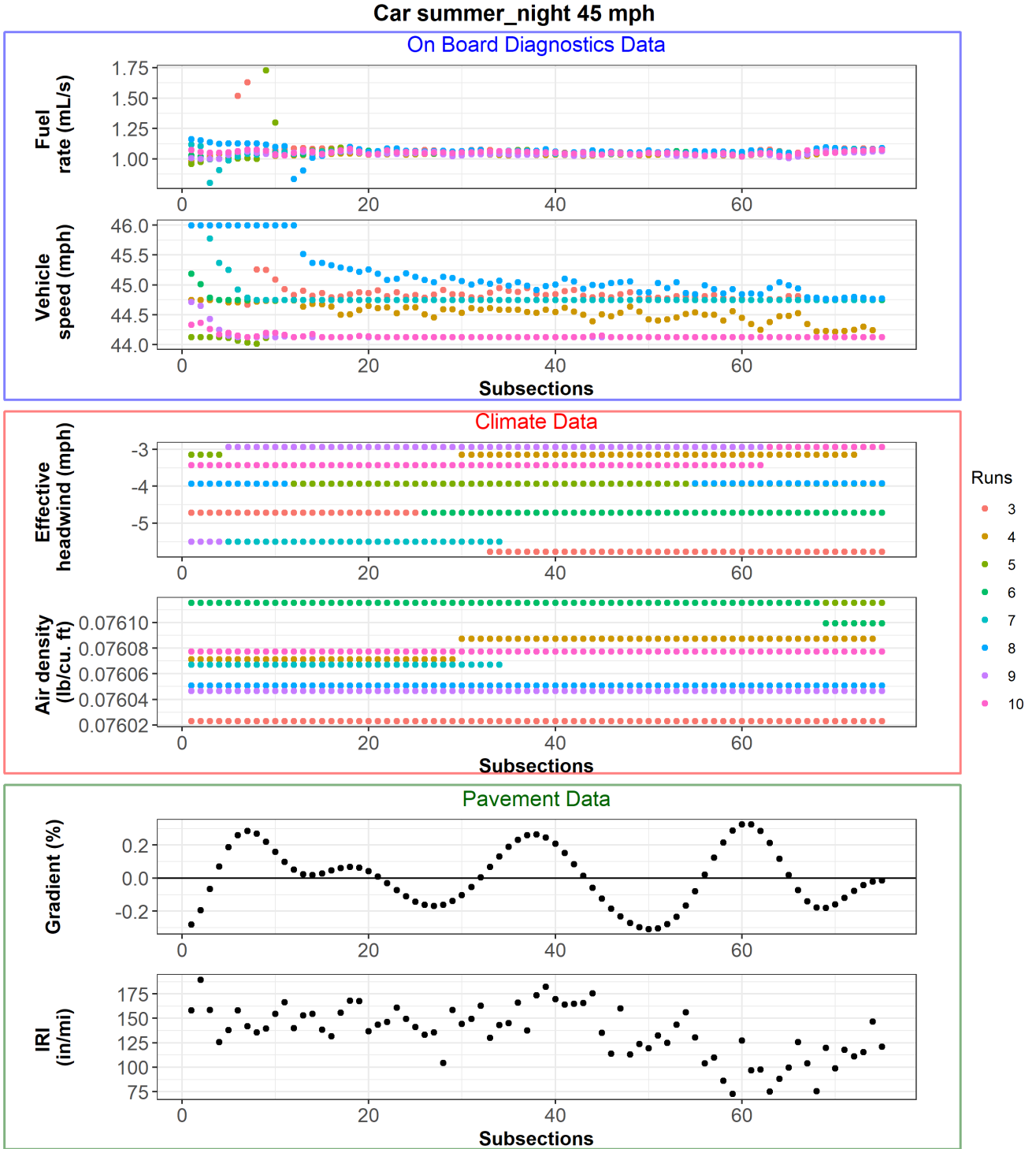
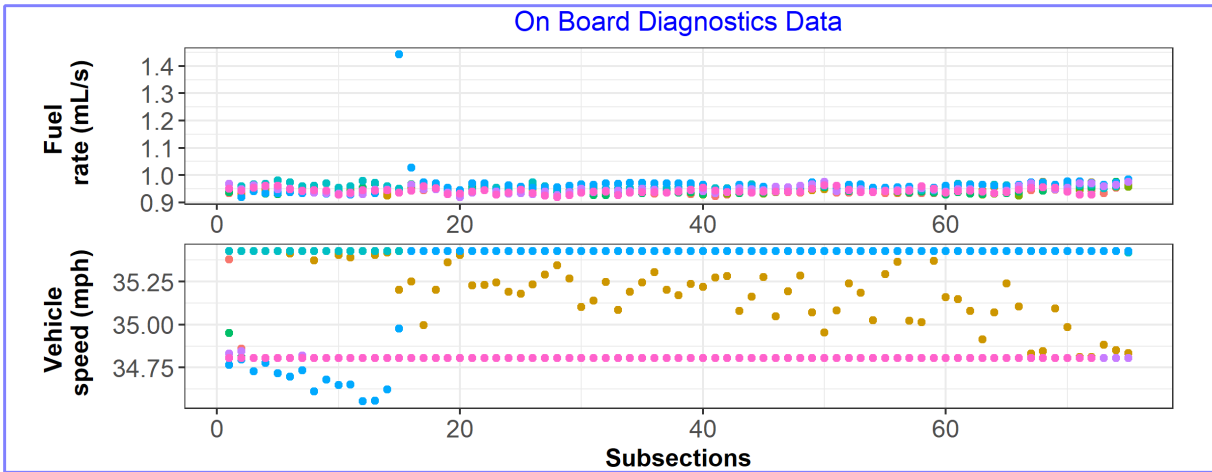


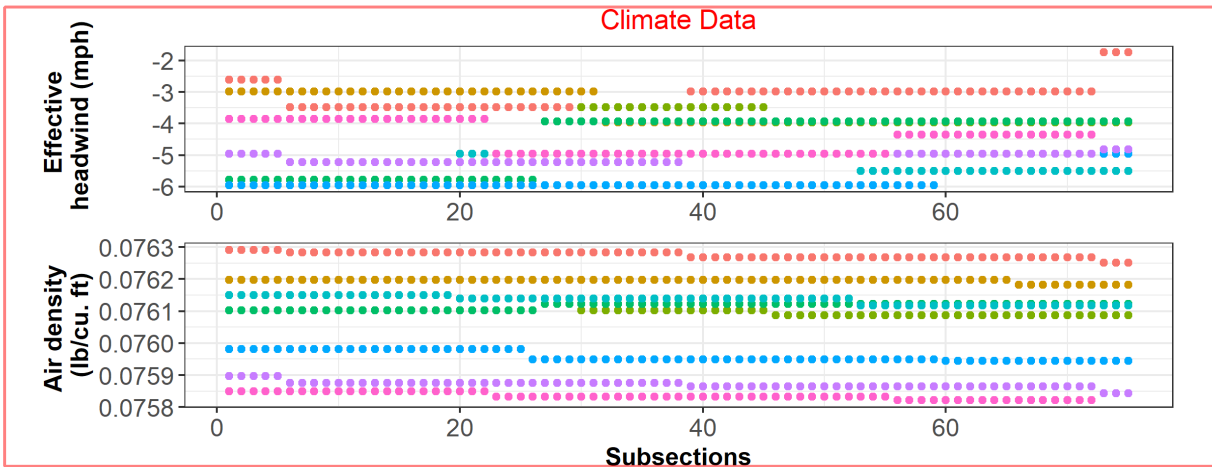
Figure P.91: Car data on Section PH23.

Car winter_day 35 mph

On Board Diagnostics Data



Climate Data



Runs

- 1
- 2
- 3
- 4
- 5
- 6
- 7
- 8

Pavement Data

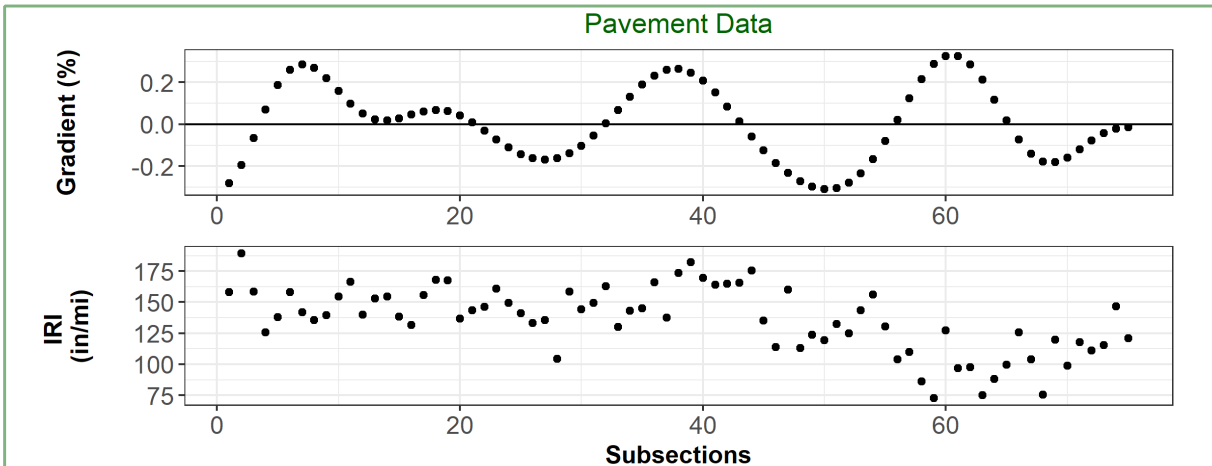


Figure P.92: Car data on Section PH23.

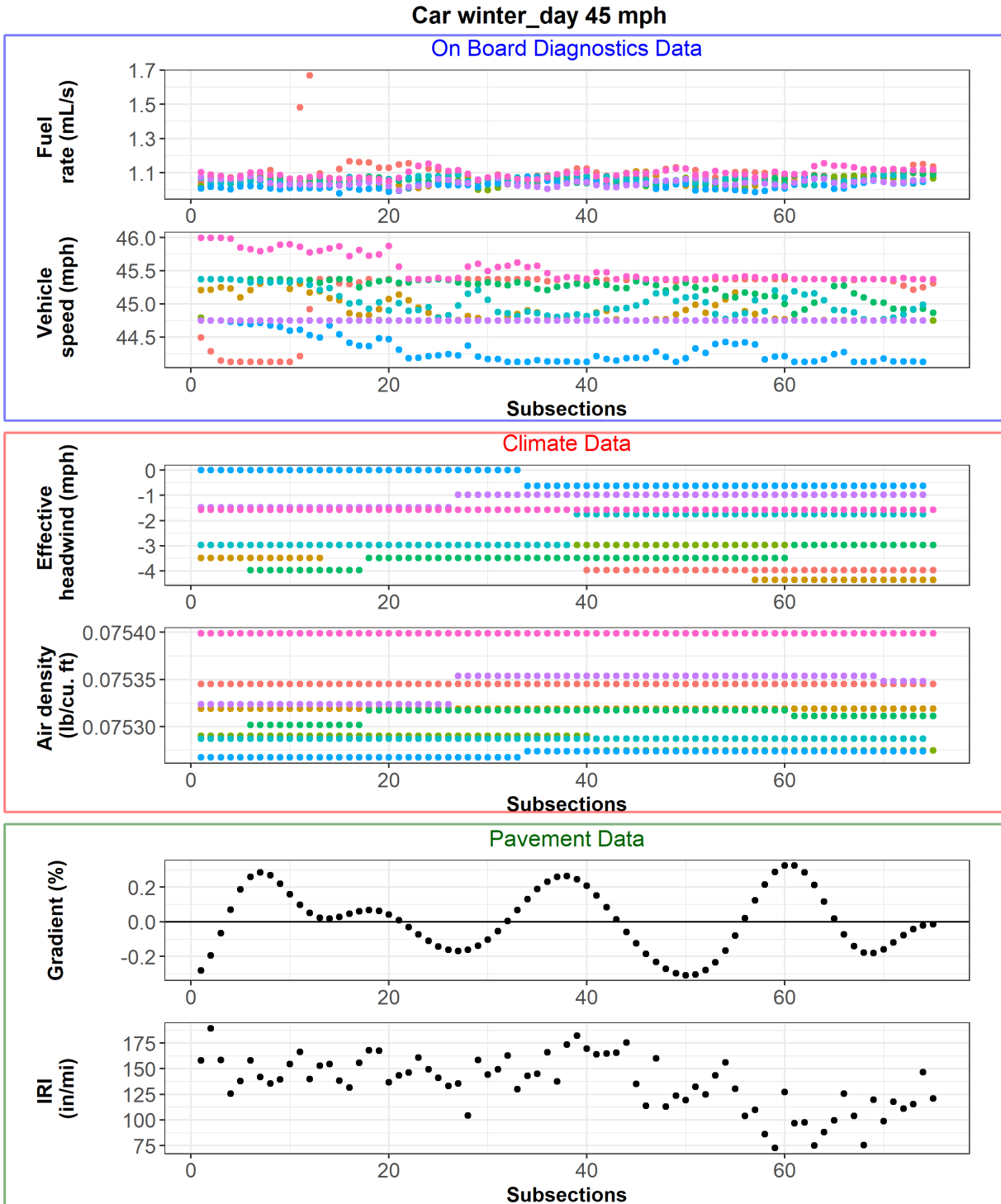


Figure P.93: Car data on Section PH23.

2. SUV Data

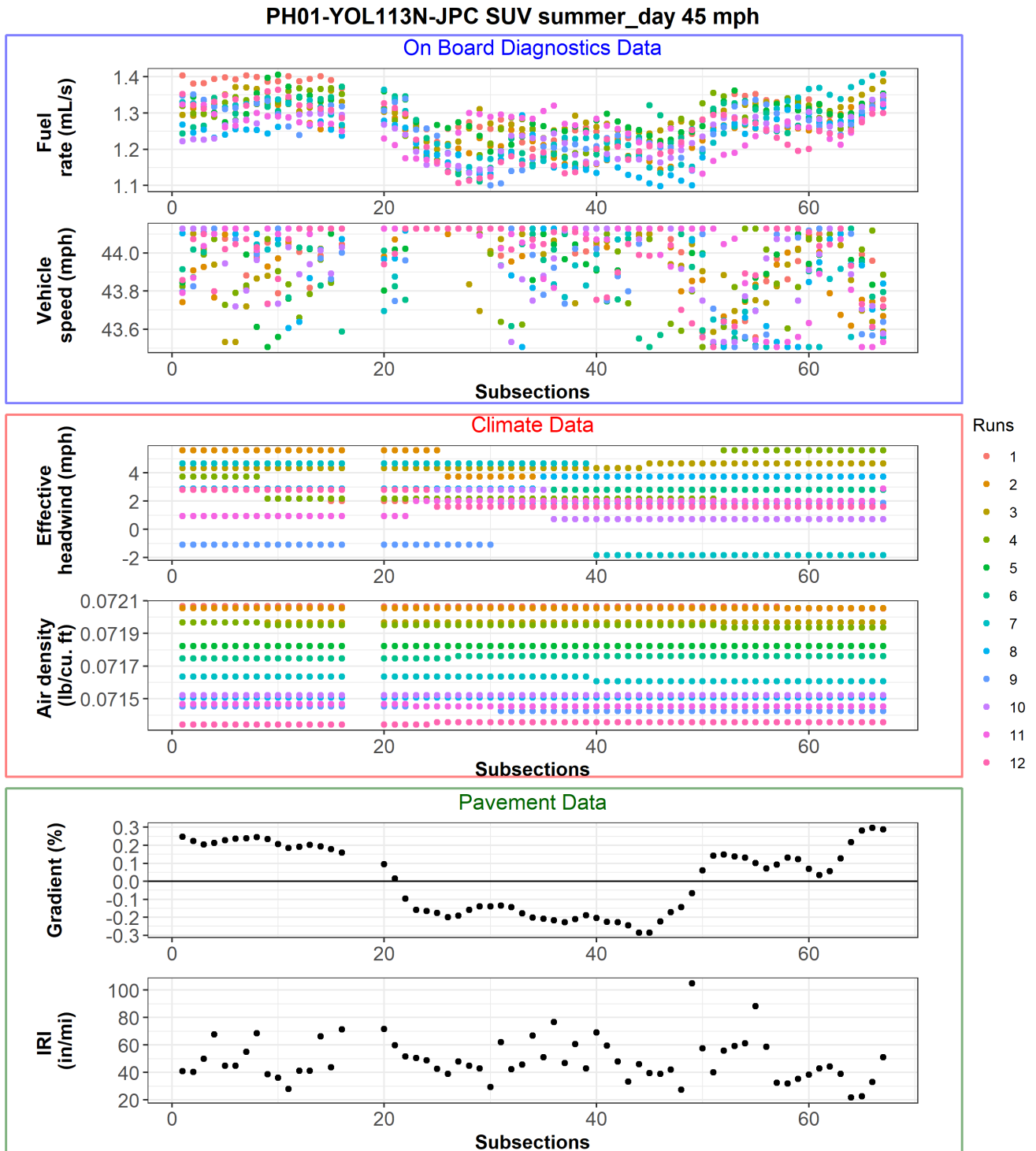


Figure P.94: SUV data on Section PH01.

PH01-YOL113N-JPC SUV summer_day 55 mph

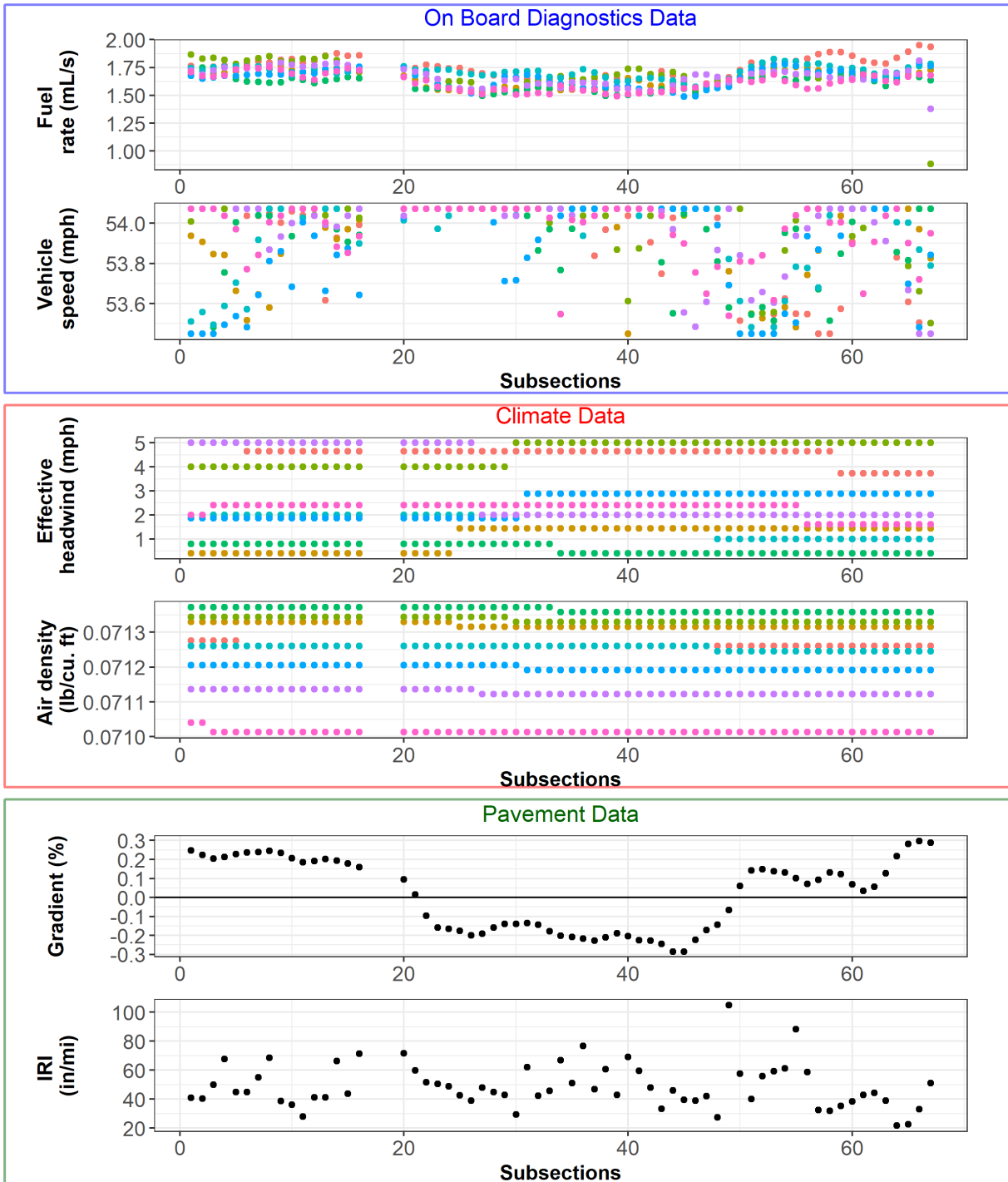


Figure P.95: SUV data on Section PH01.

PH01-YOL113N-JPC SUV summer_night 45 mph

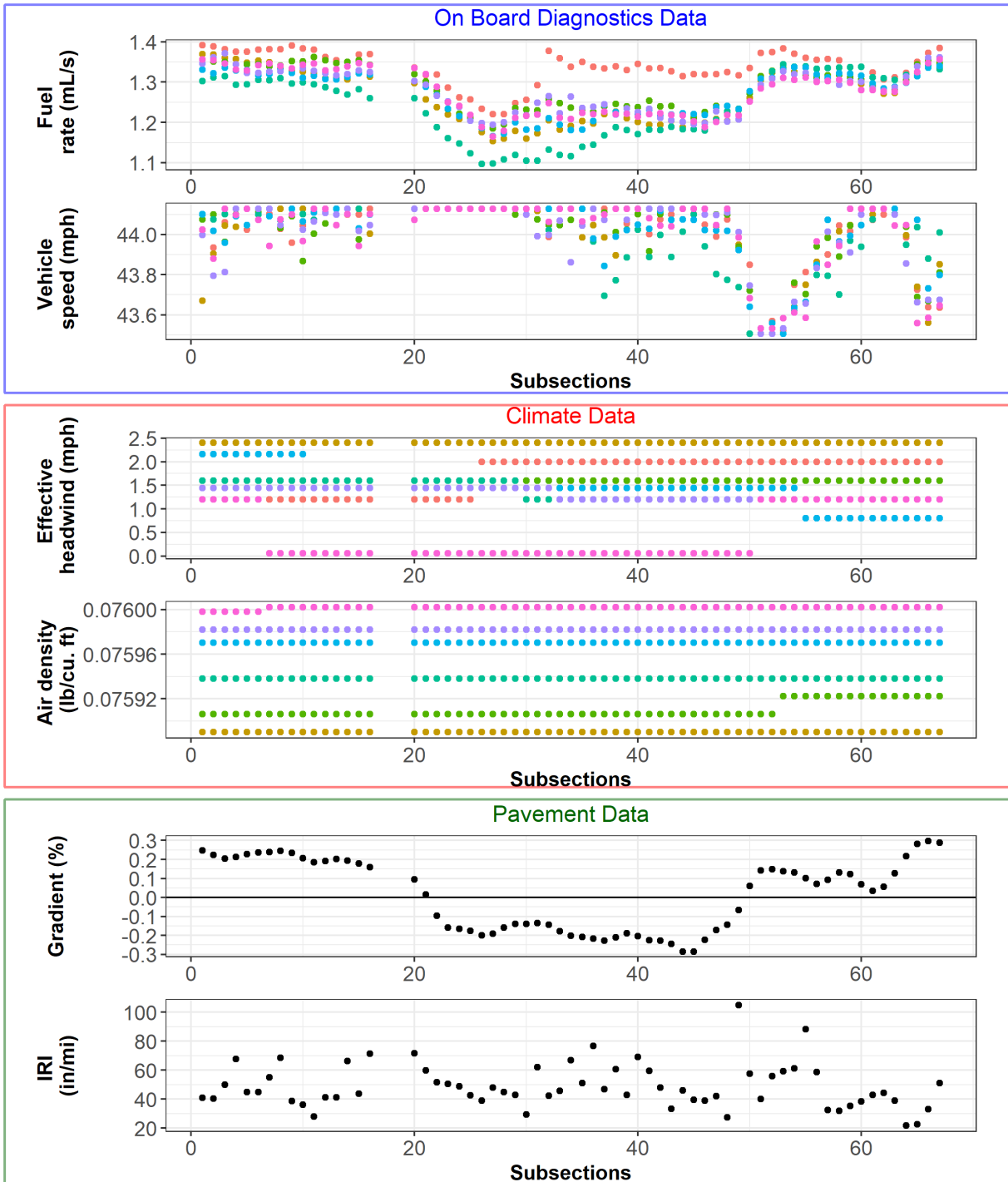


Figure P.96: SUV data on Section PH01.

PH01-YOL113N-JPC SUV summer_night 55 mph

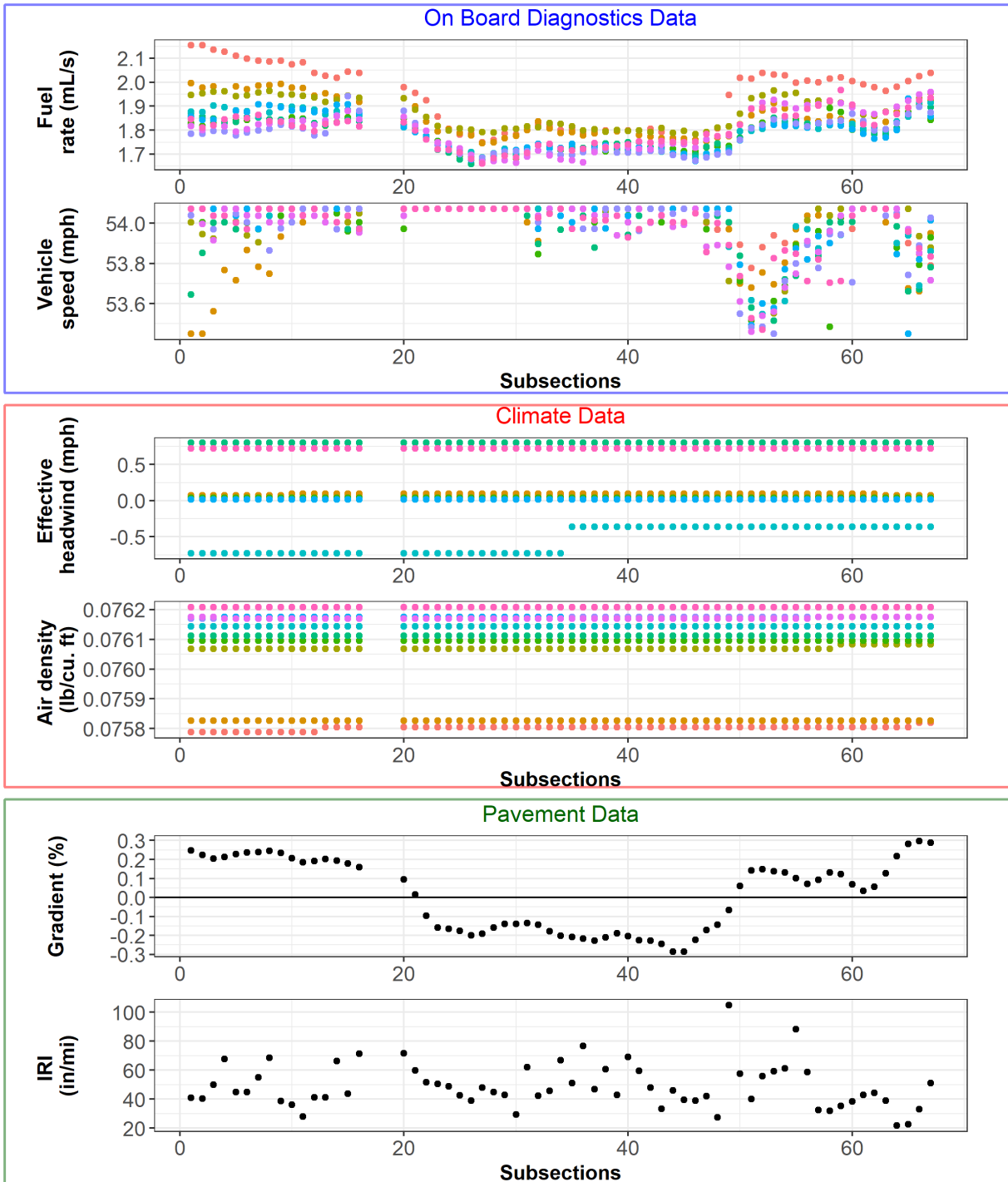


Figure P.97: SUV data on Section PH01.

PH01-YOL113N-JPC SUV winter_day 45 mph

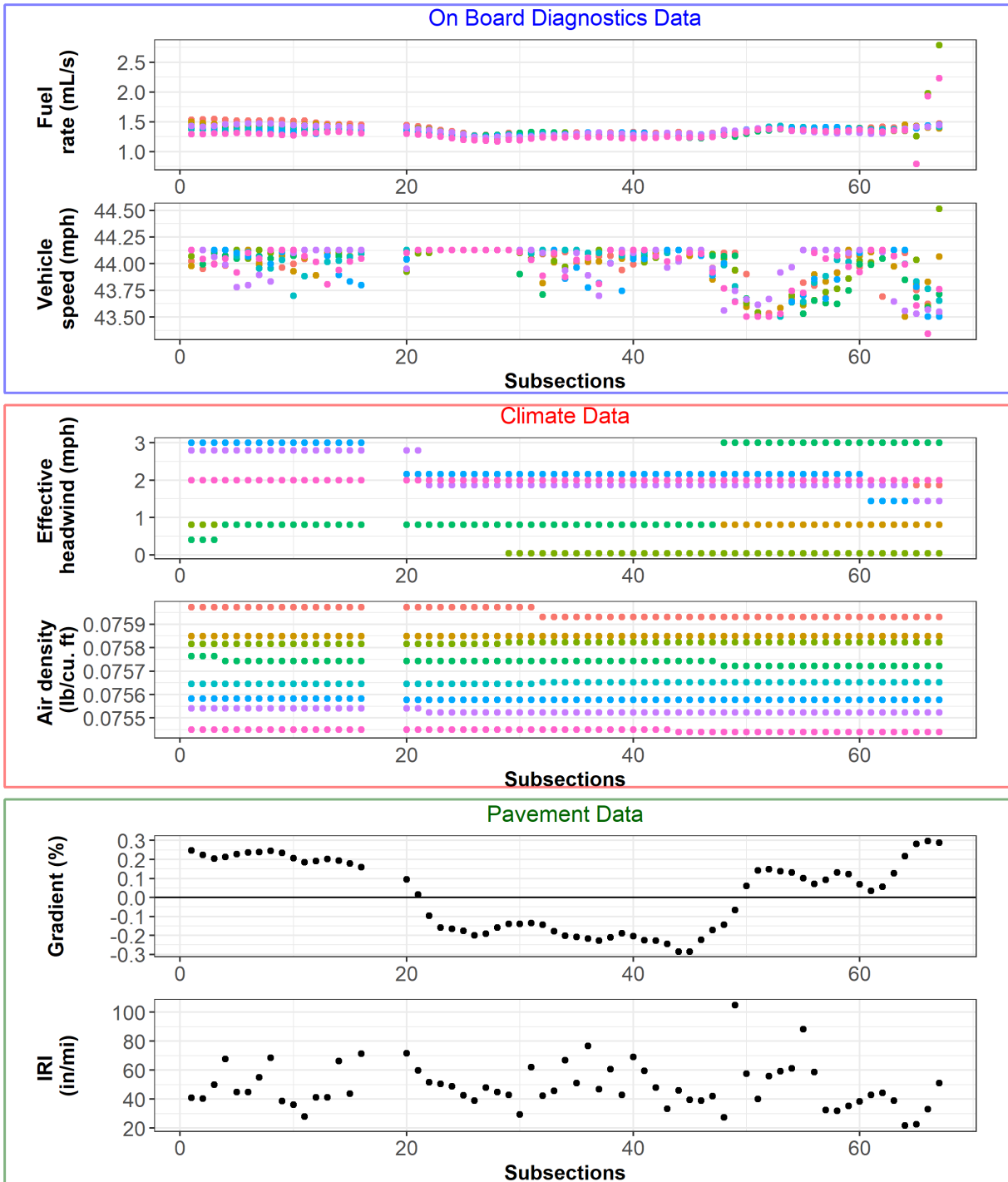


Figure P.98: SUV data on Section PH01.

PH01-YOL113N-JPC SUV winter_day 55 mph

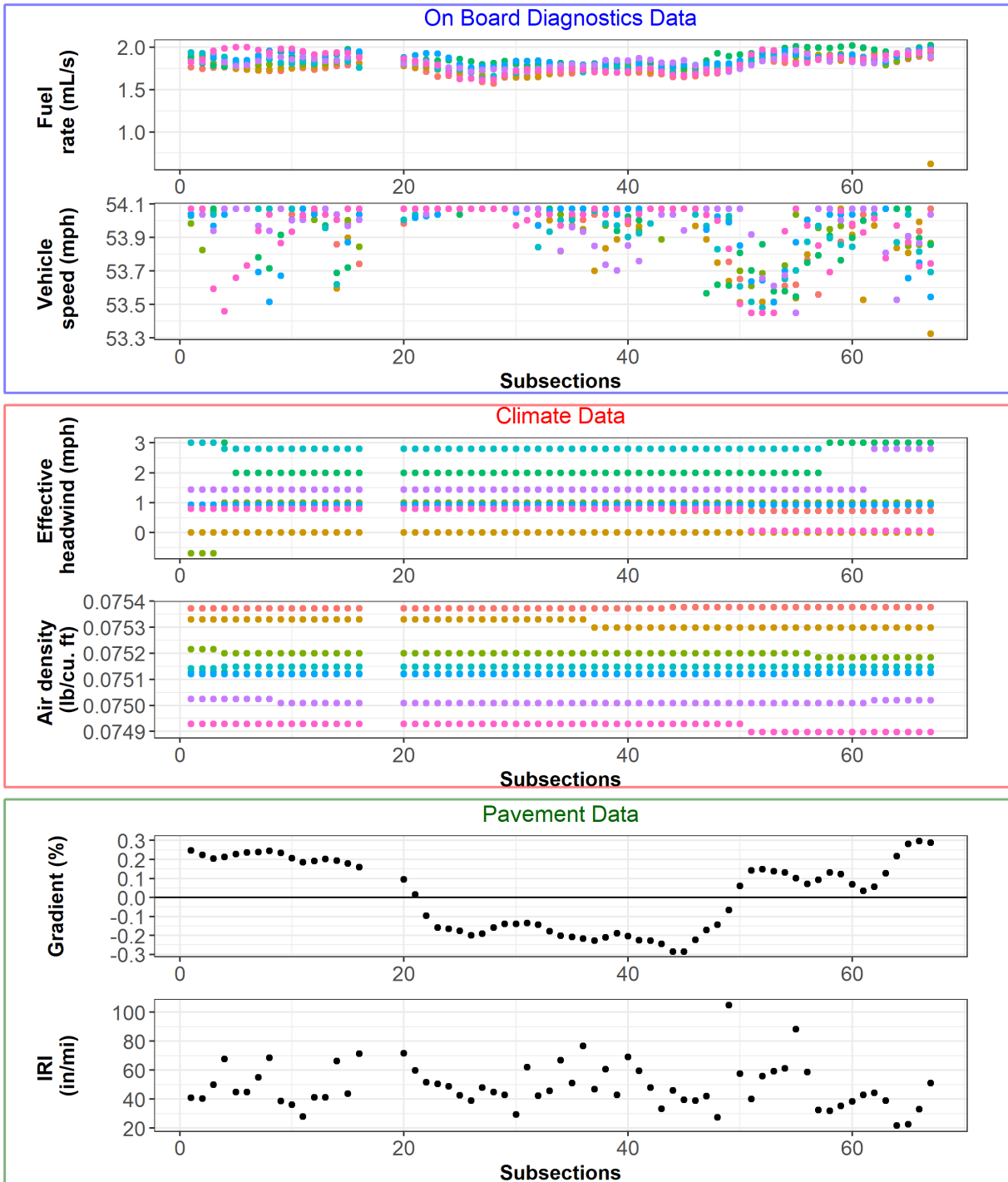
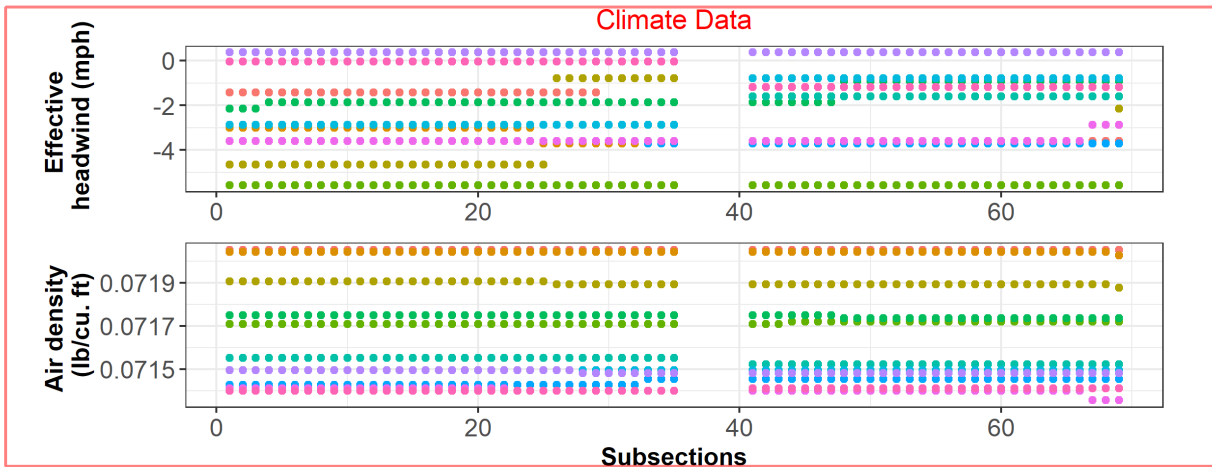
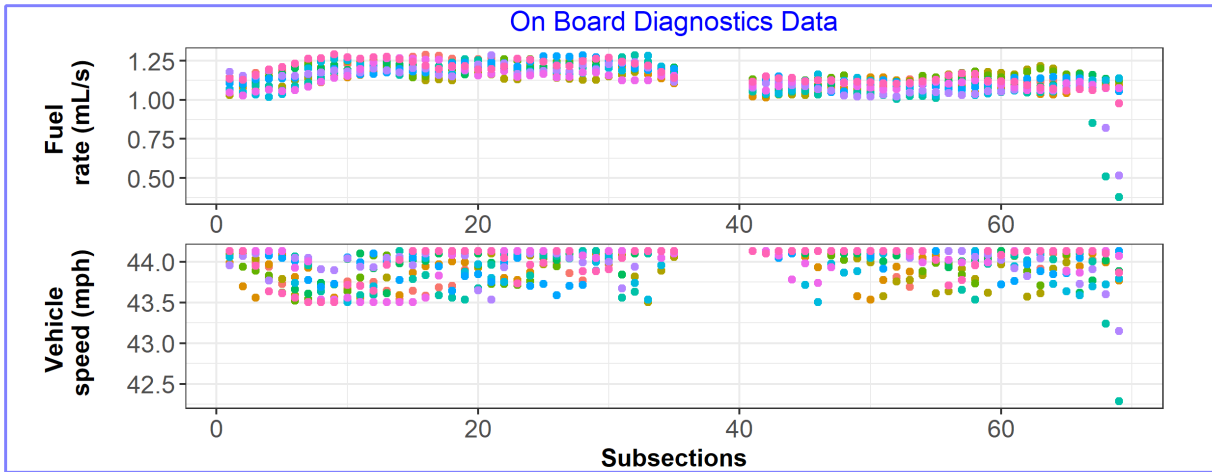


Figure P.99: SUV data on Section PH01.

PH02-YOL113S-JPC SUV summer_day 45 mph



- Runs
- 1
 - 2
 - 7
 - 8
 - 9
 - 10
 - 11
 - 12
 - 13
 - 14
 - 15

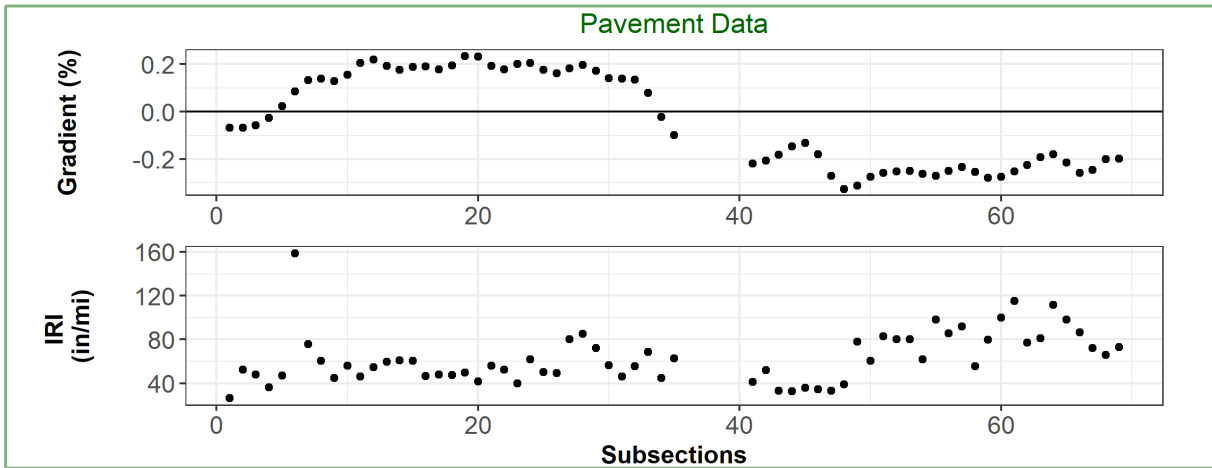


Figure P.100: SUV data on Section PH02.

PH02-YOL113S-JPC SUV summer_day 55 mph

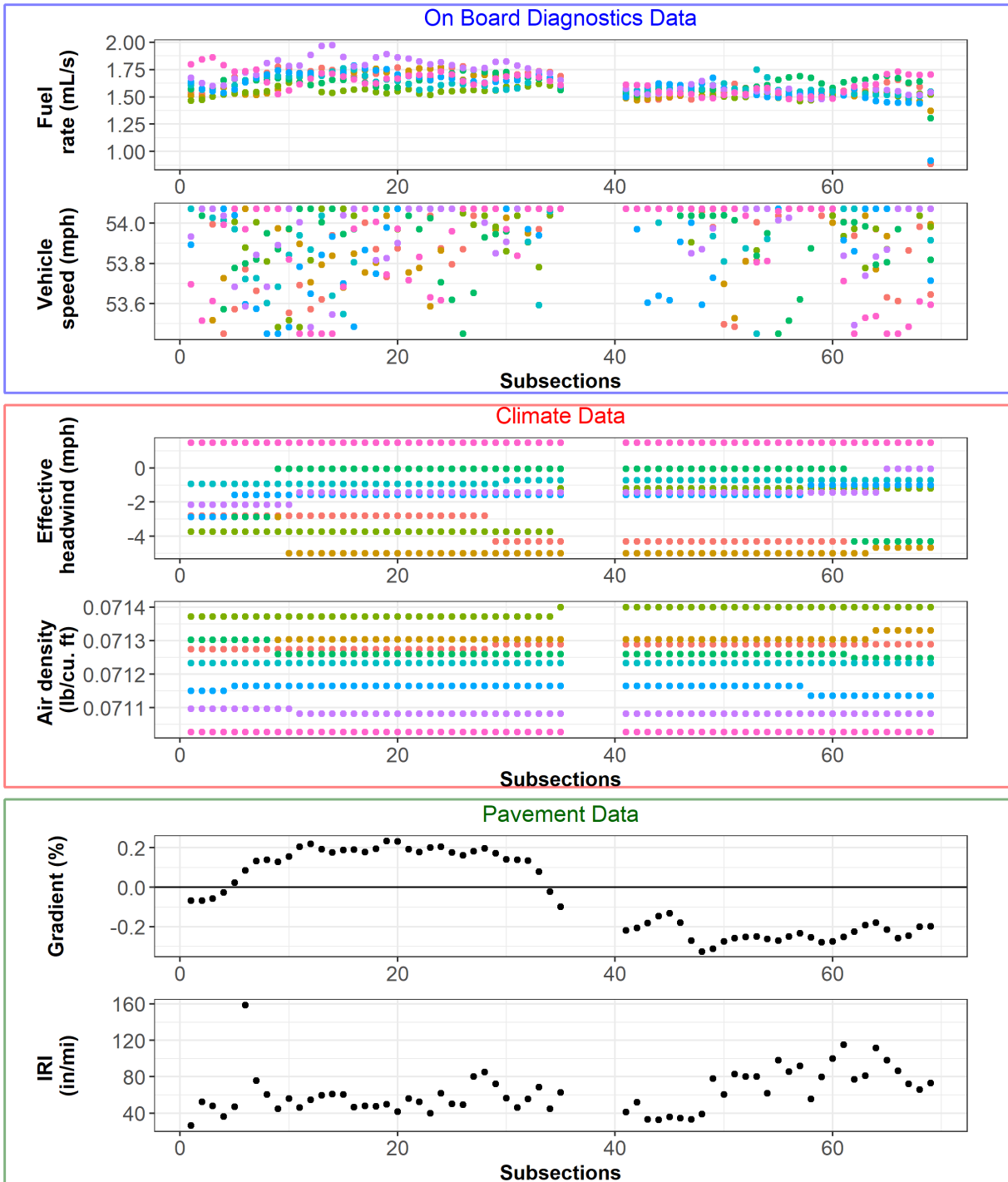


Figure P.101: SUV data on Section PH02.

PH02-YOL113S-JPC SUV summer_night 45 mph

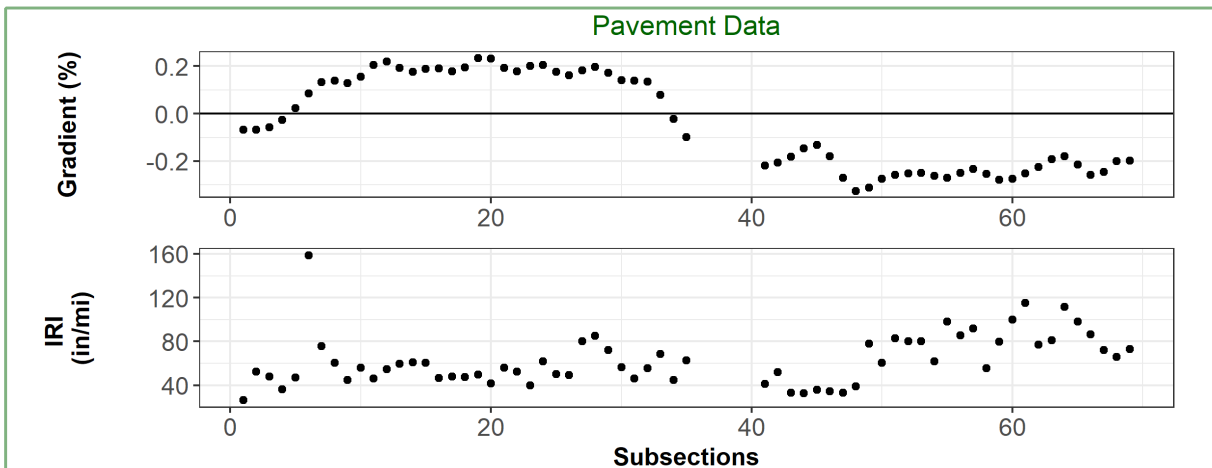
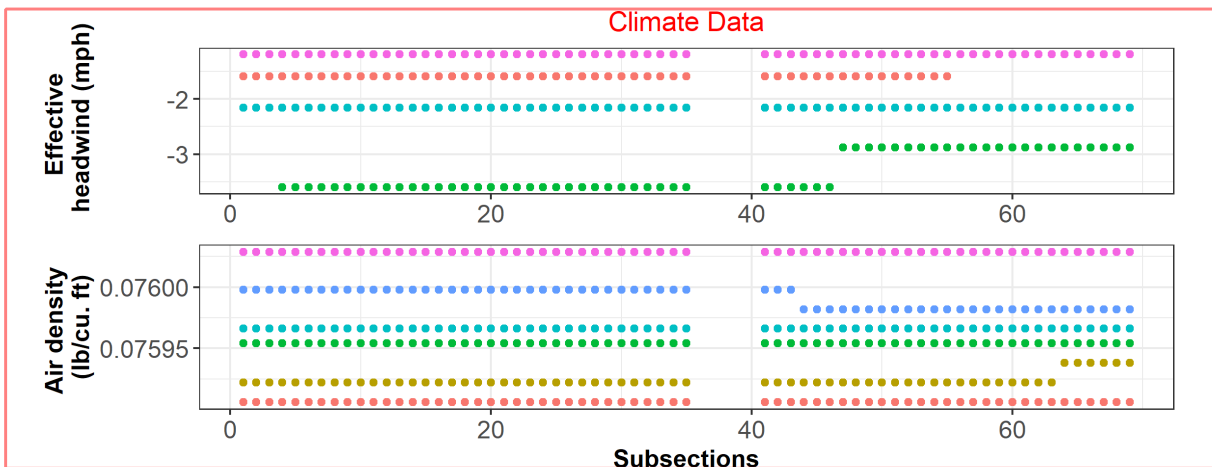
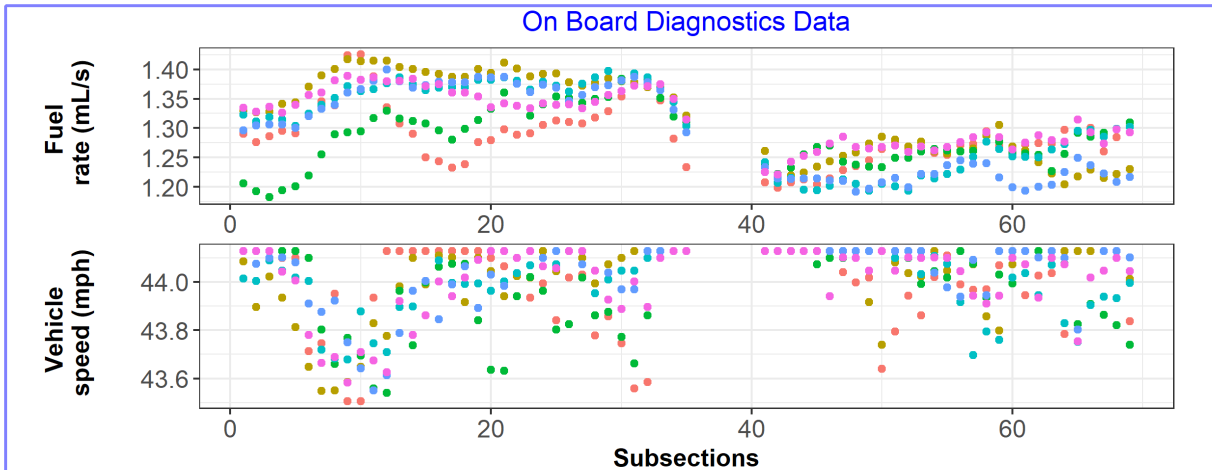


Figure P.102: SUV data on Section PH02.

PH02-YOL113S-JPC SUV summer_night 55 mph

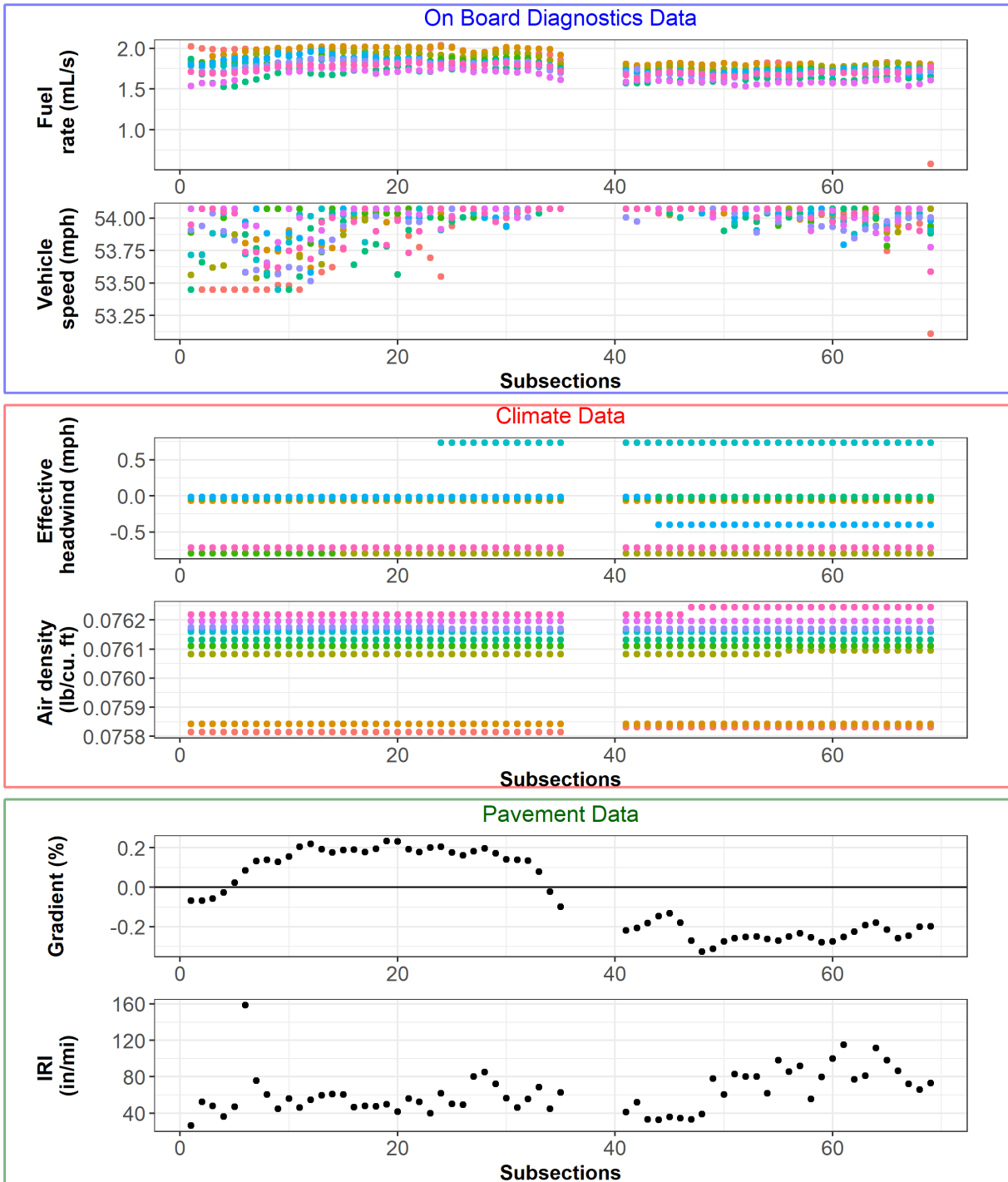


Figure P.103: SUV data on Section PH02.

PH02-YOL113S-JPC SUV winter_day 45 mph

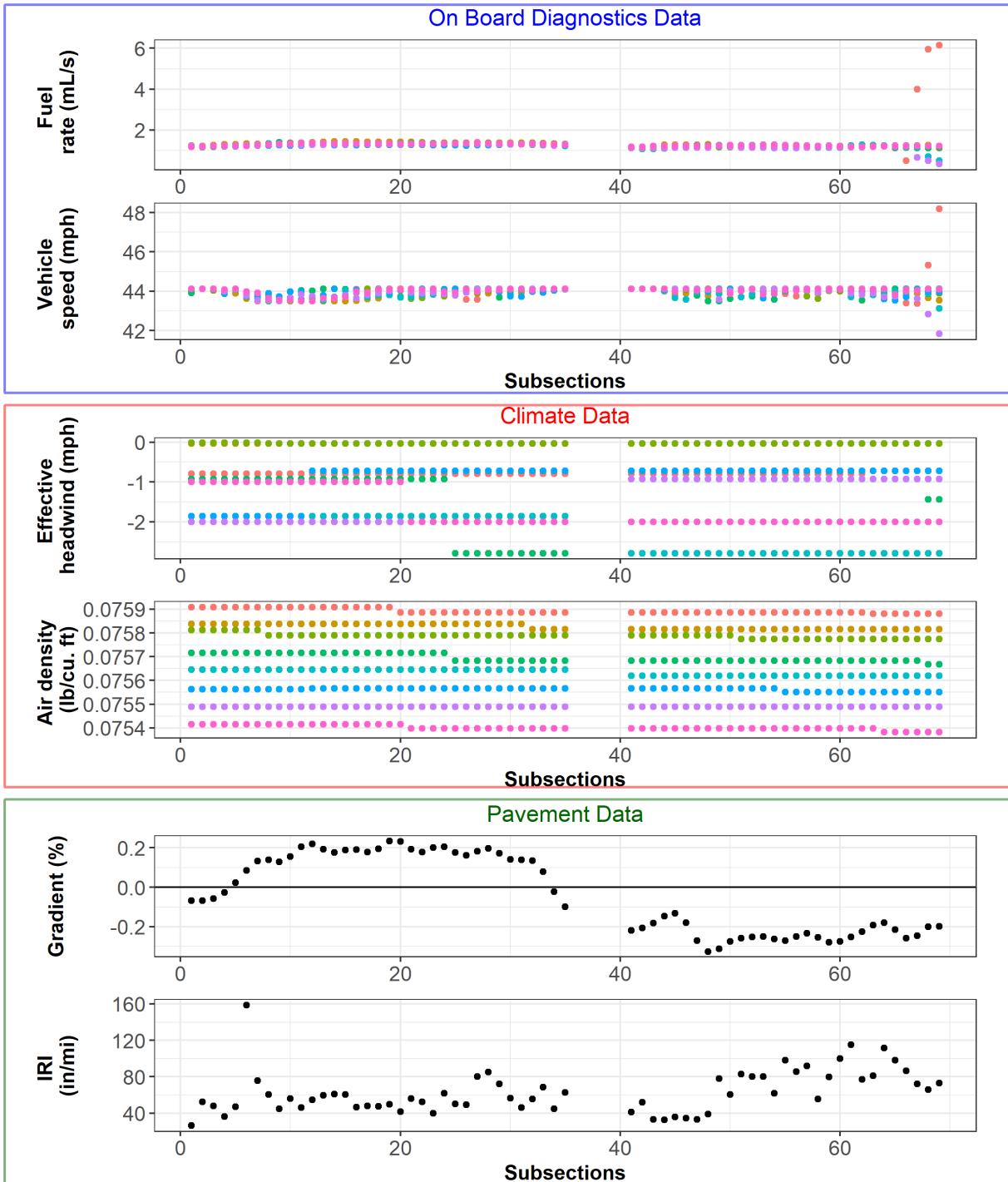


Figure P.104: SUV data on Section PH02.

PH02-YOL113S-JPC SUV winter_day 55 mph

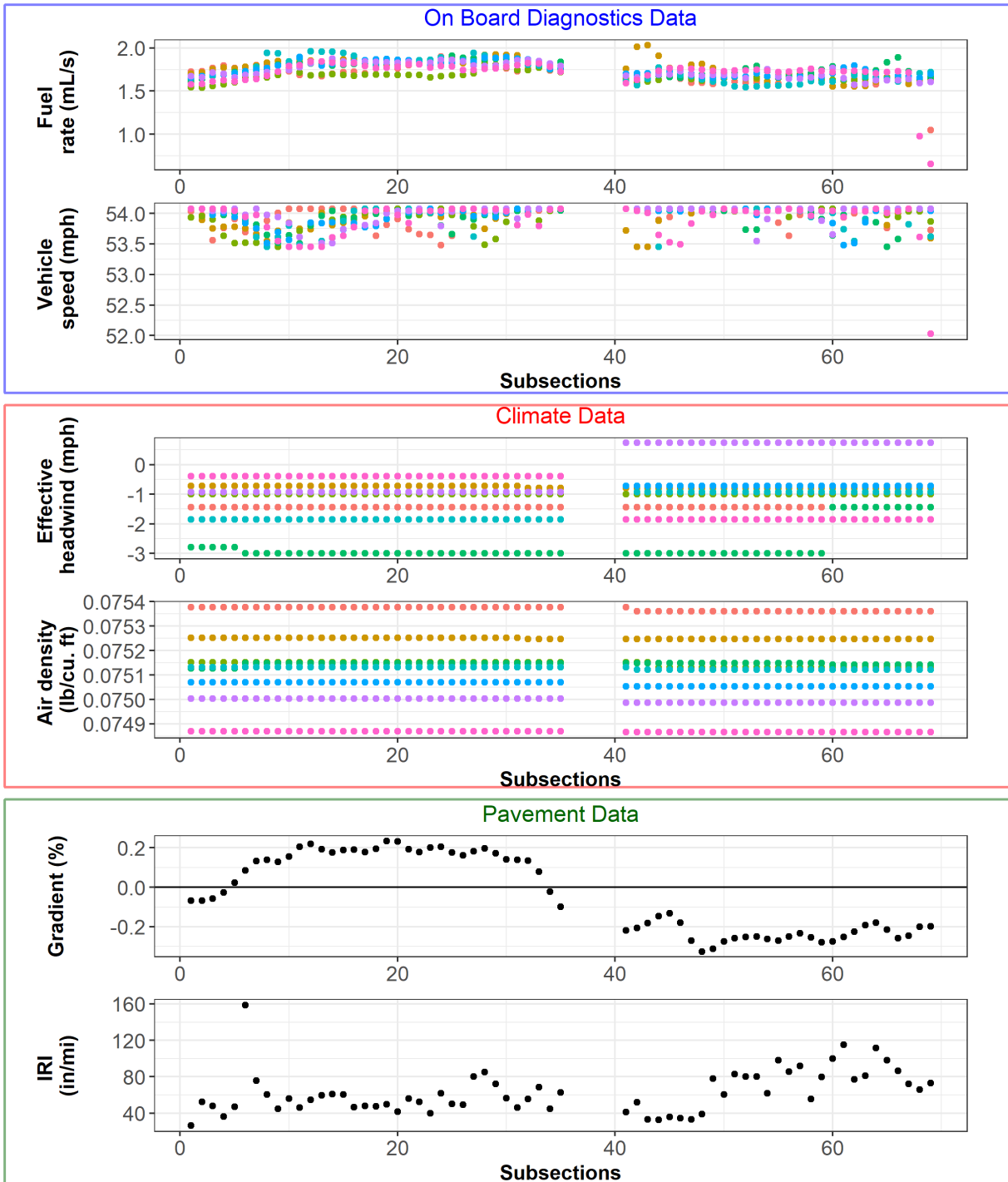


Figure P.105: SUV data on Section PH02.

PH03-YOL505N-JPC SUV summer_day 45 mph

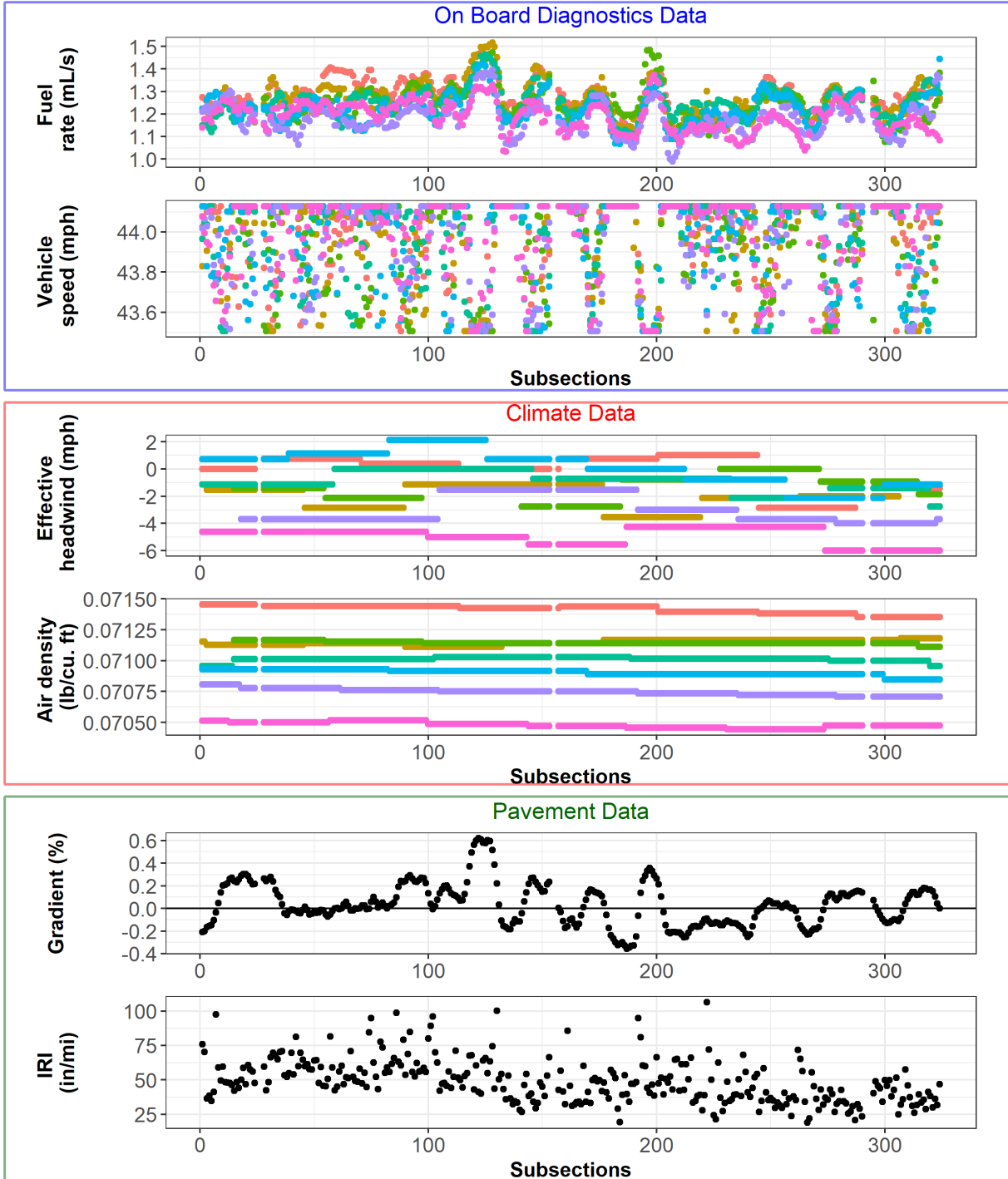


Figure P.106: SUV data on Section PH03.

PH03-YOL505N-JPC SUV summer_day 55 mph

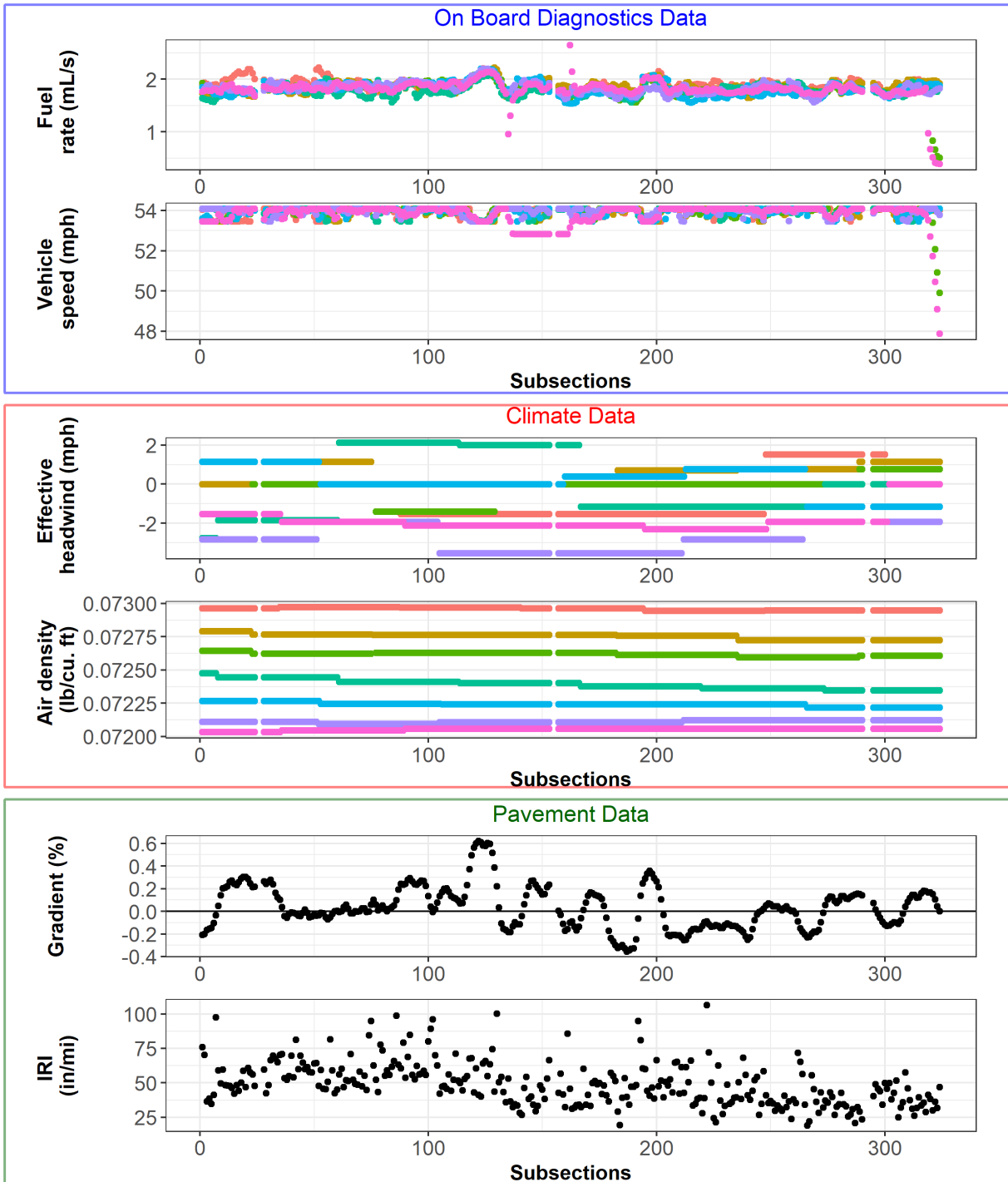


Figure P.107: SUV data on Section PH03.

PH03-YOL505N-JPC SUV summer_night 45 mph

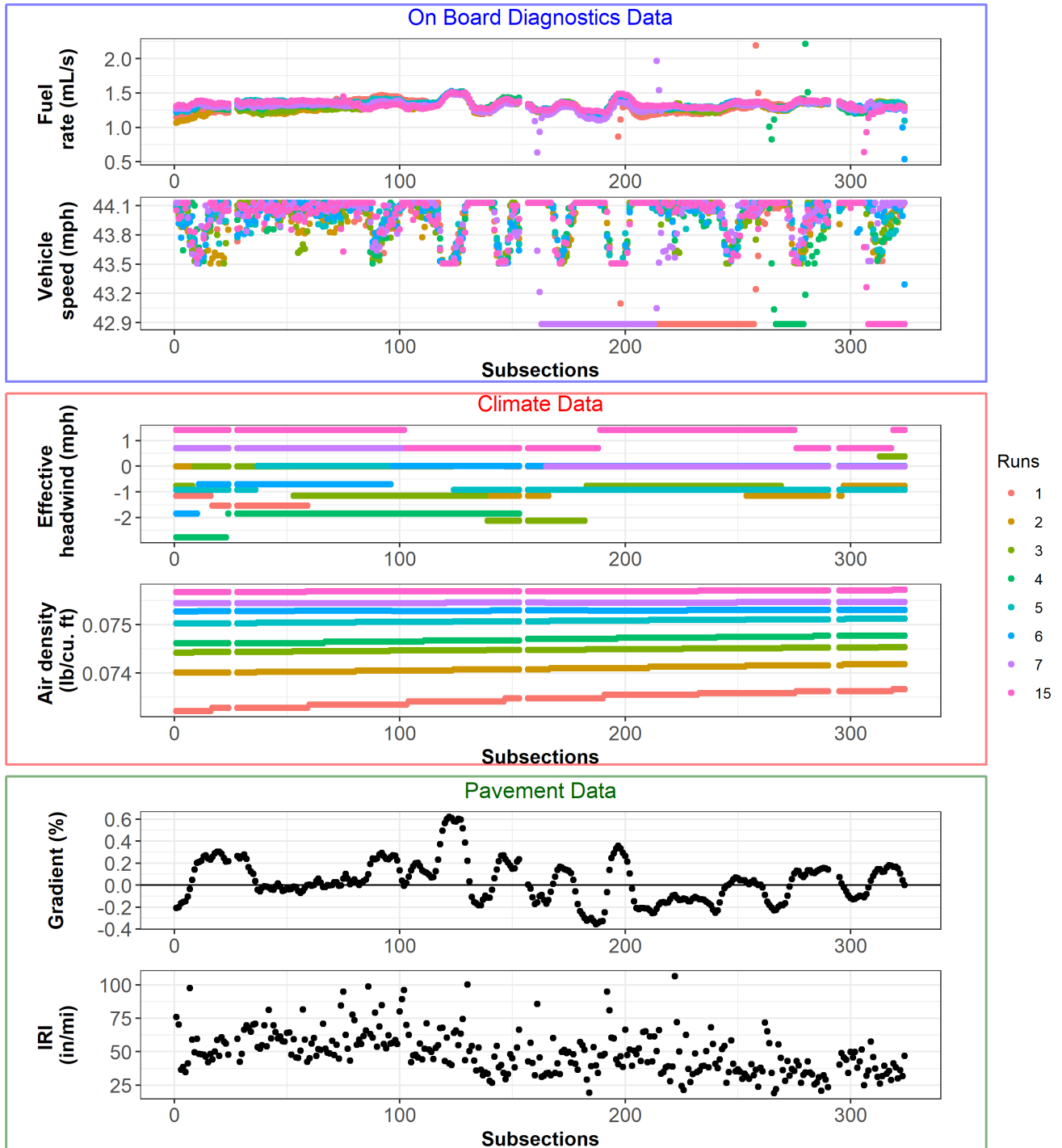


Figure P.108: SUV data on Section PH03.

PH03-YOL505N-JPC SUV summer_night 55 mph

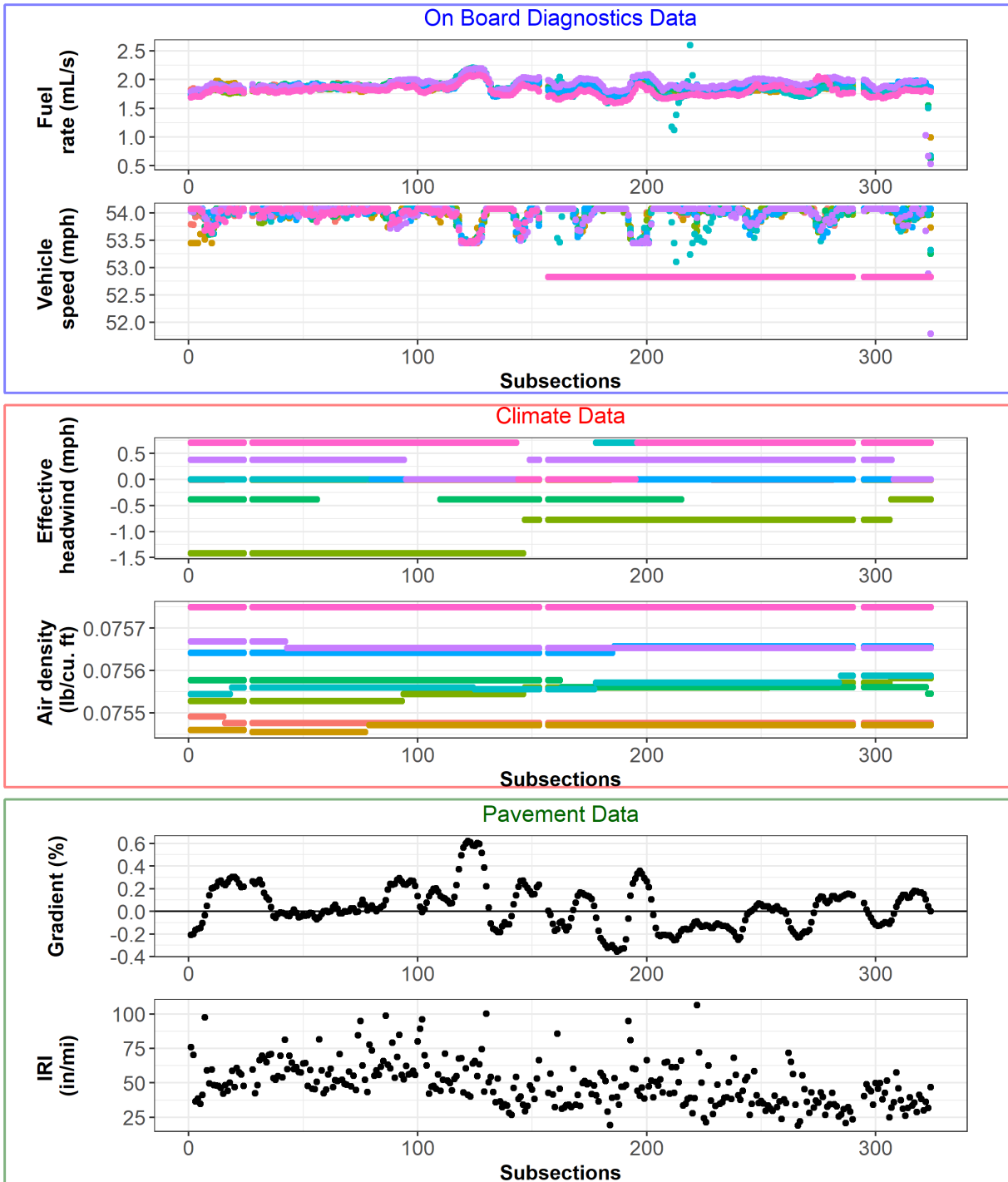


Figure P.109: SUV data on Section PH03.

PH03-YOL505N-JPC SUV winter_day 45 mph

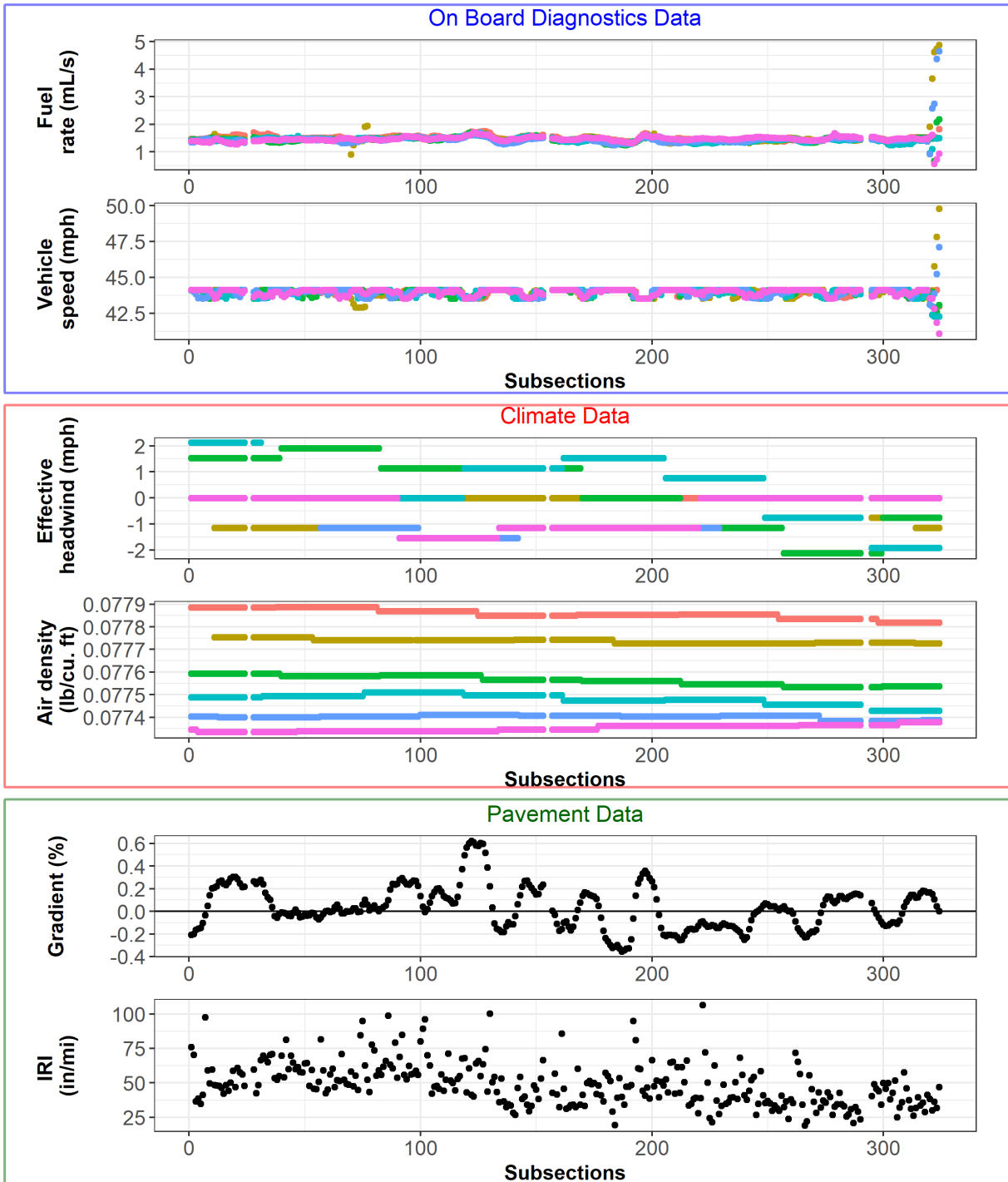


Figure P.110: SUV data on Section PH03.

PH03-YOL505N-JPC SUV winter_day 55 mph

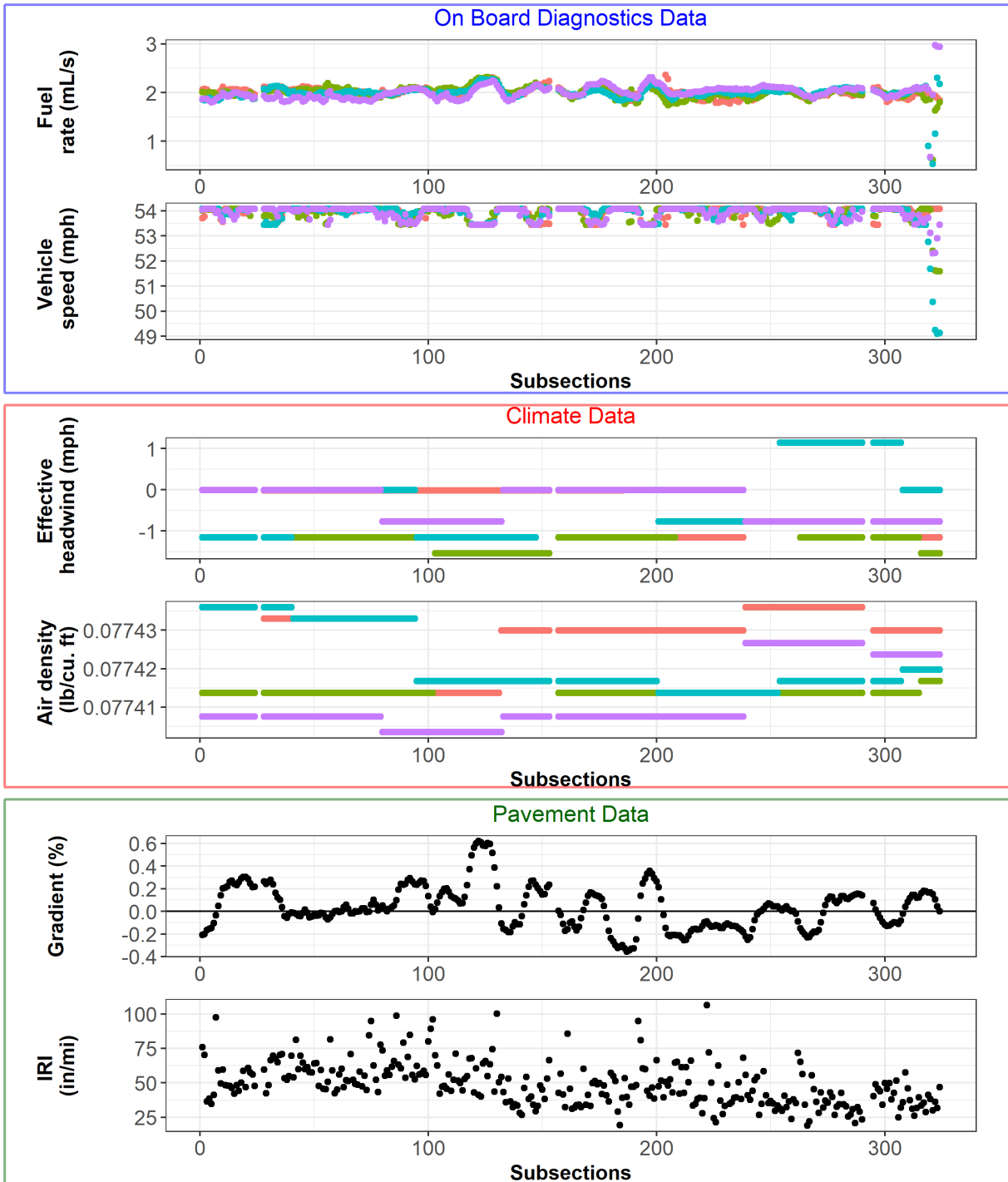


Figure P.111: SUV data on Section PH03.

PH04-YOL505S-RHMA-G SUV summer_day 45 mph

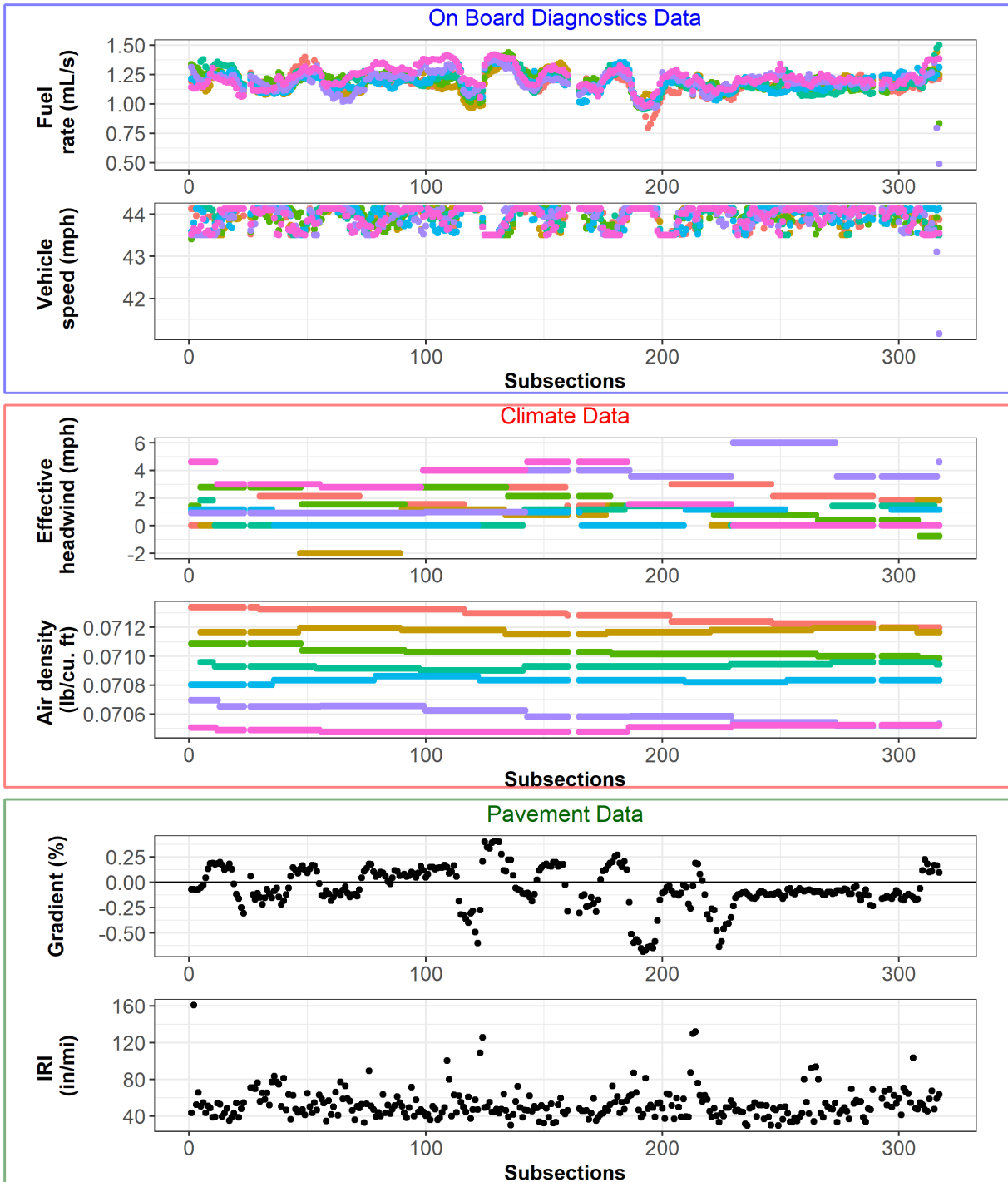


Figure P.112: SUV data on Section PH04.

PH04-YOL505S-RHMA-G SUV summer_day 55 mph

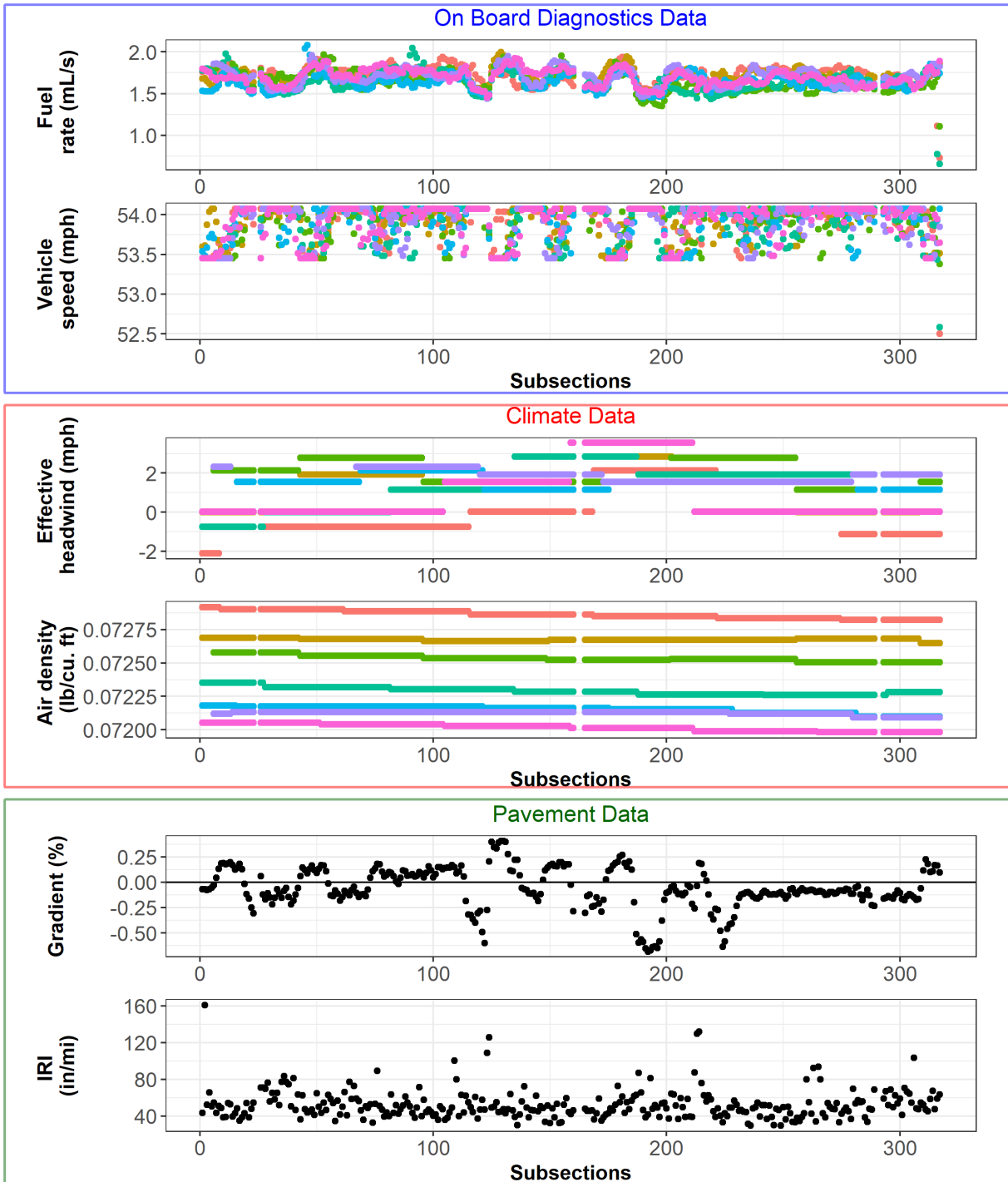


Figure P.113: SUV data on Section PH04.

PH04-YOL505S-RHMA-G SUV summer_night 45 mph

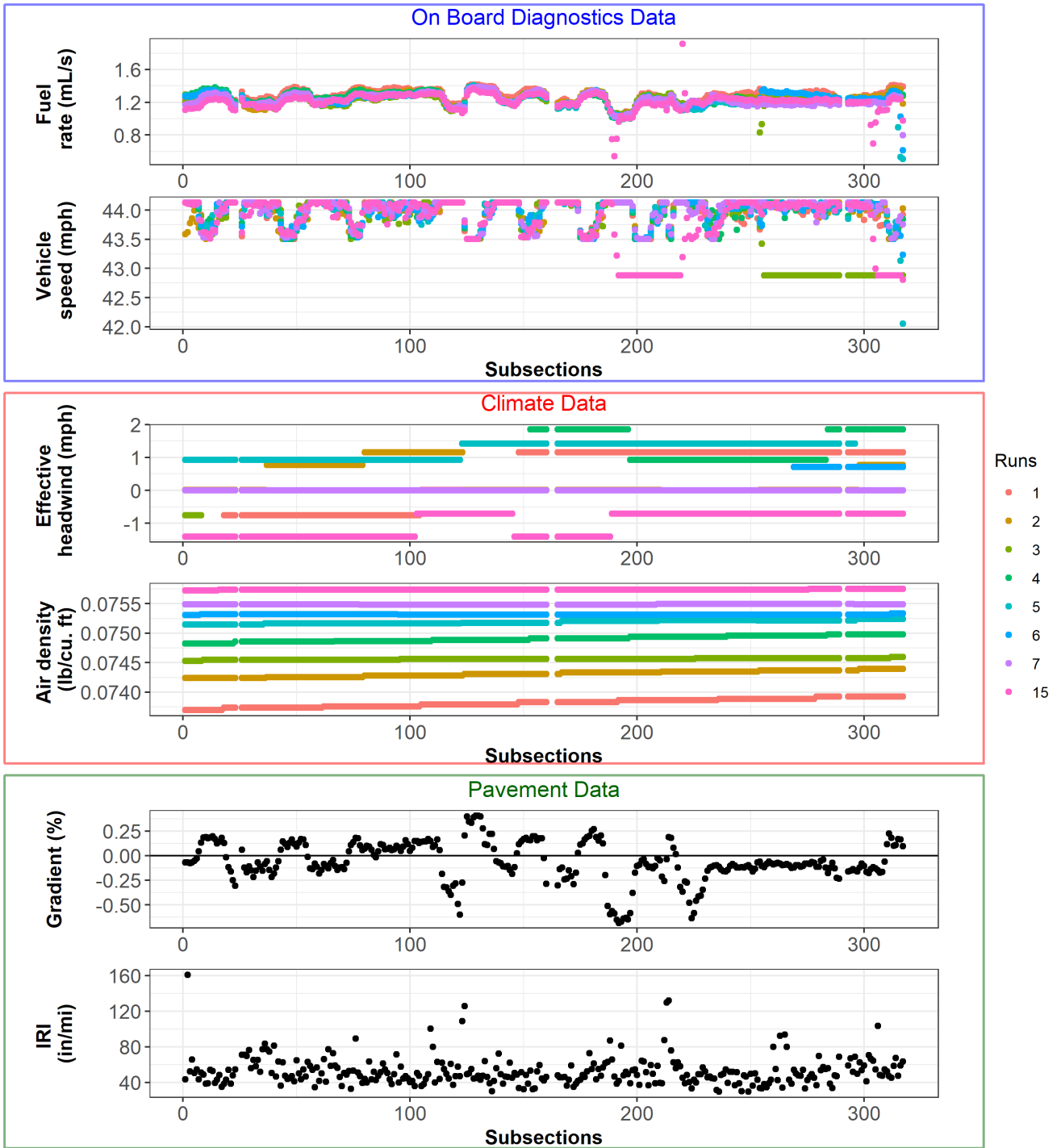


Figure P.114: SUV data on Section PH04.

PH04-YOL505S-RHMA-G SUV summer_night 55 mph

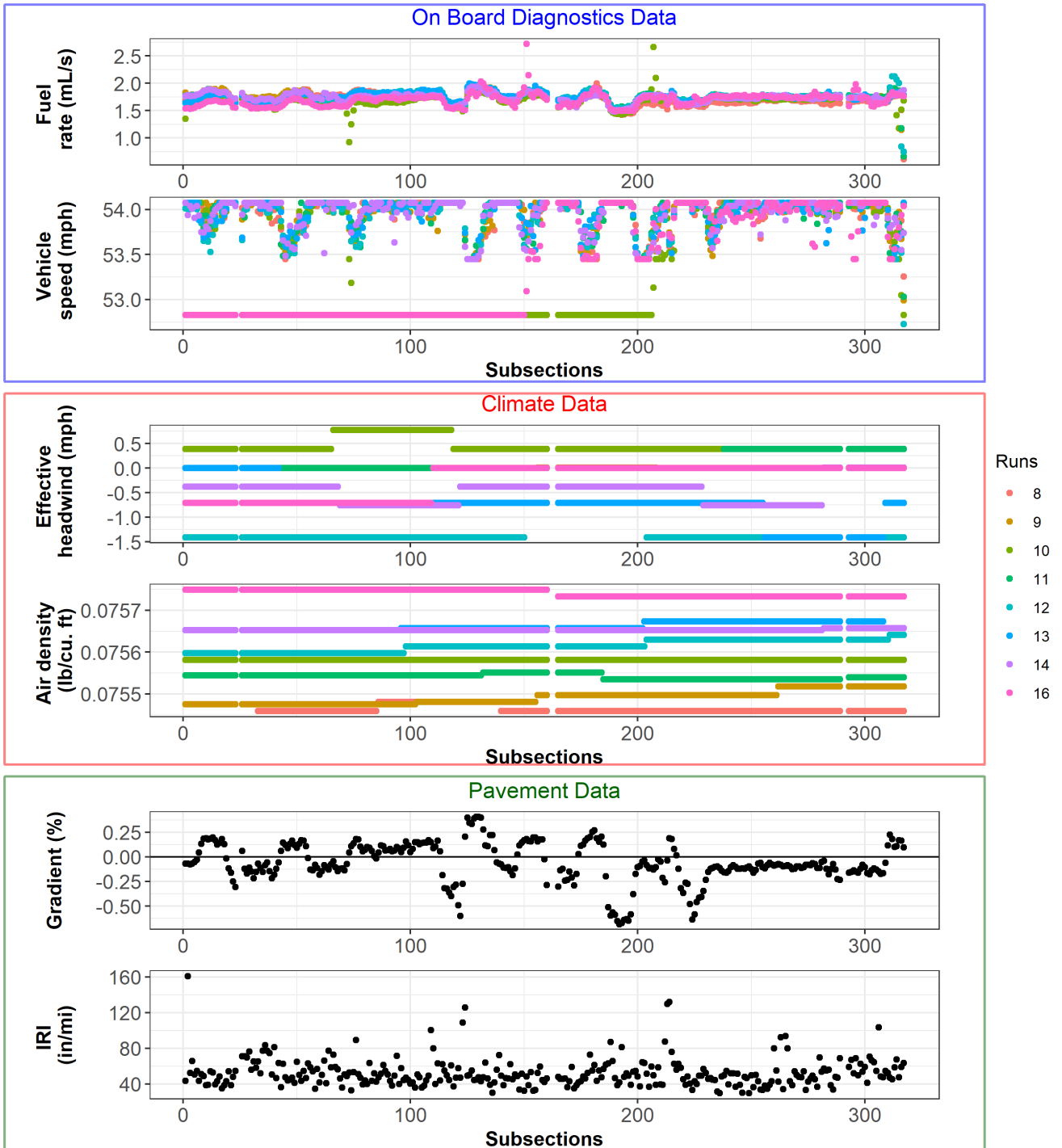


Figure P.115: SUV data on Section PH04.

PH04-YOL505S-RHMA-G SUV winter_day 45 mph

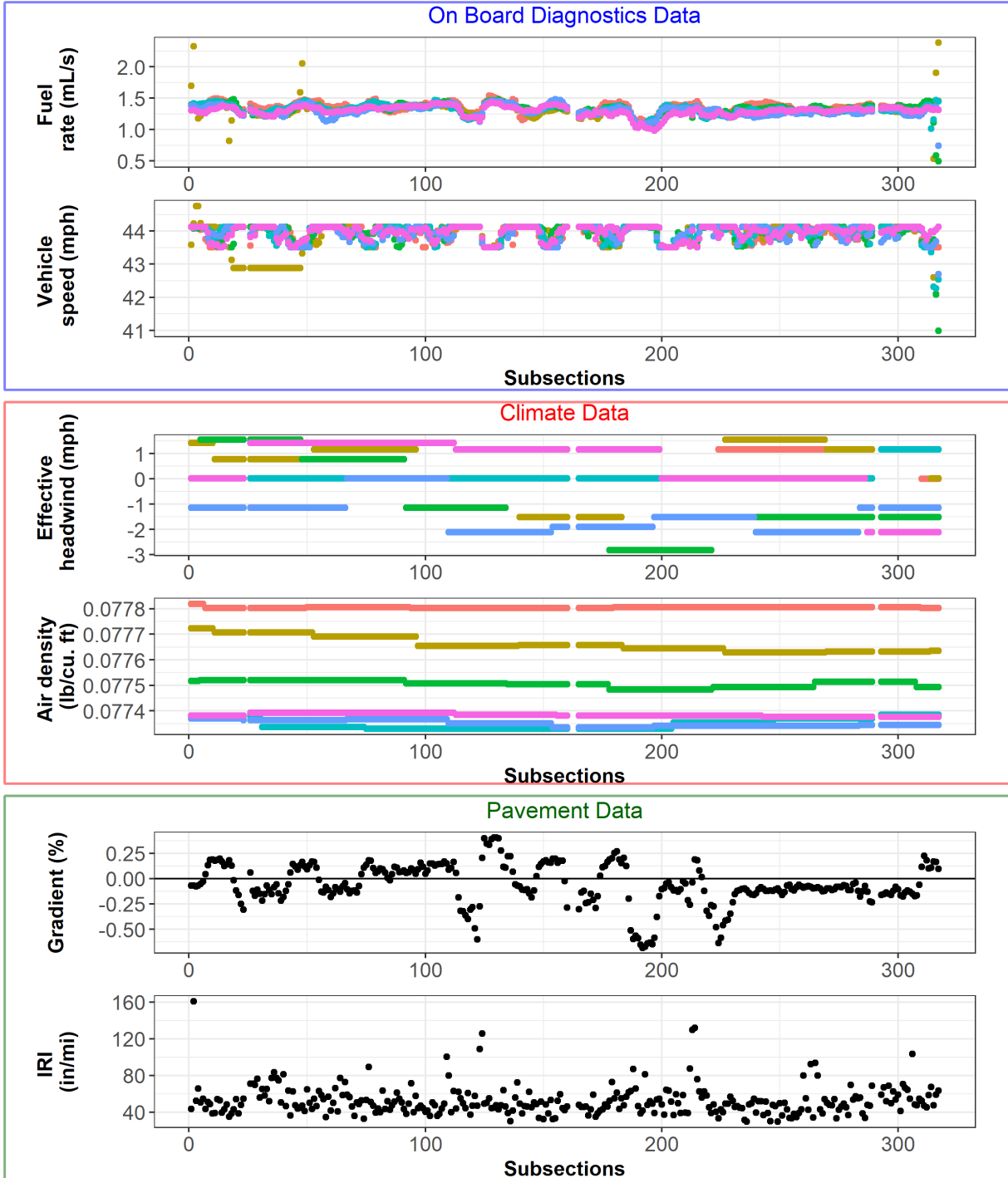


Figure P.116: SUV data on Section PH04.

PH04-YOL505S-RHMA-G SUV winter_day 55 mph

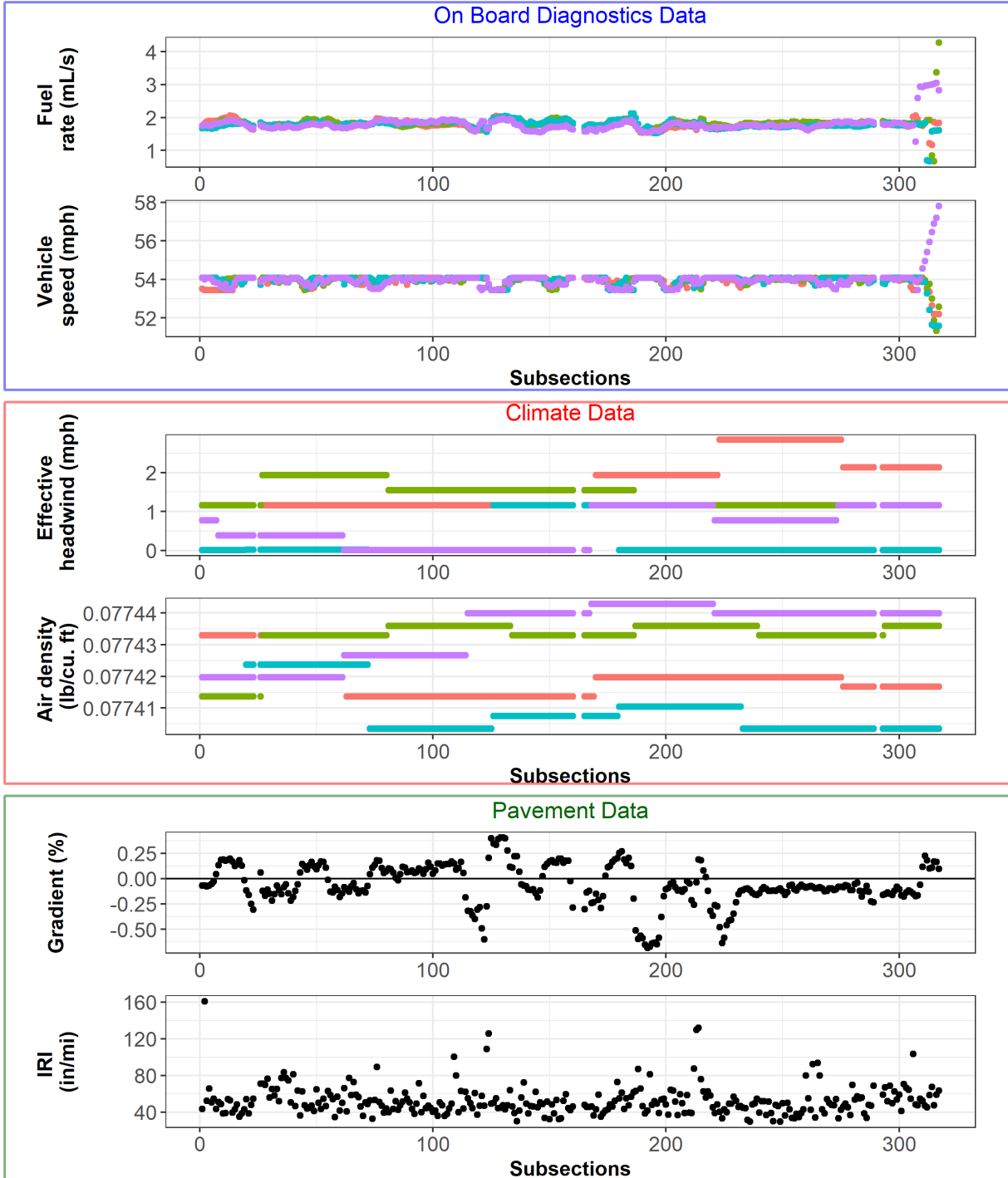


Figure P.117: SUV data on Section PH04.

PH07-YOL-CR98N-HMA SUV summer_day 35 mph

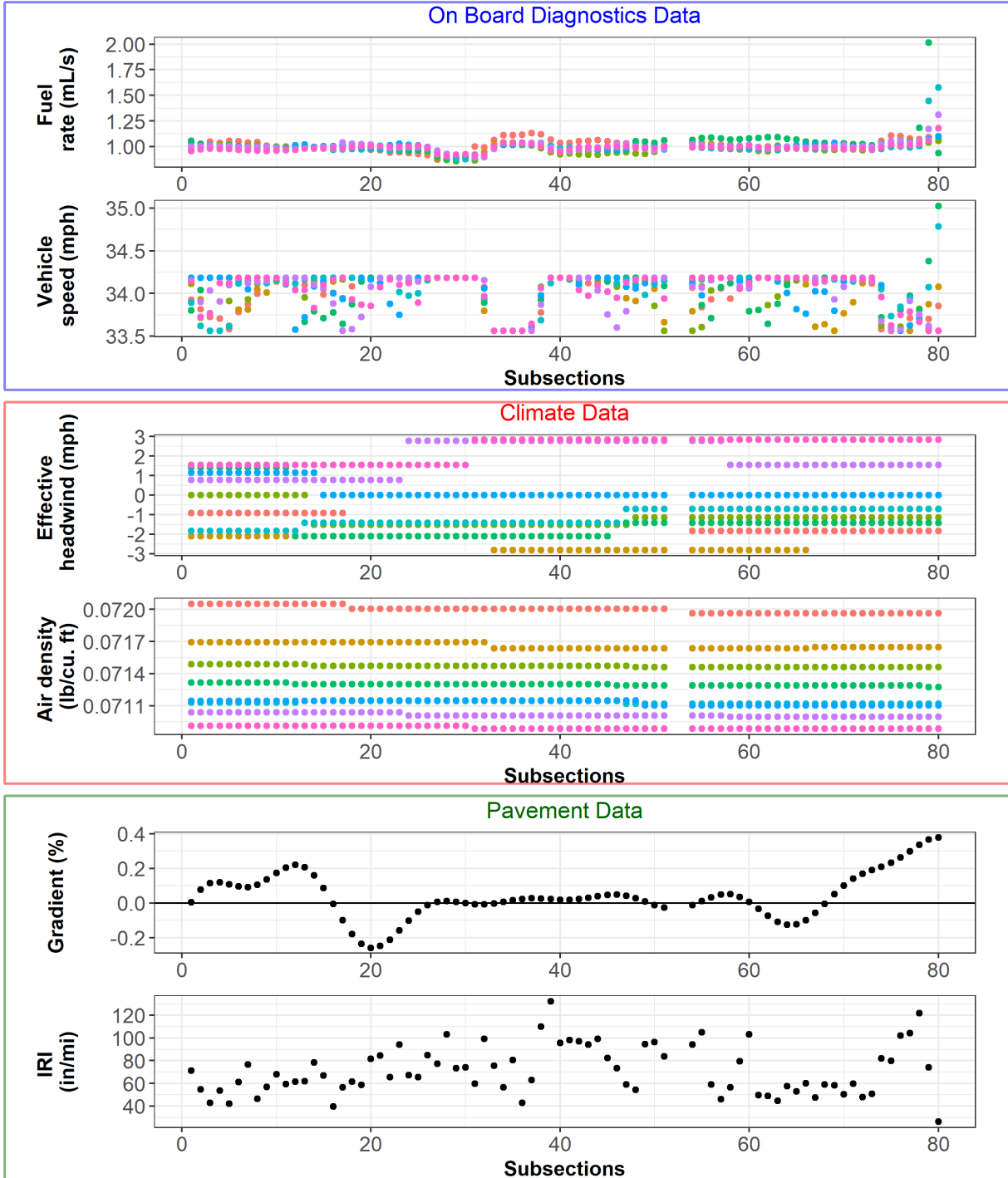


Figure P.118: SUV data on Section PH07.

PH07-YOL-CR98N-HMA SUV summer_day 45 mph

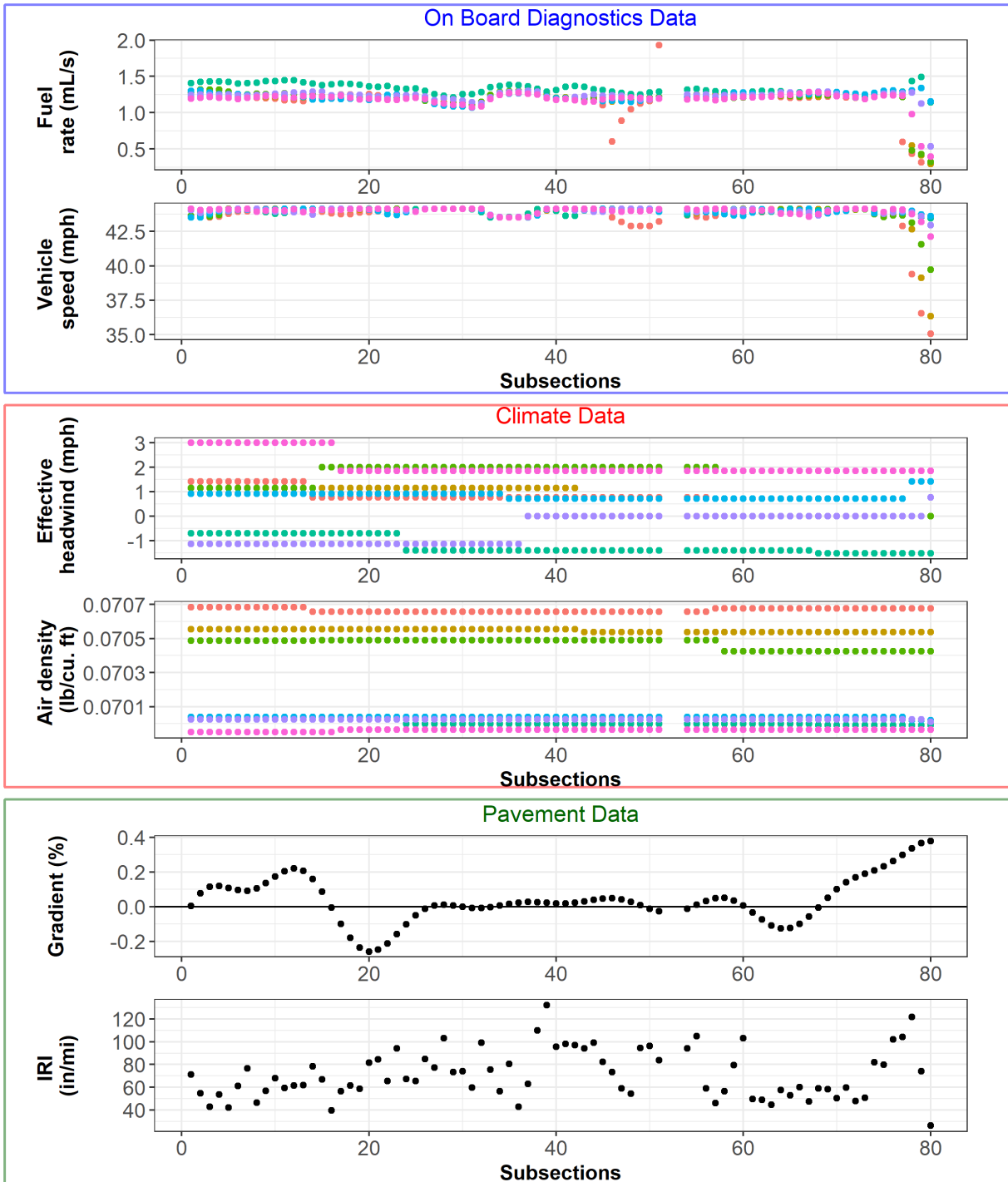


Figure P.119: SUV data on Section PH07.

PH07-YOL-CR98N-HMA SUV summer_night 35 mph

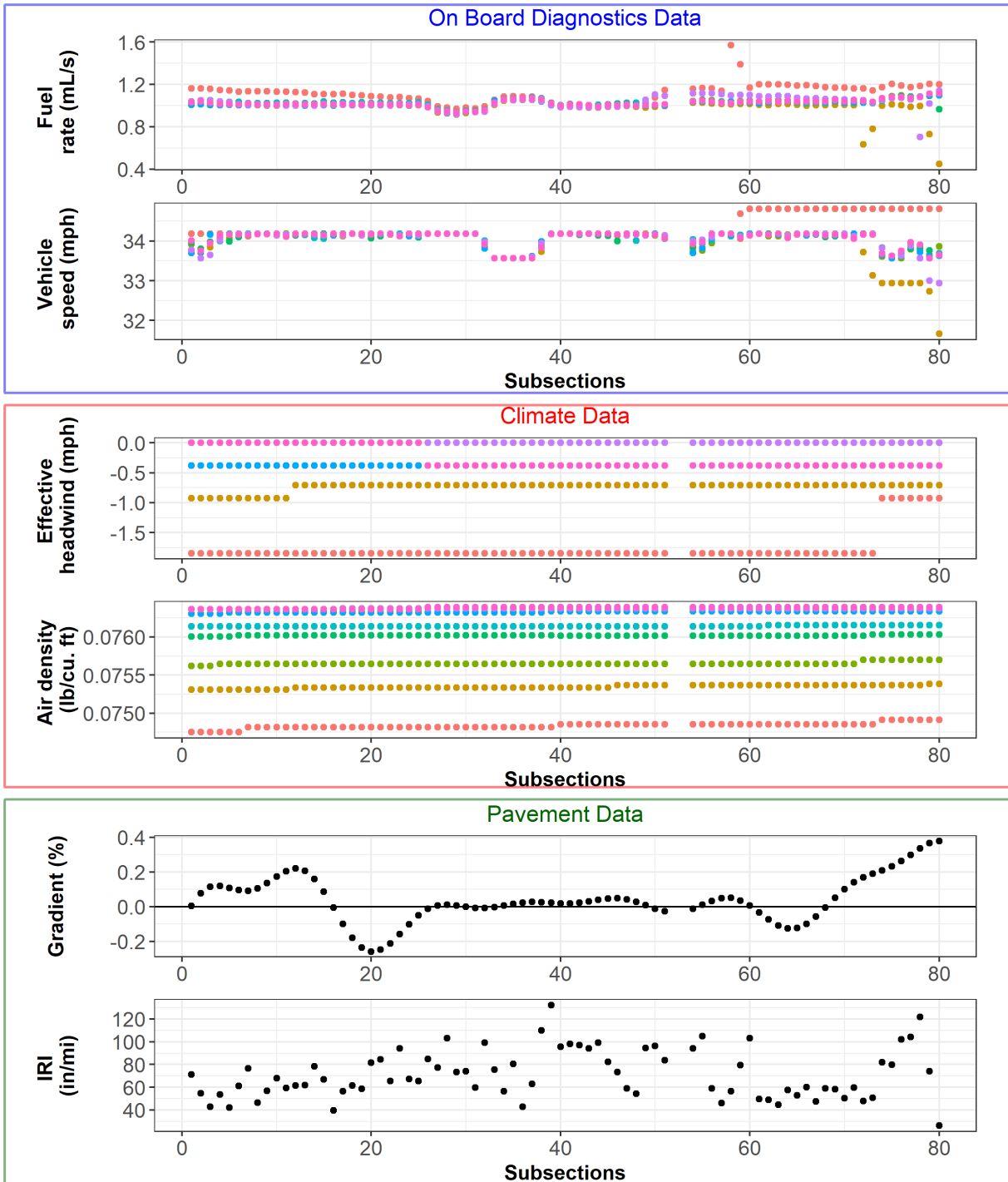


Figure P.120: SUV data on Section PH07.

PH07-YOL-CR98N-HMA SUV summer_night 45 mph

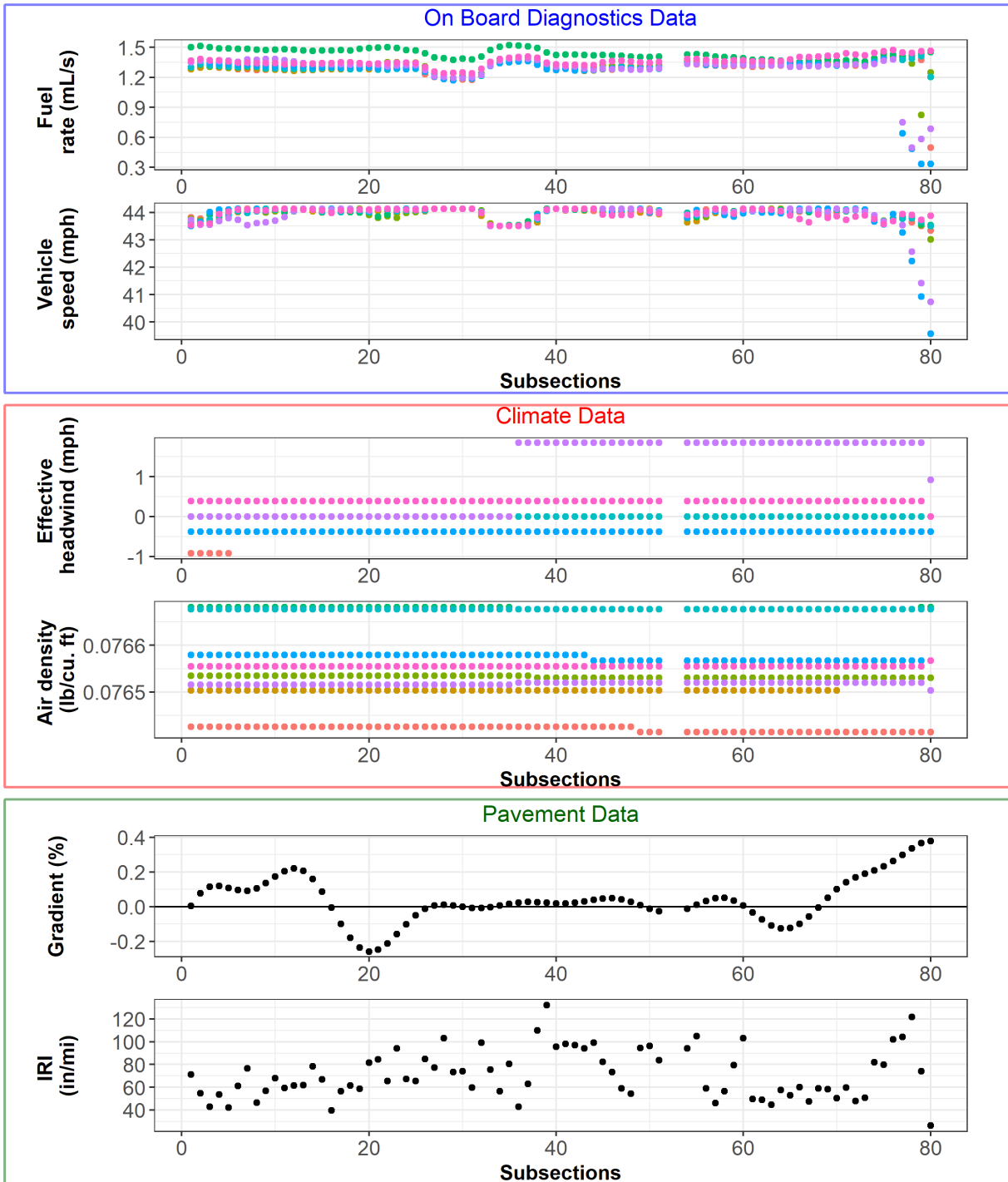


Figure P.121: SUV data on Section PH07.

PH07-YOL-CR98N-HMA SUV winter_day 35 mph

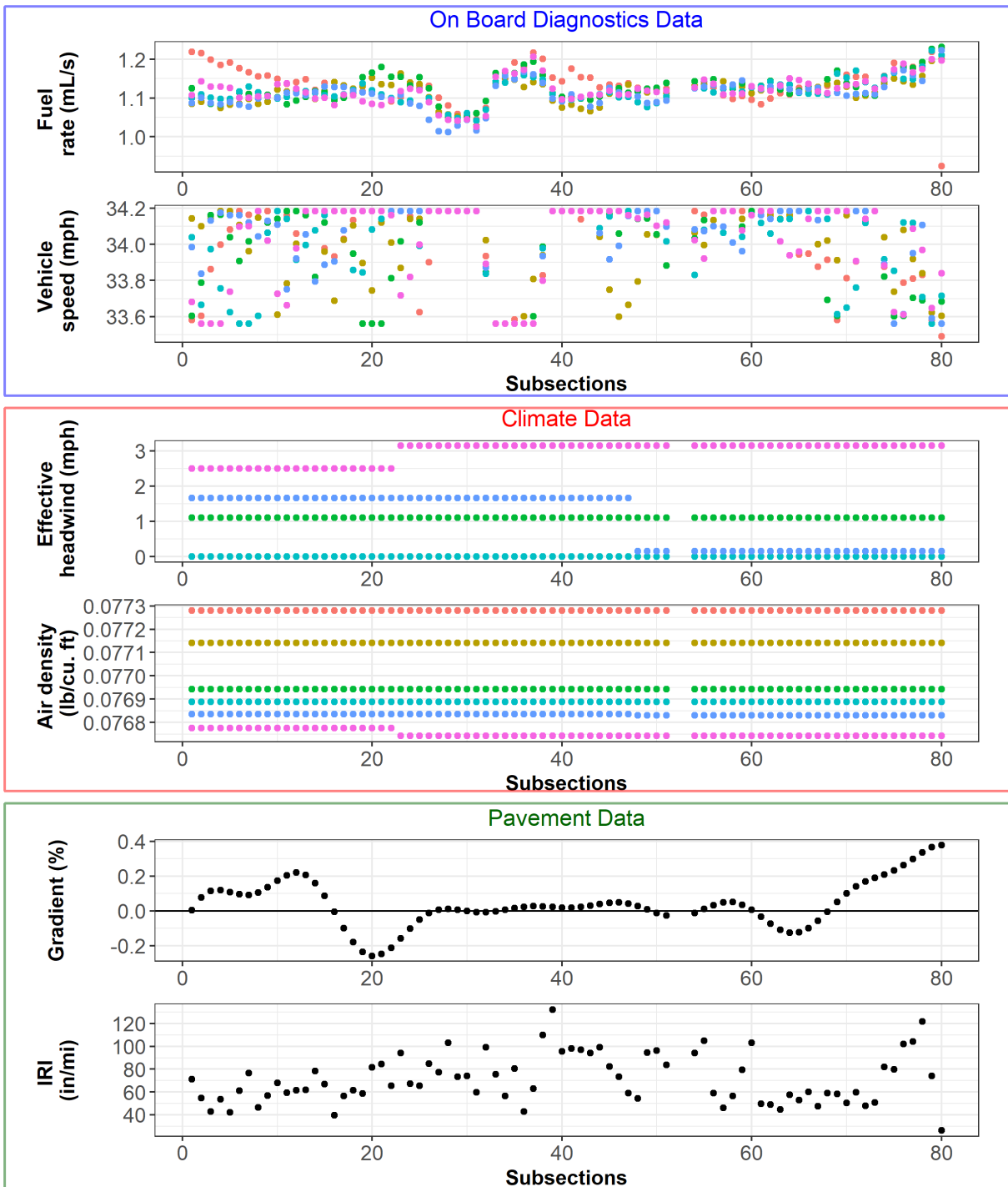


Figure P.122: SUV data on Section PH07.

PH07-YOL-CR98N-HMA SUV winter_day 45 mph

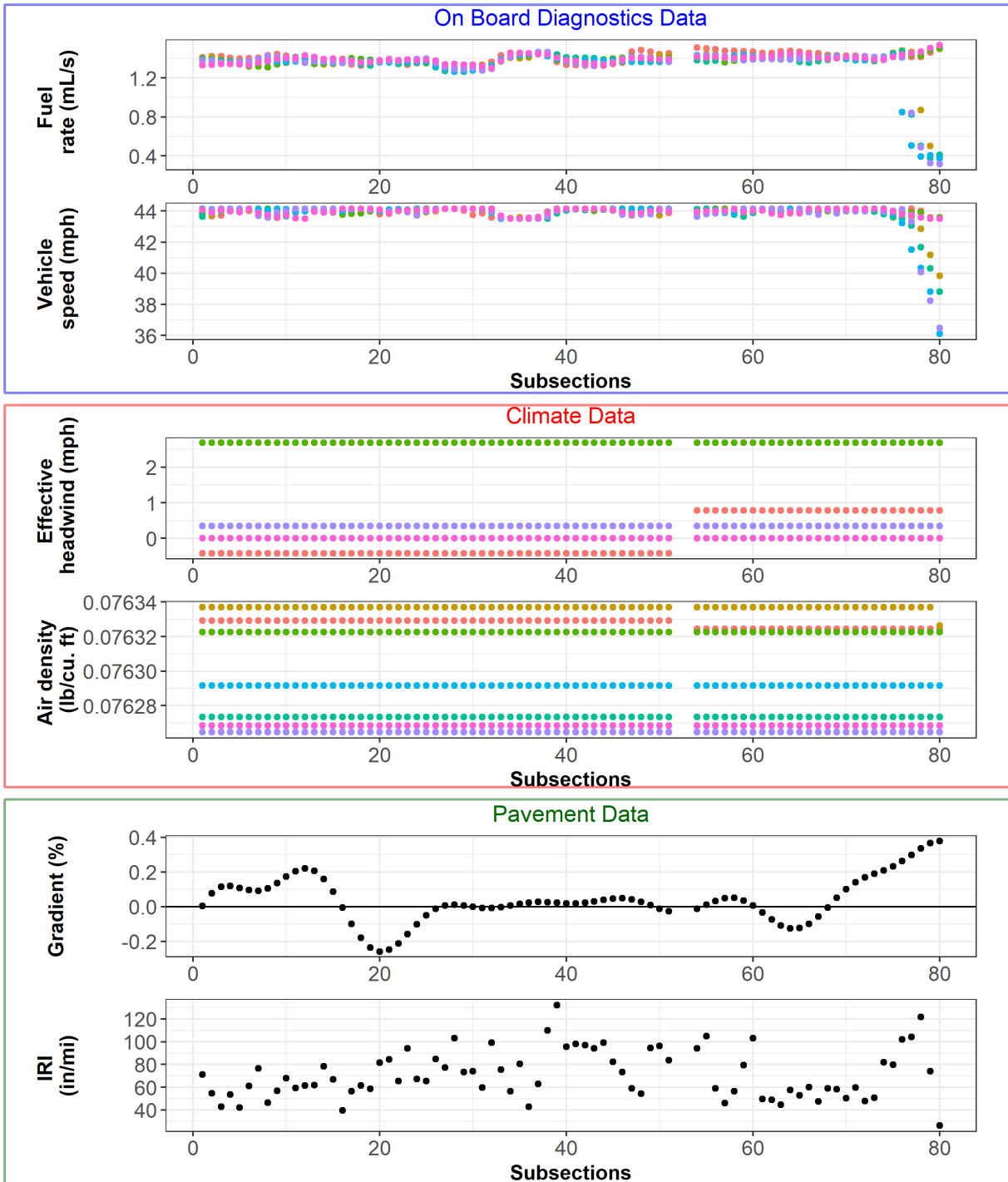


Figure P.123: SUV data on Section PH07.

PH08-YOL-CR29E-HMA SUV summer_day 35 mph

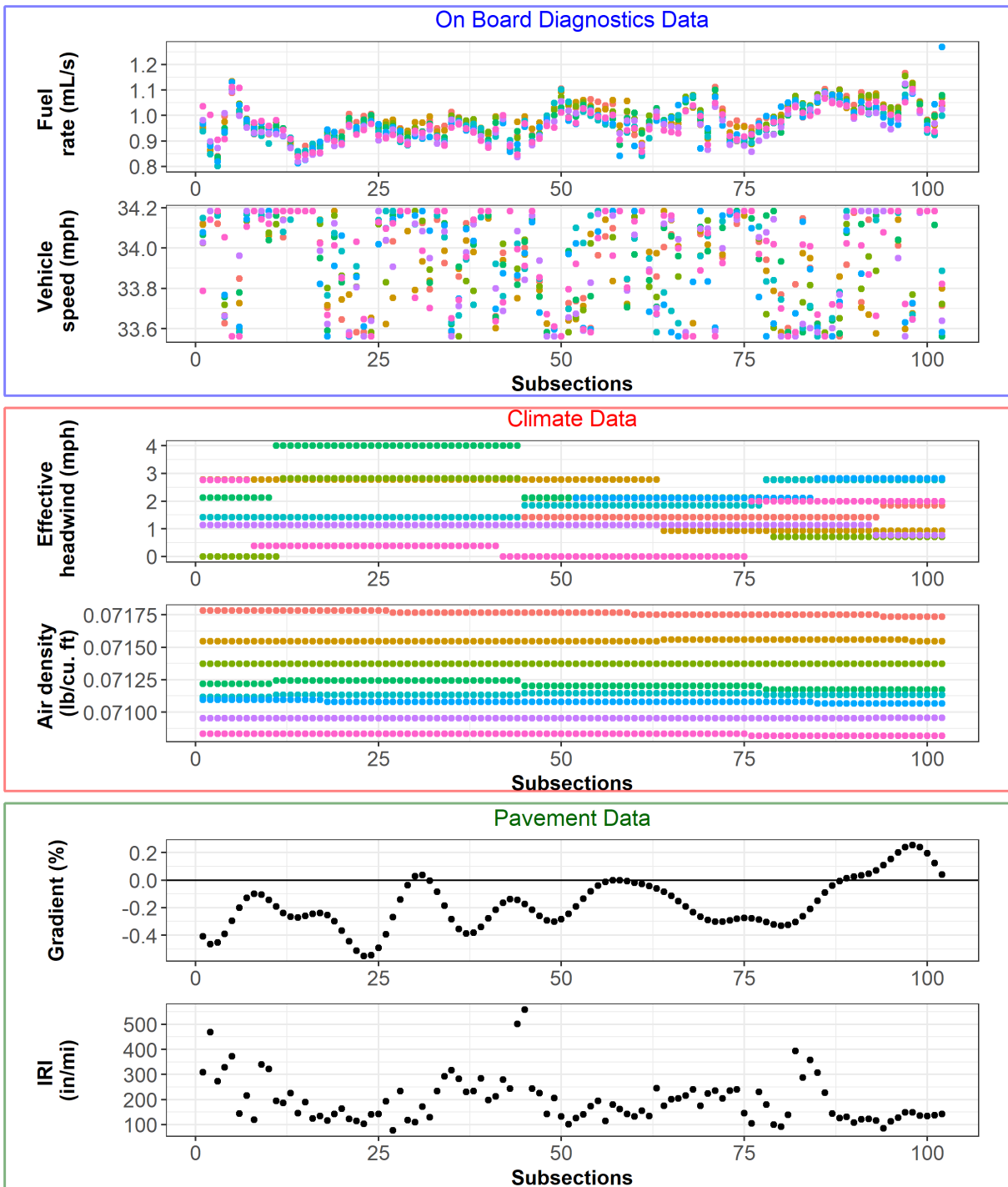


Figure P.124: SUV data on Section PH08.

PH08-YOL-CR29E-HMA SUV summer_day 45 mph

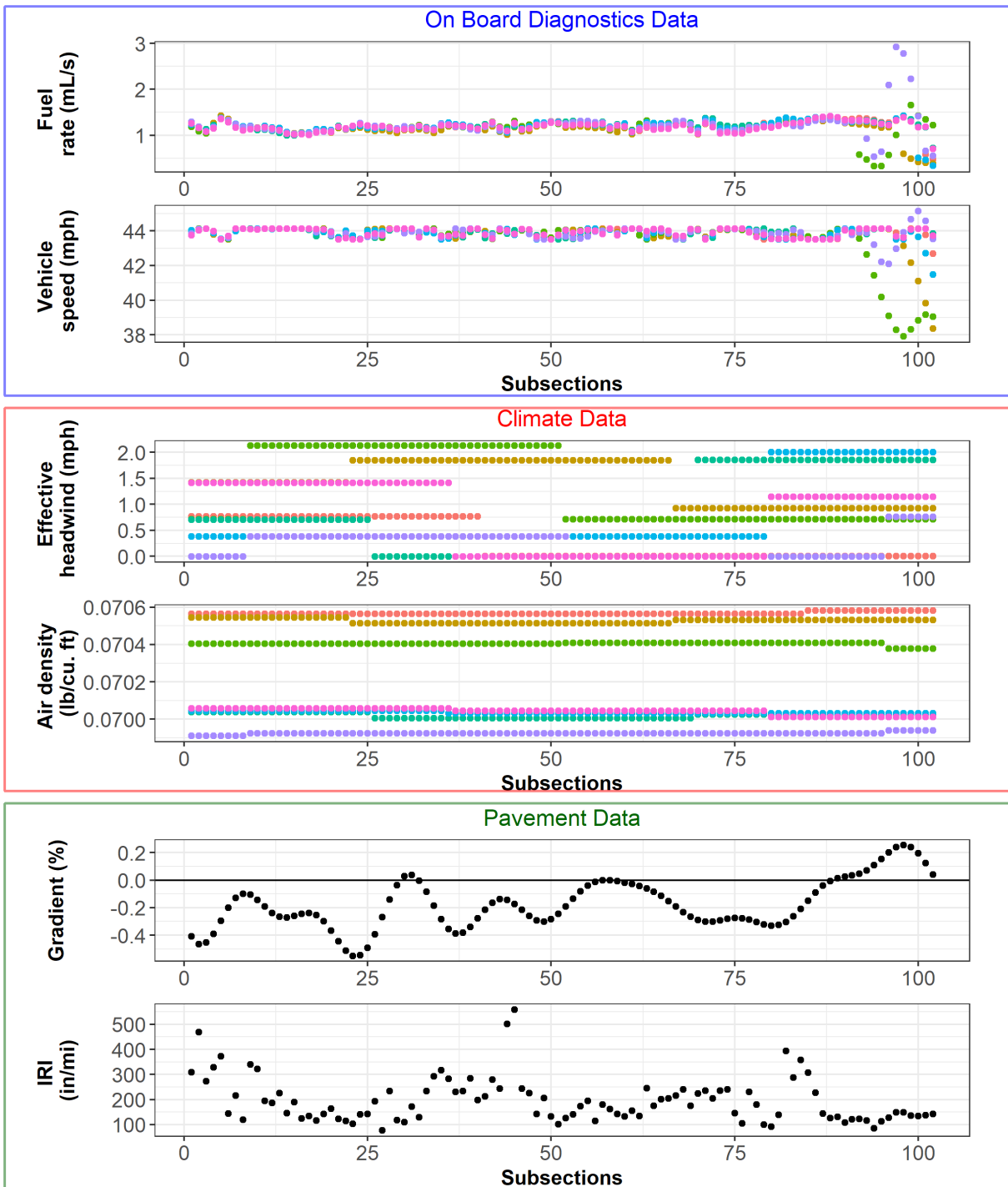


Figure P.125: SUV data on Section PH08.

PH08-YOL-CR29E-HMA SUV summer_night 35 mph

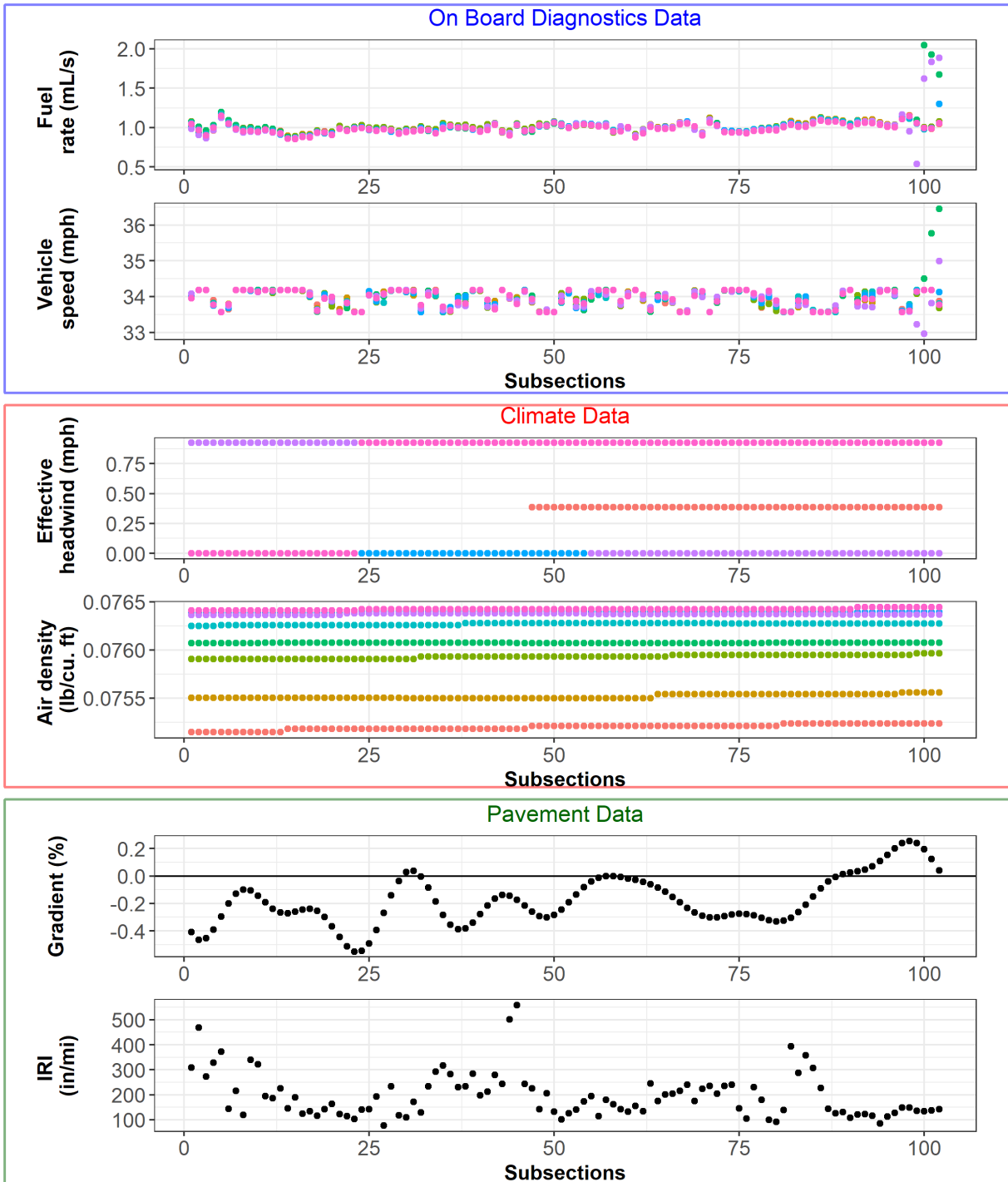


Figure P.126: SUV data on Section PH08.

PH08-YOL-CR29E-HMA SUV summer_night 45 mph

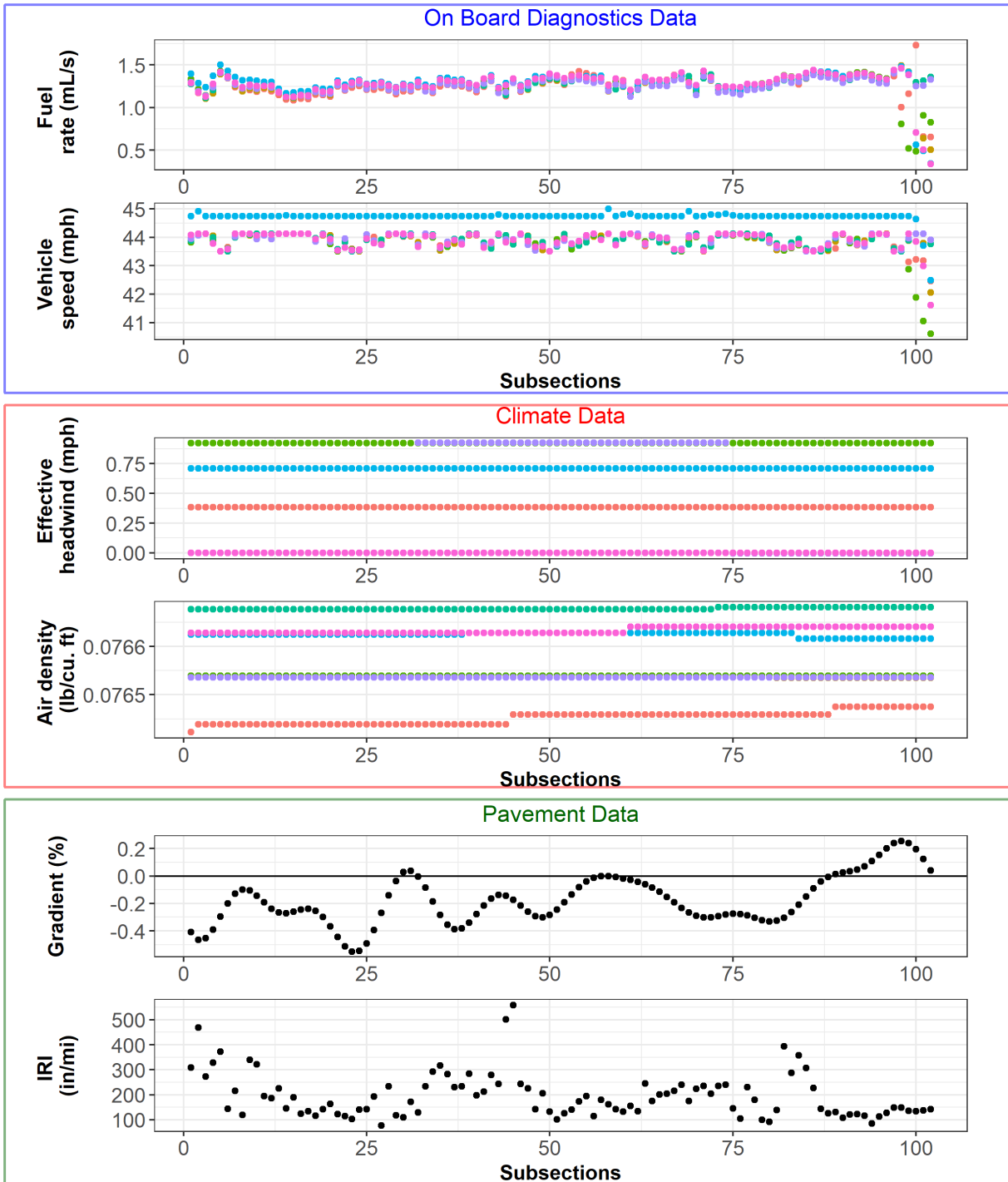


Figure P.127: SUV data on Section PH08.

PH08-YOL-CR29E-HMA SUV winter_day 35 mph

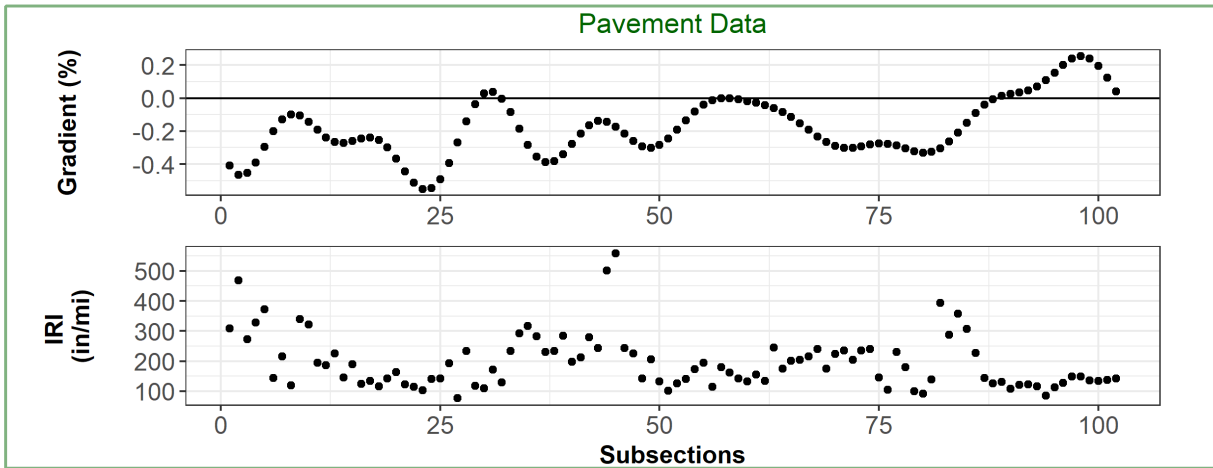
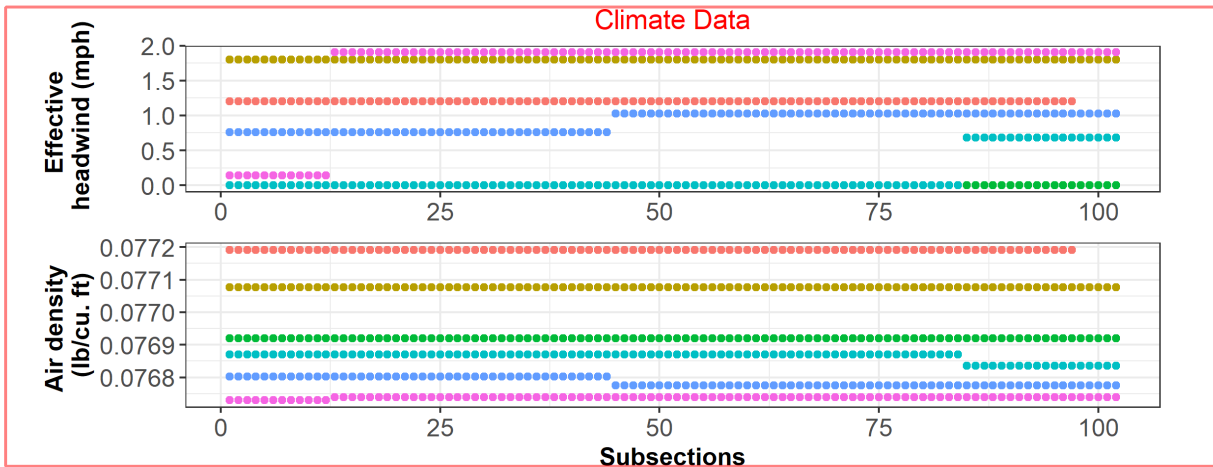
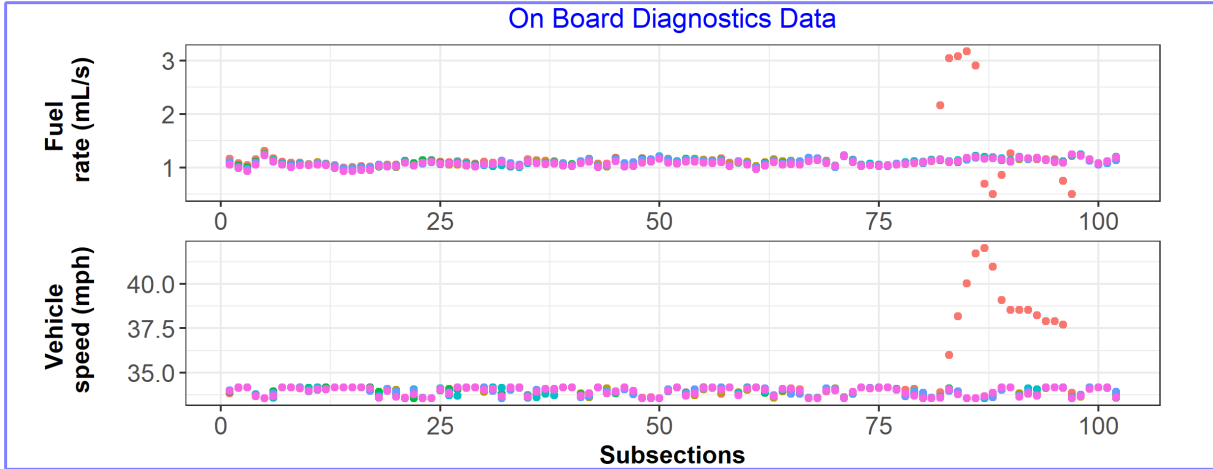


Figure P.128: SUV data on Section PH08.

PH09-SUT113N-RHMA-O SUV summer_day 45 mph

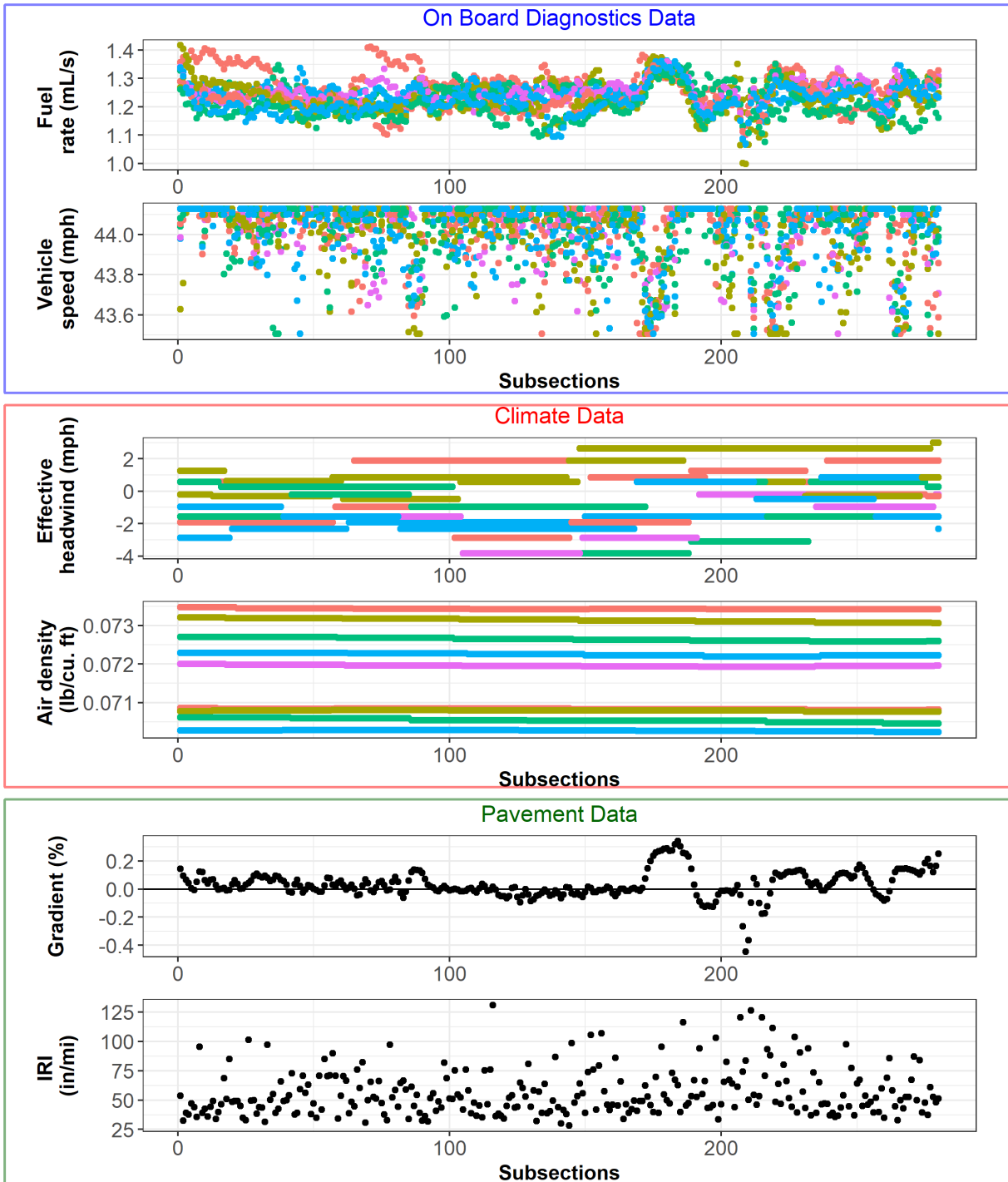


Figure P.129: SUV data on Section PH09.

PH09-SUT113N-RHMA-O SUV summer_day 55 mph

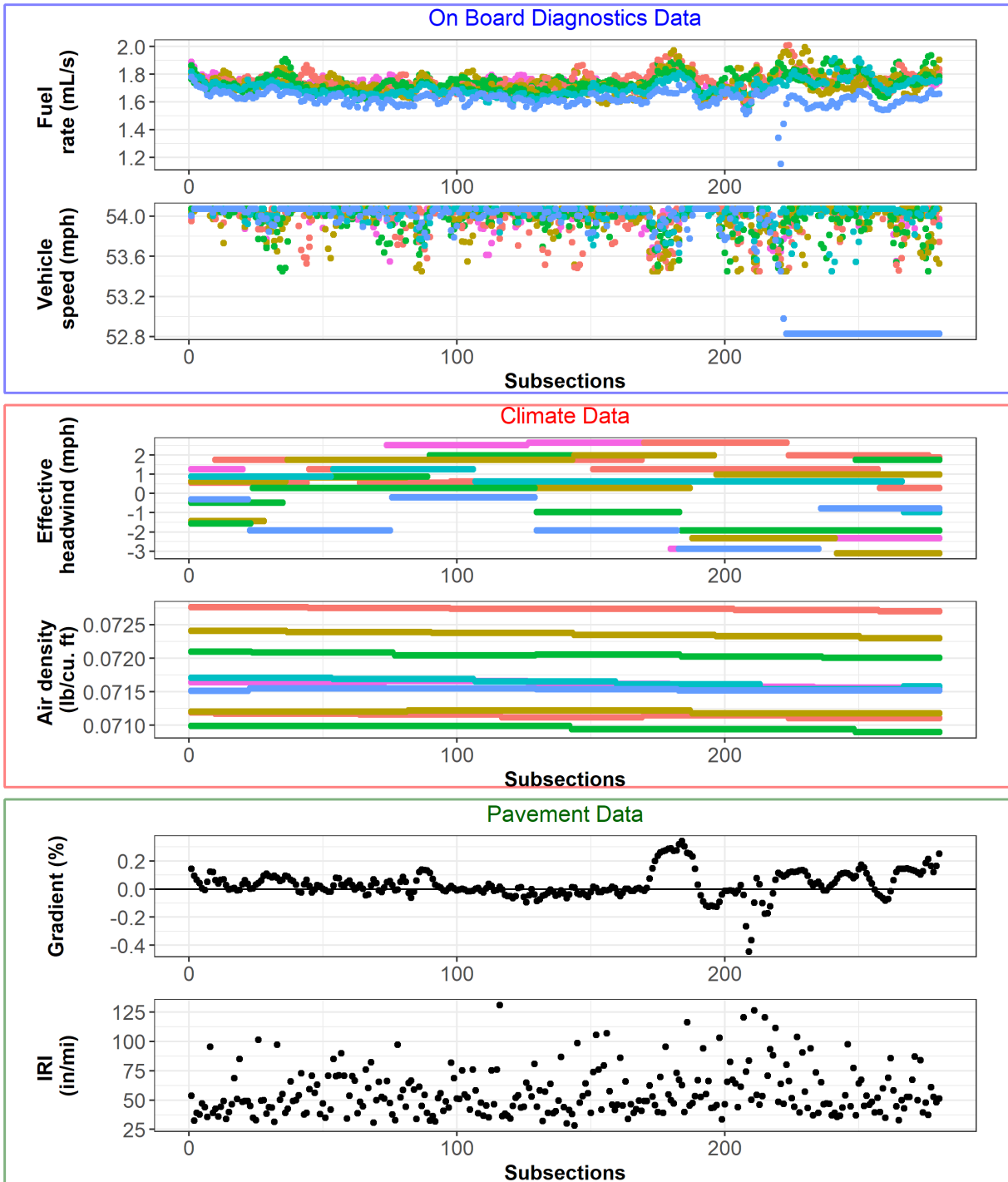


Figure P.130: SUV data on Section PH09.

PH09-SUT113N-RHMA-O SUV winter_day 45 mph

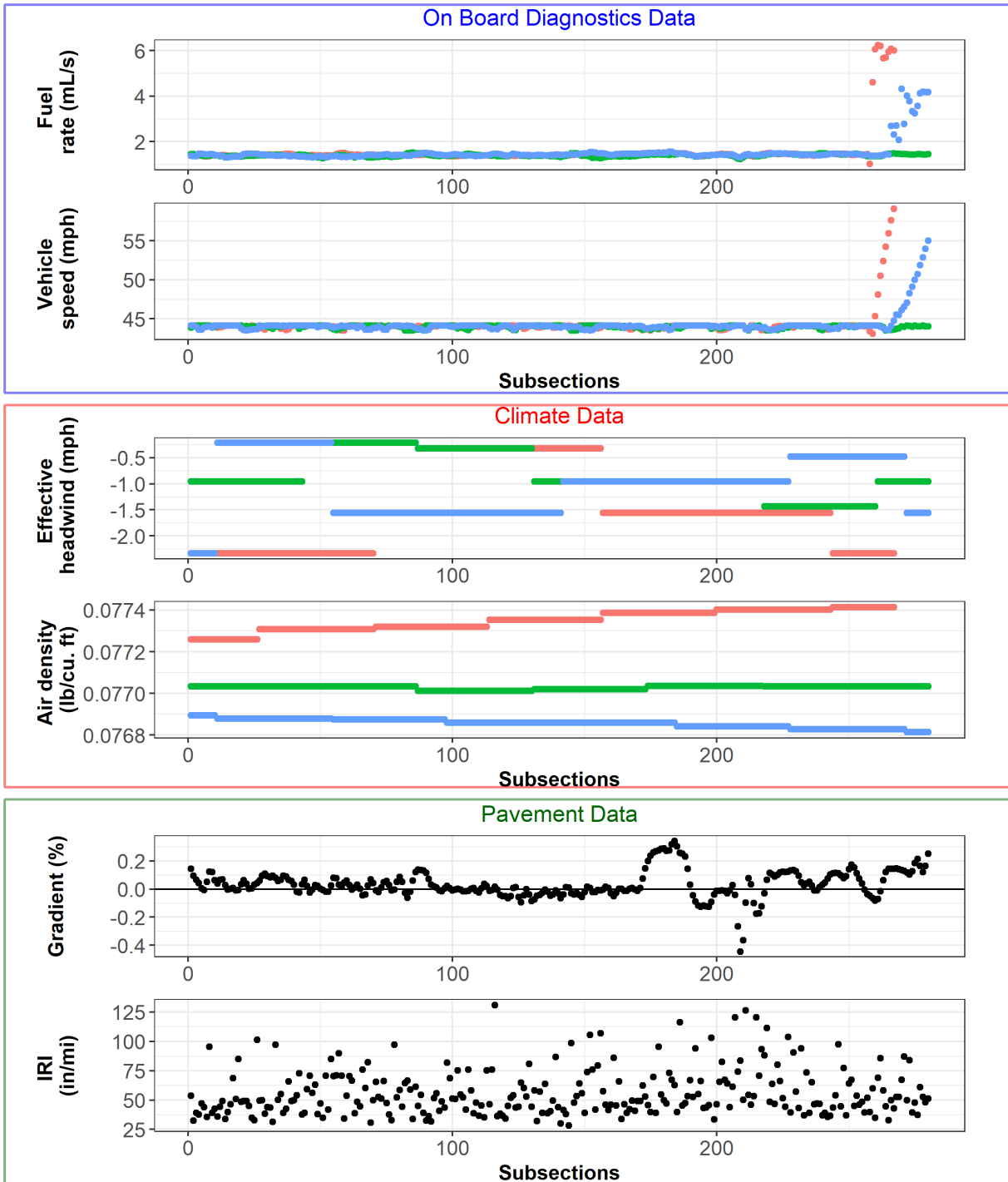


Figure P.131: SUV data on Section PH09.

PH10-SUT113S-RHMA-O SUV summer_day 45 mph

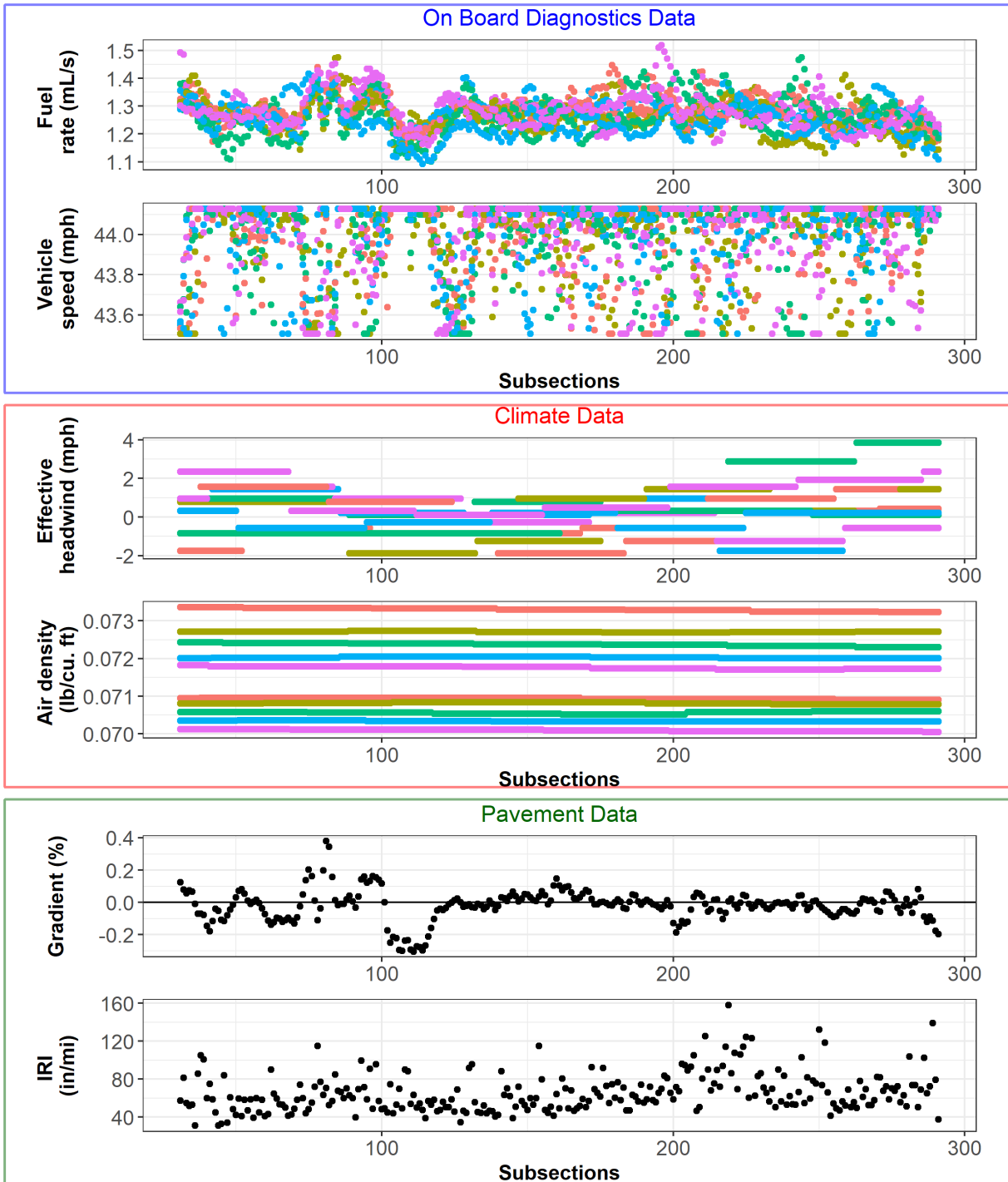


Figure P.132: SUV data on Section PH10.

PH10-SUT113S-RHMA-O SUV summer_day 55 mph

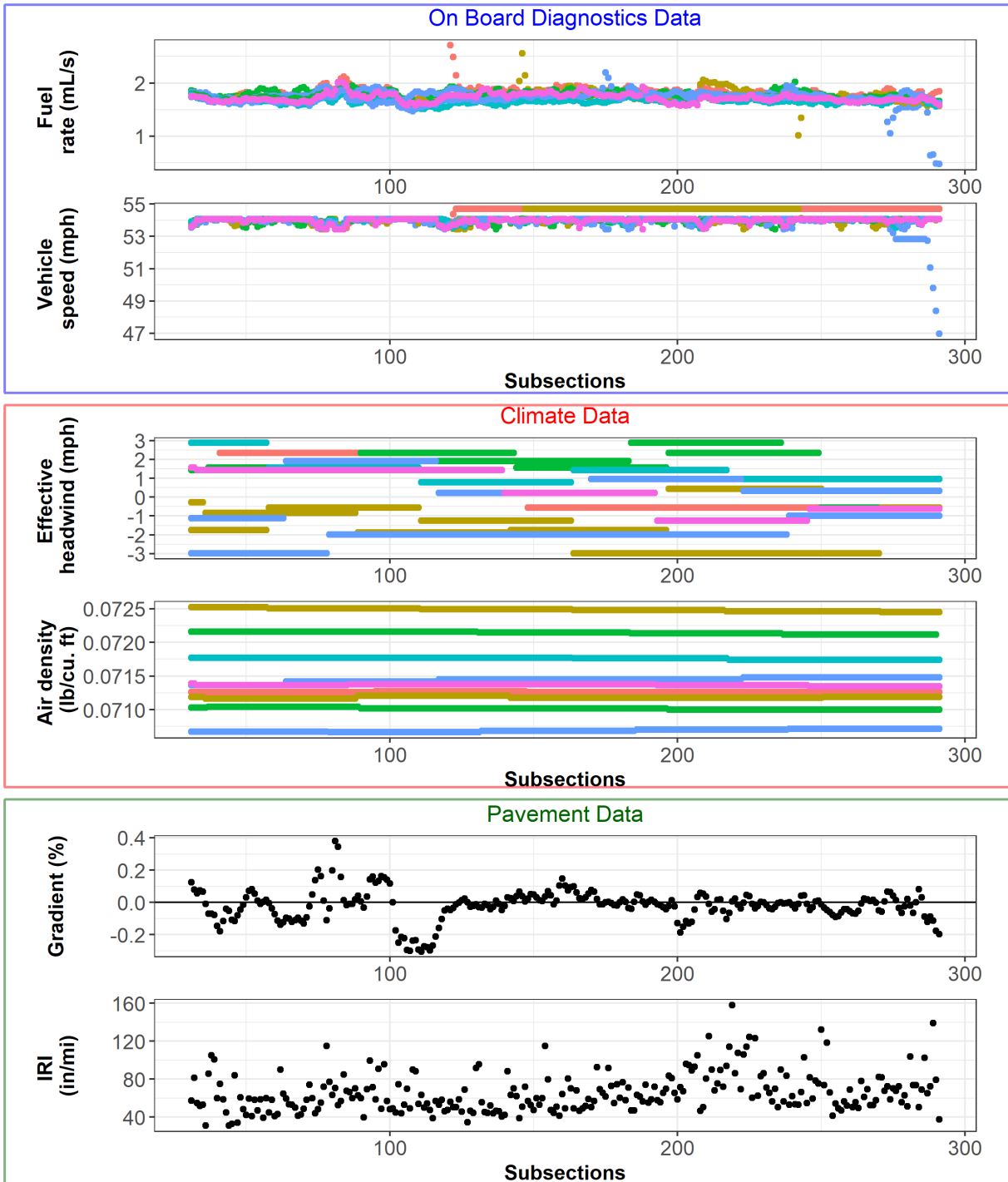


Figure P.133: SUV data on Section PH10.

PH10-SUT113S-RHMA-O SUV winter_day 45 mph

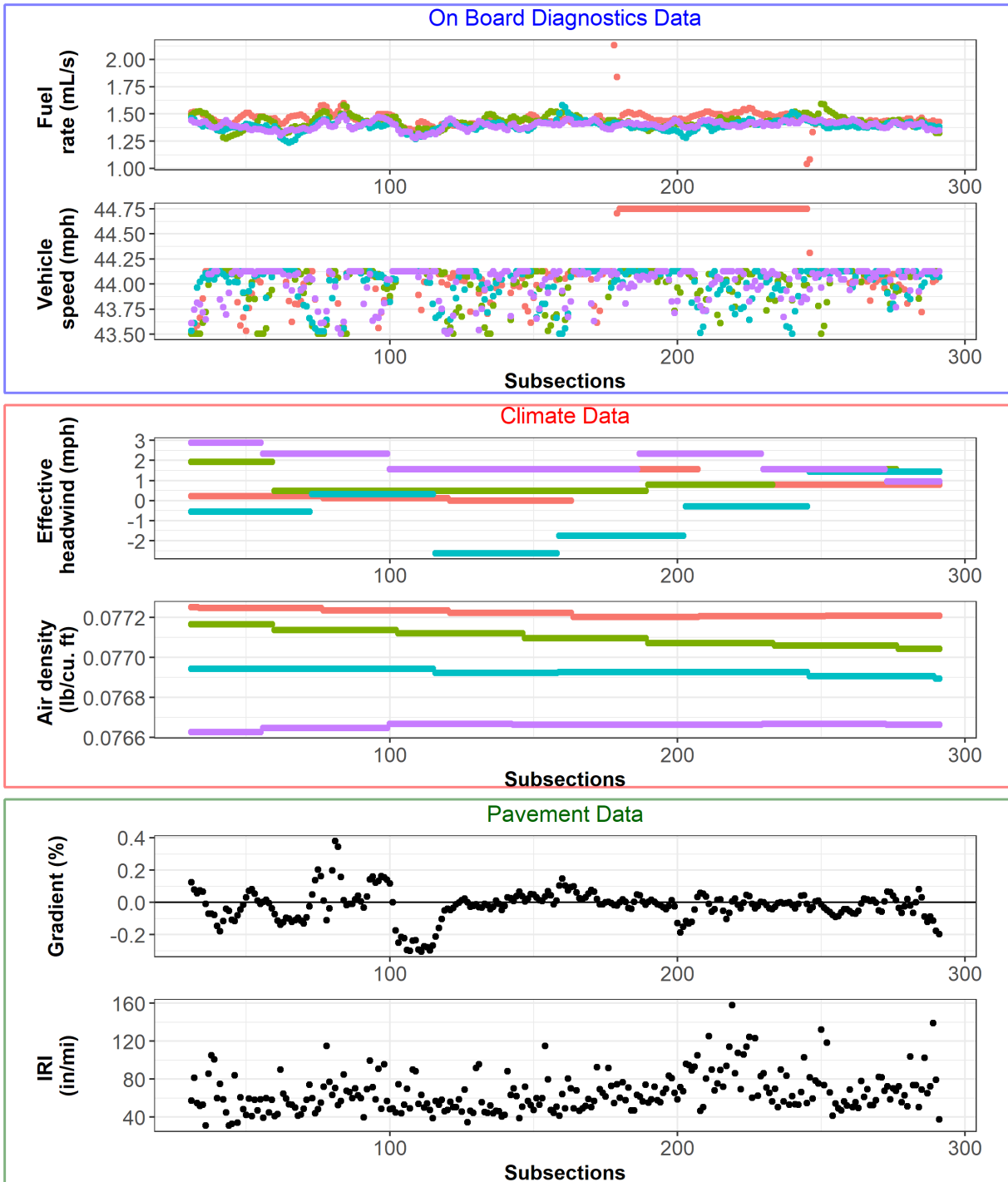


Figure P.134: SUV data on Section PH10.

PH10-SUT113S-RHMA-O SUV winter_day 55 mph

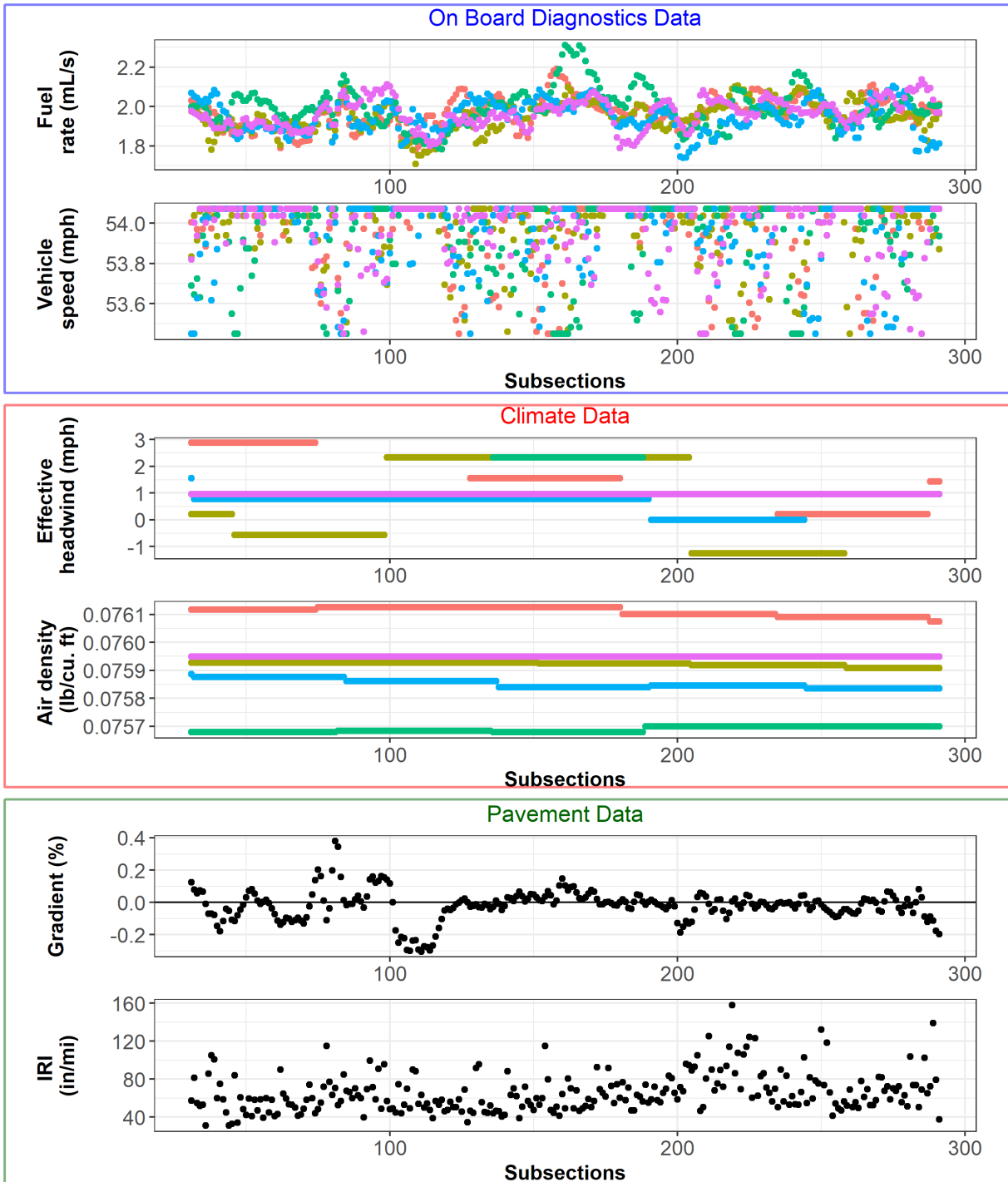


Figure P.135: SUV data on Section PH10.

PH11-SUT113N-HMA SUV summer_day 45 mph

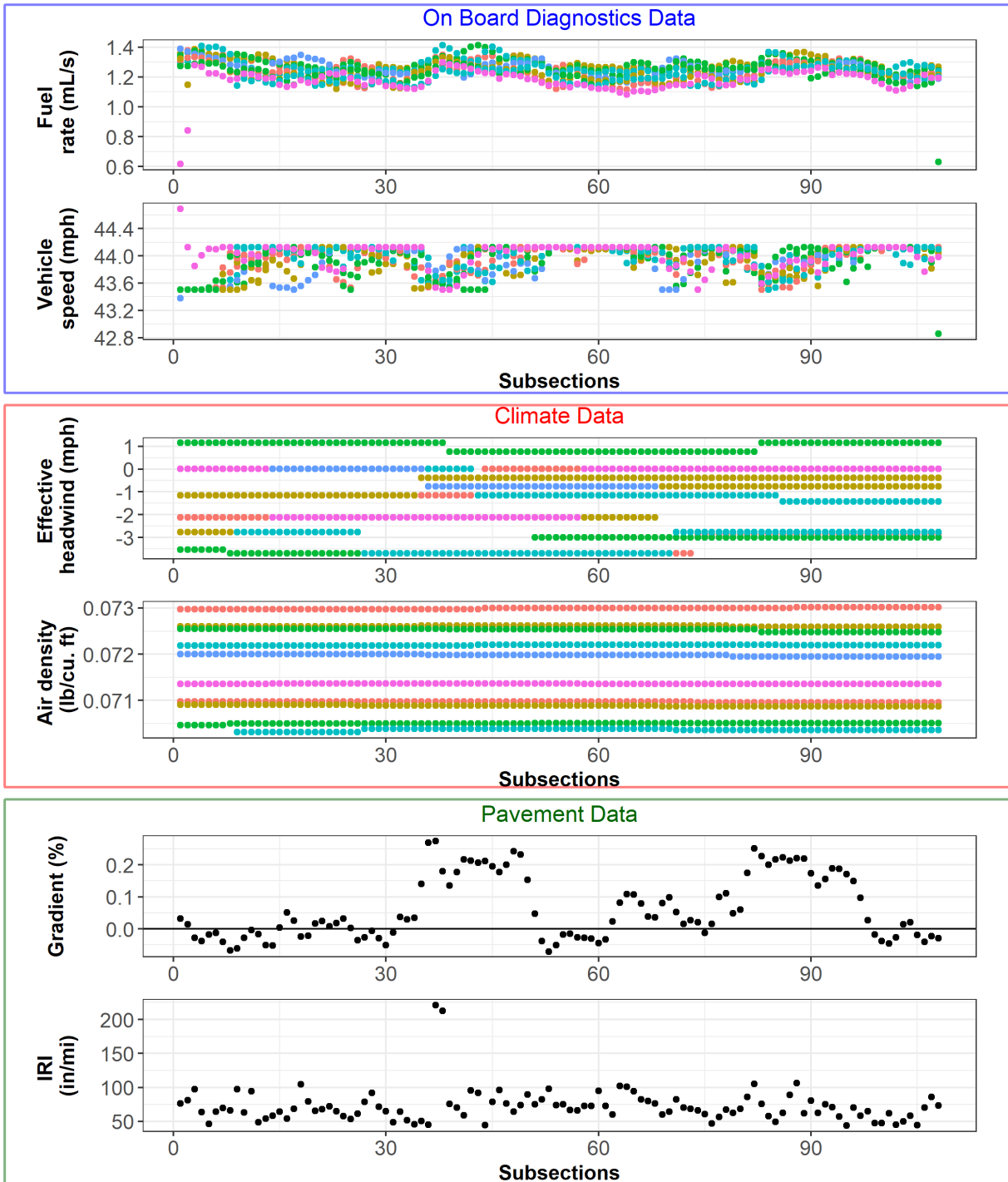


Figure P.136: SUV data on Section PH11.

PH11-SUT113N-HMA SUV summer_day 55 mph

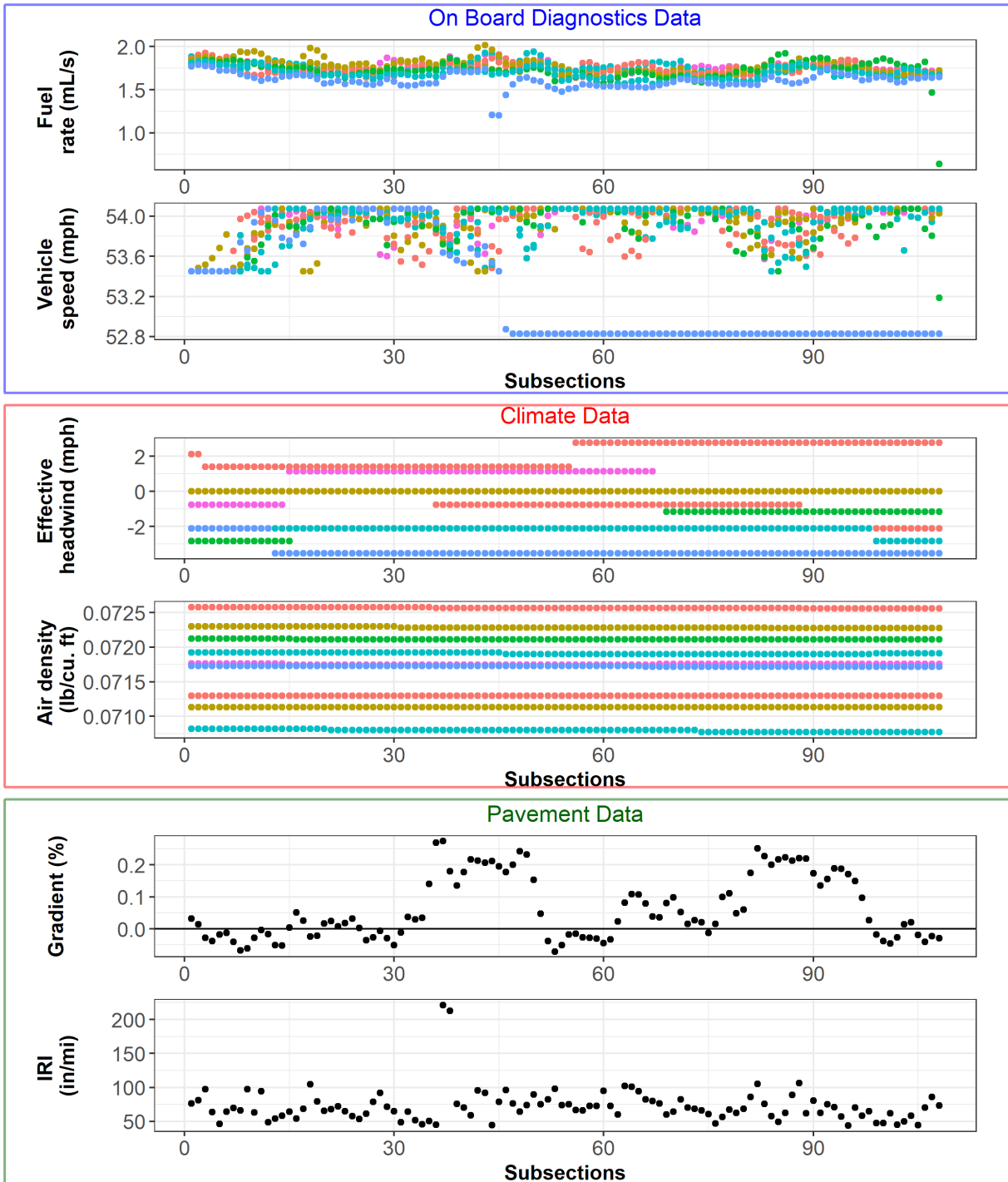


Figure P.137: SUV data on Section PH11.

PH11-SUT113N-HMA SUV winter_day 45 mph

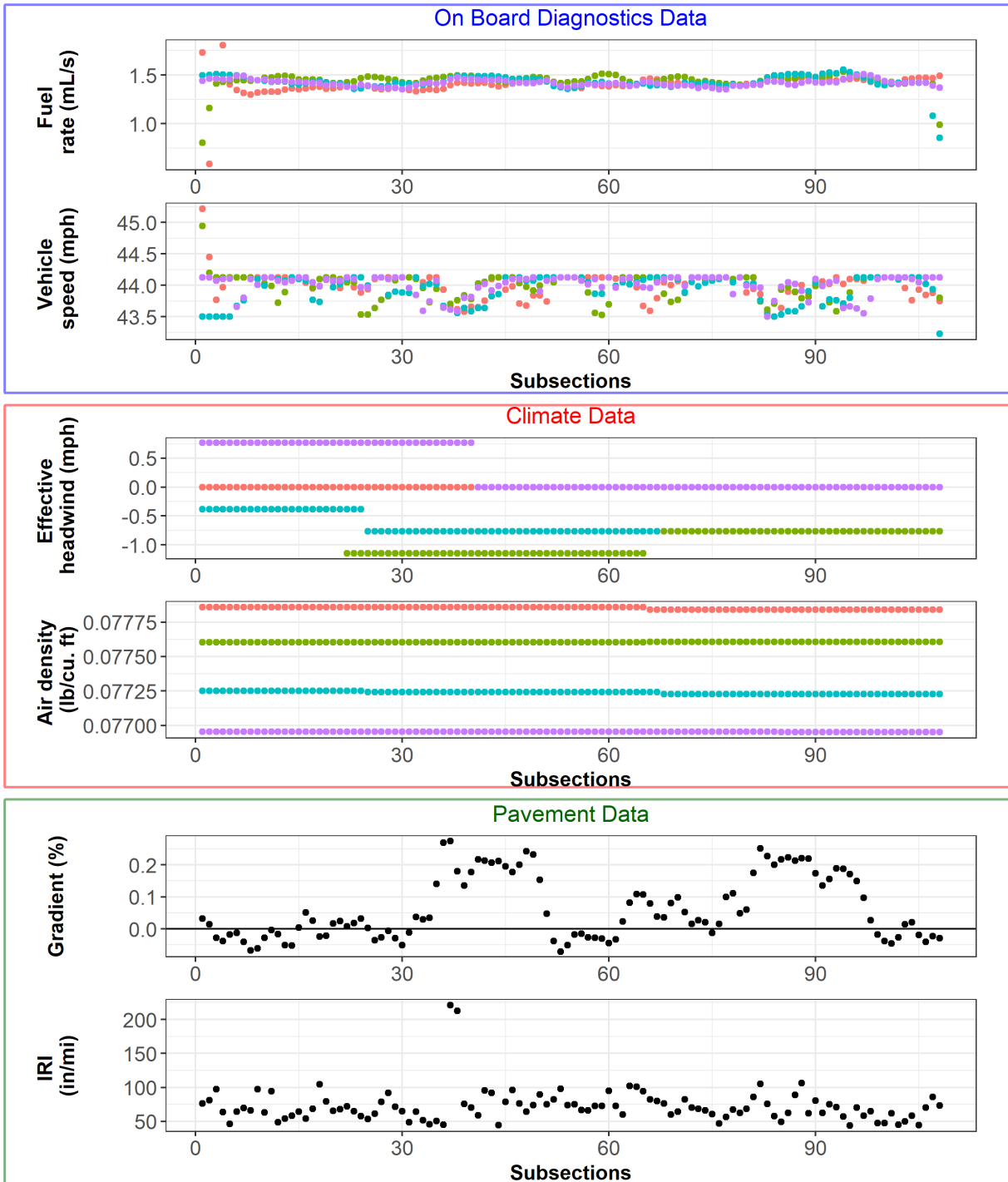


Figure P.138: SUV data on Section PH11.

PH11-SUT113N-HMA SUV winter_day 55 mph

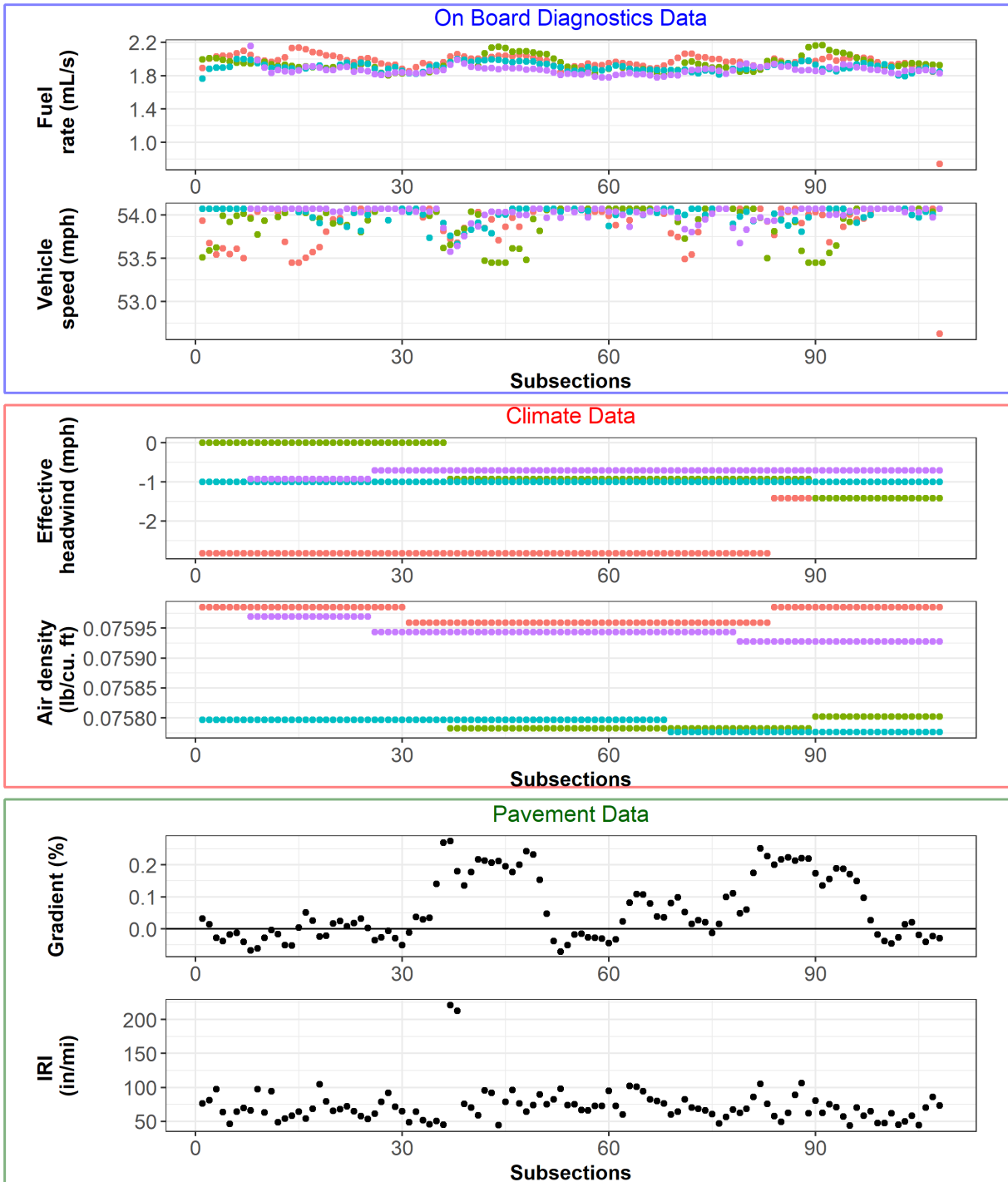


Figure P.139: SUV data on Section PH11.

PH12-SUT113S-HMA SUV summer_day 45 mph

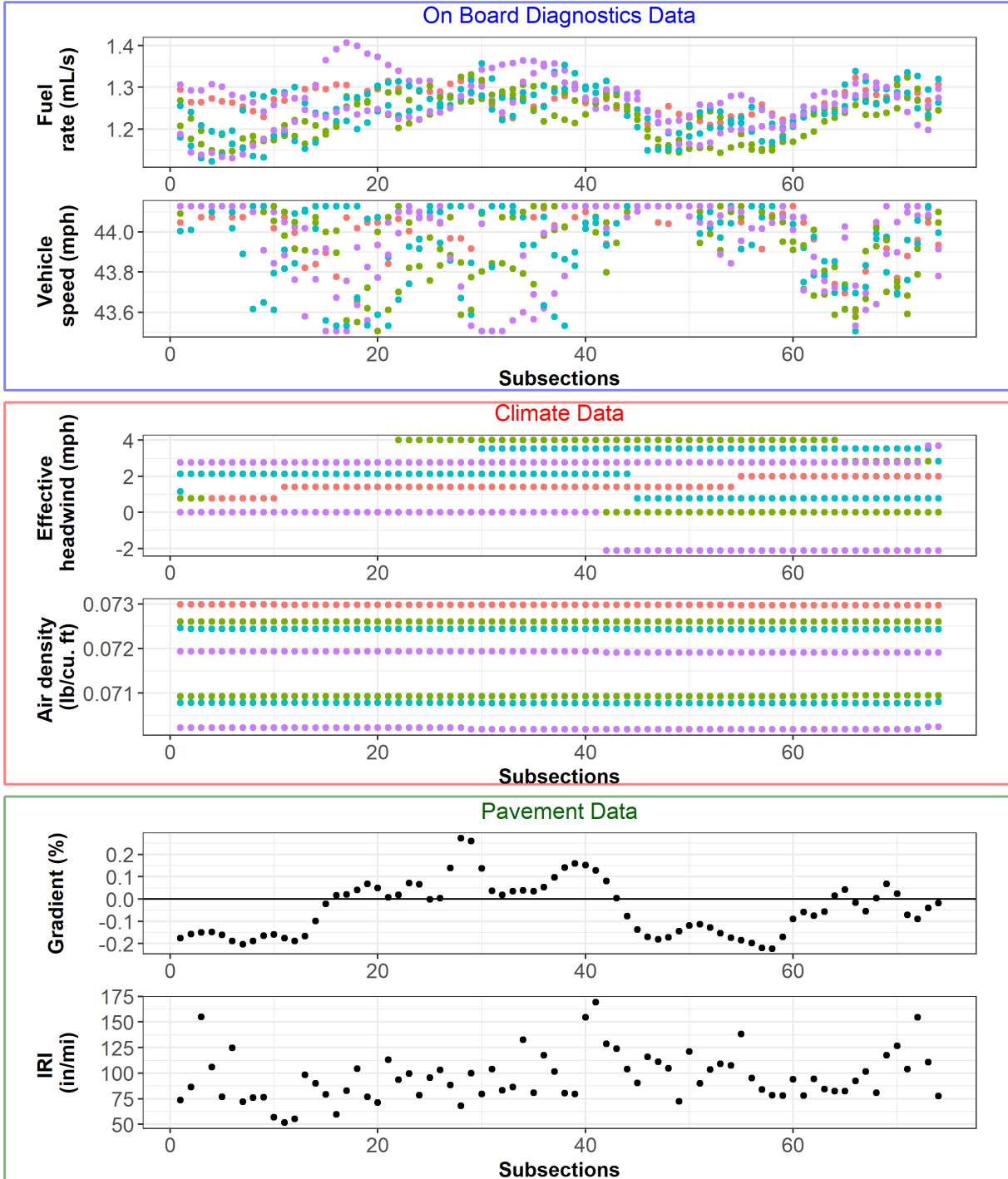


Figure P.140: SUV data on Section PH12.

PH12-SUT113S-HMA SUV summer_day 55 mph

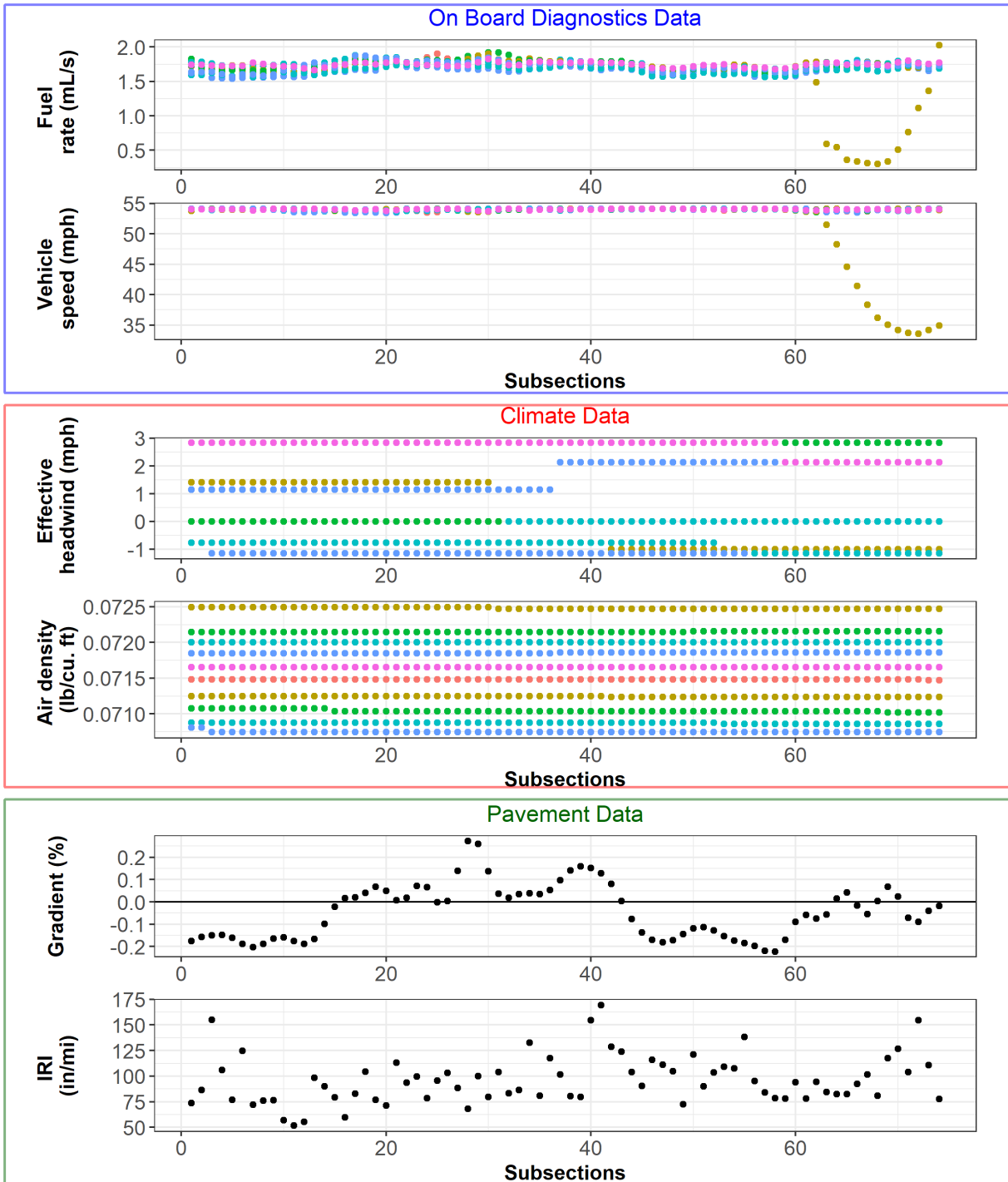


Figure P.141: SUV data on Section PH12.

PH12-SUT113S-HMA SUV winter_day 45 mph

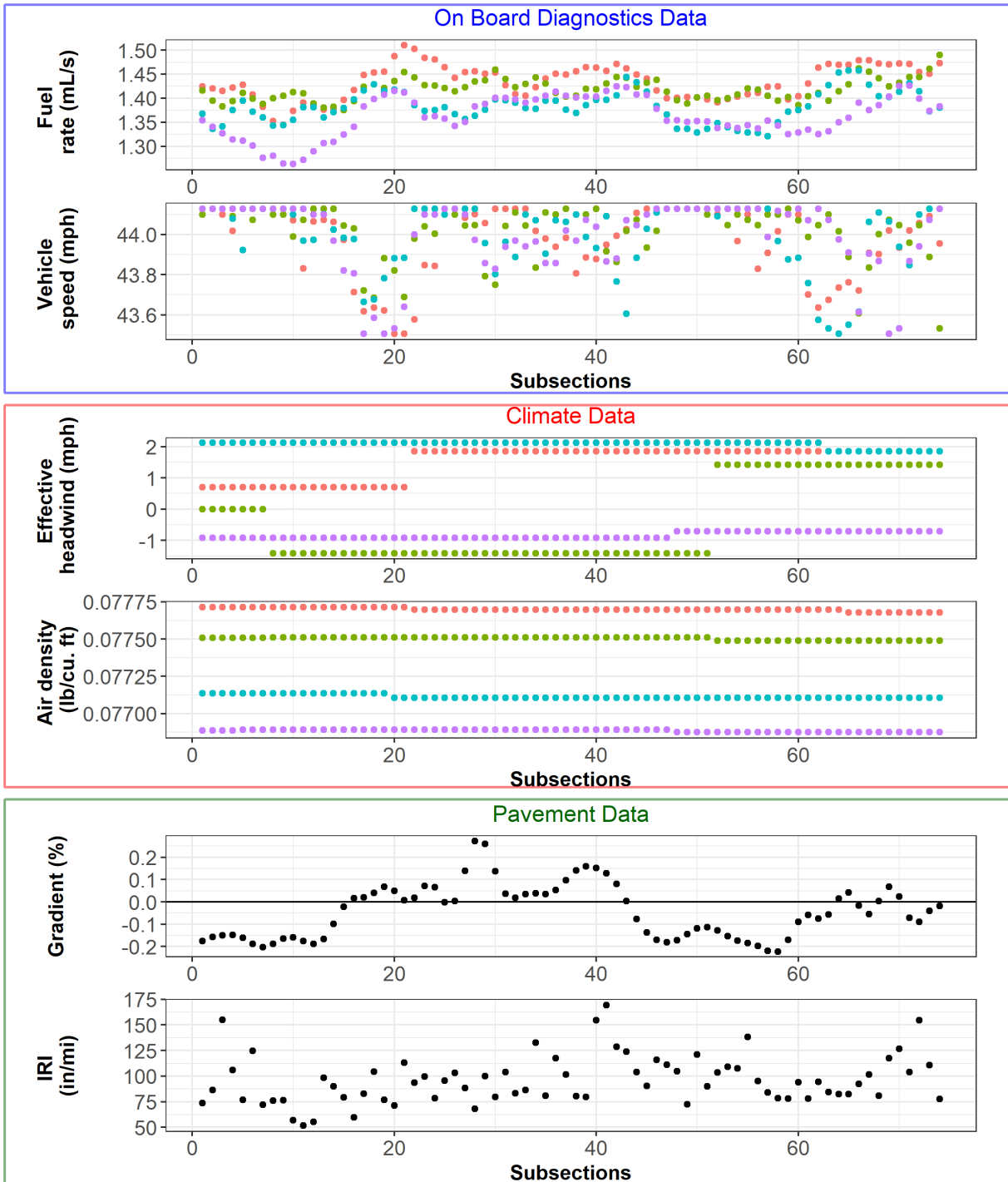


Figure P.142: SUV data on Section PH12.

PH12-SUT113S-HMA SUV winter_day 55 mph

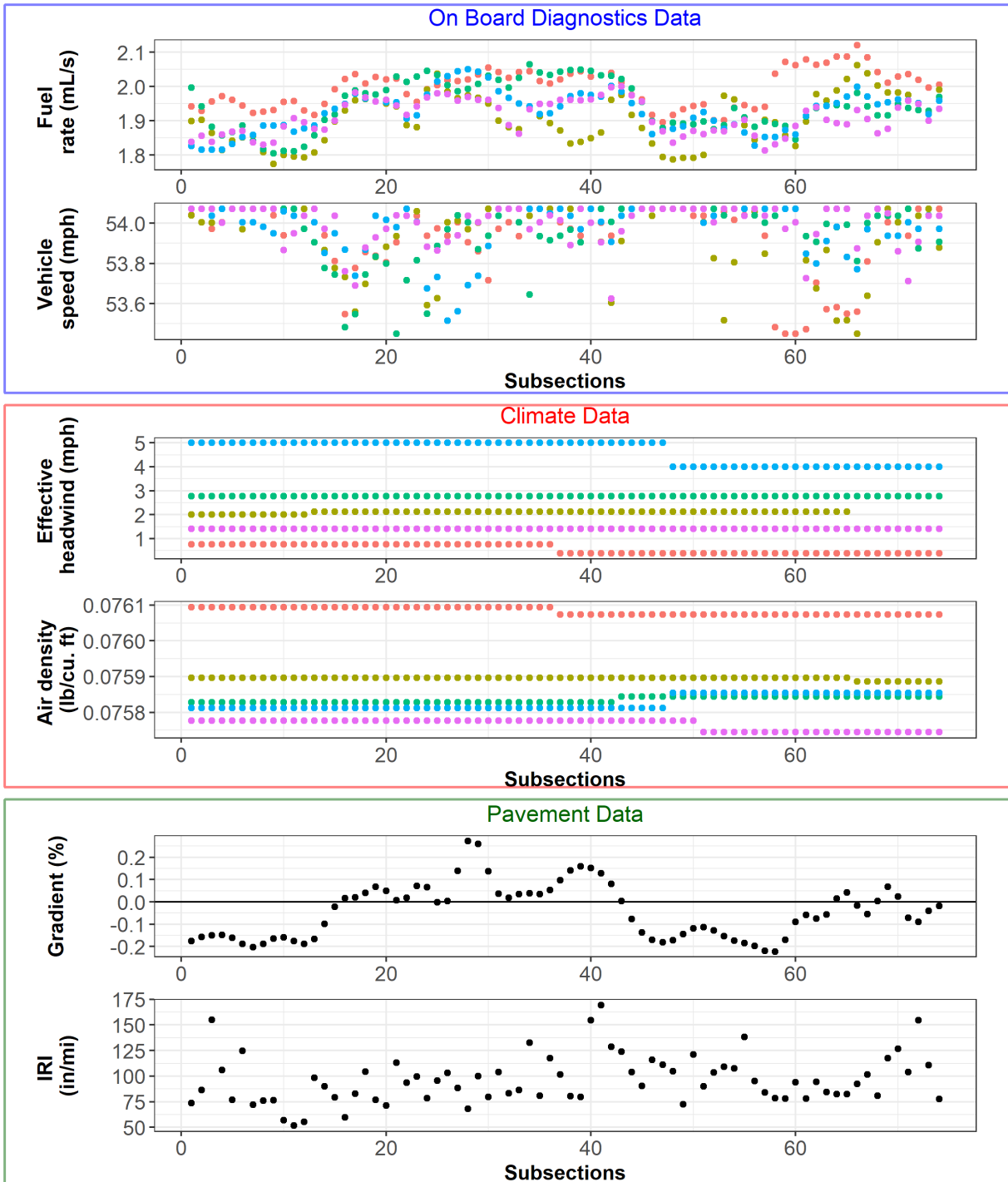


Figure P.143: SUV data on Section PH12.

PH13-SUT113N-HMA SUV summer_day 45 mph

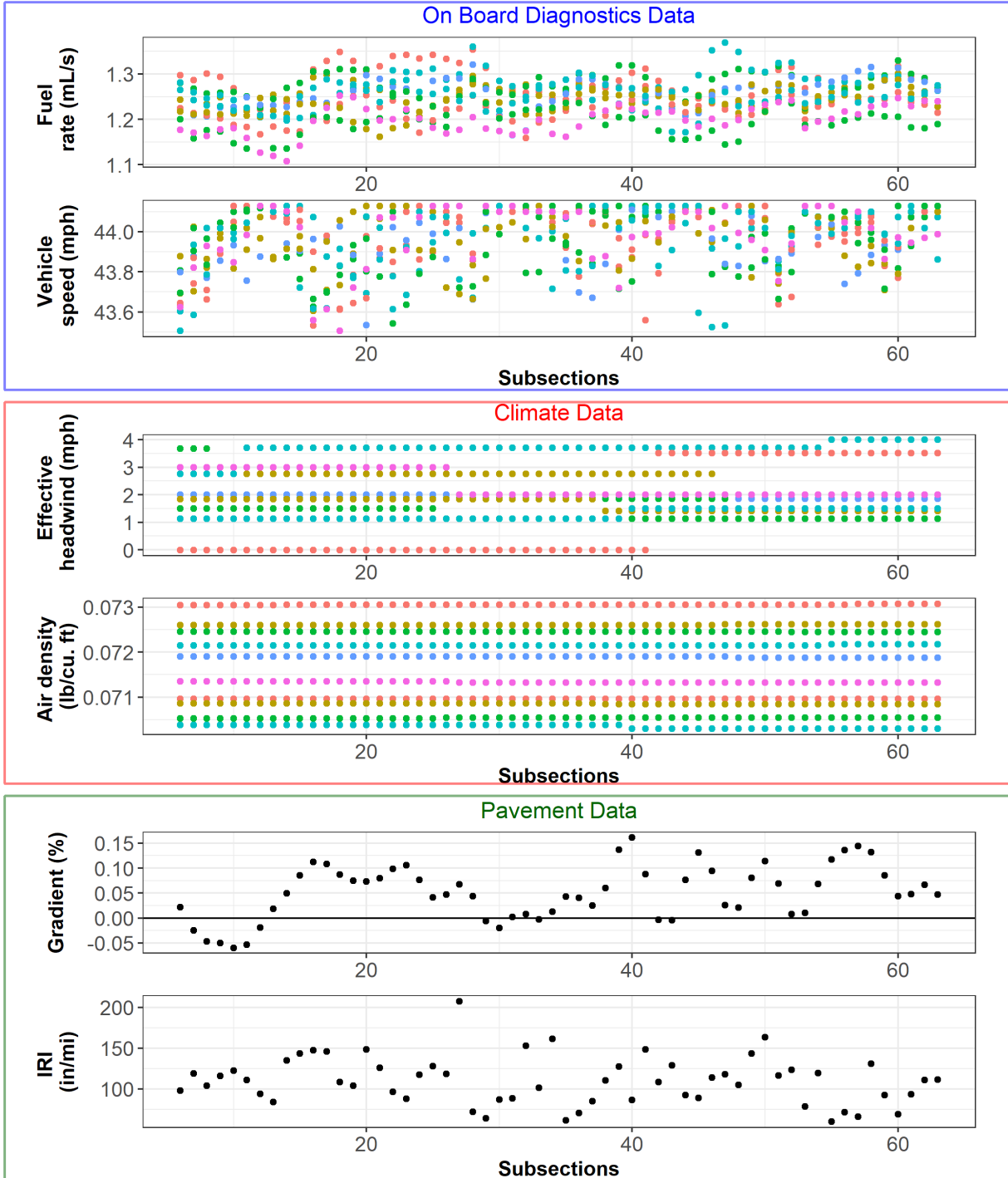


Figure P.144: SUV data on Section PH13.

PH13-SUT113N-HMA SUV summer_day 55 mph

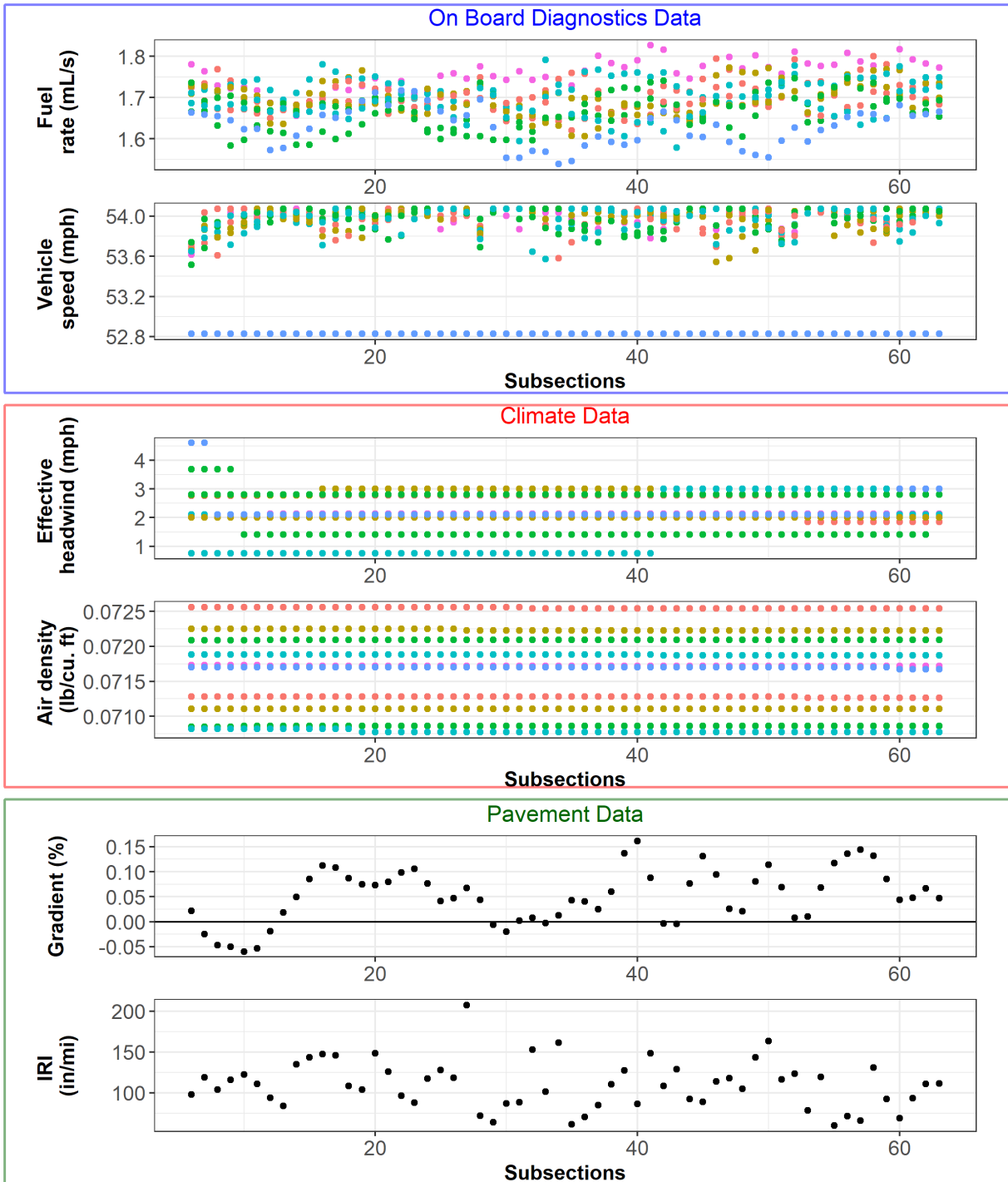


Figure P.145: SUV data on Section PH13.

PH13-SUT113N-HMA SUV winter_day 45 mph

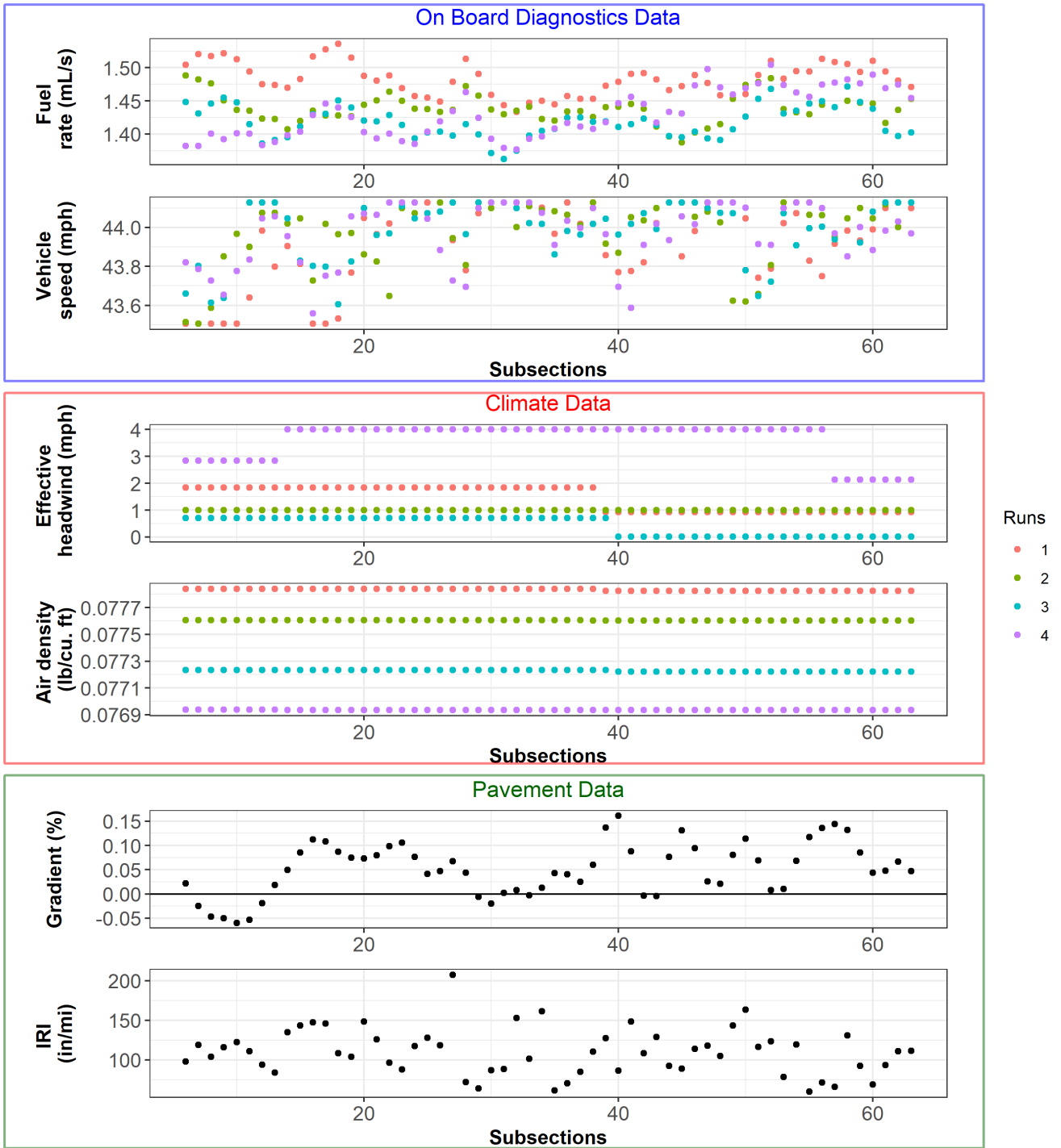


Figure P.146: SUV data on Section PH13.

PH13-SUT113N-HMA SUV winter_day 55 mph

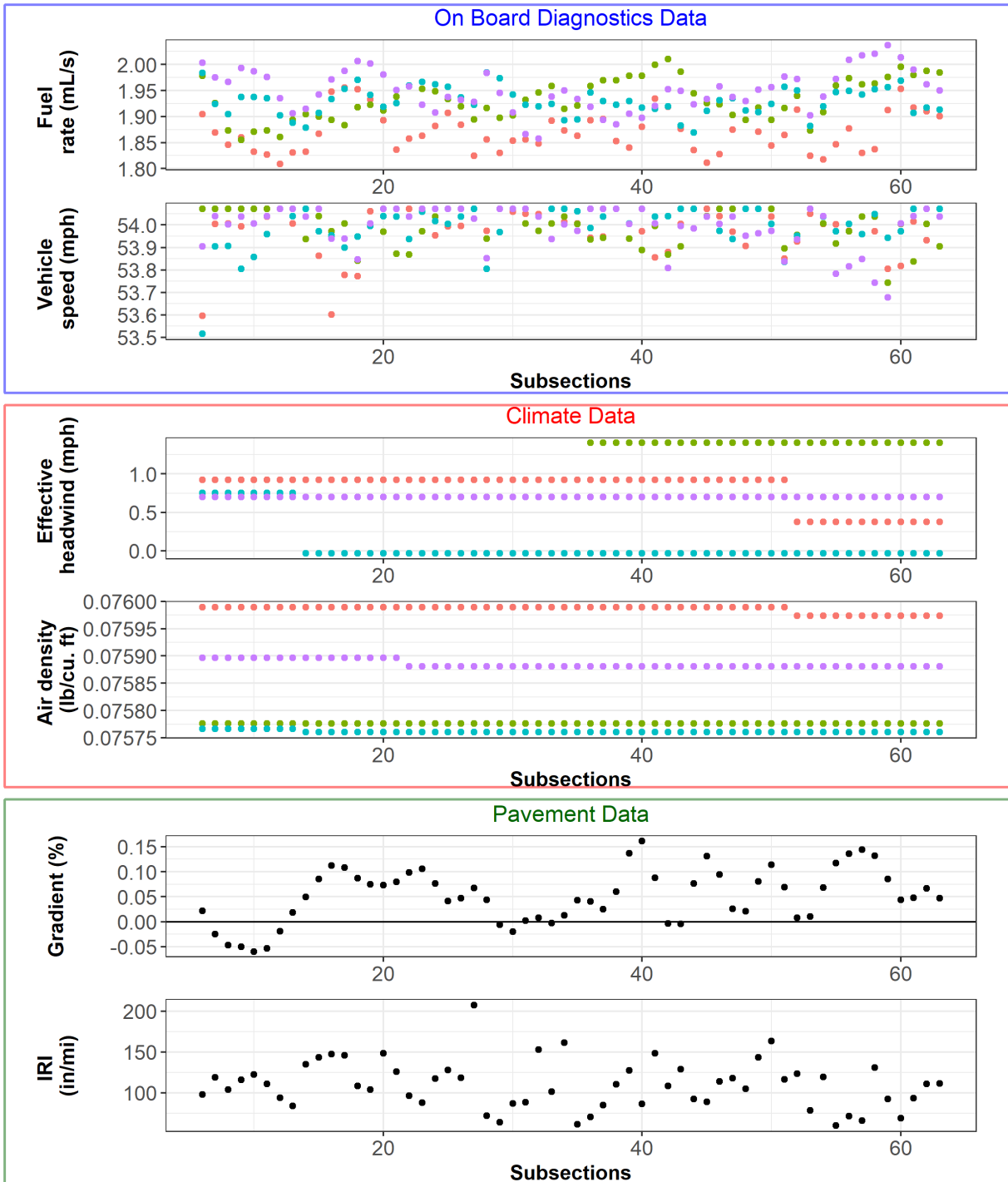


Figure P.147: SUV data on Section PH13.

PH14-SUT113S-HMA SUV summer_day 45 mph

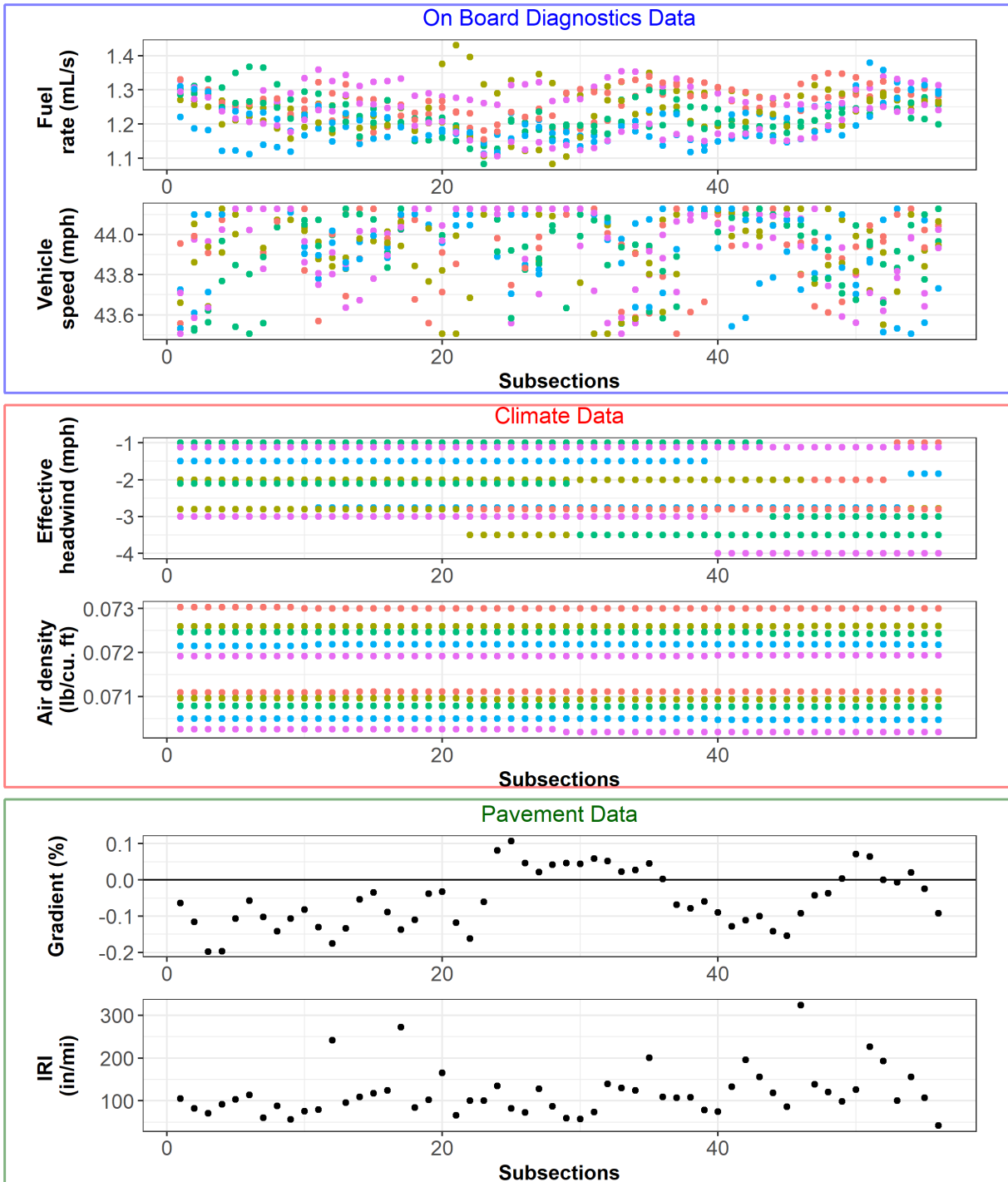


Figure P.148: SUV data on Section PH14.

PH14-SUT113S-HMA SUV summer_day 55 mph

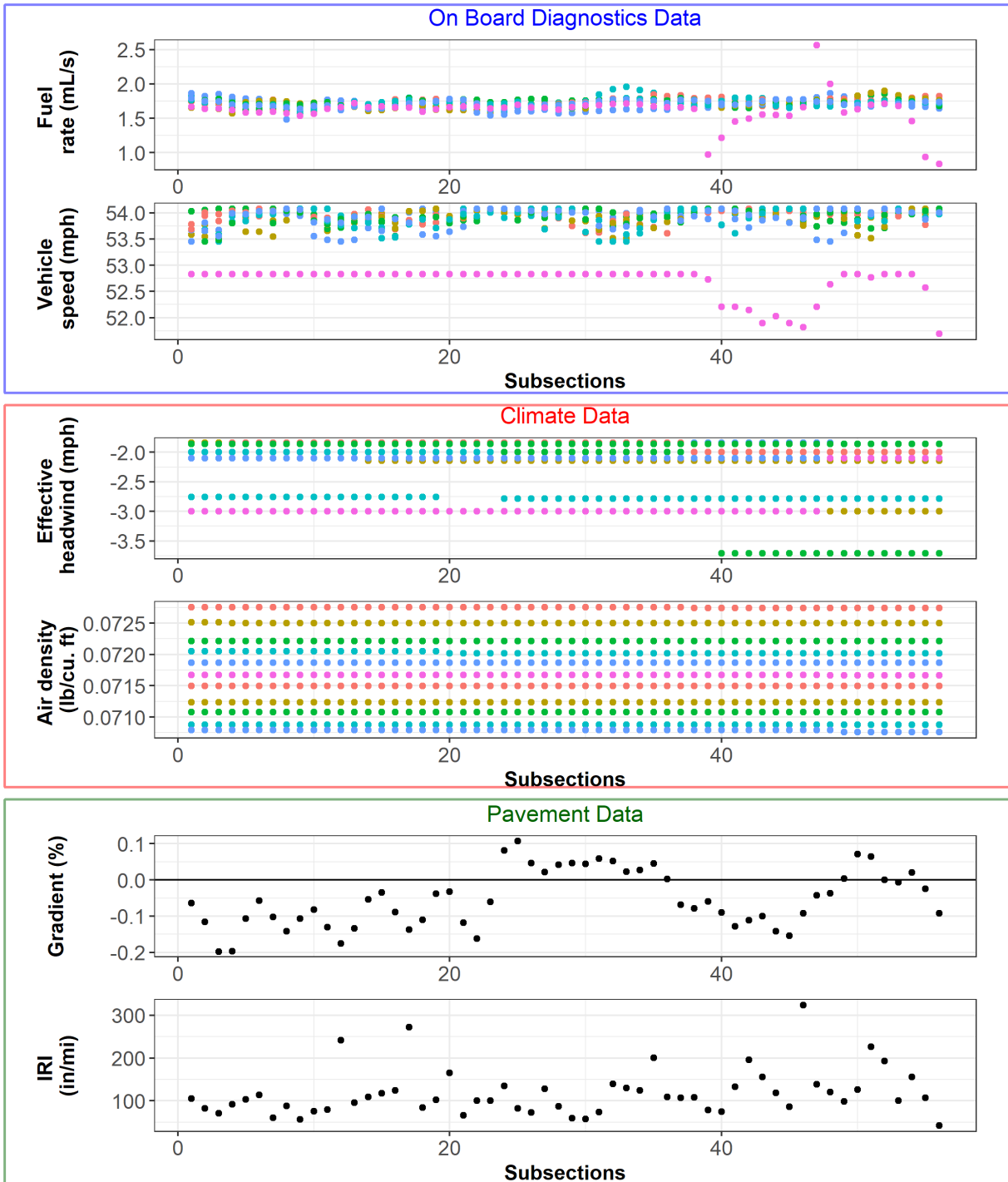


Figure P.149: SUV data on Section PH14.

PH14-SUT113S-HMA SUV winter_day 45 mph

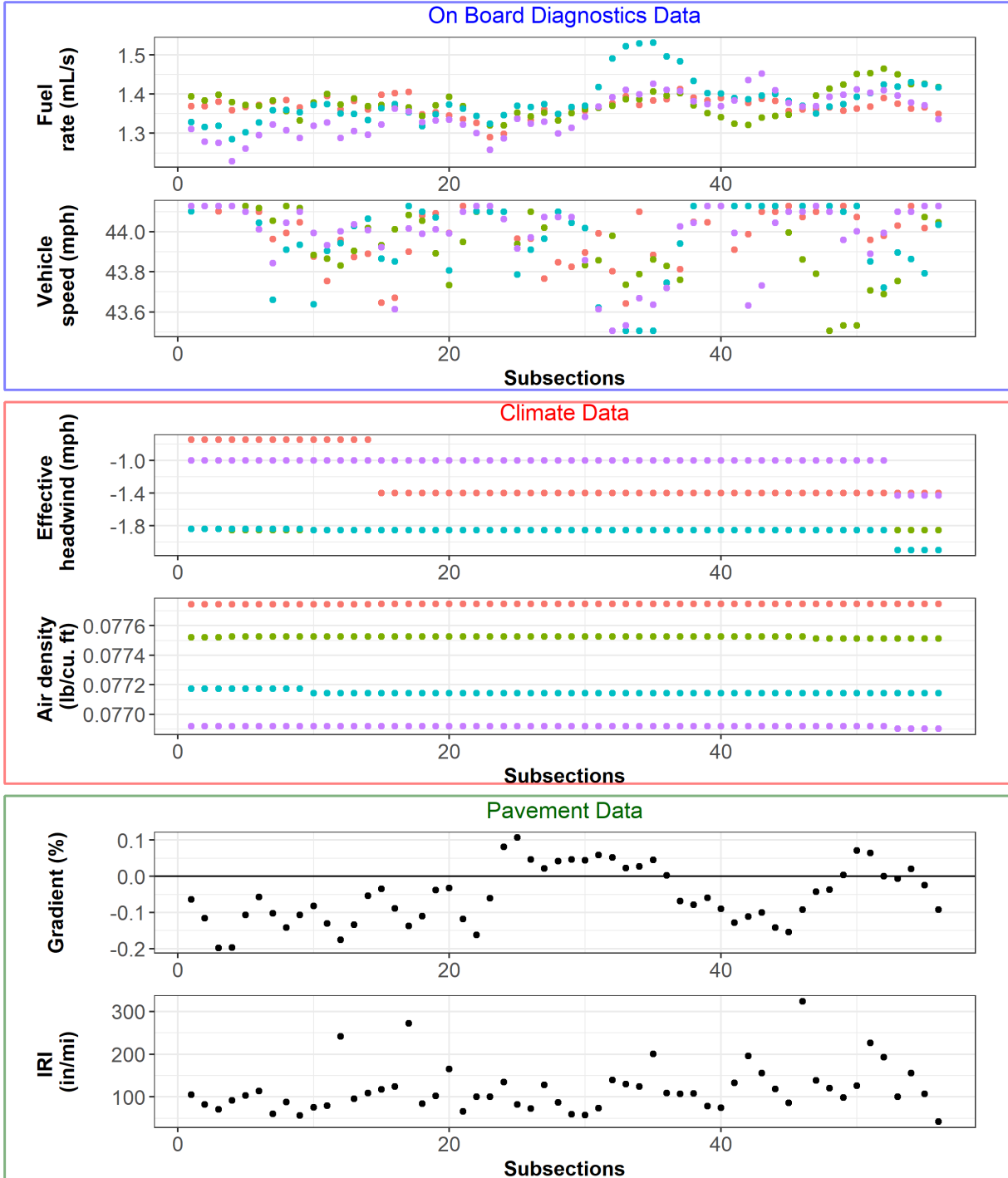


Figure P.150: SUV data on Section PH14.

PH14-SUT113S-HMA SUV winter_day 55 mph

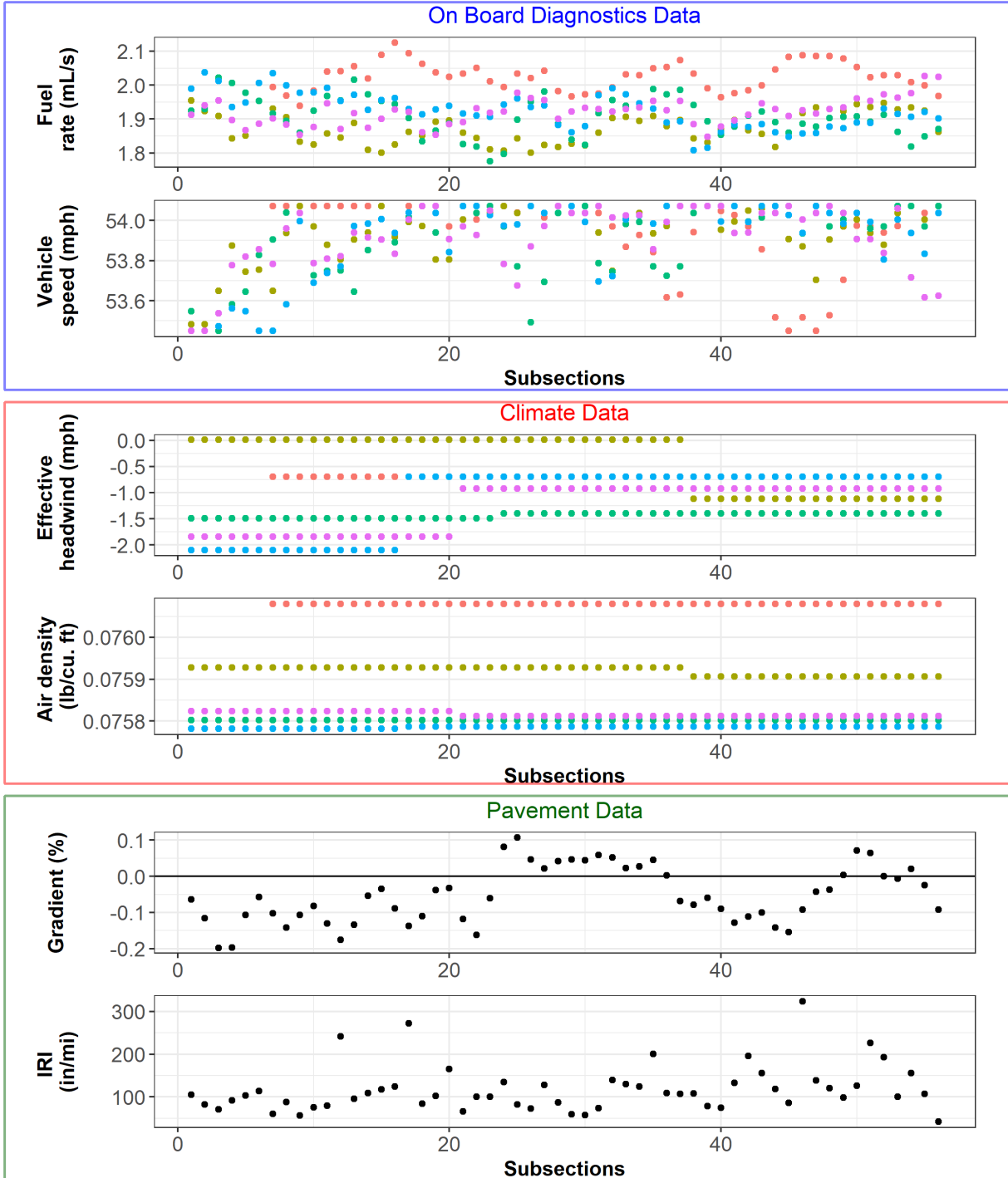


Figure P.151: SUV data on Section PH14.

PH15-YOL-CR32BE-HMA SUV summer_day 35 mph

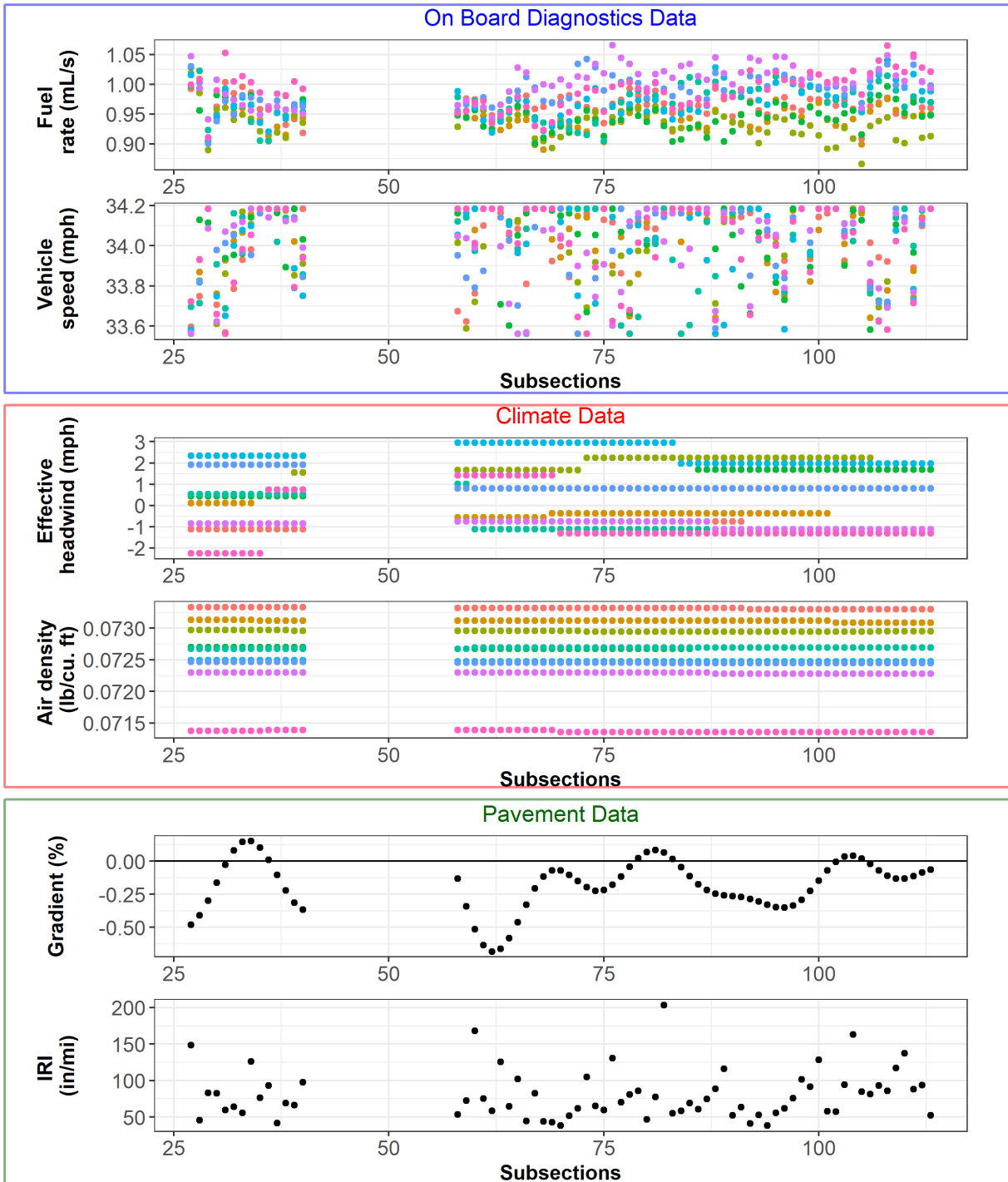


Figure P.152: SUV data on Section PH15.

PH15-YOL-CR32BE-HMA SUV summer_day 45 mph

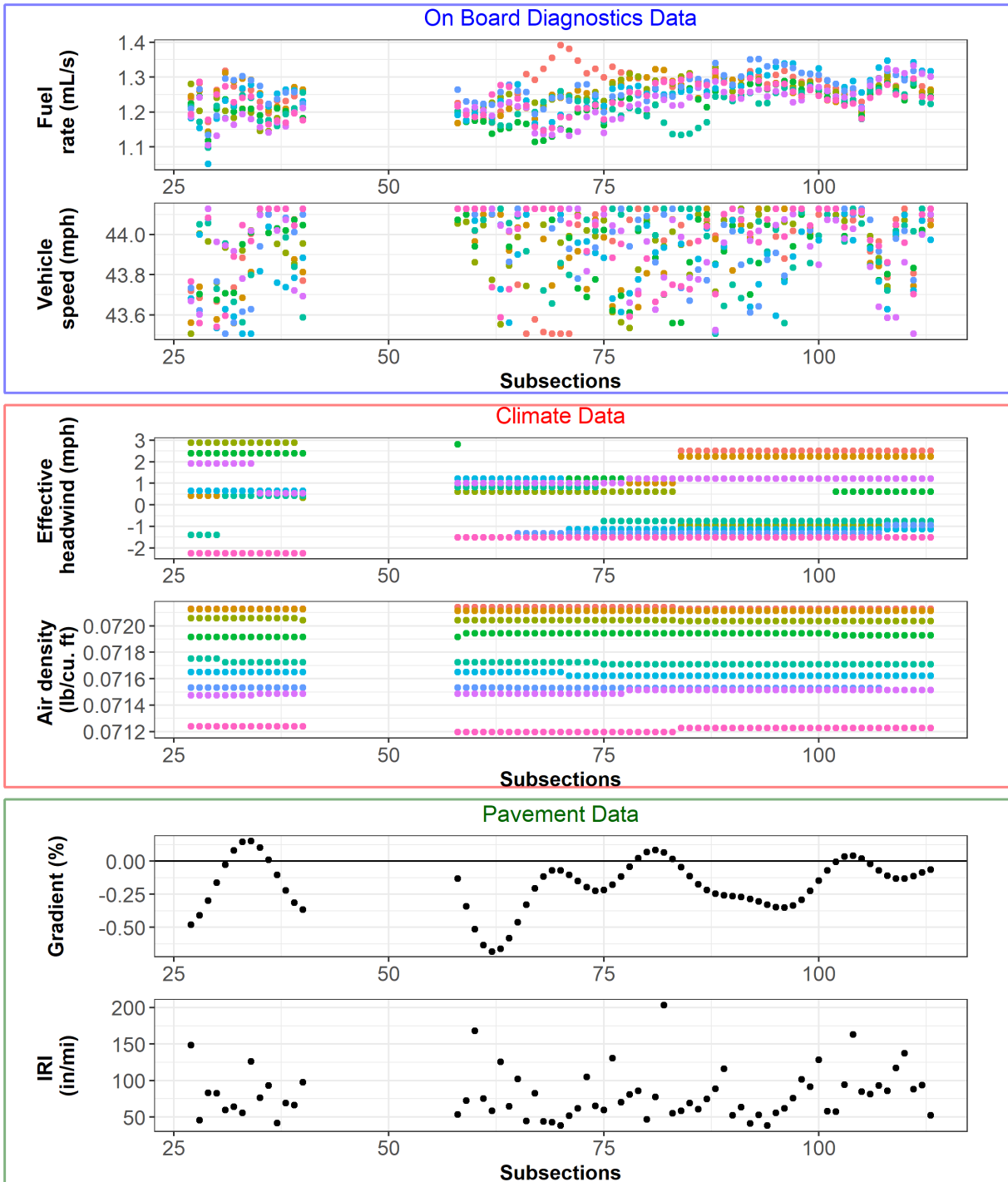


Figure P.153: SUV data on Section PH15.

PH15-YOL-CR32BE-HMA SUV summer_night 35 mph

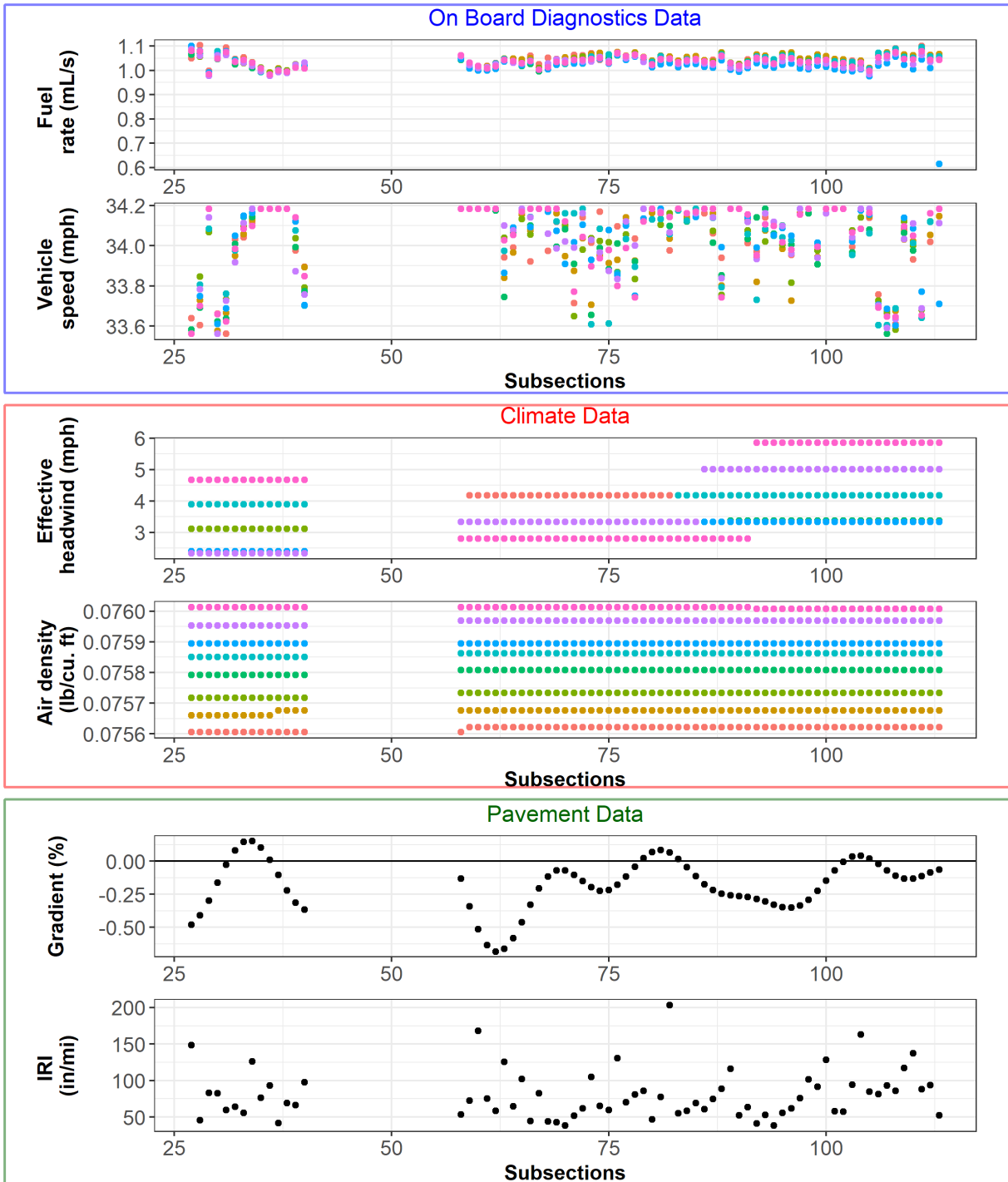


Figure P.154: SUV data on Section PH15.

PH15-YOL-CR32BE-HMA SUV summer_night 45 mph

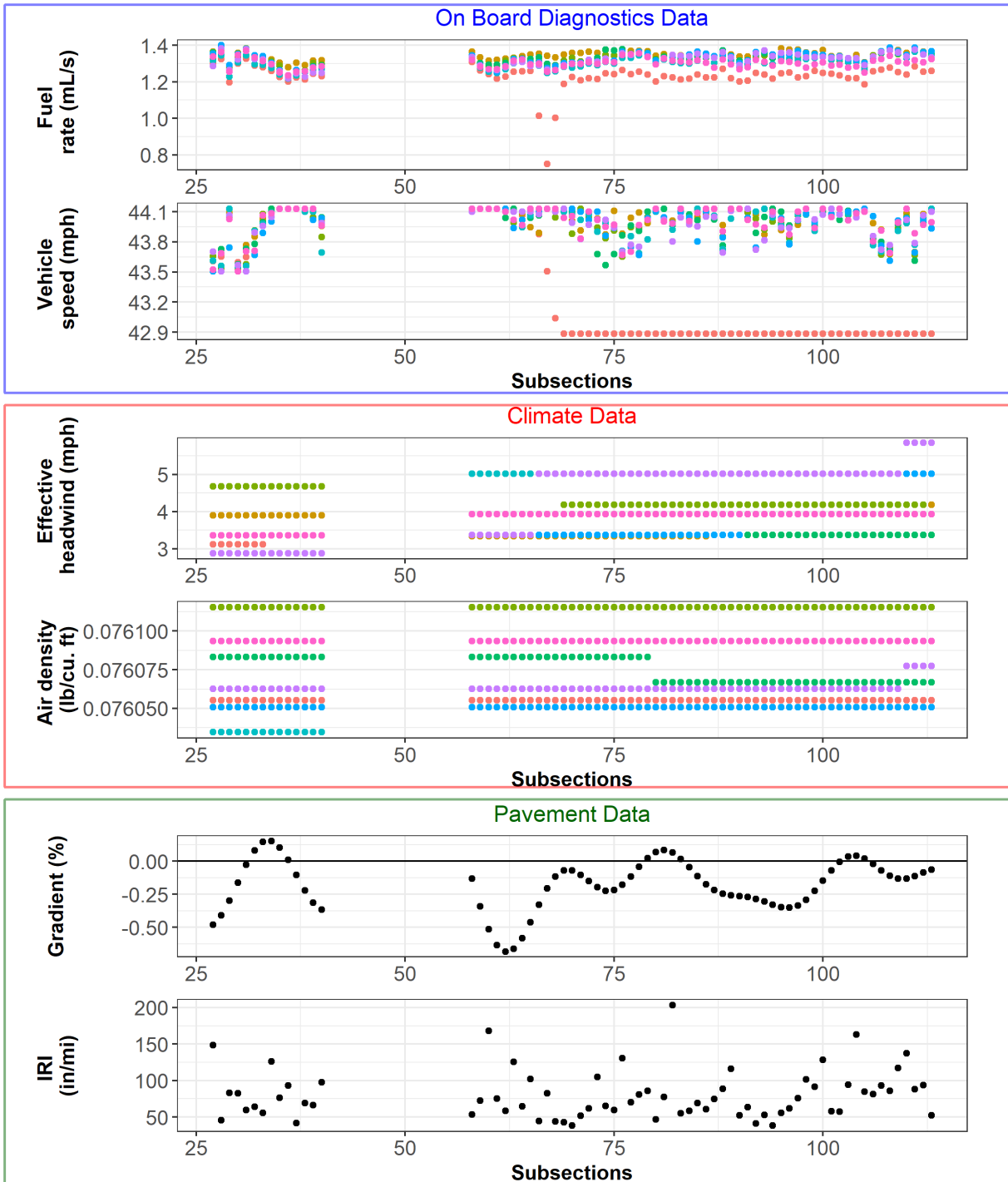


Figure P.155: SUV data on Section PH15.

PH15-YOL-CR32BE-HMA SUV winter_day 35 mph

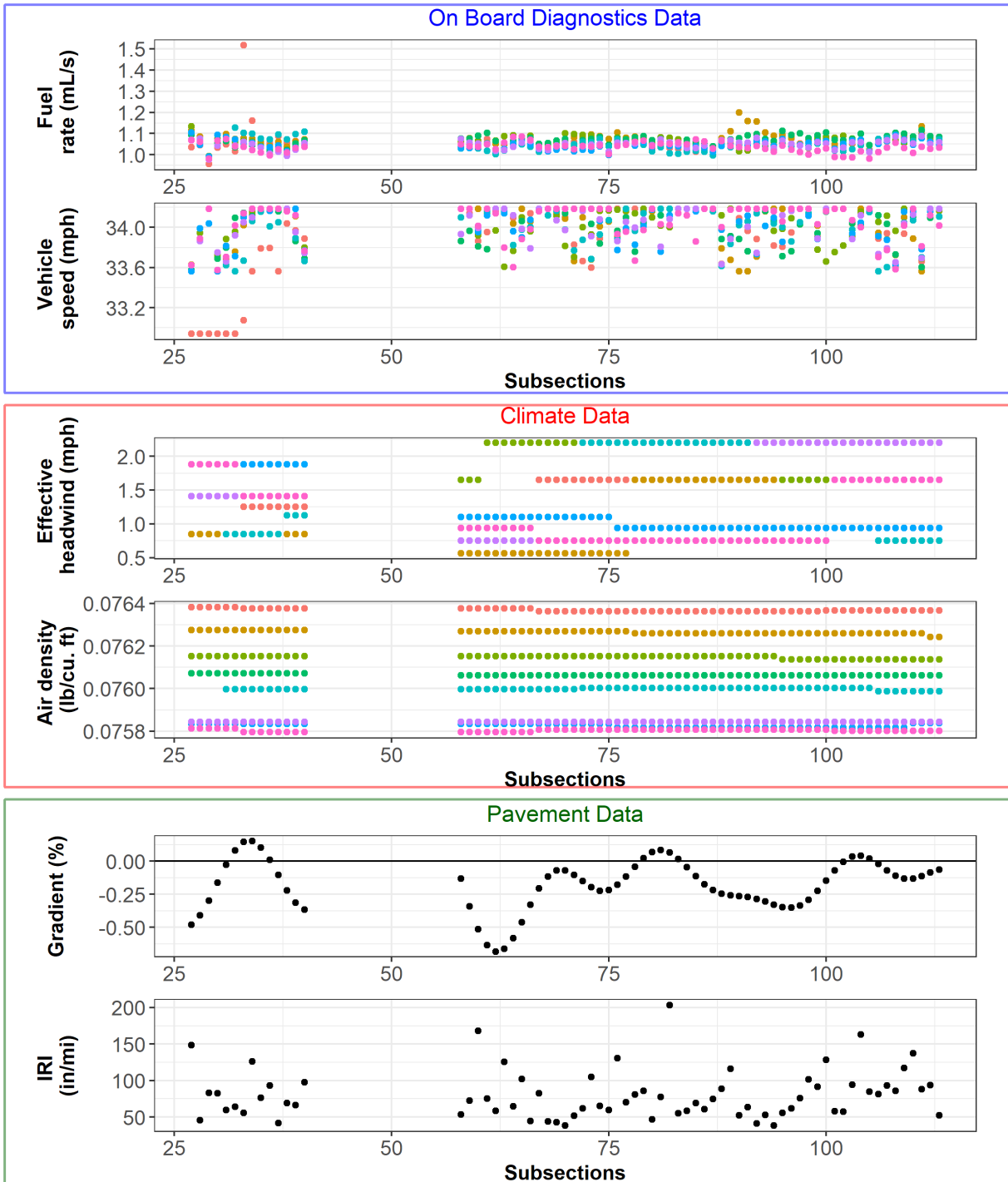


Figure P.156: SUV data on Section PH15.

PH15-YOL-CR32BE-HMA SUV winter_day 45 mph

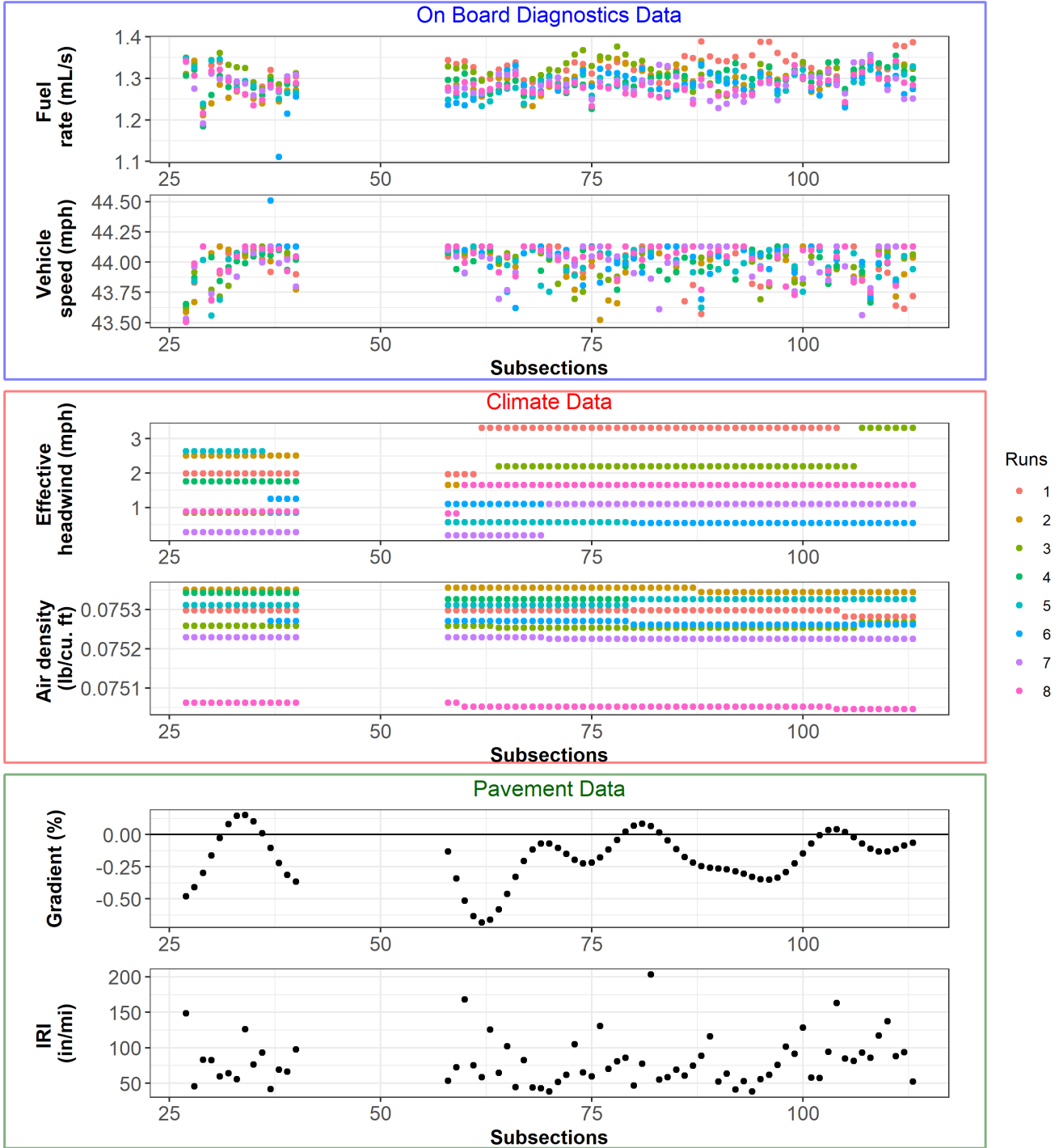


Figure P.157: SUV data on Section PH15.

PH16-STA132E-RHMA-G SUV summer_day 45 mph

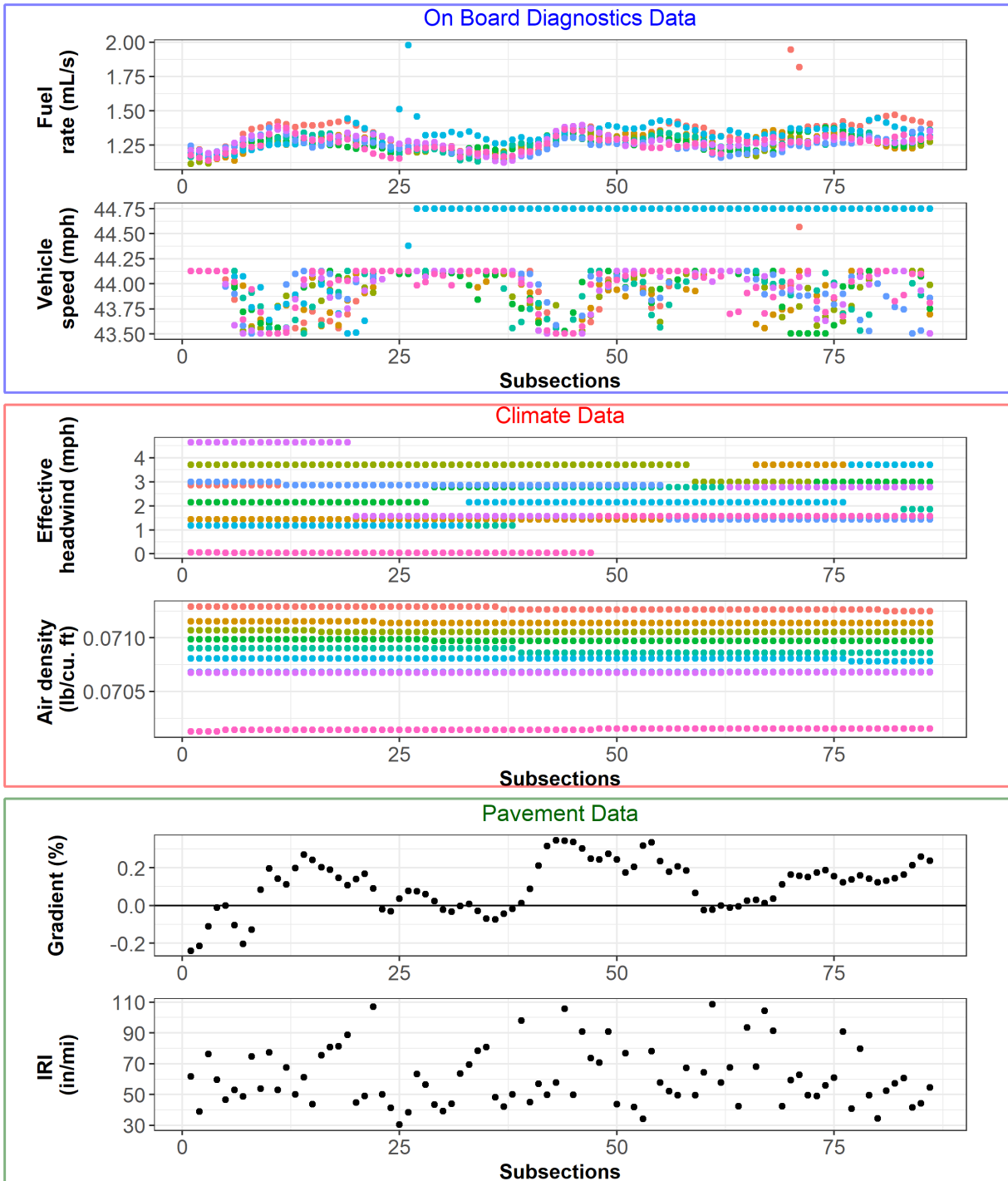


Figure P.158: SUV data on Section PH16.

PH16-STA132E-RHMA-G SUV summer_day 55 mph

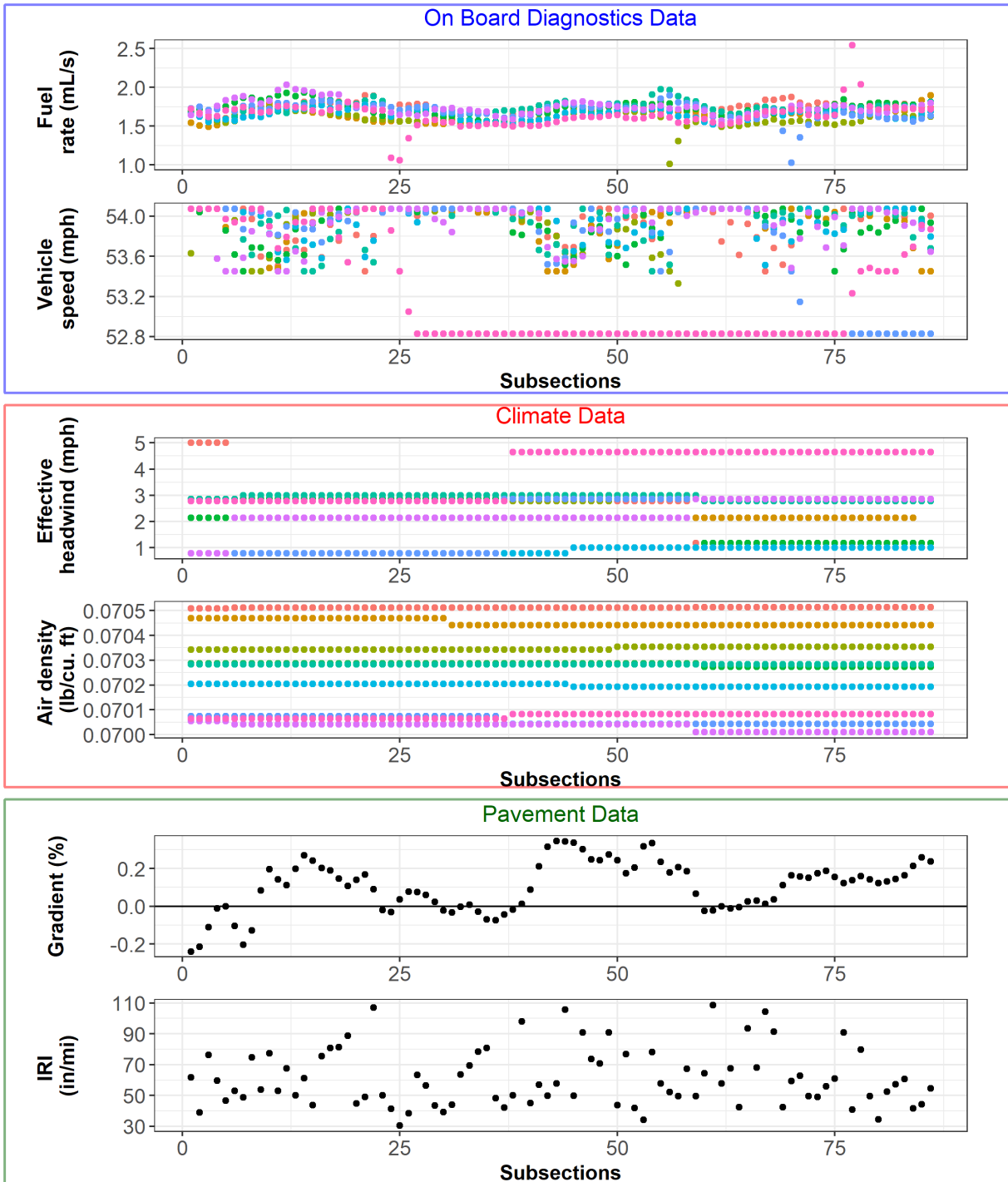


Figure P.159: SUV data on Section PH16.

PH16-STA132E-RHMA-G SUV winter_day 45 mph

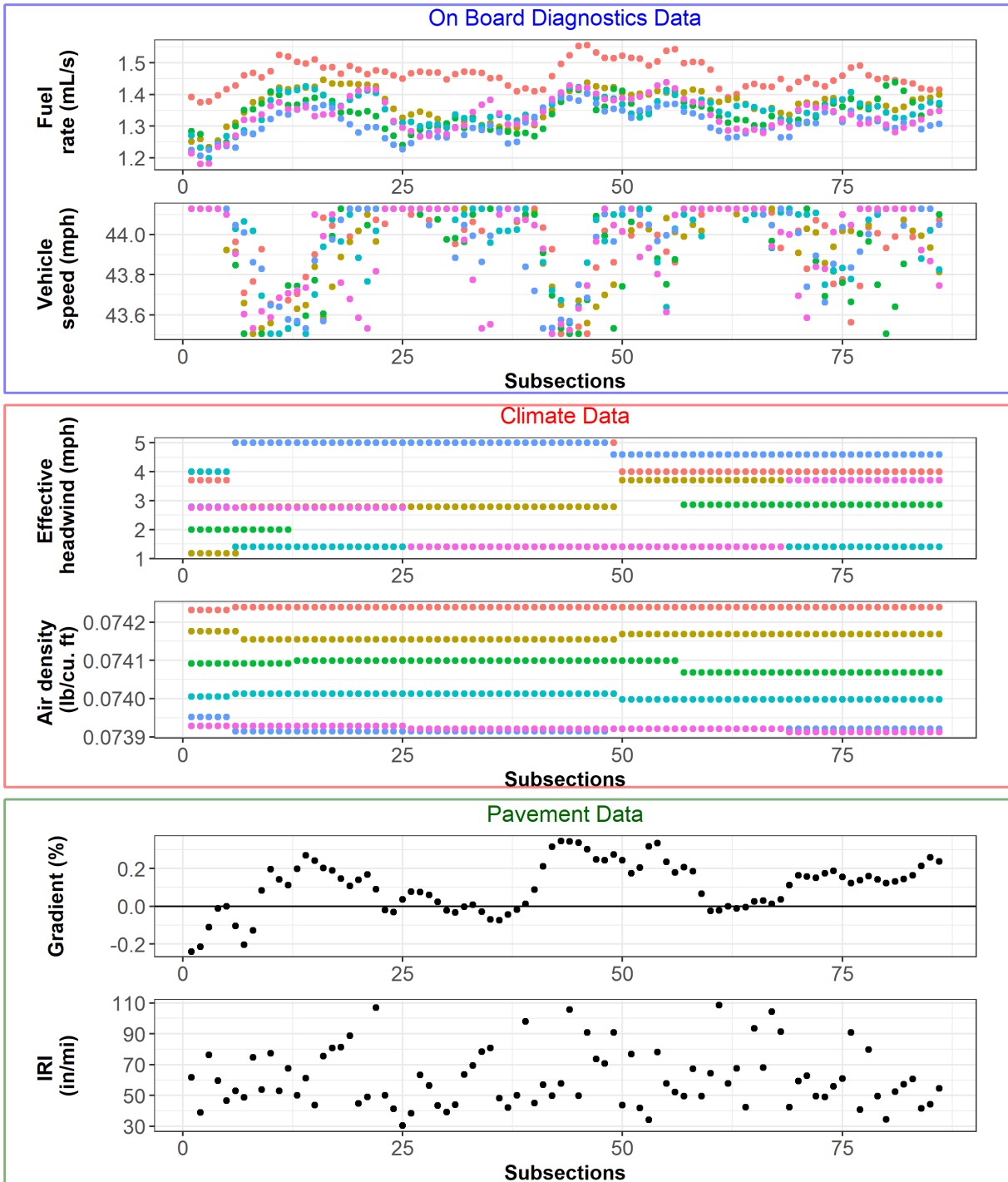


Figure P.160: SUV data on Section PH16.

PH16-STA132E-RHMA-G SUV winter_day 55 mph

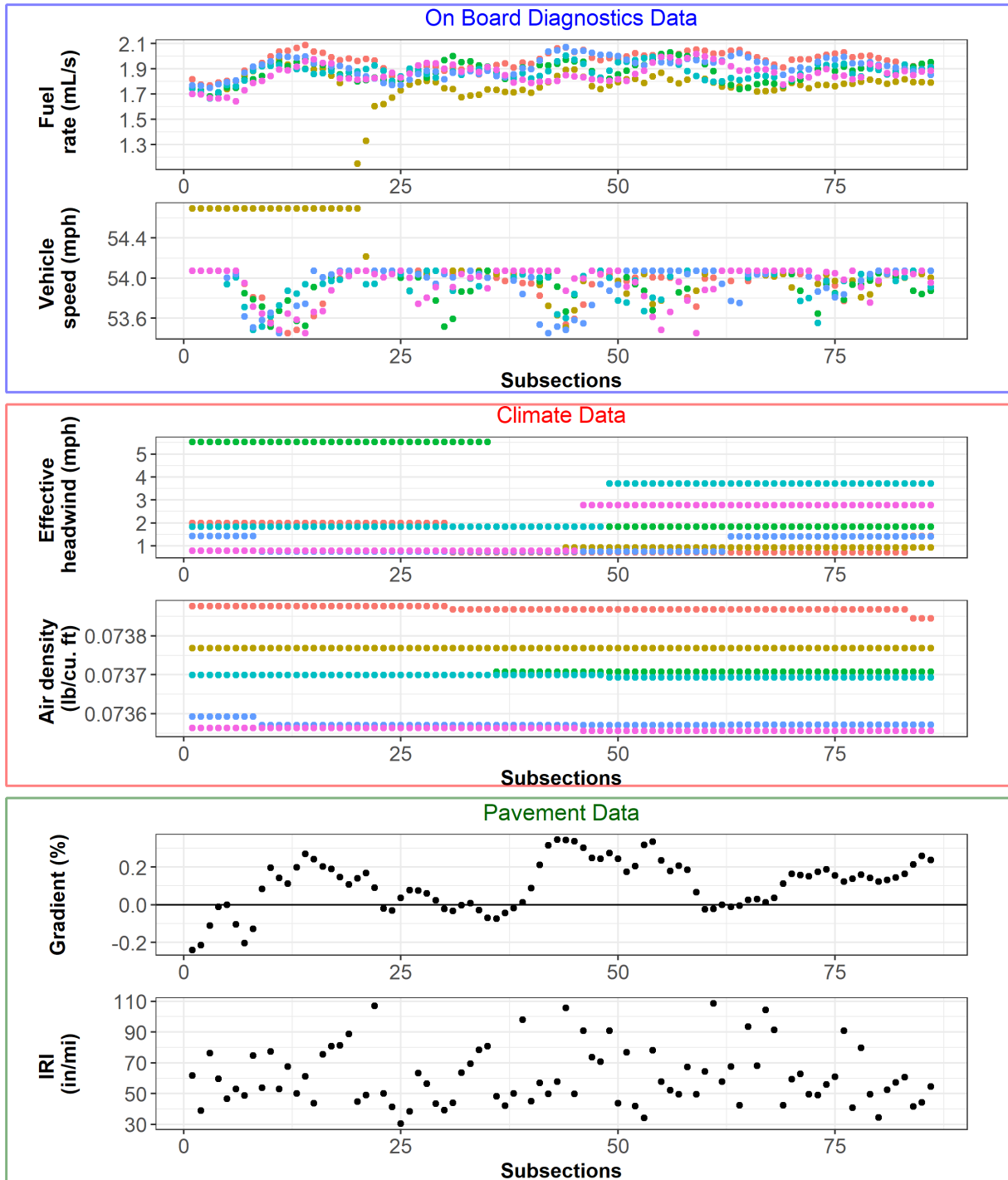


Figure P.161: SUV data on Section PH16.

PH17-STA132W-RHMA-G SUV summer_day 45 mph

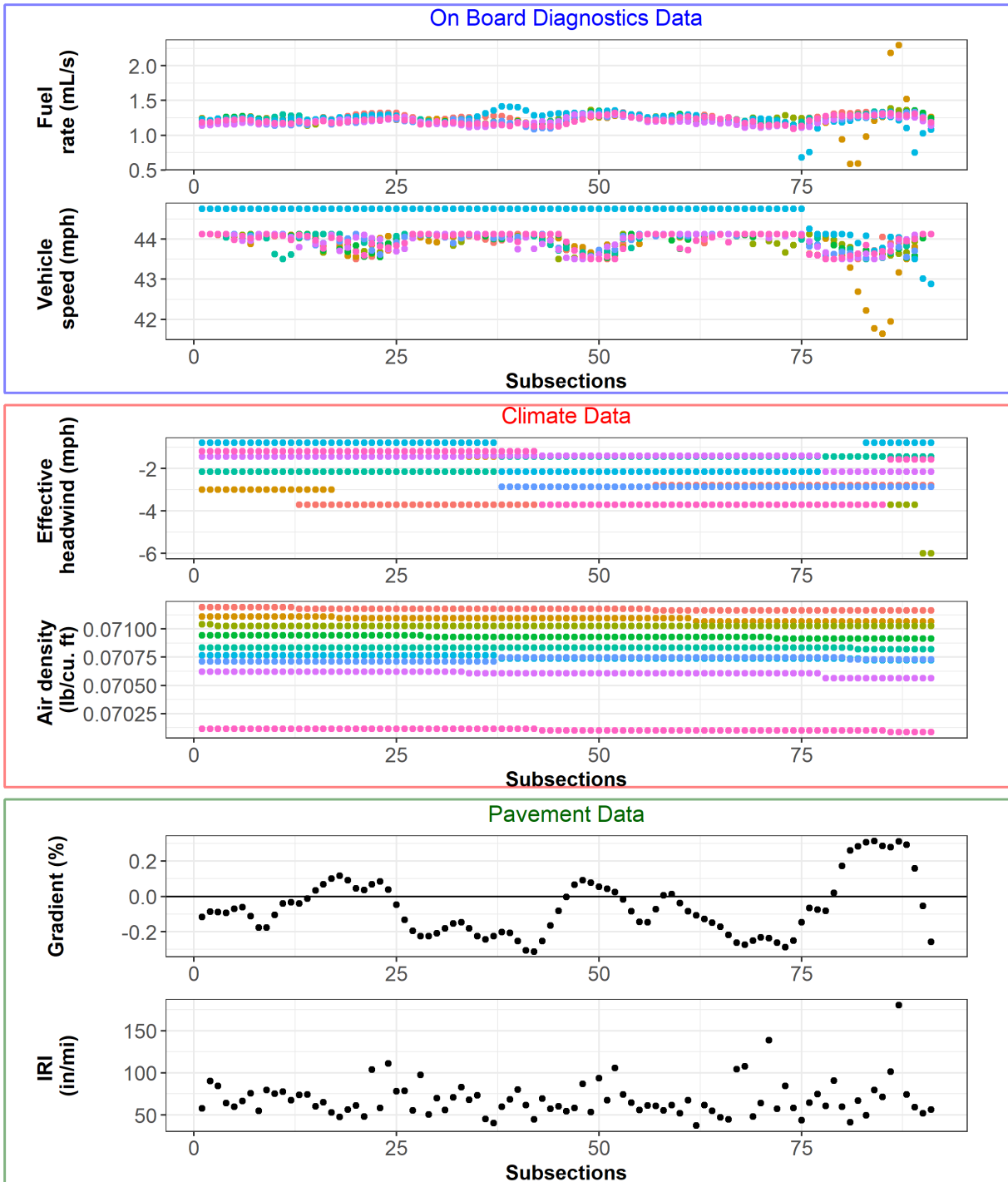


Figure P.162: SUV data on Section PH17.

PH17-STA132W-RHMA-G SUV summer_day 55 mph

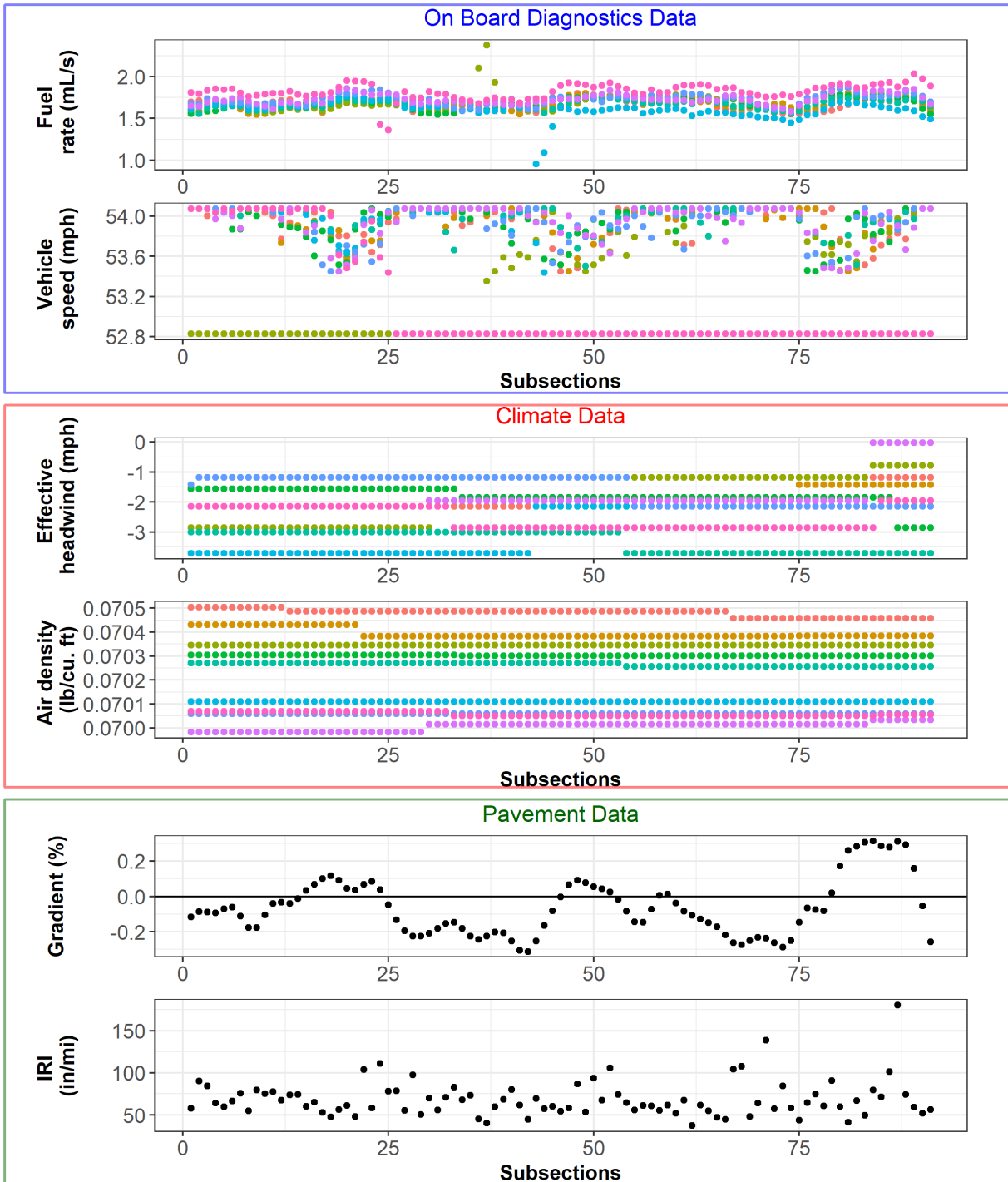


Figure P.163: SUV data on Section PH17.

PH17-STA132W-RHMA-G SUV winter_day 45 mph

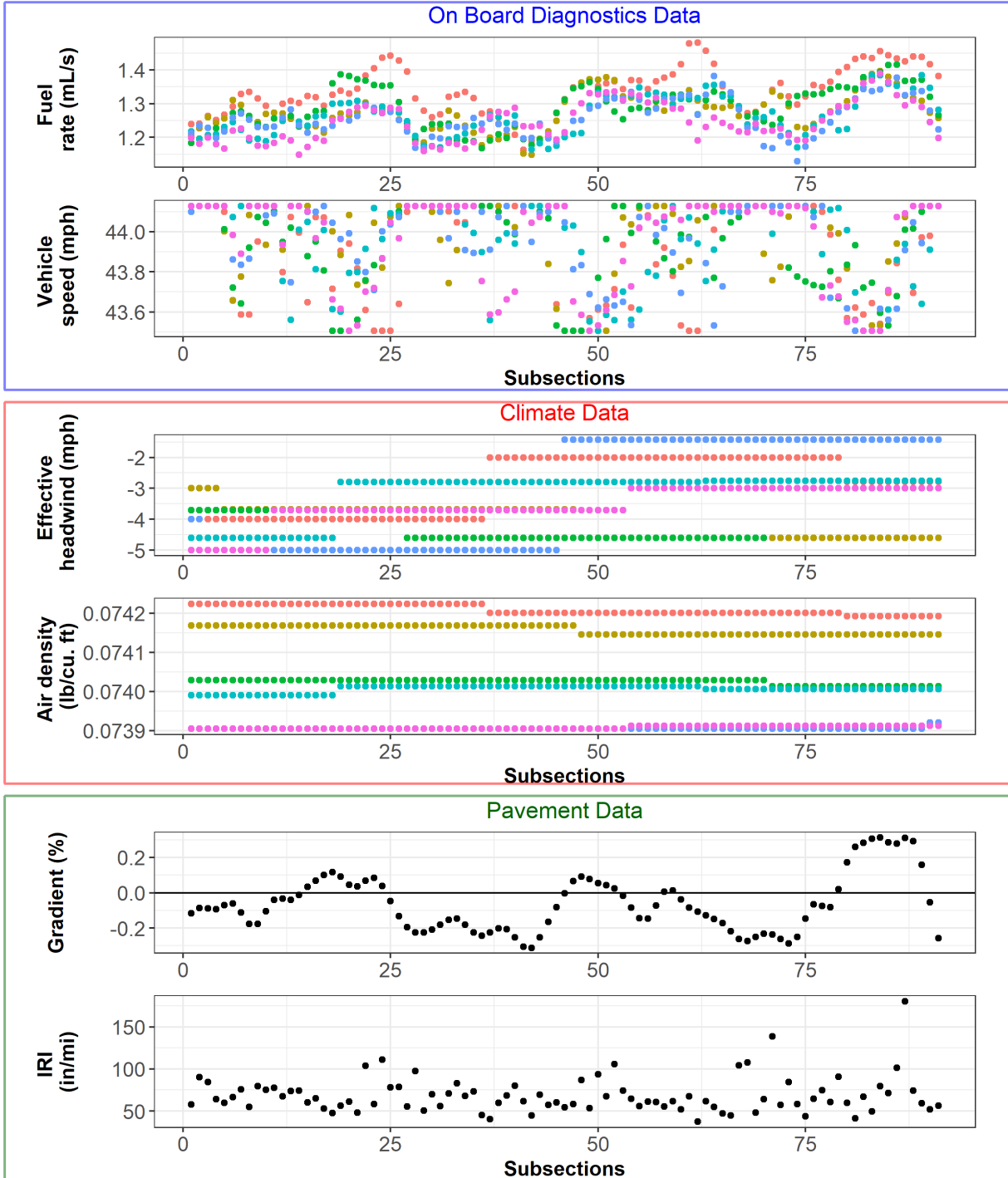


Figure P.164: SUV data on Section PH17.

PH17-STA132W-RHMA-G SUV winter_day 55 mph

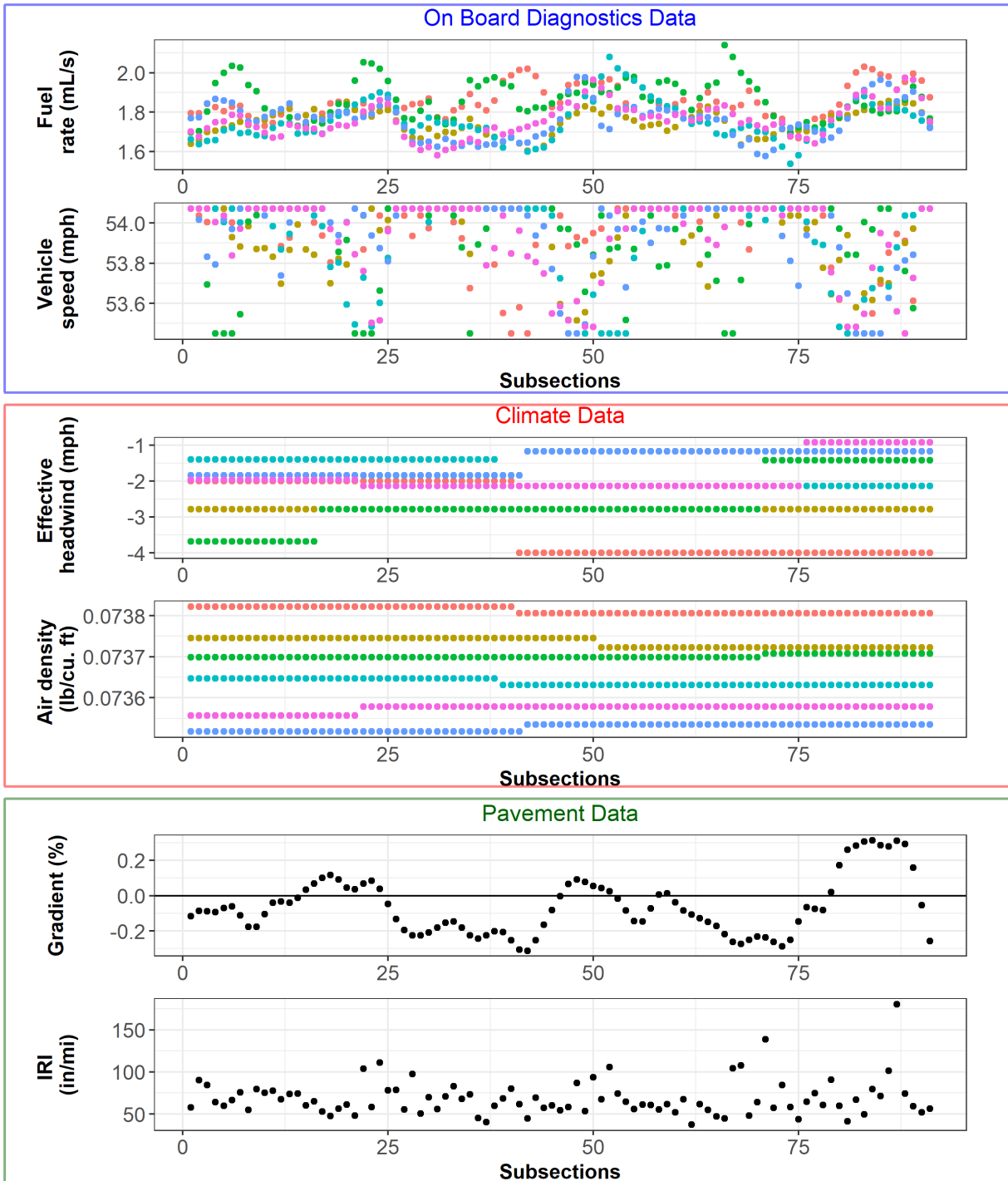


Figure P.165: SUV data on Section PH17.

PH18-KER5S-HMA-O SUV summer_day 45 mph

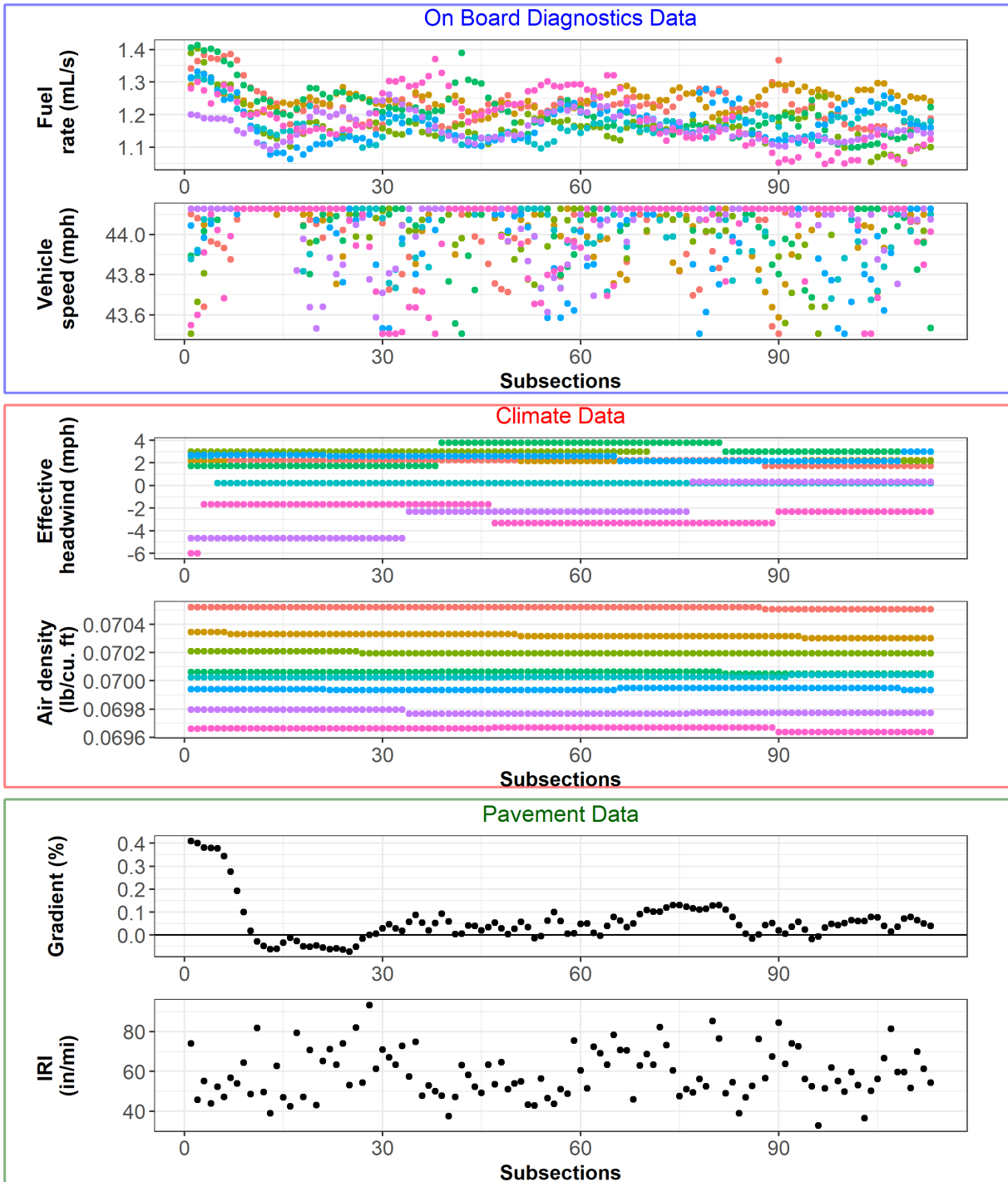


Figure P.166: SUV data on Section PH18.

PH18-KER5S-HMA-O SUV summer_day 55 mph

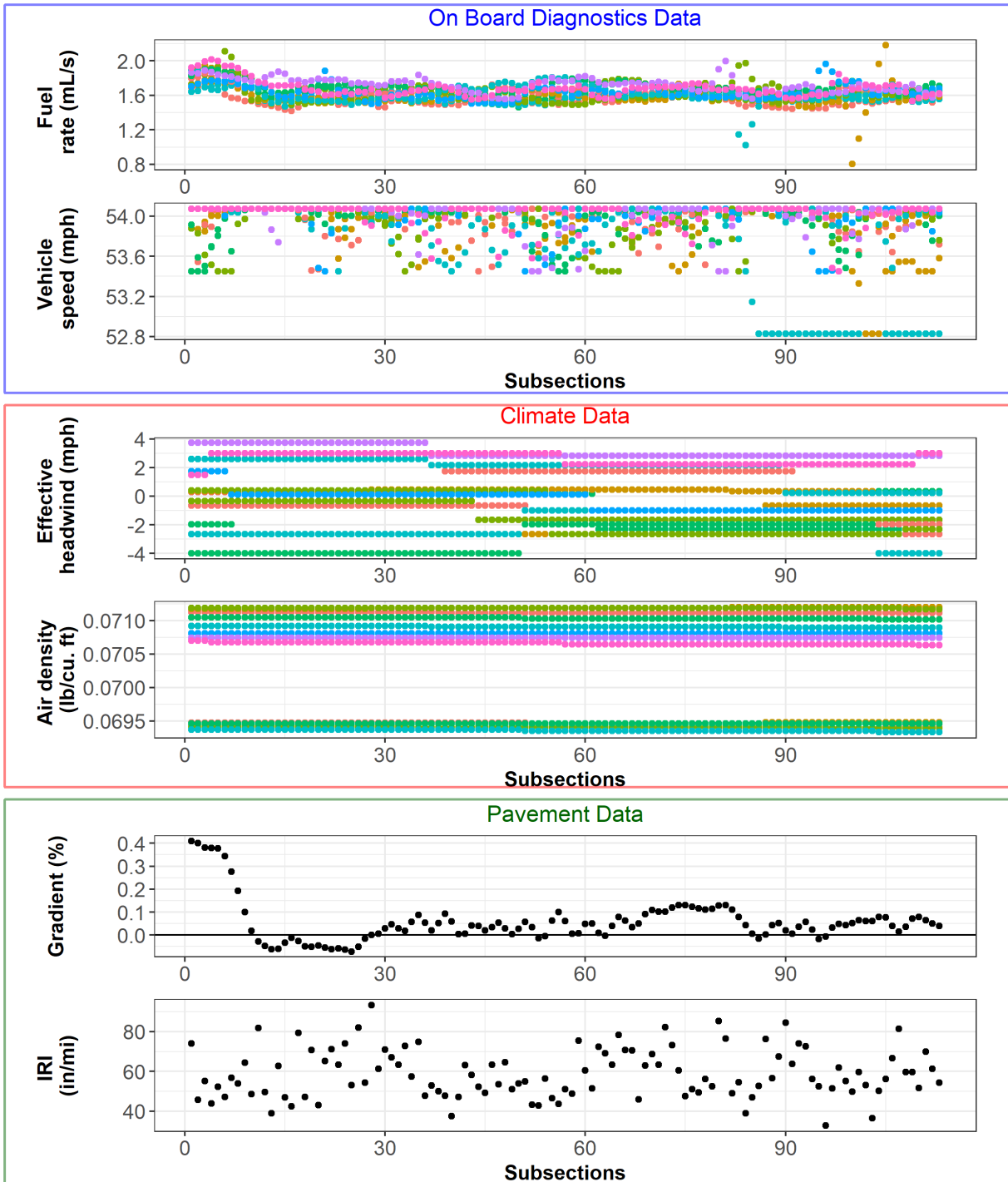


Figure P.167: SUV data on Section PH18.

PH19-KER5N- RHMA-G SUV summer_day 45 mph

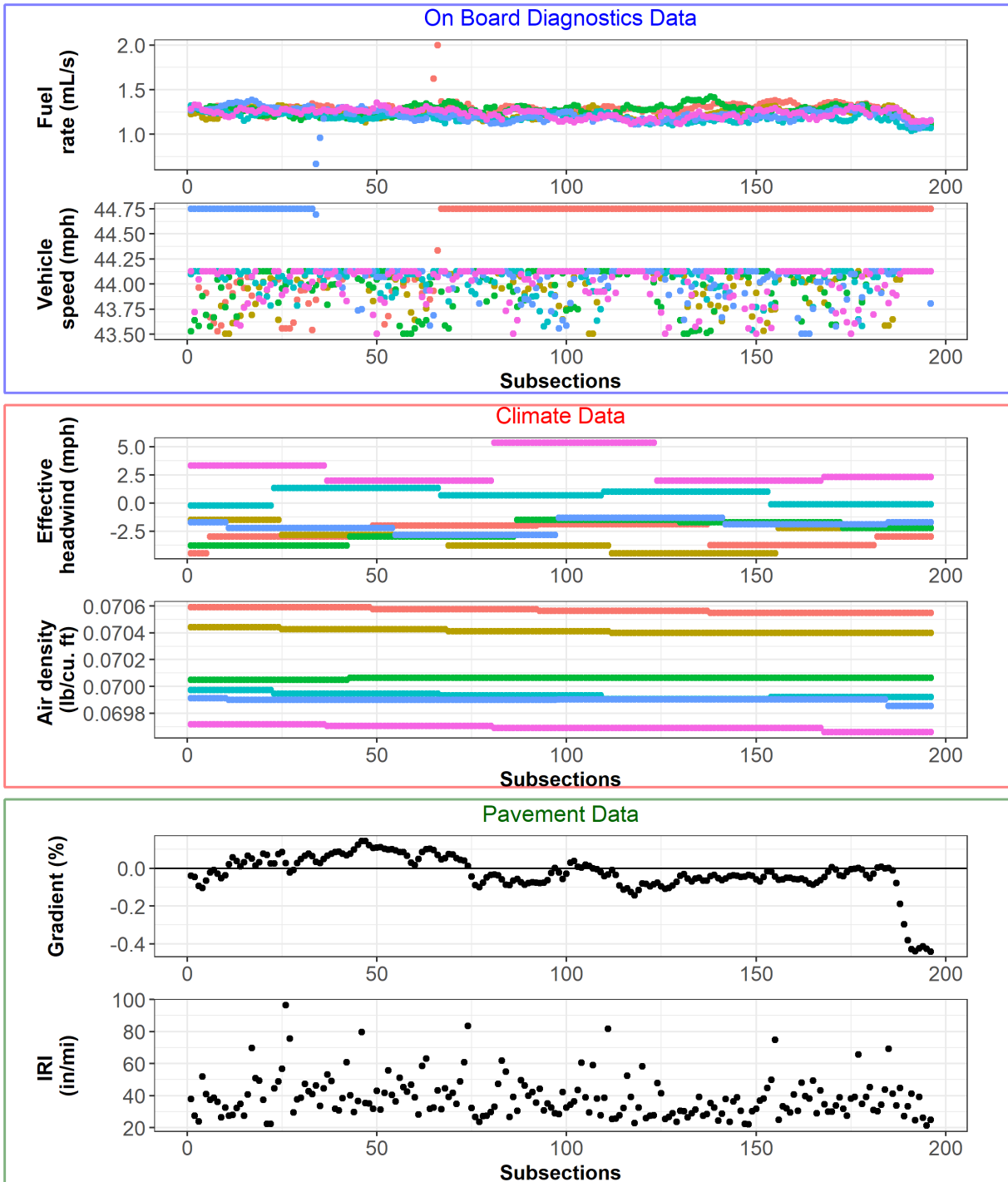


Figure P.168: SUV data on Section PH19.

PH19-KER5N- RHMA-G SUV summer_day 55 mph

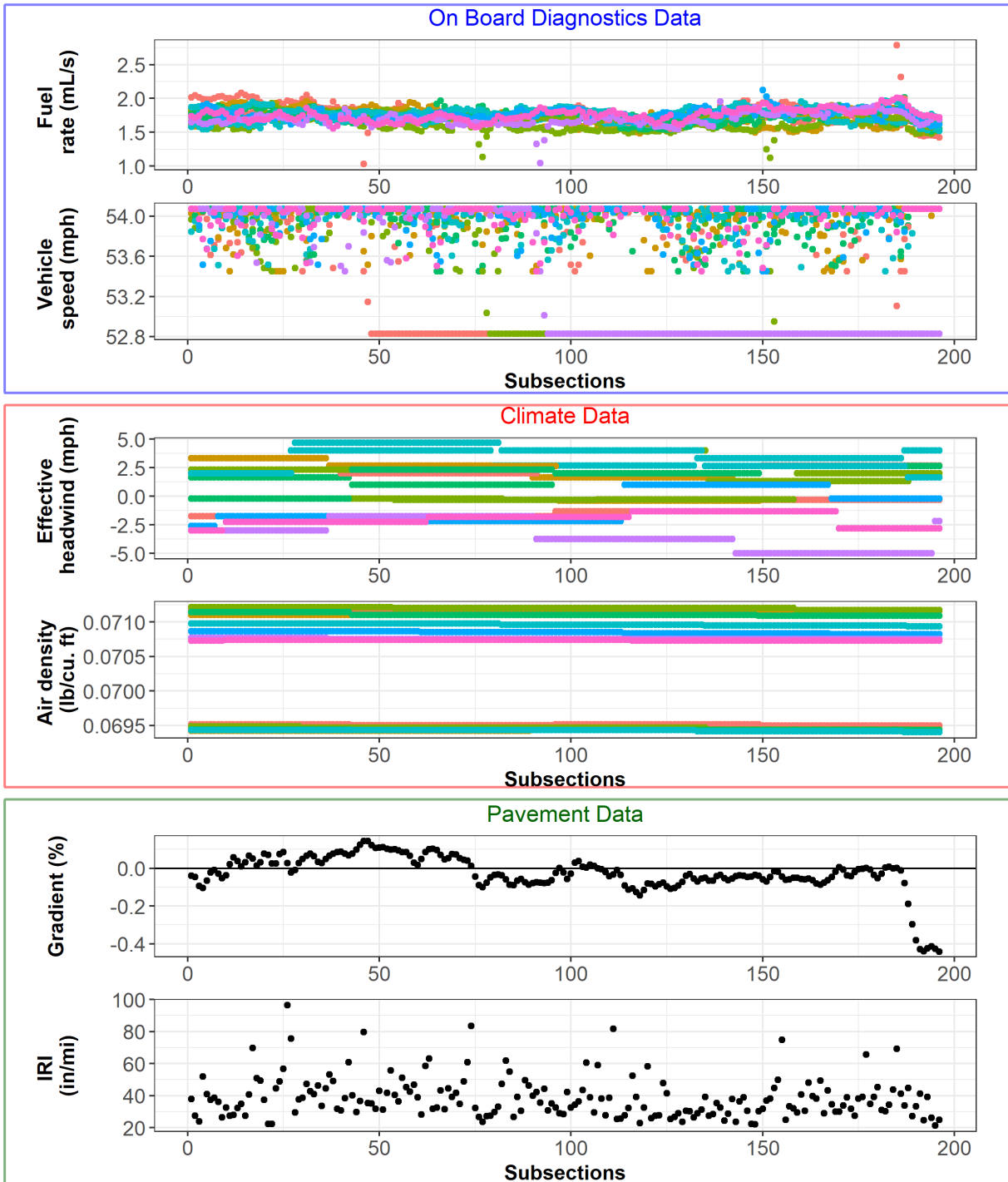


Figure P.169: SUV data on Section PH19.

PH20-KER5S-CRCP SUV summer_day 45 mph

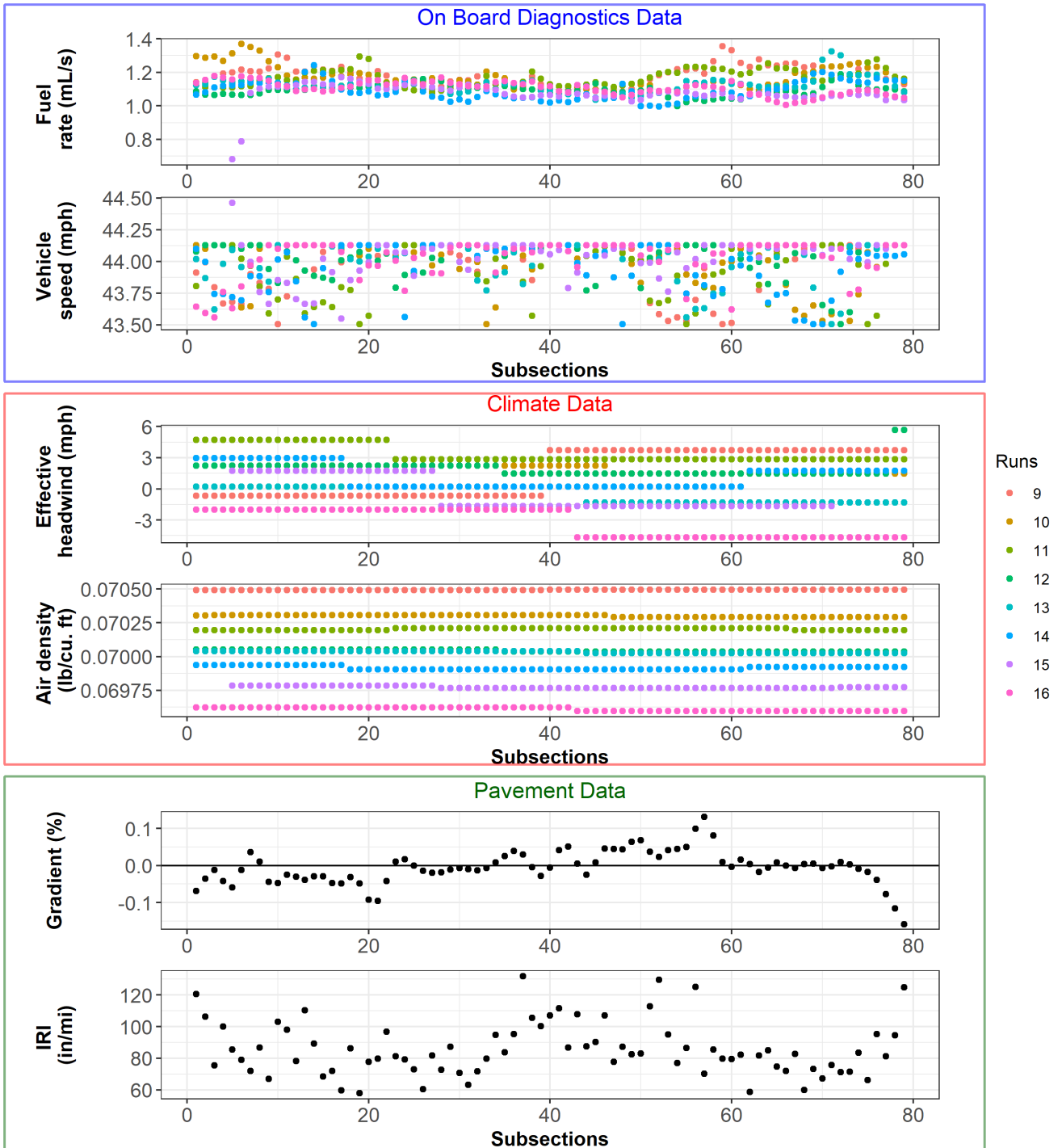


Figure P.170: SUV data on Section PH20.

PH20-KER5S-CRCP SUV summer_day 55 mph

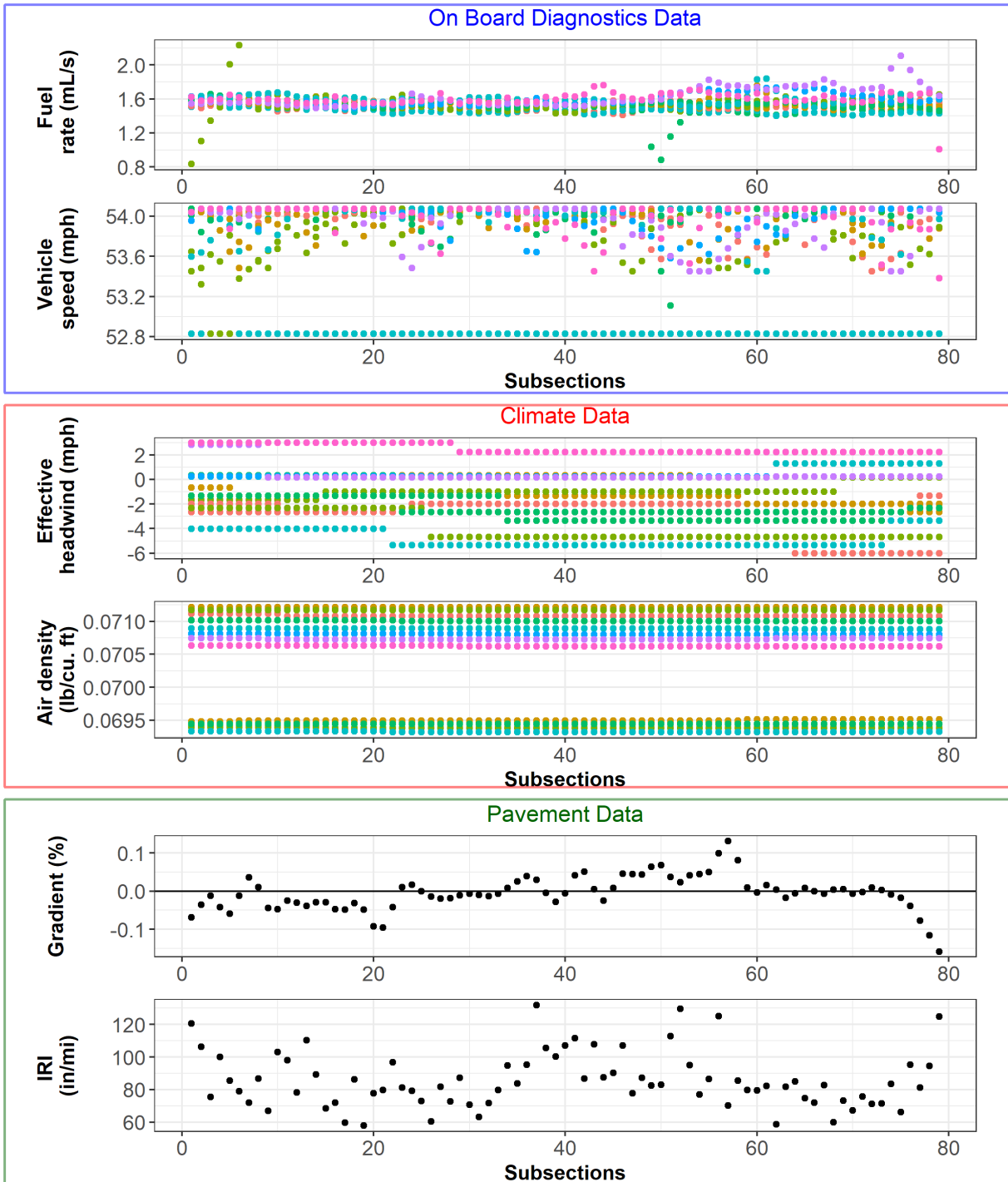


Figure P.171: SUV data on Section PH20.

PH21-YOL99N-JPC SUV summer_day 45 mph

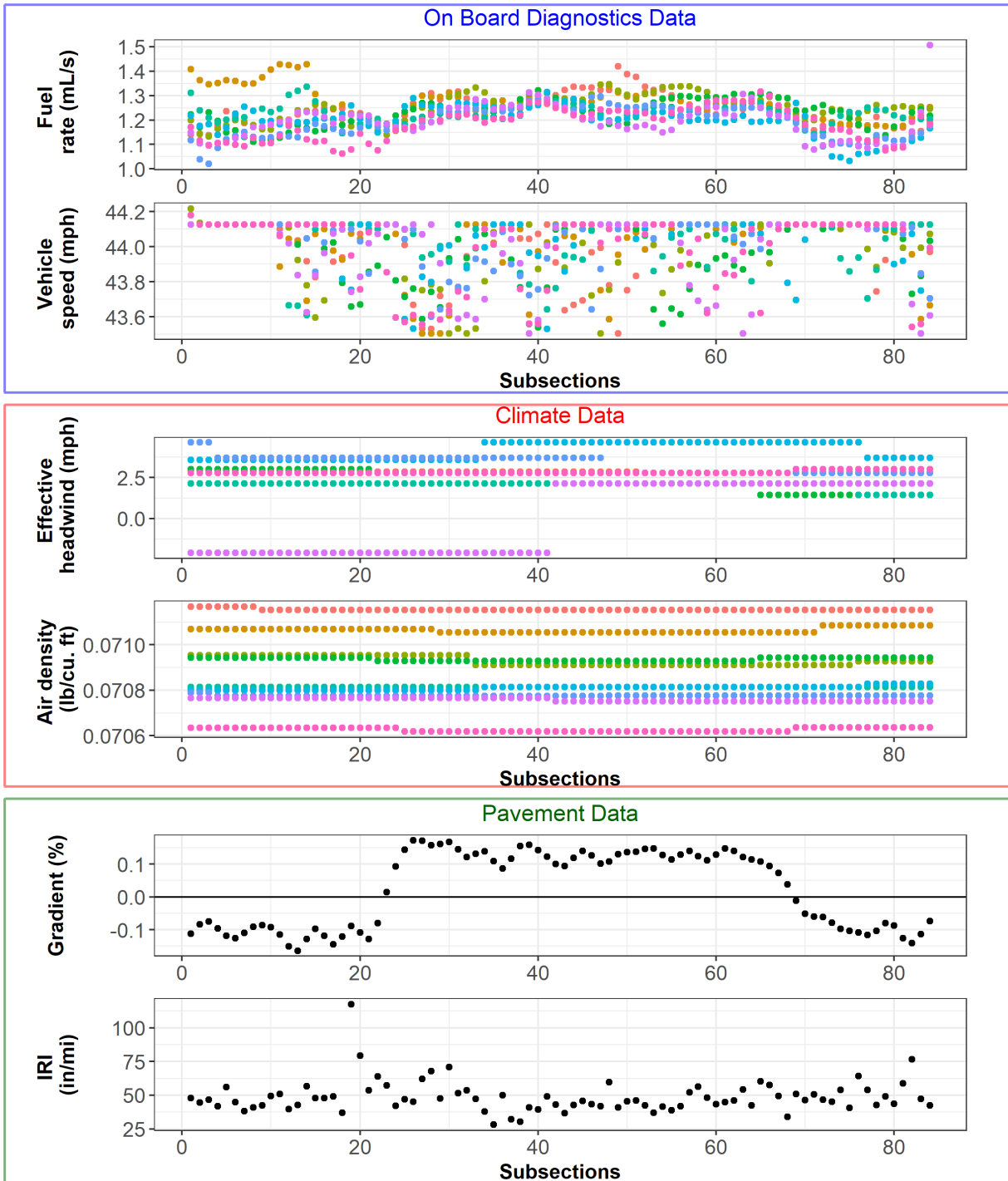


Figure P.172: SUV data on Section PH21.

PH21-YOL99N-JPC SUV summer_day 55 mph

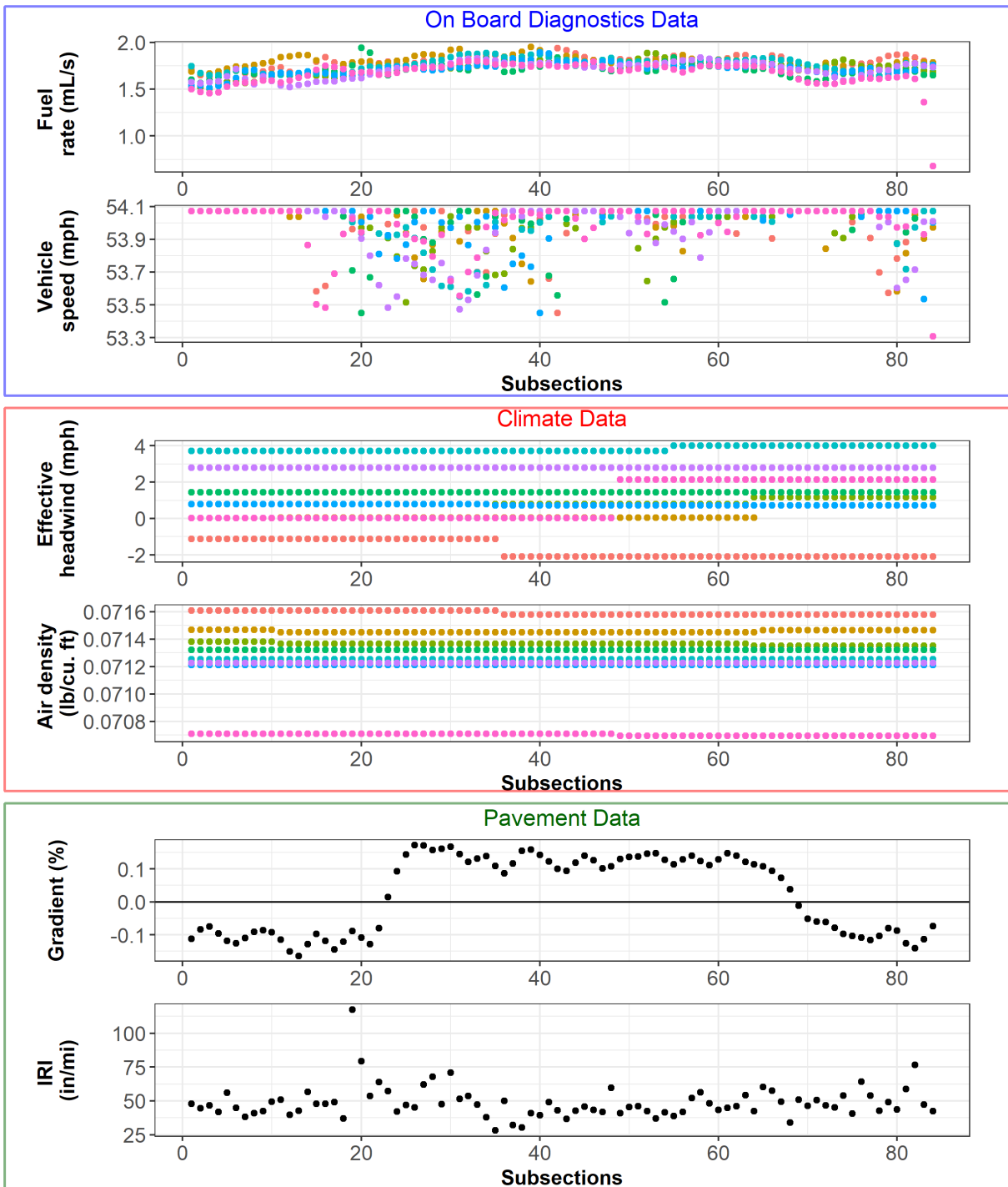


Figure P.173: SUV data on Section PH21.

PH21-YOL99N-JPC SUV winter_day 45 mph

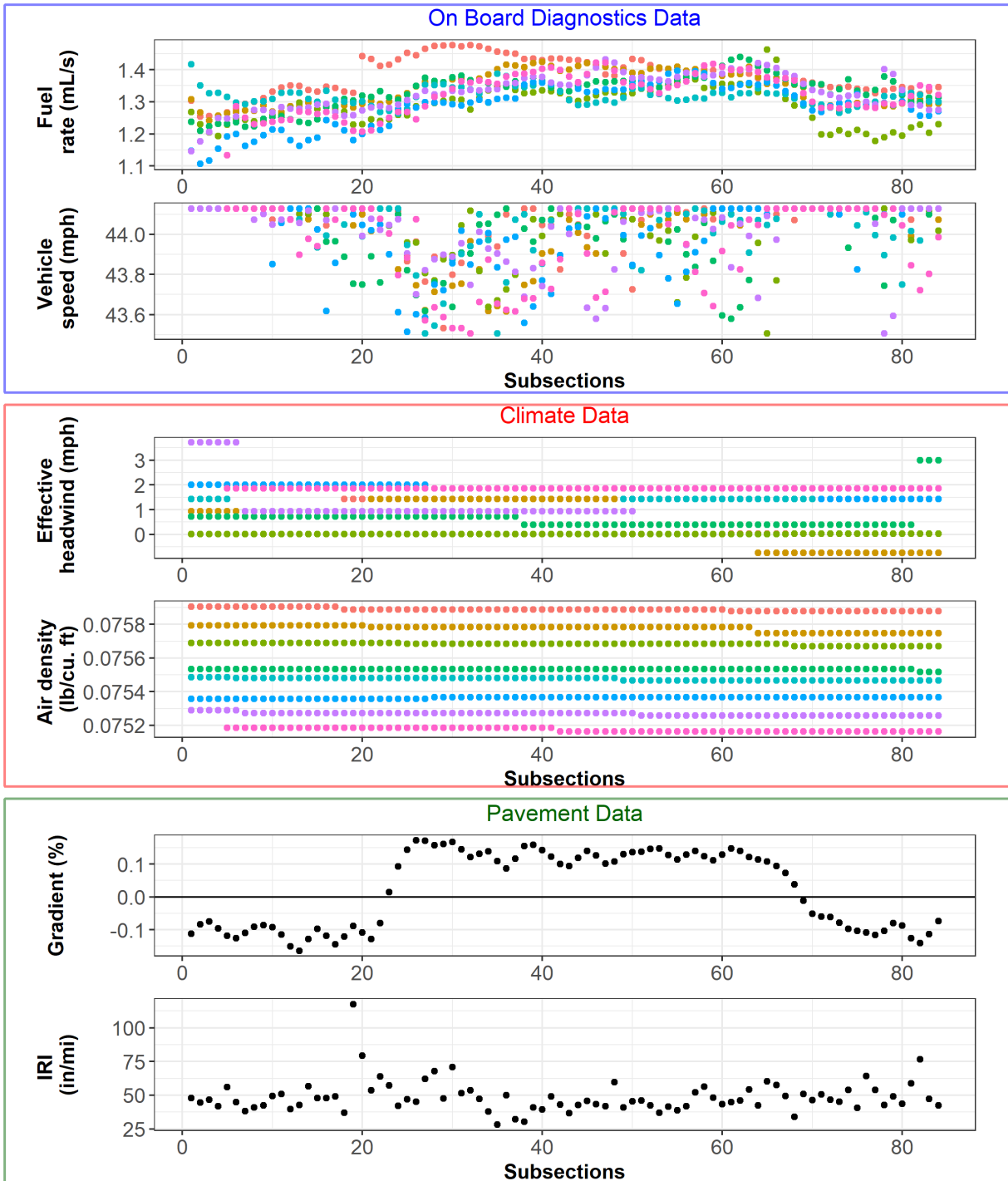


Figure P.174: SUV data on Section PH21.

PH21-YOL99N-JPC SUV winter_day 55 mph

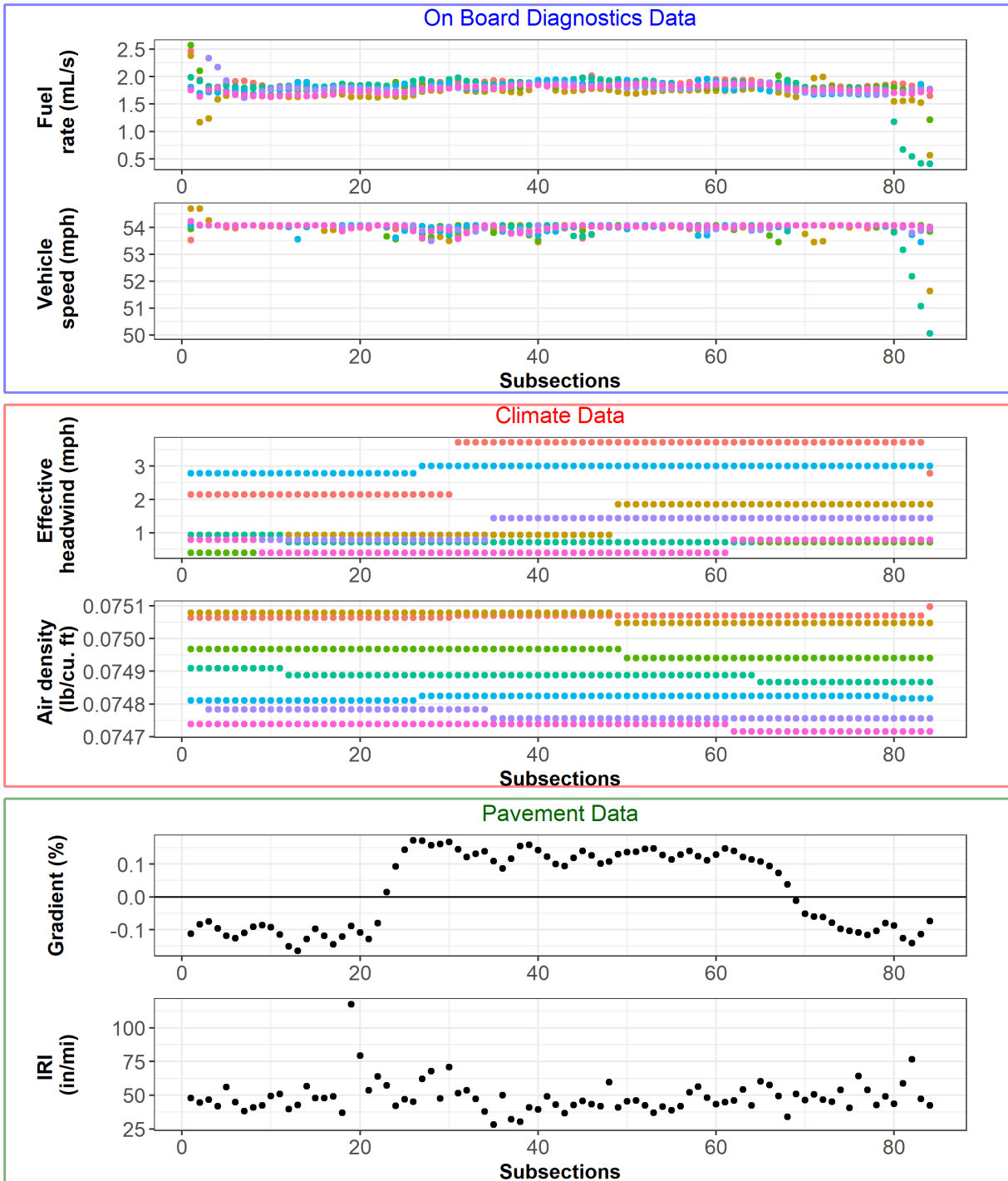


Figure P.175: SUV data on Section PH21.

PH22-YOL99S-JPC SUV summer_day 45 mph

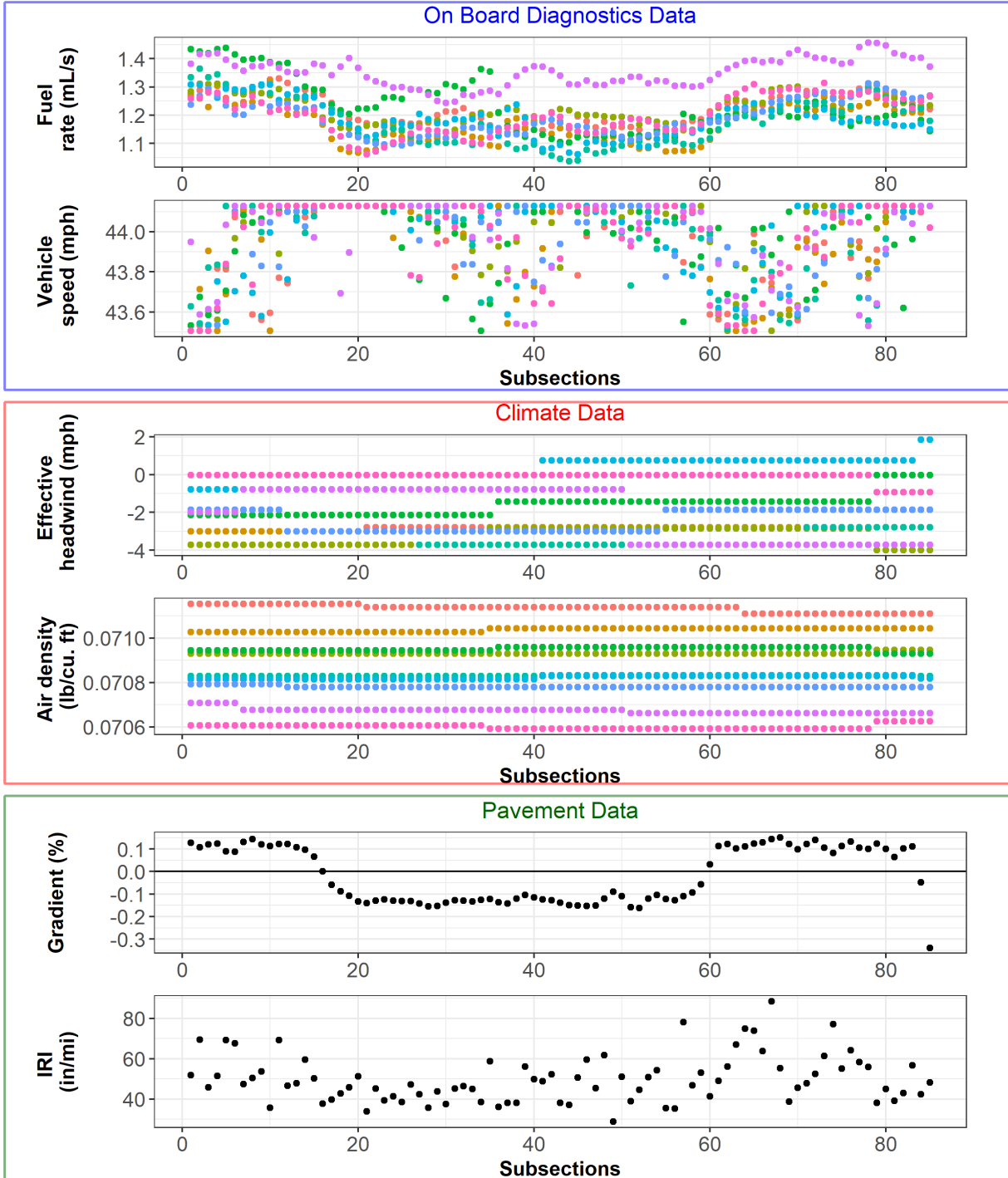
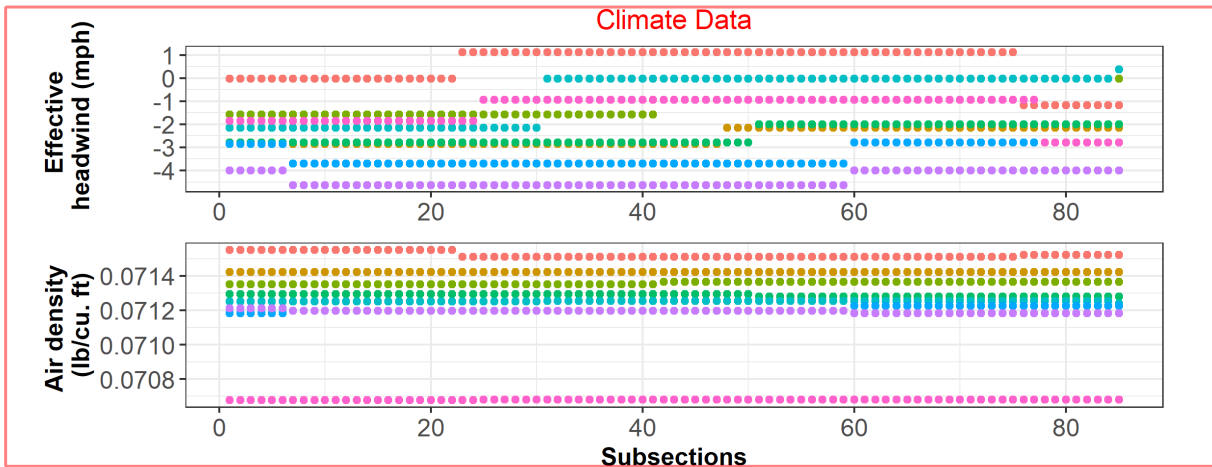
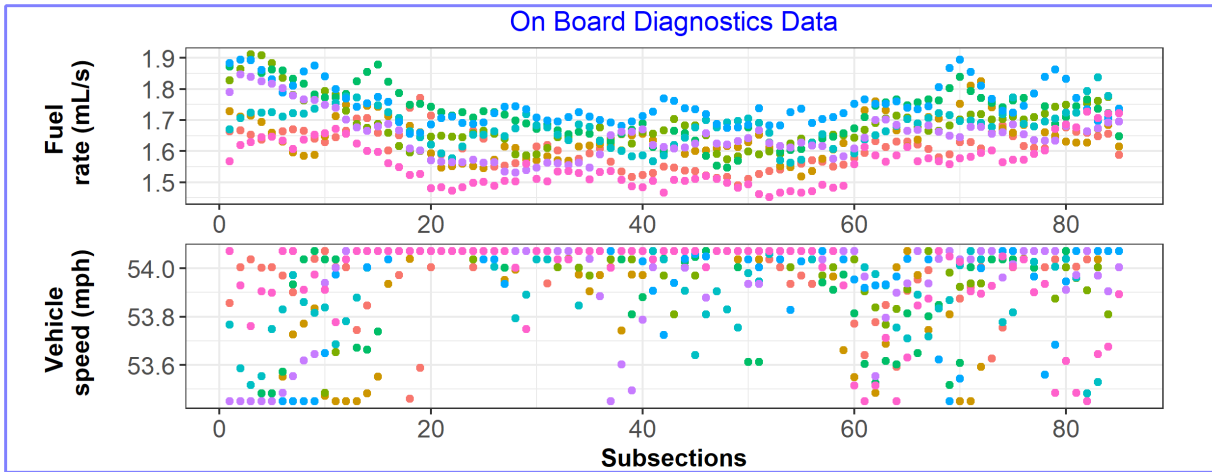


Figure P.176: SUV data on Section PH22.

PH22-YOL99S-JPC SUV summer_day 55 mph



- Runs
- 1
 - 2
 - 3
 - 4
 - 5
 - 6
 - 7
 - 16

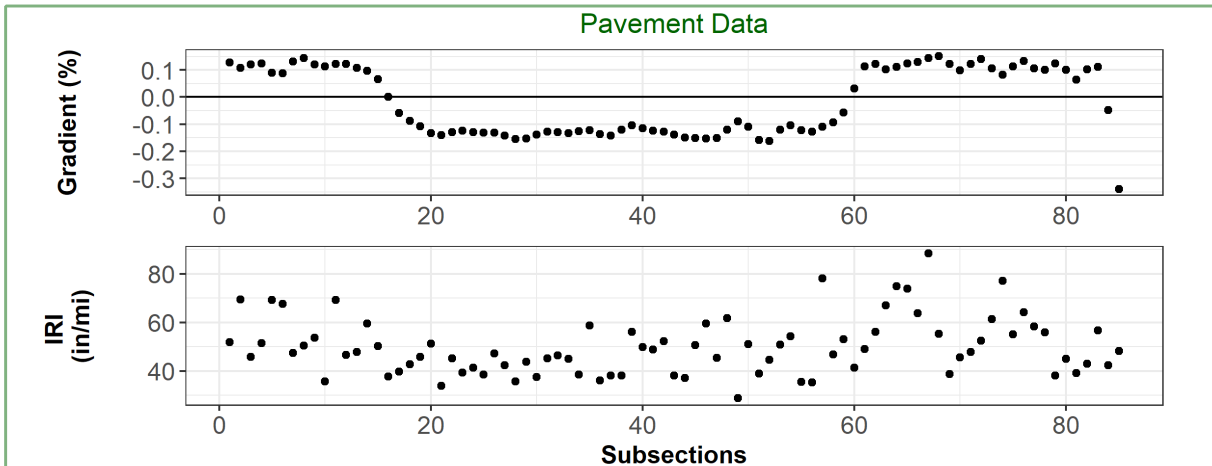


Figure P.177: SUV data on Section PH22.

PH22-YOL99S-JPC SUV winter_day 45 mph

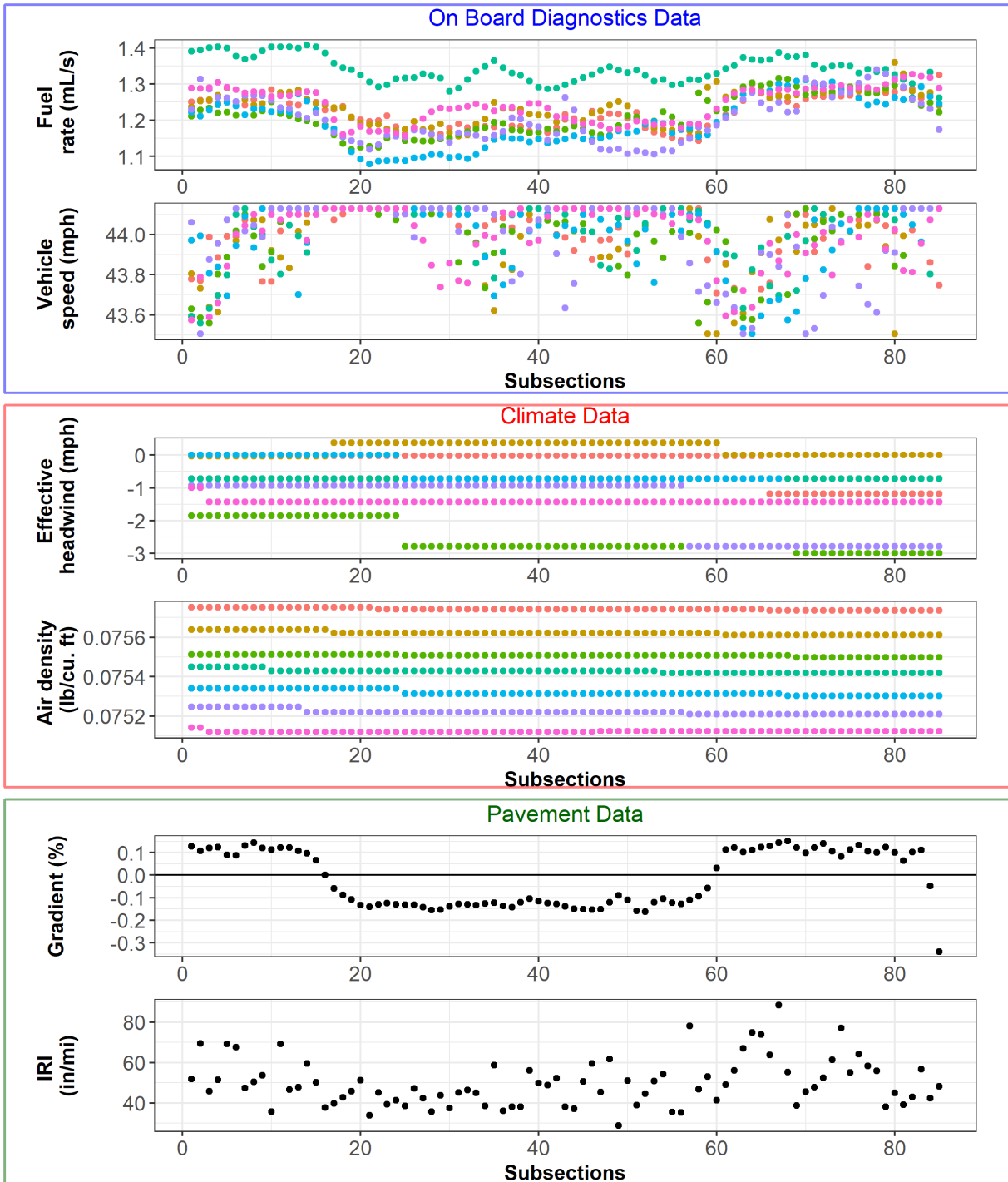


Figure P.178: SUV data on Section PH22.

PH22-YOL99S-JPC SUV winter_day 55 mph

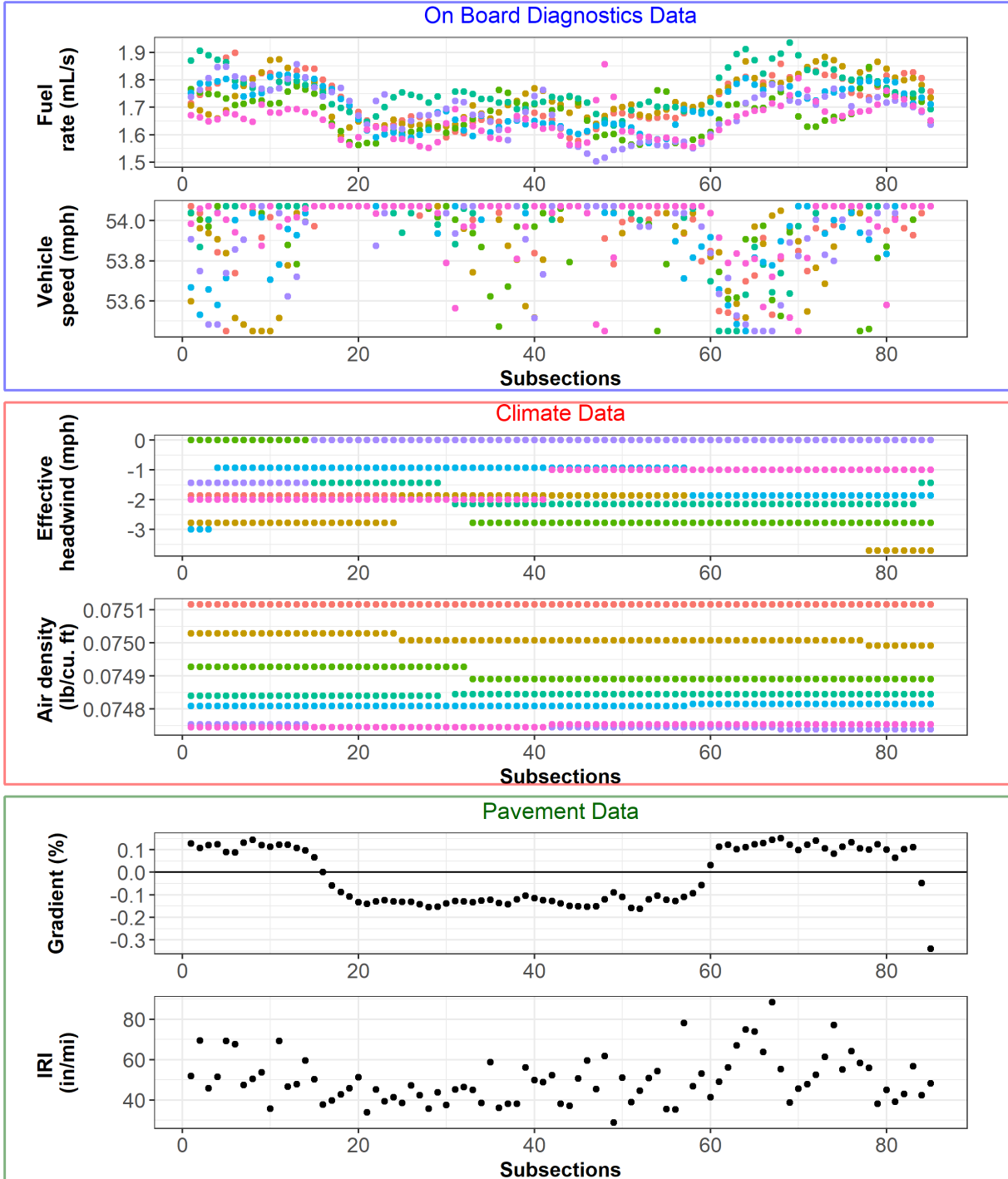


Figure P.179: SUV data on Section PH22.

PH23-YOL-CR32AW-JPC SUV summer_day 35 mph

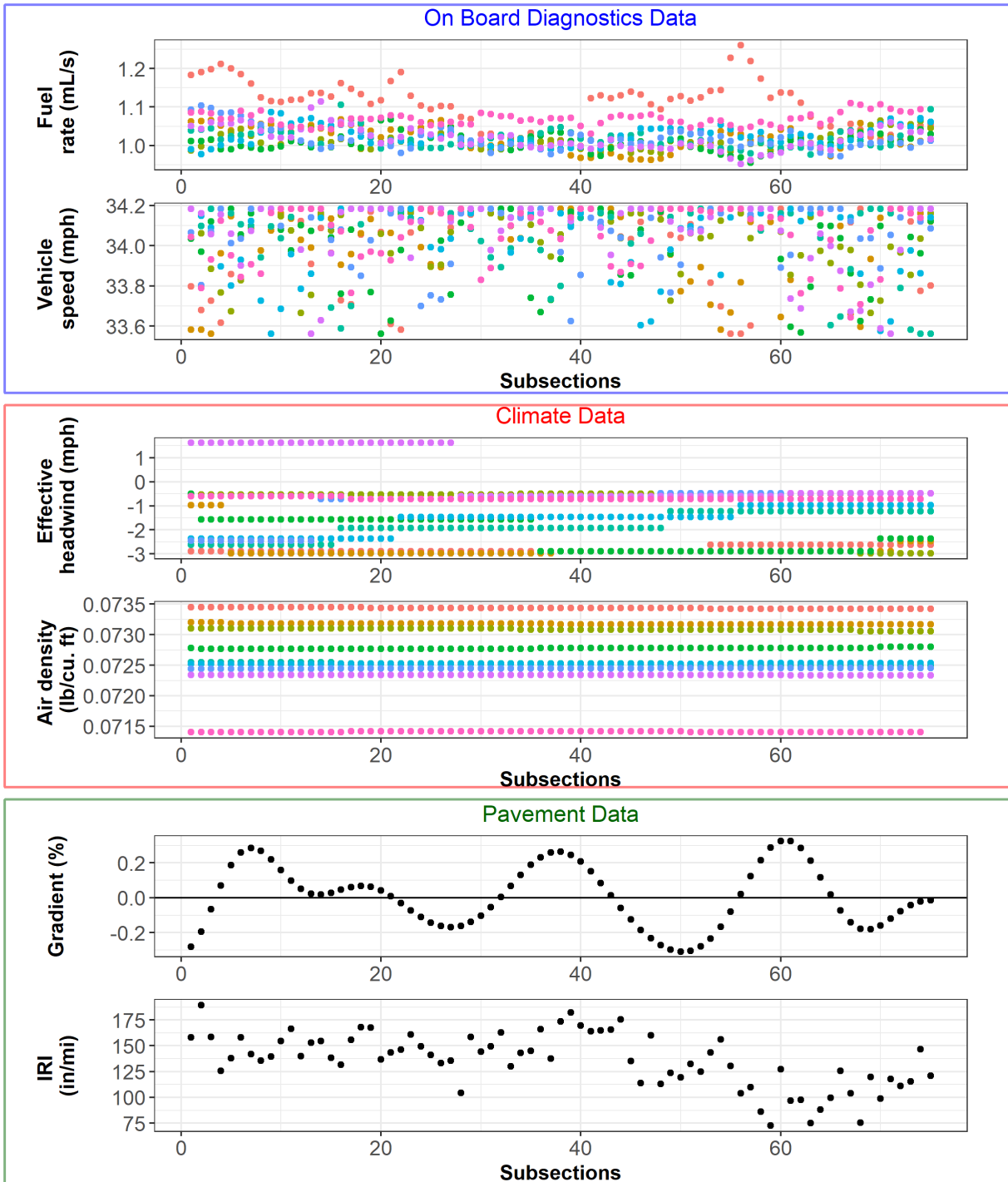


Figure P.180: SUV data on Section PH23.

PH23-YOL-CR32AW-JPC SUV summer_day 45 mph

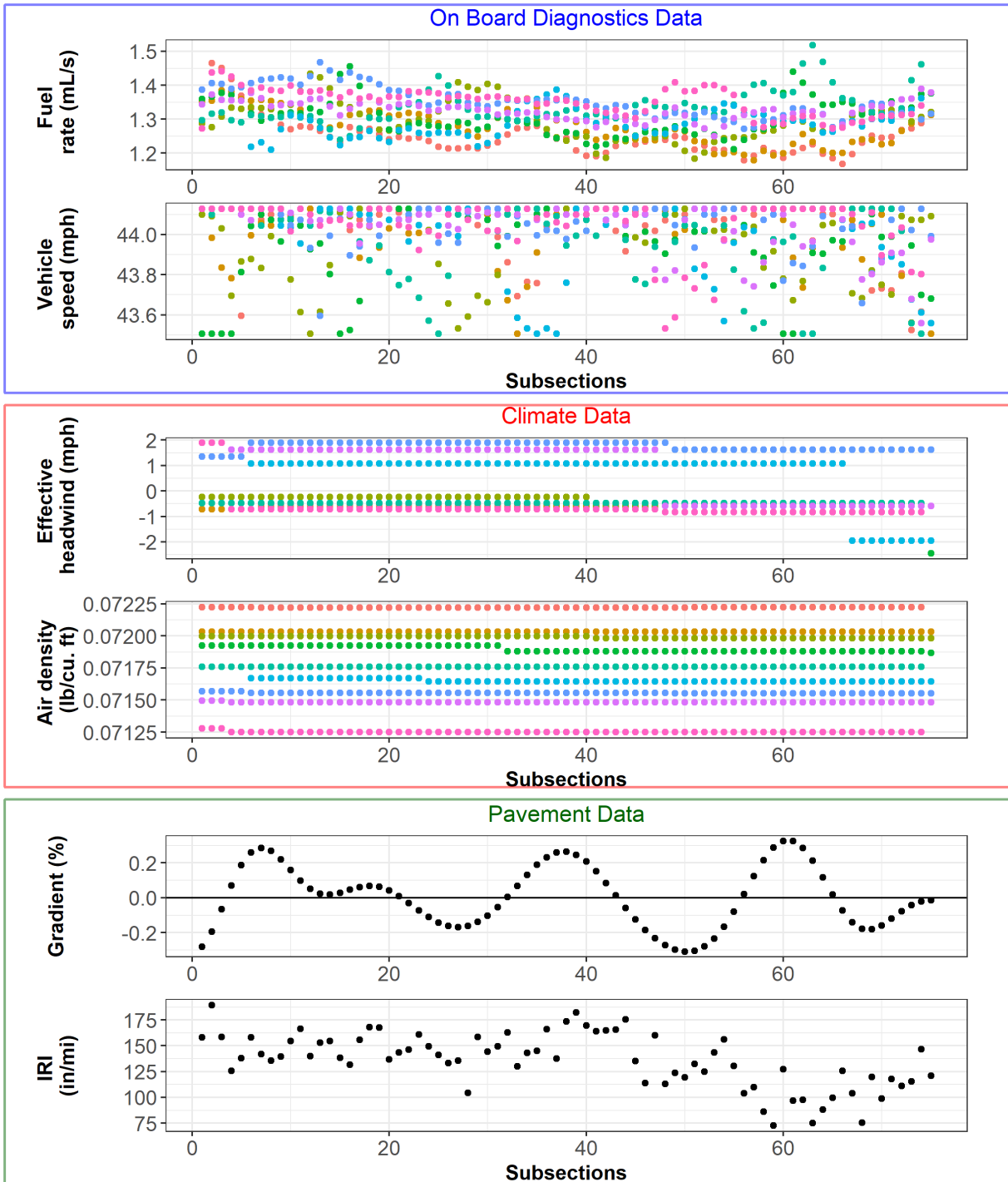


Figure P.181: SUV data on Section PH23.

PH23-YOL-CR32AW-JPC SUV summer_night 35 mph

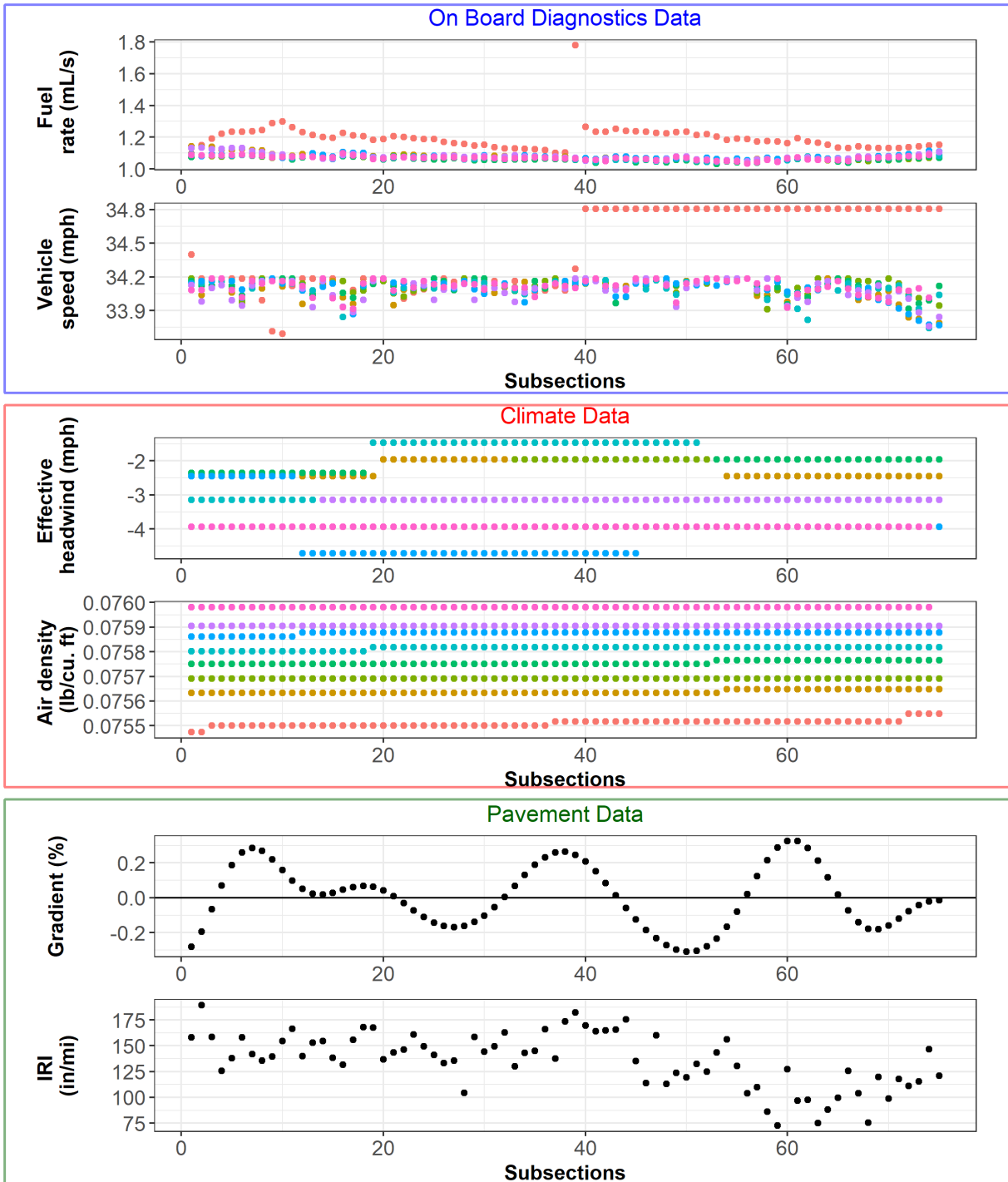


Figure P.182: SUV data on Section PH23.

PH23-YOL-CR32AW-JPC SUV summer_night 45 mph

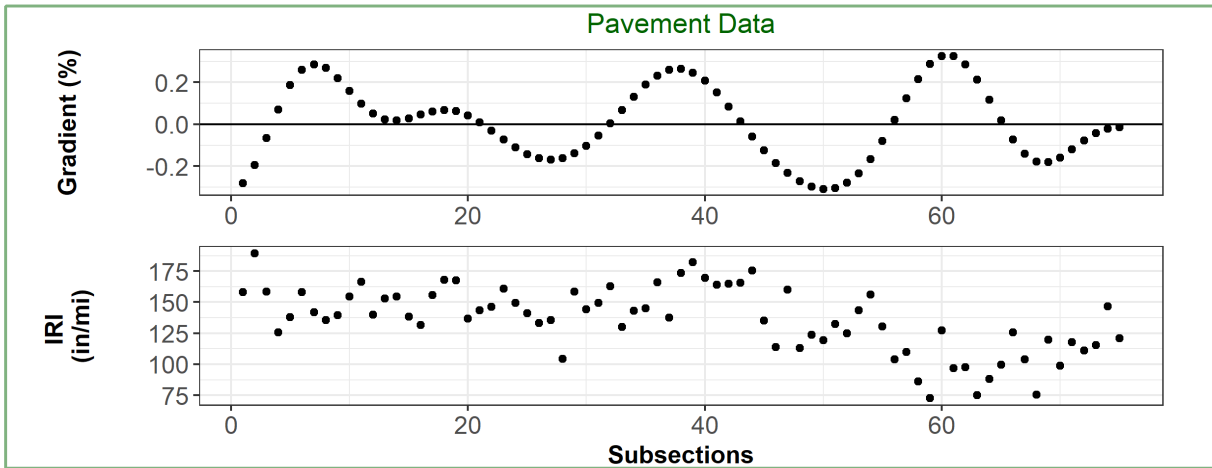
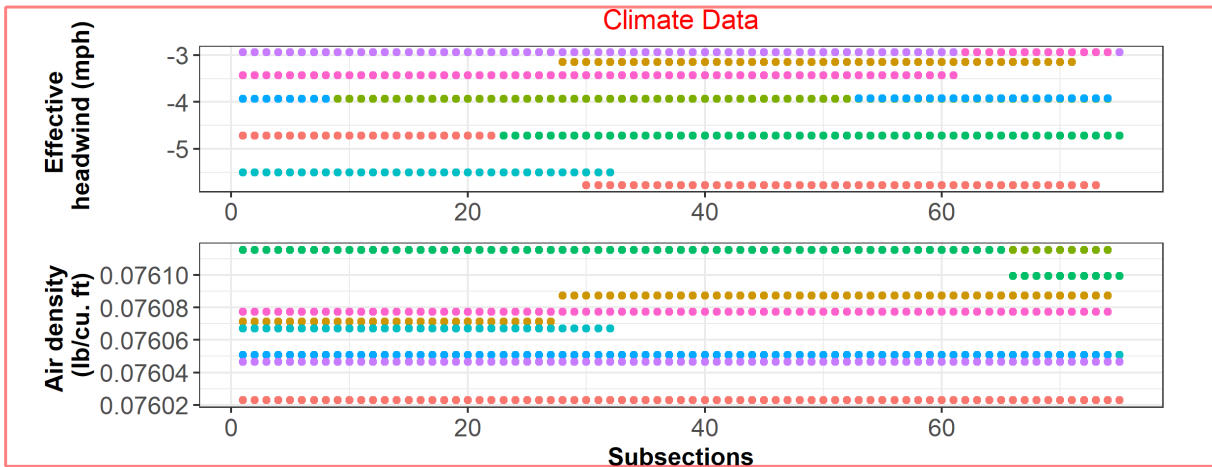
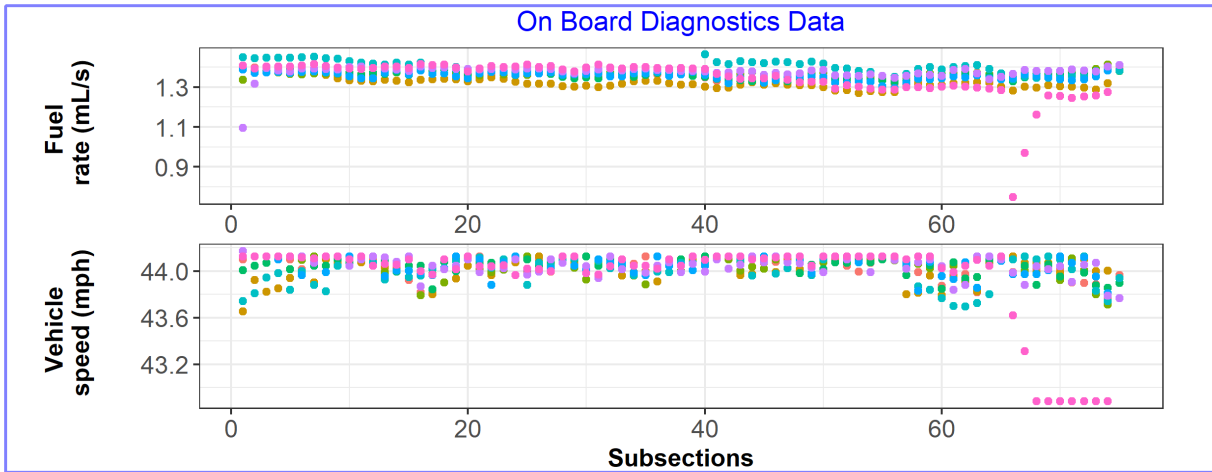


Figure P.183: SUV data on Section PH23.

PH23-YOL-CR32AW-JPC SUV winter_day 35 mph

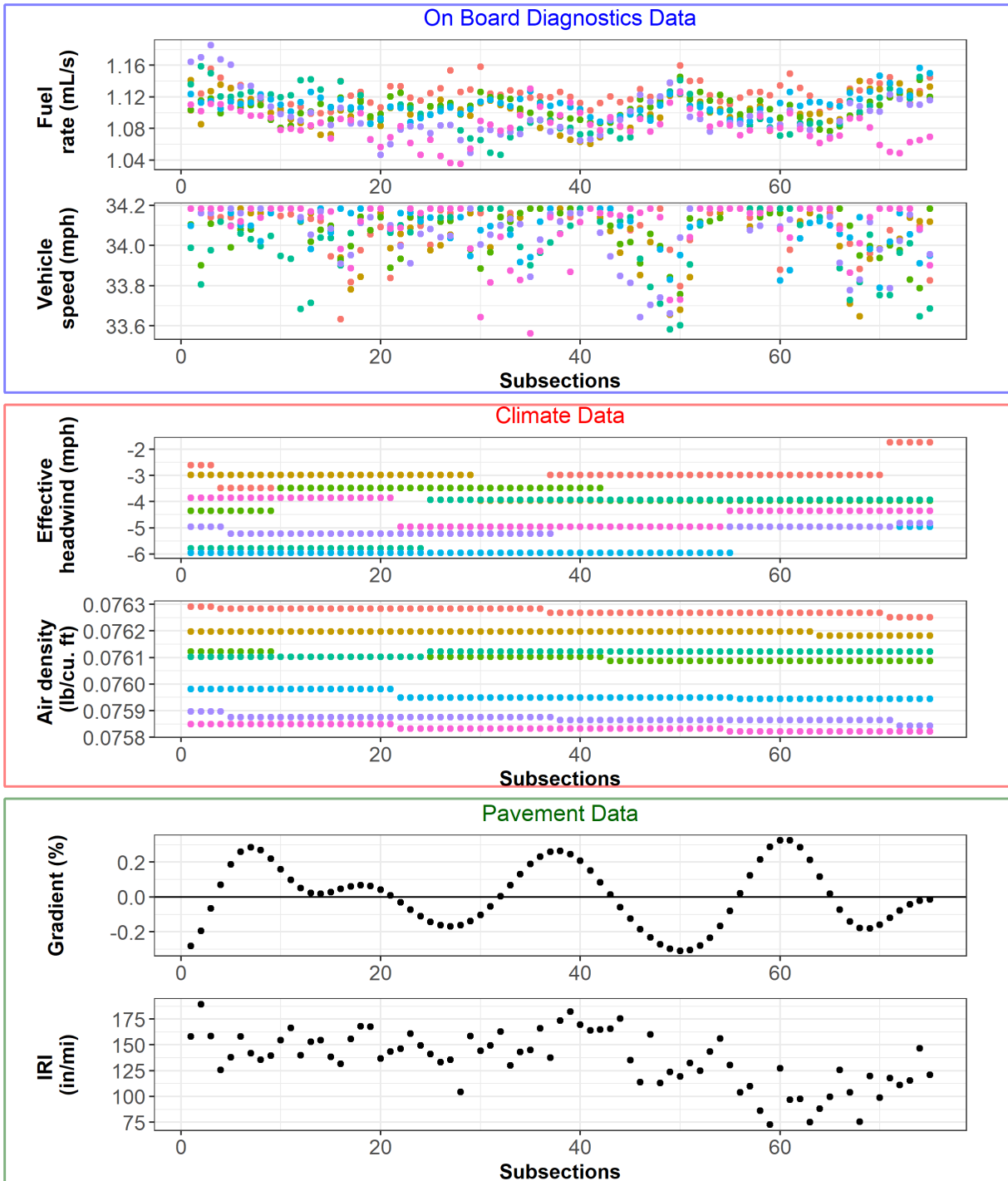


Figure P.184: SUV data on Section PH23.

PH23-YOL-CR32AW-JPC SUV winter_day 45 mph

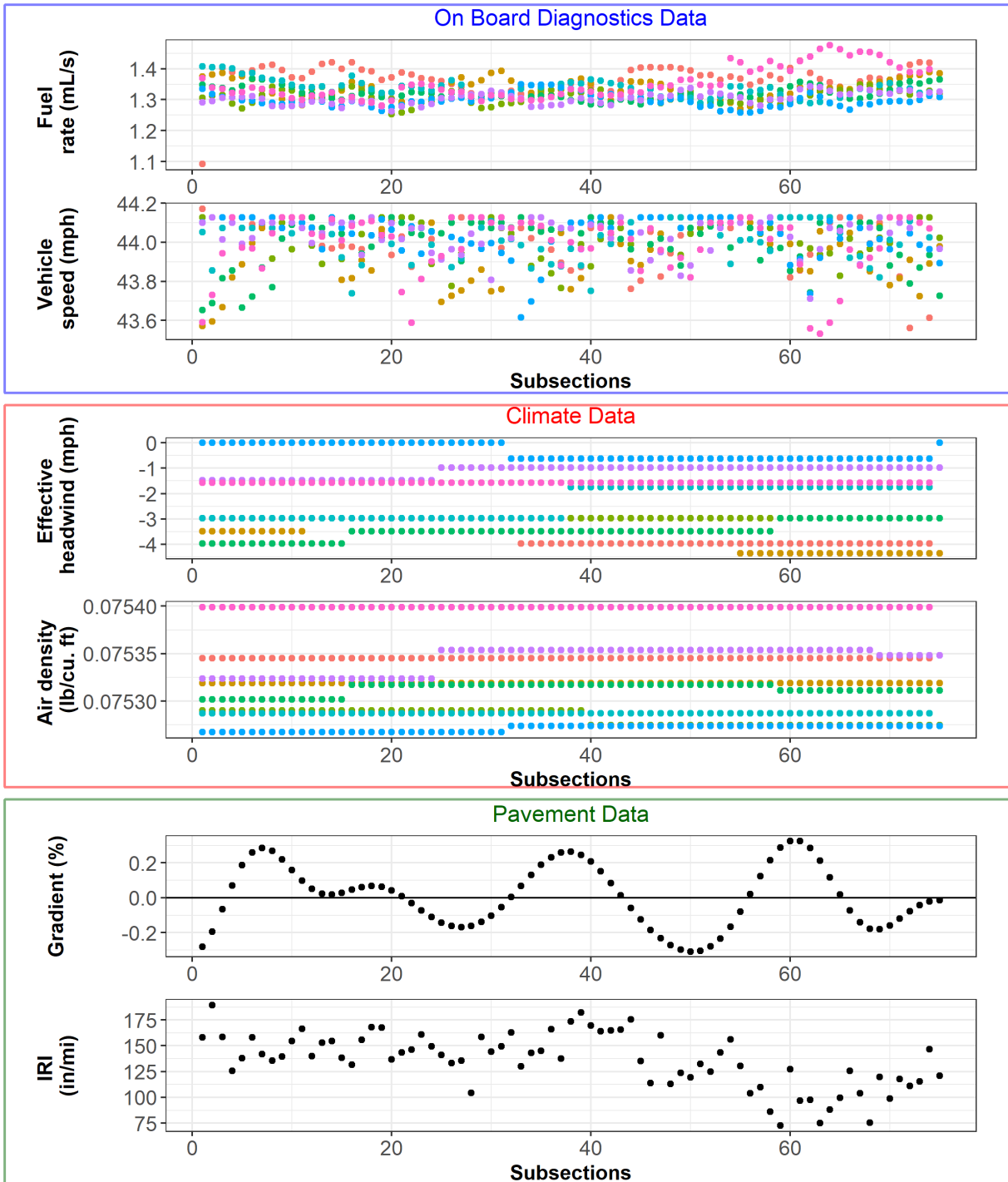


Figure P.185: SUV data on Section PH23.

3. F-450 Data

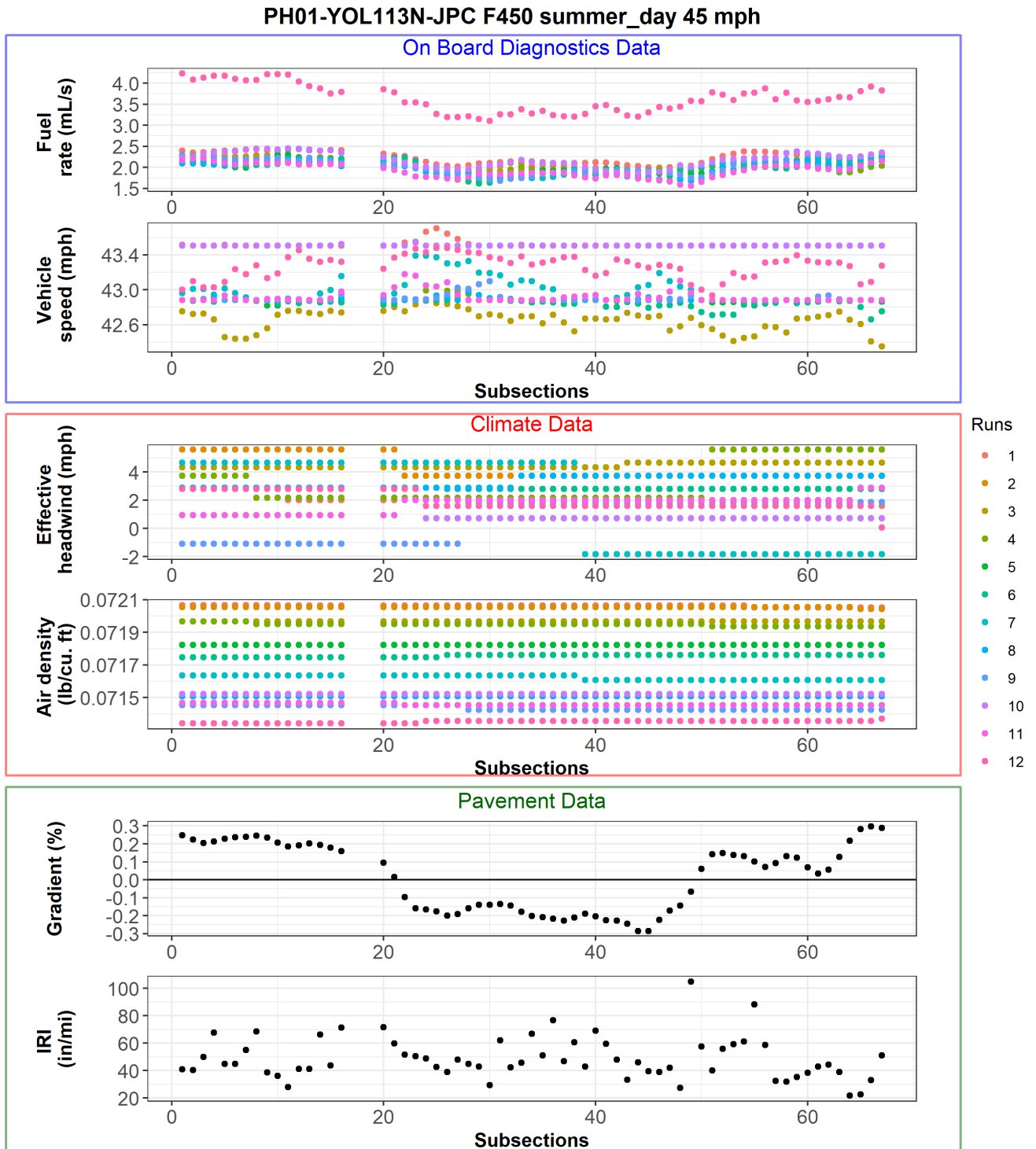


Figure P.186: F-450 data on Section PH01.

PH01-YOL113N-JPC F450 summer_day 55 mph

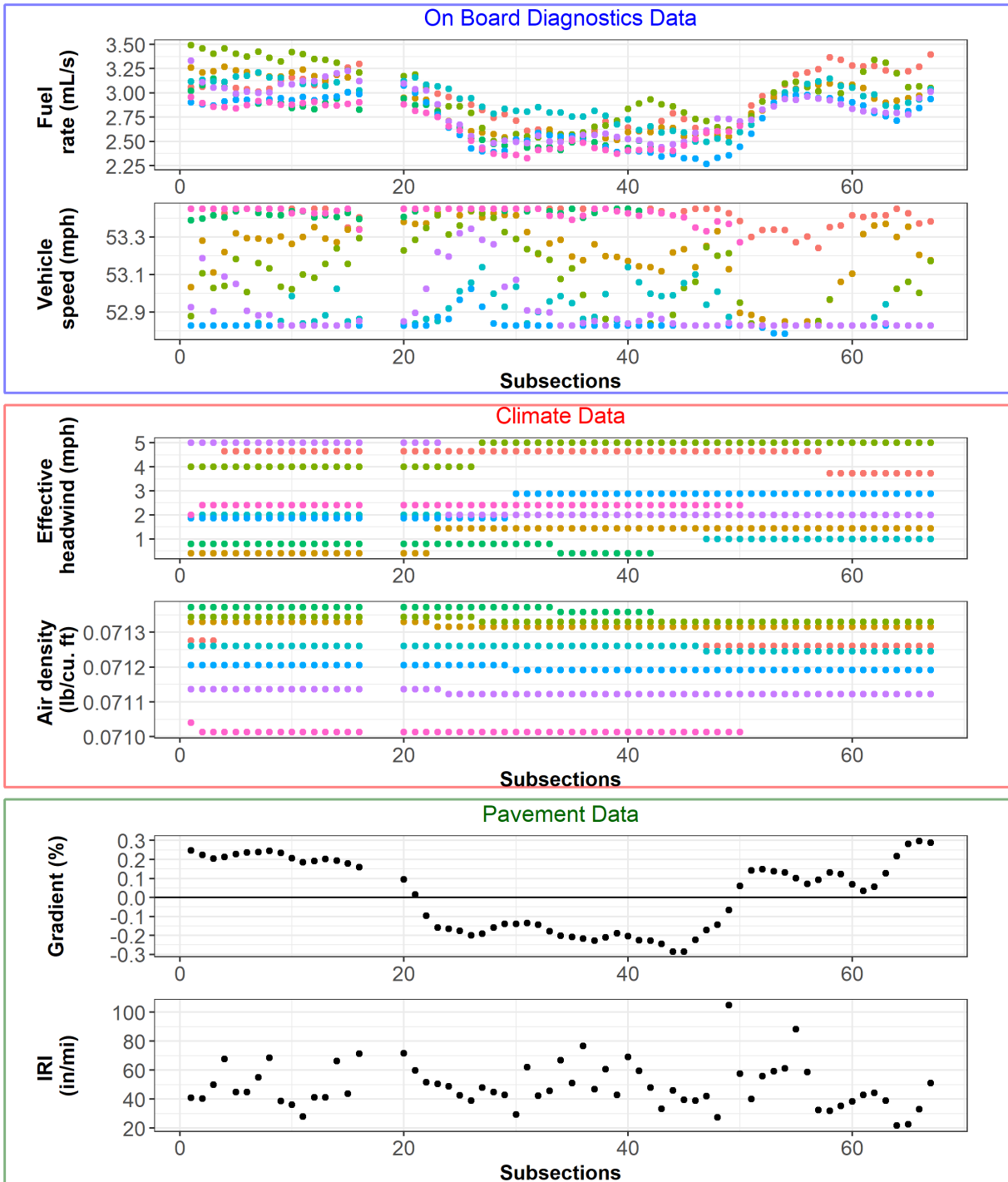


Figure P.187: F-450 data on Section PH01.

PH01-YOL113N-JPC F450 summer_night 45 mph

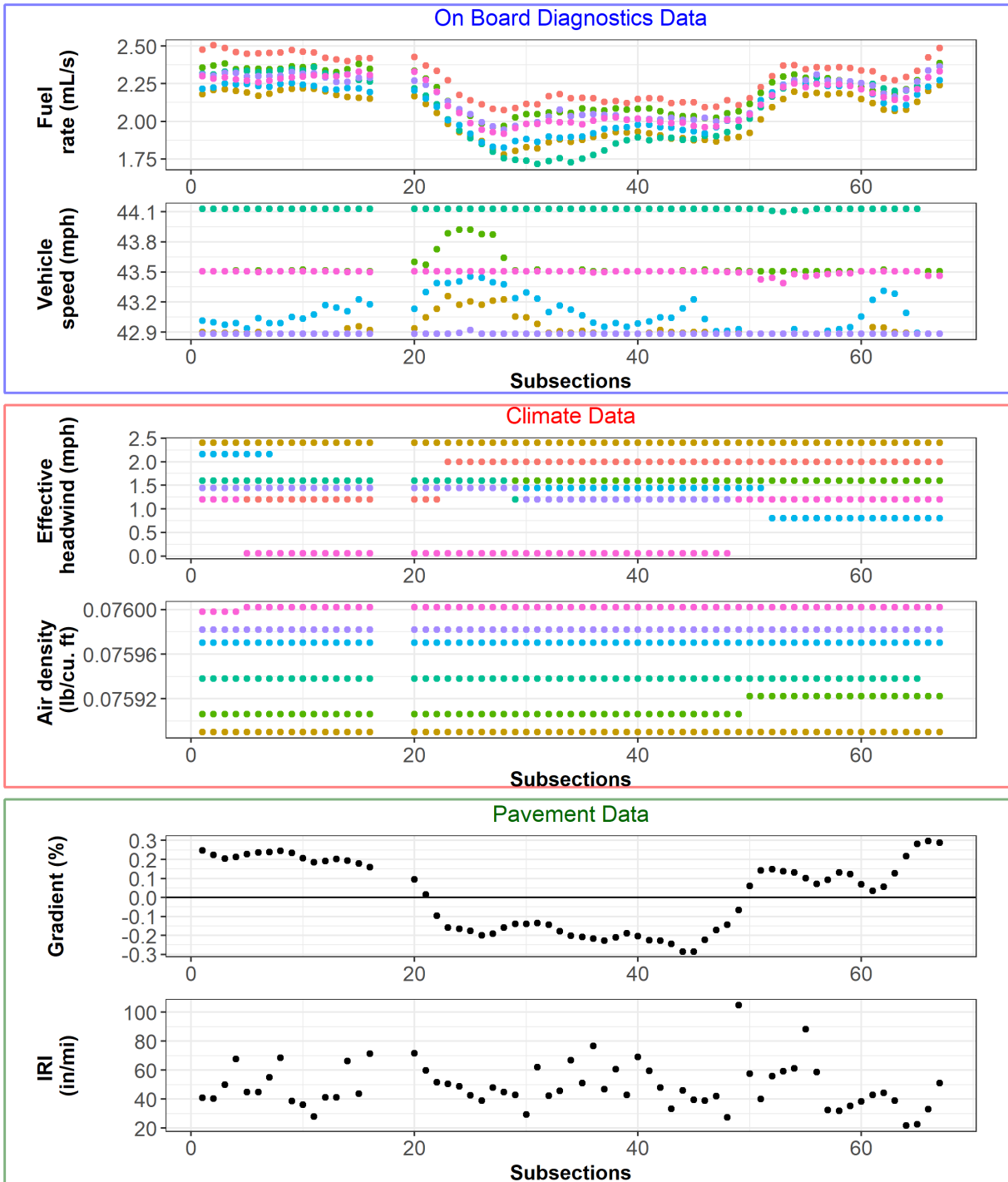


Figure P.188: F-450 data on Section PH01.

PH01-YOL113N-JPC F450 summer_night 55 mph

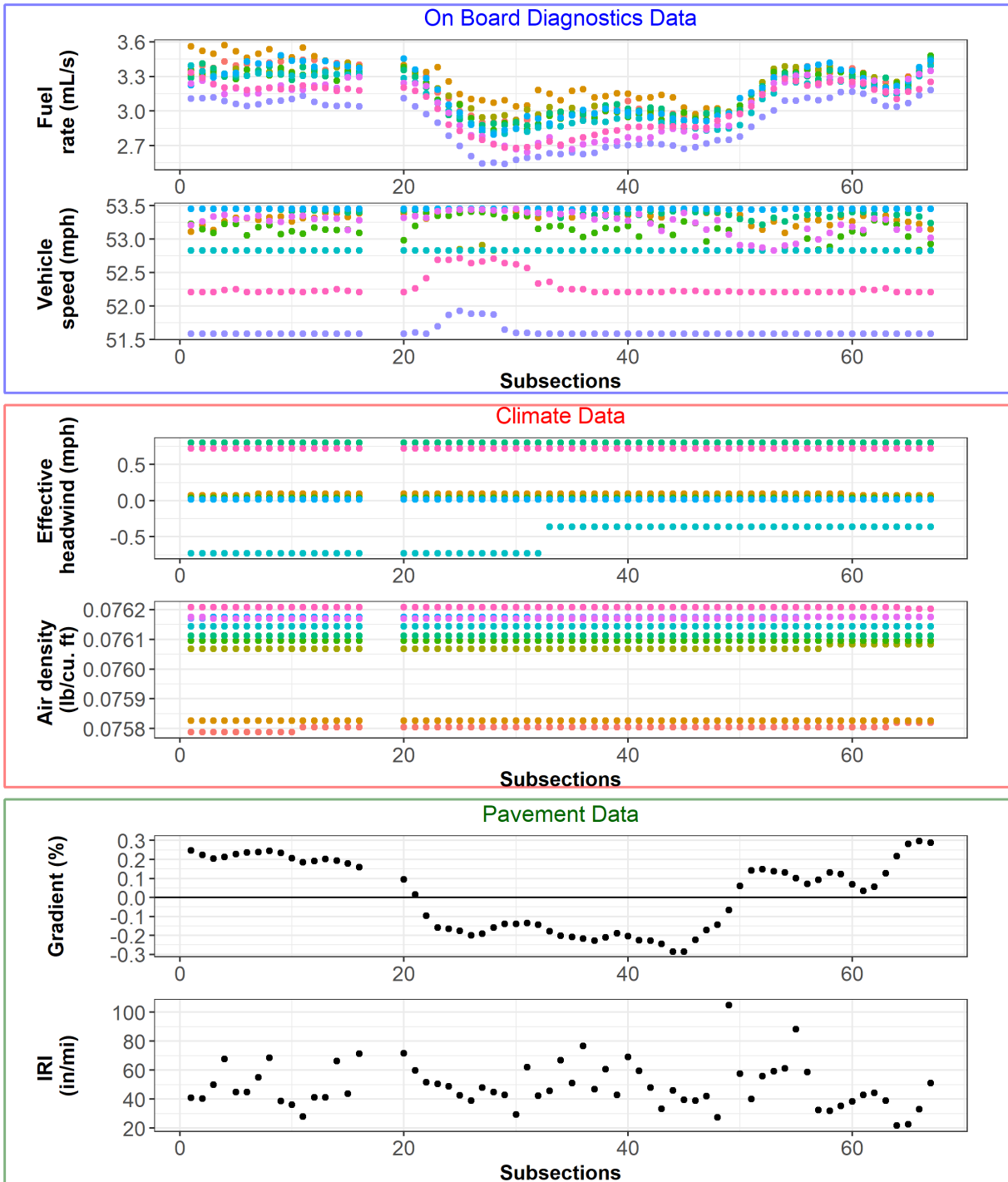


Figure P.189: F-450 data on Section PH01.

PH01-YOL113N-JPC F450 winter_day 45 mph

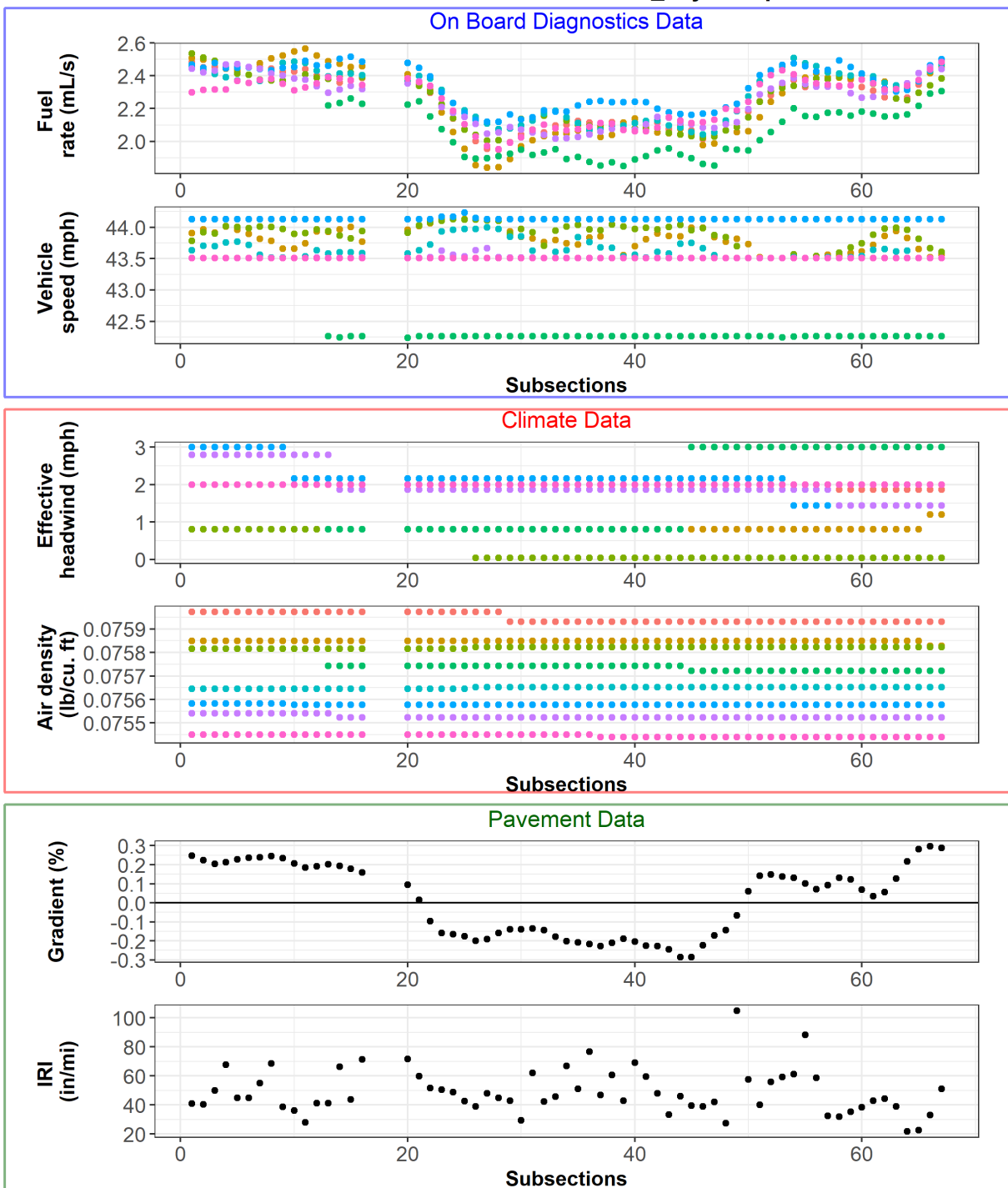


Figure P.190: F-450 data on Section PH01.

PH01-YOL113N-JPC F450 winter_day 55 mph

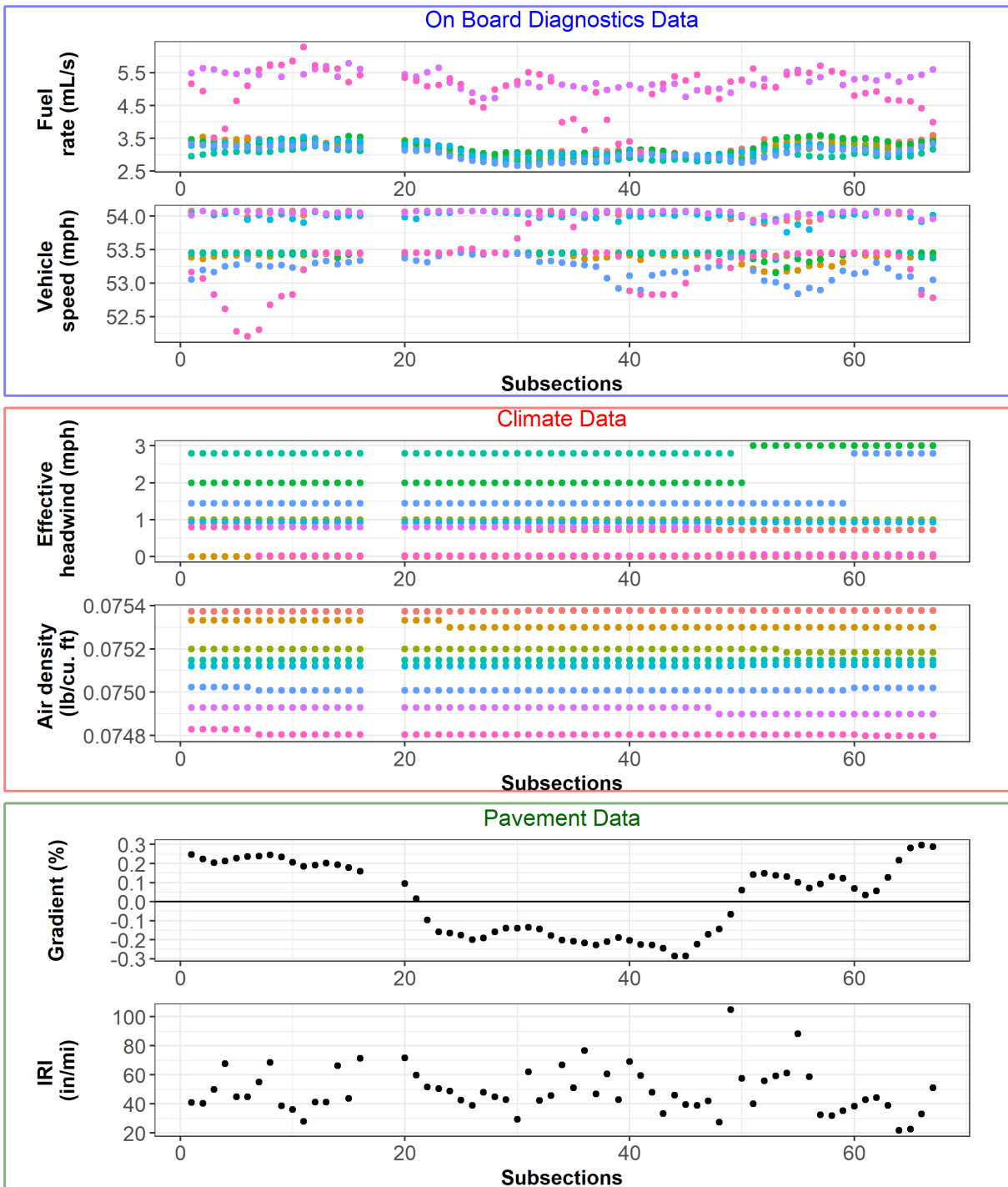
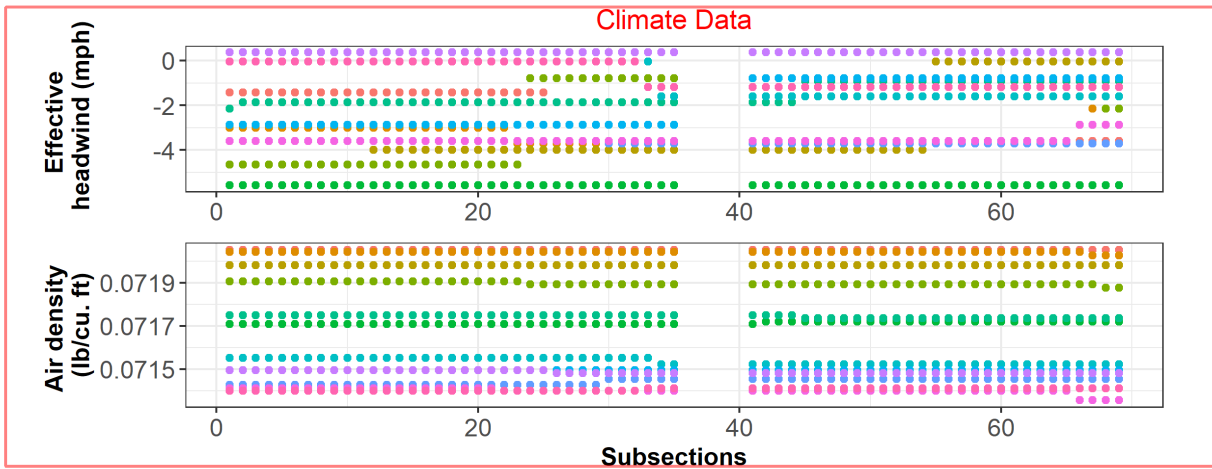
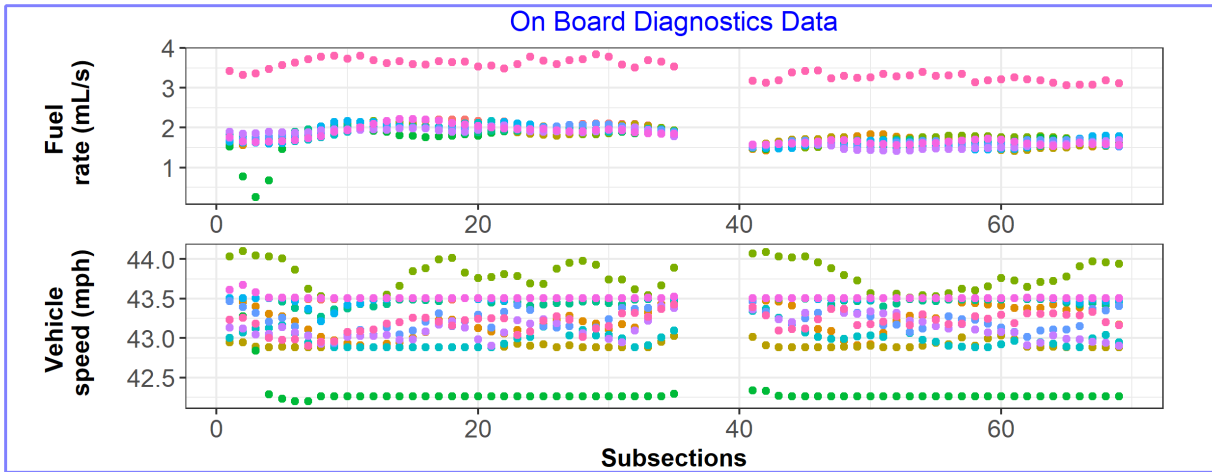


Figure P.191: F-450 data on Section PH01.

PH02-YOL113S-JPC F450 summer_day 45 mph



- Runs
- 1
 - 2
 - 3
 - 4
 - 5
 - 6
 - 7
 - 8
 - 9
 - 10
 - 11
 - 12

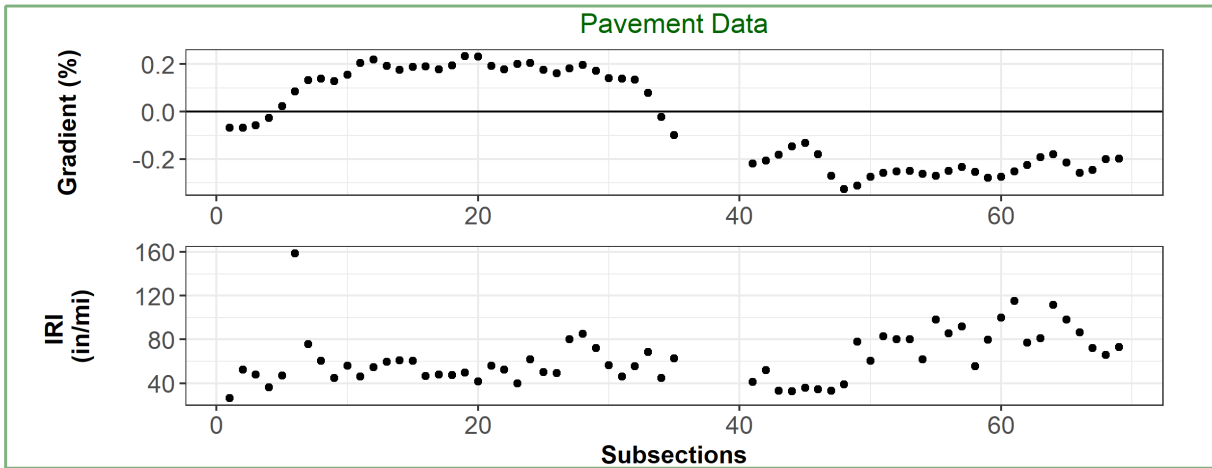


Figure P.192: F-450 data on Section PH02.

PH02-YOL113S-JPC F450 summer_day 55 mph

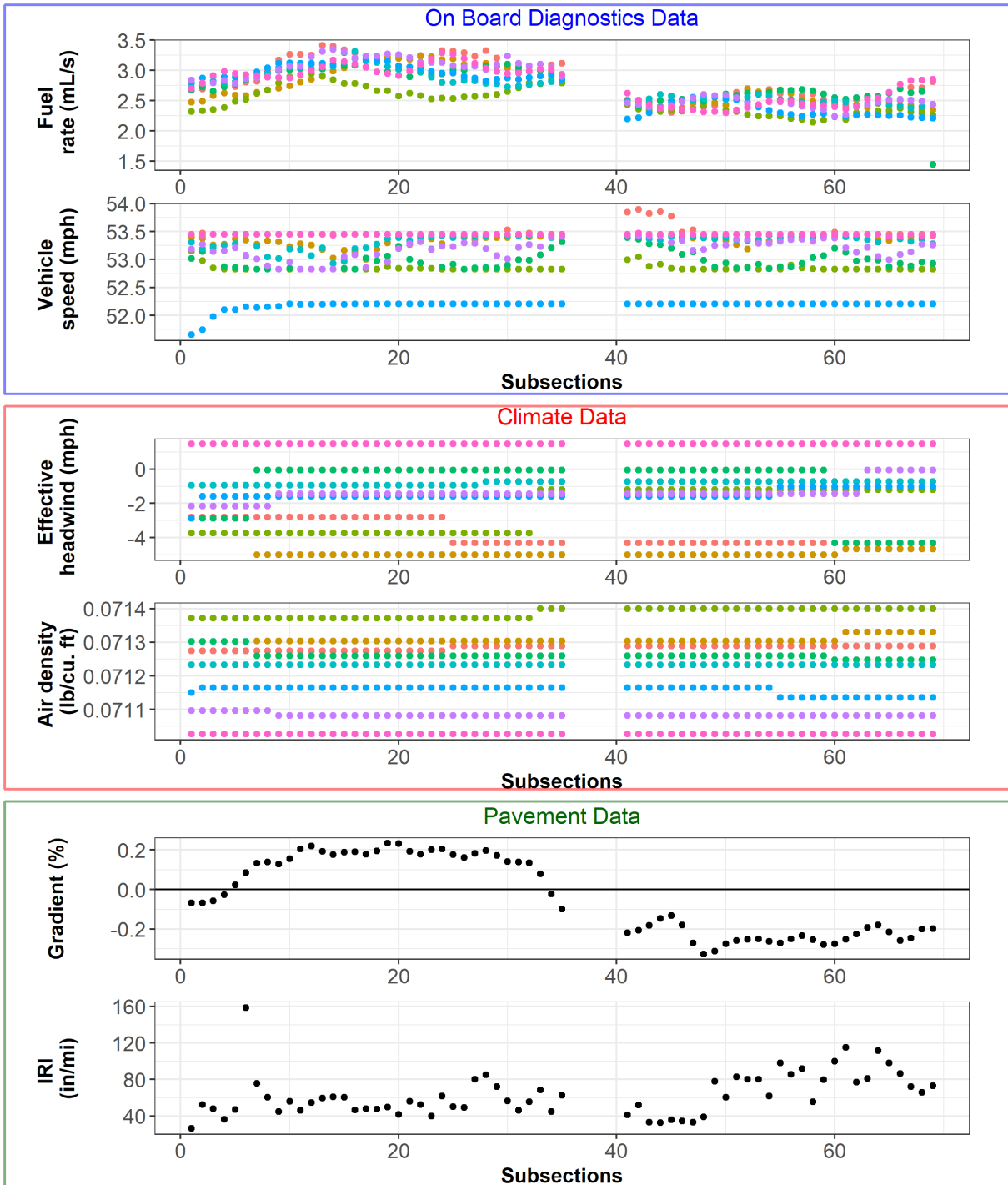


Figure P.193: F-450 data on Section PH02.

PH02-YOL113S-JPC F450 summer_night 45 mph

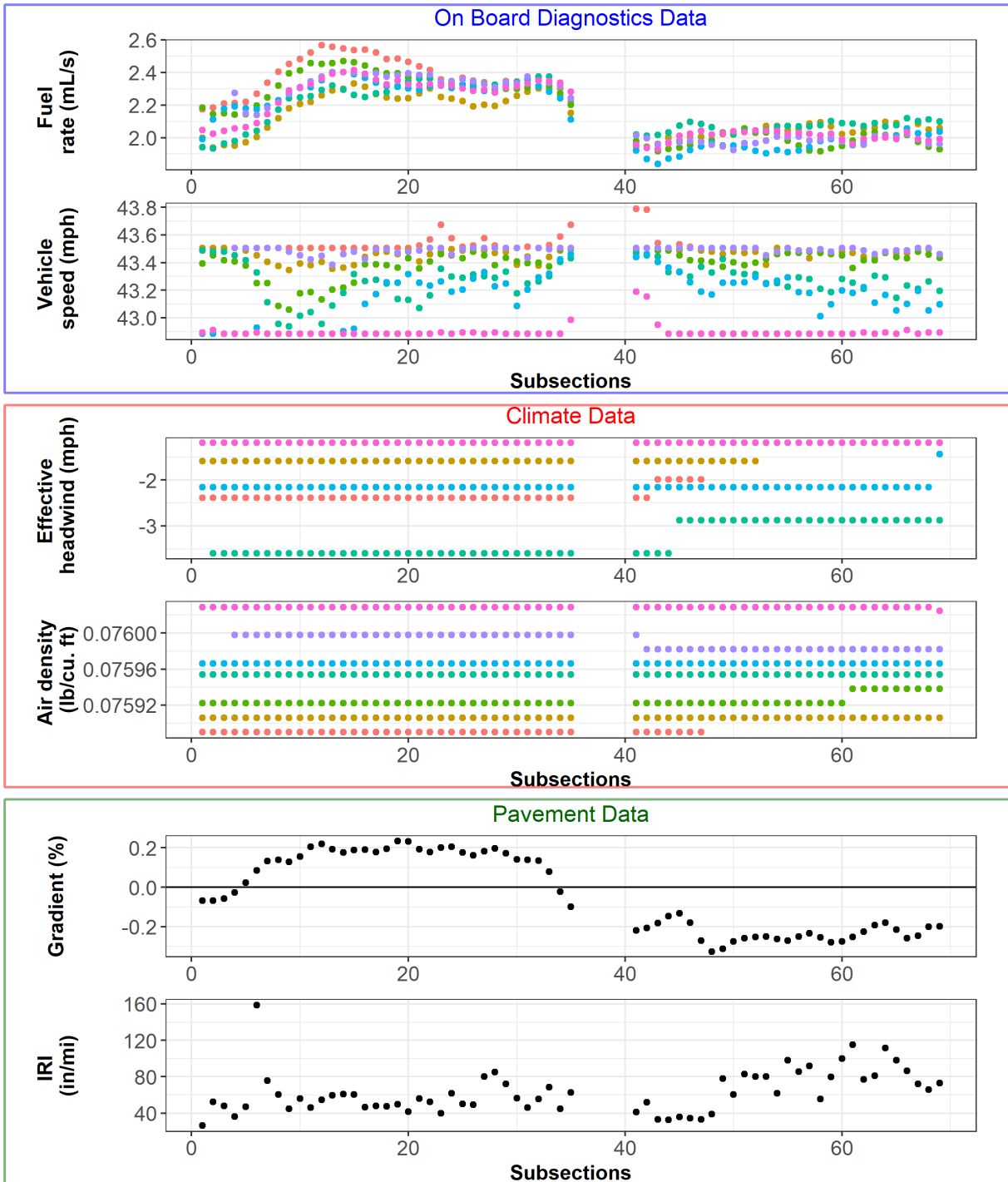


Figure P.194: F-450 data on Section PH02.

PH02-YOL113S-JPC F450 summer_night 55 mph

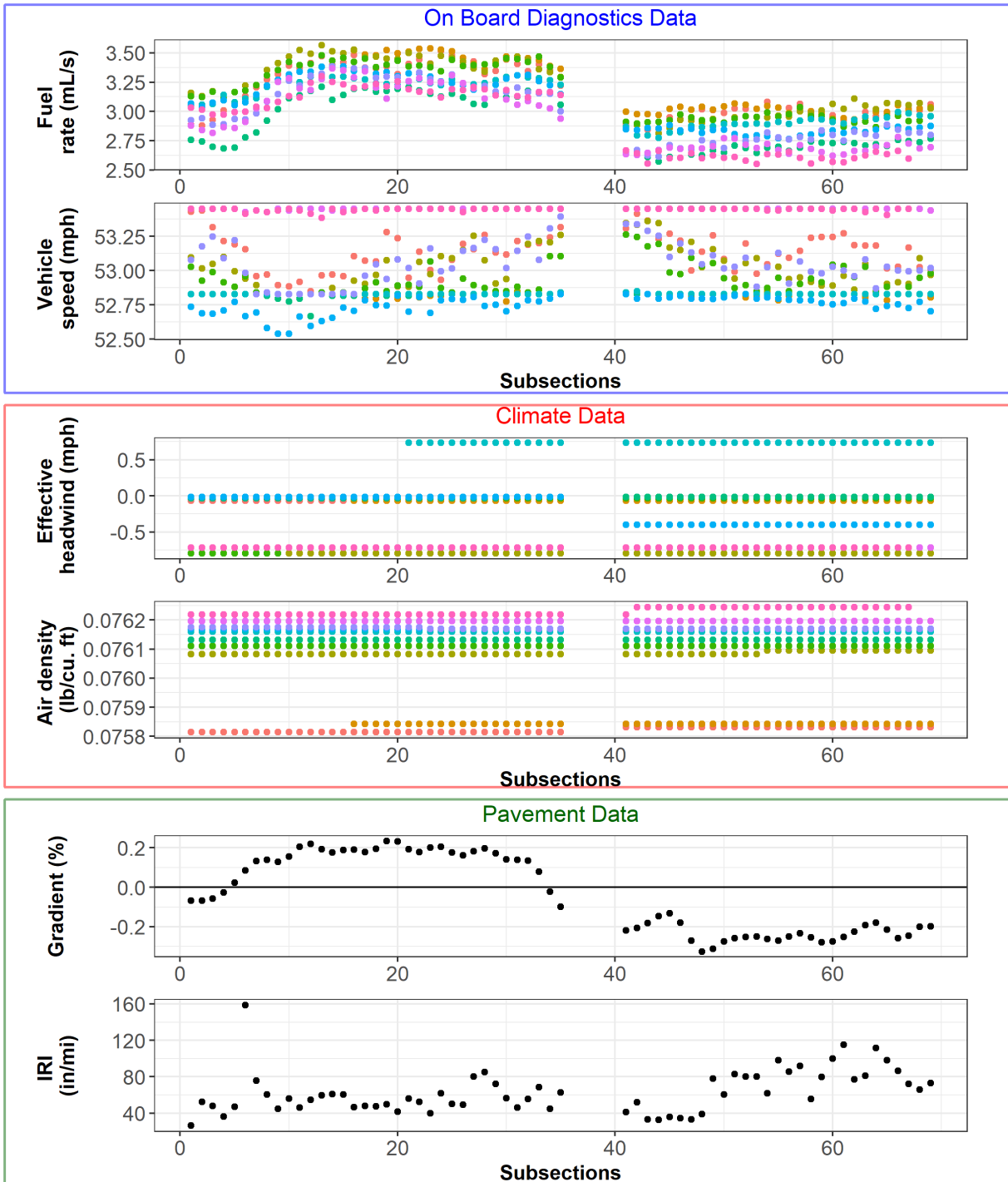


Figure P.195: F-450 data on Section PH02.

PH02-YOL113S-JPC F450 winter_day 45 mph

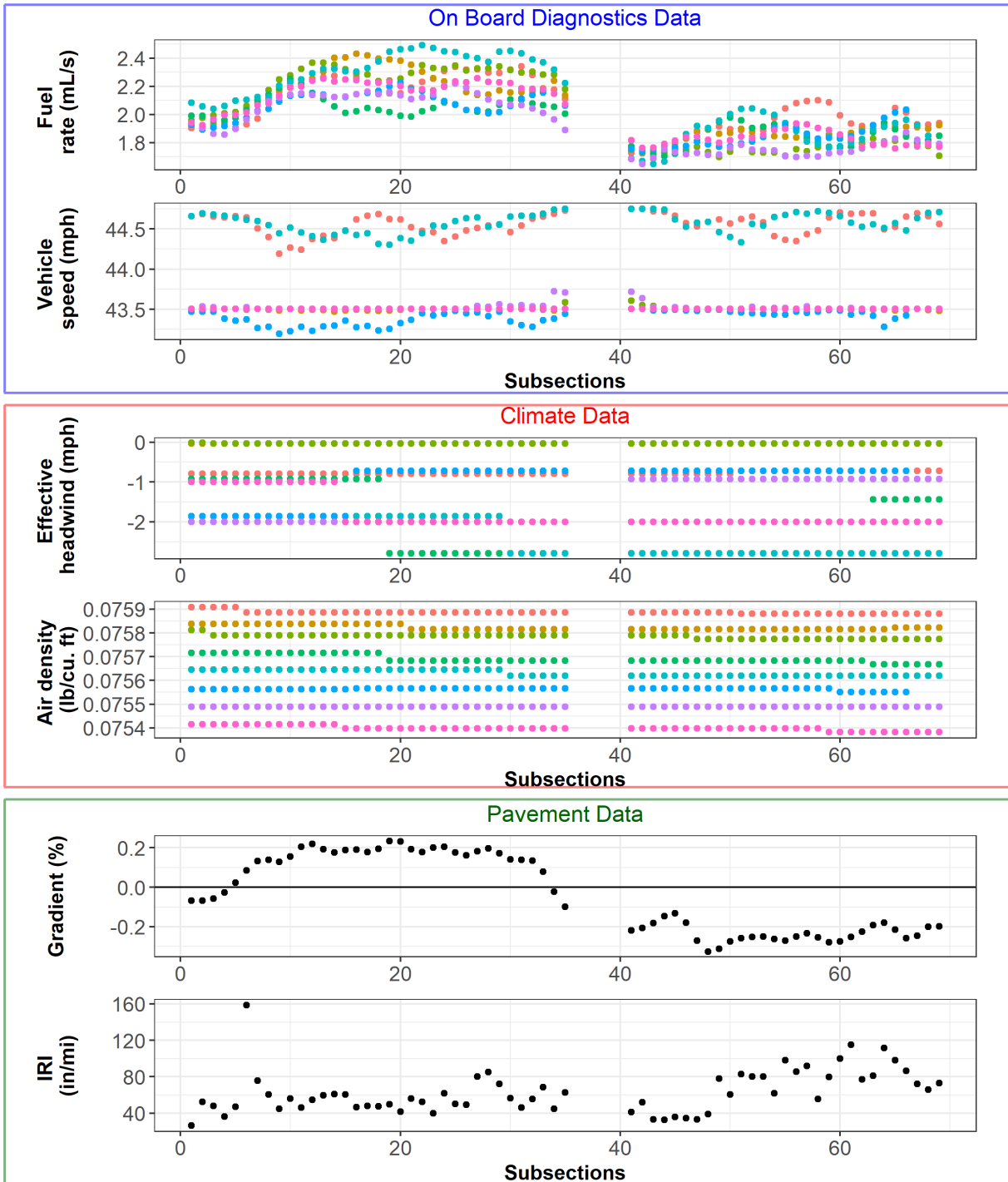


Figure P.196: F-450 data on Section PH02.

PH02-YOL113S-JPC F450 winter_day 55 mph

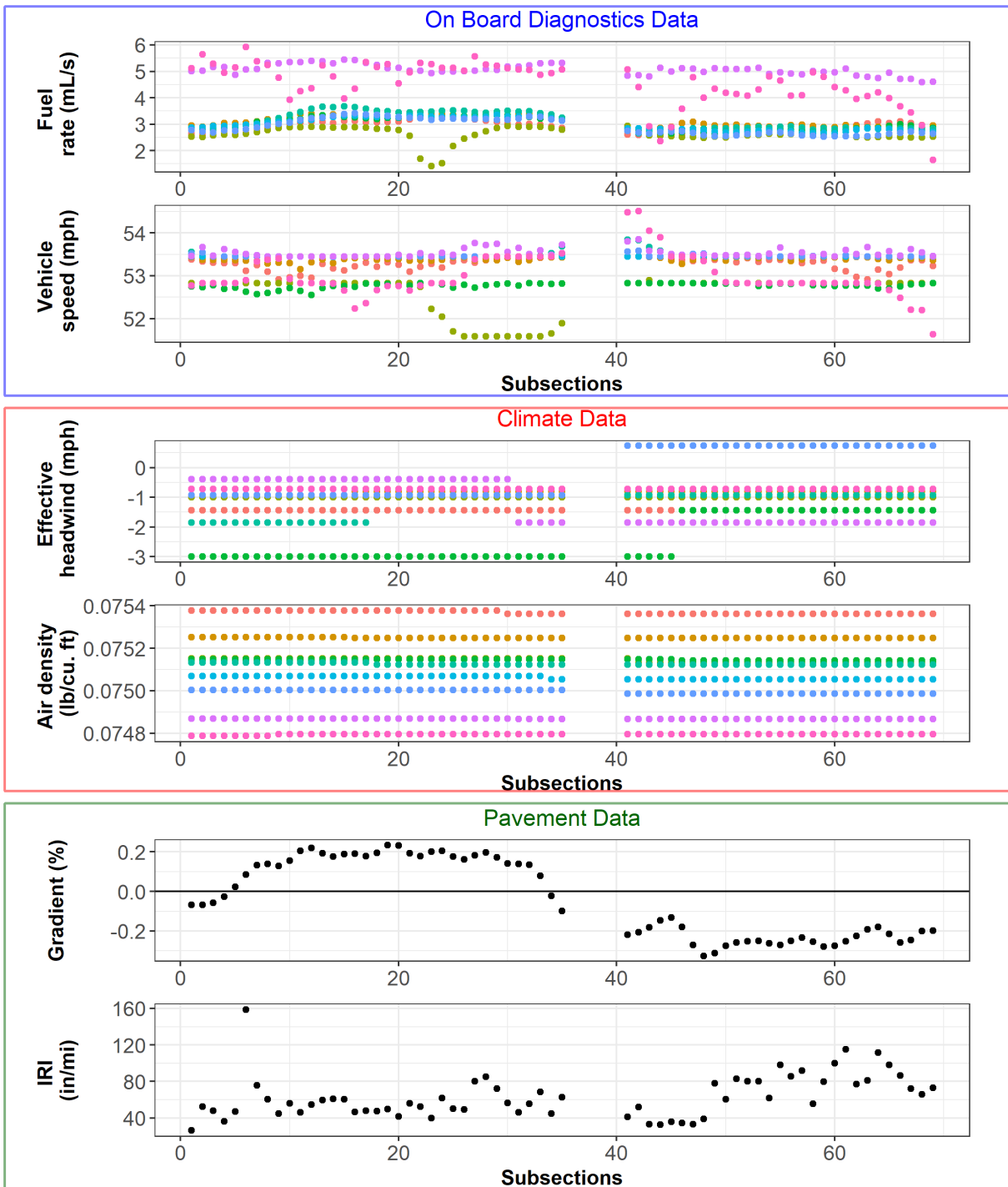


Figure P.197: F-450 data on Section PH02.

PH03-YOL505N-JPC F450 summer_day 45 mph

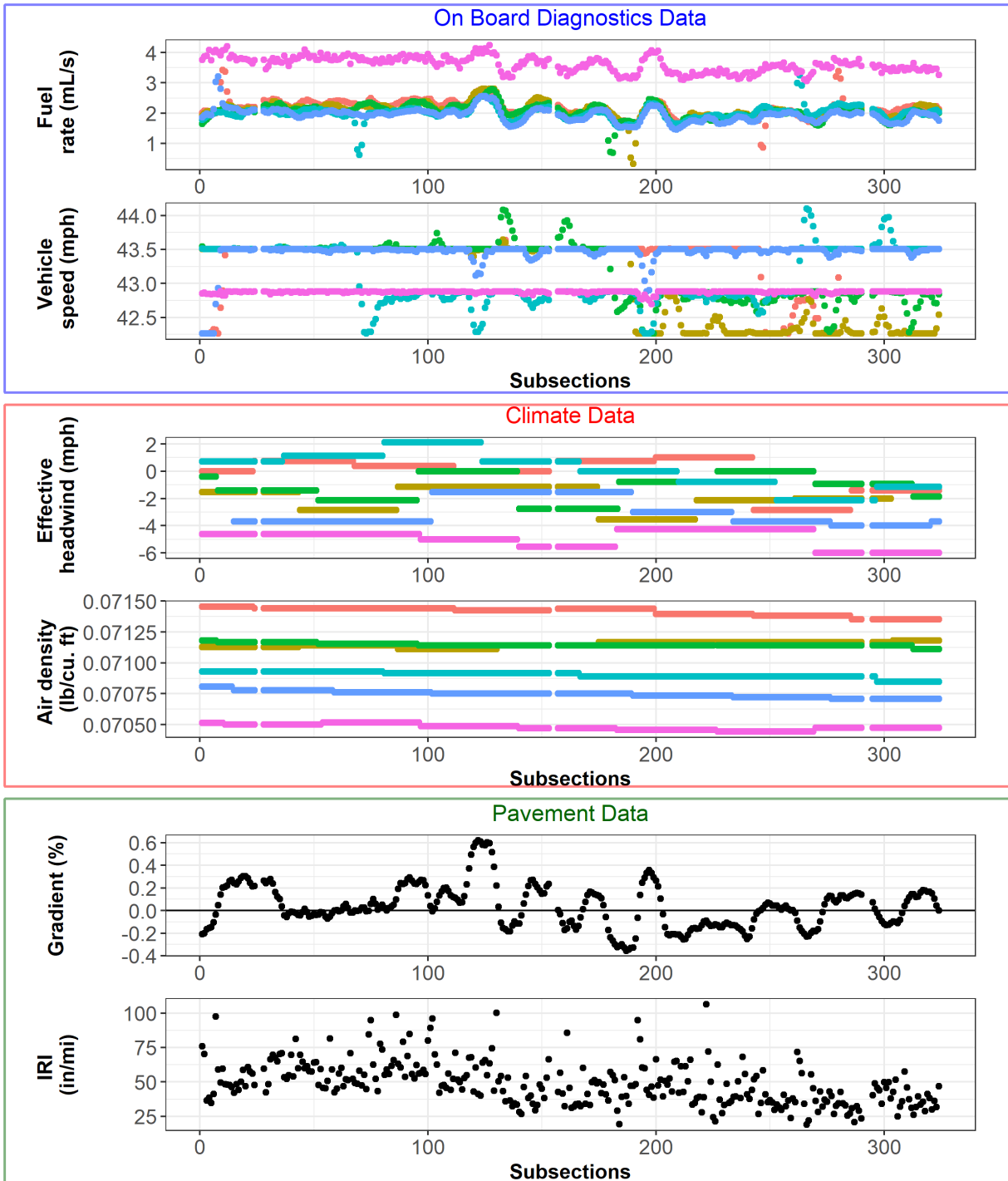


Figure P.198: F-450 data on Section PH03.

PH03-YOL505N-JPC F450 summer_day 55 mph

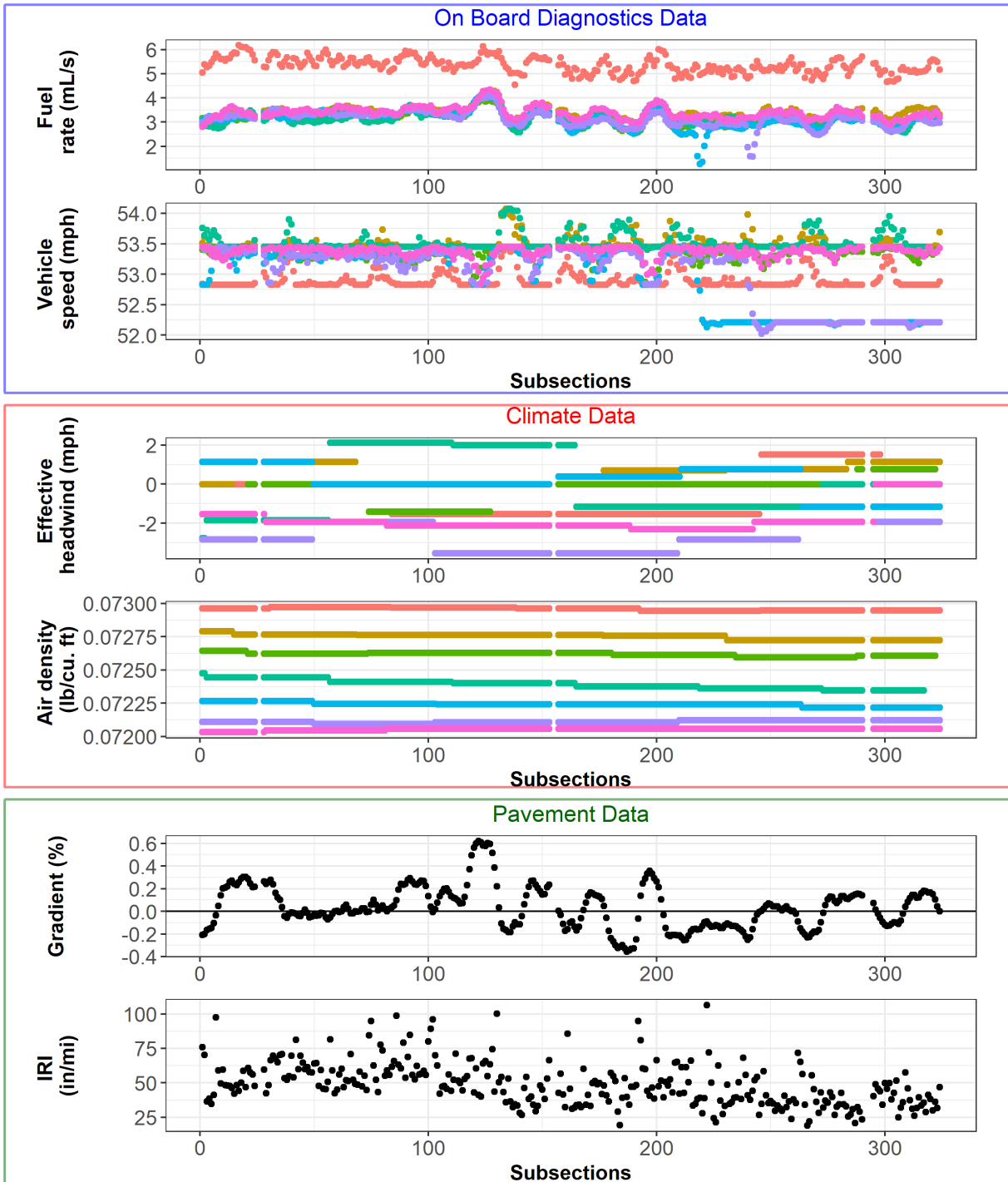


Figure P.199: F-450 data on Section PH03.

PH03-YOL505N-JPC F450 summer_night 45 mph

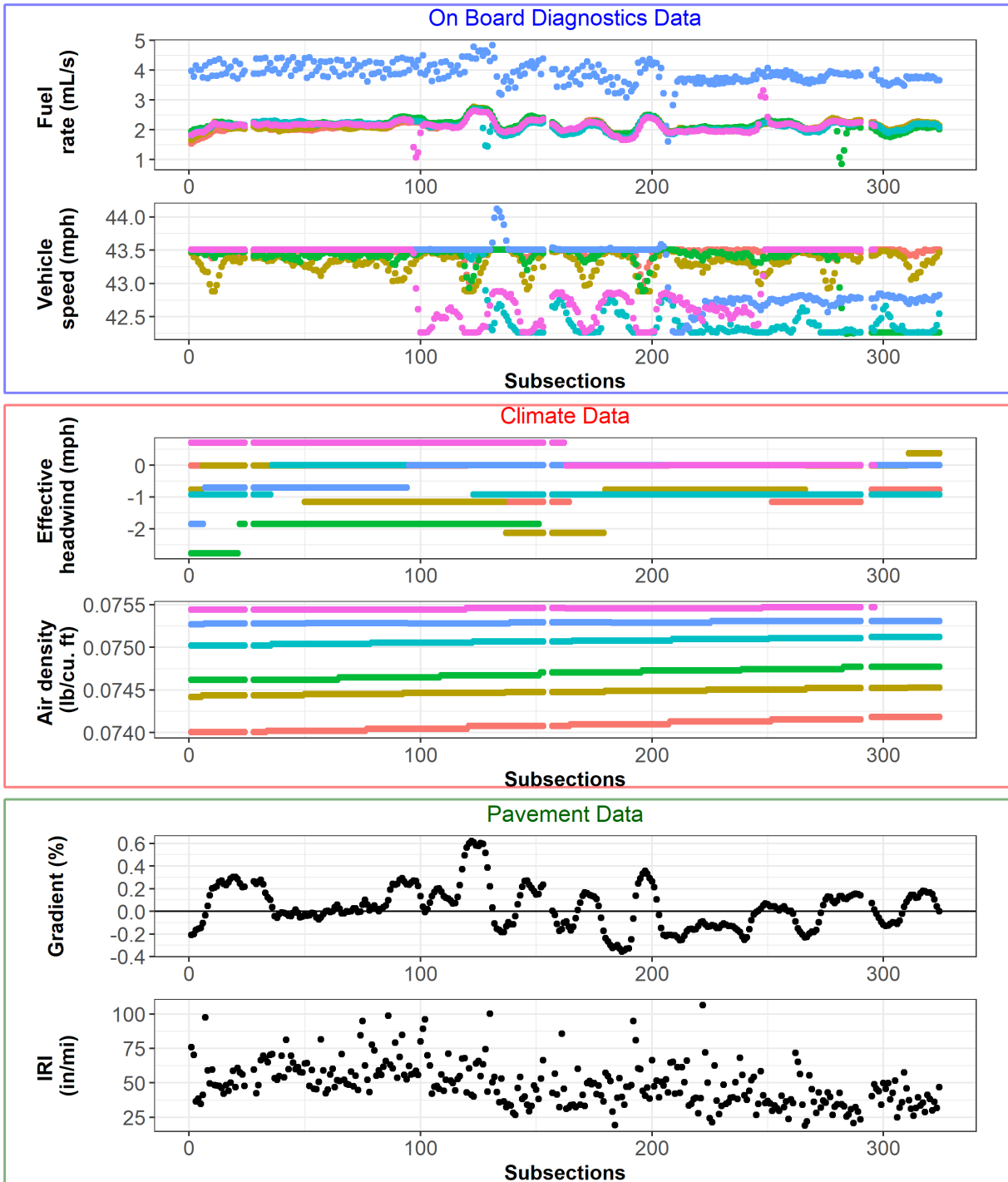


Figure P.200: F-450 data on Section PH03.

PH03-YOL505N-JPC F450 summer_night 55 mph

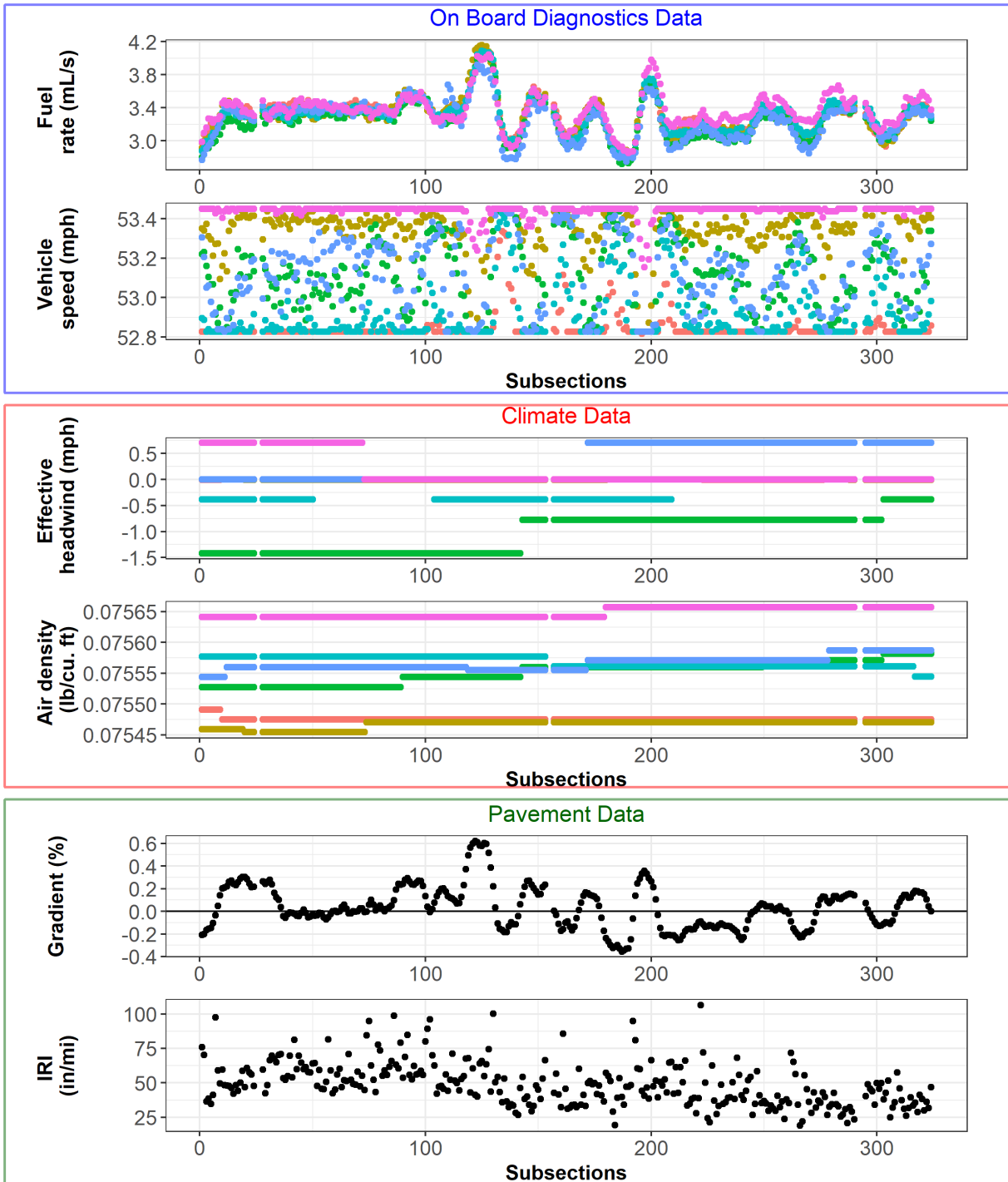


Figure P.201: F-450 data on Section PH03.

PH03-YOL505N-JPC F450 winter_day 45 mph

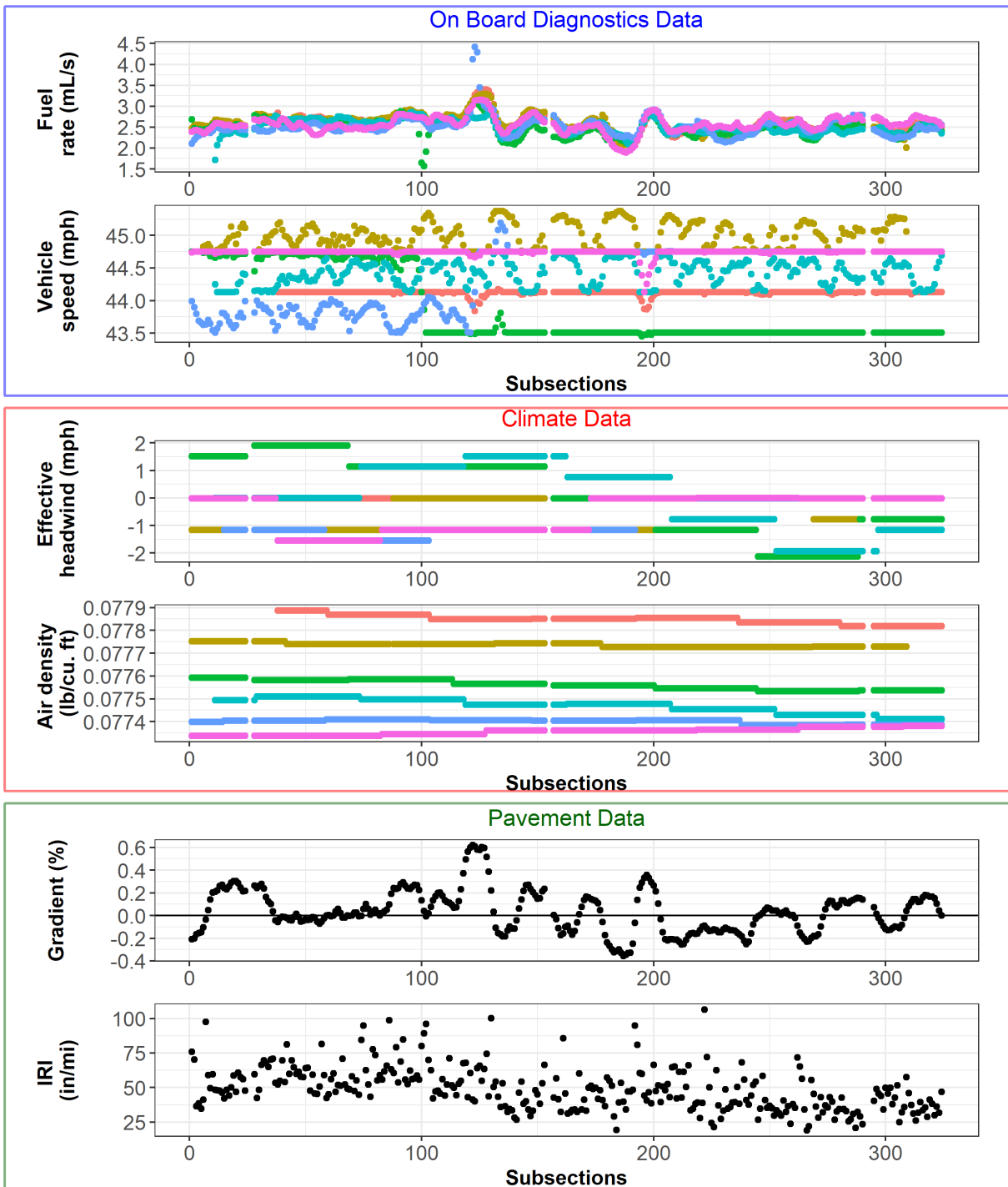


Figure P.202: F-450 data on Section PH03.

PH03-YOL505N-JPC F450 winter_day 55 mph

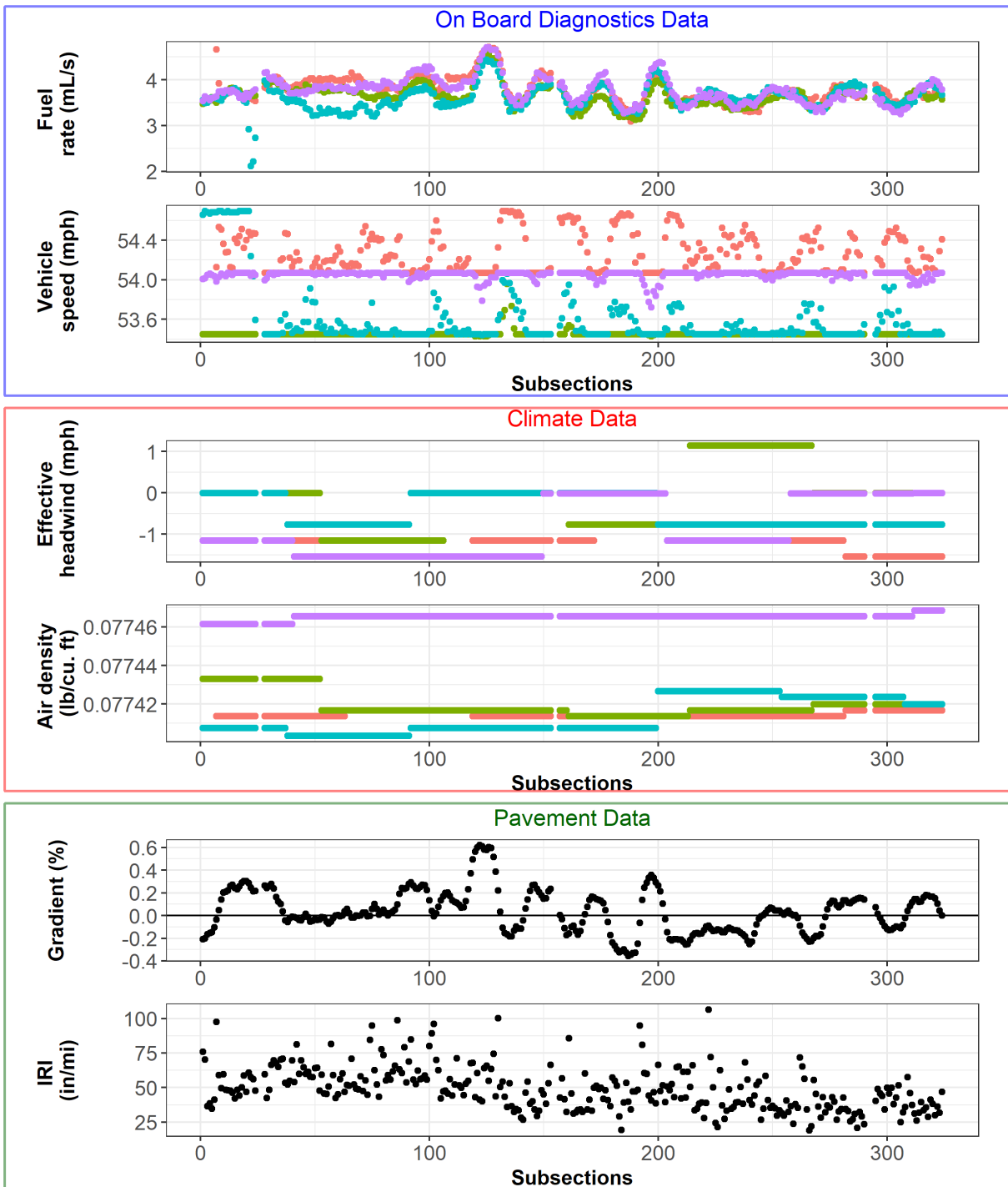


Figure P.203: F-450 data on Section PH03.

PH04-YOL505S-RHMA-G F450 summer_day 45 mph

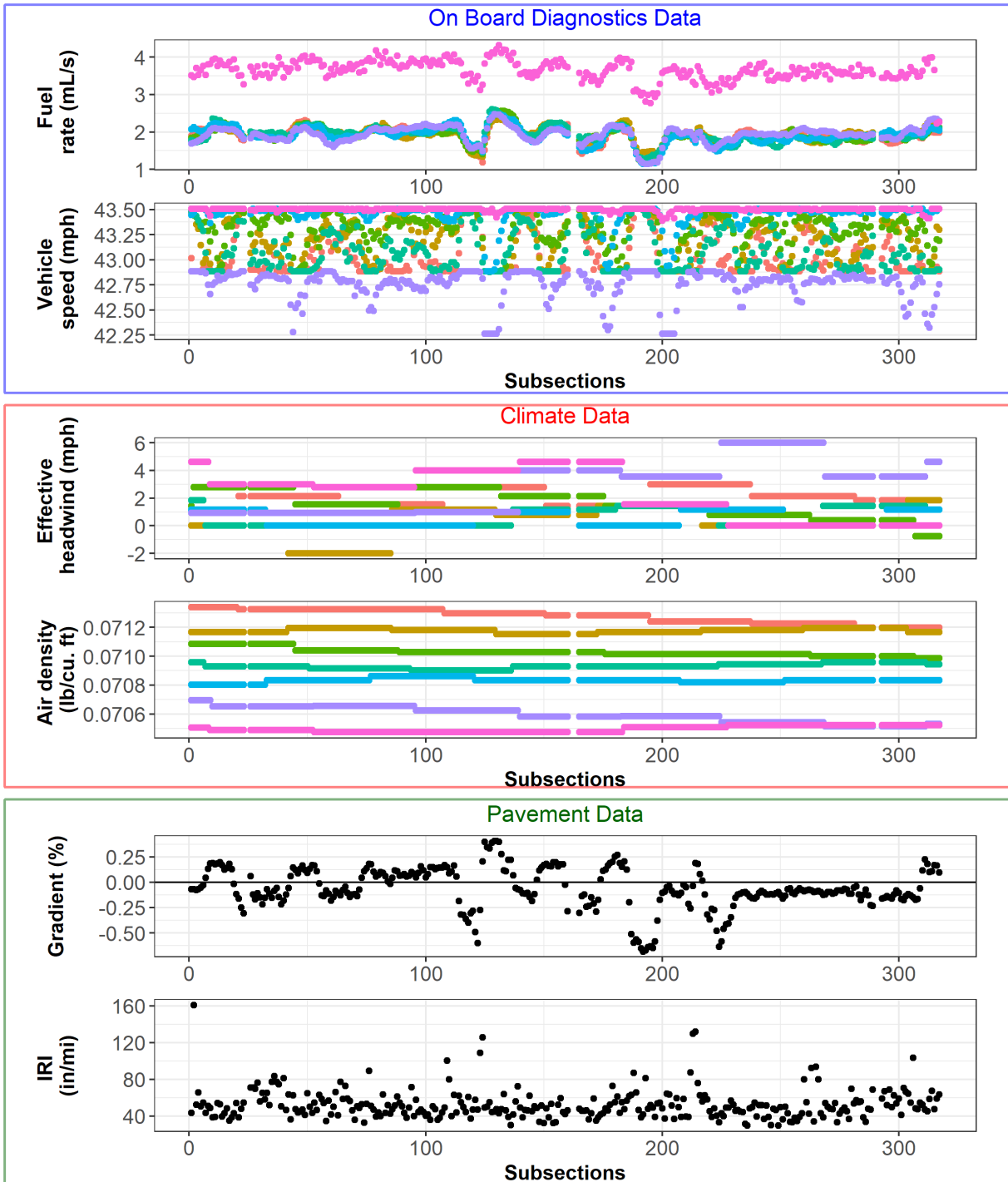


Figure P.204: F-450 data on Section PH04.

PH04-YOL505S-RHMA-G F450 summer_day 55 mph

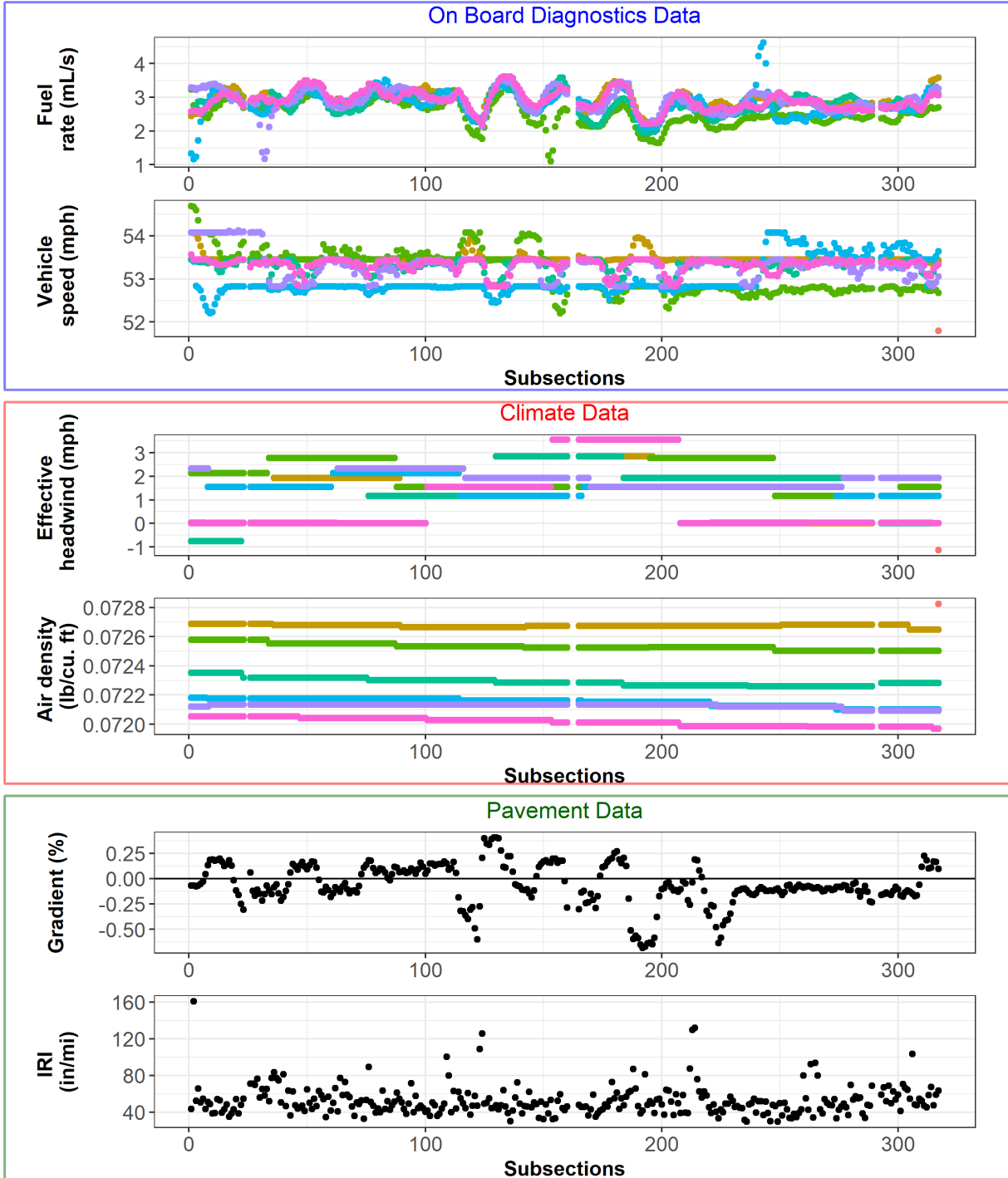


Figure P.205: F-450 data on Section PH04.

PH04-YOL505S-RHMA-G F450 summer_night 45 mph

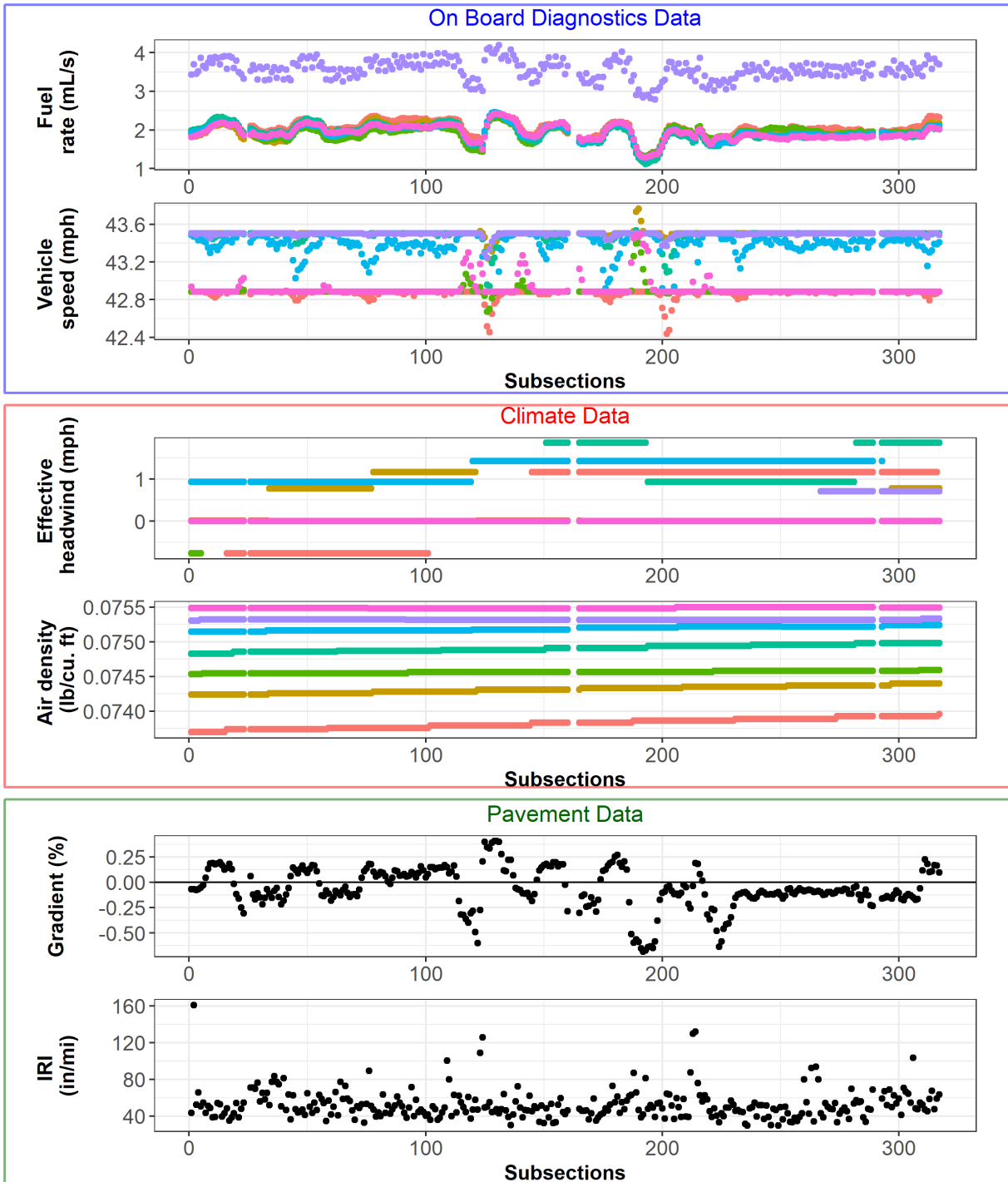


Figure P.206: F-450 data on Section PH04.

PH04-YOL505S-RHMA-G F450 summer_night 55 mph

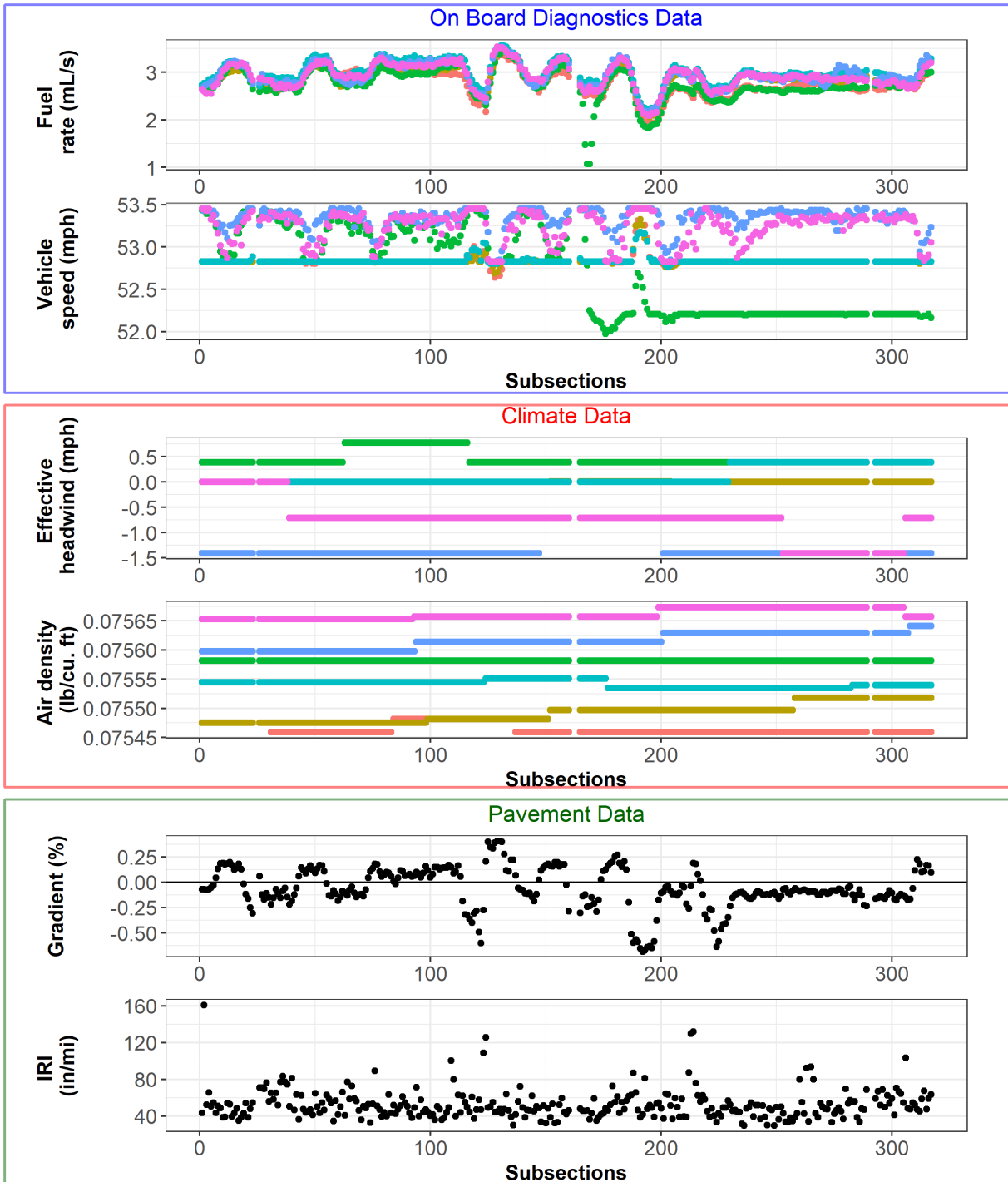


Figure P.207: F-450 data on Section PH04.

PH04-YOL505S-RHMA-G F450 winter_day 45 mph

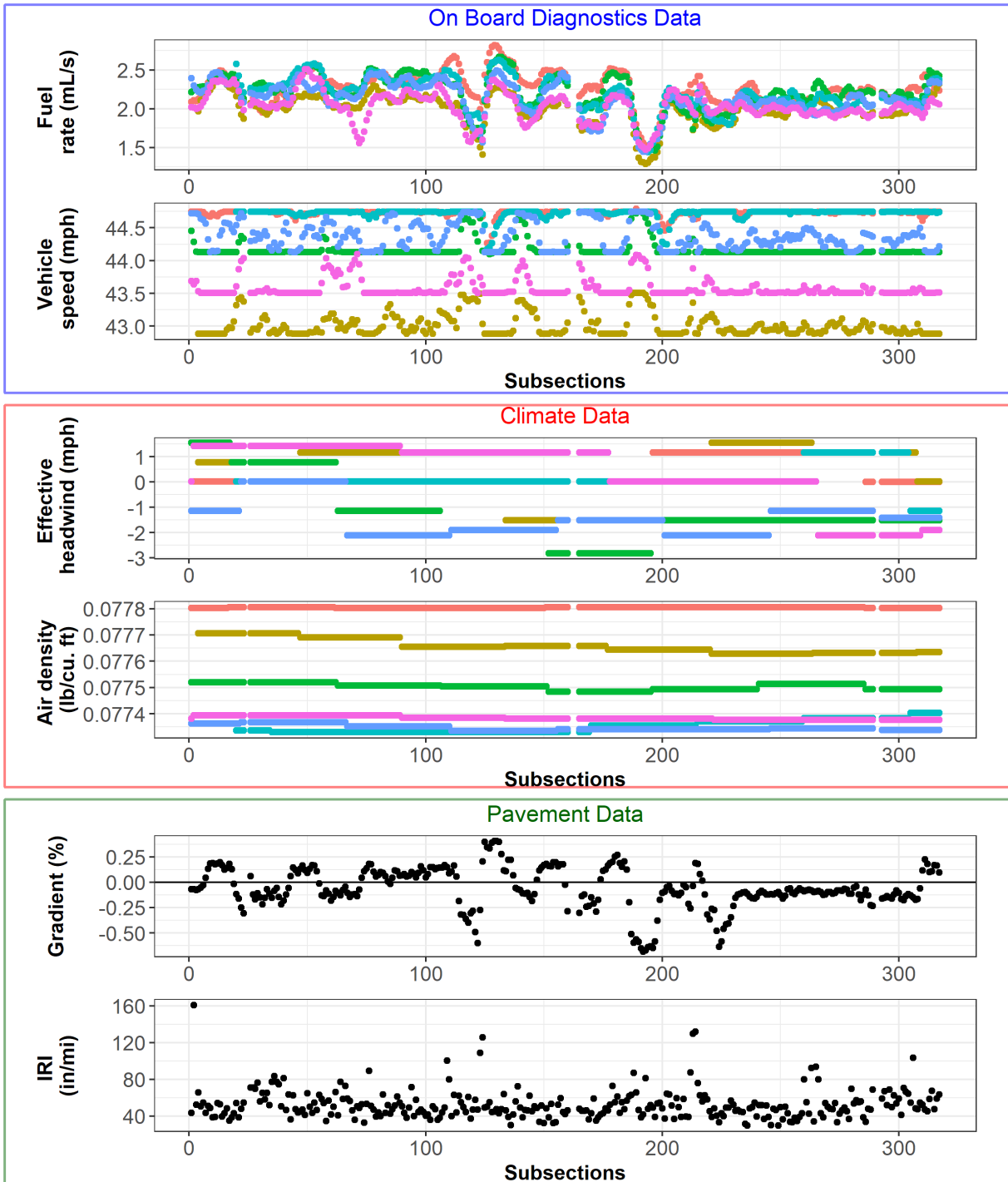


Figure P.208: F-450 data on Section PH04.

PH04-YOL505S-RHMA-G F450 winter_day 55 mph

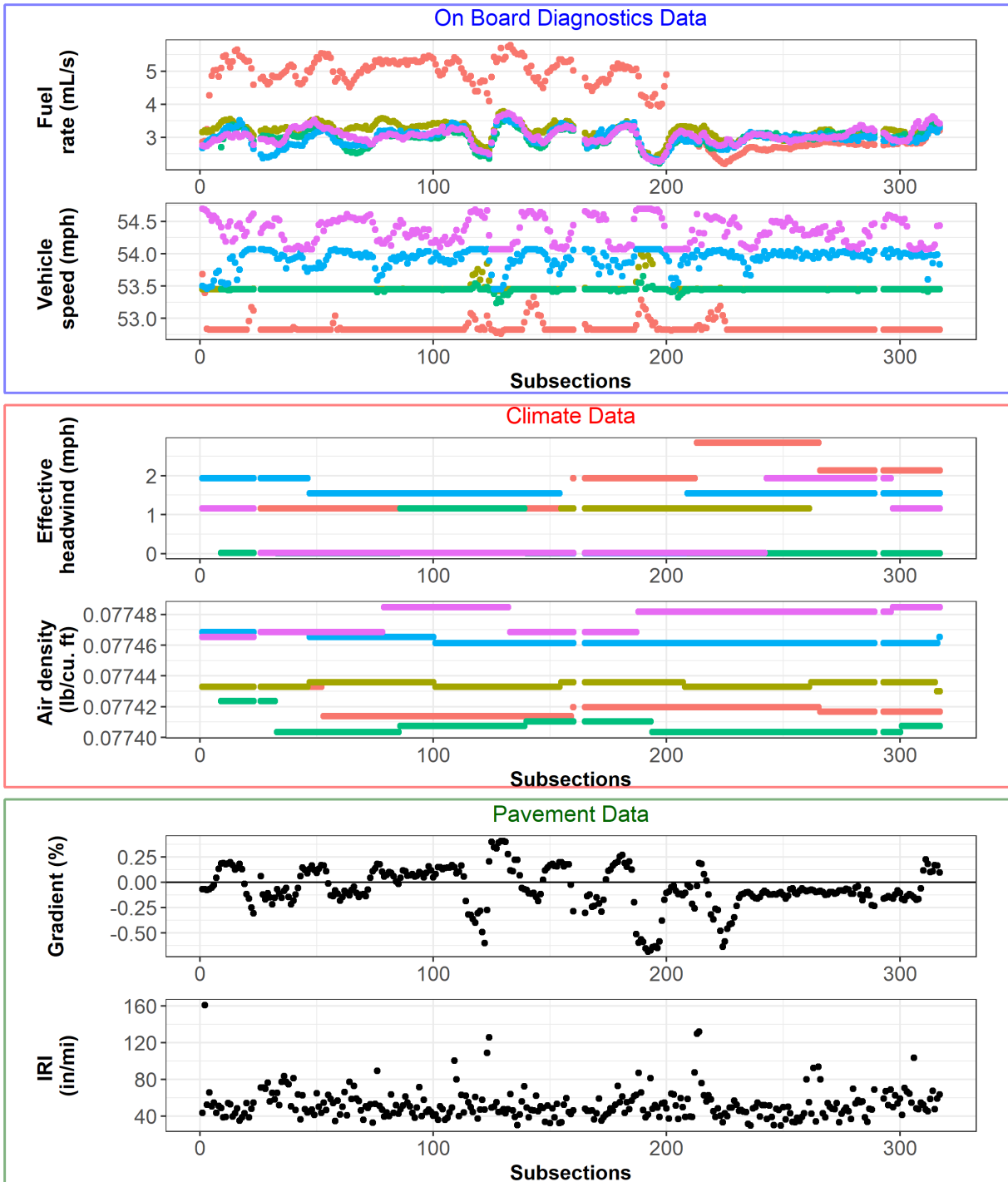


Figure P.209: F-450 data on Section PH04.

PH07-YOL-CR98N-HMA F450 summer_day 35 mph

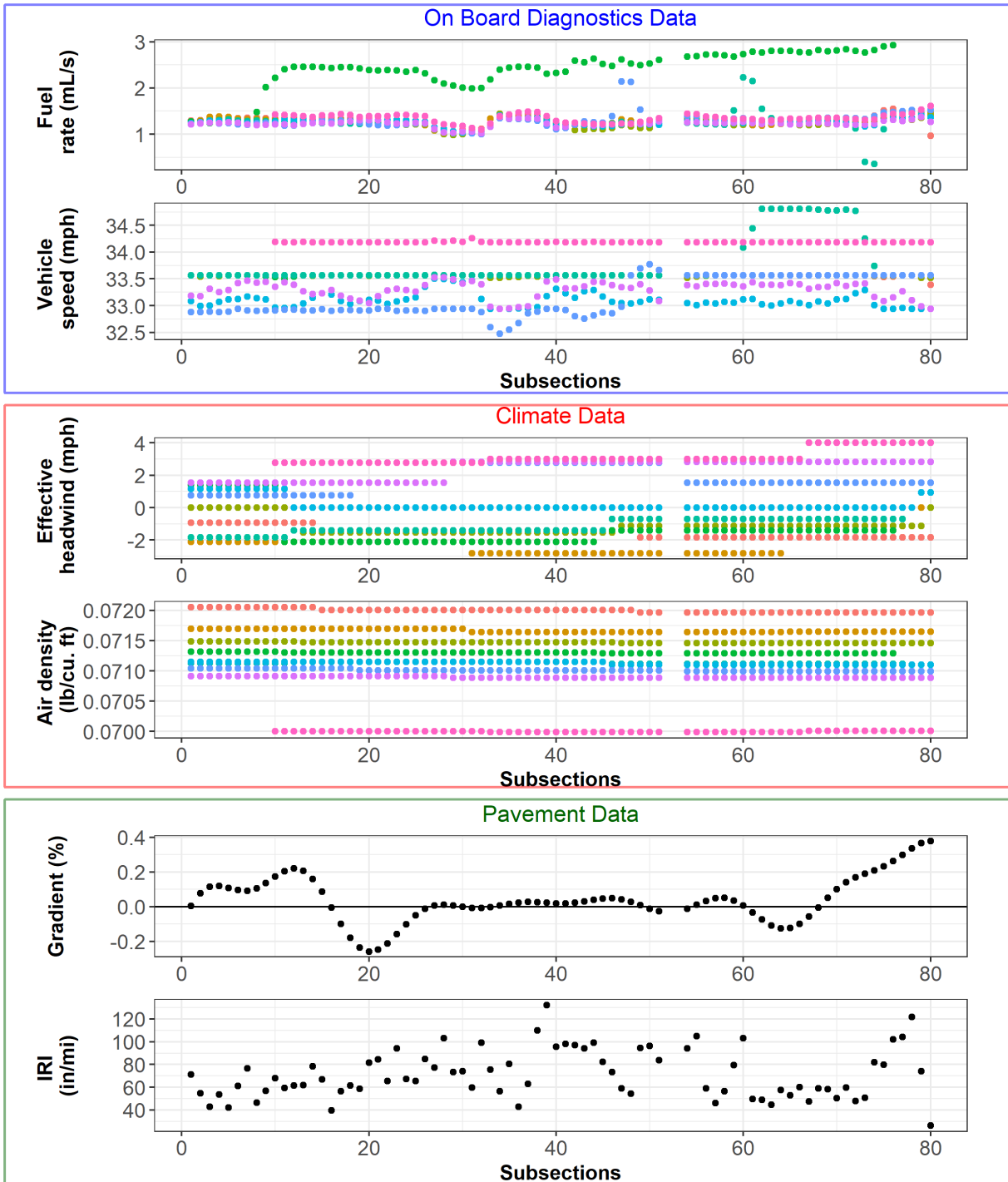


Figure P.210: F-450 data on Section PH07.

PH07-YOL-CR98N-HMA F450 summer_day 45 mph

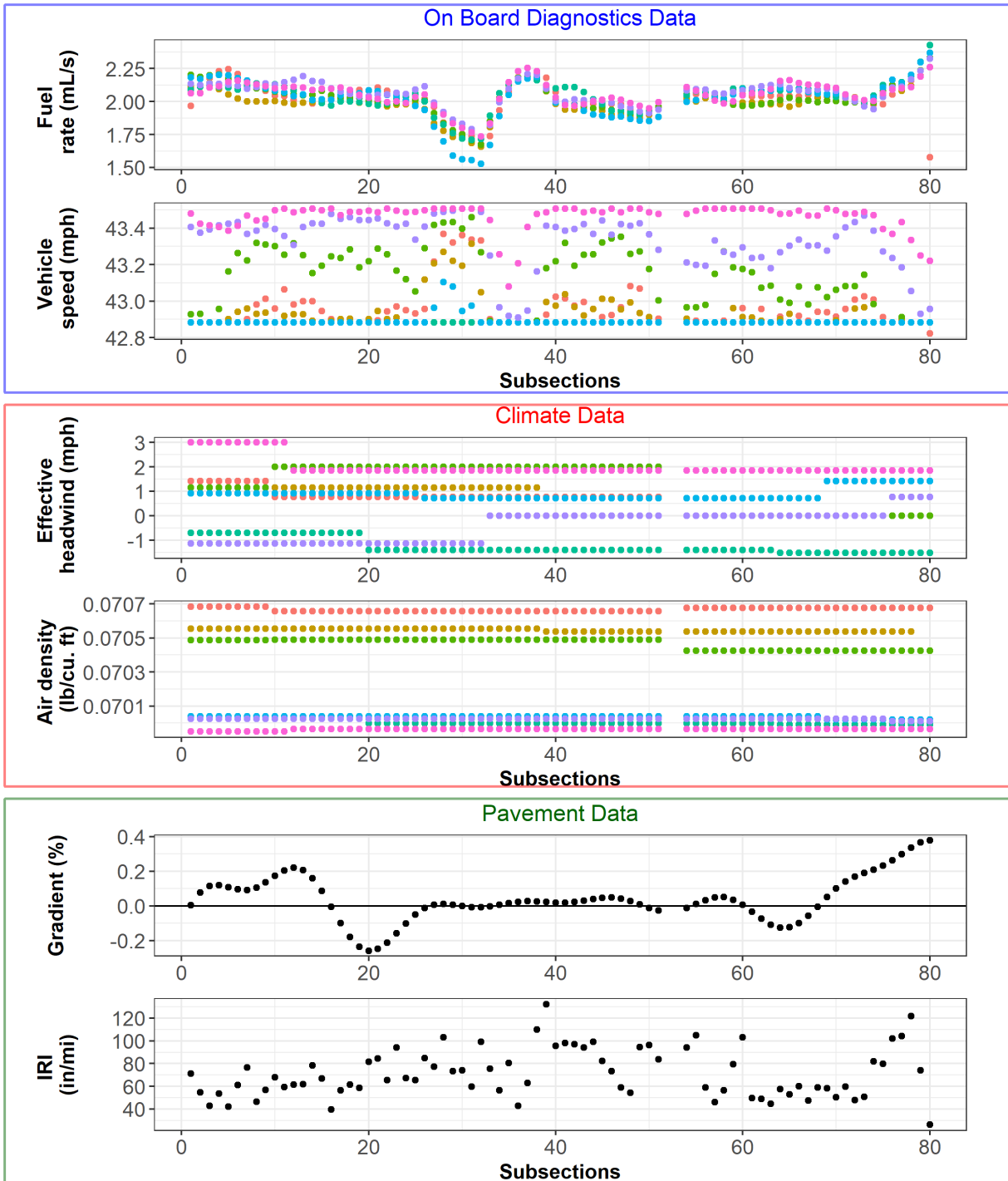


Figure P.211: F-450 data on Section PH07.

PH07-YOL-CR98N-HMA F450 summer_night 35 mph

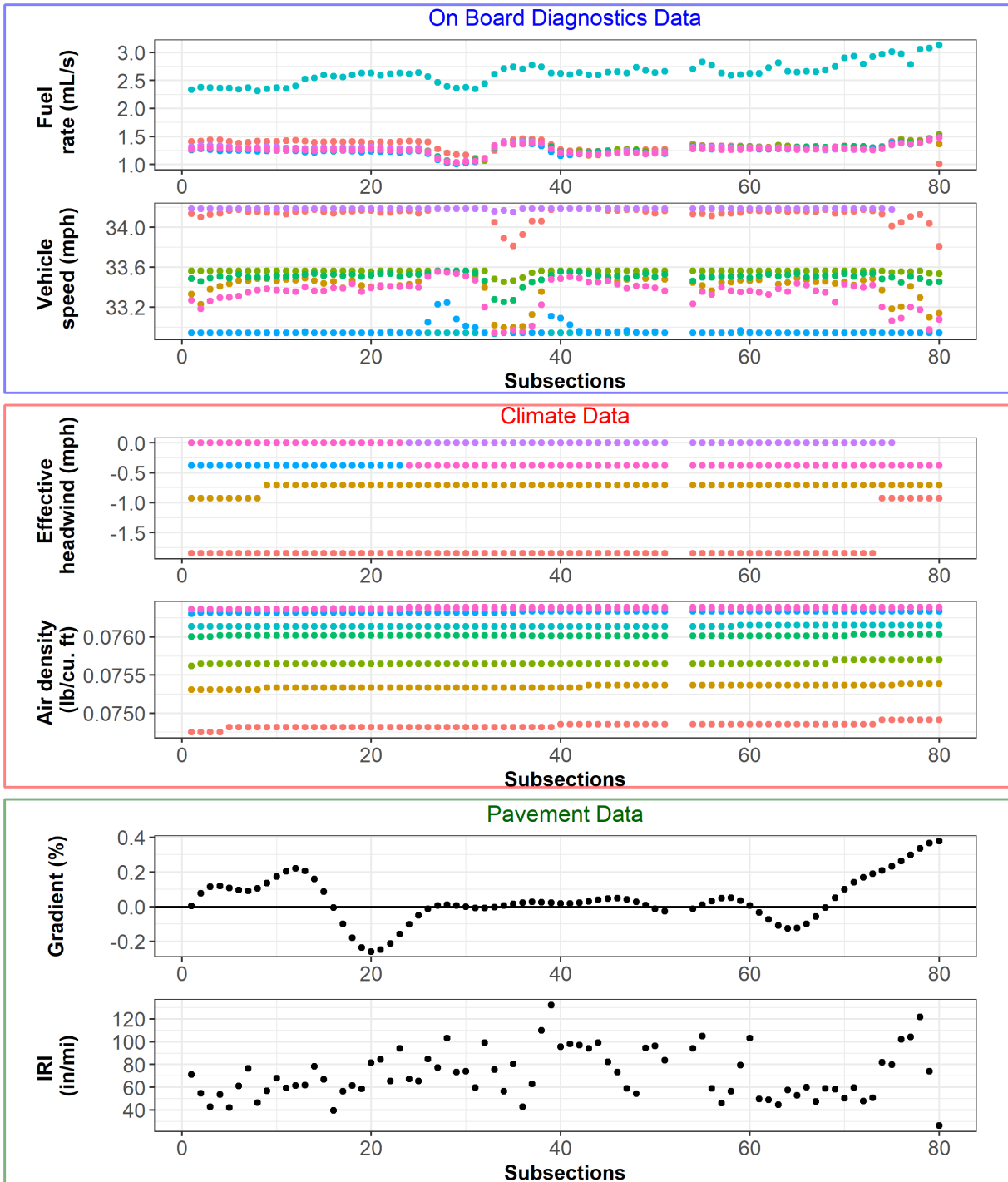


Figure P.212: F-450 data on Section PH07.

PH07-YOL-CR98N-HMA F450 summer_night 45 mph

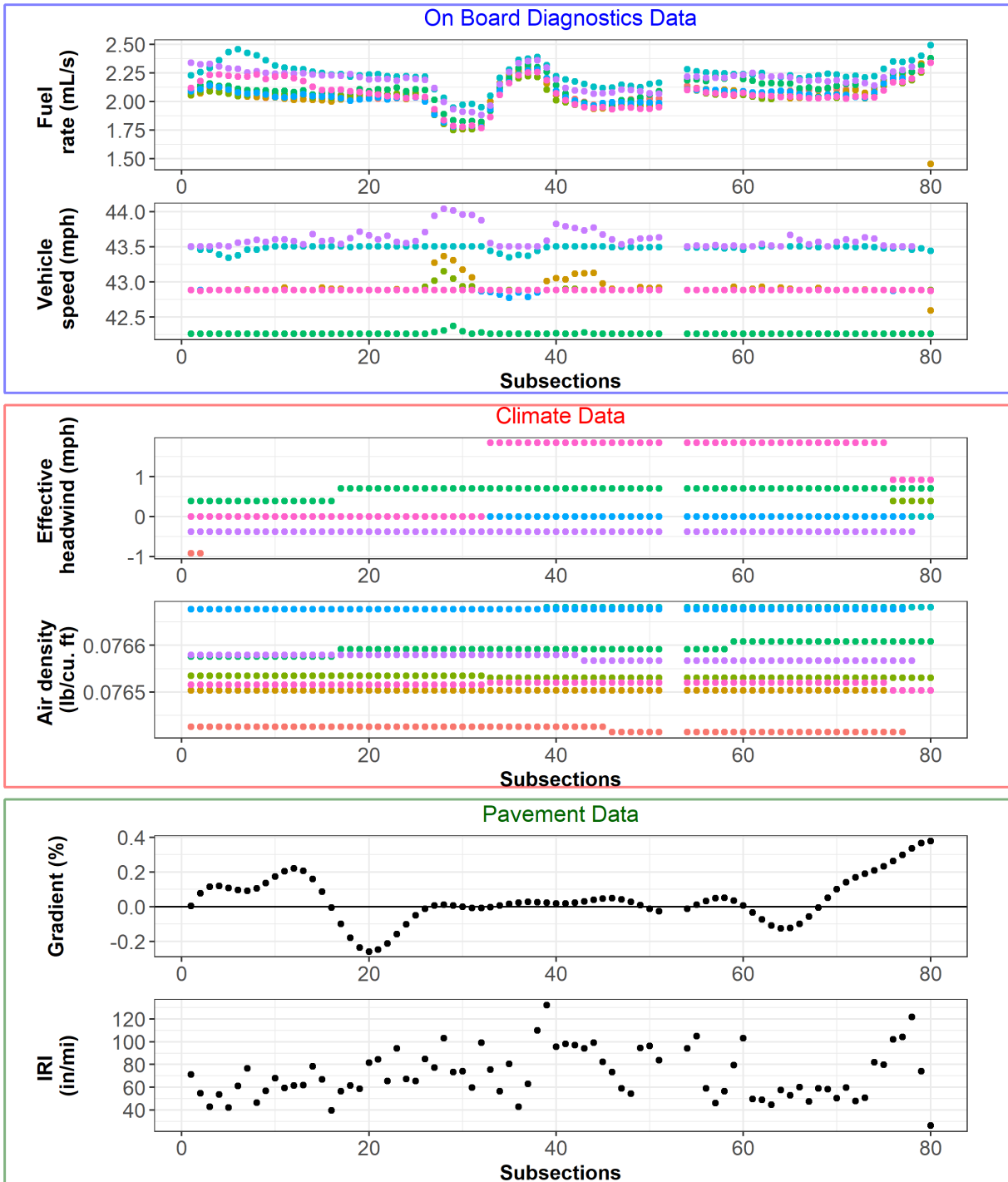


Figure P.213: F-450 data on Section PH07.

PH07-YOL-CR98N-HMA F450 winter_day 35 mph

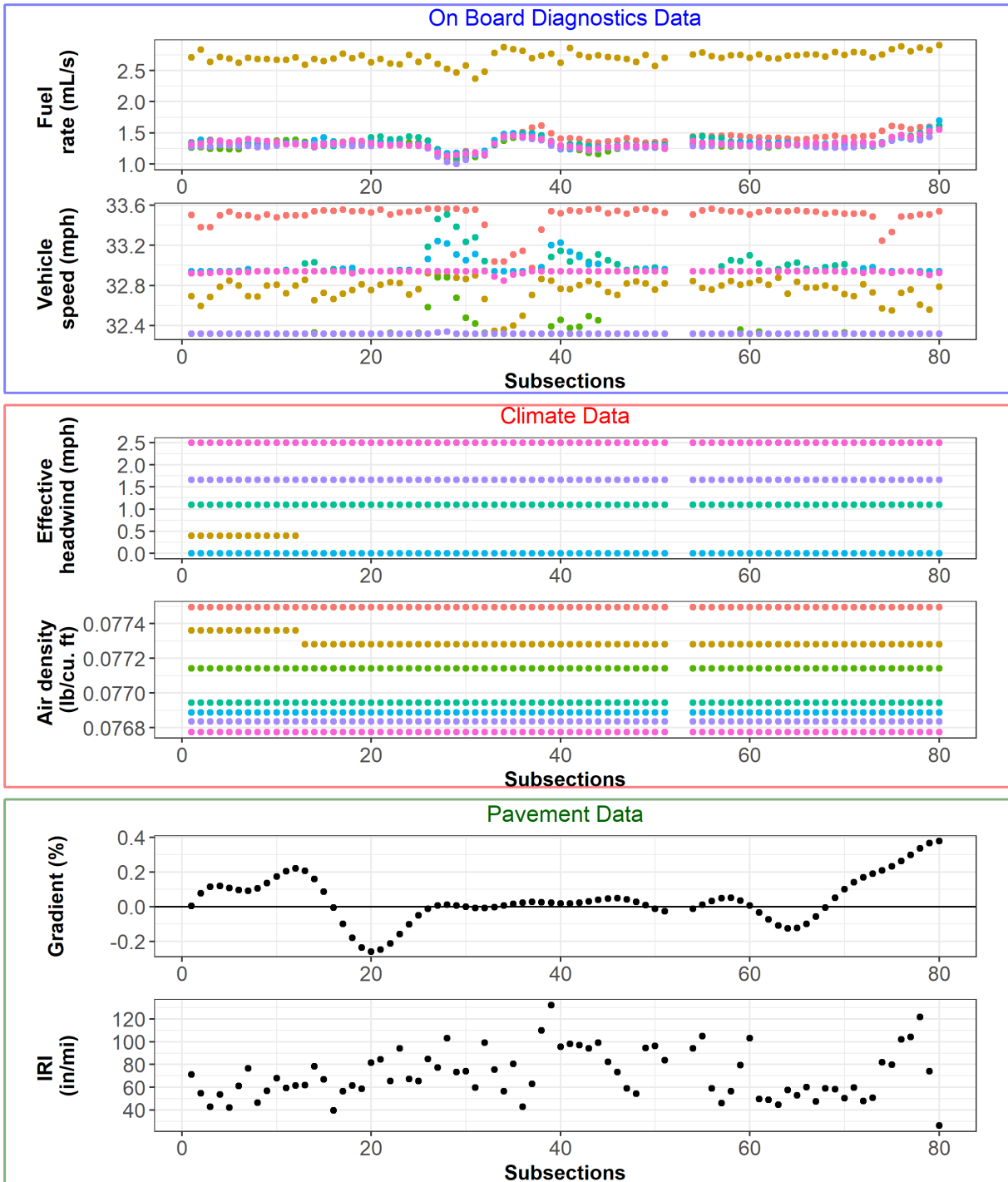


Figure P.214: F-450 data on Section PH07.

PH07-YOL-CR98N-HMA F450 winter_day 45 mph

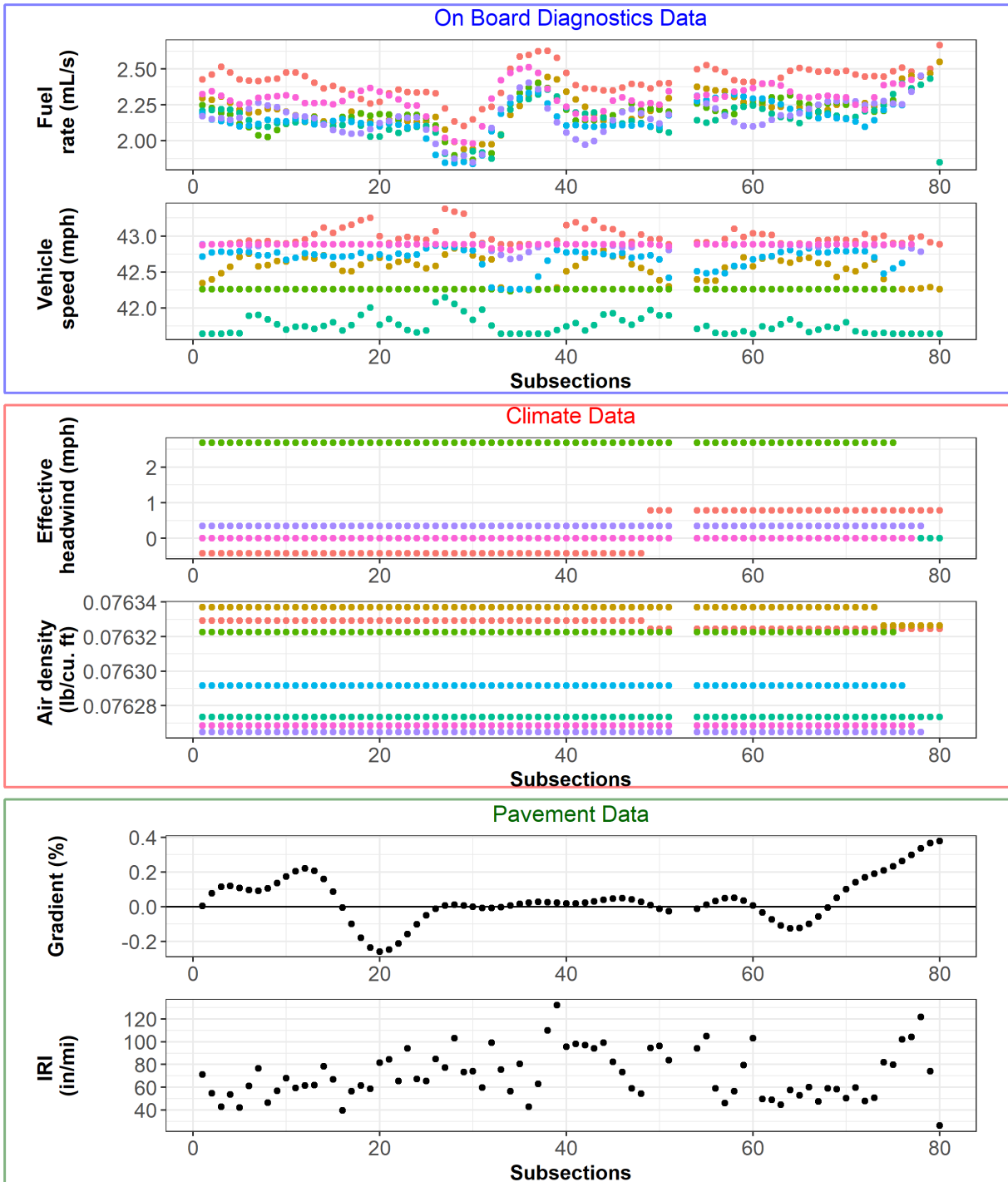


Figure P.215: F-450 data on Section PH07.

PH08-YOL-CR29E-HMA F450 summer_day 35 mph

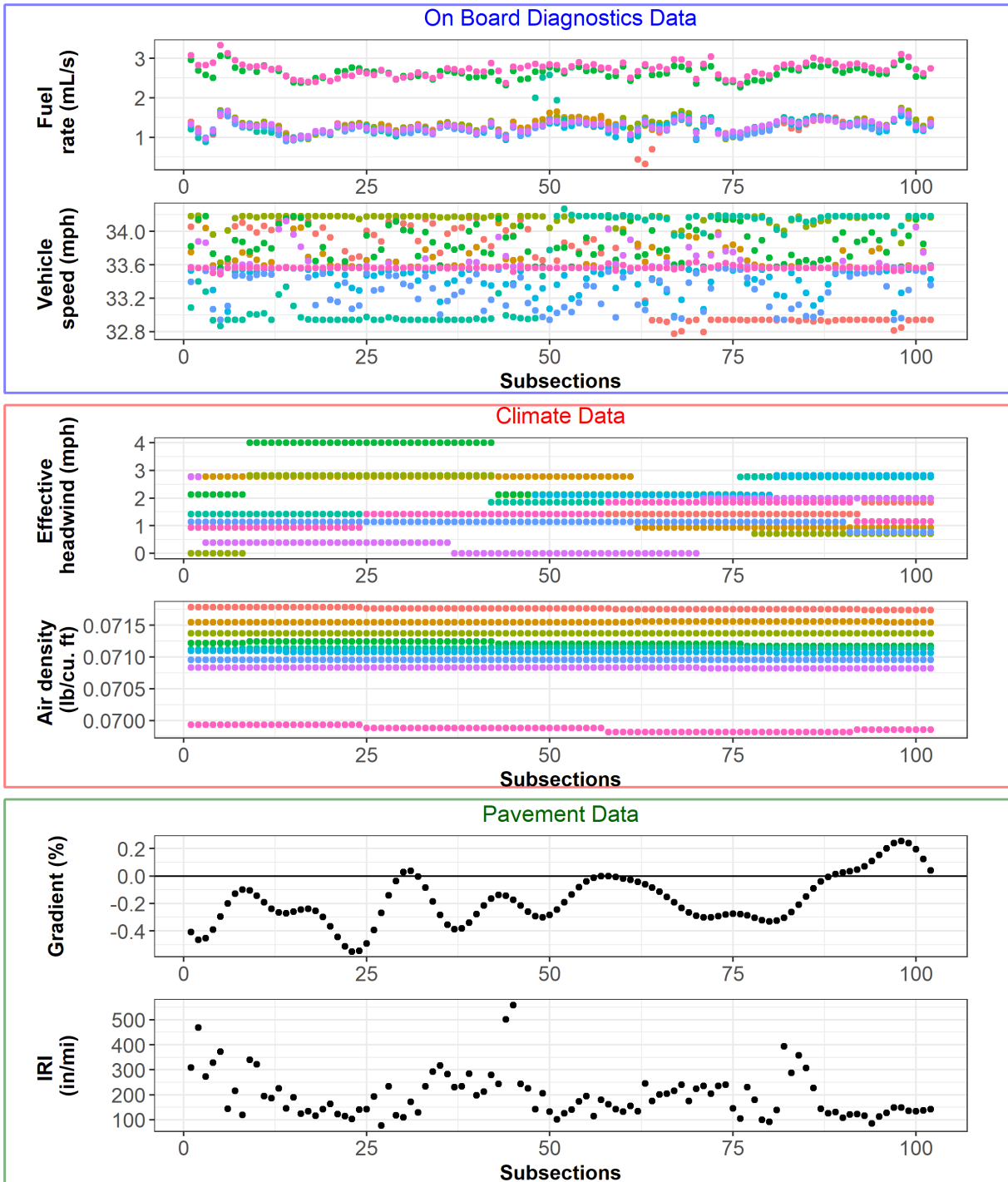


Figure P.216: F-450 data on Section PH08.

PH08-YOL-CR29E-HMA F450 summer_day 45 mph

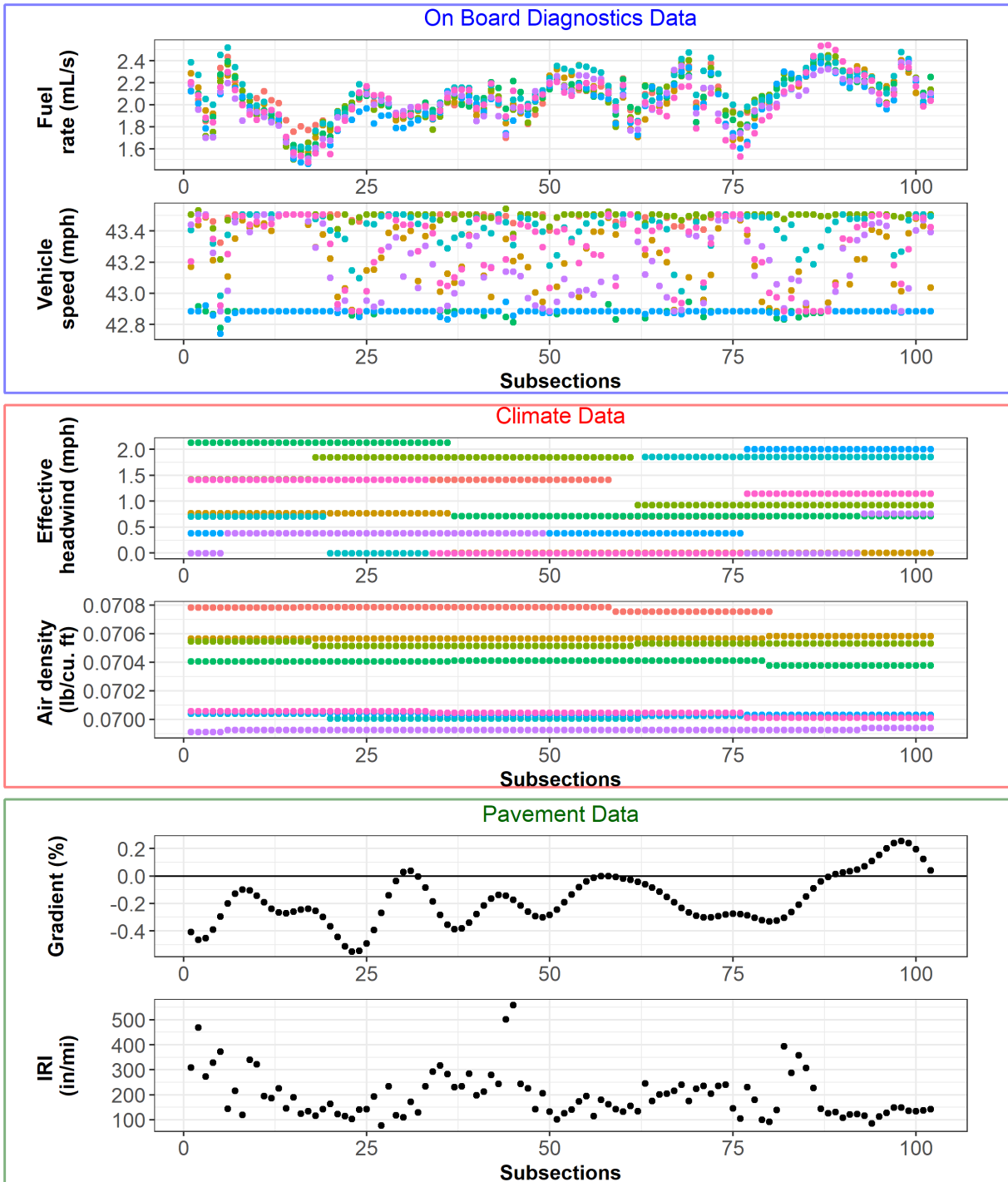


Figure P.217: F-450 data on Section PH08.

PH08-YOL-CR29E-HMA F450 summer_night 35 mph

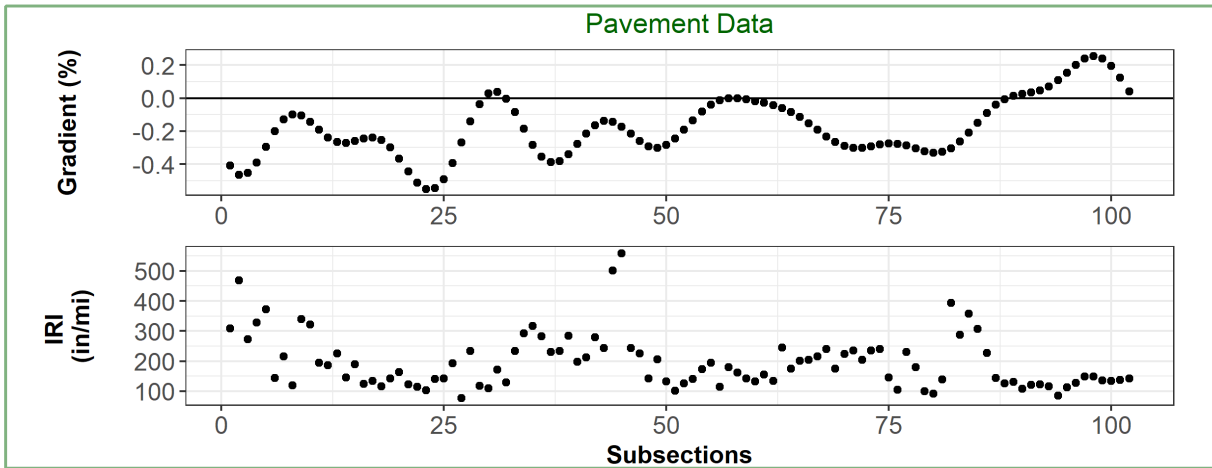
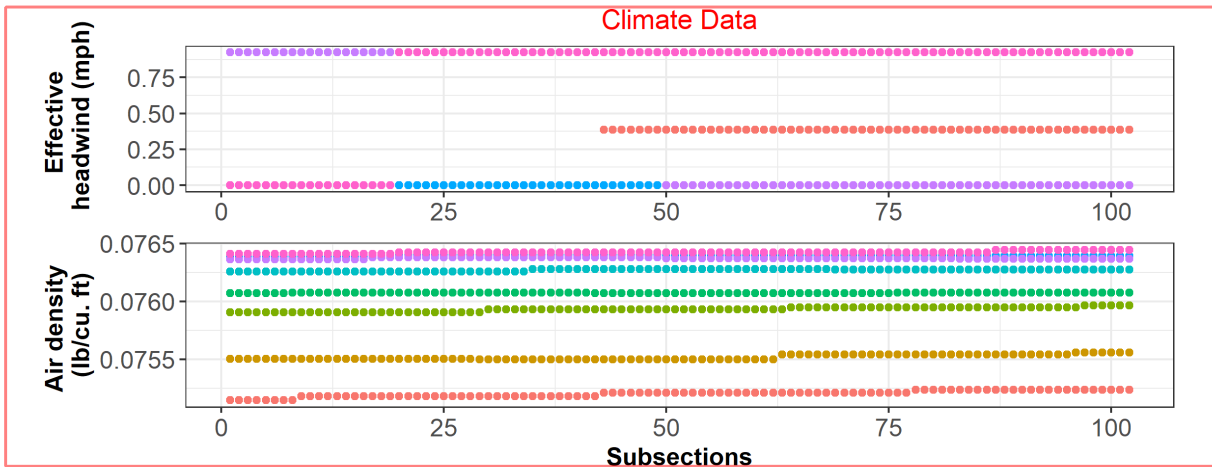
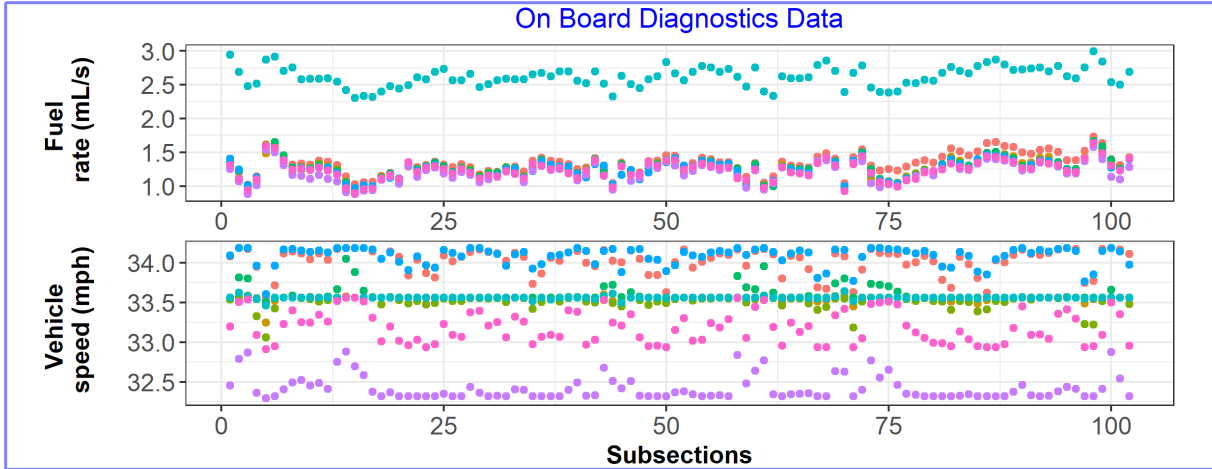


Figure P.218: F-450 data on Section PH08.

PH08-YOL-CR29E-HMA F450 summer_night 45 mph

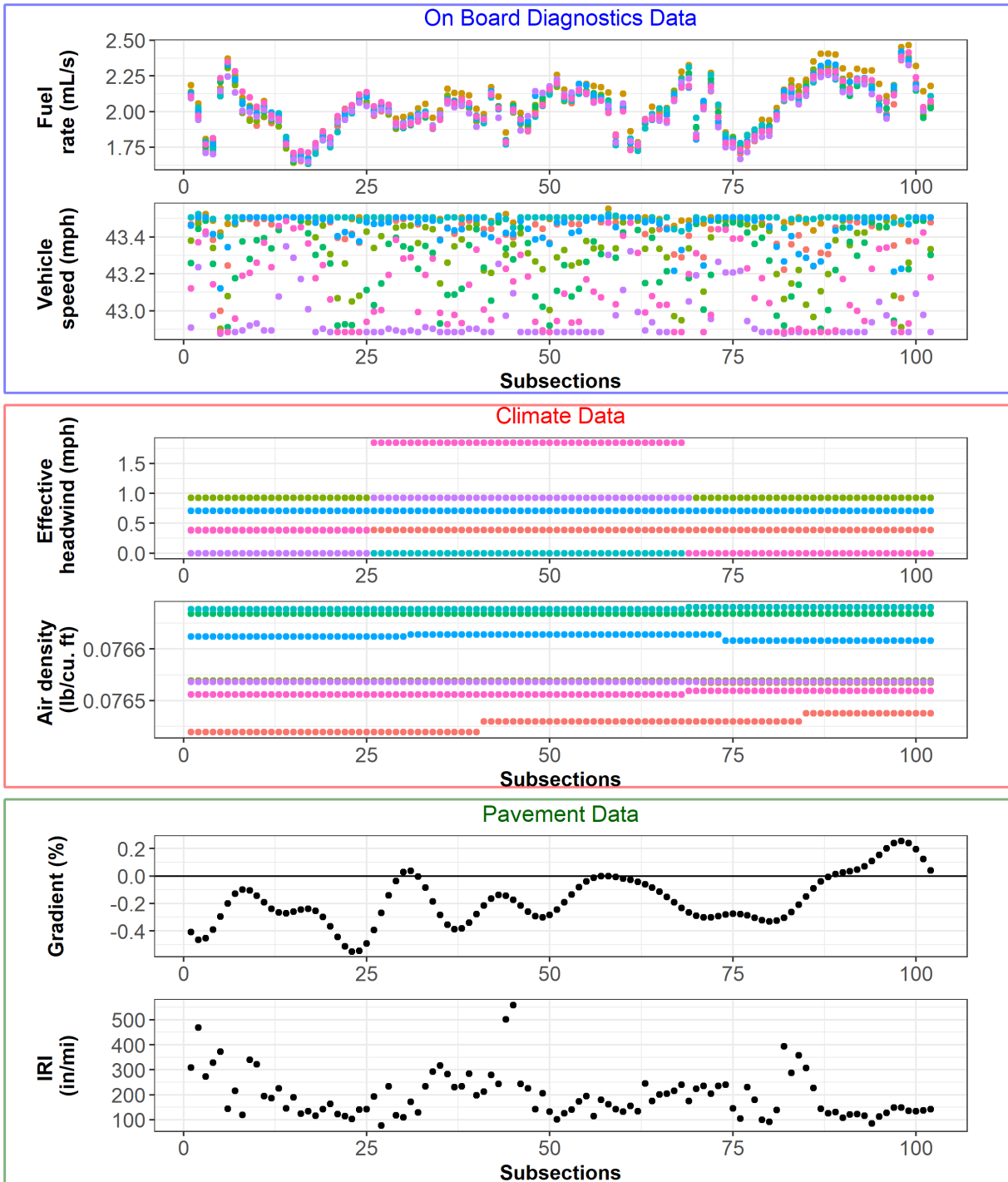


Figure P.219: F-450 data on Section PH08.

PH08-YOL-CR29E-HMA F450 winter_day 35 mph

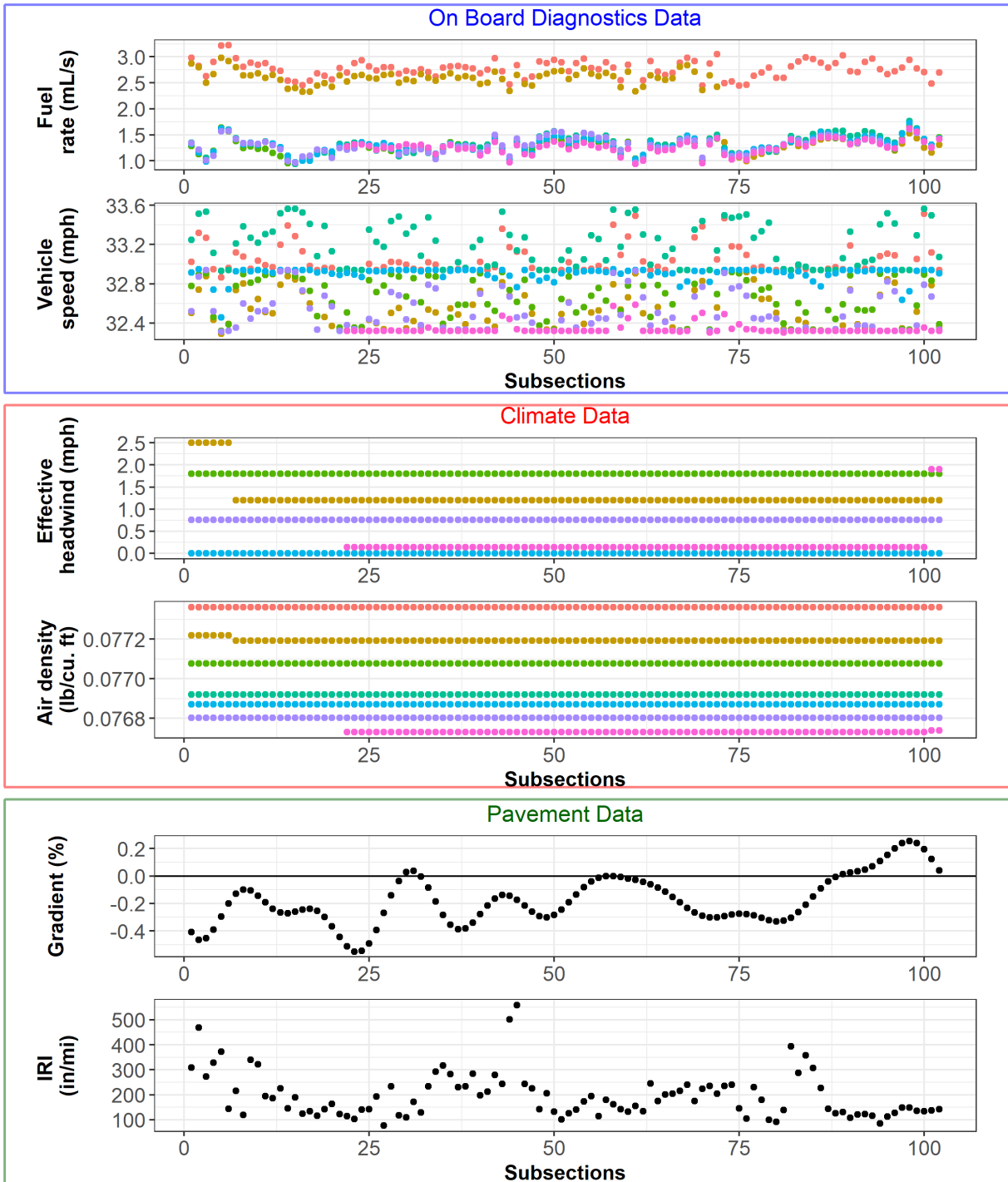


Figure P.220: F-450 data on Section PH08.

PH08-YOL-CR29E-HMA F450 winter_day 45 mph

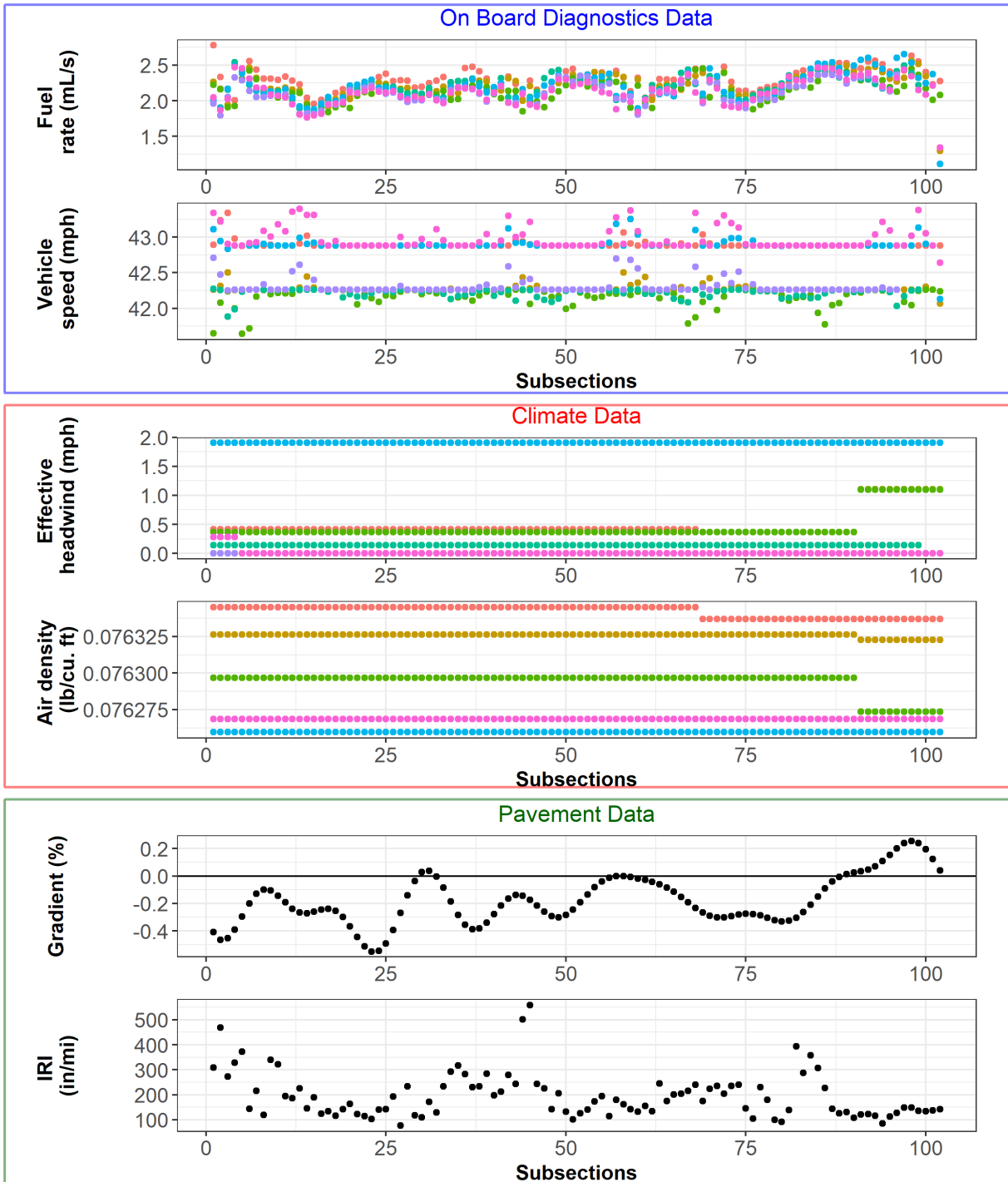


Figure P.221: F-450 data on Section PH08.

PH09-SUT113N-RHMA-O F450 summer_day 45 mph

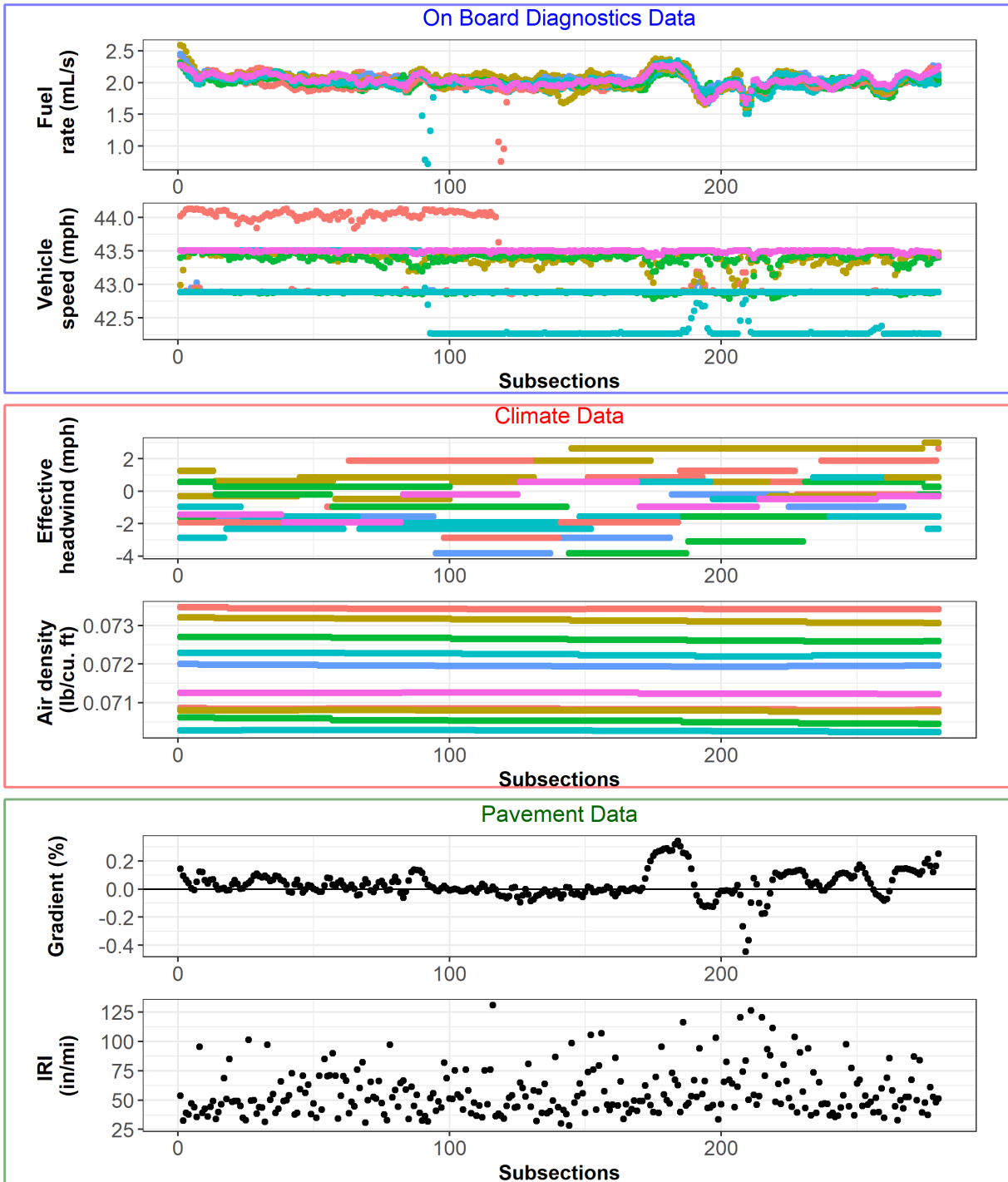


Figure P.222: F-450 data on Section PH09.

PH09-SUT113N-RHMA-O F450 summer_day 55 mph

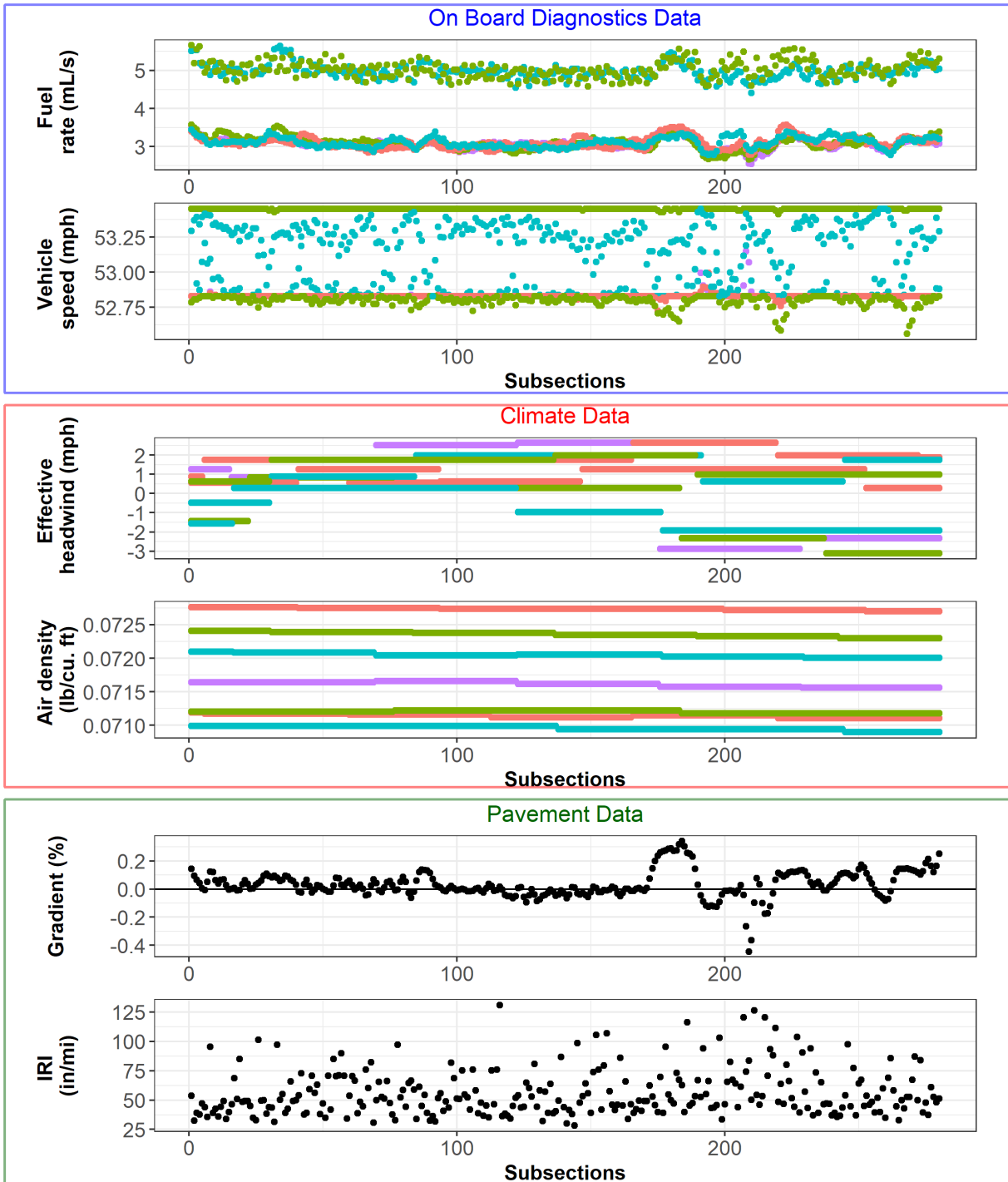


Figure P.223: F-450 data on Section PH09.

PH09-SUT113N-RHMA-O F450 winter_day 45 mph

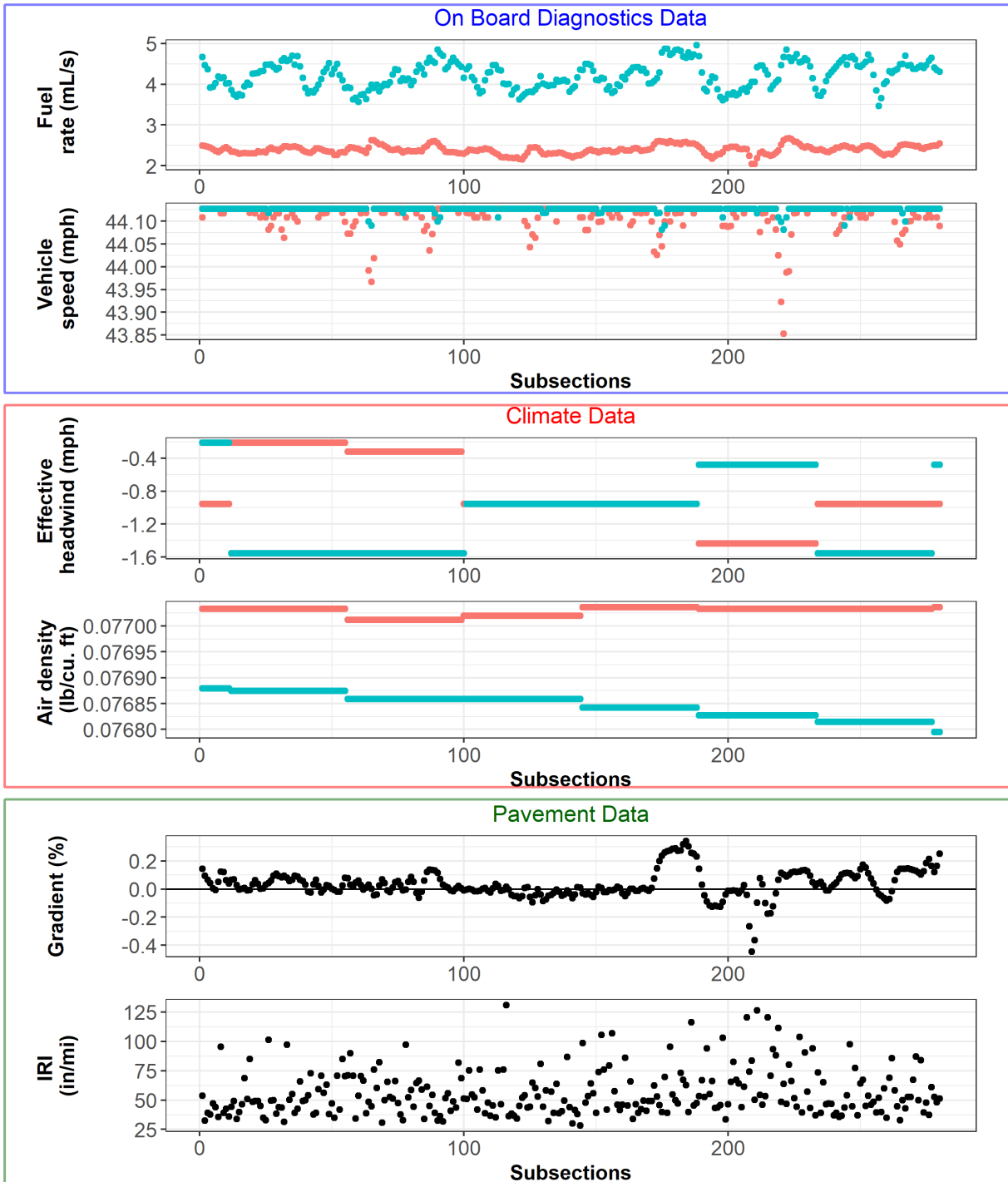


Figure P.224: F-450 data on Section PH09.

PH09-SUT113N-RHMA-O F450 winter_day 55 mph

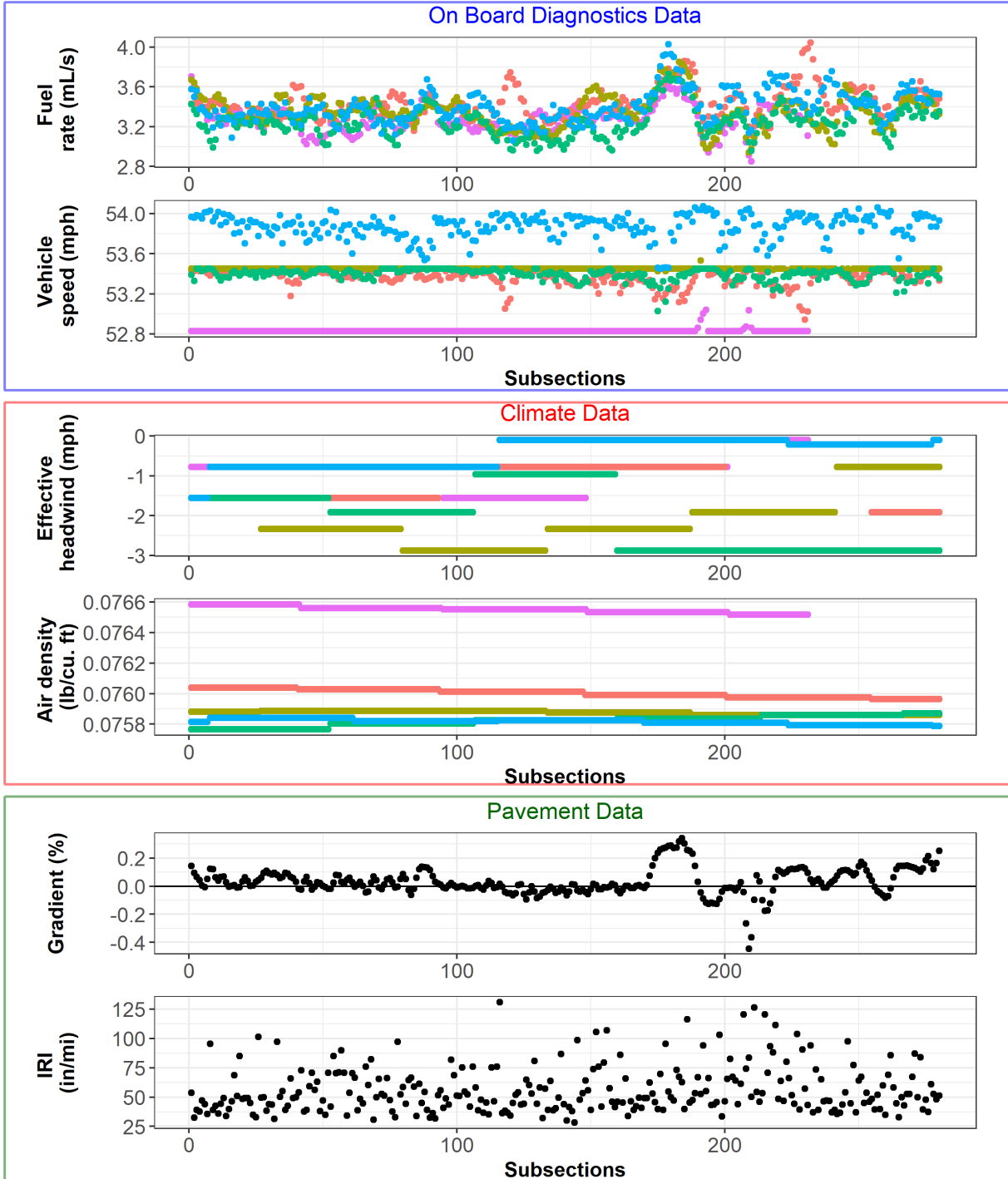


Figure P.225: F-450 data on Section PH09.

PH10-SUT113S-RHMA-O F450 summer_day 45 mph

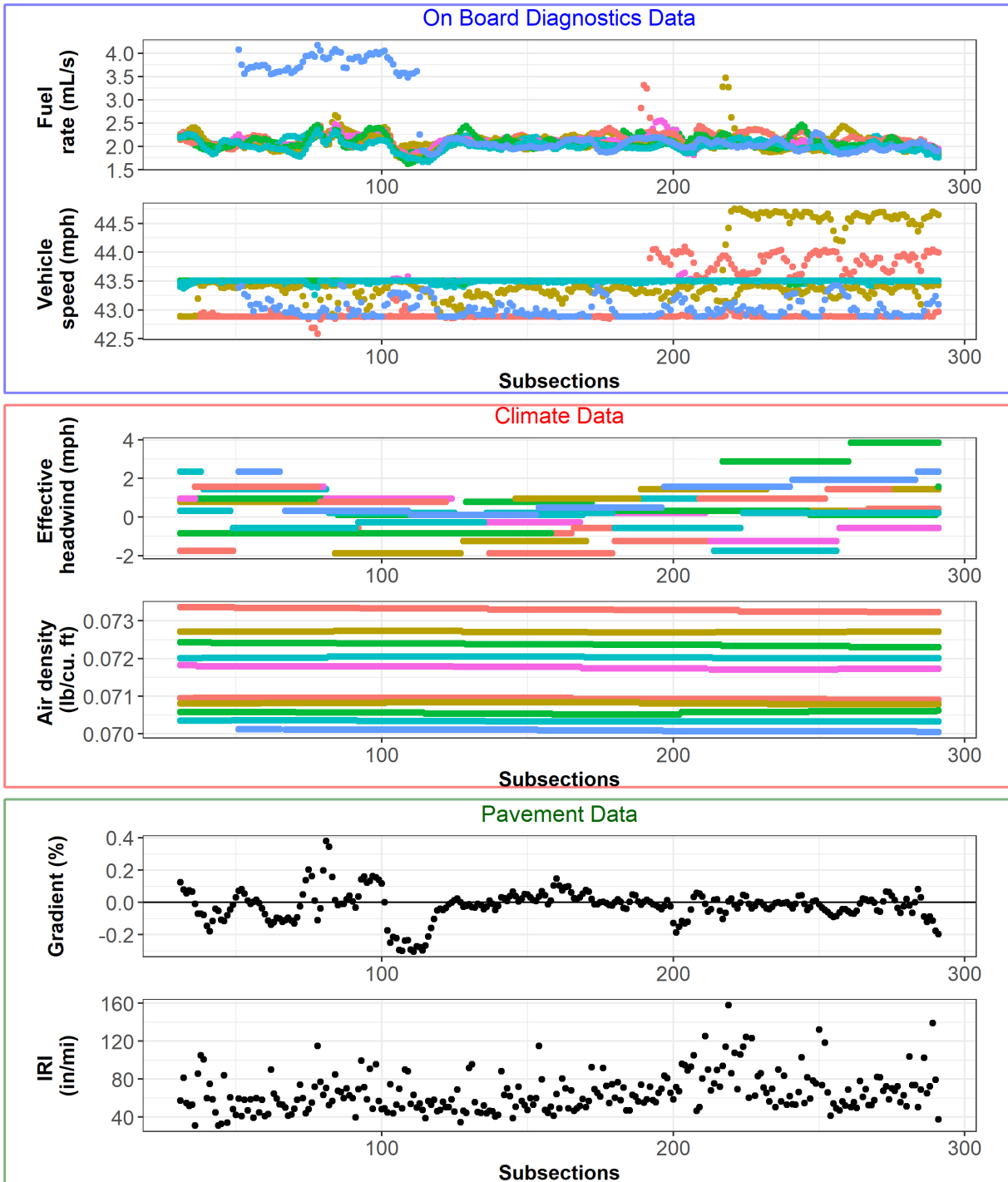


Figure P.226: F-450 data on Section PH10.

PH10-SUT113S-RHMA-O F450 summer_day 55 mph

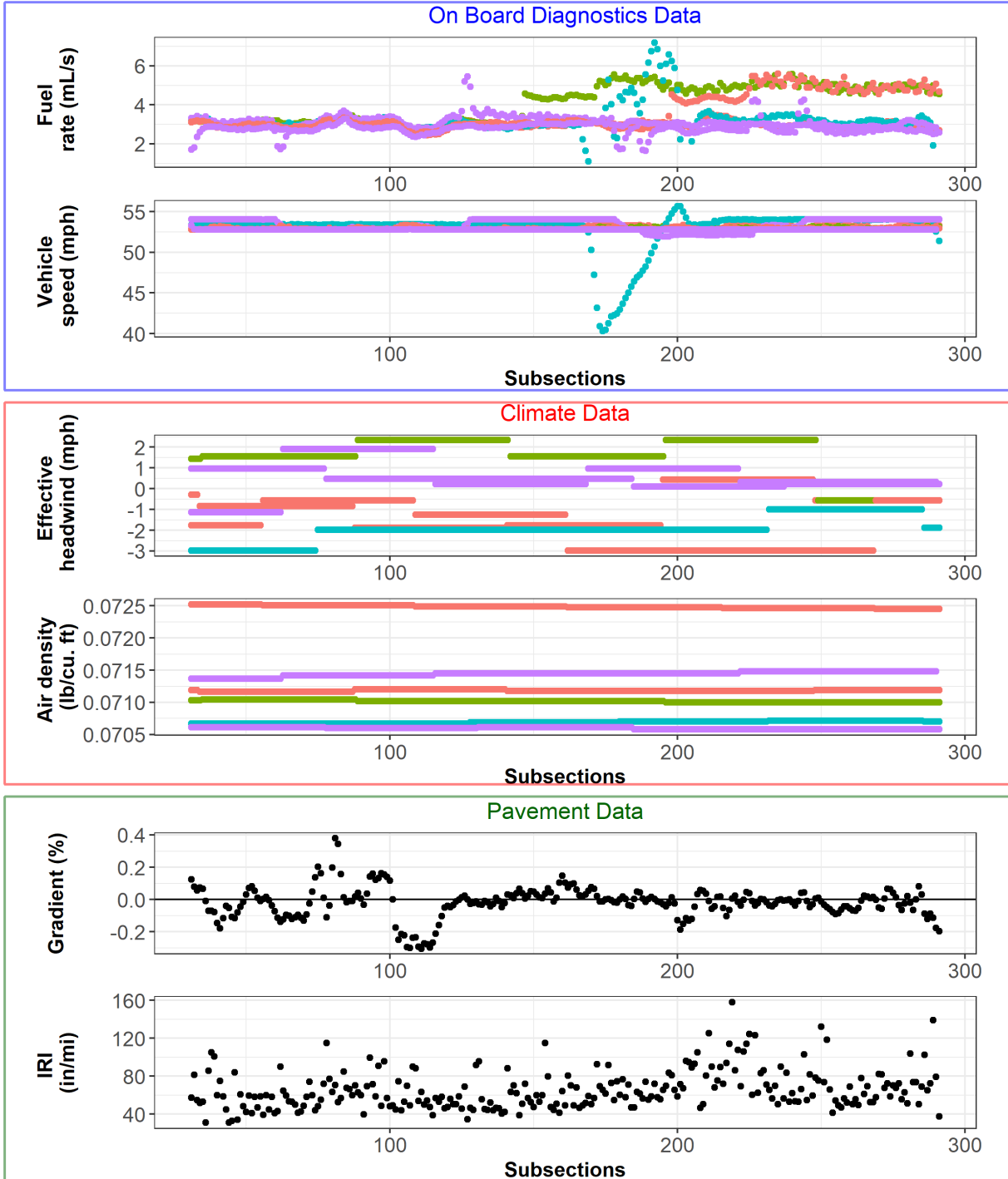


Figure P.227: F-450 data on Section PH10.

PH10-SUT113S-RHMA-O F450 winter_day 45 mph

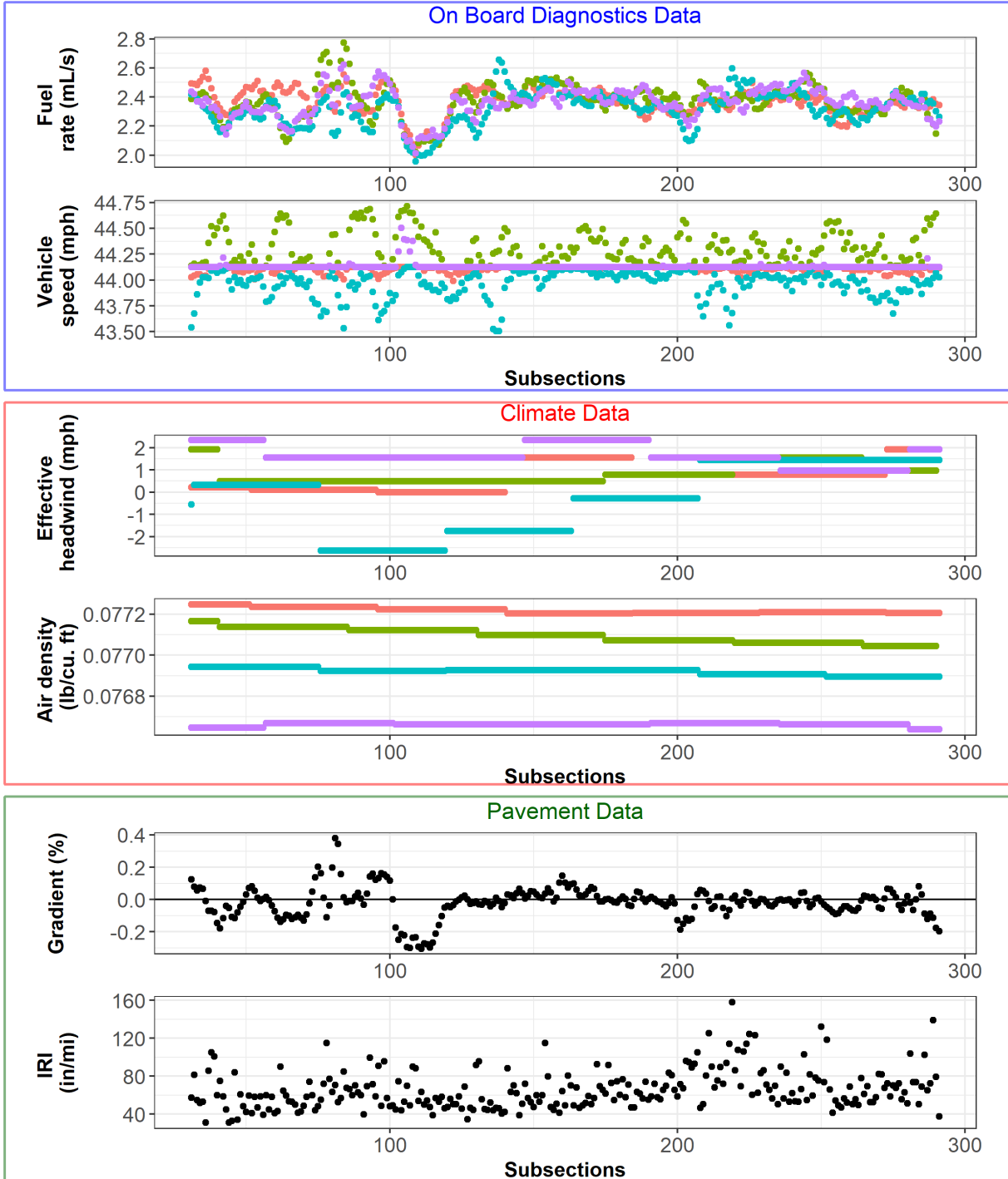


Figure P.228: F-450 data on Section PH10.

PH10-SUT113S-RHMA-O F450 winter_day 55 mph

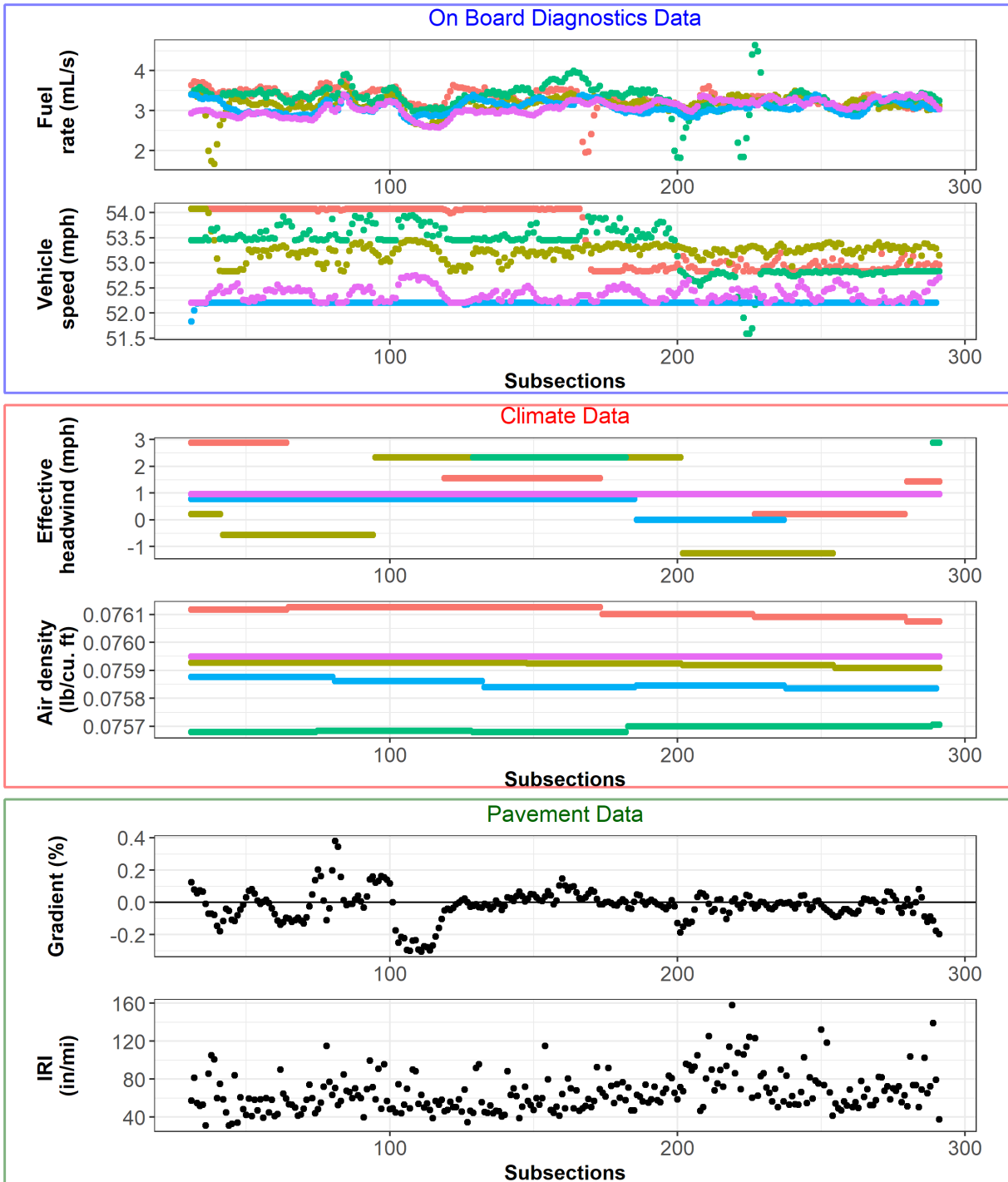


Figure P.229: F-450 data on Section PH10.

PH11-SUT113N-HMA F450 summer_day 45 mph

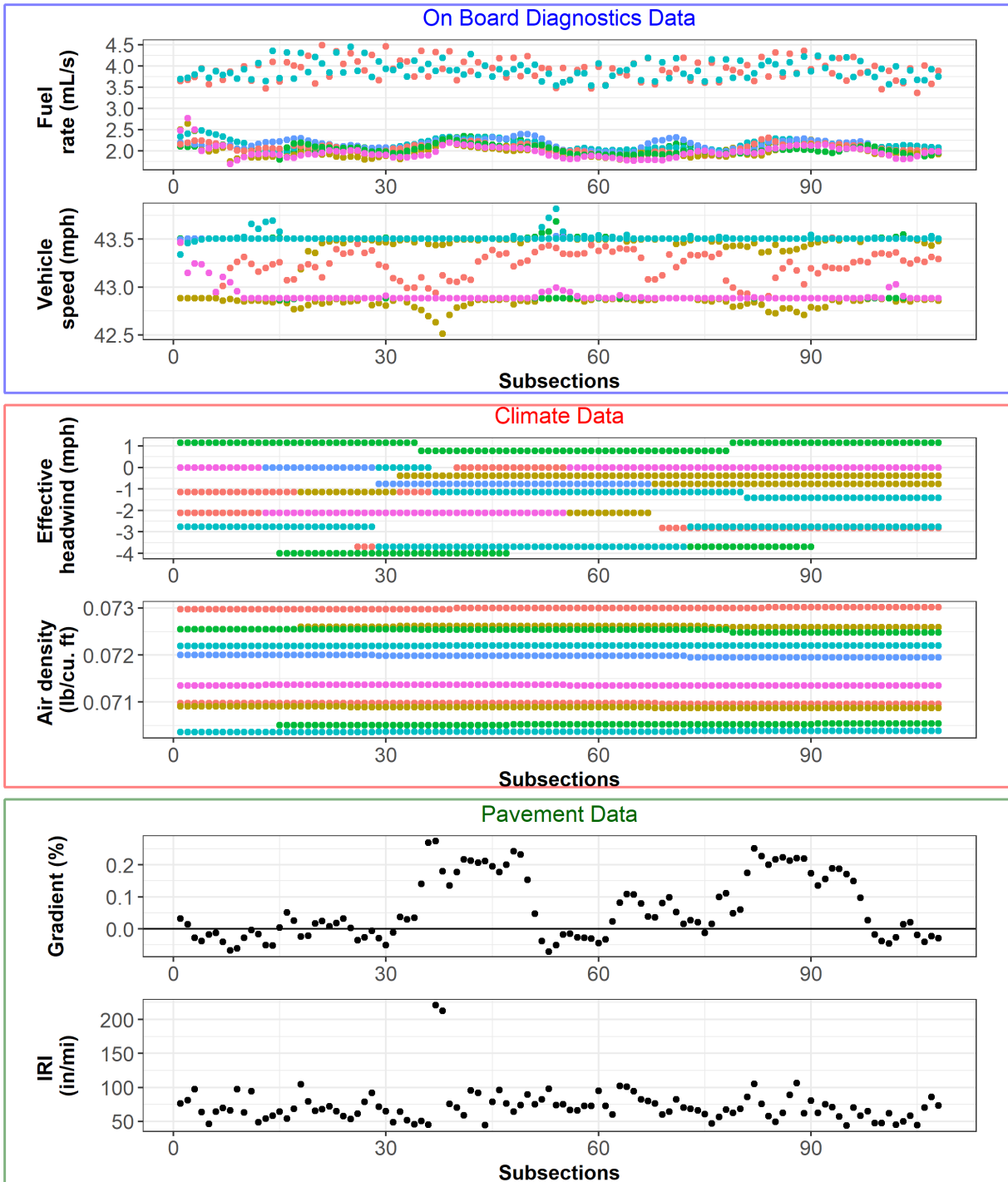


Figure P.230: F-450 data on Section PH11.

PH11-SUT113N-HMA F450 summer_day 55 mph

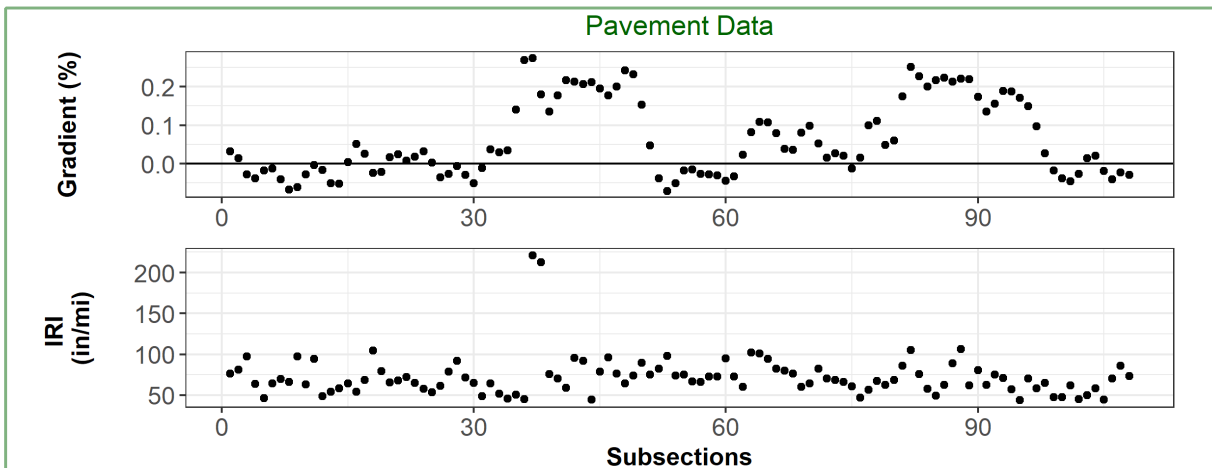
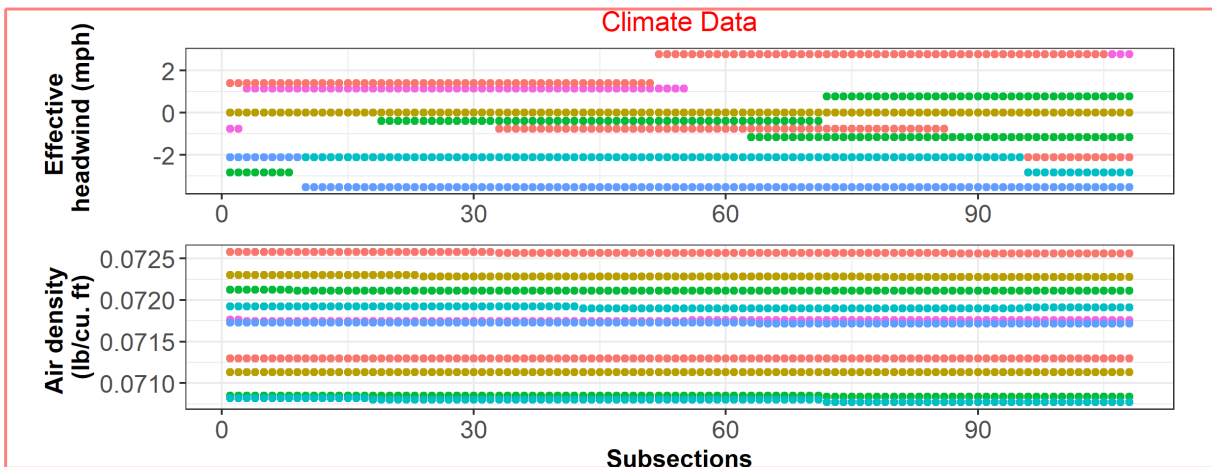
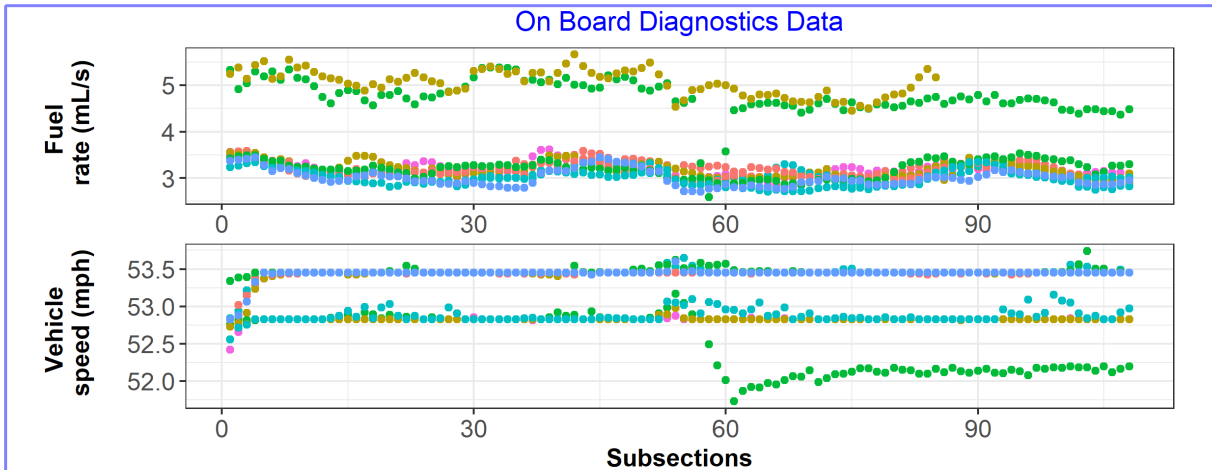


Figure P.231: F-450 data on Section PH11.

PH11-SUT113N-HMA F450 winter_day 45 mph

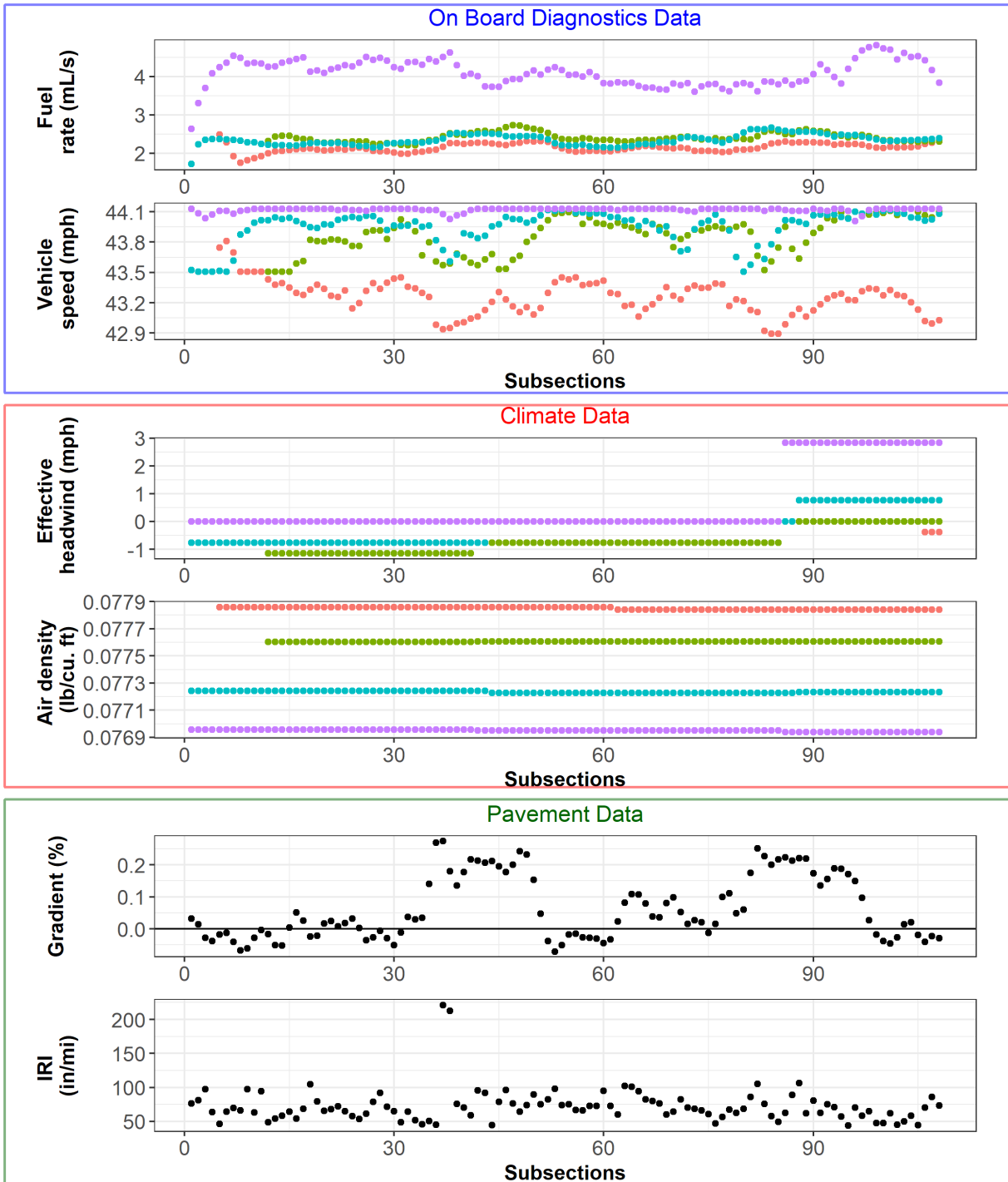


Figure P.232: F-450 data on Section PH11.

PH11-SUT113N-HMA F450 winter_day 55 mph

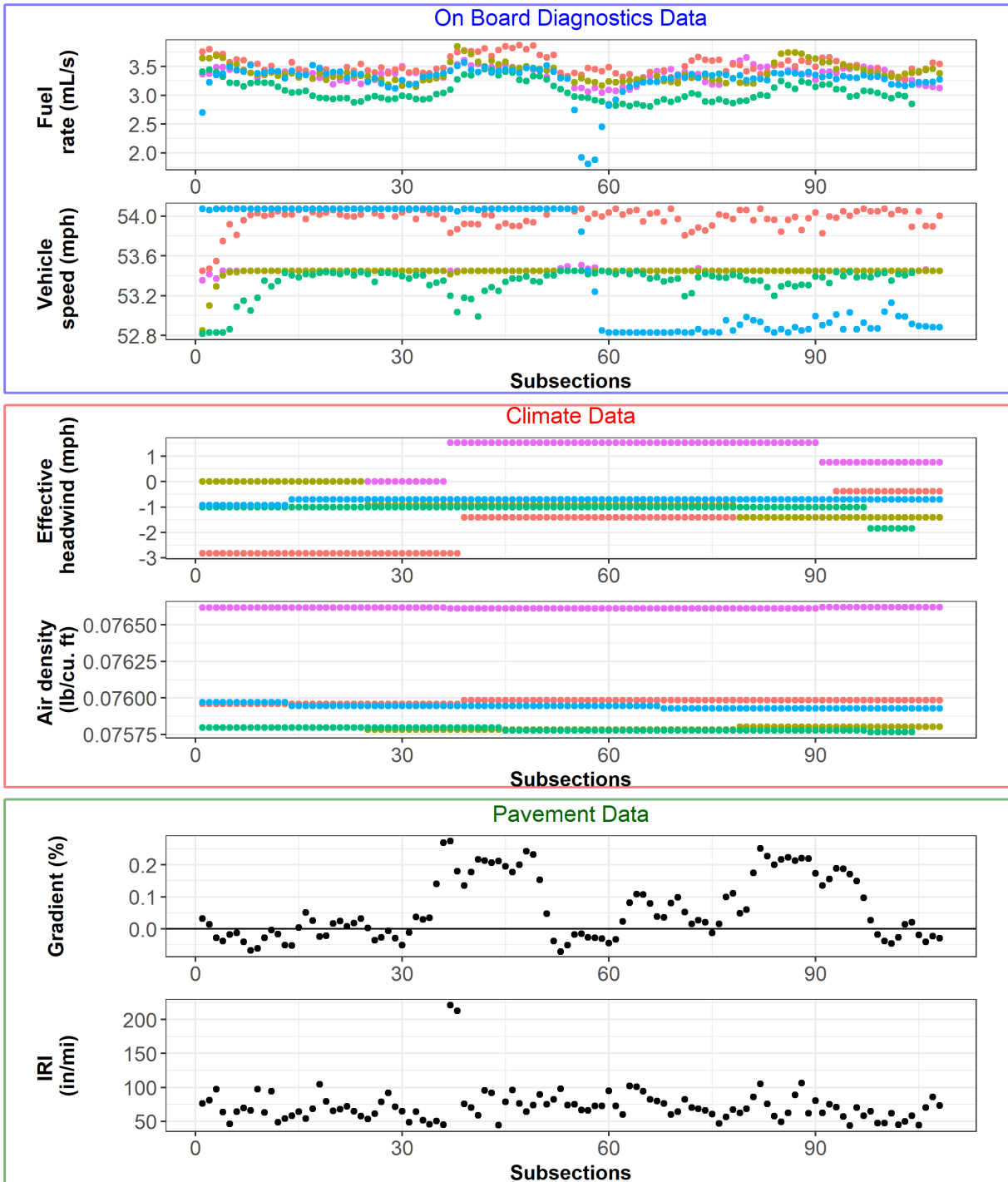


Figure P.233: F-450 data on Section PH11.

PH12-SUT113S-HMA F450 summer_day 45 mph

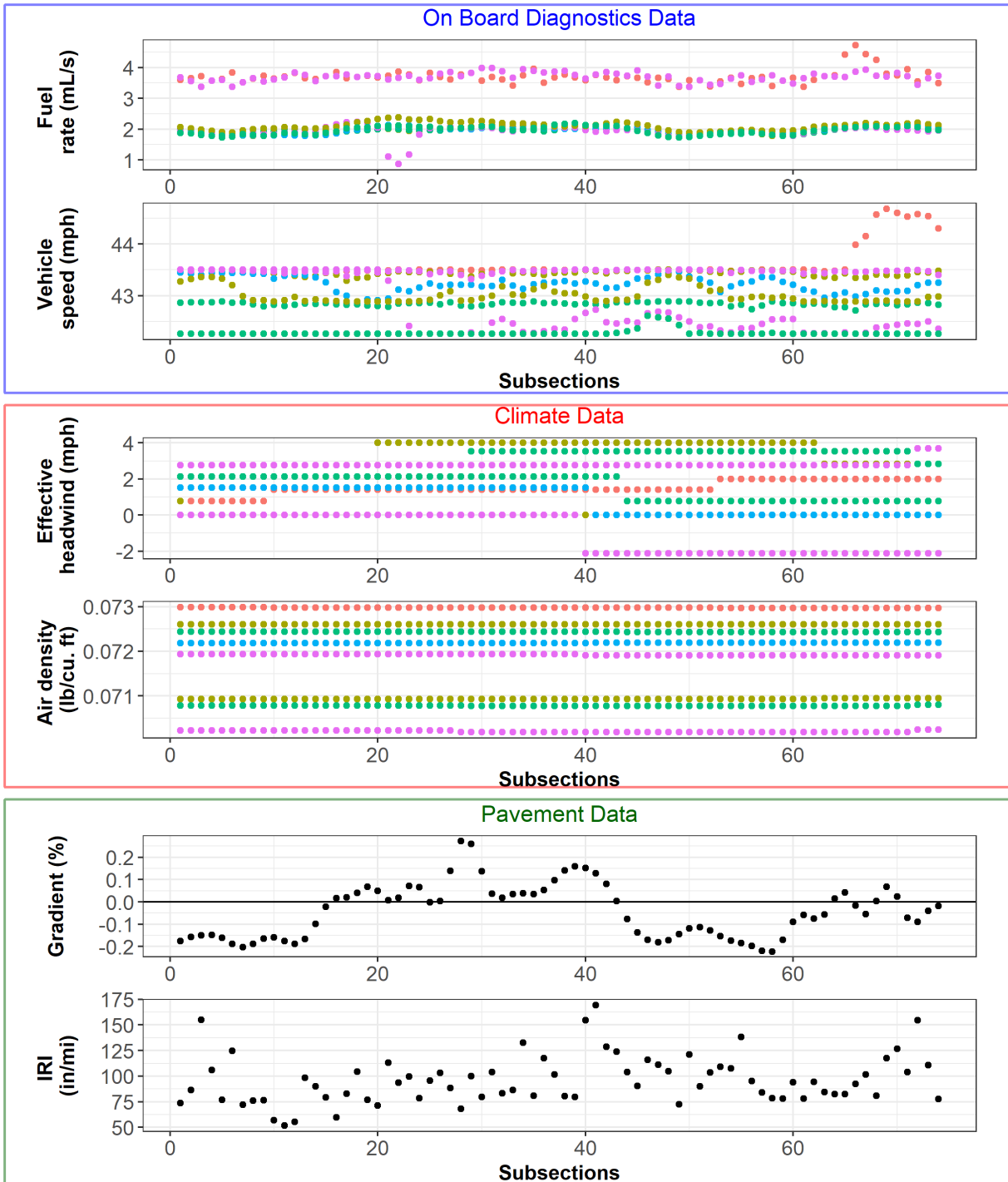


Figure P.234: F-450 data on Section PH12.

PH12-SUT113S-HMA F450 summer_day 55 mph

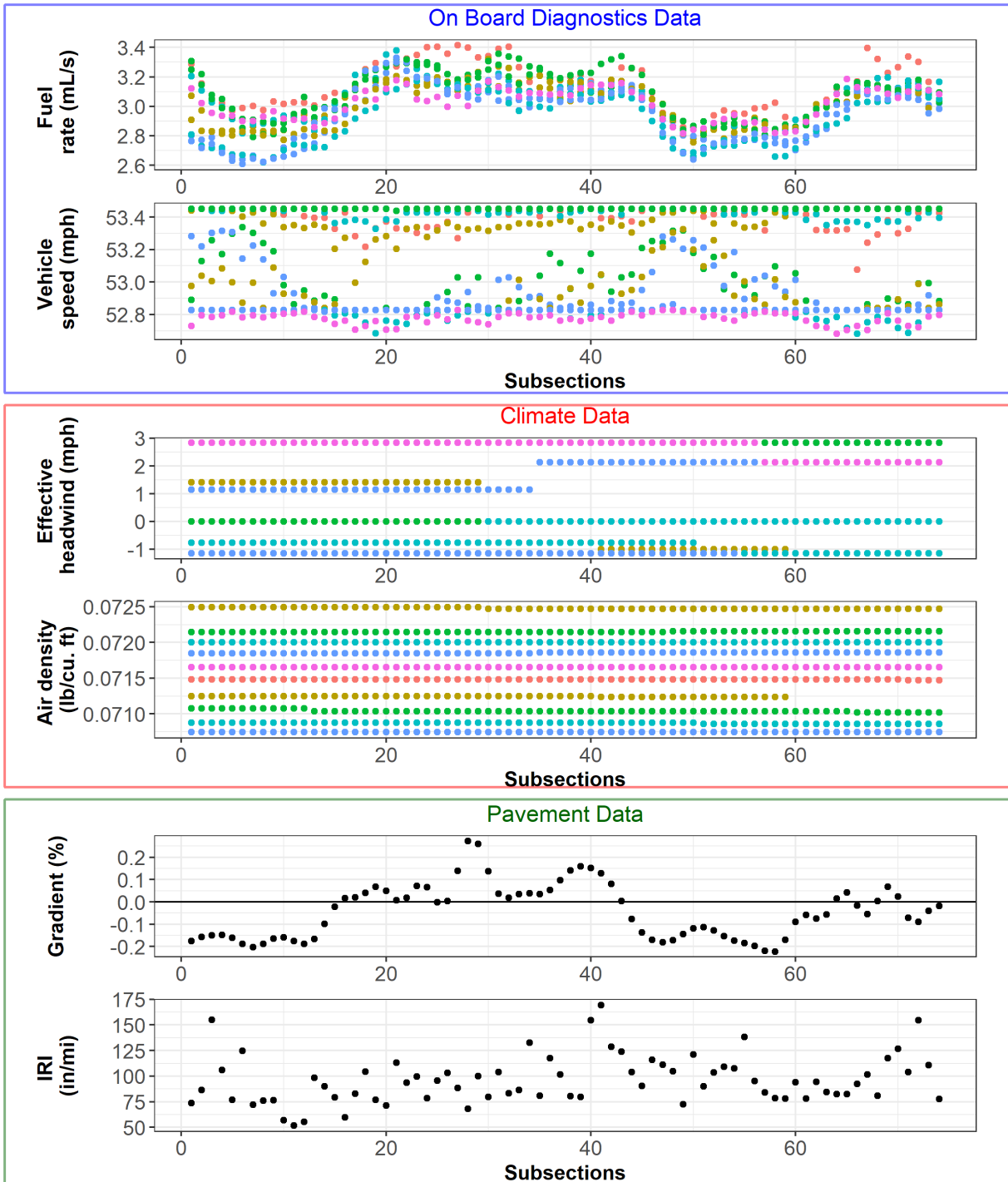


Figure P.235: F-450 data on Section PH12.

PH12-SUT113S-HMA F450 winter_day 45 mph

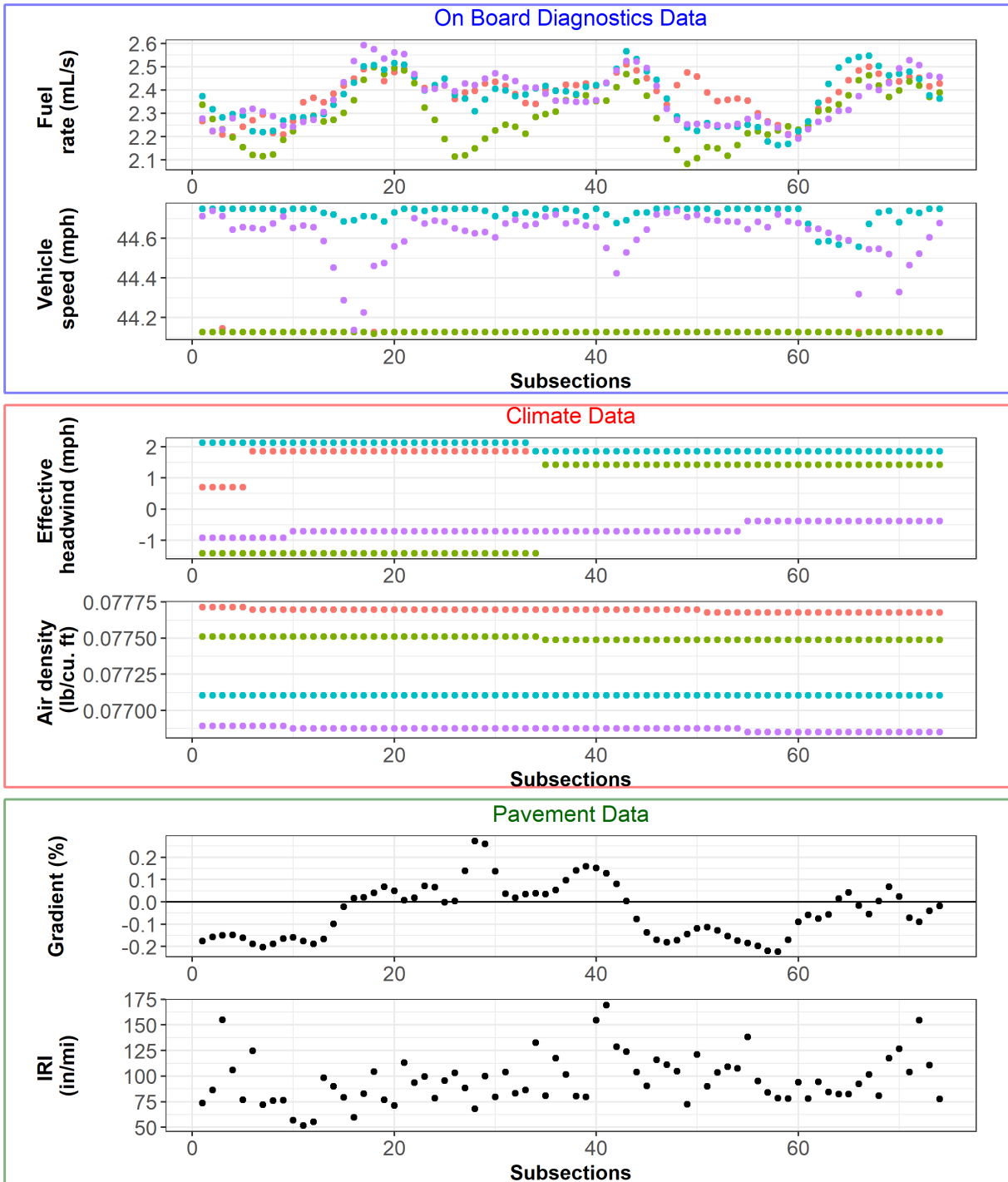


Figure P.236: F-450 data on Section PH12.

PH12-SUT113S-HMA F450 winter_day 55 mph

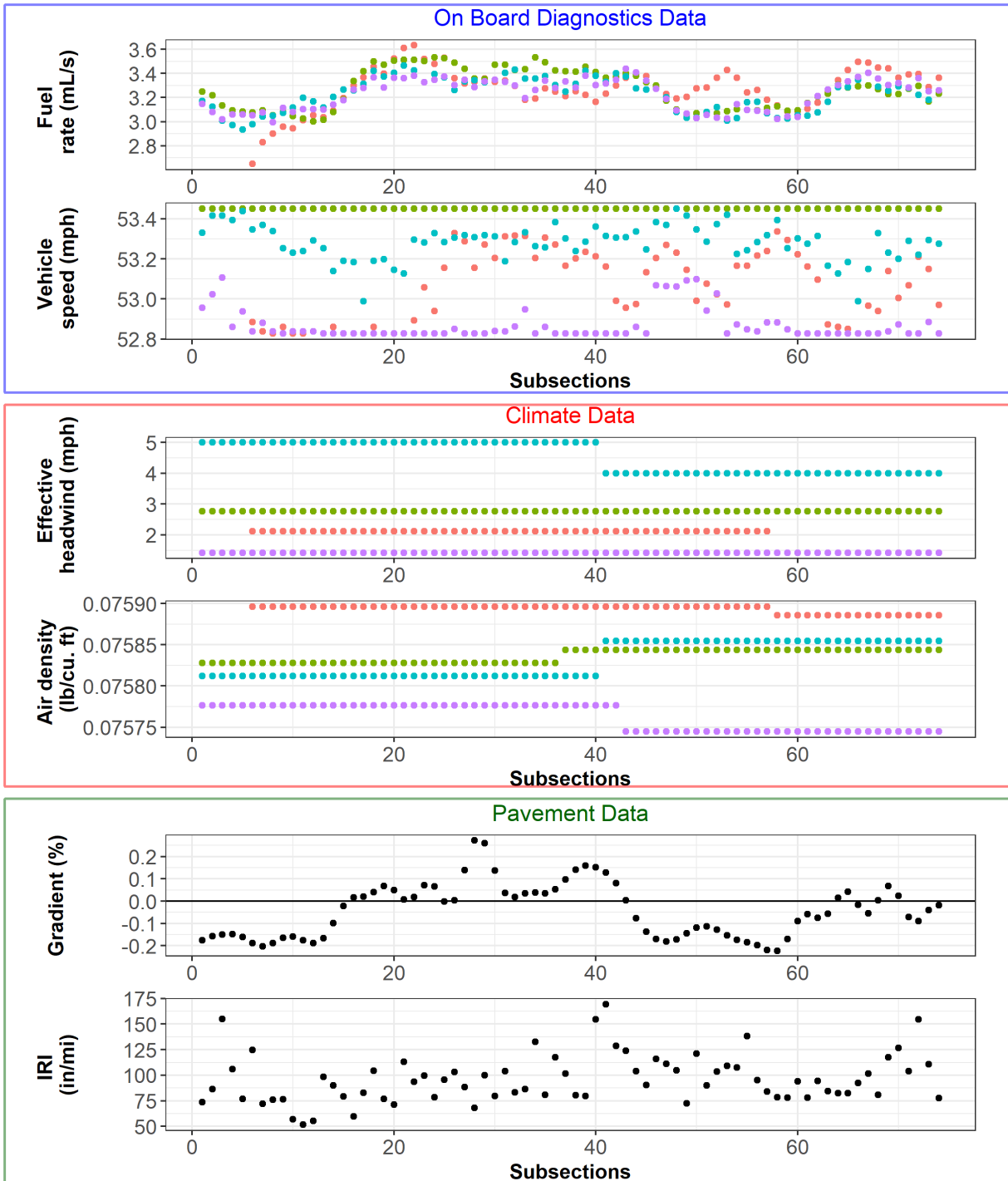


Figure P.237: F-450 data on Section PH12.

PH13-SUT113N-HMA F450 summer_day 45 mph

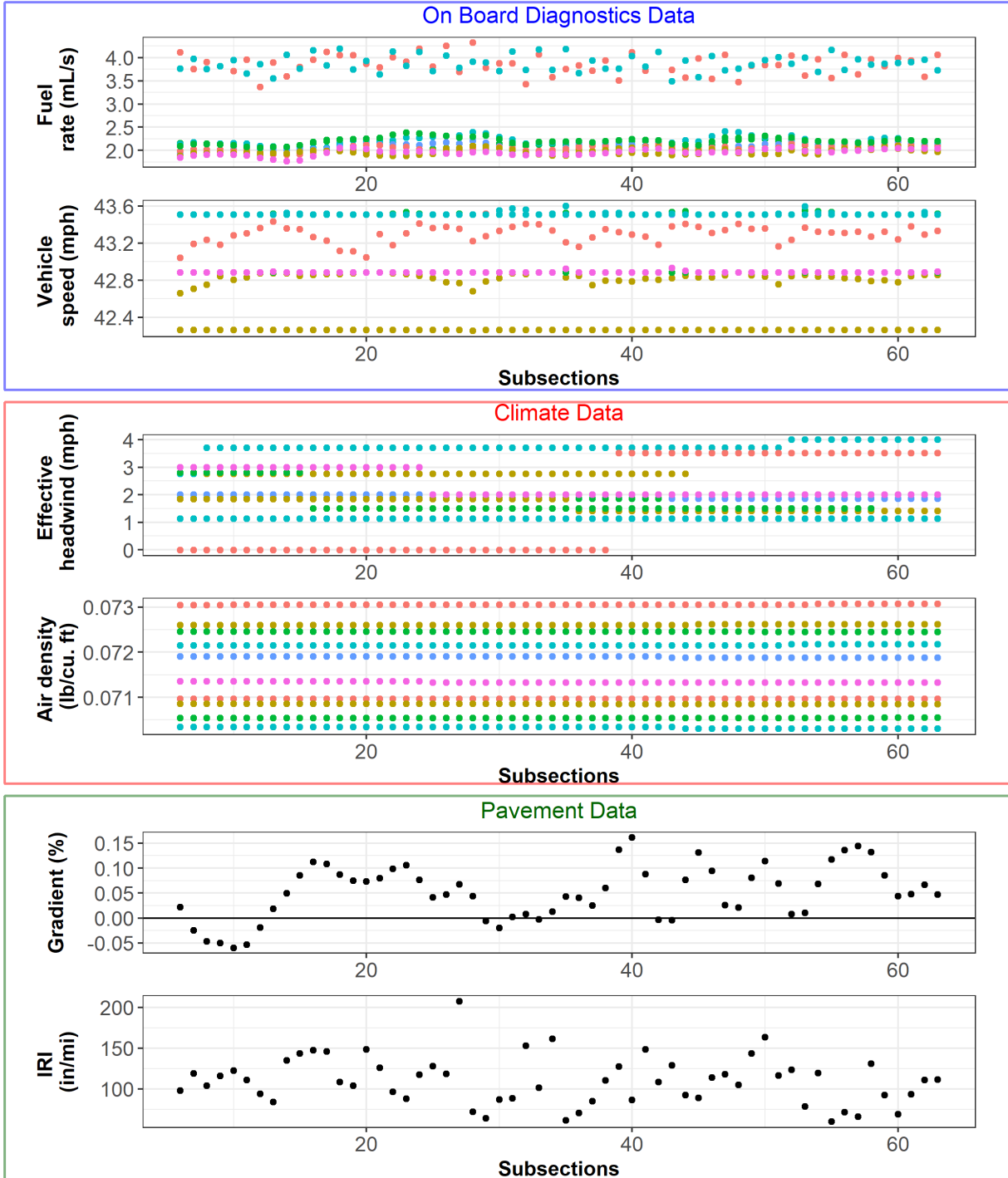


Figure P.238: F-450 data on Section PH13.

PH13-SUT113N-HMA F450 summer_day 55 mph

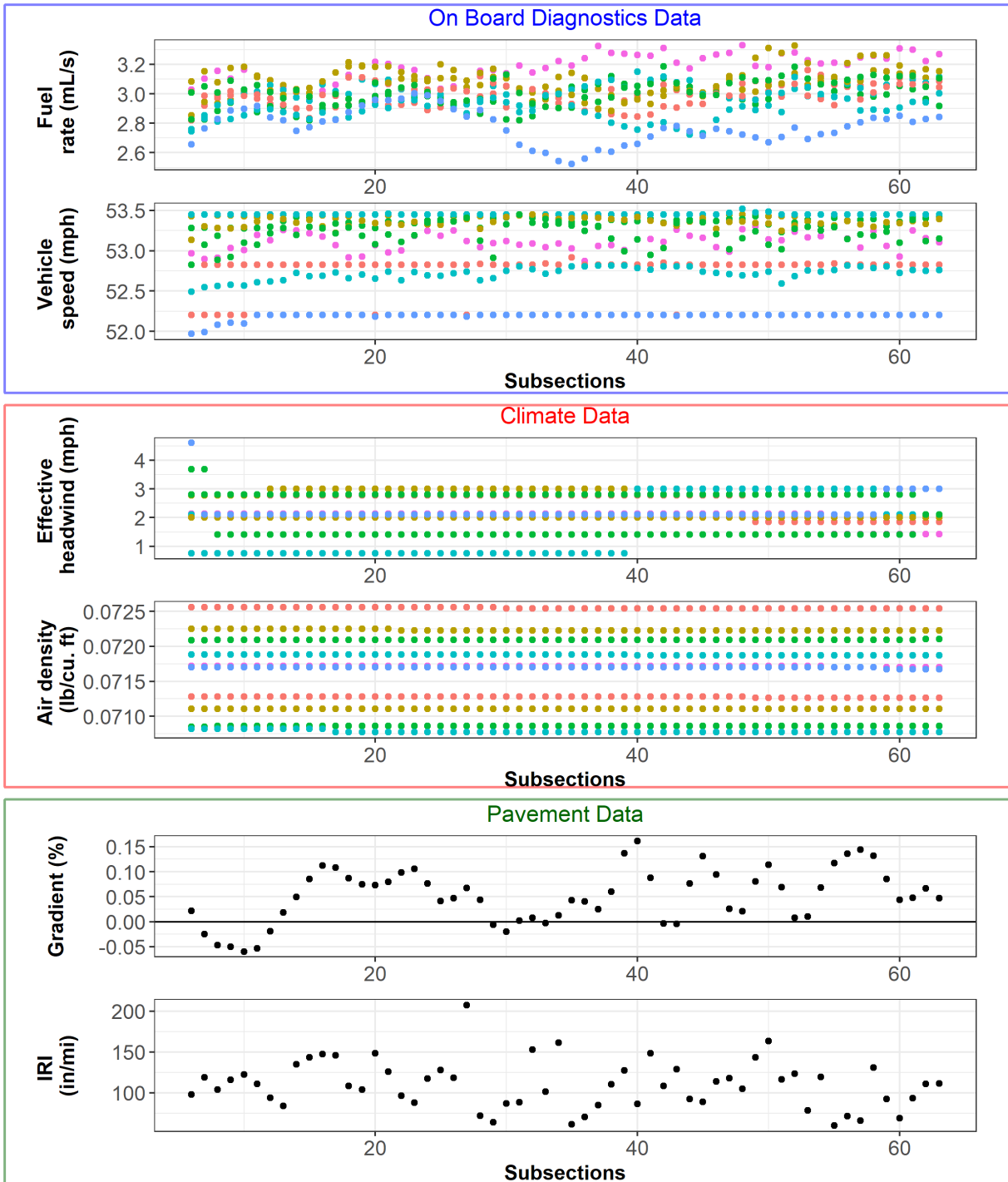


Figure P.239: F-450 data on Section PH13.

PH13-SUT113N-HMA F450 winter_day 45 mph

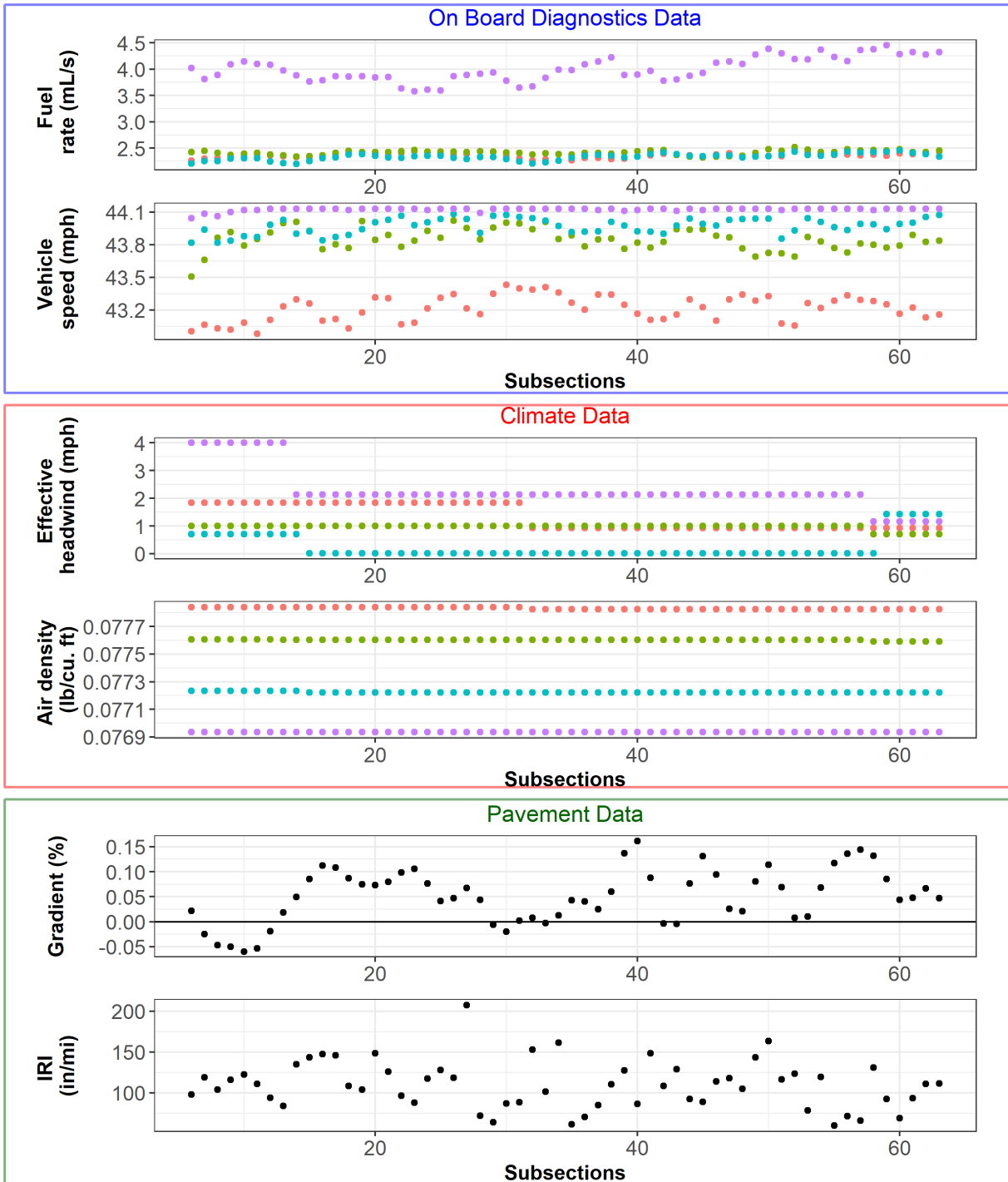


Figure P.240: F-450 data on Section PH13.

PH13-SUT113N-HMA F450 winter_day 55 mph

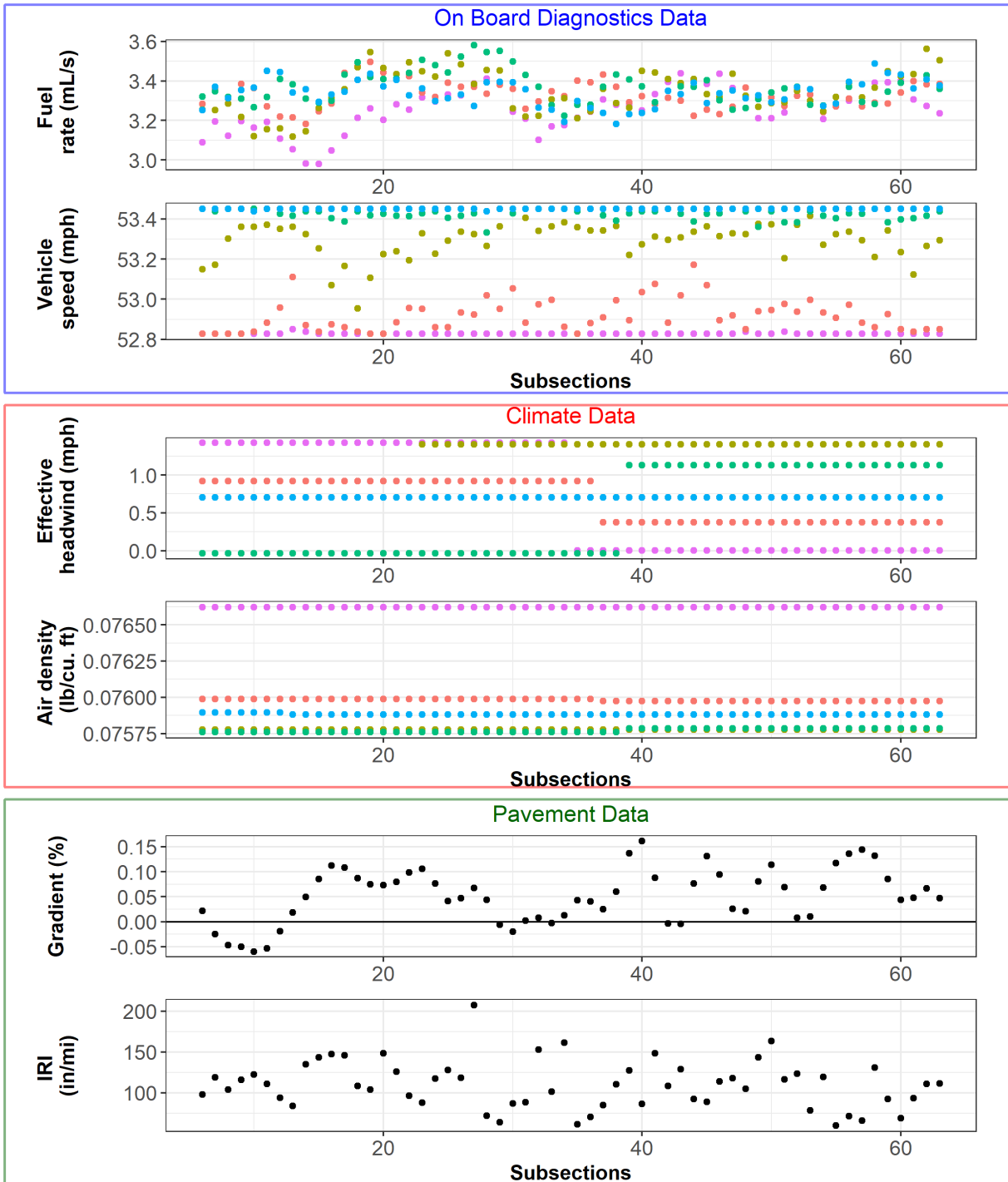


Figure P.241: F-450 data on Section PH13.

PH14-SUT113S-HMA F450 summer_day 45 mph

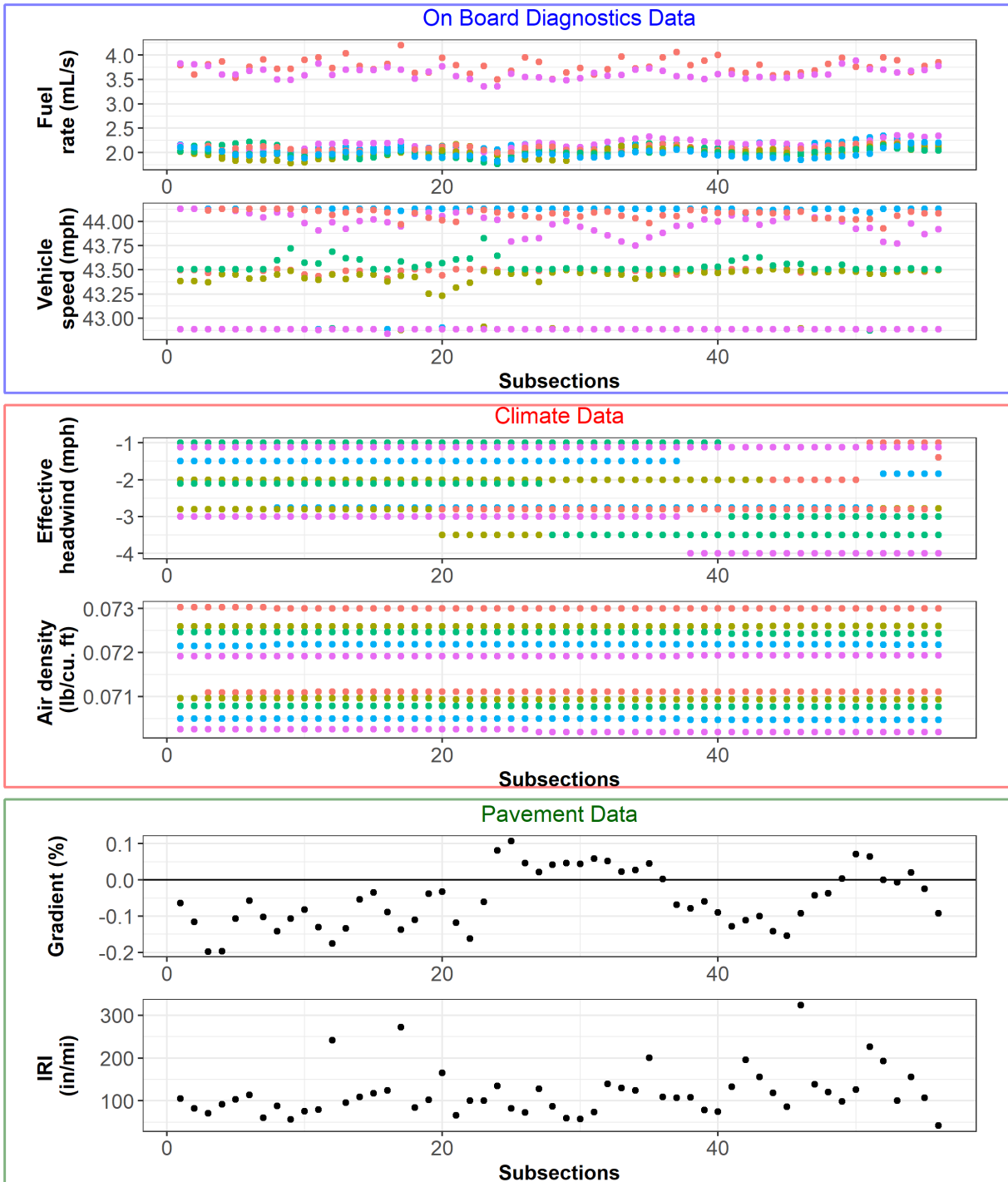


Figure P.242: F-450 data on Section PH14.

PH14-SUT113S-HMA F450 summer_day 55 mph

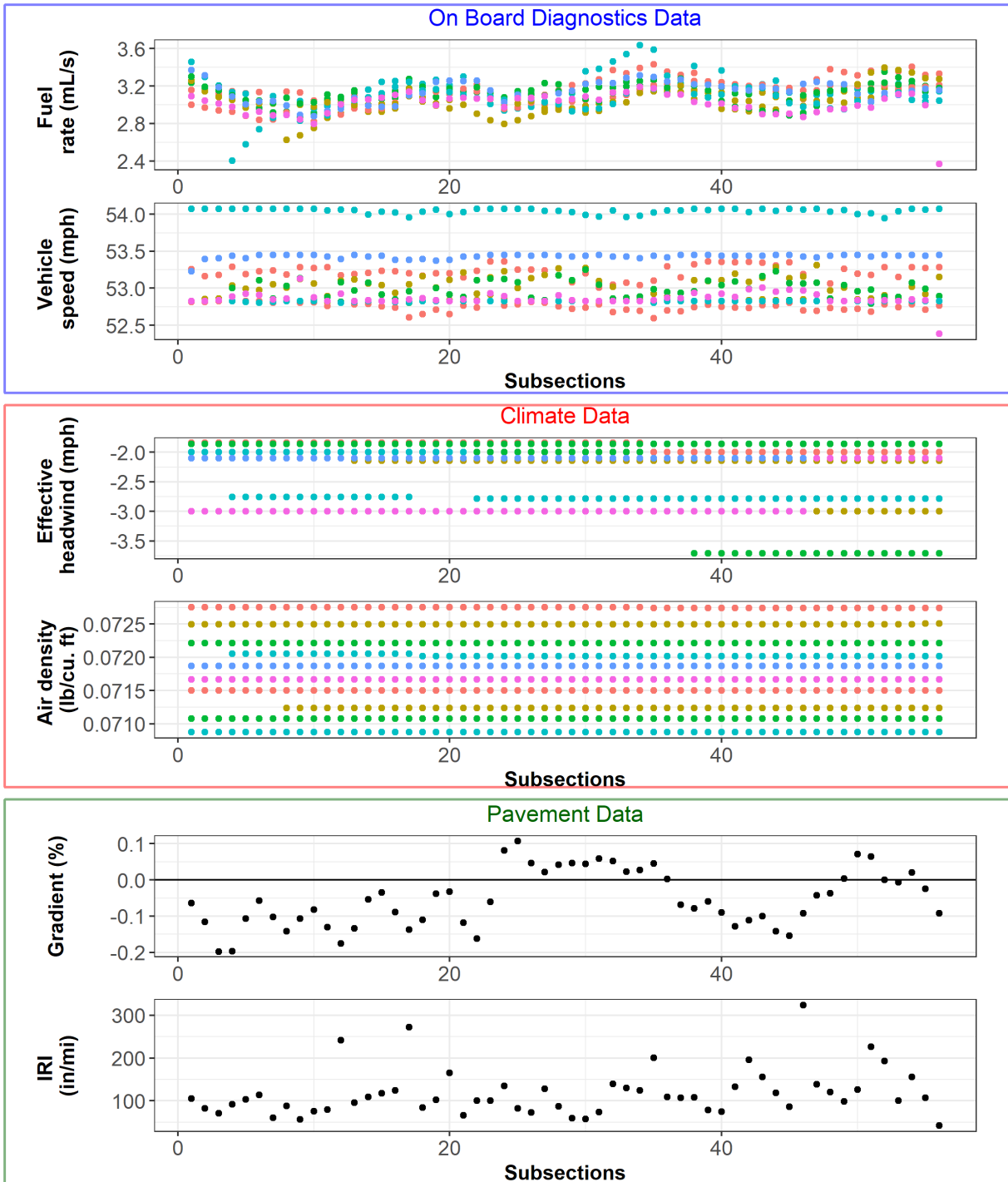


Figure P.243: F-450 data on Section PH14.

PH14-SUT113S-HMA F450 winter_day 45 mph

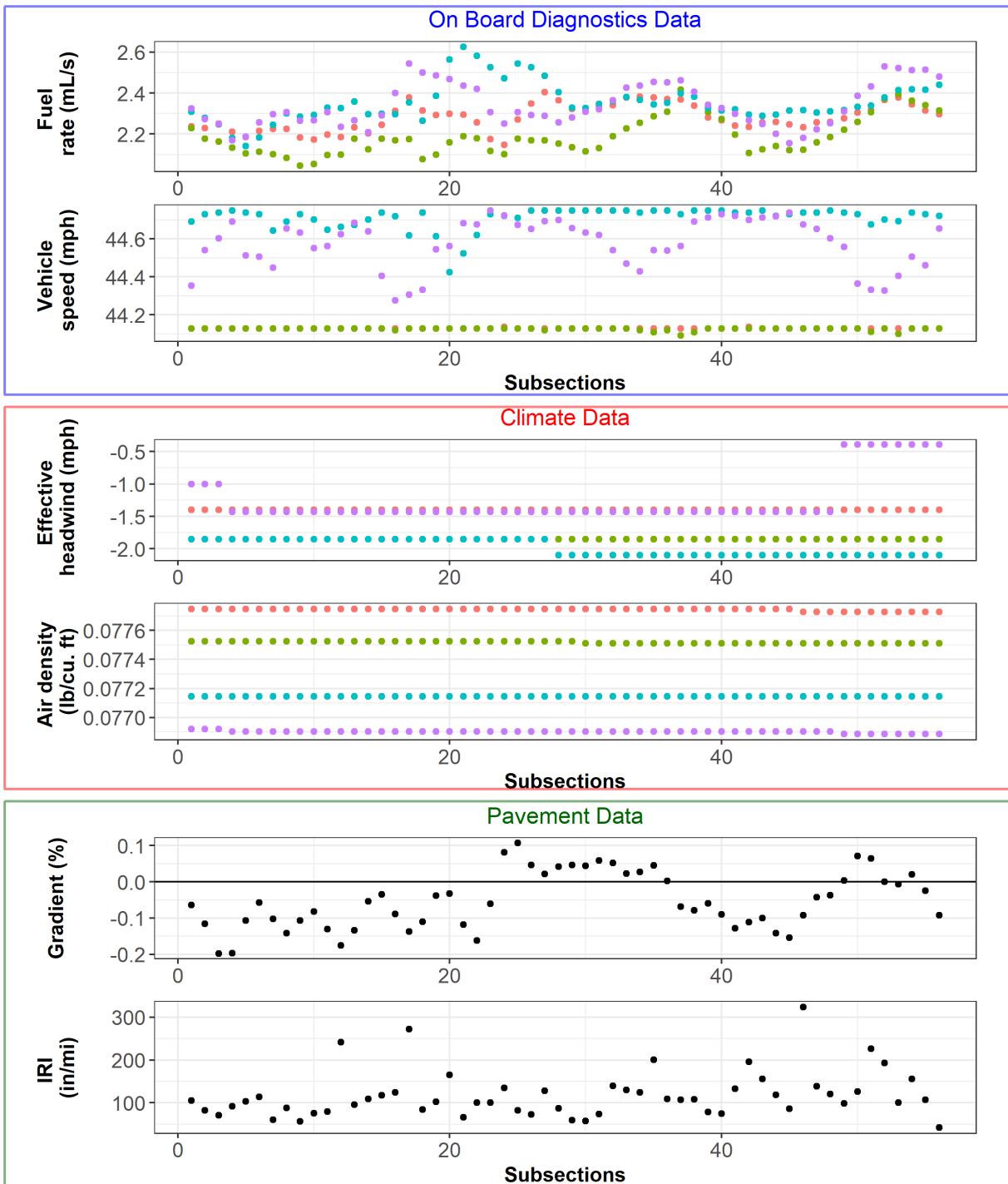


Figure P.244: F-450 data on Section PH14.

PH14-SUT113S-HMA F450 winter_day 55 mph

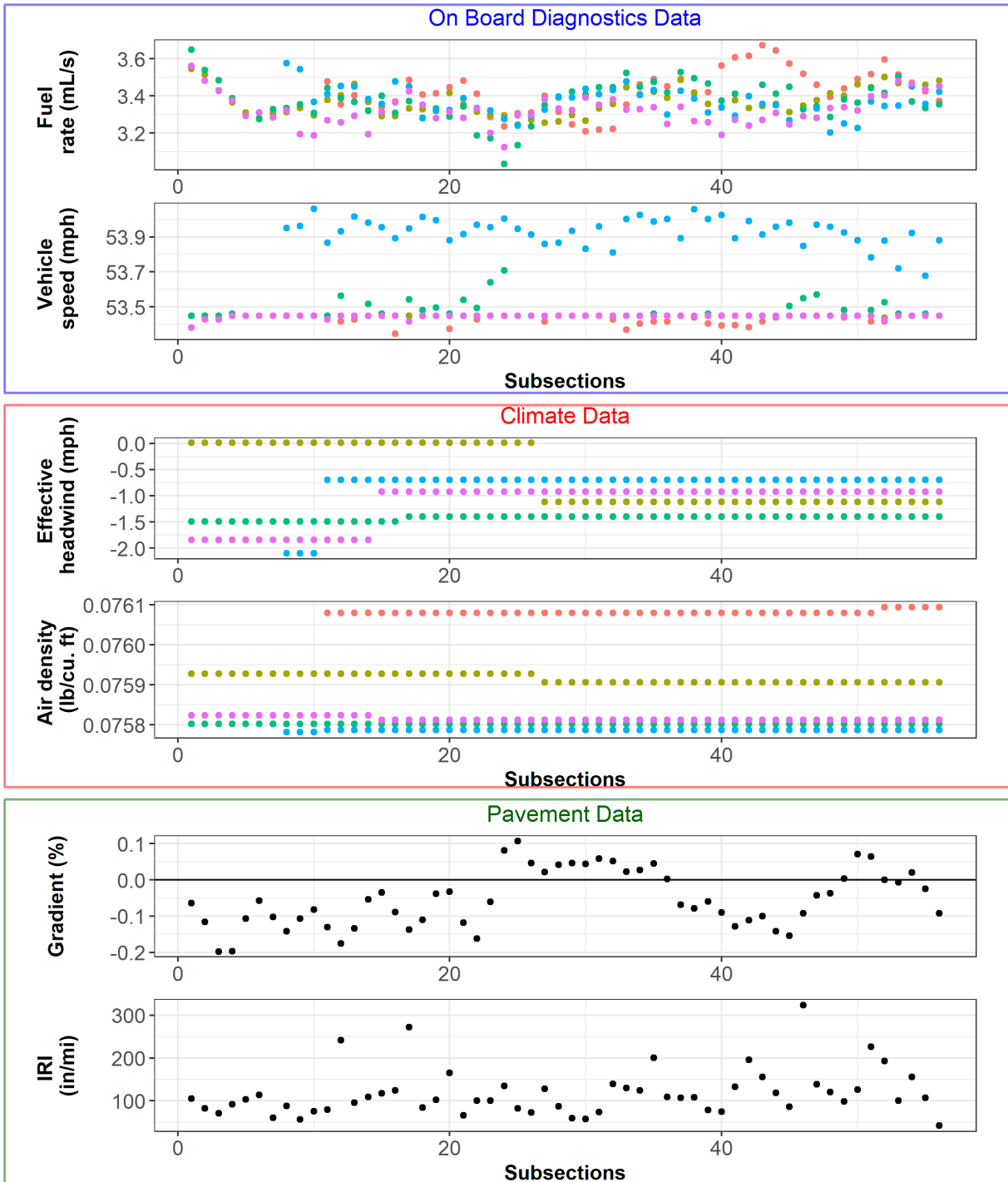


Figure P.245: F-450 data on Section PH14.

PH15-YOL-CR32BE-HMA F450 summer_day 35 mph

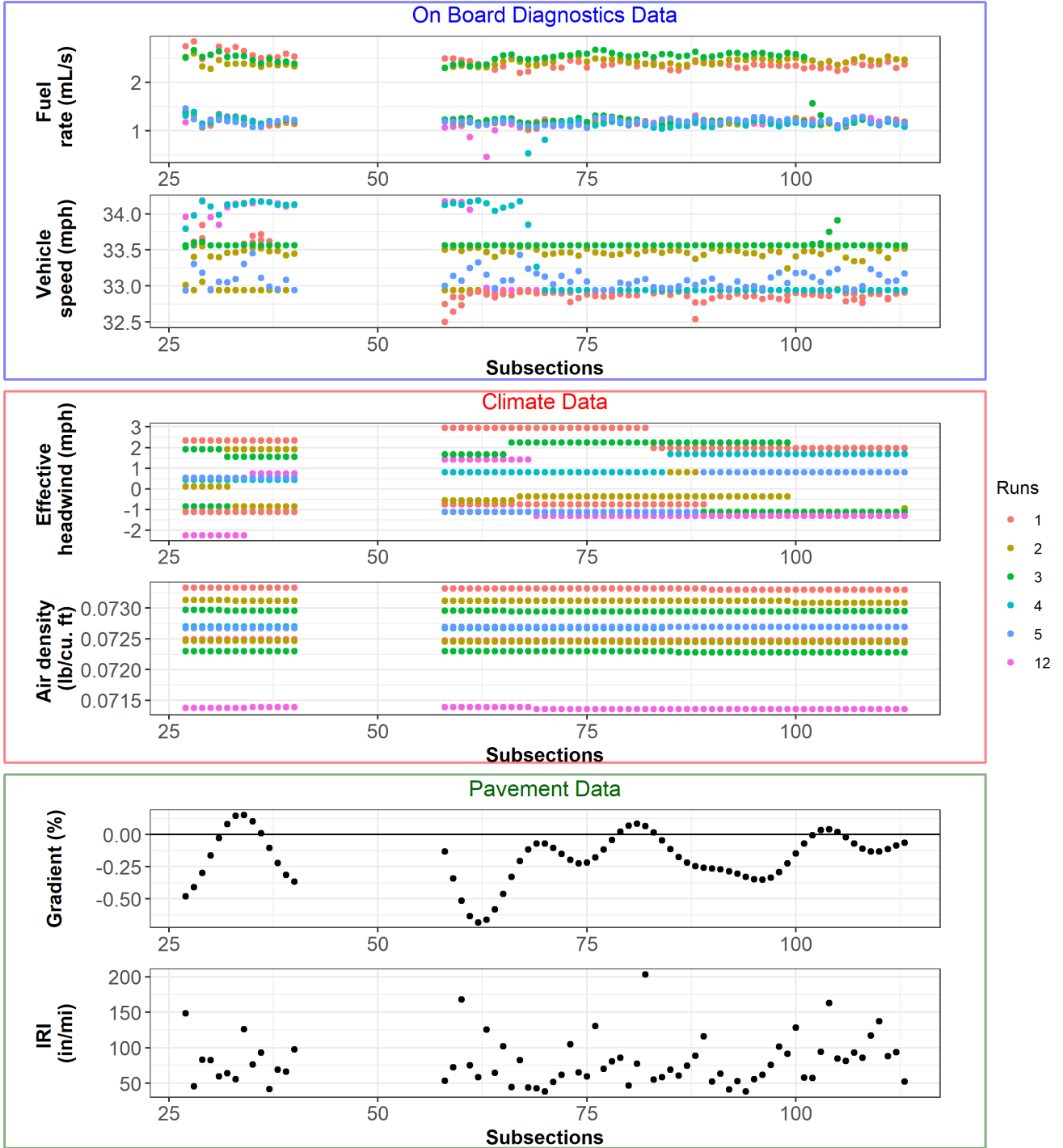


Figure P.246: F-450 data on Section PH15.

PH15-YOL-CR32BE-HMA F450 summer_day 45 mph

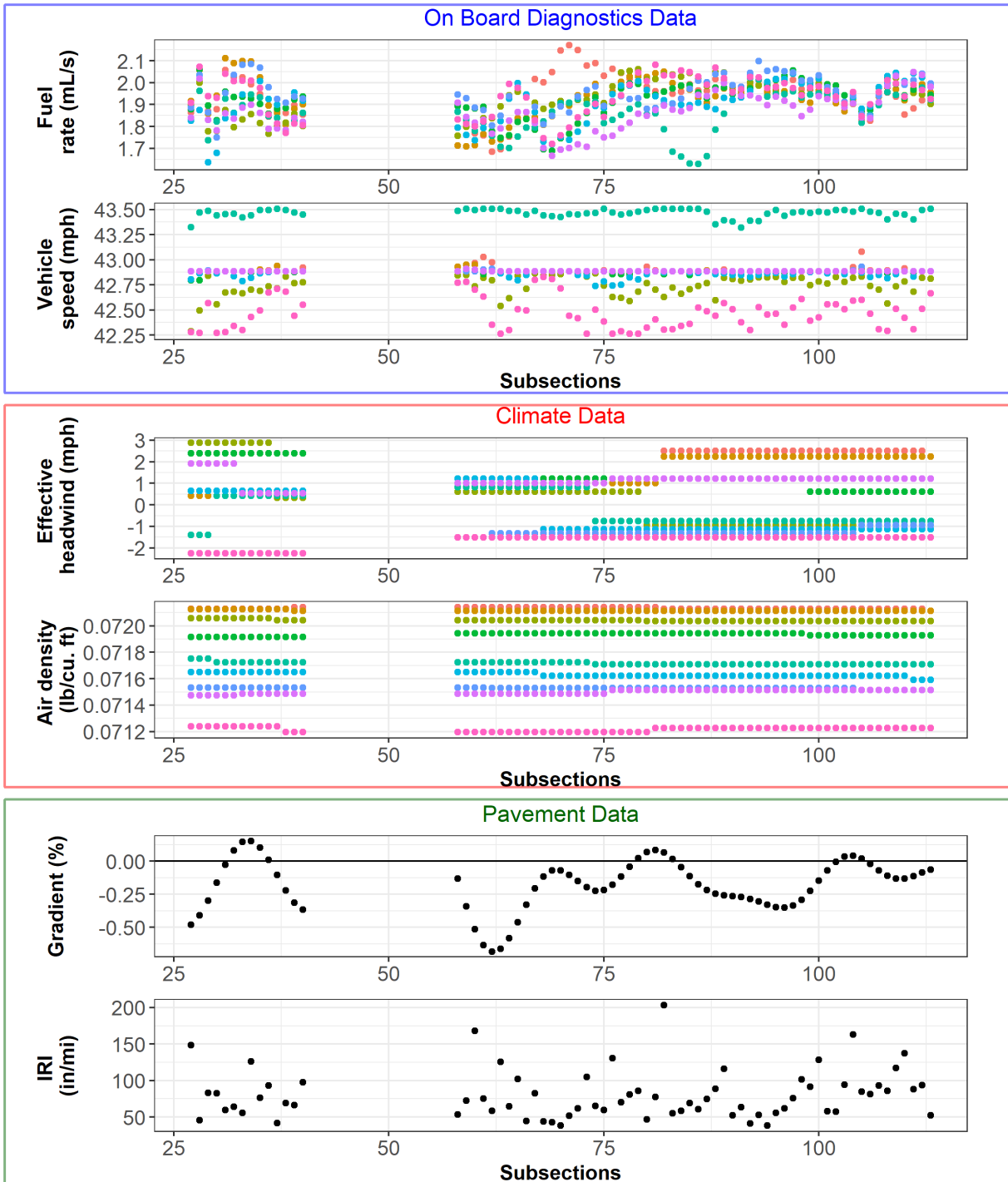


Figure P.247: F-450 data on Section PH15.

PH15-YOL-CR32BE-HMA F450 summer_night 35 mph

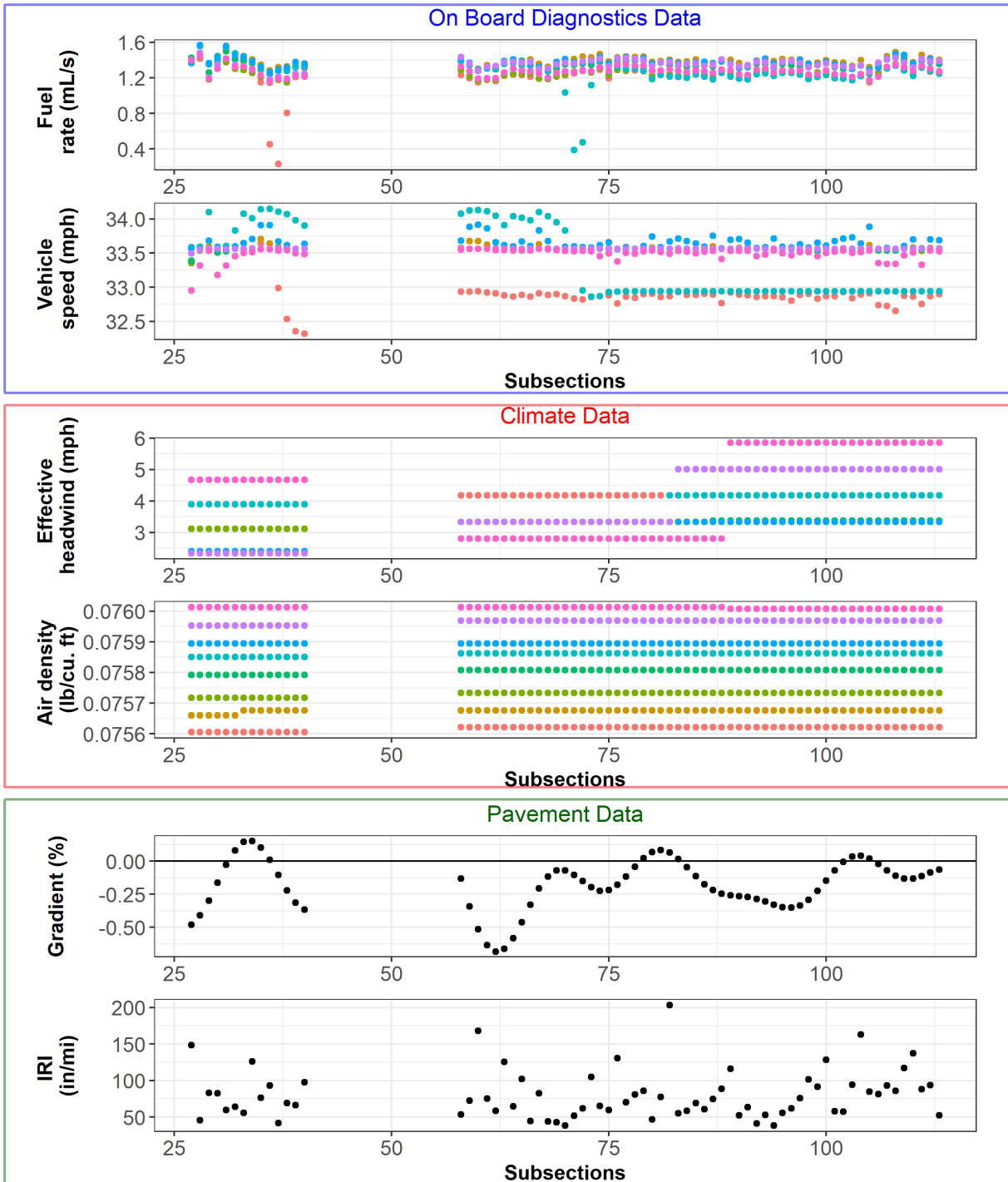


Figure P.248: F-450 data on Section PH15.

PH15-YOL-CR32BE-HMA F450 summer_night 45 mph

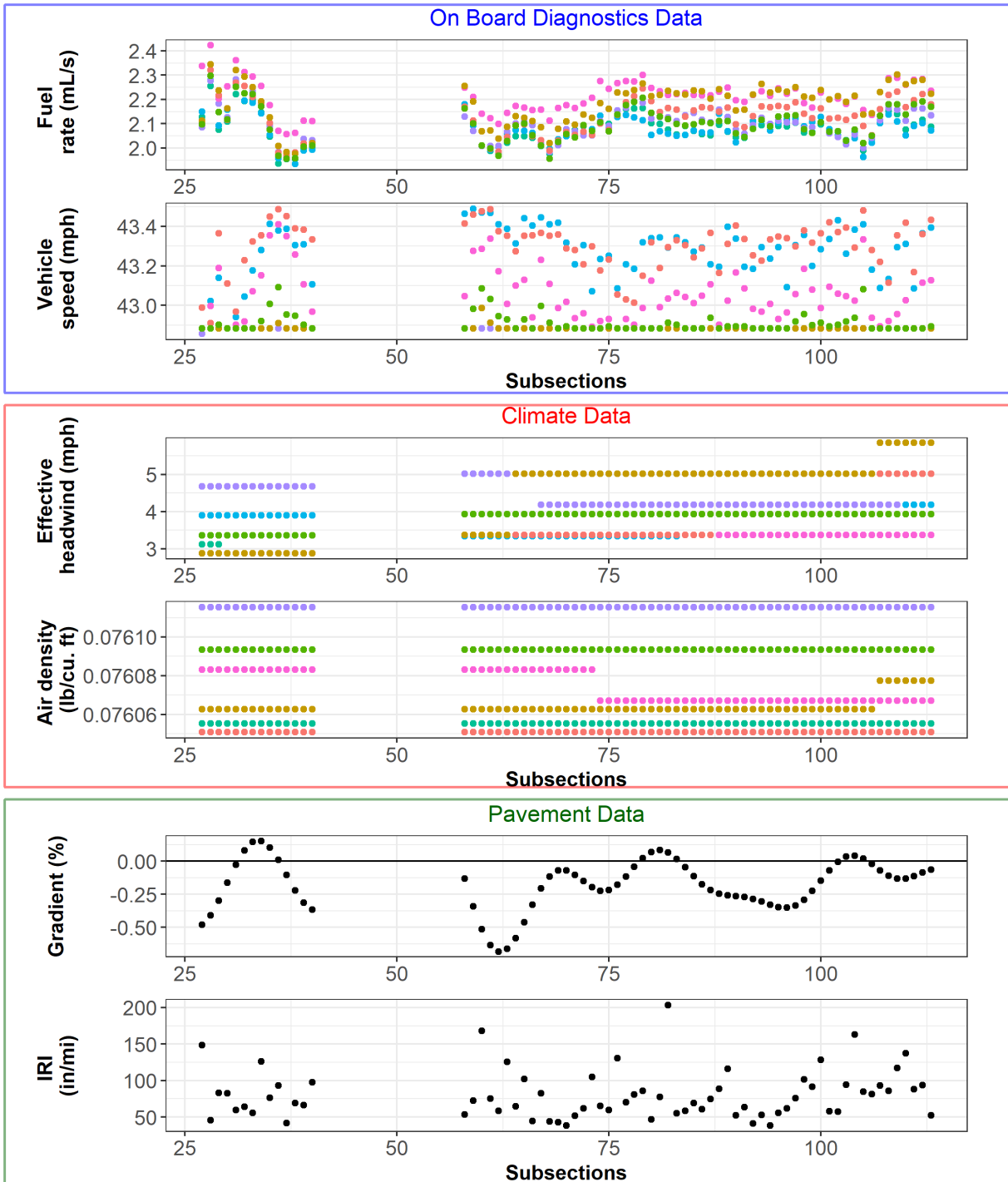


Figure P.249: F-450 data on Section PH15.

PH15-YOL-CR32BE-HMA F450 winter_day 35 mph

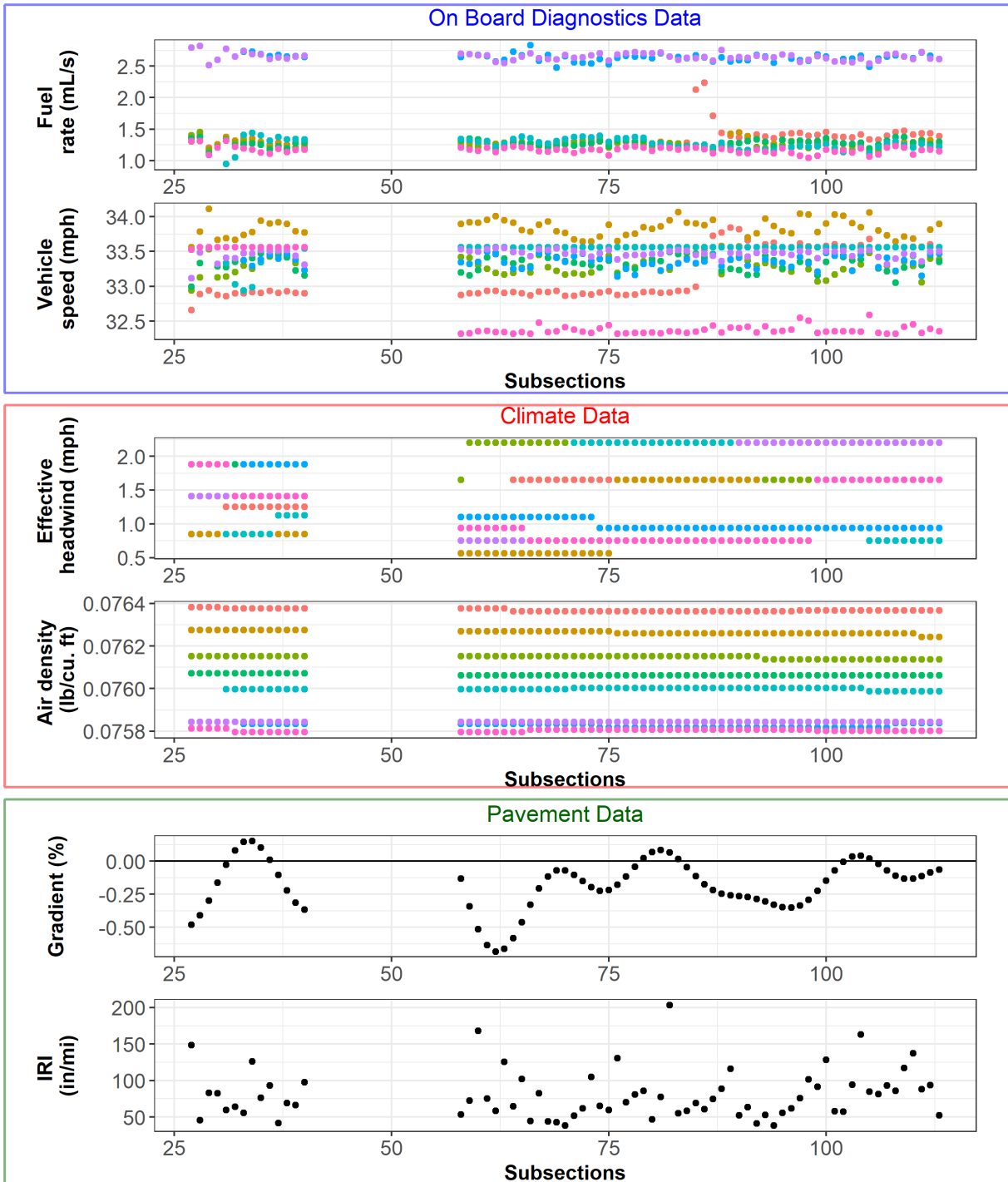


Figure P.250: F-450 data on Section PH15.

PH15-YOL-CR32BE-HMA F450 winter_day 45 mph

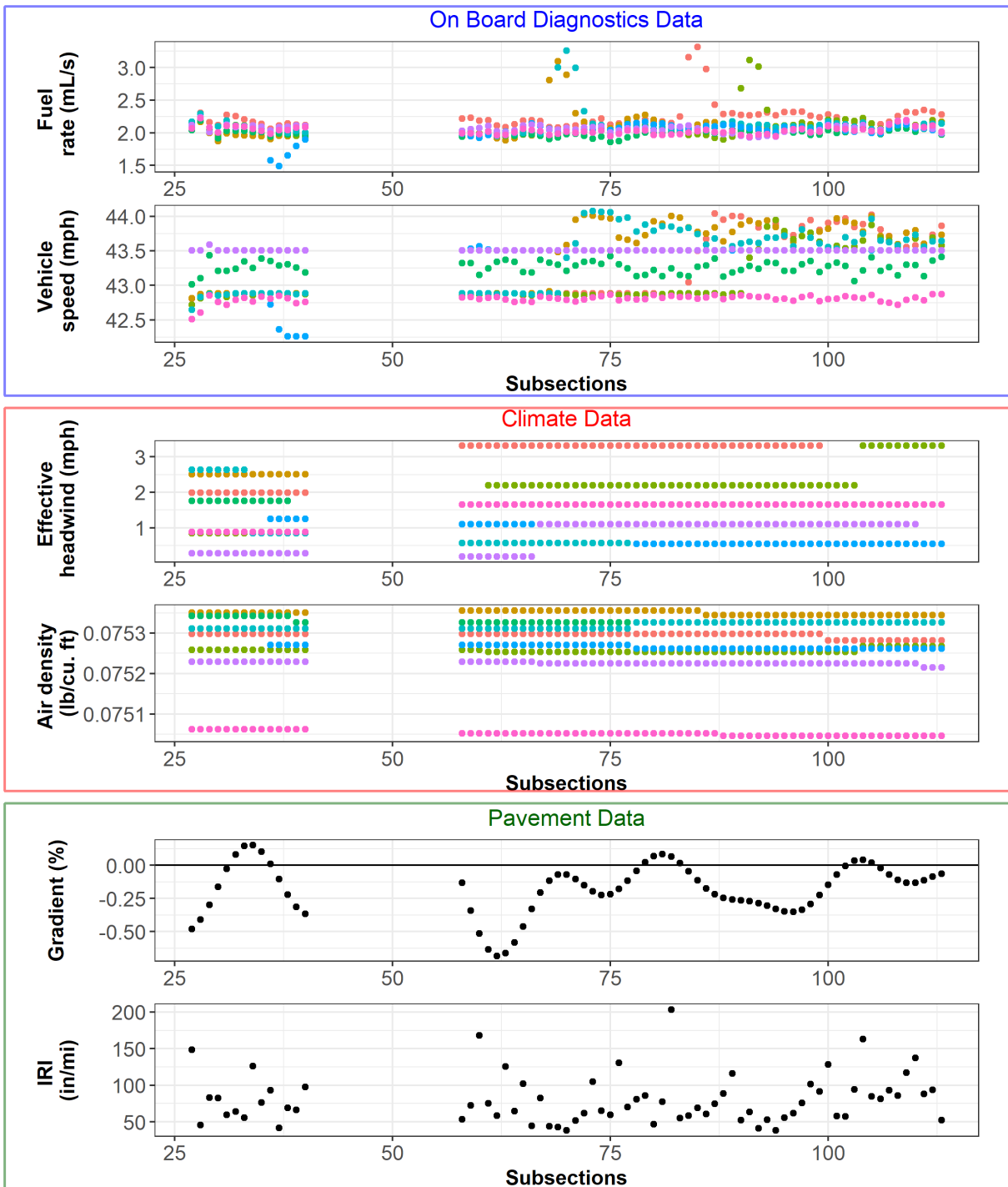


Figure P.251: F-450 data on Section PH15.

PH16-STA132E-RHMA-G F450 summer_day 45 mph

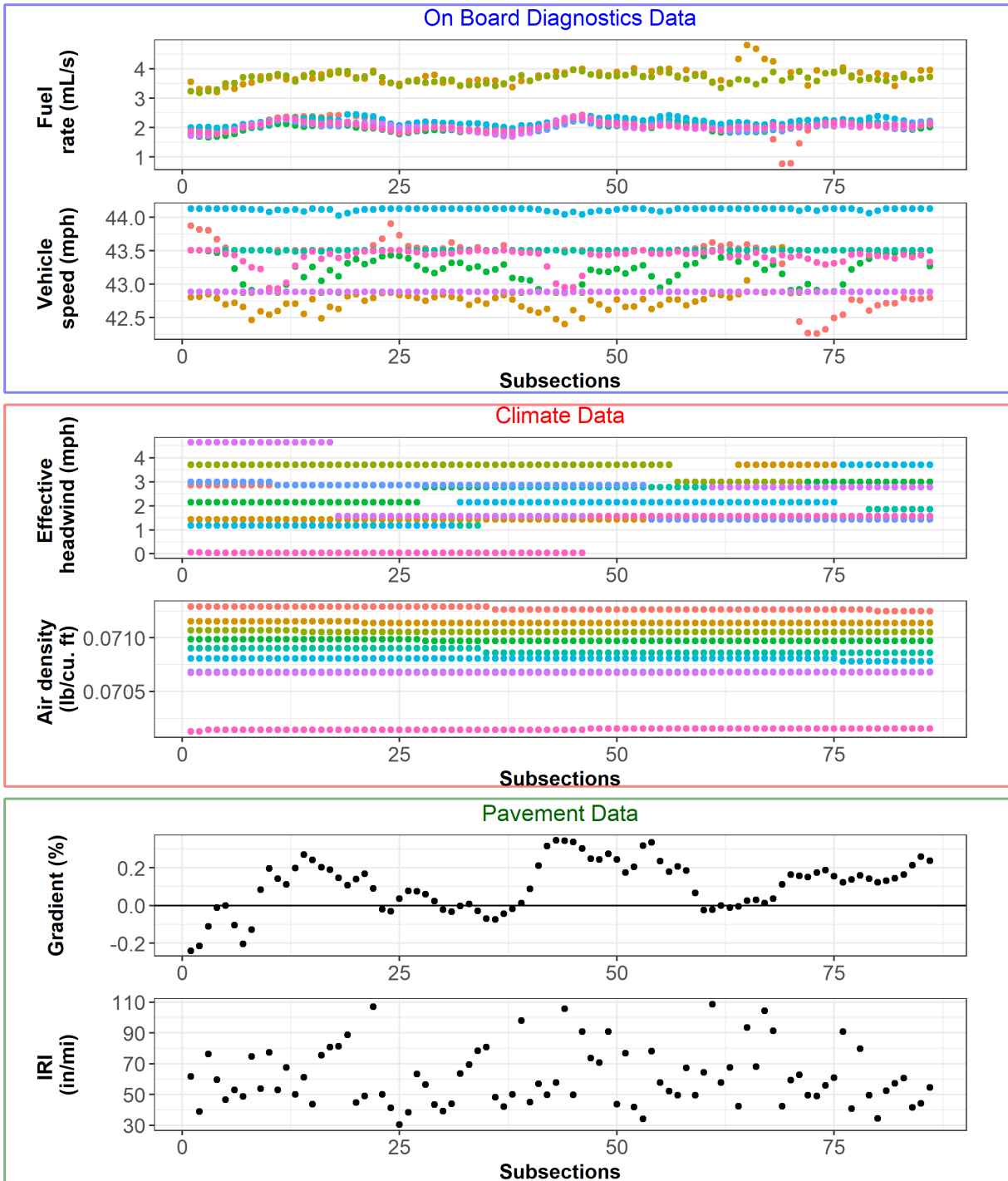


Figure P.252: F-450 data on Section PH16.

PH16-STA132E-RHMA-G F450 summer_day 55 mph

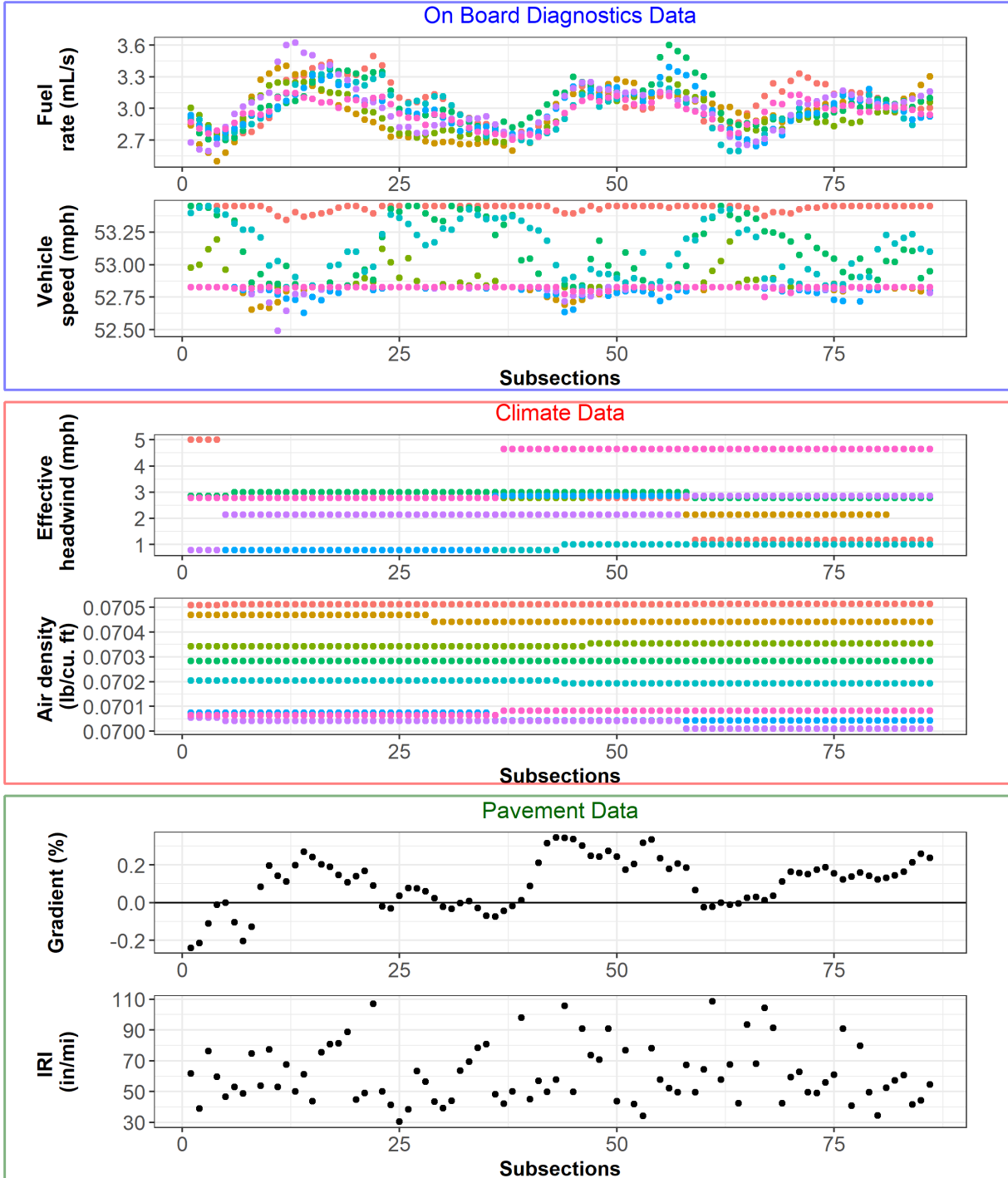


Figure P.253: F-450 data on Section PH16.

PH16-STA132E-RHMA-G F450 winter_day 45 mph

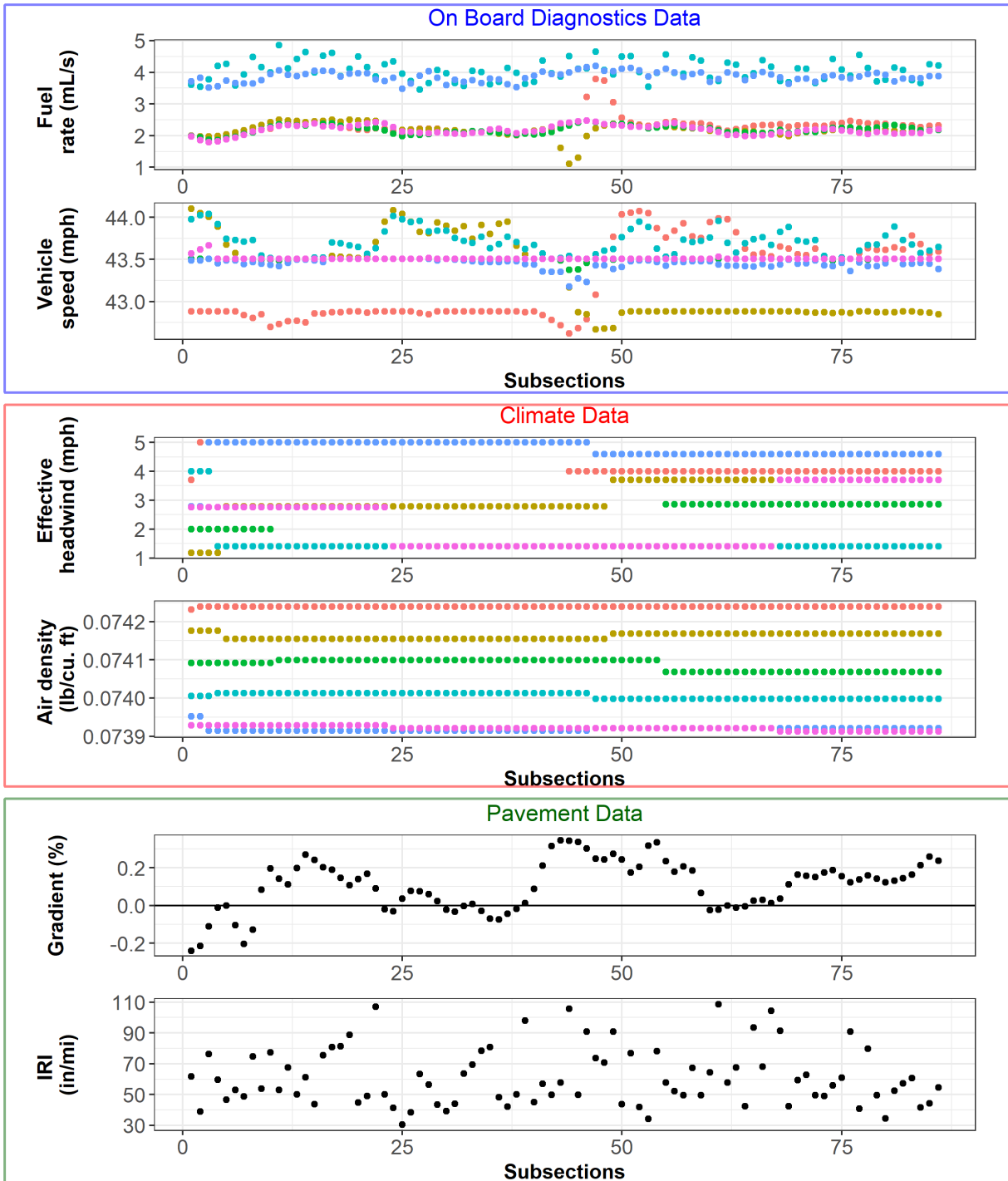


Figure P.254: F-450 data on Section PH16.

PH16-STA132E-RHMA-G F450 winter_day 55 mph

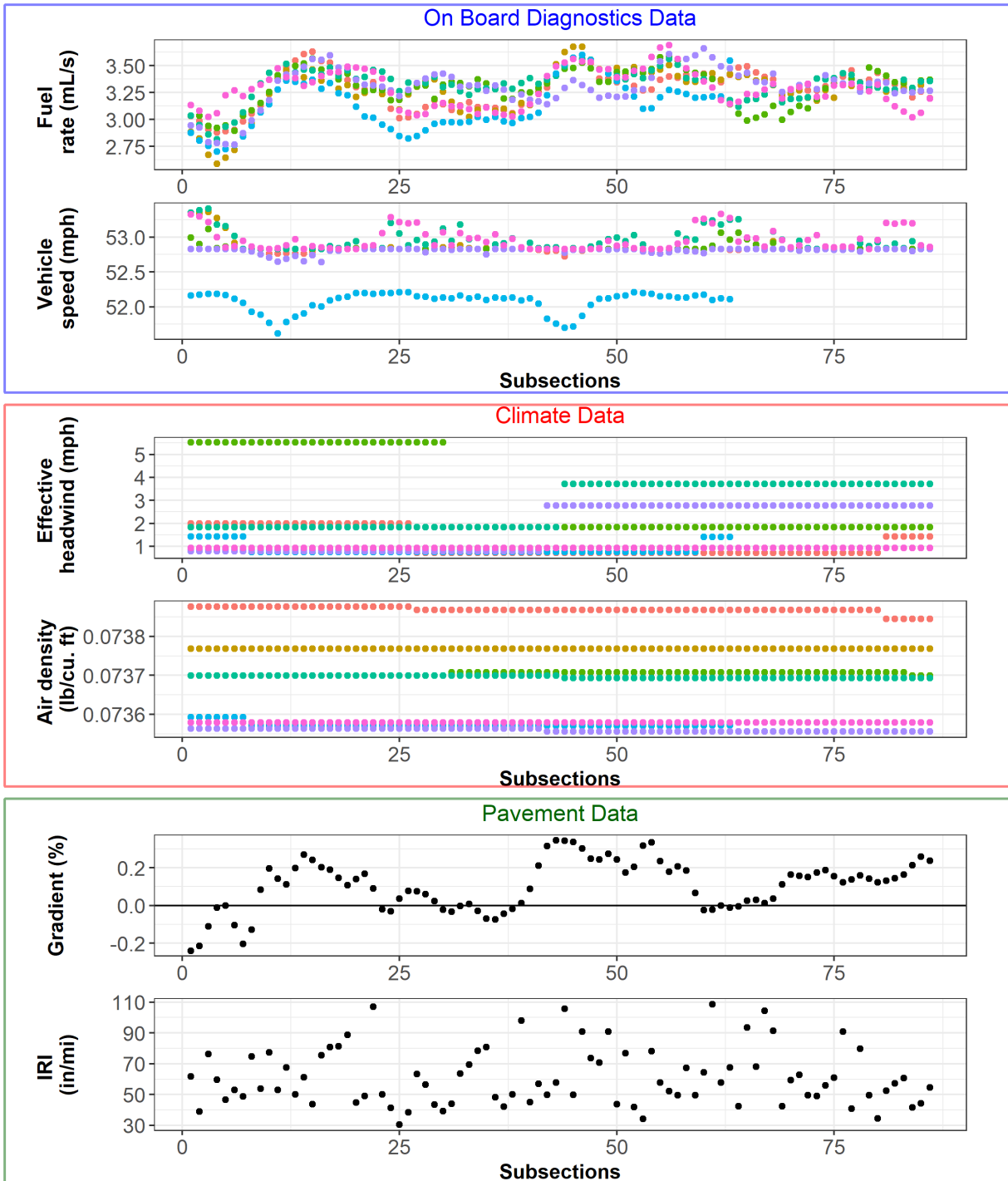


Figure P.255: F-450 data on Section PH16.

PH17-STA132W-RHMA-G F450 summer_day 45 mph

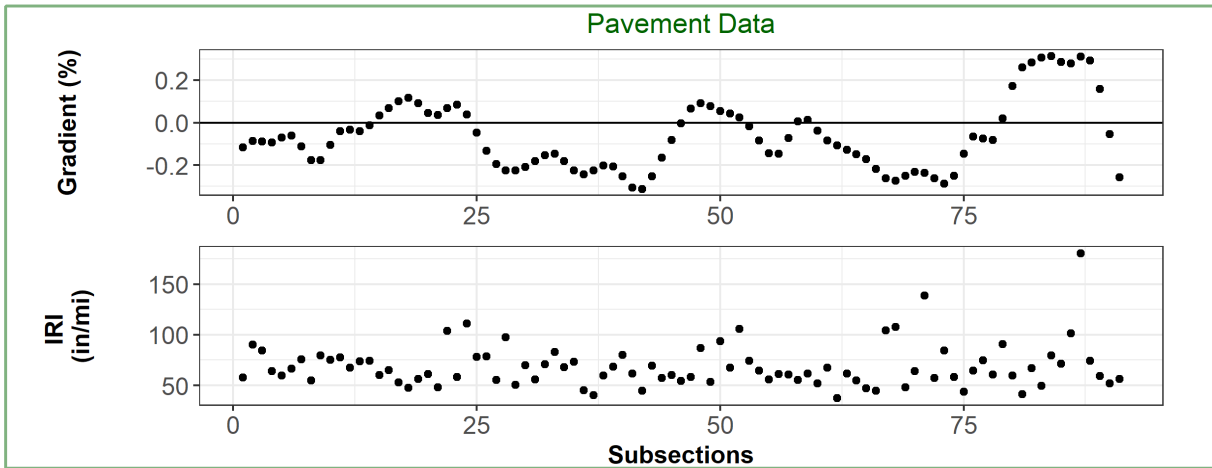
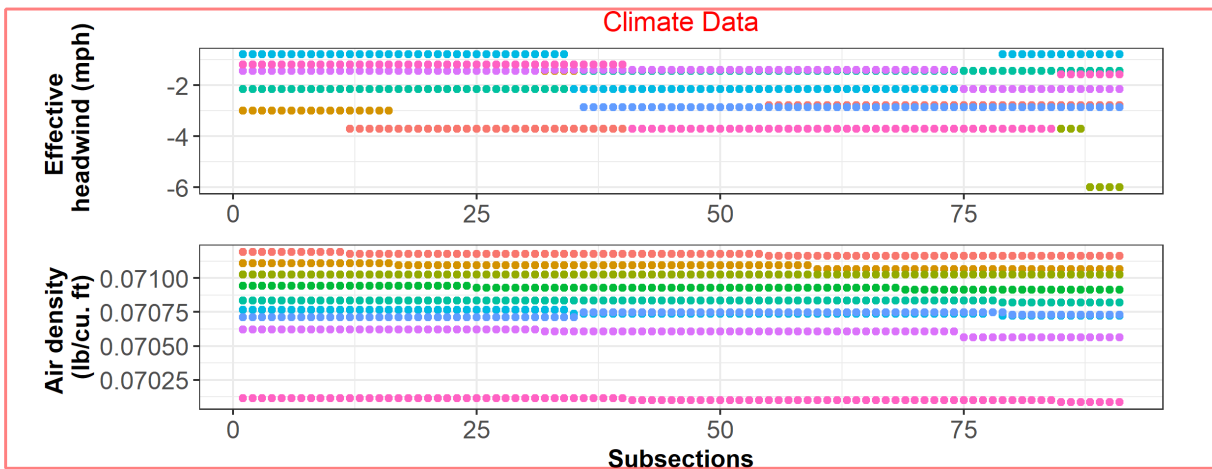
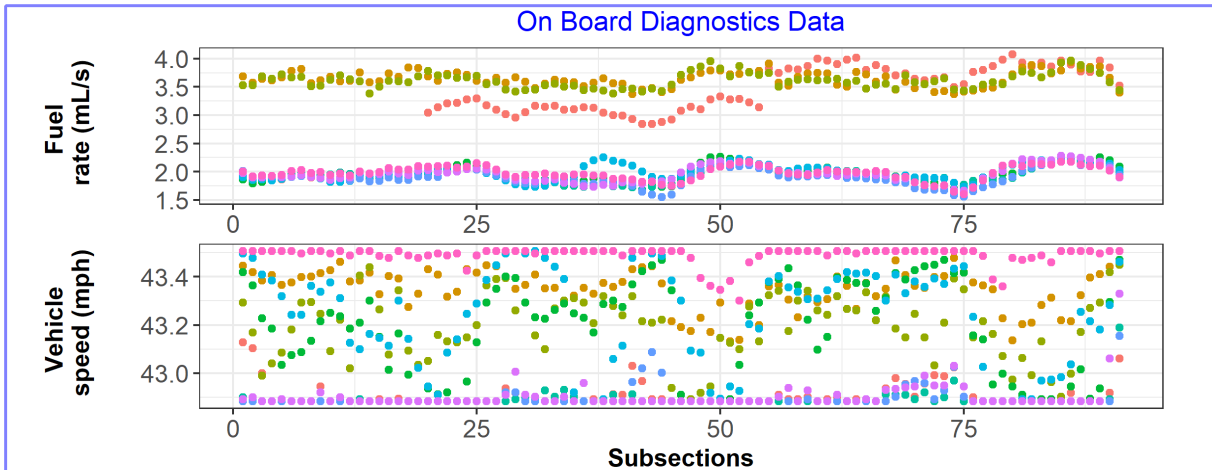


Figure P.256: F-450 data on Section PH17.

PH17-STA132W-RHMA-G F450 summer_day 55 mph

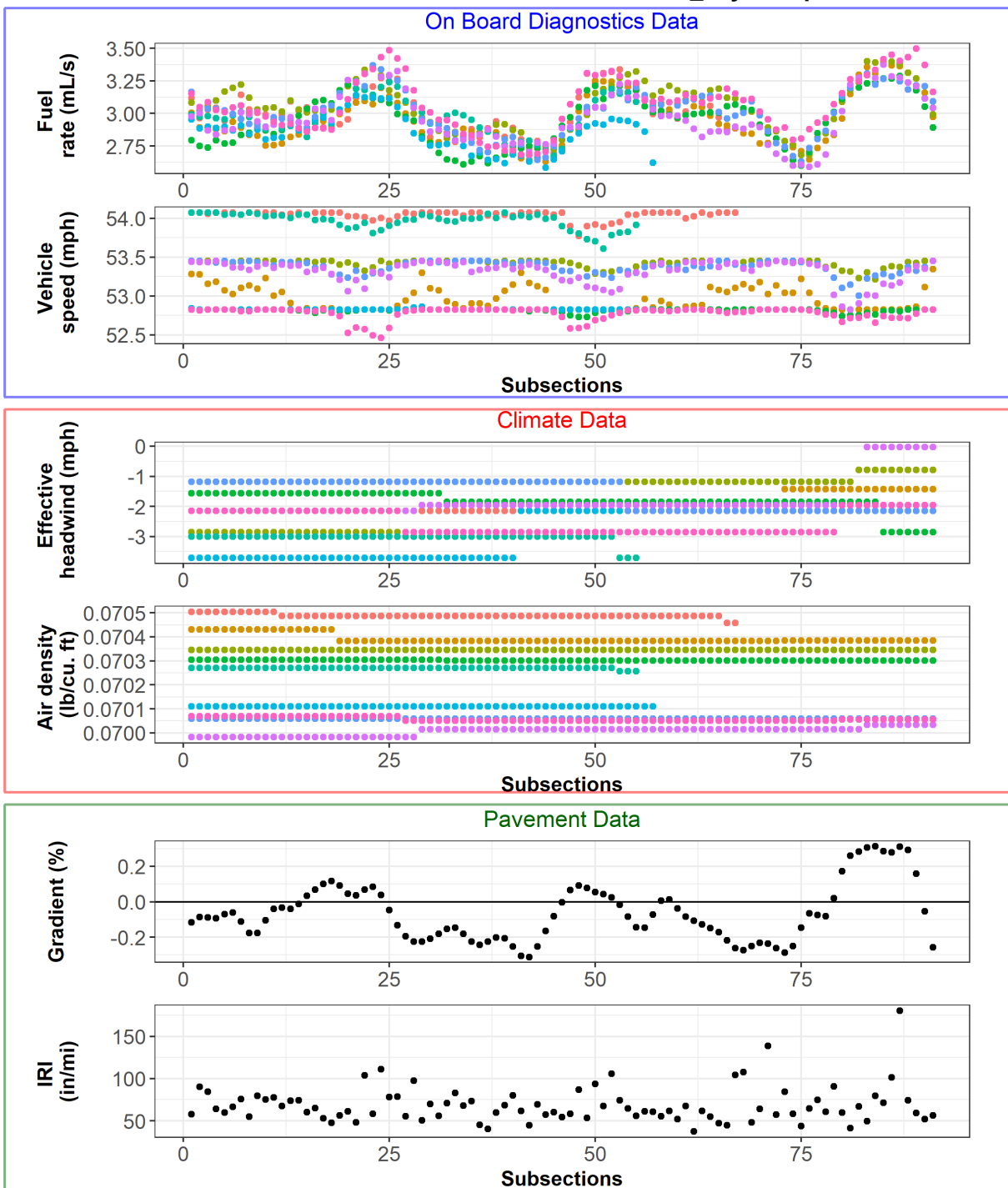


Figure P.257: F-450 data on Section PH17.

PH17-STA132W-RHMA-G F450 winter_day 45 mph

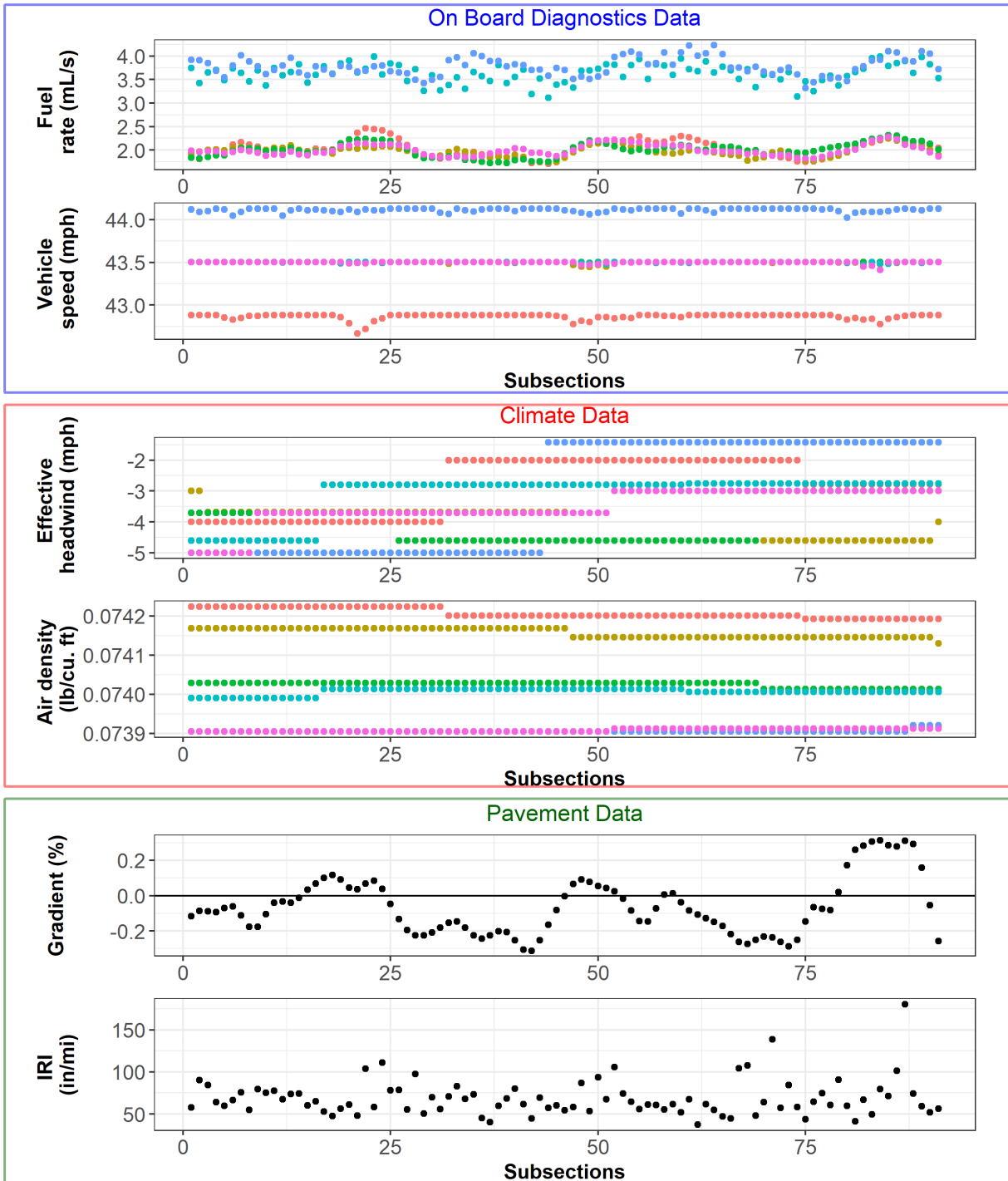


Figure P.258: F-450 data on Section PH17.

PH17-STA132W-RHMA-G F450 winter_day 55 mph

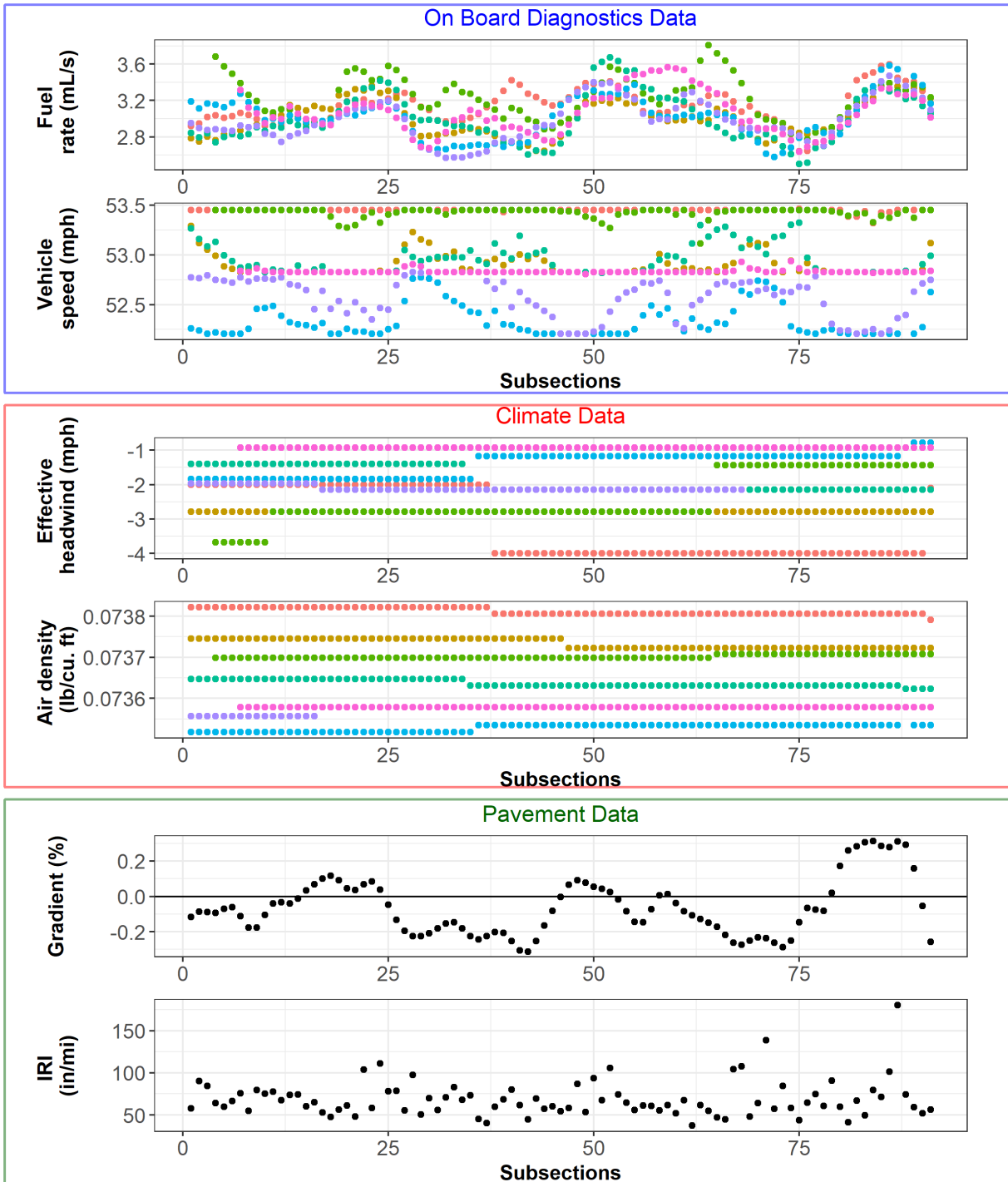


Figure P.259: F-450 data on Section PH17.

PH18-KER5S-HMA-O F450 summer_day 45 mph

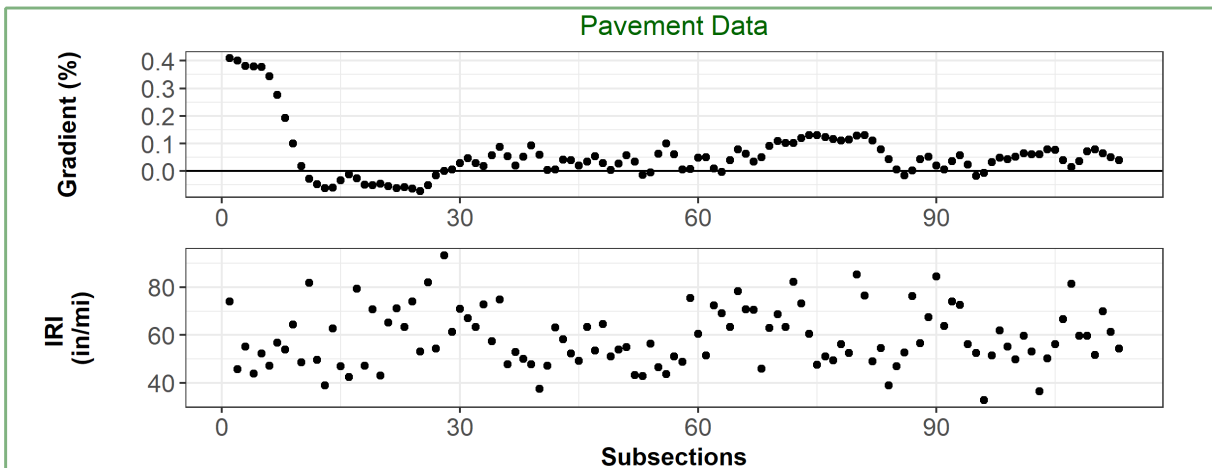
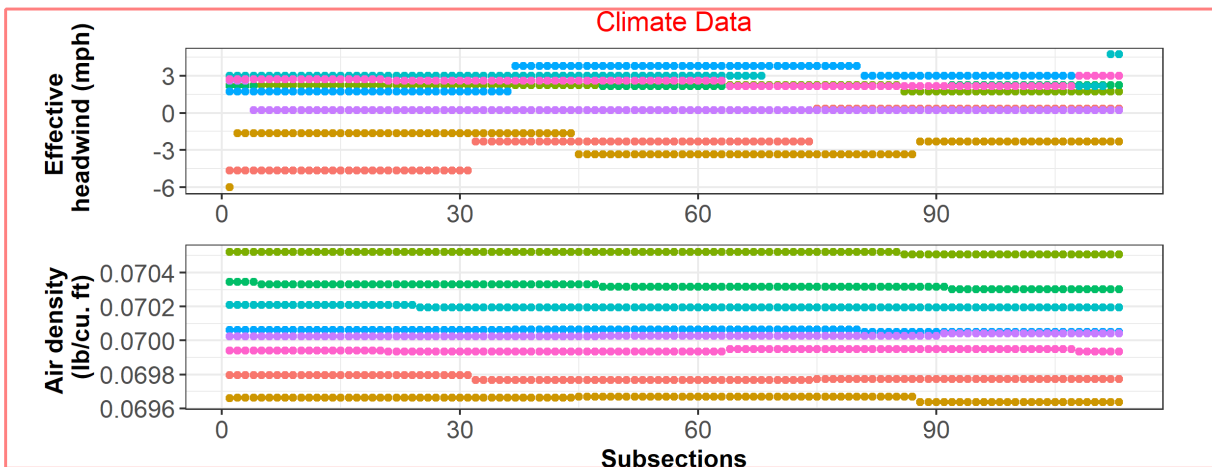
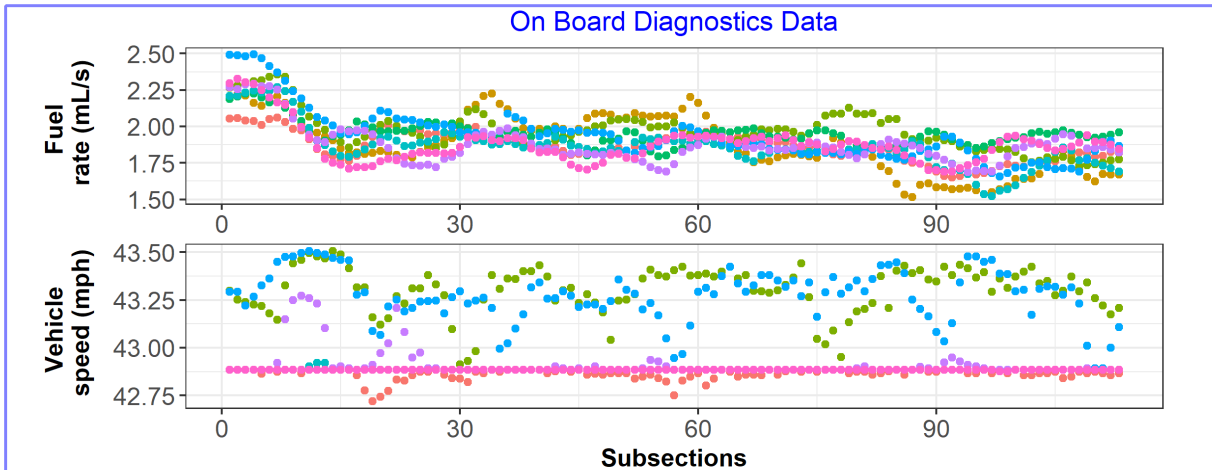
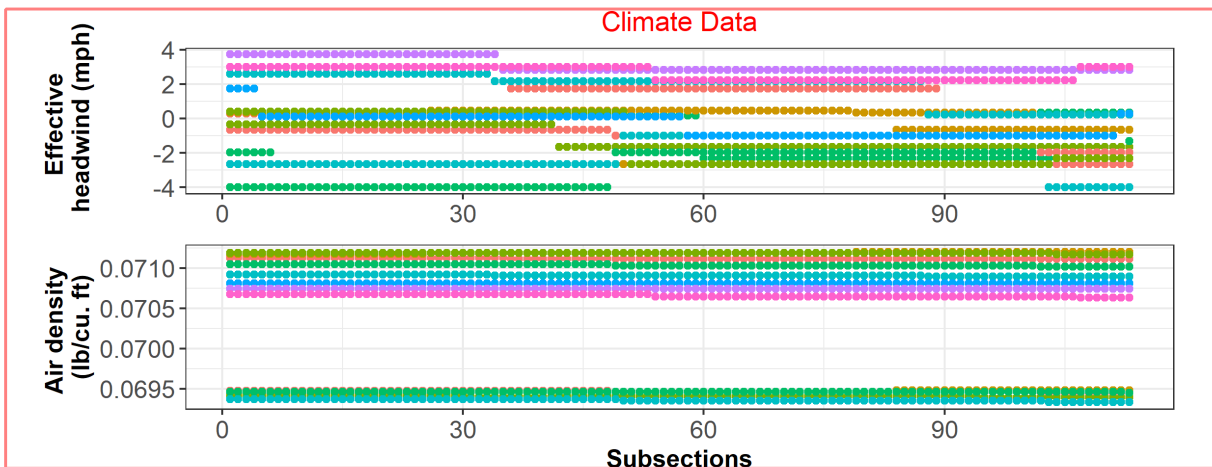
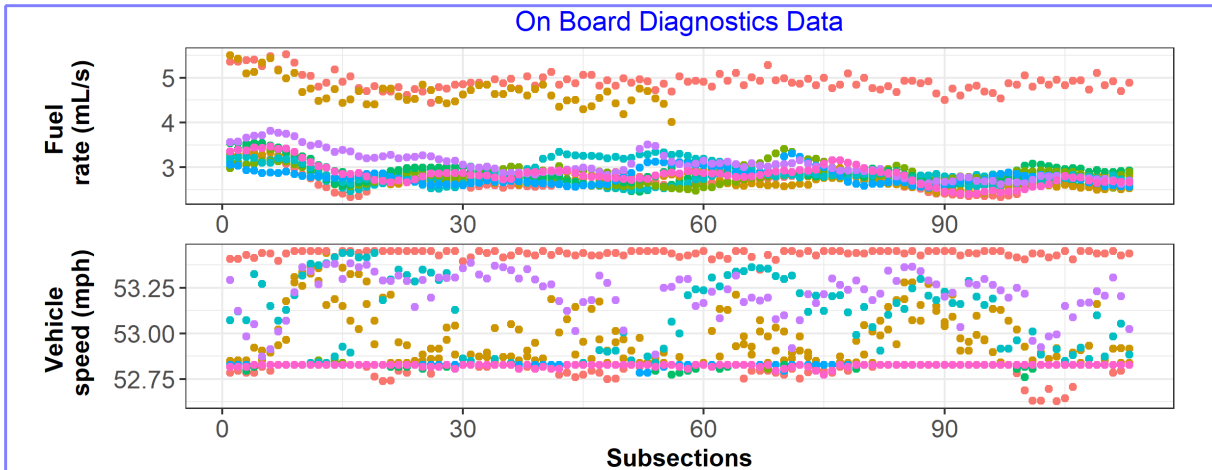


Figure P.260: F-450 data on Section PH18.

PH18-KER5S-HMA-O F450 summer_day 55 mph



- Runs
- 1
 - 2
 - 3
 - 4
 - 5
 - 6
 - 7
 - 8

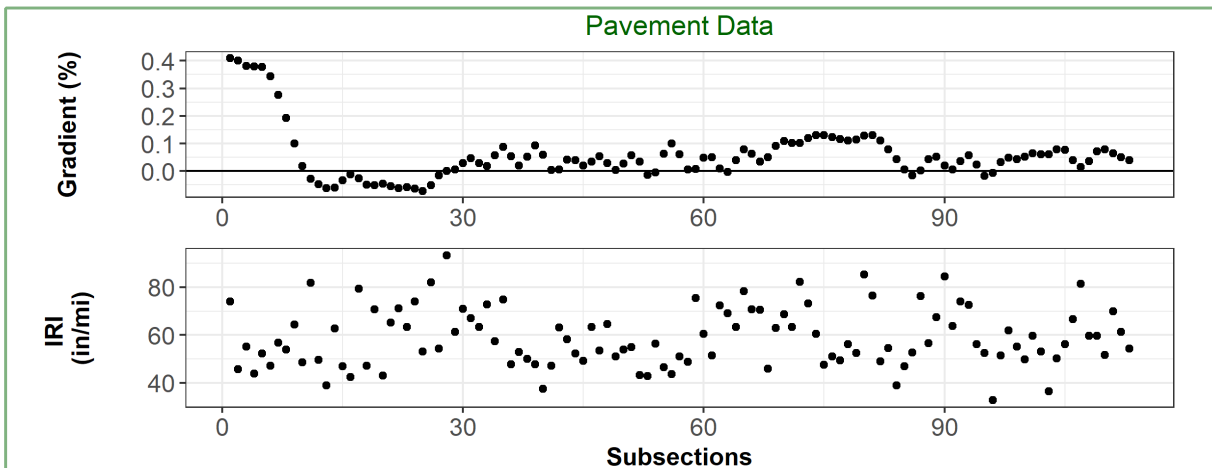


Figure P.261: F-450 data on Section PH18.

PH19-KER5N- RHMA-G F450 summer_day 45 mph

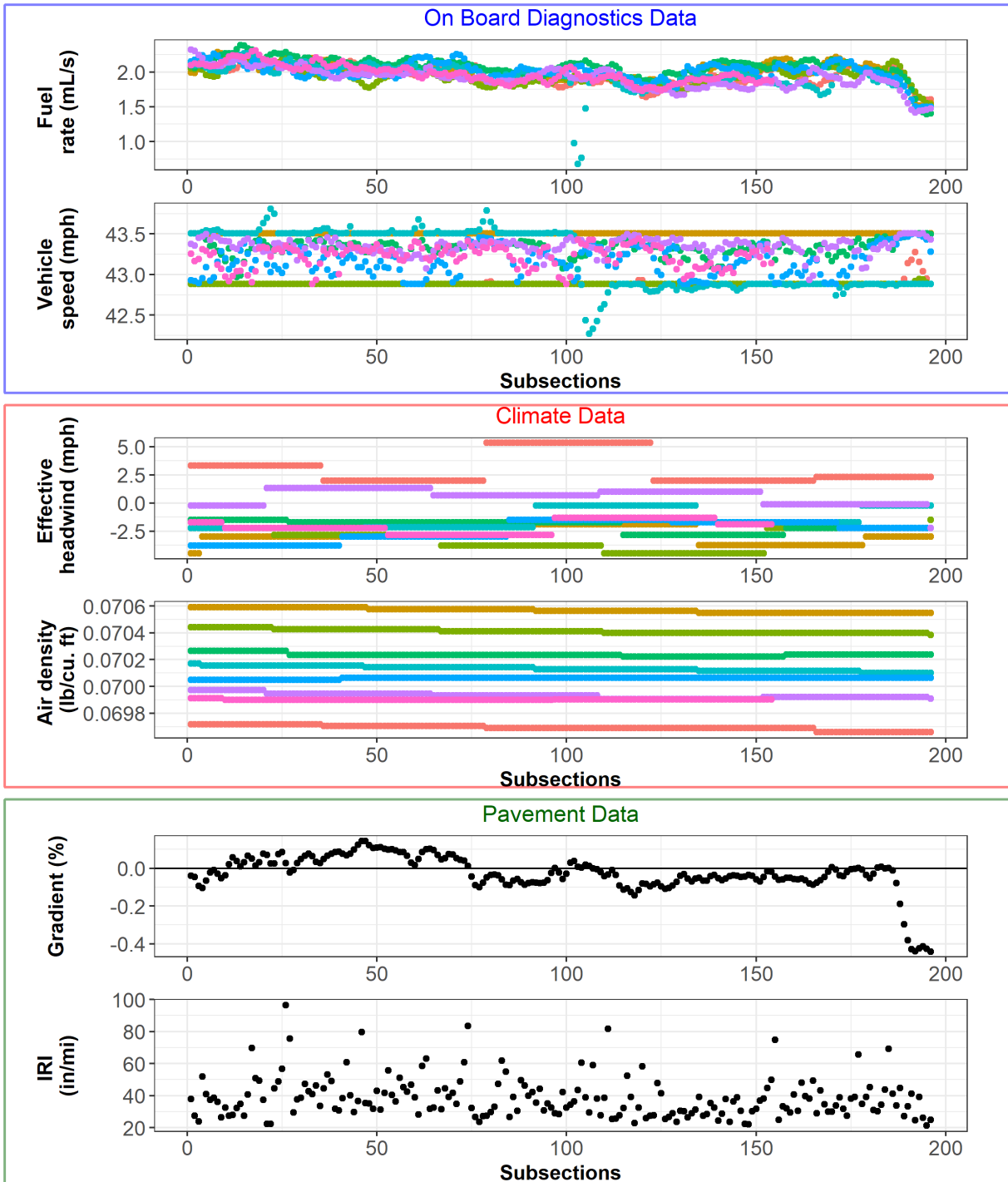


Figure P.262: F-450 data on Section PH19.

PH19-KER5N- RHMA-G F450 summer_day 55 mph

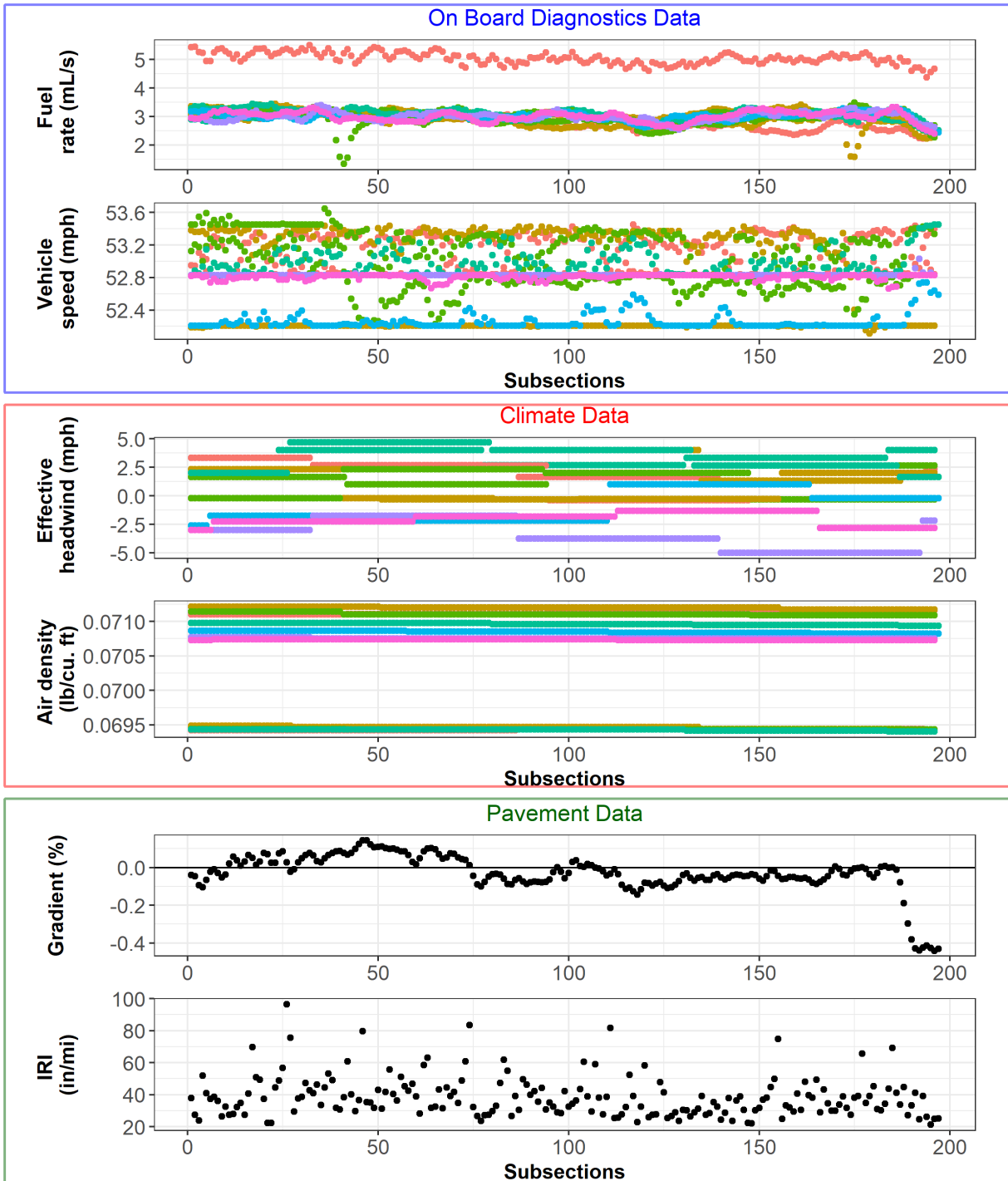
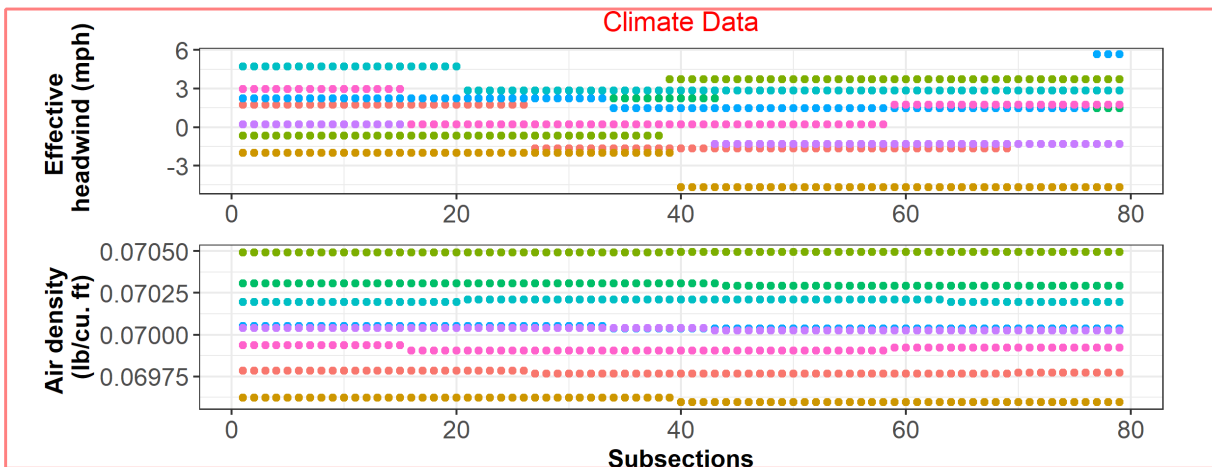
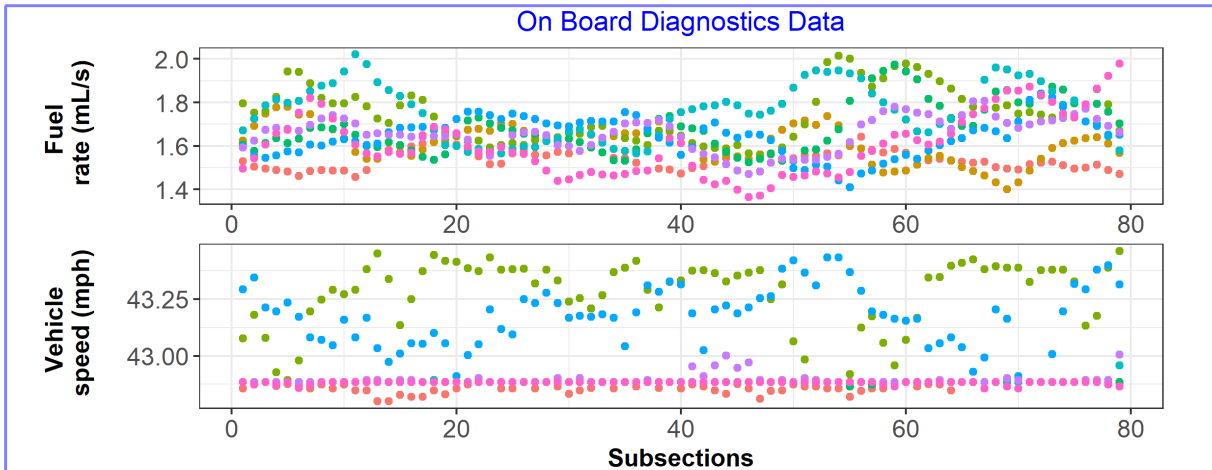


Figure P.263: F-450 data on Section PH19.

PH20-KER5S-CRCP F450 summer_day 45 mph



- Runs
- 1
 - 2
 - 9
 - 10
 - 11
 - 12
 - 13
 - 14

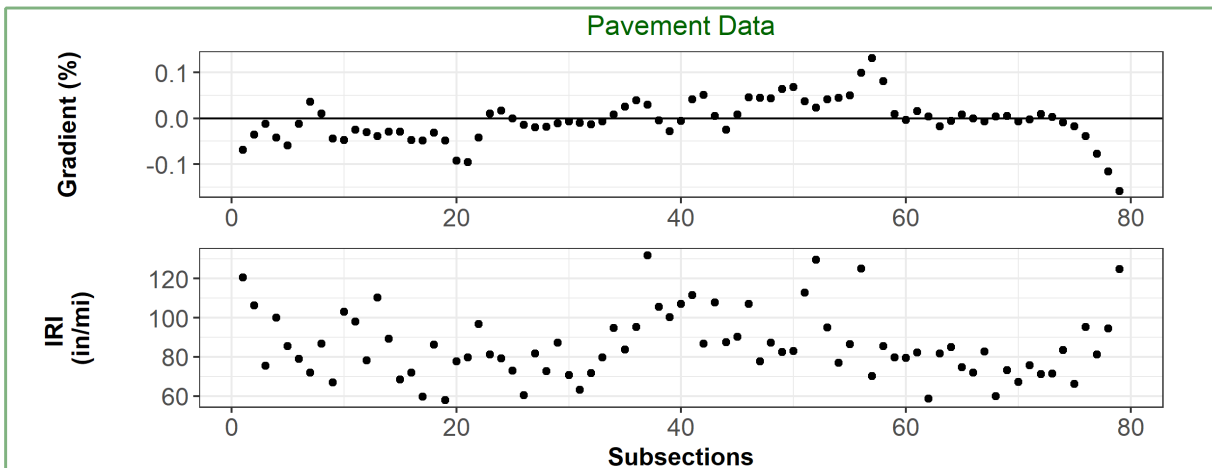


Figure P.264: F-450 data on Section PH20.

PH20-KER5S-CRCP F450 summer_day 55 mph

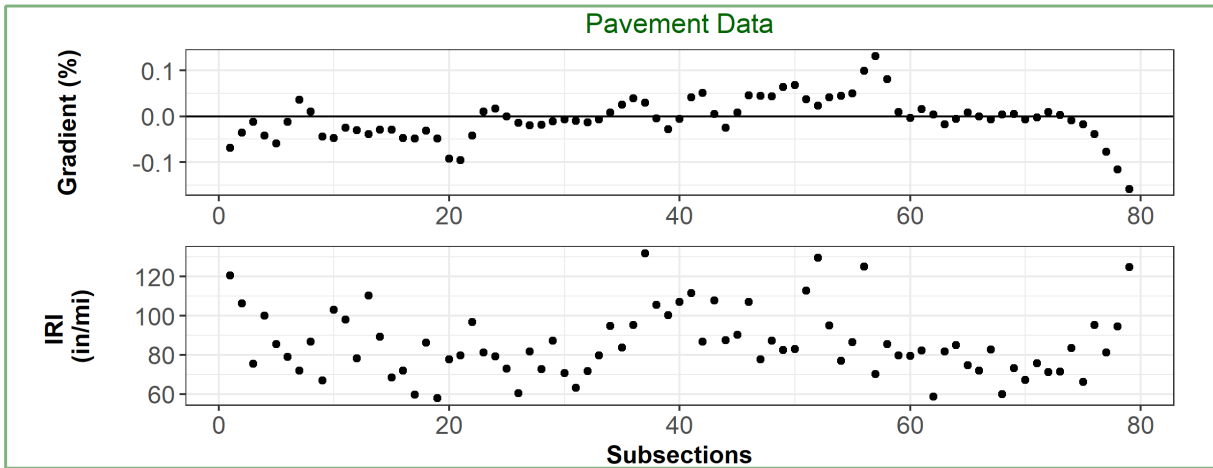
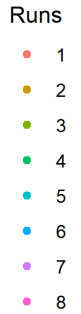
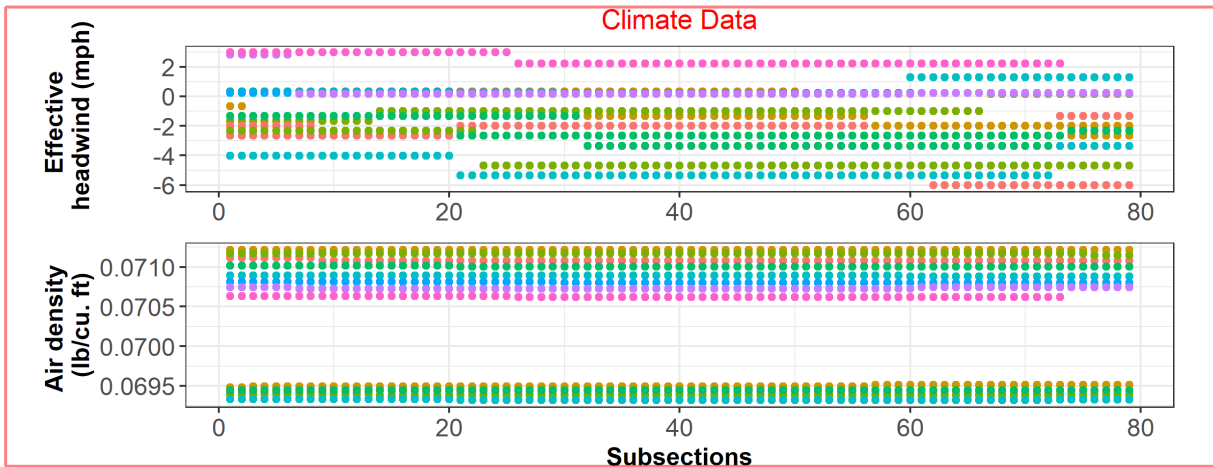
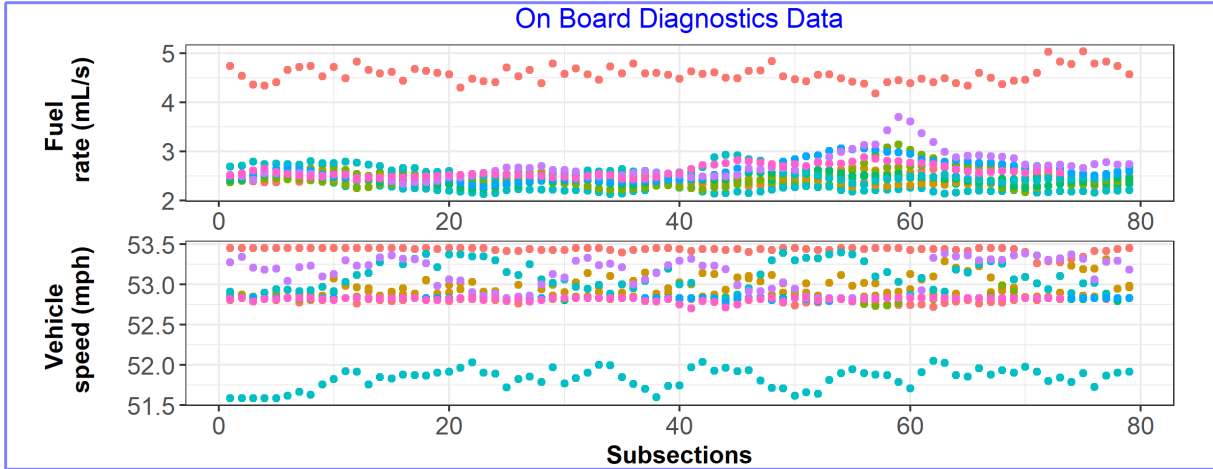


Figure P.265: F-450 data on Section PH20.

PH21-YOL99N-JPC F450 summer_day 45 mph

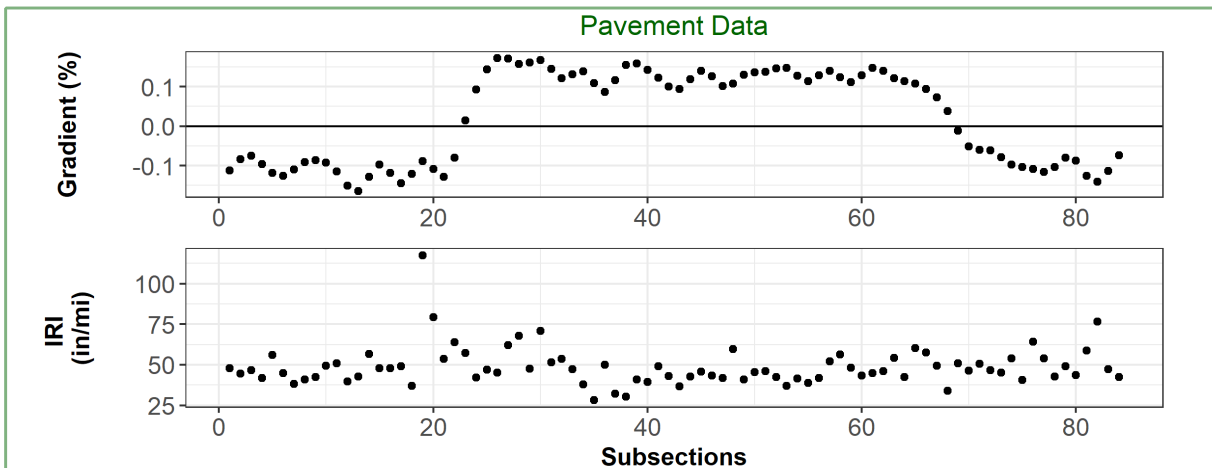
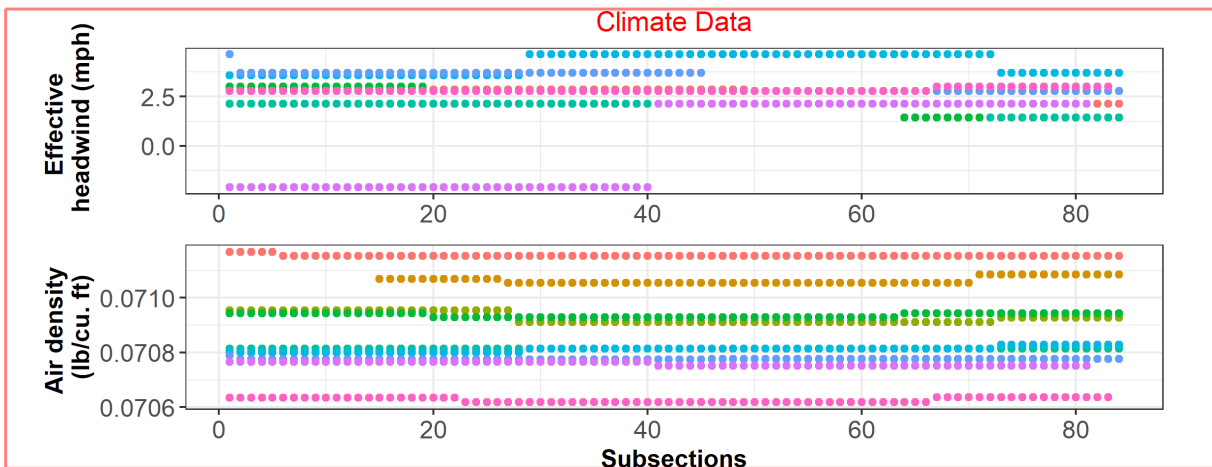
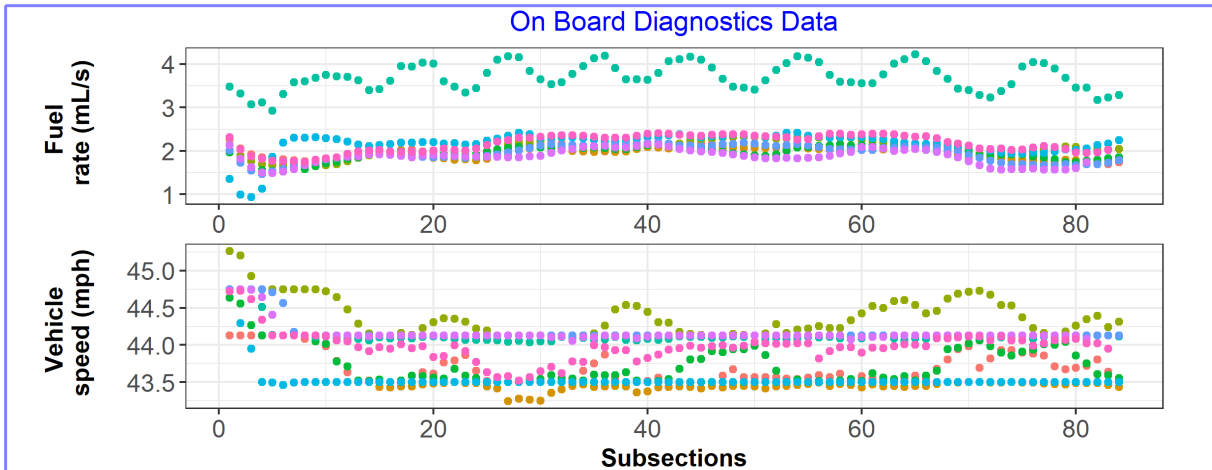


Figure P.266: F-450 data on Section PH21.

PH21-YOL99N-JPC F450 summer_day 55 mph

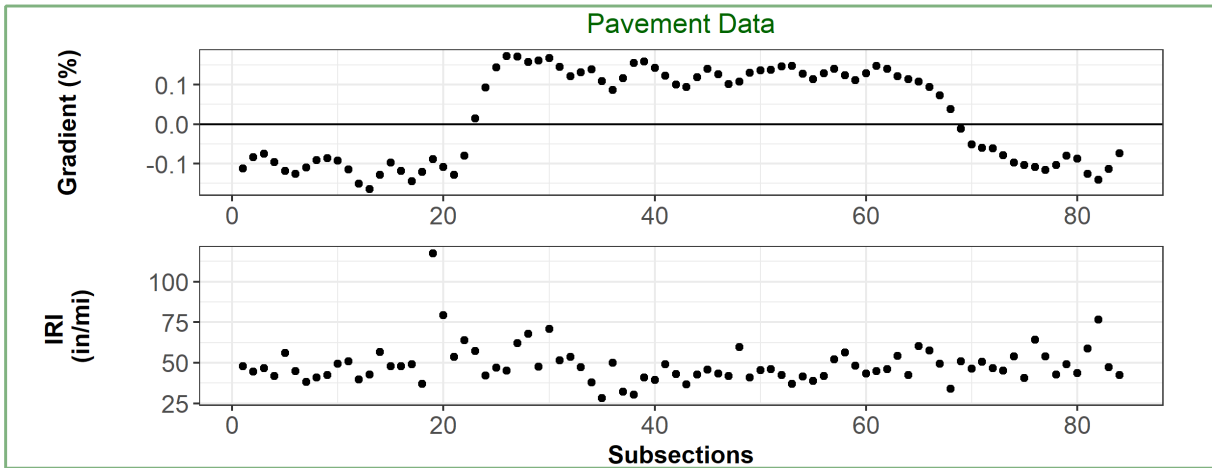
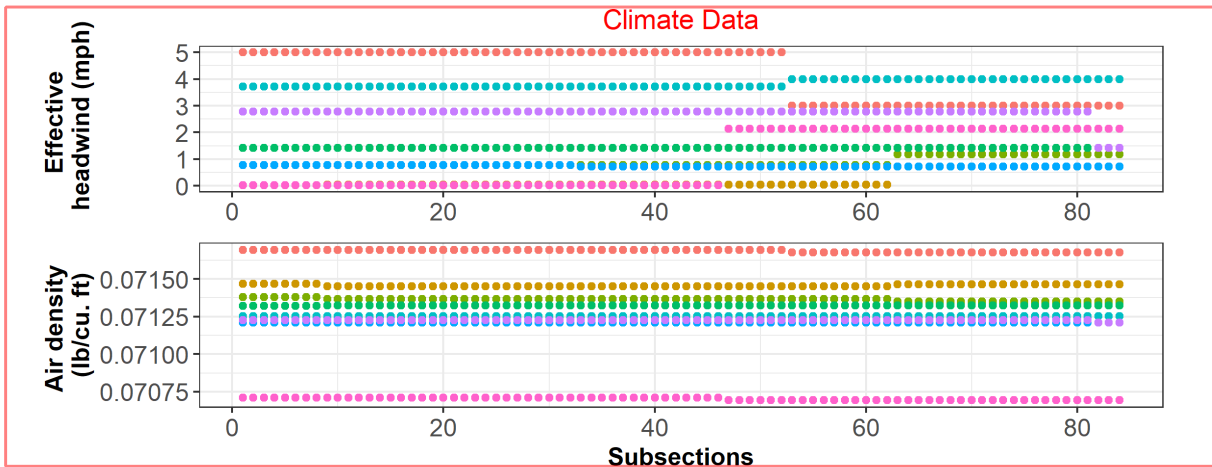
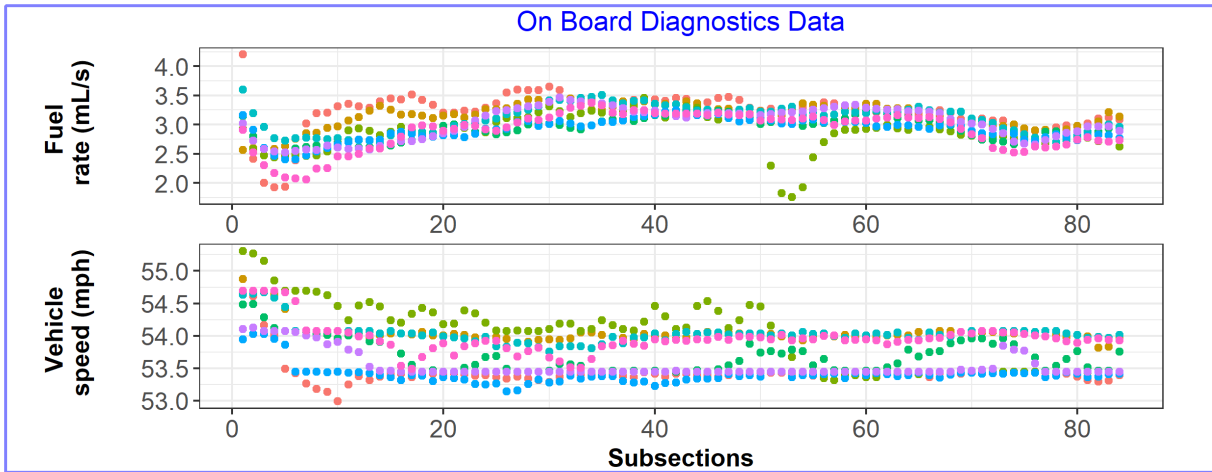
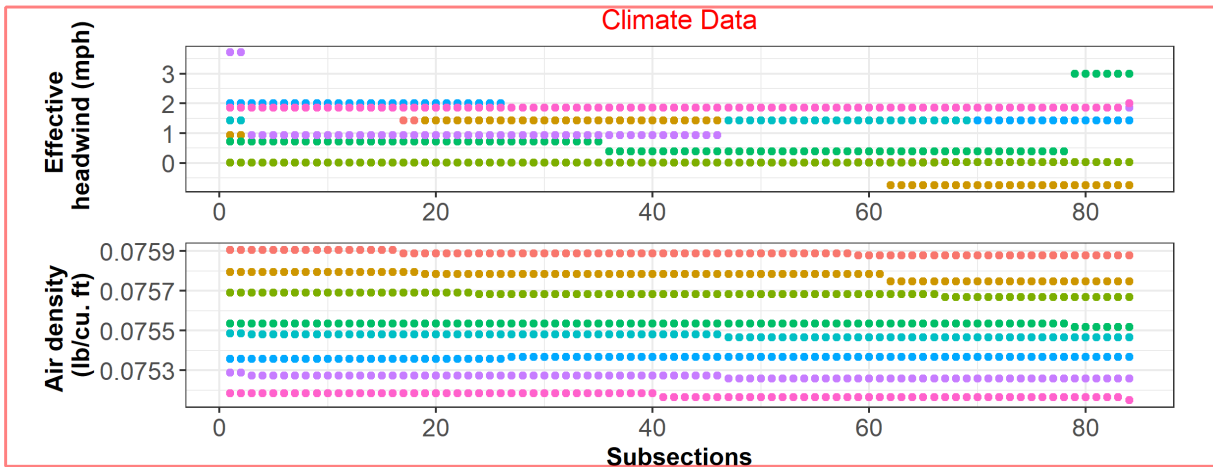
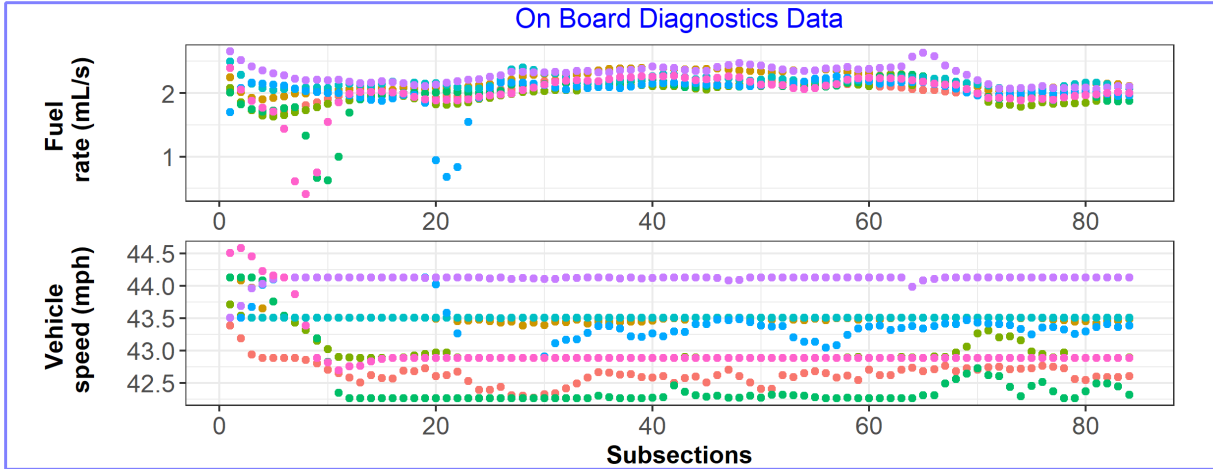


Figure P.267: F-450 data on Section PH21.

PH21-YOL99N-JPC F450 winter_day 45 mph



- Runs
- 1
 - 2
 - 3
 - 4
 - 5
 - 6
 - 7
 - 8

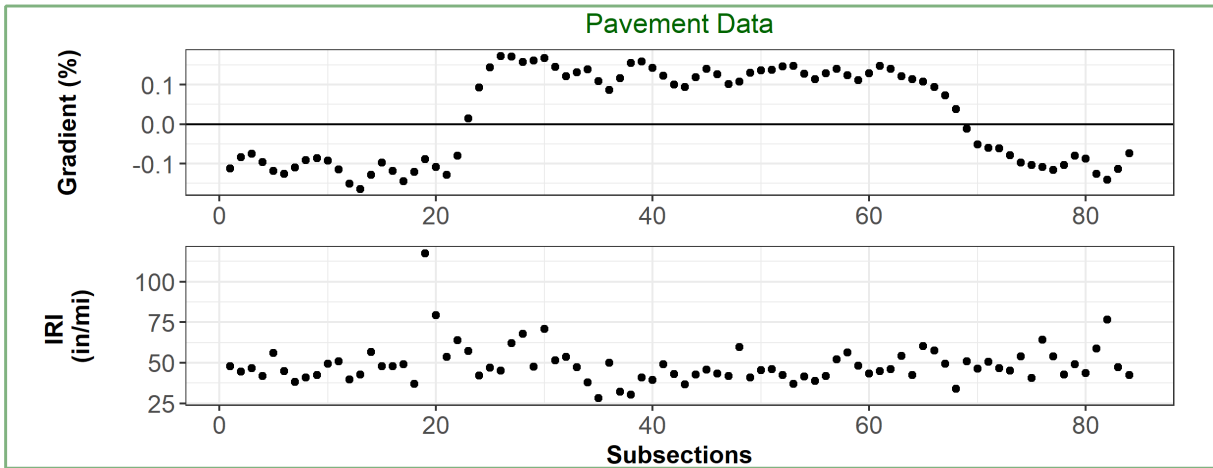


Figure P.268: F-450 data on Section PH21.

PH21-YOL99N-JPC F450 winter_day 55 mph

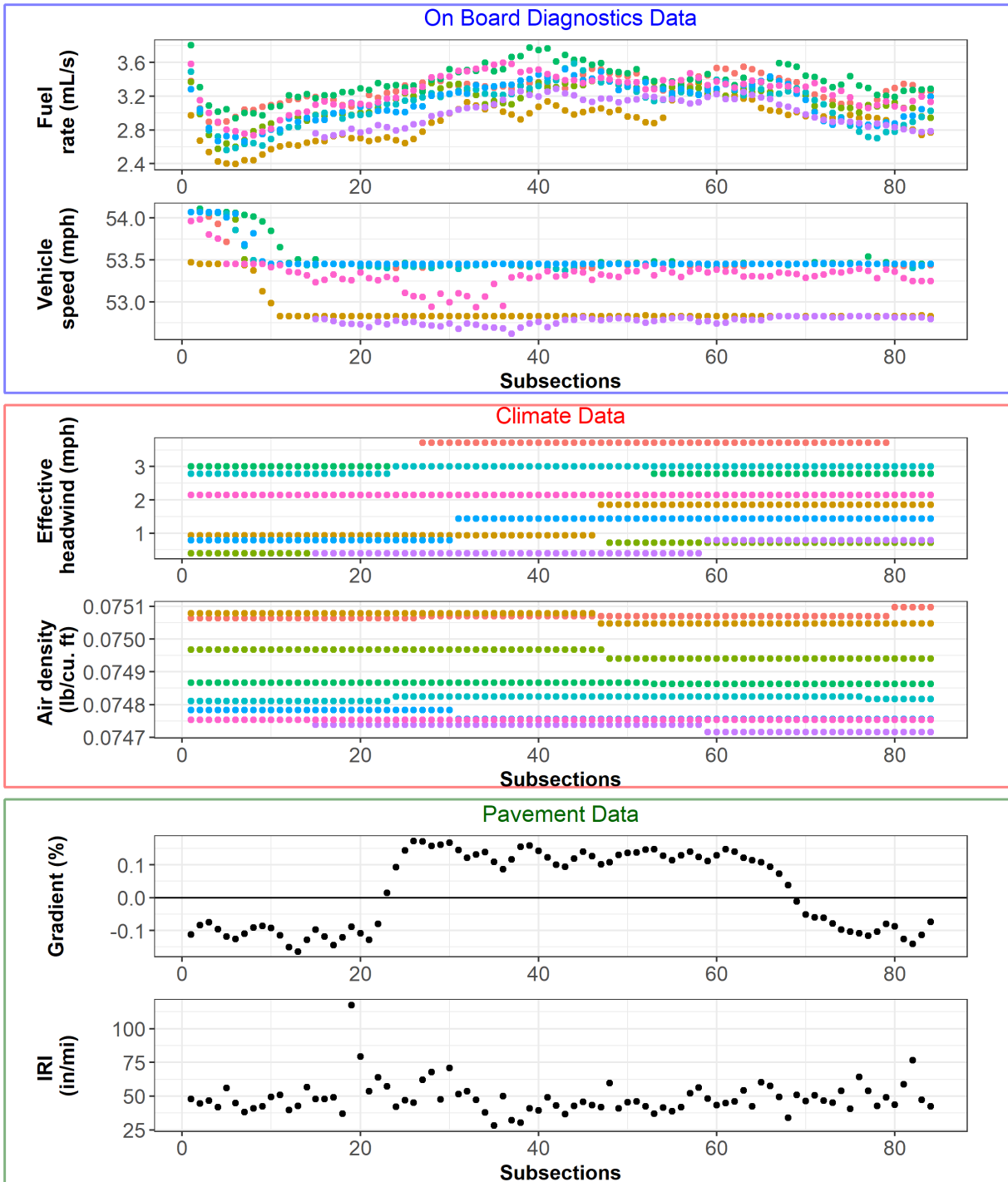


Figure P.269: F-450 data on Section PH21.

PH22-YOL99S-JPC F450 summer_day 45 mph

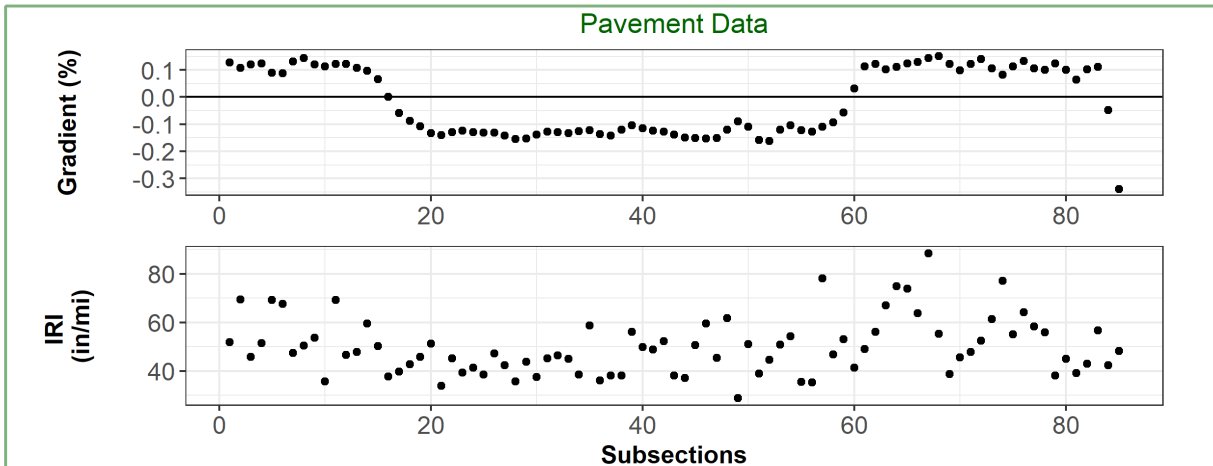
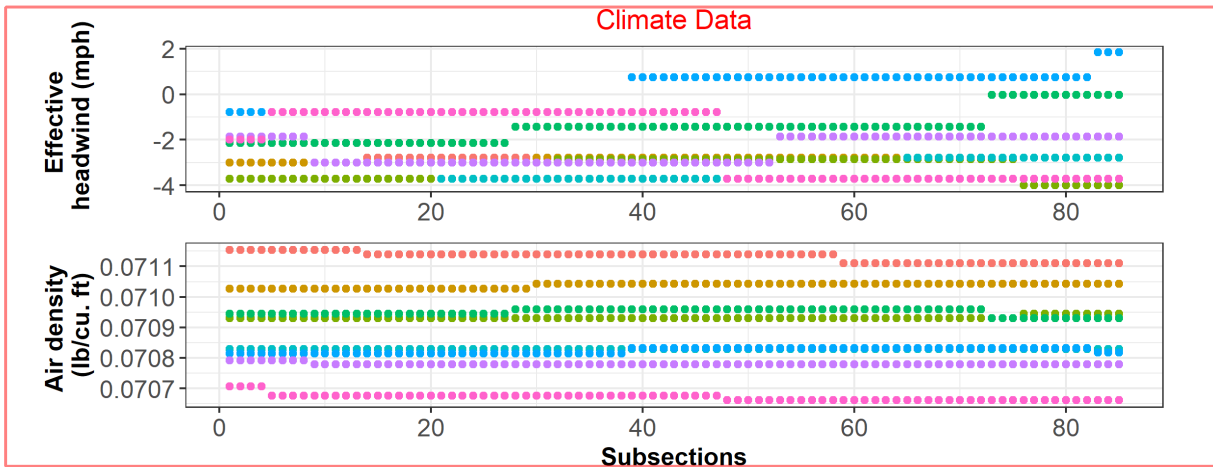
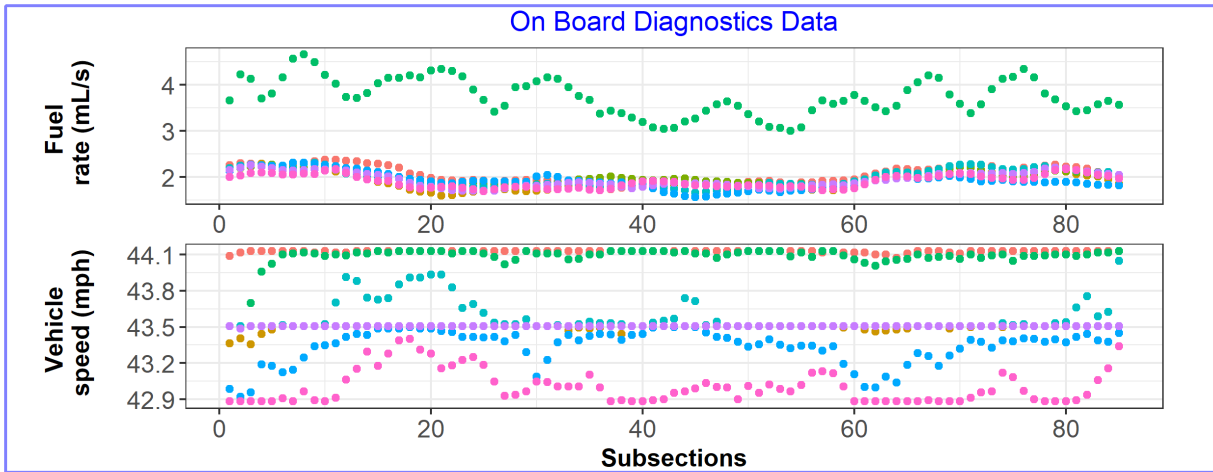


Figure P.270: F-450 data on Section PH22.

PH22-YOL99S-JPC F450 summer_day 55 mph

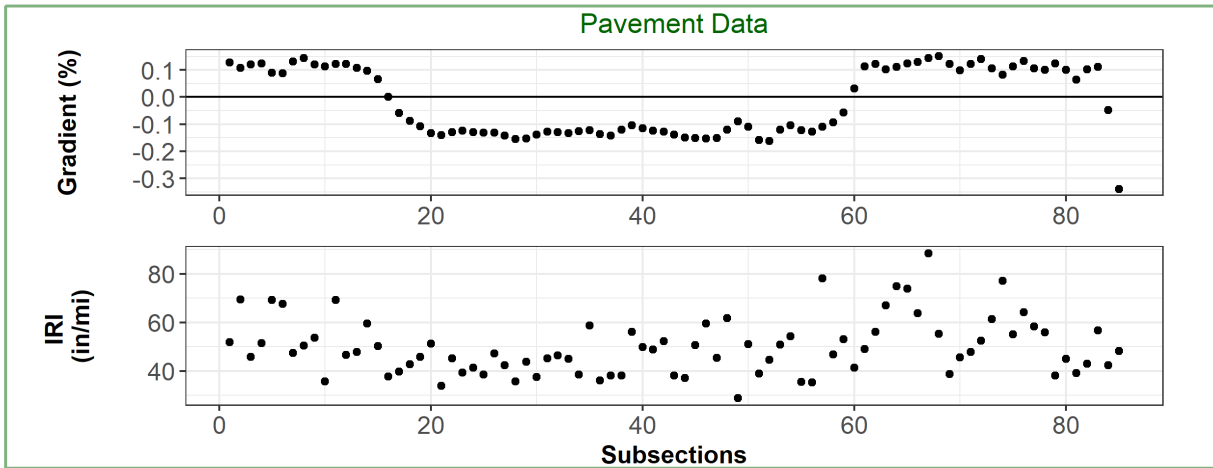
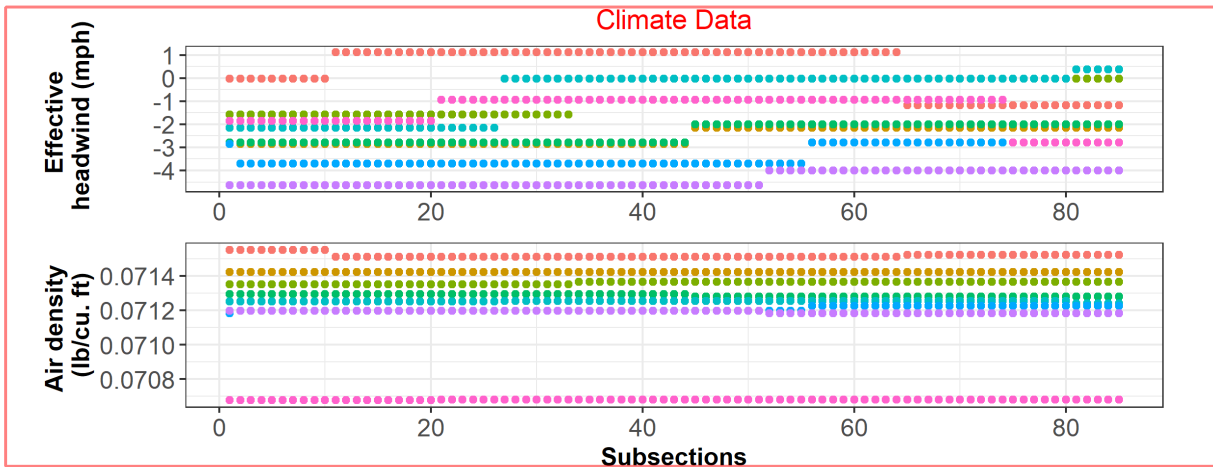
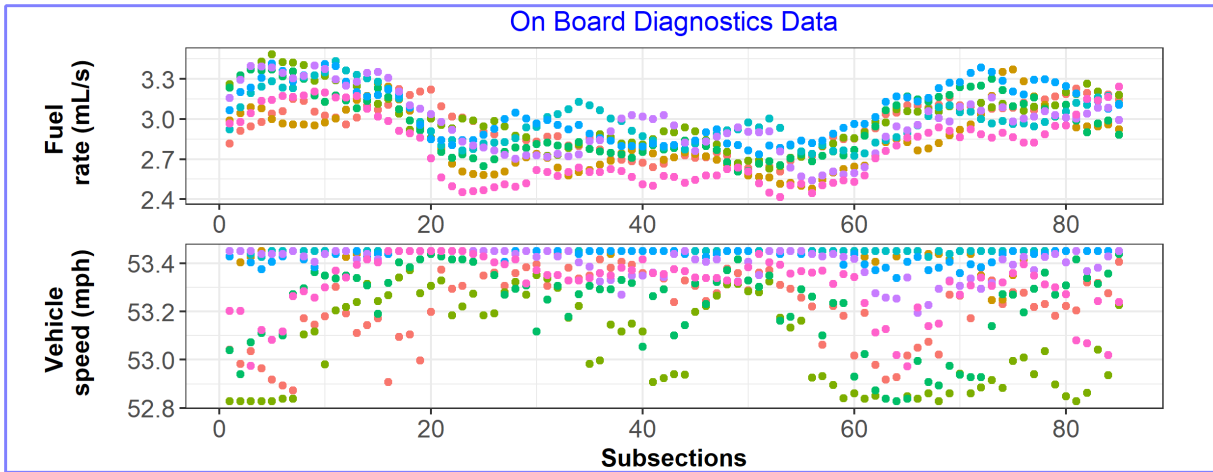


Figure P.271: F-450 data on Section PH22.

PH22-YOL99S-JPC F450 winter_day 45 mph

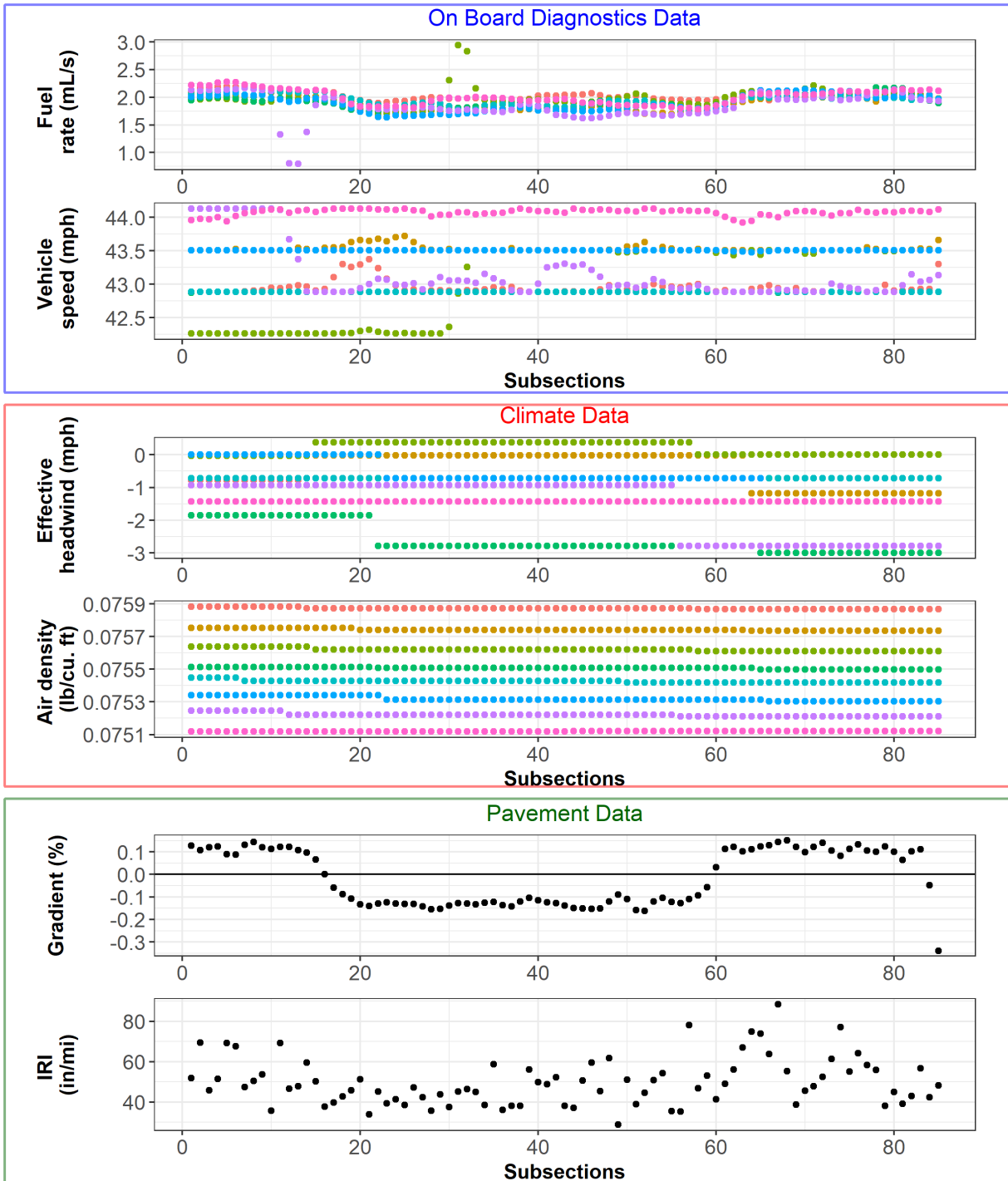


Figure P.272: F-450 data on Section PH22.

PH22-YOL99S-JPC F450 winter_day 55 mph

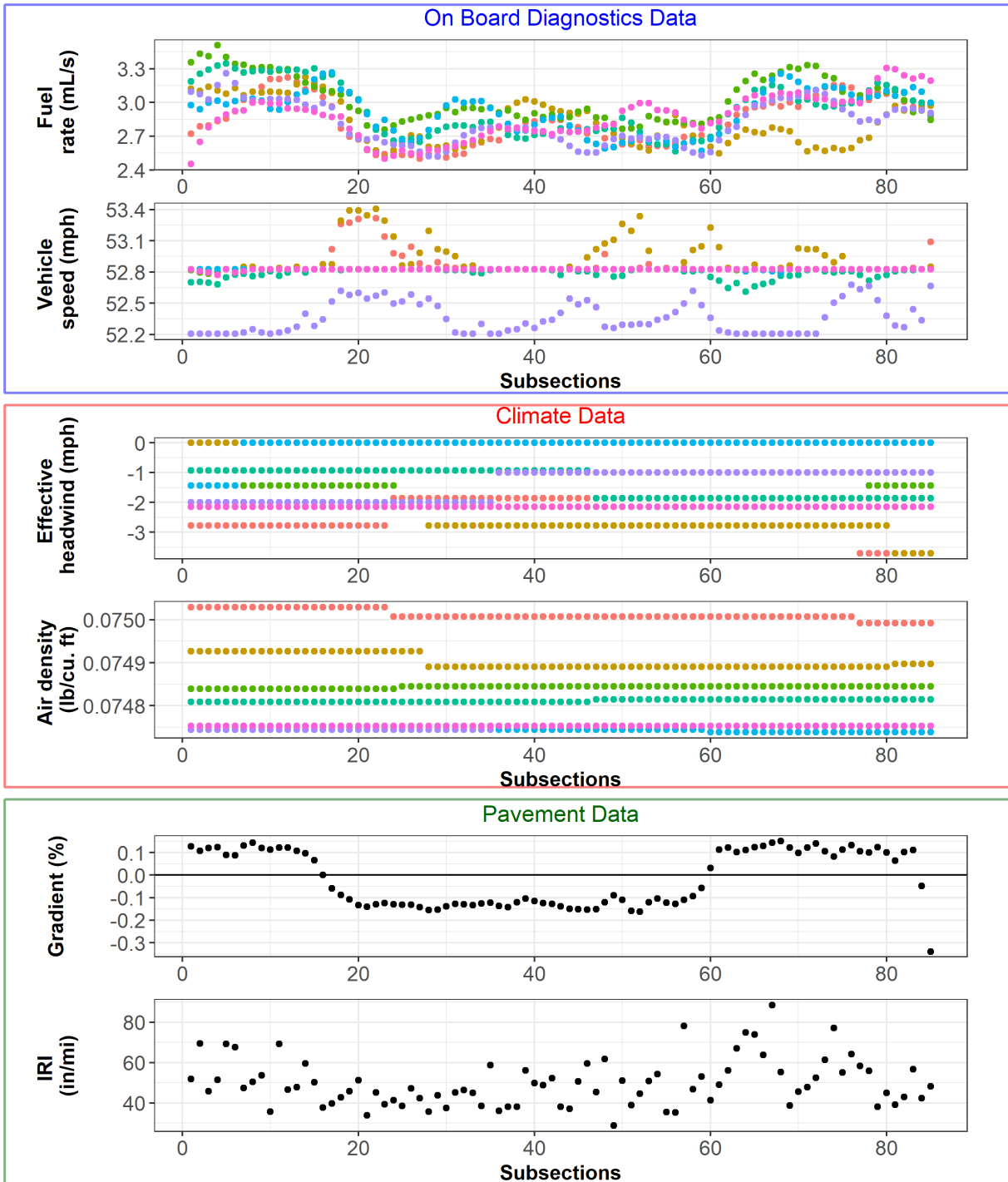


Figure P.273: F-450 data on Section PH22.

PH23-YOL-CR32AW-JPC F450 summer_day 35 mph

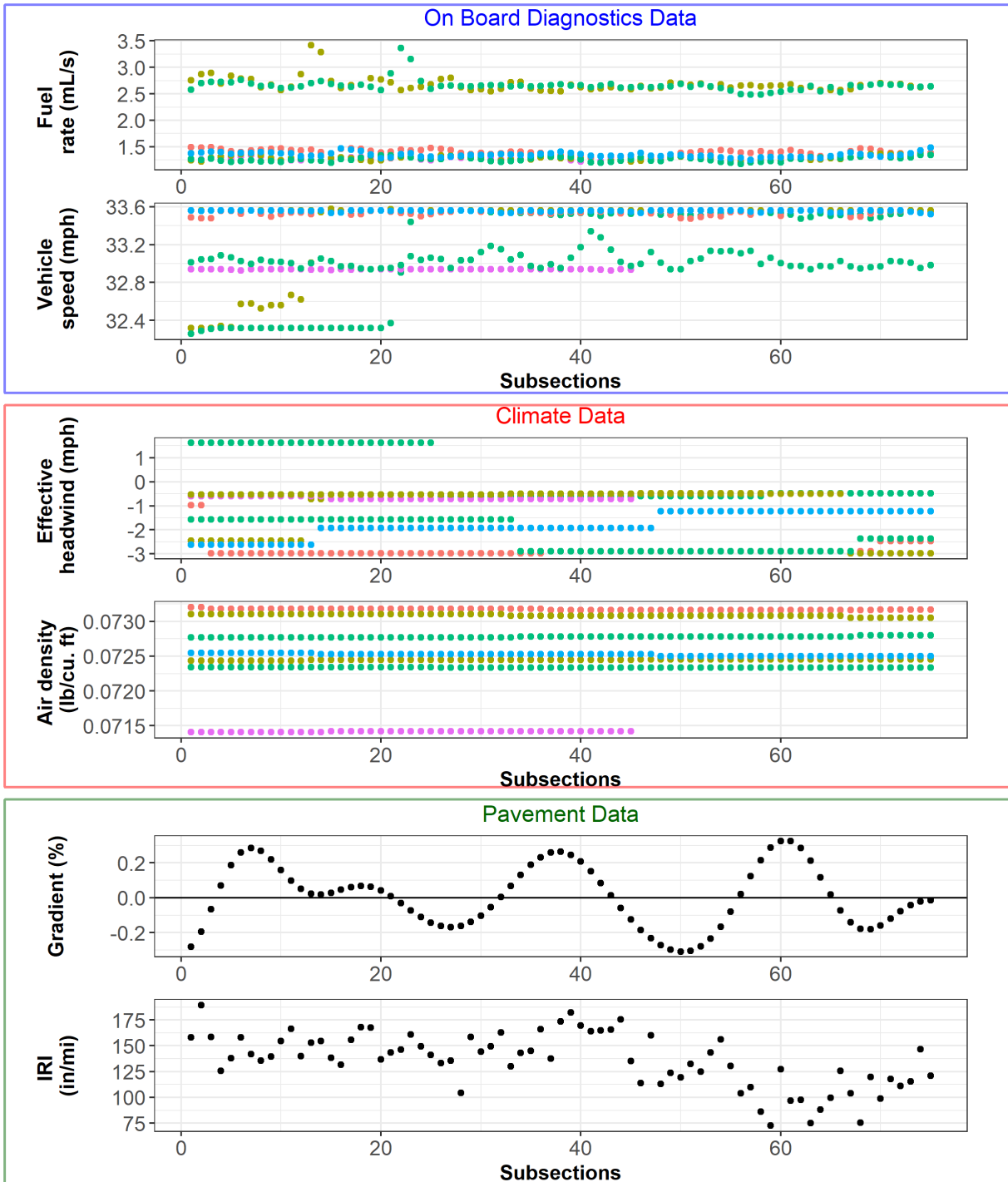


Figure P.274: F-450 data on Section PH23.

PH23-YOL-CR32AW-JPC F450 summer_day 45 mph

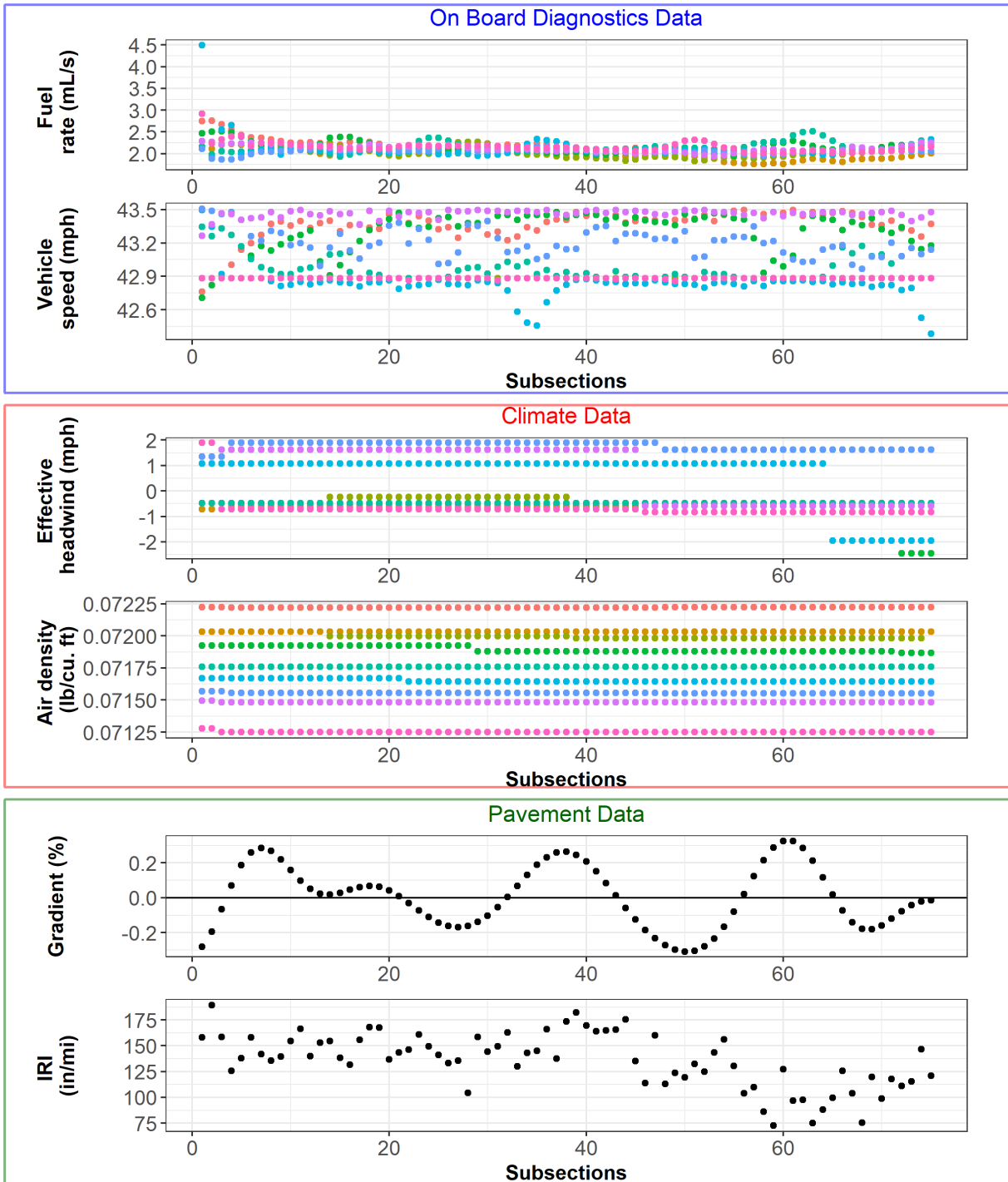


Figure P.275: F-450 data on Section PH23.

PH23-YOL-CR32AW-JPC F450 summer_night 35 mph

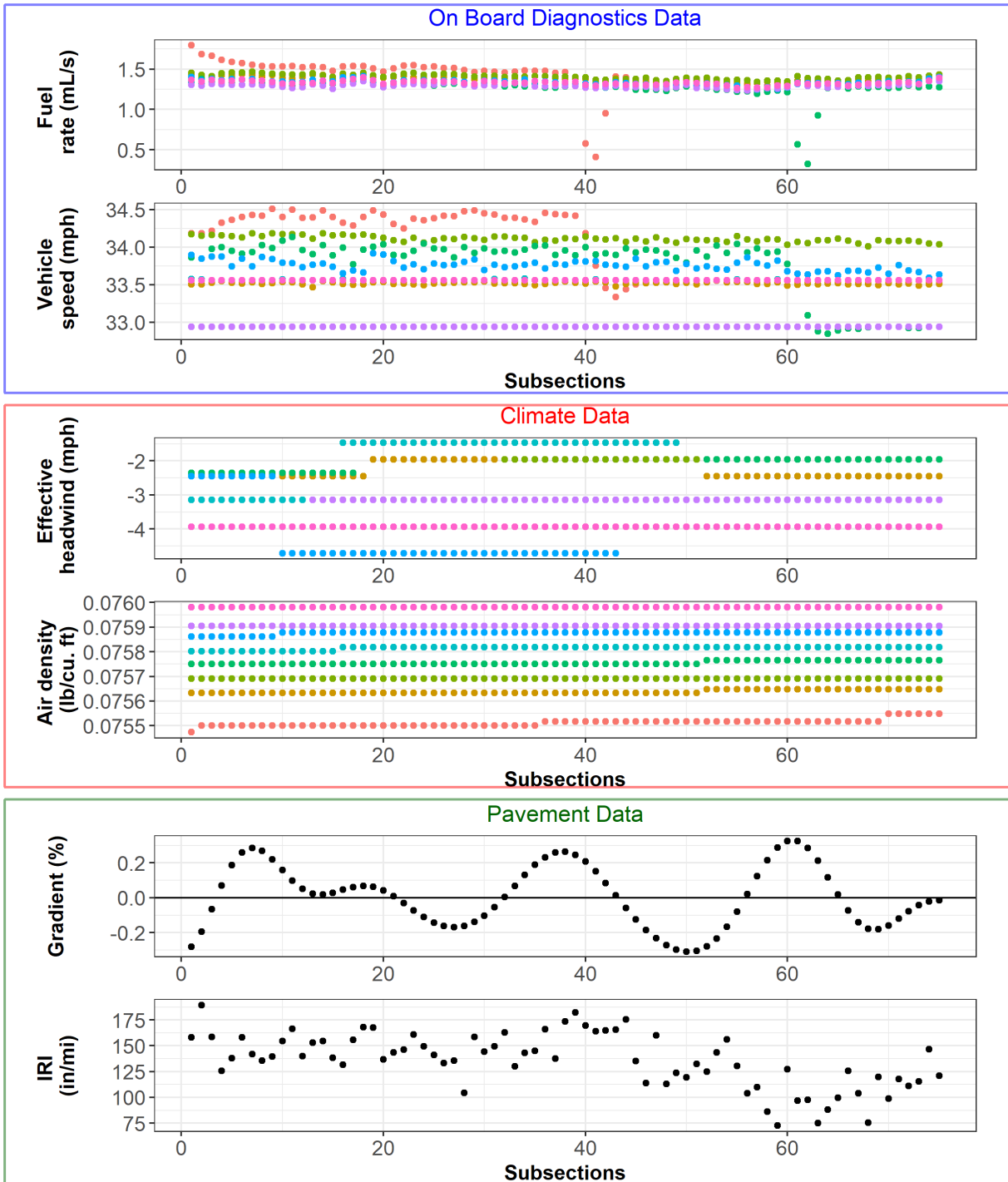


Figure P.276: F-450 data on Section PH23.

PH23-YOL-CR32AW-JPC F450 summer_night 45 mph

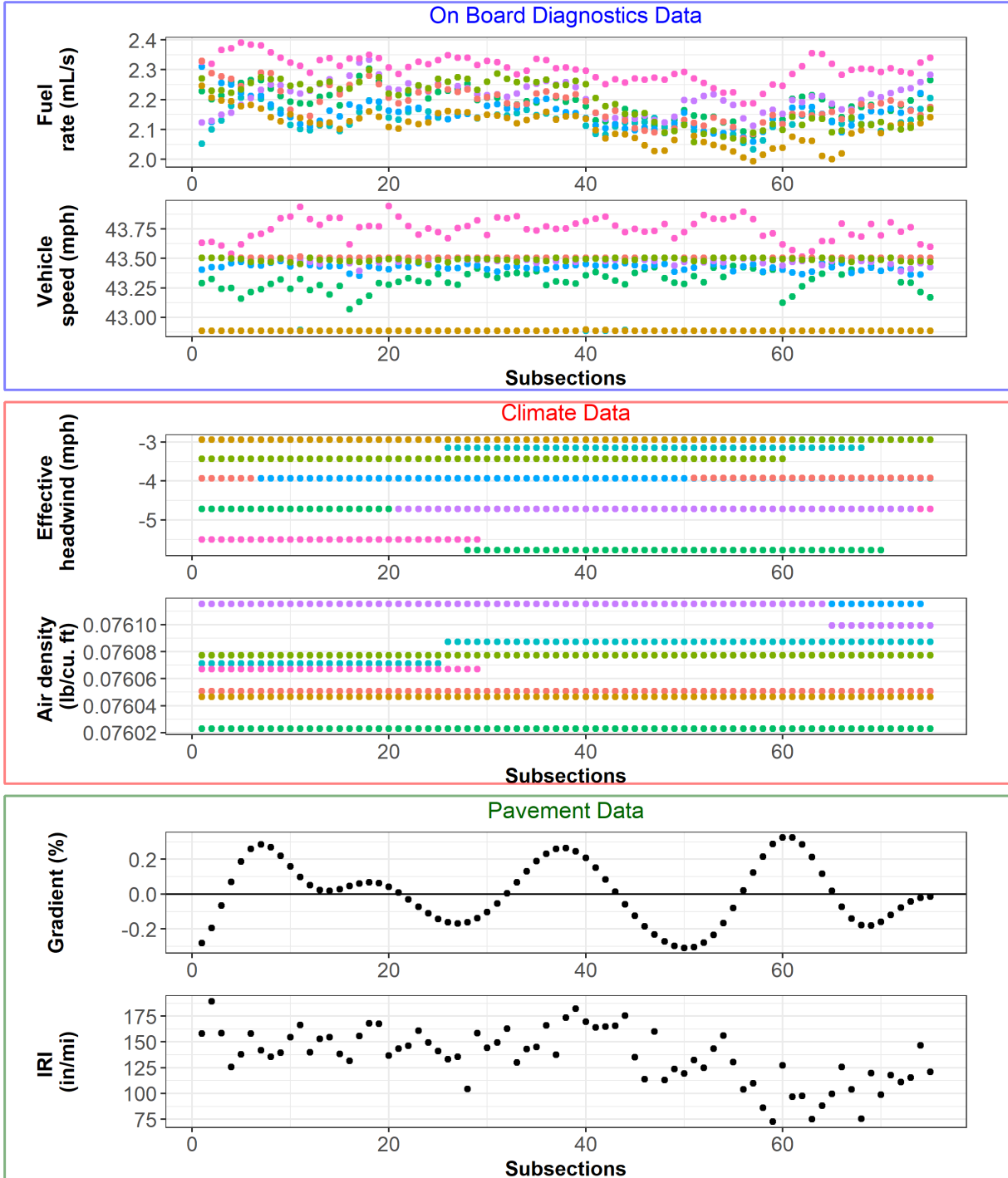


Figure P.277: F-450 data on Section PH23.

PH23-YOL-CR32AW-JPC F450 winter_day 35 mph

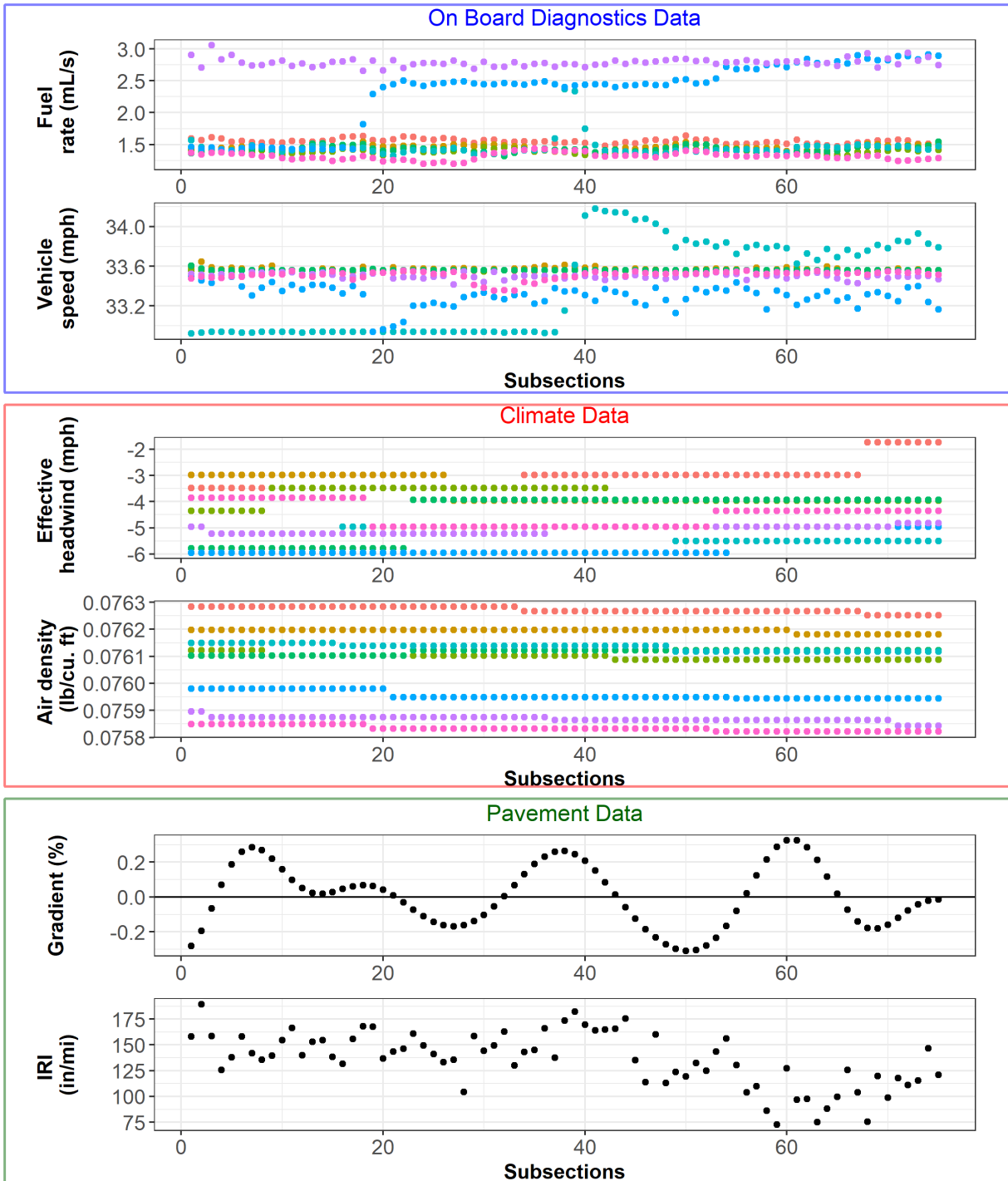


Figure P.278: F-450 data on Section PH23.

PH23-YOL-CR32AW-JPC F450 winter_day 45 mph

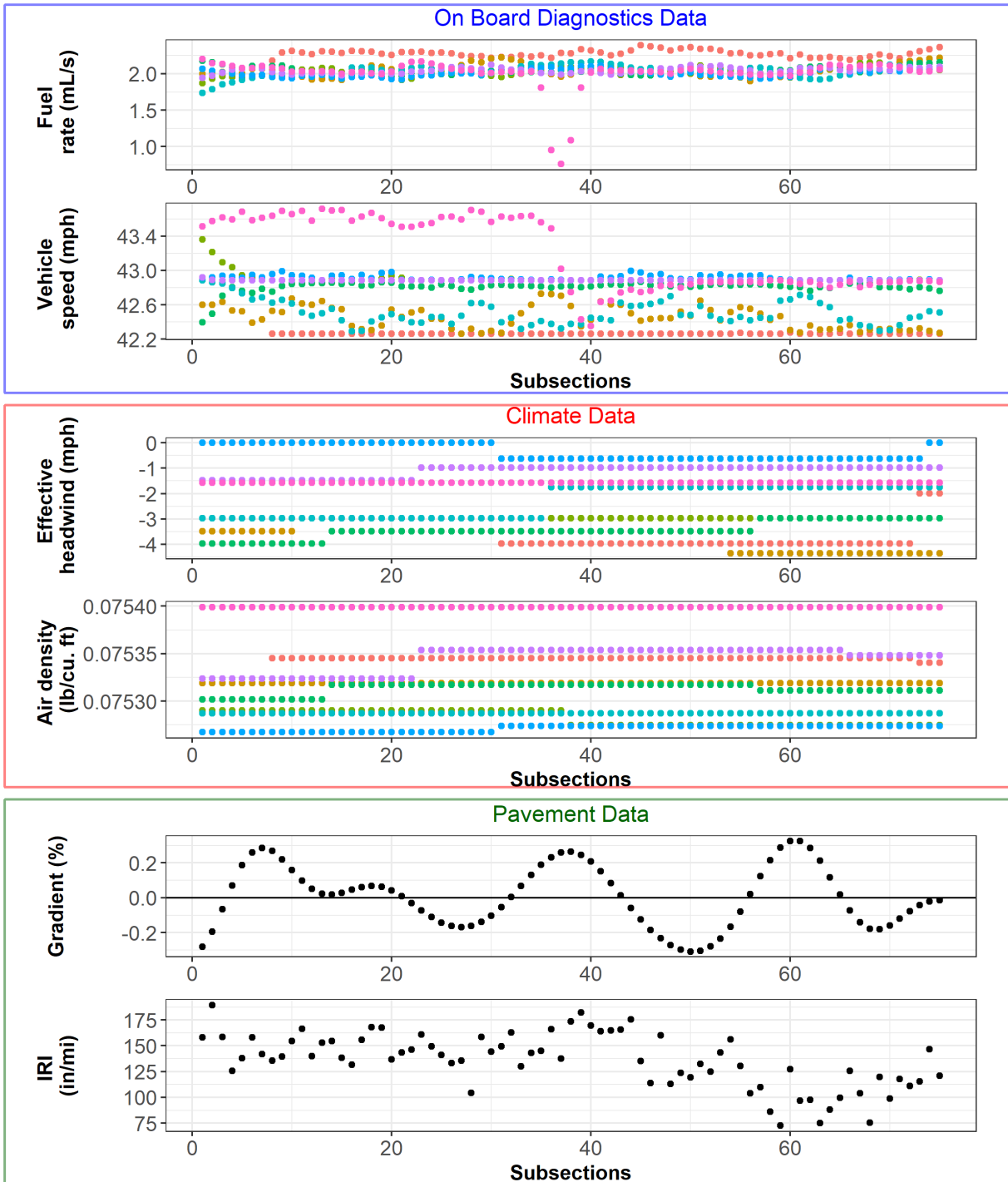


Figure P.279: F-450 data on Section PH23.

4. HHDT Data

PH01-YOL113N-JPC HHDT summer_day 45 mph

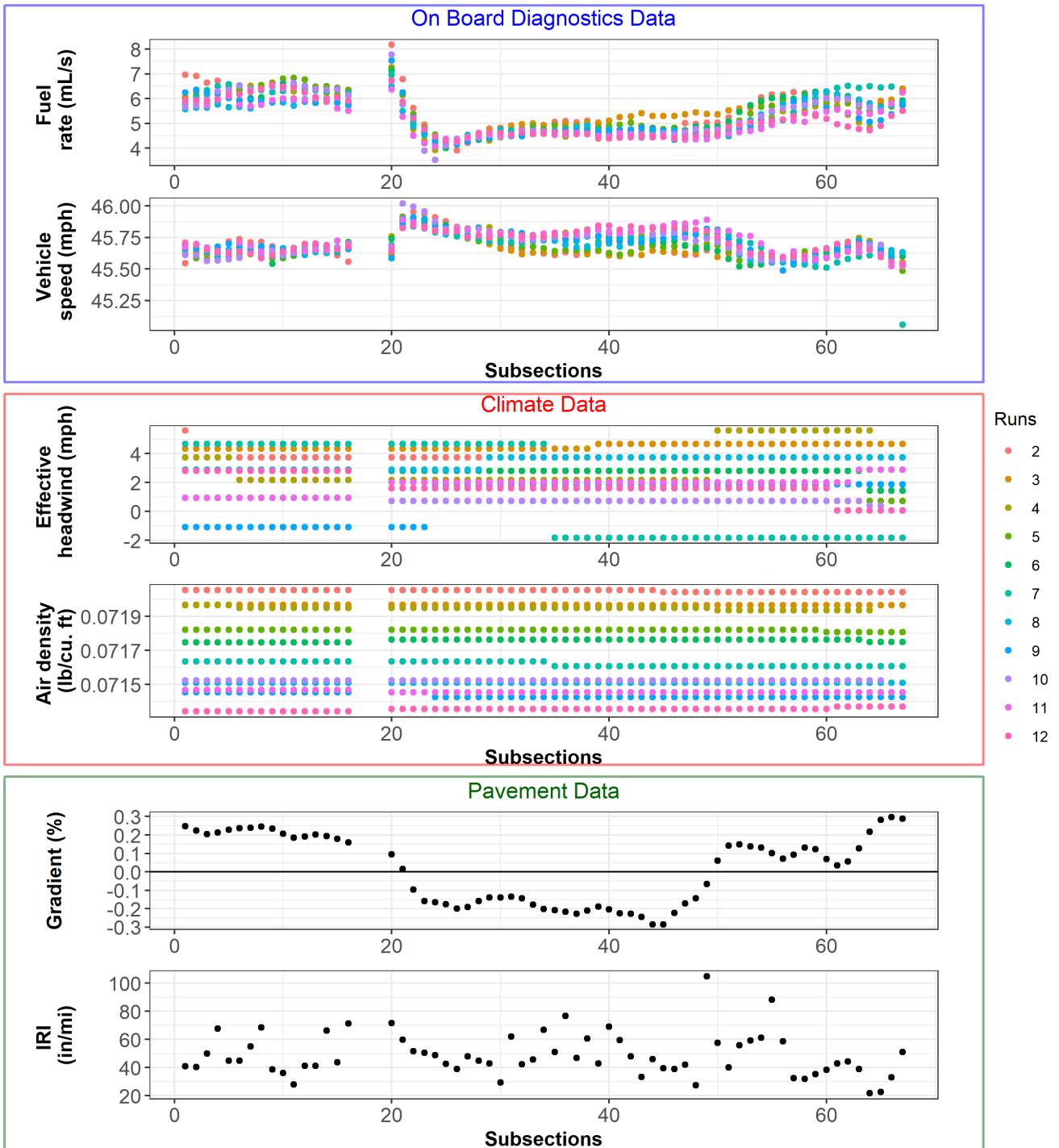


Figure P.280: HHDT data on Section PH01.

PH01-YOL113N-JPC HHDT summer_day 55 mph

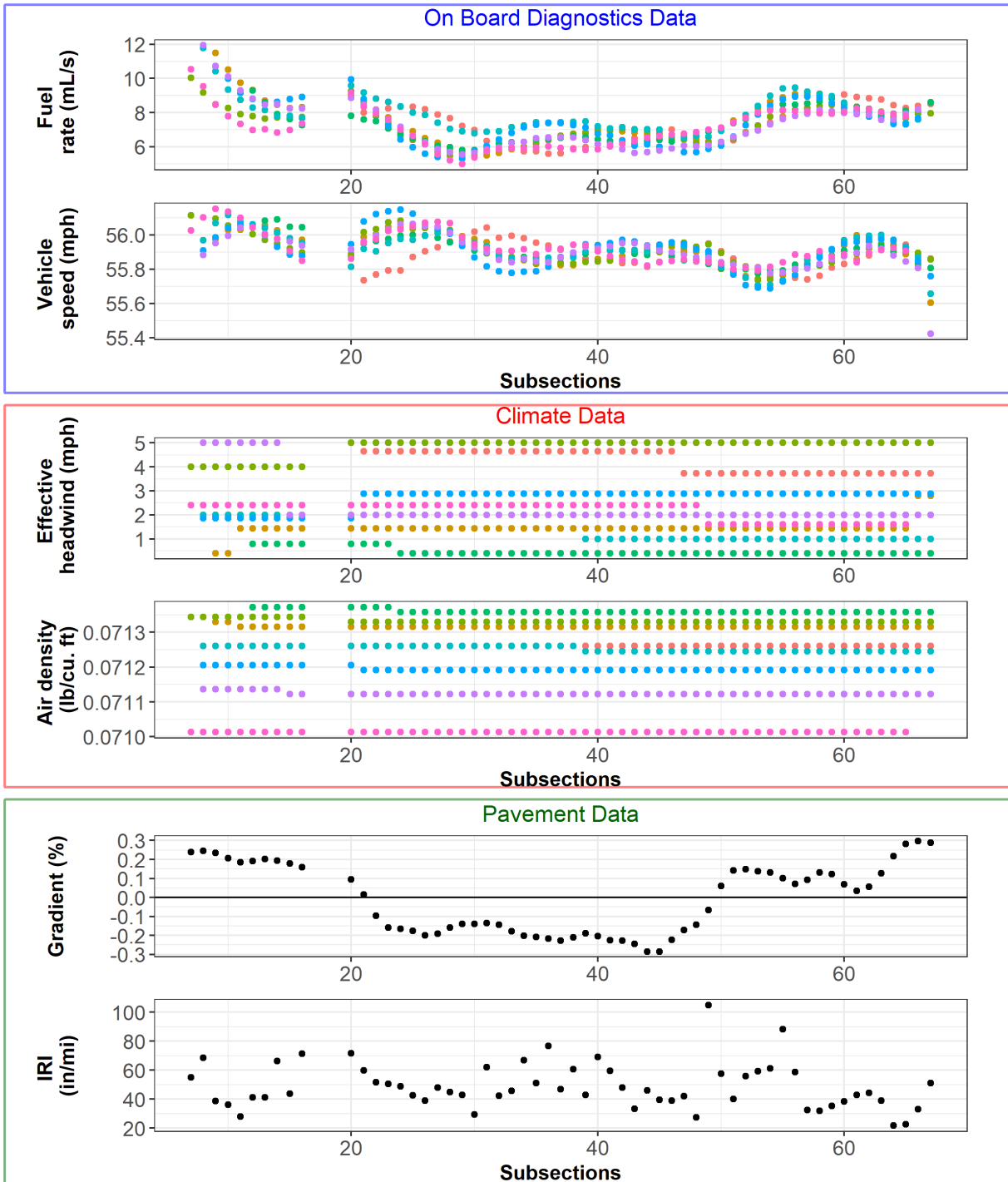


Figure P.281: HHDT data on Section PH01.

PH01-YOL113N-JPC HHDT summer_night 45 mph

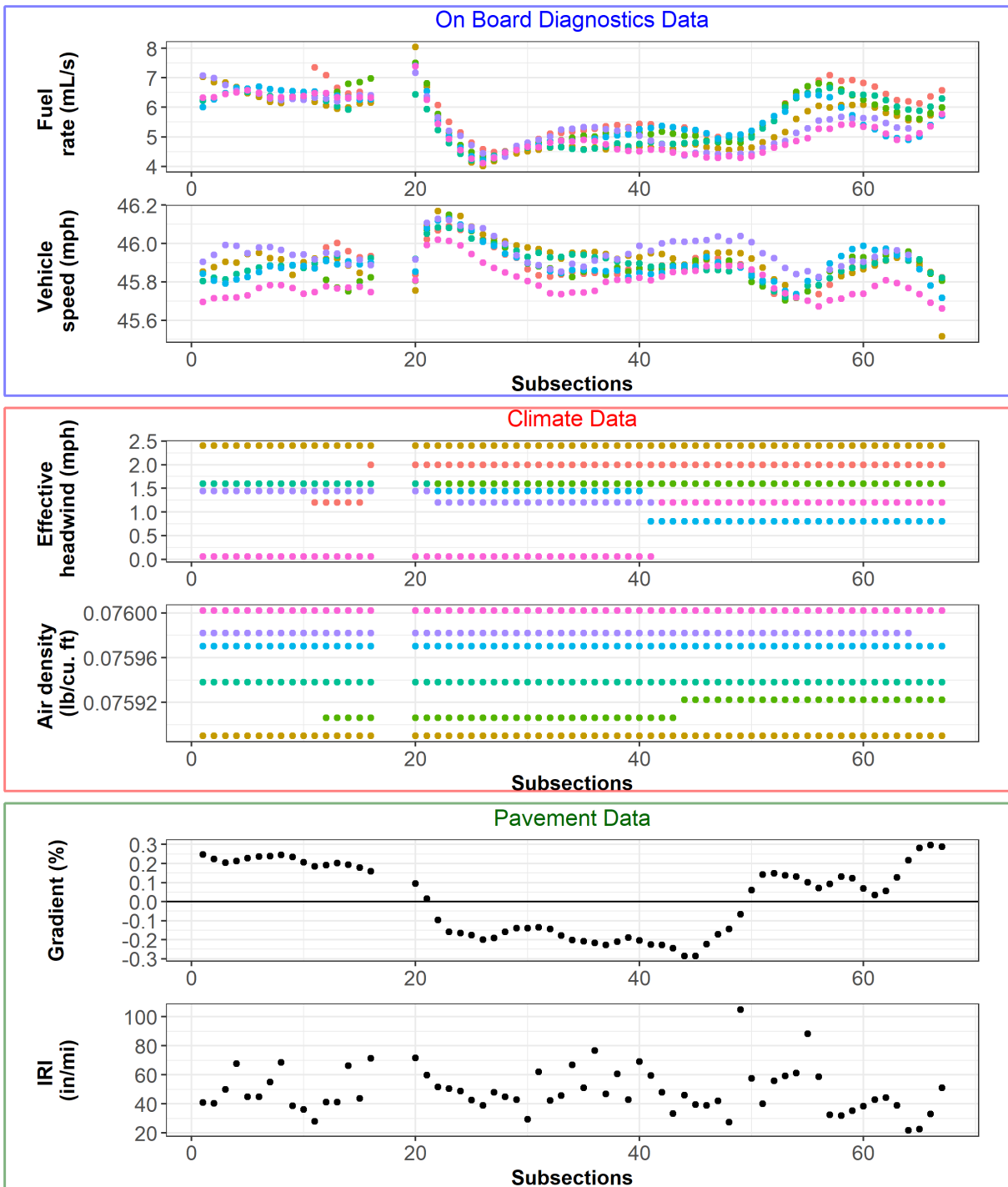


Figure P.282: HHDT data on Section PH01.

PH01-YOL113N-JPC HHDT summer_night 55 mph

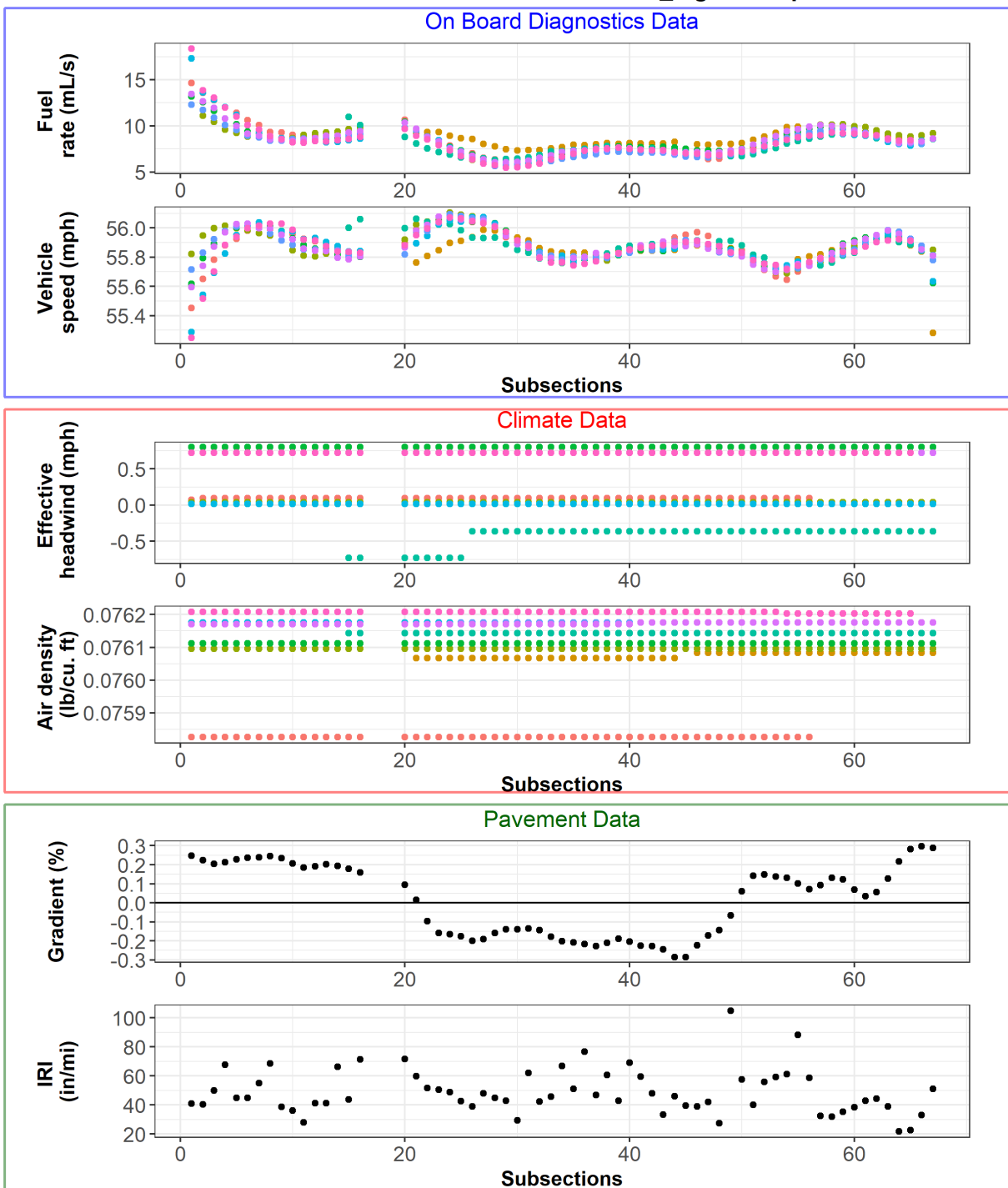


Figure P.283: HHDT data on Section PH01.

PH01-YOL113N-JPC HHDT winter_day 45 mph

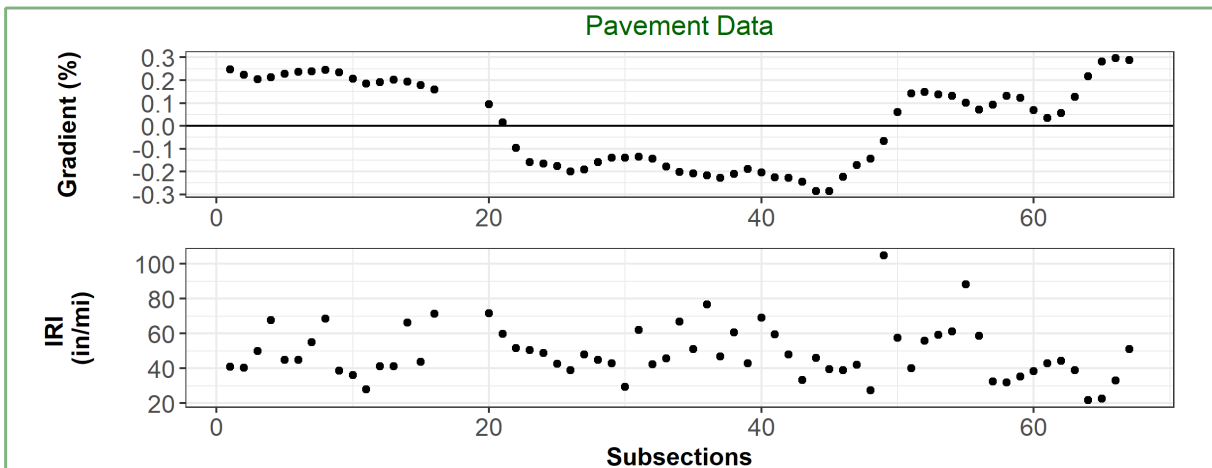
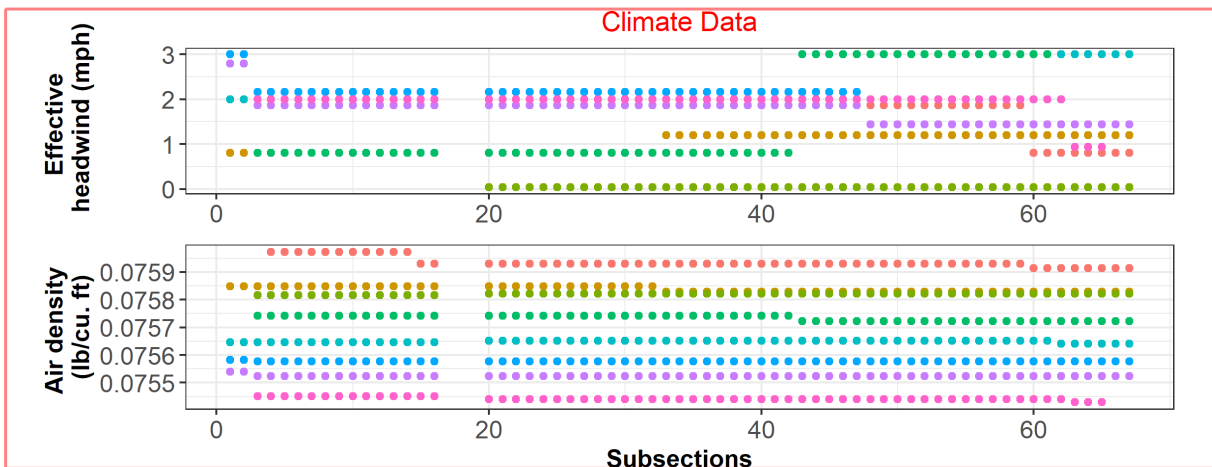
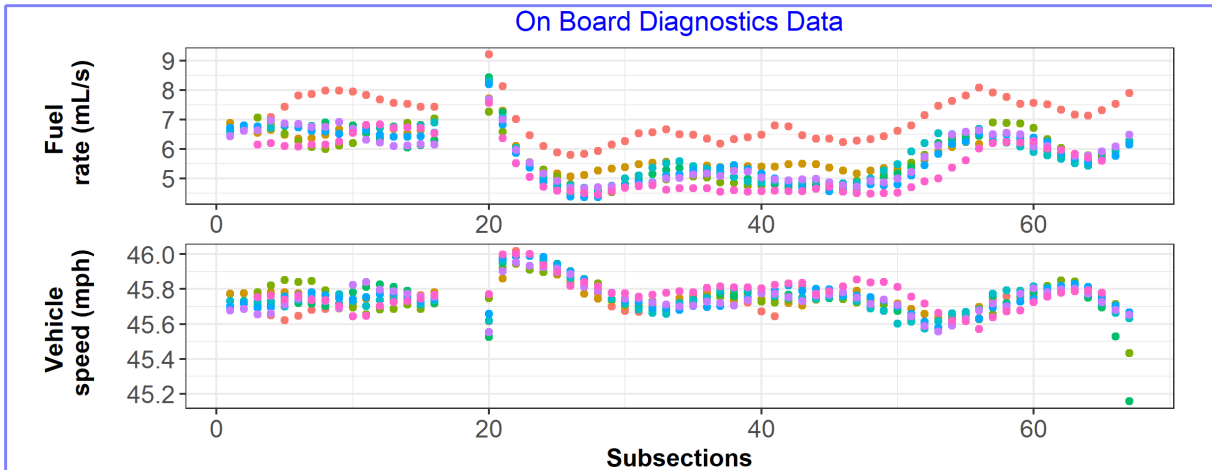


Figure P.284: HHDT data on Section PH01.

PH01-YOL113N-JPC HHDT winter_day 55 mph

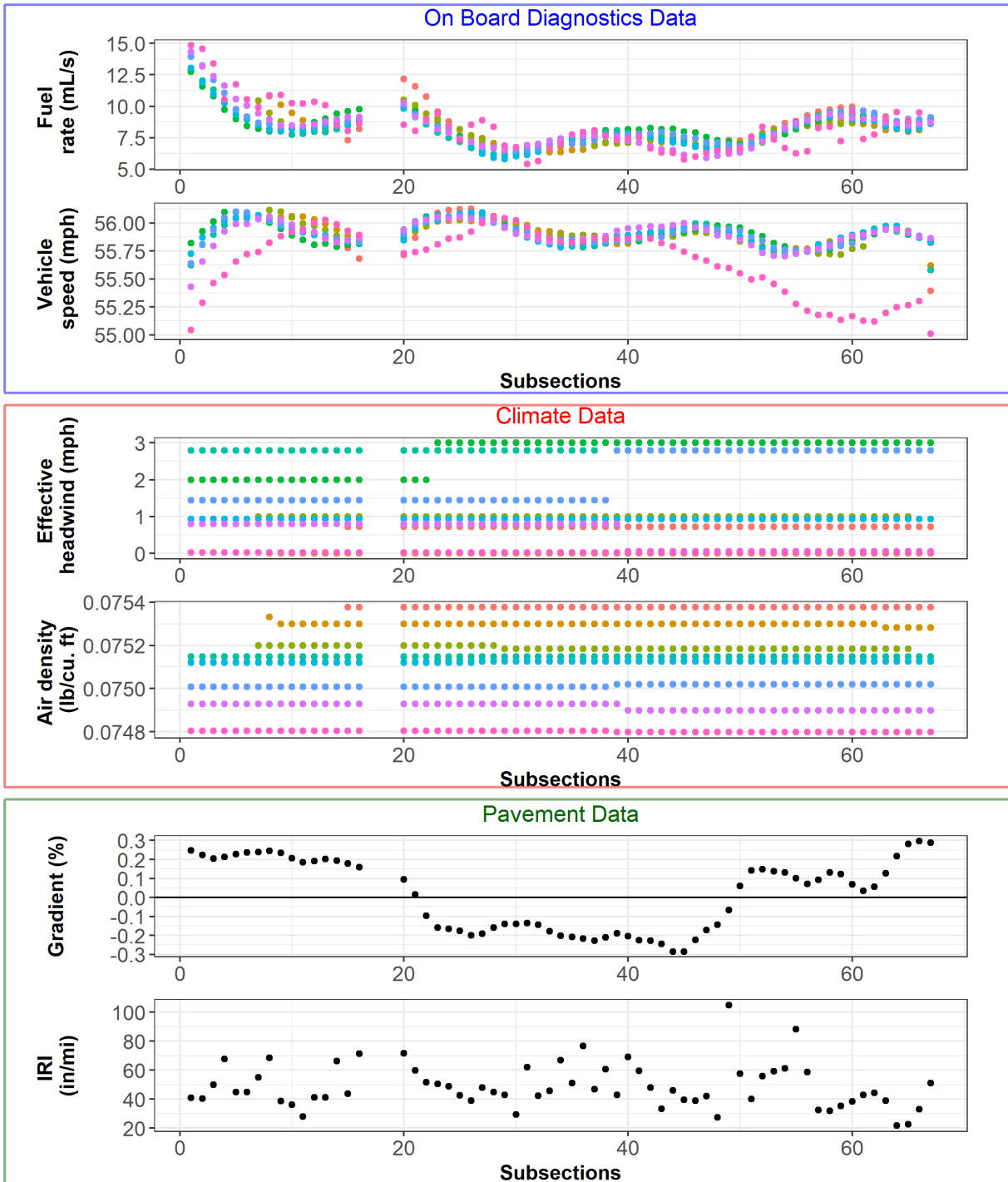
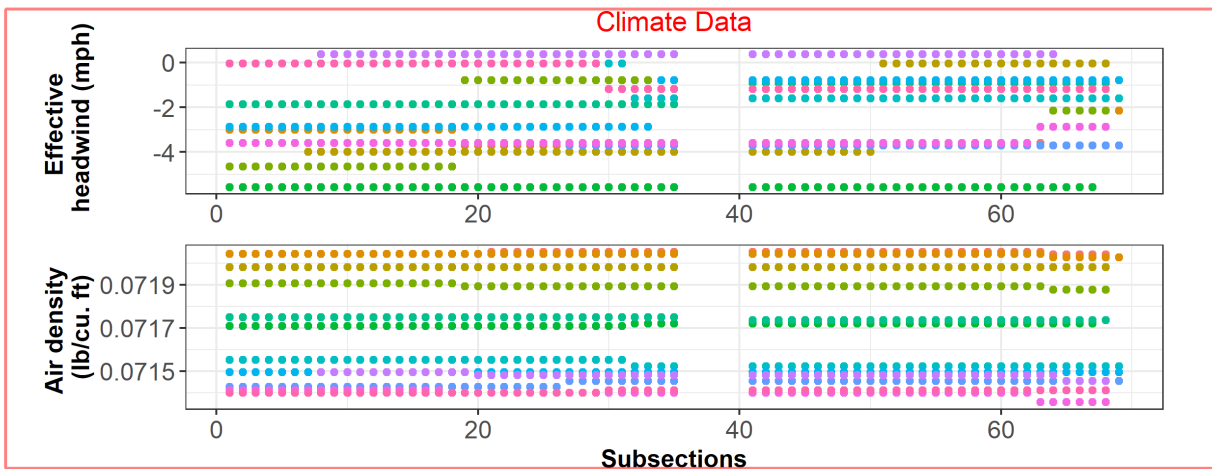
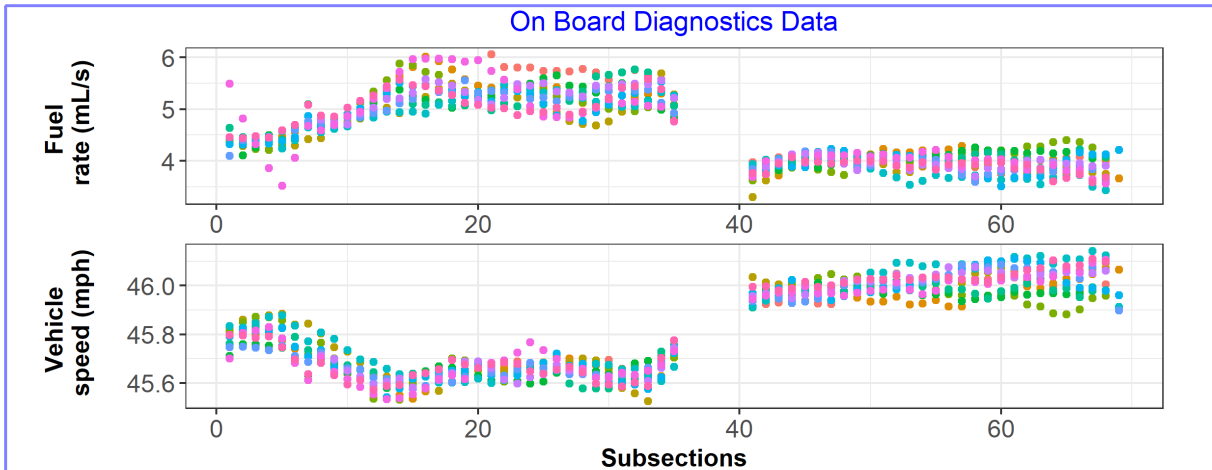


Figure P.285: HHDT data on Section PH01.

PH02-YOL113S-JPC HHDT summer_day 45 mph



- Runs
- 1
 - 2
 - 3
 - 4
 - 5
 - 6
 - 7
 - 8
 - 9
 - 10
 - 11
 - 12

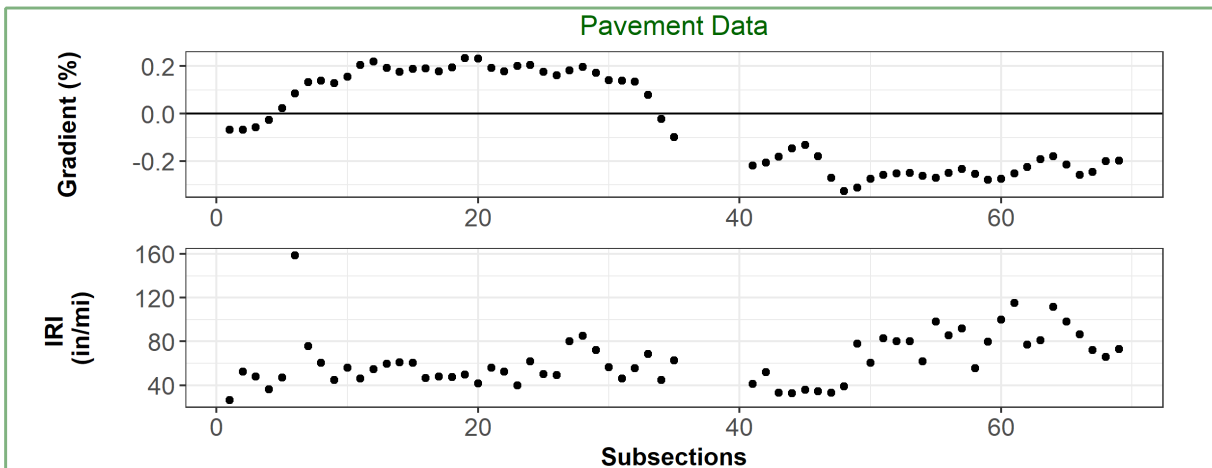


Figure P.286: HHDT data on Section PH02.

PH02-YOL113S-JPC HHDT summer_day 55 mph

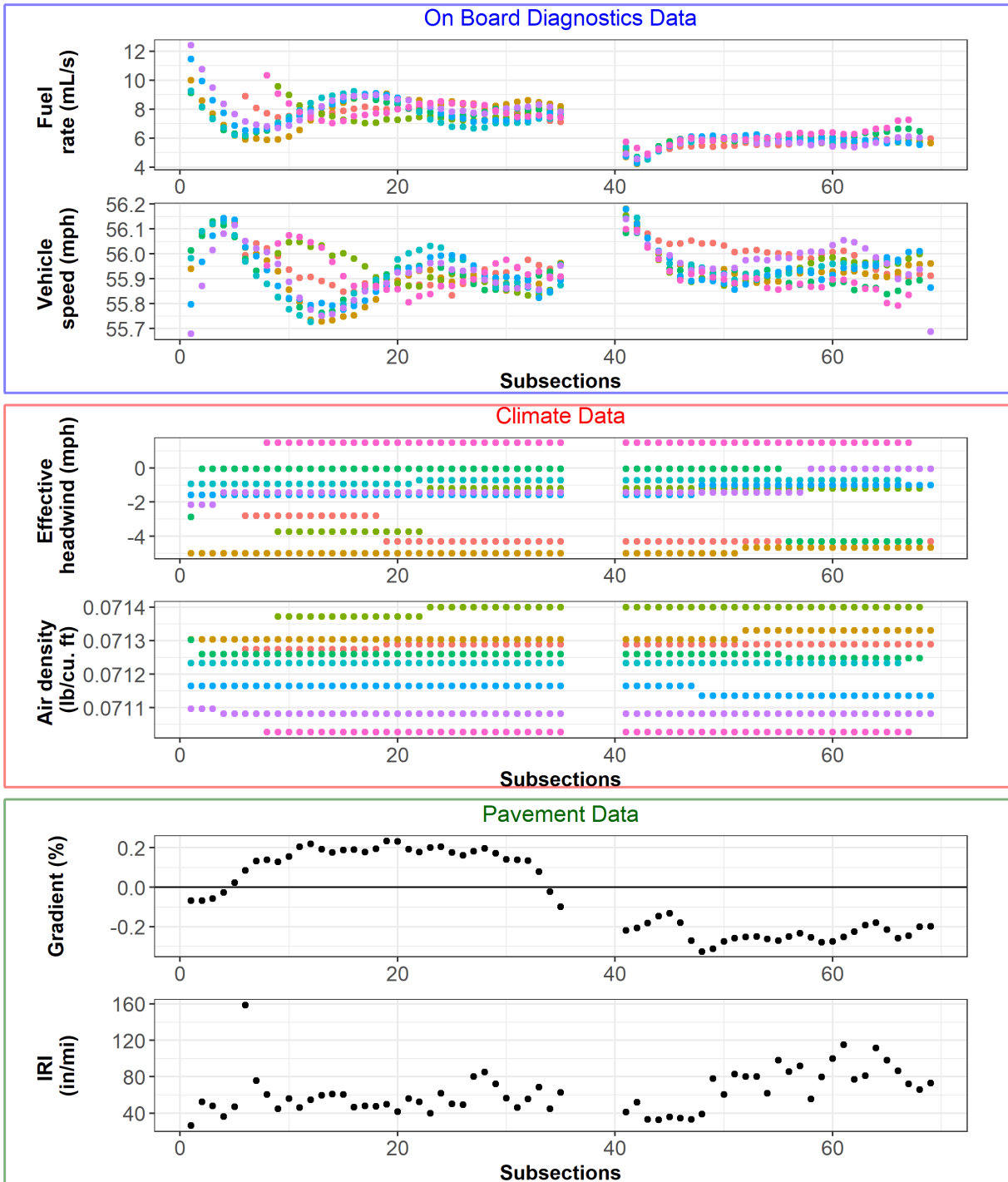


Figure P.287: HHDT data on Section PH02.

PH02-YOL113S-JPC HHDt summer_night 45 mph

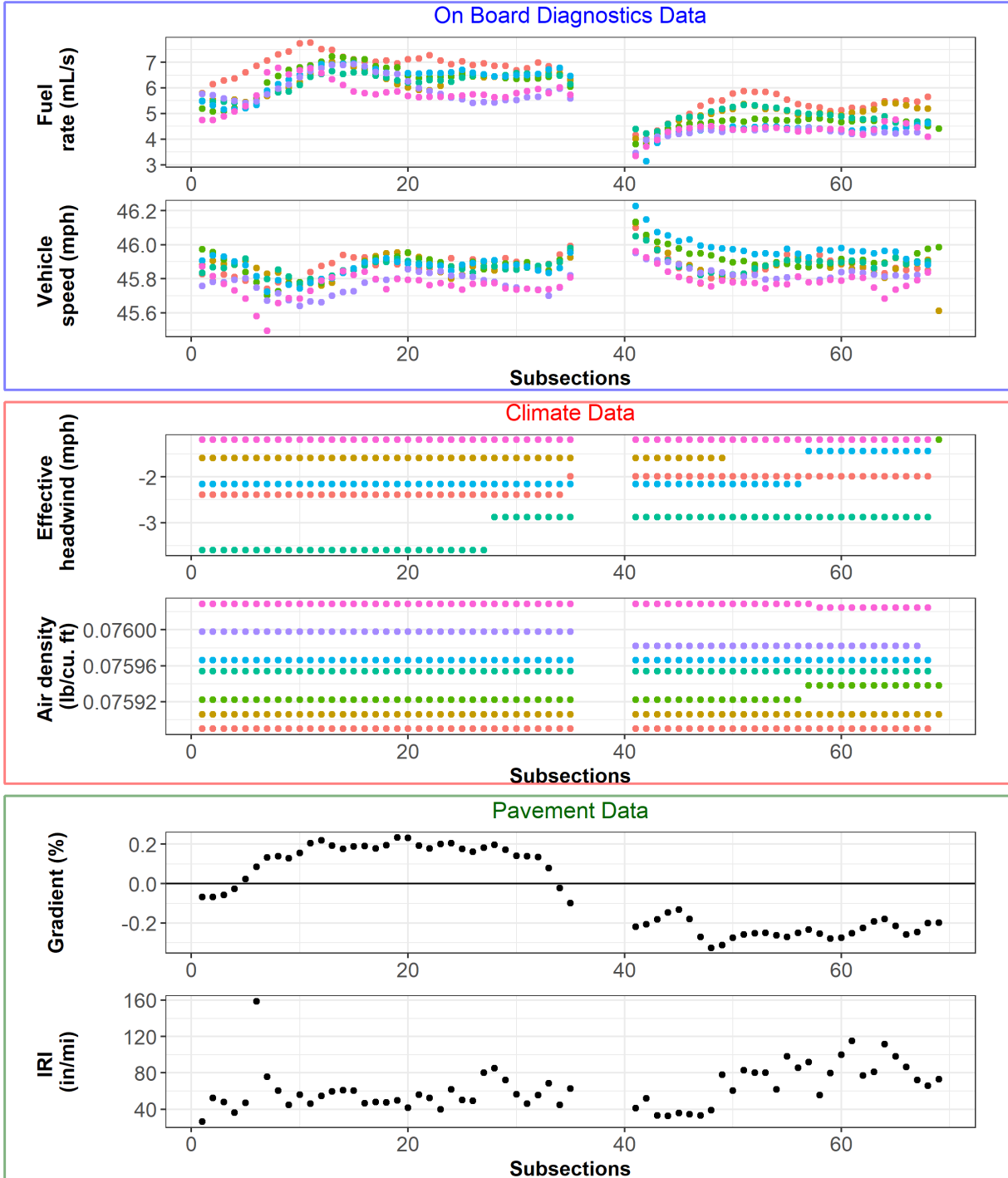


Figure P.288: HHDt data on Section PH02.

PH02-YOL113S-JPC HHDT summer_night 55 mph

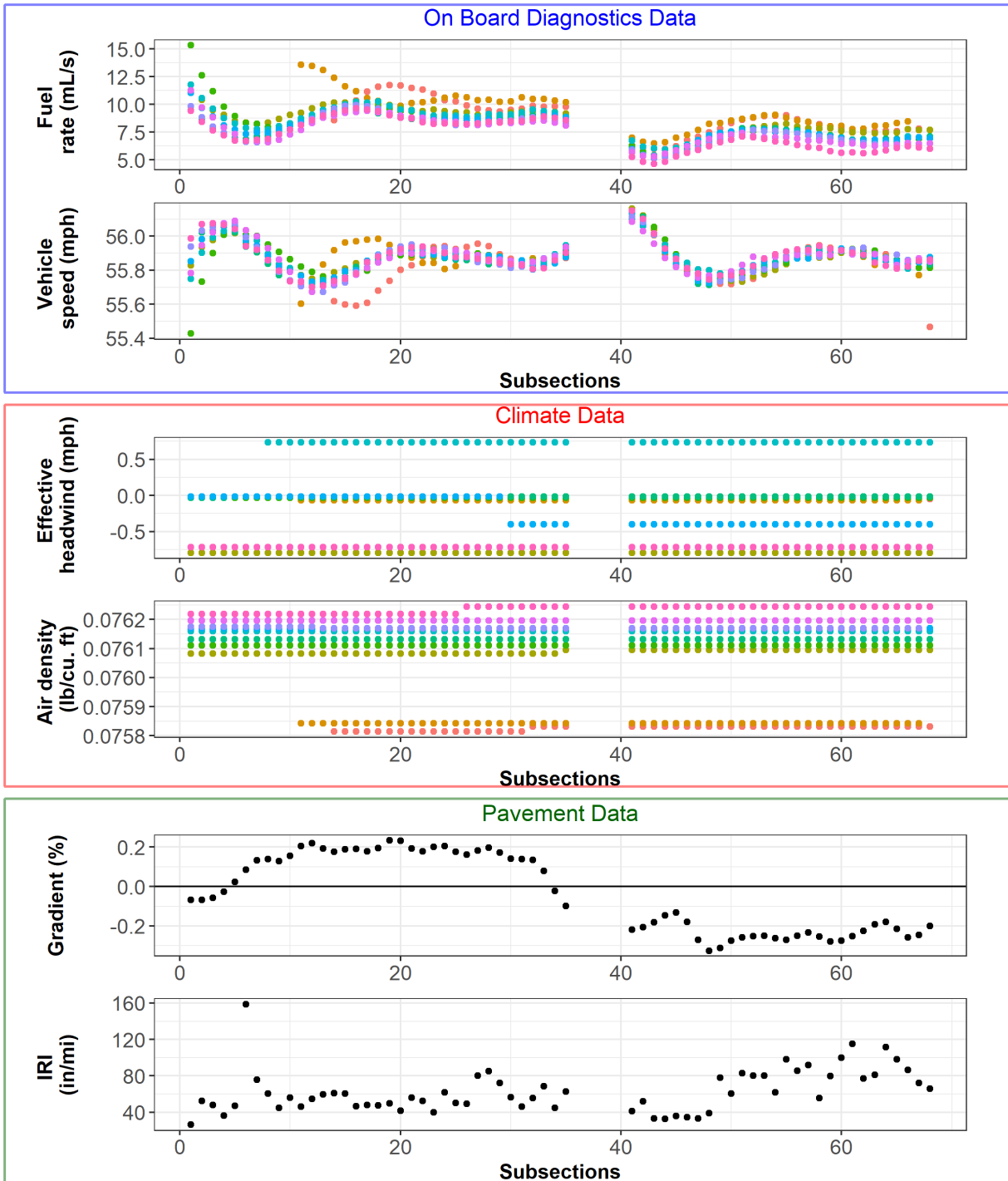


Figure P.289: HHDT data on Section PH02.

PH02-YOL113S-JPC HHDT winter_day 45 mph

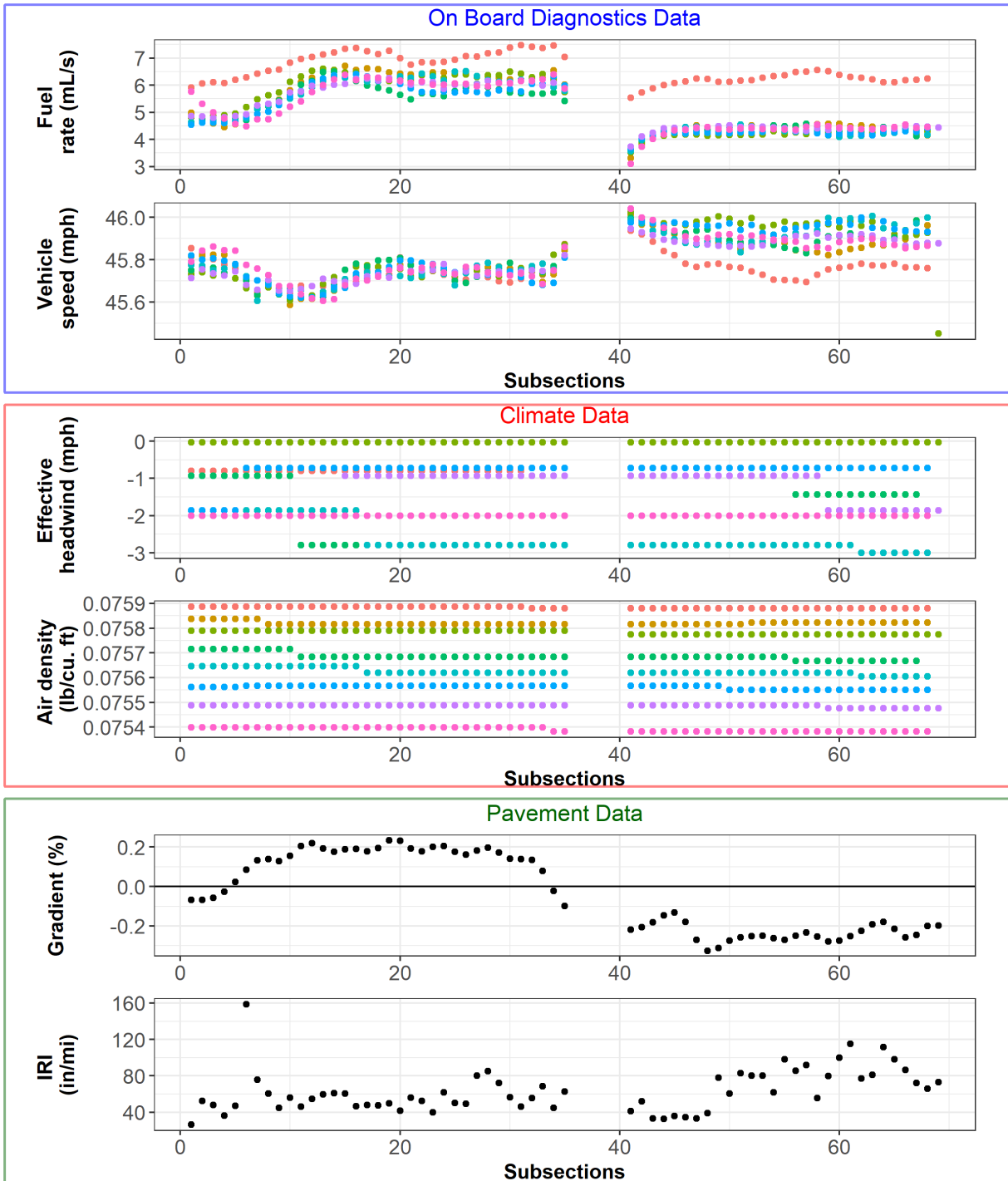


Figure P.290: HHDT data on Section PH02.

PH02-YOL113S-JPC HHDT winter_day 55 mph

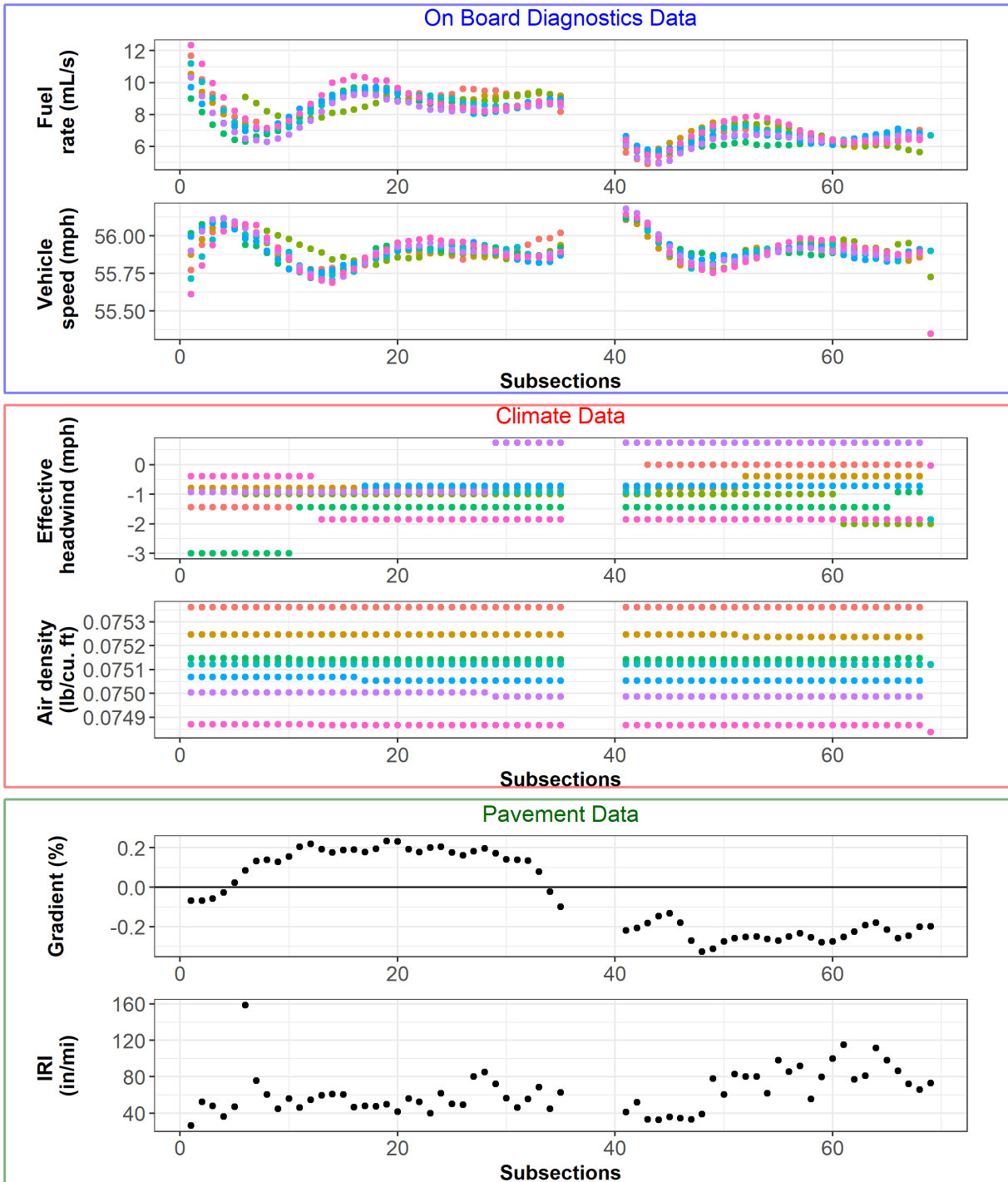


Figure P.291: HHDT data on Section PH02.

PH03-YOL505N-JPC HHDt summer_day 45 mph

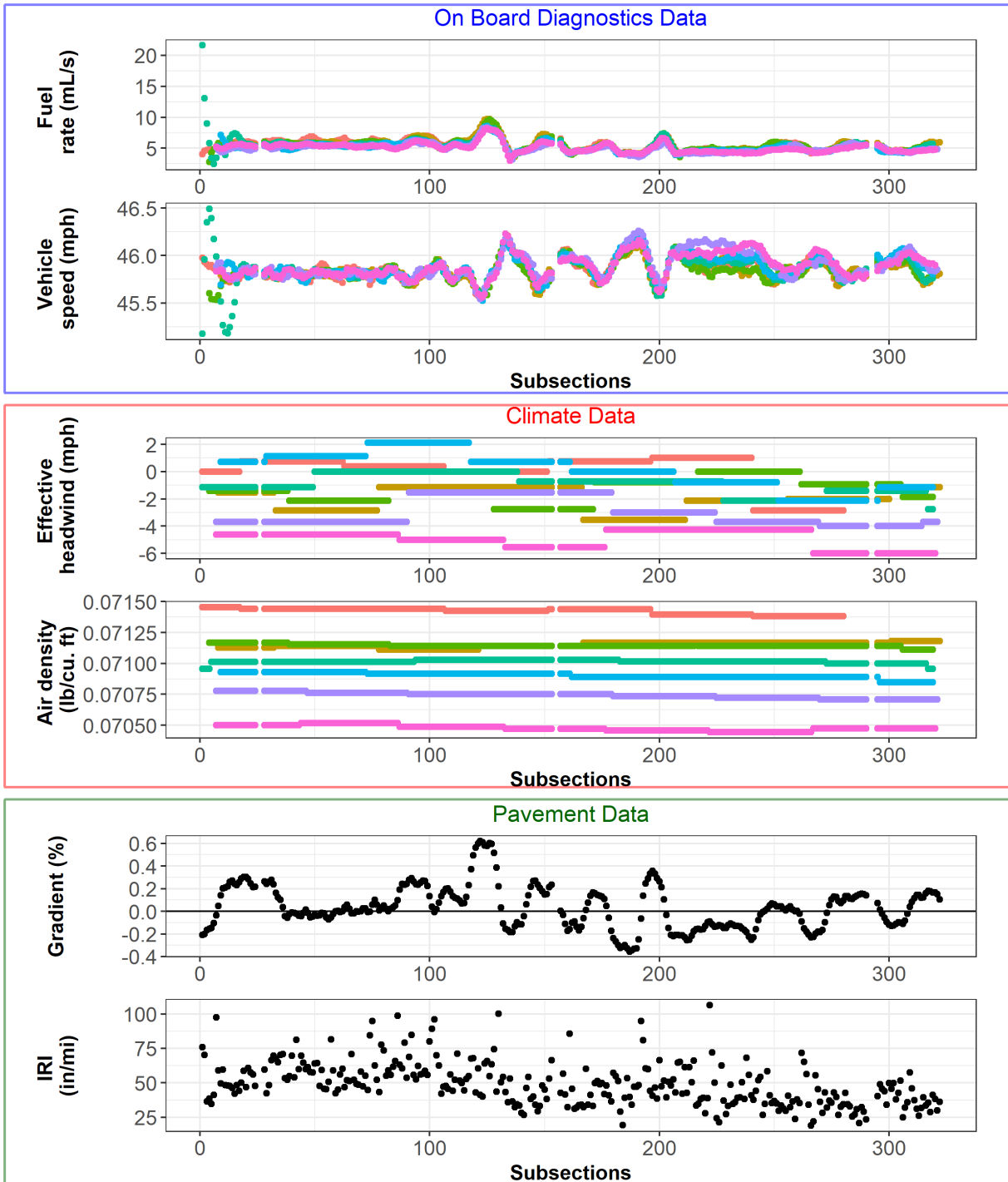


Figure P.292: HHDt data on Section PH03.

PH03-YOL505N-JPC HHDT summer_day 55 mph

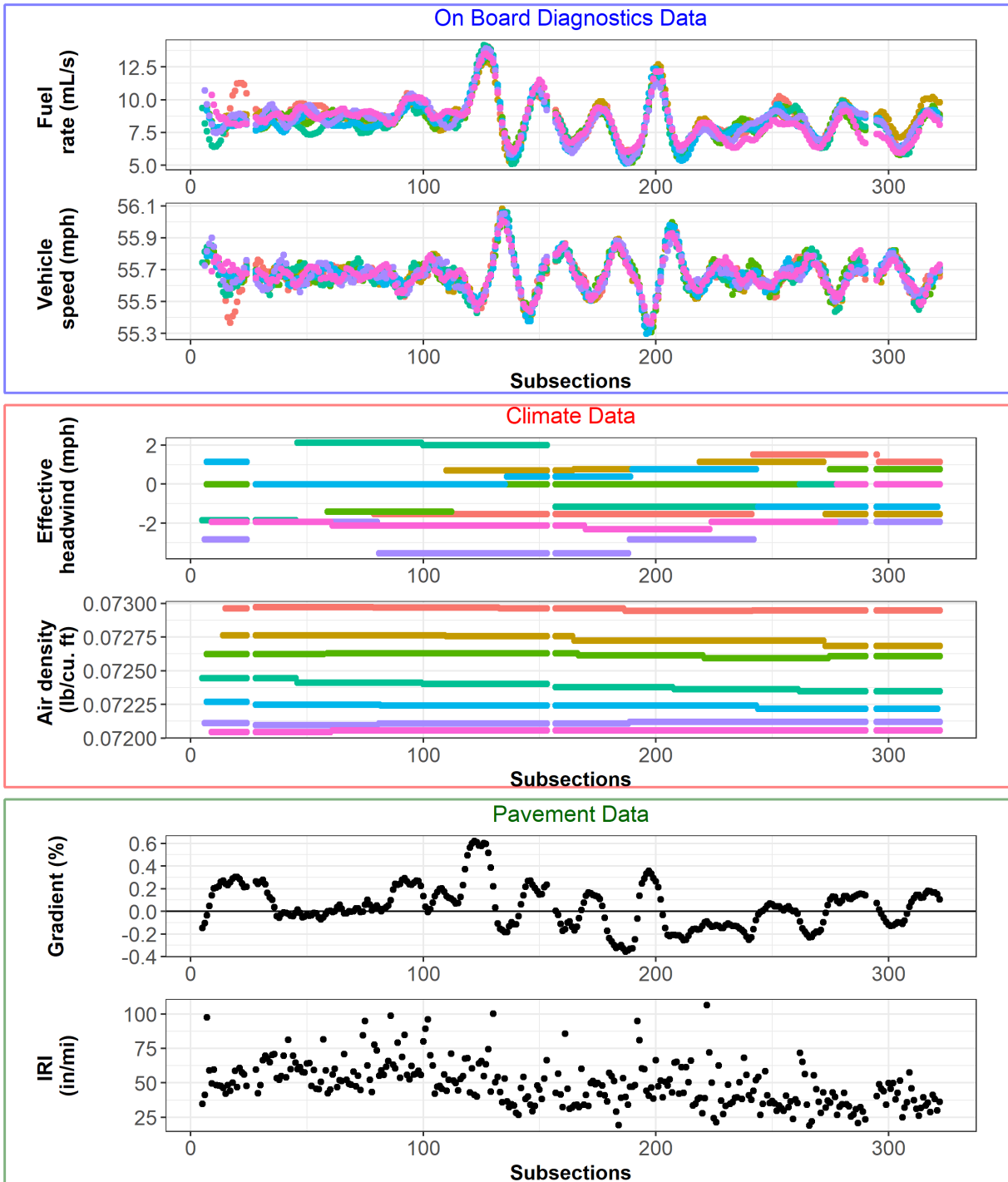


Figure P.293: HHDT data on Section PH03.

PH03-YOL505N-JPC HHDT summer_night 45 mph

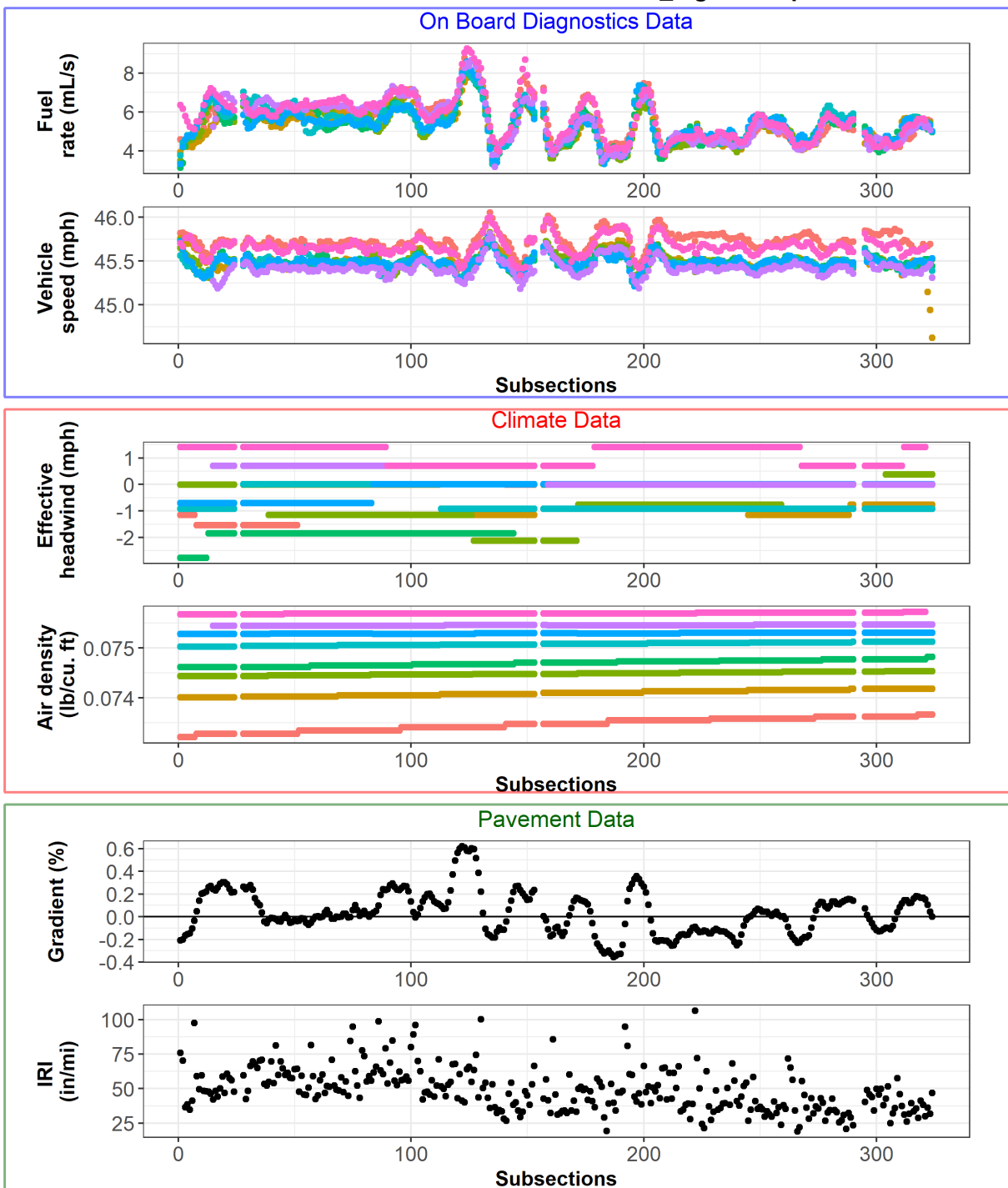


Figure P.294: HHDT data on Section PH03.

PH03-YOL505N-JPC HHDt summer_night 55 mph

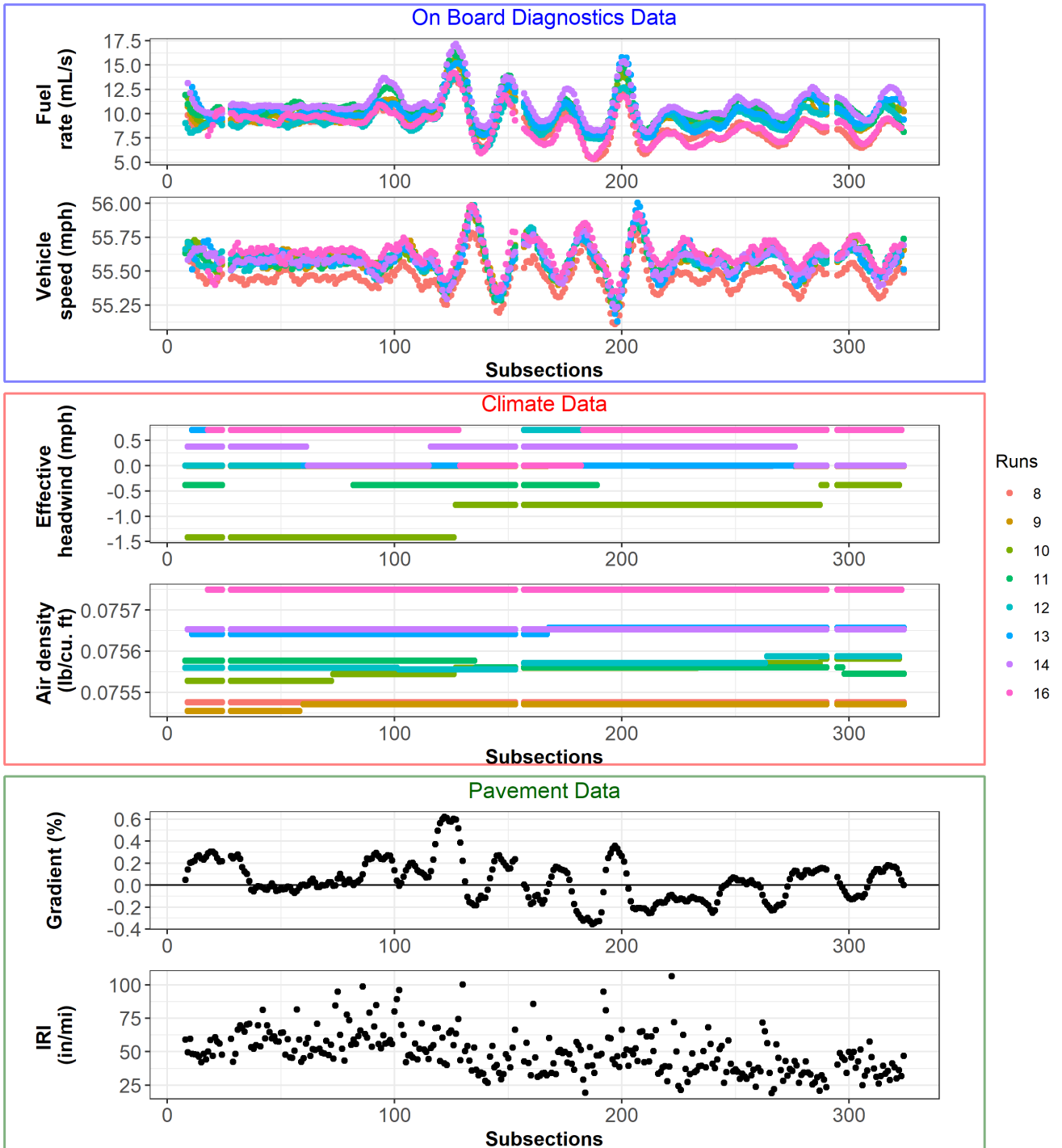


Figure P.295: HHDt data on Section PH03.

PH03-YOL505N-JPC HHDT winter_day 45 mph

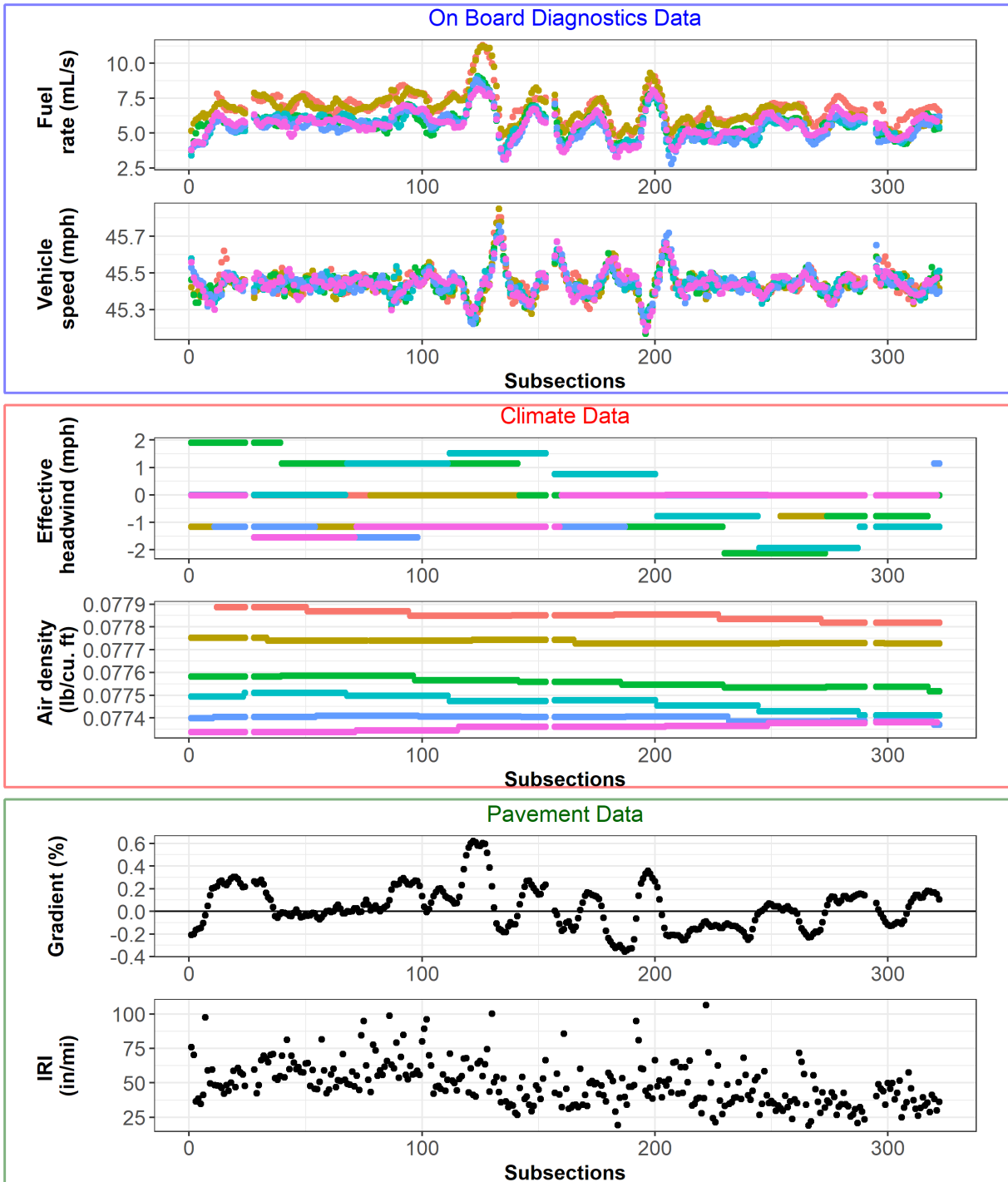


Figure P.296: HHDT data on Section PH03.

PH03-YOL505N-JPC HHDT winter_day 55 mph

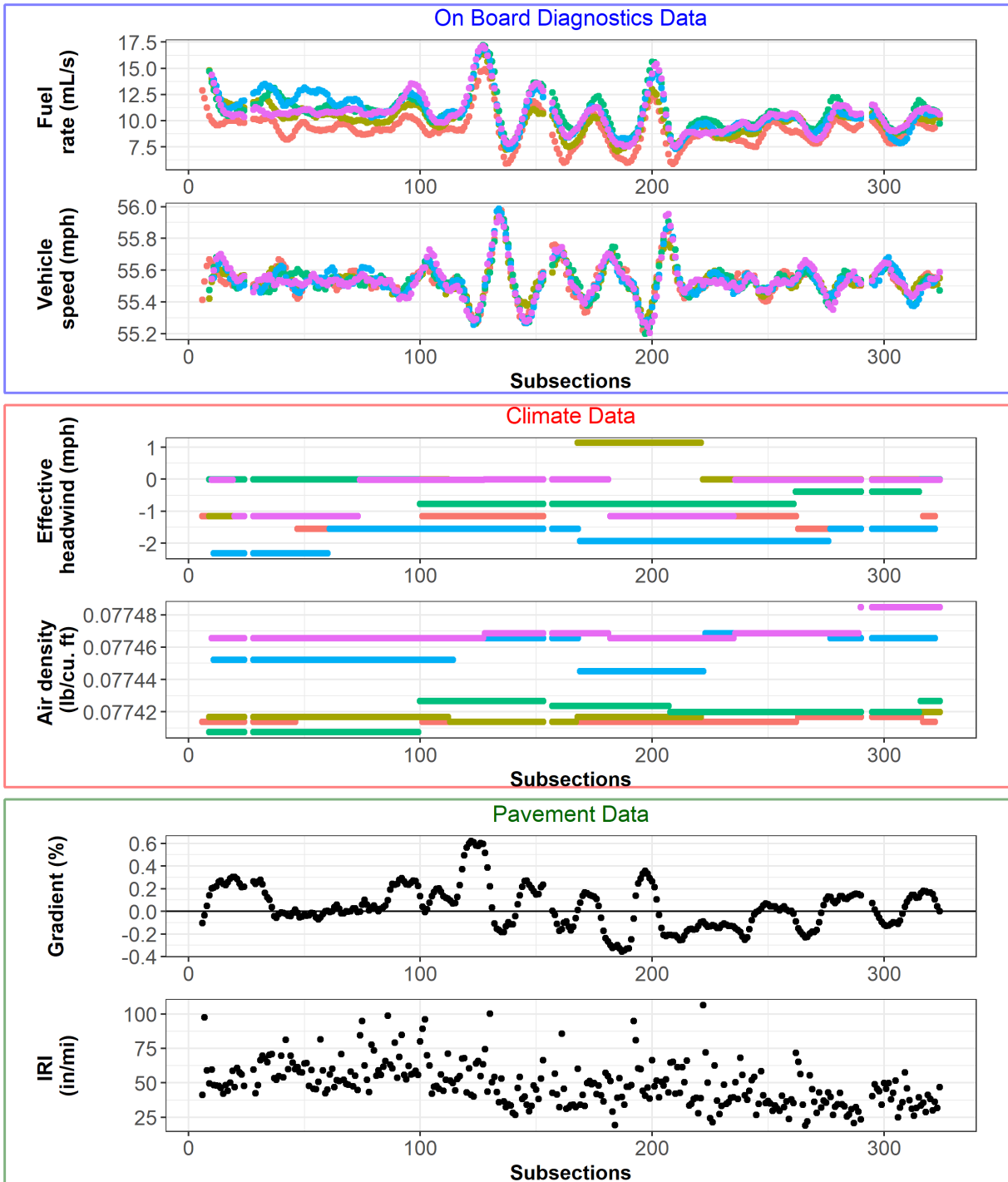


Figure P.297: HHDT data on Section PH03.

PH04-YOL505S-RHMA-G HHDT summer_day 45 mph

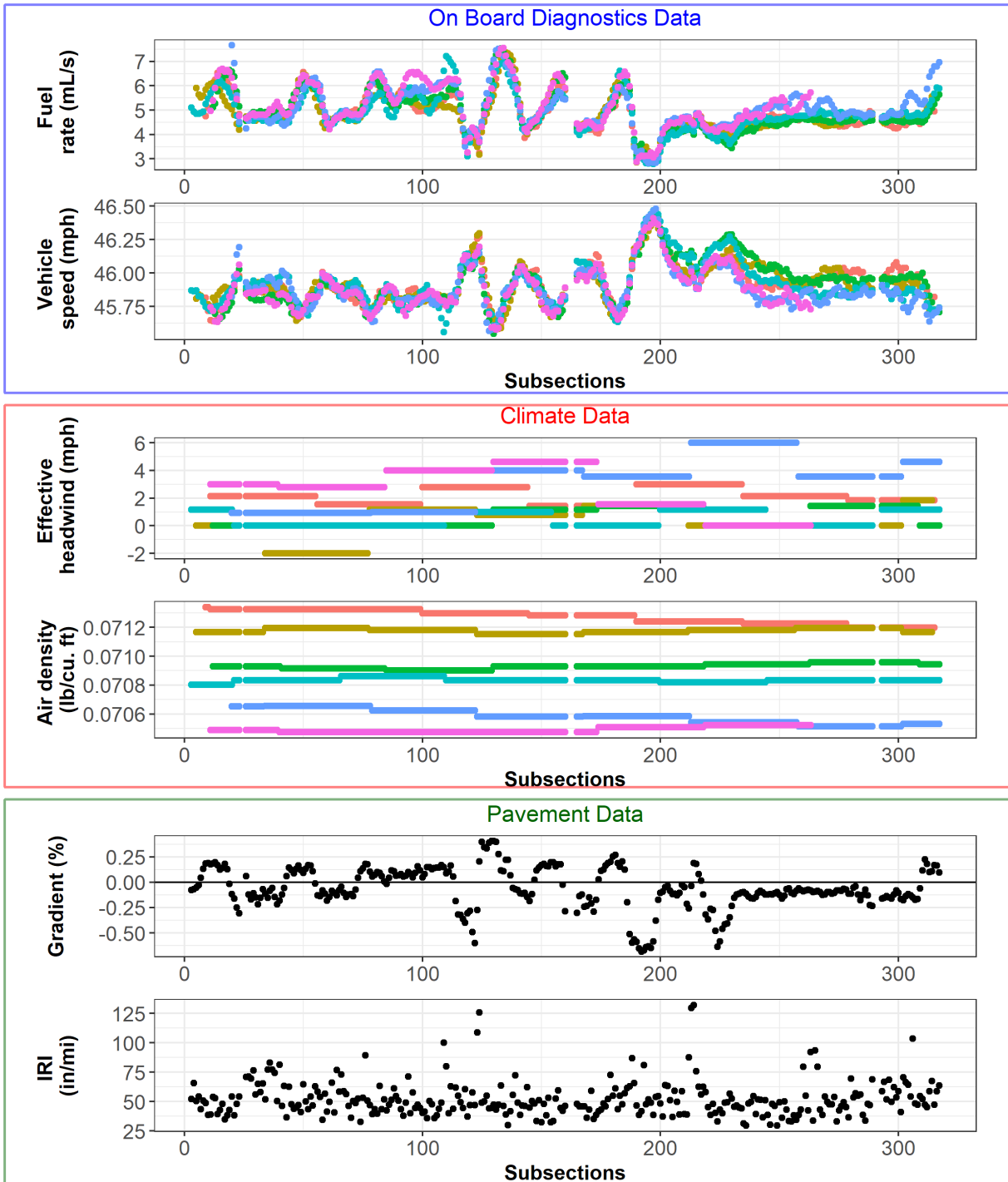


Figure P.298: HHDT data on Section PH04.

PH04-YOL505S-RHMA-G HHDt summer_day 55 mph

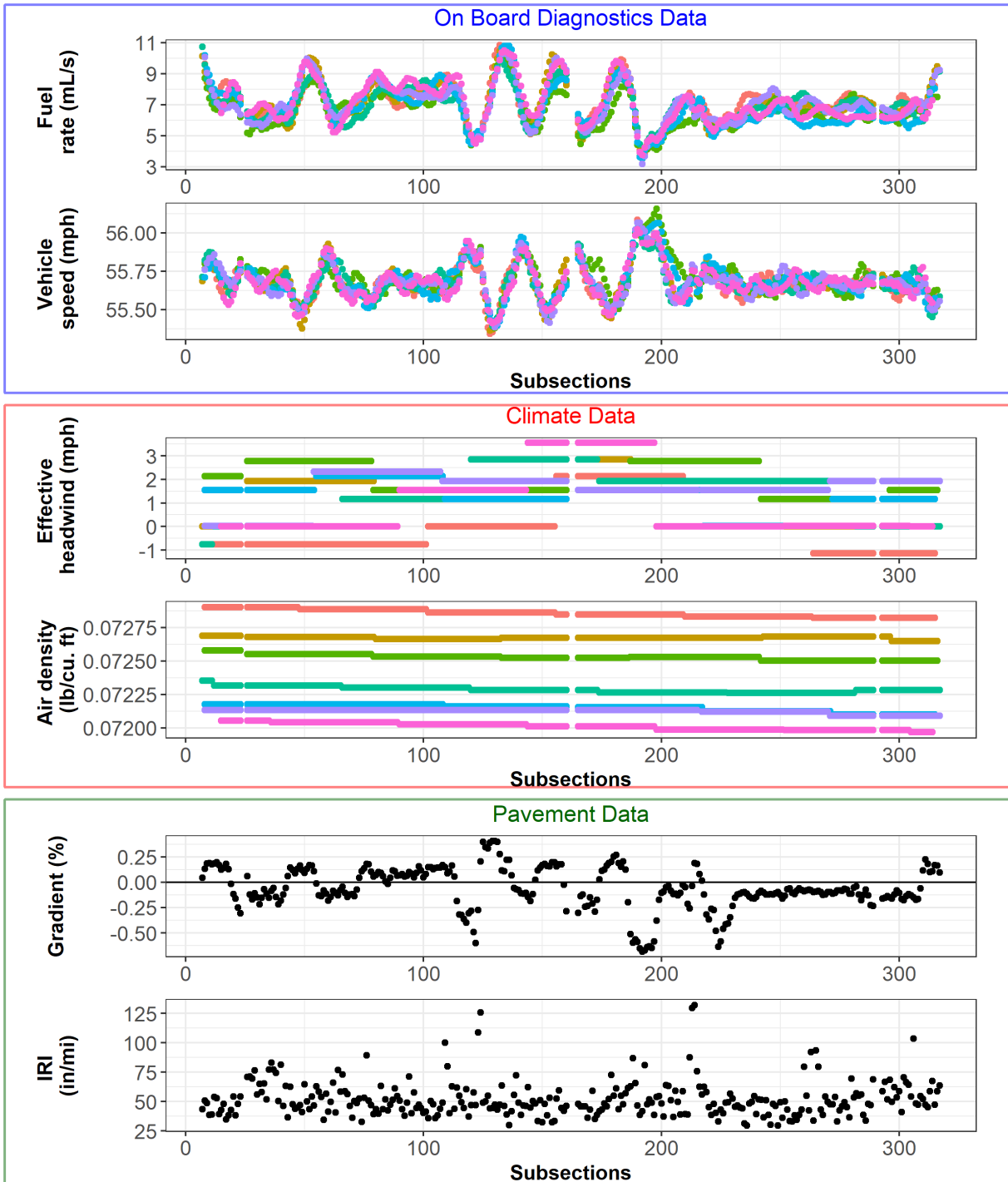


Figure P.299: HHDt data on Section PH04.

PH04-YOL505S-RHMA-G HHDt summer_night 45 mph

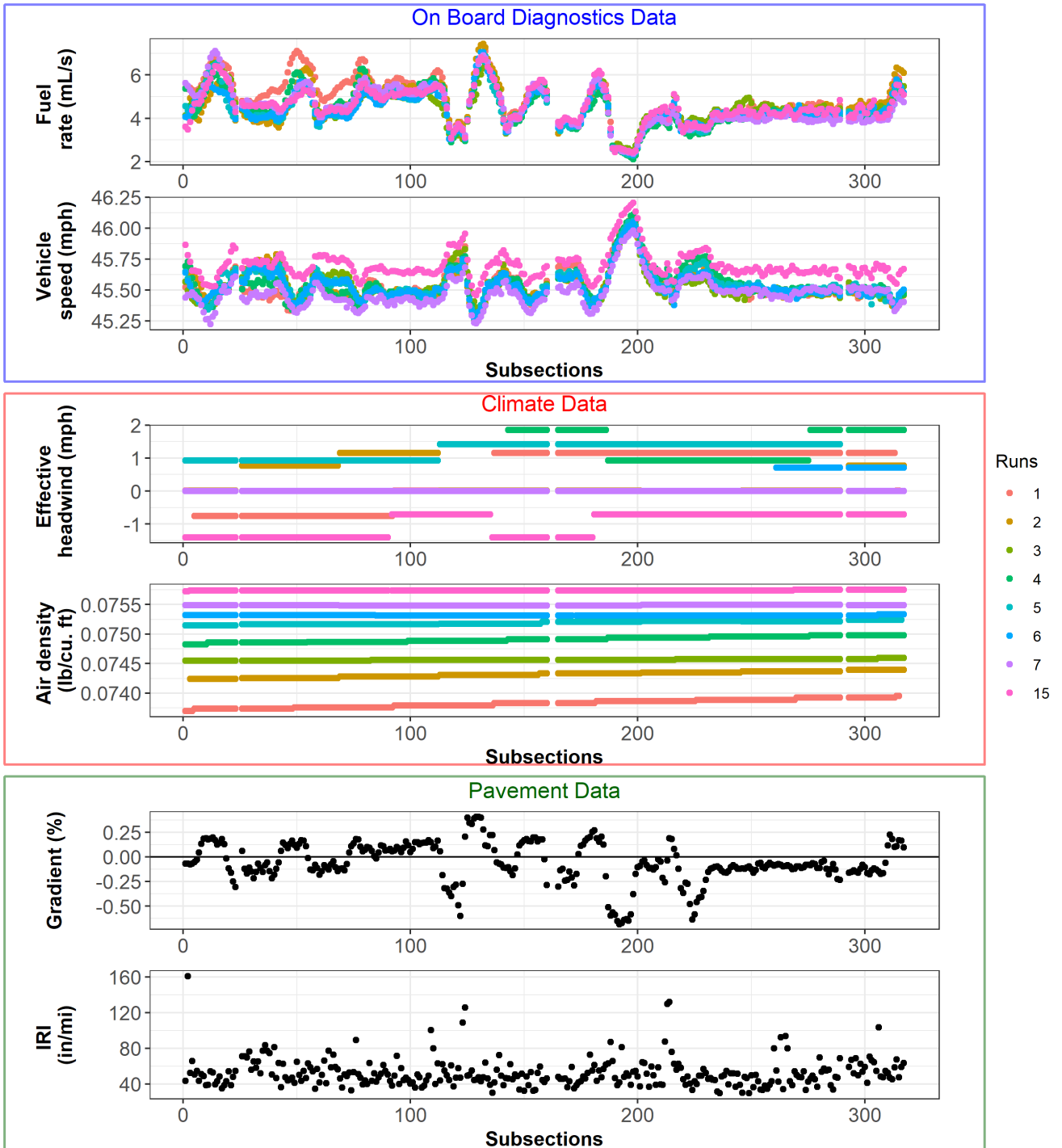


Figure P.300: HHDt data on Section PH04.

PH04-YOL505S-RHMA-G HHDt summer_night 55 mph

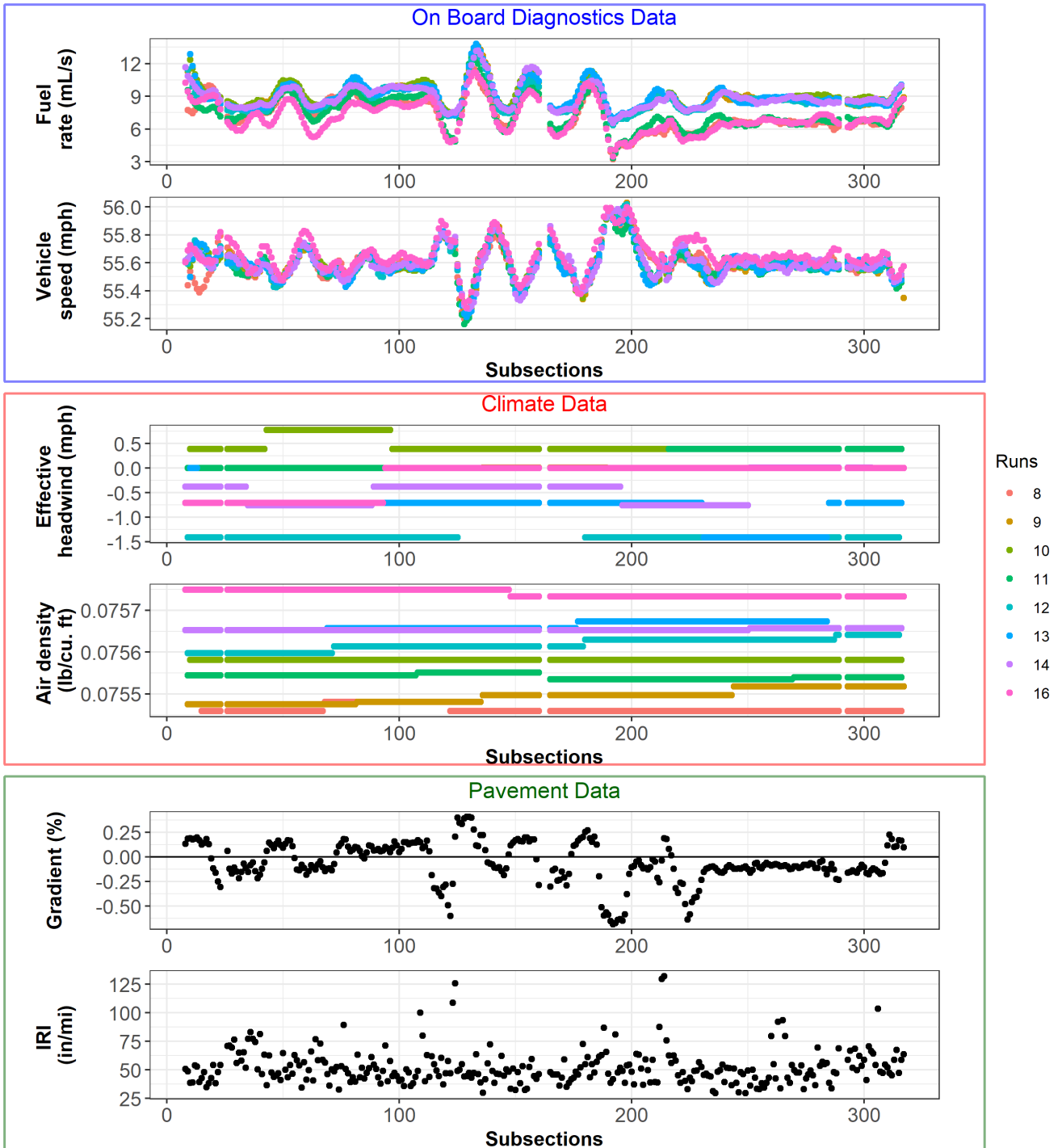


Figure P.301: HHDt data on Section PH04.

PH04-YOL505S-RHMA-G HHDT winter_day 45 mph

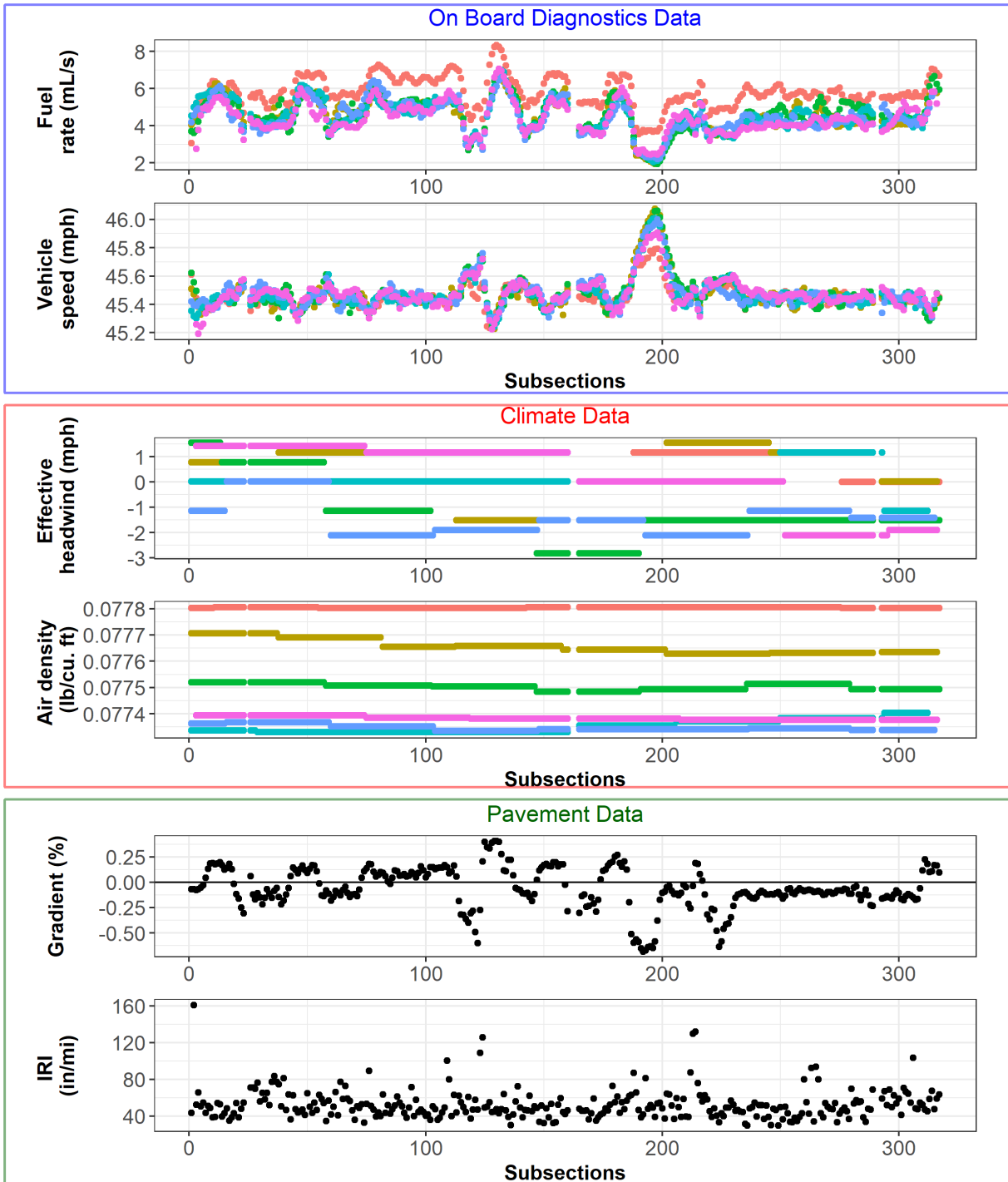


Figure P.302: HHDT data on Section PH04.

PH04-YOL505S-RHMA-G HHDt winter_day 55 mph

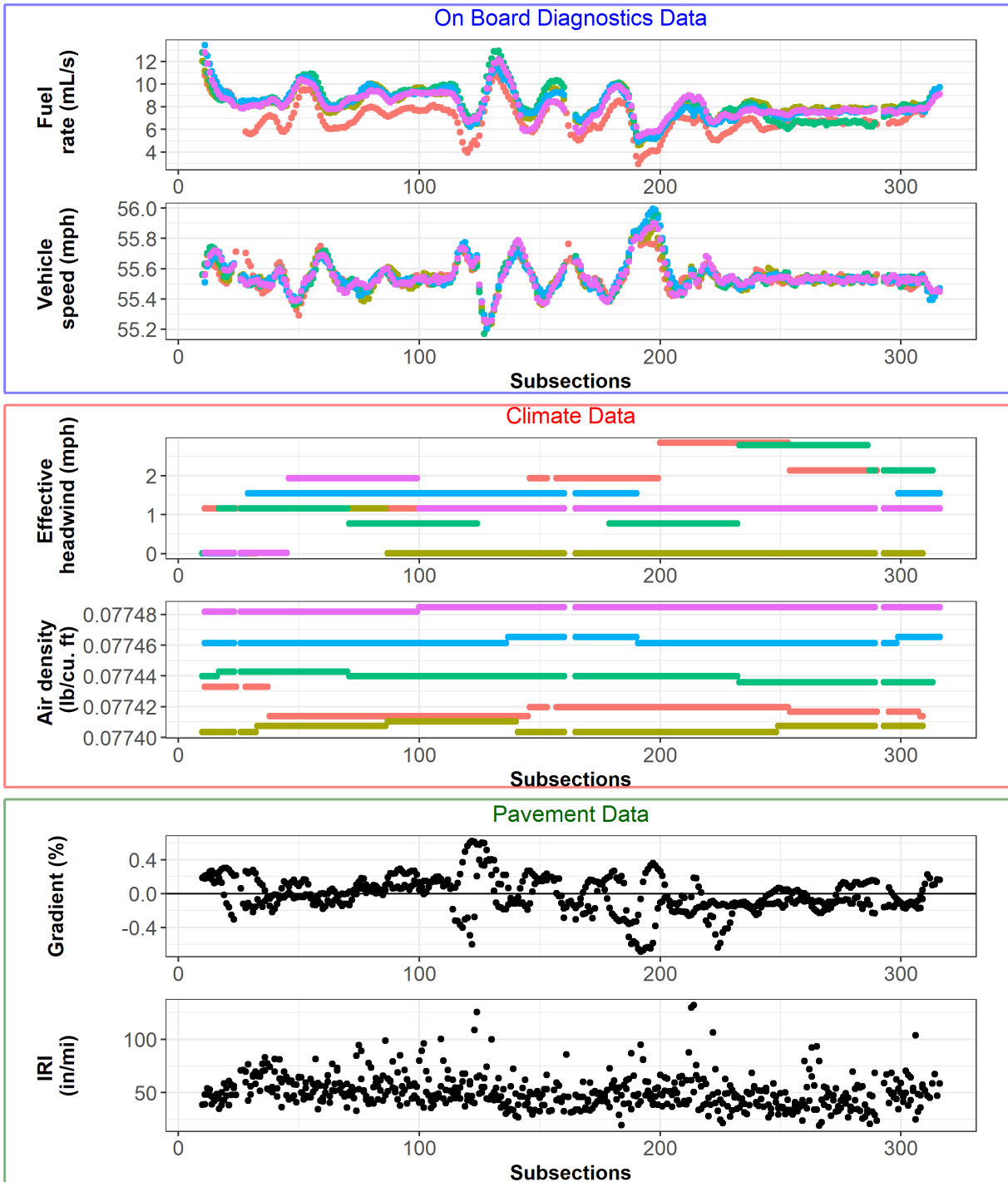


Figure P.303: HHDt data on Section PH04.

PH07-YOL-CR98N-HMA HHDt summer_day 35 mph

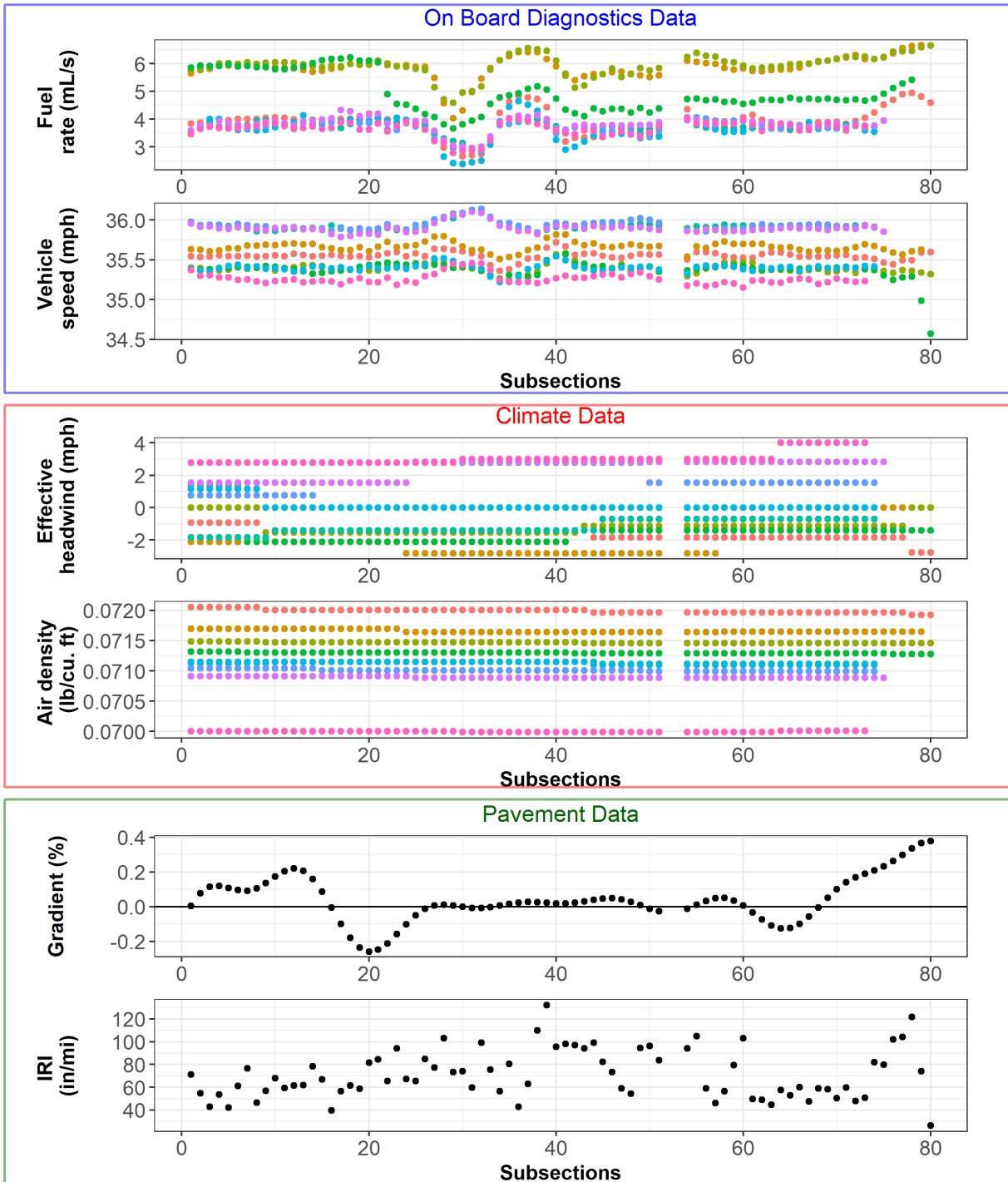


Figure P.304: HHDt data on Section PH07.

PH07-YOL-CR98N-HMA HHDT summer_day 45 mph

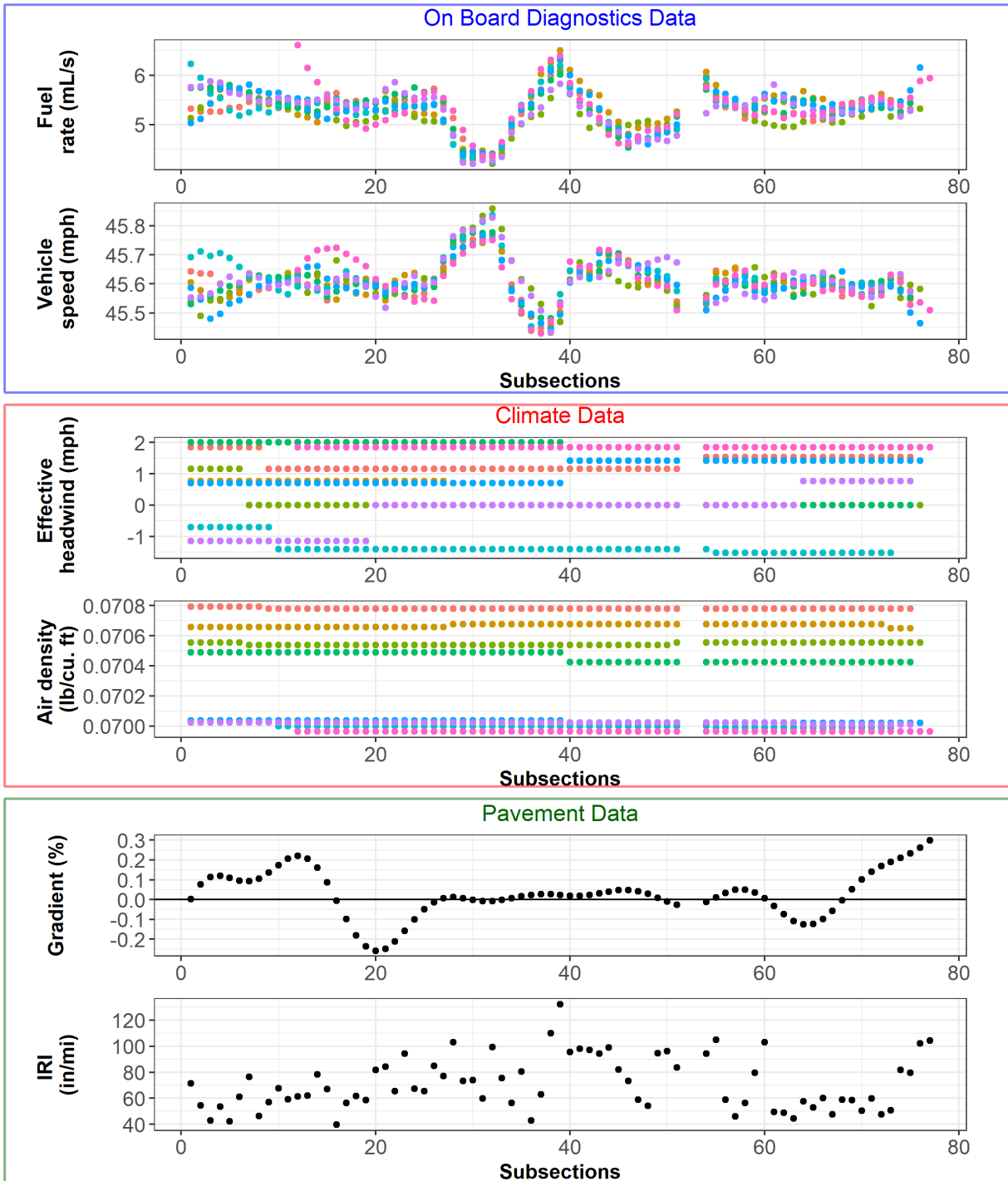


Figure P.305: HHDT data on Section PH07.

PH07-YOL-CR98N-HMA HHDT summer_night 35 mph

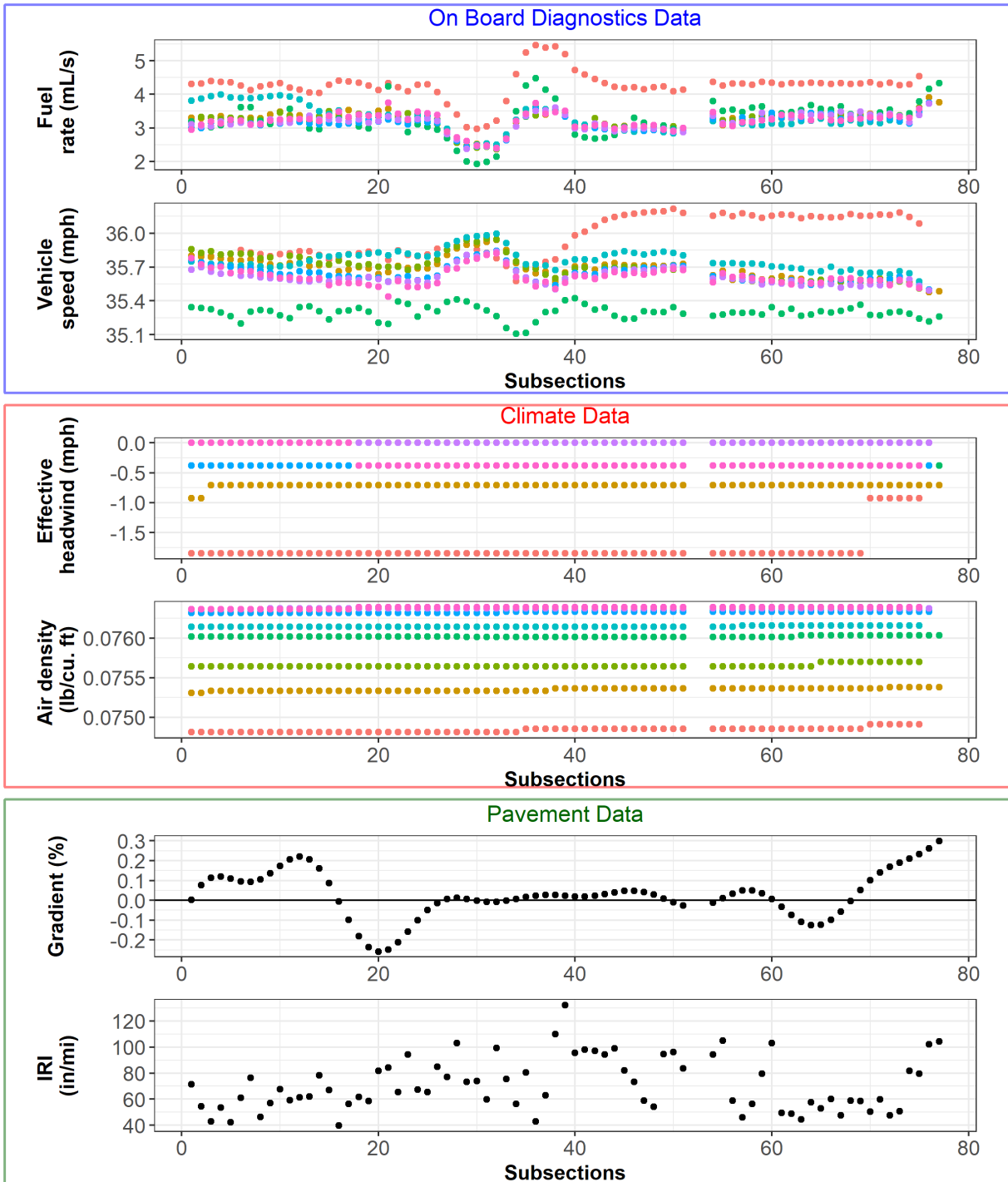


Figure P.306: HHDT data on Section PH07.

PH07-YOL-CR98N-HMA HHDT summer_night 45 mph

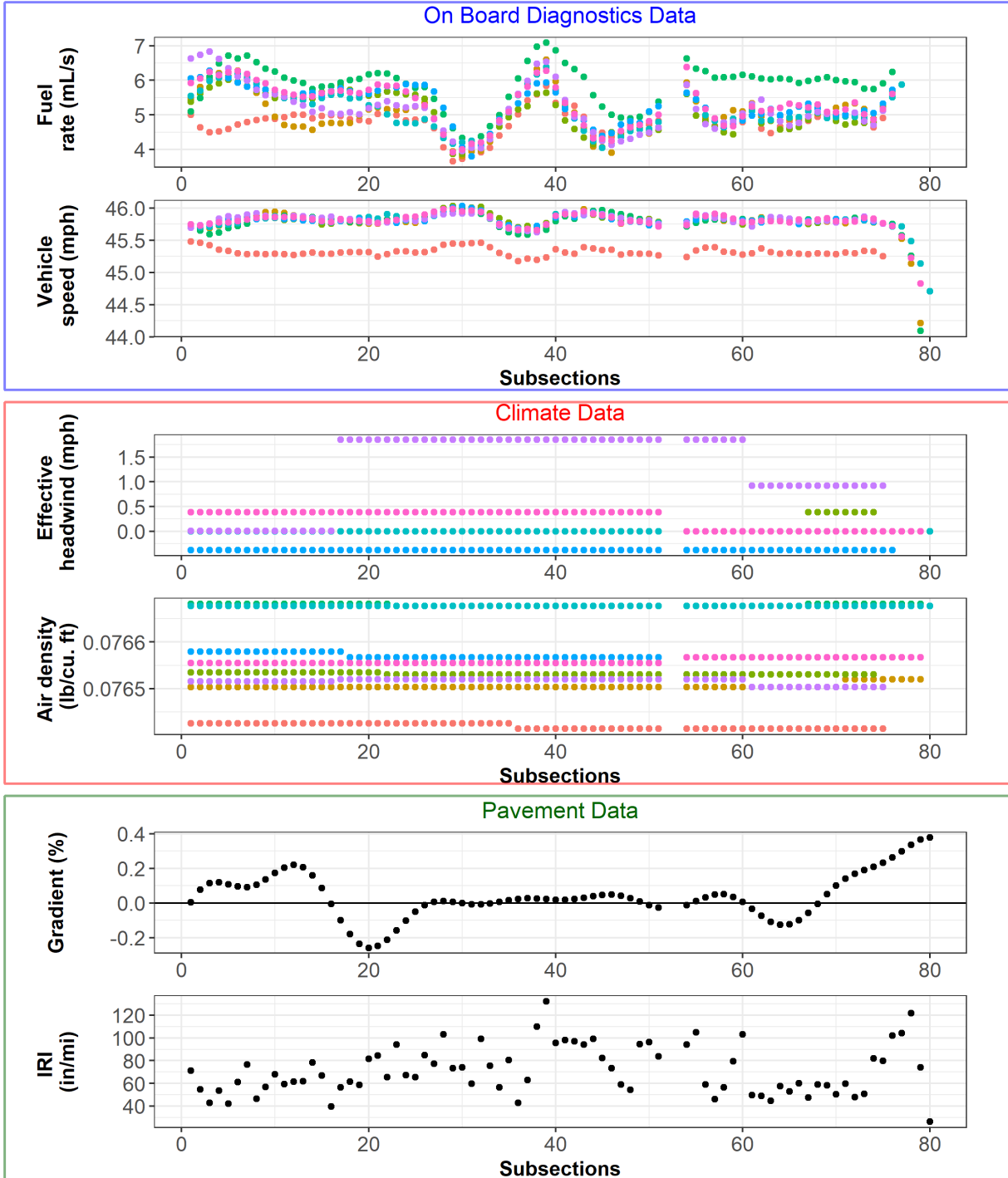


Figure P.307: HHDT data on Section PH07.

PH07-YOL-CR98N-HMA HHDT winter_day 35 mph

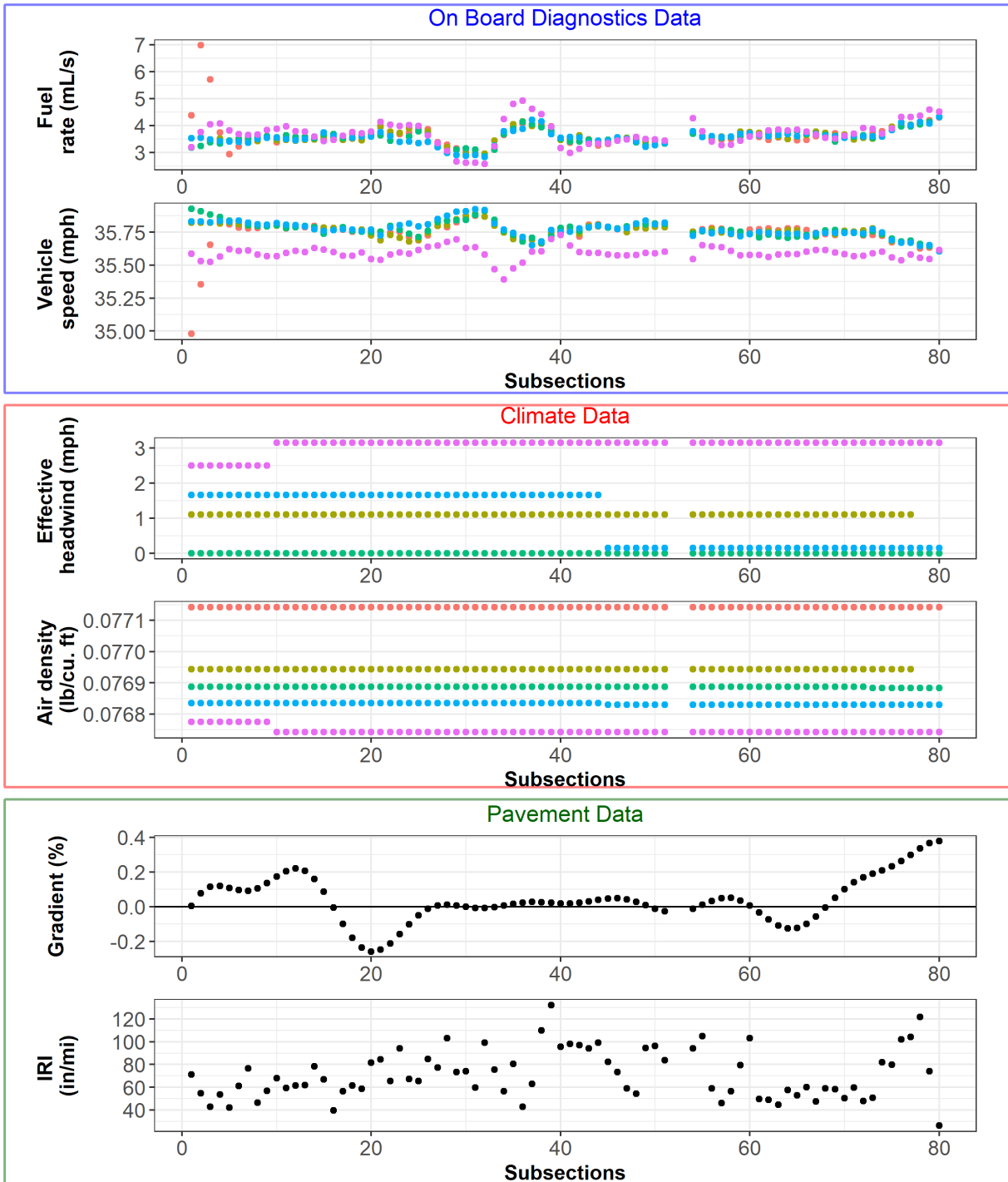


Figure P.308: HHDT data on Section PH07.

PH07-YOL-CR98N-HMA HHDT winter_day 45 mph

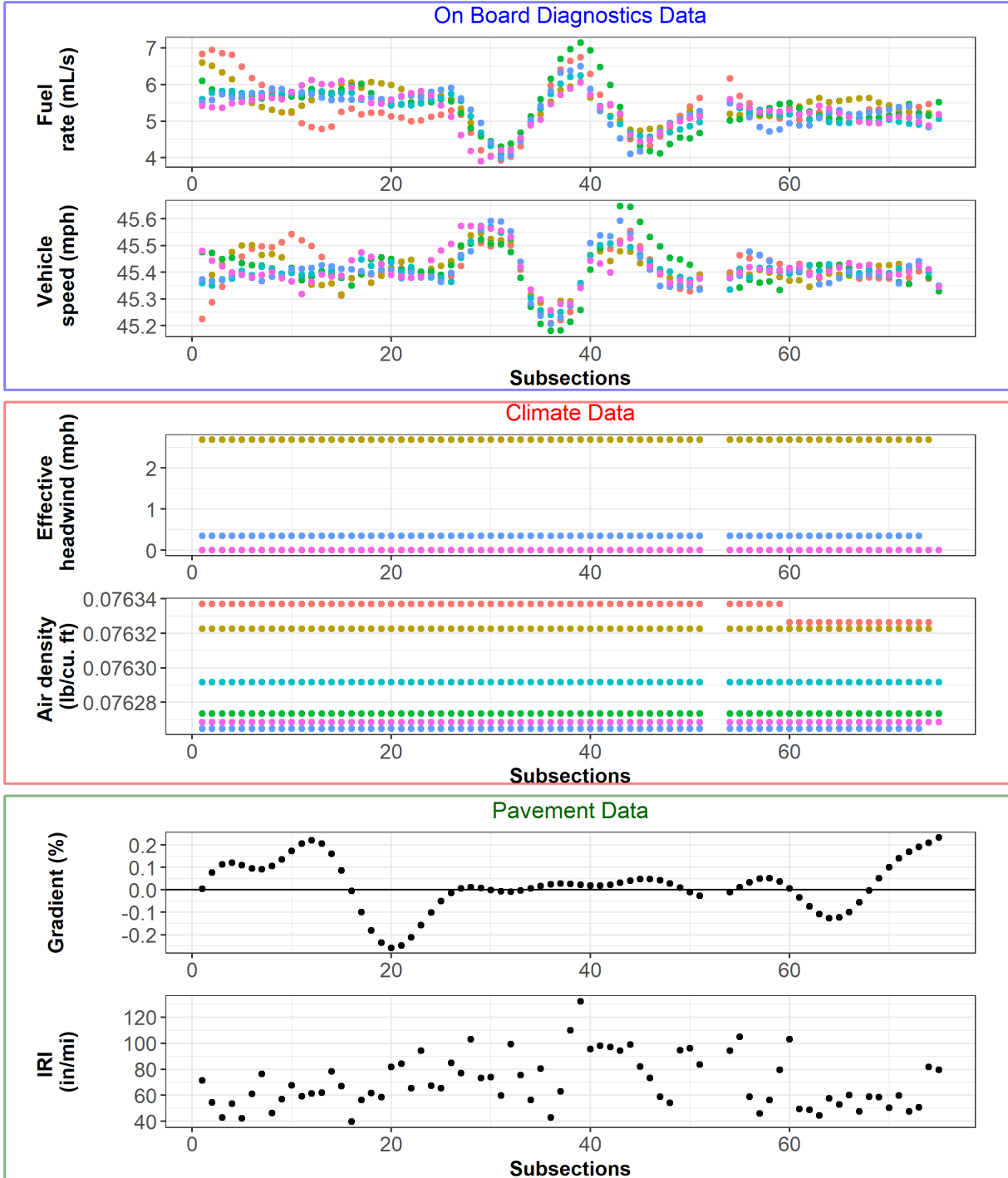


Figure P.309: HHDT data on Section PH07.

PH08-YOL-CR29E-HMA HHDT summer_day 35 mph

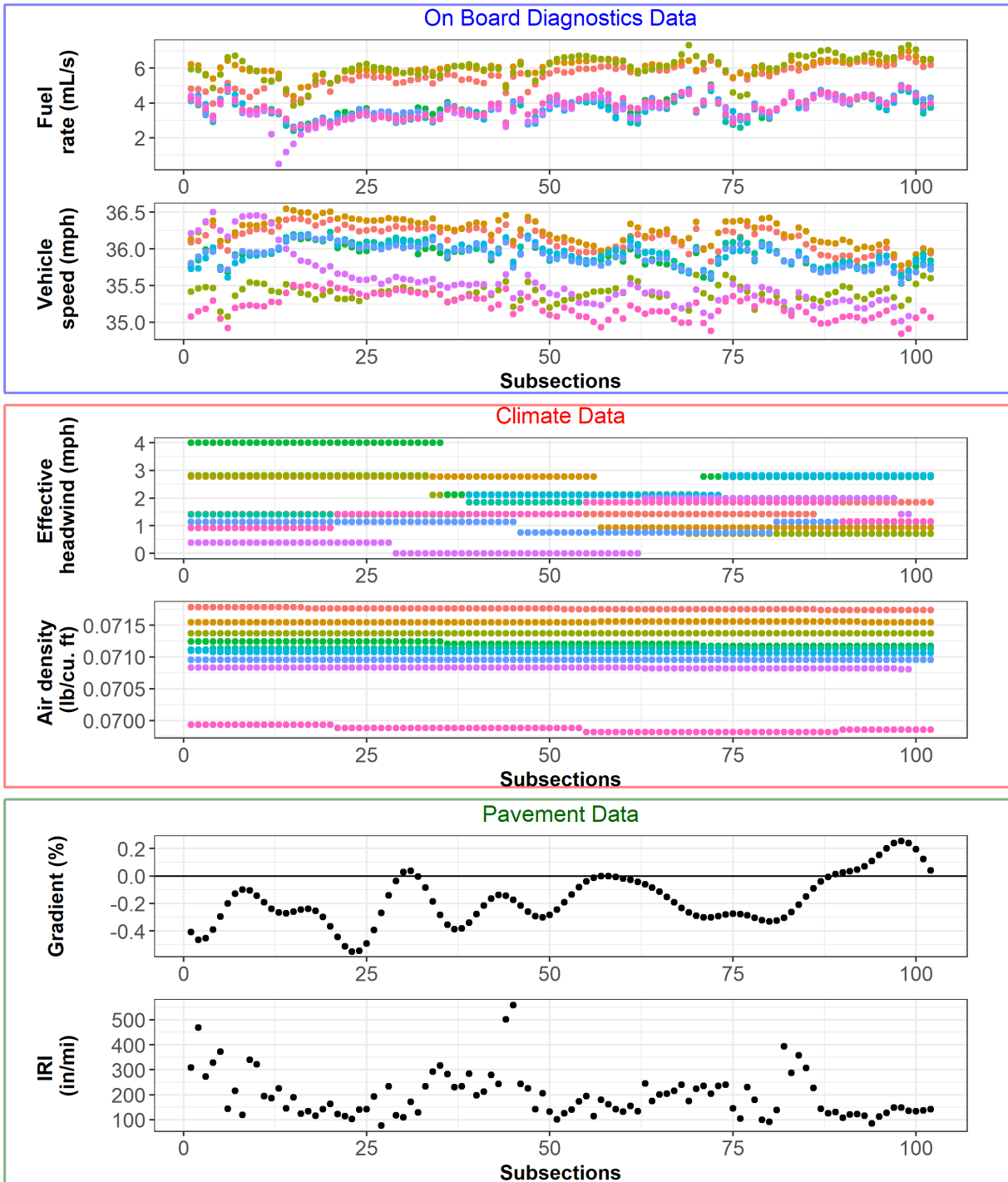


Figure P.310: HHDT data on Section PH08.

PH08-YOL-CR29E-HMA HHDT summer_day 45 mph

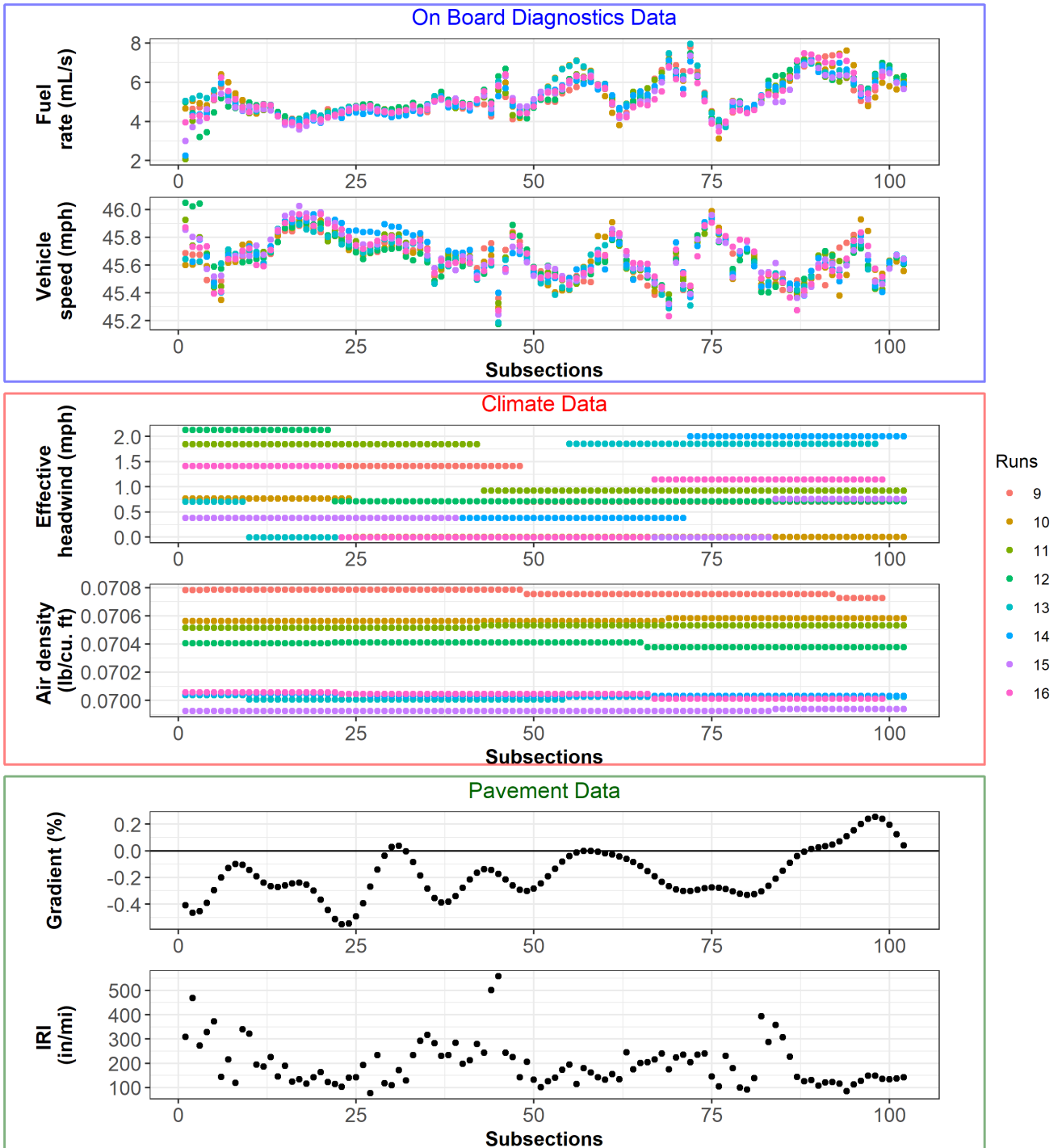


Figure P.311: HHDT data on Section PH08.

PH08-YOL-CR29E-HMA HHDT summer_night 35 mph

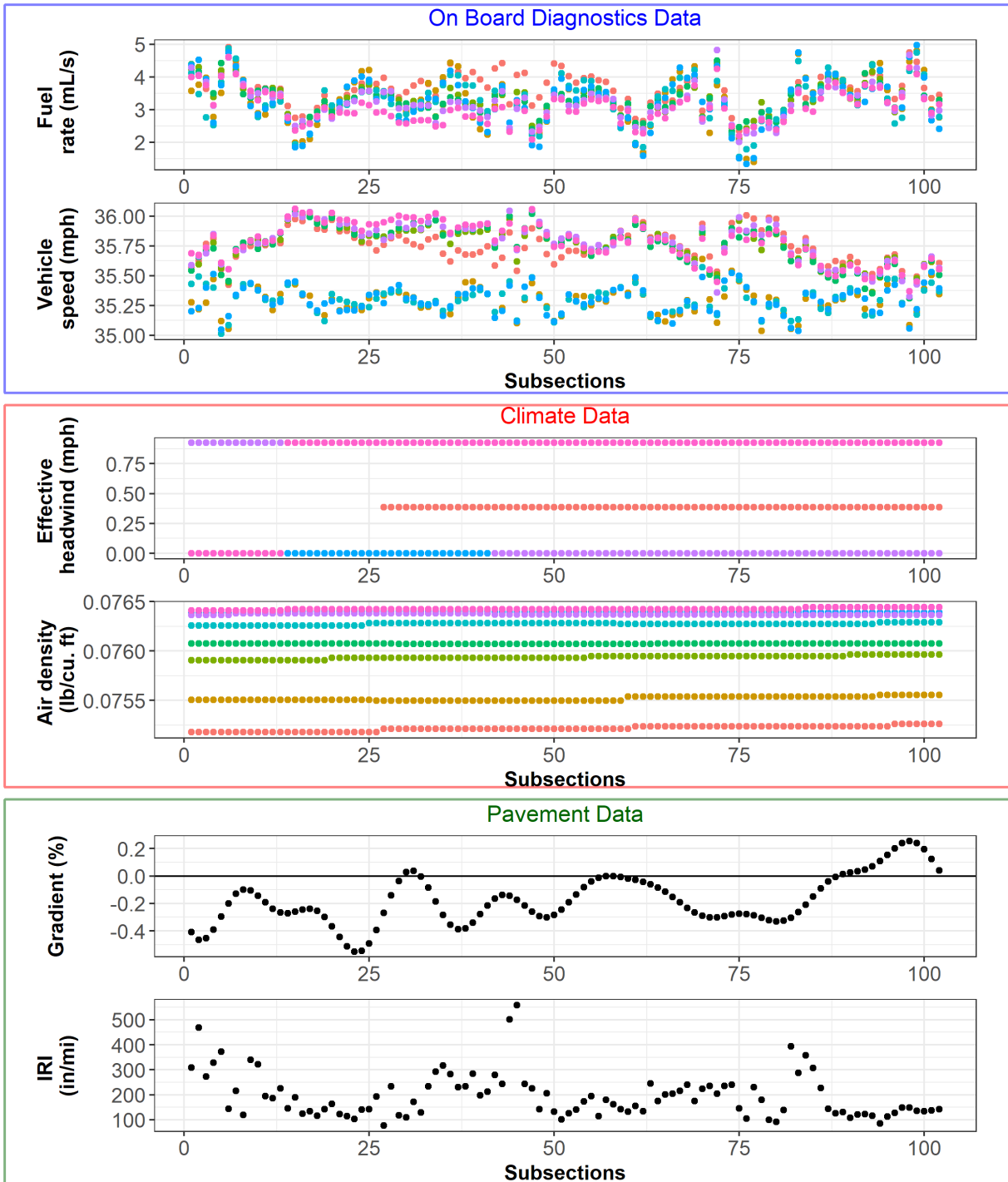


Figure P.312: HHDT data on Section PH08.

PH08-YOL-CR29E-HMA HHDt summer_night 45 mph

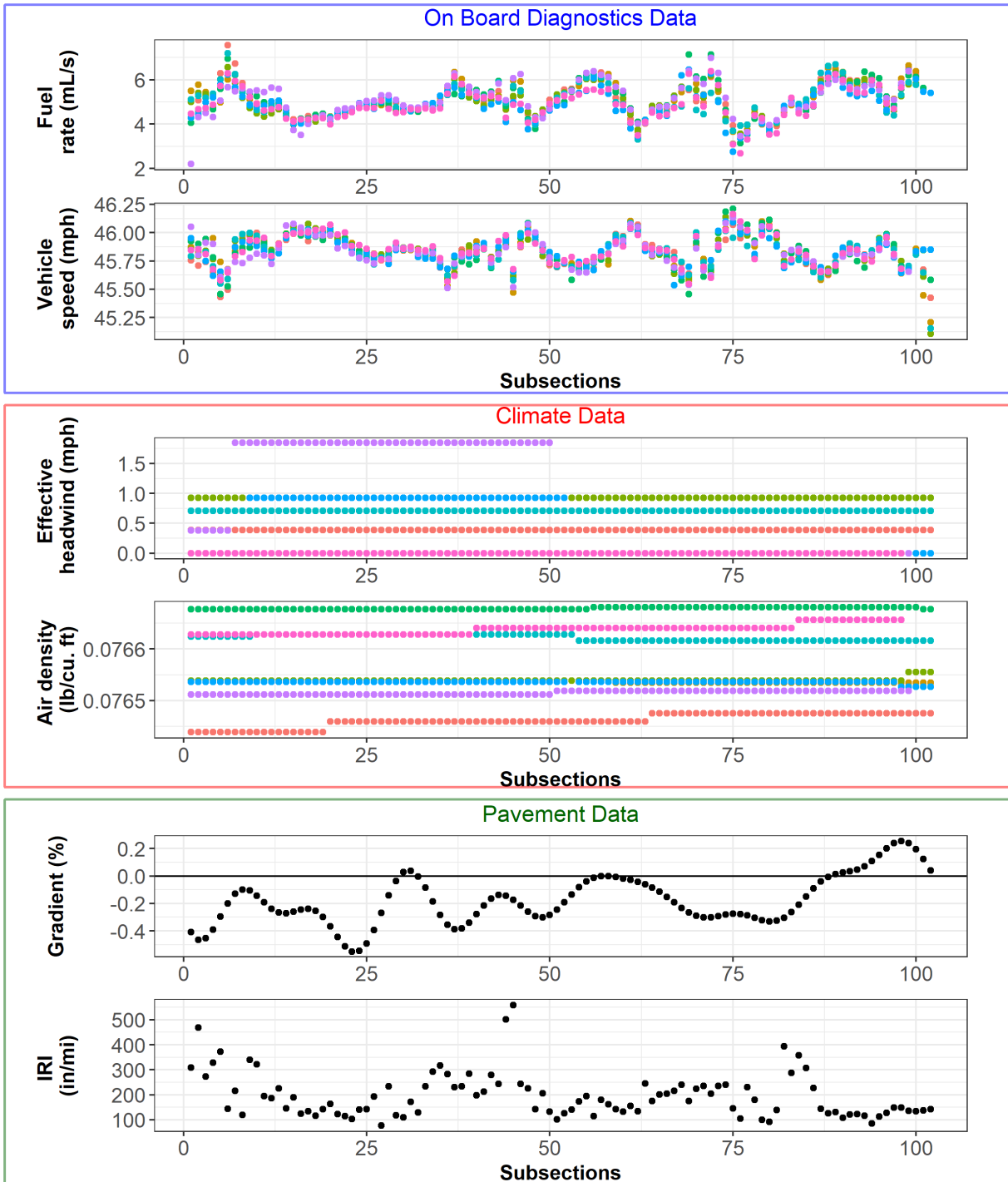


Figure P.313: HHDt data on Section PH08.

PH08-YOL-CR29E-HMA HHDT winter_day 35 mph

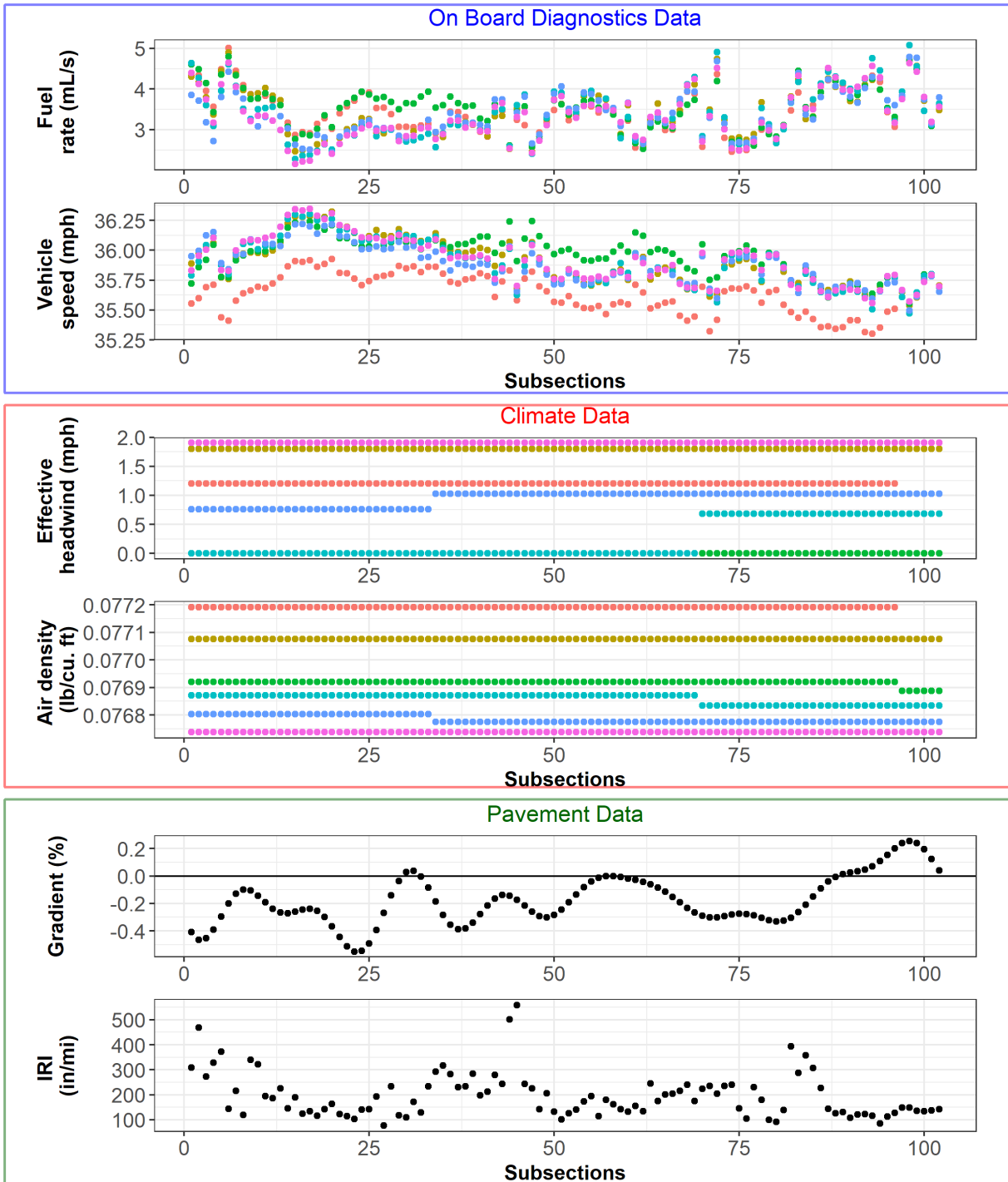


Figure P.314: HHDT data on Section PH08.

PH08-YOL-CR29E-HMA HHDT winter_day 45 mph

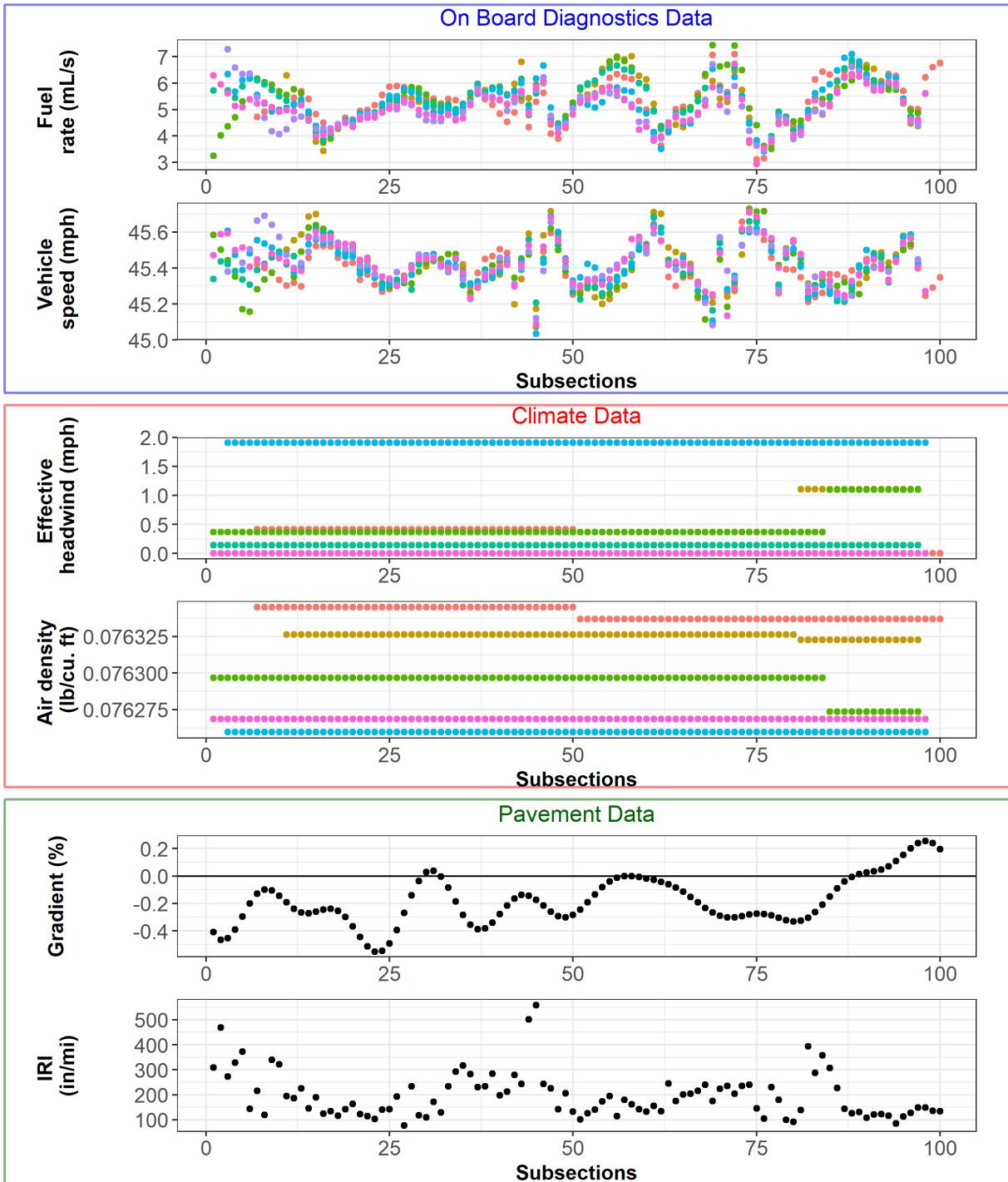


Figure P.315: HHDT data on Section PH08.

PH09-SUT113N-RHMA-O HHDt summer_day 45 mph

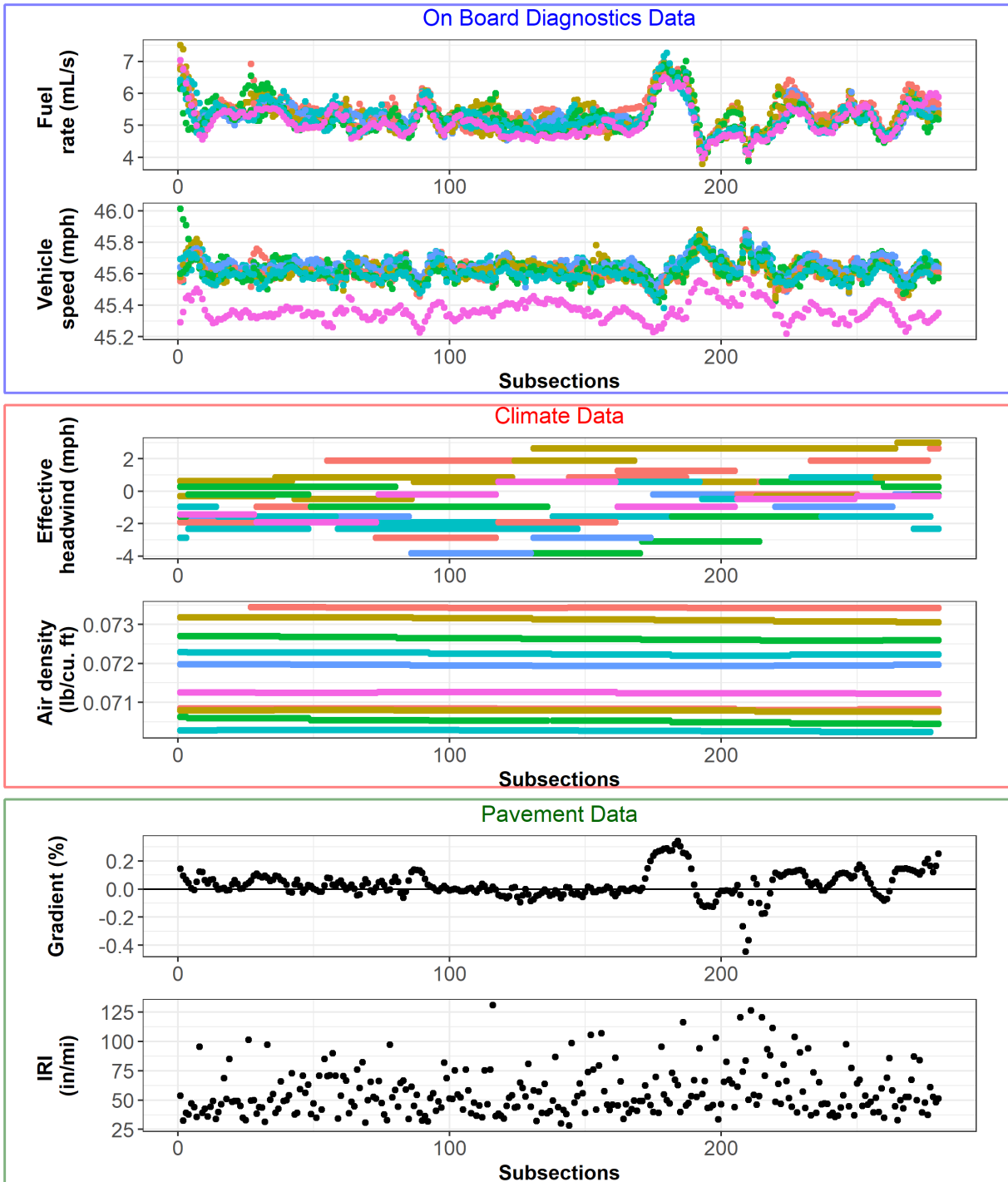


Figure P.316: HHDt data on Section PH09.

PH09-SUT113N-RHMA-O HHDT summer_day 55 mph

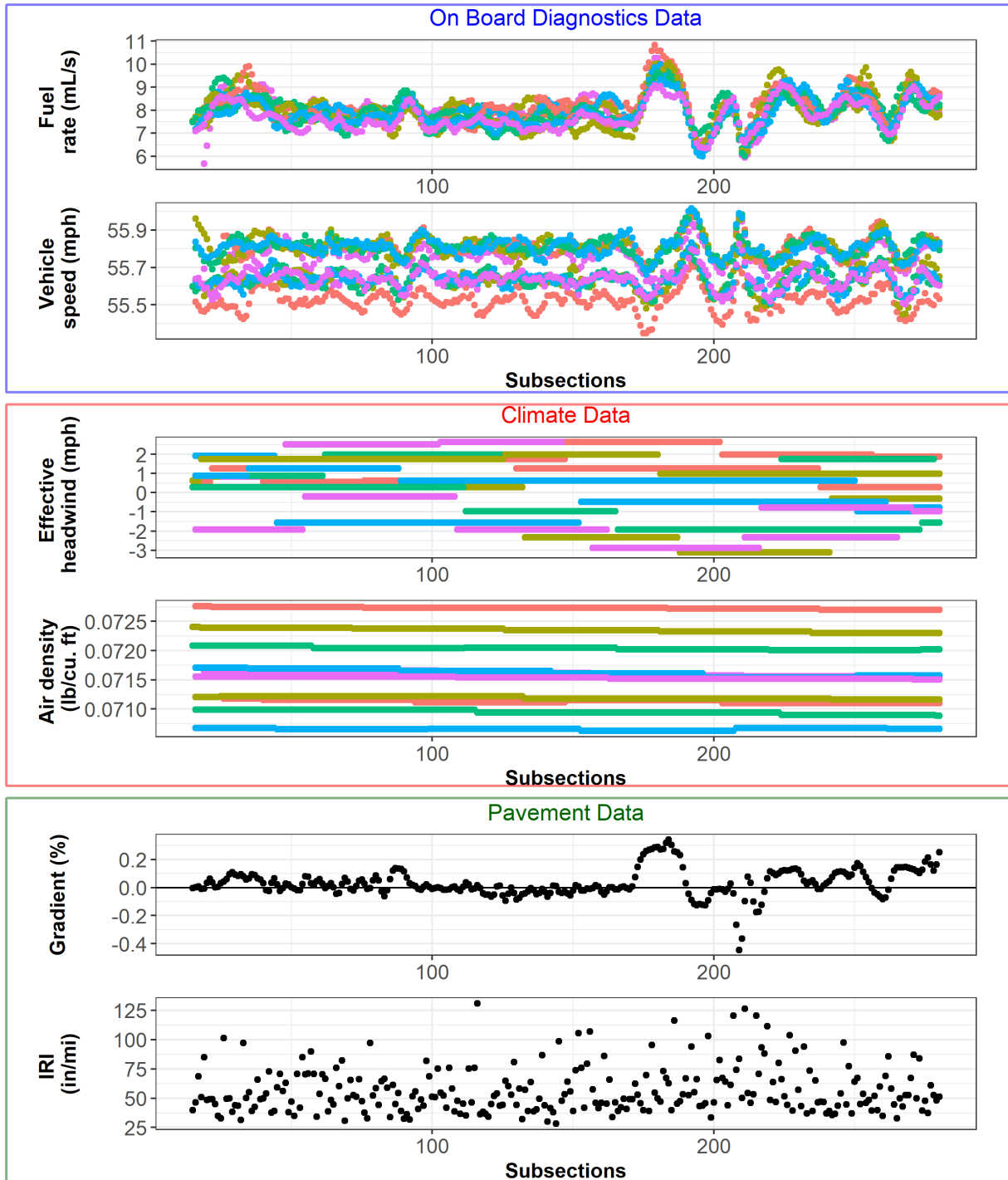


Figure P.317: HHDT data on Section PH09.

PH09-SUT113N-RHMA-O HHDt winter_day 45 mph

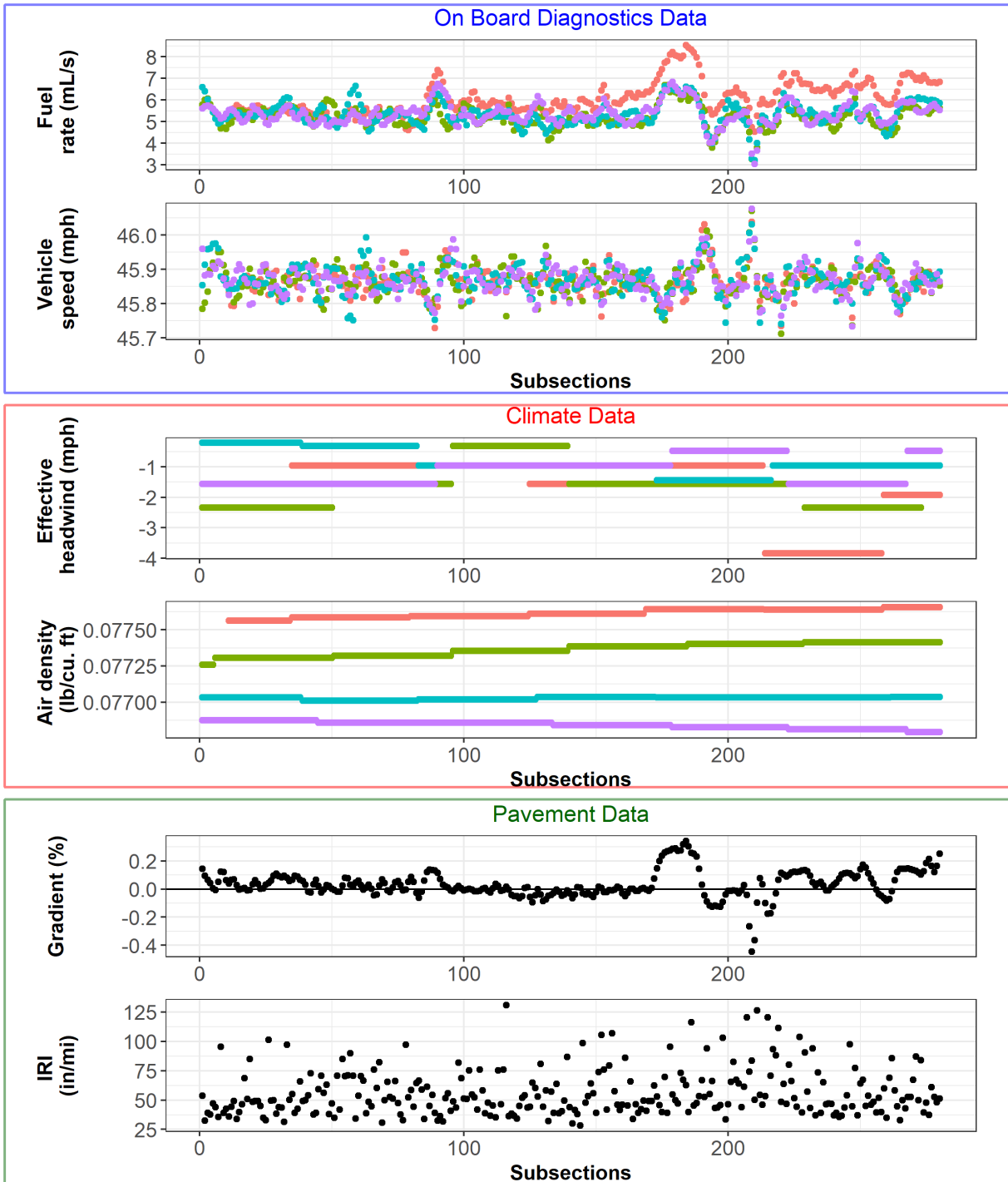


Figure P.318: HHDt data on Section PH09.

PH09-SUT113N-RHMA-O HHDt winter_day 55 mph

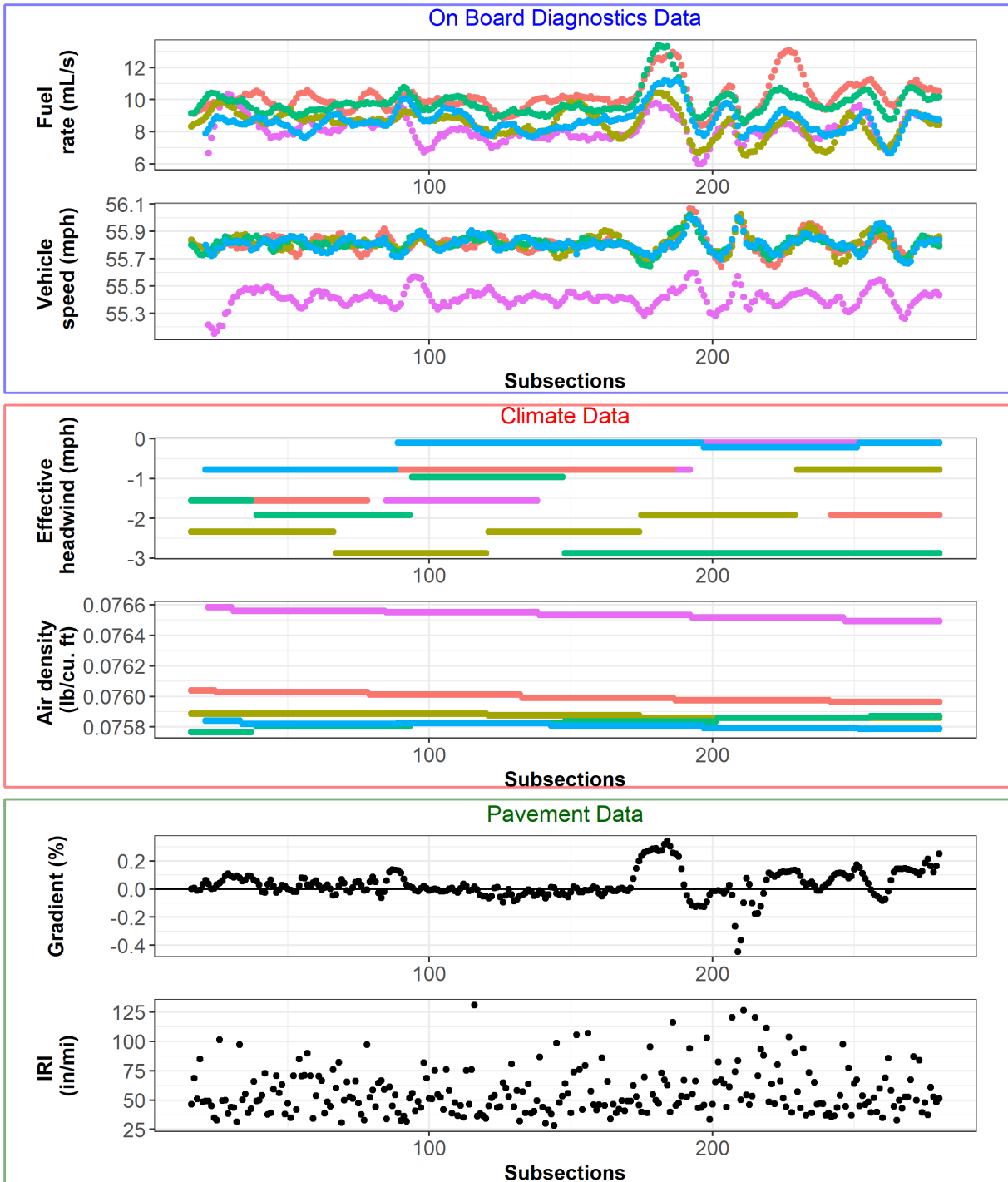


Figure P.319: HHDt data on Section PH09.

PH10-SUT113S-RHMA-O HHDt summer_day 45 mph

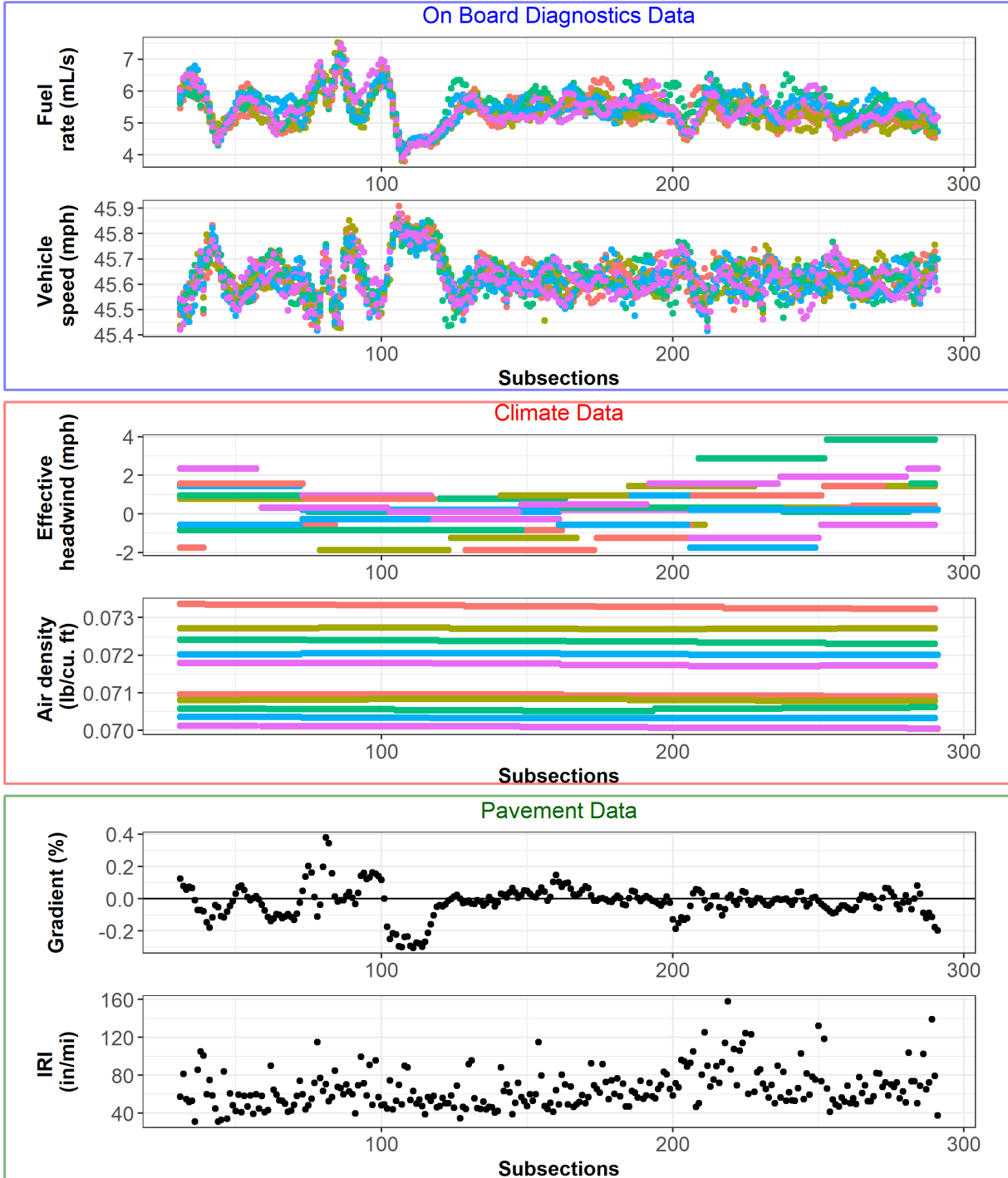


Figure P.320: HHDt data on Section PH10.

PH10-SUT113S-RHMA-O HHDT summer_day 55 mph

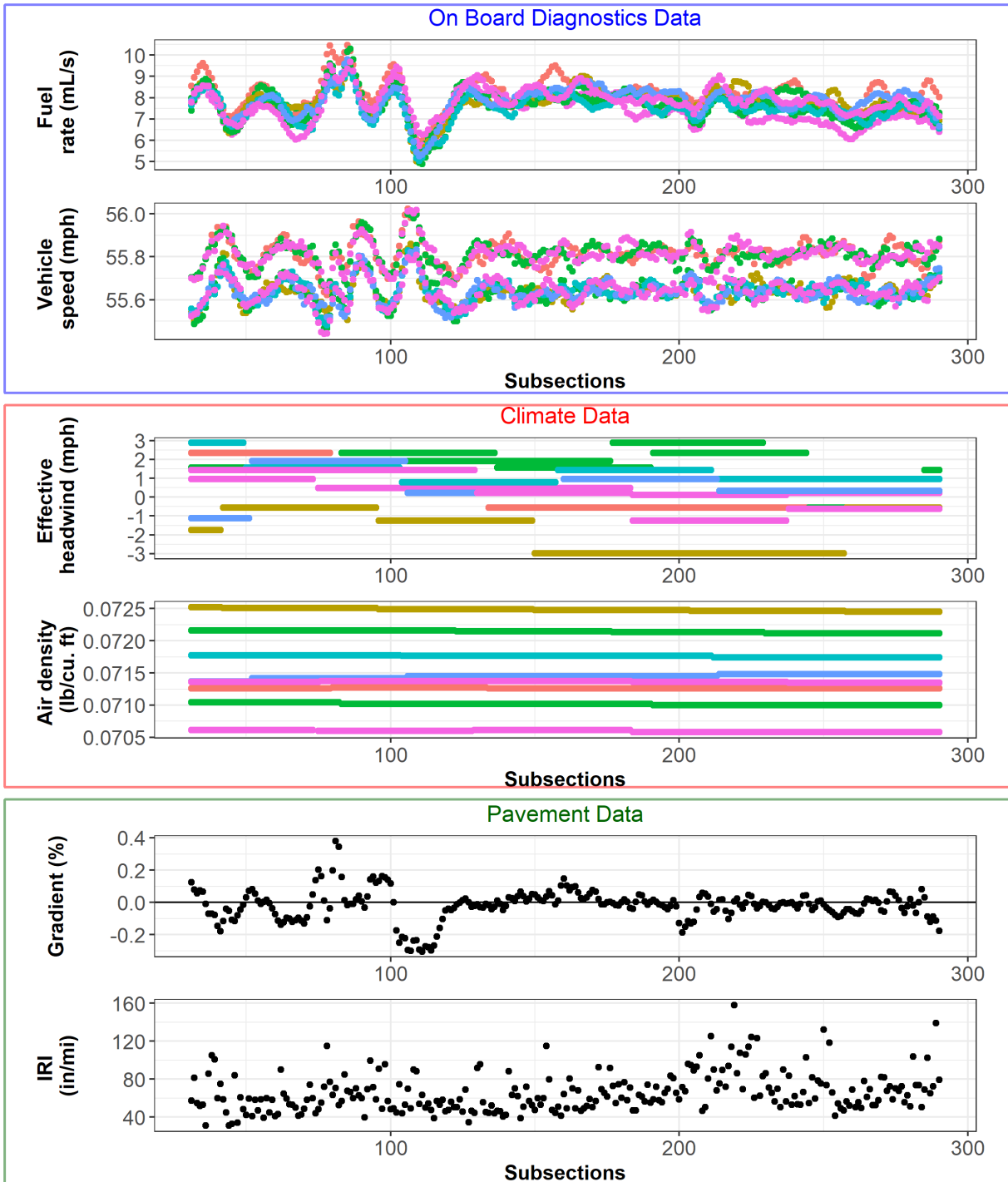


Figure P.321: HHDT data on Section PH10.

PH10-SUT113S-RHMA-O HHDt winter_day 45 mph

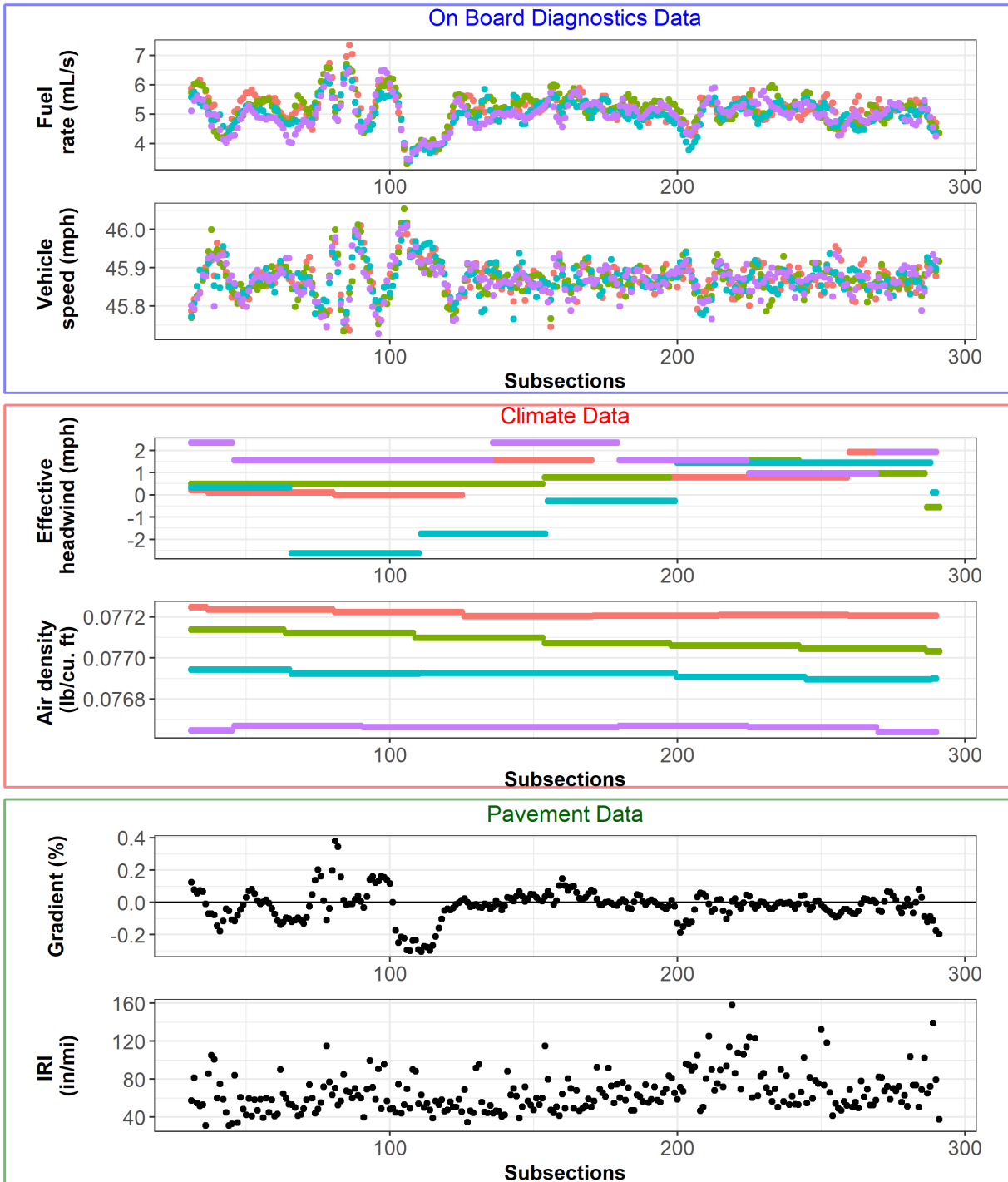


Figure P.322: HHDt data on Section PH10.

PH10-SUT113S-RHMA-O HHDt winter_day 55 mph

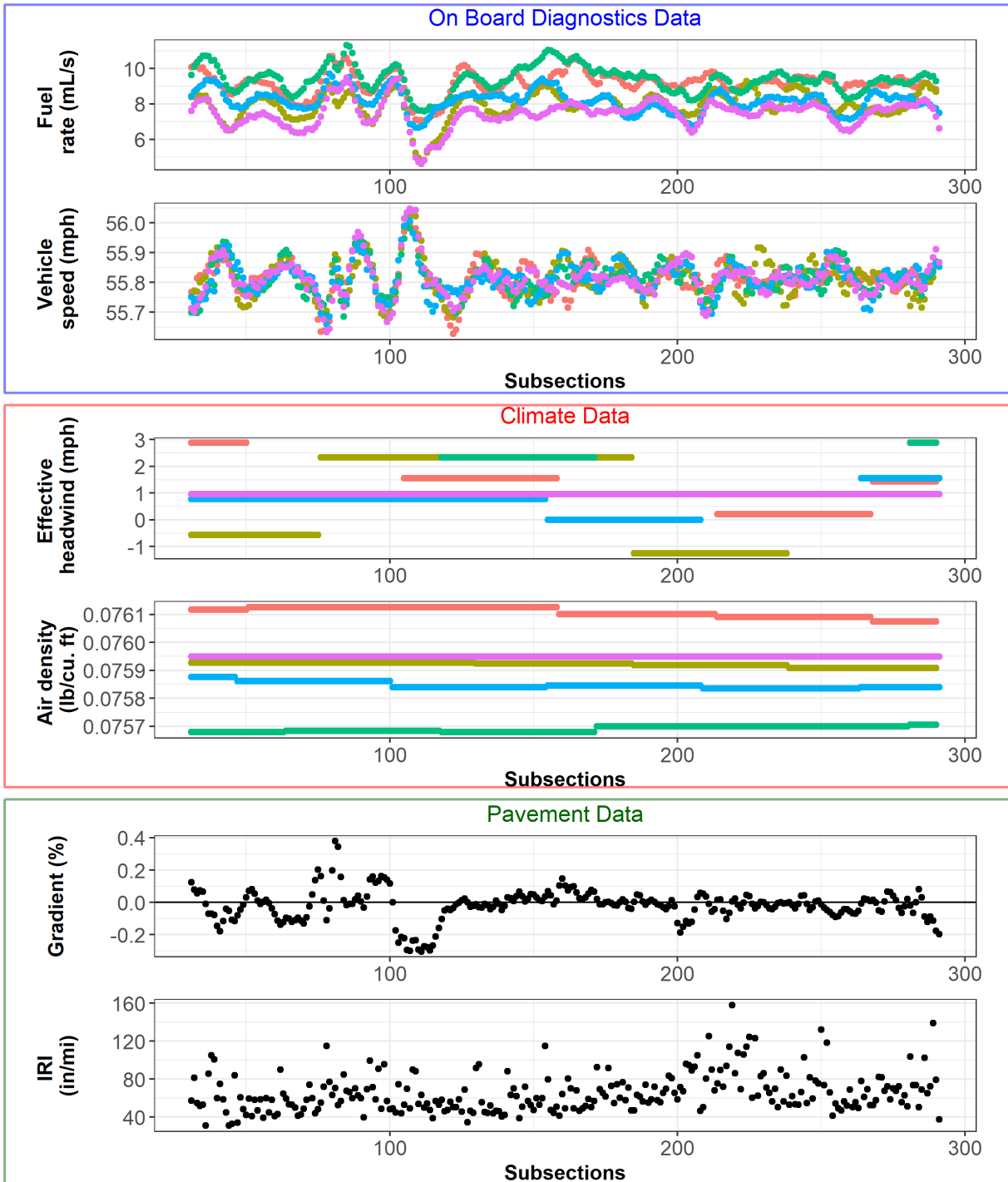


Figure P.323: HHDt data on Section PH10.

PH11-SUT113N-HMA HHDT summer_day 45 mph

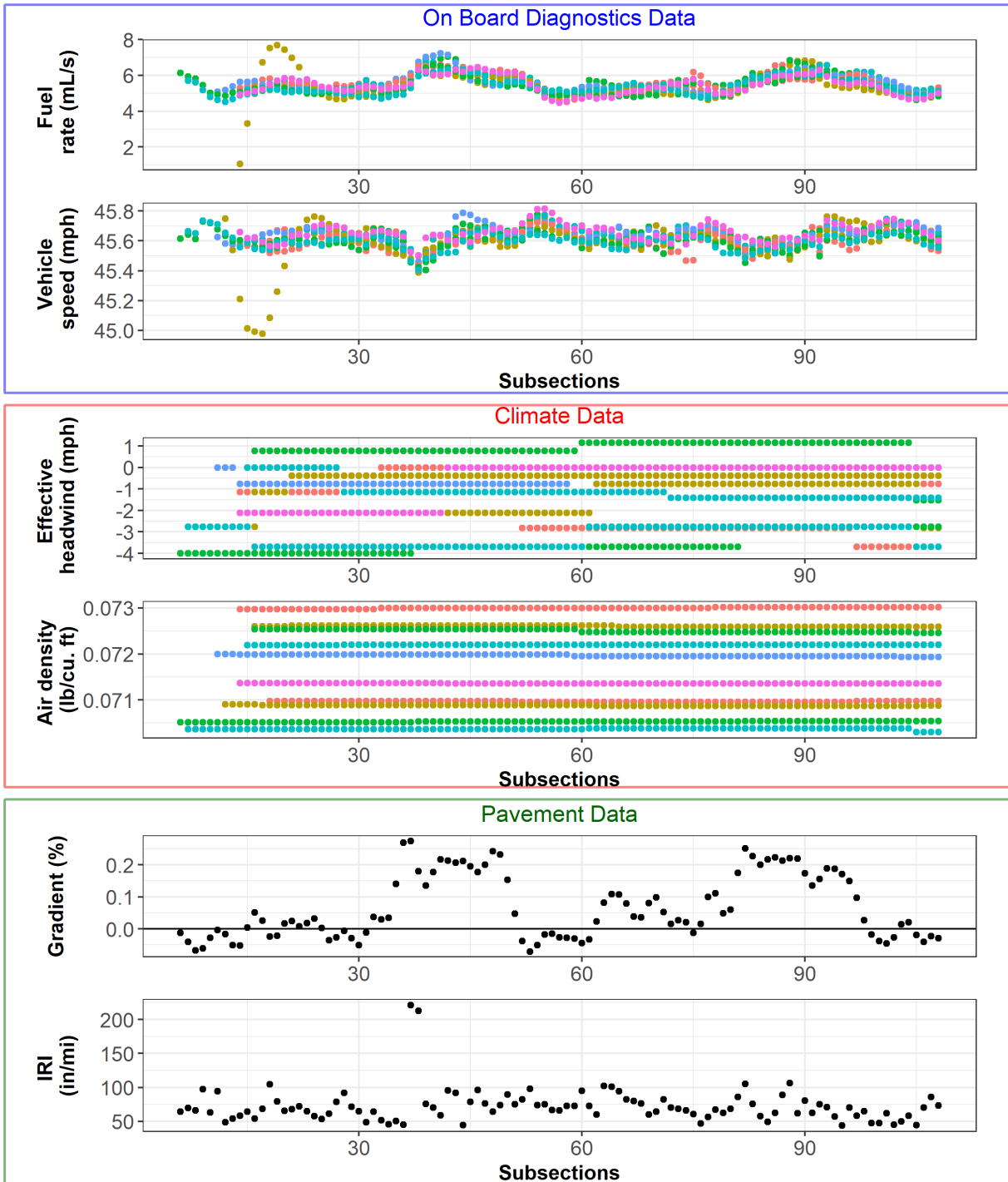


Figure P.324: HHDT data on Section PH11.

PH11-SUT113N-HMA HHDT summer_day 55 mph

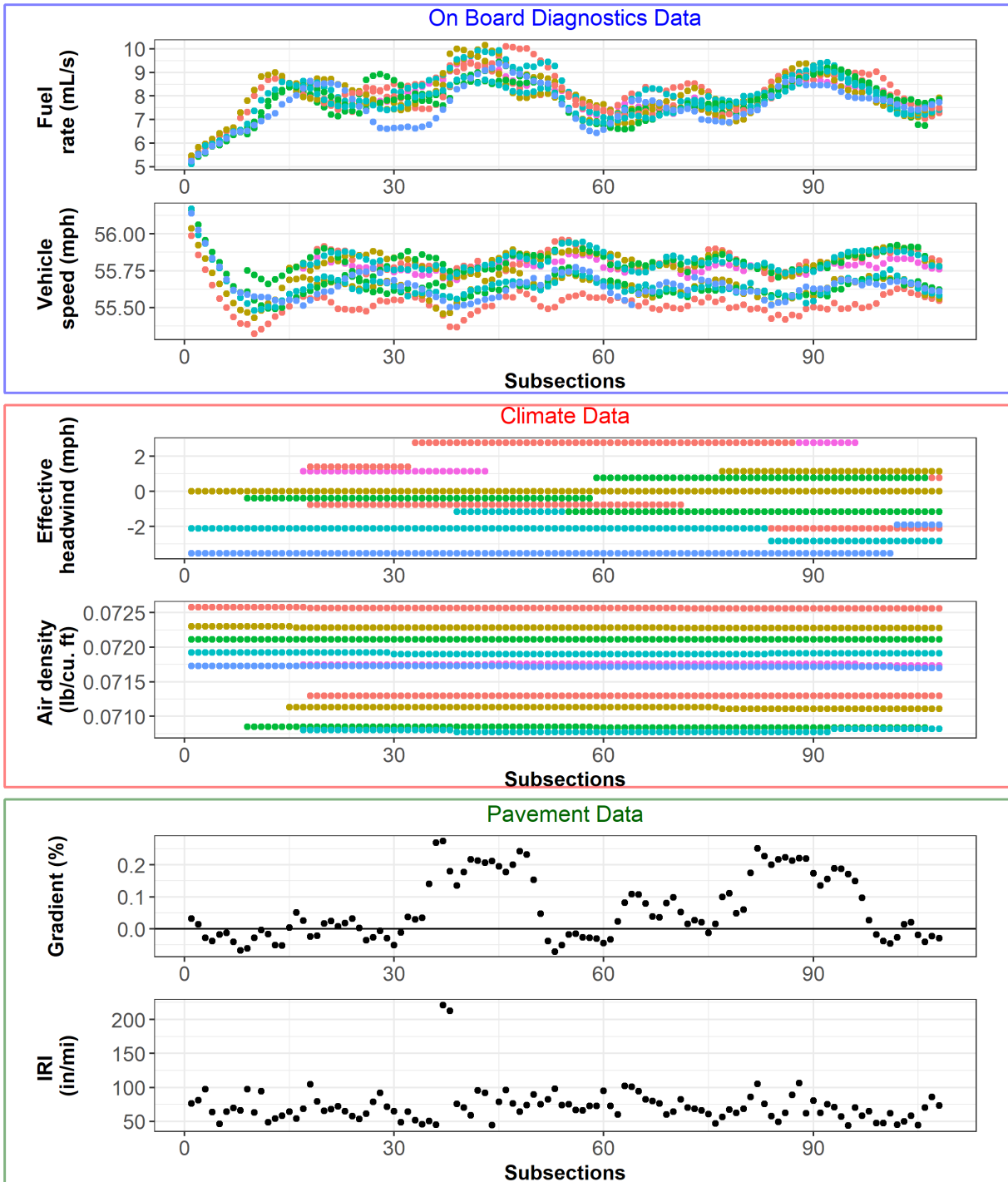


Figure P.325: HHDT data on Section PH11.

PH11-SUT113N-HMA HHDT winter_day 45 mph

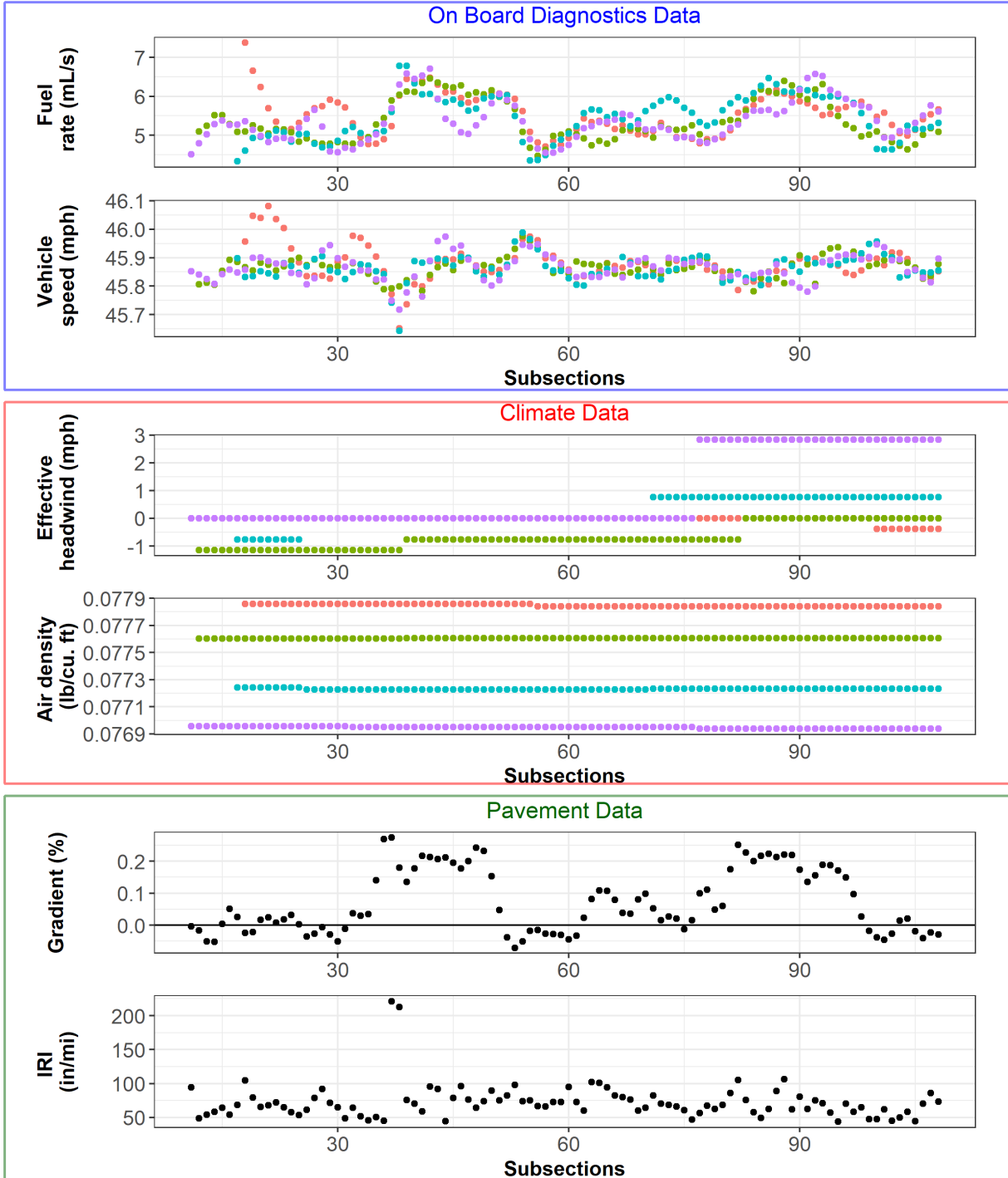


Figure P.326: HHDT data on Section PH11.

PH11-SUT113N-HMA HHDt winter_day 55 mph

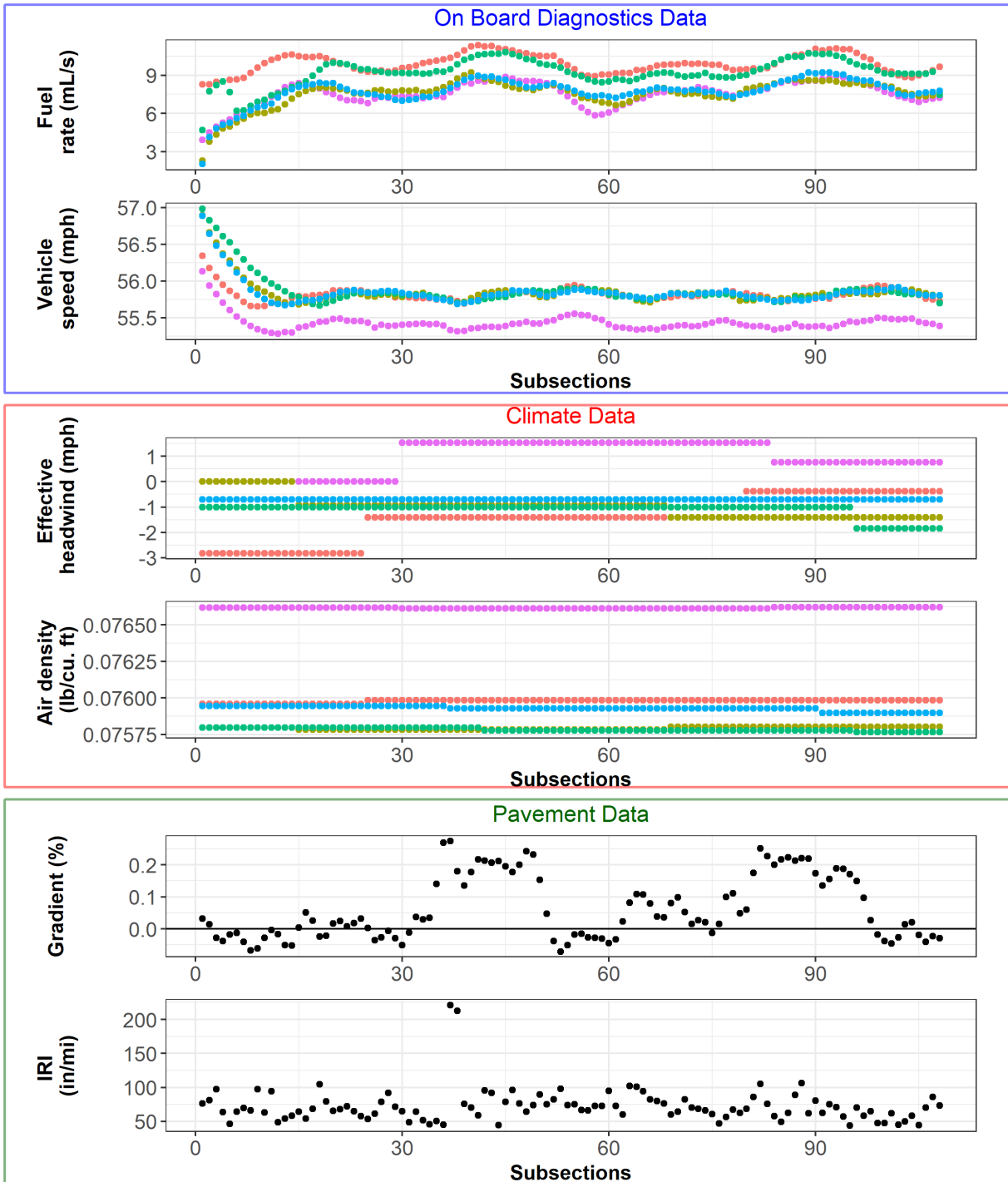


Figure P.327: HHDt data on Section PH11.

PH12-SUT113S-HMA HHDT summer_day 45 mph

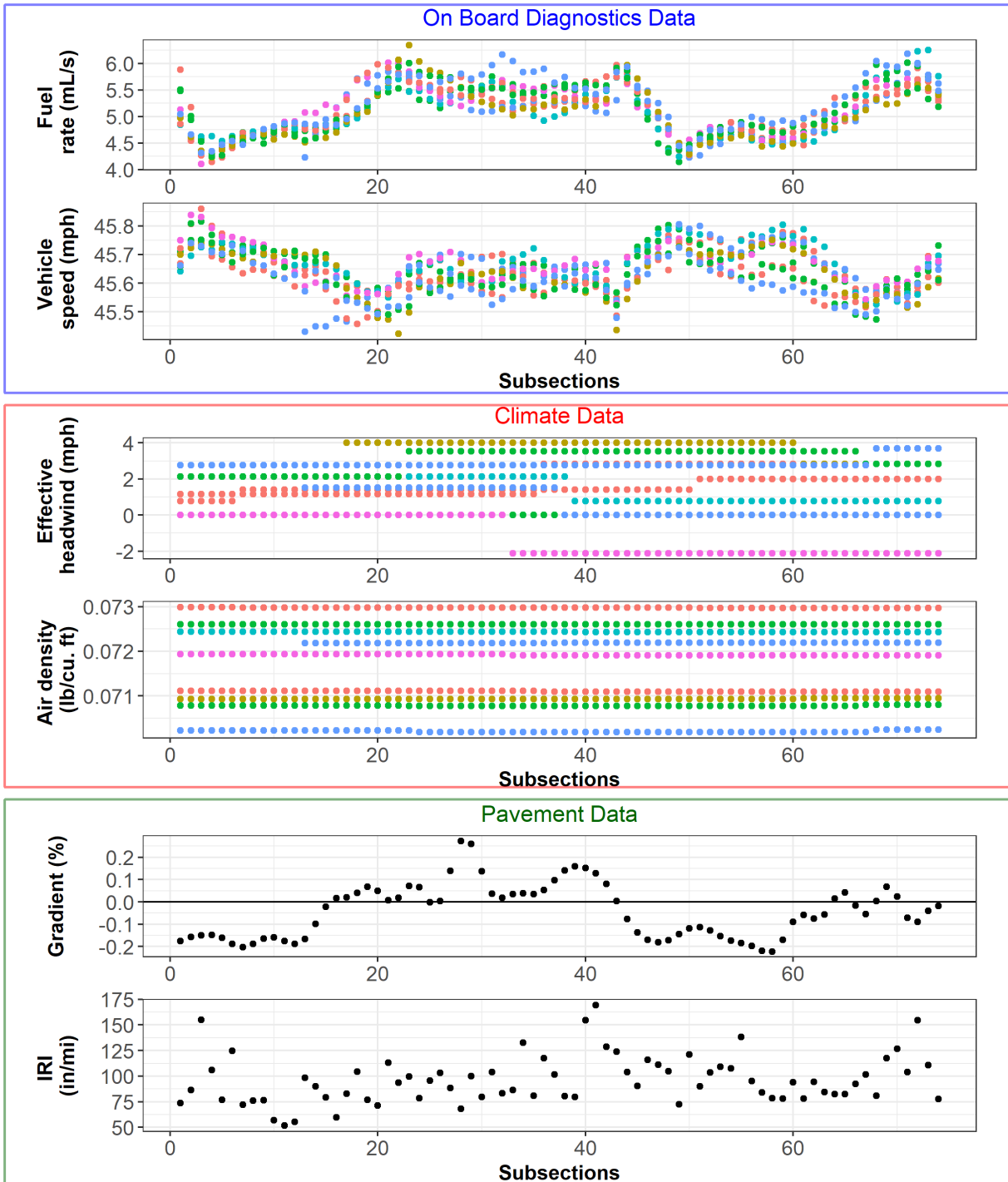


Figure P.328: HHDT data on Section PH12.

PH12-SUT113S-HMA HHDT summer_day 55 mph

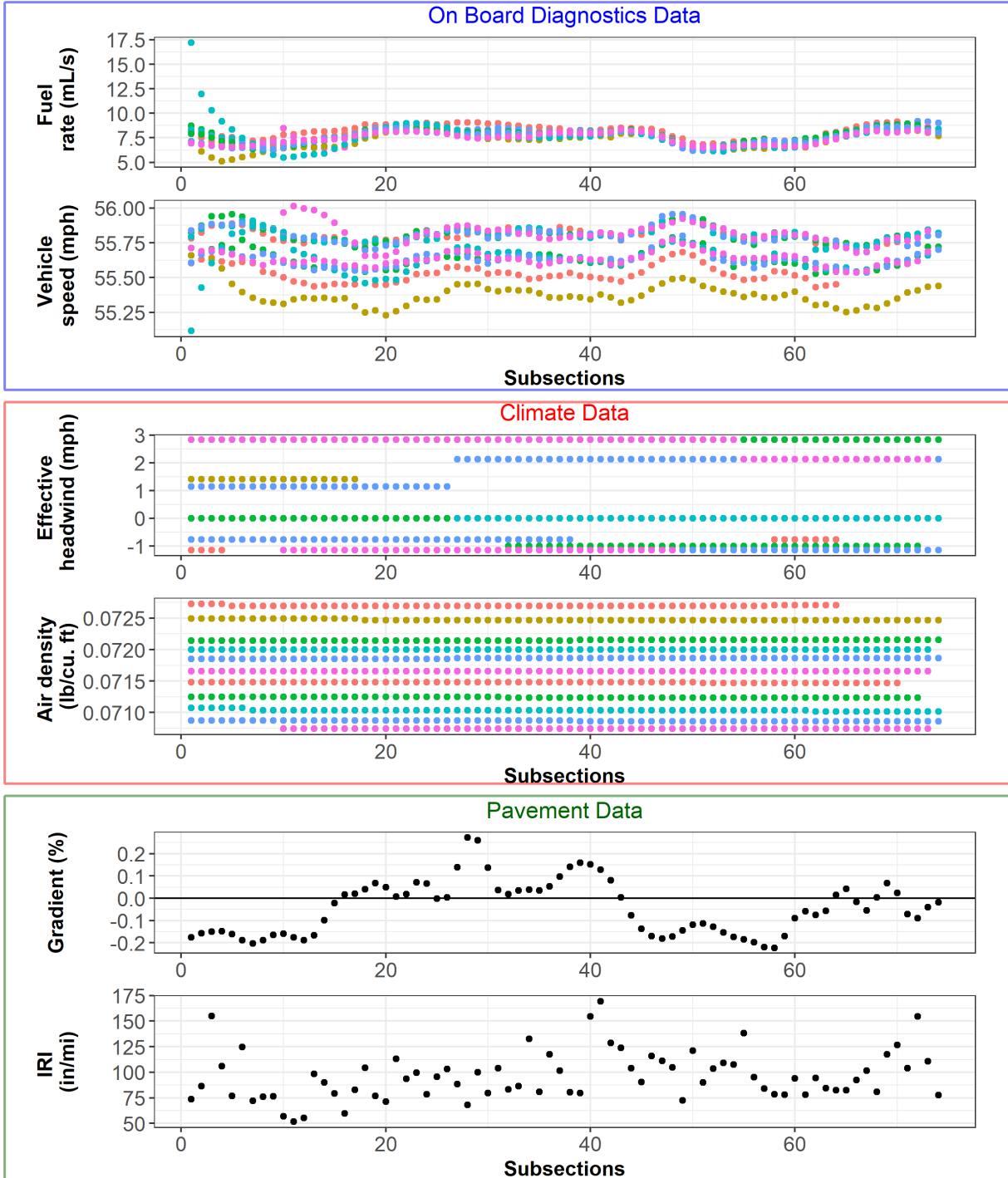


Figure P.329: HHDT data on Section PH12.

PH12-SUT113S-HMA HHDT winter_day 45 mph

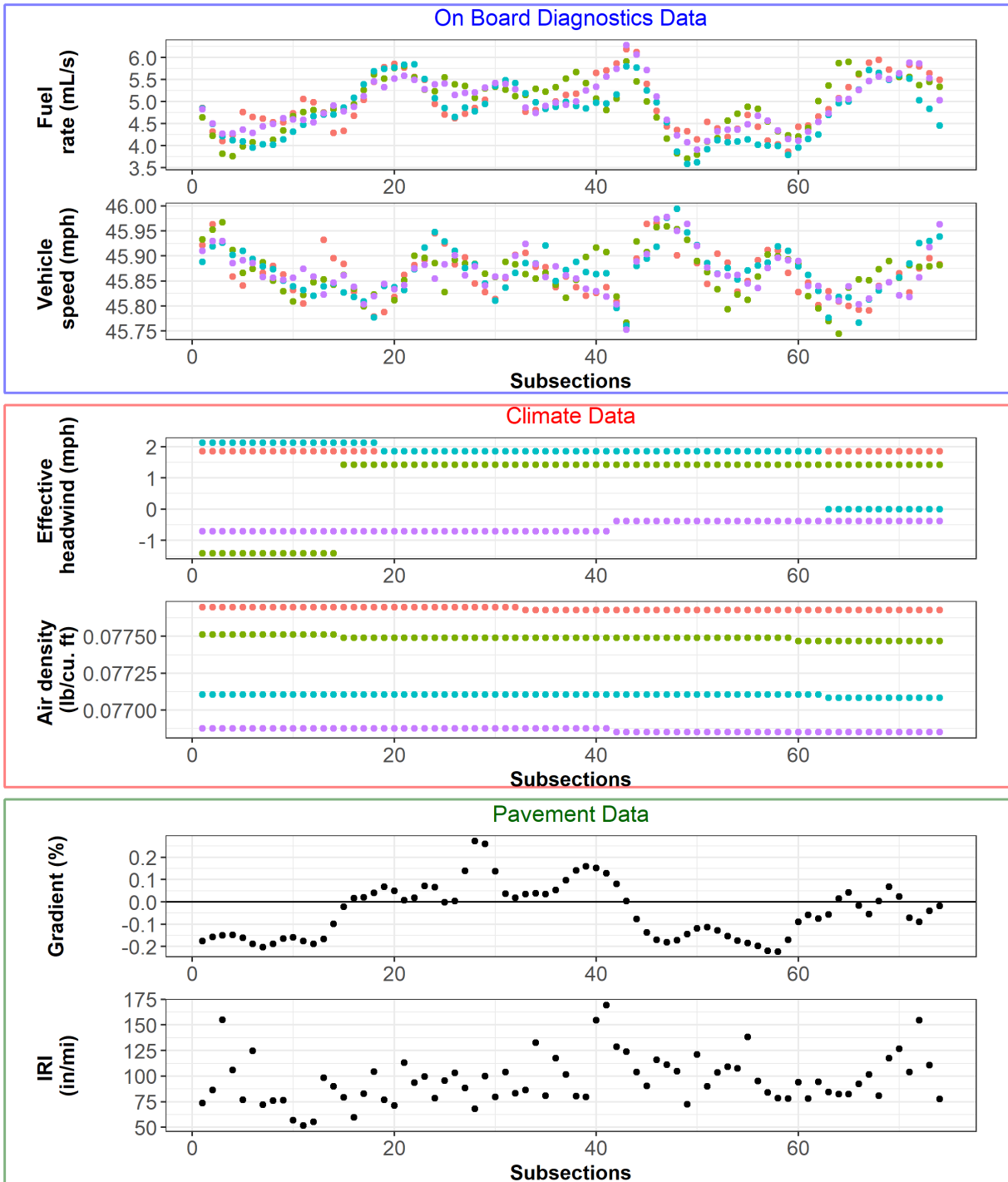


Figure P.330: HHDT data on Section PH12.

PH12-SUT113S-HMA HHDt winter_day 55 mph

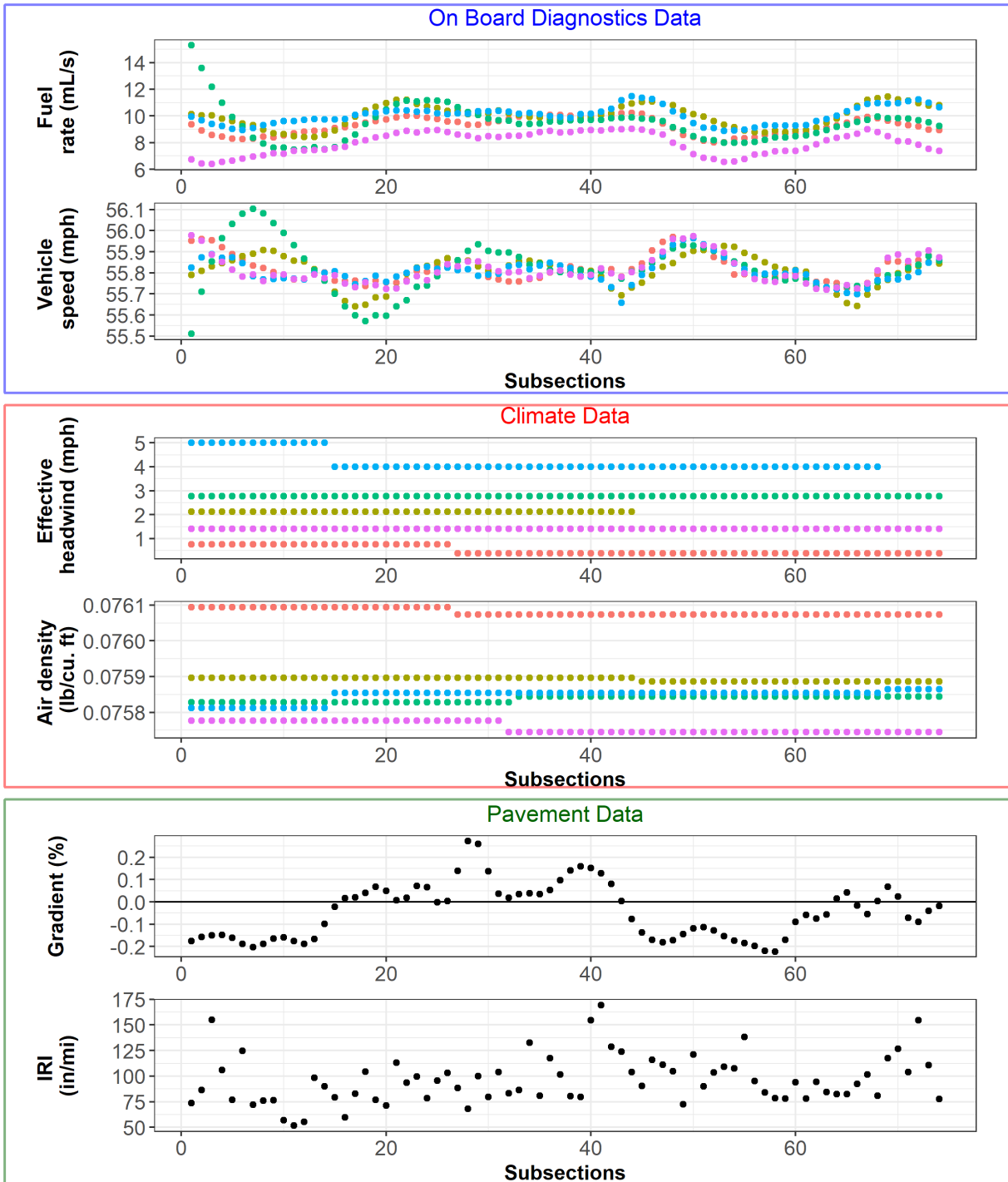


Figure P.331: HHDt data on Section PH12.

PH13-SUT113N-HMA HHDT summer_day 45 mph

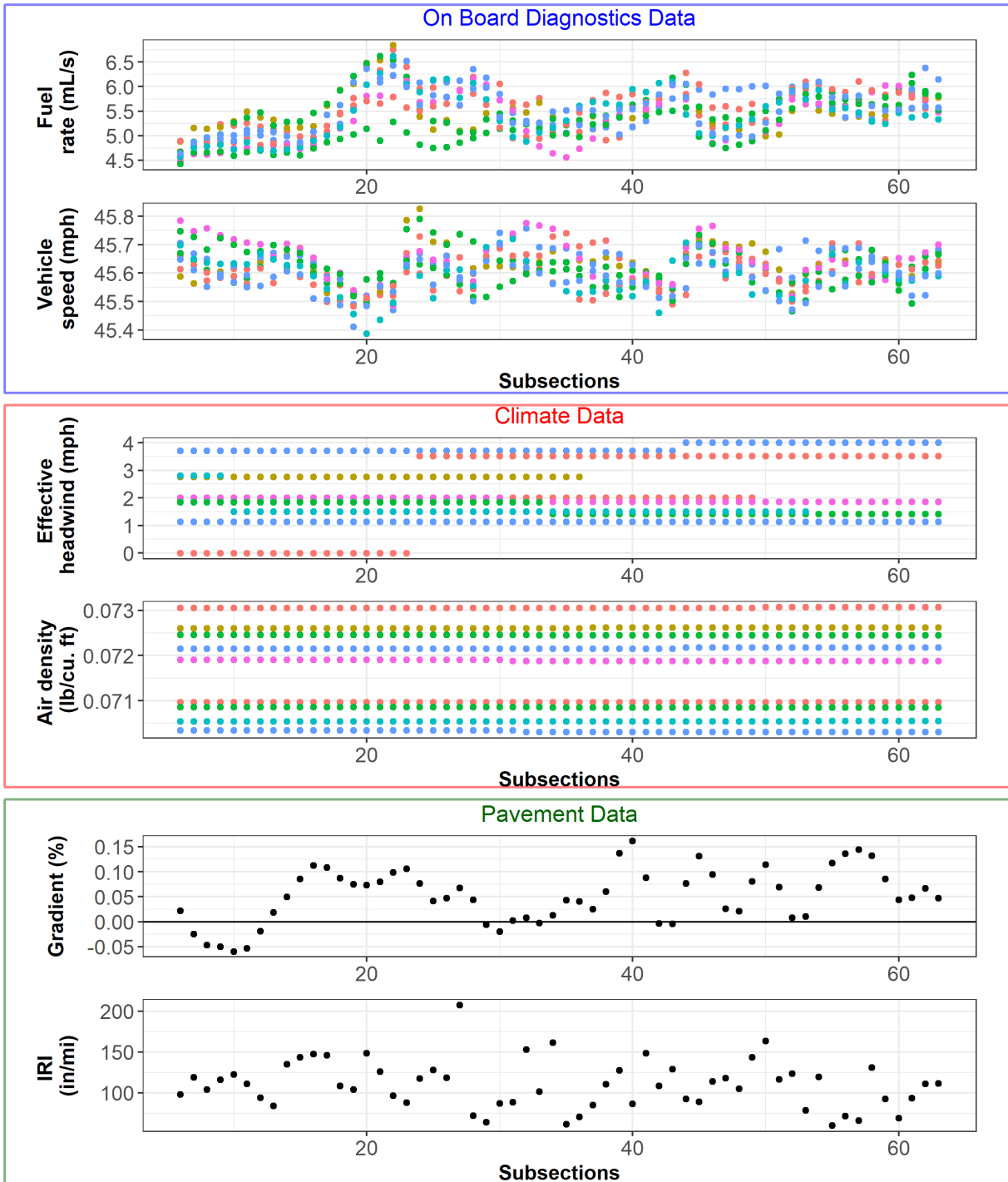


Figure P.332: HHDT data on Section PH13.

PH13-SUT113N-HMA HHDT summer_day 55 mph

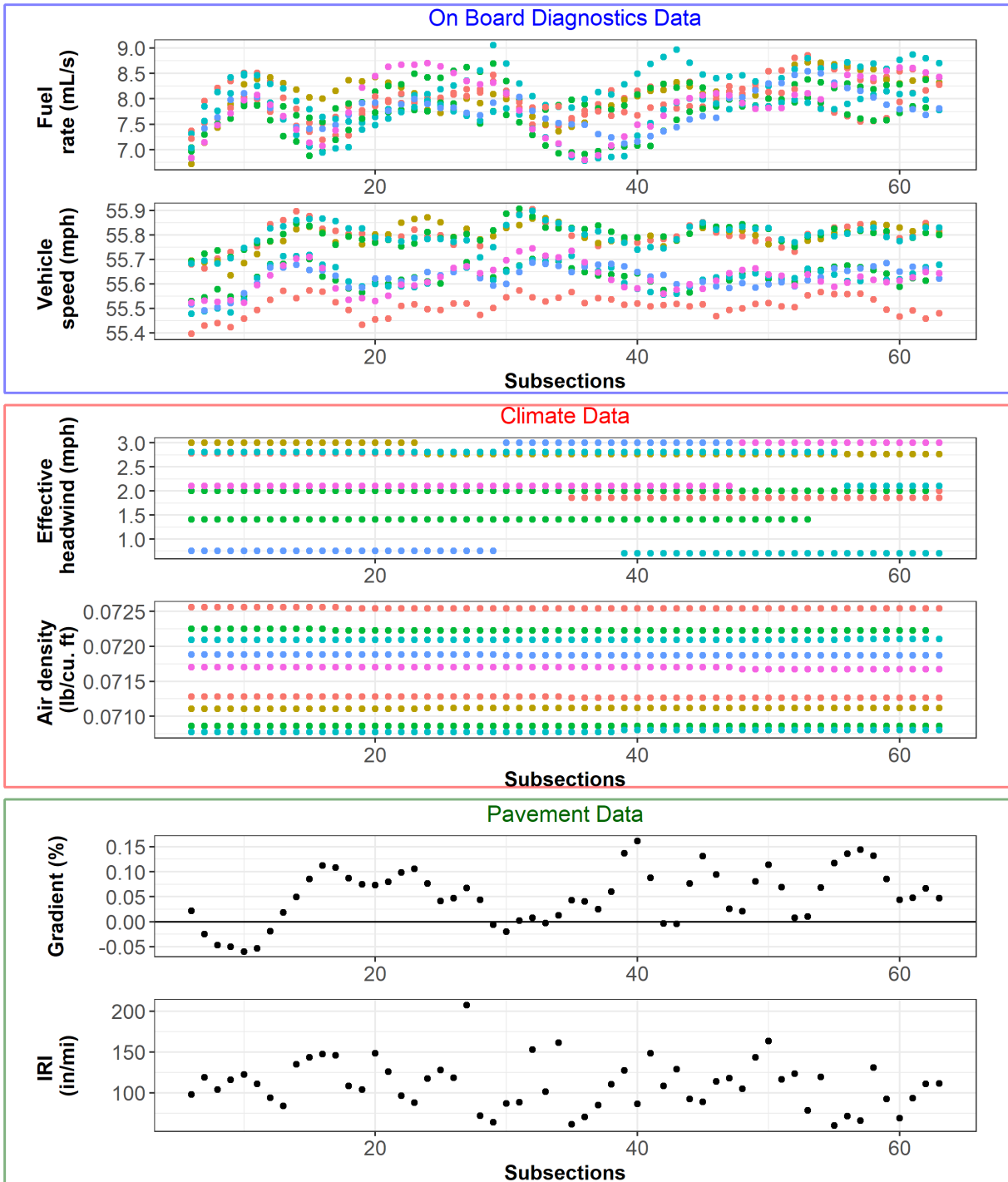


Figure P.333: HHDT data on Section PH13.

PH13-SUT113N-HMA HHDt winter_day 45 mph

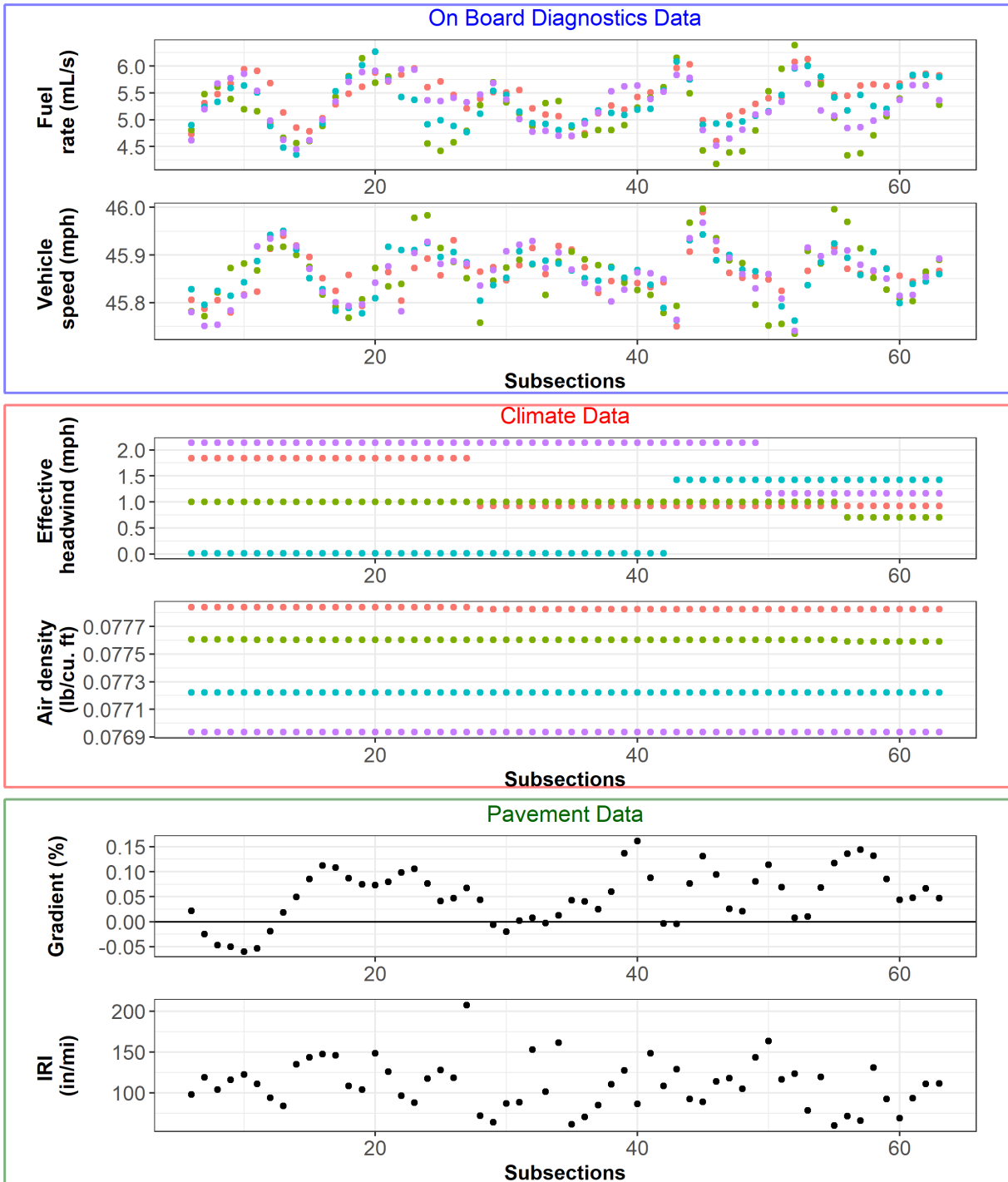


Figure P.334: HHDt data on Section PH13.

PH13-SUT113N-HMA HHDT winter_day 55 mph

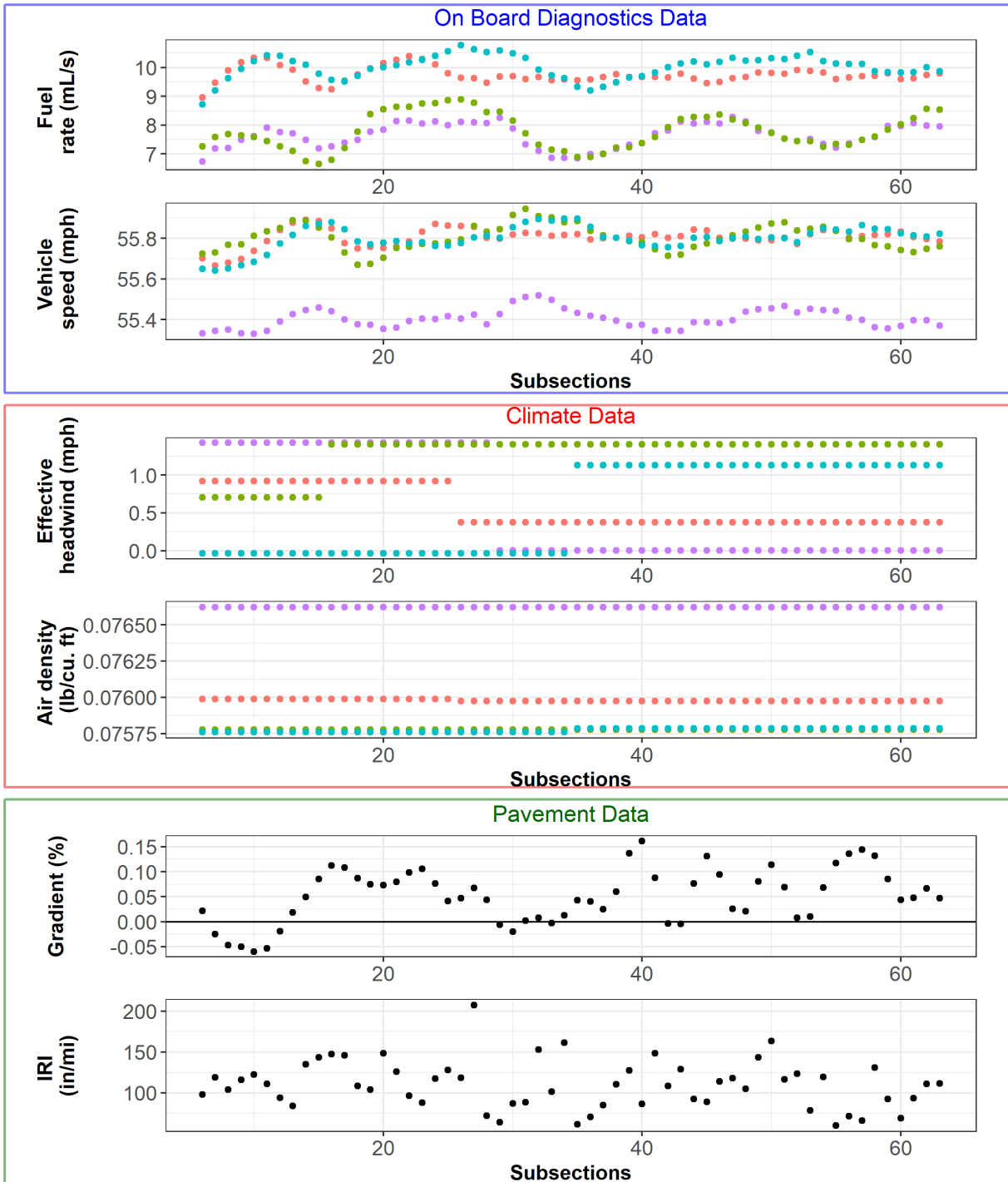


Figure P.335: HHDT data on Section PH13.

PH14-SUT113S-HMA HHDT summer_day 45 mph

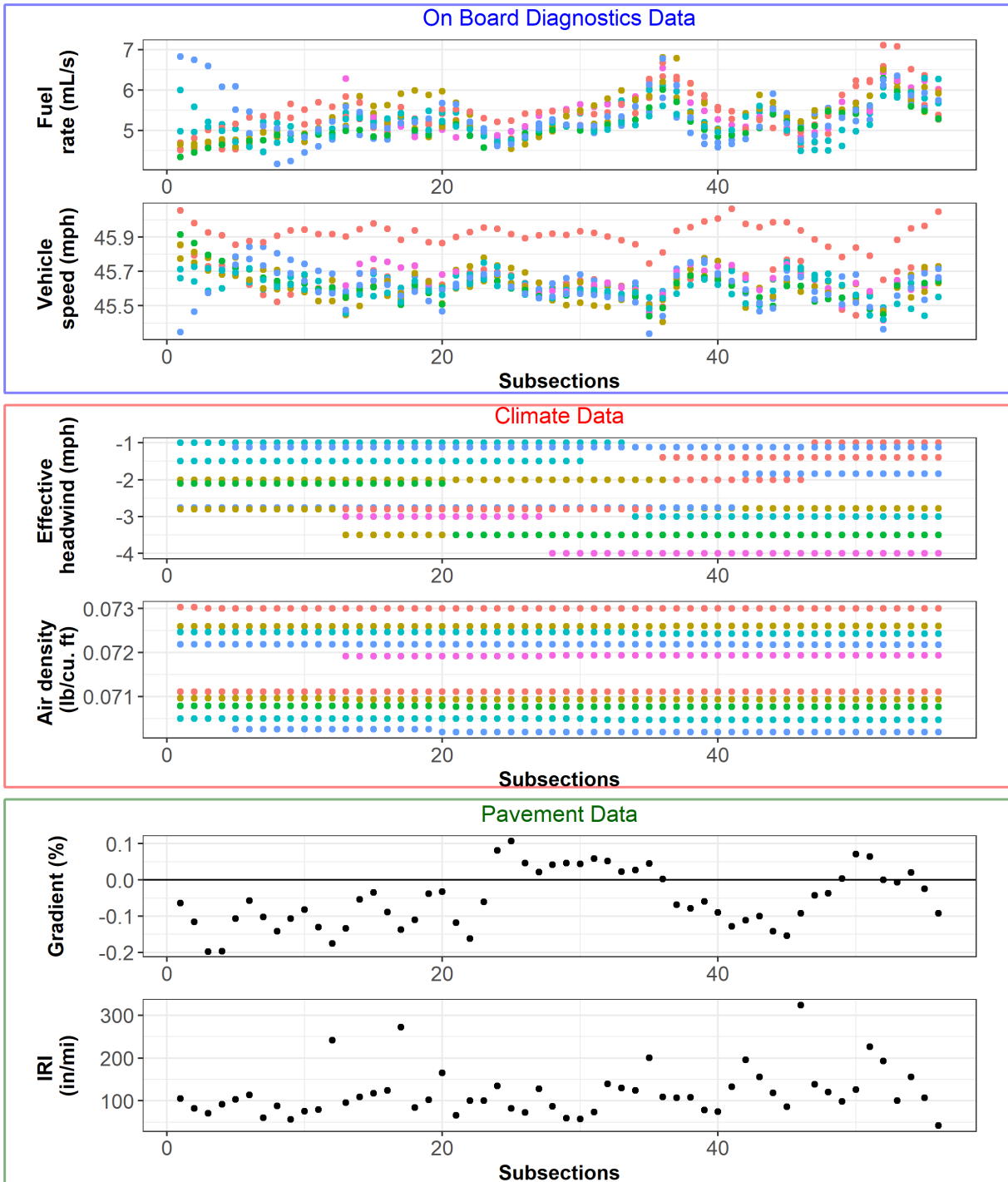


Figure P.336: HHDT data on Section PH14.

PH14-SUT113S-HMA HHDT summer_day 55 mph

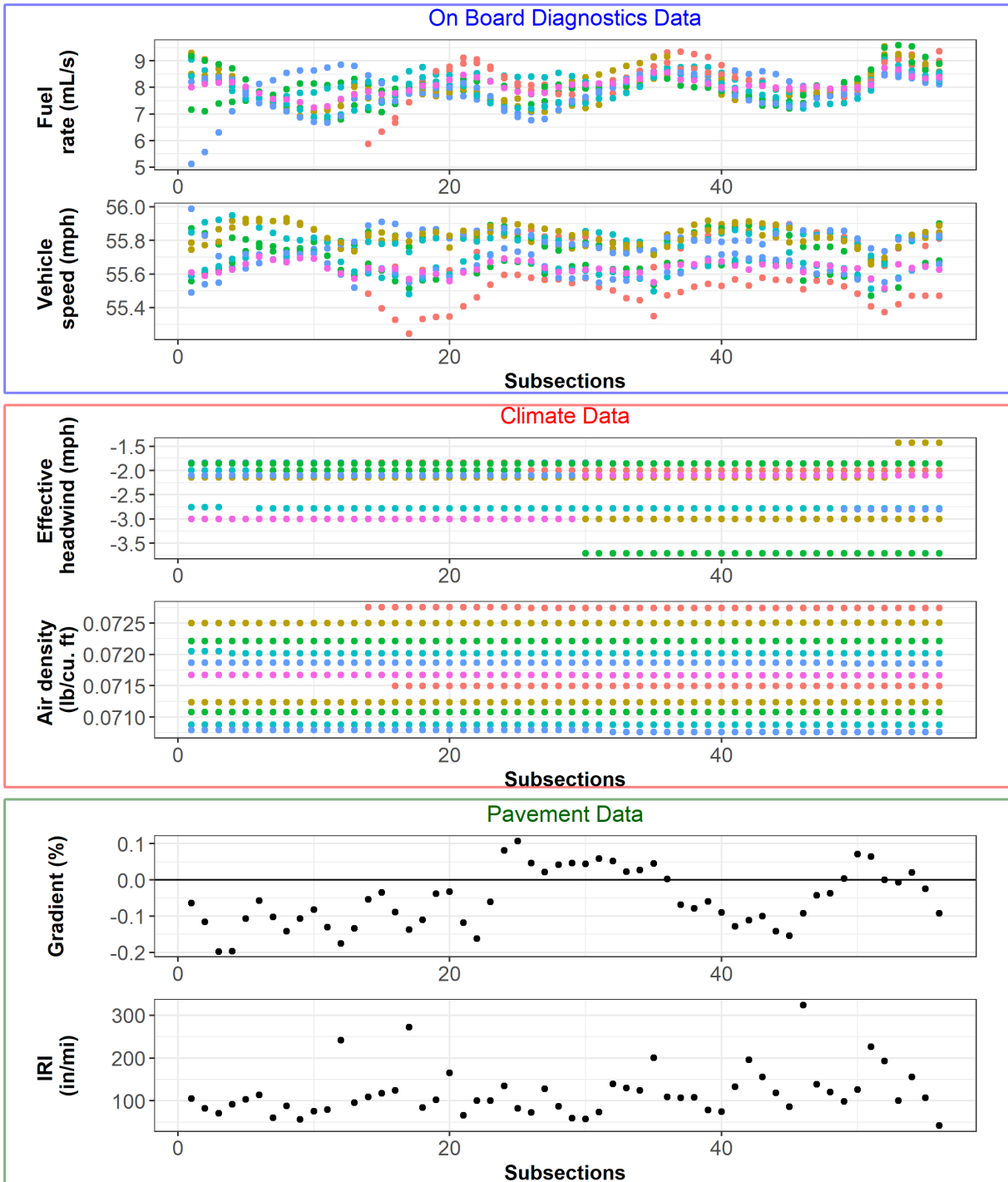


Figure P.337: HHDT data on Section PH14.

PH14-SUT113S-HMA HHDt winter_day 45 mph

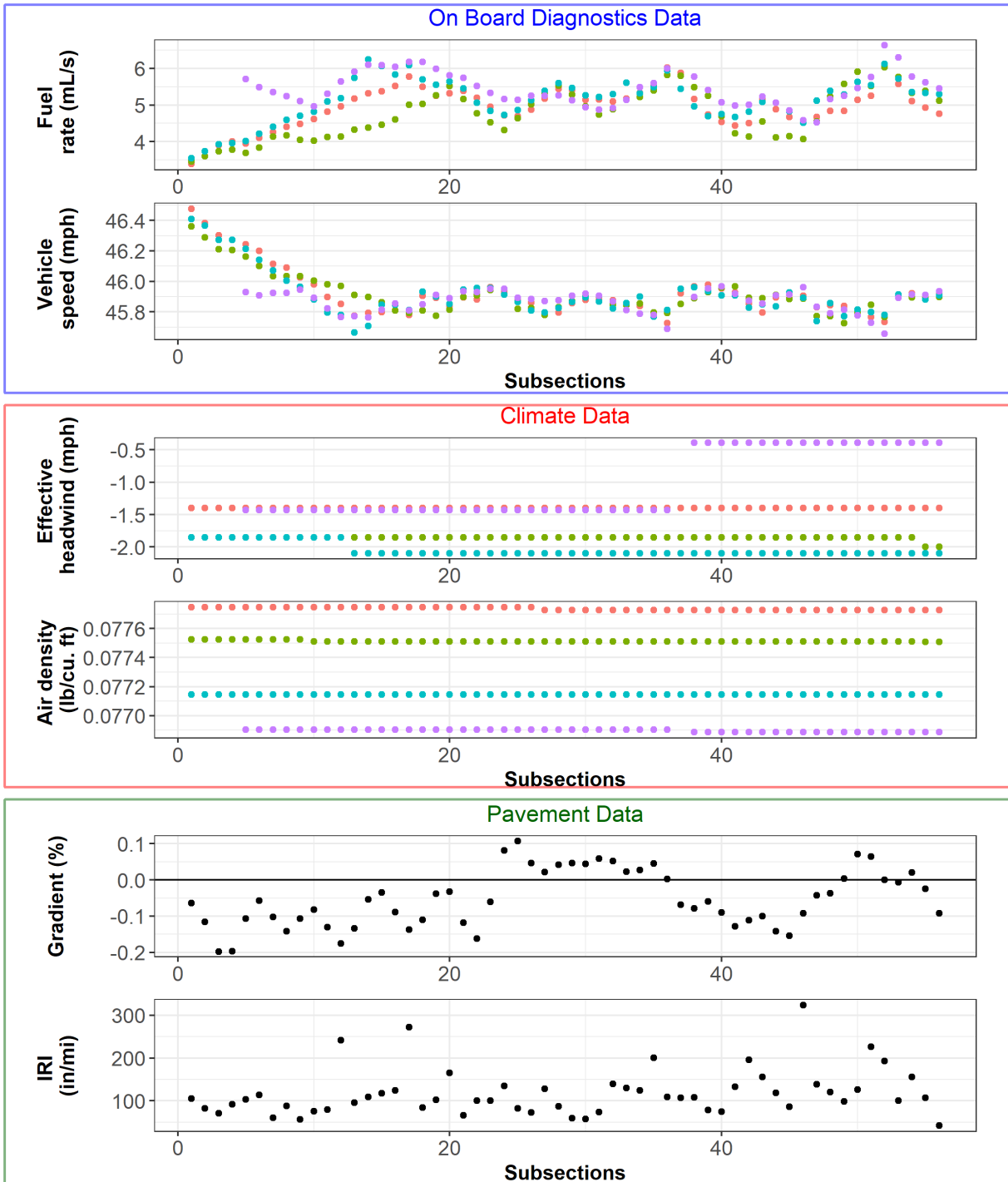


Figure P.338: HHDt data on Section PH14.

PH14-SUT113S-HMA HHDT winter_day 55 mph

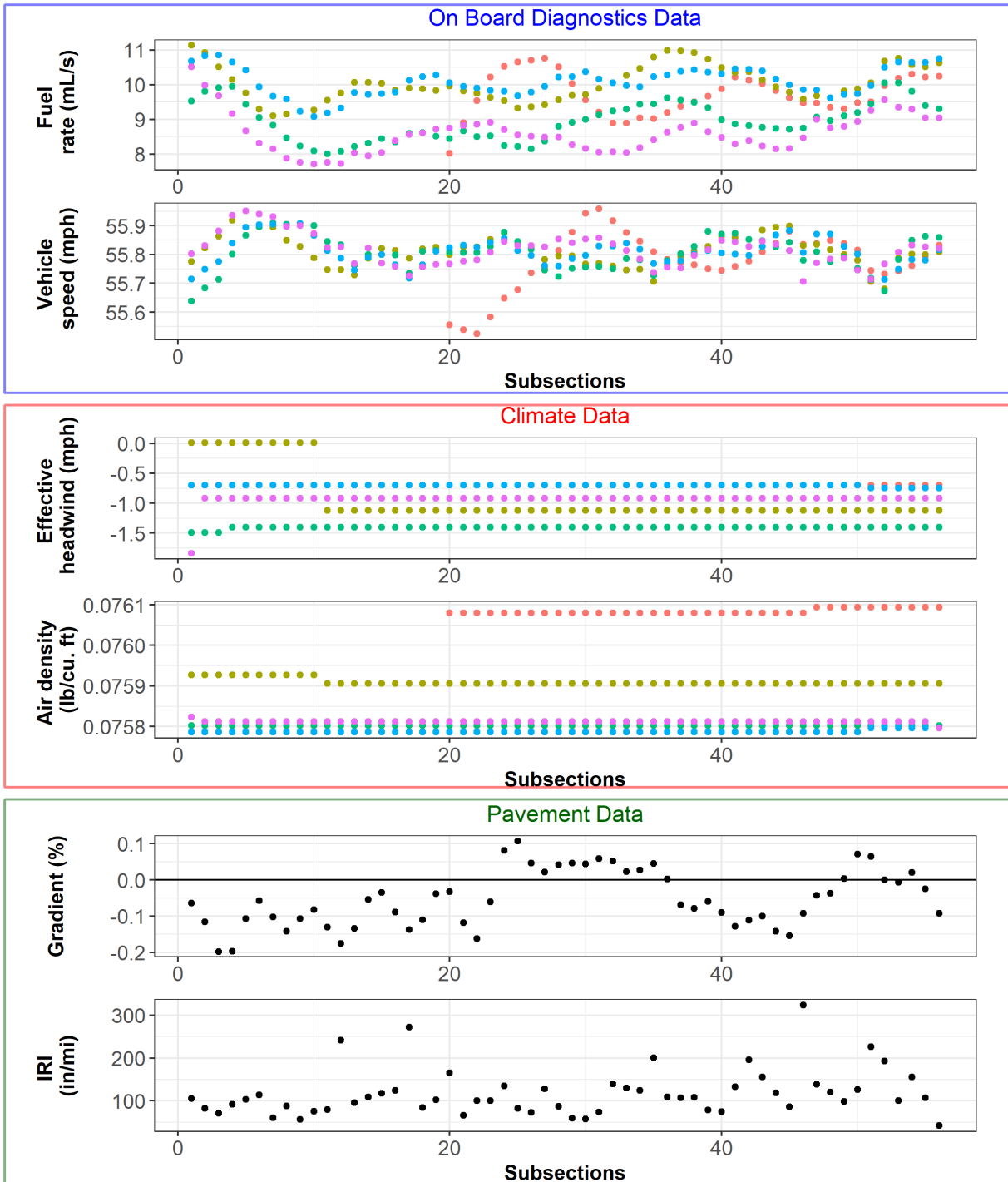


Figure P.339: HHDT data on Section PH14.

PH15-YOL-CR32BE-HMA HHDT summer_day 35 mph

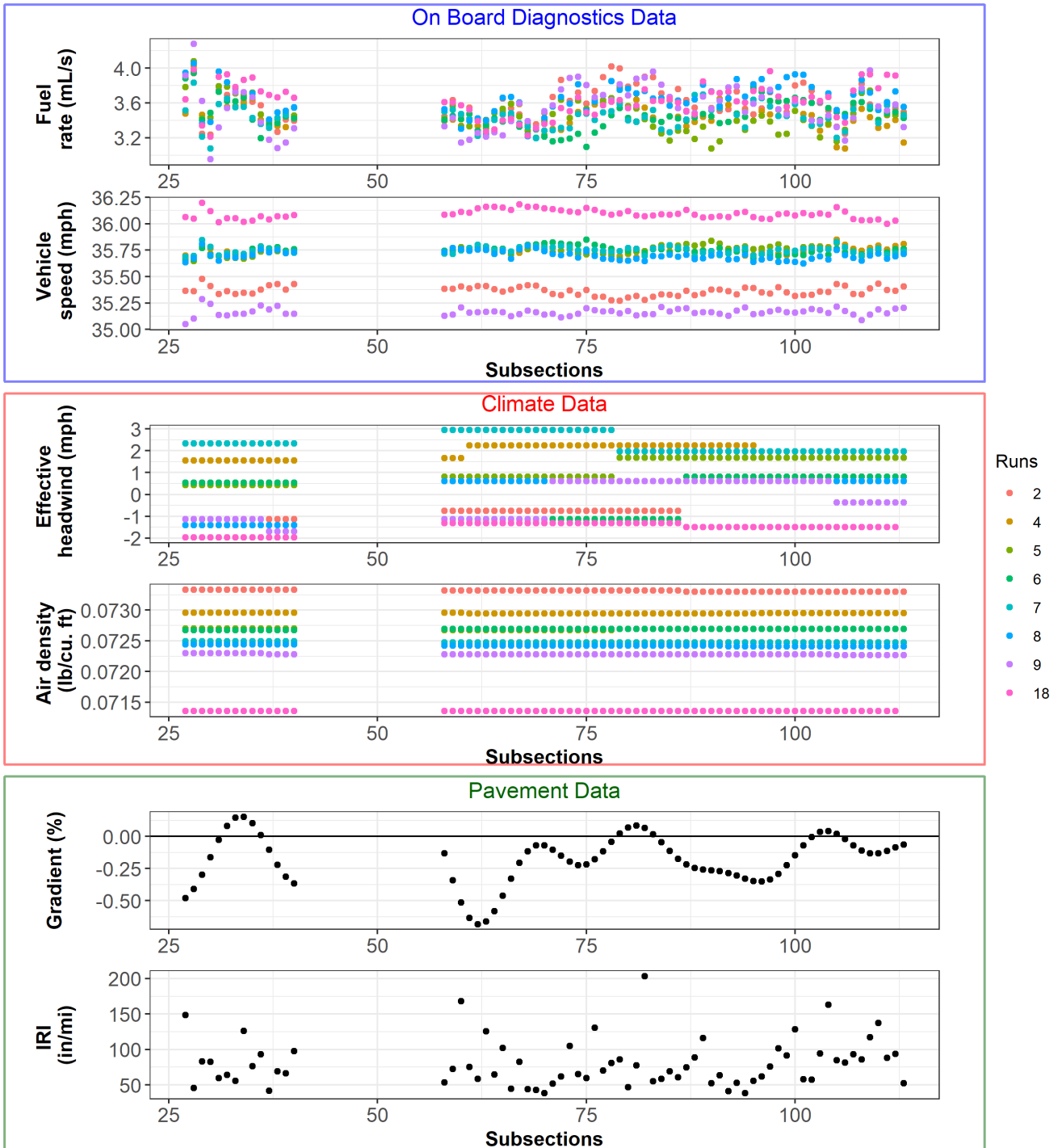


Figure P.340: HHDT data on Section PH15.

PH15-YOL-CR32BE-HMA HHDT summer_day 45 mph

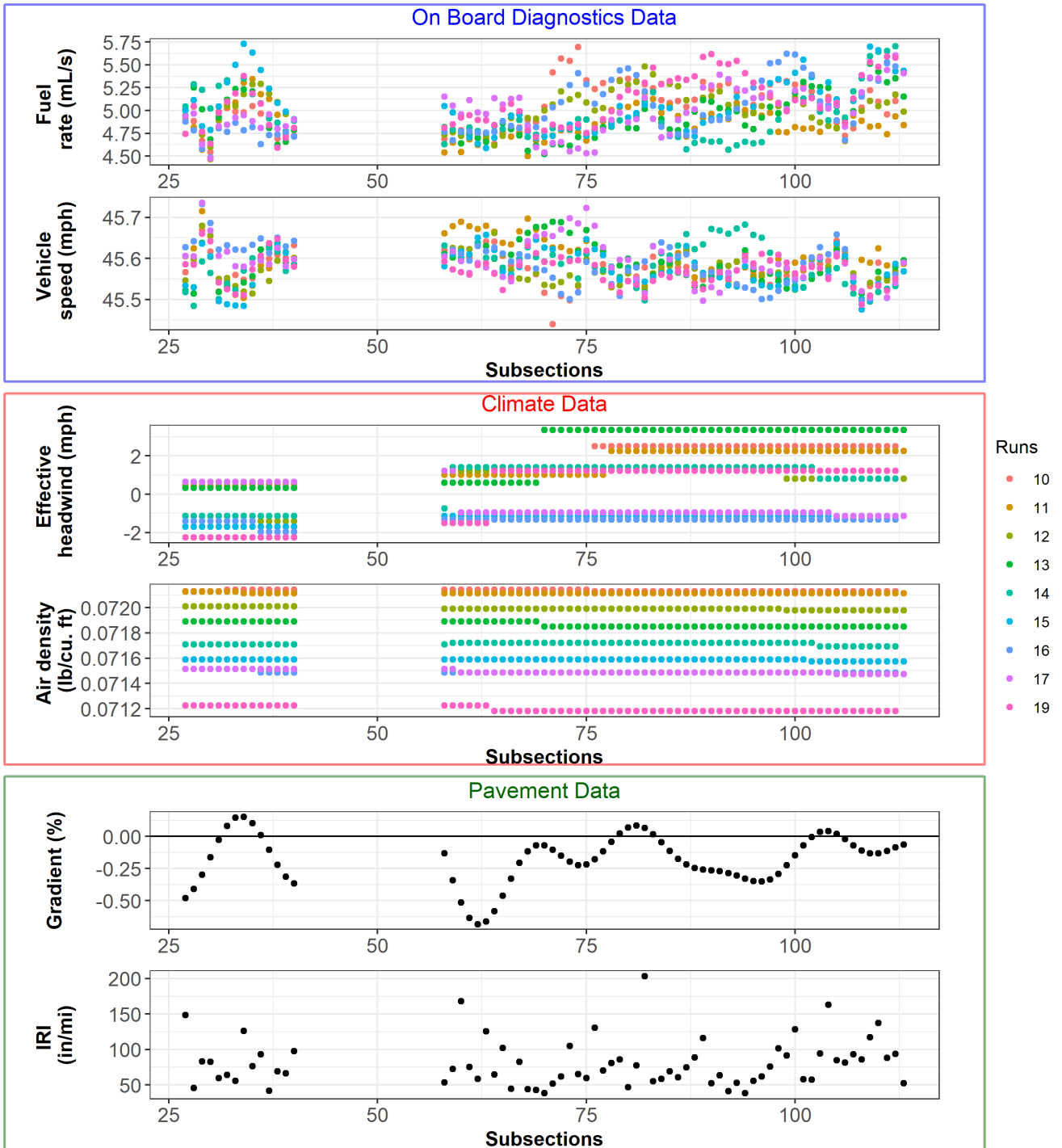


Figure P.341: HHDT data on Section PH15.

PH15-YOL-CR32BE-HMA HHDT summer_night 35 mph

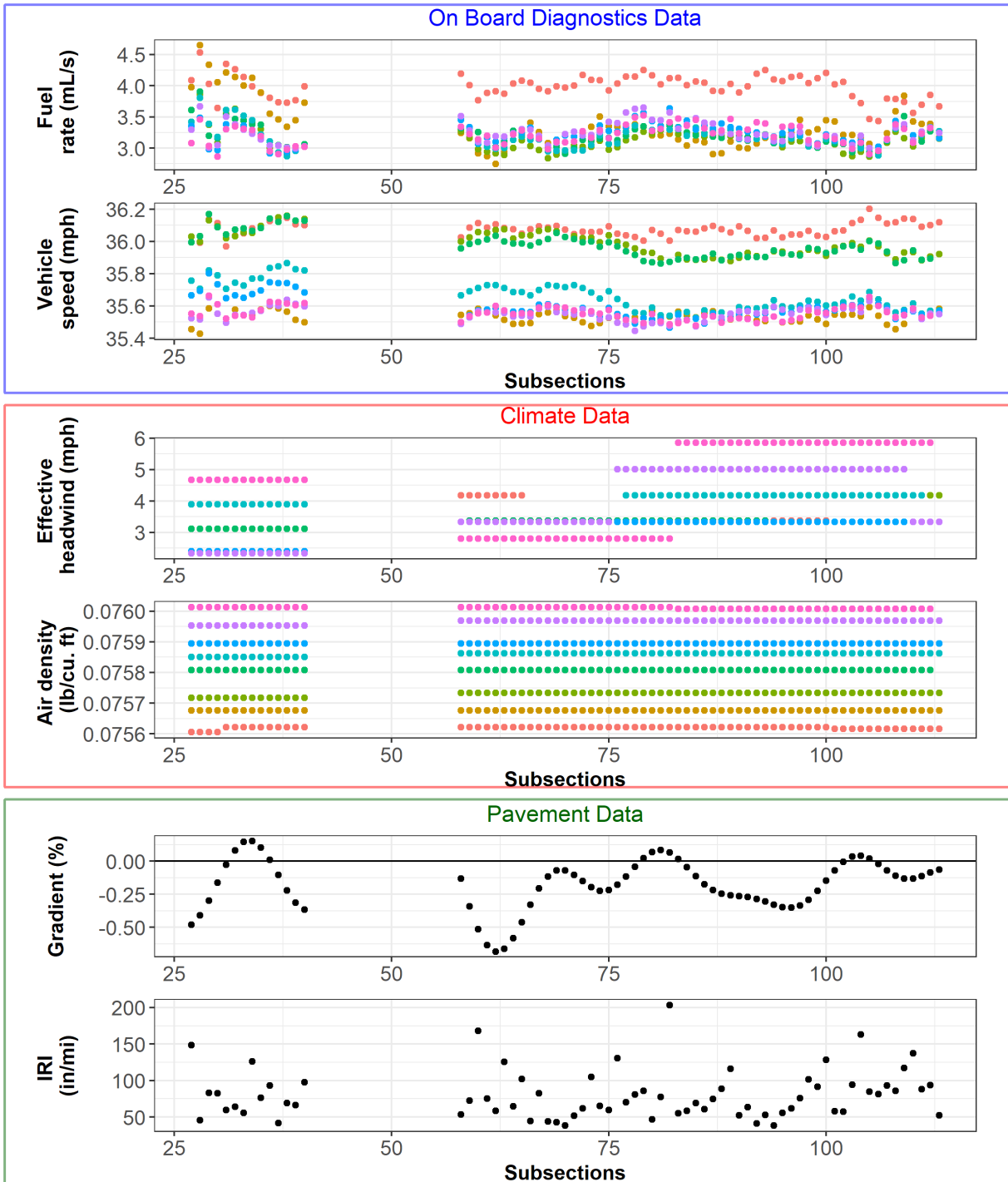


Figure P.342: HHDT data on Section PH15.

PH15-YOL-CR32BE-HMA HHDt summer_night 45 mph

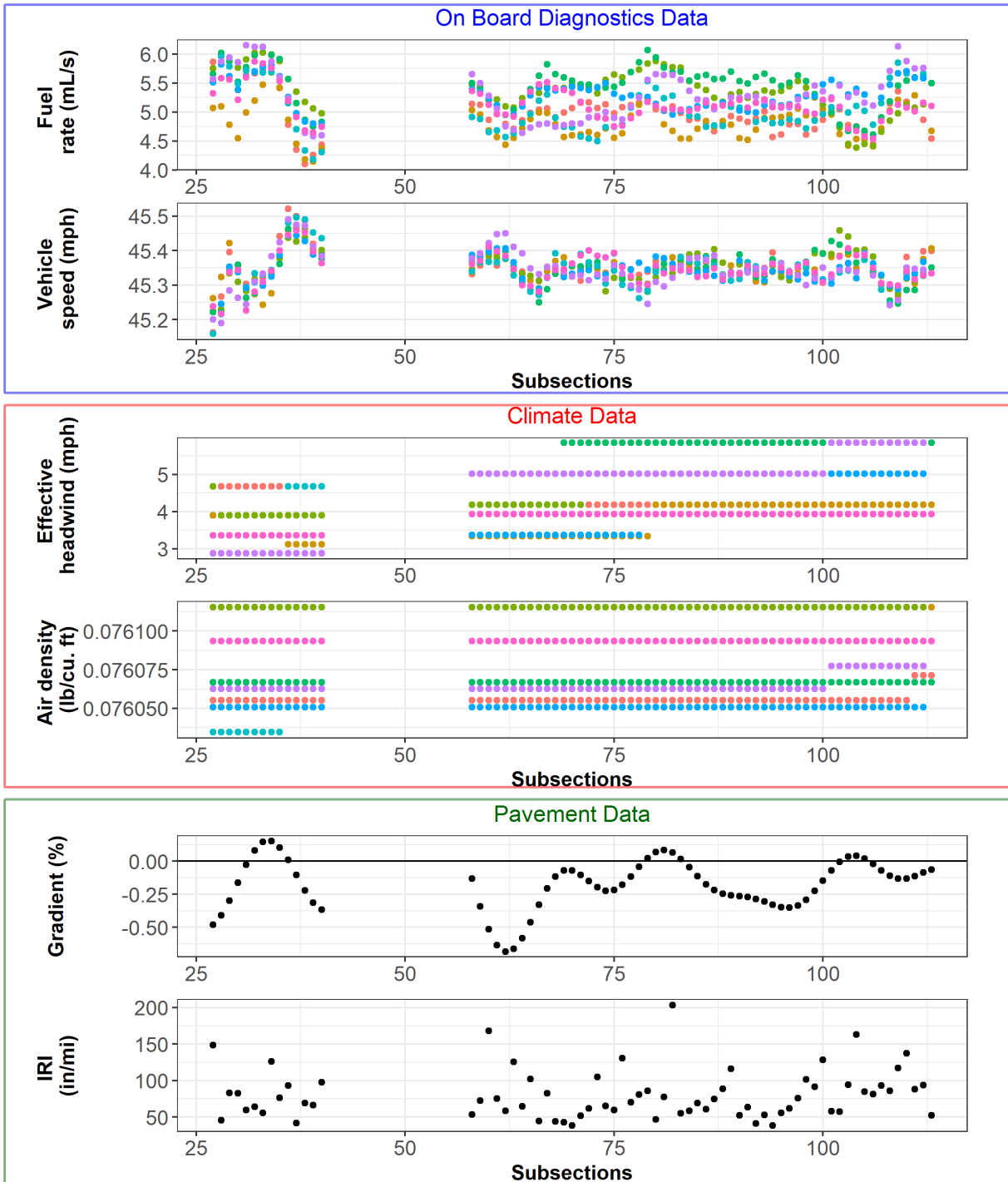


Figure P.343: HHDt data on Section PH15.

PH15-YOL-CR32BE-HMA HHDT winter_day 35 mph

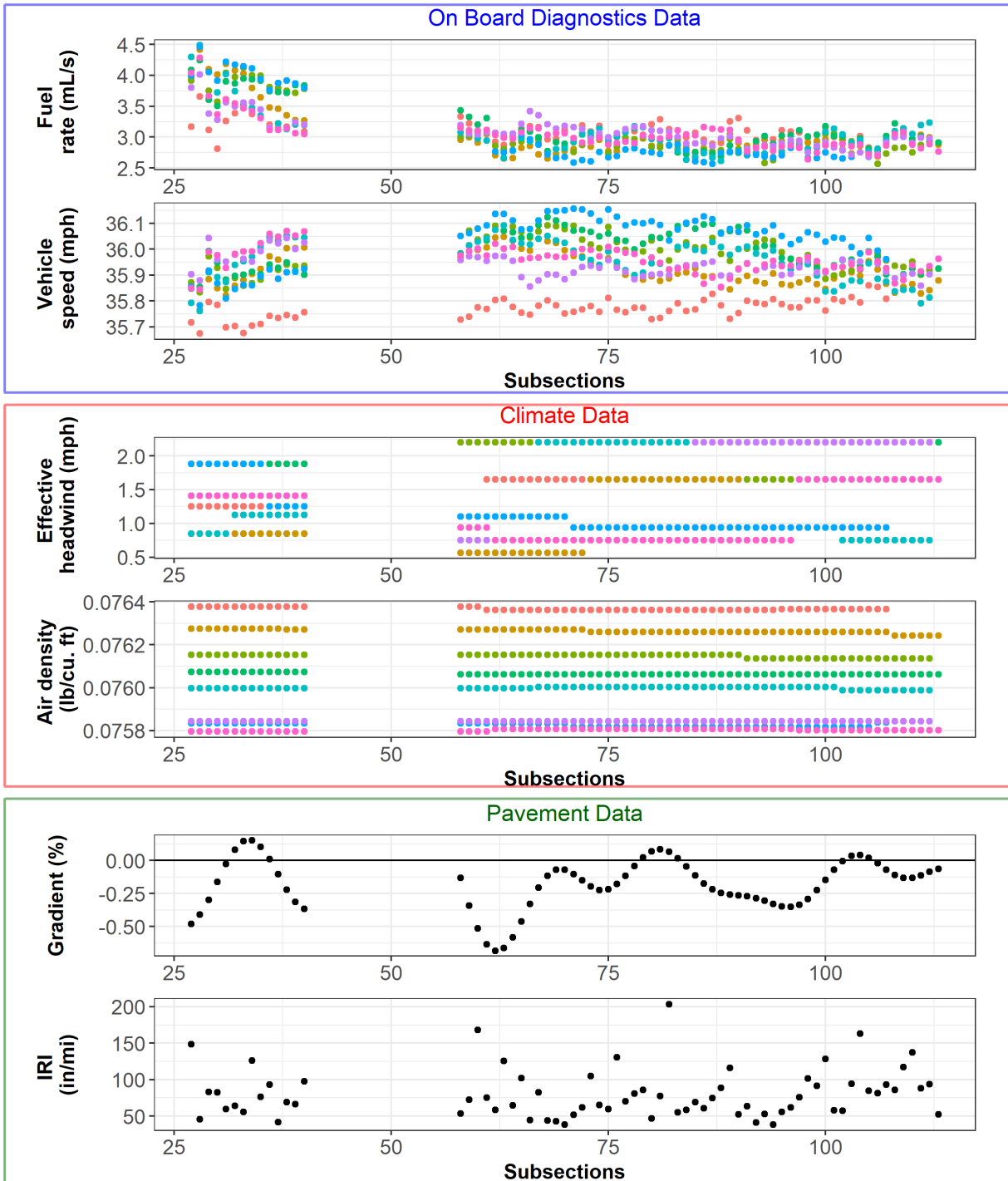


Figure P.344: HHDT data on Section PH15.

PH15-YOL-CR32BE-HMA HHDT winter_day 45 mph

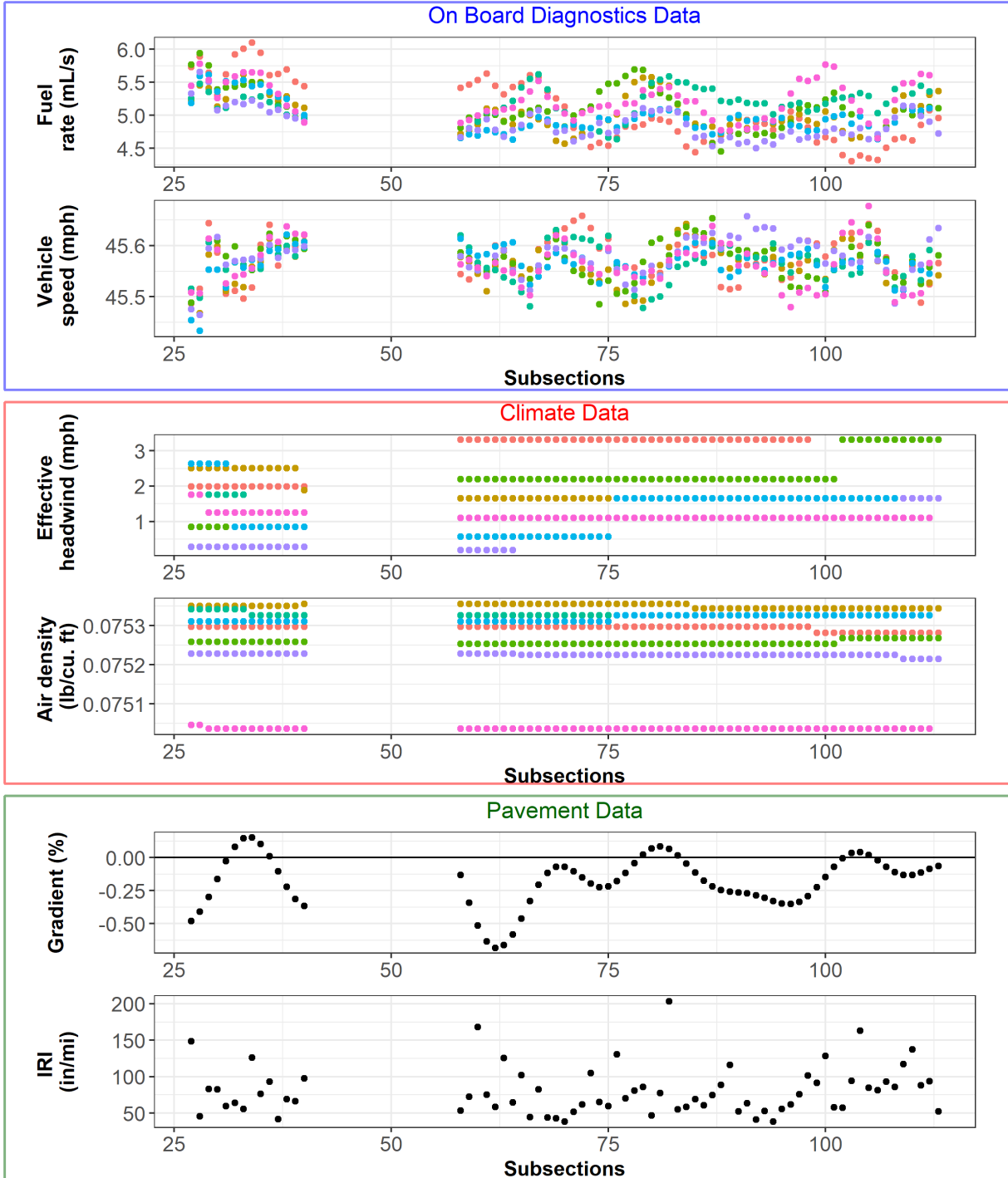


Figure P.345: HHDT data on Section PH15.

PH16-STA132E-RHMA-G HHDt summer_day 45 mph

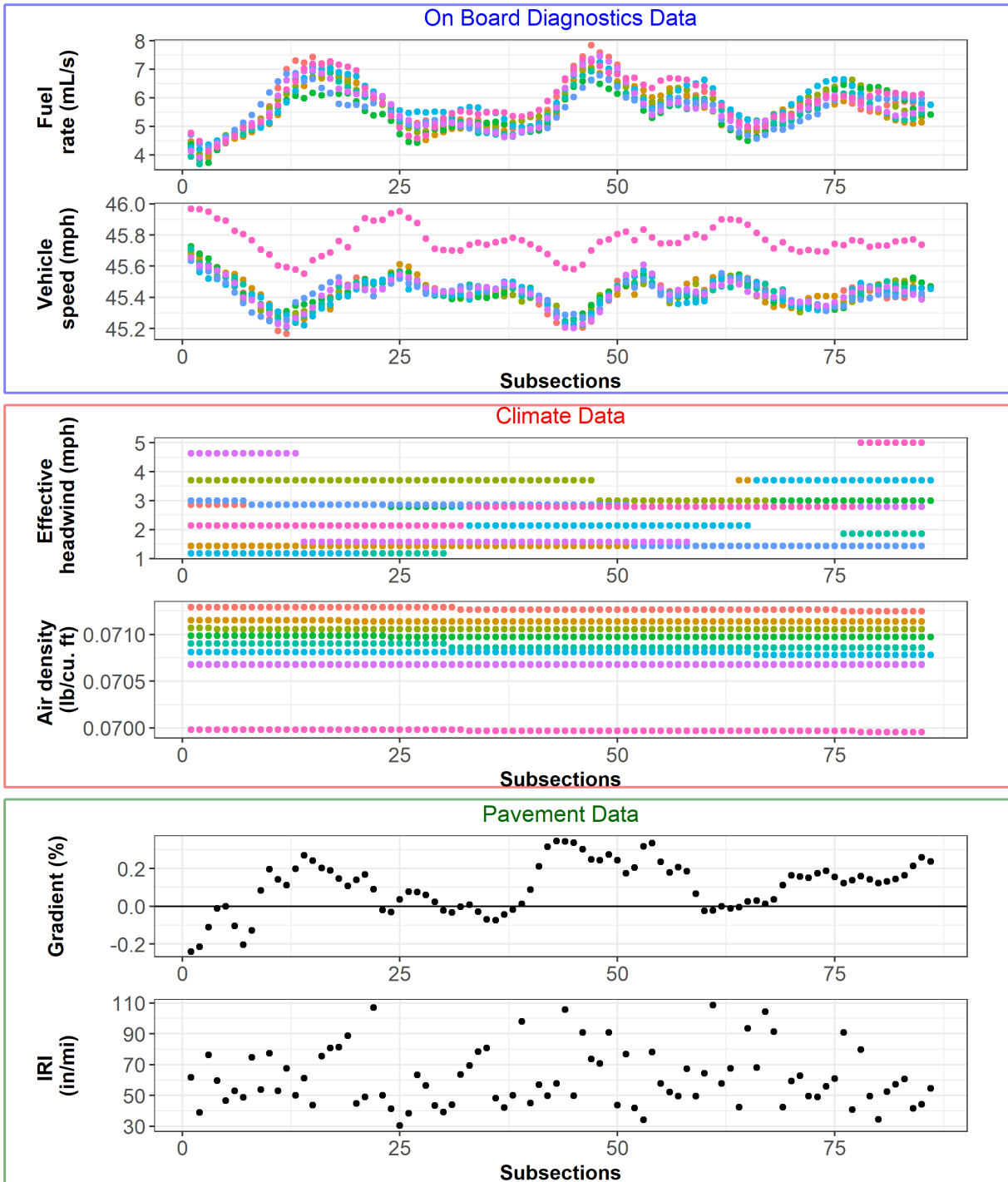


Figure P.346: HHDt data on Section PH16.

PH16-STA132E-RHMA-G HHDt summer_day 55 mph

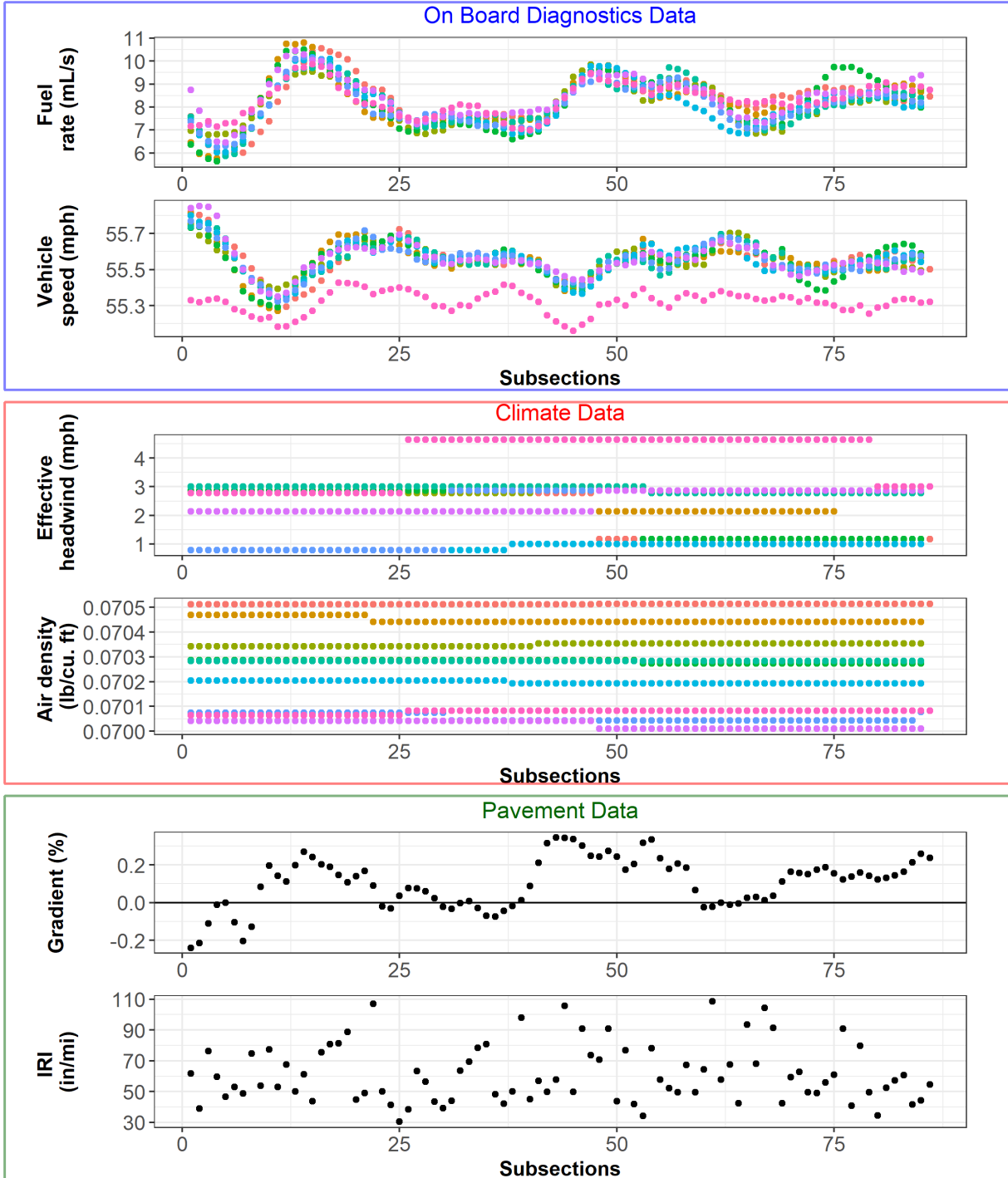


Figure P.347: HHDt data on Section PH16.

PH16-STA132E-RHMA-G HHDt winter_day 45 mph

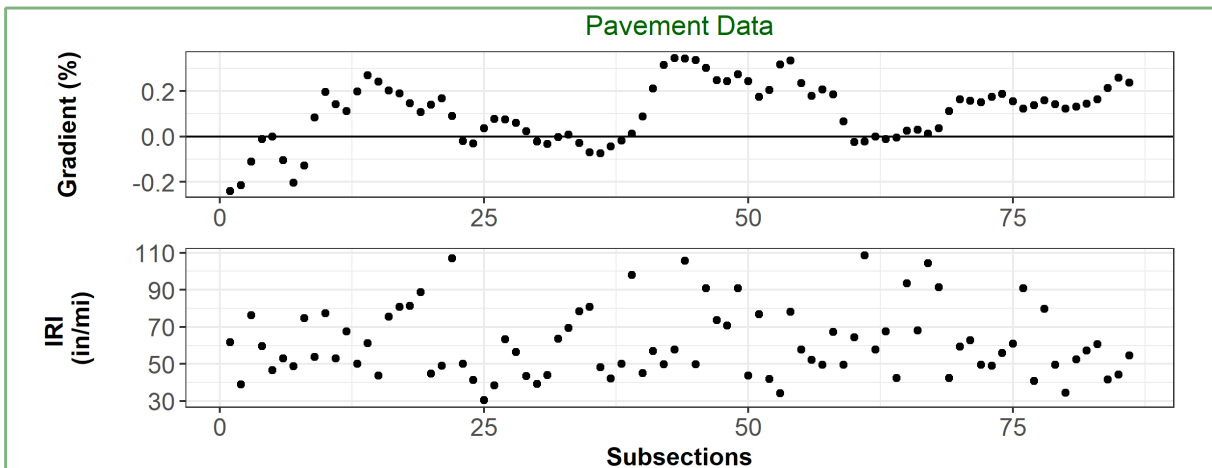
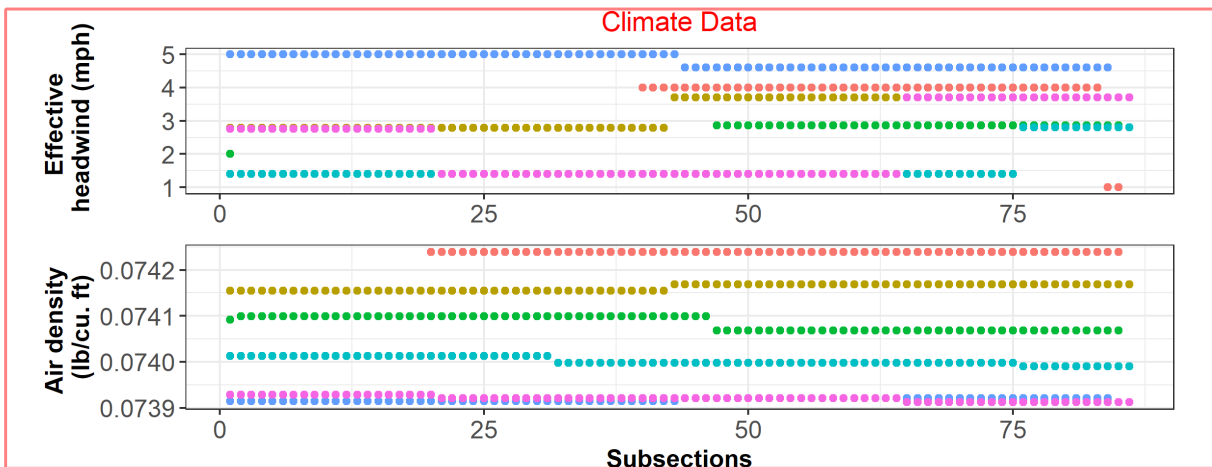
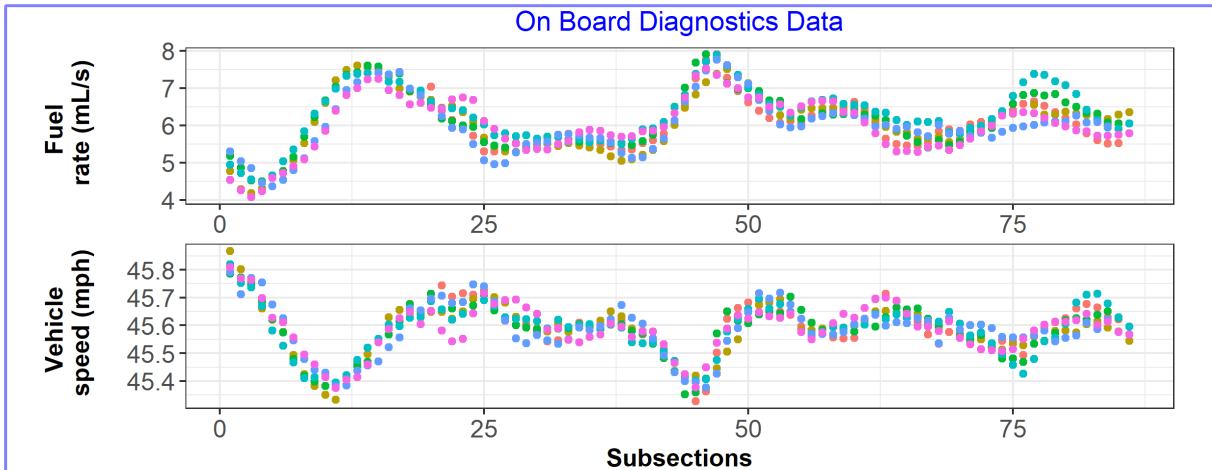


Figure P.348: HHDt data on Section PH16.

PH16-STA132E-RHMA-G HHDt winter_day 55 mph

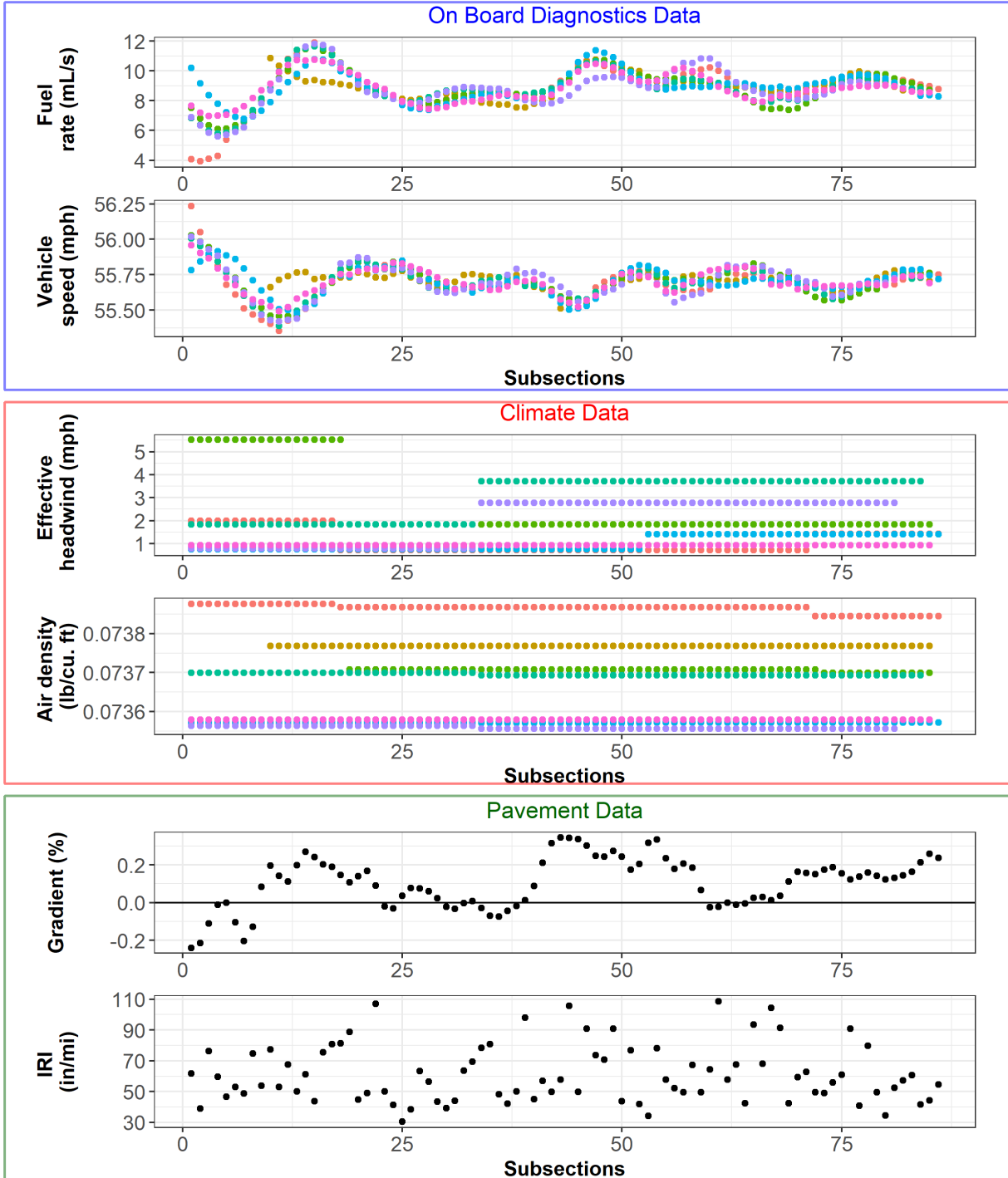


Figure P.349: HHDt data on Section PH16.

PH17-STA132W-RHMA-G HHDT summer_day 45 mph

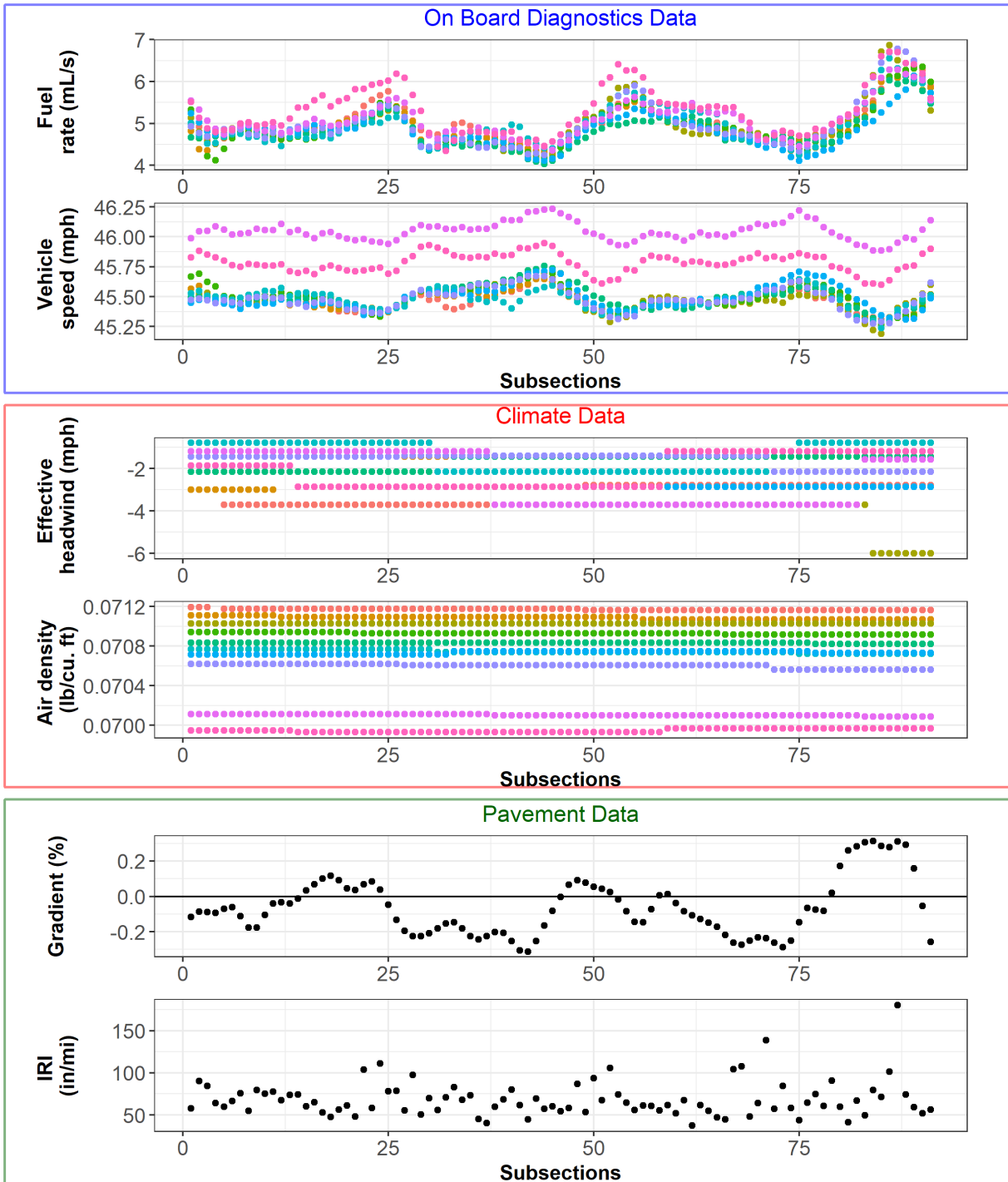


Figure P.350: HHDT data on Section PH17.

PH17-STA132W-RHMA-G HHDT summer_day 55 mph

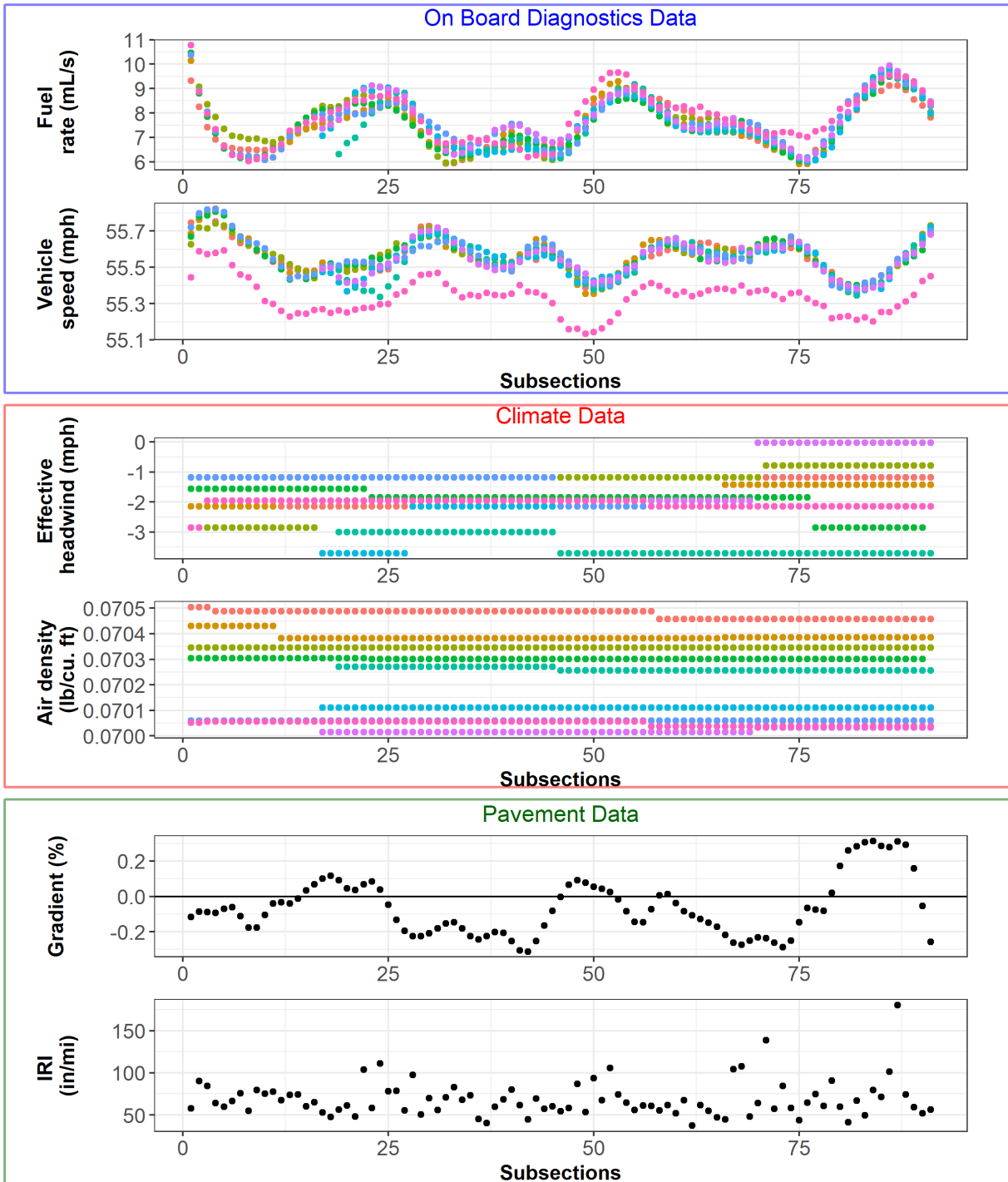


Figure P.351: HHDT data on Section PH17.

PH17-STA132W-RHMA-G HHDT winter_day 45 mph

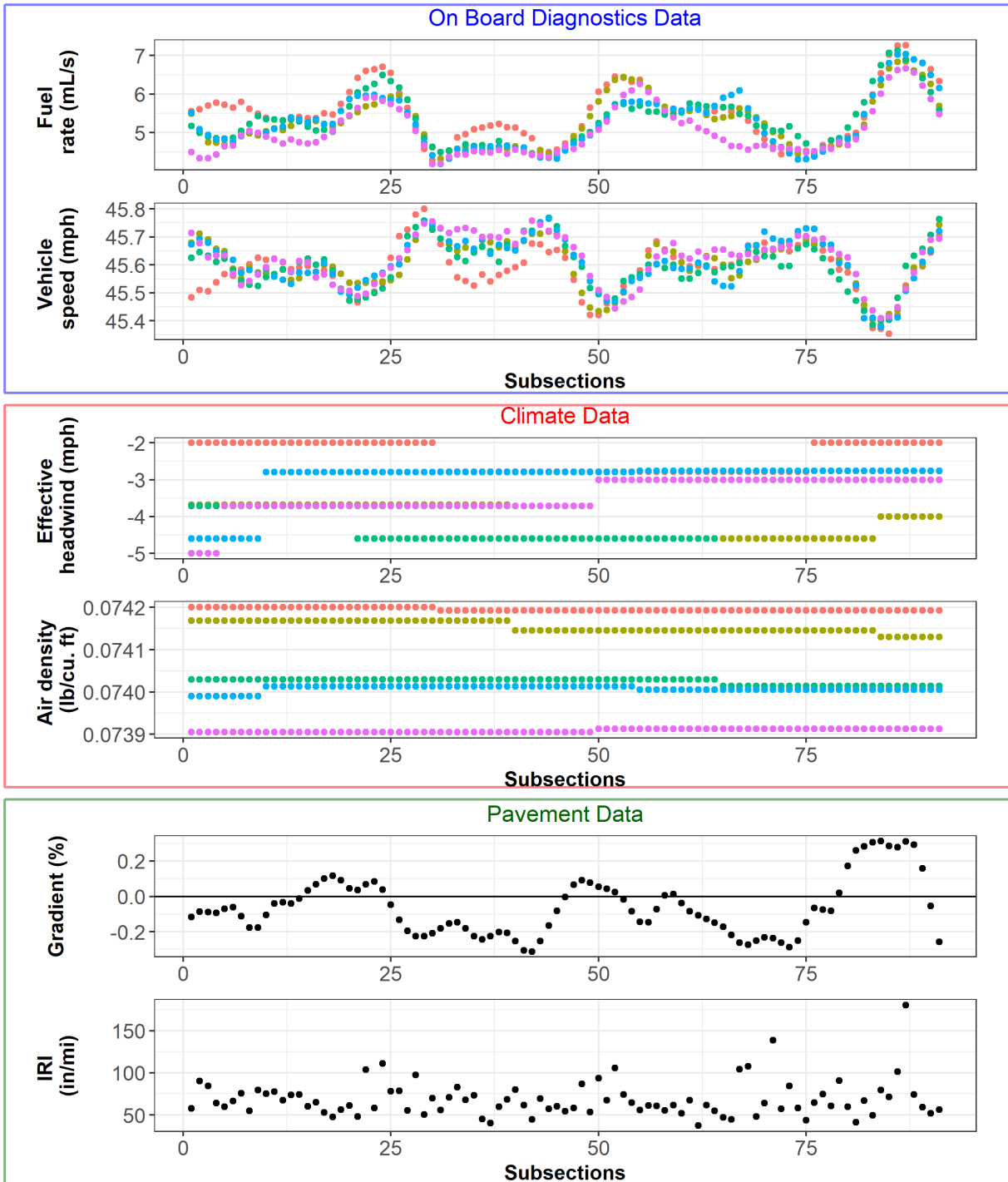


Figure P.352: HHDT data on Section PH17.

PH17-STA132W-RHMA-G HHDT winter_day 55 mph

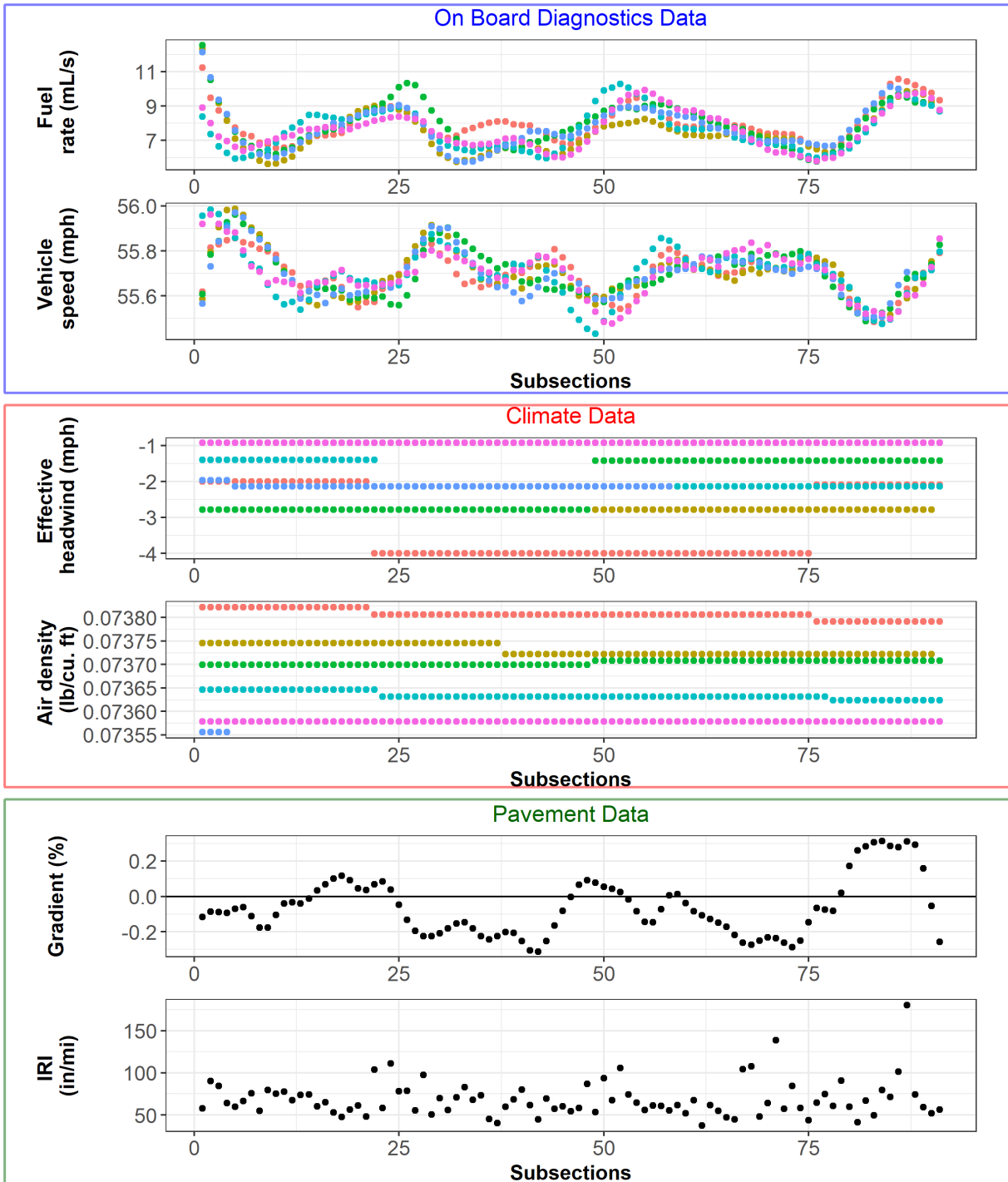


Figure P.353: HHDT data on Section PH17.

PH18-KER5S-HMA-O HHDT summer_day 45 mph

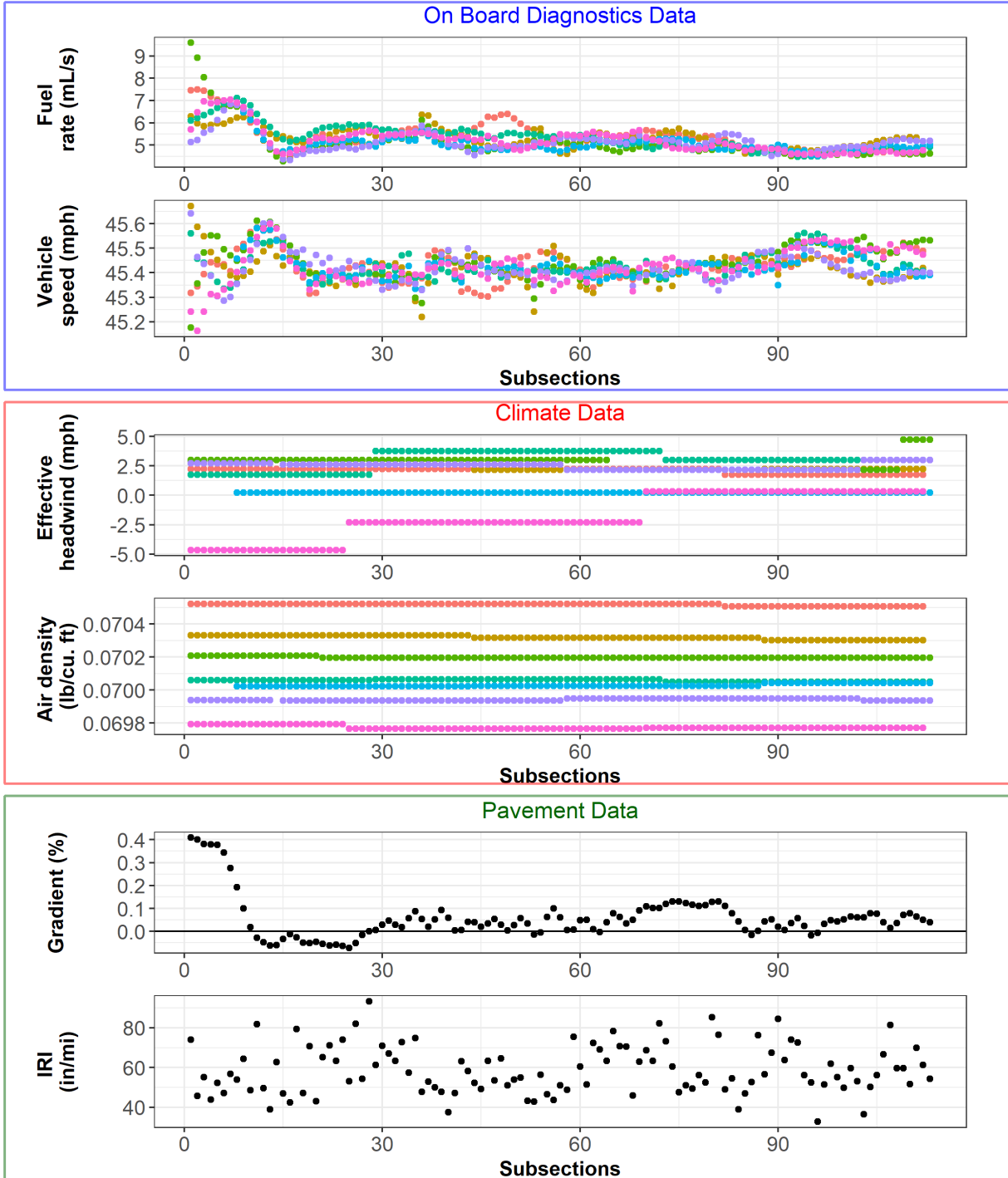


Figure P.354: HHDT data on Section PH18.

PH18-KER5S-HMA-O HHDT summer_day 55 mph

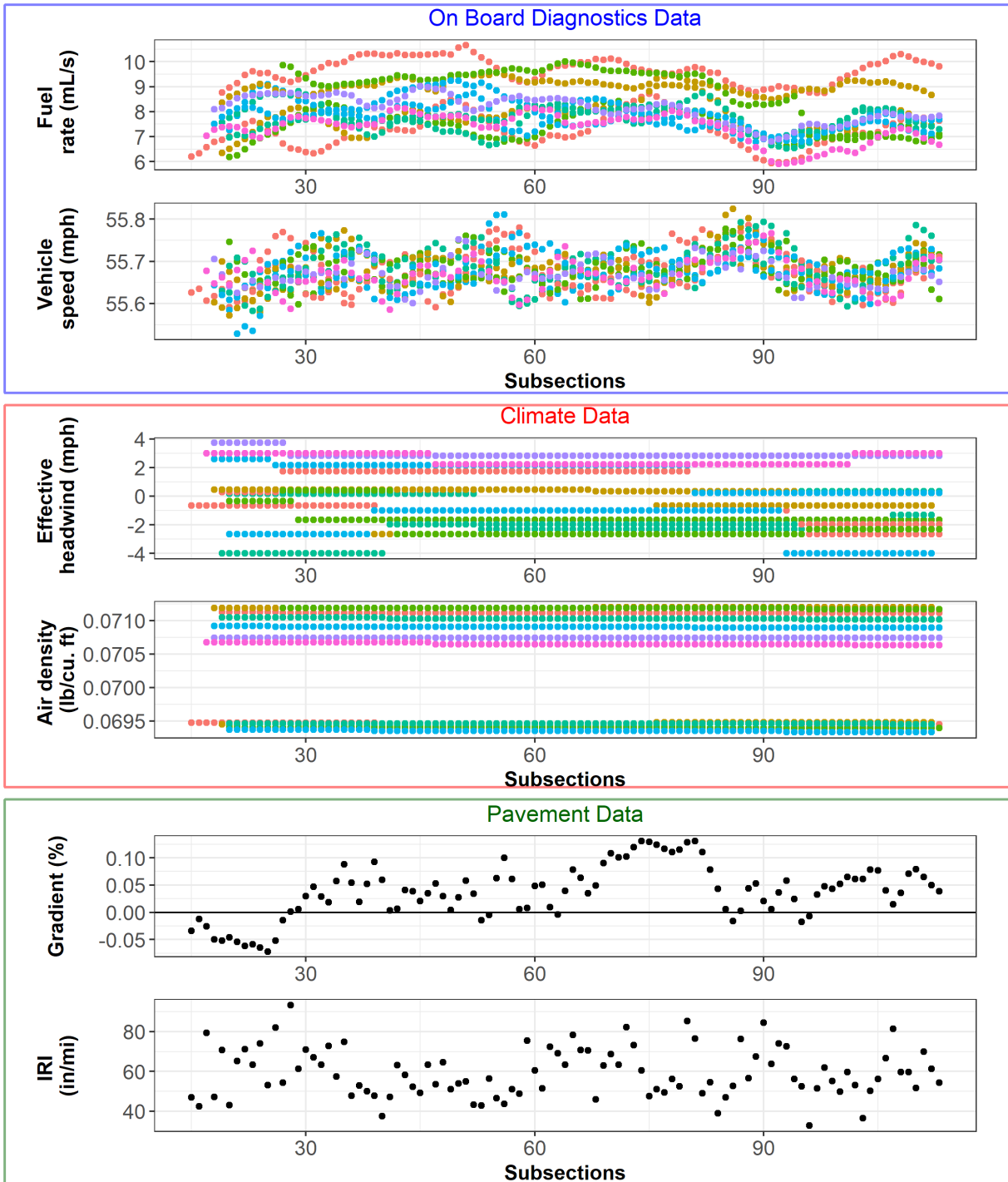


Figure P.355: HHDT data on Section PH18.

PH19-KER5N- RHMA-G HHDt summer_day 45 mph

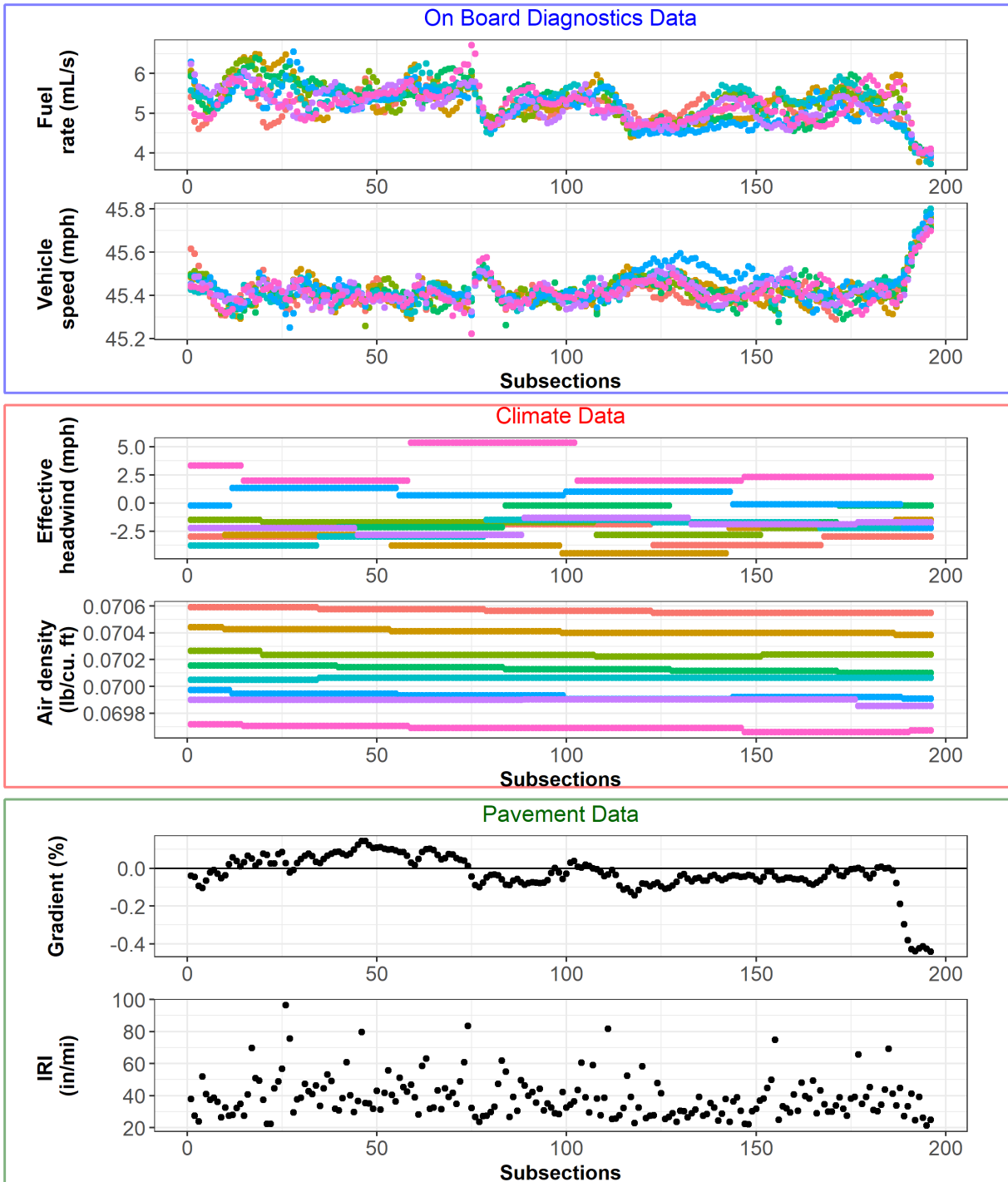


Figure P.356: HHDt data on Section PH19.

PH19-KER5N- RHMA-G HHDt summer_day 55 mph

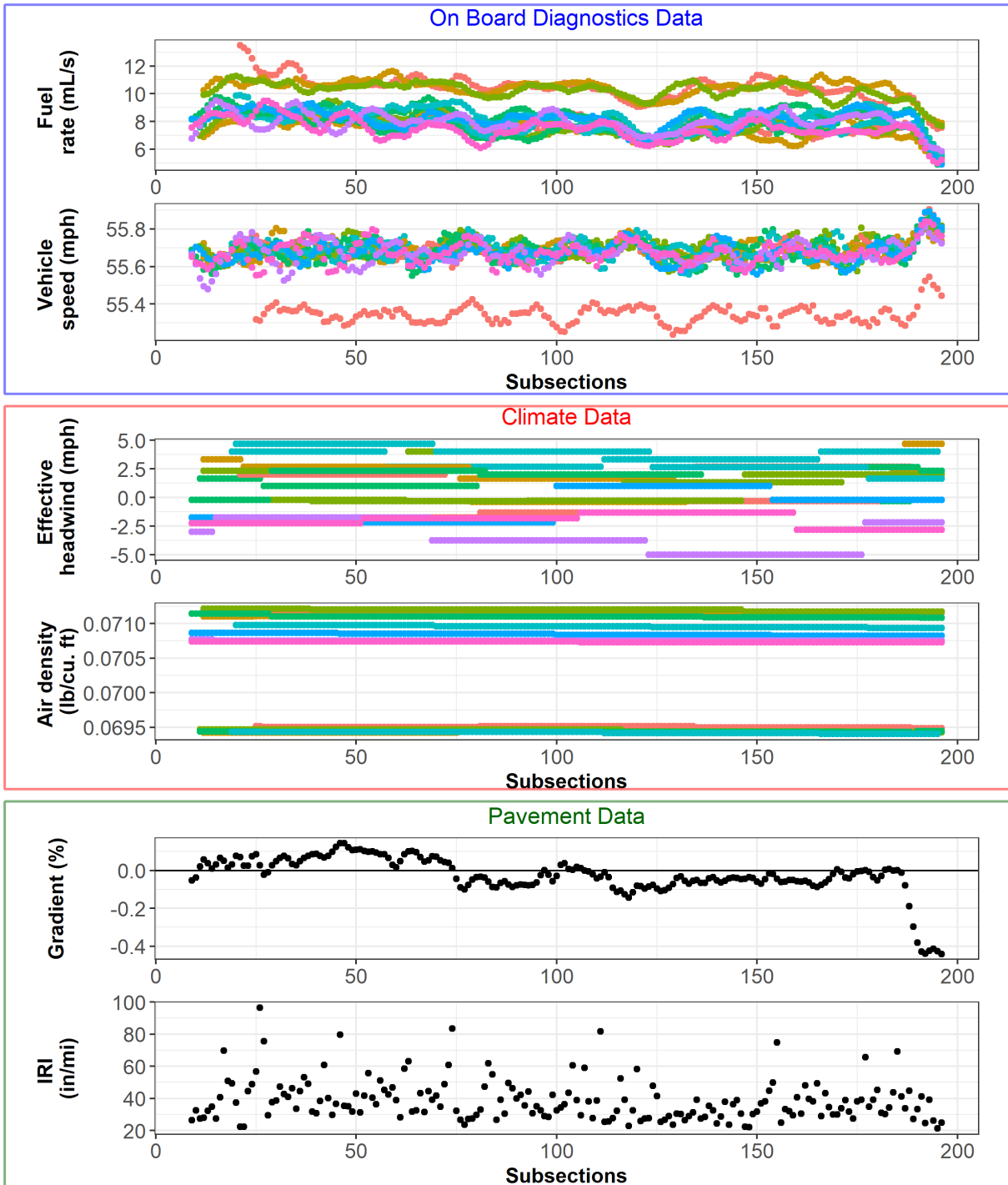


Figure P.357: HHDt data on Section PH19.

PH20-KER5S-CRCP HHDТ summer_day 45 mph

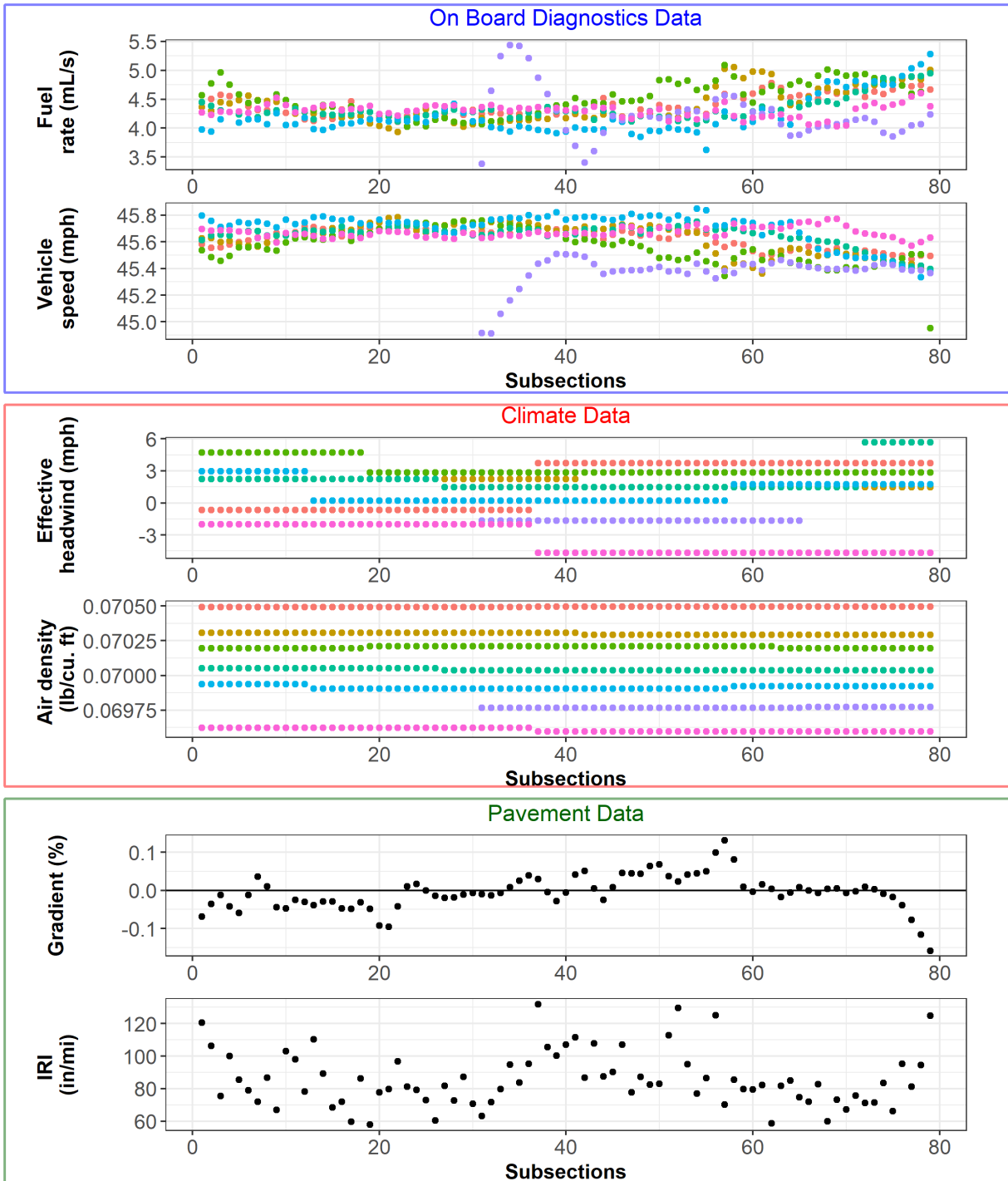


Figure P.358: HHDТ data on Section PH20.

PH20-KER5S-CRCP HHDt summer_day 55 mph

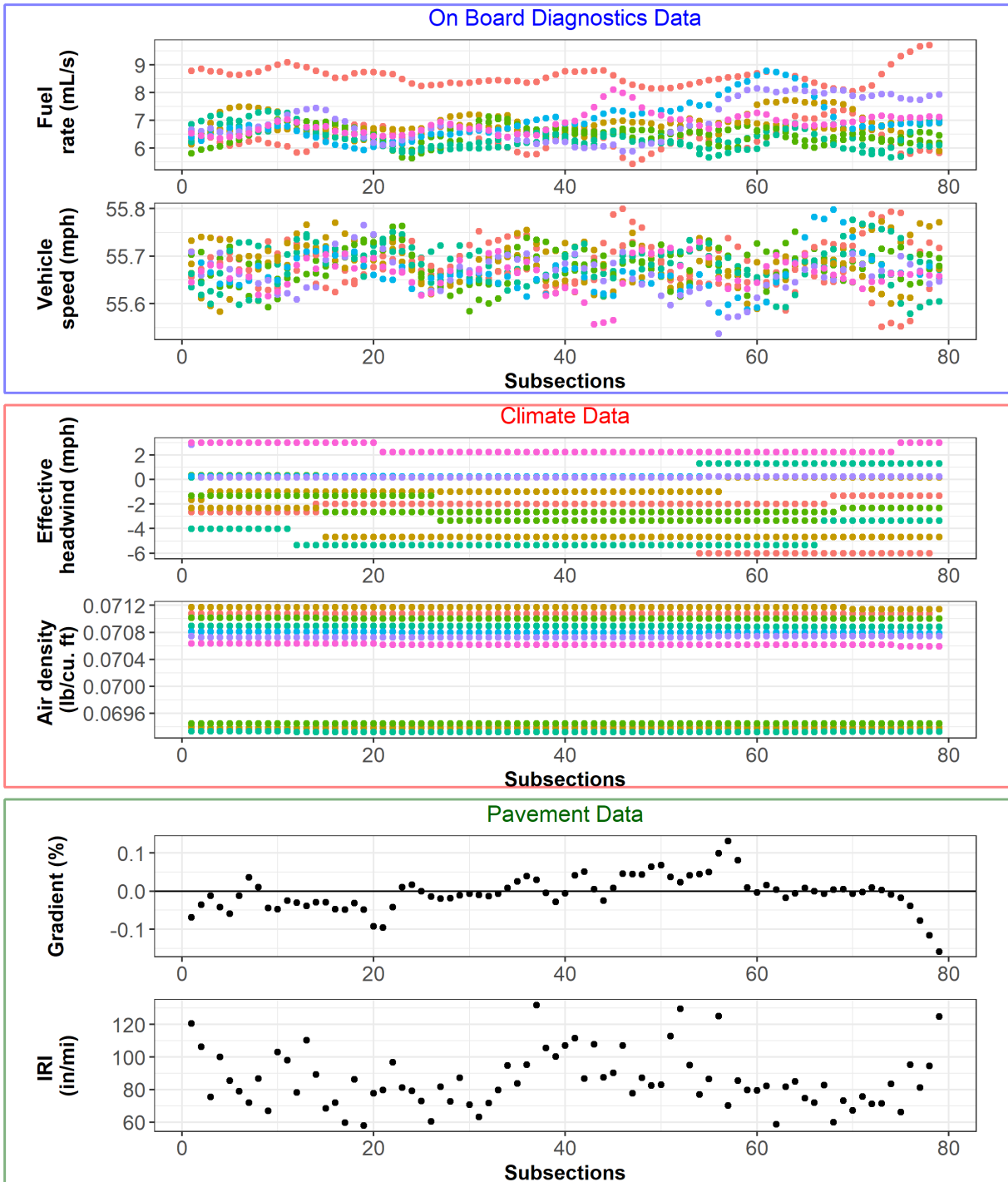


Figure P.359: HHDt data on Section PH20.

PH21-YOL99N-JPC HHDT summer_day 45 mph

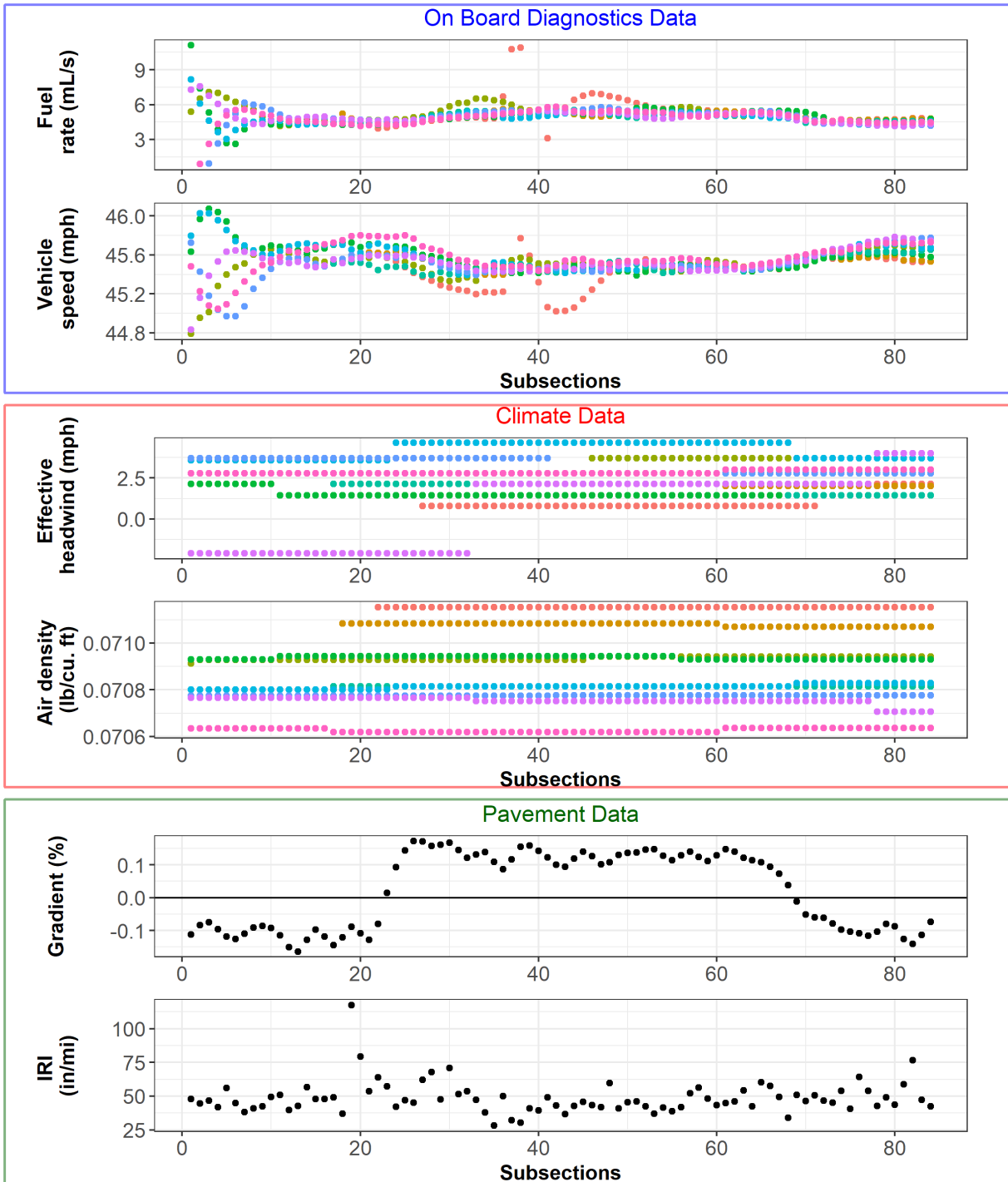


Figure P.360: HHDT data on Section PH21.

PH21-YOL99N-JPC HHDT summer_day 55 mph

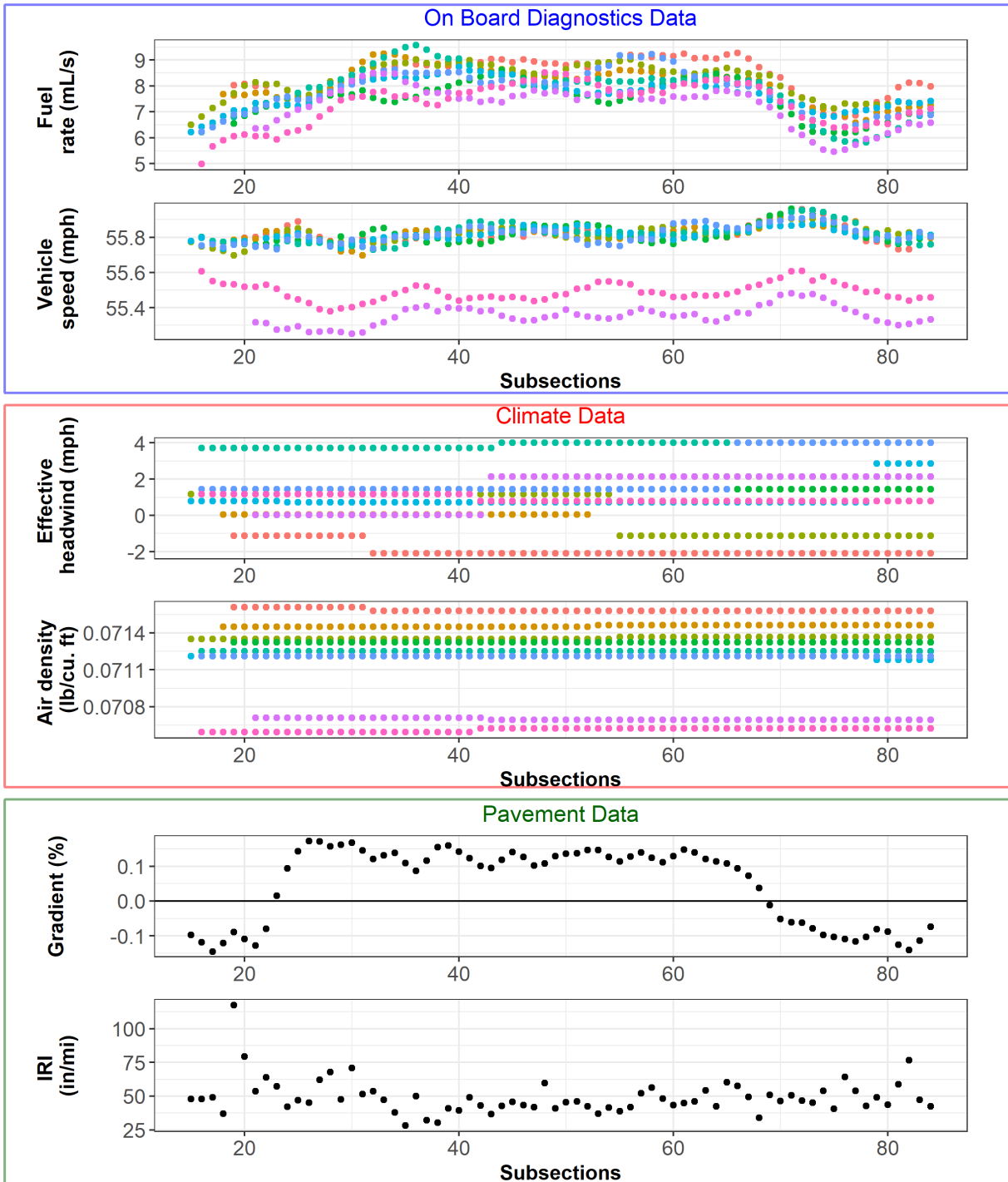


Figure P.361: HHDT data on Section PH21.

PH21-YOL99N-JPC HHDT winter_day 45 mph

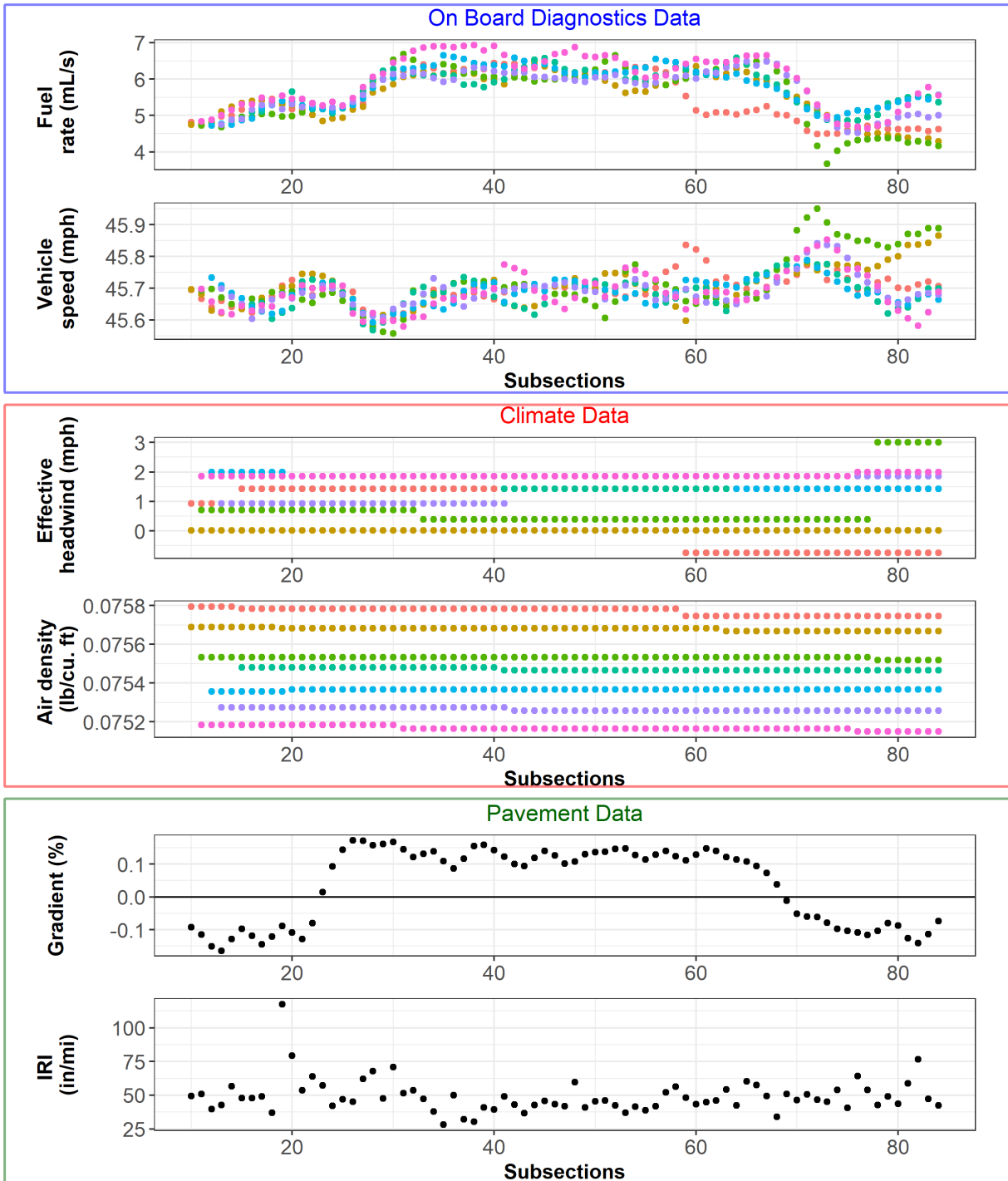


Figure P.362: HHDT data on Section PH21.

PH21-YOL99N-JPC HHDT winter_day 55 mph

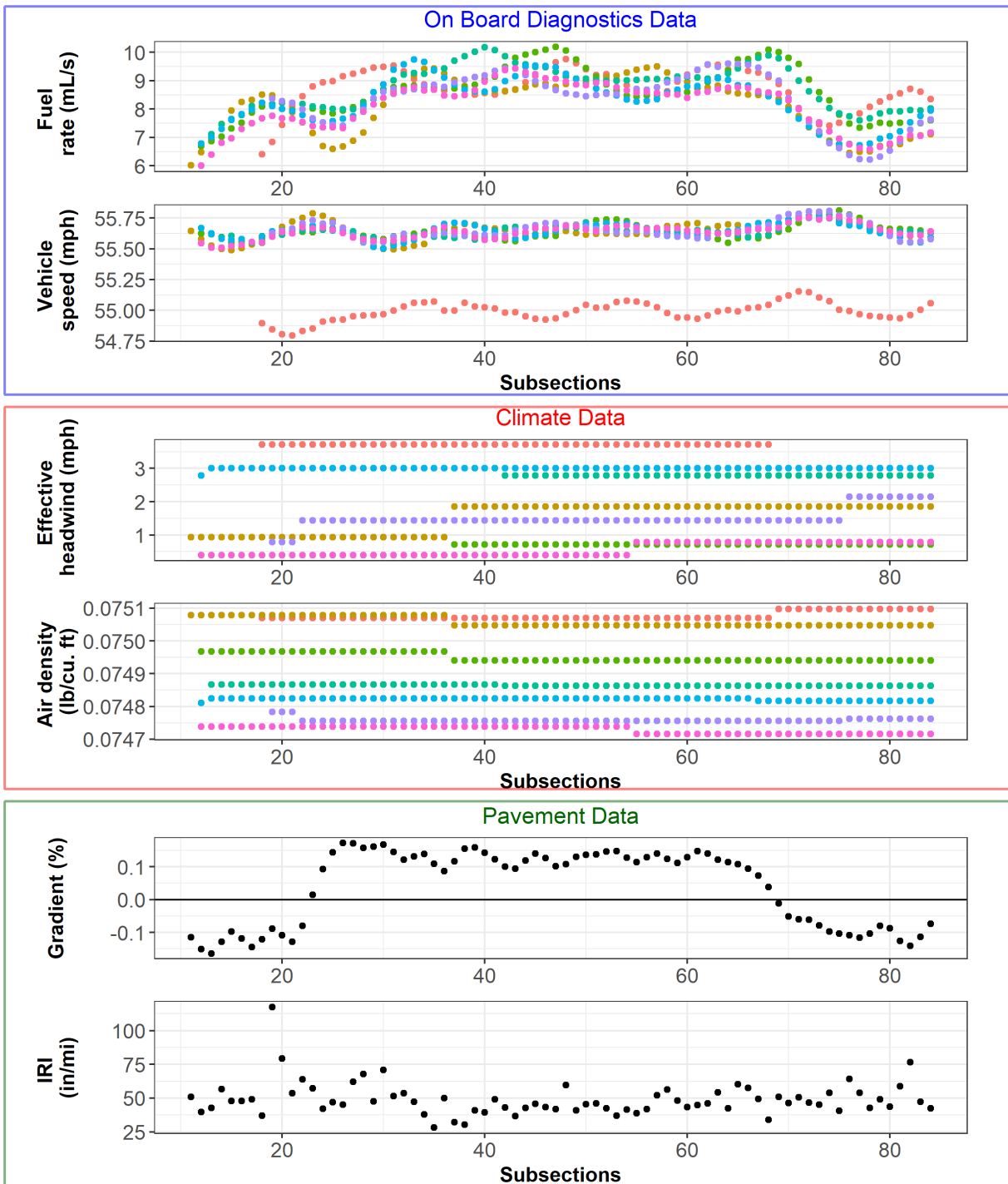


Figure P.363: HHDT data on Section PH21.

PH22-YOL99S-JPC HHDT summer_day 45 mph

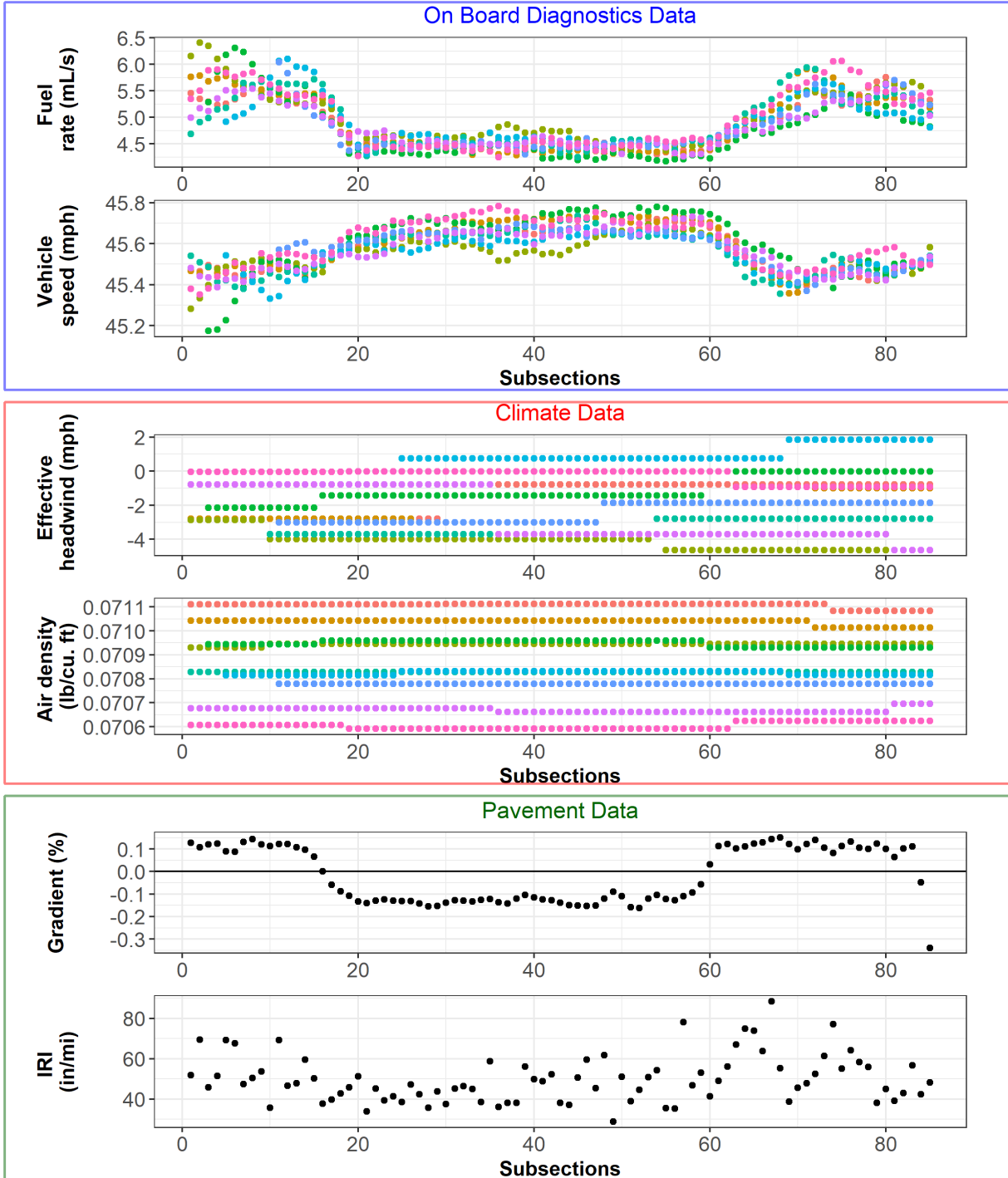


Figure P.364: HHDT data on Section PH22.

PH22-YOL99S-JPC HHDT summer_day 55 mph

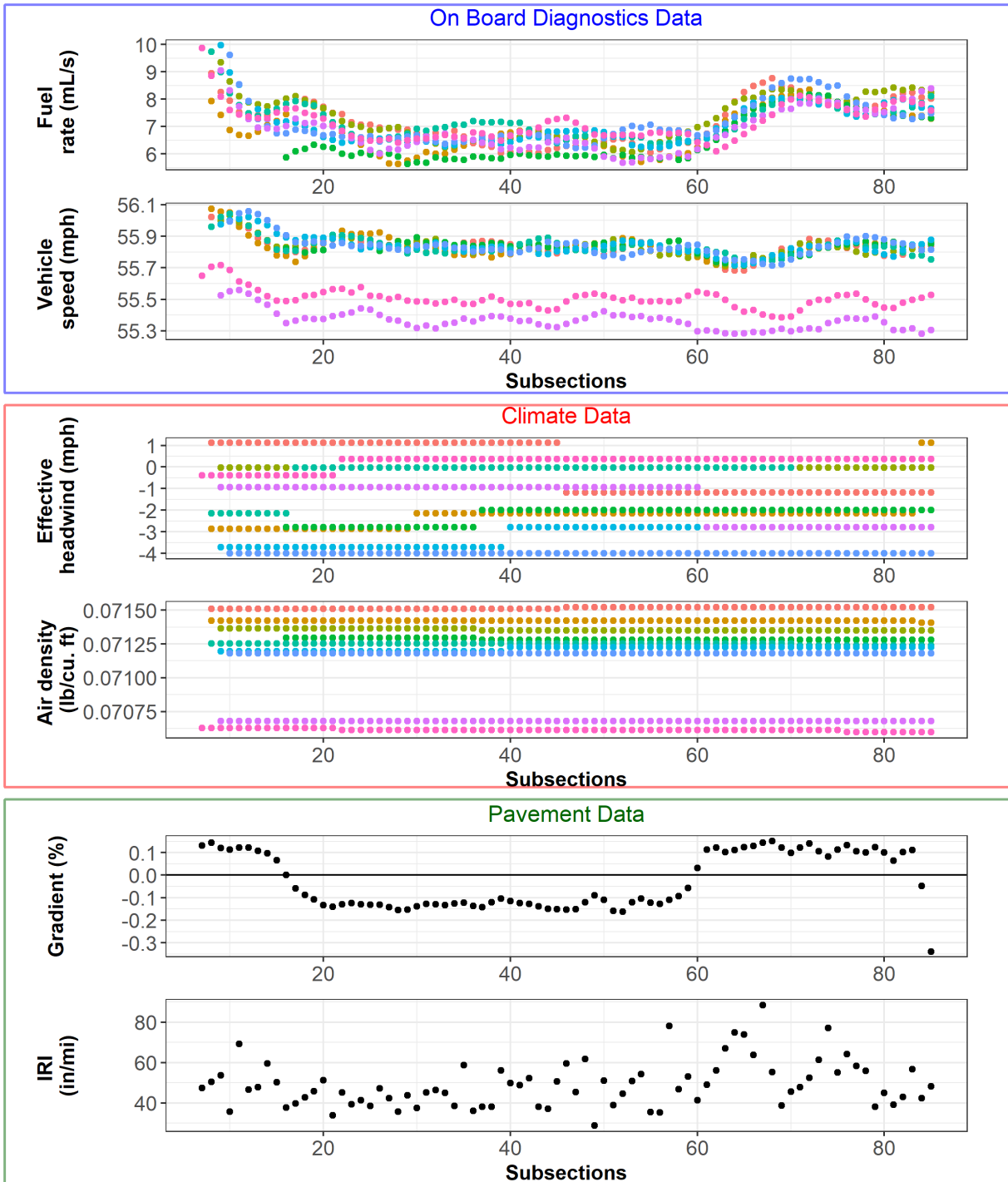


Figure P.365: HHDT data on Section PH22.

PH22-YOL99S-JPC HHDT winter_day 45 mph

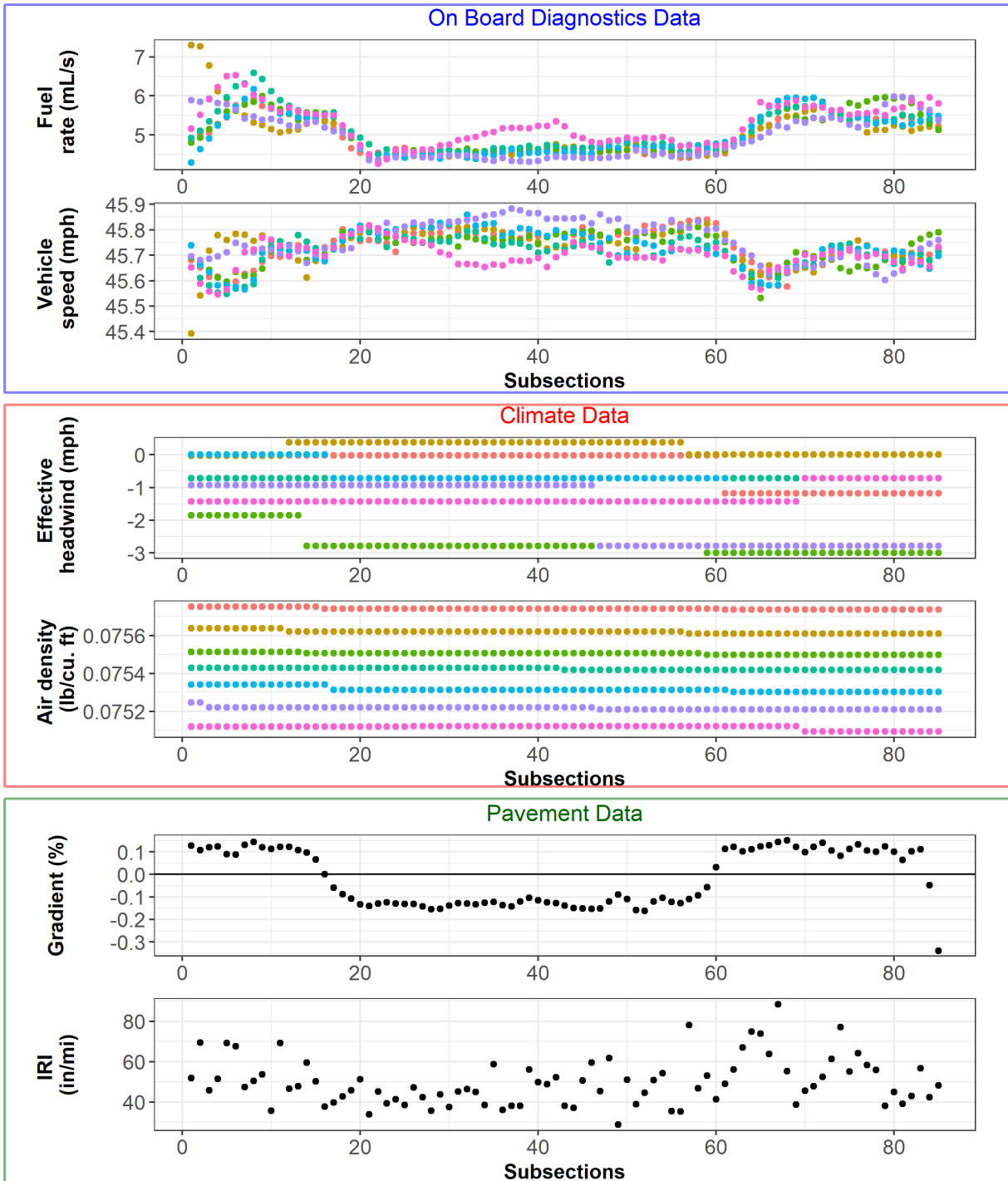


Figure P.366: HHDT data on Section PH22.

PH22-YOL99S-JPC HHDT winter_day 55 mph

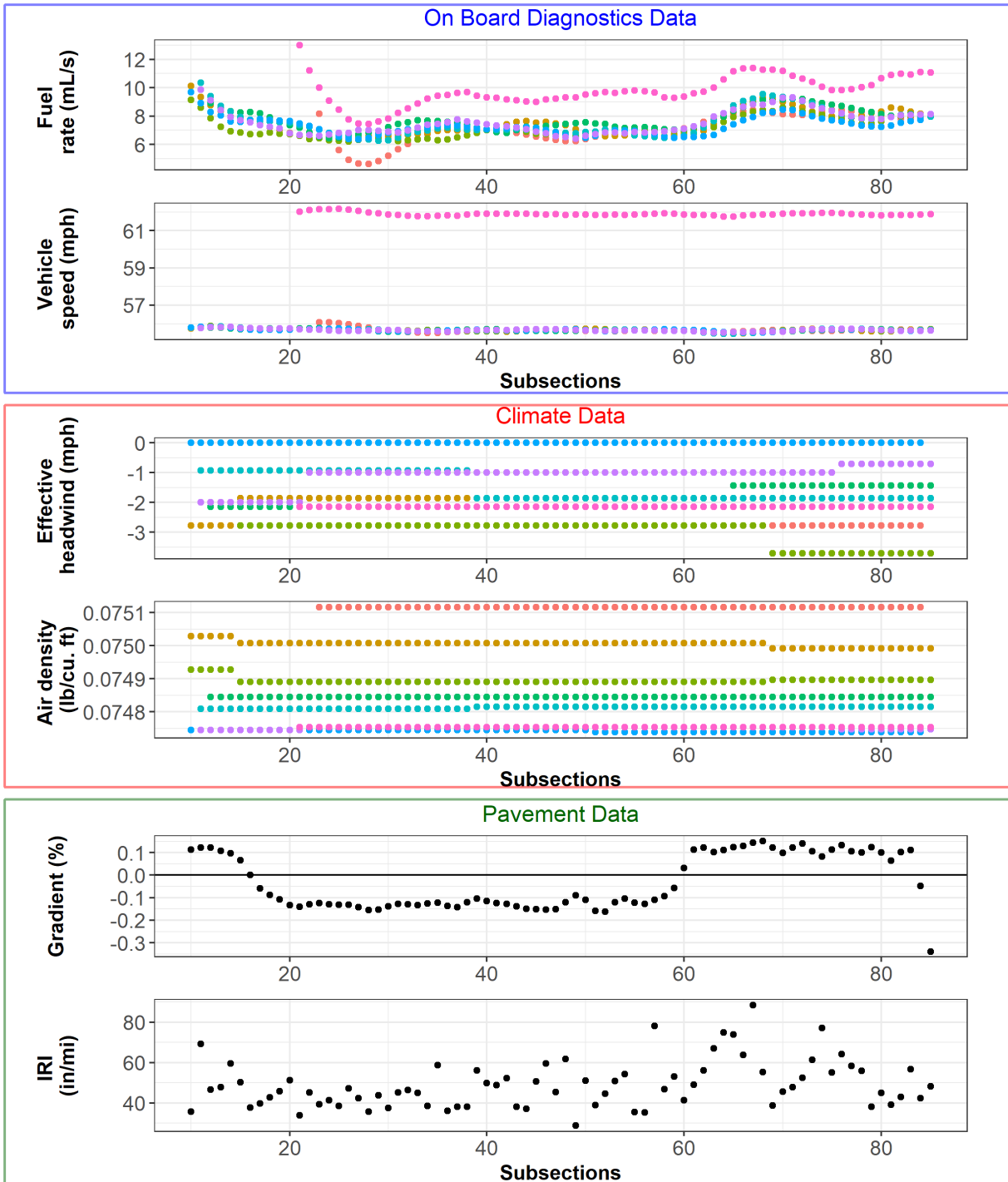


Figure P.367: HHDT data on Section PH22.

PH23-YOL-CR32AW-JPC HHDT summer_day 35 mph

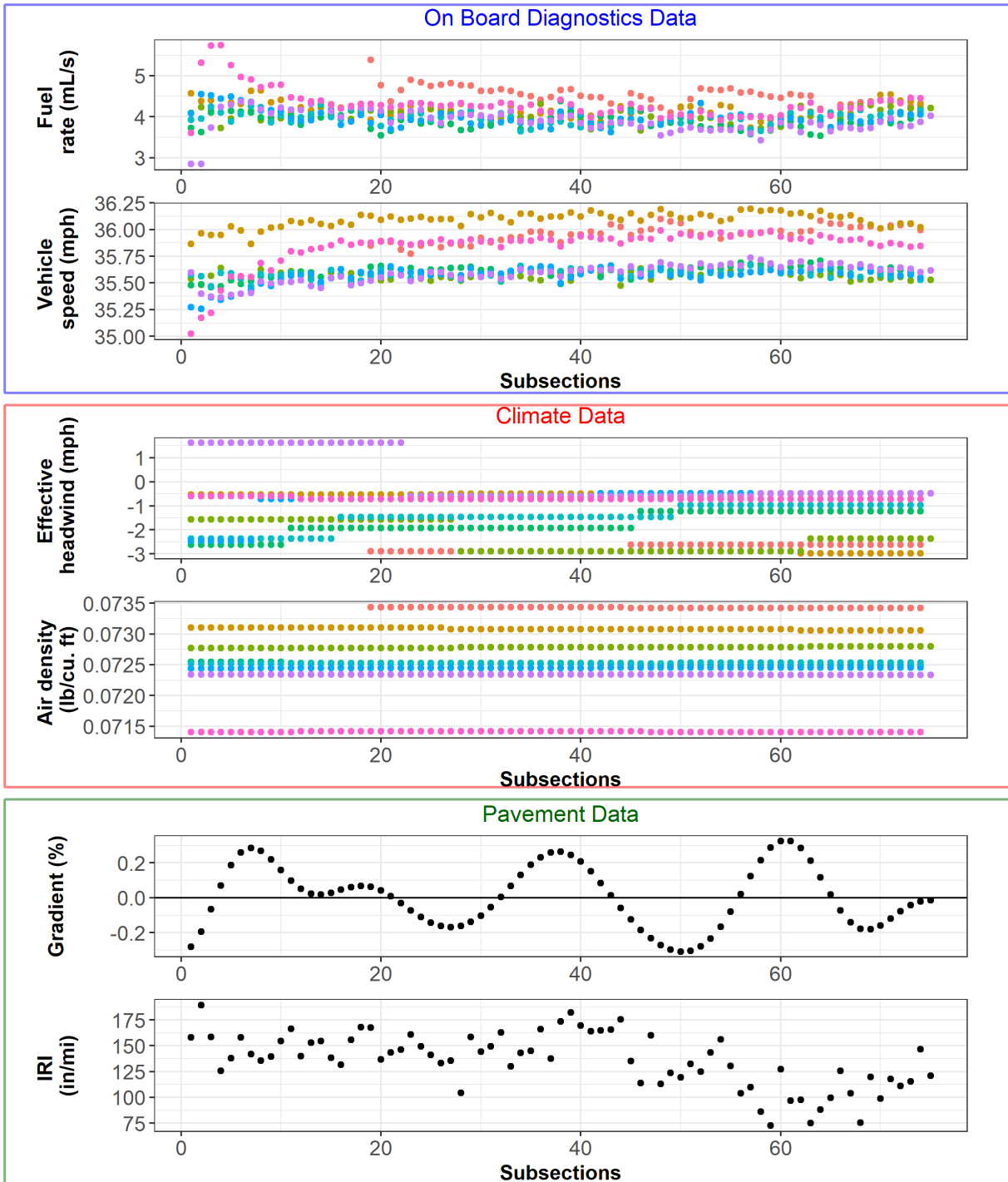


Figure P.368: HHDT data on Section PH23.

PH23-YOL-CR32AW-JPC HHDT summer_day 45 mph

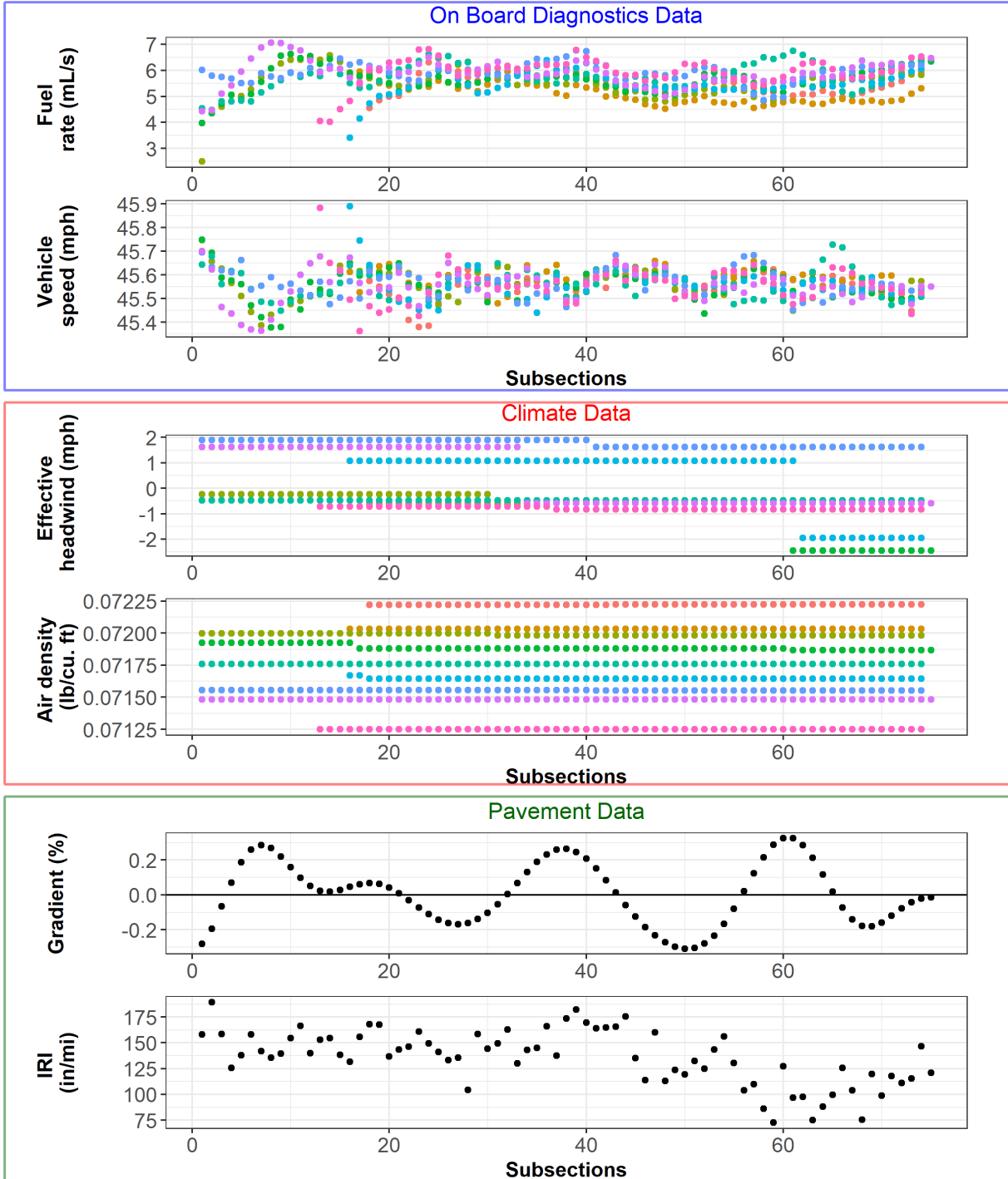


Figure P.369: HHDT data on Section PH23.

PH23-YOL-CR32AW-JPC HHDt summer_night 35 mph

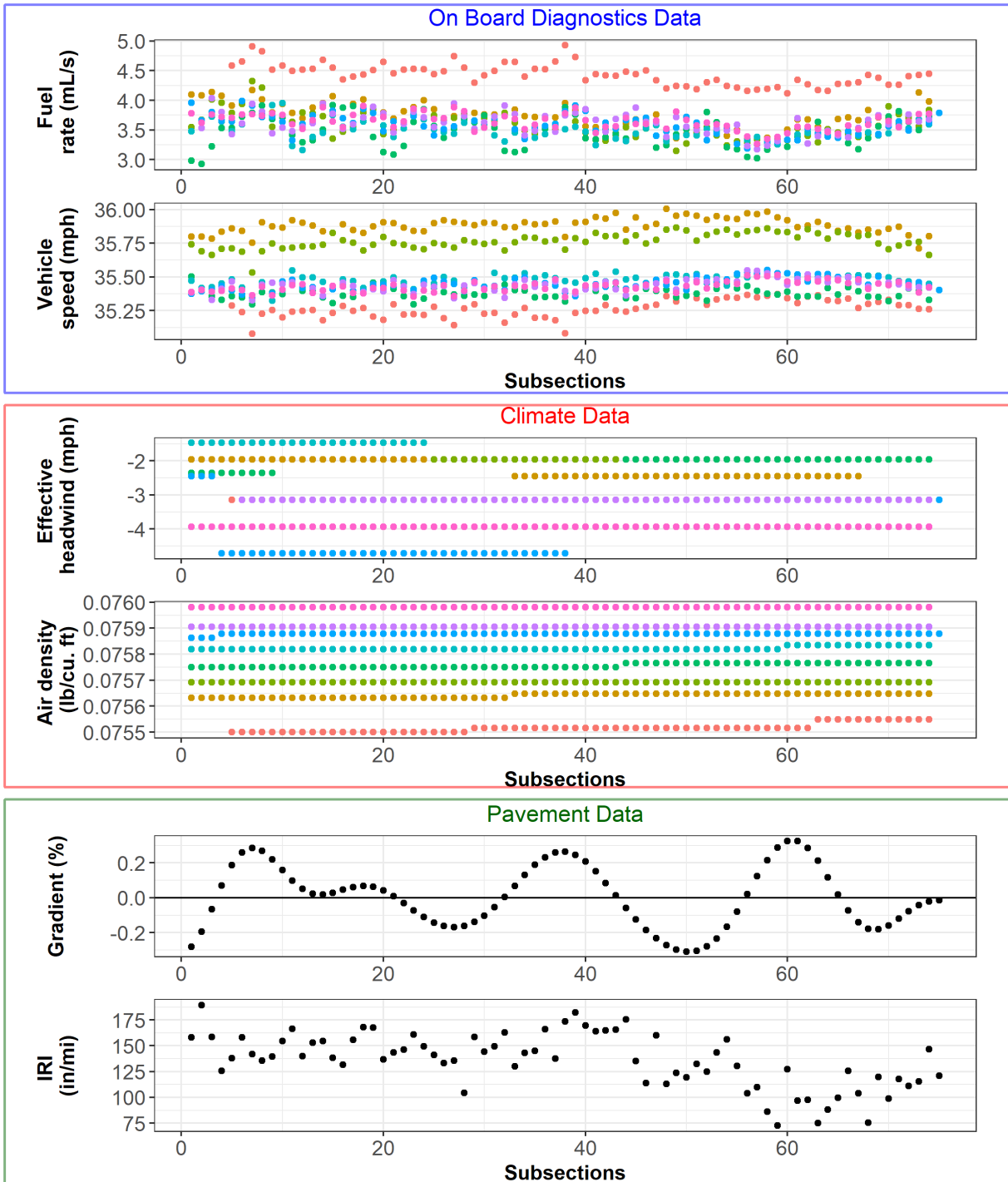


Figure P.370: HHDt data on Section PH23.

PH23-YOL-CR32AW-JPC HHDT summer_night 45 mph

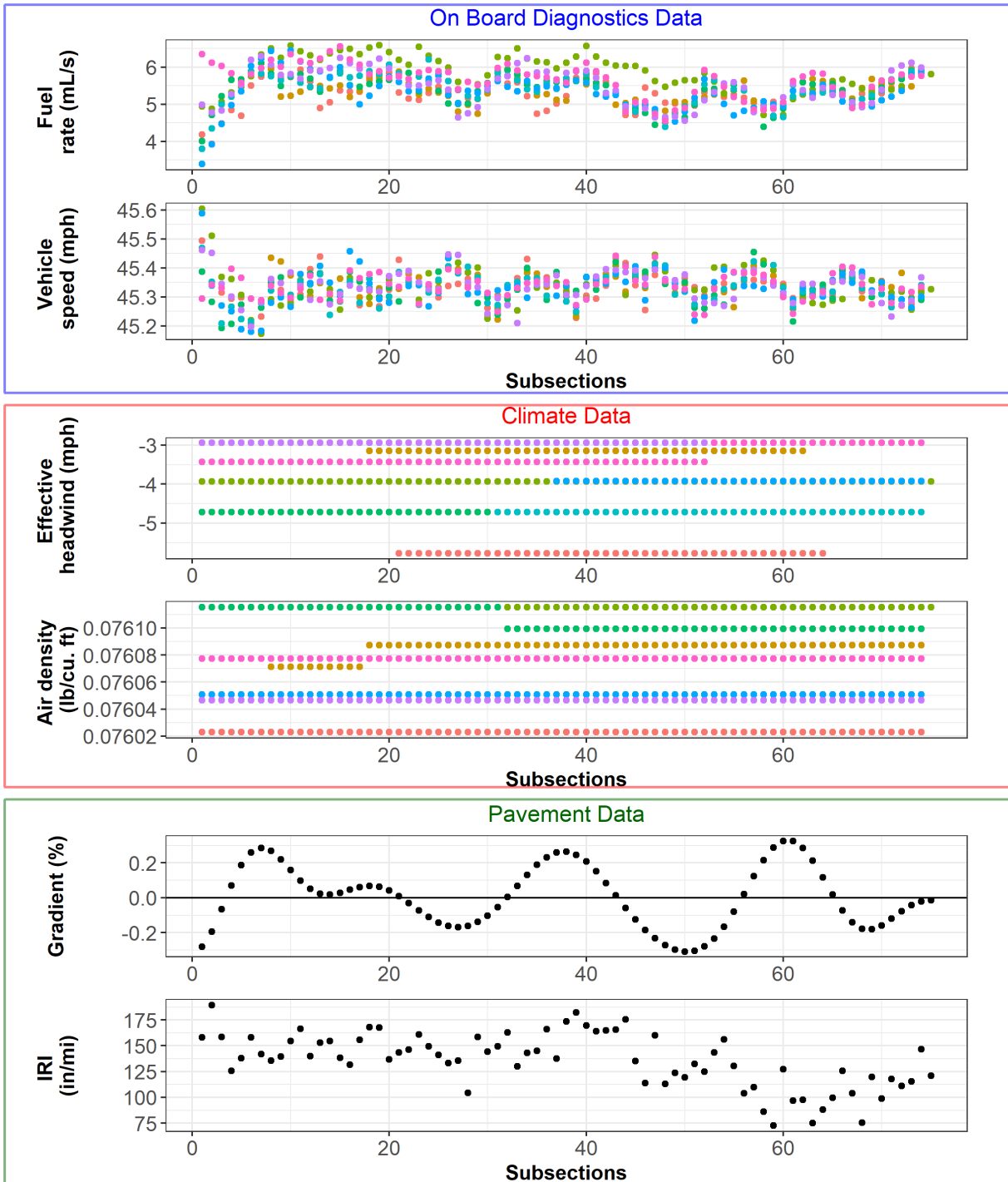


Figure P.371: HHDT data on Section PH23.

PH23-YOL-CR32AW-JPC HHDT winter_day 35 mph

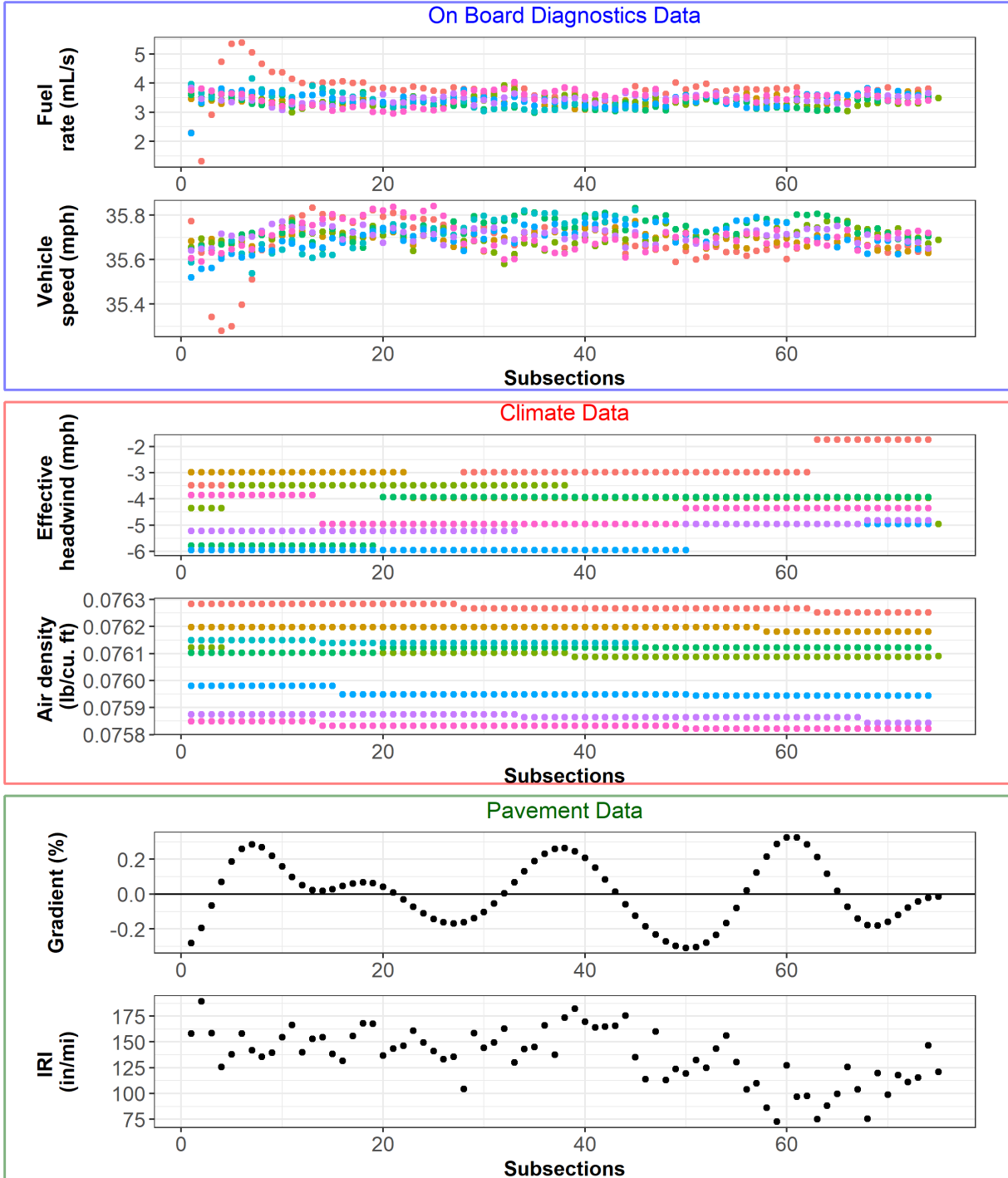


Figure P.372: HHDT data on Section PH23.

PH23-YOL-CR32AW-JPC HHDT winter_day 45 mph

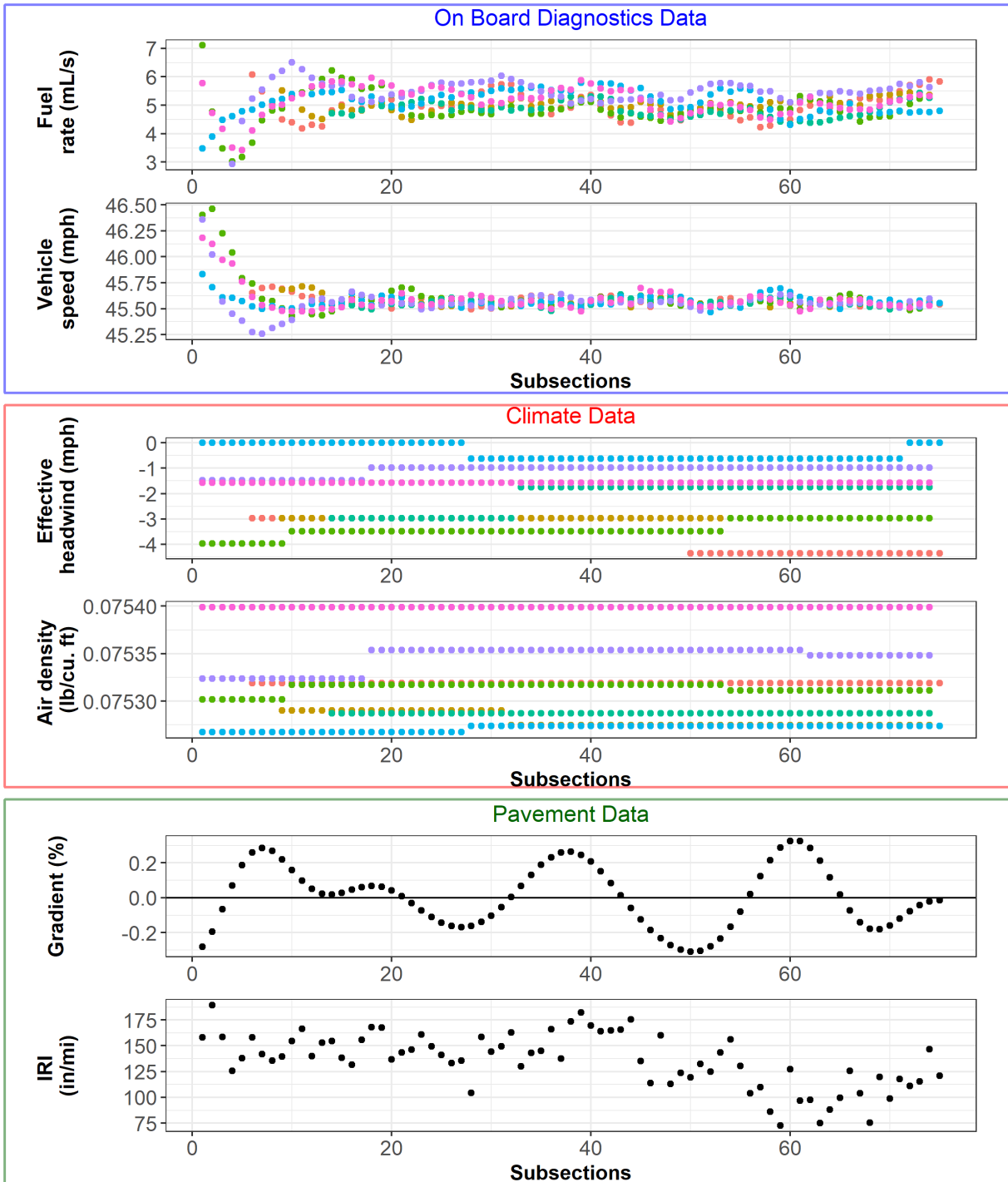


Figure P.373: HHDT data on Section PH23.

APPENDIX Q: QUANTITATIVE SUMMARIES OF VEHICLE EMPIRICAL MODELS

Table Q.1: Quantitative Summaries of Vehicle Empirical Models

Parameter	Car			SUV			F-450			HHDT		
	Mean	CI (95%)	<i>n eff</i>	Mean	CI (95%)	<i>n eff</i>	Mean	CI (95%)	<i>n eff</i>	Mean	CI (95%)	<i>n eff</i>
Correlation Structure Parameters												
auto regressive AR(1) (ρ)	0.62	0.61 - 0.62	4022	0.73	0.72 - 0.73	2555	0.94	0.94 - 0.95	2180	0.97	0.97 - 0.98	4362
Group-Level Parameters (standard deviations)												
group = road segment (ph)												
σ Intercept (35 mph)	0.04	0.03 - 0.06	629	0.05	0.04 - 0.08	810	0.22	0.13 - 0.34	785	0.80	0.47 - 1.29	930
σ 45 mph	0.01	0.00 - 0.02	241	0.01	0.00 - 0.02	359	1.03	0.66 - 1.58	510	1.07	0.73 - 1.54	970
σ 55 mph	0.03	0.02 - 0.05	714	0.03	0.02 - 0.04	792	4.06	2.24 - 6.53	650	1.86	1.30 - 2.59	1132
σ Air Temperature °F	0.02	0.01 - 0.03	526	0.03	0.01 - 0.04	402	0.34	0.24 - 0.48	990	0.31	0.14 - 0.58	463
σ 45 mph * Air Temperature °F	0.01	0.00 - 0.02	200	0.02	0.01 - 0.03	487	0.76	0.50 - 1.15	604	0.55	0.27 - 0.84	564
σ 55 mph * Air Temperature °F	0.02	0.02 - 0.04	686	0.02	0.00 - 0.04	367	9.50	5.06 - 15.07	696	1.13	0.78 - 1.68	868
σ 35 mph (in 6th gear)							0.21	0.05 - 0.67	960			
σ 45 mph (in 6th gear)							0.19	0.11 - 0.3	928			
σ 55 mph (in 6th gear)							0.16	0.03 - 0.3	506			
σ Air Temperature °F (in 6th gear)							0.92	0.43 - 1.93	1145			
σ 45 mph * Air Temperature °F (in 6th gear)							0.37	0.27 - 0.53	1223			
σ 55 mph * Air Temperature °F (in 6th gear)							0.10	0.00 - 0.27	146			
Population-Level												
Intercept (35 mph)	1.58	-0.16 - 3.38	625	1.88	0.08 - 3.69	1152	4.05	2.73 - 5.41	651	8.25	6.44 - 10.14	812
45 mph	-0.14	-1.95 - 1.60	624	-0.1	-1.89 - 1.69	1155	0.48	-0.98 - 1.90	587	-0.60	-2.50 - 1.19	859
55 mph	-0.14	-1.95 - 1.60	624	0.14	-1.66 - 1.93	1154	-0.26	-2.58 - 1.93	765	1.78	-0.29 - 3.72	928
Air Temperature °F	-0.02	-0.04 - -0.01	585	-0.09	-0.11 - -0.07	757	0.06	-0.19 - 0.32	891	0.64	0.34 - 0.99	563
Elevation Gradient (%)	0.03	0.03 - 0.03	1895	0.04	0.04 - 0.04	1661	0.04	0.03 - 0.04	1881	0.12	0.11 - 0.13	4594
Effective Tailwind	0.00	0.00 - 0.00	1879	0.00	0.00 - 0.00	1845	0.02	0.01 - 0.03	2349	0.01	-0.03 - 0.05	4269

Low Roughness (< 2.68 IRI)	-0.01	-0.01 - 0.00	2725	-0.01	-0.02 - -0.01	2474	-0.07	-0.1 - -0.04	1373	-0.04	-0.07 - 0.00	2266
Low Texture (< 1.20 MPD)	0.07	-1.74 - 1.80	623	-0.05	-1.87 - 1.75	1154	0.18	-1.16 - 1.48	631	-0.39	-2.21 - 1.33	933
45 mph * Air Temperature °F	0.00	-0.01 - 0.01	1047	0.01	-0.01 - 0.03	774	0.45	0.04 - 0.92	645	-0.69	-1.06 - -0.32	639
55 mph * Air Temperature °F	-0.01	-0.02 - 0.01	822	-0.01	-0.04 - 0.01	693	-0.65	-3.95 - 2.37	650	-1.53	-2.20 - -0.91	381
45 mph * Low Roughness (< 2.68 IRI)	0.00	-0.01 - 0.01	2601	0.01	0.00 - 0.01	2307	0.17	0.12 - 0.23	2120	0.03	-0.03 - 0.08	2491
55 mph *Low Roughness (< 2.68 IRI)	0.01	0.00 - 0.02	3240	0.01	0.00 - 0.02	2611	-0.07	-0.26 - 0.11	2775	0.02	-0.06 - 0.11	3142
45 mph * Low Texture (< 1.20 MPD)	-0.07	-1.80 - 1.75	624	0.06	-1.74 - 1.86	1155	-0.71	-2.04 - 0.62	637	0.47	-1.26 - 2.32	938
55 mph *Low Texture (< 1.20 MPD)	-0.06	-1.79 - 1.76	624	0.05	-1.74 - 1.86	1154	-0.14	-1.45 - 1.18	642	0.42	-1.32 - 2.26	930
35 mph (in 6th gear)							-0.8	-3.48 - 1.88	1916			
45 mph (in 6th gear)							-1.01	-2.37 - 0.31	658			
55 mph (in 6th gear)							-0.44	-1.81 - 0.87	673			
35 mph * Air Temperature °F (in 6th gear)							-0.21	-1.14 - 0.71	869			
45 mph * Air Temperature °F (in 6th gear)							-0.18	-0.45 - 0.10	909			
55 mph * Air Temperature °F (in 6th gear)							-0.15	-0.41 - 0.13	953			
35 mph * Low Roughness (< 2.68 IRI) (in 6th gear)							0.06	0.02 - 0.09	1539			
45 mph * Low Roughness (< 2.68 IRI) (in 6th gear)							0.07	0.04 - 0.09	1487			
55 mph *Low Roughness (< 2.68 IRI) (in 6th gear)							0.06	0.02 - 0.09	1487			
35 mph * Low Texture (< 1.20 MPD) (in 6th gear)							-0.81	-3.55 - 1.88	1903			
45 mph * Low Texture (< 1.20 MPD) (in 6th gear)							-0.14	-1.45 - 1.19	629			
55 mph *Low Texture (< 1.20 MPD) (in 6th gear)							-0.16	-1.48 - 1.18	632			
Residual standard deviation (σ)	0.07	0.07 - 0.07	1768	0.07	0.07 - 0.07	2139	0.17	0.17 - 0.17	2128	0.59	0.59 - 0.59	1843
number of observations (n)		93974			92636			89969			91777	